DESIGN OF ANALOG FILTERS

ROLF SCHAUMANN
MAC E. VAN VALKENBURG

THE OXFORD SERIES IN ELECTRICAL AND COMPUTER ENGINEERING

ADEL S. SEDRA, Series Editor, Electrical Engineering

Allen and Holberg, *CMOS Analog Circuit Design*
Bobrow, *Elementary Linear Circuit Analysis, 2nd Ed.*
Bobrow, *Fundamentals of Electrical Engineering, 2nd Ed.*
Burns and Roberts, *An Introduction to Mixed-Signal IC Test and Measurement*
Campbell, *The Science and Engineering of Microelectronic Fabrication, 2nd Ed.*
Chen, *Analog & Digital Control System Design*
Chen, *Digital Signal Processing*
Chen, *Linear System Theory and Design, 3rd Ed.*
Chen, *System and Signal Analysis, 2nd Ed.*
Comer, *Digital Logic and State Machine Design, 3rd Ed.*
Cooper and McGillem, *Probabilistic Methods of Signal and System Analysis, 3rd Ed.*
DeCarlo and Lin, *Linear Circuit Analysis, 2nd Ed.*
Dimitrijev, *Understanding Semiconductor Devices*
Fortney, *Principles of Electronics: Analog & Digital*
Franco, *Electric Circuits Fundamentals*
Granzow, *Digital Transmission Lines*
Guru and Hiziroğlu, *Electric Machinery & Transformers, 2nd Ed.*
Hoole and Hoole, *A Modern Short Course in Engineering Electromagnetics*
Jones, *Introduction to Optical Fiber Communication Systems*
Krein, *Elements of Power Electronics*
Kuo, *Digital Control Systems, 3rd Ed.*
Lathi, *Modern Digital and Analog Communications Systems, 3rd Ed.*
Martin, *Digital Integrated Circuit Design*
McGillem and Cooper, *Continuous and Discrete Signal and System Analysis, 3rd Ed.*
Miner, *Lines and Electromagnetic Fields for Engineers*
Roberts and Sedra, *SPICE, 2nd Ed.*
Roulston, *An Introduction to the Physics of Semiconductor Devices*
Sadiku, *Elements of Electromagnetics, 3rd Ed.*
Santina, Stubberud, and Hostetter, *Digital Control System Design, 2nd Ed.*
Sarma, *Introduction to Electrical Engineering*
Schaumann and Van Valkenburg, *Design of Analog Filters*
Schwarz, *Electromagnetics for Engineers*
Schwarz and Oldham, *Electrical Engineering: An Introduction, 2nd Ed.*
Sedra and Smith, *Microelectronic Circuits, 4th Ed.*
Stefani, Savant, Shahian, and Hostetter, *Design of Feedback Control Systems, 3rd Ed.*
Van Valkenburg, *Analog Filter Design*
Warner and Grung, *Semiconductor Device Electronics*
Wolovich, *Automatic Control Systems*
Yariv, *Optical Electronics in Modern Communications, 5th Ed.*

DESIGN OF ANALOG FILTERS

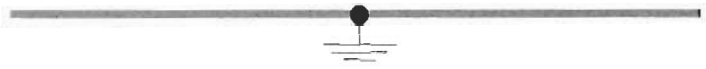

Rolf Schaumann
Portland State University

Mac E. Van Valkenburg

New York Oxford
OXFORD UNIVERSITY PRESS
2001

Oxford University Press

Oxford New York
Athens Auckland Bangkok Bogotá Buenos Aires Calcutta Cape Town
Chennai Dar es Salaam Delhi Florence Hong Kong Istanbul Karachi
Kuala Lumpur Madrid Melbourne Mexico City Mumbai Nairobi Paris
São Paulo Shanghai Singapore Taipei Tokyo Toronto Warsaw

and associated companies in
Berlin Ibadan

Published by Oxford University Press, Inc.
198 Madison Avenue, New York, New York, 10016
http://www.oup-usa.org

Oxford is a registered trademark of Oxford University Press

Library of Congress Cataloging-in-Publication Data

Schaumann, Rolf, 1941–
Design of analog filters / Rolf Schaumann, Mac E. Van Valkenburg.
p. cm. — (The Oxford series in electrical and computer engineering)
Rev. ed. of: Analog filters design / M.E. Van Valkenburg. c1982.
Includes bibliographical references.
ISBN 0-19-511877-4 (cloth)
1. Electric filters, Active—Design and construction. 2. Analog electronic systems—Design and construction. 3. Linear integrated circuits—Design and construction. 4. Operational amplifiers. I. Van Valkenburg, M. E. (Mac Elwyn), 1921– II. Van Valkenburg, M. E. (Mac Elwyn), 1921– Analog filters design. III. Title. IV. Series.
TK7872.F5 S29 2001
621.3815'324—dc21 99-035428

Printing (last digit): 9 8 7 6 5 4 3 2

Printed in the United States of America
on acid-free paper

CONTENTS

PREFACE

Filters, and more specifically analog filters, are essential in many different systems electrical engineers are called on to design. Even signal-processing systems that appear to be entirely digital often contain one or more analog continuous-time filters internally or as interface with the analog world. Thus, their wide use makes the topic of analog filters appropriate for study not only by graduate students, but also by undergraduate students as they prepare to enter their professions. Additionally, engineers in their professional careers facing new design challenges may have to upgrade their knowledge in this field. This book was written to address all these needs. As minimum prerequisites, students should have had a course in circuits and a course in mathematics that includes the Laplace transform. Beginning courses in electronics and systems are recommended as background. As the book is intended to be accessible to undergraduates, sophisticated mathematics is avoided wherever possible in favor of algebraic or intuitive derivations.

In selecting the material, the decision was made to concentrate on active "inductorless" filters. Active filters can handle almost any filtering requirement that an engineer is likely to face. They are compatible with modern microelectronic systems applications, such as controls and voice and data communications, where considerations of size and weight make the use of inductors prohibitive. In many cases, active filters can even be implemented in fully integrated monolithic form, which, except at the highest frequencies, precludes the use of inductors.

For most applications, the operational amplifier is the device that provides active filters with the required gain. The integrated-circuit operational amplifier, the "opamp," has profoundly affected the practice of analog electronic circuit design. Most electrical engineering students will have been introduced to the operational amplifier in basic circuits, electronics, or systems courses, where the opamp is often presented as an amplifier with infinite gain and bandwidth. This model has the advantage of leading to easy methods of analysis, and it often provides ready conceptual insight into the way a circuit may be designed in principle. Unfortunately, such a simple model is inadequate for designing practical filters with exacting requirements, except at very low frequencies. To undertake the design of filters with more cricial specifications requires better opamp models. Although they make circuit analysis more difficult for the student, it was deemed important to employ a realistic opamp model in the text to ensure that the resulting circuits work predictably in actual practice. As student interest is directed increasingly at engineering practice, it is important that techniques presented in courses and textbooks lead to correctly functioning designs. In addition, a filter book must provide the student with the tools that permit assessing and explaining any deviations from the expected filter performance—even if the approach and the analysis are a little more difficult to understand by the novice.

The study of filters is facilitated by access to a laboratory in which designs can be tested. This approach will not be available to many students due to high expenses and commitments of time. To provide the benefit of a laboratory setting during the study of filters, Electronics Workbench by Interactive Technologies, Ltd., was selected as a tool to verify the designs. This "simulated laboratory" allows experimentation with design alternatives and exploration of various design options rapidly and inexpensively, while gaining understanding of analog circuits and insight into filter design. At the same time students are able to experiment with models of real commercial operational amplifiers and thereby develop confidence that their circuits and filters actually perform as predicted and designed. Almost all filter examples in this text were tested with Electronics Workbench®. Using this approach should provide the student with the assurance that the filter designs developed throughout are not just "paper exercises" but lead to circuits that work in practice.

The material is organized as follows. Chapter 1 provides selected fundamental concepts and definitions to establish a common base for the study of filters. In Chapter 2, the operational amplifier is discussed and a suitable model, adequate for most active filter design procedures, is derived. The opamp is next placed into simple resistive feedback circuits, the fundamental block-diagram analysis approach is introduced, and a general method of analysis is provided that proves convenient for handling opamp circuits throughout the remainder of the book. "Experimental" examples demonstrate that the proposed models are realistic and provide predictable and practical results. This approach is followed throughout the book.

The design of filters, circuits designed intentionally to have a frequency-dependent transmission characteristic, starts in Chapter 3. The discussion begins with simple first-order blocks and illustrates the procedures by which practical filters of higher order can be obtained as cascade connections of low-order blocks. This treatment is then essentially repeated for biquads, i.e., filter sections of second order. All-pole functions are considered in Chapter 4, and functions with finite transmission zeros in Chapter 5. The presentation is restricted to only those circuits that have proven themselves in practice. Along the way, integrators, the main building blocks for all active filters, receive careful consideration. The consequences of the frequency dependence of the opamp gain, $A(s)$, on the integrator and on the second-order sections are analyzed. The discussion of the effects of $A(s)$ is contained in separate subsections and can, at the discretion of the instructor, be glossed over. The material is included in the text for the benefit of students or engineers who need to design filters with exact parameters and understand their behavior.

Next, Chapters 6 through 8 present the classical lowpass approximations, the Butterworth, Chebyshev, inverse Chebyshev, or Cauer functions that have maximally flat, equal-ripple, or elliptic magnitude characteristics. A comparison of the procedures allows the student to assess the distinct properties and the different efficiencies of these functions in approximating a given specification. Together with the frequency transformation discussed in Chapter 9, it will enable the student to design nearly all types of magnitude transmission requirements. The necessary background required for the design of delay filters is presented in Chapter 10, together with a comparison of the delay realized by different filter types. Chapter 11 addresses the design of delay equalizers.

Although alluded to earlier in the book, the discussion and the mathematics of the sensitivity of filter performance to component tolerances are left until Chapter 12. An earlier presentation would have delayed the development of actual filter circuits, and would have unnecessarily detracted from design. Nevertheless, students should comprehend the meaning of sensitivity, and have methods of sensitivity analysis in their repertory of design tools. It

enables them to compare different approaches and to understand the reasons why certain circuit structures and design methods should be avoided if the design is to perform well in practice.

In the design of filters of high order, many of the best performing circuits are based on simulating passive LC ladders. A discussion of LC ladders is included in Chapter 13 because it is considered helpful for an understanding of the origin of the LC prototypes. Conceptually, LC ladder design procedures are relatively easy, but the mathematical details tend to be formidable. The discussion is necessarily brief and concise, but is kept sufficiently general to enable the careful reader to design complete lossless ladders. Other readers may just wish to understand the LC ladder concept and the origin of useful topologies, and then consult any of the numerous design tables available in the literature and proceed with an active simulation. These simulation methods are based on two different approaches. Chapter 14 describes how the troublesome component, the inductor, can be replaced by an electronic circuit whose input impedance is inductive so that the complete filter can be realized in miniaturized form. The method discussed in Chapter 15 follows a different strategy: recognizing that capacitors and inductors in the LC ladder perform integration, their operation is simulated replacing inductors and capacitors by integrators.

In the final two chapters, the problem of designing an active filter in fully integrated, monolithic form on an integrated circuit chip is addressed. This is a topic of wide-ranging current industrial interest in which considerable research is performed. The discussion is divided into two parts. In Chapter 16, the $g_m - C$ method is considered that uses transconductance amplifiers to permit integrating continuous-time filters at the high frequencies required in modern communication systems. For these applications, opamps are often ruled out because of their relatively small bandwidth. The $g_m - C$ method leads to very simple methodical design approaches and commercially successful high-frequency filters. The techniques presented may also be used to design discrete filters, but are aimed mainly at an implementations in integrated-circuit form. In Chapter 17, switched-capacitor filters are discussed. Switched-capacitor filters are sampled-data circuits, that is, they are analog filters but no longer operate in the continuous-time domain. These integrated filters have been proven very successful at low to medium frequencies in commercial practice, but their analysis and design entail a new and different mathematical treatment that the engineer must understand to be able to develop successful products.

The book was planned as a revision of the 1982 monograph *Analog Filter Design* by Mac E. Van Valkenburg. Sadly, Profesor Van Valkenburg passed away in 1997 just as the first plans for the project were being formed, and so could, unfortunately, not participate in the revision. I have attempted to follow Mac Van Valkenburg's proven approach and have maintained the overall sequence of topics as far as possible. However considerable rewriting and shifts in emphasis were necessary, new subjects had to be included, and some topics needed more emphasis and others less, to impart a more modern flavor and to reflect the developments in the field over the past two decades.

I am indebted to numerous students on whom much of the material was tested, and to my colleagues and friends in the circuits and systems area whose research results, insights, and discussions helped clarify many concepts and ideas presented in this text. It was a pleasure to work with Peter Gordon and the staff of Oxford University Press during the production of the book. Finally, I express my gratitude to my wife Blanka for her assistance in proofreading and, in particular, for her patience and encouragement, not to mention the innumerable cups of espresso delivered during the preparation of this book.

Rolf Schauman
Portland, OR

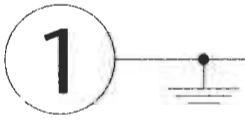

INTRODUCTION

The subject of this book is a special class of electrical circuits, commonly referred to as analog active filters. Analog filters make use of resistors R, capacitors C, and inductors L. In addition we use active devices to obtain gain. In this book we deal with miniaturized filters, which for the most part means that inductors cannot be used because, except at the highest frequencies (hundreds of megahertz, 10^8 Hz, even gigahertz, 10^9 Hz), their size cannot be reduced to a level compatible with modern integrated electronics. We shall see in the course of our study that inductors can be avoided if we have access to *gain*. In that case, the only passive components we need are resistors and capacitors, and gain is provided by operational amplifiers (opamps) or operational transconductance amplifiers (OTAs). Such filters are generally referred to as *active* filters, sometimes more specifically as *analog* active filters to distinguish them from *digital* filters. Signals in analog active filters are normally continuous functions of time, sometimes sampled, whereas in digital filters signals are digitized, that is, they are represented by ordered sets of numbers. In modern communication systems, both analog signals and digital signals must be processed. Often both analog and digital circuits and filters must be implemented together on the same integrated circuit chip for so-called *mixed-mode* signal processing. This book deals with the design of practical analog active filters and in this introductory chapter we provide some background material that will be useful in the studies to follow.

1.1 FUNDAMENTALS

Figure 1.1 shows a circuit with a voltage source $v_1(t)$ connected to the source (excitation) terminals 1–1′. The situation in Fig. 1.1a shows input and output as differential floating voltages. This is preferred for implementation in integrated circuit form for noise immunity, lower nonlinearities, and improved dynamic range. However, for most circuits in this book we find that input and output have a common terminal, Fig. 1.1b. This common terminal is

normally ground where $v(t) = 0$ and to which all signals are referenced. The output voltage $v_2(t)$ is observed or measured at the output (response) terminals 2–2′. If such a *two-port* circuit is operating in sinusoidal steady state, the two voltages

$$v_1(t) = V_1 \cos(\omega t + \theta_1) \quad \text{and} \quad v_2(t) = V_2 \cos(\omega t + \theta_2) \tag{1.1}$$

may be represented by phasors

$$\bar{V}_1 = |\bar{V}_1| e^{j\theta_1} = V_1 \angle \theta_1 \quad \text{and} \quad \bar{V}_2 = |\bar{V}_2| e^{j\theta_2} = V_2 \angle \theta_2 \tag{1.2}$$

More generally, the input and output quantities may be represented by their Laplace transforms $\bar{V}_1(s)$ and $\bar{V}_2(s)$ where $s = \sigma + j\omega$ is the frequency variable. $\bar{V}_1$ and $\bar{V}_2$ are complex numbers that along the $j\omega$-axis are expressed in terms of their magnitude and their phase,

$$\bar{V}_1 = \bar{V}_1(s)\big|_{s=j\omega} = |\bar{V}_1(j\omega)| e^{j\theta_1(\omega)} \text{ and } \bar{V}_2 = \bar{V}_2(s)\big|_{s=j\omega} = |\bar{V}_2(j\omega)| e^{j\theta_2(\omega)} \tag{1.3}$$

We also observe that both magnitude and phase are functions of the radian frequency ω. The ratio of the two Laplace transforms may be used to define a transfer function as

$$\frac{\bar{V}_2}{\bar{V}_1} = T(s) = \frac{\text{output quantity}}{\text{input quantity}} \tag{1.4}$$

Many authors define the transfer function as the reciprocal of Eq. (1.4); it is important, therefore, for us to agree on this definition throughout this text to avoid confusion. Using Eq. (1.3) in Eq. (1.4) results in

$$T(j\omega) = \frac{|\bar{V}_2(j\omega)| e^{j\theta_2(\omega)}}{|\bar{V}_1(j\omega)| e^{j\theta_1(\omega)}} = \frac{|\bar{V}_2(j\omega)|}{|\bar{V}_1(j\omega)|} e^{j[\theta_2(\omega) - \theta_1(\omega)]} = |T(j\omega)| e^{j\theta(\omega)} \tag{1.5}$$

which means that the magnitude of the transfer function equals

$$|T(j\omega)| = \frac{|\bar{V}_2(j\omega)|}{|\bar{V}_1(j\omega)|} = \left|\frac{\bar{V}_2(j\omega)}{\bar{V}_1(j\omega)}\right| \tag{1.6}$$

Rewriting Eq. (1.6) in the form

$$|\bar{V}_2| = |T(j\omega)| \, |\bar{V}_1| \tag{1.7}$$

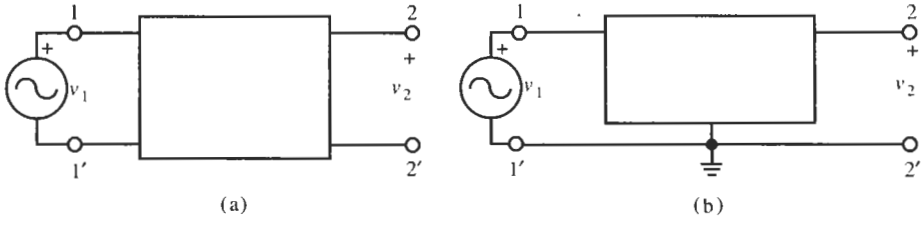

Figure 1.1 Two-port network: (a) floating input and output ports; (b) input and output have a common ground.

shows that a filter with the transfer function $T(s)$ provides information on how much the magnitude of an input signal at any given frequency ω is attenuated or magnified. Similarly, the angle of the transfer function

$$\theta(\omega) = \theta_2(\omega) - \theta_1(\omega) \tag{1.8}$$

gives information on the size of the phase shift that the input signal experiences when transmitted to the output,

$$\theta_2(\omega) = \theta_1(\omega) + \theta(\omega) \tag{1.9}$$

When we make measurements using the configuration in Fig. 1.1, we ordinarily keep the magnitude of the source voltage $|\bar{V}_1|$ constant, and we also select the phase reference arbitrarily such that $\theta_1 = 0$. Then the variations of the output $|\bar{V}_2|$ and its phase θ_2 with changes in frequency ω, in radians per second, or f, in Hertz, constitute the frequency response of the circuit. Both magnitude and phase of $T(j\omega)$ will change with frequency unless the circuit contains only resistors.

We denoted the Laplace transforms of the voltages as $\bar{V}_1$, "V_1-bar," and $\bar{V}_2$, "V_2-bar," to indicate that they are complex numbers with a magnitude and a phase. Because confusion between complex and real numbers in signals will rarely occur, we shall drop the "bar" in the remainder of this book to simplify notation. That is, we shall label the voltages simply as $V(s)$ or $V(j\omega)$, depending on whether we are concerned with the behavior in the s-plane generally, or with that on the $j\omega$-axis.

Now, if we know the circuit and the form of the input $v_1(t)$ or $V_1(s)$, we can always uniquely determine the output $v_2(t)$ or $V_2(s)$. This is called *circuit analysis*. If we know input and output, or the ratio $T(s) = V_2/V_1$, and we wish to find the circuit, we deal with *circuit design* (or synthesis). Synthesis is generally not unique; that is, there is usually more than one circuit that satisfies the prescribed transfer function behavior. Although we will frequently have to analyze circuits to understand their behavior, throughout this book we will be concerned mainly with design. This means that when magnitude and/or phase of a transfer function $T(s)$ are prescribed, our task will be to find the circuit elements and their interconnections, such that the resulting circuit performs as desired. The circuits that we design have a prescribed magnitude, phase, or related quantities as functions of frequency. These circuits are known as *filters*.

Filtering has a commonly accepted meaning of separation—something is retained, something is rejected. In electrical engineering, we filter signals, usually voltages. Any signal may be thought of as being made up of packets of signals, each at a specified frequency. Thus, if a signal is made up of two tones, one at high frequencies, such as that produced by a piccolo, and one of low frequencies, such as that produced by a tuba, we can imagine a filtering action by which one or the other is being suppressed. You will come to understand that any signal may be thought of as consisting of components, each at a given frequency. It is as if signals were generated by a large number of sinusoidal voltage sources connected in series, each characterized by a frequency, and a magnitude and phase. This concept will be formalized when you study Fourier analysis.

We reject the frequency components of a signal by designing a filter that provides *attenuation* over that band of frequencies, and we retain components of a signal through

the absence of attenuation or perhaps even gain. It is important that we distinguish between the measures of attenuation and gain. Look at Eq. (1.7). When the output signal is larger than the input, $|T(j\omega)| \geq 1$, the circuit amplifies or provides *gain*. It is customary to measure gain by a quantity $\alpha(\omega)$ defined as

$$\alpha(\omega) = 20 \log |T(j\omega)| \text{ dB} \tag{1.10}$$

where $\alpha \geq 0$ because $|T(j\omega)| \geq 1$. The same equation (1.10) is used to define loss, $|T(j\omega) < 1$, but now $\alpha < 0$ because $|T(j\omega)| < 1$. Note that α as defined is a measure of gain, that is $\alpha > 0$ is gain, whereas "negative gain," $\alpha < 0$, implies loss. This definition is consistent with the way in which most instruments (e.g., network analyzers[1]) display the measured gain or attenuation, but it is not used consistently in the literature on filters. We will *not* attach a sign to α but let the context make clear whether we mean loss (attenuation) or gain. When we speak of an amplifier providing α dB gain, it is clear that the output is larger than the input. Conversely, when a filter or a transmission channel provides α dB loss, obviously its output is smaller than its input. Only if confusion can arise will we attach a sign to α. The unit of gain and attenuation is the *decibel* (dB), with dB counted positive for gain and negative for attenuation. $\alpha = 0$ dB when $|T(j\omega)| = 1$ and input and output signals have the same magnitude. We may solve Eq. (1.10) for $|T(j\omega)|$ by dividing α by 20 and taking the antilogarithm:

$$|T(j\omega)| = 10^{\alpha(\omega)/20} = 10^{0.05\alpha(\omega)} \tag{1.11}$$

Table 1.1 provides the corresponding values of α [dB] and $|T(j\omega)|$. It is sometimes helpful to have these values in mind when designing filters. For example, a loss of $\alpha = 80$ dB means the filter's output voltage is attenuated to 1/10,000th of the input voltage, and a gain of 80 dB means the output is 10,000 times a large as the input. At the -3 dB point the output is attenuated to 70.7% of the input magnitude. This is also referred to as the "half-power point" because power is proportional to the square of the voltage and $0.707^2 = 0.5$. Other data for Table 1.1 can be filled by use of Eq. (1.10) and Eq. (1.11). For example, an amplifier with gain $\alpha = 43$ dB amplifies a signal approximately 141 times, and a filter that reduces a signal to 0.4% of the input magnitude has loss or attenuation of $\alpha \approx 48$ dB. You may also wish to remember that

-1 dB implies approximately a 10% decrease in the value of $|T|$

-2 dB implies approximately a 20% decrease in the value of $|T|$

-3 dB implies approximately a 30% decrease in the value of $|T|$

-6 dB implies approximately a 50% decrease in the value of $|T|$

You can verify from Eq. (1.11) that each additional increase of loss by $\alpha = 6$ dB reduces the value of $|T|$ by a further 50%. Also note that each increase in gain by 20 dB or attenuation by 20 dB increases or reduces, respectively, the magnitude of a transfer function by a factor of 10.

---

[1] A network analyzer will be the main (simulated) instrument that we use throughout the text to "measure" the gain, attenuation, or phase of the circuits we design. The network analyzer display will give readers confidence that their circuits behave as designed.

TABLE 1.1 Size of Attenuation or Gain and Its Values in dB

Loss		Gain	
α [dB]	$\lvert T(j\omega)\rvert$	α [dB]	$\lvert T(j\omega)\rvert$
−100	10^{-5}	100	10^5
−60	10^{-3}	60	10^3
−20	0.1	20	10
−6	0.501	6	1.995
−3	0.707	3	1.414
−1	0.891	1	1.122
−0.1	0.989	0.1	1.011

1.2 TYPES OF FILTERS AND DESCRIPTIVE TERMINOLOGY

Filters are classified according to the functions they are to perform. Over the frequency range of interest we define *passbands* and *stopbands*. In the ideal case, a passband is the range of frequencies of the filter where $|T| = 1$ and $\alpha = 0$, that is, signals are transmitted from input to output without attenuation or gain. In a stopband $|T| = 0$ and $\alpha = -\infty$, which means that transmission is blocked completely. The patterns of passbands and stopbands that give rise to the most common filters are shown in Fig. 1.2. They are defined as follows:

1. A *lowpass* filter characteristic is one in which the passband extends from $\omega = 0$ to $\omega = \omega_c$, where ω_c is known as the *cutoff frequency* (Fig. 1.2a).
2. A *highpass* filter is the complement of the lowpass filter in that the frequency range from 0 to ω_c is the stopband and from ω_c to infinity is the passband (Fig. 1.2b).
3. A *bandpass* filter is one in which the frequencies extending from ω_1 to ω_2 are passed, while signals at all other frequencies are stopped (Fig. 1.3c).
4. The *bandstop* filter is the complement of the bandpass filter where signal components at the frequencies from ω_1 to ω_2 are stopped and all others are passed (Fig. 1.2d). These filters are also sometimes referred to as *notch* filters because of the "notch" in their transmission characteristic.

There will be other kinds of filters introduced as our study progresses, such as filters specifically designed for a desired delay or filters with multiple passbands and stopbands, but filtering action can usually be visualized in terms of the basic four types of filters in Fig. 1.2.

In practice, it is not possible to realize the ideal transfer functions shown by solid lines in Fig. 1.2 with real filters consisting of a finite number of elements. We shall see throughout our study of filters that for real circuits the transfer functions defined in Eq. (1.4) are always described by *real rational functions* of the complex frequency s. A real rational function is a ratio of polynomials in s as shown in Eq. (1.12),

$$T(s) = \frac{N(s)}{D(s)} = \frac{b_m s^m + b_{m-1}s^{m-1} + \ldots + b_1 s + b_0}{a_n s^n + a_{n-1}s^{n-1} + \ldots + a_1 s + a_0} \tag{1.12}$$

where the coefficients $a_i, i = 1, \ldots, n$, and $b_j, j = 1, \ldots, m$, are real numbers. The coefficient a_n in Eq. (1.12) can arbitrarily be set to unity, $a_n = 1$, by dividing numerator and denominator by a_n. The numerator coefficients b_j can be positive, negative, or zero,

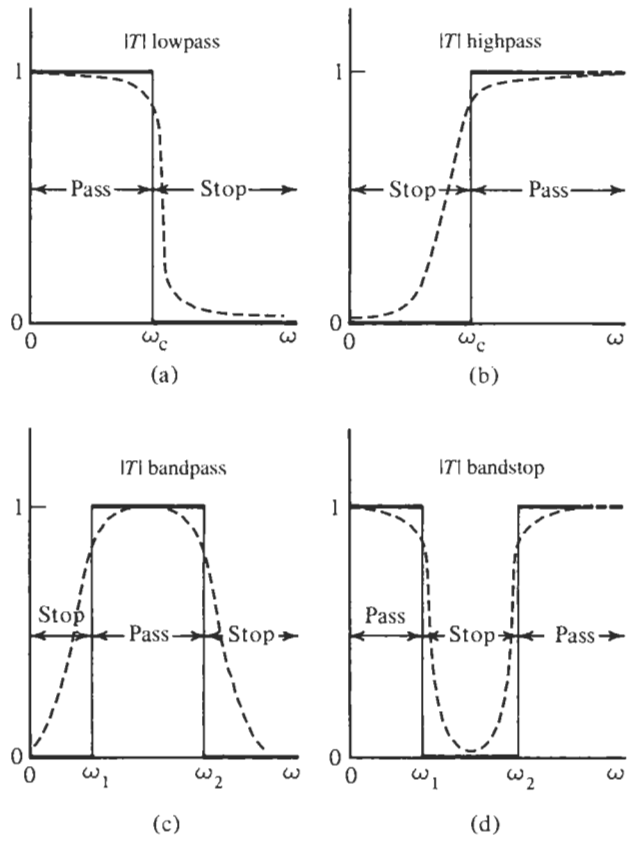

Figure 1.2 The four basic types of ideal filter functions. Solid lines: ideal function; dashed lines: real filter functions where the magnitude is a continuous function of ω.

but the denominator coefficient a_i must all be positive, $a_i > 0, i = 0, 1, \ldots, n-1$. If these restrictions are violated, the circuit will oscillate and the transfer function cannot be realized with positive elements. Also, to be realizable with a finite number of real components, the degree n of the denominator polynomial $D(s)$ must be larger than, or at least equal to, the degree m of the numerator polynomial $N(s)$, $n \geq m$. The magnitude of Eq. (1.12), when evaluated on the $j\omega$-axis, $|T(j\omega)|$, is a continuous function of frequency that cannot realize the abrupt behavior depicted by the solid lines in Fig. 1.2. Rather, realistic filter characteristics that correspond to the four basic types are shown by the dashed lines in Fig. 1.2. We will see later that the sharpness of the transition from passband to stopband, as well as the shape and width of the passband, can be controlled in the design of the filters.

In the chapters to follow we will switch from the linear magnitude or gain characteristic $|T(j\omega)|$ to the logarithmic attenuation characteristic $\alpha(\omega)$ depending on which representation makes the point more clearly. The attenuation characteristics corresponding to those of Fig. 1.2 are shown by the dashed lines in Fig. 1.3. The two quantities are related, of course, by Eq. (1.10). When specifying the desired attenuation requirements for a filter to be *design*ed, it is customary to plot attenuation as positive values of α as in Fig. 1.3. Often, frequency is plotted on logarithmic coordinates; then the curve, attenuation in dB versus logarithmic frequency, is known as a Bode plot, and the asymptotic slope is measured in multiples of 6 dB per octave

(a factor two in frequency) or 20 dB per decade (a factor 10 in frequency). This property will be examined in greater detail in Chapter 3.

Since it is impossible to realize filters with the solid-line characteristics in Fig. 1.2, having abrupt changes from passbands to stopbands and stopbands to passbands, we must learn to cope with the gradual transitions of the realistic filter transfer functions illustrated by the dashed lines in Figs. 1.2 and 1.3. The latter are used to *approximate* the ideal characteristics. The way this is accomplished is illustrated in Fig. 1.3. We will specify certain boundaries (shaded lines in Fig. 1.3) and determine the required characteristics not exactly, but only within certain tolerances in terms of attenuation α for the passbands and stopbands as follows:

1. In a passband the attenuation is always less than a maximum attenuation designated as α_{max}.
2. In a stopband the attenuation is always larger than a minimum value designated as α_{min}.
3. Bands between passbands and stopbands so defined are known as *transition* bands.

In terms of Fig. 1.3a we see that the passband extends from $\omega = 0$ to $\omega = \omega_p$, the range

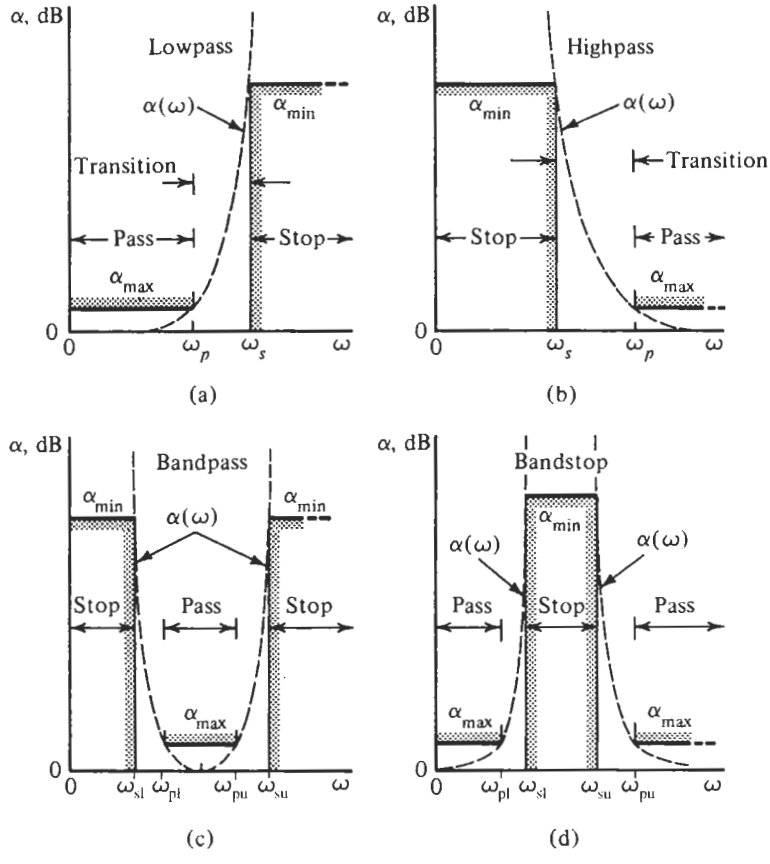

Figure 1.3 Practical filter attenuation specifications to be met by continuous functions $\alpha(\omega)$ (dashed lines).

of frequencies from ω_p to ω_s is the transition band, and all frequencies greater than ω_s constitute the stopband. In this figure, as well as in Fig. 1.3b, we have used the subscripts p and s to indicate the edges of the passbands and stopbands. The same concept applies to the bandpass and bandstop cases shown in Figs. 1.3c and d. Here there are two transition bands.

In later chapters, we will use the shaded attenuation characteristics in Fig. 1.3 as the filter *specifications*. In terms of Fig. 1.3a the design problem will be as follows: Given the four quantities α_{max}, α_{min}, ω_p, and ω_s, find an attenuation specification that satisfies the four requirements. The form of the solution, the attenuation $\alpha(\omega)$, is indicated in Fig. 1.3 by the dashed lines. Mathematically, the solution is found by a process called *approximation*; it determines the transfer function $T(s)$ in Eq. (1.12) such that $\alpha(\omega)$ defined in Eq. (1.10) meets the requirements. For the lowpass in Fig. 1.3a this means $\alpha(\omega) \leq \alpha_{max}$ in $\omega \leq \omega_p$, and $\alpha(\omega) \geq \alpha_{min}$ in $\omega \geq \omega_s$. The complementary description is true for the highpass in Fig. 1.3b. Similarly, for the bandpass specification in Fig. 1.3c we require $\alpha(\omega) \geq \alpha_{min}$ in $\omega \leq \omega_{sl}$ and $\omega \geq \omega_{su}$, and $\alpha(\omega) \leq \alpha_{max}$ in $\omega_{pl} \leq \omega \leq \omega_{pu}$, where ω_{sl} and ω_{su} are the lower and upper corners of the two stopbands, and ω_{pl} and ω_{pu} are the corners of the passband. Analogously, the complementary requirements hold for the bandstop specifications in Fig. 1.3d. The approximation problem will be studied in detail in later chapters.

Another factor must be considered in design. The attenuation curves shown thus far have a minimum value of $\alpha = 0$ dB, corresponding to $|T(j\omega)|_{max} = 1$ in Fig. 1.2. Since we are using active filters, this need not necessarily be the case, because the active elements may provide gain. If it is necessary to meet the specifications exactly, it will be necessary to provide a circuit to reduce the so-called *insertion* gain, the gain provided by inserting the filter between input and output. If the circuit provides excess attenuation as normally found in passive filters, this so-called *insertion loss* must be overcome by additional amplification. These two conditions are illustrated in Fig. 1.4 in which the characteristic bandpass curve is shifted up or down, but the shape is not changed. In filter design, such frequency-independent insertion loss or gain is usually not important.

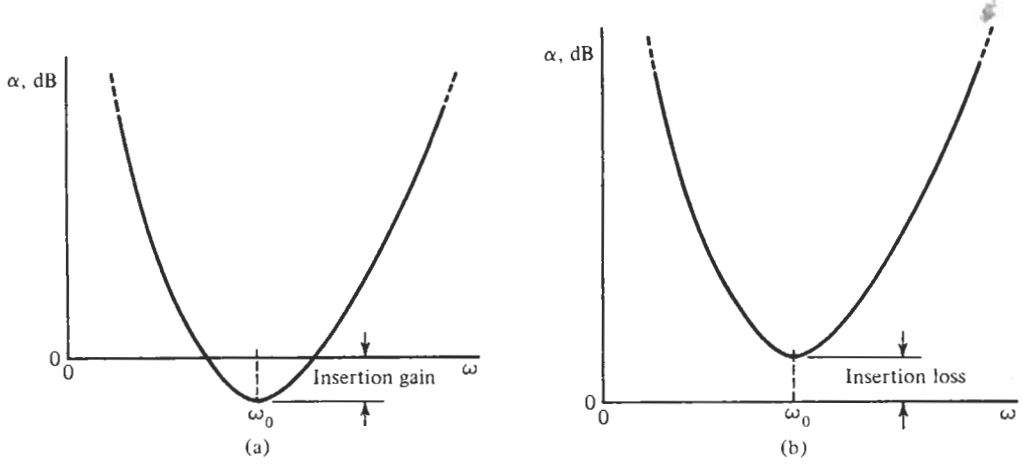

Figure 1.4 Insertion gain and loss in a bandpass characteristic.

1.3 WHY WE USE ANALOG FILTERS

The basic concepts of the electric filter were developed in 1915 independently by Wagner in Germany and Campbell in the United States. In the years since that invention, filter theory and implementation techniques have been developed to a high degree of perfection. Implementing economically an *active* filter, a filter that uses gain, became possible with the invention of the vacuum tube, and the development of feedback theory by Black, Bode, and others in the early 1930s. The present era of wide use of high-quality low-cost discrete analog active filters is due to the development of the inexpensive monolithic operational amplifier (opamp) by Widlar in 1967. In the recent trend to place ever more complicated complete systems on a monolithic integrated circuit (IC), filter designers felt pressure to devise techniques that allow the integration of analog filters onto the IC along with digital circuitry. The solution was found in the more recent developments of *switched-capacitor* filters for low to medium frequencies[2] by Fried in 1972 and by many other researchers in industry and at universities throughout the 1970s. Finally, the use of *transconductance amplifiers* led to integrated filters at high frequencies (useful from the audio range up to tens to hundreds of megahertz).

Although increasingly many filtering applications are now handled with digital signal processing techniques and digital filters, generally there remains the question of whether to choose an analog or a digital filter for a particular application. In practice, there are a number of situations in which analog continuous-time filters are either a necessity or provide a more economical solution. Among these are *interface* circuits. They connect the real-world analog signals to the digital signal processor and provide *bandlimiting* before the signals can be sampled for further processing with sampled-data or digital techniques, and reconstruction back to the analog world. Also, filtering requirements at very high frequencies where ultrafast sampling and digital circuitry may not be realistic and economical (see Fig. 1.5) may require analog techniques.

Analog active filters always use gain and capacitors. In practical discrete active filters, resistors are also used and gain is obtained from the opamp. In integrated active filters we obtain gain by making use of opamps or transconductance amplifiers (also referred to as *operational* transconductance amplifiers, known as OTAs), and we utilize capacitors, resistors, and, at the highest frequencies, integrated inductors. To be able to decide which components to use, and whether to use an active filter in preference to a filter assembled entirely out of passive components, we must consider factors such as the following:

1. The technology desired for the system implementation.
2. Availability of dc supplies for the active devices, and power consumption.
3. Cost.
4. The range of frequency of operation.
5. The sensitivity to parameter changes and stability.
6. Weight and size of the implemented circuit.
7. Noise and dynamic range of the realized filter.

[2] At the time of this writing, commercial switched-capacitor filters are limited to the range from audio frequencies up to a few hundred kilohertz.

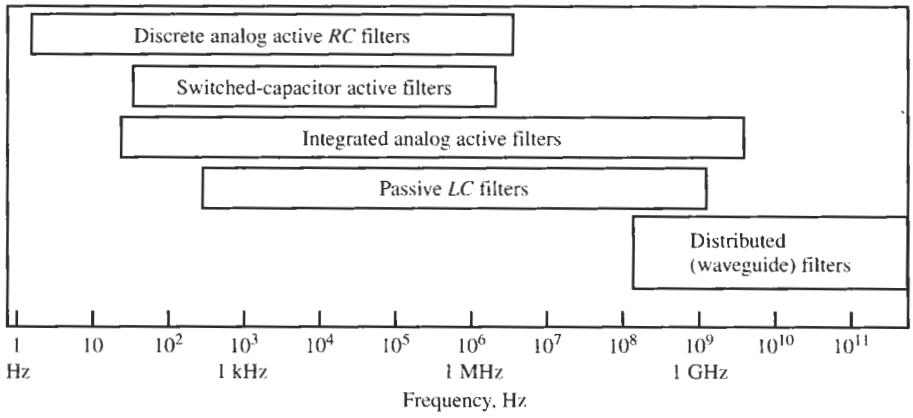

Figure 1.5 Choice of filter type as a function of the operating frequency range.

The meaning of several of these criteria will become clear as we progress in our discussion of active filters. Some guidelines for a possible choice of filter type can be obtained from Fig. 1.5 as a function of the desired frequency range of operation. The range of *LC* filters is limited at the low end by the bulk of the inductors and for high frequencies by parasitic and distributed effects. We see that compared to passive *LC* filters, discrete opamp-based active filters can realize filters for lower frequencies, but not for higher frequencies, whereas integrated analog filters, depending on the design and the type of devices used, can span the range from low audio frequencies to the gigahertz range. Switched-capacitor filters will be seen to be limited in their application range from about 10 Hz to about 1 MHz by impractical element sizes and by the bandwidth of the active devices. Microwave filters cover the highest frequency range by relying on distributed elements and waveguide designs. The indicated limitations of active filters depend, of course, on the active devices used: opamps or OTAs. The limits may be temporary and will change as technology advances and faster active devices become available.

If sensitivity to component variations and fabrication tolerances is important, passive *LC* filters often have an advantage. We will consider this aspect in Chapter 13. Although still used in large numbers, their design is not compatible with modern fully integrated systems. As our discussion progresses, we will learn that to address this difficulty many methods have been developed to simulate the performance of *LC* filters with active circuitry.

Finally, active filters require, of course, power supplies. The power supply voltages range anywhere from 1 V to 15 V, with typical designs at the time of this writing at or below 3.3 V. You will have learned in basic electronics courses that as the power supply voltage for biasing the active elements shrinks, so will the linear range over which the active devices can be used. Consequently, the usable linear signal level becomes smaller with reduced power supply voltages. Since active devices generate noise, which limits the smallest signals that can be processed, dynamic range becomes a serious concern for the designer. Dynamic range is defined as the difference between the largest undistorted signal and the noise level.

1.4 CIRCUIT ELEMENTS AND SCALING

It will become clear as our study progresses that filter design is primarily a frequency-domain matter and that we seldom make reference to time-domain quantities, such as rise time or

overshoot. Design specifications or physical measurements are made in terms of frequency f in Hertz. However, it turns out to be much more convenient to use radian frequencies ω in rad/s rather than f. We will follow this practice and use ω as long as possible and only convert to f in the last step. Experience in design will show the advantages of this choice.

We will make extensive use of both magnitude and frequency scaling, and also of normalized element values as well as normalized values of frequency. This has several reasons. It avoids the need to use very small or very large component values, such as pF (10^{-12} F) capacitors and MΩ (10^6 Ω) resistors. It permits us to design filters whose critical specifications are on the frequency axis "in the neighborhood" of $\omega = 1$ rad/s. Further, it permits us to deal with only dimensionless specifications and components without having to be concerned with units, such as Hz, Ω, F, or H. Finally, the most important reason is that much of the work of filter designers is based on the use of design tables. In these tables so-called "prototype" lowpass transfer functions are assumed to have a passband along the *normalized* frequency ω in $0 \leq \omega \leq \omega_p = 1$ and a stopband in $1 < \omega_s < \omega < \infty$. See Fig. 1.3a. In addition, these prototype filters are designed with normalized dimensionless elements from which the real physical components are obtained by denormalization. The relationships between the physical elements R, L, and C and their normalized representations R_n, L_n, and C_n are

$$L_n = \frac{\omega_S}{R_S} L, \quad C_n = \omega_S R_S C, \quad R_n = \frac{1}{R_S} R \tag{1.13a, b, c}$$

In Eq. (1.13), R_S is an arbitrary scaling resistor (in Ohms) that normalizes the impedance level and ω_S is the radian frequency (in rad/s) that scales and normalizes the frequency axis, such that $\omega/\omega_S = 1$, usually, at the passband corner. These expressions, as well as their inverses,

$$L = \frac{R_S}{\omega_S} L_n, \quad C = \frac{1}{\omega_S R_S} C_n, \quad \text{and} \quad R = R_S R_n \tag{1.14a, b, c}$$

are easy to remember by noting that R, L, and C have units of Ω, H, and F whereas R_n, L_n, and C_n are dimensionless numbers. Thus, the scaling factors ω_S and R_S do not only change the numerical values of the elements or frequency parameters, they can be seen to remove or restore the units depending on the direction of the transformation. As an example, assume that a prototype filter was designed, and design tables indicate that $R_n = 1$, $L_n = 3.239$, and $C_n = 1.455$ are the required normalized components. If the impedance level is selected as $R_S = 1{,}200\ \Omega$ and the frequency was normalized by $\omega_S = 10.8$ Mrad/s $= 10{,}800{,}000$ rad/s, we compute the real inductor value from Eq. (1.14a) as

$$L = \frac{1{,}200\ \Omega}{10.8 \times 10^6\ \text{MHz}} 3.239 = 360\ \mu\text{H}$$

Similarly, we find for the other components $R = 1.2$ kΩ and $C = 112$ pF. We still point out that *all* components with physical units (Ω, S, H, F, s, Hz) are scaled, but dimensionless parameters, such as gain, are not. Thus, in the above example where $R_S = 1{,}200\ \Omega$ was chosen as the resistor to scale the impedance level, a transconductance of value $g_m = 245\ \mu$S is normalized to

$$g_{m,n} = R_S g_m = 1200\ \Omega \times 245\ \mu\text{S} = 0.294$$

but an amplifier gain of value $K = 45$ dB keeps its value K in the normalized circuit.

TABLE 1.2 Typical Component Values in Discrete and Integrated Realizations

	Discrete	Integrated
Tolerances	1–20%	10–40% absolute 0.1–1% for ratios
Resistors		
Preferred range	1–100 kΩ	Process dependent: values
Lower limit	0.05–1 kΩ	with 10% to 30% tolerances
Upper limit	100–500 kΩ	in the range of 50 Ω–1 kΩ
Capacitors		
Readily realizable	5 pF–1 μF	0.5–5 pF
Practical	0.5 pF–10 μF	0.2–10 pF
Marginally practical	0.2 pF–500 μF	0.1–50 pF
Inductors		
Readily realizable	1 μH–10 mH	Real inductors with large losses
Practical	0.1 μH–50 mH	of the order of 10 nH or less
Marginally practical	100 nH–1 H	

It will become clear in the chapters to follow that ordinarily there is no unique solution to the design problem. One of the decisions that the designer has to make is that of element size. Making appropriate choices will become easier with experience, and selecting a suitable impedance normalization factor, R_S, will help. Table 1.2 serves in guiding the selection. Whether an element value is conveniently realizable depends on the chosen technology; here we distinguish between discrete filter designs and filters to be implemented on integrated circuits. Note that in integrated circuits, *ratios* of *like* components can be very accurate with careful layout and processing, but untuned absolute values of components can have very large tolerances. This is the reason why the parameters of integrated-circuit opamps are not predictable with any accuracy or reliability and why in the design of active filters it is very important to make the filter independent of the opamp parameters. Practical sizes of resistors and capacitors are limited by the available silicon area on an IC chip. Integrated inductors are very small and at the same time very lossy. Simulated inductors can be larger and less lossy, but they add noise; it is not difficult to implement a simulated inductor in the range of many mH or even H.

The design of active filters generally requires accurate components. Typically, resistors with 1 or 5% tolerances are used in discrete circuits, more rarely in less critical applications 10 or 20% resistors will suffice. On the other hand, capacitors with 10 or even 20% tolerances are more readily available and are preferred to save cost. As a rule, suitable capacitor values are preselected, such as 0.1 or 0.01 μF, because fewer standard capacitor values are available for the filter designer to choose from. It makes little sense to compute a capacitor for a specified filter to three or more digits and then find out that no company manufactures that capacitor. The resistors needed for the filter are determined from these predetermined values and a specified frequency. For example, frequency is set by an RC product as $f_0 = 1/(RC)$; then, for $f_0 = 12$ kHz and choosing $C = 0.01\mu$F we find $R = 1/(2\pi f_0 C) = 1.326$ kΩ. The next closest 1% resistor can be chosen for the design. If the resulting tolerances of the RC product are too large, the resistor must be trimmed. We should note that the fact that components with at best 1% tolerances are available to the filter designer does *not* mean that the computations leading to the element values can be carried out to only two or three significant digits. The numerical mathematics in filter design is as a rule very ill conditioned, especially for high-order filters,

so many digits should be retained in the calculations to achieve valid results. The problem is that many intermediate results involve small differences of two relatively large numbers. For instance, suppose a step in the algebra calls for the difference of

$$1.324495 - 1.323122 = 0.001373$$

Being mislead by the available 1% components, a designer may choose to carry only three digits, $1.32 - 1.32 = 0.00$, clearly a meaningless result. Even computing to four digits, $1.324 - 1.323 = 0.001$, leaves only one digit, which has a 38% error. Let us emphasize, therefore, that computations in filter design must be carried out with 7 to 10 or, for high-order filters, even more digits. We shall throughout this text carry out all computations to the required accuracy, but keeping practice in mind, use element values to only two or three digits. If circuit performance calls for higher accuracy tuning will be assumed in our designs.

PROBLEMS

1.1 The input voltage of a filter is $v_1(t) = \sqrt{2}\cos(\omega t + 2.68)$ and its output voltage is $v_2(t) = \sqrt{2} \cdot 5.34\cos(\omega t + 4.87)$. At the applied frequency ω, determine the gain in dB and the phase shift in degrees implemented by the filter.

1.2 At the frequency $f = 12$ kHz, a filter is designed to attenuate the input signal by 78 dB. Find the amplitude of the output signal if the 12-kHz input has an amplitude of 1 V.

1.3 A wide-band input signal of amplitude 100 mV is applied to the filter. In the stopband, the remaining signal components at the filter's output must be no larger than 45 μV. Determine the required stopband attenuation α of the filter in dB.

1.4 If an amplifier has 35 dB gain at $f_c = 100$ MHz and shifts the phase by $-42°$, determine the output signal delivered if the input is $v_{in}(t) = 2.4\cos(\omega_c t + 45°)$.

1.5 Identify the filter type (lowpass, bandpass, etc.) described by the following attenuation specifications and calculate the widths of the transition band(s).

(a) $\alpha_{max} = 0.01$ dB in $f \leq 3.4$ kHz; $\alpha_{min} = 45$ dB in $9.6\text{ kHz} \leq f \leq \infty$

(b) $\alpha_{max} = 0.01$ dB in $12.5\text{kHz} \leq f \leq 24$ kHz; $\alpha_{min} = 45$ dB in $f \leq 7$ kHz and $f \geq 40$ kHz

(c) $\alpha_{min} = 85$ dB in $12.5\text{ kHz} \leq f \leq 24$ kHz; $\alpha_{max} = 1$ dB in $f \leq 7$ kHz and $f \geq 40$ kHz

(d) $\alpha_{min} = 60$ dB in $f \leq 24$ kHz; $\alpha_{max} = 0.5$ dB in $f \geq 40$ kHz

(e) $\alpha_{max} = 0.1$ dB in $f \leq 360$ kHz; $\alpha_{min} = 80$ dB in $600\text{ kHz} \leq f$

(f) $\alpha_{max} = 3$ dB in $1\text{ MHz} \leq f \leq 2.4$ MHz; $\alpha_{min} = 75$ dB in $f \leq 730$ kHz and $\alpha_{min} = 48$ dB in $f \geq 7.8$ MHz

1.6 The transfer function of a filter is specified to equal

$$T(s) = \frac{2\left(s^2 + 9.32\right)}{s^4 + 1.322s^3 + 0.976s^2 + 0.750s + 1}$$

The frequency is normalized by $f_0 = 18$ kHz. Determine the gain in dB at dc. Calculate the rate of attenuation increase in dB per decade at high frequencies. At which frequencies is the attenuation infinite?

1.7 According to a design table, the normalized components of a passive LC filter are $L_1 = 1.2547$, $L_2 = 0.9873$, $L_3 = 0.8765$, $C_1 = 2.5632$, $C_2 = 1.5764$, and $R_S = R_L = 1$. The impedance level is normalized by $R_0 = 300\ \Omega$ and the normalizing frequency is $f_0 = 10.8$ MHz. Find the values of the denormalized components.

1.8 The normalized components of an active filter were computed to be $R_1 = 1.243$, $R_2 = R_3 = 1.677$, $R_4 = 6.888$, and $C_1 = C_2 = 0.765$; the amplifier gain is required to be $K = 1.93$. The normalizing frequency is $f_0 = 360$ kHz. Choose the impedance level such that the filter can be built with $C = 0.05$ nF capacitors and determine the remaining elements of the circuit, including the final value of amplifier gain.

1.9 Calculate the rate of attenuation increase in dB/octave and in dB/decade as f approaches zero and infinity in the function

$$T(s) = \frac{3s^2\left(s^2 + 36\right)}{s^4 + 2.344s^3 + 1.824s^2 + 1.267s + 0.987}$$

1.10 An engineer is asked to build a filter to realize the transfer function

$$T(s) = \frac{3s^6 + 2s^2 - 0.8s + 1}{s^5 + 2.5s^4 - 1.2s^2 + (1 + 3.9i)\,s + 0.6}$$

The engineer objects that the function is not realizable. List all items that are wrong with the function as stated.

2 OPERATIONAL AMPLIFIERS

In this chapter we introduce the operational amplifier (opamp), the main device used to provide gain in the design of active filters. The other gain device is the transconductor or operational transconductance amplifier (OTA). It is used mainly in filters for very high frequencies. We will delay the discussion of OTAs and OTA circuits until Chapter 16. Since the performance of active filters depends critically on the opamp, it is very important that we fully understand the behavior of opamps to be able to undertake successful filter designs. Opamps are relatively complicated electronic circuits, consisting of transistors, resistors, and capacitors. As such, the signal amplification or gain they provide must be expected to be a function of frequency. To analyze the behavior of each filter with complete transistor-level electronic circuits for the opamps is too cumbersome and prevents us from gaining the needed insights into filter behavior. We will, therefore, in the next section develop a simple model, the *integrator model*, that will prove adequate to represent the behavior of the electronic circuit for the vast majority of applications studied in this book. We will also define an even simpler model, the *ideal opamp*, that will allow us to develop circuits very rapidly and to gain preliminary insight into their behavior under carefully observed conditions, specifically, a limited frequency range. Experience has shown that even very simple models often allow us to predict a circuit's behavior

with an accuracy that is sufficient for judging the circuit's usefulness. We will, therefore, base many of the designs in this book on ideal opamp models, but we must remain aware of the limitations imposed by this model. The ultimate test of a model's validity is its success in describing and predicting circuit performance in practice, in the laboratory. Opamps are rarely used alone; instead they are used in combination with other circuit elements that provide feedback, determine gain, bandwidth, and so on. The circuit elements used in active filters in addition to opamps are capacitors and resistors. Their values and interconnections are selected to realize the specified frequency response of the filter. The simplest element used in the feedback network is the resistor, and opamp–resistor networks will be studied in this chapter.

2.1 OPERATIONAL AMPLIFIER MODELS

Opamps are differential amplifiers, familiar in modern electronics (Gray and Meyer, 1993; Sedra and Smith, 1998). They differ from ordinary amplifiers by having two inputs. Their operation is such that the output voltage v_o is the difference of the two input voltages multiplied by an overall gain factor. In terms of the voltages defined in Fig. 2.1, we have

$$v_o(t) = A[v_+(t) - v_-(t)] \tag{2.1}$$

where A is the gain of the opamp. Throughout our study, voltages will be measured relative to a 0-V ground reference. In general, the voltages can be arbitrary functions of time. Also, we will normally assume that the voltages (and all signals) are sinusoidal and we shall use capital letters for our work, implying phasors or Laplace transforms. An important property of differential amplifiers is that signals, that are common to both inputs, are not amplified: the amplifier rejects them. For example, if $v_+(t)$ and $v_-(t)$ have the same additive noise n, this noise is not transmitted to the output $v_o(t)$,

$$v_o(t) = A\{[v_+(t) + n] - [v_-(t) + n]\} = A[v_+(t) - v_-(t)] \tag{2.2}$$

resulting in a cleaner signal. Signal components that are common to both inputs, such as n in Eq. (2.2), are called *common-mode* signals and are rejected by the opamp. On the other hand, if the two inputs have no components in common, they are labeled *differential-mode* signals and each is multiplied by the gain A.

Differential amplifiers of very high gain were developed in the early 1940s by George Philbrick and others. These were intended for use in analog simulation, radar, and control systems applications. Early units employed vacuum tubes and were both bulky and expensive. The trend toward extremely small and inexpensive opamps began in the 1960s, when Philbrick, Burr Brown, and other companies developed modular solid-state units. The modern monolithic opamp, early versions of which were the LM 101 and the μA 709, was designed by Widlar in 1967. Dual and quad opamps (two and four units on an IC chip) followed in the early 1970s. The typical dimensions of an opamp on a silicon chip, depending on technology, are 1.2 × 2.0 mm. Currently, a large number of opamps and complete active filters can be implemented on the same IC chip.

A simplified circuit diagram of an IC realization of a bipolar opamp is shown in Fig. 2.2a, with pin connections for a single-opamp package indicated in Fig. 2.2b. In actual use, external components, most notably power supplies, are connected to the package as indicated in Fig. 2.2c. Since in the design of active filters, we are normally concerned only with the

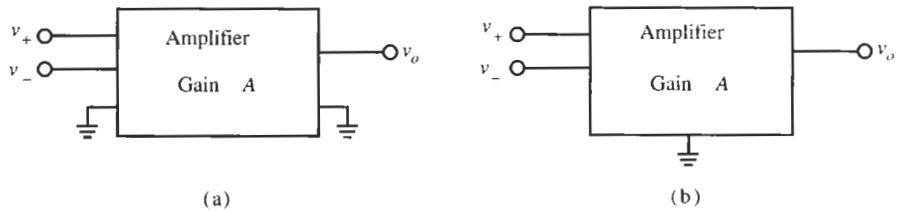

Figure 2.1 Operational amplifier. All voltages are referred to the 0-V ground terminals. Inputs and output usually have a common ground terminal as indicated in b.

signal paths, power supply connections are usually not shown explicitly in circuit diagrams. In this book we shall follow the convention of not showing power supply connections, but we must remember that the electronic circuit in the opamp requires dc power supplies to become active. Power supply voltages are found over wide ranges. They can be symmetrical as shown in Fig. 2.2c, such as ±15 or ±5 V, so that the signals are symmetrical around the 0 V ground reference. Alternatively, the power supplies can be single ended, such as 5, 3.3 V, and as low as 1.5 V, with one power supply terminal at ground. This is required, for example, in portable equipment with battery operation. In that case, the signals are floating around a nonzero dc voltage, normally one-half the power supply voltage. Generally, the trend today is toward lower power supply voltages to save power and permit ever smaller device sizes.

Similar circuit configurations as shown in Fig. 2.2a exist for other bipolar, complementary metal-oxide semiconductor (CMOS), or biCMOS designs (Johns and Martin, 1998). As is indicated in the figure, they all consist of a differential input stage g_m that provides a current

$$i(t) = -g_m[v_+(t) - v_-(t)] \tag{2.3}$$

to an inverting high-gain voltage amplification stage with gain $-A_2$. The output is obtained from a unity-gain buffer stage to drive external loads and any off-chip circuitry. The opamp is completed by the necessary bias circuitry and a compensation capacitor, C_1, as shown in Fig. 2.2a.

2.1.1 The Integrator Model

An understanding of the opamp's behavior can be gained from the simple block diagram of the opamp circuit, excluding the bias circuitry and, as we agreed, excluding the power supply. It contains the sections identified in Fig. 2.2a as shown in Fig. 2.3. We have included the resistor R to represent the large but finite output resistance of the transconductance stage g_m. Without having to concern ourselves with the details of the operation of the transconductance, g_m, and the amplifier stage, $-A_2$, we can analyze the behavior of the opamp as follows: The current I is given by

$$I = g_m (V_+ - V_-) \tag{2.4}$$

At the input of the amplifier stage $-A_2$, it divides into the resistor current V_1/R and the capacitor current $sC_1V_C = sC_1[V_1 - (-A_2V_1)]$. Thus we have from Kirchhoff's current law:

$$g_m (V_+ - V_-) + V_1[1/R + sC_1 (1 + A_2)] = 0 \tag{2.5}$$

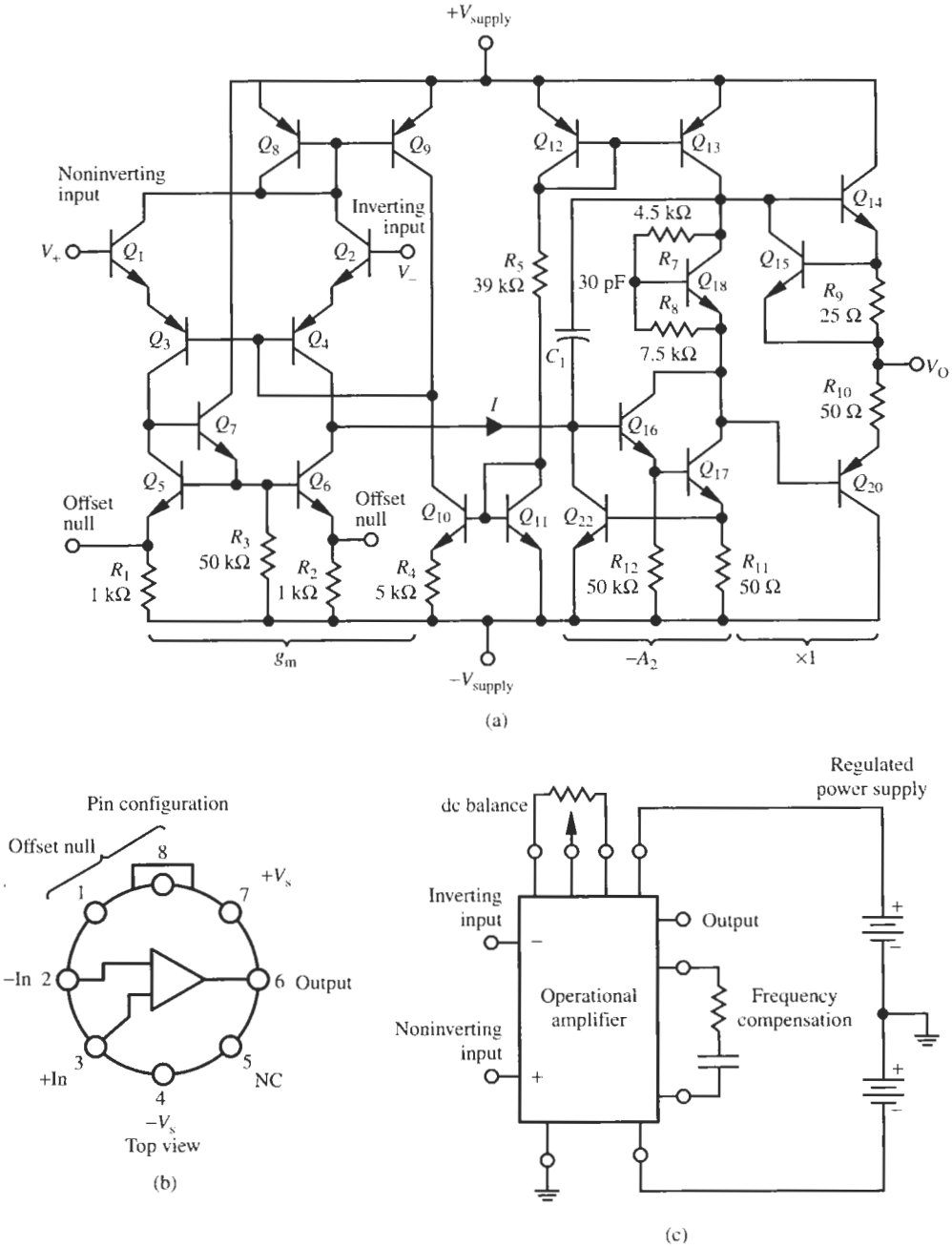

Figure 2.2 The operational amplifier. (a) Diagram of a bipolar circuit showing the three main signal blocks, g_m, $-A_2$, and a unity-gain buffer; (b) single-opamp package with pin configurations; (c) external circuitry, most notably power supplies.

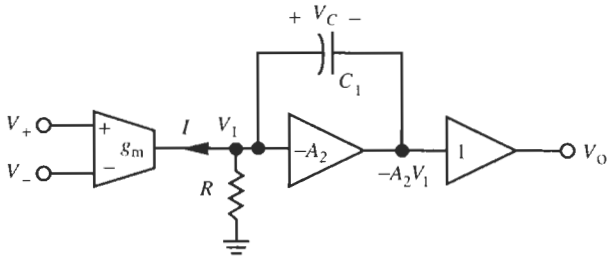

Figure 2.3 Functional parts of an opamp.

Further note from Fig. 2.3 that $-A_2V_1 = V_o$. Combining these equations and reordering the terms results in the *open-loop* transfer function of the opamp circuit in Fig. 2.3:

$$A(s) = \frac{V_o}{V_+ - V_-} = \frac{g_m}{sC_1(1 + 1/A_2) + 1/(RA_2)} \tag{2.6}$$

Open loop means that no connections are made between the opamp's output terminal and its inputs. Typically, the gain A_2 is much larger than unity, $1 \gg 1/A_2$, so that Eq. (2.6) can be simplified to read

$$A(s) \approx \frac{g_m}{sC_1 + 1/(RA_2)} = \frac{g_m/C_1}{s + 1/(RC_1A_2)} \tag{2.7}$$

To get an understanding of the frequency dependence of the opamp gain, we note first that at dc the gain equals

$$A(0) = g_m RA_2 \tag{2.8}$$

and that at the frequency

$$\omega_a = 2\pi f_a = \frac{1}{RC_1A_2} \tag{2.9}$$

the gain is reduced by 3 dB to $A(0)/\sqrt{2}$. ω_a is the open-loop bandwidth of the amplifier. Observe that the product of the dc gain, Eq. (2.8), and the bandwidth, Eq. (2.9), equals

$$A(0)\omega_a = \frac{g_m}{C_1} = \omega_t \tag{2.10}$$

Appropriately, $\omega_t = 2\pi f_t$, also labeled GB in the literature, is called the *gain-bandwidth product* of the open-loop opamp. With this notation, we can rewrite Eq. (2.7) as

$$A(s) = \frac{\omega_t}{s + \omega_a} \tag{2.11}$$

We see that $A(s)$ has a single pole at $-\omega_a$, on the negative real axis of the s-plane. The expression Eq. (2.11) is, therefore, referred to as the *one-pole model* of the opamp. To gain an understanding of the opamp's behavior in practice, let us insert realistic parameter values into these equations. The numbers depend, of course, on the opamp's specific design and the technology used, but typical values for inexpensive bipolar opamps, such as the popular 741-type devices, are

$$g_m = 200\ \mu S, \quad R = 100\ k\Omega, \quad A_2 = 10{,}000, \quad C_1 = 30\ pF \tag{2.12}$$

With these numbers we obtain from Eq. (2.8) the dc gain

$$|A(0)| = g_m R A_2 = 200\ \mu S \times 100\ k\Omega \times 10,000 = 200,000 \tag{2.13a}$$

or, using Eq. (1.10),

$$\alpha = 20\ \log\ |A(0)| = 106\ dB \tag{2.13b}$$

From Eq. (2.9), the -3 dB frequency equals

$$\omega_a = \frac{1}{RC_1A_2} = \frac{1}{100\ k\Omega \times 30\ pF \times 10,000} = 33.3\ rad/s$$
$$= 2\pi \times f_a = 2\pi \times 5.3\ Hz \tag{2.14}$$

and from Eq. (2.10) the gain-bandwidth product is

$$\omega_t = \frac{g_m}{C_1} = \frac{200\ \mu S}{30\ pF} = 6.67 \times 10^6 rad/s = 2\pi \times f_t = 2\pi \times 1.06\ MHz \tag{2.15}$$

Observe from Eq. (2.13) that an opamp has very high dc gain, from Eq. (2.14) that its -3 dB frequency f_a is very low, typically less than 10 Hz, and from Eq. (2.15) that the unity-gain frequency f_t is large, typically 1 MHz or higher. Figure 2.4a depicts the gain and phase behavior of an LM741 opamp. Unless otherwise noted, we will use the LM741 opamp throughout this text, whenever we build circuits and filters and evaluate their practical behavior. As predicted by Eq. (2.11), for frequencies much larger than ω_a, the opamp gain decreases ("rolls off") at the rate of -20 dB for each factor 10 increase in frequency (at -20 dB/decade) or at -6 dB for a doubling in frequency (at -6 dB/octave).

Table 2.1a lists many model parameters of the LM741 opamp; particularly relevant to our study are the dc open-loop gain A, the input and output resistances R_i and R_o, and the unity-gain frequency f_u.

Figure 2.4a also shows the phase of the opamp transfer function Eq. (2.11), obtained from

$$\phi(\omega) = \tan^{-1} A\,(j\omega) \approx -\tan^{-1}\,(\omega/\omega_a) \tag{2.16}$$

We see that the phase goes to zero at low frequencies, is equal to $-45°$ at $\omega = \omega_a = 1/(C_1 R_o A_2)$, and approaches $-90°$ for $\omega \gg \omega_a$. The faster gain roll-off for frequencies larger than f_t (above 1 MHz) and the increasingly negative phase ($< -90°$) at high frequencies (for $f > 70$ kHz) that are visible in Fig. 2.4a can be predicted from a more accurate analysis, specifically, by making g_m and A_2 functions of frequency. Such a description can be expressed as a two-pole model,

$$A(s) = \frac{\omega_t}{(s + \omega_a)\,(1 + s/\omega_c)} \tag{2.17a}$$

Making use of the fact that $\omega/\omega_c \ll 1$ and

$$\frac{1}{1+x} \approx 1 - x \approx e^{-x}$$

TABLE 2.1 Model Parameters for the LM741 and the HA2542-2 Opamp

(a) Opamp Model "LM741" Library "LM"			
A	Open-loop gain	2×10^5	
R_i	Input resistance	2×10^6	Ω
R_o	Output resistance	75	Ω
V_{sw+}	Positive voltage swing	21	V
V_{sw-}	Negative voltage swing	−21	V
V_{os}	Input offset voltage	0.001	V
I_{bs}	Input bias current	8×10^{-8}	A
I_{os}	Input offset current	2×10^{-8}	A
SR	Slew rate	5×10^5	V/s
f_u	Unity-gain bandwidth	1.5×10^6	Hz
f_{p2}	Location of second pole	4.5×10^6	Hz
C_c	Compensation capacitance	3×10^{-11}	F
(b) Three-Terminal Model "HA2542-2" Library "haxxxx"			
A	Open-loop gain	3×10^4	
R_i	Input resistance	1×10^5	Ω
R_o	Ourput resistance	5	Ω
V_{sw+}	Positive voltage swing	13.5	V
V_{sw-}	Negative voltage swing	−13.5	V
V_{os}	Input offset voltage	0.005	V
I_{bs}	Input bias current	1.5×10^{-5}	A
I_{os}	Input offset current	1×10^{-6}	A
SR	Slew rate	3.5×10^8	V/s
F_u	Unity-gain bandwidth	9×10^7	Hz
F_{p2}	Location of second pole	4.5×10^8	Hz
C_c	Compensation capacitance	1×10^{-12}	F

Equation (2.17a) can also be written as

$$A(s) \approx \frac{\omega_t\,(1 - s/\omega_c)}{s + \omega_a} \approx \frac{\omega_t}{s + \omega_a} e^{-j \tan^{-1}(\omega/\omega_c)} \tag{2.17b}$$

which turns out to be more convenient in many situations for the analysis of circuit and filters. The second pole $f_c = \omega_c/(2\pi)$ is typically between 3.5 and 5 MHz for inexpensive opamps. Table 1.1 lists the second pole f_{p2} at 4.5 MHz; it is the cause for much of the behavior unpredicted by the simple integrator model of Eq. (2.11). We will not explore or use this more accurate model because it is unnecessary for most of our work in this text.

Notice that f_a is a very small frequency, typically less than 10 Hz for inexpensive opamps, so that in practice most design work in active filters is concerned with frequencies $\omega \gg \omega_a$. Under these circumstances, the opamp gain, from Eq. (2.11), is inversely proportional to frequency

$$A(s) \approx \frac{\omega_t}{s} \tag{2.18}$$

In the Laplace domain, $1/s$ represents integration. The opamp model Eq. (2.18) is therefore called the *integrator model*. Note that $|A(j\omega_t)| = 1$, which gives ω_t the name *unity-gain frequency*.

The model parameters in Eq. (2.12) through Eq. (2.15), and f_c for Eq. (2.17), apply only to 741-type opamps. We shall use this opamp, specifically the LM741 with the parameters in Table 2.1a, in most of our studies in this book because the integrator model Eq. (2.18) is adequate in the range of about 100 Hz to 100 kHz, where most active filter applications are found. In this frequency range, the opamp behaves truly as an integrator, with 20 dB/decade roll-off and $-90°$ phase. To make the student aware of the behavior of more expensive high-frequency opamps, we show the frequency dependence of the HARRIS operational amplifier HA2542-2 in Fig. 2.4b, with parameters $f_a \approx 30$ kHz and $f_t \approx 90$ MHz. The most important model parameters of the HA2542-2 opamp are shown in Table 2.1b.

For our study of active filters, ω_t is the opamp parameter that is most important for determining the accuracy of active filter performance as frequency increases. Unfortunately the value of ω_t is not accurate in practical IC technologies and varies from unit to unit. Tolerances of 100% or higher must be expected. This is because by Eq. (2.10) ω_t depends on the absolute values of the input transconductance g_m of the opamp and a compensation capacitor C_1, neither of which is implemented accurately or repeatably in the manufacturing process. It is important, therefore, that a filter design is desensitized as much as possible to the value of the opamp parameters. As we will see shortly, this is accomplished, as long as the opamp gain is large, by using *feedback*.

We will find the integrator model to be sufficiently accurate for most of our work. The model is completed by noting from the circuit in Fig. 2.2a that the amplifier's input resistance R_i must be very large and its output resistance R_o low (Sedra and Smith, 1998). Again, exact values of these resistors depend on specifics of the opamp design and the technology used for the implementation, and are not accurate in practice. We shall use the typical values

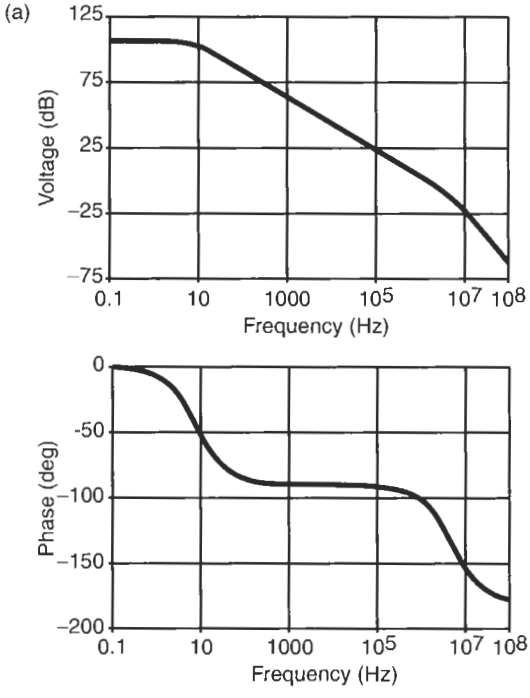

Figure 2.4 Frequency response of a real opamp. (a) Magnitude and phase of the LM741; (b) gain and phase responses of a high-frequency opamp (HA2542–2).

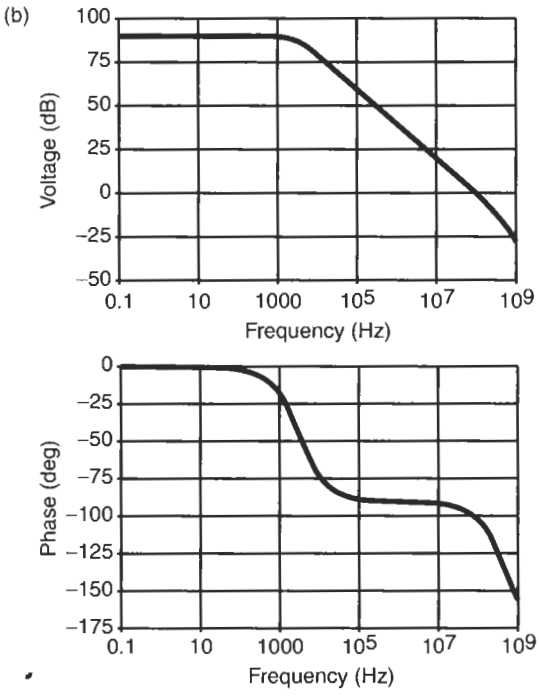

Figure 2.4 Continued

$$R_i = 1\ \text{M}\Omega, \quad R_o = 75\ \Omega \tag{2.19}$$

to arrive at the opamp model in Fig. 2.5. The triangular shape of the opamp symbol suggests the unilateral nature of the device: the difference of the input voltages determines the output, but the output voltage does not determine the input. Table 2.2 summarizes the parameters of the two models we derived.

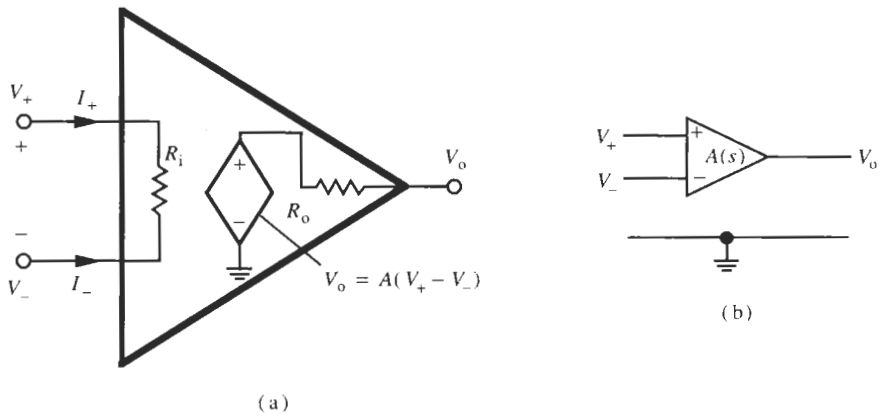

Figure 2.5 (a) Opamp model with finite input and output resistors and a controlled voltage source of gain $A(s)$; (b) opamp symbol.

TABLE 2.2 Models for Operational Amplifiers

Name	Gain $A(s)$	Input Resistance R_i	Output Resistance R_o	Comments
One-pole model	$\dfrac{\omega_t}{s+\omega_a}$	100 kΩ in bipolar	$< 75\Omega$ in bipolar	$\omega_t > 2\pi 10^6\ s^{-1}$
		100 MΩ in CMOS	$\approx 200\ \Omega$ in CMOS	$\omega_a < 2\pi 10\ s^{-1}$
Integrator model	ω_t/s	Same	Same	$\omega_t > 2\pi 10^6\ s^{-1}$
Ideal	∞	∞	0	Infinite bandwidth

2.1.2 The Ideal Operational Amplifier

We have developed a simple model that will be useful for our work in active filter design. We have seen that the gain is a function of frequency, Eqs. (2.11) or (2.18), is very large at dc, $A(0) \approx 10^5$, with a range of 10^4 to 10^6, and that the opamp has a large input resistance, $R_i = 100$ kΩ, with values reaching as high as 10^8 Ω in CMOS technology, and a small output resistance $R_o = 75$–200 Ω. To derive from this model a simpler, idealized model that is often used in the *initial* design of filters and that allows us to take a first look at a circuit's potential, we use limiting values of the opamp parameters. Specifically, we define a model with

$$A = \infty, \quad R_i = \infty, \quad R_o = 0 \tag{2.20a, b, c}$$

Table 2.2 also contains the parameters of the ideal opamp, and Fig. 2.6 shows the model and the symbol used. Equation (2.20c) implies that the opamp output is an ideal voltage source, able to drive any load, and it follows from Eq. (2.20b) that the opamp draws no input current: all input currents into an ideal opamp are zero,

$$i_+ = i_- = 0 \tag{2.21a}$$

The idealizations of Eqs. (2.20b) and (2.20c) rarely cause problems in filter design, and are used quite liberally in most circumstances. However, the one expressed in Eq. (2.20a) must be treated with great caution. It leads to the conclusion that the net input voltage into an ideal opamp must be zero,

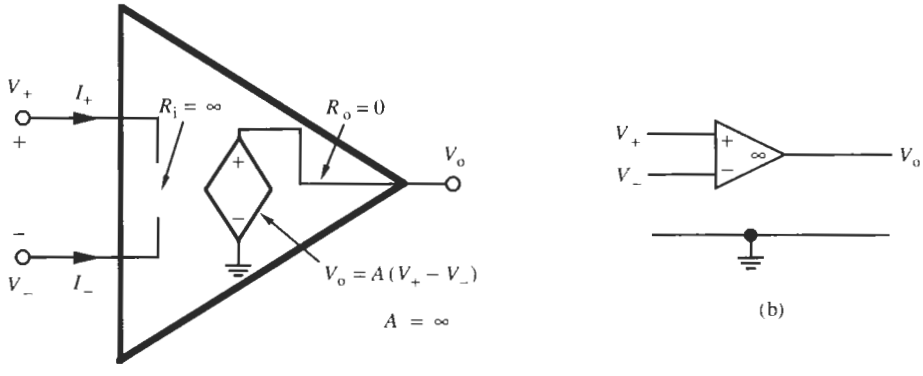

Figure 2.6 Model (a) and symbol (b) of an ideal opamp.

$$v_+ - v_- = 0 \tag{2.21b}$$

The reason is that the output voltage $v_o = A(v_+ - v_-)$ of the electronic amplifier circuit is limited by the power supply voltage, so that

$$|v_+ - v_-| = \frac{|v_o|}{A} < \frac{V_{\text{supply}}}{A} \tag{2.22}$$

Since A for the ideal opamp is assumed to be infinite, the amplifier's input voltage $v_+ - v_-$ must be zero.

Note that Eq. (2.21b) does not imply that v_+ and v_- are zero individually, but only that they are equal, $v_+ = v_-$, so that their difference is zero. In practice, of course, A is finite as depicted in Fig. 2.4. At low frequencies, where $|A|$ is very large, $|v_+ - v_-|$ can be expected to be in the millivolt or even microvolt range. The low-frequency input–output transfer curve representing Eq. (2.22) is depicted in Fig. 2.7. The steep slope for small values of $v_+ - v_-$ corresponds to the high gain of the opamp, and the output signal is limited by the power supply. The gain A decreases with increasing frequencies as indicated in Eq. (2.18) so that $|v_+ - v_-|$ will increase.

Equations (2.21a) and (2.21b) apply simultaneously at the input of the opamp, Fig. 2.6. Equation (2.21a) signifies an open circuit and Eq. (2.21b) implies a short circuit across the opamp input. This situation, where both voltage and current are zero, is known as a *virtual short*. It is depicted in Fig. 2.8. The presence of this virtual short can be used to simplify the analysis of opamp circuits as we shall see throughout the remainder of this book.

A more important consequence of Eq. (2.20a) is that the ideal opamp has *constant gain* and *infinite bandwidth*. As we have seen in the magnitude and phase plots in Fig. 2.4, this is clearly a questionable assumption, but as long as the gain is large, say $|A(j\omega)| > 1000$, useful results may nevertheless be obtained from using the ideal opamp model. Note though from Eq. (2.11) or Eq. (2.18) that for typical inexpensive opamps with a gain-bandwidth product of the

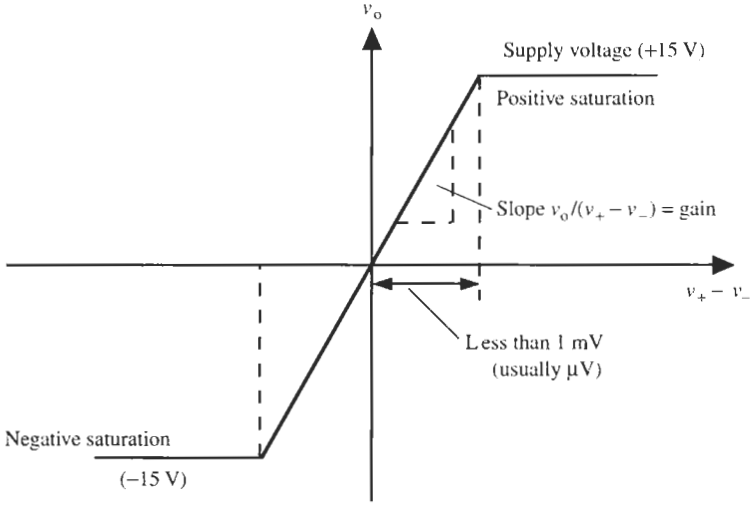

Figure 2.7 Low-frequency input–output transfer curve of an opamp. Observe the different scales chosen for the horizontal (mV or μV) and vertical (V) axes because of the large opamp gain.

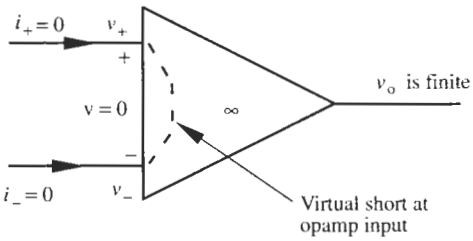

Figure 2.8 Representing a virtual short across the input terminals of an opamp.

order of 1 MHz $|A(j\omega)| > 1000$ implies that $f < 1$ kHz, too low for most filter work. Thus, whenever a filter design based on ideal opamps is intended for operation above the low audio range, the design should be treated with caution and the results carefully checked in practice.

In our work in the remainder of this book, we shall make frequent use of the ideal opamp model, simply because the analysis and initial designs are conceptually easier. This will become clear as we progress in our study. But before a design is reduced to practice, we must always check the performance with the more realistic integrator model Eq. (2.18) through careful analysis, or perform an experimental evaluation to validate the design.

2.2 OPAMP SLEW RATE

Throughout the book, almost all our discussions will be concerned with frequency-domain concepts, such as bandwidth, quality factor, gain, and phase. There is, however, one opamp parameter that specifies its time-domain performance but also affects frequency-domain designs in many important aspects. This parameter is the *slew rate*. Slew rate defines the fastest possible rate of change of the opamp's output voltage. This rate of change is limited because the electronic circuitry inside the opamp can supply only a finite current to charge or discharge the capacitor C_1 in Fig. 2.2a. Referring to the model in Fig. 2.3 and neglecting the output resistor R of the transconductance stage g_m, we calculate the capacitor charge Q, $v_o C_1$, by integrating the current $g_m(v_+ - v_-) = g_m v_{in} = i$ as follows:

$$v_o C_1 = \int g_m v_{in}\, dt = \int i\, dt$$

We assumed that $v_1 \approx 0$ because A_2 is large. The rate of change of the output voltage is obtained as

$$\frac{dv_o}{dt} = \frac{i}{C_1} = \frac{g_m}{C_1} v_{in} \tag{2.23}$$

The maximum of this slope is the slew rate SR,

$$SR = \left.\frac{dv_o}{dt}\right|_{max} = \left.\frac{i}{C_1}\right|_{max} \tag{2.24}$$

The maximum current is given by the bias current of the input stage of the opamp; in a 741-type opamp, typically it is 20 μA so that together with $C_1 = 30$ pF we have

$$SR = \frac{20\ \mu\text{A}}{30\ \text{pF}} = 0.67\ \text{V}/\mu\text{s} \tag{2.25}$$

Instrumentation-type opamps can have slew rates of several hundred or even thousand of volts per microsecond.

Interesting for our study of analog filters is the observation that the maximum slope of a sinusoidal output voltage $v_o(t) = V_o \sin \omega t$ is ωV_o. Thus,

$$\left.\frac{dv_o}{dt}\right|_{max} = SR = \omega V_o \tag{2.26}$$

The equation tells us that the maximum signal that an opamp can handle for a given frequency is SR/ω,

$$V_o|_{max} < SR/\omega \tag{2.27}$$

For a larger signal, the opamp's electronic circuitry cannot follow the signal and distortion will result. For example, assuming that the power supply is larger than 5 V (see Fig. 2.7), in an LM741 opamp a 20-kHz signal should be smaller than $\approx$ 5 V. Figure 2.9 illustrates what happens to the signal if slew rate limits are violated: the opamp voltage rises or falls at a constant rate, the slew rate, rather than following the faster rate the signal frequency demands.

The slew rate is a measure of the opamp's quality because it determines how fast the opamp output can follow an input signal. For example, if the input v_{in} is a step V_{in} applied at $t = 0$, we have from Eq. (2.23)

$$v_o(t) = \int_0^t \frac{g_m}{C_1} V_{in}\, dt = \frac{g_m}{C_1} V_{in} t = \text{const} \times t \tag{2.28}$$

that is, the output is a ramp. We can relate slew rate SR to frequency parameters by forming the Laplace transform of Eq. (2.23),

$$sV_o = \frac{g_m}{C_1} V_{in}, \quad \text{i.e.,} \quad \frac{V_o}{V_{in}} = \frac{g_m}{sC_1}$$

Since $V_o/V_{in} = 1$ at the unity gain frequency $\omega_t = g_m/C_1$ [see Eq. (2.10)], we have with Eq. (2.24) the result

$$1 = \frac{g_m}{\omega_t} \frac{1}{C_1} = \frac{g_m}{\omega_t} \frac{SR}{i|_{max}}$$

or

$$SR = \frac{\omega_t}{g_m} i|_{max} \tag{2.29}$$

SR increases with increasing ω_t and power-supply current. We see that we have no control over SR; it is a parameter set by the opamp designer.

To avoid distortion, we will for the most part pay attention to keeping the signal level in our designs smaller than the restriction imposed by slew rate limits. If the occasion should call for large signals and frequencies, we shall point out the problems that may arise. With signal-level restrictions obeyed, we can assume, therefore, throughout most of the book that $SR = \infty$.

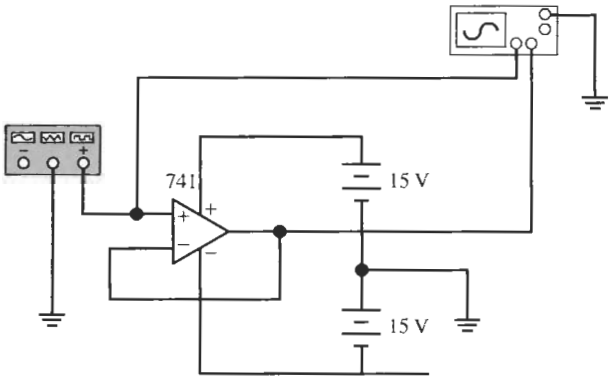

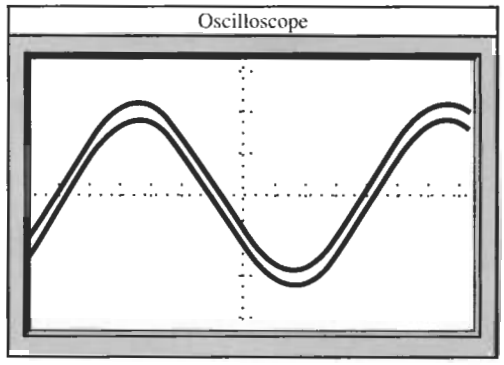

(a)

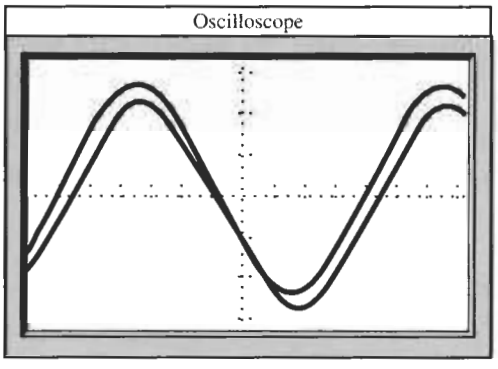

(b)

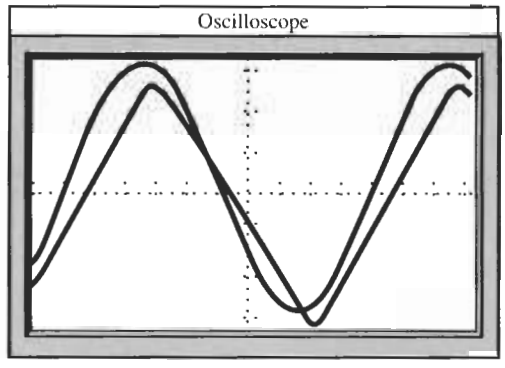

(c)

Figure 2.9 A 741-type opamp in unity-gain configuration with $SR = 0.67\text{V}/\mu s$. A 20-kHz sine wave is applied from the function generator. The power supply is ± 15 V. Input and output are measured on two traces of the oscilloscope **that is in all cases set to 5.00 μs/div and 2 V/div for both channels:** the traces are separated on the display by + and −, respectively, 0.2-V offset to be able to see the two curves; input signal amplitude is (a) 4 V, resulting in no distortion, (b) 5 V, beginning distortion is visible, and (c) 6 V, distortion is large, the amplifier is slewing, and the output waveform is essentially triangular.

2.3 THE OPERATIONAL AMPLIFIER WITH RESISTIVE FEEDBACK: NONINVERTING AND INVERTING AMPLIFIERS

To help us gain an understanding of opamp behavior, and to appreciate the use of the models we introduced, we will study two important circuits, the noninverting and the inverting finite-gain amplifiers built with opamps. Amplifiers are used to increase the amplitude or the power of a signal. Ideally, this amplification should be performed without loading the signal source, and the amplified signal should be able to drive arbitrary loads. This implies that no current should be drawn by the amplifier from the source, i.e., the amplifier's input resistance should be very large, ideally infinite. Being able to drive arbitrary loads in turn implies that the output of the amplifier should appear like an ideal voltage source, i.e., it should have a very small, ideally zero, output resistance. Figure 2.10 depicts the situation and shows a model for the amplifier of gain K. We can obtain a formal representation of the statements just made by writing equations

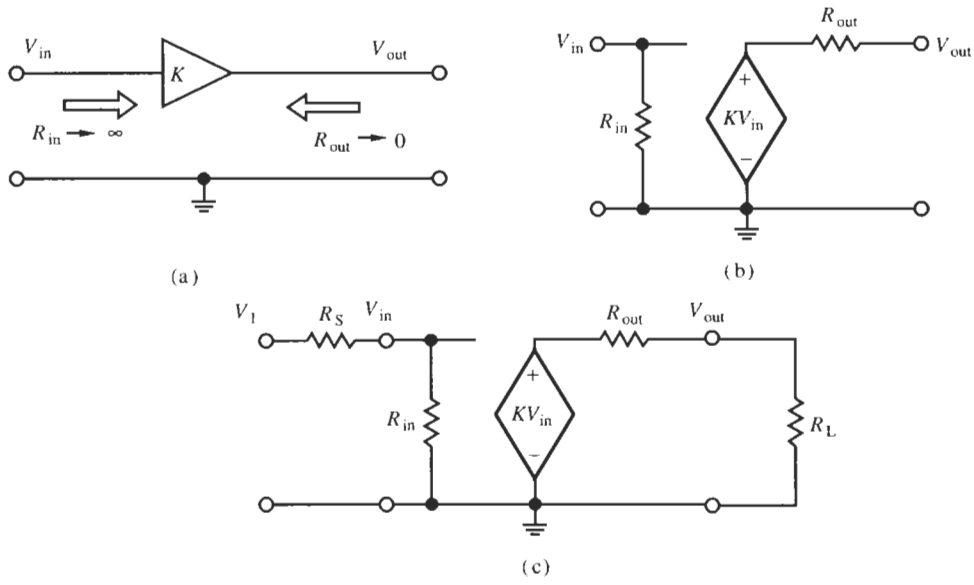

Figure 2.10 (a) Symbol of an amplifier with gain K; (b) controlled-source model; (c) amplifier connected to a resistive source and a resistive load.

for the gain of the amplifier circuit in Fig. 2.10c with resistive source and load. Using voltage division at input and output, we find

$$V_{out} = \frac{R_L}{R_{out} + R_L} K V_{in} = \frac{R_L}{R_{out} + R_L} K \frac{R_{in}}{R_{in} + R_S} V_I \tag{2.30}$$

The equation shows that the amplifier's gain is reduced if the amplifier's input resistance R_{in} is finite and the output resistance R_{out} is nonzero. Thus, a good amplifier should have its input resistance as large as possible and its output resistance as small as possible. It is important, therefore, that we determine these two resistances in any practical amplifier design.

As mentioned, it is very difficult, if not impossible, to design accurately the electronic variables that determine the opamp parameters, Eqs. (2.8), (2.9), and (2.10). Furthermore, they vary from opamp to opamp. Therefore, in practice, circuit and filter designers have to make their designs as independent of the opamp parameters as possible. This feat is accomplished by using feedback. It places the opamp into a harness of passive components that determines the amplifier's and ultimately the filter's performance. In the following, we shall see how this is accomplished in noninverting amplifiers.

2.3.1 The Noninverting Amplifier

Figure 2.11 shows the opamp placed into a harness made up of two resistors. To emphasize that the following discussion is valid for arbitrary signals, lower-case symbols are used. The input v_1 is applied to the noninverting input terminal and a fraction v_a of the output voltage, determined by voltage division,

$$v_a = \frac{R_1}{R_1 + R_2} v_2 \tag{2.31}$$

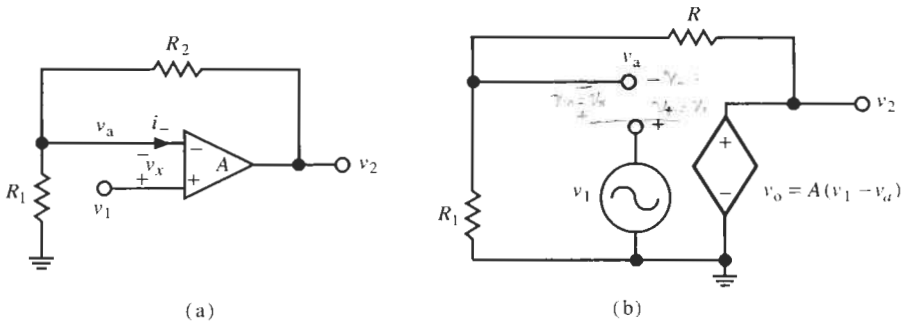

Figure 2.11 The noninverting amplifier. (a) The opamp circuit; (b) a controlled-source model arranged in a form convenient for analysis.

is applied ("fed back") to the inverting input. To analyze the circuit, we remember that the opamp output is obtained by multiplying the input by the gain A,

$$v_o = A(v_+ - v_-) = A(v_1 - v_a) = Av_x \tag{2.32}$$

Combining Eqs. (2.31) and (2.32), and noting that $v_2 = v_o$, results in

$$v_2 = A\left(v_1 - \frac{R_1}{R_1 + R_2} v_2\right) \tag{2.33}$$

or

$$v_2\left(1 + A\frac{R_1}{R_1 + R_2}\right) = Av_1$$

Solving this equation for v_2/v_1 gives the gain of the noninverting amplifier as

$$\frac{v_2}{v_1} = \frac{A}{1 + A\dfrac{R_1}{R_1 + R_2}} = \left(1 + \frac{R_2}{R_1}\right)\frac{1}{1 + (1 + R_2/R_1)/A} \tag{2.34}$$

Now, if the opamp gain is very large, in the limit infinite ($A = \infty$) for an ideal opamp, we obtain from Eq. (2.34)

$$\frac{v_2}{v_1} = K_P = 1 + \frac{R_2}{R_1} \tag{2.35}$$

Thus, we see that the circuit in Fig. 2.11 is an amplifier whose positive (noninverting) gain K_P is determined by two resistors, and is—to the first order, for large gain A—independent of the opamp gain A. By choosing the proper values of the two resistors, the gain is determined. For example, $R_1 = 1\ \text{k}\Omega$ and $R_2 = 9\ \text{k}\Omega$ gives an amplifier with a gain of $K_P = 10$. Note that the gain is always larger than unity, $K_P > 1$.

A comment is appropriate at this point about the kind of feedback necessary to achieve a stable circuit. Note from Fig. 2.11 that the fraction v_a of the output signal, Eq. (2.31), is fed back to the *inverting* (negative) input terminal of the opamp. This choice, *negative*

feedback, results in the minus sign in Eq. (2.33) so that increasing v_2 tends to make the opamp's input v_x smaller, which in turn decreases v_2. The stable point is reached as $v_x \to 0$ so that the output voltage stabilizes at a finite value. If we were to mix our connections and instead feed the fraction of v_2 to the noninverting (positive) opamp input in Fig. 2.11 (*positive feedback*), the minus sign on the right-hand side of Eq. (2.33) would be replaced by a plus sign, resulting in increasing values of v_x. This, in turn, leads to increasing values for v_2 on the left side, leading to further increases of v_x, and so on, until the opamp's limit, $|v_2| \leq V_{\text{supply}}$, is reached. The opamp is said to "latch up" to a constant output level, the positive or negative power supply voltage. When designing feedback circuits, as is always the case with active filters, we must avoid positive feedback, because linear operation breaks down, the gain becomes zero (in the horizontal part of the curve in Fig. 2.7), and the filter will not function at all.

We promised earlier that the assumption of ideal opamps in circuit design would simplify the analysis. To verify this claim, note that by Eq. (2.22) $A = \infty$ implies $v_x = 0$. This means from Eq. (2.32) that $v_a = v_1$. Consequently, with Eq. (2.31),

$$\frac{R_1}{R_1 + R_2} v_2 = v_1 \tag{2.36}$$

and the final result Eq. (2.35) follows directly. Since Eq. (2.36) is obtained by inspection from Fig. 2.11, using voltage division along with the property of a virtual short, the analysis of the amplifier based on an ideal opamp can be written down almost in one line.

We went through the complete analysis of the circuit with finite values of A for two reasons. First, we must become familiar with the analysis methods as early as possible so that we become comfortable with the process. Second, we wished to derive Eq. (2.34); it permits us to gauge the differences in amplifier performance when compared to the ideal behavior predicted by Eq. (2.35). To be able to investigate the frequency response, we use Laplace transforms. To be specific, let us take the integrator model of Eq. (2.18) and rewrite Eq. (2.34) using the gain K_P defined in Eq. (2.35). The result is

$$\frac{V_2}{V_1} = \frac{K_P}{1 + K_P/A(s)} = \frac{K_P}{1 + K_P s/\omega_t}\bigg|_{s=j\omega} = \frac{K_P}{1 + K_P(j\omega/\omega_t)} \tag{2.37}$$

This is an important equation. It tells us, that at low frequencies, $s = j\omega \to 0$, the amplifier has indeed the gain K_P as predicted by Eq. (2.35) for an ideal opamp model, but *the gain is not constant*. Rather, evaluating the amplifier on the $j\omega$-axis as done on the right-hand side of Eq. (2.37), we see that the -3 dB bandwidth of the amplifier, where the gain is reduced to $K_P/\sqrt{2}$, equals

$$\omega_{-3\text{ dB}} = \omega_t / K_P \tag{2.38}$$

Thus, we note that the bandwidth of the noninverting amplifier in Fig. 2.11 depends on the gain K_P that we wish to realize. Specifically, the bandwidth is inversely proportional to K_P. An additional insight can be obtained by rewriting Eq. (2.38) as

$$K_P \omega_{-3\text{ dB}} = \omega_t \tag{2.39}$$

Recall from Eq. (2.10) that ω_t is the product of the open-loop bandwidth ω_a of the opamp and the dc gain $A(0)$, and from Eq. (2.38) that ω_t is the bandwidth for the gain $K_P = 1$. Equation Eq. (2.39) generalizes this result. It says that

The product of realized gain and bandwidth of the amplifier is constant.

For example, assuming again an LM741 opamp with $f_t = 1.5$ MHz, we find the realized amplifier bandwidth is 150 kHz for gain $K_P = 10$, but is only 1.5 kHz for $K_P = 1000$. Figure 2.12 depicts the situation graphically. Evidently, the bandwidth of the circuit in Fig. 2.11 is far from constant, contrary to what is suggested by the simple analysis leading to Eq. (2.35), based on an ideal opamp. The student is encouraged to keep this picture in mind when designing opamp circuits with gains significantly larger than unity.

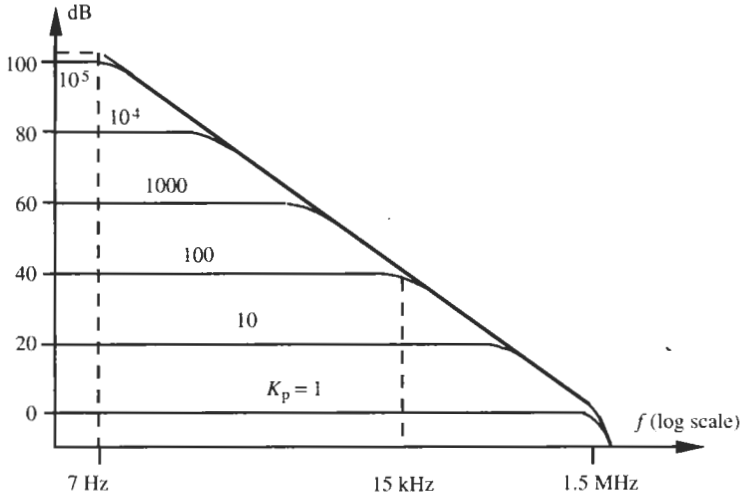

Figure 2.12 Bandwidth of amplifiers with different gains built as in Fig. 2.11. The opamp has the characteristic of Fig. 2.4a.

EXAMPLE 2.1

Design an amplifier with 14-dB gain using an LM741 opamp.

Solution

First we determine the necessary resistor ratio. A gain of 14 dB means by Eq. (1.11) that the voltage ratio Eq. (2.35) is

$$\frac{V_2}{V_1} = K_P = 1 + \frac{R_2}{R_1} = 10^{14/20} = 5.01$$

Now note that gain is a dimensionless parameter, determined by a *ratio* of resistors. One of them may be chosen arbitrarily. Consequently, choosing, e.g., $R_1 = 3.3$ kΩ, we find $R_2 = 13.2$ kΩ. The bandwidth of the amplifier we obtain from Eq. (2.38):

$$f_{-3\text{ dB}} = \frac{f_t}{K_P} = \frac{1.5 \times 10^6\text{ Hz}}{5.01} \approx 300\text{ kHz}$$

Figure 2.13 shows the circuit and the frequency response curve.

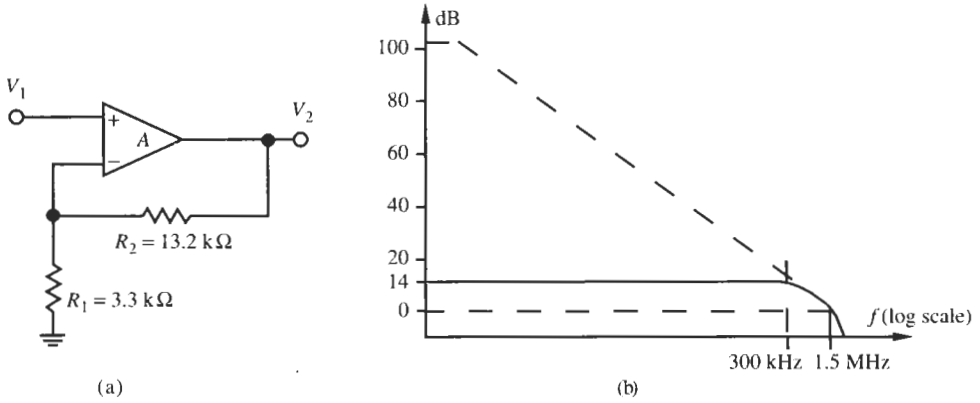

Figure 2.13 (a) Opamp circuit with gain $K_P = 5$; (b) frequency response of the circuit assuming an LM741 opamp.

We have derived the gain of the noninverting amplifier, both under the assumption of ideal opamps and using the more realistic model that results in the amplifier's finite bandwidth. For a complete description of the amplifier, we still need to derive the circuit's input and output resistances. To this end, we insert the opamp model of Fig. 2.5a into the circuit into Fig. 2.11. The result is shown in Fig. 2.14. To compute the resistances, we note the definitions

$$R_{in} = \left.\frac{V_1}{I_i}\right|_{I_o=0} \quad \text{and} \quad R_{out} = \left.\frac{V_2}{I_o}\right|_{V_1=0} \tag{2.40}$$

and compute from Fig. 2.14

$$I_i = \frac{1}{R_i}(V_1 - V_-) \tag{2.41}$$

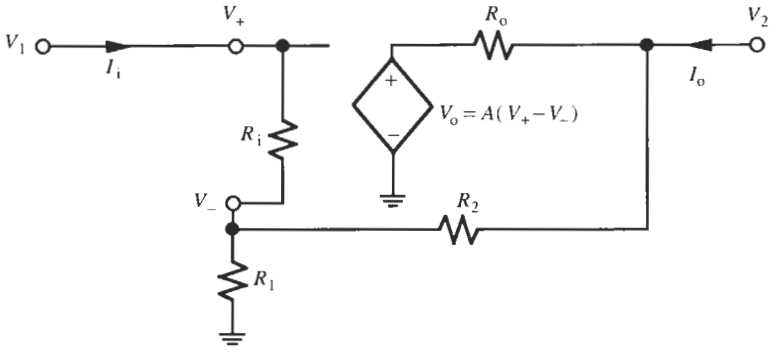

Figure 2.14 Small-signal model to compute the input and output impedances of the noninverting amplifier.

Under the reasonable assumption that the opamp's R_i is much larger than R_1 and R_2 we can neglect the current through R_i compared to that through R_2, when computing the current through R_1. Thus, we obtain by simple voltage division

$$V_- = \frac{R_1}{R_1 + R_2} V_2 = \frac{V_2}{K_P} \tag{2.42}$$

where K_P was defined in Eq. (2.35). Recalling from Eq. (2.37) that

$$\frac{V_2}{V_1} = \frac{K_P}{1 + K_P/A} \tag{2.43}$$

we insert Eqs. (2.42) and (2.43) into Eq. (2.41) and obtain

$$I_i = \frac{1}{R_i}\left(V_1 - \frac{V_2}{K_P}\right) = \frac{1}{R_i}\left(V_1 - \frac{V_1}{1 + K_P/A}\right) = \frac{V_1}{R_i}\frac{1}{1 + A/K_P}$$

The input resistance is therefore

$$R_{in} = \frac{V_1}{I_i} = R_i\left(1 + \frac{A}{K_P}\right) \tag{2.44}$$

We observe that the amplifier's input resistance R_{in} depends on the opamp's input resistance R_i, on the realized gain K_P, and, of course, on the opamp gain A. In particular we note that R_{in} is *very* large because normally $A > K_P$, at least at low frequencies (see Fig. 2.12). For an LM741 opamp, for example, with $|A| = 200{,}000$, $R_i = 2\ \text{M}\Omega$ and $K_P = 10$, we find $R_{in} = 40 \times 10^9\ \Omega = 40\ \text{G}\Omega$, which is a close approximation for our requirement that the input resistance of the amplifier be infinite. We must remember, though, that A is a function of frequency, $A = A(s)$, so that "R_{in} becomes frequency dependent," i.e., it is an impedance

$$Z_{in}(s) = \frac{V_1}{I_i} = R_i\left[1 + \frac{A(s)}{K_P}\right] = R_i\left[1 + \frac{\omega_t}{(s + \omega_a)\,K_P}\right] \tag{2.45a}$$

where we have used the single-pole model Eq. (2.11) for the opamp gain. If we rewrite Eq. (2.45a) as

$$Z_{in}(s) = R_i + \frac{1}{s\dfrac{K_P}{R_i\omega_t} + \dfrac{1}{\dfrac{R_i\omega_t}{\omega_a K_P}}} = R_i + \frac{1}{sC_p + \dfrac{1}{R_p}} \tag{2.45b}$$

we recognize that the amplifier's input impedance is capacitive as is indicated in the equivalent circuit in Fig. 2.15a, with a capacitor

$$C_p = \frac{K_P}{R_i\omega_t} \tag{2.46}$$

For $R_i = 2\ \text{M}\Omega$, $f_t = 1.5\ \text{MHz}$, and $K_P = 10$, we find $C_p \approx 0.53\ \text{pF}$. Z_{in} has a low-frequency ($s \to 0$) value

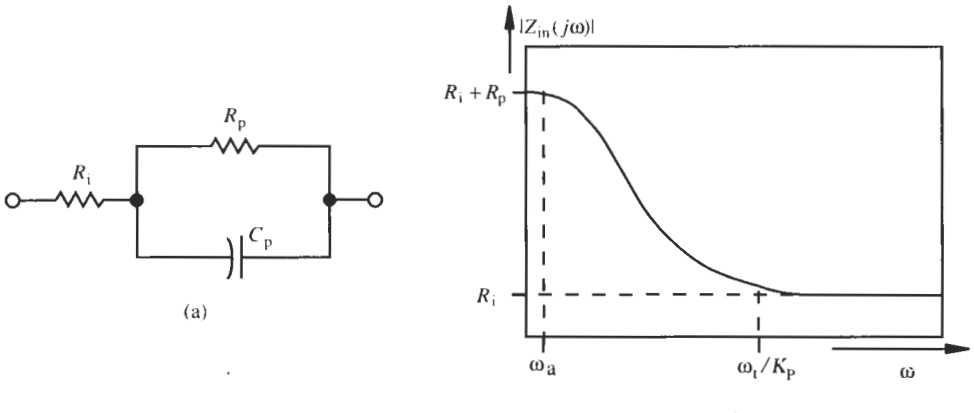

Figure 2.15 Input impedance of the noninverting amplifier: (a) model; (b) frequency dependence.

$$Z_{in}(0) = R_i + R_p = R_i\left(1 + \frac{\omega_t}{\omega_a K_P}\right) \approx \frac{R_i \omega_t}{\omega_a K_P} \tag{2.47}$$

and a high-frequency ($s \to \infty$) value

$$Z_{in}(\infty) = R_i \tag{2.48}$$

$|Z_{in}|$ is plotted versus ω in Fig. 2.15b. For our work it is important to remember that the input impedance of the amplifier is not purely resistive, and that it is very large for all frequencies of interest.

Consider next the output impedance of the circuit in Fig. 2.14. To compute Z_{out}, by Eq. (2.40), we have to determine I_o. Remembering that $V_1 = 0$, using the same assumptions as above for computing R_{in}, and $R_o \ll R_1 + R_2$, we find from Fig. 2.14

$$I_o = \frac{V_2}{R_1 + R_2} + \frac{V_2 - (-AV_-)}{R_o} \tag{2.49}$$

Substituting Eq. (2.42) into this equation results in

$$I_o = \frac{V_2}{R_1 + R_2} + \frac{V_2 + AV_2/K_P}{R_o} = V_2\left(\frac{1}{R_1 + R_2} + \frac{1 + A/K_P}{R_o}\right) \tag{2.50}$$

and gives the output impedance

$$Z_{out} = \frac{V_2}{I_o} = \left.\frac{R_o}{\dfrac{R_o}{R_1 + R_2} + 1 + \dfrac{A}{K_P}}\right|_{R_o \ll R_1 + R_2} \approx \frac{R_o}{1 + \dfrac{A}{K_P}} \tag{2.51}$$

At low frequencies, where usually $A/K_P \gg 1$, $R_{out} = Z_{out}(0)$ is seen to be very small, less than R_o of the open-loop opamp. To understand the behavior at higher frequencies, we insert the model Eq. (2.18) into Eq. (2.51) to obtain

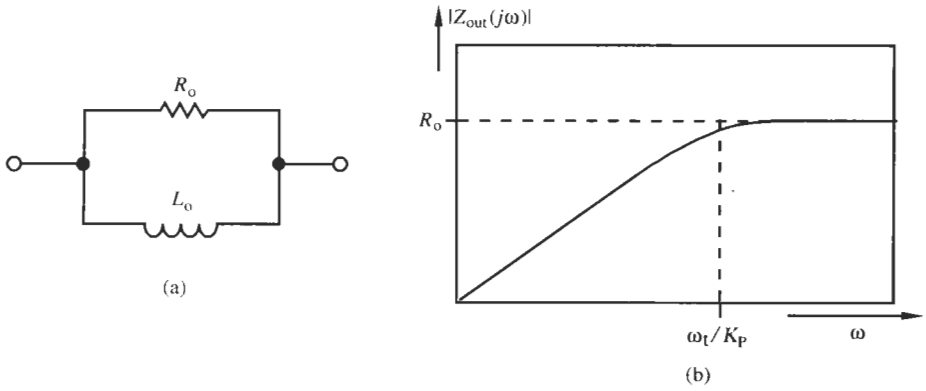

Figure 2.16 Output impedance of the noninverting amplifier: (a) model; (b) frequency dependence.

TABLE 2.3 Amplifier Circuits for Opamp Models

Circuit	Parameter and Equation No.	$A(s)$ Approximate Equations	Ideal ($A = \infty$) Equations
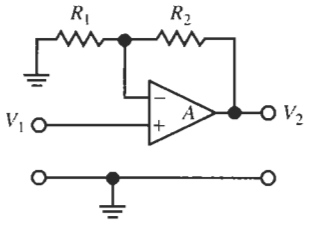	Gain (2.37)	$\frac{V_2}{V_1} = \frac{K_P}{1 + K_P/A}$	$\frac{V_2}{V_1} = K_P$
	Input resistor (2.44)	$R_{in} = R_i\left(1 + \frac{A}{K_P}\right)$	$R_{in} = \infty$
	Output resistor (2.51)	$R_{out} = \frac{R_o}{1 + A/K_P}$	$R_{out} = 0$
$(K_P = 1 + R_2/R_1)$ *Noninverting amplifier*	Bandwidth (2.38)	$\omega_{-3\,dB} = \frac{\omega_t}{K_P}$	$\omega_{-3\,dB} = \infty$
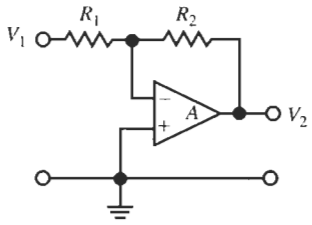	Gain (2.57)	$\frac{V_2}{V_1} = -\frac{K_N}{1 + (1 + K_N)/A}$	$\frac{V_2}{V_1} = -K_N$
	Input resistor (2.61)	$R_{in} \approx R_1 + \frac{R_2}{1 + A}$	$R_{in} = \infty$
	Output resistor (2.51)	$R_{out} = \frac{R_o}{1 + A/(1 + K_N)}$	$R_{out} = 0$
$(K_N = R_2/R_1)$ *Inverting amplifier*	Bandwidth (2.58)	$\omega_{-3\,dB} = \frac{\omega_t}{1 + K_N}$	$\omega_{-3\,dB} = \infty$
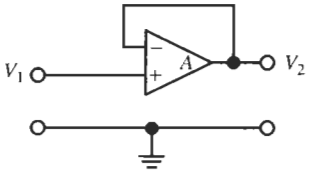	Gain (2.82)	$\frac{V_2}{V_1} = \frac{1}{1 + 1/A}$	$\frac{V_2}{V_1} = 1$
	Input resistor (2.84)	$R_{in} = R_i(1 + A)$	$R_{in} = \infty$
	Output resistor (2.85)	$R_{out} = \frac{R_o}{1 + A}$	$R_{out} = 0$
Voltage follower	Bandwidth (2.86)	$\omega_{-3\,dB} = \omega_t$	$\omega_{-3\,dB} = \infty$

$$Z_{\text{out}} \approx \frac{R_\text{o}}{1+\dfrac{1}{K_\text{P}}\dfrac{\omega_\text{t}}{s}} = \frac{1}{\dfrac{1}{R_\text{o}}+\dfrac{1}{s}\dfrac{\omega_\text{t}}{R_\text{o}K_\text{P}}} = \frac{1}{\dfrac{1}{R_\text{o}}+\dfrac{1}{sL_\text{o}}} = \frac{sL_\text{o}}{1+sL_\text{o}/R_\text{o}} \tag{2.52}$$

We notice that Z_{out} consists of R_o in parallel with an inductor L_o. The inductor value is, using $K_\text{P} = 10$, $R_\text{o} = 75\ \Omega$, and $f_\text{t} = 1.5$ MHz,

$$L_\text{o} = \frac{R_\text{o}K_\text{P}}{\omega_\text{t}} = \frac{75\ \Omega \times 10}{2\pi \times 1.5 \times 10^6\ \text{s}^{-1}} \approx 80\ \mu\text{H} \tag{2.53}$$

The equivalent circuit of the output impedance and a plot of its frequency dependence are shown in Fig. 2.16. We want to remember for our future work that the output impedance magnitude is very small over the frequency range of interest. Table 2.3 shows the circuit diagram and a collection of relevant equations characterizing the noninverting amplifier.

2.3.2 The Inverting Amplifier

The circuit just considered is a noninverting amplifier. This suggests that there is also an inverting amplifier that we shall discuss next. The circuit is shown in Fig. 2.17. In this case both input and output signals are connected through resistors to the inverting opamp input terminal for negative feedback. The analysis proceeds as follows: summing the currents at node a, and remembering that the opamp input current i_- is zero, results in the equation

$$\frac{v_1 - v_\text{a}}{R_1} + \frac{v_2 - v_\text{a}}{R_2} = 0 \tag{2.54}$$

Of course, the opamp imposes the condition $v_x = 0 - v_\text{a} = -v_\text{a} = v_2/A$. If we combine these equations and reorder terms, we obtain from Eq. (2.54)

$$\frac{v_2}{v_1} = -\frac{R_2}{R_1}\frac{1}{1+(1+R_2/R_1)/A} \tag{2.55}$$

Interpreting this expression proceeds similarly to the discussion following Eq. (2.34). If the opamp gain is very large, in the limiting case infinite ($A = \infty$), we obtain from Eq. (2.55)

$$\frac{v_2}{v_1} = -K_\text{N} = -\frac{R_2}{R_1} \tag{2.56}$$

The circuit is an inverting amplifier of gain $-K_\text{N}$. As in the noninverting amplifier, the gain is set by two chosen resistors. It is (at low frequencies) independent of A, and the minus sign indicates a signal inversion (positive input results in a negative output; see Fig. 2.18). Again the assumption of an ideal opamp would have permitted us to obtain the result in Eq. (2.56) immediately. Observe that for $A \to \infty$ we find $v_\text{a} \to 0$ in Eq. (2.54) and the result [Eq. (2.56)] follows from Fig. 2.17 by inspection. We just write Kirchhoff's current law at the inverting input node and make use of the concept of a virtual short. Using again Laplace transforms to

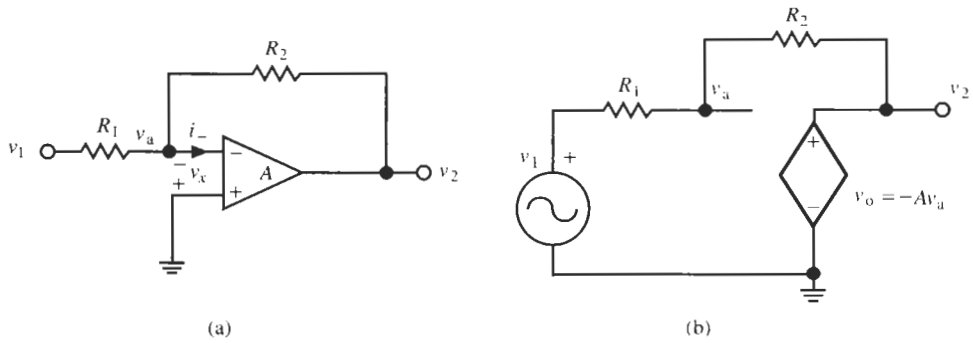

Figure 2.17 The inverting amplifier: (a) circuit; (b) controlled-source model.

permit us to study the frequency response, we obtain from Eq. (2.55), with Eqs. (2.35), (2.56), and the integrator model Eq. (2.18)

$$\frac{V_2}{V_1} = -\frac{K_N}{1 + K_P/A(s)} = -K_N \left.\frac{1}{1 + K_P s/\omega_t}\right|_{s=j\omega} = -K_N \frac{1}{1 + j\omega K_P/\omega_t} \tag{2.57}$$

Note that far from being constant, the gain of the inverting amplifier is also a function of frequency. The equation shows that at low frequencies the gain equals $-K_N$ for $A \to \infty$ as predicted by Eq. (2.56). For higher frequencies, the frequency dependence is like the one of the noninverting amplifier in Eq. (2.37), that is, the bandwidth of the inverting amplifier equals

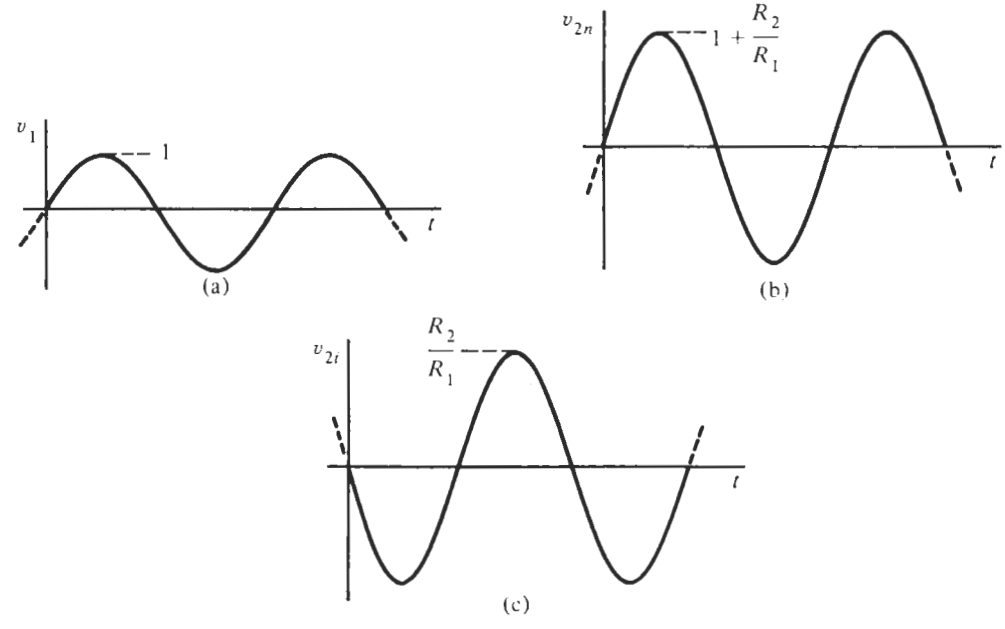

Figure 2.18 Interpretation of (b) noninverting and (c) inverting amplifier gain. The input signal is shown in (a).

$$\omega_{-3\text{ dB}} = \frac{\omega_t}{K_P} = \frac{\omega_t}{1 + K_N} \tag{2.58}$$

EXAMPLE 2.2

A 150-mV, 55-kHz voltage signal must be amplified to 2.2 V. Design an amplifier using the inverting opamp circuit in Fig. 2.17a and determine whether an LM741 opamp will have adequate bandwidth.

Solution

The required gain equals

$$K_N = \frac{R_2}{R_1} = \frac{2.2\text{ V}}{150\text{ mV}} = 14.67$$

Resistors with values $R_1 = 3.3\,\text{k}\Omega$ and $R_2 = 48.4\,\text{k}\Omega$ will provide the necessary feedback network. To check on the bandwidth requirement, we compute from Eq. (2.58)

$$f_{-3\text{ dB}}(1 + K_N) = 55\text{ kHz} \times (1 + 14.67) \approx 862\text{ kHz}$$

Evidently, an LM741 opamp with 1.5-MHz bandwidth is adequate for the task.

It remains for us to compute the input and output impedances of the inverting amplifier. Starting from the circuit diagram in Fig. 2.19, we proceed similarly as for the noninverting amplifier. The input current I_i equals

$$I_i = G_1(V_1 - V_-) = G_1 V_1 \left(1 - \frac{V_-}{V_1}\right) \tag{2.59}$$

and V_-/V_1 is obtained from the node equation at node V_-:

$$V_- \left(G_1 + \frac{1}{R_2 + R_o} + G_i\right) = V_1 G_1 - \frac{AV_-}{R_2 + R_o} \tag{2.60}$$

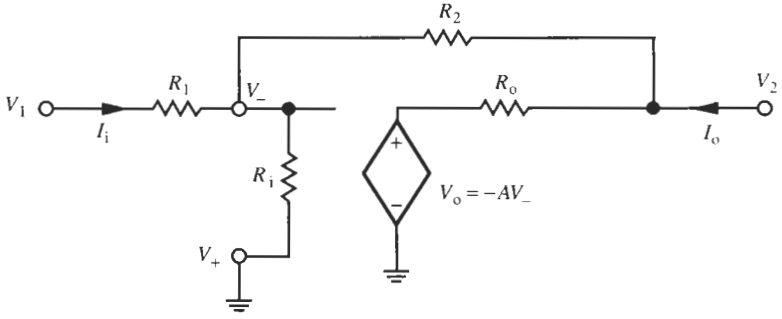

Figure 2.19 Small-signal model to compute the input and output impedances of the inverting amplifier.

Note that we used conductances, $G_i = 1/R_i$, for convenience of notation. Assuming $R_2 \gg R_o$, we obtain from Eq. (2.60)

$$\frac{V_-}{V_1} = \frac{G_1}{G_1 + G_2(1 + A) + G_i}$$

which is inserted into Eq. (2.59):

$$I_i = G_1 V_1 \left[1 - \frac{G_1}{G_1 + G_2(1 + A) + G_i}\right]$$

This equation yields the expression for the input impedance

$$Z_{in} = \frac{V_1}{I_i} = R_1 \left.\frac{G_1 + G_2(1 + A) + G_i}{G_2(1 + A) + G_i}\right|_{G_i \ll G_2} \approx R_1 \frac{R_2/R_1 + 1 + A}{1 + A}$$

which can be rewritten as

$$Z_{in} \approx R_1 + \left.\frac{R_2}{1 + A}\right|_{A \gg 1} \approx R_1 + \frac{R_2}{A} \tag{2.61}$$

We see that the input impedance of the inverting amplifier consists essentially of the resistor R_1 in series with R_2/A, which has a negligibly small value at low frequencies. If we make use of the integrator model Eq. (2.18), Eq. (2.61) with Eq. (2.56) can be expressed as

$$Z_{in} \approx R_1 \left(1 + \frac{R_2/R_1}{A}\right) = R_1 \left(1 + s\frac{K_N}{\omega_t}\right) = R_1 + sL_1 \tag{2.62}$$

i.e., the input impedance behaves like a resistor only at low frequencies; it is inductive with a 3-dB bandwidth f_t/K_N. The inductor value is

$$L_1 = \frac{R_1 K_N}{\omega_t} = \frac{R_2}{\omega_t} \tag{2.63}$$

The output impedance of the inverting amplifier is the same as that of the noninverting amplifier, Eq. (2.51), as is seen from the fact that the circuits in Figs. 2.14 and 2.19 are the same under the condition $V_1 = 0$. The equations for the inverting amplifier are also summarized in Table 2.3.

2.4 ANALYZING OPAMP CIRCUITS

Throughout this book, we will spend considerable time and effort analyzing and designing opamp circuits, specifically active filters. Rather than attempting to develop new and different analysis techniques specifically for each situation we encounter, let us digress for a moment from our discussion of amplifier circuits and reflect on a suitable method of analysis that will serve us well throughout our study. To help in this undertaking, we note that in any opamp circuit, a number of circuit branches will be connected to the opamps' input and output terminals. An example is seen in Fig. 2.11a where $v_- = v_a$ is connected to two resistive branches, where v_+ is connected to one branch (a voltage source), and where the output has one connection back to the inverting input. Similarly, in Fig. 2.17 we see one branch from v_+

to ground, and two branches from $v_- = v_a$, one through R_2 to the opamp output v_o and one through R_1 and the voltage source to ground. Figure 2.20 attempts to generalize the concept. We show three branches at V_+ and at V_o, and two at V_-. All are connected through resistors to other nodes in the circuit that are labeled by their respective voltages V_i, $i = 1, \ldots, 6$. The analysis now proceeds as follows.

In almost all situations, it is more convenient to base the analysis of opamp circuits on Kirchhoff's current law, i.e., on writing node equations. The reason for this choice is the very high input impedance of opamps that results in the opamp's input currents being (approximately) zero. The result is that the opamp input nodes are current summing nodes where all currents entering from other parts of the circuit must add up to zero. Making use of that fact, we simply sum the currents flowing toward the opamp input nodes. Because "current = voltage × conductance," we still note that it is generally easier and is recommended to convert resistance to conductance, $G = 1/R$, before the equations are written. Then, using Kirchhoff's current law we find at V_+ in Fig. 2.20:

$$I_1 + I_2 + I_4 = 0 \quad \text{or} \quad (V_1 - V_+)\,G_1 + (V_2 - V_+)\,G_2 + (V_4 - V_+)\,G_4 = 0 \tag{2.64a}$$

and at V_-:

$$I_3 + I_0 = 0 \quad \text{or} \quad (V_3 - V_-)\,G_3 + (V_o - V_-)\,G_0 = 0 \tag{2.64b}$$

The corresponding equations are written when the branches are *not* purely resistive. In our case it normally means they would be capacitive, in which case the conductance G of the particular branch is replaced by sC. Next we solve these two equations for the opamp input voltages V_+ and V_-:

$$V_+ = \frac{V_1G_1 + V_2G_2 + V_4G_4}{G_1 + G_2 + G_4}, \quad \text{and} \quad V_- = \frac{V_3G_3 + V_oG_0}{G_0 + G_3} \tag{2.65}$$

Observe that the two voltages at the opamp input terminals are determined solely by the circuitry surrounding the opamp, and not by the opamp itself. Also note that no equation needs to be written for the opamp's output voltage V_o. The reason is that the output is assumed to be (is modeled as) an ideal voltage source so that the value V_o is independent of any components that may be connected to it. Considering now the effect of the opamp on Eq. (2.65), we must

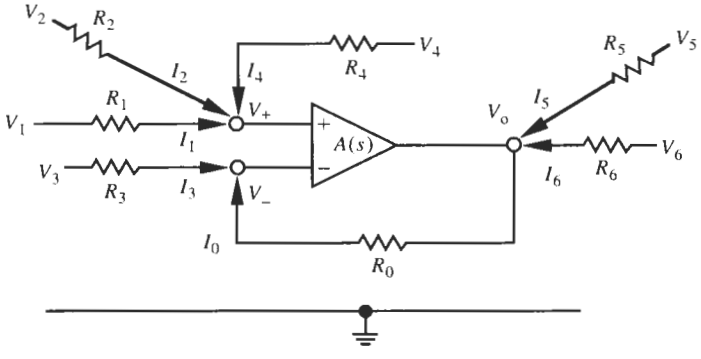

Figure 2.20 General connections to an opamp to illustrate analysis methods.

distinguish between (a) an analysis assuming ideal opamps and (b) the one based on real opamps with finite gain $A(s)$.

In Case (a), we set, according to Eq. (2.21b), $V_+ = V_-$ or $V_+ - V_- = 0$, that is

$$\frac{V_1G_1 + V_2G_2 + V_4G_4}{G_1 + G_2 + G_4} - \frac{V_3G_3 + V_oG_0}{G_0 + G_3} = 0$$

and solve for the opamp output voltage,

$$V_o = \frac{G_0 + G_3}{G_0}\left(\frac{V_1G_1 + V_2G_2 + V_4G_4}{G_1 + G_2 + G_4} - \frac{V_3G_3}{G_0 + G_3}\right) \tag{2.66a}$$

In Case (b), with finite gain A, we set $V_+ - V_- = V_o/A$ to yield

$$\frac{V_1G_1 + V_2G_2 + V_4G_4}{G_1 + G_2 + G_4} - \frac{V_3G_3 + V_oG_0}{G_0 + G_3} = \frac{V_o}{A}$$

that is,

$$V_o\left(1 + \frac{1}{A}\frac{G_0 + G_3}{G_0}\right) = \frac{G_0 + G_3}{G_0}\left(\frac{V_1G_1 + V_2G_2 + V_4G_4}{G_1 + G_2 + G_4} - \frac{V_3G_3}{G_0 + G_3}\right) \tag{2.66b}$$

We note that, as must be expected, Eq. (2.66b) reduces to Eq. (2.66a) for $A = \infty$. This simple and transparent procedure will always work and must be used for every opamp in the circuit. Normally, there will be no more than two or three opamps in a filter.

EXAMPLE 2.3

Use the procedure just described to find the output voltage V_o of the circuit in Fig. 2.21.

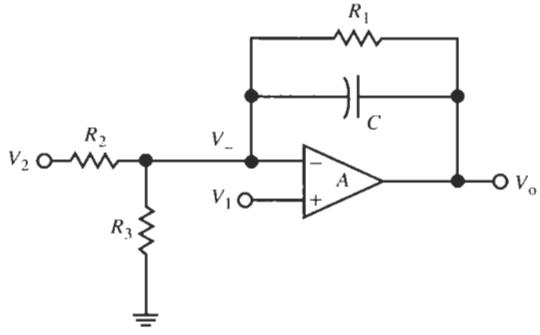

Figure 2.21 Opamp circuit for Example 2.3.

Solution

Clearly we have $V_+ = V_1$; writing Kirchhoff's current law to sum the currents flowing from the inverting input terminal yields

$$V_-G_3 + (V_- - V_2)\,G_2 + (V_- - V_o)\,(sC + G_1) = 0$$

or

$$V_-(G_1 + G_2 + G_3 + sC) = V_2G_2 + V_o(sC + G_1) \tag{2.67}$$

If we are dealing with an ideal opamp, we have $V_- = V_1$ because the opamp input voltage $V_+ - V_-$ must be zero. Thus, Eq. (2.67) gives the solution directly:

$$V_o = \frac{V_1(G_1 + G_2 + G_3 + sC) - V_2G_2}{sC + G_1} \tag{2.68}$$

If we are instead required to deal with a real opamp of finite gain A, modeled as in Eq. (2.18), the analysis is only slightly more complicated: We need one additional equation to describe the opamp:

$$V_1 - V_- = \frac{V_o}{A}$$

Combined with Eq. (2.67), we have

$$V_o\frac{1}{A} = V_1 - \frac{V_2G_2 + V_o(sC + G_1)}{G_1 + G_2 + G_3 + sC} \tag{2.69}$$

or

$$V_o\left[1 + \frac{G_1 + G_2 + G_3 + sC}{A(sC + G_1)}\right] = \frac{V_1(G_1 + G_2 + G_3 + sC) - V_2G_2}{sC + G_1} \tag{2.70}$$

As a check we observe that this equation reduces to Eq. (2.68) for $A \to \infty$. The terms in Eq. (2.70) can be further organized to show explicitly the output voltage as a function of frequency using the suggested opamp model (2.18):

$$V_o = \frac{V_1(G_1 + G_2 + G_3 + sC) - V_2G_2}{sC + G_1 + \dfrac{G_1 + G_2 + G_3 + sC}{A}} = \frac{V_1(G_1 + G_2 + G_3 + sC) - V_2G_2}{s^2\dfrac{C}{\omega_t} + s\left(C + \dfrac{G_1 + G_2 + G_3}{\omega_t}\right) + G_1} \tag{2.71}$$

To complete the example, we make a number of observations:

First, as was expected, the results, Eq. (2.68) and Eq. (2.71), are identical if $A = \infty$ (note that $A = \infty$ is the same as imposing $\omega_t = \infty$).

Second, we observe that the analysis with finite-gain opamps is not more difficult, although it is more laborious, than the one assuming ideal opamps.

Third, if A becomes a function of frequency, we must expect potentially substantial changes in the circuit's transfer function compared with that obtained for ideal opamps: note that the first-order function (2.68) is changed into the second-order function (2.71) by the opamp model $A(s) = \omega_t/s$. This last observation is the main reason why at all but the lowest frequencies we must be very careful with filter designs that are based on ideal opamp models. We will encounter this difficulty throughout the book.

2.5 BLOCK DIAGRAMS AND FEEDBACK

We mentioned earlier that opamp parameters are not well determined in manufacture and that filter designers will have to strive to make their designs as independent as possible of the opamps. As long as the opamp gain is large, this can be achieved by feedback as we have just

seen by comparing Eq. (2.43) with Eq. (2.35) for the noninverting, and Eq. (2.55) with Eq. (2.56) for the inverting amplifier. We shall show next that the results do not hold just for these two special cases, but that feedback is a more general principle, useful in active filter design and beyond. We start by introducing the representation of circuits by block diagrams as an aid to visualizing feedback. The equation

$$v_1 T = v_2 \tag{2.72}$$

may be represented by the block diagram in Fig. 2.22a. Both the equation and the block diagram tell us that when v_1 is multiplied by the function T, the result is v_2. The arrows associated with the blocks indicate the unilateral nature of the operation. Usually, all signals in block diagrams are voltages so that the functional blocks are dimensionless, such as the voltage ratio $T = v_2/v_1$. This is not necessary, though; the signals can be currents, or they can even be of mixed dimensions, such as in the block diagram in Fig. 2.22b, where Ohm's law, $iR = v$, is represented.

The equation

$$v_1 T_1 T_2 = v_2 \tag{2.73}$$

implies the *cascade* connection of two blocks as shown in Fig. 2.22c. It is often convenient for the analysis of block diagrams to identify intermediate variables, as we did for v_3 in Fig. 2.22c, so that we may write

$$v_1 T_1 = v_3 \quad \text{and} \quad v_3 T_2 = v_2$$

which combine to give Eq. (2.73).

The next block diagram operation, addition and subtraction, is represented in Fig. 2.23a. The $\pm$ sign next to the circle denotes the fact that to arrive at v_2 we may either add the signal v_3 to v_1 or subtract it from v_1. The diagram is equivalent to the equation

$$v_2 = v_1 \pm v_3 \tag{2.74}$$

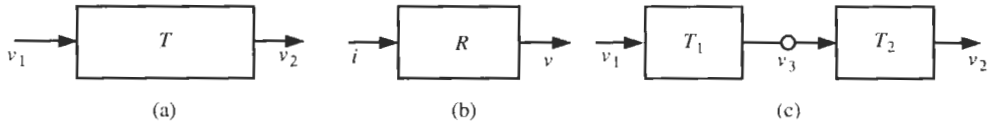

Figure 2.22 Block diagram representations: (a) a voltage gain block T; (b) a resistive path block R; (c) a cascade of two blocks T_1 and T_2.

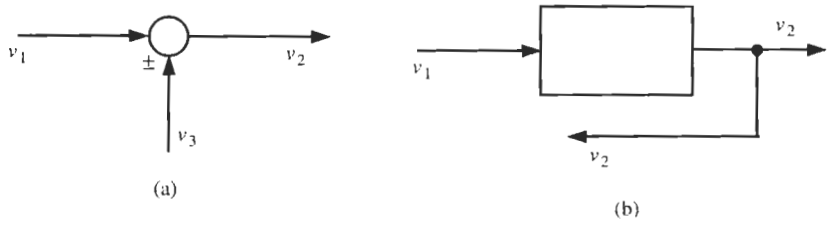

Figure 2.23 Block diagram representations: (a) signal addition or subtraction; (b) pick-off point where the signal is split into two paths.

indicating that v_2 is either the sum or the difference of v_1 and v_3. Figure 2.23b illustrates a *pick-off point*: a signal line drawn from another signal line, frequently with a heavy dot to point out the connection, indicating that the signal follows two paths. Here v_2 is an output, but it is also connected to another part of the system.

The connection of blocks in the form of Fig. 2.24 is known as an *elementary feedback system*. Here v_1 is the input and v_2 the output, and feedback is accomplished by feeding back v_2 through the block H. Then v_2H is either added to or subtracted from v_1 to form a signal e. A minus sign implies negative feedback; a plus sign implies positive feedback. If $H = 1$, and negative feedback is used, then e is simply the difference between input and output, which may be referred to as the *error*. Many feedback systems are designed to minimize this error so that the output follows closely the input. The voltage follower discussed in Section 2.6, Fig. 2.27d, is an example.

Two equations describe the block diagram of Fig. 2.24:

$$v_2 = Ae \tag{2.75}$$

and

$$e = v_1 \pm Hv_2 \tag{2.76}$$

Substituting Eq. (2.76) into Eq. (2.75) and rearranging the result, we have

$$\frac{v_2}{v_1} = \frac{A}{1 \mp AH} = \frac{1}{\mp H + 1/A} \tag{2.77}$$

Here, the plus sign indicates negative feedback and the minus sign indicates positive feedback. Now if A becomes very large, then $1/A$ is negligible compared to H and the function Eq. (2.77) realized by the feedback system in Fig. 2.24 becomes

$$\frac{v_2}{v_1} \approx \mp\frac{1}{H} \tag{2.78}$$

independent of A. Thus, if A in the feedforward path in Fig. 2.24 represents an opamp, the function realized by the feedback system is determined by the passive circuit elements as we saw in Eq. (2.35) and Eq. (2.56); it tends to be independent of the opamp gain A, as long as A is large. We begin to see how an "infinite-gain opamp" might be an attractive device to have, because it would render the circuit function completely independent of A.

We still note the simple steps necessary to obtain the frequency response of the feedback system. If the frequency response is desired, the input signal v_1 is sinusoidal and we can find

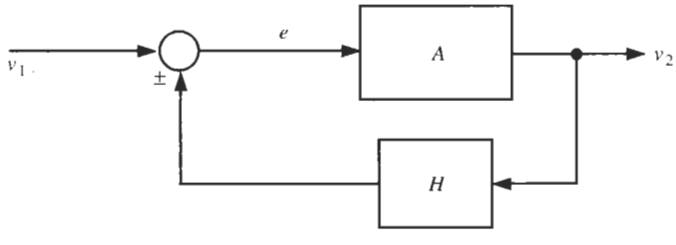

Figure 2.24 Elementary feedback block diagram.

its Laplace transform $V_1(s)$. Since the system is linear, the output is sinusoidal as well so that we may write the voltage as $V_2(s)$. Finally, we must assume that the blocks have frequency-dependent transfer characteristics, $A(s)$ and $H(s)$. Thus, the frequency response of the system in Fig. 2.24 is

$$\frac{V_2}{V_1} = \frac{A(s)}{1 \mp A(s)H(s)} = \frac{1}{\mp H(s) + 1/A(s)}\bigg|_{A\to\infty} \approx \mp\frac{1}{H(s)} \tag{2.79}$$

To see how these equations might apply to a practical circuit, let us review the derivation of the equations of the noninverting amplifier circuit in Fig. 2.11, Eq. (2.31) to Eq. (2.35), in light of the present discussion of feedback. There, the feedback factor H was simply a voltage divider ratio

$$H = \frac{v_a}{v_2} = \frac{R_1}{R_1 + R_2}$$

see Eq. (2.31), and the block A represents directly the opamp. This is depicted in Fig. 2.25a. Using this case for H in Eq. (2.77) and using the plus sign, since negative feedback was applied in Figs. 2.11 and 2.25, yield after rearranging of terms the equation

$$\frac{v_2}{v_1} = \frac{1}{H}\frac{1}{1 + \dfrac{1}{A}\dfrac{1}{H}} = \frac{R_1 + R_2}{R_1}\frac{1}{1 + \dfrac{1}{A}\dfrac{R_1 + R_2}{R_1}}$$

We recognize this result as identical to Eq. (2.34). Now setting $A = \infty$ results in Eq. (2.78) (with a plus sign), which corresponds to Eq. (2.35). The noninverting amplifier is a voltage-controlled voltage source that can be represented as in Fig. 2.25b, assuming that $A = \infty$. We note that the input terminals appear as an open circuit because the input current i_+ is zero so that

$$R_{in} = \frac{v_1}{i_+} = \infty \tag{2.80}$$

Also, the amplifier acts like an ideal voltage source with

$$R_{out} \approx 0 \tag{2.81}$$

because the output is taken directly from the opamp whose output resistance is assumed to be zero (or at least very small).

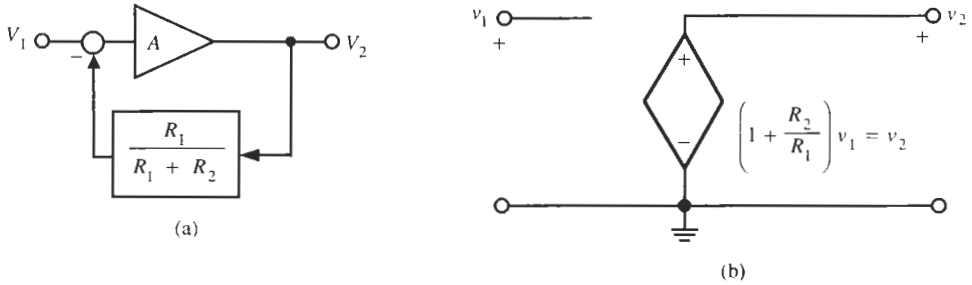

Figure 2.25 Noninverting amplifier: (a) block diagram representation; (b) controlled-source (small-signal) model.

2.6 THE VOLTAGE FOLLOWER

The voltage follower is a special case of the noninverting amplifier circuit of Figs. 2.11 or 2.25. The steps in the evolution of the voltage follower are shown in Fig. 2.26. Starting with Fig. 2.11a we let $R_1 = \infty$ and obtain the circuit in Fig. 2.26a. Since the opamp input resistor is infinite, the current i_- through R_2 is zero and so, by Ohm's law, is the voltage across it. Thus, R_2 may be replaced by a short circuit as indicated in Fig. 2.26b. This circuit is the voltage follower in question. If we set $R_1 = \infty$ in Eq. (2.34) we get

$$\frac{v_2}{v_1} = \frac{A}{1+A} = \frac{1}{1+1/A} \tag{2.82}$$

which for ideal opamps ($A \to \infty$) results in

$$\frac{v_2}{v_1} = 1 \quad \text{or} \quad v_2 = v_1 \tag{2.83}$$

so that the input and output voltages are identical, "v_2 follows v_1." A block diagram representation of this circuit in shown in Fig. 2.26c from which Eq. (2.82) can be derived directly. The input and output impedances of the voltage follower can be obtained directly from the noninverting amplifier, Eqs. (2.44) and (2.51), after setting $K_P = 1$:

$$Z_{in} = R_i(1 + A) \tag{2.84}$$

and

$$Z_{out} \approx \frac{R_o}{1+A} \tag{2.85}$$

Note that $|Z_{out}|$ is very small and $|Z_{in}|$ is very large for all frequencies of interest to our work with active filters. For ideal opamps it follows that the circuit is an amplifier with gain $K = 1$, input resistance $R_{in} = \infty$, and output resistance $R_{out} = 0$.

To determine why we would not achieve the same result simply by connecting two wires between input v_1 and output v_o, we look more carefully at the circuit and its operation. The circuit's function can be explained with the help of the equivalent circuit in Fig 2.27. The input is an open circuit and draws no current from the source, and the output is an ideal voltage source that can provide (theoretically) any power required by the load. The voltage follower's main role is to provide isolation between parts of a circuit that are required not to interact. The circuit is also called a *unity-gain buffer* because of the isolation it provides between input and output. To show the buffering action, consider an example.

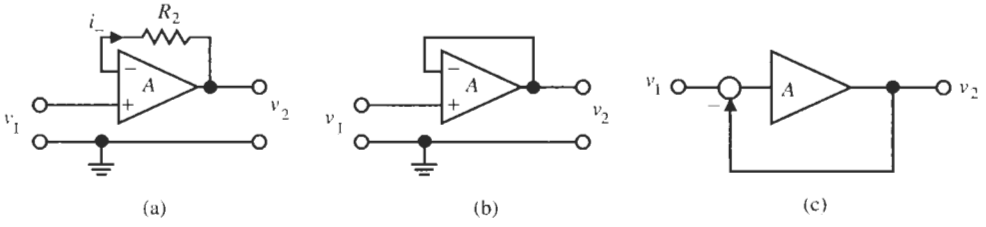

Figure 2.26 Evolution of unity-gain buffer from Fig. 2.11 (see text): (a) $R_1 = \infty$; (b) $R_1 - \infty$ and $R_2 = 0$; (c) block diagram representation.

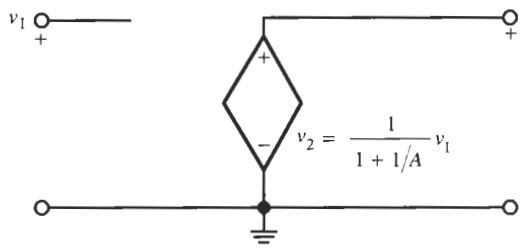

Figure 2.27 Controlled-source model of the unity-gain buffer.

EXAMPLE 2.4

A signal generator produces a voltage of 0.1 V. The internal resistance of the generator is 1000 Ω, and a load resistor of 100 Ω is to be connected to this source. The circuit is shown in Fig. 2.28. Find the load voltage without and with the use of a unity-gain buffer amplifier.

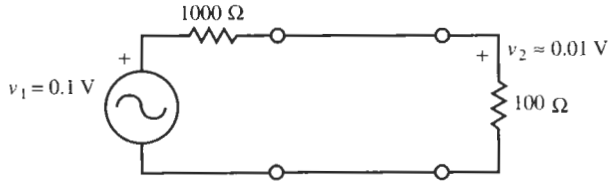

(a)

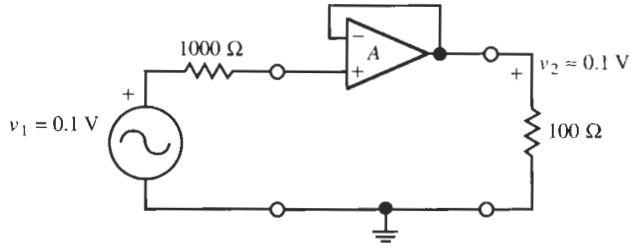

(b)

Figure 2.28 Load voltage obtained (a) without buffer; (b) with buffer.

Solution

With the connection illustrated in Fig. 2.28a, voltage-divider action results in the load voltage of

$$v_2 = \frac{100\ \Omega}{100\ \Omega + 1000\ \Omega} 0.1\text{V} \approx 0.009\text{V}$$

whereas 0.1 V − 0.009 V = 0.091 V is "lost" on the 1000-Ω generator resistance. If a buffer is employed as illustrated in Fig. 2.28b, there is no voltage drop across the generator resistor because $i_i = 0$ and the full 0.1 V is available on the 100-Ω load, provided that the opamp can deliver the required current $i = 0.1\ \text{V}/100\ \Omega = 1$ mA without exceeding its maximum output current. This example illustrates the utility of buffers as building blocks in circuit design.

Finally, to understand the frequency dependence of the buffer, we insert the integrator model Eq. (2.18) into Eq. (2.82). The result is

$$\frac{V_2}{V_1} = \frac{1}{1 + 1/A} \approx \frac{1}{1 + s/\omega_t} \tag{2.86}$$

It shows that the unity-gain buffer has the bandwidth $\omega_{-3\,\mathrm{dB}} = \omega_t$. This result was to be expected, of course, from Eq. (2.38) with $K_P = 1$. We have collected all-important equations for the voltage follower in Table 2.3.

2.7 ADDITION AND SUBTRACTION

Opamp circuits to add and subtract voltages were highly developed in connection with analog computers in the early 1940s. The ideas involved are simple and useful in our subsequent work. As we shall see shortly, they follow directly from the inverting and noninverting amplifiers and the fact that an opamp input is a current-summing node. Consider that a second input signal is connected via a resistor R_2 to the inverting opamp input in Fig. 2.17. Figure 2.29a shows the resulting circuit on which we apply the analysis method recommended in Section 2.4. Labeling the output voltage V_o, the node equation at node n takes the form

$$(V_1 - V_-)\,G_1 + (V_2 - V_-)\,G_2 + (V_o - V_-)\,G_F = 0$$

or

$$V_-\,(G_1 + G_2 + G_F) = V_1 G_1 + V_2 G_2 + V_o G_F \tag{2.87}$$

where the feedback resistor was called R_F. Further we remember that the opamp is described by

$$V_o = A\,(V_+ - V_-) \tag{2.88}$$

where in this case, of course, $V_+ = 0$. Therefore, we substitute $V_- = -V_o/A$ in Eq. (2.87) to obtain

$$V_o\left(G_F + \frac{G_1 + G_2 + G_F}{A}\right) = -\,(V_1 G_1 + V_2 G_2) \tag{2.89}$$

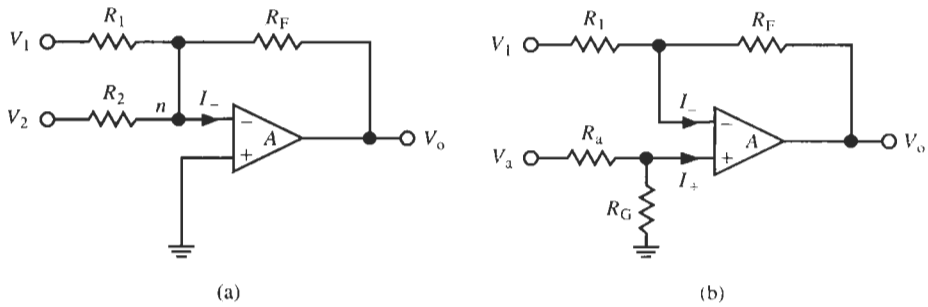

Figure 2.29 Resistive opamp circuits to (a) add and (b) subtract two voltages.

As long as A is very large, in the limit infinite, we have the simple result

$$V_o = -\left(\frac{R_F}{R_1}V_1 + \frac{R_F}{R_2}V_2\right) = -(K_1V_1 + K_2V_2) \tag{2.90}$$

It indicates that the output voltage of the circuit in Fig. 2.29a is the inverting sum of the (scaled) input voltages, where the scale factors K_i, $i = 1, 2$, are determined by the designer through resistor ratios. If we choose $R_1 = R_2$, then $K_1 = K_2 = K$ and the circuit simply inverts the two input voltages and adds them after scaling by a factor K. Note that for $V_2 = 0$, and substituting R_F for R_2, Eq. (2.90) reduces to Eq. (2.56) as must be expected.

It is not difficult to appreciate that the summer function can be extended to any number of additional inputs. For example, if we connected a signal V_3 through a resistor R_3 to node n, we would find instead of Eq. (2.90)

$$V_o = -\left(\frac{R_F}{R_1}V_1 + \frac{R_F}{R_2}V_2 + \frac{R_F}{R_3}V_3\right) = -(K_1V_1 + K_2V_2 + K_3V_3)$$

Let us emphasize again that the bandwidth of the summing circuit is, of course, not infinite as the idealized result Eq. (2.90) would suggest. To determine the bandwidth we use the integrator model (2.18) in Eq. (2.89) and employ again the same procedure used several times before. We obtain

$$V_o\left(1 + s\frac{1 + K_1 + K_2}{\omega_t}\right) = -(V_1K_1 + V_2K_2)$$

or

$$V_o = -\frac{V_1K_1 + V_2K_2}{1 + s(1 + K_1 + K_2)/\omega_t} \tag{2.91}$$

The reader will recall that the circuit's 3-dB frequency is defined as that frequency at which the denominator of Eq. (2.91) has the magnitude

$$\left|1 + j\frac{\omega}{\omega_t/(1 + K_1 + K_2)}\right| = \sqrt{2}$$

Thus,

$$\omega = \omega_{-3\,dB} = \frac{\omega_t}{1 + K_1 + K_2} \tag{2.92}$$

EXAMPLE 2.5

Build a circuit that adds the signal $v_1(t) = 3\cos(1.6 \times 10^6)t$ multiplied by 1.9 and the signal $v_2(t) = -2e^{-5t}$ multiplied by $K_2 = 2$ to the dc voltage $V_3 = 4.5$. All voltages are measured in volts [V] and the frequency is in rad/s. Will an LM741 opamp be adequate for the task?

Solution

We have chosen a different time dependence for each of the three inputs to emphasize that the summing function holds for arbitrary voltages. We then apply the three inputs v_i through

three resistors R_i to the inverting input node of the opamp. Since the multiplying factors are dimensionless ratios of resistors, we can again choose one of the resistors arbitrarily. Choosing $R_F = 10\ \text{k}\Omega$, we obtain

$$R_1 = \frac{R_F}{K_1} = \frac{10\text{k}\Omega}{1.9} \approx 5.26\ \text{k}\Omega, \quad R_2 = \frac{R_F}{K_2} = \frac{10\ \text{k}\Omega}{2} = 5\ \text{k}\Omega, \quad \text{and}$$

$$R_3 = \frac{R_F}{K_3} = \frac{10\ \text{k}\Omega}{1} = 10\ \text{k}\Omega$$

The output voltage is then

$$v_o(t) = -[4.5 + 5.7\cos\left(1.6 \times 10^6\right)t - 4e^{-5t}]$$

Using an LM741 opamp, the 3-dB bandwidth of this four-input circuit is by Eq. (2.92)

$$f_{-3\text{ dB}} = \frac{f_t}{1 + K_1 + K_2 + K_3} = \frac{f_t}{1 + 1.9 + 2 + 1} = \frac{1.5MHz}{5.9} \approx 254\ \text{kHz}$$

Since the applied frequency equals $\omega = 1.6 \times 10^6$ rad/s $= 2\pi \times 254$ kHz, the bandwidth may not be high enough because the signal v_1 is reduced by a factor of $1/\sqrt{2}$ (-3 dB corresponds to 0.707).

We have seen throughout our study so far that an opamp forms its output voltage by multiplying the difference of its input voltages by the gain A [see Eq. (2.88)]. This should enable us to form the difference of two input signals, if we were to generate v_+ from an applied voltage rather than setting it to zero (ground) as done for the inverting summer in Fig. 2.29a. The way to do this is pictured in Fig. 2.29b where we set by voltage division

$$V_+ = \frac{R_G}{R_a + R_G} V_a = \frac{G_a}{G_a + G_G} V_a \tag{2.93}$$

The voltage V_- is obtained as before from a node equation at the inverting input node as

$$V_- = \frac{G_1 V_1 + G_F V_o}{G_1 + G_F} \tag{2.94}$$

and the opamp imposes the restriction $V_+ - V_- = V_o/A$. Thus we have with Eqs. (2.93) and (2.94)

$$\frac{V_o}{A} = \frac{G_a}{G_a + G_G} V_a - \frac{G_1 V_1 + G_F V_o}{G_1 + G_F}$$

that is

$$V_o\left(1 + \frac{1}{A}\frac{G_1 + G_F}{G_F}\right) = \frac{G_1 + G_F}{G_a + G_G}\frac{G_a}{G_F} V_a - \frac{G_1}{G_F} V_1 = K_a V_a - K_1 V_1 \tag{2.95}$$

where we have defined gain constants K_a and K_1 as indicated to simplify notation in the following discussion. Observe that K_a can be made a simple ratio of two resistors, $K_a = R_F/R_a$,

by selecting $R_F = R_G$ and $R_a = R_1$. Assume for the moment that we deal with ideal opamps, or simply that A is so large that

$$1 \gg \frac{1}{A}\frac{G_1 + G_F}{G_F} = \frac{1 + K_1}{A} \tag{2.96}$$

Then we observe that the circuit in Fig. 2.29b is the desired difference amplifier: it forms the difference between two applied input signals, each multiplied by a gain constant determined by the chosen resistor values.

If the opamp is not ideal, nothing changes except that, as we know and expect by now, the bandwidth of the circuit is finite. Modeling the opamp as an integrator, Eq. (2.18), we find from Eq. (2.95)

$$V_o = \frac{K_a V_a - K_1 V_1}{1 + s\,(1 + K_1)/\omega_t}$$

that is, the 3-dB bandwidth is

$$\omega_{-3\text{ dB}} = \omega_t \frac{G_F}{G_1 + G_F} = \frac{\omega_t}{1 + K_1} \tag{2.97}$$

We point out here that the bandwidth is determined by the opamp (ω_t) and the feedback network ($1 + K_1$), i.e., the blocks A and H in Fig. 2.24. The resistive input voltage divider determining V_+ does not affect the bandwidth.

2.8 APPLICATIONS OF OPAMP RESISTOR CIRCUITS

Thus far in this chapter, we have described circuits that provide amplification, isolation, addition, and subtraction. Let us still give a number of additional examples of useful applications of resistor–opamp circuits.

We wish to develop a circuit that generates an output voltage proportional to a change ΔR in a resistor. This change may be effected, for example, by a change in pressure, humidity, or other causes. Let us assume we want to measure temperature and that we have a temperature-dependent resistor

$$R = R_0[1 - \alpha\,(T - T_0)] = R_0 - \Delta R \tag{2.98}$$

where α is a temperature coefficient, T is the temperature, T_0 is a nominal reference temperature, and R_0 is the value of R at $T = T_0$.

A suitable circuit is shown in Fig. 2.30. It is derived from the difference amplifier in Fig 2.29b where we combined the two inputs, placed the variable resistor into the feedback path, and labeled the remaining resistors in a manner that is convenient for the task at hand. Since the operation is at dc, powered by a battery V_B, we can safely assume the opamp is ideal. Following the procedure of Section 2.4, making use of the virtual short at the opamp's input yields by direct analysis

$$V_+\,(G_1 + G_0) = V_B G_1 \quad \text{and} \quad V_-\left(G_1 + \frac{1}{R_0 - \Delta R}\right) = V_B G_1 + V_o \frac{1}{R_0 - \Delta R} \tag{2.99}$$

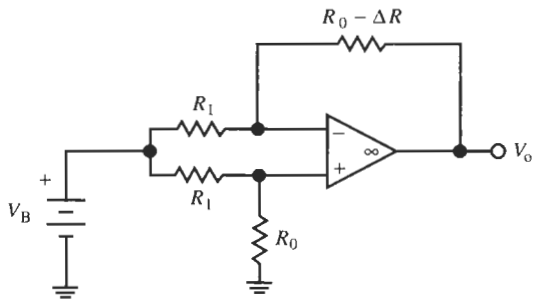

Figure 2.30 An opamp circuit to measure ΔR.

Together with $V_+ = V_-$ for our ideal opamp, this results in the equation

$$\left(\frac{G_1}{G_1 + G_0} - \frac{G_1}{G_1 + 1/(R_0 - \Delta R)}\right) V_B = \frac{1/(R_0 - \Delta R)}{G_1 + 1/(R_0 - \Delta R)} V_o \tag{2.100}$$

Bringing the left-hand side of Eq. (2.100) on its common denominator yields

$$\frac{G_1\left(G_1 + \dfrac{1}{R_0 - \Delta R}\right) - G_1(G_1 + G_0)}{(G_1 + G_0)\left(G_1 + \dfrac{1}{R_0 - \Delta R}\right)} V_B = \frac{\dfrac{1}{R_0 - \Delta R}}{G_1 + \dfrac{1}{R_0 - \Delta R}} V_o \tag{2.101}$$

We may now eliminate common factors to obtain

$$\frac{G_1[1/(R_0 - \Delta R)] - G_1 G_0}{G_1 + G_0} V_B = \left(\frac{1}{R_0 - \Delta R}\right) V_o \tag{2.102}$$

Finally, multiplying both sides of Eq. (2.102) by $R_0 - \Delta R$ and using Eq. (2.98) gives the desired result:

$$V_o = \frac{\Delta R}{R_0 + R_1} V_B = \frac{\alpha(T - T_0)}{1 + R_1/R_0} V_B \tag{2.103}$$

It indicates that the opamp output voltage is directly proportional to the temperature difference. Notice that the result Eq. (2.103) could also have been obtained immediately from Eq. (2.95) by relabeling the components of Fig. 2.29b as in Fig. 2.30.

The following circuit is an instrumentation amplifier that has very low input currents and can be tuned to a desired gain by one resistor. Instrumentation amplifiers are normally used at low frequencies, such as in biomedical applications, so that we are justified to work with the ideal opamp model. The circuit is shown in Fig. 2.31, and the tuning resistor is identified as R_g. Although the connection is new to us, it is composed of circuits we have studied previously: the inverting and noninverting amplifiers, and the difference amplifier. We make use of the fact that the input voltage of the ideal amplifier is zero (being a virtual short) such that v_1 appears at both nodes A and B and v_2 at nodes C and D. Then, using superposition,

$$v_4 = (1 + R_1/R_g)\, v_1 + (-R_1/R_g)\, v_2 \tag{2.104a}$$

$$v_5 = (1 + R_1/R_g)\, v_2 + (-R_1/R_g)\, v_1 \tag{2.104b}$$

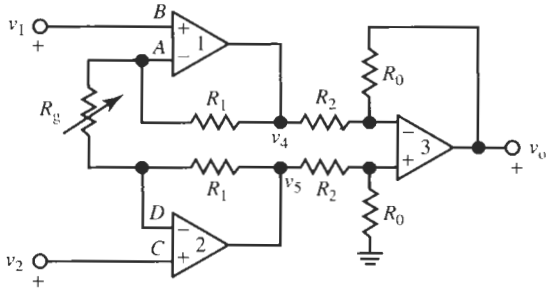

Figure 2.31 Instrumentation amplifier.

We see from the circuit in Fig. 2.31 that v_4 and v_5 are combined by opamp 3 to give

$$v_o = -\frac{R_0}{R_2}v_4 + \frac{R_0}{R_0 + R_2}\left(1 + \frac{R_0}{R_2}\right)v_5 = \frac{R_0}{R_2}(v_5 - v_4)$$

Substituting v_4 and v_5 from Eq. (2.104) into this equation gives

$$v_o = \left(1 + \frac{2R_1}{R_g}\right)\frac{R_0}{R_2}(v_2 - v_1) = K(v_2 - v_1) \tag{2.105}$$

where K is the circuit gain. Thus the circuit is a differential amplifier whose gain K is adjusted by changing R_g. The input resistance is very high because the input voltages are applied to the + input terminals of opamps 1 and 2.

As an example assume that an instrumentation amplifier has the element values $R_1 = 75\ \text{k}\Omega$, $R_2 = R_g = 5\ \text{k}\Omega$, and $R_0 = 160\ \text{k}\Omega$. Then from Eq. (2.105) we determine the gain to be

$$K = \left(1 + \frac{2 \times 75\ \text{k}\Omega}{5\ \text{k}\Omega}\right)\left(\frac{160\ \text{k}\Omega}{5\ \text{k}\Omega}\right) = 993$$

Fine adjustments of the value of gain can be made by tuning R_g.

As the next example we study an opamp circuit that is useful for providing a stage of high gain. Since, as we saw, high gain implies low bandwidth, we shall limit the application to low frequencies and base our analysis on ideal opamps. The gain of the inverting amplifier, shown again in Fig. 2.32a, is $K_N = -R_2/R_1$. We see that the gain can be increased either by making R_2 larger, or by making R_1 smaller. But R_1 is the input resistance of the inverting amplifier [see Eq. (2.61)], and so there is a preference for making R_2 larger. As a result we may need to implement a very large resistor, which is undesirable in many technologies, such as in integrated circuits. For example, if we wish to increase the gain by a factor α, we could do this by increasing R_2 to $R_2' = \alpha R_2$ as shown in Fig. 2.32b, with the mentioned difficulty. We shall see that the design we present next avoids this problem, at the cost of two additional resistors.

The circuit we will use to realize a large-gain amplifier is shown in Fig. 2.33. It is the inverting amplifier of Fig. 2.32a, augmented by two additional resistors R_3 and R_4, which help further to reduce by voltage division the fraction of the voltage v_2 that is fed back to the opamp's input. The goal is to reduce the gain of the feedback path H in Fig 2.24 because it will increase total circuit gain, which is inversely proportional to H by Eq. (2.78).

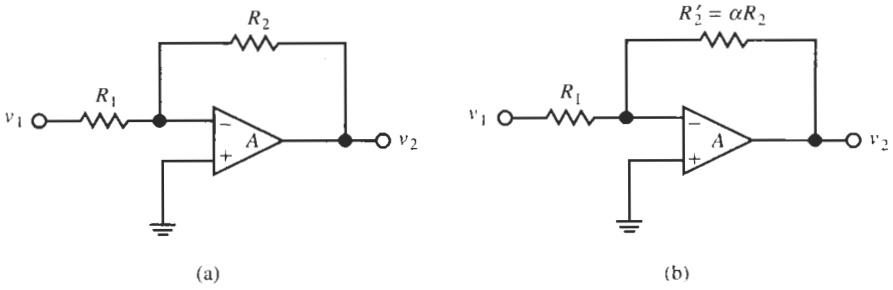

Figure 2.32 (a) Inverting amplifier; (b) modification for increased gain.

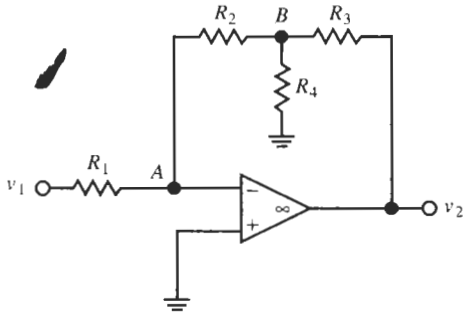

Figure 2.33 Circuit configuration suitable for high-gain amplifiers.

Remembering that $v_- = 0$ (the inverting input node is at virtual ground), we have from Kirchhoff's current law at node A

$$v_1 G_1 + v_B G_2 = 0 \tag{2.106}$$

and at node B

$$v_B G_2 + v_B G_4 + (v_B - v_2) G_3 = 0 \tag{2.107}$$

Substituting v_B from Eq. (2.106) into this equation gives

$$\frac{v_2}{v_1} = -\frac{G_1 (G_2 + G_3 + G_4)}{G_2 G_3} = -\frac{R_2}{R_1}\left(1 + \frac{G_2 + G_4}{G_3}\right) = -\alpha \frac{R_2}{R_1} = -\alpha K_N \tag{2.108}$$

We notice that we have implemented the gain $K_N = R_2/R_1$, increased by a factor $\alpha > 1$ as would be realized by Fig. 2.32b, but we have obtained the factor α from the resistive T-network in the feedback path of the opamp rather than from an increase in R_2.

There are many ways to choose the resistors to make the factor

$$\alpha = 1 + \frac{G_2 + G_4}{G_3} = 1 + \frac{R_3}{R_2} + \frac{R_3}{R_4} \tag{2.109}$$

large without again incurring excessive resistor values. One possibility is to choose $R_3 = R_2$ and $R_4 < R_2$ to achieve that α becomes large. For example, if a gain $K_N = 3000$ is required along with $R_1 \geq 10$ kΩ to maintain an adequate input impedance, the standard inverting

amplifier would call for $R_2 = 30\ \text{M}\Omega$. With the technique in Fig. 2.33, we can choose $R_2 = R_3 = 100\ \text{k}\Omega$ and $R_4 = 336\Omega$ to get

$$\frac{v_2}{v_1} = -\frac{100\ \text{k}\Omega}{10\ \text{k}\Omega}\left(2 + \frac{100\ \text{k}\Omega}{336\Omega}\right) \approx -3000$$

As the last example of this chapter we consider a circuit idea that will guide us through a practical design and make use of much of what we learned in previous sections. It will demonstrate succinctly that assuming ideal opamps may be very misleading and lead to dangerous misconceptions about the circuit's behavior in practice.

Assume a student engineer is asked to design an inverting audiofrequency amplifier with a gain of $K_N = 500$ in the frequency range $f \leq f_{-3\,\text{dB}} = 30\text{kHz}$. The circuit is to be very inexpensive and should use, if possible, LM741 opamps. The student is concerned that with 741s, the bandwidth may be too low for her needs. After all, by Eq. (2.58) the expected bandwidth is only

$$f_{-3\,\text{dB}} = \frac{1.5\ \text{MHz}}{501} \approx 3\ \text{kHz}$$

if an LM741 opamp is used. Striving to keep cost low, the student tries to avoid a more expensive high-frequency amplifier and proposes to build a two-stage amplifier by putting two 741 opamps in cascade to achieve higher active-device gain. The circuit is shown in Fig. 2.34. We note that A_1 is connected in the inverting and A_2 in the noninverting mode so that the loop gain is negative and negative feedback is applied. Let us assume that the opamps are identical, $A_1 = A_2 = A$, for example, dual opamps (two devices) on the same integrated circuit. The analysis of the circuit is trivial: a node equation at the input of A_1 yields

$$V_-(G_1 + G_2) = V_1 G_1 + V_2 G_2 \tag{2.110}$$

which together with

$$V_2 = (-A_1 \times A_2)\, V_- = -A^2 V_- \tag{2.111}$$

gives the circuit function

$$\frac{V_2}{V_1} = -\frac{G_1}{G_2 + \dfrac{G_1 + G_2}{A^2}} = -\frac{R_2}{R_1}\frac{1}{1 + \dfrac{1 + R_2/R_1}{A^2}} = -K_N \frac{1}{1 + \dfrac{1 + K_N}{A^2}} \tag{2.112}$$

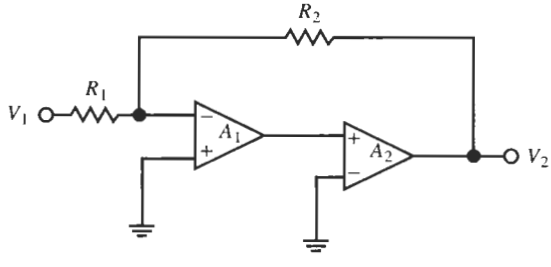

Figure 2.34 Inverting amplifier using two opamps.

This is precisely the result expected, with A replaced by A^2 in Eq. (2.55). A gain of 500 requires, for example, $R_1 = 1\ \text{k}\Omega$ and $R_2 = 500\ \text{k}\Omega$. Since

$$|A(j\omega)|^2 \geq \left(\frac{1.5\ \text{MHz}}{30\ \text{kHz}}\right)^2 = 2500$$

is large compared to 501 over the prescribed frequency range, the student assumes that the gain will be reasonably constant at 500, or 54 dB, as she requires. Attempting to compute the bandwidth, she inserts the integrator model (2.18) into Eq. (2.112) to obtain, for $s = j\omega$,

$$\frac{V_2}{V_1} = -K_N \frac{1}{1 + s^2\left[(1 + K_N)/\omega_t^2\right]_{s=j\omega}} = -\frac{500}{1 - \omega^2\left(501/\omega_t^2\right)} \tag{2.113a}$$

This is a worrisome result because it indicates that at

$$f = \frac{f_t}{\sqrt{501}} = \frac{1.5\ \text{MHz}}{22.4} \approx 67\ \text{kHz} \tag{2.113b}$$

the amplifier gain becomes infinite. Although our student does not believe that in real life voltages can become infinite, she is curious, and wanting to be a cautious and careful designer, she builds the circuit and measures its performance on a network analyzer. The experimental circuit and result are seen in Fig. 2.35, which shows that the gain is a constant 54 dB only up to about 9 kHz, after which it rises to a peak value of over 127 dB at 66.9 kHz.[1] The peak is, of course, finite but it is at the frequency predicted in Eq. (2.113b); for higher frequencies the gain drops at the rate −40 dB per decade. The −40-dB/decade roll-off is understandable because $|V_o/V_1|$ decreases as ω^{-2} for large frequencies as seen in Eq. (2.113a). The student finds that her approach to increasing the bandwidth has worked: it has increased by a factor three compared with that of a single-amplifier design, but the bandwith is still a factor three lower than the required 30 kHz and the peaking gain is unacceptable. To find a solution, the student consults an experienced designer. He suggests[2] that "the circuit Q is too large; try to dampen the peak by putting a feedback resistor across A_1." The student proceeds to do so, and the bandwidth indeed widens with the peak being reduced. After some trial-and-error experimentation, she produces the circuit in Fig. 2.36a with the experimental result in Fig. 2.36b. We observe that the gain is almost perfectly flat at 54 dB until 36 kHz, with the −3-dB bandwidth now at 71 kHz (see the cursor), more than twice what is required. Although the specifications are met with a wide margin, our student engineer has a final worry: will they still be met if the amplifiers' unity-gain frequency changes from the assumed 1.5 MHz? We recall that f_t is only a very poorly controlled parameter. Fortunately, further measurements with different lots of opamps (or better: circuit simulations) quickly show that everything is fine as long as $f_t \geq 750$ kHz, allowing for a comfortable −50% manufacturing error. (The circuit performance, of course, improves only if $f_t \geq 1.5$ MHz.)

[1] The numbers are obtained by displaying the performance with higher resolution.

[2] The reader should not be concerned with the meaning of this cryptic statement. (Q is the "quality factor" of the circuit.) A rational explanation along with the complete theory will become clear as we progress in our study of filters.

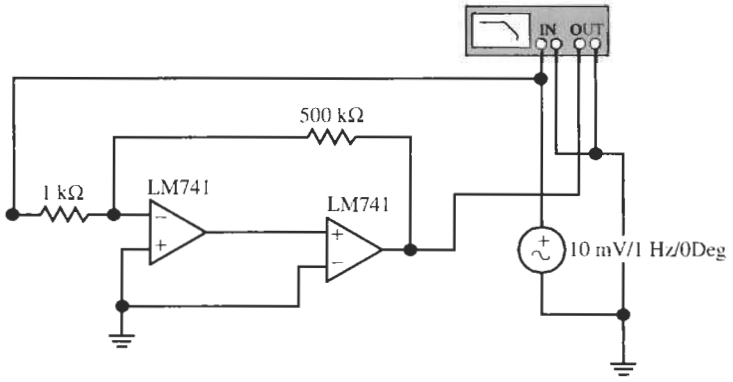

(a)

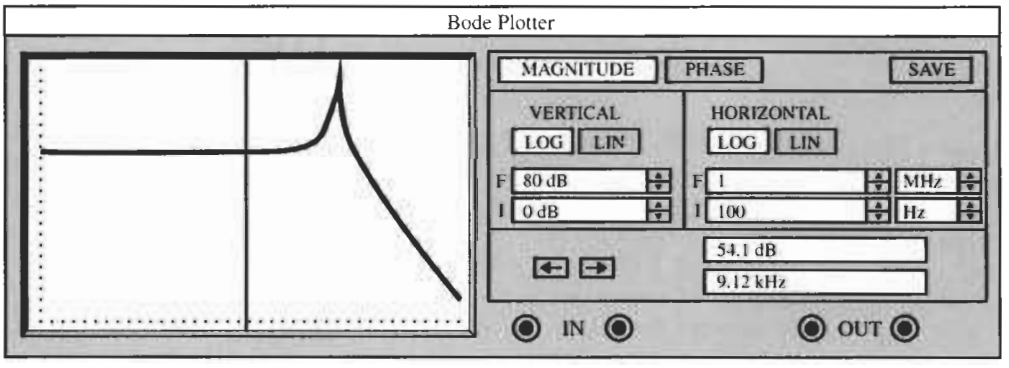

(b)

Figure 2.35 Experimental performance of the circuit in Fig. 2.34 for 54-dB gain. The Bode Plotter's frequency range is 100 Hz to 1 MHz, the vertical scale is set from 0 dB to +80 dB, and the cursor is at 9.12 kHz and reads 54.1 dB at the edge of the constant-gain range. To measure the frequency response of the circuit, we connect its input and output terminals to the *IN* and *OUT* terminals, respectively, of the network analyzer. It is dubbed "Bode Plotter" in the program "Electronics Workbench" by Interactive Image Technologies, Ltd. In Fig. 2.35, we measure the circuit's performance with LM741 opamps. The circuit is driven by a 10-mV–1-Hz input signal. The input signal and the circuit's output signal are measured by the Bode Plotter. When the Bode Plotter is activated, it overrides the settings of the voltage source by the parameters chosen for the display: in Fig. 2.35, where we specified to measure *Magnitude*, the frequency range for the abscissa starts (I) at 100 Hz and goes to 1 MHz (F). The vertical range is set to go from 0 dB (I) to 80 dB (F). "I" and "F" are the initial and final points of the axes. Both vertical and horizontal axes are set to *LOG* scale so that the display is a Bode plot (see Section 3.3). The vertical line on the display is the cursor that can be moved by the right and left arrows below the *VERTICAL* readout (or by dragging with the mouse pointer); it intersects the measured display curve of the measured response at the point [54.1 dB, 9.12 kHz] as is shown below the *HORIZONTAL* readout. In the remaining figures, when Bode plots are measured, only the Bode Plotter readout will be shown, but not the complete front panels. The Bode Plotter settings will always be identified in the figure headings.

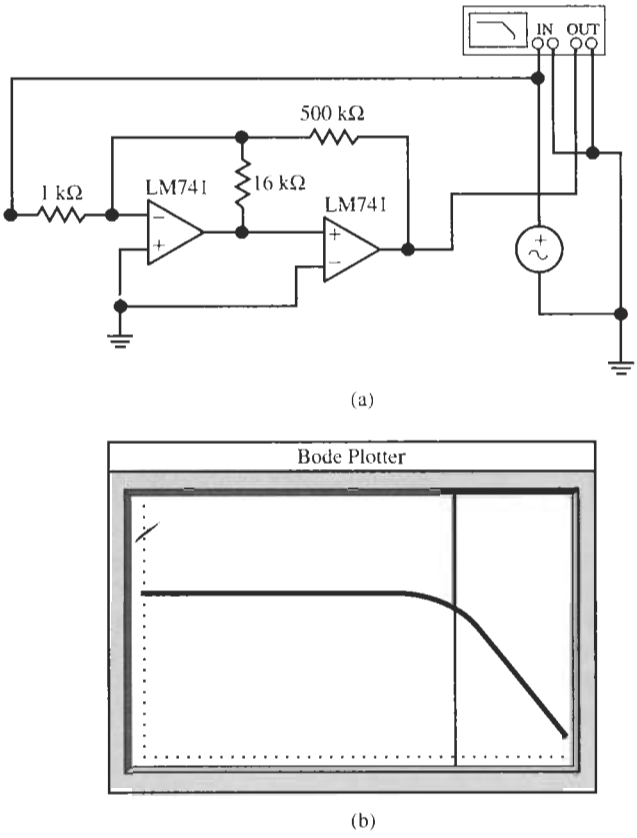

Figure 2.36 (a) Improved circuit; (b) experimental performance. Bode Plotter settings as in Fig 2.35. The cursor readout is 50.7 dB at 71.0 kHz.

REFERENCES

A. S. Sedra and K. C. Smith, *Microelectronic Circuits*, Fourth Edition, Oxford University Press, New York, 1998.

P. R. Gray and R. G. Meyer, *Analysis and Design of Analog Integrated Circuits*, 3rd ed. John Wiley, New York, 1993.

D. A. Johns and K. Martin, *Analog Integrated Circuit Design*. John Wiley, New York, 1998.

PROBLEMS

2.1 The circuit in Fig. P2.1 uses a potentiometer and an opamp to build an amplifier with adjustable noninverting gain K. The opamp is modeled as in Eq. (2.18). Determine the range of K and find the bandwidth as a function of the wiper position.

2.2 Repeat Problem 2.1 but for a configuration with inverting gain.

2.3 For $K = +5$ and $K = -5$, respectively, verify your designs in Problems 2.1 and 2.2 by testing their performance with the program Electronics Workbench (EWB).

2.4 The circuit in Fig. P2.4 can be used to provide a voltage proportional to an input current I.

(a) Assuming the opamp is ideal, compute V_0 as a function of I and of the feedback resistor R.

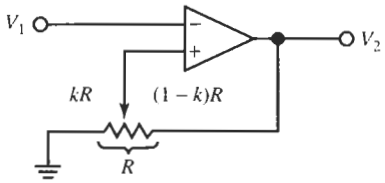

Figure P2.1

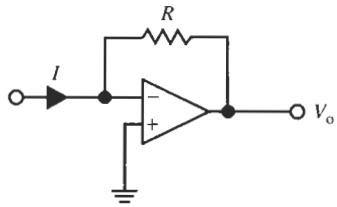

Figure P2.4

(b) Investigate the circuit's behavior if the opamp has finite gain $A = \omega_t/s$.

(c) Set $R = 1$ kΩ and verify your design by testing its performance with EWB.

2.5 The opamp circuit in Fig. P2.5 is required to implement the function

$$v_o = \frac{1}{3}v_2 - 2v_1$$

(a) Determine the values of R_a and R_b that give the desired relationship.

(b) Suppose that $v_2 = V_2 = +10$ V and $v_1 = V_1 = -10$ V find the current in each resistor and the power dissipated in each resistor.

2.6 (a) Design a circuit with a single opamp to realize

$$V_0 = V_1 - 4V_2$$

where V_1 and V_2 are two input voltages.

(b) Select the resistor values so that no more than 0.25 W is dissipated in any resistor when the input voltages are no larger than 10 V.

(c) If your design uses an LM741 opamp, determine the bandwidth of your circuit.

(d) Verify your design by testing its performance with EWB.

2.7 Use the data in Table 2.1 to identify the parameters of the model of Eq. (2.17a) for the LM741 and the HA2542–2 operational amplifiers.

2.8 From the plots in Fig. 2.4a and b determine the range over which the integrator model of Eq. (2.28) can be expected to provide reasonable accuracy when representing (a) the LM741 and (b) the HA2541–2 opamps.

2.9 The circuit in Fig. P2.9 is used to produce an output voltage proportional to the key that is depressed. It operates with a standard keyboard incorporated into the resistive feedback path of the inverting circuit. The output of this circuit is then added to the input by means of an adder-inverter circuit. Pressing a key on the keyboard connects together points that are the horizontal and vertical projections of points A, B, C, D, E, F, G, and H from the key. For example, pushing Key 1 connects points D and E such that $R_2 = \frac{15}{16}R$, pushing Key 11 connects B and G so that $R_2 = \frac{5}{16}R$, pushing Key 13 connects A and E so that $R_2 = \frac{3}{16}R$, and so on. Show that in general we have, with $R_1 = R$,

$$\frac{v_a}{v_1} = -\left(1 - \frac{n}{16}\right)$$

and

$$v_2 = -\frac{n}{16}v_1$$

2.10 Design an opamp circuit to realize $V_o = 4V_1 + 2V_2 - 2V_3$ where V_o is the output and the other voltages are inputs. Determine the resistor values such that no resistor dissipates more than 1/8 W.

2.11 The circuit in Fig. P2.11 must amplify a 1-m V–25-kHz signal to a level of 8 V. The input impedance should be no less than 10 kΩ. The circuit should use as many identical resistors as possible. Design the circuit and determine whether a 741-type opamp is adequate for the job. Verify your design by testing its performance with EWB.

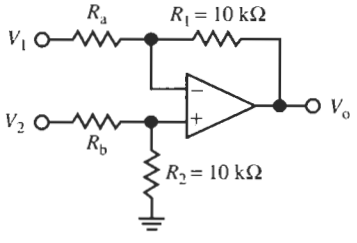

Figure P2.5

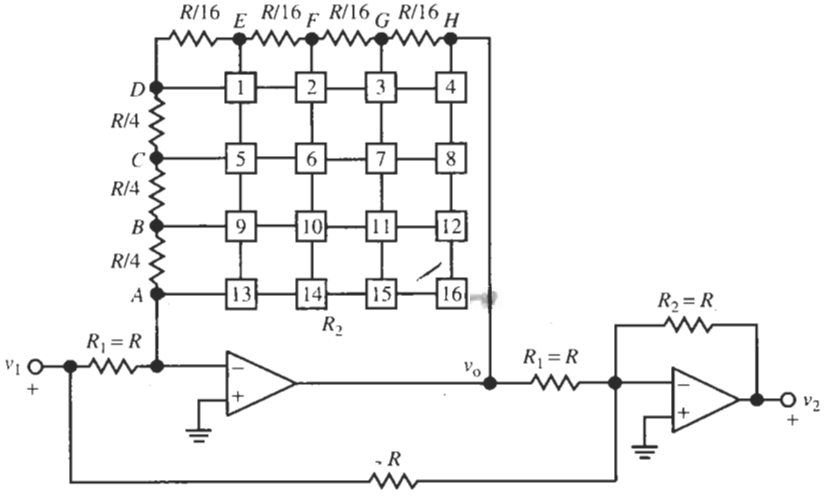

Figure P2.9

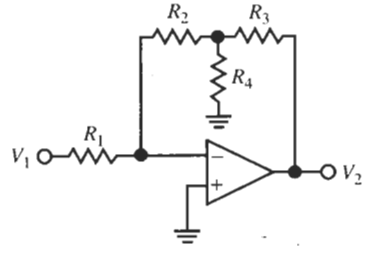

Figure P2.11

2.12 Find the output and the input impedances of the amplifiers analyzed in Problems 2.1 and 2.2.

2.13 A 60-kHz sinusoidal signal is applied to an amplifier with a gain of $K = 2$. The circuit is built with an LM741 opamp with power supplies ± 13 V. Find the largest amplitude the signal may have before it is limited by slew rate constraints. Determine the limits if the amplifier is replaced by an HA2542-2 unit. Verify your answers by testing the circuits with EWB.

2.14 What is the highest frequency of a 10-V peak-to-peak triangular wave that can be reproduced by an LM741 opamp without experiencing slew rate distortion? What is the largest amplitude of a sine wave of the same frequency that the opamp can process with no distortion? Verify your answers by testing the circuit with an opamp in unity-gain configuration with EWB.

2.15 Use the analysis procedure suggested in Section 2.4 to show that the circuit in Fig. P2.15 realizes the voltage gain

$$\frac{V_2}{V_1} = T(s) = \frac{(G_1 + G_2)\,G_3}{(G_3 + G_5)\,G_2 - G_1 G_4}$$

Let all resistors be equal to R except R_4 and sketch T as a function of R_4. Explain the behavior when $R_4 = R/2$.

2.16 Show that the opamp circuit of Fig. P2.16 can be used to form the difference of sums of signals.

(a) Show by routine analysis that

$$\frac{V_o}{A} = \frac{G_a V_a + G_b V_b}{G_a + G_b + G_G} - \frac{G_1 V_1 + G_2 V_2 + G_F V_o}{G_1 + G_2 + G_F}$$

and solve the equation for V_o. Determine the result for ideal opamps.

(b) Determine the bandwidth of the amplifier summer when the opamp's bandwidth is ω_t.

2.17 (a) Use the analysis procedure suggested in Section 2.4 to find the input impedance of the

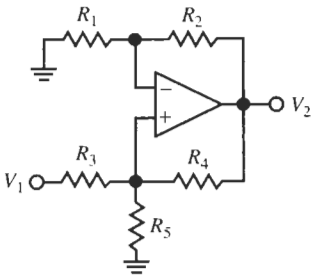

Figure P2.15

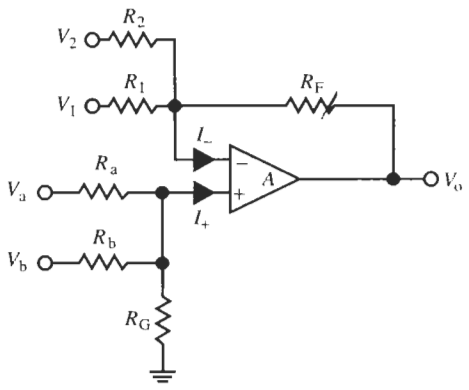

Figure P2.16

circuit in Fig. P2.17 under the assumption that the opamp is ideal. Interpret the result.

(b) Assume $Z = sL$, $L = 1$ mH, and verify your design by devising a test with EWB.

2.18 Design an instrumentation amplifier as in Fig. 2.32 to realize a gain in $1 \leq K \leq 25$. Use as many identical resistors as possible. Find the bandwidth of the amplifier as a function of K if the circuit is designed with three identical LM741 opamps. Verify your design by testing its performance with EWB.

2.19 The circuit in Fig. P2.19 is to provide any gain between -10 (when $k = 0$) and $+10$ (when $k = 1$) by adjusting the potentiometer in the range $0 \leq k \leq 1$.

(a) Determine the gain $T = V_2/V_1$ as a function of the component values and of k.

(b) Find suitable values for R_a and R_b and determine the value of k for which $V_2 = 0$.

(c) Assume the circuit is built with a 741-type operational amplifier and model the opamp's gain as ω_t/s. Determine the frequency response of T.

2.20 (a) Find the input impedance of the circuit in Fig. P2.20 under the assumption that the opamp is ideal. Interpret the result.

(b) Repeat for the case in which the opamp is modeled as ω_t/s and compare the results.

2.21 (a) Analyze the circuit in Fig. P2.21 to find the output voltage V_0 as a function of the resistors and the input voltages V_i, $i = 1, 2, \ldots, n$, and V_j, $j = n+1, \ldots, m$. Express the result as

$$V_0 = \sum_{j=n+1}^{m} a_j V_j - \sum_{i=1}^{n} b_i V_i$$

(b) Investigate the possibility of adjusting the coefficients a_j and b_i independently.

(c) Find the bandwidth of the circuit in Fig. P2.21 if the opamp is represented by the integrator model of Eq. (2.18).

2.22 (a) Analyze the circuit in Fig. P2.22 and verify that V_2/V_1 is the function of an ideal integrator if the opamp can be assumed to be ideal.

(b) Investigate the changes in performance if the integrator model of Eq. (2.18) is used for the opamp.

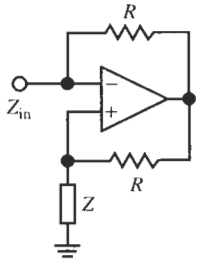

Figure P2.17

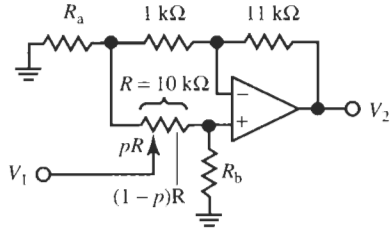

Figure P2.19

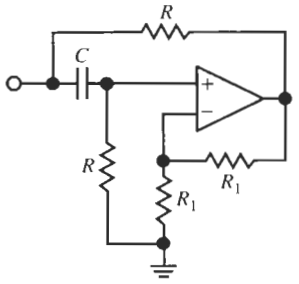

Figure P2.20

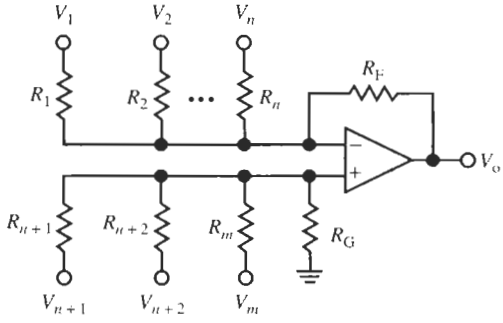

Figure P2.21

(c) Show that the nominal performance can be improved by placing a small resistor r in series with the capacitor in the feedback loop.

2.23 The circuit in Fig. P2.23 realizes a lowpass filter.

(a) Use the method discussed in Section 2.4 and find the transfer function V_2/V_1, assuming the opamp is ideal.

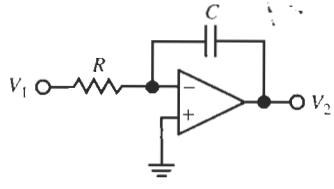

Figure P2.22

(b) Investigate the changes in the transfer function caused by an opamp with finite gain $A = \omega_t/s$.

(c) Design the lowpass filter to have a dc gain of 0 dB and the -3 dB frequency of 6 kHz. Verify your design by testing the circuit's performance with EWB.

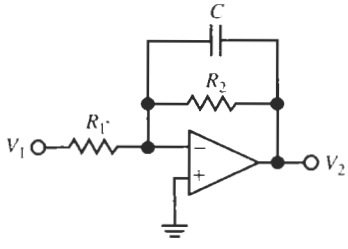

Figure P2.23

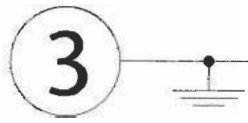

FIRST-ORDER FILTERS: BILINEAR TRANSFER FUNCTIONS AND FREQUENCY RESPONSE

In Chapter 2, we considered operational amplifier circuits with purely resistive feedback. Any frequency dependence arose from the operational amplifier itself. However, since opamps have poorly controlled parameters, we saw that it is generally not advisable to let filter performance be determined by these parameters. We must, therefore, rely on the opamp to have large (even if finite) gain and make the feedback characteristic H frequency dependent. This was indicated in Eq. (2.79). To accomplish this goal, we will in this chapter extend our studies from Chapter 2 by adding the capacitor as component to the resistor in the feedback network. Also, since we shall be interested from now on mainly in the frequency response, we shall always assume sinusoidal sources and steady-state operation. Although we will remind ourselves from time to time of time-domain responses, the language of filter design is predominantly that of the frequency domain. This means that $v(t)$ and $i(t)$ will be represented by phasors or Laplace transforms $V(s)$ and $I(s)$. Earlier, we labeled the *ratio of output to input* of a circuit the gain. In the following we shall refer to this ratio as the *transfer function* and assign again the symbol T or $T(s)$. We will also characterize the circuit elements, individual ones or combinations, by their impedances $Z(s) = V/I$ or admittances $Y(s) = I/V$. This was done on occasion before, when we needed to consider frequency-domain concepts, such as the bandwidth of a design.

We pointed out in Chapter 1 that the transfer function of a filter with a finite number of discrete components must be a real rational function. This was shown in Eq. (1.12), which we repeat here as Eq. (3.1) for convenience:

$$T(s) = \frac{N(s)}{D(s)} = \frac{b_m s^m + b_{m-1}s^{m-1} + \cdots + b_1 s + b_0}{a_n s^n + a_{n-1}s^{n-1} + \cdots + a_1 s + a_0} \tag{3.1}$$

s is the frequency parameter and the coefficients a_i and b_j are real numbers. In this chapter we treat the simplest special case of this expression, the first-order or *bilinear* transfer function. We will start the presentation of the bilinear transfer function with passive *RC* circuits and will leave the extension to active opamp-*RC* circuits until later. We hope this approach, starting from familiar circuits and analysis methods, will distract minimally from the notion of transfer function, its gain and phase, Bode plots, and related definitions and concepts, which are important for our subsequent discussion of filters.

3.1 BILINEAR TRANSFER FUNCTION AND ITS PARTS

With $m = n = 1$, we have from Eq. (3.1) the first-order function

$$T(s) = \frac{N(s)}{D(s)} = \frac{b_1 s + b_0}{a_1 s + a_0} \tag{3.2}$$

whose coefficients are real constants; the coefficients b_i of the numerator polynomial $N(s)$ may be positive, negative, or zero, but the coefficients a_i of the denominator $D(s)$ must be nonnegative to ensure that the roots of $D(s)$ are not in the right half-plane. You will have learned in prior circuits or controls courses that that would result in an unstable circuit.

$T(s)$ is also referred to as *bilinear* because it is a ratio of two straight line equations (or first-order polynomials)

$$N(s) = b_1 s + b_0 \quad \text{and} \quad D(s) = a_1 s + a_0 \tag{3.3}$$

where frequency, s, is the independent variable. We can rewrite Eq. (3.2) in the form

$$T(s) = \frac{N(s)}{D(s)} = \frac{b_1}{a_1}\frac{s + b_0/b_1}{s + a_0/a_1} = K\frac{s + z_1}{s + p_1} \tag{3.4}$$

where z_1 is the zero of $T(s)$ and p_1 is its pole. In the s plane these two quantities are located at

$$s = -z_1 = -\frac{b_0}{b_1} \quad \text{and} \quad s = -p_1 = -\frac{a_0}{a_1} \tag{3.5}$$

Since the coefficients a_i and b_j are real numbers, we see that the pole and the zero are located on the real axis in the complex s-plane. As mentioned, the pole p_1 will always be on the negative real axis, whereas the zero z_1 may be either on the positive or the negative part of the real axis since the b coefficients may be negative. Figure 3.1 shows typical pole-zero locations in the s-plane. These correspond to

$$T_a(s) = K_a\frac{s+3}{s+1}, \quad T_b(s) = K_b\frac{s+1}{s+4}, \quad T_c(s) = K_c\frac{s-2}{s+2} \tag{3.6}$$

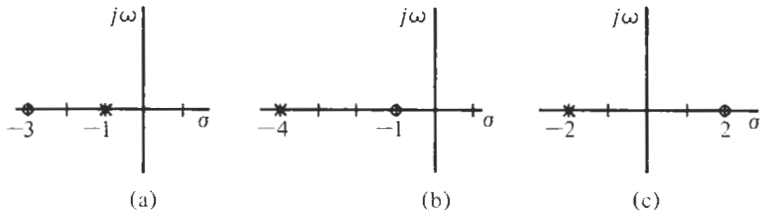

Figure 3.1 Pole-zero plots corresponding to Eq. (3.6). Poles are crosses (×); zeros are circles (○).

It should be clear from the examples that specifying the poles and zeros does not specify the constants K_i. We also pointed out in Chapter 1 that filter designers normally evaluate the transfer function on the $j\omega$-axis,

$$T(j\omega) = \frac{N(j\omega)}{D(j\omega)} = K\frac{j\omega + z_1}{j\omega + p_1} \tag{3.7}$$

This is a complex number that we can split into its real and imaginary parts,

$$T(j\omega) = \text{Re}\,T(j\omega) + j\,\text{Im}\,T(j\omega) \tag{3.8}$$

Alternatively, and used much more frequently, we can employ polar coordinates and split $T(j\omega)$ into magnitude and phase,

$$T(j\omega) = |T(j\omega)|\,e^{j\theta(\omega)} \tag{3.9}$$

as we did in Eq. (1.5). The magnitude provides information on the gain (or loss) of the filter as a function of frequency [see Eq. (1.7)] and the phase tells us how much the phase of a sinusoidal signal was shifted from input to output [see Eq. (1.8)]. Although we need both forms, ordinarily we will deal in magnitude and phase information in the design of filters. The relationships between real and imaginary parts and magnitude and phase are familiar from elementary studies. They are

$$|T(j\omega)| = \sqrt{[\text{Re}\,T(j\omega)]^2 + [\text{Im}\,T(j\omega)]^2} \tag{3.10}$$

and

$$\theta(\omega) = \tan^{-1}\left[\frac{\text{Im}\,T(j\omega)}{\text{Re}\,T(j\omega)}\right] \tag{3.11}$$

Although these equations are correct, they are often inconvenient to evaluate in our study of active filters, where the transfer function is always a ratio of two complex numbers. [$N(j\omega)$ and $D(j\omega)$ are themselves complex.] To develop more suitable expressions, we return to Eq. (3.7) and write instead of Eq. (3.8)

$$T(j\omega) = \frac{\text{Re}\,N(j\omega) + j\,\text{Im}\,N(j\omega)}{\text{Re}\,D(j\omega) + j\,\text{Im}\,D(j\omega)} \tag{3.12}$$

We then make use of the fact that

$$T(j\omega) = \frac{|N(j\omega)|\, e^{j\theta_N(\omega)}}{|D(j\omega)|\, e^{j\theta_D(\omega)}} = \left|\frac{N(j\omega)}{D(j\omega)}\right| e^{j[\theta_N(\omega)-\theta_D(\omega)]} \tag{3.13}$$

i.e., we note that "the magnitude of a ratio of two complex numbers is equal to the ratio of their magnitudes" and "the phase angle of a ratio of two complex numbers is equal to the difference of their phases." These obvious and well-known facts will make our computations much simpler. Thus, using Eq. (3.13) leads to the magnitude

$$|T(j\omega)| = \frac{\sqrt{[\mathrm{Re}\, N(j\omega)]^2 + [\mathrm{Im}\, N(j\omega)]^2}}{\sqrt{[\mathrm{Re}\, D(j\omega)]^2 + [\mathrm{Im}\, D(j\omega)]^2}} \tag{3.14}$$

and the phase

$$\theta(\omega) = \theta_N(\omega) - \theta_D(\omega) = \tan^{-1}\left[\frac{\mathrm{Im}\, N(j\omega)}{\mathrm{Re}\, N(j\omega)}\right] - \tan^{-1}\left[\frac{\mathrm{Im}\, D(j\omega)}{\mathrm{Re}\, D(j\omega)}\right] \tag{3.15}$$

3.2 REALIZATION WITH PASSIVE ELEMENTS

Let us now contemplate how the bilinear function of Eq. (3.2) and its various special cases can be realized with passive components. To this end consider the voltage divider in Fig. 3.2. It is characterized by impedances, phasor voltages, and currents. The analysis follows well-known elementary procedures. If $I_2 = 0$, we have

$$V_1 = (Z_1 + Z_2)I \quad \text{and} \quad V_2 = Z_2 I \tag{3.16}$$

then, with $Y = 1/Z$,

$$\frac{V_2}{V_1} = T(s) = \frac{Z_2}{Z_1 + Z_2} = \frac{Y_1}{Y_1 + Y_2} \tag{3.17}$$

an equation that could also have been written directly by voltage division. Remembering that we do not wish to use inductors, we can use the simple *RC* circuit in Fig. 3.3. With $G_i = 1/R_i$, we see that

$$Y_1 = G_1 + sC_1 \quad \text{and} \quad Y_2 = G_2 + sC_2 \tag{3.18}$$

so that the transfer function (3.17) becomes

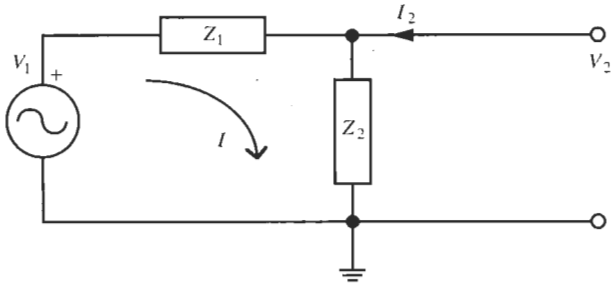

Figure 3.2 Passive voltage divider to realize a bilinear function.

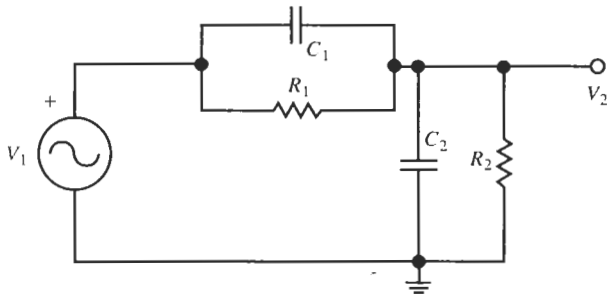

Figure 3.3 *RC* voltage divider to realize Eq. (3.4).

$$T(s) = \frac{sC_1 + G_1}{s(C_1 + C_2) + G_1 + G_2} \tag{3.19}$$

Clearly, it is a bilinear expression with real coefficients as required. If we bring this equation into the form of Eq. (3.4),

$$T(s) = \frac{C_1}{C_1 + C_2} \frac{s + G_1/C_1}{s + (G_1 + G_2)/(C_1 + C_2)} = K\frac{s + z_1}{s + p_1} \tag{3.20}$$

we see that the zero and the pole for the circuit in Fig. 3.3 are located at

$$s = z_1 = -\frac{G_1}{C_1} = -\frac{1}{R_1C_1} \tag{3.21a}$$

$$s = p_1 = -\frac{G_1 + G_2}{C_1 + C_2} = -\frac{1}{[R_1R_2/(R_1 + R_2)](C_1 + C_2)} \tag{3.21b}$$

Observe that pole and zero have units of $1/time$, i.e., they are frequencies set by *RC* time constants. We will find that this is always the case. Also note that pole and zero are on the negative real axis as we predicted because the coefficients of Eq. (3.20) are positive, and further that we may have $z_1 < p_1$ or $z_1 > p_1$ depending on how the element values are chosen. Equation (3.20) is, therefore, a relatively general bilinear function with only few restrictions on possible pole-zero locations. Observe, for example, that we cannot realize a pole at the origin, $s = 0$, because that requires $G_1 = G_2 = 0$, or equivalently $R_1 = R_2 = \infty$, which reduces the circuit to a capacitive voltage divider with no pole or zero

$$T(s) = K = \frac{C_1}{C_1 + C_2}$$

There are many ways in which we can select components to implement different bilinear functions. Some of them will be considered in the Problems at the end of the chapter. Here, consider the circuit in Fig. 3.4, a special case of the circuit in Fig. 3.3 where C_1 and G_2 are removed (have zero values). By direct analysis, or from Eq. (3.19), we obtain

$$T(s) = \frac{G_1}{sC_2 + G_1} = \frac{1}{sC_2R_1 + 1} \tag{3.22}$$

Although Eq. (3.22) is not a very good approximation of the ideal, so-called *brick wall*, lowpass characteristic of Fig. 1.2a, it is intuitively clear that the circuit in Fig. 3.4 is a lowpass

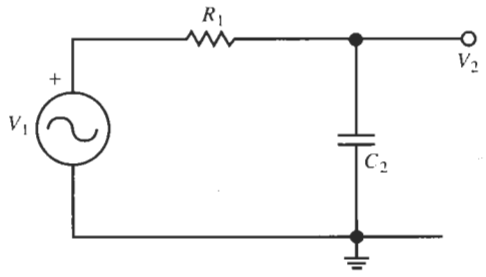

Figure 3.4 First-order RC lowpass filter.

filter. We note that at low frequencies, the capacitive impedance $|Z_2(j\omega)| = 1/\omega C_2$ is large so that low-frequency signals get through to the output, whereas at higher frequencies the capacitor increasingly shorts out the signal and the output voltage $|V_2|$ decreases. $T(s)$ reflects these facts.

EXAMPLE 3.1

Compute magnitude, phase, pole, and zero of $T(s)$ in Eq. (3.22). Assume $R_1 = 12$ kΩ and $C_2 = 100$ nF.

Solution

The pole is obtained directly from Eq. (3.22), or from Eq. (3.21b) with $C_1 = G_2 = 0$, as

$$p_1 = -\omega_c = -\frac{1}{R_1 C_2} = -\frac{1}{12{,}000 \times 10^{-7}\text{s}} = -833.3 \text{ rad/s}$$

and the zero is at $z_1 = \infty$. Using Eq. (3.14), the magnitude of Eq. (3.22) is computed as

$$|T(j\omega)| = \frac{1}{\sqrt{1 + (\omega C_2 R_1)^2}} = \frac{1}{\sqrt{1 + (\omega/\omega_c)^2}} \tag{3.23}$$

and the phase follows from Eq. (3.15):

$$\theta(\omega) = -\tan^{-1}(\omega C_2 R_1) = -\tan^{-1}(\omega/\omega_c) \tag{3.24}$$

Taking the natural logarithm of Eq. (3.9) enables us to separate magnitude and phase information of the transfer function $T(s)$,

$$\ln T(j\omega) = \ln|T(j\omega)| + j\theta(\omega) \tag{3.25}$$

We will make separate plots of the two parts of this equation. Customarily, however, not the natural logarithm is plotted but the base-10 logarithm and it is multiplied by 20. This quantity,

$$\alpha(\omega) = 20 \log|T(j\omega)| \text{ dB} \tag{3.26}$$

is labeled in dB (decibel) as in Eq. (1.10). The phase function is usually plotted in degrees, less frequently in radians. There are different coordinates that can be used to plot magnitude and phase. The scales we will use most often are those depicted in Fig. 3.5a and b.

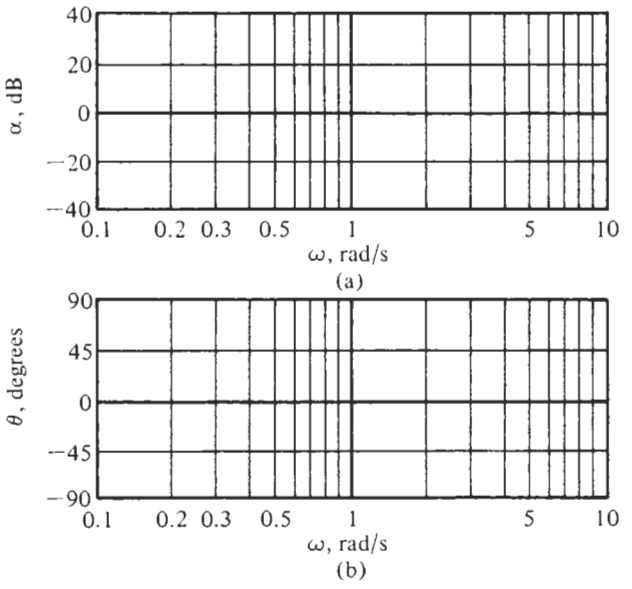

Figure 3.5 The customary magnitude (a) and phase (b) coordinates for Bode plots.

EXAMPLE 3.2

Plot magnitude and phase of the first-order lowpass $T(s)$ of Eq. (3.22).

Solution

Expressions for both magnitude and phase were found in Eqs. (3.23) and (3.24) of Example 3.1. It is an easy matter to plot these two simple functions versus frequency. Let us again use the abbreviation $C_2R_1 = 1/\omega_c$ so that

$$|T(j\omega)| = \frac{1}{\sqrt{1 + (\omega/\omega_c)^2}} \quad \text{and} \quad \theta(\omega) = -\tan^{-1}(\omega/\omega_c) \tag{3.27}$$

and use linear scales. The result is shown in Fig. 3.6. Observe that at $\omega = \omega_{-3\text{ dB}} = \omega_c$, $|T|$ is reduced to the value $|T(j\omega_c)| = |T(0)|/\sqrt{2}$, and the phase equals $\theta(\omega_c) = -\tan^{-1} 1 = -45°$. As was pointed out in Chapter 1, this is the half-power frequency where the voltage is reduced by 3 dB and the power delivered to the output by the source is reduced to one-half the power available at $s = 0$. By convention, the half-power frequency is often referred to as the bandwidth or also as the *cut-off* frequency of the filter. Note still that the phase of this lowpass is negative for all frequencies.

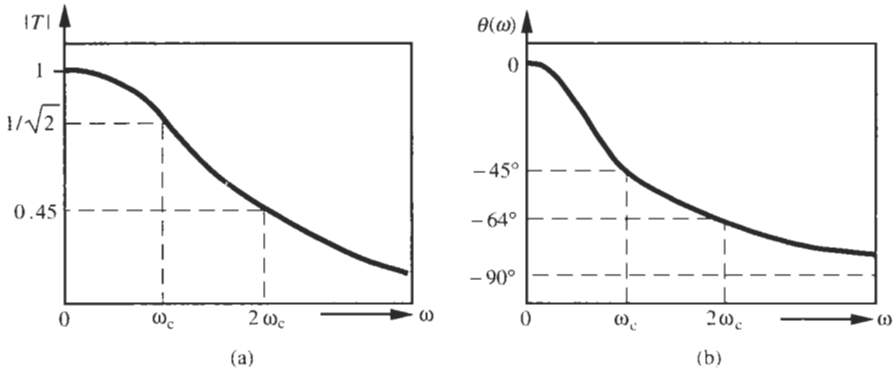

Figure 3.6 Magnitude (a) and phase (b) of the first-order lowpass function of Eq. (3.22).

Filters whose phase is always negative are labeled *lag* filters because the output lags the input in time. In contrast, filters whose phase is positive are called *lead* filters. To clarify this result let us assume that the input voltage of a filter, in sinusoidal as well as phasor representation, is

$$v_1(t) = V_1 \sin \omega t, \quad V_1 = |V_1| \angle 0 \tag{3.28}$$

and its output voltage

$$v_2(t) = V_2 \sin(\omega t + \theta), \quad V_2 = |V_2| \angle \theta \tag{3.29}$$

The transfer function relating these two voltages would be

$$T(j\omega) = \frac{|V_2| \angle \theta}{|V_1| \angle 0} = \left| \frac{V_2}{V_1} \right| \angle \theta = |T(j\omega)| e^{j\theta} \tag{3.30}$$

Then we say that v_2 *leads* v_1 if the phase is positive, $\theta > 0$, and T is a lead filter; otherwise v_2 *lags* v_1 and T is a lag filter. A graphic interpretation is shown in the time-domain diagram in Fig. 3.7. A more intuitive explanation of the terms "leading" and "lagging" can be obtained

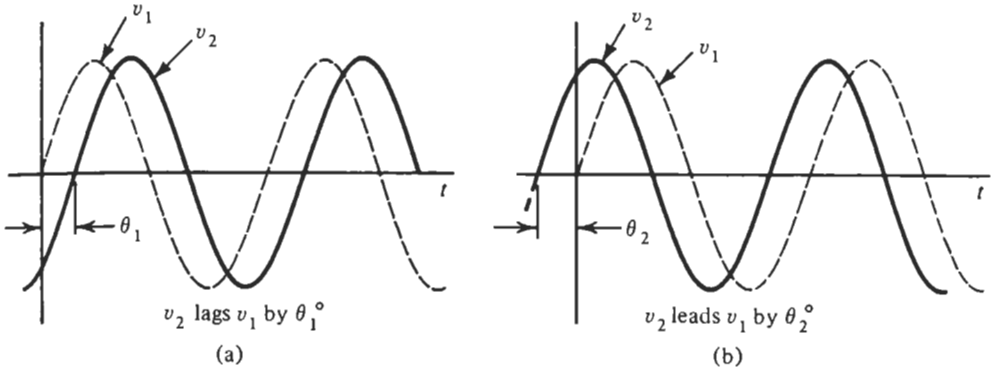

Figure 3.7 Illustration of (a) lagging and (b) leading phase in the time domain.

from the phasor diagram in Fig. 3.8. We see that V_2 *leads* V_1 as the two phasors rotate around the origin with angular velocity ωt if $\theta > 0$. If $\theta < 0$, V_2 lags V_1.

An example of a lead filter is obtained from the circuit in Fig. 3.3 with $C_2 = 0$ and $R_1 = \infty$. Figure 3.9 shows the circuit. The transfer function is obtained by voltage division or from Eq. (3.19) as

$$T(s) = \frac{sC_1}{sC_1 + G_2} = \frac{sC_1R_2}{sC_1R_2 + 1} \tag{3.31}$$

Let us define again the RC product as the frequency $\omega_c = 1/(C_1R_2)$ and evaluate T on the $j\omega$-axis,

$$T(j\omega) = \frac{j\omega/\omega_c}{1 + j\omega/\omega_c} \tag{3.32}$$

Then the magnitude and phase of Eq. (3.32) are

$$|T(j\omega)| = \frac{\omega/\omega_c}{\sqrt{1 + (\omega/\omega_c)^2}} \quad \text{and} \quad \theta(\omega) = \frac{\pi}{2} - \tan^{-1}\left(\frac{\omega}{\omega_c}\right) \tag{3.33}$$

In spite of the poor approximation of the ideal highpass characteristic in Fig. 1.2b, the function is recognized as a highpass because $|T(j\omega)|$ is small at low frequencies and approaches the value $|T(j\omega)| = 1$ as $\omega \to \infty$. The shape of the phase function is the same as that of the lowpass [Eq. (3.27)], except that a constant 90° is added. Figure 3.10 shows plots of Eq. (3.33).

At this point let us go through a design example to practice some of the points we discussed.

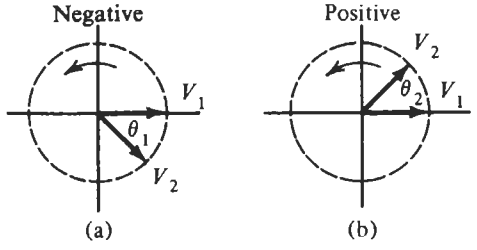

Figure 3.8 Illustration of (a) lagging and (b) leading phase in the phasor domain.

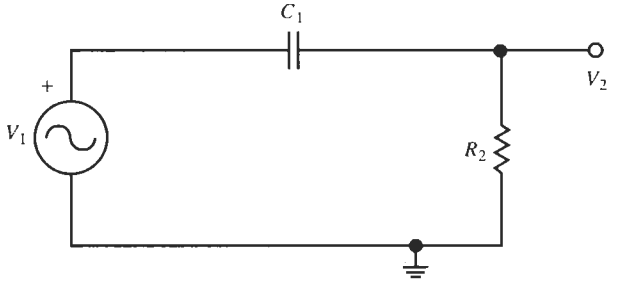

Figure 3.9 A first-order highpass filter.

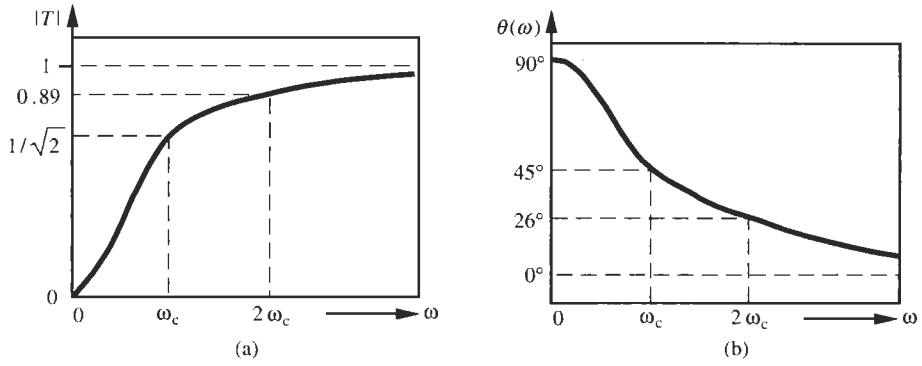

Figure 3.10 Magnitude (a) and phase (b) of the highpass circuit in Fig. 3.9.

EXAMPLE 3.3

Design a first-order passive highpass filter such that its dc gain $T(0) = 0.3$ and the gain at high frequencies is equal to $T(\infty) = 1$. The filter must have a zero on the negative real axis at $f_z = -159$ Hz. Plot the magnitude and phase of the filter.

Solution

To solve this problem we observe first that the simple highpass circuit in Fig. 3.9 will not work because its gain at the origin is zero. We consult, therefore, the more general circuit in Fig. 3.3 and Eq. (3.19), which indicates that we must set $C_2 = 0$ because of the requirement $T(\infty) = 1$. The resulting circuit is shown in Fig. 3.11. The circuit realizes, from Eq. (3.19),

$$T(s) = \frac{V_2}{V_1} = \frac{sC_1 + G_1}{sC_1 + G_1 + G_2} = \frac{s + G_1/C_1}{s + (G_1 + G_2)/C_1} \tag{3.34}$$

At dc the function equals

$$T(0) = \frac{G_1}{G_1 + G_2} = \frac{R_2}{R_1 + R_2} \tag{3.35}$$

and it has a zero at

$$z_1 = -\frac{G_1}{C_1} = -\frac{1}{R_1 C_1} \tag{3.36a}$$

which is required to be located at -159 Hz, i.e., at

$$z_1 = -2\pi \times 159 \text{ Hz} \approx -1000 \text{ s}^{-1} = -\frac{1}{R_1 C_1} \tag{3.36b}$$

We have three components but only two specific requirements, f_z and $T(0)$, so that one element may be chosen freely. Let us pick $C_1 = 1\ \mu$F, which from Eq. (3.36b) leads directly to $R_1 = 1$ kΩ. The second resistor is computed from Eq. (3.35): We find

$$T(0) = 0.3 = \frac{R_2}{R_1 + R_2} = \frac{1}{1 + R_1/R_2} \quad \text{or} \quad \frac{R_1}{R_2} = \frac{1}{0.3} - 1 = 2.33$$

resulting in $R_2 = R_1/2.33 \approx 429\ \Omega$. We still note that the function (3.34) has a pole at

$$p_1 = -\frac{G_1 + G_2}{C_1} = -\frac{1}{C_1}\left(\frac{1}{R_1} + \frac{1}{R_2}\right) = -10^6\left(10^{-3} + \frac{10^{-3}}{0.429}\right)\ \text{s}^{-1} \approx -3.33\ \text{ks}^{-1}$$

which is larger, that is more negative, than the zero. The final transfer function is

$$T(j\omega) = \frac{j\omega + 1000}{j\omega + 3330} = \frac{1 + j(\omega/1000)}{3.33 + j(\omega/1000)} \tag{3.37}$$

where for convenience we have scaled the frequency by $1000\ \text{s}^{-1}$. With Eqs. (3.14) and (3.15) we find the magnitude and phase of Eq. (3.37) as follows:

$$|T(j\omega)| = 0.3\sqrt{\frac{1 + (\omega/1000)^2}{1 + 0.09(\omega/1000)^2}} \tag{3.38a}$$

$$\theta(\omega) = \theta_z - \theta_p = \tan^{-1}\frac{\omega}{1000} - \tan^{-1}\frac{\omega/1000}{3.33} \tag{3.38b}$$

Plots of these two equations are shown in Fig. 3.12. It is worthwhile to point out the construction of the phase curve: The two solid curves in Fig. 3.12b are θ_z and $-\theta_p$, drawn in a fashion analogous to Fig. 3.6b. The final dashed phase curve is simply a graphic addition of $\theta_z + (-\theta_p)$. Since $\theta > 0$, we recognize the circuit as a lead filter.

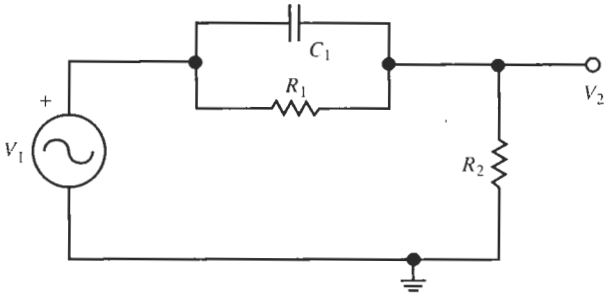

Figure 3.11 Highpass circuit for Example 3.3.

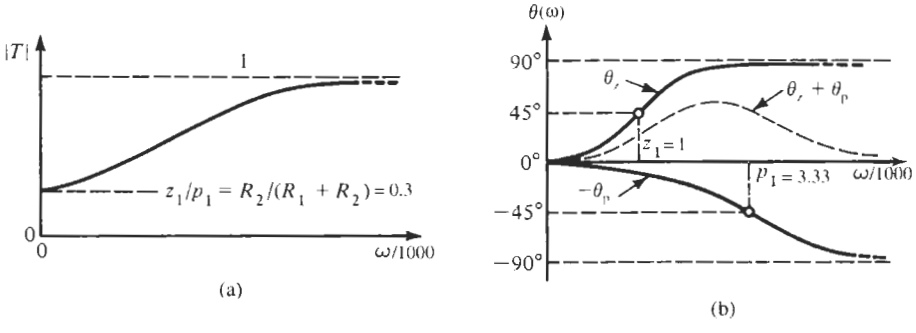

Figure 3.12 (a) Magnitude and (b) phase of the circuit in Fig. 3.11. Notice the scaled frequency axes.

It is clear from Eq. (3.19) that the circuit in Fig. 3.3 can realize only transfer functions with positive coefficients. If we want to implement Eq. (3.2) with a negative coefficient in the numerator, such as T_c in Eq. (3.6), we need to consider a different circuit configuration that can generate a minus sign. The circuit in Fig. 3.13a is a suitable structure that has a different (nonplanar) appearance from those considered earlier. It is known as a *lattice*. An equivalent form in which it may appear is shown in Fig. 3.13b. In this form it is known as a *bridge* circuit and is simpler to analyze. We will often find it convenient to redraw a circuit in a form where the structure becomes easier for the analysis. Proceeding thus with Fig. 3.13b, we observe that the output voltage is the difference of the voltages at nodes A and B,

$$V_2 = V_A - V_B \tag{3.39}$$

where clearly, with equal resistors,

$$V_A = \frac{V_1}{2}$$

The other voltage, V_B, comes directly from Eq. (3.31):

$$V_B = \frac{sCR}{sCR + 1} V_1 \tag{3.40}$$

Substituting these two results into Eq. (3.39), we have

$$V_2 = \left(\frac{1}{2} - \frac{sCR}{sCR + 1}\right) V_1 = \frac{1}{2} \frac{1 - sCR}{1 + sCR} V_1 \tag{3.41}$$

The pole-zero description of this equation is shown in Fig. 3.14a where we have let $RC = 1/\omega_c$. Notice that the function has a zero in the right half-plane and a pole in the left half-plane, both on the real axis, and with equal distances from the origin. If we let $s = j\omega$, the magnitude function becomes

$$|T(j\omega)| = \frac{1}{2} \frac{|1 - j\omega/\omega_c|}{|1 + j\omega/\omega_c|} \tag{3.42}$$

Observe next that the numerator and denominator have identical magnitudes so that

$$|T(j\omega)| = \frac{1}{2} \quad \text{for all } \omega \tag{3.43}$$

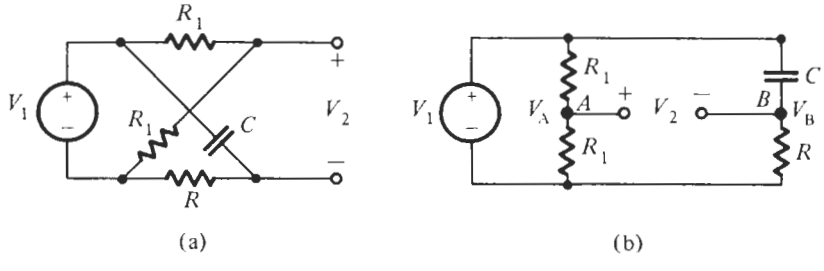

Figure 3.13 (a) Lattice or (b) bridge circuit to realize a right half-plane zero.

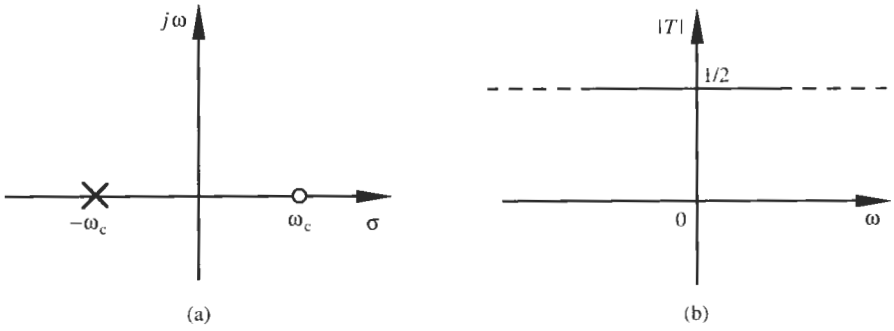

Figure 3.14 (a) Pole-zero plot of the allpass characteristic in Eq. (3.41); (b) magnitude of allpass characteristics in Eq. (3.42).

The only apt description of this characteristic, shown in Fig. 3.14b, is *allpass*, and the concept of a cut-off frequency has no meaning. A circuit having this characteristic is known as an *allpass filter*.

The student may well wonder at this point what good such a circuit is and why it is not simply replaced by a resistive voltage divider, such as in the left branch of Fig. 3.13b. The answer is that an allpass filter provides frequency-dependent phase shift without changing the magnitude. For instance, we can find from Eq. (3.41)

$$\theta(\omega) = -2\tan^{-1}(\omega CR) = -2\tan^{-1}(\omega/\omega_c) \tag{3.44}$$

Notice that the allpass filter has twice the phase of the lowpass filter in Eq. (3.27). Allpass filters are important in many communications applications where they are used as phase equalizers for transmission channels, a topic we will study in more detail in Chapters 10 and 11.

Table 3.1 presents the different types of bilinear transfer functions, their pole-zero patterns, and their magnitude and phase responses. Many of these first-order functions can be realized by the circuits in Fig. 3.3 or 3.13, but some pole-zero patterns, such as the integrator K/s, cannot be implemented with passive circuits. Although "a capacitor is an integrator," $Z_C = 1/(sC)$,[1] it is an impedance and not a transfer function. Also, passive implementations of bilinear functions have another problem: they cannot be loaded without destroying the transfer function. For example if we need to develop the output voltage V_2 of the lowpass filter in Fig. 3.4 across a prescribed load resistor R_L, such as in Fig. 3.15, we would seriously alter the behavior of the filter. Using voltage division or Eq. (3.19), the transfer function of this circuit is readily derived as

$$T(s) = \frac{G_1}{G_1 + G_L + sC_2} = \frac{G_1}{G_1 + G_L}\frac{1}{sC_2/(G_1 + G_L) + 1} \tag{3.45}$$

Comparing this expression with the nominal lowpass filter function (3.22) with $G_L = 0$ shows that not only has the dc gain $T(0)$ changed, but, what is more important and generally more

[1] We shall make use of this interpretation of a capacitor's function later when we develop active simulations of high-order filters.

TABLE 3.1

$T_n(s)$[a]	Pole and Zero	Magnitude Response	Phase Response
$\frac{K_1}{s}$	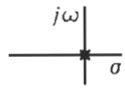	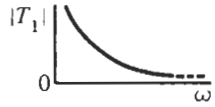	
$K_2 s$			
$\frac{K_3}{s+p_1}$	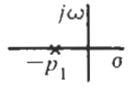		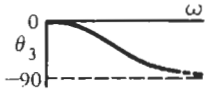
$K_4(s+z_1)$	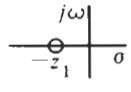	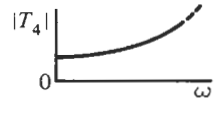	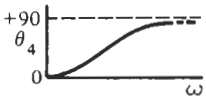
$K_5\frac{s+z_1}{s+p_1}$	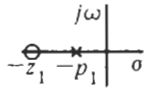	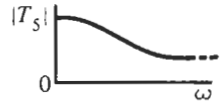	
$K_6\frac{s}{s+p_1}$	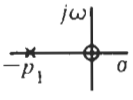	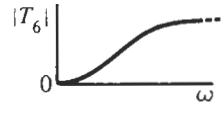	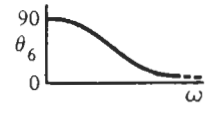
$K_7\frac{s+z_1}{s+p_1}$	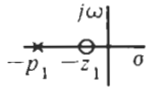	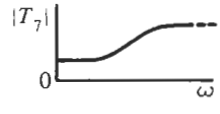	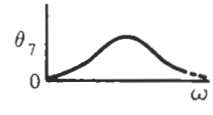
$K_8\frac{s-\sigma_1}{s+\sigma_1}$	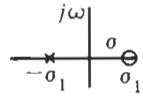	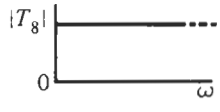	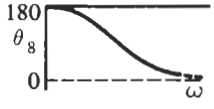

[a] All K_j are assumed positive.

troublesome, the pole position has shifted. This means that the 3-dB frequency has increased from $1/(R_1C_2)$ to $(1 + R_1/R_L)/(R_1C_2)$ as you can show from Eq. (3.45). Such shifts in a filter's poles (and zeros) are normally not acceptable because the specified transmission behavior is destroyed. An additional problem for some applications is that zeros and poles are not independently adjustable or *tunable*. Assume, for example, that z_1 and p_1 of the circuit in Fig. 3.3 have been designed as per specifications, but that after fabrication the zero turned out to be incorrect because of component tolerances. Thus, the zero must be tuned by adjusting either R_1 or C_1. Now note from Eq. (3.21) that varying the components R_1 and C_1 to set the correct z_1 will always adjust p_1 as well so that iterative tuning of parameters is normally necessary.

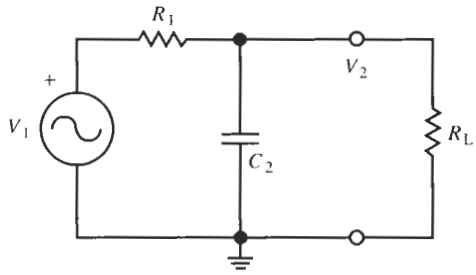

Figure 3.15 The lowpass filter of Fig. 3.4 with a load resistor R_L.

For these reasons we are motivated to look for other ways to implement first-order filters. We shall find that using operational amplifiers in the design will help solve all three difficulties: arbitrary sets of real-axis poles and zeros can be realized, loading effects are minimized, and poles and zeros may be independently adjusted. Consequently, active *RC* realizations will be discussed in Section 3.4. First, though, let us look in more detail at the customary method of representing the transfer function graphically: the *Bode plot*.

3.3 BODE PLOTS

We will find it most convenient when describing filter requirements to use a graphic representation. Filter behavior is normally specified over very wide ranges of frequency, for example, over the frequency range 100 Hz $\leq f \leq$ 10 MHz, that is, five orders of magnitude. Similarly, the required gain (or loss) performance is prescribed over wide ranges of gain (or loss), for example, $100 \geq K \geq 0.0001$, that is, six orders of magnitude. To be able to picture these ranges graphically without losing all detail at the extremes, engineers have long used logarithmic plots. As pointed out in Chapter 1, Eq. (1.10), or in Eq. (3.26), the magnitude is customarily represented by the logarithmic measure

$$\alpha(\omega) = 20 \log |T(j\omega)| \text{ dB} \tag{3.46}$$

and is plotted versus ω on a logarithmic scale. Similarly, the phase in degrees is plotted versus $\log(\omega)$. The axes were shown in Figs. 3.5a and b. The plots of magnitude and phase characteristics on these coordinates are referred to as *Bode plots* after Hendrik Bode.[2] Observe that both sets of coordinates identify *semilog* plots, i.e., the abscissas have linear scales, but note that $\alpha(\omega)$ is a logarithmic measure, even if plotted on a linear scale. Let us demonstrate on a specific example, the first-order function discussed in this chapter, how a Bode plot is generated. We start from the transfer function of Eq. (3.7), evaluated on the $j\omega$-axis,

$$T(j\omega) = \frac{N(j\omega)}{D(j\omega)} = K\frac{j\omega + z_1}{j\omega + p_1} = K\frac{z_1}{p_1}\frac{1 + j\omega/z_1}{1 + j\omega/p_1} \tag{3.47}$$

We are interested in plotting magnitude and phase of $T(j\omega)$ versus logarithmic coordinates. The magnitude function of Eq. (3.47) is

[2] Hendrik Bode (pronounced *boh dah*) grew up in Urbana, Illinois, and spent most of his professional life at Bell Laboratories. After his retirement from Bell Labs, he became a professor at Harvard University.

$$T(j\omega) = \left| K \frac{z_1}{p_1} \right| \frac{|1 + j\omega/z_1|}{|1 + j\omega/p_1|} \tag{3.48}$$

From this we see that $\alpha(\omega)$, defined in Eq. (3.46), is

$$\alpha(\omega) = 20 \log \left| K \frac{z_1}{p_1} \right| + 20 \log \left| 1 + \frac{j\omega}{z_1} \right| - 20 \log \left| 1 + \frac{j\omega}{p_1} \right| \tag{3.49}$$

and the phase function is

$$\theta(\omega) = \theta_K + \tan^{-1}\left(\frac{\omega}{z_1}\right) - \tan^{-1}\left(\frac{\omega}{p_1}\right) \tag{3.50}$$

where $\theta_K = 0°$ or $180°$ depending on whether $K > 0$ or $K < 0$. The first term in Eq. (3.49) is a constant; the second and third terms are similar, except for the sign. We will first study the second term and then consider the others in Eq. (3.49). It is

$$\alpha_2(\omega) = 20 \log \left| 1 + \frac{j\omega}{z_1} \right| \tag{3.51}$$

or, since z_1 is real,

$$\alpha_2(\omega) = 20 \log \sqrt{1 + \left(\frac{\omega}{z_1}\right)^2} = 10 \log \left[1 + \left(\frac{\omega}{z_1}\right)^2 \right] \tag{3.52}$$

We gain insight into the form of $\alpha(\omega)$ if we consider the low-frequency and high-frequency asymptotes. When $\omega \ll z_1$, then

$$\alpha_2(\omega) = 20 \log(1) = 0 \text{ dB} \tag{3.53}$$

At high frequencies, when $\omega \gg z_1$, the 1 in Eq. (3.52) can be neglected, and we obtain

$$\alpha_2(\omega) = 20 \log \left(\frac{\omega}{z_1}\right) \tag{3.54}$$

This is the equation of a straight line in Bode coordinates, i.e., plotted versus $\log(\omega)$. To describe this line we make a number of observations. First we see that $\alpha_2 = 0$ when $\omega = z_1$. We also see that the straight line has a positive slope. What is this slope, and how can it be described? Note that if the frequency increases by a factor of 10, i.e., if $\omega \to 10\omega$, we find from Eq. (3.54)

$$\alpha_2(10\omega) = 20 \log \left(\frac{10\omega}{z_1}\right) = 20 \log 10 + 20 \log \left(\frac{\omega}{z_1}\right) = 20 + \alpha_2(\omega) \text{ dB}$$

Thus, for each increase in frequency by a factor of 10, the attenuation increases by 20 dB. The slope of the straight line is 20 dB per decade of frequency. This result is easy to generalize. If frequency increases by several, say n, factors of 10, the attenuation increases by $20n$ dB:

$$\alpha_2\left(10^n \omega\right) = 20n \log 10 + 20 \log \left(\frac{\omega}{z_1}\right) = 20n + \alpha_2(\omega) \text{ dB} \tag{3.55}$$

Alternatively, we see that for each increase in frequency by a factor of two the attenuation increases by $\log 2 = 6.0206n$ dB, and by $\log 2^n = 6.0206n$ dB for increases by a factor of 2^n:

$$\alpha_2(2^n\omega) = 20 \log\left(\frac{2^n\omega}{z_1}\right) = 20n \log 2 + 20 \log\left(\frac{\omega}{z_1}\right) = 6.02n + \alpha_2(\omega) \text{ dB} \quad (3.56)$$

The exact value 6.02... dB is customarily rounded down to 6 dB. Doubling the frequency is referred to as increasing it by an *octave*. Thus we see that the slope of the straight line in Eq. (3.54) can be described by either

$$\frac{6 \text{ dB}}{\text{octave}} \quad \text{or} \quad \frac{20 \text{ dB}}{\text{decade}} \quad (3.57)$$

The line that we just described is shown in Fig. 3.16. We observe that if the low-frequency asymptote of 0 dB is extended, it intersects the high-frequency asymptote at the frequency $\omega = z_1$. These two asymptotes constitute the asymptotic plot of Eq. (3.52).

For many applications the asymptotic plot alone will suffice. If we require accuracy, then a plot may be made using Eq. (3.52). The equation is well suited for use of a calculator. However, for a simple though approximate method of plotting the actual curve, the following steps may be taken:

1. Plot the straight-line asymptotes, as in Fig. 3.16.
2. The difference between the actual and the asymptotic curves will be as follows:
   a. At z_1 (called the *break frequency*) the difference is 3 dB.
   b. One octave above and one octave below the break frequency, the difference is 1 dB.

These three points allow you to rough in the actual response with fair accuracy. This is summarized in Fig. 3.17.

Now let us return to Eq. (3.49) and compare the second and third terms. The second

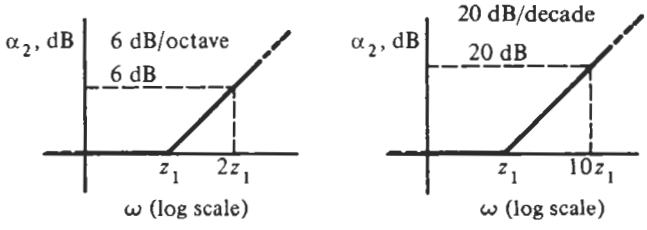

Figure 3.16 Asymptotic straight lines representing Eq. (3.52).

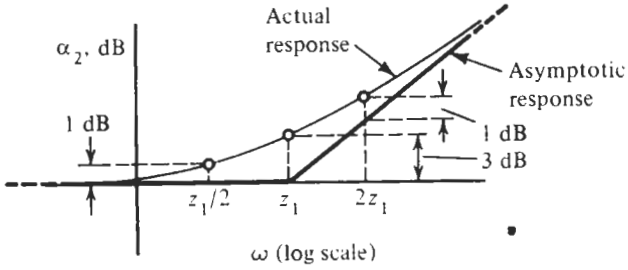

Figure 3.17 Constructing the actual response from the asymptotes of a zero term.

involves z_1, whereas the third involves p_1, but these are simply break frequencies as identified in Fig. 3.16. The significant difference is the sign, which is negative. This simply means that the slope of the high-frequency asymptotic curve will be negative, as shown in Fig. 3.18. Otherwise everything that has been described for the second term applies to the third.

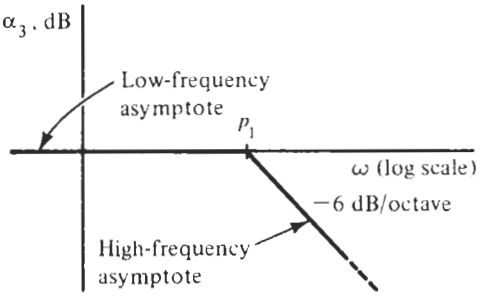

Figure 3.18 Asymptotic Bode plot of a pole term.

EXAMPLE 3.4

Create a Bode plot for the bilinear transfer function

$$T(s) = \left.\frac{s+0.5}{s+3}\right|_{s=j\omega} = \frac{1}{6}\frac{1+j\omega/0.5}{1+j\omega/3} \tag{3.58}$$

Solution

The form of the transfer function indicates that there is a zero at $z_1 = -0.5$ and a pole at $p_1 = -3$. The gain constant equals $K = 1/6$. The Bode plot is generated from

$$\alpha(\omega) = 20\log(1/6) + 10\log\left[1+\left(\frac{\omega}{0.5}\right)^2\right] - 10\log\left[1+\left(\frac{\omega}{3}\right)^2\right] \tag{3.59}$$

and

$$\theta(\omega) = \tan^{-1}\left(\frac{\omega}{0.5}\right) - \tan^{-1}\left(\frac{\omega}{3}\right) \tag{3.60}$$

The last two terms in Eq. (3.59) are plotted in asymptotic form in Fig. 3.19a. Adding these two terms gives the total response in both asymptotic and actual forms as indicated in the figure. The first term in Eq. (3.59), $20\log(1/6) = -15.6$ dB, must be added to the total. The result is shown in Fig. 3.19b. Observe that the response at high frequencies is $T(\infty) = 1$, or 0 dB, as prescribed by Eq. (3.58); the transfer function is that of a highpass. Finally, Fig. (3.19c) shows the phase as plotted from Eq. (3.60). To draw the curve, it helps to remember that the $\tan^{-1}$ curve goes from 0° to 90° and $\tan^{-1}(1) = 45°$; thus, at $\omega = 0.5$ the phase of the first term equals 45°, and at $\omega = 3$ the phase of the second term is −45°. These two points are marked in Fig. 3.19c. The total phase (dashed curve) is simply the sum of the two solid lines.

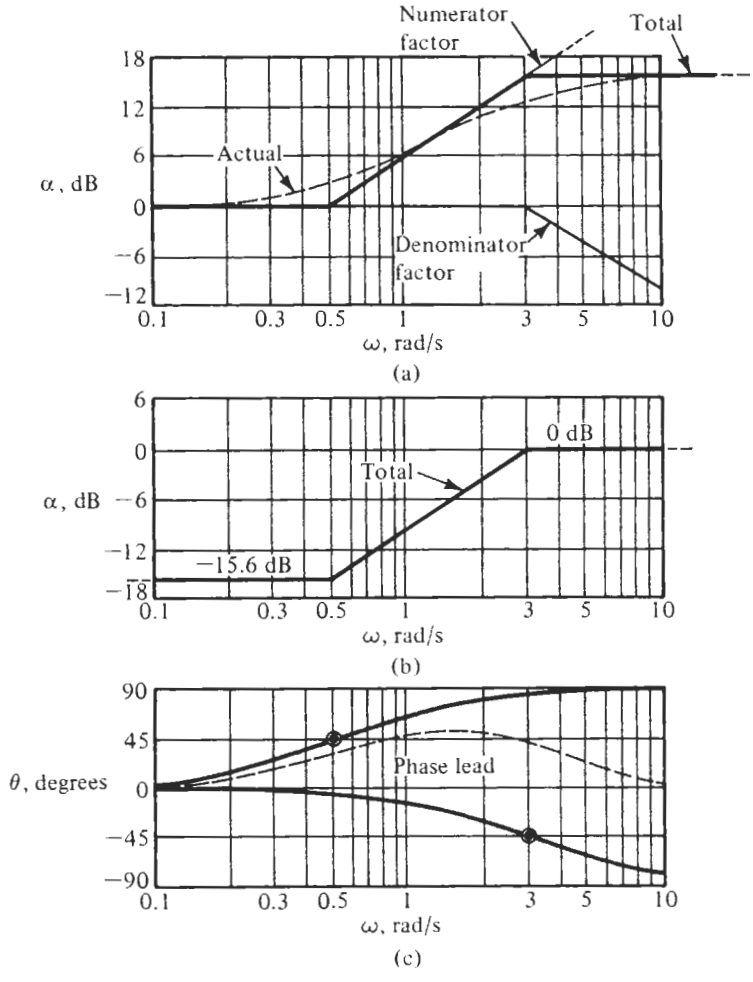

Figure 3.19 Magnitude and phase plots for Eq. (3.58).

Finally we remark that the various plots of the amplifier gains in Chapter 2, Fig. 2.4, are of course, Bode plots of Eq. (2.17). This we can recognize immediately by bringing Eq. (2.17) into the appropriate form displaying the break points (the two poles) and the gain constant:

$$A(j\omega) = \frac{\omega_t}{(j\omega + \omega_a)(1 + j\omega/\omega_c)} = \frac{\omega_t}{\omega_a} \frac{1}{(1 + j\omega/\omega_a)(1 + j\omega/\omega_c)} \tag{3.61}$$

For $\omega \ll \omega_a$ the gain is constant at, for 741-type opamps, $\omega_t/\omega_a \approx 10^6/6 \approx 167{,}000$ or 104 dB as Fig. 2.4a shows. It is 3 dB down at ω_a, and in the range $\omega_a < \omega < \omega_t$ the gain decreases by 20 dB per decade of frequency. Finally, for $\omega > \omega_c$ the attenuation increases at the rate of −40 dB/decade due to the second pole. Note that for $\omega \to \infty$ we have

$$|A(j\infty)| \to \frac{\omega_t \omega_c}{\omega^2} \propto \frac{1}{\omega^2} \tag{3.62}$$

implying a −40-dB/decade roll-off.

In summary, compared to linear plots, Bode plots offer a number of features that will be important in filter design:

1. With frequency plotted on a logarithmic scale, each octave and each decade are equal linear distances, as shown in Fig. 3.20.
2. Using a logarithmic measure for the magnitude of T makes it possible to add and subtract rather than multiply and divide. For example, if

$$T = \frac{T_1 T_2 T_3}{T_4} \tag{3.63}$$

then

$$\alpha_t = \alpha_1 + \alpha_2 + \alpha_3 - \alpha_4 \tag{3.64}$$

just as is the case for angles,

$$\theta_t = \theta_1 + \theta_2 + \theta_3 - \theta_4 \tag{3.65}$$

Figure 3.21 shows how simple it is to add lines to obtain segments of lines for $\alpha_t = \alpha_1 + \alpha_2 + \alpha_3$.

3. The slope of all lines for bilinear functions is ±6 dB per octave or ±20 dB per decade. In the general case all asymptotic lines are integer multiples of these two numbers as shown in Eq. (3.55) and Eq. (3.56).
4. In many applications we deal only with the asymptotic plots without "filling in the corners" to obtain the actual plots. In some sense the asymptotic plots are a short-hand notation with which we can sketch out our design ideas.
5. Because of item 1, the shape of a Bode magnitude plot is maintained when frequency is scaled, as shown by Fig. 3.22. This makes it possible to use templates with these characteristic shapes for magnitude and phase and the template can be moved to the right or left and up or down.
6. The phase angle plots for first-order factors are shown in Figs. 3.19c. These have a different appearance than the linear plots, but there is nothing distinctive about them. As indicated by Eq. (3.65), angle plots are added and subtracted to obtain total angle response.

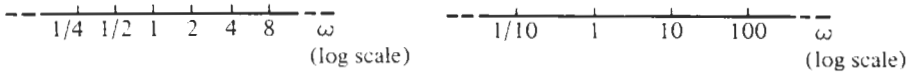

Figure 3.20 Logarithmic frequency axes showing "octaves" and "decades."

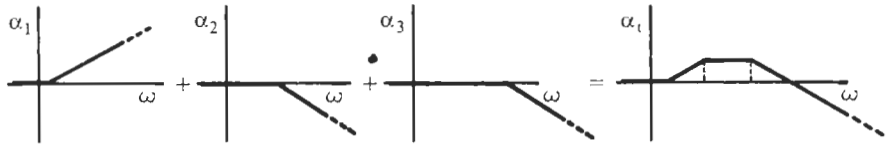

Figure 3.21 Adding asymptotes to obtain the total attenuation.

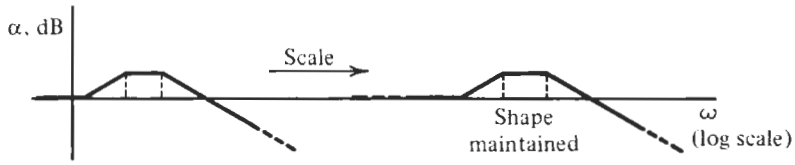

Figure 3.22 Scaling the frequency axis simply shifts the Bode plot.

3.4 ACTIVE REALIZATIONS

3.4.1 Inverting Opamp Circuits

We mentioned at the end of Section 3.2 that passive realizations of the function

$$T(s) = \frac{N(s)}{D(s)} = K\frac{s+z_1}{s+p_1} \tag{3.66}$$

have a number of problems that we proposed to solve with the aid of operational amplifiers. To determine the circuit that might provide a solution, we consult Chapter 2 and notice that the inverting amplifier may be suitable if we replace the resistors by impedances. Figure 3.23 shows the circuit. The analysis of this circuit is no different from its resistive version in Chapter 2. We sum the currents at the inverting input node of the opamp or, for simplicity, consult Eq. (2.55) and replace R_i by Z_i. The result is

$$\frac{V_2}{V_1} = -\frac{Z_2}{Z_1}\frac{1}{1+\dfrac{1}{A(s)}\left(1+\dfrac{Z_2}{Z_1}\right)} = -\frac{Y_1}{Y_2}\frac{1}{1+\dfrac{1}{A(s)}\left(1+\dfrac{Y_1}{Y_2}\right)} \tag{3.67a}$$

On the right-hand side we have used admittances, $Y = 1/Z$, because in the following, as is often the case in active filter work, the treatment will be simpler and more transparent if it is based on admittances. Also, we have included in Eq. (3.67a) the effect on the transfer function of finite and frequency-dependent opamp gain $A(s)$ to remind ourselves that this is a concern we must address. Initially, however, we shall assume $A = \infty$ so that we can focus on the main issues involved in designing first-order circuits. Thus we base our further treatment on

$$T(s) = \frac{V_2}{V_1} \approx -\frac{Z_2}{Z_1} = -\frac{Y_1}{Y_2} \tag{3.67b}$$

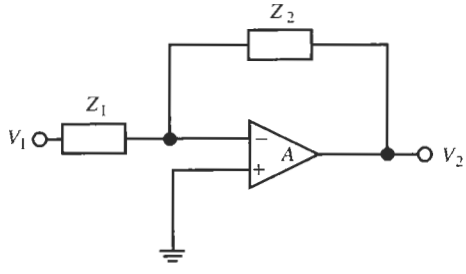

Figure 3.23 Inverting amplifier with impedances in the passive feedback network.

and contemplate how the bilinear function of Eq. (3.66), multiplied, of course, by -1, can be realized by the circuit in Fig. 3.23,

$$T(s) = -\frac{Z_2}{Z_1} = -\frac{Y_1}{Y_2} = -K\frac{s+z_1}{s+p_1} \tag{3.68}$$

The problem to be considered may be formulated in terms of this equation. We assume that the specifications of the design problem are the values K, z_1, and p_1. These may be found from a Bode plot—the break frequencies and the gain at some frequency—or obtained in any other convenient way. The solution to the design problem involves finding a circuit and the elements in that circuit. We will assume that inductors are excluded from our considerations. Hence we need to find the values of the Rs and Cs and their interconnections. Once the components are found, they are adjusted by appropriate frequency scaling and impedance-level scaling as discussed in Chapter 1, Section 4, to obtain convenient element values. Finally, the components may be tuned as necessary to realize the prescribed behavior exactly.

The procedure we will follow requires that some parts of the prescribed right-hand side of Eq. (3.68) be assigned to Y_1 and Y_2. The assignments are not unique, resulting in several different design strategies and circuits. Since inductors are excluded, we must avoid making the identifications $Y = 1/(sL)$ or $Z = sL$. One of several possibilities that suggests itself is to make the admittances linear functions of frequency,

$$Y_1 = sC_1 + G_1 \quad \text{and} \quad Y_2 = sC_2 + G_2 \tag{3.69}$$

to give

$$T(s) = -\frac{Y_1}{Y_2} = -\frac{sC_1 + G_1}{sC_2 + G_2} = -\frac{C_1}{C_2}\frac{s + G_1/C_1}{s + G_2/C_2} \tag{3.70}$$

from which we can identify

$$z_1 = \frac{G_1}{C_1} = \frac{1}{C_1R_1}, \quad p_1 = \frac{G_2}{C_2} = \frac{1}{C_2R_2}, \quad \text{and} \quad K = \frac{C_1}{C_2} \tag{3.71}$$

The circuit is shown in Fig. 3.24. With Eq. (3.71) it is easy to find the component values for a prescribed design.

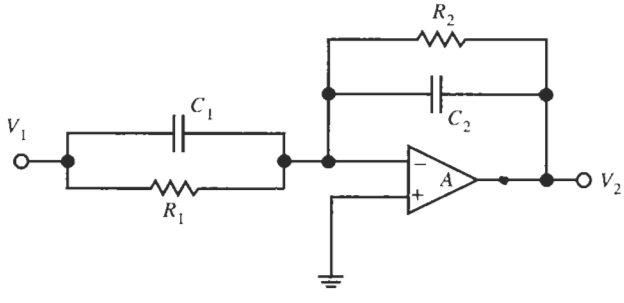

Figure 3.24 Active circuit realizing the bilinear function of Eq. (3.70).

EXAMPLE 3.5

Design a circuit to realize the bilinear transfer function with a zero at $f_z = 830$ Hz, a pole at $f_p = 13$ kHz, and a high-frequency gain of 23 dB.

Solution

On a linear scale, the high-frequency gain corresponds to

$$K = 10^{23/20} = 14.125$$

Thus, the transfer function of the circuit is

$$T(s) = -14.125\frac{s + 2\pi \times 830 \text{ Hz}}{s + 2\pi \times 13{,}000 \text{ Hz}} \tag{3.72}$$

Although the element values could be calculated directly from this equation with the help of Eq. (3.71), let us gain some practice in normalizing equations. If the frequency parameter is scaled by $\omega_S = 2\pi \times 1000$ rad/s, the result is

$$T(s) = -14.125\frac{s_n + 0.83}{s_n + 13} \tag{3.73}$$

where $s_n = s/\omega_S$. We have then, with normalized elements (identified by the subscript n),

$$G_{1n}/C_{1n} = 0.83, \quad G_{2n}/C_{2n} = 13, \quad \text{and} \quad C_{1n}/C_{2n} = 14.125 \tag{3.74}$$

Since we have four elements and only three constraints, we are free to choose one component arbitrarily. Let us select C_1 and determine the remaining elements as functions of C_1:

$$R_{1n} = \frac{1}{0.83C_{1n}}, \quad C_{2n} = \frac{C_{1n}}{14.125}, \quad \text{and} \quad R_{2n} = \frac{1}{13C_{2n}} = \frac{14.125}{13C_{1n}}$$

Letting now $C_1 = 50$ nF $= 0.05$ μF, and recalling that the frequency is normalized by $\omega_S = 2\pi \times 1000$ rad/s, results in

$$R_1 = \frac{1}{2\pi \times 830 \text{ Hz} \times 50 \text{ nF}} = 3.835 \text{ k}\Omega, \quad C_2 = \frac{C_1}{14.125} = 3.54 \text{ nF}$$

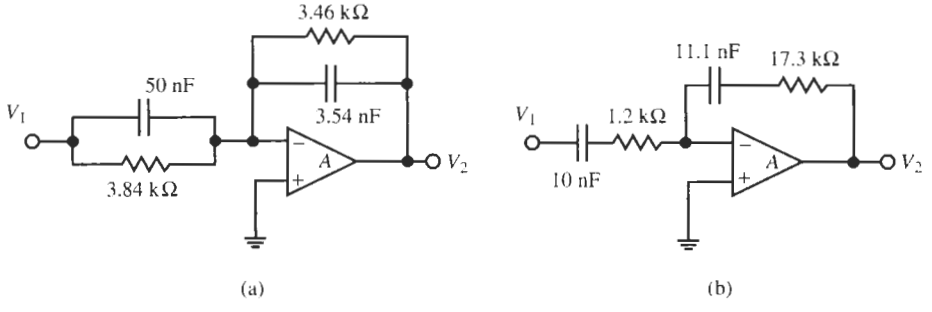

Figure 3.25 Circuit of (a) Example 3.5; (b) Example 3.6. Both circuits realize the same transfer function, Eq. (3.72).

and

$$R_2 = \frac{1}{2\pi \times 13{,}000\ \text{s}^{-1} \times C_2} = 3.458\ \text{k}\Omega$$

We see that at the origin $T(0) = -R_2/R_1 = -0.901$ and at high frequencies $T(\infty) = -C_1/C_2 = -14.125$. The circuit, an (inverting) highpass filter, is shown in Fig. 3.25a.

A comment is appropriate at this point concerning the problems we pointed out at the end of Section 3.2. Observe first that the filter in Fig. 3.23 can be loaded without affecting the transfer function in any substantial way because of the low (ideally zero) output impedance of the opamp. Second, as mentioned, it is clear from Eq. (3.70) that pole and zero can be adjusted independently. Since the zero is provided by $Y_1 = 1/Z_1$ and the pole is given by $Y_2 = 1/Z_2$, varying the zero by R_1 or C_1 will not affect the pole and, conversely, varying R_2 or C_2 will not change the zero. Finally, apart from being on the negative real axis, there are no restrictions on the pole or zero locations. For instance, we may choose and $C_1 = R_2 = 0$ to obtain the circuit in Fig. 3.26a. It realizes

$$T(s) = -\frac{Y_1}{Y_2} = -\frac{1}{sC_2R_1} \tag{3.75}$$

This is an inverting ideal integrator, a function that could not have been realized with only passive elements. Its attenuation can be written as

$$\alpha(\omega) = 20 \log |T(j\omega)| = -20 \log(\omega\tau) = -20 \log\left(\frac{\omega}{1/\tau}\right) \tag{3.76}$$

where $\tau = C_2R_1$ is the integrator time constant, and the phase is $\theta(\omega) = 180° - 90°$. In this equation, 180° arises from the minus sign in Eq. (3.75) and the integration itself, $1/(s\tau)$, contributes −90°. Figure 3.27a shows a Bode plot of the integrator magnitude with its breakpoint $1/\tau$. We will find integration, and therefore the ideal integrator, to be very important and fundamental in the design of active filters. A separate section, Section 4.4, will be devoted to its design.

A second function that cannot be implemented with only passive components is the differentiator with transfer function

$$T(s) = \frac{V_2}{V_1} = s\tau \tag{3.77}$$

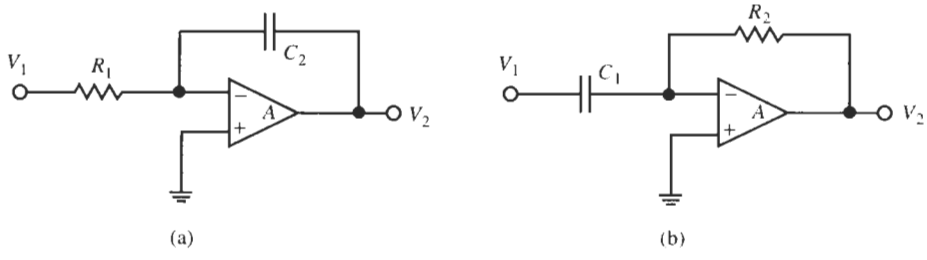

Figure 3.26 (a) Integrator; (b) differentiator.

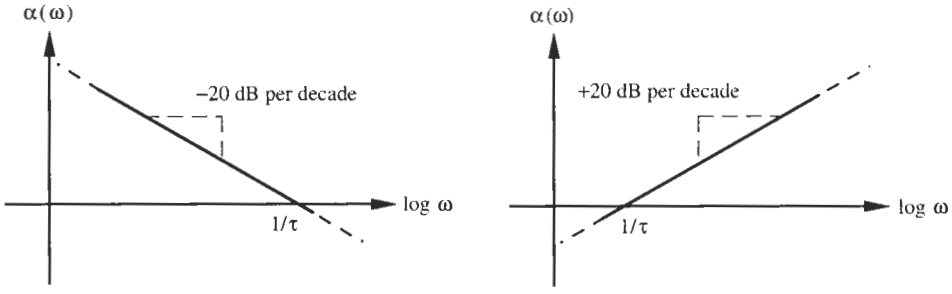

Figure 3.27 Bode plot of the magnitude of (a) an ideal integrator (note: α is infinite at $\omega = 0$) and (b) an ideal differentiator.

If we accept a minus sign for an inverting differentiator, the function is readily implemented by the circuit in Fig. 3.24 with $R_1 = C_2 = 0$ as shown in Fig. 3.26b. It realizes

$$T(s) = \frac{V_2}{V_1} = -\frac{sC_1}{G_2} = -sC_1R_2 = -s\tau \tag{3.78}$$

where $\tau = C_1R_2$ is the differentiator time constant and sets the breakpoint on the Bode plot. The Bode plot of the differentiator gain is shown in Fig. 3.27b.

We mentioned earlier that there are several possibilities for identifying the impedances in Fig. 3.23 such that the circuit realizes the bilinear transfer function of Eq. (3.66). In other words, circuit design does not normally lead to a unique solution. To demonstrate another general solution to our problem, let us identify instead of Eq. (3.69) the first-order impedances

$$Z_1(s) = R_1 + \frac{1}{sC_1} \quad \text{and} \quad Z_2(s) = R_2 + \frac{1}{sC_2} \tag{3.79}$$

to obtain the circuit in Fig. 3.28. Inserting these values into Eq. (3.68) results in

$$T(s) = -\frac{Z_2}{Z_1} = -\frac{R_2 + 1/(sC_2)}{R_1 + 1/(sC_1)} = -\frac{R_2}{R_1}\frac{s + 1/(C_2R_2)}{s + 1/(C_1R_1)} = -K\frac{s + z_1}{s + p_1} \tag{3.80}$$

where we have

$$K = \frac{R_2}{R_1}, \quad z_1 = \frac{1}{C_2R_2}, \quad \text{and} \quad p_1 = \frac{1}{C_1R_1} \tag{3.81}$$

Again, we observe that the pole and the zero may be set independently anywhere on the negative real axis, such as at the origin and at infinity. To illustrate that design is not unique, let us repeat the design of Example 3.5 for the circuit in Fig. 3.28.

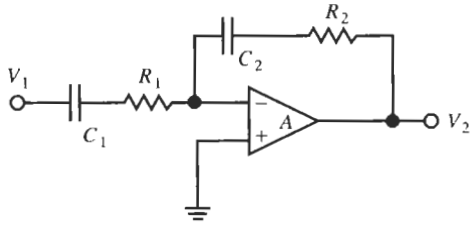

Figure 3.28 Alternative active realization of a bilinear function.

EXAMPLE 3.6

The transfer function of the circuit was given in Eqs. (3.72) and (3.73):

$$T(s) = -14.125\frac{s + 2\pi \times 830 \text{ Hz}}{s + 2\pi \times 13000 \text{ Hz}} \tag{3.82}$$

Solution

Using no scaling, we obtain directly with Eq. (3.81)

$$\frac{R_2}{R_1} = 14.125, \quad \frac{1}{C_2R_2} = 2\pi \times 830 \text{ Hz}, \quad \text{and} \quad \frac{1}{C_1R_1} = 2\pi \times 13 \text{ kHz} \tag{3.83}$$

Choosing $C_1 = 10 \text{ nF} = 0.01 \ \mu\text{F}$, results in the components

$$R_1 = \frac{1}{2\pi \times 13 \text{ kHz} \times 10 \text{ nF}} = 1.224 \text{ k}\Omega, \quad R_2 = 14.125R_1 = 17.289 \text{ k}\Omega$$

$$C_2 = \frac{1}{2\pi \times 830 \text{ Hz} \times 17.289 \text{ k}\Omega} = 11.09 \text{ nF}$$

The resulting circuit is seen in Fig. 3.25b. As the transfer function implemented by the two circuits in Fig. 3.25 is the same, we have demonstrated that design is not unique.

Further possibilities for the design of the circuit of Fig. 3.23 in selecting one capacitor and one resistor each for Z_1 and Z_2 are the following. We note that we could contemplate mixing the series and parallel connections of capacitor and resistor for the input branch and the feedback branch, i.e., place the parallel branch in the feedback path and the series connection in the input branch, or vice versa. This is shown in Fig. 3.29a and b. The transfer functions of these circuits are obtained most easily by noting from Eq. (3.67b) that for Fig. 3.29a:

$$T(s) = -\frac{1}{Z_1Y_2} \tag{3.84a}$$

Inserting the elements, we obtain

$$T(s) = -\frac{1}{Z_1Y_2} = -\frac{1}{[R_1 + 1/(sC_1)]\,(G_2 + sC_2)} = -\frac{sC_1R_2}{(sC_1R_1 + 1)\,(sC_2R_2 + 1)} \tag{3.85a}$$

For Fig 3.29b we use

$$T(s) = -Y_1Z_2 \tag{3.84b}$$

so that

$$T(s) = -Y_1Z_2 = -\,(G_1 + sC_1)\left(R_2 + \frac{1}{sC_2}\right) = -\frac{(sC_1R_1 + 1)\,(sC_2R_2 + 1)}{sC_2R_1} \tag{3.85b}$$

We observe that both circuits in Fig. 3.29 lead to *second-order* functions. It suggests that the manner in which the capacitors are connected determines the order of the transfer function

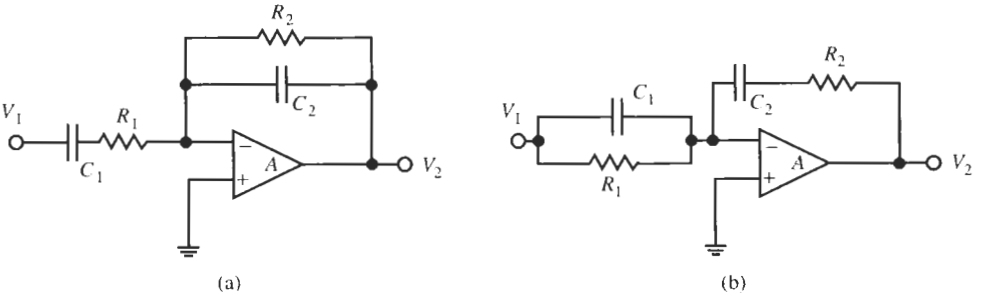

Figure 3.29 Two alternative filter structures.

realized. Equation (3.85a) has two negative real poles, and zeros at the origin and at infinity. The function is that of a bandpass as illustrated in Figs. 1.2c or 1.3c.

It is interesting to investigate the circuit in Fig. 3.29b more carefully. It is not useful because the (theoretical) poles at $s = 0$ and $s = \infty$ would imply infinite gain at the origin and at infinity. To understand the behavior suggested by Eq. (3.85b), we note that at $s = 0$ C_1 and C_2 are open circuits and the *opamp operates in open loop*. Further, V_1 is directly connected to the inverting input terminal of the opamp because at dc the current through R_1 is zero.[3] Thus the opamp would apply infinite gain to V_1, unconstrained by feedback. At very high frequencies, V_1 is again directly connected to the opamp (by C_1) and feedback is supplied via R_2. The gain $|R_2/Z_1|$ of the inverting amplifier becomes infinite because Z_1 appears to be zero (is a short circuit). In reality the gain will stay finite, of course, because, as was pointed out in Chapter 2, the electronic circuitry in the opamp will not support any voltage larger than the power supply. So, the increasing gain at $s \to 0$ and $s \to \infty$ will result in nonlinear opamp operation so that the result of Eq. (3.85b) is meaningless.

Let us point out in connection with this case that the student should always carefully examine a circuit when the analysis suggests a result that is physically meaningless. The cause for such unrealistic predictions is almost always found in poor or overly simplified device models being used for the mathematical analysis. In the case under discussion, we mistakenly assumed that, first, the opamp gain is infinite at high frequencies (neglecting the frequency dependence), and that, second, the opamp gain is linear (neglecting the limits placed on the magnitude of the output voltage). The result of Eq. (3.85b) was based on an unrealistic device model and is, therefore, not valid.

We have seen that for the appropriate choice of components the circuits in Figs. 3.24 and 3.28 can realize any bilinear function with negative real poles and zeros, including at the origin and at infinity, as long as the gain is inverting. Fortunately, in most applications this inversion, a phase shift of 180°, is unimportant. As we shall see later in our study, higher order filters are often designed by *cascading* low-order sections. We wish to make certain, therefore, that sections later in the cascade do not load the earlier sections. This means that their input impedances must be high, a condition not necessarily satisfied by the circuit in Fig. 3.23 whose input impedance was derived in Chapter 2 to be finite (it is equal to Z_1). On the other hand, the input impedance of a noninverting amplifier stage is essentially an open circuit. Let us, therefore, in the next section investigate the possibility of a circuit that delivers positive gain.

[3] Since both the opamp input and the capacitor C_2 are open circuits at dc, no dc current can flow through R_1.

3.4.2 Noninverting Opamp Circuits

Recalling our discussions from Chapter 2, we seek to utilize the noninverting amplifier of Fig. 2.11a with resistors replaced by impedances. This circuit is shown in Fig. 3.30. By direct analysis, or by analogy with Eq. (2.34), we obtain its transfer function as

$$\frac{V_2}{V_1} = \left(1 + \frac{Z_2}{Z_1}\right) \frac{1}{1 + \dfrac{1}{A(s)}\left(1 + \dfrac{Z_2}{Z_1}\right)} \tag{3.86}$$

Again we have shown the dependence on $A(s)$ because we must be mindful of its effect. For now let us assume the ideal case, $A(s) = \infty$, and consider the design possibilities of the function

$$T(s) = \frac{V_2}{V_1} = 1 + \frac{Z_2}{Z_1} = 1 + \frac{Y_1}{Y_2} = K\frac{e_n s + z_1}{e_d s + p_1} \tag{3.87}$$

In Eq. (3.87) we have temporarily introduced the two coefficients e_n and e_d in the numerator and the denominator. Both coefficients will be equal to either 1 or 0, depending on whether the s-terms are present or absent. This notation will help us state more clearly the conditions that the bilinear function must satisfy to be realizable by the circuit in Fig. 3.30.

The design will proceed by identifying possible impedances from

$$\frac{Z_2}{Z_1} = \frac{Y_1}{Y_2} = K\frac{e_n s + z_1}{e_d s + p_1} - 1 = \frac{(e_n K - e_d)\, s + K z_1 - p_1}{e_d s + p_1} \tag{3.88}$$

As for the inverting-amplifier case, we recognize several possibilities: we assume normalized and scaled components and identify them by the subscript n. We may then set

$$Y_1 = sC_{1n} + G_{1n} = s\,(e_n K - e_d) + K z_1 - p_1 \tag{3.89a}$$

and

$$Y_2 = sC_{2n} + G_{2n} = e_d s + p_1 \tag{3.89b}$$

When we work with impedances, we cannot simply equate the numerators and denominators of

$$\frac{Z_2}{Z_1} = \frac{(e_n K - e_d)\, s + K z_1 - p}{e_d s + p_1}$$

because that would lead us to inductances. Rather, we use the step of dividing numerator and denominator by s to obtain

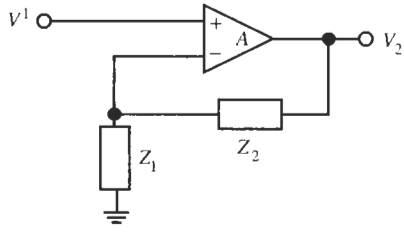

Figure 3.30 Noninverting amplifier with impedances in the feedback network.

$$\frac{Z_2}{Z_1} = \frac{[(e_n K - e_d)s + Kz_1 - p_1]/s}{(e_d s + p_1)/s} = \frac{(e_n K - e_d) + (Kz_1 - p_1)/s}{e_d + p_1/s} \tag{3.90}$$

We can then identify

$$Z_1 = R_{1n} + \frac{1}{sC_{1n}} = e_d + \frac{p_1}{s} \tag{3.91a}$$

$$Z_2 = R_{2n} + \frac{1}{sC_{2n}} = (e_n K - e_d) + \frac{Kz_1 - p_1}{s} \tag{3.91b}$$

In the design, nothing changes compared with the inverting-opamp case except that we need to observe the two restrictions that $T(s)$ must satisfy to be realizable with the circuit in Fig. 3.30. Since the resistors and capacitors are positive elements, it follows from Eqs. (3.89) and (3.91) that to be realizable we must have

$$e_n K - e_d \geq 0, \quad \text{and} \quad Kz_1 - p_1 \geq 0 \tag{3.92}$$

Of course, we must take the more restrictive of the two conditions. We note that these conditions will normally limit the minimum value that K can take on. The gain constant K is usually not important; it affects only the gain without changing the shape of the transmission behavior; recall that in constructing the Bode plot the effect of K is only to add a *constant* value $\alpha = 20 \log K$ to the frequency characteristics. If the prescribed value of K is too small, we can simply increase it as required to satisfy the constraints of Eq. (3.92), and then, if necessary, follow the filter by an appropriate attenuation. Some bilinear characteristics, however, cannot be realized by the noninverting circuit. Note from Eq. (3.92) that the s-term in the numerator of Eq. (3.87) must be present ($e_n = 1$) and that a zero at the origin is not permitted ($z_1 > 0$). For example, the first-order lowpass ($e_n = 0$) or highpass ($z_1 = 0$) functions

$$T_{LP}(s) = \frac{K}{s + p_1} \quad \text{and} \quad T_{HP}(s) = \frac{Ks}{s + p_1}$$

are not realizable with the circuit in Fig. 3.30. An example will illustrate the procedure.

EXAMPLE 3.7

Repeat Example 3.5 for a design leading to Fig. 3.30.

Solution

The specified transfer function (with the minus sign omitted) was

$$T(s) = 14.125 \frac{s_n + 0.83}{s_n + 13} \tag{3.93}$$

where the frequency parameter is scaled by $\omega_S = 2\pi \times 1000$ rad/s. First we check Eq. (3.92); we require

$$K - 1 = 14.125 - 1 > 0 \quad \text{and} \quad Kz_1 - p_1 = 0.83 \times 14.125 - 13 = -1.28 < 0$$

Clearly, the prescribed K is too small. To proceed with the design, we increase K to its minimum value

$$K = \frac{13}{0.83} = 15.663$$

because that will save one component (R_1) in the admittance approach in Eq. (3.89):

$$Y_1 = sC_{1n} + G_{1n} = s(15.663 - 1) + 15.663 \times 0.83 - 13 = 14.663s \tag{3.94a}$$

and

$$Y_2 = sC_{2n} + G_{2n} = s_n + 13 \tag{3.94b}$$

Next we need to denormalize the normalized components. We select arbitrarily $R_S = 1000\ \Omega$ along with $\omega_S = 2\pi \times 1000$ rad/s as identified earlier. Then we find from Eq. (1.14) in Chapter 1,

$$C_1 = \frac{1}{\omega_S R_S} C_{1n} = \frac{14.663}{2\pi \times 1000 \times 1000}\ \text{F} = 2.333\ \mu\text{F},$$

$$C_2 = \frac{1}{\omega_S R_S} C_{2n} = \frac{1}{2\pi \times 10^6}\ \text{F} = 159\ \text{nF}$$

$$R_1 = R_S R_{1n} = \frac{R_S}{G_{1n}} = \frac{1000}{0}\ \Omega = \text{"open circuit,"}$$

$$R_2 = R_S R_{2n} = \frac{R_S}{G_{2n}} = \frac{1000}{13}\ \Omega \approx 77\ \Omega$$

We mentioned in Chapter 1 that the denormalizing resistor R_S would be chosen to obtain convenient element values. The value $R_S = 1\ \text{k}\Omega$ chosen above leads to large capacitors with nonstandard values and a very small resistor. As R_S may be chosen freely, a better value for R_S might be $R_S = 116.7\ \text{k}\Omega$. Then we obtain for the design elements

$$C_1 = \frac{1}{\omega_S R_S} C_{1n} = \frac{14.663}{1.167 \times 10^5 \times 2\pi \times 10^3}\ \text{F} \approx 20\ \text{nF}$$

$$C_2 = \frac{1}{\omega_S R_S} C_{2n} = \frac{1}{2\pi \times 1.167 \times 10^8}\ \text{F} = 1.36\ \text{nF}$$

$$R_2 = R_S R_{2n} = \frac{1.167 \times 10^5}{13}\ \Omega \approx 8.977\ \text{k}\Omega$$

Figure 3.31a shows the circuit.

Let us also derive the circuit based on the impedance approach in Eq. (3.91) to illustrate once more that design problems do not normally have a unique solution. For the numbers derived, we obtain the expressions

$$Z_1 = R_{1n} + \frac{1}{sC_{1n}} = 1 + \frac{13}{s}, \quad \text{and} \quad Z_2 = R_{2n} + \frac{1}{sC_{2n}} = 14.663$$

from which the component values are computed. Let us here choose $R_S = 1.225\ \text{k}\Omega$ to obtain

$$R_1 = R_S R_{1n} = 1.225\ \text{k}\Omega, \quad C_1 = \frac{C_{1n}}{\omega_S R_S} = \frac{1}{13 \times 1.225\ \text{k}\Omega \times 2\pi \times 1000\ \text{rad/s}} = 10\ \text{nF}$$

$$R_2 = R_S R_{2n} = 17.96\ \text{k}\Omega$$

The resulting circuit is shown in Fig. 3.31b. Of the two circuits, the one in Fig. 3.31b may be preferable because resistors are less expensive than capacitors. Naturally, this judgment depends on the technology used to implement the design.

To realize the transfer function of Eq. (3.93) with the noninverting circuits, we had to increase the prescribed gain constant from $K = 14.125$ to $K = 15.993$, a factor 1.11. If this is not acceptable, we can precede[4] the circuit by a voltage divider that reduces the overall gain by $1/1.11 = 0.90$. The circuits modified in this form are shown in Fig. 3.32. Note that the simple voltage divider may be used here without buffering because the input impedance into the opamp is infinite so that no current is drawn. We have chosen resistors in the voltage dividers that are large to keep the input impedances into the filters high: $R_{in} = 110\ \text{k}\Omega$.

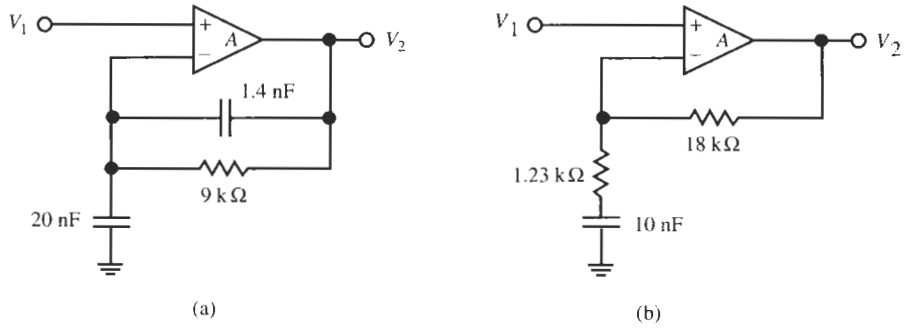

Figure 3.31 Circuits realizing the function (3.93) with an increased gain of $K = 15.663$ using (a) the admittance approach and (b) the impedance approach.

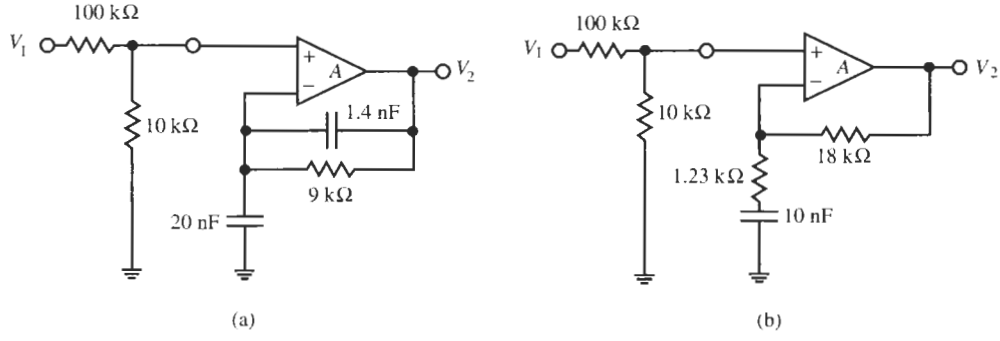

Figure 3.32 Circuits realizing the function (3.93) with an corrected gain of $K = 14.125$ using (a) the admittance approach and (b) the impedance approach.

[4]The voltage divider must precede rather than follow the first-order filter so that a load can be driven by the opamp. If the divider is connected at the opamp output any load would change the function of the divider because the output would no longer be a low impedance.

3.4.3 Differential Opamp Circuits Allpass Filters: Phase Shaping

The first-order active circuits we have discussed so far can realize arbitrary poles and zeros on the *negative* real axis. Zeros on the positive real axis, such as are needed, for example, for allpass filters, Eq. (3.41), cannot be obtained because the circuits in Figs. 3.24, 3.28, 3.29, and 3.30 cannot generate a negative coefficient in the numerator. A different circuit configuration is necessary. Suitable is a circuit that uses a voltage difference to generate a minus sign, as was done in Fig. 3.12 and Eq. (3.41). To help us locate a suitable structure, we again consult the opamp circuits in Chapter 2, where we found that the differential amplifier in Fig. 2.29b could be used to take the difference of two input signals, V_1 and V_a, each multiplied by a constant as in Eq. (2.95). For our application, of course, only a single input is required. Thus, if we contemplate tying the two inputs together, i.e., $V_a = V_1$, we obtain the circuit in Fig. 3.33. By direct analysis, or using Eq. (2.95), we find the circuit realizes the transfer function

$$T(s) = \frac{V_o}{V_1} = \left(\frac{G_1 + G_F}{G_F}\frac{G_a}{G_a + G_G} - \frac{G_1}{G_F}\right)\frac{1}{1 + \dfrac{1 + G_1/G_F}{A}}$$

$$= \frac{\left(1 + \dfrac{G_1}{G_F}\right)G_a - \dfrac{G_1}{G_F}(G_a + G_G)}{G_a + G_G}\,\frac{1}{1 + \dfrac{1 + G_1/G_F}{A}}$$

which can be further simplified to read

$$T(s) = \frac{V_o}{V_1} = \frac{G_a - \dfrac{G_1}{G_F}G_G}{G_a + G_G}\,\frac{1}{1 + \dfrac{1 + G_1/G_F}{A}} \tag{3.95}$$

As we did earlier in this section, we will for now assume ideal opamps ($A = \infty$) so that we may concentrate first on the nominal circuit behavior, that is

$$T(s) = \frac{V_o}{V_1} = \frac{G_a - kG_G}{G_a + G_G} \tag{3.96}$$

where we introduced the constant $k = R_F/R_1$.

The student will recognize that this expression is exactly what we are looking for. As is always the case in circuit design, there are several different possibilities. A simple solution that suggests itself is to replace the conductor G_a by a capacitor C as in Fig. 3.34a to get the function

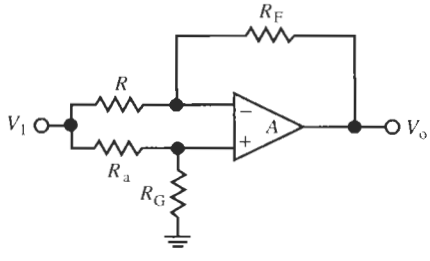

Figure 3.33 Fundamental opamp circuit to generate negative numerator coefficients.

$$T(s) = \frac{V_o}{V_I} = \frac{sC - kG_G}{sC + G_G} = \frac{s - k/(CR_G)}{s + 1/(CR_G)} \tag{3.97}$$

Observe that Eq. (3.97) provides us with a general bilinear function with a pole on the negative real axis at

$$p_1 = -\frac{1}{CR_G} \tag{3.98}$$

and a zero in the right half-plane at

$$z_1 = \frac{k}{CR_G} = k\,|p_1| \tag{3.99}$$

We also note that the zero location can be less than, larger than, or equal to $|p_1|$, depending on the choice of the constant $k < 1$, $k > 1$, or $k = 1$.

Of particular interest is $k = R_F/R_1 = 1$ so that the circuit in Fig. 3.34a realizes

$$T(s) = \frac{s - 1/(CR_G)}{s + 1/(CR_G)} = \frac{s - z_1}{s + z_1} = \frac{m_n \angle\theta_n}{m_d \angle\theta_d} \tag{3.100}$$

where we have called the complex numbers in numerator and denominator $m_n\angle\theta_n$ and $m_d\angle\theta_d$, respectively. The magnitude of $T(j\omega)$ is

$$|T(j\omega)| = \left|\frac{j\omega - z_1}{j\omega + z_1}\right| = \frac{m_n}{m_d} = \frac{\sqrt{1 + \omega^2/z_1^2}}{\sqrt{1 + \omega^2/z_1^2}} \equiv 1 \tag{3.101}$$

for all frequencies. A comparison with Eq. (3.42) shows that the circuit is an allpass, that is, signals at all frequencies are transmitted equally, without gain or attenuation between input and output. The phase and its sign follow from Eq. (3.100) as

$$\theta(\omega) = \theta_n - \theta_d = \tan^{-1}\left(\frac{\omega}{-z_1}\right) - \tan^{-1}\left(\frac{\omega}{z_1}\right) \tag{3.102}$$

Before we are misled by the $-z_1$ term in Eq. (3.102), let us consult Fig. 3.35. It helps explain which branch of the multivalued $\tan^{-1}$ curve to use, and clarifies the phase and its sign: we have indicated the two complex numbers of numerator and denominator of Eq. (3.100) with

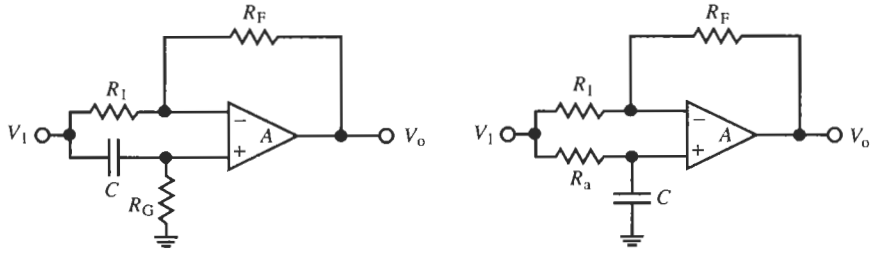

Figure 3.34 Two active circuits to realize a bilinear function with a zero in the right half-plane. Choose $R_1 = R_F$ for allpass functions.

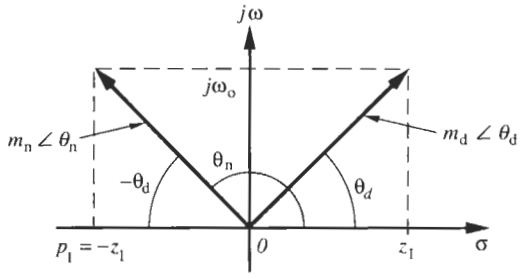

Figure 3.35 Complex plane showing the two complex numbers in the numerator and denominator of Eq. (3.100) with their phases θ_n and θ_d.

their rectangular coordinates p_1, z_1, and the operating frequency $j\omega_o$, and their phases θ_n and θ_d. Observe that as ω_o increases from 0 to ∞, θ_d increases from 0° to 90° and θ_n decreases from 180° to 90° and can be written as $\theta_n = 180° - \theta_d$. As a function of ω, the total phase, Eq. (3.102), of the allpass circuit decreases therefore from 180° to 0° as

$$\theta(\omega) = 180° - 2\theta_d = 180° - 2\tan^{-1}\frac{\omega}{z_1} \tag{3.103}$$

The phase is positive for all frequencies, with $\theta(\omega) = 180° - 2 \times 45° = 90°$ at $\omega = z_1$. Magnitude and phase of Eq. (3.100) are shown in Fig. 3.36.

The circuit in Fig. 3.34a is a lead filter. If the application calls for a lag filter, i.e., a negative phase, we need to find a way to shift the θ-curve below the ω-axis in Fig. 3.36b, i.e., we need to subtract[5] 180° from θ. Since a 180° phase shift corresponds to a sign inversion, we need in effect to be able to find a way to multiply Eq. (3.97) by -1. Returning to Eq. (3.96), we notice that instead of G_a we can select to replace G_G by a capacitor C to obtain

$$T(s) = \frac{V_o}{V_I} = \frac{G_a - \dfrac{G_I}{G_F}sC}{G_a + sC} = -\frac{R_F}{R_I}\frac{s - \dfrac{R_I}{R_F}\dfrac{1}{CR_a}}{s + \dfrac{1}{CR_a}} = -k\frac{s - \dfrac{1}{kCR_a}}{s + \dfrac{1}{CR_a}} \tag{3.104}$$

where the constant $k = R_F/R_I$ was defined earlier. Similar to the function (3.97), $T(s)$ has a pole on the negative real axis at

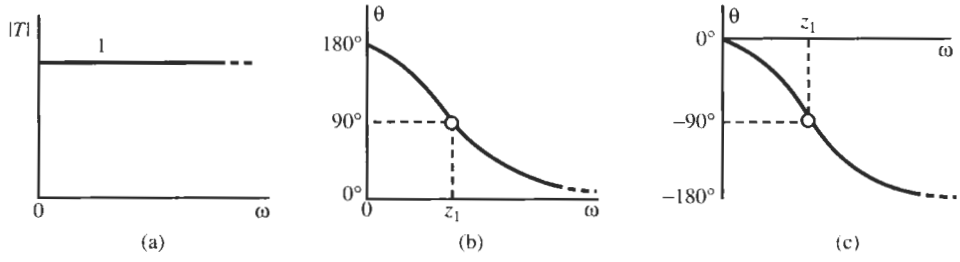

Figure 3.36 (a) Magnitude of the allpass circuits in Fig. 3.34; phase of the circuit (b) of Fig. 3.34a and (c) of Fig. 3.34b.

[5] Note that is does not matter whether we add or subtract 180° because the difference, 360°, leaves the function unchanged.

$$p_1 = -\frac{1}{CR_a} \tag{3.105}$$

and a zero at

$$z_1 = \frac{|p_1|}{k} \tag{3.106}$$

on the positive real axis. As before, the zero location can be less than, larger than, or equal to $|p_1|$, depending on the choice of the constant $k > 1$, $k < 1$, or $k = 1$. To generate an allpass filter, we choose $k = 1$ to obtain a function identical in behavior to the one in Eq. (3.100), except for the phase inversion caused by the multiplication by -1. Thus, the only difference is that the phase is always negative, moving with increasing ω from 0° to −180°,

$$\theta(\omega) = -2\tan^{-1}\frac{\omega}{z_1} = -2\tan^{-1}\omega CR_a \tag{3.107}$$

The corresponding circuit is shown in Fig. 3.34b and its phase and gain are also sketched in Fig. 3.36.

EXAMPLE 3.8

Design a circuit that provides a set of three 60-Hz voltages of equal magnitudes but lagging each other in phase by 120° as shown in Fig. 3.37.

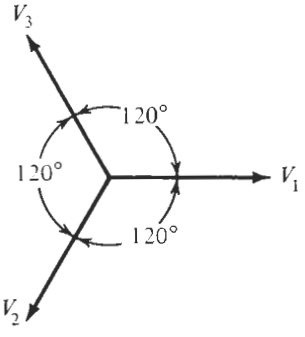

Figure 3.37 Voltages for a lagging three-phase system.

Solution

The design proceeds exactly as in the previous example, but now using the lag circuit in Fig. 3.34b. We start from the phase realized, Eq. (3.107):

$$\theta(\omega_0) = -2\tan^{-1}\omega_0 CR_a \Rightarrow -120^\circ$$

from which we determine, for a chosen capacitor $C = 1\ \mu\text{F}$,

$$R_a = \frac{\tan(60^\circ)}{\omega_0 C} = \frac{1.7321}{2\pi \times 60\text{s}^{-1} \times 10^{-6}\text{F}} = 4.59\ \text{k}\Omega$$

We again pick $R_1 = R_F = 10\ \text{k}\Omega$ to complete one section of the phase-shifting circuit. The complete three-phase network is shown in Fig. 3.38.

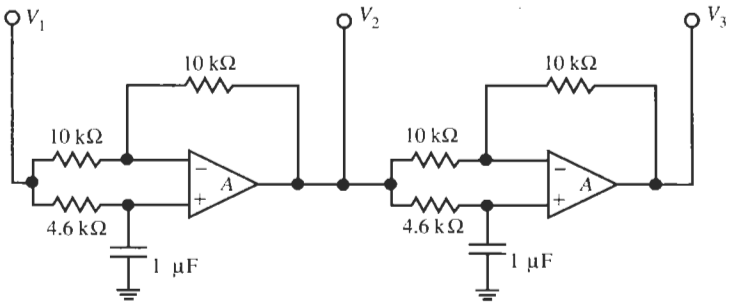

Figure 3.38 Three-phase circuit for Example 3.8.

3.5 THE EFFECT OF $A(s)$

In Section 3.4 we developed a number of active implementations of bilinear transfer functions. To be able to concentrate on the nominal behavior of the circuits, we assumed that the opamp gain was so large that its influence on the transfer function could be neglected. However, throughout Chapter 2 we encountered many examples of the limitations on operation imposed by the finite bandwidth of opamps. In this section we shall examine, therefore, how far the infinite gain and bandwidth assumptions are valid for first-order opamp circuits. We will determine when and under which conditions we need to be careful before we use any of the presented circuit design ideas with real operational amplifiers.

To begin, let us look at the behavior of the circuits using the inverting opamp connection in Fig. 3.23. The circuit was described by Eq. (3.67a), repeated here for convenience:

$$\frac{V_2}{V_1} = -\frac{Z_2}{Z_1}\frac{1}{1+(1+Z_2/Z_1)/A(s)} \tag{3.108}$$

Equation (3.108) contains explicitly the finite and frequency-dependent opamp gain $A(s)$ so that we may examine its effect on the transfer function. Since we are dealing with bilinear functions in this chapter, we insert for the impedance ratio Eq. (3.68),

$$\frac{Z_2}{Z_1} = K\frac{s+z_1}{s+p_1} \tag{3.109}$$

and obtain the expression

$$\begin{aligned}\frac{V_2}{V_1} &= -K\frac{s+z_1}{s+p_1}\frac{1}{1+\dfrac{1}{A(s)}\left(1+K\dfrac{s+z_1}{s+p_1}\right)} \\ &= -K\frac{s+z_1}{s+p_1+\dfrac{1}{A(s)}\left[s+p_1+K\,(s+z_1)\right]}\end{aligned} \tag{3.110}$$

To proceed further, we substitute for the opamp gain the integrator model of Eq. (2.18). Recall that for 741-type opamps the integrator model is expected to give reasonably realistic results from 100 Hz to several hundred kilohertz. At lower frequencies the opamp model must be extended to the single-pole model, Eq. (2.11), to account for the low-frequency pole at f_a (approximately 10 Hz); at higher frequencies the second pole at f_c, Eq. (2.17), must be considered. The result from using the integrator model in Eq. (3.110) is

$$\begin{aligned}\frac{V_2}{V_1} &= -K\frac{s+z_1}{s+p_1+(s/\omega_t)\,[s+p_1+K\,(s+z_1)]}\\ &= -K\frac{s+z_1}{s^2\dfrac{1+K}{\omega_t}+s\left(1+\dfrac{p_1+Kz_1}{\omega_t}\right)+p_1}\end{aligned} \tag{3.111}$$

It is comforting to see that Eq. (3.111) reverts back to the ideal equation, Eqs. (3.68) or (3.109), for $\omega_t \to \infty$, i.e., for opamps with infinite bandwidth. The most important effect of the finite opamp gain is that the order of the transfer function has increased by one: the denominator is now of second order with two poles in the left half-plane. One of the two poles is *near* the nominal pole p_1 and the second one is a new *parasitic* pole p_p. The perturbation Δp_1 that shifts the nominal pole p_1 to $p_1 + \Delta p_1$, and p_p are caused by the opamp. Thus the transfer function is now of the form

$$\frac{V_2}{V_1} = -\tilde{K}\frac{s+z_1}{(s+p_1+\Delta p_1)\,(s+p_p)} \tag{3.112}$$

Whether this causes problems in circuit operation depends on the specific filter parameters and, especially, the operating frequency range. To have minimal deviations from the nominal behavior, we need to have the parasitic pole far away from the frequency range of interest, and naturally, the error Δp_1 as small as possible. Δp_1 and p_p depend on the poles, zeros, gain, or other filter parameters, and the opamp's gain-bandwidth product. But as we may expect, accurate predictions depend on specific parameter values and can rarely be made in general terms. Let us consider an example to study the methods used for the analysis and to see the actual limits imposed by the opamp.

EXAMPLE 3.9

Design a circuit with the transfer function (3.72) of Example 3.5. Use an LM741 opamp and determine the limitations and errors caused by this real operational amplifier.

Solution

The transfer function was

$$T(s) = -14.125\frac{s+2\pi\times 830\ \text{Hz}}{s+2\pi\times 13000\text{Hz}}$$

or, after scaling the frequency by $\omega_S = 2\pi \times 1000$ rad/s,

$$T(s) = -\frac{Z_2}{Z_1} = -14.125\frac{s_n+0.83}{s_n+13} \tag{3.113}$$

We substitute the values from this equation into Eq. (3.111) to obtain

$$\begin{aligned}\frac{V_2}{V_1} &= -14.125\frac{s_n + 0.83}{s_n^2\dfrac{1 + 14.125}{\omega_t} + s_n\left(1 + \dfrac{13 + 14.125 \times 0.83}{\omega_t}\right) + 13} \\ &= -14.125\frac{s_n + 0.83}{s_n^2\dfrac{15.125}{1.5 \times 10^3} + s_n\left(1 + \dfrac{24.724}{1.5 \times 10^3}\right) + 13} \\ &= -14.125\frac{s_n + 0.83}{10.08 \times 10^{-3}s_n^2 + 1.016s_n + 13} \qquad (3.114)\end{aligned}$$

Note that s_n is a normalized frequency and that $\omega_t = 2\pi \times 1.5$ Mrad/s must be scaled by ω_S along with all other frequency parameters in the computations. We observe that the zero of the transfer function is unchanged because $A(s)$ affects only the denominator. To determine the poles, we factor Eq. (3.114) to find

$$\begin{aligned}\frac{V_2}{V_1} &= -14.125\frac{s_n + 0.83}{10.08 \times 10^{-3}\left(s_n^2 + 100.8s_n + 129\right)} \\ &= -1401\frac{s_n + 0.83}{(s_n + 15.05)(s_n + 85.75)} \qquad (3.115)\end{aligned}$$

This equation shows that the dc gain has not changed as we might expect because at dc the opamp is ideal. But notice that the (normalized) pole at $p_1 = -13$ has shifted by $\Delta p_1 = -2.05$ to -15.05, and that a parasitic pole was generated at $p_p = -85.75$. Figure 3.42 contains an asymptotic Bode plot that shows the low-frequency gain at -0.9 dB, the first break point at 0.83, the second break point at 15.05, and the final (parasitic) break point at 85.75. We have also indicated the ideal Bode asymptote at a gain of 23 dB that would be realized if ideal opamps were available. The actual performance will follow the asymptotic curve with rounded corners as explained in Section 3.3. As mentioned, for frequencies larger than about 300 or 400 kHz deviations from the Bode plot in Fig. 3.39 must be expected because the integrator model is inadequate at these frequencies. To verify the circuit's behavior, let us build the filter and obtain

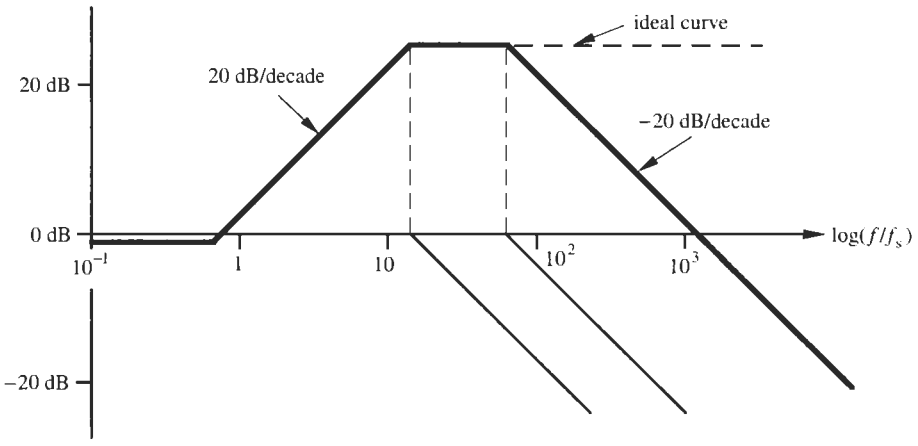

Figure 3.39 Bode plot for Example 3.9.

an experimental result in the range $f \leq 1$ MHz. Figure 3.40 contains the result that clearly shows the third break point at ≈ 85 kHz (cursor) and roll-off at high frequencies. The roll-off is larger than -20 dB/decade and not predicted by our equations because of the too simplistic opamp model. The example demonstrates that it is crucial for the engineer to investigate the effects of real opamps on the design. In this example we note that the circuit behaves nearly as predicted at low frequencies (up to the nominal pole), but that substantial deviations from the ideal performance are found at higher frequencies.

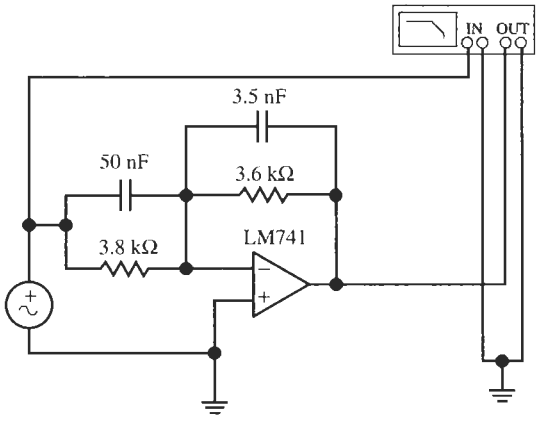

(a)

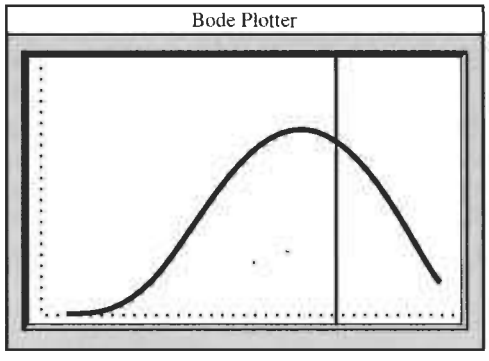

(b)

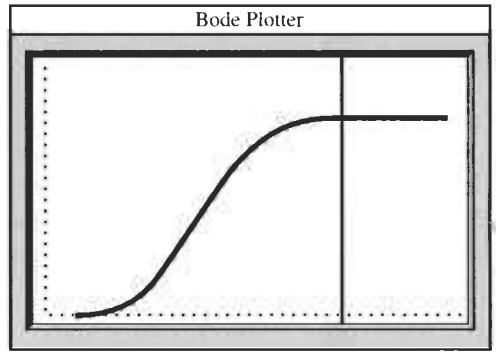

(c)

Figure 3.40 (a) Circuit and test set-up of Example 3.9; (b) test performance observed with a network analyzer (Bode Plotter), cursor at (21.83 dB, 85.25 kHz); (c) performance with an ideal opamp, cursor at (23 dB, 85.25 kHz). (In both cases the frequency range is from 100 Hz to 1 MHz and the vertical axis goes from 0 dB to +30 dB.)

The deviation in practical performance from the ideal one of the remaining inverting opamp structures we discussed is identical to the one just presented because their transfer functions are the same. A small difference is found in the noninverting structure of Fig. 3.30. Nothing changes in principle, but the formulation is slightly altered because of the different expression of the bilinear function in terms of the impedance ratio in Eq. (3.87). To investigate the difference we proceed in a manner identical to the one used for the inverting configuration. The transfer function was given in Eq. (3.86), repeated here for convenience:

$$\frac{V_2}{V_1} = \left(1 + \frac{Z_2}{Z_1}\right) \frac{1}{1 + \dfrac{1}{A(s)}\left(1 + \dfrac{Z_2}{Z_1}\right)} \tag{3.116}$$

If we substitute from Eq. (3.87)

$$1+\frac{Z_2}{Z_1}=K\frac{s+z_1}{s+p_1} \tag{3.117}$$

and use again the integrator model for the opamp, we obtain

$$\frac{V_2}{V_1}=\quad K\frac{s+z_1}{s+p_1+(s/\omega_t)K\,(s+z_1)}=K\frac{s+z_1}{s^2K/\omega_t+s\,(1+Kz_1/\omega_t)+p_1} \tag{3.118}$$

We observe again that the dc gain and the zero have not changed, and that the function reverts to the ideal one for $\omega_t=\infty$. The order of the function increases by one due to the influence of the nonideal opamp.

EXAMPLE 3.10

Repeat Example 3.9 for a noninverting design.

Solution

From Eq. (3.118) we find

$$\frac{V_2}{V_1}=\omega_t\frac{s+z_1}{s^2+s\,(\omega_t/K+z_1)+\omega_t p_1/K}$$

and for the given numbers after normalizing the frequency by 1000 rad/s

$$\frac{V_2}{V_1}=1500\frac{s_n+0.83}{s_n^2+107s_n+1381}=1500\frac{s_n+0.83}{(s_n+15)\,(s_n+92.02)}$$

[compare Eq. (3.115)]. As we predicted, there are no surprises in this result. The dominant pole has shifted from $p_1=-13$ to $p_1=-15$ due to the finite gain-bandwidth product of the opamp, and the parasitic pole is at $p_p=-92.02$, slightly further away than in the inverting case. Apart from the 180° phase shift caused by the inversion, the two circuits behave essentially the same.

Let us still examine bilinear functions realized with real opamps using their differential inputs; in Eq. (3.95) we found:

$$T(s)=\frac{V_o}{V_1}=\frac{G_a-\dfrac{G_1}{G_F}G_G}{G_a+G_G}\,\frac{1}{1+\dfrac{1+G_1/G_F}{A(s)}} \tag{3.119}$$

Recall that in all our circuits we used a constant k for the ratio R_F/R_1 so that the "correction factor," with the integrator model for the opamp, is

$$\frac{1}{1+\dfrac{1+G_1/G_F}{A(s)}}=\frac{1}{1+s\dfrac{1+k}{\omega_t}}=\frac{\omega_t/(1+k)}{s+\omega_t/(1+k)} \tag{3.120}$$

It is a lowpass function with dc gain equal to unity and the 3-dB frequency equal to $\omega_t/(1+k)$. This lowpass has no other consequences than to multiply the nominal transfer function. Note that the error term is the same for the two structures in Fig. 3.34.

The examples in this section should have provided the student with some understanding of methods of determining errors in nominal frequency response caused by real opamps. The procedures are relatively straightforward but often cumbersome and laborious to execute. It should have become clear that the careful designer *must* take the time to examine circuit performance with real opamps, either by simulation with adequate opamp models, or by experiment. Basing a design on ideal opamps will prove inadequate in practice at frequencies above the low audio range.

3.6 CASCADE DESIGN

Throughout this chapter we presented a variety of passive and active circuits that can implement the bilinear transfer function with only few restrictions. Naturally, to keep the circuits stable, that is to prevent them from oscillating, the poles are restricted to the negative real axis. The zeros, however, can be anywhere on the positive or negative real axis, depending on the circuit structure. With the exception of the circuit in Fig. 3.29a, which can have two negative real poles, all the circuits discussed are limited to only a single pole and a single zero. The question of how we can build filters of higher order, with several poles and zeros, so that more complicated transfer functions can be implemented, therefore arises. Although in this chapter we are discussing first-order circuits, the solution to be presented is much more general and not limited to first-order modules.

We encountered previously an example, in Fig. 3.38, in which a second-order circuit was built out of a chain, a so-called *cascade connection*, of two first-order sections. Let us in the following generalize this procedure and derive the conditions under which the method can be employed. A cascade of low-order sections, normally of first or second order, is the most widely used method of implementing high-order filters. It is easy, general, and has several practical advantages that make it commercially attractive. We must, therefore, develop a clear understanding of this design approach.

The method proposes to connect n lower-order building blocks with transfer functions $T_i(s)$ in cascade as shown in Fig. 3.41 such that the total higher-order transfer function is the product of the individual functions

$$T(s) = T_1 T_2 T_3 \cdots T_n \tag{3.121}$$

For this simple method to work, the low-order sections must satisfy certain conditions that we can understand readily by considering the circuit depicted in Fig. 3.42. We have shown two ideal transfer blocks

$$T_1(s) = \frac{V_{n1}}{V_1} \quad \text{and} \quad T_2(s) = \frac{V_{n2}}{V_2}$$

V_{n1} and V_{n2} are the voltages at the respective internal nodes n_1 and n_2 in Fig. 3.42. To be realistic, we have indicated that in practice the circuitry of each block will have a fi-

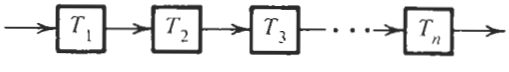

Figure 3.41 Cascade connection of n sections.

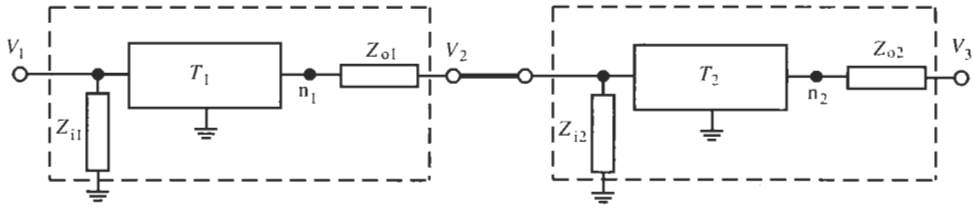

Figure 3.42 Two-section cascade.

nite input impedance $Z_i(s)$ and output impedance $Z_o(s)$, i.e., the realistically modeled sections are contained in the dashed boxes. Assume now that V_1 is an ideal voltage source so that Z_{i1} has no effect, and that there is an open circuit at V_3 so that no current flows through Z_{o2}. If we analyze the configuration in Fig. 3.42, starting from the output, we find

$$V_3 = T_2(s)V_2 = T_2(s) \times \frac{Z_{i2}(s)}{Z_{i2}(s) + Z_{o1}(s)} V_{n1} = T_2(s) \times \frac{Z_{i2}(s)}{Z_{i2}(s) + Z_{o1}(s)} \times T_1(s)V_1 \quad (3.122)$$

that is, the transfer function of the two-section cascade is

$$T(s) = \frac{V_3}{V_1} = T_1(s)T_2(s) \times \frac{Z_{i2}(s)}{Z_{i2}(s) + Z_{o1}(s)} \quad (3.123)$$

rather than the simple product T_1T_2 we intended. The problem is that the current through Z_{o1} is not zero, i.e., Section 1 is loaded by Section 2. Equation (3.123) indicates that the desired result is achieved under the condition

$$|Z_{i2}(j\omega)| \gg |Z_{o1}(j\omega)| \quad (3.124)$$

ideally, $Z_{i2} = \infty$ and $Z_{o1} = 0$. In words this says that the input impedance of the loading section must be much larger than the output impedance of the driving section so that the voltage divider factor that multiplies the ideal product T_1T_2 in Eq. (3.123) is as close to unity as possible. We have on purpose written the voltage divider ratio in terms of impedances as functions of s or $j\omega$ to emphasize that the designer in practice needs to contend with more than a resistor ratio that would simply multiply T_1T_2 by a frequency-independent constant.

To illustrate this point consider a second-order lowpass being built by cascading two identical first-order sections of the form shown in Fig. 3.4,

$$T_1(s) = T_2(s) = \frac{1}{sCR + 1} \quad (3.125)$$

The intent is to multiply their transfer functions so that

$$T(s) = \frac{V_3}{V_1} = T_1(s)T_2(s) = \frac{1}{sCR + 1} \times \frac{1}{sCR + 1} = \frac{1}{(sCR)^2 + 2sCR + 1} \quad (3.126)$$

The proposed circuit is shown in Fig. 3.43. Using the formalism in Eq. (3.123) and Eq. (3.125), we find with

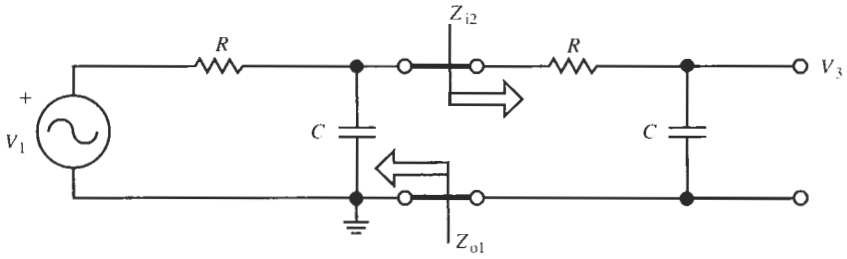

Figure 3.43 Cascade connection of two first-order passive lowpass sections.

$$Z_{i2} = R + \frac{1}{sC} \quad \text{and} \quad Z_{o1} = \frac{1}{sC + 1/R}$$

the transfer function

$$T(s) = \frac{V_3}{V_1} = \left(\frac{1}{sCR+1}\right)^2 \times \frac{R + \dfrac{1}{sC}}{\left(R + \dfrac{1}{sC}\right) + \left(\dfrac{R}{sCR+1}\right)}$$

$$= \frac{1}{(sCR+1)^2} \frac{(sCR+1)^2}{(sCR)^2 + 3sCR + 1} = \frac{1}{(sCR)^2 + 3sCR + 1} \tag{3.127}$$

This result can be confirmed by direct analysis of the circuit in Fig. 3.43. Comparing Eqs. (3.126) and (3.127), we see that the finite frequency-dependent input and output impedances changed the desired transfer function in a substantial way. Using the voltage follower of Fig. 2.26b, we can remedy the situation by *buffering* the sections as in Fig. 3.44 so that no current is drawn from the first section and the second section is driven by a nearly ideal voltage source.

To summarize the discussion, we repeat the important condition that must be satisfied if two circuits are to be connected in cascade: the trailing section must not load the leading section. The circuits to be cascaded can be of low order, high order, active, passive, or any desired combination; the loading restriction does not change. For designing high-order active filters, we shall see that the cascade connection normally consists of first- and second-order *active* building blocks because they can be cascaded directly with no need for buffering. Since active circuits usually have an opamp output as their output terminal [see e.g. Figs. (3.23), (3.30), and (3.34)], unbuffered cascading is possible because the opamp output resistance in a feedback network is very small (see Table 2.2). On the other hand, we can expect intuitively that *passive* circuits can generally not be connected in cascade without buffering because the condition (3.124) will rarely be satisfied. We mentioned at the end of Section 3.2 that the

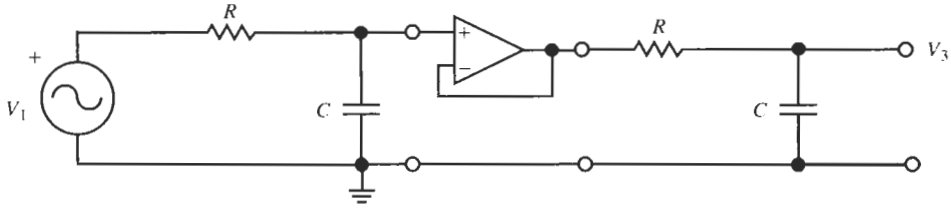

Figure 3.44 Two lowpass modules isolated by an opamp buffer.

possibility of loading a circuit without destroying the designed transfer function is a major benefit of active realizations. This advantage will come therefore to good use in the design of higher-order filters. For example, in the phase shifting network of Example 3.8, Fig. 3.38, the cascade connection causes no problems because the output impedance of the left amplifier is small compared to the input impedance of the following stage.

3.7 AND NOW DESIGN

We are now prepared to introduce some aspects of circuit design that will be amplified throughout the book. We do this in terms of some of the circuits analyzed earlier in this and in previous chapters, and we will make use of what we learned about opamp behavior. The design procedure may be summarized in the following steps:

Specification Some aspects of the required magnitude or phase response must be given along the frequency axis so that poles and zeros, i.e., the transfer function, can be identified. For example, if we describe filter requirements by a Bode plot, the break frequencies permit us to locate poles and zeros by a graphic trial-and-error procedure. We shall discuss in subsequent chapters a more rigorous mathematical process that provides the poles and zeros needed for the design without trial and error.

Requirement We require the complete circuit with element values in a practical range, consistent with the technology chosen.

Procedure The following steps are suggested:

1. Proceed from the specifications to determine the transfer function with its pole and zero locations. Poles and zeros are always needed before proceeding with filter design.
2. Select a circuit that promises to be able to satisfy the required magnitude or phase variation with frequency.
3. Use scaling and normalization, if desired, to reduce pole and zero locations to small numbers of the order on unity (eliminating high positive or negative powers of 10) and to be able to deal with dimensionless numbers for the components.
4. Determine the element values from the values of the poles and zeros.
5. If scaling was used, invert Step 3 to arrive at suitable practical component values.
6. Since a design problem never has a unique solution, investigate whether other circuit solutions exist that may be better suited to practical implementation in teems of component use, power consumption, or other factors.

The student may want to review some of the examples presented earlier in light of the six steps. A number of additional examples to point out various aspects of the design process follow.

EXAMPLE 3.11

Design a filter whose transfer characteristic satisfies the asymptotic Bode plot in Fig. 3.45a. It is that of a bandstop filter. There is no loss at high and low frequencies, but 20 dB attenuation is provided in the intermediate range 1000 rad/s $\leq \omega \leq$ 10000 rad/s.

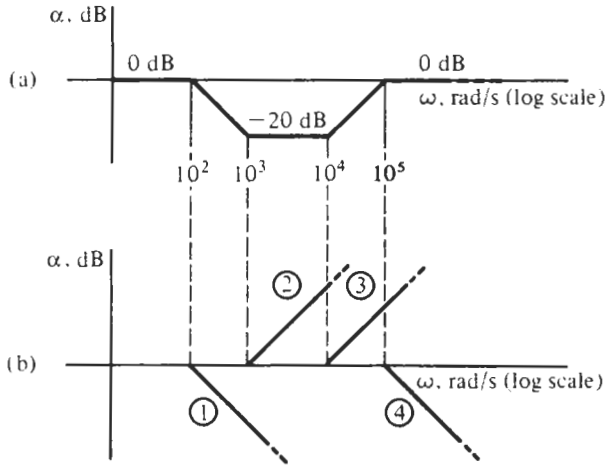

Figure 3.45 Specifications for Example 3.11.

Solution

The composite plot may be decomposed into four first-order factors as shown in Fig. 3.45b. Those marked 1 and 4 represent poles, whereas those marked 2 and 3 are zero factors. In other words, we see that

$$\alpha(\omega) = \alpha_0 - \alpha_1(\omega) + \alpha_2(\omega) + \alpha_3(\omega) - \alpha_4(\omega)$$

α_0 accounts for the possibility of a frequency-independent gain constant. From the given break frequencies and the 20-dB/decade slopes, we see that

$$T(j\omega) = K\frac{(1 + j\omega/10^3)(1 + j\omega/10^4)}{(1 + j\omega/10^2)(1 + j\omega/10^5)} \tag{3.128}$$

Written in this form, it is clearly seen that when $\omega = 0$, $T(j0) = K$. From the figure we see that the low-frequency value of $\alpha(\omega) = \alpha_0 = 0$ dB, so that by Eq. (2.26), $K = 1$. Substituting s for $j\omega$ in Eq. (3.128) gives us the transfer function

$$T(s) = \frac{(s + 10^3)(s + 10^4)}{(s + 10^2)(s + 10^5)} \tag{3.129}$$

With experience it will be possible to write $T(s)$ in this form directly from the asymptotic Bode plot, bypassing the intermediate steps.

We next write $T(s)$ as a product of bilinear functions. The choice is arbitrary, but one possibility is

$$T(s) = T_1(s)T_2(s) = \frac{s + 10^3}{s + 10^2} \times \frac{s + 10^4}{s + 10^5} \tag{3.130}$$

For a circuit realization of T_1 and T_2, we next decide to use the inverting opamp circuit in Fig. 3.24. Using the formulas for element values give in Eq. (3.71), we obtain for the first section

$$\frac{1}{C_{11}R_{11}} = 1000 \text{ rad/s} \quad \text{and} \quad \frac{1}{C_{21}R_{21}} = 100 \text{ rad/s}$$

and for the second section

$$\frac{1}{C_{12}R_{12}} = 10,000 \text{ rad/s} \quad \text{and} \quad \frac{1}{C_{22}R_{22}} = 100,000 \text{ rad/s}$$

It is convenient to choose all capacitors of the same value; let us select $C = 0.01\ \mu$F. Then we obtain

$$R_{11} = \frac{1}{1000 \text{ rad/s} \times 0.01\ \mu\text{F}} = 100\ \text{k}\Omega \quad \text{and} \quad R_{21} = \frac{1}{100 \text{ rad/s} \times 0.01\ \mu\text{F}} = 1\ \text{M}\Omega$$

$$R_{12} = \frac{1}{10{,}000 \text{ rad/s} \times 0.01\ \mu\text{F}} = 10\ \text{k}\Omega \quad \text{and} \quad R_{22} = \frac{1}{100{,}000 \text{ rad/s} \times 0.01\ \mu\text{F}} = 1\ \text{k}\Omega$$

The element values that result are shown in Fig. 3.46a and the design is complete. A characteristic of design that again becomes apparent is that there is no unique solution. If, e.g., the spread of resistor sizes in Fig. 3.46a is too large, then we begin the design process again and obtain a different result. This process may be repeated several times until a satisfactory solution is obtained.

To consider the effect of a real opamp on the transfer function of Eq. (3.130) we insert the specified poles and zeros of the two sections into Eq. (3.111):

$$T_1(s) = -\frac{s + 10^3}{2s^2/\omega_t + s\,(1 + 1100/\omega_t) + 100} \quad \text{and}$$

$$T_2(s) = -\frac{s + 10^4}{2s^2/\omega_t + s\,(1 + 11 \times 10^4/\omega_t) + 10^5} \tag{3.131}$$

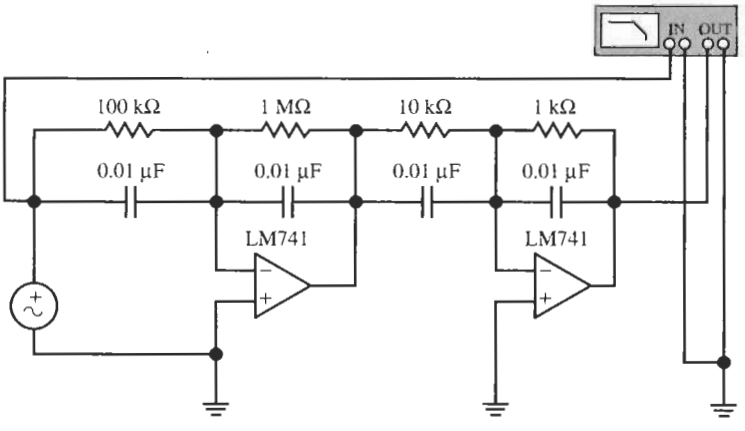

(a)

Figure 3.46 (a) Circuit realizing Eq. (3.128) of Example 3.11 and test set-up; (b) measured circuit performance with LM741 opamps (cursor readout is 100 kHz, 1.495 dB); (c) measured circuit performance with HA2542-2 opamps (cursor at 540.3 Hz, −19.17 dB). (The frequency scale of the Bode Plotter is set from 1 Hz to 1 MHz; the vertical axis goes from −20 dB to +10 dB.)

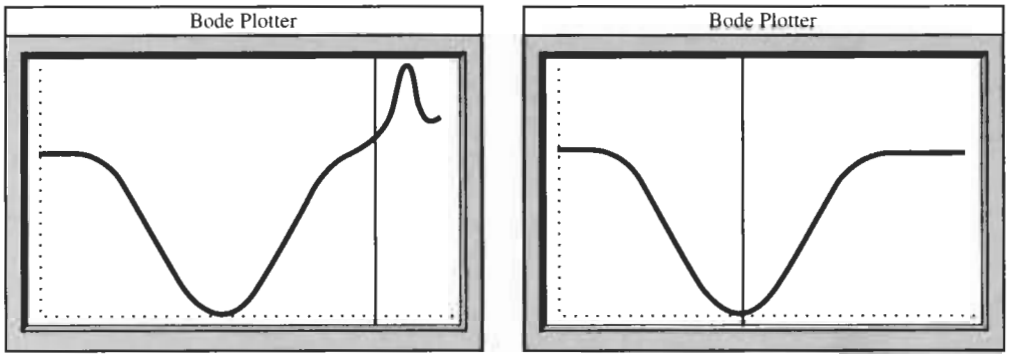

(b) (c)

Figure 3.46 Continued

This allows us to assess the shift of the nominal pole position and the parasitic pole for each section contributed by the opamp. With the highest frequency in the band of interest less than 100 kHz, we can assume that the design with real amplifiers will behave nearly as the specifications in Fig. 3.45 demand. Experimentally, the circuit's performance is indeed as specified until approximately 100 kHz. At higher frequencies, Figure 3.46b shows peaking in the transfer function caused by higher-order poles in the opamp model. This behavior may or may not be acceptable in practice; if it is not acceptable, a faster opamp must be used. Figure 3.46c shows the performance obtained with HA2542-2 opamps; it is ideal until 1 MHz.

EXAMPLE 3.12

The asymptotic Bode plot of Fig. 3.47a describes a *band-enhancement* filter or *gain equalizer*. We wish to obtain additional gain over a narrow band of frequencies, e.g., to compensate for the loss elsewhere in the transmission channel, leaving the gain at higher and lower frequencies unchanged. An additional specification is that all capacitors have the value $C = 0.01\ \mu$F.

Solution

This particular problem specifies that the peak gain of the *asymptotic* plot is 6 dB. Note that the *real* gain obtained after filling in a smooth curve in the asymptotic plot will be about 3 to 4 dB below the 6-dB peak. An asymptotic plot increases by 6 dB per octave, so that $\omega_a = 200$ rad/s. Since the plot returns to 0 dB, ω_b must be one octave greater than ω_a, or $\omega_b = 400$ rad/s. Next, the first-order factors that make up the Bode plot are shown in Fig. 3.47b. As frequency increases, the first break frequency identifies a zero factor; next comes a double pole factor, followed by another zero factor. The pole-zero plot corresponding to these factors is shown in Fig. 3.47c. From this information we construct $T(j\omega)$ as

$$T(j\omega) = K\frac{(1 + j\omega/100)(1 + j\omega/400)}{(1 + j\omega/200)^2} \tag{3.132}$$

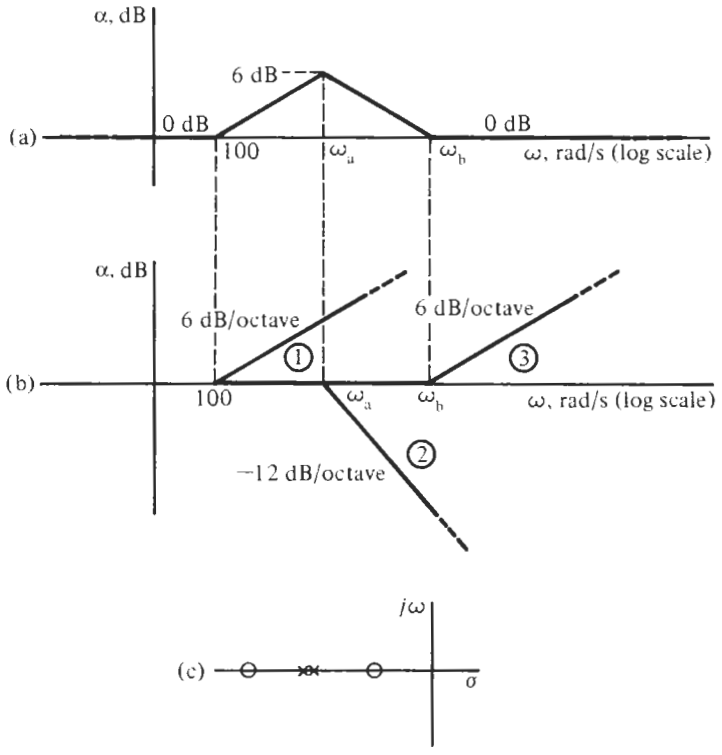

Figure 3.47 The decomposition of the band-enhancement filter magnitude response of (a) into component parts shown in (b), having poles and zeros for $T(s)$ as indicated in (c).

Since $T(0) = 0$ dB we have $K = 1$, and $T(s)$ is

$$T(s) = T_1(s)T_2(s) = \frac{(s+100)(s+400)}{(s+200)^2} = \frac{(s+100)}{(s+200)}\frac{(s+400)}{(s+200)} \tag{3.133}$$

The frequencies are in rads/second, i.e., no normalization is used. If we employ the same strategy that we used for Example 3.11, we obtain the circuit shown in Fig. 3.48a with the performance in Fig. 3.48b. But in design there are always many possibilities. Suppose we try for this example a design that uses the noninverting opamp circuit of Fig. 3.30 and the admittance-based approach in Eqs. (3.88) and (3.89). From Eq. (3.89), we obtain for Module 1

$$Y_{11} = s(k_1 - 1) + 100k_1 - 200 \quad \text{and} \quad Y_{21} = s + 200$$

and for Module 2

$$Y_{12} = s(k_2 - 1) + 400k_2 - 200 \quad \text{and} \quad Y_{22} = s + 200$$

Clearly, to realize these equations with positive element values, we require $k_1 \geq 2$ and $k_2 \geq 1$. Choosing $k_1 = 2$ and $k_2 = 1$ to save one resistor and one capacitor, results in

$$Y_{11} = s, \quad Y_{12} = 200, \quad \text{and} \quad Y_{21} = Y_{22} = s + 200$$

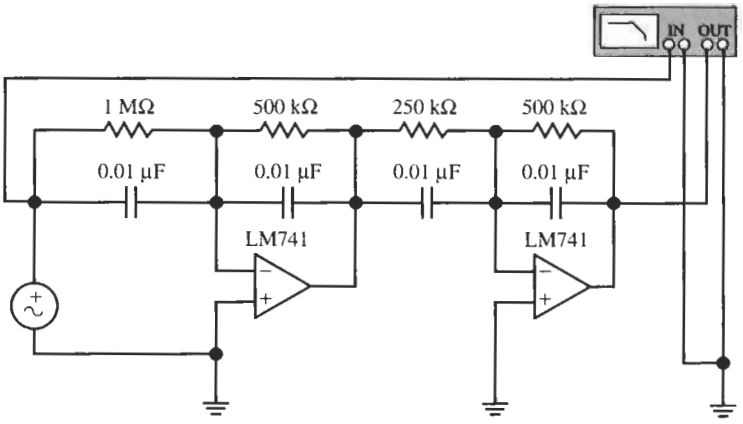

(a)

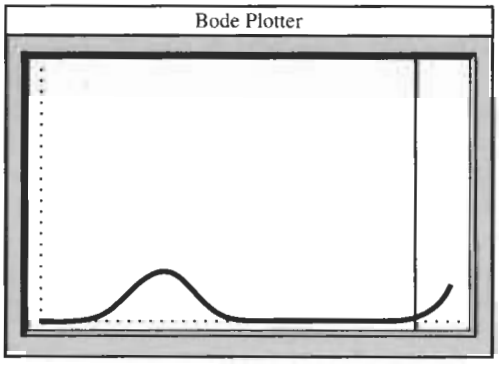

(b)

Figure 3.48 Two implementations of Eq. (3.133) and test results. (Bode Plotter scales: 1 Hz to 100 kHz; 0 dB to +10 dB). Circuit using (a) inverting opamp sections with test result in (b) and the cursor is at 35.5 kHz, 0.187 dB; (c) noninverting opamp circuits with test results in (d) and the cursor is at 31.85 Hz, 1.938 dB.

Since C is specified to equal 0.01 μF and no frequency normalization was used, we find the three resistors to be equal to

$$R = \frac{1}{200 \text{ rad/s} \times 0.01\ \mu\text{F}} = 500\ \text{k}\Omega$$

Finally, since we chose $k_1 = 2$, the filter realizes a gain of two (6 dB) rather than the specified gain of unity. If the exact gain must be realized, we can precede the active blocks by a voltage divider of gain equal to 1/2, since no current is drawn from the divider. The final circuit and its performance are seen in Figs. 3.48c and 3.48d.

As an example for mixing passive and active sections, consider realizing the same transfer function with one section of Eq. (3.133) implemented by the circuit in Fig. 3.3. It realizes, from Eq. (3.20),

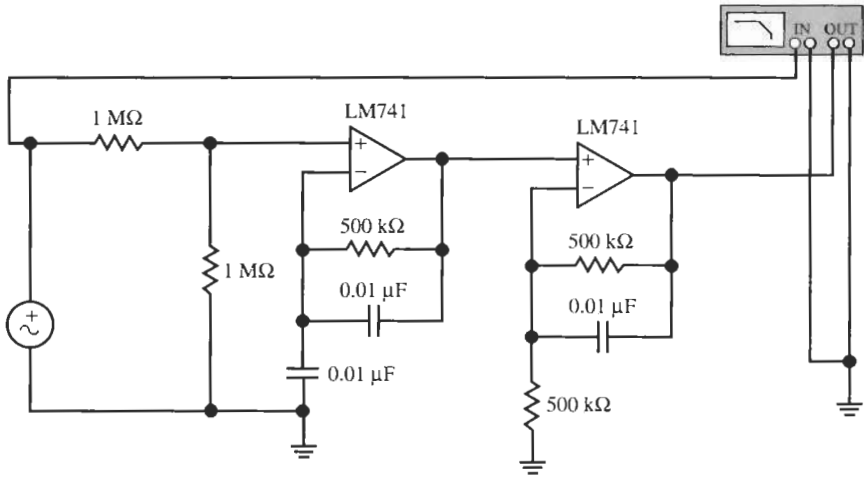

(c)

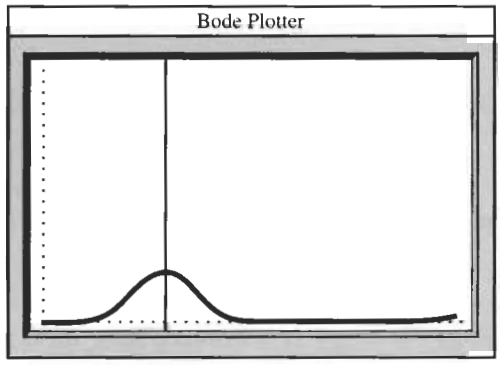

(d)

Figure 3.48 Continued

$$T(s) = \frac{C_1}{C_1 + C_2} \frac{s + G_1/C_1}{s + (G_1 + G_2)/(C_1 + C_2)} = K \frac{s + z_1}{s + p_1} \tag{3.134}$$

Note that $K < 1$. Let us, for convenience, label $K = 1/k$ with $k > 1$, and rewrite Eq. (3.133) as

$$T(s) = T_1 T_2 = \frac{1}{k} \frac{s + 400}{s + 200} \times k \frac{s + 100}{s + 200}$$

to maintain the prescribed gain. The second section we implement by the noninverting active circuit in Fig. 3.30, realizing, from Eq. (3.88),

$$\frac{Z_2}{Z_1} = \frac{(k-1)s + 100k - 200}{s + 200} \tag{3.135}$$

Note that we have reordered T_1 and T_2. The reason for this reordering will become clear momentarily.

Considering the requirement that capacitor values are $C = 0.01\ \mu$F we have $k = 1/K = 2$. As a result, Eq. (3.135) becomes

$$\frac{Z_2}{Z_1} = \frac{s}{s+200} = \frac{1}{1+200/s} = \frac{R_2}{R_1 + 1/(sC)}$$

and we find

$$C_1 = 0.01\ \mu\text{F}, \quad C_2 = 0, \quad \text{and} \quad R_1 = R_2 = \frac{1}{200\ \text{rad/s} \times 0.01\ \mu\text{F}} = 500\ \text{k}\Omega$$

For the passive circuit we obtain from Eq. (3.134)

$$z_1 = -400 = -\frac{1}{R_1 C} \quad \text{and} \quad p_1 = -200 = -\frac{1}{2CR_1R_2/(R_1+R_2)}$$

Consequently, we can complete the design for the passive circuit as

$$R_1 = \frac{1}{400C} = \frac{10^6}{4}\ \Omega = 250\ \text{k}\Omega \quad \text{and} \quad R_2 = \left(\frac{1}{400C} - 1\right) R_1 = 6.25\ \text{G}\Omega$$

The resistor value R_2 is unrealistically large. Let us, therefore, relax the requirement that all capacitors have the value 0.01 μF and choose instead $C = 1\ \mu$F in the passive module. Then we obtain

$$R_1 = \frac{1}{400C} = \frac{10^6}{400}\ \Omega = 2.5\ \text{k}\Omega \quad \text{and} \quad R_2 = \left(\frac{1}{400C} - 1\right) R_1 = 6.2\ \text{M}\Omega$$

The value of R_2 is still large, but more realistic. The circuit and its performance with an LM741 opamp are shown in Fig. 3.49a and b.

The designer will have to decide now which of the three realizations in Fig. 3.48 or 3.49 to select for implementation. The decision involves value judgments, trade-offs in cost and power consumption, and a comparison of performance. The circuits in Fig. 3.48 have little to recommend themselves over each other; both use two opamps and eight passive components, but in Fig. 3.48c we used one capacitor less, a slight cost advantage. In Fig. 3.49, we succeeded in a realization with only one opamp and seven passive components, but were forced by otherwise unrealistic resistor values to abandon the requirement of identical 0.01-μF capacitors. Considering that the frequencies of interest are below 1 kHz, experimentally, the three circuits have the same performance; only for frequencies above 400 kHz do we observe substantial peaking, much more so for the circuits in Fig. 3.48 than for the one-opamp design in Fig. 3.49. Saving one opamp together with the improved behavior at high frequencies may provide a deciding advantage in cost and power consumption compared with the other two realizations. The example shows quite clearly that the designer will have to consider many different points and performance characteristics before a final choice of circuit can be made.

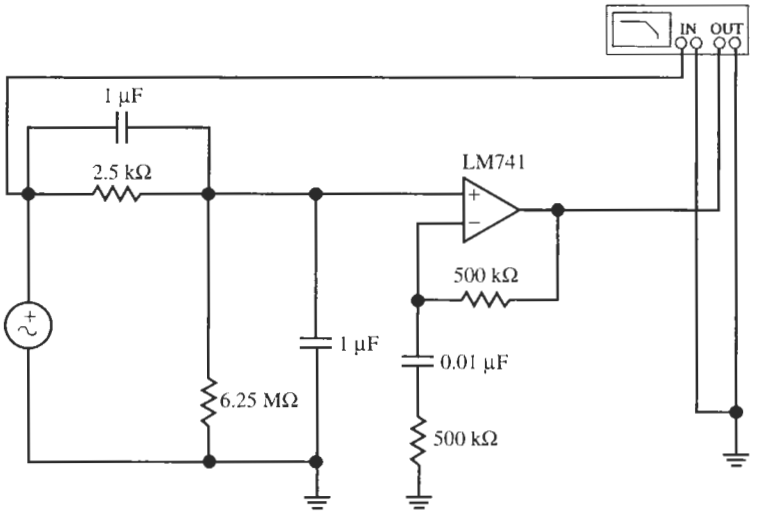

(a)

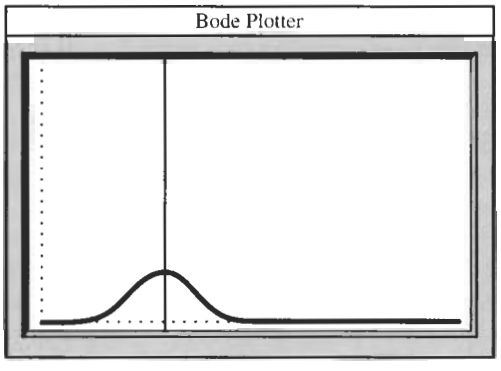

(b)

Figure 3.49 (a) A third circuit realizing Eq. (3.123); (b) test performance. (Bode Plotter scales: 1 Hz to 100 kHz; 0 dB to +10 dB; cursor at 31.62 Hz, 1.936 dB.)

Example 3.12 called for a maximum gain enhancement of 6 dB. Let us generalize this problem as follows: given a maximum gain enhancement of h dB at a center frequency of ω_0, find the two break frequencies ω_1 and ω_2; all the quantities are identified in Fig. 3.50. With ω_1 and ω_2 determined, $T(s)$ may be found following the steps in the last two examples.

We first observe that the distances AB and BC in Fig. 3.50 are equal because the slope of one line is 6 dB per octave and that of the other line is −6 dB per octave. Then

$$\log \omega_0 - \log \omega_1 = \log \omega_2 - \log \omega_0 \tag{3.136}$$

or

$$2 \log \omega_0 = \log \omega_2 + \log \omega_1 = \log \omega_1 \omega_2$$

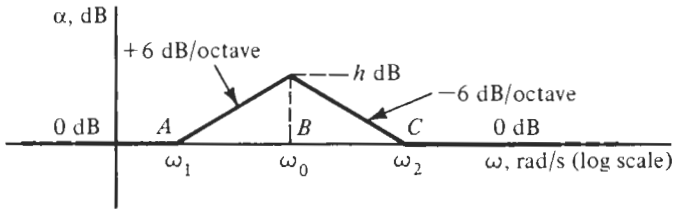

Figure 3.50 Diagram to support the derivation of Eq. (3.137).

so that finally

$$\omega_0^2 = \omega_1 \omega_2 \tag{3.137}$$

Note that ω_0 is the geometric mean of the two break frequencies. This is an important relationship that will be used frequently in the chapters that follow. Returning to Fig. 3.50, we make two observations. Let the frequencies ω_1 and ω_2 be separated by n octaves so that

$$\frac{\omega_2}{\omega_1} = 2^n \tag{3.138}$$

If the line of positive slope is extended to ω_2, then its value will be $\alpha = 2h$ dB, so that

$$n \times 6 = 2h \text{ dB} \tag{3.139}$$

Combining these two equations gives

$$\frac{\omega_2}{\omega_1} = 2^{h/3} \tag{3.140}$$

Combining this result with Eq. (3.137) gives us the values for the two break frequencies

$$\omega_1 = \omega_0 2^{-h/6}, \qquad \omega_2 = \omega_0 2^{+h/6} \tag{3.141}$$

As a check, note that $h = 6$ dB gives the values found for Example 3.12.

A similar strategy can be followed to determine the midband frequency f_0 when the gain of the frequency band of interest is flat and a central peak as in Fig. 3.50 is not identified. This situation is shown in Fig. 3.51 where we have indicated two Bode asymptotes of ±20 dB/decade and a horizontal constant midband gain between the frequencies f_1 and f_2. The midband frequency f_0 is then found graphically as is shown in the figure by extending the ±20 dB/decade asymptotes until they meet. In equations, we write from the top triangle in Fig. 3.51

$$\log f_0 - \log f_1 = \log f_2 - \log f_0$$

so that, as in Eq. (3.137),

$$f_0 = \sqrt{f_1 f_2} \tag{3.142}$$

is again the geometric mean of the two 3-dB corner frequencies.

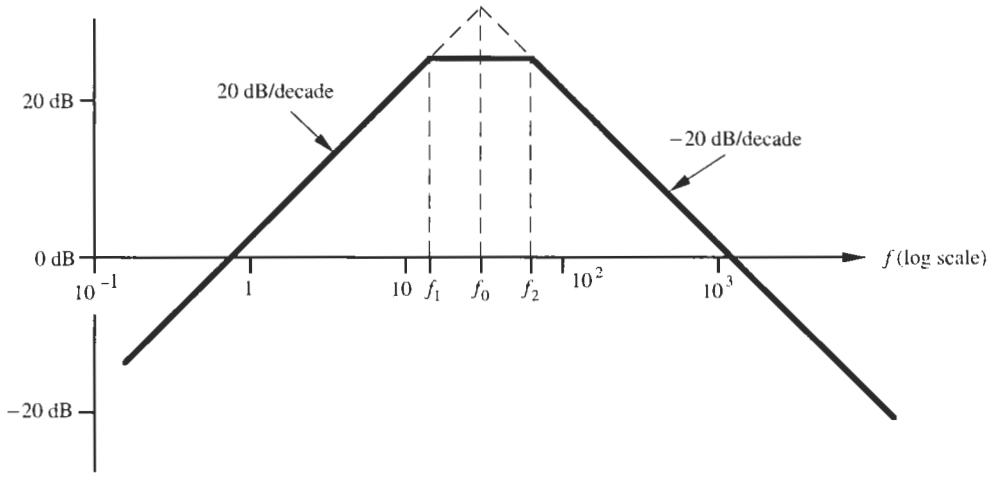

Figure 3.51 Diagram to support the derivation of Eq. (3.142).

We have shown in this chapter how a variety of useful filters can be designed by a very simple procedure: using passive and active bilinear sections by themselves or in cascade. It is a limitation of these filters that their building blocks, the first-order sections, have only simple real-axis poles and zeros. One consequence of this restriction is that the attenuation in the stopband increases at a slope of only 20 dB/decade. The designer can attempt to increase this roll-off by connecting more sections in cascade, adding the corresponding Bode plots (the attenuation in dB). However, this approach generally also narrows the passband. We see that a convenient workable solution is not as simple as multiplying the number of sections. Quite apart from increasing the cost of the design in proportion to the number of sections, a complete redesign of all sections would be needed each time a section is added to the filter. The problem is the restriction of poles and zeros to the real axis. If we can shift these *critical frequencies* away from the real axis into the complex s-plane, we gain considerable freedom in shaping transfer functions for filters with steeper transition regions. The different second-order or higher order circuit structures to achieve this goal will be discussed in the next chapter.

PROBLEMS

3.1 Find the magnitude and phase of the following transfer functions as a function of frequency. Express the low- and high-frequency values of the functions in dB.

(a) $T_1(s_n) = K\dfrac{s_n + z_1}{s_n + p_1}$

(b) $T_2(s_n) = 5\dfrac{s_n + 2}{s_n + 1}$; s_n is normalized with respect to ω_c where $f_c = 19$ kHz.

(c) $T_3(s_n) = -2\dfrac{9 - s_n}{3 + s_n}$; s_n is a normalized with respect to $\omega_c = 4\pi$ Mrad/s.

(d) $T_4(s) = \dfrac{s - 2700}{s + 2700}$

3.2 Derive an inverting allpass function to have $|T| = 1$ and a phase shift of $\phi = 38°$ at $f = 9.2$ kHz.

3.3 Construct a first-order function $T(s)$ such that $T(0) = 1, T(\infty) = 0.2$. Determine the remaining degrees of freedom to set the function's pole at $f_p = -2$ kHz.

3.4 Find the real and imaginary parts of the following transfer functions:

(a) $T_1 = 2\dfrac{s+400}{s+1200}$

(b) $T_2 = \dfrac{s-1400}{s+1400}$

(c) $T_3 = 9\dfrac{s/12000+1}{s/24000+1}$

3.5 Realize the functions of Problem 3.1 and Problem 3.4 with the passive bilinear filters of Fig. 3.2 or Fig. 3.13 as appropriate. Determine the components such that $C_{max} = 0.1\ \mu$F. Find alternative realizations if possible by interpreting the impedances Z_1 and Z_2 in Fig. 3.2 either as a parallel or as a series connection of a resistor and a capacitor.

3.6 A first-order lowpass filter is to be designed with $T(0) = 0.9$ and the 3-dB frequency of $f = 1.2$ MHz. No power supply is available, i.e., the circuit must be passive. Verify your design with Electronics Workbench (EWB).

3.7 Design a passive first-order lowpass filter to have dc gain of unity and a lagging phase of 28° at $f = 460$ kHz. Verify your design with EWB.

3.8 In the circuit of Problem 3.7, interchange the positions of the resistor and the capacitor. Characterize the resulting filter; give its low-frequency and high-frequency values, the 3-dB frequency, and compute the phase shift at 460 kHz. Verify your result with EWB.

3.9 Design a first-order passive highpass filter such that the dc gain is zero and the attenuation is at least 12 dB for $f < 15.6$ kHz. Verify your design with EWB.

3.10 Design a passive allpass filter to realize the gain $|T| = 0.5$ such that the phase equals $-45°$ at $f = 4.8$ kHz. Verify your design with EWB.

3.11 The phase of a first-order passive allpass filter should be less than 120° for $f \geq 600$ kHz. Derive the circuit with a suitable set of practical component values. Verify your design with EWB.

3.12 Prepare an asymptotic Bode plot for both magnitude and phase for the following transfer functions. In making the plots it is useful to make use of four- or five-cycle semilog paper. Assume that the frequency parameter in all functions is normalized by $\omega_1 = 1000$ rad/s.

(a) $T(s) = 2\dfrac{s+2}{s+9}$

(b) $T(s) = -100\dfrac{s+10^4}{s+10^2}$

(c) $T(s) = 1000\dfrac{(1+0.25s)(1+0.1s)}{(1+s)(1+0.025s)}$

(d) $T(s) = \dfrac{(1+0.1s)(1+0.01s)}{(1+s)(1+0.001s)}$

(e) $T(s) = \dfrac{1000s}{(1+0.01s)(1+0.0025s)}$

(f) $T(s) = 180\dfrac{s(1+0.01s)}{(1+0.05s)(1+0.001s)}$

(g) $T(s) = 50\dfrac{(1+0.025s)}{s(1+0.05s)}$

(h) $T(s) = \dfrac{100}{s(1+0.01s)(1+0.001s)}$

(i) $T(s) = 1000\dfrac{s^2}{(1+0.17s)(1+0.53s)}$

3.13 Figure P3.13 shows only the asymptotes of a Bode magnitude plot. The characteristic response is used for gain enhancement—increasing the gain over a band of frequencies, but not changing either high- or low-frequency behavior. For this response, determine $T(s)$, evaluating all constants.

3.14 Repeat Problem 3.13 for the Bode magnitude plot shown in Fig. P3.14.

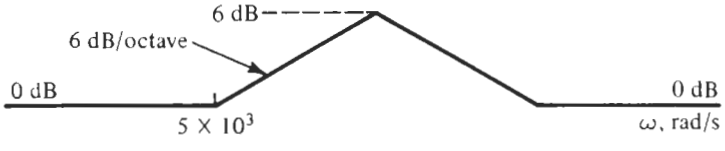

Figure P3.13

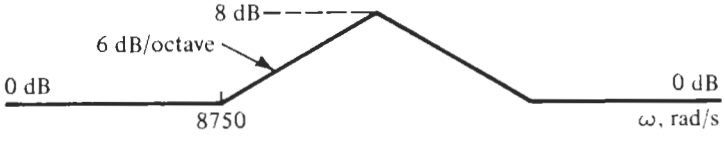

Figure P3.14

3.15 Reconsider Problem 3.13 where it is specified that the peak gain of the *asymptote* is 6 dB. Estimate the actual gain, not that of the asymptote, at the peak frequency.

3.16 Redesign the function of Problem 3.13 such that the actual peak gain, not that of the asymptote, is 6 dB. Aim for the same peak frequency, i.e., midband at 10 krad/s, as in Problem 3.13 and adjust the lower and upper break frequencies accordingly.

3.17 The bandpass response shown in Fig. P3.17 is given as a specification. As the first step in the design of the circuit determine $T(s)$, evaluating all constants.

3.18 The problem is to design an amplifier-filter having the Bode asymptotic plot shown in Fig. P3.18. Determine $T(s)$, evaluating all constants.

3.19 Given the Bode asymptotic plot for a notch filter as shown in Fig. P3.19, determine $T(s)$, evaluating all constants.

3.20 The transfer function corresponding to the asymptotic Bode plot shown in Fig. P3.20 has only real poles and zeros. Construct $T(s)$, determining all constants.

3.21 The asymptotic Bode plot shown in Fig. P3.21a represents a filter-amplifier having a break frequency of 1000 rad/s. Determine a transfer function $T_0(s)$ that when multiplied by $T(s)$ of Fig. P3.21a gives that specified in Fig. P3.21b.

3.22 Figure P3.22 shows the asymptotic of a Bode plot.

(a) Determine the half-power frequency for this plot, the point 3 dB below $T(0)$.

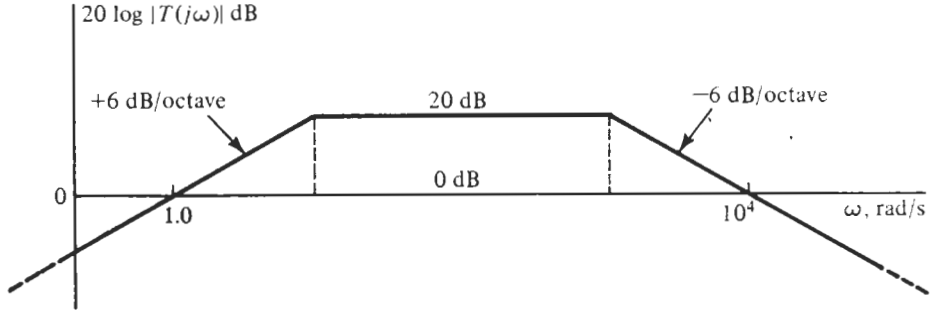

Figure P3.17

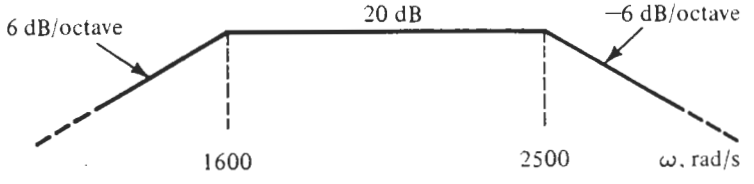

Figure P3.18

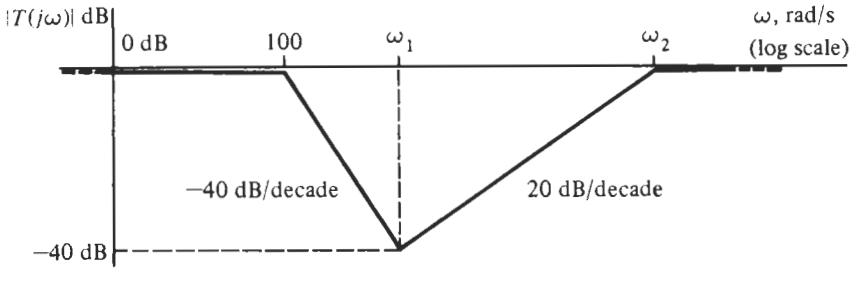

Figure P3.19

(b) Determine $T(s)$, evaluating all constants.

3.23 For the circuit given in Fig. P3.23, prepare an asymptotic Bode plot for the magnitude of $T(j\omega)$. Carefully identify slopes and low- and high-frequency asymptotes.

3.24 The circuit shown in Fig. P3.24 consists of the cascade connection of two opamp circuits. For this circuit, determine $T(s)$ and plot the Bode asymptotic magnitude function. Identify slopes and the low- and high-frequency asymptotes.

3.25 For the circuit given in Fig. P3.25, prepare the asymptotic Bode plot for the magnitude of $T(j\omega)$. Carefully identify all slopes and low- and high-frequency asymptotes.

3.26 The circuit given in Fig. P3.26 consists of the cascade connection of three sections. The first is an inverting stage in which the input is the sum of voltages V_0 and V_1; the second stage is a passive RC circuit; and the third stage is a noninverting opamp circuit. In the total circuit, all Cs are equal, and all Rs are equal.

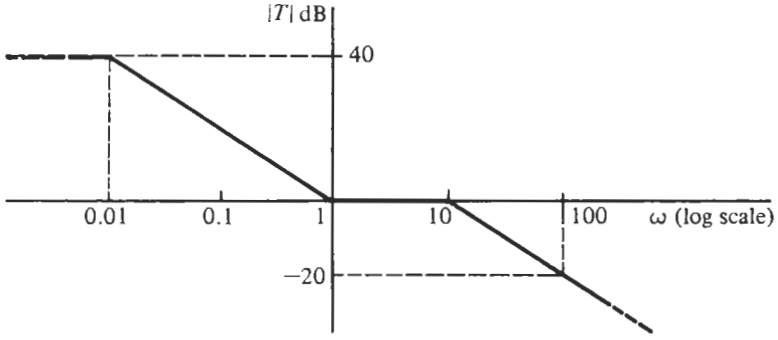

Figure P3.20

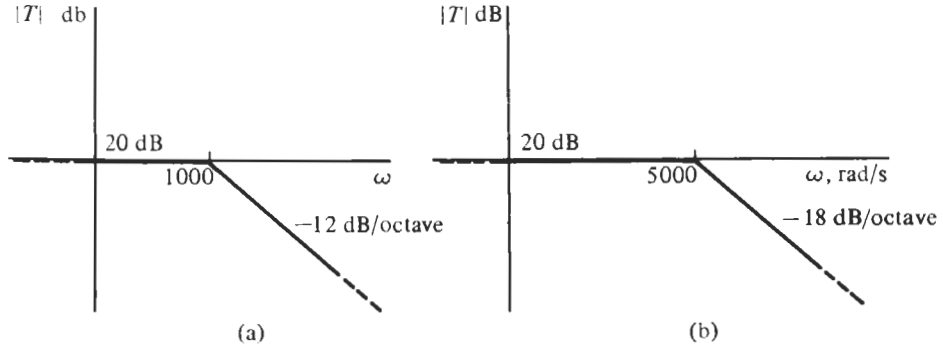

Figure P3.21

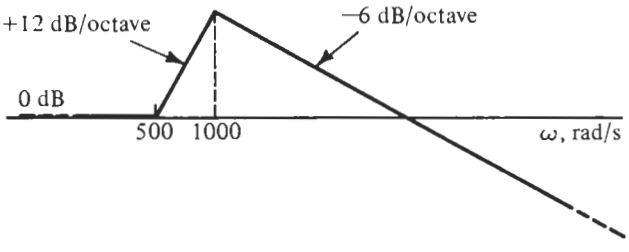

Figure P3.22

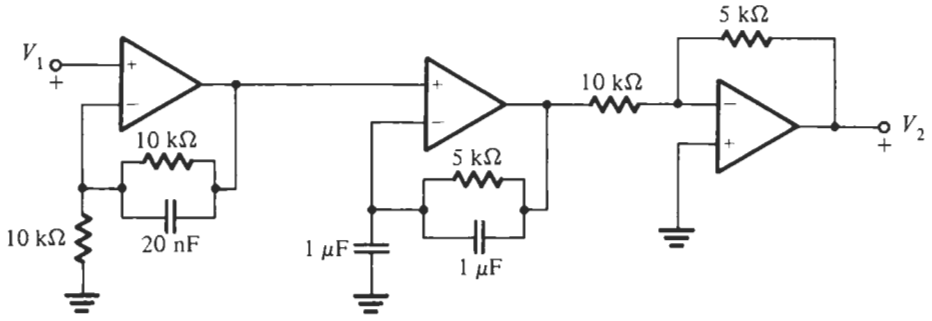

Figure P3.23

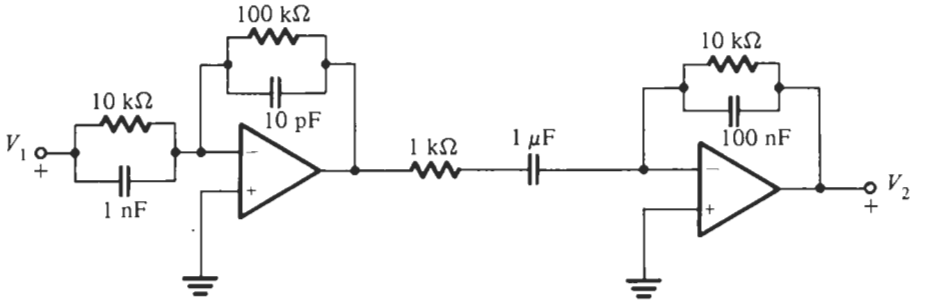

Figure P3.24

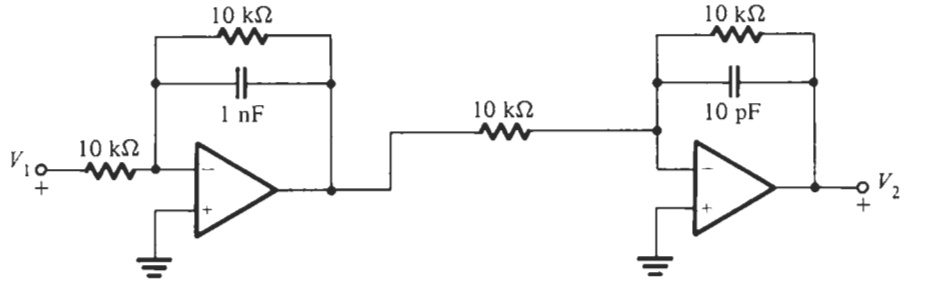

Figure P3.25

(a) Let $V_o = 0$ and find the transfer function $T = V_2/V_1$.

(b) Connect node 0 to node 2 such that $V_o = V_2$, and determine the transfer function under this condition.

3.27 Choose an appropriate active filter structure to implement the transfer functions of Problem 3.1. Use suitable opamps and verify each of the designs with EWB.

3.28 Choose a suitable active filter structure to implement the transfer functions of Problem 3.4. Use LM741 opamps and verify each of the designs with EWB.

3.29 Implement the first-order transfer functions of Problems 3.12a and b. Use an LM741 opamp and test each of the designs with EWB.

3.30 Design and test with EWB a noninverting active first-order lowpass filter such that $|T(0)| = 1$ and $|T(\infty)| = 1$. The 3-dB point must be at $f = 3.7$ kHz.

3.31 Design and test with EWB an active first-order highpass filter such that $|T(0)| = 0.1$ and $|T(\infty)| = 1$.

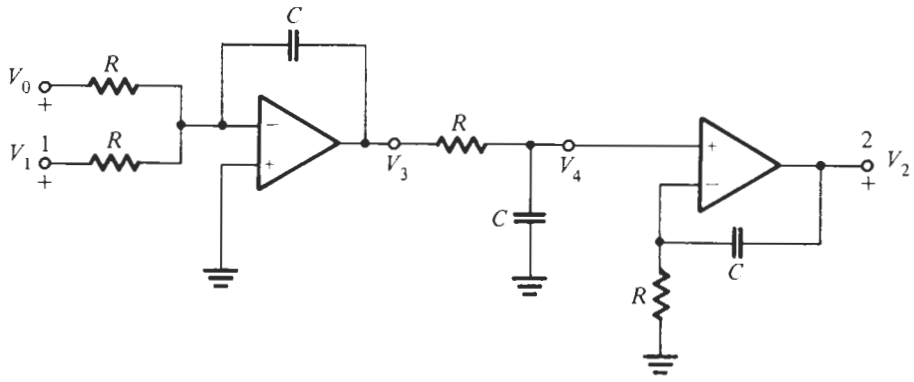

Figure P3.26

The gain should be 3 dB below its maximum at $f = 8.9$ kHz. The gain must be inverting. Use an LM741 opamp.

3.32 Implement the second-order transfer functions of Problems 3.12c through i. Use LM741 opamps and test each of the designs with EWB.

3.33 Design an active filter to realize the function derived in Problem 3.15. Use appropriate opamps and test the designs with EWB.

3.34 Design an amplifier-filter having the Bode asymptotic plot shown in Fig. P3.34. Find the circuit and give the schematic and element values. Scale so that the element values are in a practical range.

3.35 In the function derived in Problem 3.20, the frequency is normalized by 10^3 rad/s. Design an active filter with LM741 opamps to realize the function. Make certain that only practical component values are used and test your design with EWB.

3.36 Design and test a circuit to realize the transfer function derived in Problem 3.13.

3.37 Design and test a circuit to realize the transfer function derived in Problem 3.14.

3.38 Design and test a circuit to realize the transfer function derived in Problem 3.16.

3.39 Design and test a circuit to realize the transfer function derived in Problem 3.19.

3.40 Design and test a circuit to realize the transfer function derived in Problem 3.21.

3.41 Design and test a bandpass filter having the asymptotic Bode plot shown in Fig. P3.41. Use a minimum number of opamps in your realization. Scale element values until they are in a practical range.

3.42 Figure P3.42 shows the asymptotic Bode plot for a bandpass filter. Design and test a circuit that realizes the given frequency response. Give the schematic, and indicate element values chosen for your design.

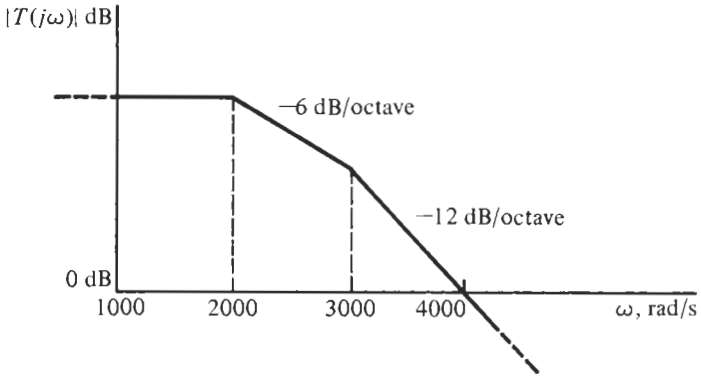

Figure P3.34

3.43 Design and test an *RC* opamp filter to realize the bandpass response shown in Fig. P3.43. Use a minimum number of opamps in your design, and scale so that the elements are in a practical range.

3.44 The asymptotic of the Bode plot shown in Fig. P3.44 represent a characteristic that has the objective opposite to that described in Problem 3.13. In this case, we wish to reduce the gain over a band of frequencies. Find a circuit that will realize the given specification characteristic. Design and test the circuit that satisfies the requirements.

3.45 The asymptotic Bode plot shown in Fig. P3.45 represents a lowpass filter with gain enhancement over a range of frequencies. Design and test a circuit using no more than two opamps that will have this magnitude characteristic using one or both of the circuits shown in Fig. P3.45b and c.

3.46 The characteristic shown in the asymptotic Bode plot of Fig. P3.46 indicates that considerable gain enhancement is required over a large band of frequencies, but there should be no change in gain at low and high frequencies. Design and test an opamp circuit that realizes these specifications.

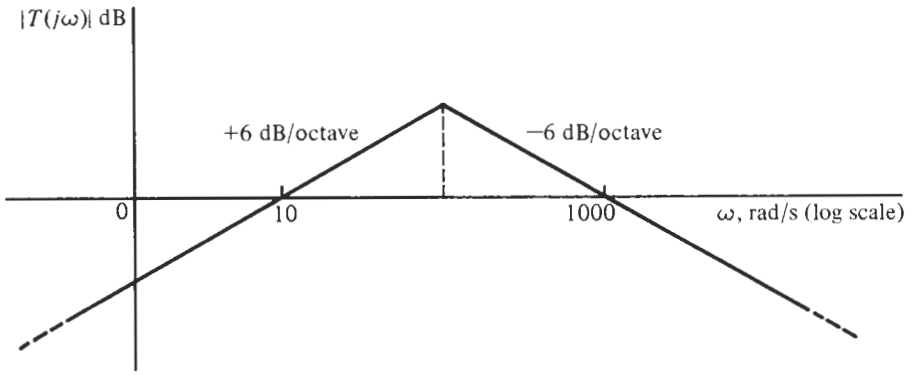

Figure P3.41

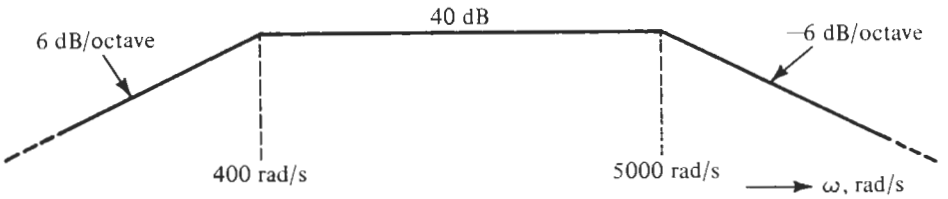

Figure P3.42

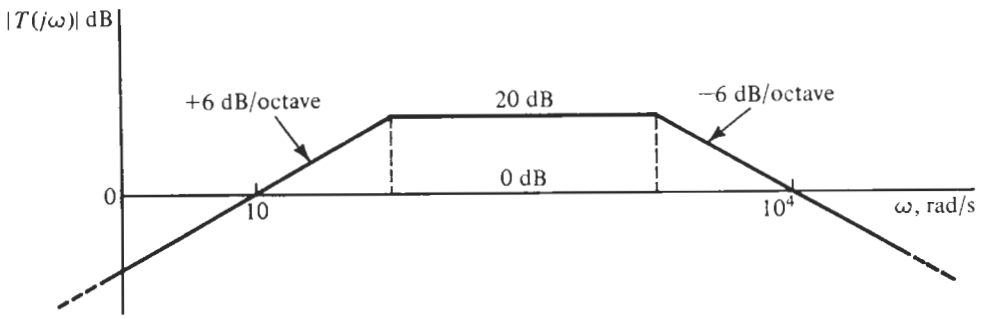

Figure P3.43

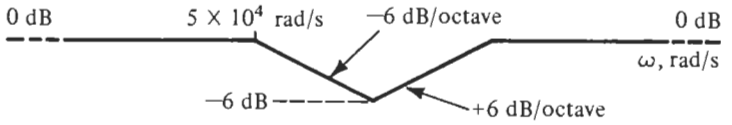

Figure P3.44

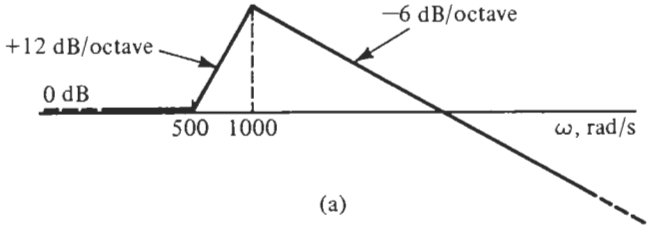

(a)

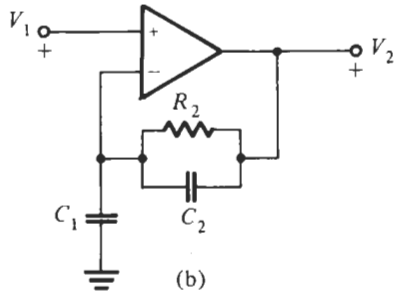

(b)

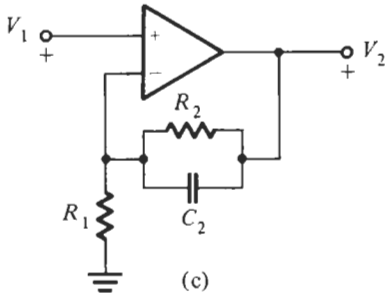

(c)

Figure P3.45

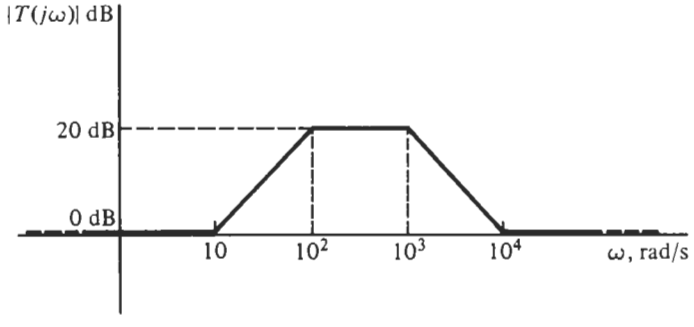

Figure P3.46

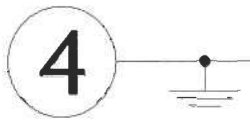

SECOND-ORDER LOWPASS AND BANDPASS FILTERS

Second-order filters, often referred to as *biquads*, are among the most useful circuits when electrical engineers have to solve analog signal processing requirements. Sections of second order can be configured to be universal filters: their poles are complex conjugates in the left half of the s-plane and zeros are also complex conjugates that may lie anywhere in the s-plane. Cascade connections of biquads are used most frequently when filters of higher order are to be designed. We will discuss in this chapter specifically second-order lowpass and bandpass filters and leave the more general biquads to Chapter 5. We shall start by defining a few basic terms and the notation used by filter designers and we shall then investigate how fundamentally a biquad can be designed to meet arbitrary requirements.

4.1 DESIGN PARAMETERS Q AND ω_0

Jargon fills a special need for the engineer. It is a shorthand that permits the experession of ideas quickly and concisely. "Design a bandpass filter with a Q of 5 and an ω_0 of 10,000." In this section we will explore what this statement means.

We begin with the RLC circuit shown in Fig. 4.1, which has the now familiar form of a voltage-divider circuit. We can anticipate the form of the transfer function $T(s) = V_L(s)/V_1(s)$

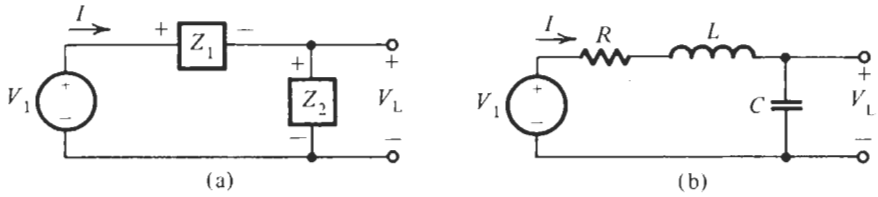

Figure 4.1 Voltage divider representation (a) of an RLC circuit (b) with complex poles. V_L is a lowpass output.

by considering the behavior of the elements at low and high frequencies. At low frequencies C behaves as an open circuit; thus there is no current in R and L, and so $V_L = V_1$ approximately. At high frequencies the capacitor C behaves as a short circuit so that V_L approaches the value $V_L = 0$ in the limit. We have used the label V_L for the voltage at the output because we see that the circuit is a lowpass filter of the type familiar from studies in the last two chapters. From the voltage-divider equation,

$$T(s) = \frac{V_L(s)}{V_1(s)} = \frac{Z_2}{Z_1 + Z_2} = \frac{1/(Cs)}{Ls + R + 1/(Cs)} \tag{4.1}$$

Dividing numerator and denominator by L and multiplying by s, we obtain

$$T(s) = \frac{1/(LC)}{s^2 + (R/L)s + 1/(LC)} \tag{4.2}$$

This result may be put into a *standard form* by defining two new quantities. First we observe that when the circuit is lossless with $R = 0$, then the denominator reduces to the simple form from which the pole positions may be determined:

$$s^2 + \frac{1}{LC} = 0 \tag{4.3}$$

or

$$s_1, s_2 = \pm j\sqrt{\frac{1}{LC}} = \pm j\omega_0 \tag{4.4}$$

This means that the poles are on the imaginary axis and are conjugates. The other parameter that we require originated in studies of lossy coils for which a *quality factor* Q was defined as Q_L/R_{Loss}, which is the ratio of reactance at the frequency ω to resistance. Here we define similarly at the frequency $\omega = \omega_0$.

$$Q = \frac{\omega_0 L}{R} = \frac{1}{R}\sqrt{\frac{L}{C}} \tag{4.5}$$

The historical identification of Q with a lossy coil is no longer appropriate, of course, and we will identify many kinds of circuits with the parameter Q. The last equation may be solved for the ratio R/L in Eq. (4.2):

$$\frac{R}{L} = \frac{\omega_0}{Q} \tag{4.6}$$

Substituting this equation and Eq. (4.4) for $1/(LC)$ into Eq. (4.2), we obtain

$$T(s) = \frac{\omega_0^2}{s^2 + (\omega_0/Q)s + \omega_0^2} = \frac{N(s)}{D(s)} \tag{4.7}$$

This is the desired standard form. Before studying $T(j\omega)$, we turn our attention to the s-plane location for the poles of $T(s)$.

The poles of $T(s)$ are the values for which $D(s) = 0$ in Eq. (4.7). Let their s-plane location be $-\alpha \pm j\beta$ so that

$$\begin{aligned} D(s) &= (s + \alpha + j\beta)(s + \alpha - j\beta) \\ &= s^2 + 2\alpha s + (\alpha^2 + \beta^2) \end{aligned} \tag{4.8}$$

Equating like terms of this equation and $D(s)$ in Eq. (4.7), we find that

$$\alpha = \frac{\omega_0}{2Q} \tag{4.9}$$

or

$$Q = \frac{\omega_0}{2\alpha} \tag{4.10}$$

Similarly, equating the constant terms in $D(s)$ in Eqs. (4.7) and (4.8):

$$\omega_0^2 = \alpha^2 + \beta^2 \tag{4.11}$$

Combining this with Eq. (4.9) and solving for β gives

$$\beta = \omega_0\sqrt{1 - \frac{1}{4Q^2}} \tag{4.12}$$

All of these relationships are shown in Fig. 4.2. In this figure we also define the angle ψ with respect to the negative real axis as

$$\psi = \cos^{-1}\left(\frac{\alpha}{\omega_0}\right) = \cos^{-1}\left(\frac{1}{2Q}\right) \tag{4.13}$$

Figure 4.3 shows important contours in the s-plane. Contours of constant ω_0 are cir-

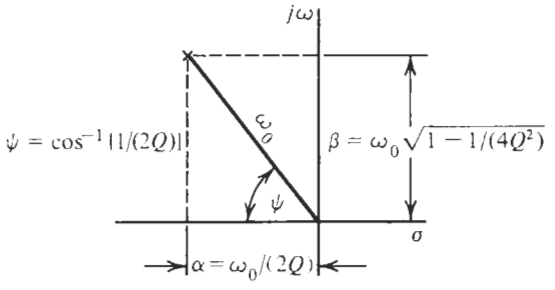

Figure 4.2 Definitions of parameters related to pole positions.

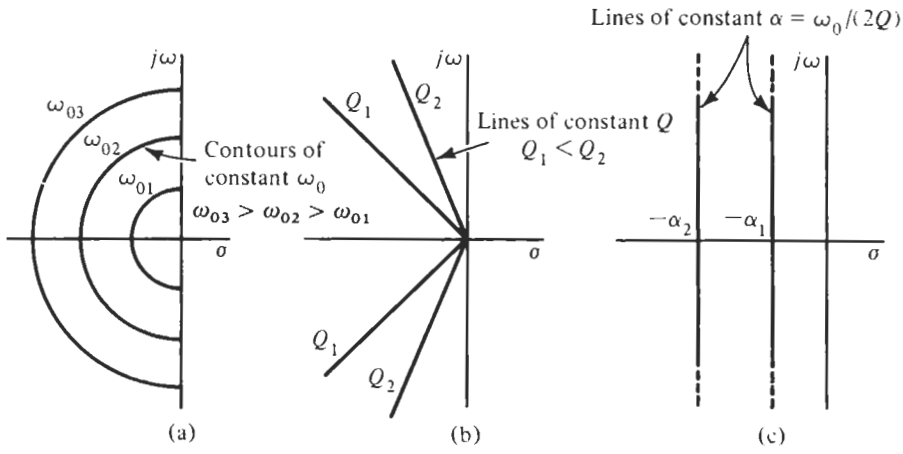

Figure 4.3 Contours in the s-plane.

cles of radius ω_0 with their centers at the origin, as shown in Fig. 4.3a. From Eq. (4.13) we see that lines of constant Q are lines of constant angle ψ, as shown in Fig. 4.3b. Finally, lines of constant ratio $\omega_0/(2Q)$ are lines parallel to the imaginary axis, as shown in Fig. 4.3c.

In circuit design we will ordinarily deal with Q values greater than 1. This has implications with respect to pole positions. From Eq. (4.13) we make the following tabulation:

Q	ψ (degrees)
0.707	45
1	60
2	75.52
5	84.3
20	88.5
100	89.7

Hence we conclude that we will normally be interested in a small sector of the s-plane, which is shaded in Fig. 4.4. Observe that when Q is greater than 5, then Eq. (4.12) for β simplifies to $\beta \approx \omega_0$ with an error less than 1%.

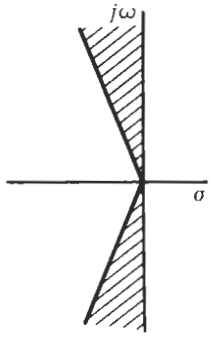

Figure 4.4 Sectors of usual pole locations.

EXAMPLE 4.1

The two poles of a given $T(s)$ are located in the s-plane on lines of slope ± 2, as shown in Fig. 4.5. (a) Determine an expression for the Q of these poles. (b) Express the pole locations $-\alpha \pm j\beta$ in terms of ω_0.

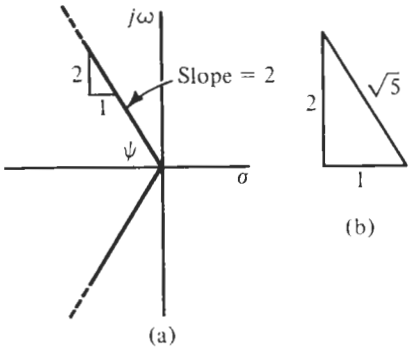

Figure 4.5 (a) Identifying Q in Example 4.1 from the angle (b) of their locus in the s plane.

Solution

Since the slope of the s-plane line is 2, then $\tan \psi = 2$. For this angle, shown in Fig. 4.5b, $\cos \psi = 1/\sqrt{5}$. Combining this result with Eq. (4.13), we see that

$$\cos \psi = \frac{1}{2Q} = \frac{1}{\sqrt{5}} \tag{4.14}$$

so that

$$Q = \frac{\sqrt{5}}{2} \tag{4.15}$$

Once Q is determined, then Eqs. (4.9) and (4.12) give the pole location as

$$\alpha = \frac{1}{2Q}\omega_0 = \frac{\omega_0}{\sqrt{5}}, \qquad \beta = \omega_0\sqrt{1 - \frac{1}{4Q^2}} = \frac{2}{\sqrt{5}}\omega_0 \tag{4.16}$$

If ω_0 is also specified, then the pole locations are fixed.

Returning to the circuit of Fig. 4.1b and the associated transfer function which described it, Eq. (4.2), we see that the three element values R, L, and C completely specify $T(s)$. But we have now shown that the two parameters Q and ω_0 also specify $T(s)$, as given by Eq. (4.7). We now have to relate Q and ω_0 to the magnitude and phase responses, which we will in turn relate to filter specifications.

4.2 THE SECOND-ORDER CIRCUIT

The transfer function for the lowpass filter derived as Eq. (4.7) was written in a normalized form such that $T(j0) = 1$. A more general form for $T(s)$ in active circuits will recognize the

possibility of gain and also that the associated circuit may be inverting or noninverting. Such a transfer function is

$$T(s) = \frac{\pm H\omega_0^2}{s^2 + (\omega_0/Q)s + \omega_0^2} \tag{4.17a}$$

and can be represented by the block diagram in Fig. 4.6. Next we do what will be done frequently in the chapters to follow: we scale the frequency by dividing s by ω_0, i.e., we use the normalized frequency $s_n = s/\omega_0$. To accomplish this step, we divide numerator and denominator of Eq. (4.17a) by ω_0^2,

$$T(s) = \frac{\pm H}{(s/\omega_0)^2 + (1/Q)(s/\omega_0) + 1} = \frac{\pm H}{s_n^2 + (1/Q)s_n + 1} \tag{4.17b}$$

Note that the result obtained is the same as if we had simply set $\omega_0 = 1$ in Eq. (4.17a). When in the discussions to follow we refer to "setting $\omega_0 = 1$" we mean the normalization (or scaling) just discussed. However, to keep the notation simple, we shall in the following drop the subscript n from the frequency parameter s and remember that in most filter work we deal in normalized frequencies. The context will always make clear what is meant. Thus, in what follows, s is a normalized frequency. We also choose the negative sign in Eq. (4.17), meaning that we anticipate an inverting realization of the transfer function. Then Eq. (4.17b) becomes

$$T(s) = \frac{V_L}{V_1} = \frac{-H}{s^2 + (1/Q)s + 1} \tag{4.18}$$

We wish to manipulate this equation until it has a form that can be identified with the simple circuits studied previously. We begin by rewriting Eq. (4.18) as

$$\left(s^2 + \frac{1}{Q}s + 1\right) V_L = -HV_1 \tag{4.19}$$

Let us take a small excursion into the time domain to see what steps to take next and help us develop a circuit whose output is V_L. We remind ourselves that s in the Laplace domain represents the differentiation operator, so that Eq. (4.19) is the Laplace transform of a second-order differential equation,

$$\frac{d^2v_L(t)}{dt^2} + \frac{1}{Q}\frac{dv_L(t)}{dt} + v_L(t) = -Hv_1(t)$$

Thus, to determine the output voltage $v_L(t)$ from the input $v_1(t)$ we need to perform two integrations. But since dividing by s is an easier operation than integration ($1/s$ is the integration operator), let us return to the frequency domain and recast Eq. (4.19) in a form that lets us identify integration, $1/s$. We obtain

$$s(s + 1/Q)V_L = -(HV_1 + V_L)$$

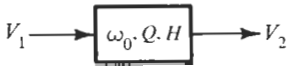

Figure 4.6 Block diagram of second-order section.

or

$$sV_L = -\frac{1}{s+1/Q}(HV_1 + V_L) = V_B \tag{4.20}$$

We see that V_L is obtained by integrating the voltage on the right-hand side, identified as V_B:

$$V_L = \frac{1}{s}V_B = \frac{1}{s}\left[-\frac{1}{s+1/Q}(HV_1 + V_L)\right] \tag{4.21}$$

To further resolve the operation in the brackets, we rewrite Eq. (4.20) as

$$(s + 1/Q)V_B = -HV_1 - V_L$$

or

$$V_B = -\frac{1}{s}\left(HV_1 + V_L + \frac{1}{Q}V_B\right) = -\frac{1}{s}V_H \tag{4.22}$$

Equation (4.22) says that V_B is obtained by integrating, with a sign inversion, the voltage V_H, which in turn is obtained by summing three scaled voltages,

$$V_H = HV_1 + V_L + \frac{1}{Q}V_B \tag{4.23}$$

Thus we have identified the double integration to obtain V_L

$$V_L = \left(\frac{1}{s}\right) \times \left[\left(-\frac{1}{s}\right) \times V_H\right] \tag{4.24}$$

with V_H obtained from the sum in Eq. (4.23). A block diagram depicting our result is shown in Fig. 4.7a. We see that the summing node realizes the weighted sum of the three voltages V_1, V_L, and V_B as prescribed in Eq. (4.23), followed by an inverting integrator to produce V_B as in Eq. (4.22) and a final noninverting integrator to obtain the lowpass output V_L as Eq. (4.21) demands. It is interesting to observe the functions realized at the other outputs, V_B and V_H. V_B is seen to be obtained by multiplying V_L by s and V_H by multiplying V_B by $-s$. With Eq. (4.18), the results are

$$V_L = \frac{-H}{s^2 + (1/Q)s + 1}V_1 = T_L V_1 \tag{4.25a}$$

$$V_B = \frac{-Hs}{s^2 + (1/Q)s + 1}V_1 = T_B V_1 \tag{4.25b}$$

$$V_H = \frac{Hs^2}{s^2 + (1/Q)s + 1}V_1 = T_H V_1 \tag{4.25c}$$

that is, at the three nodes the block diagram realizes not only a lowpass function T_L, but also what will be recognized as a *bandpass* T_B and a *highpass* T_H. Note that V_B equals HQ at $s = \pm j(\omega = \omega_0 = 1)$ and goes to zero at low and at high frequencies as was sketched in Fig. 1.2c. The voltage V_H at the highpass output equals zero at $s = 0$ and then increases with frequency, reaching HQ at $s = \pm j$ and H at $s = \infty$.

Having developed a simple block diagram to realize the transfer functions of Eq. (4.25), we need to consider next how to implement the circuit with real components. To this end we return to the circuits we developed in Chapters 2 and 3 and recall that we were able to realize an ideal inverting integrator, Fig. 3.2a, but not an ideal noninverting integrator. But two inverting integrators cannot be used directly because we must ensure stability, which requires negative feedback in all loops. To solve this difficulty, we introduce a minor modification into the block diagram of Fig. 4.7a and realize a noninverting integrator as a cascade connection of an inverting integrator and an inverter, $(1/s) = (-1/s) \times (-1)$, as is shown in Fig. 4.7b. This approach provides the additional advantage of letting us realize a *non*inverting lowpass function at the output $-V_L$. We can now use two of the inverting integrators of Fig. 3.2a, T_2 in Fig. 4.8, followed by the inverter of Fig. 2.17a with $R_1 = R_2 = 1$, T_3 in Fig. 4.8. At the input we need the summer of Fig. 2.29a, which we can combine (merge) with the integrator by replacing R_F by a resistor and capacitor in parallel; this circuit is shown as T_1 in Fig 4.8. The module T_1 realizes, assuming an ideal opamp, $V_B/A \approx 0$,

$$1 \times V_L + H \times V_I + (1/Q + s) \times V_B \approx 0$$

that is, as required in Eq. (4.20),

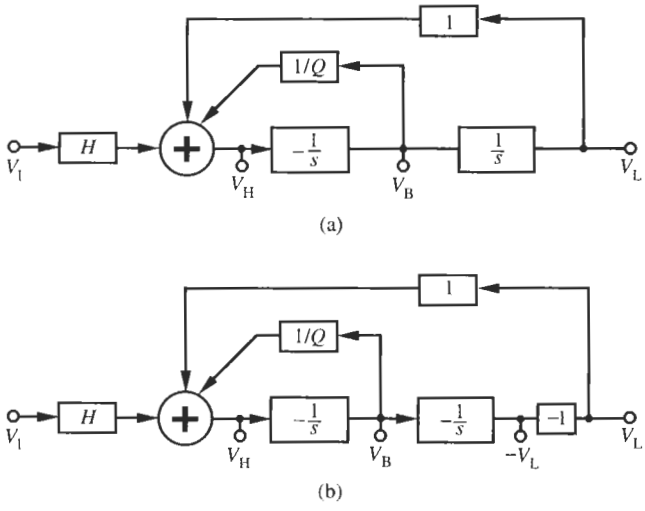

Figure 4.7 Block diagram (*two-integrator loop*) to implement Eq. (4.18); (a) using an inverting and a noninverting integrator; (b) using two inverting integrators and an inverter.

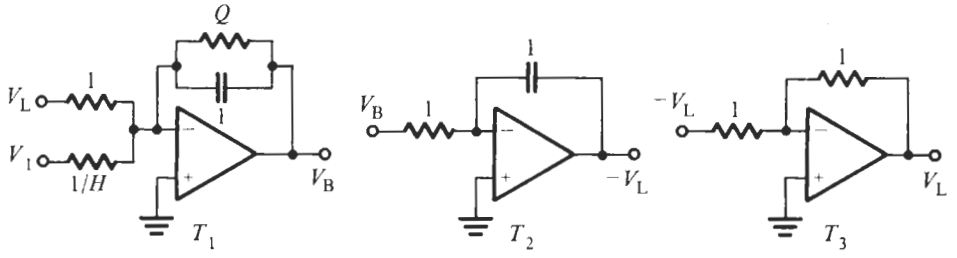

Figure 4.8 Circuit modules to implement the block diagram of Fig. 4.7b.

$$V_B = -\frac{1}{s + 1/Q}(V_L + HV_1) \tag{4.26}$$

Notice that the feedback resistor across the ideal (lossless) integrator makes the integrator lossy. Combining this equation with

$$-V_L = -\frac{1}{s}V_B \quad \text{and} \quad V_L = (-1)(-V_L)$$

and making the connections suggested by the labels at the terminals of the three modules results in the full circuit in Fig. 4.9. This filter is the so-called *Tow–Thomas* biquad (Tow, 1968; Thomas, 1971). To see how the elements of the circuit enter the transfer function explicitly, let us label them as in Fig. 4.10. Routine analysis results in the lowpass and bandpass functions

$$T_L(s) = -\frac{1/(R_3R_4C_1C_2)}{s^2 + s/(R_1C_1) + 1/(R_2R_4C_1C_2)} \tag{4.27a}$$

$$T_B(s) = (-sC_2R_4) \times [-T_L(s)] = -\frac{(R_1/R_3) \cdot s/(R_1C_1)}{s^2 + s/(R_1C_1) + 1/(R_2R_4C_1C_2)} \tag{4.27b}$$

The circuit cannot realize the highpass output because we have chosen to merge the summing block with the first integrator. If the highpass output is required, an additional opamp is

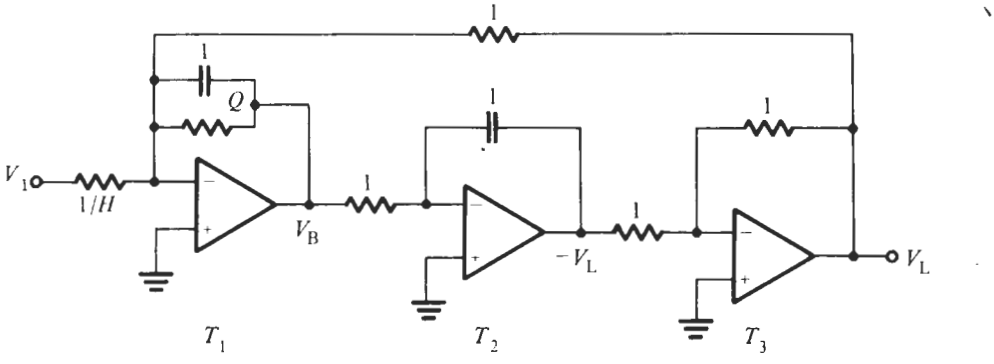

Figure 4.9 The Tow–Thomas biquad with normalized elements.

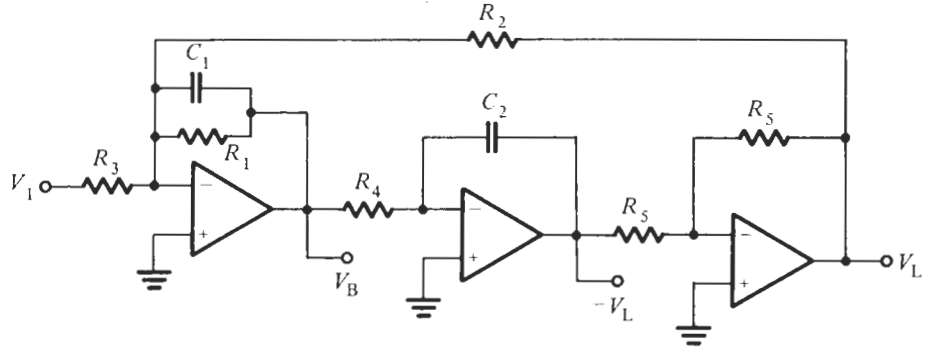

Figure 4.10 The Tow–Thomas biquad.

needed to permit realizing the summing operation (Fig. 2.29a) and the integration (Fig. 3.26a) separately.

Comparing Eq. (4.27a) to the standard form of Eq. (4.17), we identify the appropriate coefficients with the element values as

$$\omega_0^2 = \frac{1}{R_2 R_4 C_1 C_2}, \quad Q = \frac{R_1}{\sqrt{R_2 R_4}}\sqrt{\frac{C_1}{C_2}}, \quad \text{and} \quad H = \frac{R_2}{R_3} \tag{4.28}$$

We can now determine the element values to satisfy the given design parameters. This is a typical situation in active filter design: we have more components (here six) than parameters (here three). We will therefore select arbitrarily three of the components and then examine the consequences on the remaining three. Since we used frequency scaling ($\omega_0 = 1$) and intend to use magnitude scaling as well, we make the following choices:

$$C_1 = C_2 = 1 \quad \text{and} \quad R_4 = 1$$

and obtain from Eq. (4.28)

$$R_1 = Q, \quad R_2 = 1, \quad \text{and} \quad R_3 = 1/H$$

These element values give us exactly the circuit previously derived in Fig. 4.9.

An important property of the biquad circuit is that it can be *orthogonally* tuned. By this we mean that

1. R_2 can be adjusted to a specified value of ω_0.
2. R_1 can then be adjusted to give the specified value of Q without changing ω_0, which has already been adjusted.
3. Finally R_3 can be adjusted to give the desired value of H or gain for the circuit, without affecting either ω_0 or Q, which have already been set.

These steps are often called the *tuning algorithm*. This algorithm provides for orthogonal tuning. If this tuning is not possible, then the tuning is called *iterative*, meaning that we try to adjust successively each of the tuning elements until all specifications are met. Orthogonal tuning is always much preferred, especially when the filter is to be produced on a production line with a laser used to adjust each circuit element value.

An example will help us understand the design process:

EXAMPLE 4.2

A lowpass filter is to be designed whose poles in the normalized s-plane are located at $-0.577 \pm j0.8165$. The dc ($\omega \to 0$) gain is to be 2. The frequency is scaled by $\omega_0 = 20,000$ rad/s ($f_0 = 3183$ Hz). Find the values of the pole frequency and pole quality factor, and design a circuit to realize the specifications.

Solution

From Eqs. (4.10) and (4.11) we find $\omega_0 = 1$ and $Q = 0.877 = \sqrt{3}/2$. Also, from Eq. (4.17), $H = 2$. Let us choose $C_1 = C_2 = C = 0.01\ \mu$F and the normalizing resistor $R_S = 10\ \text{k}\Omega$. Choosing $R_2 = R_4$ in Eq. (4.28) with the given value of ω_0 we find

$$R_2 = R_4 = \frac{1}{\omega_0 C} = \frac{1}{2 \times 10^4 \text{s}^{-1} \times 10^{-8} \text{F}} = 5 \text{ k}\Omega$$

and

$$R_3 = \frac{R_2}{H} = 2.5 \text{ k}\Omega, \quad R_1 = \sqrt{R_2 R_4} Q = 5 \times 10^3 \ \Omega \times 0.877 = 4.33 \text{k}\Omega$$

The two resistors of the inverter are also chosen as 10 kΩ. The circuit and its test performance are shown in Fig. 4.11. We notice that the circuit is a lowpass filter with a dc gain of $H = 2$, i.e., 6 dB as specified. The passband corner is at $\approx$ 3.7 kHz (a little higher than 20,000 rad/s divided by 2π, see Fig. 4.13); it has a small peak near the passband edge, and the attenuation increase for frequencies above 3.7 kHz is 20 dB per decade (6 dB per octave), because $T(s)$ decreases as $1/s^2$. We also observe an unexpected dip in the attenuation curve at approximately 350 kHz that can be shown to be caused by higher-order poles in the opamp model.

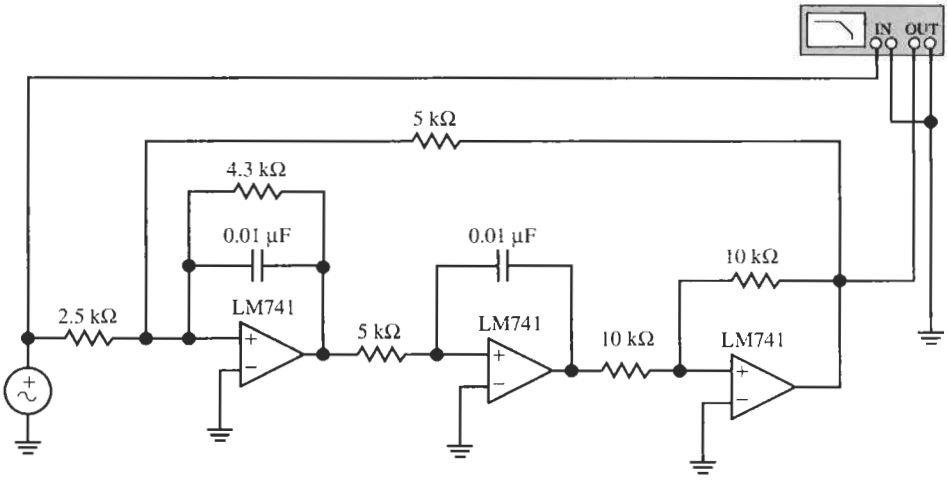

(a)

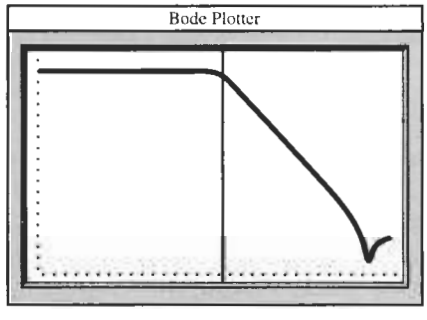

(b)

Figure 4.11 (a) Circuit for Example 4.2 and (b) its performance. (Bode Plotter scales: 10 Hz to 700 kHz; −100 dB to +10 dB; cursor at 3.70 kHz, 3.10 dB.)

The test performance shown in Fig. 4.11b will be explained as we discuss the frequency response of the biquad in detail in the following section. Previously in this chapter, we considered the opamps to be ideal, as always a reasonable assumption for low-frequency, low-Q designs as in Example 4.2. As operating frequency and circuit Q increase, nonideal opamp effects will be seen to become more pronounced. We shall consider these effect in Section 4.4.

4.3 FREQUENCY RESPONSE OF LOWPASS AND BANDPASS CIRCUITS

We have found that the biquad circuit in Fig. 4.9 is described by two transfer functions, depending on the output chosen. To begin, let the output be V_L so that the transfer function is that given by Eq. (4.25a). We are interested in the magnitude and phase of this function. Since the gain H is just a constant multiplier with no effect on the frequency response, let us simplify the equations by scaling T by H, i.e., we assume $H = 1$. Also, let us drop the minus sign, i.e., we assume a noninverting circuit. Then

$$T(j\omega) = \frac{1}{1 - \omega^2 + j\omega/Q} \tag{4.29}$$

From this complex quantity we find that the magnitude is

$$|T(j\omega)| = \frac{1}{\sqrt{(1-\omega^2)^2 + (\omega/Q)^2}} \tag{4.30}$$

and the phase is

$$\theta = -\tan^{-1}\left(\frac{\omega/Q}{1-\omega^2}\right) \tag{4.31}$$

These two functions are plotted in Fig. 4.12 for a given value of Q. We have marked a number of values of $|T|$ of interest for our future work, specifically $|T(j0)|$, $|T(j1)|$, and the peak value and the frequency at which it occurs. For the magnitude function we see that

$$|T(j0)| = 1, \qquad |T(j1)| = Q, \qquad |T(j\infty)| \to 0 \tag{4.32}$$

and that for large ω, $|T(j\omega)| \approx 1/\omega^2$. Similarly for the phase

$$\theta(j0) = 0°, \qquad \theta(j1) = -90°, \qquad \theta(j\infty) \to -180° \tag{4.33}$$

The magnitude plot on Bode coordinates is shown in Fig. 4.13 for a range of values of Q from 0.707 to 10. The asymptotic Bode plot decreases at the rate of -12 dB per octave, and this is sometimes described as *two-pole roll-off*.

These responses can be visualized in terms of the pole locations of the transfer function. We start with Eq. (4.29), with $j\omega = s$:

$$T(s) = \frac{1}{s^2 + (1/Q)s + 1} \tag{4.34}$$

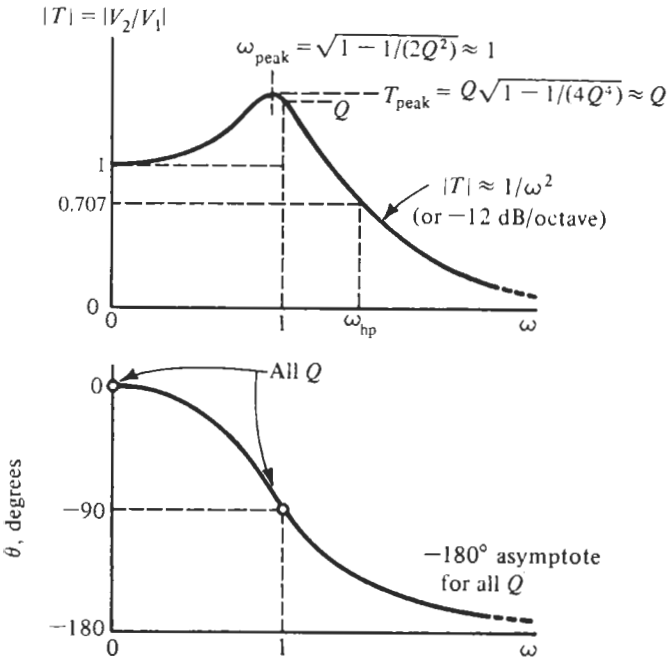

Figure 4.12 Magnitude and phase of the lowpass function (4.29).

The poles of this function are located on a circle of radius 1 and at an angle with respect to the negative real axis of

$$\psi = \cos^{-1}\left(\frac{1}{2Q}\right) \tag{4.35}$$

This equation can be combined with the previous one to give an alternative representation:

$$T(s) = \frac{1}{s^2 + (2\cos\psi)s + 1} \tag{4.36}$$

In terms of the poles shown in Fig. 4.14,

$$T(s) = \frac{1}{(s + p_1)(s + \bar{p}_1)} \tag{4.37}$$

where $\bar{p}_1$ is the conjugate of p_1. With $s = j\omega$, the two factors in this equation become

$$j\omega + p_1 = m_1\angle\phi_1 \qquad \text{and} \qquad j\omega + \bar{p}_1 = m_2\angle\phi_2 \tag{4.38}$$

In terms of these quantities, the magnitude and phase are

$$|T(j\omega)| = \frac{1}{m_1 m_2} \tag{4.39}$$

and

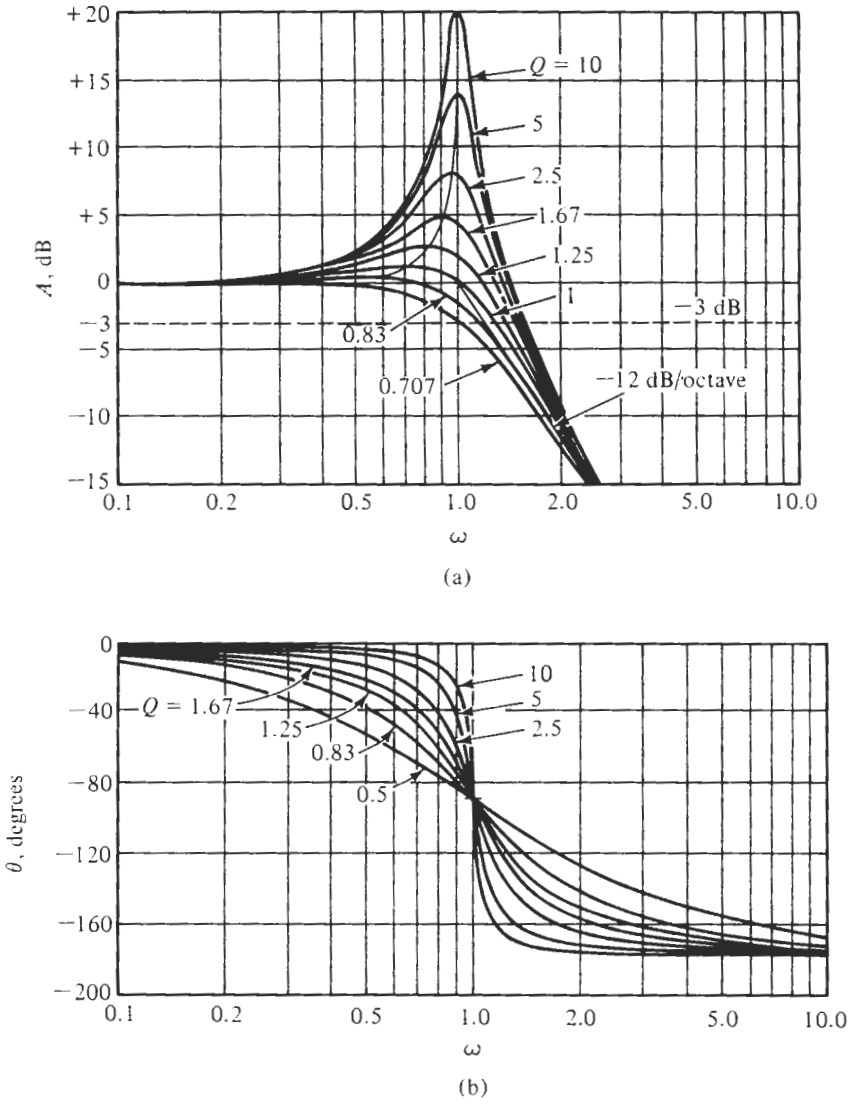

Figure 4.13 Magnitude (a) and phase (b) of Eq. (4.34) as functions of Q.

$$\theta = -(\phi_1 + \phi_2) \tag{4.40}$$

Phasors representing Eq. (4.38) are shown in Fig. 4.15. The figure shows the values computed using these last two equations for three different values of frequency—one below ω_0, one at ω_0, and one above ω_0. From this construction we see that the short length m_2 near the frequency ω_0 is the reason why the magnitude function reaches a peak near ω_0. These plots are useful in visualizing the behavior of the circuit. In solving problems, Eqs. (4.30) and (4.31) may be evaluated readily by a hand-held calculator.

For a lowpass filter, the usual specifications will be the *half-power frequency* ω_{hp} and the value of $|T|_{peak}$; these quantities are identified in Fig. 4.12. As mentioned earlier, the term

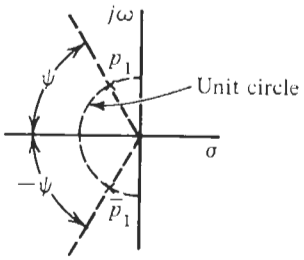

Figure 4.14 Conjugate complex poles of Eq. (4.34).

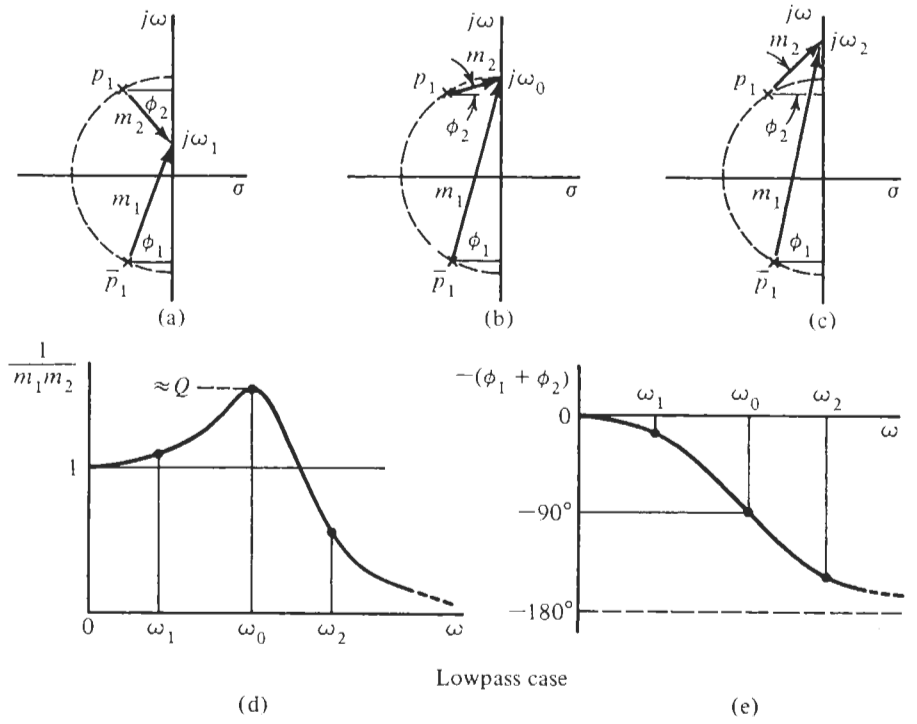

Lowpass case

Figure 4.15 Evaluation of magnitude (d) and phase (e) of $T(j\omega)$ from given pole positions for the frequencies ω_1, ω_0, and ω_2 in (a), (b), and (c).

half-power comes from the equation for power, $P = V^2/R$, from which we see that if P is to be reduced by one-half, then V must be reduced by $1/\sqrt{2}$, i.e., by 3 dB. So we see that ω_{hp}, the −3-dB frequency, is the frequency at which $|T(j\omega)|$ is reduced to 0.707 of its dc value, $|T(0)|$. Note that the value of $|T|_{peak}$ is approximately equal to Q. Specifying a relatively flat magnitude in the passband implies, therefore, a low value of Q. Figure 4.13 indicates that $Q < 0.9$ will be necessary if noticeable peaking must be avoided. More accurate methods of designing filters with flat passband characteristics will be discussed in Chapter 6.

We now return to the biquad circuit of Fig. 4.9 and consider the case in which the output voltage is taken to be V_B, so that Eq. (4.25b) applies. This bandpass transfer function differs from that of the lowpass case essentially in that it has a zero at the origin. The denominators of the two transfer functions are identical, of course. The gain constant H in Eq. (4.25) was

defined as the gain of the lowpass filter, Eq. (4.25a), at $s = 0$; it has no meaning in a bandpass filter. Let us, therefore, define the bandpass function as

$$T_B(s) = \frac{Ks}{s^2 + (\omega_0/Q)\,s + \omega_0^2} \tag{4.41}$$

We have shown the pole frequency ω_0 explicitly to help us keep track of what happens to it in the following derivations. The constant K is now to be determined such that the circuit has a specified gain H at $\omega = \omega_0$. Setting $s = j\omega_0$ in Eq. (4.41) and equating the result to H, we see that the first and last terms in the denominator cancel and

$$K = H\omega_0/Q \tag{4.42}$$

so that Eq. (4.41) becomes

$$T_B(s) = \frac{H\,(\omega_0/Q)\,s}{s^2 + (\omega_0/Q)\,s + \omega_0^2} \tag{4.43}$$

H may be either positive or negative, depending on the specifications and the circuit. For example, returning to Fig. 4.10 and Eq. (4.27b), we see that

$$H = -R_1/R_3 \tag{4.44}$$

The expressions for Q and ω_0 are the same as those for the lowpass filter in Eq. (4.28).

We now return to scaled frequencies, i.e., we set $\omega_0 = 1$ in Eq. (4.43), to obtain

$$T_B\,(j\omega) = \frac{(H/Q)j\omega}{1 - \omega^2 + j\omega(1/Q)}$$

with magnitude

$$|T_B\,(j\omega)| = \frac{H\,(\omega/Q)}{\sqrt{\left(1 - \omega^2\right)^2 + (\omega/Q)^2}} \tag{4.45}$$

and phase

$$\theta = 90^\circ - \tan^{-1}\left(\frac{\omega/Q}{1 - \omega^2}\right) \tag{4.46}$$

Plots of these two functions for one value of Q are given in Fig. 4.16 with $H = 1$. From the magnitude response we see that it starts with zero value at $\omega = 0$, increases to unit value at $\omega = 1$, and then decreases at the rate of 6 dB per octave, or with *one-pole roll-off*. The phase response differs from that found for the lowpass case only in that 90° is added to all values. Hence it has a value of 90° when $\omega = 0$, 0° when $\omega = 1$, and then approaches −90° as ω increases.

An analysis similar to that given in terms of the pole locations in Fig. 4.15 is presented for this case in Fig. 4.17. The difference here from the lowpass case is that a zero at the origin has been added, which contributes the factor $j\omega = \omega\angle 90^\circ = M_1\angle\theta_1$ to the magnitude and phase characteristics.

We next compute the half-power frequencies for the bandpass response. If we let $H = 1$ and impose the requirement that $|T_B|^2 = \frac{1}{2}$ in Eq. (4.45), then we obtain an equation for which there are four solutions. Selecting only those that are positive, we have

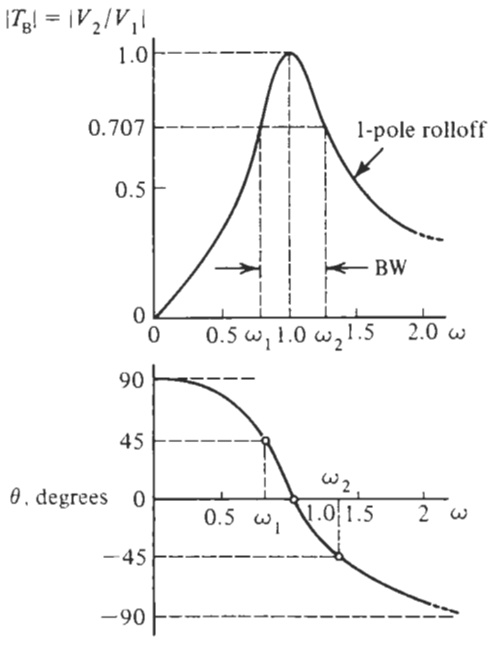

Figure 4.16 Important parameters of magnitude and phase curves of a second-order bandpass function.

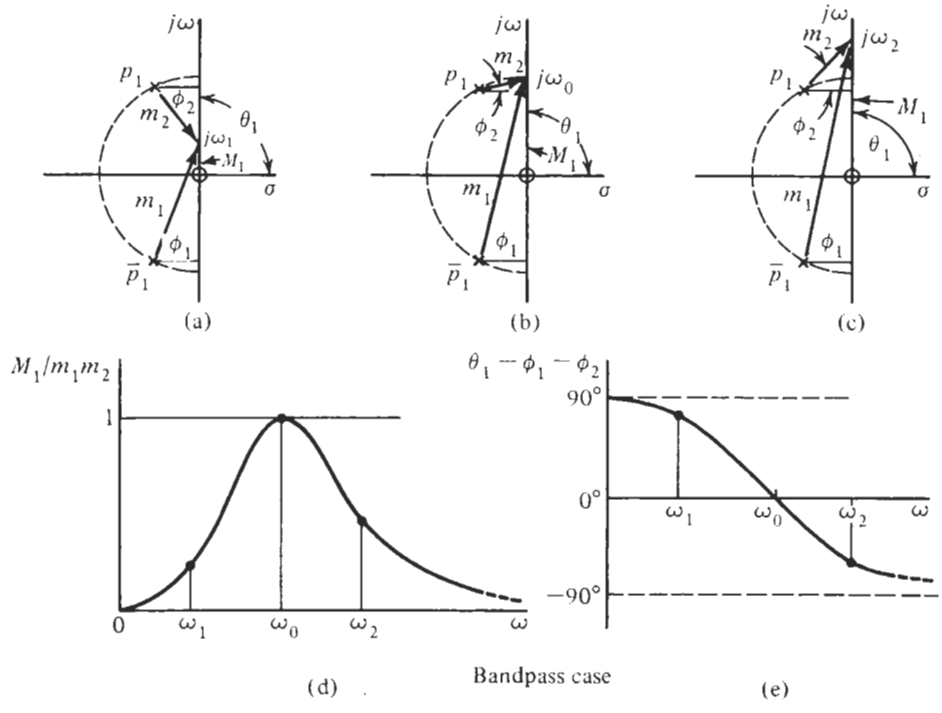

Figure 4.17 Construction of magnitude (d) and phase (e) of a bandpass function from pole and zero positions for the frequencies ω_1, ω_0, and ω_2 in (a), (b), and (c).

$$\omega_2, \omega_1 = \sqrt{1 + \left(\frac{1}{2Q}\right)^2} \pm \frac{1}{2Q} \tag{4.47}$$

These frequencies are identified in Fig. 4.16. The product and difference of these two frequencies are

$$\omega_1\omega_2 = 1 \qquad \text{and} \qquad \omega_2 - \omega_1 = \frac{1}{Q} \tag{4.48}$$

Restoring ω_0, i.e., denormalizing Eq. (4.48), gives

$$\omega_1\omega_2 = \omega_0^2 \qquad \text{and} \qquad \omega_2 - \omega_1 = \frac{\omega_0}{Q} \tag{4.49}$$

This frequency difference is defined as the bandwidth (BW); so we see that

$$\text{BW} = \frac{\omega_0}{Q} \tag{4.50}$$

or

$$Q = \frac{\omega_0}{\text{BW}} = \frac{\omega_0}{\omega_2 - \omega_1} \tag{4.51}$$

These equations tell us that Q and BW are inversely related, as shown in Fig. 4.18. We can use these results to show that there is symmetry in this response in that, see also Fig. 4.16,

$$|T_B(j\omega_1)| = |T_B(j\omega_2)| \tag{4.52}$$

and

$$\theta(j\omega_1) = -\theta(j\omega_2) \tag{4.53}$$

We also observe that Eq. (4.43) with $H = 1$ can be written

$$T_B(s) = \frac{\text{BW}s}{s^2 + \text{BW}s + \omega_0^2} \tag{4.54}$$

However, this applies only for the bandpass case.

With the experience gained in this chapter, let us revisit the example at the end of Section 2.8, where a student engineer proposed to use the two-opamp circuit of Fig. 2.35 to build a wide-band high-gain amplifier. We can now understand perfectly what the experienced engineer meant by the suggestion that the observed peaking (Fig. 2.36) could be eliminated by "dampening the high Q by placing a feedback resistor across the first opamp," and why the improved circuit in Fig. 2.37 achieved the desired result:

Remember that a real opamp is an integrator so that the circuit in Fig. 2.37, consisting of an inverting and a noninverting integrator in a feedback network is nothing but a standard two-integrator loop of the form depicted in Fig. 4.7a. Analyzing the circuit in Fig. 2.37, repeated for convenience in Fig. 4.19, results in the following node equation at the input of the first opamp:

$$-\frac{V_2}{A^2}(G_1 + G_2 + G_3) = G_1V_1 + G_2V_2 + G_3\frac{V_2}{A}$$

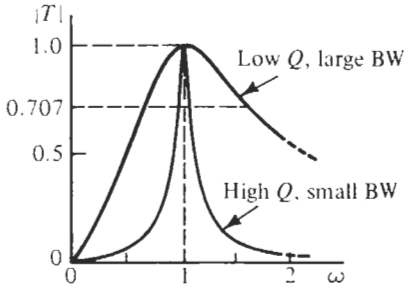

Figure 4.18 Illustration of low-Q and high-Q bandpass functions.

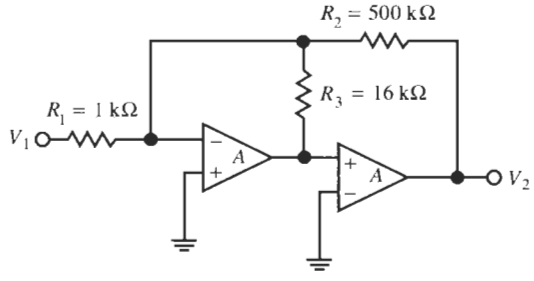

Figure 4.19 A "capacitorless" second-order lowpass filter.

Now letting $G_1 + G_2 + G_3 = G$, the transfer characteristic becomes

$$\frac{V_2}{V_1} = -\frac{G_1}{G_2 + G_3/A + G/A^2} = -\frac{R_2}{R_1}\frac{G_2/G}{1/A^2 + G_3/(GA) + G_2/G} \tag{4.55}$$

To show the frequency dependence explicitly, we insert the integrator model of Eq. (2.18), $A(s) = \omega_t/s$, into Eq. (4.55) and obtain

$$\frac{V_2}{V_1} = \frac{-\left(\frac{R_2}{R_1}\right)\left(\frac{G_2}{G}\omega_t^2\right)}{s^2 + \frac{G_3}{\sqrt{G_2 G}}\left(\sqrt{\frac{G_2}{G}}\omega_t\right)s + \left(\frac{G_2}{G}\omega_t^2\right)} = \frac{-H\omega_0^2}{s^2 + \frac{\omega_0}{Q}s + \omega_0^2} \tag{4.56}$$

We have brought Eq. (4.56) into the standard form of Eq. (4.18) so that we can directly identify the filter parameters

$$H = \frac{R_2}{R_1}, \quad \omega_0 = \sqrt{\frac{G_2}{G}}\omega_t, \quad \text{and} \quad Q = \frac{\sqrt{G_2 G}}{G_3} = \frac{R_3}{\sqrt{R_2}}\sqrt{G} \tag{4.57}$$

Now notice that for the component values in Fig. 4.19 the dc gain of the filter is $H = 500$ as required, and that for LM741 opamps,

$$f_0 = \frac{\omega_t/(2\pi)}{\sqrt{501}} = \frac{1.5\text{ MHz}}{2.238} = 67\text{ kHz} \tag{4.58}$$

as in Eq. (2.121b). Finally, if we set $R_3 = \infty$, as in the circuit proposed originally in Fig.

2.35, we find $Q = \infty$ (ideally) with excessive peaking (Fig. 2.36). This result is suggested by the design curves in Fig. 4.13a. If, however, we dampen the large Q by using the finite value $R_3 = 16$ kΩ, found experimentally as an optimal value in Chapter 2, we compute from Eq. (4.57):

$$Q = \frac{16,000}{\sqrt{500,000}}\sqrt{\left(\frac{1}{500} + \frac{1}{16} + 1\right) \times 10^{-3}} = 0.738$$

According to the design curves in Fig. 4.13a, this value results in approximately an optimally flat passband with no peaking, as was indeed verified experimentally in Fig. 2.37b.

This explanation should have answered any lingering questions about the design leading to the circuit in Fig. 2.37a. Knowing what we know now, it will be clear that the circuit also implements a bandpass filter at the output of the first opamp. We leave an investigation of that behavior to the problems. These circuits are called *active R filters* in the literature (Brand and Schaumann, 1978) because they use no *external* capacitors. The student will realize that the term is misleading, because no filtering function can be built without capacitors when designing active filters. In active R filters, the capacitors are simply *internal* to the opamps (see Fig. 2.3), where they are responsible for the integrator behavior. Active R filters generally are not useful for commercial applications and always require careful adjustments (tuning) because their critical frequency parameter ω_0 is proportional to the opamp's ω_t [see Eq. (4.57)] and, therefore, not designable. Recall from our discussions in Chapter 2 that the gain-bandwidth product of opamps is poorly controlled, may vary from unit to unit, and furthermore depends on environmental factors, such as temperature and supply voltages. What the so-called active R filters demonstrate quite clearly, though, is that *opamps are integrators*, and by no means can be assumed to be amplifiers with large constant gain, except at very low frequencies.

To add to our experience with second-order filters, let us consider next two examples of bandpass filters, one at low frequencies and with a moderate value of Q and, second, a more demanding design at higher frequencies with a larger Q.

EXAMPLE 4.3

Use the circuit of Fig. 4.10 to design a bandpass filter with a center frequency of $\omega_0 = 1000$ rad/s ($f_0 = 159$ Hz) and a bandwidth of 200 rad/s. The midband gain must be $H = 1$.

Solution

From Eq. (4.51) we find $Q = 5$. Choosing $C_1 = C_2 = C = 0.1$ μF, $R_2 = R_4$, and using Eqs. (4.44) and (4.28), we find

$$R_2 = R_4 = \frac{1}{\omega_0 C} = \frac{10^6\ \Omega}{0.1 \times 1000} = 10\ \text{k}\Omega, \quad \text{and} \quad R_1 = QR_2 = 50\ \text{k}\Omega = R_3$$

Figure 4.20 shows the circuit and its experimental performance. This low-frequency circuit behaves as desired in the frequency range of interest, but at high frequencies we notice an increase in gain after reaching a minimum, behavior caused by unmodeled opamp dynamics.

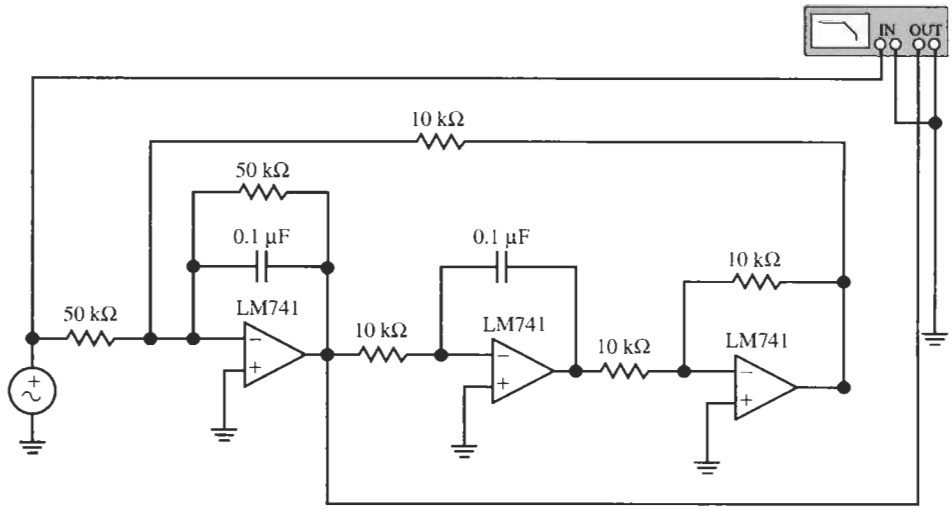

(a)

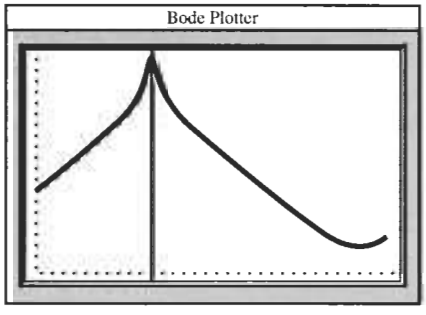

(b)

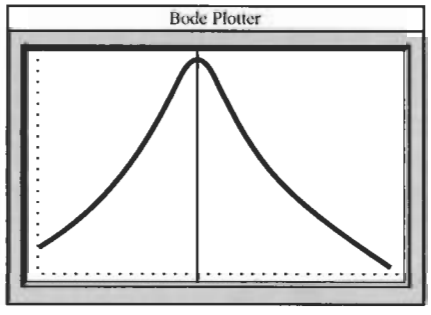

(c)

Figure 4.20 (a) Bandpass biquad for Example 4.3; (b) and (c) circuit performance. [Bode Plotter scales: (b) 3 Hz to 500 kHz; −80 dB to 0 dB; cursor at 160 Hz, 0.01 dB; (c) 80 Hz to 360 Hz; −20 dB to 0 dB; cursor at 160 Hz, 0.01 dB.]

EXAMPLE 4.4

Use again the biquad of Fig. 4.10, but design a bandpass filter with a center frequency of $f_0 = 38$ kHz; the −3-dB passband should be located between 34.8 and 41.1 kHz, and the midband gain must be $H = 1$. Use LM741 operational amplifiers.

Solution

In this case, we have the more challenging task of designing a circuit with a higher center frequency and a somewhat larger value of Q,

$$Q = \frac{41.1 - 34.8}{38} \approx 6$$

Choosing $C_1 = C_2 = C = 0.01\ \mu$F to accommodate the larger frequency and again $R_2 = R_4$, we find from Eqs. (4.44) and (4.28)

$$R_2 = R_4 = \frac{1}{\omega_0 C} = \frac{10^6\ \Omega}{0.01 \times 2\pi \times 38000} = 419\ \Omega, \quad \text{and}$$
$$R_3 = R_1 = QR_2 = 6 \times 419\ \Omega = 2.513\ \text{k}\Omega$$

The inverter we build again with two equal 10-kΩ resistors. Figure 4.21 shows the circuit and its performance. The center frequency $f_0 = 36.8$ kHz is approximately as specified, but the realized midband gain is 11.2 dB rather than 0 dB as required, and the quality factor is 21.7, far larger than the specified $Q = 6$ (Fig. 4.21b). If we simulate the circuit with ideal opamps, however, or build it with faster opamps such as the HA2542–2, the performance is as specified in the design requirements (Fig. 4.21c). Clearly, the errors are unacceptable and we need to investigate from where these problems arise and how to fix or at least predict them.

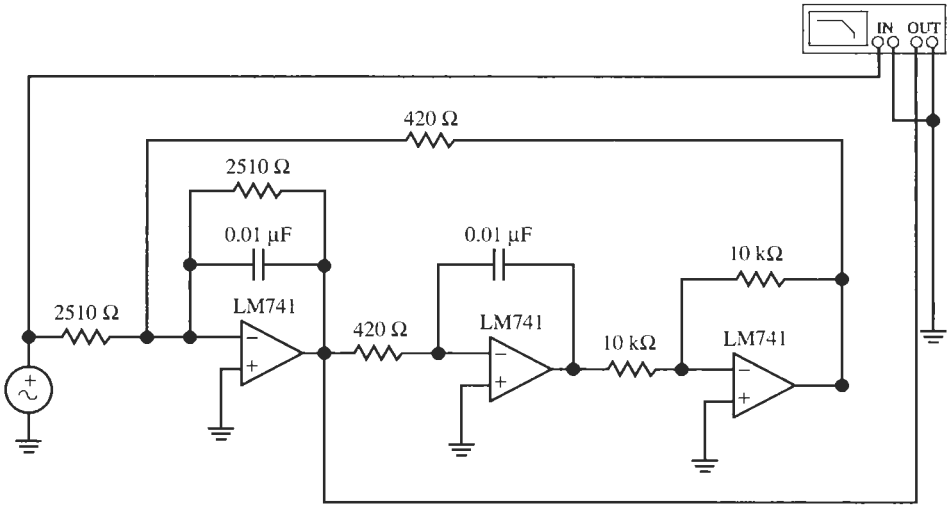

(a)

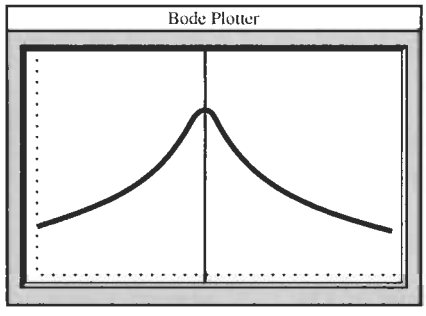

(b)

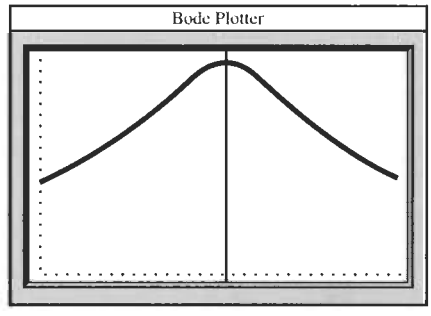

(c)

Figure 4.21 (a) Bandpass biquad for Example 4.4; (b) passband performance. (Bode Plotter scales: 28 kHz to 50 kHz; −20 dB to +20 dB; cursor at 36.8 Hz, 11.2 dB.) (c) with HA 2542-2 opamps. (Bode Plotter scales: 28 Hz to 50 kHz; −20 dB to 0 dB; cursor at 38.0 kHz, −0.01 dB.)

This example illustrates the serious errors that must be expected if an idealistic and inadequate opamp model is used in filter design. It serves as a reminder that opamp effects must be considered in all but the most undemanding designs and when frequencies are not small relative to the opamp's gain-bandwidth product. In the next section we shall determine the reasons for the unexpected circuit performance we found in the previous example.

4.4 INTEGRATORS: THE EFFECTS OF $A(s)$

We have seen in Example 4.4 that the frequency dependence of opamps can cause huge errors to appear in filter performance. To be able to arrive at predictable designs, we clearly need to be able to determine where these errors arise and how to eliminate or at least minimize them. To this end, we could reanalyze the circuit in Fig. 4.10 with frequency-dependent opamp gain $A(s)$ to arrive at the modified transfer function, corresponding to Eq. (4.27a), which includes opamp effects. This approach will certainly work; it will lead, however, into a large amount of algebra and prevent us from gaining the desired insight into circuit behavior. Let us instead use a much more transparent approach. It will give insight into integrator performance and will be generally useful for our subsequent filter design work.

We note that the biquad was designed under the assumption of ideal inverting and noninverting integrators (see Fig. 4.7a). The only effect that frequency-dependent opamp gain can have is to change the performance of the integrators from their ideal behavior, $\pm 1/s$, to a different function of frequency. Thus let us concentrate on the "quality" of integrators built with real opamps. We define the "quality of active integrators" analogously to the quality of a passive capacitor C, through losses. In a capacitor, losses are modeled via a resistor $R_C = 1/G_C$, as shown in Fig. 4.22. A lossy capacitor generates a voltage by integrating a current; in the time domain,

$$v(t) = \frac{1}{C}\int_0^t \left(i - \frac{v}{R_C}\right) dt$$

or in the Laplace domain

$$V(s) = \frac{1}{sC}\left[I(s) - \frac{V(s)}{R_C}\right]$$

On the $j\omega$-axis, the equation becomes

$$V = \frac{1}{j\omega C + G_C} I = \frac{1}{Y(j\omega)} I \tag{4.59}$$

An ideal capacitor has no losses, i.e., the real part of its admittance Y is zero.

$$\text{Re}\, Y(j\omega) = G_C = 0 \tag{4.60}$$

Related to this concept, the literature defines the *quality factor* of a capacitor as

$$Q = \frac{\text{Im}Y(j\omega)}{\text{Re}Y(j\omega)} = \frac{\omega C}{G_C} = \omega C R_C \tag{4.61}$$

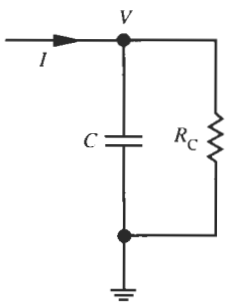

Figure 4.22 Lossy capacitor performing integration.

so that Q is infinite—the capacitor is ideal and the loss is zero—if the parallel loss resistor is infinite and draws no current, i.e., $\mathrm{Re}Y(j\omega) = 0$. The integration is described by

$$V = \frac{I}{Y(j\omega)} = \frac{I}{sC + G_C}\bigg|_{s=j\omega} = \frac{1}{j\omega C\left[1 - j\dfrac{G_C}{\omega C}\right]} I = \frac{1}{j\omega C\left[1 - j\dfrac{1}{Q(\omega)}\right]} I \tag{4.62}$$

Analogously, we define a general integrator function $F(s)$ as

$$\frac{V_2}{V_1} = \frac{1}{F(j\omega)} = \frac{1}{j\mathrm{Im}F(j\omega) + \mathrm{Re}F(j\omega)} = \frac{1}{j\omega\tau + q} = \frac{1}{j\omega\tau\left[1 - j\dfrac{q}{\omega\tau}\right]} \tag{4.63}$$

and refer to the integrator as ideal,

$$\frac{1}{F(s)} = \frac{1}{s\tau} \tag{4.64}$$

if its "losses," represented by q, are zero. τ is the integrator time constant, usually an RC product set by the designer. We can then classify different integrators by the amount of loss, q, or equivalently by their "integrator Q," Q_I, defined analogously to Eq. (4.61) as

$$Q_I(\omega) = \frac{\mathrm{Im}F(j\omega)}{\mathrm{Re}F(j\omega)} = \frac{\omega\tau}{q} \tag{4.65}$$

For an ideal integrator with no losses, $Q_I(\omega) \to \infty$ and $q \to 0$. Alternatively, we will find it useful to classify integrators by their phase error: from Eq. (4.63) we find the phase of $1/F(j\omega)$ to be

$$\theta(\omega) = -\tan^{-1}\left(\frac{\omega\tau}{q}\right) = -90^o + \tan^{-1}\left(\frac{q}{\omega\tau}\right) = -90^o + \theta_\varepsilon(\omega) \tag{4.66}$$

where $-90°$ is the phase of an ideal integrator and $\theta_\varepsilon(\omega)$ is the phase error caused by integrator nonidealities, i.e., nonzero losses, $q \neq 0$.

We are now ready to consider the active integrators. These circuits are the fundamental building blocks of almost all types of active filters, of first, second, or higher order, and built in different technologies. We will, therefore, study various practically useful integrator circuits in some detail and characterize them by their sign and by their loss q as expressed in

$$\frac{V_2}{V_1} = \pm\frac{1}{F(j\omega)} = \pm\frac{1}{j\omega\tau + q} \tag{4.67}$$

These parameters will prove to be very important in our further study of filter design.

Our goal is to determine the errors caused by real opamps in the two-integrator loop, whose fundamental structure is depicted in Fig. 4.7a and leads, e.g., to the circuit in Fig. 4.10. Along the way we shall study the performance of a number of active integrators that have been proven useful in practice, and we shall get experience in investigating causes of errors.

4.4.1 Inverting Integrators

Let us start with the inverting integrator in Fig. 4.23a. We can analyze the circuit directly or use Eq. (3.108) with $Z_2(s) = 1/(sC)$ and $Z_1 = R$; the result is

$$\frac{V_2}{V_1} = -\frac{1}{sCR}\frac{1}{1 + [1 + 1/(sCR)]/A(s)} \tag{4.68}$$

Let us employ the integrator model of Eq. (2.18) for the opamp and evaluate Eq. (4.68) on the $j\omega$-axis. Bringing the result into the form of Eq. (4.67) gives

$$\begin{aligned}\frac{V_2}{V_1} &= -\frac{1}{sCR}\frac{1}{1 + s/\omega_t + 1/(\omega_t CR)} \approx -\frac{1}{sCR}\frac{1}{1 + s/\omega_t}\Bigg|_{s=j\omega} \\ &= -\frac{1}{j\omega CR - \omega^2 CR/\omega_t}\end{aligned} \tag{4.69}$$

where we assumed that $1/(\omega_t CR) \ll 1$. We notice that the integrator acquired a parasitic pole at $s \approx -\omega_t$. The loss of the so-called *Miller integrator* is then

$$q = -\frac{\omega^2 CR}{\omega_t} = -\frac{\omega CR}{|A(j\omega)|} \tag{4.70a}$$

We observe that q is *negative*. Also, it increases with the square of the frequency, and is inversely proportional to the magnitude of the opamp gain at the frequency of interest. We will find the latter observations to be true in all integrators to be discussed, indicating that problems with integrator nonidealities get worse at higher frequencies. The literature also often labels the Miller integrator by its quality factor, which by Eq. (4.65) equals

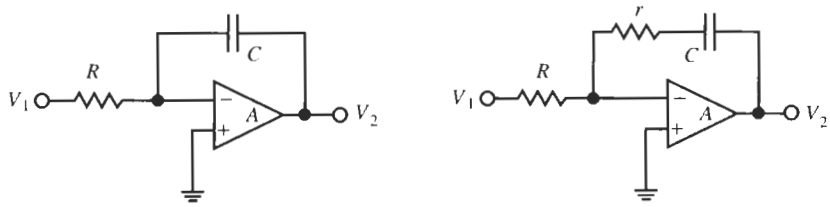

Figure 4.23 (a) Miller integrator; (b) passive compensation for opamp effects.

$$Q_1 = -\frac{\omega CR}{q} = -\frac{\omega_t}{\omega} = -|A(j\omega)| \tag{4.70b}$$

For example, at the center frequency $f_0 = 38$ kHz in Example 4.4, the magnitude of the integrator Q is only about 40, far too small to design high-quality filters with critical specifications. With $CR = \omega_0$, the loss term q equals -0.025.

To remedy the problem and design a better integrator, we need to make $q = 0$ or at least reduce it. A glance at Eq. (4.69) shows that the loss term disappears if we create a zero at $s \approx -\omega_t$, which cancels the parasitic pole at $s \approx -\omega_t$. To do this we notice that a zero can be created in Eq. (4.69) by replacing sC by $sC/(1 + sCr)$. This equation indicates that we need to place a resistor r in series with the capacitor C as shown in Fig. 4.23b. This gives

$$\frac{V_2}{V_1} = -\frac{1}{\dfrac{sC}{1+sCr}R}\,\frac{1}{1 + \dfrac{s}{\omega_t} + \dfrac{1+sCr}{\omega_t CR}} = -\frac{1}{sCR}\,\frac{1+sCr}{1 + \dfrac{1}{\omega_t CR} + \dfrac{s}{\omega_t}\left(1 + \dfrac{r}{R}\right)}$$

This expression shows that pole-zero cancellation occurs when

$$Cr = \frac{\dfrac{1}{\omega_t}\left(1 + \dfrac{r}{R}\right)}{1 + \dfrac{1}{\omega_t CR}} = \frac{1 + \dfrac{r}{R}}{\omega_t + \dfrac{1}{CR}} \quad \text{or} \quad \omega_t Cr + \frac{r}{R} = 1 + \frac{r}{R}$$

That is, as long as the opamp model of Eq. (2.18) is valid, the compensation resistor

$$r = \frac{1}{\omega_t C} \tag{4.71}$$

will result in an ideal inverting integrator with $q = 0$ or $Q_1 = \infty$:

$$\frac{V_2}{V_1} = -\frac{1}{sCR[1 + 1/(\omega_t CR)]} \approx -\frac{1}{sCR}$$

Thus the solution to the losses of the Miller integrator is a small resistor r in series with the integrating capacitor.

A problem with passive compensation is that we are attempting to equate two electrically dissimilar components, that is, circuit elements depending on different manufacturing processes and physical parameters. As seen from Eq. (4.71), we are trying to match the passive rC product to the active electronic parameter ω_t. To be more explicit, since $g_m = \omega_t C_1$ where C_1 is an opamp-internal capacitor [see Eq. (2.10)], we are attempting to match $1/r$ to the opamp's transconductance parameter g_m. Although C and C_1 can be made to match very well and track over time and temperature, the bias- and processing-dependent transconductance can generally not be assumed to match, much less track the passive resistor r. Thus, although this scheme is usable for achieving inexpensive first-order compensation of opamp effects, careful tuning of r for each opamp in the circuit would be required to achieve superior results—not a feasible method for mass production.

A better method would need to make the position of the compensating zero track that of the parasitic pole, with no need for fine tuning or further processing steps. To achieve this, the zero must also be generated by an opamp. Figure 4.24 shows a possible circuit. We have

replaced the direct connection of the capacitor to the opamp output V_2 by a buffer. We can derive the node equation at the inverting opamp input, where $V_- = -V_2/A$, as follows:

$$-\frac{V_2}{A}(G+sC) = GV_1 + sC\frac{1}{1+1/A_1}V_2$$

so that

$$V_2\left(\frac{sC}{1+1/A_1} + \frac{G+sC}{A}\right) = -GV_1 \tag{4.72}$$

As $1/|A_1| \ll 1$ for any useful frequency of operation, let us now use a Taylor expansion,

$$\frac{1}{1+1/A_1} \approx 1 - \frac{1}{A_1} + \frac{1}{A_1^2} - \frac{1}{A_1^3} + \cdots$$

so that Eq. (4.72) can be written as

$$\frac{V_2}{V_1} \approx -\frac{G}{sC\left(1 - \frac{1}{A_1} + \frac{1}{A_1^2} - \frac{1}{A_1^3} + \cdots\right) + \frac{sC+G}{A}} \tag{4.73}$$

Using the opamp integrator model and evaluating Eq. (4.73) on the $j\omega$-axis results in

$$\begin{aligned}\frac{V_2}{V_1} &\approx -\frac{1}{j\omega CR\left(1 - \frac{j\omega}{\omega_{t1}} - \frac{\omega^2}{\omega_{t1}^2} + j\frac{\omega^3}{\omega_{t1}^3} + \cdots\right) - \frac{\omega^2 CR - j\omega}{\omega_t}} \\ &\approx -\frac{1}{j\omega CR\left(1 + \frac{1}{\omega_t CR} - \frac{\omega^2}{\omega_{t1}^2}\right) + \frac{\omega^2 CR}{\omega_{t1}}\left(1 - \frac{\omega^2}{\omega_{t1}^2} - \frac{\omega_{t1}}{\omega_t}\right)}\end{aligned} \tag{4.74}$$

Thus, the loss equals

$$q = \frac{\omega^2 CR}{\omega_{t1}}\left(1 - \frac{\omega^2}{\omega_{t1}^2} - \frac{\omega_{t1}}{\omega_t}\right) = \frac{\omega CR}{|A_1(j\omega)|}\left(1 - \frac{1}{|A_1(j\omega)|^2} - \frac{\omega_{t1}}{\omega_t}\right) \tag{4.75}$$

In this circuit we must be careful before we neglect higher-order terms: if the two opamps are perfectly matched, i.e., if $\omega_{t1} = \omega_t$, we find the circuit in Fig. 4.24 has very low losses.

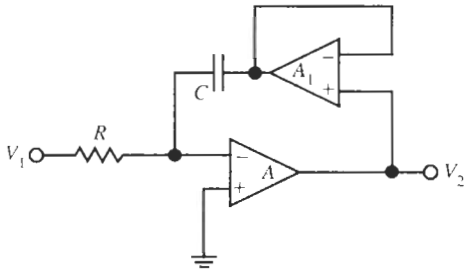

Figure 4.24 Active compensation of a Miller integrator.

$$q = -\frac{\omega CR}{|A_1(j\omega)|^3} \tag{4.76a}$$

In the more realistic case of a slight mismatch between the amplifiers, the mismatch term will dominate and we have

$$q = \frac{\omega CR}{|A_1(j\omega)|}\left(1 - \frac{1}{|A_1(j\omega)|^2} - \frac{\omega_{t1}}{\omega_t}\right) \approx \frac{\omega CR}{|A_1(j\omega)|}\left(1 - \frac{\omega_{t1}}{\omega_t}\right) \tag{4.76b}$$

Note that there is an uncertainty as to the sign of q. The loss term can be positive or negative depending on whether $\omega_{t1} < \omega_t$ or $\omega_{t1} > \omega_t$, respectively.

4.4.2 Noninverting Integrators

We have established the effect of $A(s)$ on the inverting integrator and have presented a couple of compensation techniques to minimize the loss. We will next consider the noninverting integrator. In the biquad of Fig. 4.10 we have simply used a cascade of a Miller integrator and an inverter as shown in Fig. 4.25a. The transfer function is obtained readily by multiplying the transfer functions of the two blocks, Eqs. (4.68) and (2.55) for $R_1 = R_2 = R$. Assuming matched amplifiers, $A = A_1$, we have

$$\begin{aligned}\frac{V_2}{V_1} &= -\frac{1}{sCR}\frac{1}{1 + \frac{1}{A(s)}\left(1 + \frac{1}{sCR}\right)} \times \frac{-1}{1 + \frac{2}{A(s)}} \\ &= \frac{1}{sCR}\frac{1}{1 + \frac{3}{A} + \frac{1}{sCRA} + \frac{2}{A^2} + \frac{2}{sCRA^2}}\end{aligned} \tag{4.77}$$

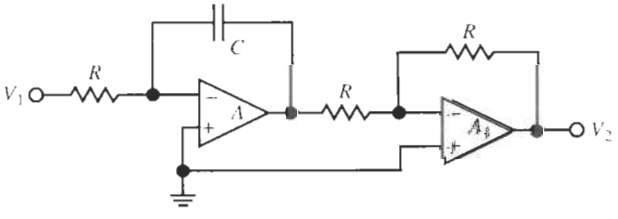

(a)

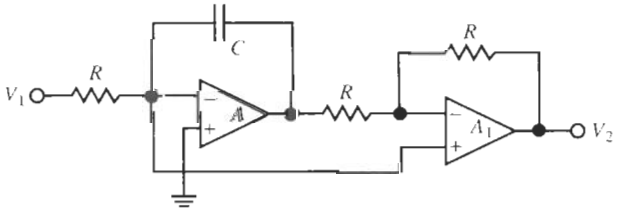

(b)

Figure 4.25 Noninverting integrator: (a) the Miller-inverter cascade; (b) modified circuit to reduce the loss by a factor of 3.

We next proceed as before: evaluate Eq. (4.77) on the $j\omega$-axis and neglect all terms involving A^{-2}. The result is

$$\frac{V_2}{V_1} \approx \frac{1}{j\omega CR[1 + 1/(CR\omega_t)] - 3\omega^2 CR/\omega_t} \approx \frac{1}{j\omega CR - 3\omega^2 CR/\omega_t} \tag{4.78}$$

where we again assumed that $\omega_t CR \gg 1$. The loss for this noninverting integrator is seen to equal

$$q = -\frac{3\omega^2 CR}{\omega_t} = -\frac{3\omega CR}{|A(j\omega)|} \tag{4.79}$$

Thus, the Miller-Inverter Cascade has also a negative loss term, but three times larger than that of the Miller integrator.

There is a simple wiring change that reduces q of Eq. (4.79) by a factor of three. Consider the circuit in Fig. 4.25b, where we removed the noninverting input of opamp A_1 from ground and connected it to virtual ground at the inverting input of opamp A. Analyzing that circuit is not difficult (see the problems); for matched amplifiers, the result is the transfer function of Eq. (4.68), multiplied by the term

$$-\frac{1 + 2/A}{1 + 2/A_1} \approx -1$$

i.e.,

$$\frac{V_2}{V_1} = -\frac{1}{sCR}\frac{1}{1 + 1/A + 1/(sCRA)}\left(-\frac{1 + 2/A}{1 + 2/A_1}\right) \tag{4.80}$$

so that q is given by Eq. (4.70a), three times smaller than in Eq. (4.79).

An alternative way of building a noninverting integrator is to start from the inverting amplifier in Fig. 2.17a with R_2 replaced by $1/(sC)$, and the plus and minus terminals of the opamp interchanged. To keep the circuit stable, the loop gain of the feedback loop must be negative. Thus, similar to how we handled the case in Fig. 4.7b, we have to have an inverter in the loop. Figure 4.26 shows the circuit. The analysis proceeds from the node equation at the noninverting input of amplifier A,

$$\frac{V_2}{A}(G + sC) = GV_1 + sC\frac{-1}{1 + 2/A_1}V_2$$

Using again the Taylor series, this expression can be manipulated to arrive at the transfer function as follows:

$$\frac{V_2}{V_1} = \frac{G}{\dfrac{sC}{1 + 2/A_1} + \dfrac{G + sC}{A}} \approx \frac{1}{sCR\left(1 - \dfrac{2}{A_1} + \dfrac{4}{A_1^2} - \ldots\right) + \dfrac{1 + sCR}{A}} \tag{4.81}$$

From this equation we calculate, assuming matched opamps and using the same methods as before,

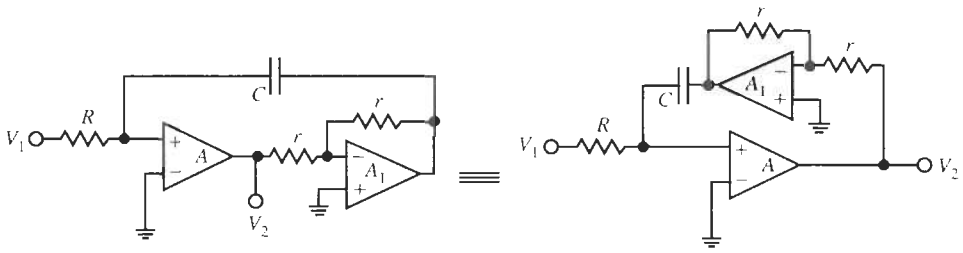

Figure 4.26 Noninverting integrator; q is given in Eq. (4.82).

$$q = \frac{\omega^2 CR}{\omega_t} = \frac{\omega CR}{|A(j\omega)|} \tag{4.82}$$

The size of the loss term is the same as for the inverting integrator, but it is worth noting that here q is *positive*.

We can also develop a low-loss noninverting integrator to match the one in Fig. 4.24, by combining the ideas of Figs. 4.24 and 4.25b. The resulting circuit is shown in Fig. 4.27. The analysis of this three-opamp circuit seems daunting, but is actually quite simple if we proceed methodically and remember the functions of the buffer (A_1) and difference amplifier (A_2). We introduce for convenience the intermediate variable V_3; then we start as always with Kirchhoff's current law at the inverting input of amplifier A,

$$-\frac{V_3}{A}(G + sC) = GV_1 + sC\frac{V_3}{1 + 1/A_1} \quad \text{or} \quad V_3\left(\frac{G + sC}{A} + \frac{sC}{1 + 1/A_1}\right) = -GV_1 \tag{4.83}$$

and follow by the operation of the difference amplifier

$$V_2 = A_2\left(-\frac{V_3}{A} - \frac{GV_3 + GV_2}{2G}\right) \quad \text{or} \quad V_3\left(\frac{1}{A} + \frac{1}{2}\right) = -V_2\left(\frac{1}{A_2} + \frac{1}{2}\right) \tag{4.84}$$

Eliminating now the unneeded voltage V_3 from Eqs. (4.83) and (4.84) and assuming matching between amplifiers A and A_2, we obtain

$$\frac{V_2}{V_1} = \frac{G}{sC/(1 + 1/A_1) + (G + sC)/A} \tag{4.85}$$

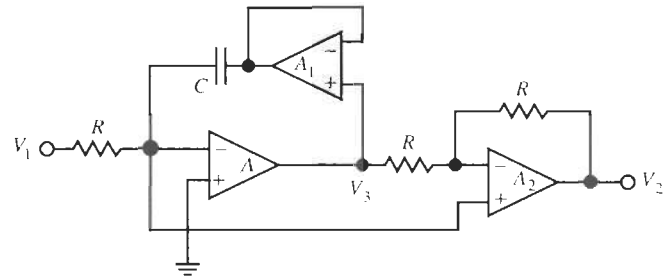

Figure 4.27 Noninverting integrator; q is given in Eq. (4.75).

which is identical to Eq. (4.72), except for the sign. Consequently, the circuit in Fig. 4.27 is a noninverting low-loss integrator, with q given by Eq. (4.75). Table 4.1 summarizes the different integrators we discussed and their losses.

4.4.3 The Effects of $A(s)$ on the Biquad

We have established that the effect of frequency-dependent opamp gain $A(s)$ is to make the integrators lossy,

$$\frac{V_2}{V_1} = \pm\frac{1}{s\tau + q} \tag{4.86}$$

where τ is the integrator time constant, normally an RC product, and q is the error caused by nonideal opamps. As seen in Table 4.1, q can be positive or negative, is a function of frequency (proportional to $\omega CR = \omega\tau$), and is inversely proportional to the opamp gain at the frequency of interest. Thus, q rises proportionally at least to ω^2, which makes the loss effects worse as operating frequencies increase.

Having determined in which way the integrator function is altered by a realistic opamp model, we are now ready to investigate the behavior of the two-integrator loop biquad in Fig. 4.7a. To do this, we replace the ideal integrators, $\pm 1/s$, by Eq. (4.86) as shown in Fig. 4.28. We labeled the multiplier of the input voltage K and recall from our earlier discussion that $K = H$, the dc gain of the lowpass or the high-frequency gain of the highpass function. In case of a bandpass filter, $K = H(\omega_0/Q)$ so that H is the midband gain. Let us analyze the circuit for its bandpass function T_B, noting that in Fig. 4.7a the frequency is normalized, $\omega_0 = 1$. Instead of the bandpass function in Eq. (4.25b), we have

$$T_B(s) = \frac{V_B}{V_1} = -\frac{H(1/Q)(s\tau_2 + q_2)}{(s\tau_1 + q_1)(s\tau_2 + q_2) + (1/Q)(s\tau_2 + q_2) + 1}$$

TABLE 4.1 Active Integrators

Circuit	Loss q; Quality Factor $Q_t = \omega RC/q$	
Inverting		
Miller integrator (Fig. 4.23a)	$q = -\frac{\omega^2 CR}{\omega_t} = -\frac{\omega CR}{\lvert A(j\omega)\rvert}$	Eq. (4.70a)
High-Q Miller integrator—active compensation (Fig. 4.24)	$q = \frac{\omega^2 CR}{\omega_{t1}}\left(1 - \frac{\omega^2}{\omega_{t1}^2} - \frac{\omega_{t1}}{\omega_t}\right)$	Eq. (4.75)
Noninverting		
Miller-inverter cascade (Fig. 4.25a)	$q = -\frac{3\omega^2 CR}{\omega_t} = -\frac{3\omega CR}{\lvert A(j\omega)\rvert}$	Eq. (4.79)
Modified Miller-inverter cascade (Fig. 4.25b)	$q = -\frac{\omega^2 CR}{\omega_t} = -\frac{\omega CR}{\lvert A(j\omega)\rvert}$	Eq. (4.70a)
Positive loss term (Fig. 4.26)	$q = +\frac{\omega^2 CR}{\omega_t} = +\frac{\omega CR}{\lvert A(j\omega)\rvert}$	Eq. (4.82)
High-Q integrator (Fig. 4.27)	$q = \frac{\omega^2 CR}{\omega_{t1}}\left(1 - \frac{\omega^2}{\omega_{t1}^2} - \frac{\omega_{t1}}{\omega_t}\right)$	Eq. (4.75)

$$= -\frac{\dfrac{H}{\tau_1 \tau_2 Q}(s\tau_2 + q_2)}{s^2 + s\left(\dfrac{q_1}{\tau_1} + \dfrac{q_2}{\tau_2} + \dfrac{1}{\tau_1 Q}\right) + \left(1 + q_1 q_2 + \dfrac{q_2}{Q}\right)\dfrac{1}{\tau_1 \tau_2}} \tag{4.87}$$

As a check on our computations, we note that for lossless integrators ($q_i = 0$) and t_i normalized to 1, the denominator of Eq. (4.87) reduces to that in Eq. (4.25b).

Let us compare Eq. (4.87) with the standard form in Eq. (4.43) to get an idea of the errors caused by the opamps. If we use the subscript r to label the parameters *realized* in the filter built with real opamps,

$$T_B(s) = -\frac{H_r\,(\omega_{0r}/Q_r)\,s}{s^2 + (\omega_{0r}/Q_r)\,s + \omega_{0r}^2} \tag{4.88}$$

we see that the circuit realizes the pole frequency

$$\omega_{0r} = \frac{1}{\sqrt{\tau_1 \tau_2}}\sqrt{1 + q_1 q_2 + \frac{q_2}{Q}} \tag{4.89}$$

and the pole Q

$$Q_r = \frac{\omega_{0r}}{\dfrac{q_2}{\tau_2} + \dfrac{q_1}{\tau_1} + \dfrac{1}{\tau_1 Q}} = Q\frac{\omega_{0r}\tau_1}{1 + Q\,(q_1 + q_2\tau_1/\tau_2)} \tag{4.90}$$

In addition, the bandpass realizes the midband gain (at $\omega = \omega_{0r}$)

$$H_r \approx H\frac{1}{1 + Q\,(q_1 + q_2\tau_1/\tau_2)} \tag{4.91}$$

and has a parasitic zero at

$$s = -q_2/\tau_2 \tag{4.92}$$

close to, but *not at* the origin as required in a bandpass filter. The effect of having shifted the zero away from the origin can be neglected in most applications, but it causes the dc gain of the bandpass filter to be finite.

Equations (4.89) to (4.92) provide the information we were seeking: the deviations in filter performance caused by the frequency dependence of the opamps. Understanding these results

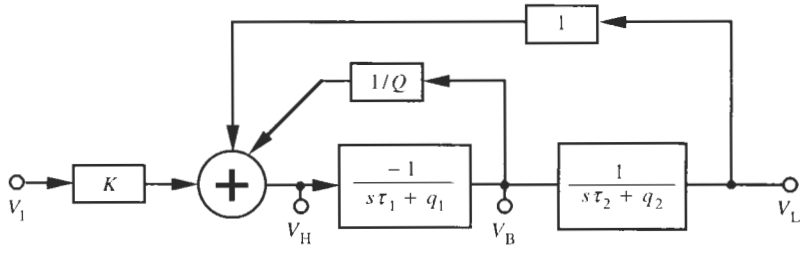

Figure 4.28 Two-integrator loop with nonideal integrators.

will enable us to anticipate the errors to be expected when implementing a transfer function by a circuit with real opamps, and permit us to take corrective steps during the design phase. To help in the interpretation, let us assume, as is usually the case (see, e.g., Example 4.4), that

$$\tau_1 = \tau_2 = \tau = 1/\omega_0$$

Further, in practice the integrator losses will always be fairly small, $q_i \ll 1$; note that q is inversely proportional to $|A|$ as shown earlier in this section. Under these conditions we obtain from Eq. (4.89)

$$\omega_{0r} \approx \frac{1}{\tau}\left[1 + \frac{1}{2}\left(q_1 q_2 + \frac{q_2}{Q}\right)\right] \approx \omega_0 + \Delta\omega_0 \tag{4.93a}$$

with

$$\Delta\omega_0 \approx \frac{1}{2\tau}\left(q_1 q_2 + \frac{q_2}{Q}\right) = \frac{\omega_0}{2}\left(q_1 q_2 + \frac{q_2}{Q}\right) = \frac{\omega_0}{2} q_2 \left(q_1 + \frac{1}{Q}\right) \tag{4.93b}$$

In Eq. (4.93), we made use of the Taylor expansion $\sqrt{1+x} \approx 1 + x/2$ for $x \ll 1$. It is seen that $\Delta\omega/\omega_0 \ll 1$ so that integrator losses have only a small effect on ω_0. Recall from our discussion in Sections 4.4.1 and 4.4.2 (Table 4.1) that integrator losses are mostly negative. Because normally $Q < |q_1|$, it follows that $\Delta\omega_0$ must be expected to be negative, that is, $\omega_{0r} < \omega_0$.

From Eqs. (4.90) and (4.91) we note that errors of the quality factor Q caused by integrator losses in the two-integrator loop are approximately the same as those of the midband gain H, i.e.,

$$\frac{Q_r}{Q} \approx \frac{H_r}{H} = \frac{1}{1 + Q\,(q_1 + q_2)} \tag{4.94}$$

where we assumed that $\omega_{0r}\tau \approx 1$. These errors can be, and often are, large because the small term $(q_1 + q_2)$ is multiplied by Q. We must pay particular attention to the problem when large Q values are to be designed and when the loss terms q_i are negative, as they mostly are in practical integrators (Table 4.1). For instance, for the nominal value of $f_t = 1.5$ MHz in Example 4.4, we have $q_1 \approx -0.025$ and $q_2 = 3q_1 \approx -0.076$. For this case the denominator of Eq. (4.94) goes to zero, that is Q_r and H_r become infinite, if the design value of Q equals or exceeds

$$Q \approx \frac{1}{q_1 + q_2} = \frac{1}{0.101} = 9.87$$

Physically, infinite Q_r means that the filter oscillates and is not useful as a signal processing circuit. We note that Eq. (4.94) imposes serious restrictions on the realizable values of Q, i.e., $Q < 1/(q_1 + q_2)$, unless corrective measures are taken.

Equations (4.89) to (4.94) are the desired results. They predict and explain the errors in the realized parameters in a two-integrator-loop biquad circuit, and they suggest possible approaches we can take to reduce the deviations. For example, Eq. (4.94) could be used to determine the necessary design value Q that will result in the required value Q_r realized. We simply solve the equation for Q,

$$Q = \frac{Q_r}{1 - Q_r(q_1 + q_2)} \tag{4.95}$$

which lets us determine Q, given Q_r and integrator losses. For example, with $q_1 + q_2 = 0.101$ and the required value of $Q_r = 6$ in Example 4.4, we need to design the filter for a nominal value $Q = 3.73$. We refer to this process as *predistorting* the design so that realizing the filter with real opamps will enhance Q to the desired value Q_r. We might contemplate a similar approach for the center frequency ω_0: design the circuit with a value $(\omega_0 - \Delta\omega_0)$ so that the integrator losses by Eq. (4.93a) result in the correct value ω_0. Although *predistortion* does work in principle and may reduce the observed errors, a weakness is that it assumes that the q_i-values, and therefore the gain-bandwidth products ω_t of the opamps, are known. Unless ω_t is first measured, this is not normally a realistic assumption because of the wide variability of ω_t from opamp to opamp. To illustrate the difficulty, let us revisit Example 4.4 and check the measured performance against the above equations.

EXAMPLE 4.5

Explain the measured performance in Example 4.4. Determine the actual value of f_t and compare it with the nominal value of 1.5 MHz.

Solution

In this example we designed a bandpass biquad with $Q = 6$, midband gain $H = 1$ (0 dB), and $f_0 = 38$ kHz. The measured performance was $Q = 21.7$, midband gain $H = 11.3$ dB, and $f_0 = 36.8$ kHz. The opamps we used were LM741 with $f_t = 1.5$ MHz nominally. We chose $R_2 = R_4 = R = 1/(\omega_0 C)$ so that $\omega_0 RC = 1$ in the equations for the integrator loss, q. The biquad was built with an inverting Miller integrator and a Miller-inverter cascade. The loss terms are, therefore, from Eqs. (4.70a) and (4.79) and evaluated at the center frequency,

$$q_1 = -\frac{\omega^2 CR}{\omega_t} = -\frac{\omega}{\omega_t} = -\frac{38}{1500} = -0.0253 \quad \text{and} \quad q_2 = -\frac{3\omega^2 CR}{\omega_t} = -3q_1 = -0.0760$$

We note first that the ratio of realized to designed Q equals $21.7/6 = 3.62$, which corresponds to 11.12 dB. This is approximately the observed gain enhancement as the theory in Eq. (4.94) predicts. The actual predicted values are, from Eq. (4.94),

$$\frac{Q_r}{Q} = \frac{H_r}{H} = \frac{1}{1 + Q\,(q_1 + q_2)} = \frac{1}{1 - 6 \times 0.101} = 2.54$$

leading to $H = 8.1$ dB and $Q = 15.2$. Further, by Eq. (4.93a), the center frequency is reduced to

$$f_{0r} \approx f_0 \left[1 + \frac{1}{2}\left(0.0253 \times 0.0760 - \frac{0.0760}{6}\right)\right] \approx 37.9 \text{ kHz}$$

Clearly, the predictions are incorrect (too small), although they are in the right direction. The inconsistencies between equations and measurement can be explained by an incorrect value of f_t and with a further refinement of the opamp model, compare Eq. (2.17). To find the experimental value of f_t, we solve Eq. (4.94) for $q_1 + q_2$,

$$q_1 + q_2 = 4q_1 = \frac{Q - Q_r}{QQ_r} = \frac{6 - 21.7}{6 \times 21.7} = -0.1206$$

where we used that $q_2 = 3q_1$. With $\omega_0 CR = 1$, it follows from Eq. (4.70a) that

$$q_1 = -0.0301 = -\frac{f_0}{f_t} = -\frac{38 \text{ kHz}}{f_t}$$

that is $f_t = 1.26$ MHz, rather than the nominal $f_t = 1.5$ MHz we assumed for the design. Since the actual value of f_t is smaller than the nominal value on which the design was based, we have $|A|$ smaller than assumed, the losses are larger, and the filter parameter errors in Example 4.4 are larger than expected.

The example illustrates that predistortion is normally not a practical approach for achieving accurate and reliable circuits. A better method will use integrators with lower loss, such as the actively compensated Miller integrator in Fig. 4.24 and its noninverting counterpart in Fig. 4.27. Alternatively, we may seek to eliminate the loss in the two-integrator loop completely by noticing from Eq. (4.94) that the errors are reduced to zero if $q_1 = -q_2$. Consulting Table 4.1, we see that this can be achieved by pairing the inverting Miller integrator with the noninverting integrator of Fig. 4.26. The resulting biquad, the so-called *Åckerberg–Mossberg* circuit, is shown in Fig. 4.29.

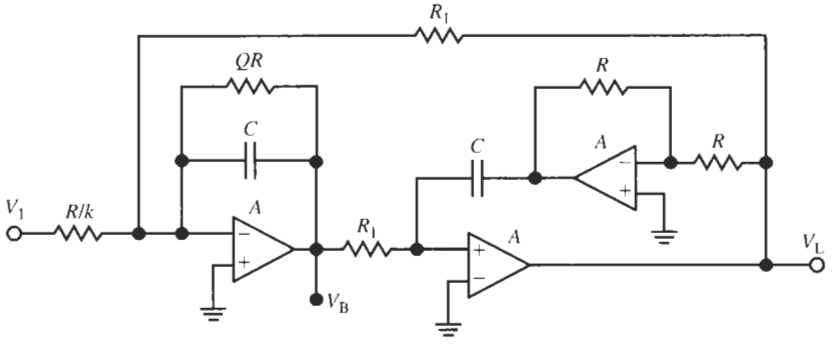

Figure 4.29 The Åckerberg–Mossberg filter.

EXAMPLE 4.6

Design an Åckerberg–Mossberg bandpass with the frequency and gain specifications given in Example 4.4, but with a quality factor $Q = 15$. Use LM741 opamps.

Solution

The design process follows exactly Example 4.4. The circuit with component values to realize the filter specified is shown in Fig. 4.30a[1] and the frequency response with real amplifiers is

[1]We have used in this example resistor values with unrealistically low tolerances to ensure that any errors arise from the opamp and not from component tolerances.

given in Fig. 4.30b. Although we based the design on ideal amplifiers, the performance with real opamps is nearly as predicted: The experimental midband gain is 1.24 rather than 1, and Q equals 14.3 rather than 15 as specified. As in the previous two-integrator loop structures, the experimental center frequency equals 36.9 kHz.

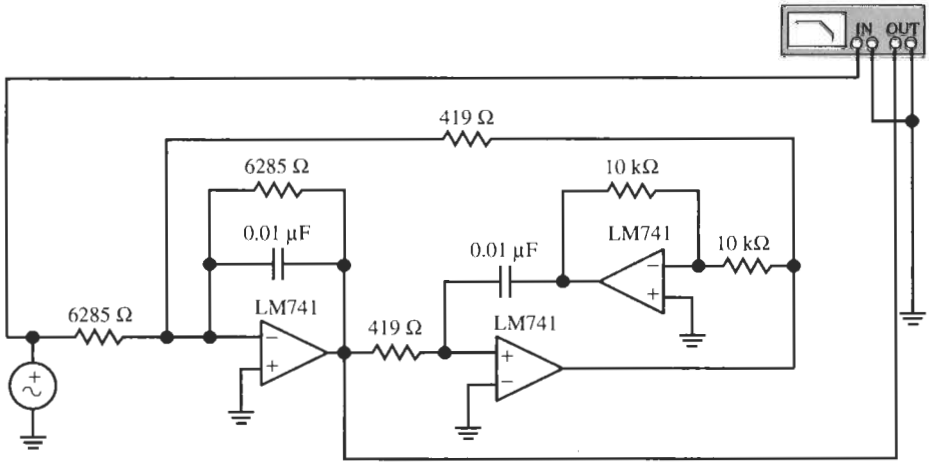

(a)

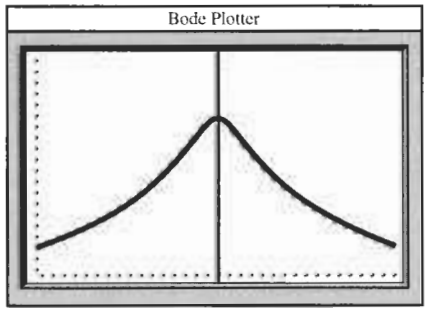

(b)

Figure 4.30 (a) Filter designed for Example 4.6; (b) experimental performance. (Bode Plotter scales: 30 to 45 kHz; −20 dB to +10 dB; cursor at 36.9 kHz, 1.86 dB.)

This example demonstrates that the Åckerberg–Mossberg biquad is a filter that can be designed reliably for higher frequencies and large quality factors without incurring large unpredictable Q and gain errors. Frequency deviations are, of course, not affected by this circuit structure because, by Eq. (4.89), q cancellations do not influence f_0.

We have now analyzed in great detail the two-integrator-loop (Tow–Thomas) biquad in Fig. 4.10 and a number of modifications. With the help of our study of integrators, we arrived at the alternate implementations. The understanding gained showed us that finite integrator losses are the cause of errors in biquad performance. In particular, we discovered that at least the errors in quality factor could be eliminated entirely by pairing an

integrator with a positive loss term with one with a negative loss term. This resulted in the Åckerberg–Mossberg biquad of Fig. 4.29. Observe that the improved performance over that of the Tow-Thomas biquad in Fig. 4.10 is obtained at no additional cost. It requires only a wiring change. We will, therefore, in the remainder of this book deal only with the Åckerberg–Mossberg biquad whenever we need to use a two-integrator loop circuit. Nevertheless, the literature on active filters contains a great number of second-order circuits developed for a variety of applications. In the next section we shall study a few of them to present the student with a choice of circuits that may be called on to realize a design requirement.

4.5 OTHER BIQUADS

In addition to the three-amplifier biquads of Section 4.4, engineers have invented biquads that use two opamps or even only one opamp. The number of opamps does, of course, affect cost and power consumption, but the main differences between different circuits are their sensitivity to component tolerances, to be discussed in Chapter 12, and their versatility in being able to realize different transfer functions.

4.5.1 Sallen–Key Circuits

Sallen–Key filters were among the first active filters that appeared in the literature (Sallen and Key, 1955). This reference contains a whole catalog of possible structures that permit the realization of various types of transfer functions. One such structure to realize a lowpass function is shown in Fig. 4.31a. To analyze the circuit for its transfer function we obtain first by voltage division

$$\frac{V_2}{V_-} = 1 + \frac{R_B}{R_A} = K \tag{4.96}$$

and write node equations at nodes V_a and V_b:

$$(sC_2 + G_2)\, V_a = G_2 V_b \tag{4.97}$$

$$V_b\,(G_1 + G_2 + sC_1) = G_1 V_1 + sC_1 V_2 + G_2 V_a \tag{4.98}$$

For an ideal opamp we have $V_a - V_- = 0$ and we can solve the previous three equations for the transfer function V_2/V_1. Let us instead assume a real opamp with finite gain $A(s)$ and use $V_a - V_- = V_2/A$ to be able to investigate the effects of A. We next solve Eq. (4.98) for V_b and substitute the result into Eq. (4.97):

$$\left(sC_2 + G_2 - \frac{G_2^2}{G_1 + G_2 + sC_1}\right) V_a = G_2 \frac{G_1 V_1 + sC_1 V_2}{G_1 + G_2 + sC_1}$$

Solving for V_a, we obtain

$$V_a = \frac{G_1 G_2 V_1 + sC_1 G_2 V_2}{s^2 C_1 C_2 + s[C_2\,(G_1 + G_2) + C_1 G_2] + G_1 G_2}$$

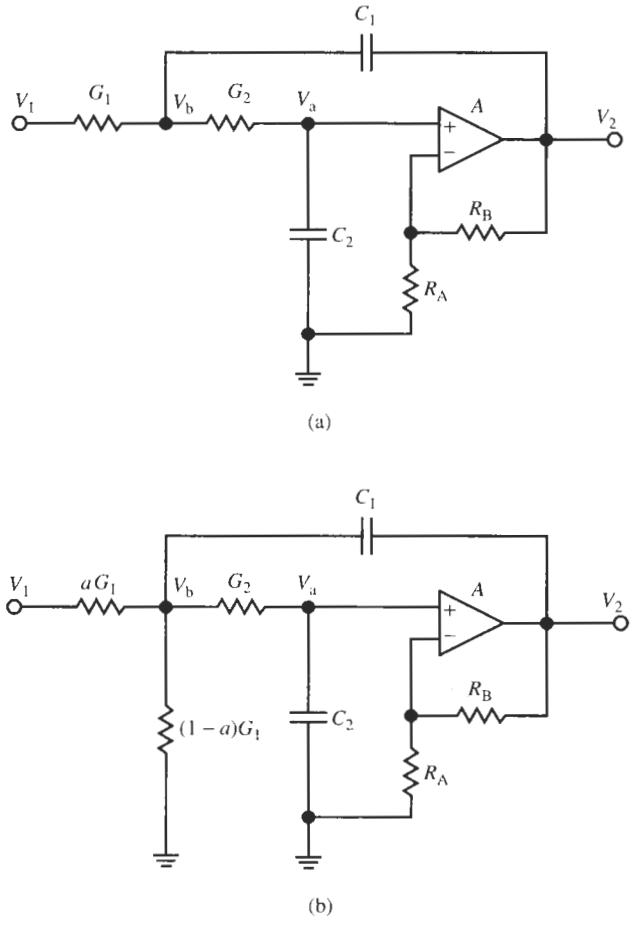

Figure 4.31 Sallen–Key lowpass filter; (a) dc gain $H = K$; (b) dc gain $H = aK$.

which with Eq. (4.96) and $V_a - V_- = V_2/A$ results in

$$T(s) = \frac{V_2}{V_1} = \frac{K G_1 G_2 \dfrac{1}{1 + K/A}}{s^2 C_1 C_2 + s\left[C_2 (G_1 + G_2) + C_1 G_2 \left(1 - K \dfrac{1}{1 + K/A}\right)\right] + G_1 G_2} \tag{4.99}$$

To derive the design equations, let us assume for now an ideal opamp, $A = \infty$. We then have the lowpass function

$$T(s) = \frac{V_2}{V_1} = \frac{K G_1 G_2}{s^2 C_1 C_2 + s[C_2 (G_1 + G_2) + C_1 G_2 (1 - K)] + G_1 G_2} \tag{4.100}$$

For convenience we set $C_1 = C_2 = C$ to obtain

$$T(s) = \frac{KG_1G_2/C^2}{s^2 + s[G_1 + G_2(2-K)]/C + G_1G_2/C^2} = \frac{H\omega_0^2}{s^2 + s\omega_0/Q + \omega_0^2} \tag{4.101}$$

We have again expressed the function in its standard form as in Eq. (4.17a) that lets us identify how the three filter parameters are expressed in terms of components:

$$\omega_0^2 = \frac{G_1G_2}{C^2} \tag{4.102}$$

$$Q = \frac{\sqrt{G_1G_2}}{G_1 + G_2(2-K)} \tag{4.103}$$

$$H = K > 1 \tag{4.104}$$

In selecting the four elements C, G_1, G_2, and K to realize the three filter parameters we have some freedom of choice. Since, in practice, the available capacitor values are usually limited, let us choose a convenient value for C. Also, let us assume that the dc gain is not important and can be fixed at $H = K$. Then we may select $R_1 = R_2 = R$ and obtain with

$$Q = \frac{1}{3-K} \tag{4.105}$$

the element values

$$R = \frac{1}{\omega_0 C} \quad \text{and} \quad K = 3 - \frac{1}{Q} = 1 + \frac{R_B}{R_A}, \quad \text{i.e.,} \quad R_B = (2 - 1/Q)R_A \tag{4.106}$$

R_A is arbitrary and can be chosen equal to R to minimize the number of different resistor values.

EXAMPLE 4.7

Design a Sallen–Key lowpass filter with $f_0 = 12.5$ kHz and no peaking. The dc gain is not specified. Use an LM741 opamp.

Solution

According to Fig. 4.13 a value $Q = 0.707$ is required to avoid peaking. Choosing $C = 0.01\mu$F results in

$$R_1 = R_2 = R_A = \frac{1}{2\pi \times 12.5 \times 10^{+4} \times 10^{-8}}\ \text{k}\Omega = 1.273\ \text{k}\Omega,$$
$$R_B = R_A(2 - 1/0.707) = 746\ \Omega$$

from Eq. (4.106). Figure 4.32 shows the circuit and its performance. The dc gain equals 4 dB as designed, and $f_0 = 12.5$ kHz. The dip and subsequent rise in gain at high frequencies are caused by higher-order opamp dynamics.

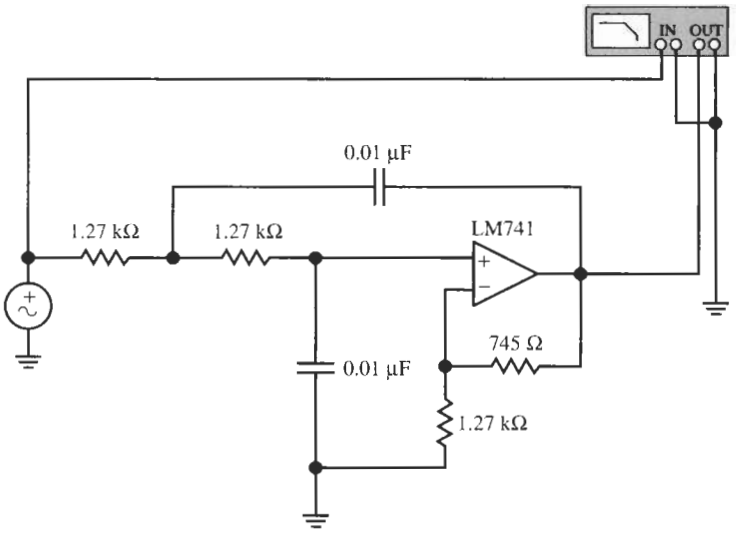

(a)

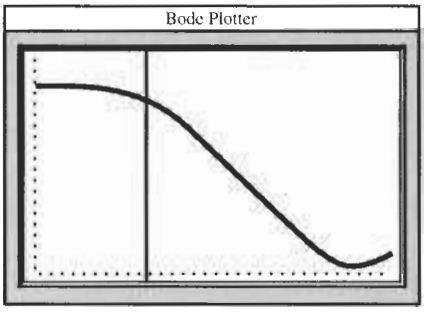

(b)

Figure 4.32 The circuit design for Example 4.7 and test results. (Bode Plotter scales: 3 to 300 k/Hz; −40 to +10 dB.) The cursor is at the −3 dB point (cursor readout: 12.5 kHz, 1.02 dB).

Observe that the Sallen–Key circuit has a potential problem: it is clear from Eq. (4.105) that for large Q, when K must be close to 3, Q is critically dependent on the exact realization of K. To get a measure of how sensitive Q is to the value K, let us use Eq. (4.105) and look at the slope of the function $Q(K)$ versus K,

$$\frac{dQ(K)}{dK} = \frac{d}{dK}\left(\frac{1}{3-K}\right) = \frac{1}{(3-K)^2} = Q^2 \tag{4.107}$$

In terms of finite differences, this equation can be recast as $\Delta Q \approx Q^2 \Delta K$ or

$$\frac{\Delta Q}{Q} \approx K\,Q\frac{\Delta K}{K} = (3Q-1)\frac{\Delta K}{K} \tag{4.108}$$

It says that *the percentage error in Q equals $K\,Q = 3Q - 1$ times the percentage error in K.* The ratio

$$S_K^Q = \frac{dQ/Q}{dK/K} \approx \frac{\Delta Q/Q}{\Delta K/K} \tag{4.109}$$

is called the *sensitivity* of Q to K. We shall study sensitivity in more detail in Chapter 12. For now we just note that for large values of Q the Q-sensitivity becomes very large. For instance, if we need to design a peaking lowpass with $Q = 10$ (see Fig. 4.13) the sensitivity, with Eq. (4.108), is 29, that is, a 1% error in amplifier gain K is predicted to result in approximately a 30% error in quality factor. Such large errors in filter parameters will generally not be acceptable. They either require expensive processes to get very tight component tolerances, such as a 0.1% error in K to reduce the expected error in Q to 3%, or call for tuning. For a lowpass design, however, where Q is of the order of unity and $K \approx 2$, a 1% error in K results in $\approx 2\%$ error in quality factor. We can conclude, therefore, that Sallen–Key filters are useful only for small values of Q as are normally required in lowpass filters. For high-Q filters we need to develop alternative realizations. They will be discussed in Sections 4.5.2 and 4.5.3.

Gain Adjustment in Sallen–Key Filters

Another limitation of Sallen–Key lowpass filters is that their dc gain is fixed at $H = K = 3 - 1/Q$. We shall see later that, in particular for cascade designs, the biquad gain must be adjustable if filters with good dynamic range are to be designed. Naturally, we could solve the problem by cascading the Sallen–Key circuit with an opamp-based amplifier of gain less than or larger than 1, but this solution may be too expensive. Let us look at a modification of the circuit that avoid additional opamps.

Consider first the problem of realizing a desired value of $H < K$. We can reduce the gain by including a voltage divider into the circuit in such a way that the poles do not get changed. Observe that the filter has a resistor R_1 in series with the input so that the resistance seen from V_b to the left in Fig. 4.31a equals R_1. We may replace that resistor by a voltage divider consisting of

$$R_a = \frac{R_1}{a} \quad \text{and} \quad R_b = \frac{R_1}{1-a} \tag{4.110}$$

as shown in Fig. 4.31b. Then R_a and R_b in parallel equal R_1,

$$R_1 = \frac{1}{G_1} = \frac{1}{G_a + G_b} = \frac{R_1}{a + (1-a)}$$

and the effect of this step multiplies V_1 in Eq. (4.98) by $a < 1$. The transfer function will not change except for a multiplying factor a, so that the gain equals $H = aK$ as desired:

$$T(s) = \frac{V_2}{V_1} = \frac{aKG_1G_2}{s^2C_1C_2 + s[C_2(G_1+G_2) + C_1G_2(1-K)] + G_1G_2} \tag{4.111}$$

The opposite problem, increasing the dc gain above the value K, is not as easy to solve. Normally, an additional opamp is necessary to provide the required gain.

The Effect of $A(s)$ on the Sallen–Key Circuit

Let us investigate what deviations are caused by the operational amplifier. Anticipating this concern, we did include in the circuit analysis leading to Eq. (4.99) the finite amplifier gain A. Starting from that equation we find with $C_1 = C_2 = C$ and $G_1 = G_2 = G$

$$T(s) = \frac{K\omega_0^2 \dfrac{1}{1 + K/A}}{s^2 + s\omega_0\left(3 - K\dfrac{1}{1 + K/A}\right) + \omega_0^2}$$

To get a manageable expression for the errors, we make the approximation $1/(1 + K/A) \approx 1 - K/A$ for $|A| \gg K$. This leads to the equation

$$T(s) \approx \frac{K\omega_0^2(1 - K/A)}{s^2 + s\omega_0[3 - K(1 - K/A)] + \omega_0^2}$$

Using the opamp integrator model of Eq. (2.18), $A(s) \approx \omega_t/s$, we have

$$T(s) \approx \frac{K\omega_0^2(1 - sK/\omega_t)}{s^2(1 + \varepsilon) + s\omega_0(3 - K) + \omega_0^2} \tag{4.112}$$

where we introduced the error term

$$\varepsilon = \frac{\omega_0}{\omega_t}K^2 = \frac{K^2}{|A(j\omega_0)|} \tag{4.113}$$

Equation (4.112) can be manipulated into the following form by dividing numerator and denominator by $1 + \varepsilon$:

$$T(s) = \frac{K\left(\dfrac{\omega_0}{\sqrt{1+\varepsilon}}\right)^2(1 - sK/\omega_t)}{s^2 + s\dfrac{\omega_0}{\sqrt{1+\varepsilon}}\left(\dfrac{3 - K}{\sqrt{1+\varepsilon}}\right) + \left(\dfrac{\omega_0}{\sqrt{1+\varepsilon}}\right)^2} \rightarrow \frac{H_L\omega_{0R}^2}{s^2 + s\dfrac{\omega_{0R}}{Q_R} + \omega_{0R}^2} \tag{4.114}$$

As indicated, this expression describes the *realized* filter. The notation shows that the realized pole frequency f_{0R} is decreased to

$$f_{0R} = \frac{f_0}{\sqrt{1+\varepsilon}} \approx f_0\left(1 - \frac{\varepsilon}{2}\right) = f_0 - \Delta f_0 \tag{4.115}$$

and the realized quality factor has increased:

$$Q_R = \frac{1}{3 - K}\sqrt{1+\varepsilon} = Q\sqrt{1+\varepsilon} \approx Q\left(1 + \frac{\varepsilon}{2}\right) = Q + \Delta Q \tag{4.116}$$

The dc gain is realized correctly, $H_L = K$, but $T(s)$ has acquired a zero on the positive real axis at $s = \omega_t/K$. Because Q_R must be finite and positive, Eq. (4.105) requires $K < 3$. This zero is, therefore, too far from the operating frequencies of the filter to cause noticeable errors in the transfer behavior.

Let us interpret these results: Notice from Eq. (4.113) that $\varepsilon < 9/|A(j\omega_0)|$ ($\varepsilon < 0.06$ for an LM741 at 10 kHz). In Example 4.7 with $K = 1.59$, this frequency error is $\Delta f_0/f_0 \approx -1\%$ and the error in quality factor is $\Delta Q/Q \approx +1\%$. We can state, therefore, that the Sallen–Key filter provides a good *lowpass* filter with very small ω_t-caused deviations *for low values of*

Q. We mentioned already that alternative realizations are needed for high-Q circuits, such as bandpass filters.

Changing a Lowpass Filter to a Highpass Filter: The RC–CR Transformation

We shall discuss in Chapter 9 a general process of frequency transformation that will allow us to convert a given lowpass specification and design into a highpass, bandpass, or other type of filter. The *RC–CR* transformation is a simple special case of the general method suitable for active *RC* filters. We shall discuss it here specifically for the Sallen–Key circuit although it is applicable for other *RC*–opamp configurations.

Consider the Sallen–Key lowpass circuit in Fig. 4.31a described by Eq. (4.100), repeated here for convenience as $T_L(s)$ in Eq. (4.117):

$$T_L(s) = \frac{V_2}{V_1} = \frac{KG_1G_2}{s^2C_1C_2 + s[C_2(G_1 + G_2) + C_1G_2(1 - K)] + G_1G_2} \tag{4.117}$$

Now let us replace the conductances G_j in the lowpass circuit by the capacitors C_j, and the capacitors C_k by conductances G_k, respectively,

$$\begin{aligned} G_j &\rightarrow C_j, \quad \text{i.e.,} \quad C_j = G_j = 1/R_j \\ C_k &\rightarrow G_k, \quad \text{i.e.,} \quad G_k = 1/R_k = C_k \end{aligned} \tag{4.118}$$

Amplifier gains are not affected, that is, the parameter K and, therefore, the resistors R_A and R_B are not changed. The result of this transformation is the circuit in Fig. 4.33 with the highpass transfer function

$$T_H(s) = \frac{V_2}{V_1} = \frac{Ks^2C_1C_2}{G_1G_2 + s[G_2(C_1 + C_2) + G_1C_2(1 - K)] + s^2C_1C_2} \tag{4.119}$$

This equation can be obtained by analyzing the circuit in Fig. 4.33 or directly from Eq. (4.117) by replacing G_j by sC_j, $j = 1, 2$, and sC_k by G_k, $k = 1, 2$. Comparing the result with Eq. (4.117), we see that the corresponding coefficients have the same numerical values because of the transformation (4.118). More specifically we recognize that the dc gain of the lowpass and

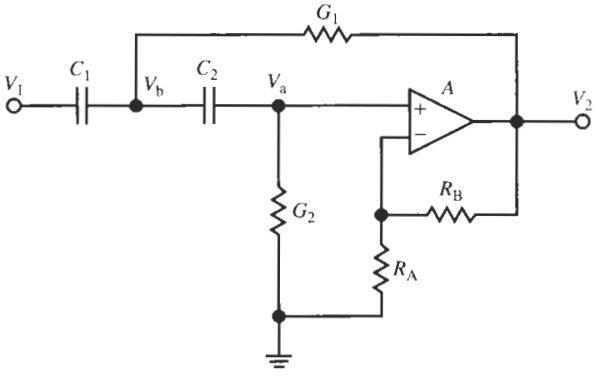

Figure 4.33 Sallen–Key highpass circuit obtained by the *RC–CR* transformation from the lowpass in Fig. 4.31a.

the high-frequency gain of the highpass are K, that the pole frequency ω_0 in both functions is given by

$$\omega_0^2 = \frac{G_1 G_2}{C_1 C_2} \tag{4.120}$$

as in Eq. (4.102), and that Q in both functions is identical, determined by the expression in brackets.

Let us still observe that the transformation (4.118) as written assumes a normalized frequency parameter, s/ω_0, and, therefore, normalized elements. The physical element values are obtained by denormalizing the frequency by ω_0, that is the highpass elements R_{HP} and C_{HP} are obtained from the known lowpass elements R_{LP} and C_{LP} as follows:

$$R_{j,\text{HP}} \to \frac{1}{\omega_0 C_{j,\text{LP}}}, \quad \text{and} \quad C_{k,\text{HP}} = \frac{1}{\omega_0 R_{k,\text{LP}}} \tag{4.121}$$

Any components that do not affect the frequency parameter and enter the transfer function only as a ratio, such as R_{A} and R_{B} to set K,, are not changed. Note that we may still preselect a convenient value for C and choose identical resistors $R = 1/G$ as in the lowpass filter to obtain from Eq. (4.119)

$$T_{\text{H}}(s) = \frac{Ks^2}{s^2 + s\omega_0(3 - K) + \omega_0^2} \tag{4.122}$$

where

$$Q = \frac{1}{3 - K} \tag{4.123}$$

as in Eq. (4.105). An example will illustrate the method.

EXAMPLE 4.8

Design a Sallen–Key lowpass filter with $f_0 = 1.25$ kHz and $Q = 5$. The dc gain is not specified. Use the *RC–CR* transformation to design a highpass with the same specifications of pole frequency and quality factor. LM741 opamps are to be used.

Solution

The process is identical to the one in Example 4.7. Choosing $C = 0.1\ \mu$F results in

$$R_1 = R_2 = R_A = \frac{1}{2\pi \times 1.25 \times 10^{+4} \times 10^{-7}}\ \text{k}\Omega = 1.273\ \text{k}\Omega,$$
$$R_{\text{B}} = R_{\text{A}}(2 - 1/5) = 2.29\ \text{k}\Omega$$

Figure 4.34 shows the lowpass and highpass circuits and their performance. The dc gain of the

lowpass and the high-frequency gain of the highpass are 9.25 dB as designed, and $f_0 = 12.5$ kHz. The dip and subsequent rise in gain at high frequencies are caused by higher-order opamp dynamics. Note that gain at $s = j\omega_0$ is $T(j\omega_0) = KQ = 14.3$ or 23.1 dB.

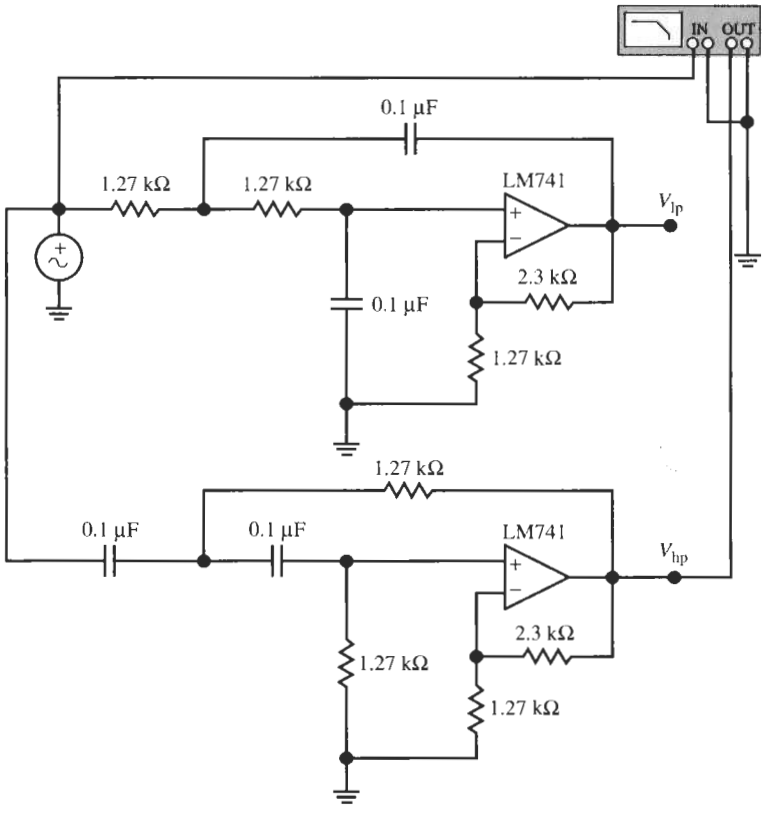

(a)

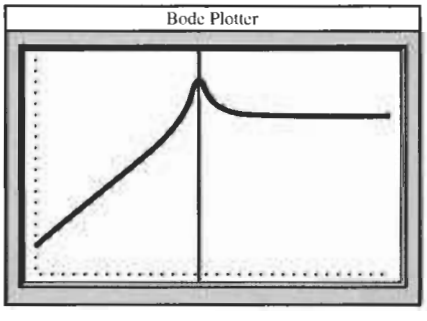

(b)

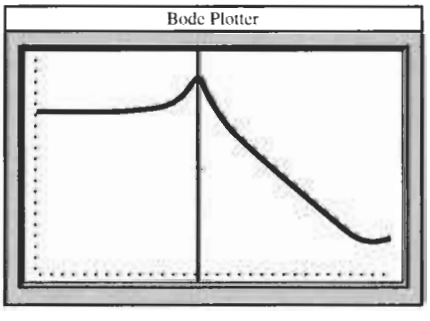

(c)

Figure 4.34 (a) The lowpass and highpass circuits for Example 4.8 and test set-up; the test performance measured at (b) the highpass output V_{hp}; and (c) the lowpass output V_{lp}. The cursor is at the peak frequency. (Bode Plotter scales for both curves: 50 Hz to 55 kHz; −60 dB to +30 dB: cursor at 1.25 kHz, 23.4 dB).

Since the *RC–CR* transformation did not change the filter poles, the earlier warning concerning the sensitivity of Q to the gain K is still valid, as are the discussion and results on the effect of finite opamp gain. Observe further that if a highpass with smaller gain is required, a procedure analogous to the one used for the lowpass in Fig. 4.31b can be used. The difference is that now we have a capacitor in series with the input so that we obtain a capacitive voltage divider with elements aC_1 and $(1-a)C$. For example, if in the previous example a high-frequency gain of 0 dB is specified, i.e., $a = 1/K = 0.357$, the $C = 0.1$-μF capacitor will have to be split into a series capacitor of 35.7 nF and a shunt capacitor of 64.3 nF.

4.5.2 The Single-Amplifier Biquad (SAB)

A useful bandpass circuit using only one operational amplifier was developed by T. Delyiannis (1968) and J. J. Friend (1970). It is shown in its bandpass configuration in Fig. 4.35. Both capacitors are labeled C because these filters are normally built with identical capacitors. We can determine the circuit's operation by writing a node equation for the inverting input terminal of the opamp, and one for the node labeled V_x. The two equations are

$$(2sC + G_1)\,V_x = aG_1V_1 + sCV_2 + sCV_- \tag{4.124}$$

$$(sC + G_2)\,V_- = sCV_x + G_2V_2 \tag{4.125}$$

with

$$V_- = -V_2/A \tag{4.126}$$

We have again assumed finite opamp gain A to be able to investigate later which effect A may have on filter parameters with no need to repeat the analysis. For an ideal opamp, $V_- = 0$ and the terms multiplied by V_- will simply be absent. To solve these equations for the transfer function V_2/V_1, we solve Eq. (4.125) for V_x and insert the result into Eq. (4.124). We find

$$V_x = -\frac{1}{sC}\left(G_2 + \frac{sC + G_2}{A}\right)V_2$$

and

$$V_2\left[\frac{1}{sC}\left(G_2 + \frac{sC + G_2}{A}\right)(2sC + G_1) + sC - \frac{sC}{A}\right] = -aG_1V_1$$

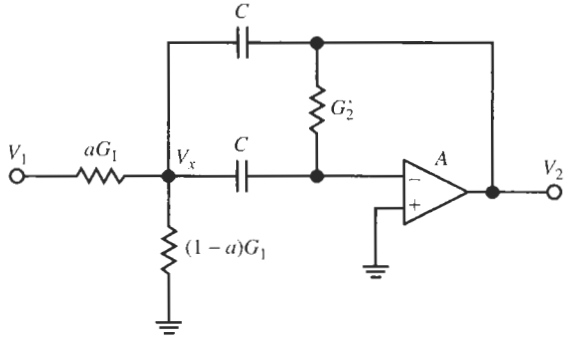

Figure 4.35 Delyiannis–Friend bandpass circuit.

This equation gives us the transfer function as

$$T(s) = \frac{V_2}{V_1} = \frac{N(s)}{D(s)} = -\left(\frac{A}{1+A}\right)\frac{saG_1/C}{s^2 + s\left(\frac{2G_2}{C} + \frac{G_1/C}{1+A}\right) + \frac{G_1G_2}{C^2}} \tag{4.127}$$

The parameter a to set the gain is obtained by a feed-in voltage divider in the same manner as for the Sallen–Key circuit in Fig. 4.31b. We observe that the first effect of finite opamp gain is the multiplying factor $A/(1+A)$. This is simply the gain of a voltage buffer, Eq. (2.82), and can be neglected for frequencies less than the opamp's unity-gain frequency, $f < f_t$. The second effect is determined by the term $(G_1/C)/(1+A)$ in the denominator. We shall investigate its consequences later and assume for now an ideal opamp, i.e., we consider the ideal transfer function

$$T(s) = -\frac{saCG_1}{s^2C^2 + 2sCG_2 + G_1G_2} = -\frac{saG_1/C}{s^2 + s2G_2/C + G_1G_2/C^2} \tag{4.128}$$

Let us rewrite Eq. (4.128) in the standard form with center frequency ω_0 and quality factor Q_0,

$$T(s) = \frac{V_2}{V_1} = -\frac{sH\,(\omega_0/Q_0)}{s^2 + s\,(\omega_0/Q_0) + \omega_0^2} \tag{4.129}$$

We can then identify the filter parameters as

$$\omega_0 = \sqrt{\frac{1}{R_1R_2C^2}}, \quad Q_0 = \frac{1}{2}\omega_0CR_2 = \frac{1}{2}\sqrt{\frac{R_2}{R_1}}, \quad \text{and} \quad H = \frac{1}{2}a\frac{R_2}{R_1} = 2aQ_0^2 \tag{4.130}$$

Conversely, we can also express the element values directly in terms of the filter parameters. From Eq. (4.130) we find the design equations as follows:

$$R_1R_2 = \frac{1}{\omega_0^2C^2}, \quad \frac{R_2}{R_1} = 4Q_0^2, \quad \text{and} \quad a = \frac{H}{2Q_0^2} \tag{4.131}$$

so that for a chosen value C we have

$$R_2 = 2Q_0\frac{1}{\omega_0C}, \quad R_1 = \frac{R_2}{4Q_0^2}, \quad \text{and} \quad a = \frac{H}{2Q_0^2} \tag{4.132}$$

Note that we require $H < 2Q_0^2$ because a is defined to be less than 1.

EXAMPLE 4.9

Design a Delyiannis–Friend bandpass circuit with $f_0 = 12.5$ kHz, $Q_0 = 10$, and midband gain $H = 26$ dB. Use an LM741 opamp.

Solution

On a linear scale, the gain equals $H = 19.95$; choosing $C = 5$ nF, we find from Eq. (4.132)

$$R_2 = \frac{20}{3.927 \times 10^{-4}} = 50.9\ \text{k}\Omega, \quad R_1 = \frac{R_2}{400} = 127\ \Omega, \quad a = \frac{19.95}{200} = 0.0998 \approx 0.1$$

and

$$R_1/a = 1.27\ \text{k}\Omega, \quad R_1/(1-a) = 141\ \Omega$$

The circuit and performance are shown in Fig. 4.36. Compared to the specified values, the measured center frequency and quality factor are $f_0 = 11.6$ kHz, reduced by 7.2% from the design value, and $Q_0 \approx 10.8$, an increase of $\approx 8\%$. The gain is $H = 26.2$ dB.

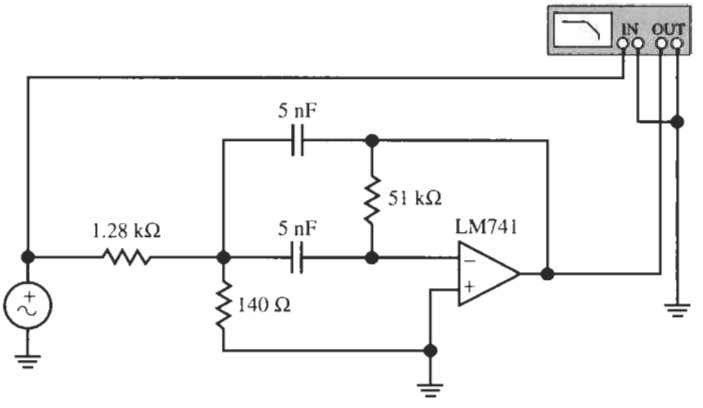

(a)

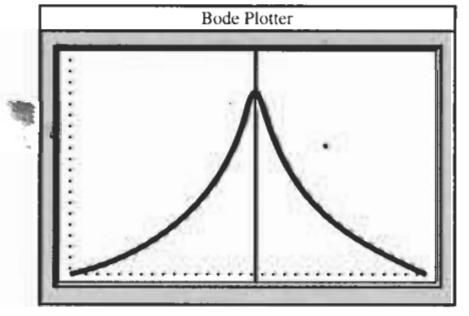

(b)

Figure 4.36 Bandpass circuit of Example 4.9 and test performance. (Bode Plotter scales: 5 to 25 kHz; 0 dB to +30 dB; cursor at 11.6 kHz, 26.1 dB.)

Q-Enhancement

Notice from Eq. (4.131) that the component ratio R_2/R_1 in the Delyiannis–Friend circuit equals $4Q_0^2$. Thus, implementing large quality factors with this circuit is not practical because of the required large resistor ratios. To alleviate this difficulty, we should have available some means of Q enhancement; that is, we wish to use some additional circuitry, such that the basic Delyiannis–Friend circuit operates with a small(er) value of Q_0 but the total circuit has a large

quality factor. This feat is accomplished by using a small amount of positive feedback as shown in Fig. 4.37. The analysis proceeds exactly as for the previous circuit; the difference is that we now have $V_+ \neq 0$, so that instead of Eq. (4.126) we obtain

$$V_- = -\frac{V_2}{A} + V_+ \tag{4.133}$$

Inserting this expression into Eqs. (4.124) and (4.125) results in

$$(2sC + G_1)\, V_x = aG_1 V_1 + sCV_2 + sC\,(V_+ - V_2/A) \tag{4.134}$$

and

$$(sC + G_2)\,(V_+ - V_2/A) = sCV_x + G_2 V_2 \tag{4.135}$$

From the circuit we derive

$$V_+ = KV_2 \tag{4.136}$$

Next, we insert Eq. (4.136) into Eqs. (4.134) and (4.135) and eliminate the internal voltage V_x. After a little algebra, we obtain the transfer function

$$\begin{aligned} T(s) = \frac{V_2}{V_1} &= -\left[\frac{A}{1+(1-K)A}\right] \frac{saG_1C}{s^2C^2 + 2sCG_2 - \dfrac{sCG_1\,(K-1/A)}{1-K+1/A} + G_1G_2} \\ &= -\left[\frac{A}{1+(1-K)A}\right] \frac{saG_1/C}{s^2 + s\dfrac{2G_2}{C}\left(1 - \dfrac{G_1}{2G_2}\dfrac{K-1/A}{1-K+1/A}\right) + \dfrac{G_1G_2}{C^2}} \end{aligned} \tag{4.137}$$

Note that Eq. (4.127) is a special case of Eq. (4.137) obtained for $K = 0$. Let us use the standard notation and the parameters introduced in Eqs. (4.129) and (4.130), and again assume for now that we are dealing with an ideal opamp, $|A| = \infty$. This yields

$$T(s) = -\left(\frac{1}{1-K}\right) \frac{sH\omega_0/Q_0}{s^2 + s\omega_0\left(1 - 2\alpha Q_0^2\right)/Q_0 + \omega_0^2} \tag{4.138}$$

where we introduced the parameter

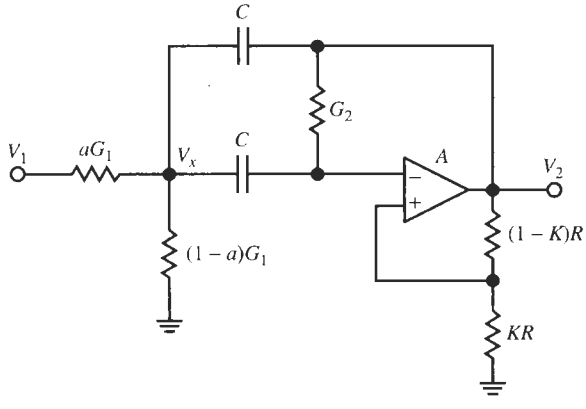

Figure 4.37 Delyiannis–Friend circuit with Q enhancement.

$$\alpha = \frac{K}{1-K} \tag{4.139}$$

to achieve a more convenient notation in the following derivations. Equation (4.138) is the result we sought. We see that the center frequency ω_0 has not changed from that of the Delyiannis–Friend circuit, but that the quality factor is now enhanced to

$$Q = \frac{Q_0}{1-2\alpha Q_0^2} \tag{4.140}$$

where Q_0 was the quality factor without positive feedback. The midband gain H_B of the Q-enhanced bandpass is also increased; it has the value

$$H_B = \frac{H}{1-2\alpha Q_0^2}\frac{1}{1-K} = H\frac{Q}{Q_0}\frac{1}{1-K} \tag{4.141}$$

The design of this circuit with prescribed values of ω_0, Q, and H_B proceeds as follows: First we have to select a value Q_0 for the quality factor of the Delyiannis–Friend circuit without Q enhancement. Q_0 determines the resistor spread by Eq. (4.131). There is a great deal of freedom in picking Q_0, but a study (Schaumann et al., 1990) of the circuit's sensitivities to the opamp's gain-bandwidth product and to the passive component values shows that an optimum choice is

$$Q_0 \approx 1.5 \tag{4.142}$$

We shall choose this value for our designs. Next, we find the parameter α from Eq. (4.140)

$$\alpha = \frac{1}{2Q_0^2}\left(1-\frac{Q_0}{Q}\right) \tag{4.143}$$

With Eq. (4.139), this gives the design value

$$K = \frac{\alpha}{1+\alpha} \tag{4.144}$$

which determines the amount of positive feedback in Fig. 4.37. From Eq. (4.141) we have

$$H = H_B\frac{Q_0}{Q}(1-K) \tag{4.145}$$

and the remaining element values, along with a choice of C, are obtained from Eq. (4.132) as

$$R_2 = 2Q_0\frac{1}{\omega_0 C}, \quad R_1 = \frac{R_2}{4Q_0^2}, \quad \text{and} \quad a = \frac{H}{2Q_0^2} \tag{4.146}$$

We still note from Eq. (4.140) that for $2\alpha Q_0^2 \to 1$, Q is a fairly sensitive function of α, i.e., of the tap position K. By varying K, Q can be tuned easily to the desired value. K is increased to increase Q; if Q needs to be lowered we reduce K. ω_0 is not affected by this step, but H_B rises and falls with Q.

Let us consider an example.

EXAMPLE 4.10

Repeat the design of Example 4.9 but with a Q-enhanced Delyiannis–Friend bandpass circuit with $f_0 = 12.5$ kHz, $Q = 10$, and midband gain $H_B = 26$ dB. Use an LM741 opamp.

Solution

On a linear scale, the gain equals $H_B = 19.95$; we choose again $C = 5$ nF. First we pick $Q_0 = 1.5$ as suggested in Eq. (4.142), and compute from Eqs. (4.143) and (4.144),

$$\alpha = \frac{1}{2Q_0^2}\left(1 - \frac{Q_0}{Q}\right) = \frac{1}{4.5}\left(1 - \frac{1.5}{10}\right) = 0.189 \quad \text{and} \quad K = \frac{\alpha}{1+\alpha} = \frac{0.189}{1.189} = 0.159$$

With these numbers,

$$H = H_B \frac{Q_0}{Q}(1 - K) = 19.95\frac{1.5}{10}(1 - 0.159) = 2.517$$

so that from Eq. (4.146) we find

$$R_2 = \frac{3}{3.927 \times 10^{-4}} = 7.64\ \text{k}\Omega, \quad R_1 = \frac{R_2}{9} = 849\ \Omega, \quad a = \frac{H}{2Q_0^2} = \frac{2.517}{4.5} = 0.559$$

and

$$R_1/a = 1.52\ \text{k}\Omega, \quad R_1/(1-a) = 1.93\ \text{k}\Omega$$

Finally, we choose R. Note that this resistor loads the opamp; it should not be chosen too small. Let us pick $R = 10.0$ kΩ and tap the resistor at

$$KR = 1.59\ \text{k}\Omega, \quad [(1-K)R = 8.41\ \text{k}\Omega]$$

The performance is shown in Fig. 4.38. Compared to the specified values, the measured center frequency and quality factor are $f_0 = 12.2$ kHz, reduced by 2.4% from the design value, and $Q_0 \approx 10.17$, an increase of $\approx 1.7\%$. The gain is $H = 26.2$ dB.

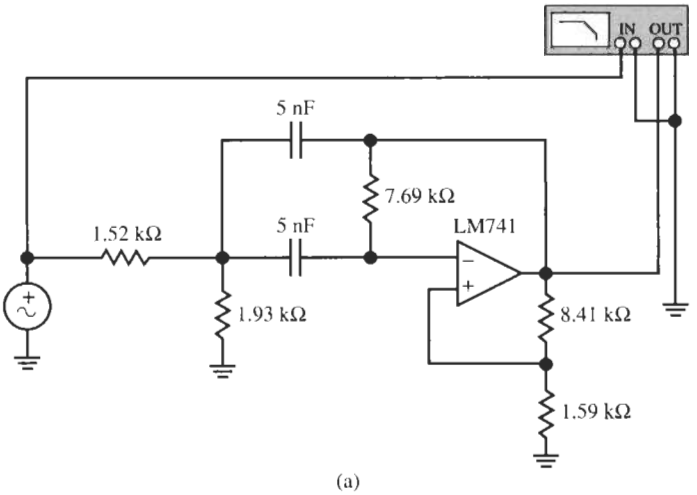

(a)

Figure 4.38 The enhanced-Q bandpass of Example 4.10 and its performance. Note the reduced center frequency error compared to that in Example 4.9. (Bode Plotter scales: 5 to 25 kHz; 0 dB to +25 dB; cursor at 12.2 kHz, 26.2 dB.)

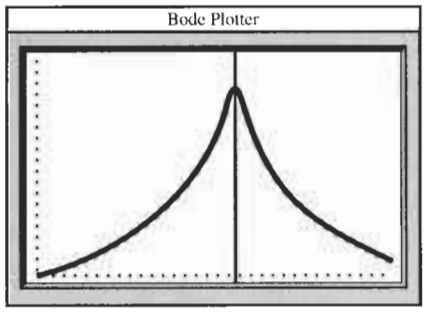

(b)

Figure 4.38 Continued

The Effect of $A(s)$ on the Single-Amplifier Biquad

We notice that the center frequency and quality factor again have noticeable errors compared with an implementation based on an ideal opamp. Let us, therefore, reiterate that it is necessary to consider the effects caused by real opamps before we can hope to arrive at a predictable design. To help in this task, we have in Eqs. (4.127) and (4.137) already presented the transfer functions $T(s)$ including their dependence on $A(s)$. Consider Eq. (4.137): If we use the integrator model for A, Eq. (2.18), it should be clear that $T(s)$ is a function of third order. Rather than attempting to find the poles and zeros of that expression, let us be content with an approximation to give an indication of the errors. We saw that the dominant effect was the A-dependent term in the denominator $D(s)$. Using the standard notation with ω_0 and Q_0, we found in Eq. (4.138) that $D(s)$ equals

$$D(s) = s^2 + s\frac{\omega_0}{Q_0}\left(1 - 2Q_0^2\frac{K - 1/A}{1 - K + 1/A}\right) + \omega_0^2 \tag{4.147}$$

We recast this equation into the form

$$D(s) = s^2 + s\frac{\omega_0}{Q_0}\left[1 - 2Q_0^2\alpha\frac{1 - 1/(KA)}{1 + 1/[(1 - K)A]}\right] + \omega_0^2$$

where we used Eq. (4.139). Although the frequency dependence of this expression seems quite difficult to evaluate, we can make it manageable by making reasonable approximations. Let us assume that $|(1 - K)A(j\omega)| \gg 1$ and make use of $1/(1 + x) \approx 1 - x$ for $x \ll 1$. Then we obtain

$$\begin{aligned} D(s) &\approx s^2 + s\frac{\omega_0}{Q_0}\left\{1 - 2Q_0^2\alpha\left(1 - \frac{1}{KA}\right)\left[1 - \frac{1}{(1 - K)A}\right]\right\} + \omega_0^2 \\ &\approx s^2 + s\frac{\omega_0}{Q_0}\left\{1 - 2Q_0^2\alpha\left[1 - \frac{s}{\omega_t}\left(\frac{1}{K} + \frac{1}{1 - K}\right)\right]\right\} + \omega_0^2 \end{aligned} \tag{4.148}$$

In this equation we used the opamp integrator model and we further neglected the term that is proportional to $1/A^2$. If we collect the s^2-terms we obtain

$$D(s) \approx s^2(1 + \varepsilon) + s\frac{\omega_0}{Q_0}\left(1 - 2Q_0^2\alpha\right) + \omega_0^2 \tag{4.149}$$

where we labeled the error term ε,

$$\varepsilon = \frac{2Q_0}{\omega_t/\omega_0}\frac{\alpha}{K(1-K)} = \frac{2Q_0}{|A(j\omega_0)|}\frac{1}{(1-K)^2} \tag{4.150}$$

With Eq. (4.149), the transfer function $T(s)$ of Eq. (4.138) becomes

$$T(s) \approx -\left(\frac{A}{1+(1-K)A}\right)\frac{sH\dfrac{\omega_0}{Q_0}}{s^2(1+\varepsilon)+s\dfrac{\omega_0}{Q_0}\left(1-2Q_0^2\alpha\right)+\omega_0^2}$$

Because $K < 1$, the first factor is approximately equal to $1/(1-K)$ over the frequency range of interest, so that T can be rewritten as

$$\begin{aligned} T(s) &\approx -\frac{1}{1-K}\frac{sH\dfrac{\omega_0}{Q_0(1+\varepsilon)}}{s^2+s\dfrac{\omega_0}{Q_0(1+\varepsilon)}\left(1-2Q_0^2\alpha\right)+\dfrac{\omega_0^2}{1+\varepsilon}} \\ &= -\frac{s\dfrac{H}{1-K}\dfrac{\omega_0/\sqrt{1+\varepsilon}}{Q_0\sqrt{1+\varepsilon}}}{s^2+s\dfrac{\omega_0/\sqrt{1+\varepsilon}}{Q_0\sqrt{1+\varepsilon}}\left(1-2Q_0^2\alpha\right)+\left(\dfrac{\omega_0}{\sqrt{1+\varepsilon}}\right)^2} \\ &= -\frac{sH_R\omega_{0R}/Q_R}{s^2+s\omega_{0R}/Q_R+\omega_{0R}^2} \end{aligned} \tag{4.151}$$

This result indicates that the center frequency ω_0 is reduced, and the quality factor has increased over its enhanced value Q in Eq. (4.140); the *realized* parameters are

$$\omega_{0R} \approx \frac{\omega_0}{\sqrt{1+\varepsilon}}, \quad Q_R = \frac{Q_0}{1-2Q_0^2\alpha}\sqrt{1+\varepsilon} = Q\sqrt{1+\varepsilon} \tag{4.152}$$

and the *realized* gain is approximately unaffected by the opamp, $H_R = H_B$ of Eq. (4.141). For instance, for the design parameters in Example 4.9 we have from Eq. (4.150)

$$\varepsilon = \frac{2Q_0}{|A(j\omega_0)|}\frac{1}{(1-K)^2} = \frac{3}{1500/12.5}\frac{1}{(1-0.159)^2} = 0.035$$

that is, the frequency error equals -1.7% and the Q error is $+1.7\%$. In the Delyiannis–Friend circuit with no Q enhancement, we had $K = 0$ and $Q_0 = Q = 10$; the error then becomes

$$\varepsilon = \frac{2Q}{|A(j\omega_0)|} = \frac{20}{1500/12.5} = 0.17$$

and the errors would be equal to -8% and $+8\%$ for frequency and Q, respectively, as was observed in Example 4.9. We note, therefore, that Q enhancement brings two notable advantages for the small price of two resistors. The component ratio is substantially reduced (from 400 in Example 4.9 to nine in Example 4.10) and the errors in frequency and quality

factor are significantly smaller (by about a factor of five in these examples). In the remainder of this book we will always use the Q-enhanced Delyiannis–Friend circuit in Fig. 4.37 when a single-amplifier biquad is needed.

4.5.3 The General Impedance Converter (GIC) Circuit

The next biquad structure we shall discuss is based on the second-order passive *RLC* circuit in Fig. 4.39. Using voltage division, we derive that this circuit realizes the bandpass transfer function

$$T(s) = \frac{V_L}{V_1} = \frac{sG/C_1}{s^2 + sG/C_1 + 1/(LC_1)} \tag{4.153}$$

Because we do not wish to use inductors for the filters developed in this book we need to investigate whether there are methods that let us *simulate* the behavior of an inductor with some active electronic circuit. This means we wish to find a circuit, Fig. 4.40, whose input impedance looks inductive, but that consists of only resistors, capacitors, and active devices. Such a circuit is an *impedance converter*, also referred to as *gyrator*, and can be described by the equations

$$I_1 = -\frac{1}{r}V_2 \quad \text{and} \quad I_2 = \frac{1}{r}V_1 \tag{4.154}$$

We have labeled the constant as $1/r$ to remind us that it has units of 1/Ohm or Siemens [S]. The gyrator symbol is shown in Fig. 4.41. Using Eq. (4.154) we derive the input impedance of the gyrator as

$$Z_{in}(s) = \frac{V_1}{I_1} = -\frac{rI_2}{(1/r)V_2} = r^2\frac{-I_2}{V_2} = \frac{r^2}{Z_{load}(s)} \tag{4.155}$$

which lets us define the gyrator as a twoport whose input impedance is inversely proportional to the load impedance. It is clear then how an inductor can be simulated with a gyrator (Fig. 4.42). If we load the gyrator by a capacitor, $Z_{load} = 1/(sC_2)$, the input impedance is that of an inductor:

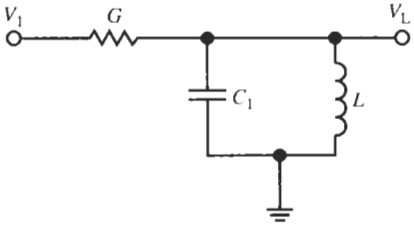

Figure 4.39 *RLC* bandpass filter.

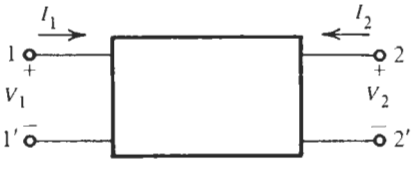

Figure 4.40 Twoport used to derive an inductor circuit.

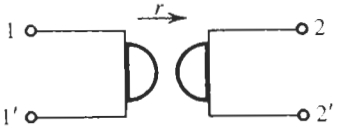

Figure 4.41 Gyrator symbol.

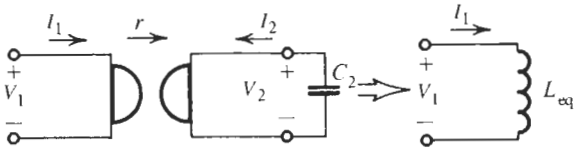

Figure 4.42 An inductor built via a gyrator loaded by a capacitor.

$$Z_{in}(s) = \frac{r^2}{1/(sC_2)} = sr^2C_2 = sL_{eq} \tag{4.156}$$

where the equivalent inductor is

$$L_{eq} = r^2C_2 \tag{4.157}$$

The constant r is called the *gyration resistance.*

We shall see later in this book that a natural and very simple implementation of a gyrator uses two *transconductors*, circuits that relate an output current to an input voltage. For now, however, we will concentrate on building an impedance converter with opamps, that is, we wish to find an RC-opamp circuit to put into the twoport of Fig. 4.40 so that a circuit is created whose input impedance is inductive. To minimize interaction let us also require that the RC-opamp circuit to be found has infinite input impedance and zero output impedance. The necessary inductive input current, therefore, must flow past that circuit. We provide a resistor R_1 for this purpose. Figure 4.43 shows the contemplated circuit where we have labeled the input voltage V_L because it will be the voltage at the inductor terminal. We find

$$I_1 = G_1(V_L - V_2) = G_1V_L\left(1 - \frac{V_2}{V_L}\right)$$

so that the input admittance is

$$Y_{in}(s) = \frac{I_1}{V_L} = G_1\left(1 - \frac{V_2}{V_L}\right) = \frac{1}{sL_{eq}}$$

It is to be inductive as indicated. It follows that the circuit in Fig. 4.43 must realize the transfer function

$$\frac{V_2}{V_L} = 1 - \frac{R_1}{sL_{eq}} = 1 - \frac{1}{s\tau} \tag{4.158}$$

where we abbreviated the time constant L_{eq}/R_1 as τ. To be able to focus on the circuit design, we shall assume ideal opamps and leave the discussion of the effects of finite ω_t until later.

The realization of the circuit is quite easy if we recognize from Eq. (4.158) that we need to subtract an integration, $1/(s\tau)$, from a constant, specifically from 1. We can accomplish this

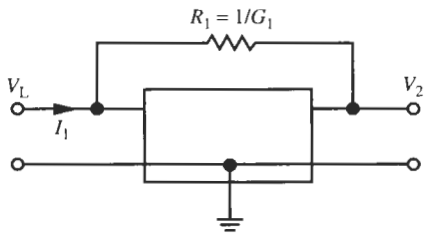

Figure 4.43 Conceptual circuit to realize an inductor.

with the difference amplifier of Fig. 2.29b, tying the inputs together and replacing the feedback resistor R_F by a capacitor. The resulting circuit is shown in Fig. 4.44b. It realizes

$$V_+ = \frac{G_4}{G_4 + G_5} V = \frac{1}{H} V \quad \text{and} \quad V_- = \frac{sC_2V_2 + G_3V}{sC_2 + G_3}$$

where we labeled

$$1 + \frac{G_5}{G_4} = H > 1 \tag{4.159}$$

Because the opamps are assumed to be ideal, we have $V_+ = V_-$ so that

$$\left(\frac{1}{H} - \frac{G_3}{sC_2 + G_3}\right) V = \frac{sC_2}{sC_2 + G_3} V_2$$

or

$$\begin{aligned} \frac{V_2}{V} &= \frac{1}{H} \frac{sC_2 + G_3}{sC_2} - \frac{G_3}{sC_2} = \frac{1}{H}\left[1 - \frac{1}{sC_2R_3}(H-1)\right] \\ &= \frac{1}{H}\left(1 - \frac{1}{sC_2R_3R_5/R_4}\right) \to \frac{1}{H}\left(1 - \frac{R_1}{sL_{eq}}\right) \end{aligned} \tag{4.160}$$

From the indicated comparison with Eq. (4.158) we see that the circuit realizes an inductor of value

$$L_{eq} = C_2R_1R_3\frac{R_5}{R_4} \tag{4.161}$$

Comparing this equation with Eq. (4.157) we see that r was realized as $r = \sqrt{R_1R_3R_5/R_4}$. To realize Eq. (4.158) exactly we still must remove the multiplying factor $1/H$ in Eq. (4.160). Rewriting the equation as

$$\frac{V_2}{V/H} = 1 - \frac{R_1}{sL_{eq}}$$

we notice that to do this we need to generate a voltage $V_L = V/H$. This relationship can be implemented by the opamp circuit in Fig. 4.44a if we can assume the connection labeled V/H closes the feedback loop around the amplifier A_1 so that the opamp's input voltage is zero,

$$V_L - V/H = 0$$

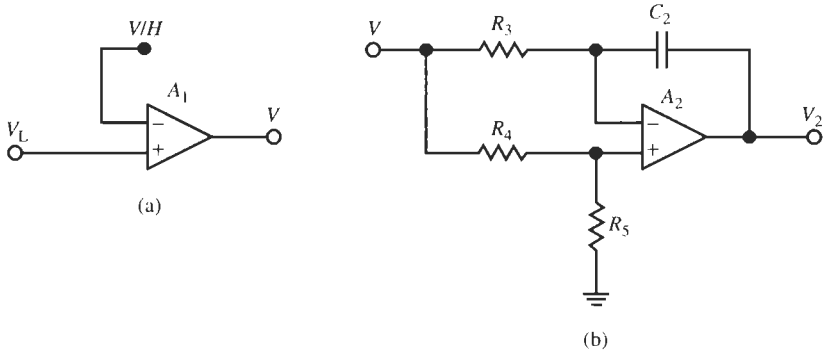

Figure 4.44 (a) Circuit realizing $V = HV_L$; (b) circuit realizing the function of Eq. (4.160).

Because $V_+ = V/H$ and $|A_2| = \infty$, the voltage V/H is available at the inverting input node of A_2 in Fig. 4.44b. Making that connection closes the loop around A_1 and results in Fig. 4.45a to realize the conceptual circuit in Fig. 4.43. To check our derivation, let us analyze the circuit after redrawing it in the more standard form of Fig. 4.45b. The analysis is made easy if we note that

$$V_L = V_3 \quad \text{and} \quad V_3 = V_5 \tag{4.162}$$

because we assumed ideal opamps. Consequently we find with $V_L = V_3 = V_5$

$$V_4 = V_L\left(1 + \frac{G_5}{G_4}\right), \quad I_4 = G_3(V_L - V_4) = G_3V_L\left(1 - \frac{V_4}{V_L}\right) = -\frac{G_3G_5}{G_4}V_L = I_3 \tag{4.163}$$

$$V_2 = V_L + I_3\frac{1}{sC_2} = \left(1 - \frac{G_3G_5}{sC_2G_4}\right)V_L,$$

$$I_1 = G_1(V_L - V_2) = G_1V_L\left(1 - \frac{V_2}{V_L}\right) = \frac{G_1G_3G_5}{sC_2G_4}V_L$$

so that the input impedance becomes

$$Z_{in}(s) = \frac{V_L}{I_1} = sL_{eq} = s\frac{C_2G_4}{G_1G_3G_5} \tag{4.164}$$

as in Eq. (4.161). This result verifies that the circuit simulates an inductor. We can generalize this result by replacing the resistors and the capacitor in Fig. 4.45b by impedances:

$$Z_{in}(s) = \frac{V_L}{I_1} = \frac{Y_2Y_4}{Y_1Y_3Y_5} = \frac{Z_1Z_3Z_5}{Z_2Z_4} \tag{4.165}$$

Note that a variety of different input impedances can be realized by this *general impedance converter* (GIC) circuit by selecting the impedances $Z_i, i = 1, \ldots, 5$, appropriately. For instance, in the so-called GIC I in Fig. 4.45b we may interchange the positions of C_2 and R_4. The result is the GIC II that realizes inductor

$$L_{eq}' = s\frac{G_2C_4}{G_1G_3G_5} \tag{4.166}$$

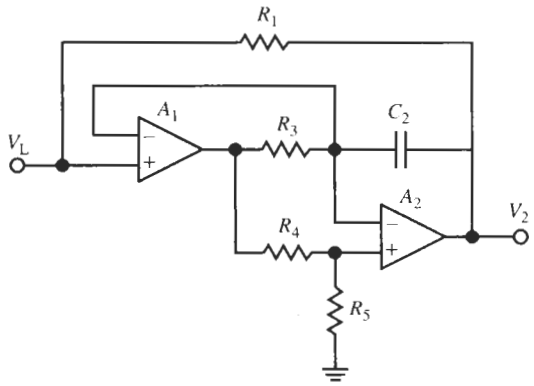

(a)

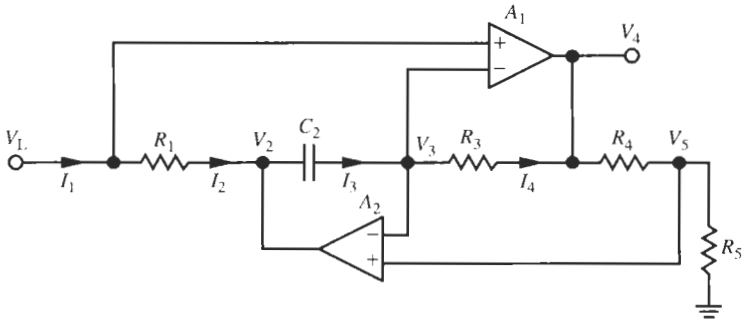

(b)

Figure 4.45 The general impedance converter (GIC). (a) Circuit obtained by combing Figs. 4.44a and b; (b) standard representation of the GIC.

We shall return to the GIC II structure later when we realize general high-order filters by simulating *LC* ladders. For our present situation, biquads, we use the GIC I.

We have succeeded in building an opamp circuit whose input impedance looks like an inductor. Consequently, if we substitute that circuit, Fig. 4.45b, for the inductor in Fig. 4.39, we ought to arrive at an active bandpass biquad. There is still a small problem to be resolved: the biquad output voltage V_L must be taken from the inductor terminal that is not an opamp output and, hence, cannot be loaded without affecting filter performance. Naturally, we could use an opamp buffer, but that would require use of a third opamp. Fortunately, a simpler solution is available: recall that we found in Eq. (4.163) that the opamp output V_4 in Fig. 4.45b is proportional to V_L,

$$V_4 = V_L\left(1 + \frac{G_5}{G_4}\right) = V_L H \tag{4.167}$$

We shall, therefore, use the output V_4 as the output terminal of our bandpass. The final circuit is shown in Fig. 4.46a, where we have the filter output relabeled V_2. This circuit is among the best performing second-order bandpass sections available. Its transfer function is obtained

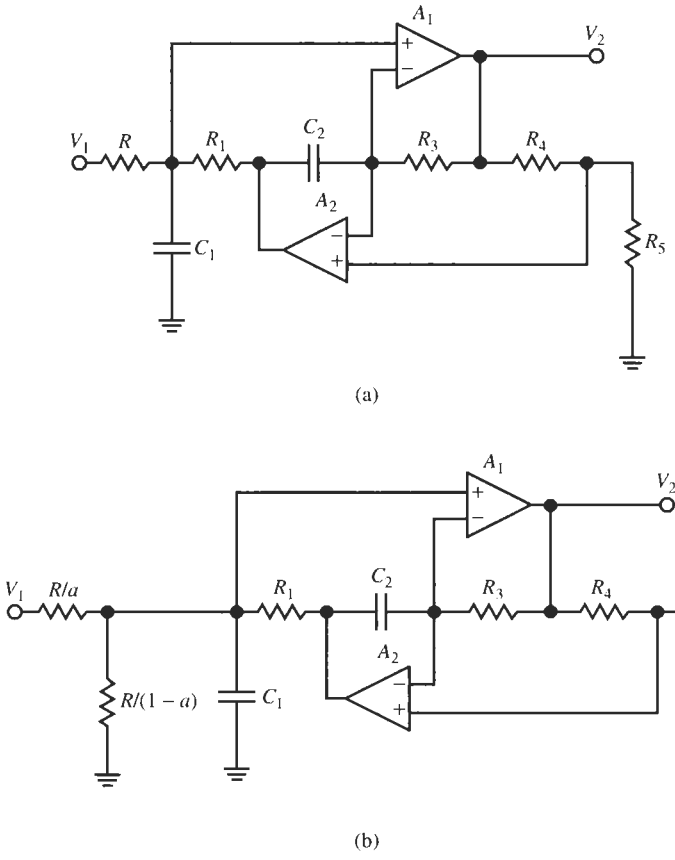

Figure 4.46 (a) The GIC bandpass circuit for gain $H = 1 + R_4/R_5$; (b) the circuit for gain aH, $a < 1$. The optimal component choice is given in Eq. (4.170).

by substituting Eq. (4.161) for L in Eq. (4.153) and remembering that the output is taken at $V_4 = HV_L$. We obtain

$$T(s) = \frac{V_2}{V_1} = \frac{s\left(1 + \dfrac{G_5}{G_4}\right)\dfrac{G}{C_1}}{s^2 + s\dfrac{G}{C_1} + \dfrac{G_1G_3G_5}{C_1C_2G_4}} \tag{4.168a}$$

Let us again pick $C_1 = C_2 = C$. The bandpass circuit then has the center frequency ω_0, quality factor Q, and midband gain H

$$\omega_0 = \sqrt{\frac{G_1G_3G_5}{C^2G_4}}, \quad Q = \frac{\omega_0 C}{G} = \frac{1}{G}\sqrt{\frac{G_1G_3G_5}{G_4}}, \quad H = 1 + \frac{G_5}{G_4} \tag{4.169a}$$

In principle, any value of $H > 1$ can be used. However, we shall demonstrate shortly that

$R_4 = R_5$, i.e., $H = 2$, is the optimal choice. Let us, therefore, choose $R_4 = R_5$ and select, arbitrarily, $R_3 = R_1$. Then we obtain

$$\omega_0 = \frac{1}{CR_1}, \quad Q = \frac{\omega_0 C}{G} = \frac{R}{R_1}, \quad \text{and} \quad H = 2 \tag{4.169b}$$

Because nothing can be gained from unequal resistors, we have for given ω_0 and a suitable choice of C the following simple design equations for the GIC bandpass circuit:

$$R_1 = R_3 = R_4 = R_5 = \frac{1}{\omega_0 C} \quad \text{and} \quad R = QR_1 \tag{4.170}$$

H is fixed at the value 2. A design with $H > 2$ is possible according to Eq. (4.181a) by selecting $R_4 > R_5$, but as shown in the following it will cause the errors in ω_0 and Q to increase. If $H < 2$ is required, say $H = 2a$ with $a < 1$, it can be implemented with no ill effects on circuit performance by replacing the resistor R by a voltage divider as shown in Fig. 4.46b. The two resistors in the divider must equal R when connected in parallel so as not to affect the pole position. The circuit in Fig. 4.46b realizes

$$T(s) = \frac{V_L}{V_1} = \frac{sa\left(1 + \dfrac{G_5}{G_4}\right)\dfrac{G}{C_1}}{s^2 + s\dfrac{G}{C_1} + \dfrac{G_1 G_3 G_5}{C_1 C_2 G_4}} \tag{4.168b}$$

An example will illustrate the design process.

EXAMPLE 4.11

Repeat the design of Example 4.10, but for a GIC biquad. The filter should have 0-dB midband gain; use LM741 opamps.

Solution

Specified were $f_0 = 12.5$ kHz and $Q = 10$. Choosing $C = 5$ nF, we obtain according to Eq. (4.170)

$$R_1 = R_3 = R_4 = R_5 = \frac{1}{\omega_0 C} = \frac{10^4}{3.927}\ \Omega = 2.55\ \text{k}\Omega, \quad R = 25.5\ \text{k}\Omega$$

Because 0-dB gain is specified, i.e., $aH = 2a = 1$, we need to set $a = 0.5$. The resistor R is split, therefore, into two 51-kΩ resistors in parallel.

$$R/a = R/(1 - a) = 51\ \text{k}\Omega$$

The circuit and its performance are shown in Fig. 4.47. We see that $f_0 = 12.3$ kHz for an error of -1.6% and $Q \approx 10.08$, increased by $\approx 0.8\%$ over the specifications. The midband gain is 0 dB as designed.

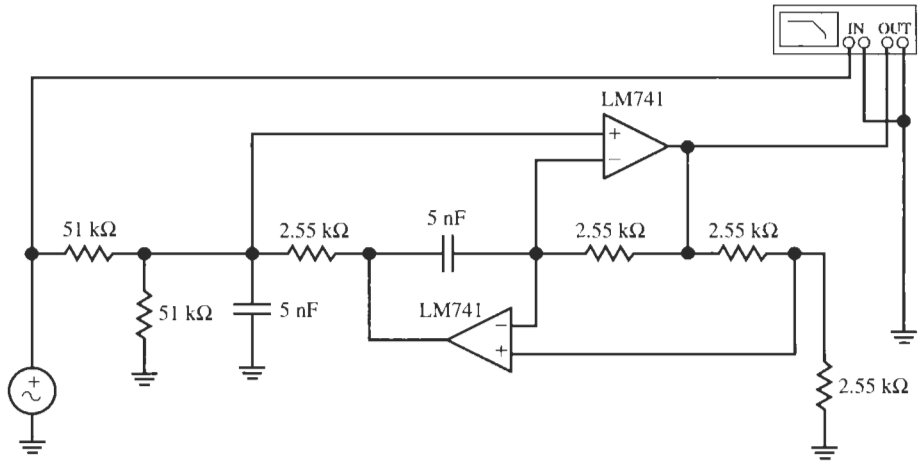

(a)

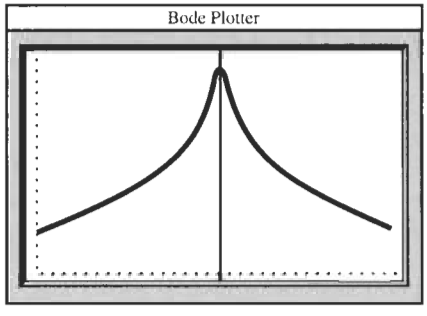

(b)

Figure 4.47 GIC bandpass design for Example 4.11 and test results. (Bode Plotter scales: 3 to 45 kHz; −40 dB to 0 dB; cursor at 12.3 kHz, −0.01 dB.)

We notice that this circuit has smaller errors than the previous designs for the same specifications. We shall next consider the effects of finite ω_t to try to verify the good performance theoretically.

The Effect of $A(s)$ on the GIC Biquad

The analysis of the GIC circuit with finite values of $A_i(s)$, $i = 1, 2$, is not difficult, but quite tedious. We shall not go through the details but just note that the assumption of ideal opamps resulted in Eq. (4.162), i.e., in $V_L = V_3 = V_5$. If the opamp gains A_i are finite, Eq. (4.162) should instead read

$$V_L - V_3 = \frac{V_4}{A_1(s)} \quad \text{and} \quad V_5 - V_3 = \frac{V_2}{A_2(s)} \tag{4.171}$$

and these expressions should be used in the equations (4.163). Because the opamp dependence is contained in the inductor L_{eq}, we need not investigate the behavior of the biquad, but can

concentrate on L_{eq}. Carrying out the algebra and neglecting all terms that are proportional to $1/(A_1A_2)$ results in

$$\begin{aligned} Z_{in}(j\omega) &\approx j\omega L_{eq}\frac{1+H\left(\dfrac{1}{A_1}+\dfrac{1}{A_2}\dfrac{G_3}{j\omega C_2}\right)}{1+\dfrac{H}{H-1}\left(\dfrac{1}{A_2}+\dfrac{1}{A_2}\dfrac{j\omega C_2}{G_3}\right)} \\ &= j\omega L_{eq}\frac{1+H\left(\dfrac{j\omega}{\omega_{t1}}+\dfrac{G_3}{\omega_{t2}C_2}\right)}{1+\dfrac{H}{H-1}\left(\dfrac{j\omega}{\omega_{t2}}-\dfrac{\omega^2C_2}{\omega_{t1}G_3}\right)} \end{aligned} \tag{4.172}$$

H and L_{eq} were defined in Eqs. (4.169) and (4.166), and we have used the integrator model for the opamps. As done before, we next use the approximation $1/(1+x)\approx 1-x$ for small x and obtain

$$\begin{aligned} Z_{in}(j\omega) &\approx j\omega L_{eq}\left[1+H\left(\frac{j\omega}{\omega_{t1}}+\frac{G_3}{\omega_{t2}C_2}\right)\right]\left[1-\frac{H}{H-1}\left(\frac{j\omega}{\omega_{t2}}-\frac{\omega^2C_2}{\omega_{t1}G_3}\right)\right] \\ &\approx j\omega L_{eq}\left[1+H\left(\frac{j\omega}{\omega_{t1}}+\frac{G_3}{\omega_{t2}C_2}\right)-\frac{H}{H-1}\left(\frac{j\omega}{\omega_{t2}}-\frac{\omega^2C_2}{\omega_{t1}G_3}\right)\right] \\ &\approx j\omega L_{eq}\left[1+H\frac{G_3}{\omega_{t2}C_2}+\frac{H}{H-1}\frac{\omega^2C_2}{\omega_{t1}G_3}+\frac{j\omega}{\omega_{t1}}H\left(1-\frac{1}{H-1}\frac{\omega_{t1}}{\omega_{t2}}\right)\right] \end{aligned} \tag{4.173}$$

Thus, the impedance is of the form

$$Z_{in}(j\omega)\approx j\omega L_{eq}\left(1+\frac{\Delta L}{L_{eq}}\right)-\frac{\omega L_{eq}H}{|A_1(j\omega)|}\left(1-\frac{1}{H-1}\frac{\omega_{t1}}{\omega_{t2}}\right) \tag{4.174}$$

Again, terms proportional to $|1/(A_1A_2)|$ were neglected. Now note that the real part of Eq. (4.174) is a (negative) resistor that represents the inductor losses. For matched opamps, $\omega_{t1}=\omega_{t2}$, it becomes zero if we choose $H=2$, i.e., $R_4=R_5$. That is, the GIC circuit in Fig. 4.45 simulates an ideal inductor if $R_4=R_5$. Furthermore, we observe that for $H=2$ and matched opamps, $\omega_{t1}=\omega_{t2}$, the error

$$\Delta L\approx\frac{2}{|A_1(j\omega)|}L_{eq}\left(\frac{\omega_{t1}}{\omega_{t2}}\frac{G_3}{\omega C_2}+\frac{\omega C_2}{G_3}\right) \tag{4.175}$$

of the inductor value is minimized if we choose

$$\omega_cC_2=G_3=\frac{1}{R_3} \tag{4.176}$$

at some critical frequency ω_c. In our case, $\omega_c=\omega_0$, the center of the passband.

This analysis verifies our earlier assertion that $H=2$ is the optimal choice. We can readily verify from Eqs. (4.173) and (4.174) that both the error ΔL in inductor value and the inductor

losses will increase if $H > 2$. For $H = 2$ and matched opamps the inductor losses are zero. Using Eqs. (4.175) and (4.176), the remaining inductor error equals

$$\Delta L \approx \frac{4}{|A_1(j\omega_0)|} L_{eq} = \frac{4}{|A_1(j\omega_0)|} \frac{1}{\omega_0^2 C} \tag{4.177}$$

For the numbers in Example 4.11 we find $L_{eq} = 32.4$ mH and

$$\Delta L \approx \frac{4}{|A_1(j\omega_0)|} L_{eq} = \frac{4 \times 12.5}{1500} 32.4 \text{ mH} \approx 1 \text{ mH}$$

for an inductor error of +3.3%. Since the error in f_0 is proportional to $1/\sqrt{L_{eq}}$, the corresponding frequency deviation is $\Delta f_0 \approx -1.6\%$ in agreement with the test result in Example 4.11. Because our inductor is essentially lossless, Q is realized nearly exactly. Our analysis and the sample numbers indicate that the GIC bandpass is the best of the ones presented in this chapter.

We have now developed a variety of bandpass sections, or as they are often called, *resonators*, which have been tested extensively and have proven their performance in practice. In the next chapter we extend our study of active filters by augmenting these resonators so that the circuits can realize general *biquadratic* transfer functions. This will then enable us to implement filters with arbitrary transmission zeros.

REFERENCES

J. R. Brand and R. Schaumann, "Active R Filters: Review of Theory and Practice," *IEE J. Electr. Circuits Sys.*, Vol. 2, pp.89–101, July 1978.

T. Delyiannis, "High-Q Factor Circuit with Reduced Sensitivities," *Electron. Lett.*, Vol. 4, p. 577, December 1968.

J. J. Friend, "A Single Operational Amplifier Biquadratic Filter Section." *1970 Digest Tech. Papers*, p. 189, 1970.

S. K. Mitra, "A Network Transformation for Active *RC* Networks," *Proc. IEEE*, Vol. 55, pp. 2021–2022, 1967.

R. P. Sallen and E. L. Key, "A Practical Method of Designing *RC* Active Filters," *IRE Trans. Circuit Theory*, Vol. CT-2, pp. 74–85, 1955.

R. Schaumann, M. S. Ghausi, and K. R. Laker, *Design of Analog Filters: Passive, Active RC, and Switched Capacitor*, Prentice-Hall, Englewood-Cliffs, NJ, 1990, Chapter 5.2.

J. Tow, "Active *RC* Filters—A State-Space Realization," *Proc. IEEE*, Vol. 56, pp. 1137–1139, 1968.

L. C. Thomas, "The Biquad: Part I—Some Practical Design Considerations," *IEEE Trans. Circuits Syst.*, Vol. CAS-18, pp. 350–357, 1971, and "The Biquad: Part II—A Multipurpose Active Filtering System," *IEEE Trans. Circuits Syst.*, Vol. CAS-18, pp. 358–361, 1971.

PROBLEMS

4.1 A second-order passive lowpass filter as in Fig. 4.1b is designed with $R = 120\ \Omega$, $L = 16$ mH, and $C = 0.05\ \mu$F.

(a) Derive the transfer function.

(b) Find the poles and zeros of the function.

(c) Calculate ω_0 and Q. What is the dc gain of the circuit? What is the peak gain and at which frequency is it observed?

(d) Redesign the circuit to raise its quality factor to 12 without changing ω_0.

(e) Test the original and the redesigned circuits with Electronics Workbench (EWB).

4.2 In the circuit Problem 4.1 interchange the inductor and capacitor and repeat Parts a through e. What kind of filter does this circuit realize?

4.3 Bring the function derived in Problem 4.1a into the form of Eqs. (4.17a) and (4.17b). Do the coefficients agree with the results obtained in Problem 4.1c?

4.4 Derive Eqs. (4.27a) and (4.27b).

4.5 The biquad of Fig. 4.10 is to be used to design a bandpass filter with center frequency $f_0 = 3.2$ kHz, $Q = 7.5$, and midband gain 24 dB.

(a) What is the filter's 3-dB bandwidth?

(b) Construct the filter, using practical component values and LM741 opamps.

(c) Test magnitude and phase performance of the circuit with EWB. Consider also the outputs at the remaining two output nodes.

(d) Compare the test results with the nominal responses. Discuss any deviations from the performance expected for ideal opamps.

4.6 Use the circuit of Fig. 4.10 to design a lowpass filter with the specifications: cut-off frequency $f_c = 145$ kHz, $Q = 9$, and dc gain of 0 dB. Use practical component values.

(a) Devise a convenient tuning algorithm to vary noninteractively, if possible, f_c, Q, and the dc gain.

(b) Test the magnitude and phase of the circuit with LM741 opamps.

(c) Test the magnitude and phase of the circuit with HA2542-2 opamps.

(d) Compare and discuss the circuit performances for the two types of amplifiers. Do they agree with predictions? Comment on any deviations from the nominal performances.

4.7 Consult the design curves in Fig. 4.13 to design a Tow–Thomas biquad with a peak gain of 10 dB at the cutoff frequency f_c. The dc gain should be 0 dB and f_c is prescribed to be 4.85 kHz. Test your design with EWB.

4.8 Repeat Problem 4.7 but for a design with dc gain equal to 5 dB.

4.9 Determine the poles and zeros for your design in Problem 4.6 and use them to sketch a magnitude and phase plot. Consult Fig. 4.17 for a possible procedure.

4.10 Consider the two-integrator-loop circuit in Fig. 2.37a, redrawn as Fig. 4.19, and determine the transfer function V_3/V_1 (V_3 is at the output of amplifier A_1) as a function of the three resistors. Use the integrator model for Eq. (2.18) for the amplifier gain.

(a) For LM741 opamps and the resistor values in Fig. 4.19 compute the transfer function and calculate center frequency, quality factor, and midband gain. What changes if $R_3 = \infty$?

(b) Verify your result with EWB.

(c) Repeat Parts a and b for a design with an HA2542-2 opamp. Are the results as expected? Explain.

4.11 This problem examines the consequences of using a more complete opamp model.

(a) Redesign the circuit of Fig. 4.19 to realize a bandpass with a quality factor of $Q = 15$ and test your design with EWB. Comment on any unexpected behavior.

(b) Replace the integrator model of the LM741 opamp, Eq. (2.18), by the pole-zero model of Eq. (2.17b) with $\omega_a = 0$ and examine any changes to the transfer function. Use your result to explain the test performance observed in Part a.

4.12 The inverting integrator of Fig. 4.24 is constructed with two nominally identical LM741 opamps for an operating frequency of 50 kHz. The integrator time constant is 25 μs.

(a) Determine the quality factor of the integrator. Use reasonable approximations.

(b) Repeat the calculations of Part a under the assumption that the gain-bandwidth products of the opamps are mismatched by 1.5%.

4.13 A Miller integrator (Fig. 4.23a) is designed with $R = 3.3\,\text{k}\Omega$, $C = 0.2\,\mu\text{F}$, and an LM741 operational amplifier.

(a) Using a resistor, design a passive compensation circuit to eliminate the finite pole created by the opamp.

(b) Use a capacitor in a compensation circuit to eliminate the pole created by the opamp.

4.14 Derive the transfer function (4.80) of the noninverting integrator in Fig. 4.25b.

4.15 Derive the result in Eq. 4.82.

4.16 The noninverting integrator discussed in the text uses at least two opamps. This problem presents a method to design such an integrator with only one opamp.

(a) Show that the circuit in Fig. P4.16a is a noninverting integrator if R_2 can be negative. Determine the appropriate size of R_2.

(b) Show that the circuit in Fig. P4.16b is a noninverting integrator with transfer function $V_2/V_1 = 2/(sCR)$. Consulting the result of Part a, this indicates that a negative resistor can be simulated with an opamp and three resistors. (How to create negative components will be discussed in Section 14.7.)

4.17 The Tow–Thomas biquad in Fig. 4.10 is designed as a bandpass filter for the parameters $f_0 = 10.8$ kHz, $Q = 14$, and midband gain $\hat{H}_M = 1$. The circuit is built with LM741 opamps. Estimate the deviations in filter parameters f_0, Q, and H_0 that must be expected in the design. Verify your results with EWB.

4.18 Repeat Problem 4.17, but let the center frequency be $f_0 = 10.8$ MHz and use HA2542-2 amplifiers. Verify your results with EWB.

4.19 A lowpass filter as in Fig. 4.10 is designed for the parameters $f_0 = 3.6$ kHz, $Q = 4$, and dc gain of 7 dB. Estimate the minimum gain-bandwidth product the opamps must have if the errors in frequency contributed by the opamp must be no larger than 1% and those of the quality factor must be no more than 2%.

4.20 A Tow–Thomas bandpass filter, Fig. 4.10, is designed with 5% capacitors and 2% resistors. Estimate the errors in Q and f_0 that must be expected in the design.

4.21 In the design of Problem 4.20, choose one resistor to tune f_0 and determine the range over which it must be variable to tune f_0 to its exact value. Choose a second but different resistor to tune Q and determine the necessary tuning range to tune Q exactly.

4.22 The biquad designed in Problem 4.17 is to be predistorted to account for the nominal Q errors caused by the opamps. Choose a suitable resistor and its value to accomplish this goal.

4.23 Repeat Problems 4.17 and 4.18 for the Åckerberg–Mossberg filter in Fig. 4.29.

4.24 Estimate the highest center frequency of an Åckerberg–Mossberg bandpass filter if the frequency error caused by LM741 opamps must be restricted to 0.5%.

4.25 This problem is designed to provide practice in filter design. Use LM741 opamps, practical component values, and test the designs with EWB. Build an Åckerberg–Mossberg filter to realize a

(a) lowpass for $f_c = 3.2$ kHz, $Q = 0.707$, $H_0 = 4$ dB

(b) lowpass for $f_c = 900$ Hz, $Q = 3$, $H_0 = 1$

(c) lowpass for $f_c = 13$ kHz, $Q = 0.707$, $H_0 = 10$ dB

(d) lowpass for $f_c = 24$ kHz, $Q = 6$, $H_0 = 0$ dB

(e) bandpass for $f_c = 3.6$ kHz, $Q = 3$, $H_0 = 9$ dB

(f) bandpass for $f_c = 500$ Hz, $Q = 30$, $H_0 = 2$

(g) bandpass for $f_c = 18$ kHz, $Q = 25$, $H_0 = 0$ dB

(h) bandpass for $f_c = 8$ kHz, $Q = 7.5$, $H_0 = 5$

4.26 Repeat Problems 4.25a, b, c, and d for an appropriate version of a Sallen–Key section.

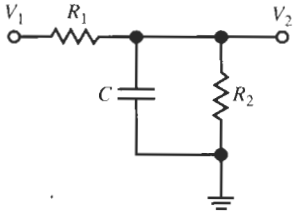

(a)

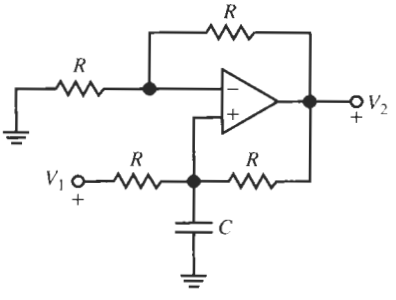

(b)

Figure P4.16

4.27 A Sallen–Key lowpass filter is designed for the parameters $f_c = 4.8$ kHz, $Q = 5$, and dc gain $H = 3$. Estimate the errors in filter parameters if the circuit is built with an LM741 opamp.

4.28 Use the *RC–CR* transformation to convert the circuits of Problem 4.26 into highpass filters. Test your designs with EWB.

4.29 Design the Delyiannis–Friend single-amplifier biquad (SAB) of Fig. 4.37 to realize a bandpass filter with the parameters

(a) $f_0 = 4.5$ kHz, $Q = 9$, $H_M = 26$ dB; use an LM741 opamp and test the design.

(b) $f_0 = 4.5$ MHz, $Q = 9$, $H_M = 26$ dB; use an HA2542–2 opamp and test the design.

4.30 Analyze the effects of finite gain-bandwidth products in the designs of Problem 4.29. Compare your results with the tests performed in Problem 4.29.

4.31 The impedance converter of Fig. 4.45b with impedances in the branches realizes the impedance of Eq. (4.165). Find the elements required such that the impedance is a frequency-dependent negative resistor (FDNR) described by $Z_{in}(j\omega) = -1/(\omega^2 D)$ where D is a real number. Of course, no inductors are to be used. (The FDNR is a component that can be used to simulate high-order filters, see Section 14.5.)

4.32 Realize a GIC bandpass filter with the parameters $f_0 = 25$ kHz, $Q = 8.7$, and $H = 2$. Use LM741 opamps and test the design with EWB. Discuss the deviations if any.

4.33 Repeat the design of Problem 4.32 but for $H = 10$. Test the design and carefully evaluate any deviations in performance compared with those found in Problem 4.32.

4.34 Repeat the design of Problem 4.32 but for $H = 0.4$. Test the design and carefully evaluate any deviations in performance compared to those found in Problem 4.32.

4.35 Design the bandpass filters of Problems 4.25e, f, g, and h for a GIC section.

4.36 Derive Eq. (4.172), which shows the effect of finite opamp bandwidth on the GIC performance.

4.37 For an optimal GIC design with $\omega_c C_2 = G_3$ and identical opamps, sketch the inductor error ΔL and the loss term of the simulated inductor as functions of gain H. [Refer to Eqs. (4.173) and (4.174)].

4.38 In many circuits the sensitivity to component variations and component spread is proportional to the quality factor Q or even to Q^2. We found this to be the case in the Delyiannis–Friend circuit of Fig. 4.35 and solved the difficulty in a simple way by Q enhancement with two resistors as in Fig. 4.37. If such a simple procedure cannot be employed, a different method can be used that needs an additional opamp. The configuration is shown for the case of a Delyiannis–Friend biquad in Fig. P4.38. If the section T realizes

$$T(s) = -\frac{sH\omega_0/Q}{s^2 + s\omega_0/Q + \omega_0^2}$$

show that the transfer function of the configuration in Fig. P4.38 is

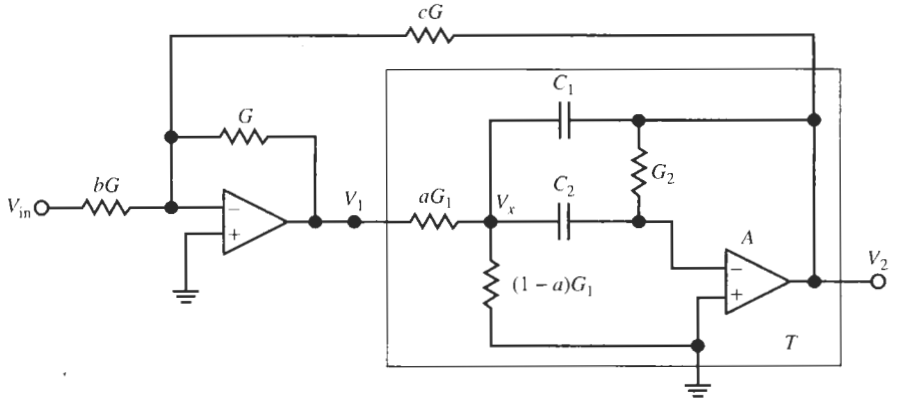

Figure P4.38

$$T(s) = b\frac{sH\omega_0/Q}{s^2 + s(\omega_0/Q)(1 - cH) + \omega_0^2}$$

We see both Q and the gain H are enhanced by the factor $(1 - cH)$. This method allows the designer to build the intrinsic second-order section with a lower quality factor Q_0 but realize the selectivity implied by the increased quality factor $Q_0/(1-cH)$. Note that the sensitivity becomes large when cH approaches the value 1, that is Q enhancement must not be chosen "too large." Test this approach by designing an enhanced-Q Delyiannis–Friend bandpass filter with $f_0 = 12.5$ kHz, $Q = 40$, and $H = 26$ dB. Use the intrinsic quality factor $Q_0 = 5$ and gain $H = 1$. Build the circuit with LM741 opamps and test the performance with EWB.

5 SECOND-ORDER FILTERS WITH ARBITRARY TRANSMISSION ZEROS

In the previous chapter we presented four excellent second-order filters, the Åckerberg–Mossberg two-integrator loop circuit of Fig. 4.29, the Sallen–Key circuit of Fig. 4.31b, the Delyiannis–Friend single-amplifier biquad of Fig. 4.37, and the GIC circuit of Fig. 4.46. They are accepted in practice and will be used for most designs in the remainder of this book. A problem is that these circuits in the form presented can implement only limited types of transfer functions: lowpass or highpass functions for the Sallen–Key circuit, lowpass and bandpass functions for the Åckerberg–Mossberg circuit, and bandpass functions for the Delyiannis–Friend and the GIC filters. The circuits are too limited indeed to be useful in many practical applications that require the realization of transmission zeros anywhere in the s-plane. What is required is a second-order section to realize the *biquadratic* function

$$T(s) = \frac{N(s)}{D(s)} = \frac{k_2 s^2 + k_1 s + k_0}{s^2 + s(\omega_0/Q) + \omega_0^2} \tag{5.1}$$

where the numerator coefficients k_i may be positive, negative, or zero. We would like to derive *biquads* based on the good filter circuits developed previously without destroying their excellent properties. Because these properties depend on the poles, this implies that we must be able to generate the numerator $N(s)$, i.e., the transmission zeros, without changing the circuits' pole positions. The numerator $N(s)$ is determined by the output node we choose in the filter. We saw an example in the two-integrator loop in Fig. 4.10 where a bandpass and an inverting and a noninverting lowpass output were available at different nodes. Also, the numerator depends on the location of the input, which is to say, the transmission zeros depend

on where in the circuit and through which components we connect the input signal. It is our goal in this chapter to show how arbitrary transmission zeros and, therefore, more versatile filters can be generated out of the structures discussed in Chapter 4 without affecting their poles. We shall employ two generally useful methods to accomplish this task. The first technique uses summing of different filter outputs. The second method injects the input signal into appropriate nodes and thereby generates full second-order numerators in the second-order sections.

5.1 BY USING SUMMING

We will consider this technique on the Åckerberg–Mossberg circuit in Fig. 4.29, repeated here in the upper part of Fig. 5.1 for ease of reference. We found in Eq. (4.27) that at the lowpass and bandpass outputs the filter realizes, for $C_1 = C_2 = C$ and the indicated resistors

$$T_L(s) = \frac{V_L}{V_I} = -\frac{k(G/C)^2}{s^2 + s(G/C)/Q + (G/C)^2} = -\frac{k\omega_0^2}{s^2 + s\omega_0/Q + \omega_0^2} \tag{5.2a}$$

$$T_B(s) = \frac{V_B}{V_I} = -\frac{skG/C}{s^2 + s(G/C)/Q + (G/C)^2} = -\frac{skQ\,(\omega_0/Q)}{s^2 + s\omega_0/Q + \omega_0^2} \tag{5.2b}$$

ω_0 is given by G/C. In addition, at the third opamp output terminal we have available the negative of the lowpass output,

$$-T_L(s) = \frac{-V_L}{V_I} = \frac{k(G/C)^2}{s^2 + s(G/C)/Q + (G/C)^2} = \frac{k\omega_0^2}{s^2 + s\omega_0/Q + \omega_0^2} \tag{5.2c}$$

We have chosen in Fig. 5.1 two identical capacitors to keep with common practice, and have identified the quantities k and Q at the corresponding resistors that determine these filter parameters. The two resistors R_A of the inverter are arbitrary. Let us employ a fourth opamp as a summer, shown in the lower part of Fig. 5.1. Using four opamps causes no great expense because four opamps on an IC package are sold commercially, so that the fourth device is readily available.

In Chapter 4 we analyzed in great detail the effects of the finite gain-bandwidth product ω_t on the Åckerberg–Mossberg circuit; let us here briefly consider the additional effect of the summer. Assuming finite opamp gain and writing a node equation at the inverting opamp input, we find

$$V_{out} + aV_I + bV_B + cV_L + d(-V_L) = -\frac{V_{out}}{A}(1 + a + b + c + d)$$

which is brought into the form

$$V_{out} = -\frac{aV_I + bV_B + (c - d)V_L}{1 + (1 + a + b + c + d)/A(s)} \tag{5.3}$$

It lets us judge what effect the finite opamp gain has. Using the integrator model of Eq. (2.18), we notice that the summer's 3-dB bandwidth is given by

$$\omega_{-3\,dB} = \frac{\omega_t}{1 + a + b + c + d} \tag{5.4}$$

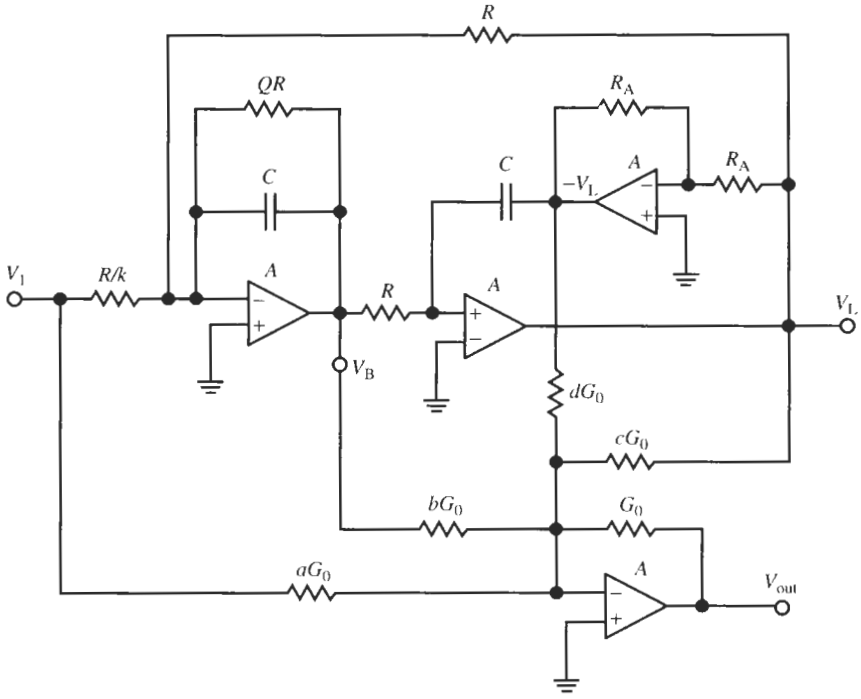

Figure 5.1 The Åckerberg–Mossberg circuit with V_{out} generated by summing the input voltage to the bandpass and lowpass outputs. $\omega_0 = G/C$.

Evidently then, the designer must control the size of the summer coefficients so that the summer's bandwidth does not limit the usable frequency range of the filter being developed. This is important, especially in circuits such as highpass filters, where operation at higher frequencies is specified.

We shall keep Eq. (5.4) in mind and assume next ideal opamps for the derivation of the design equations. From Eq. (5.3) we form

$$\frac{V_{out}}{V_I} = -\left[a + b\frac{V_B}{V_I} + (c-d)\frac{V_L}{V_I}\right]$$

and insert the three transfer functions of Eq. (5.2); we obtain

$$\frac{V_{out}}{V_I} = -\frac{as^2 + s(\omega_0/Q)\,[a - b(kQ)] + \omega_0^2\,[a - (c-d)k]}{s^2 + s\omega_0/Q + \omega_0^2} \tag{5.5}$$

This function is of the desired form of Eq. (5.1). Note that we may choose the terms in brackets, that is the coefficients k_1 and k_0, to be positive, negative, or zero. There is, of course, no interest in building a lowpass or a bandpass filter with this technique because these functions can be implemented with the basic Åckerberg–Mossberg circuit at the outputs V_B and V_L. But a highpass filter is obtained by choosing components such that $[a - b(kQ)] = 0$ and $[a - (c-d)k] = 0$. This filtering function was lost in the two-integrator loop because we merged the input summer with the first integrator (see Fig. 4.10).

EXAMPLE 5.1

Design a highpass filter with a cut-off frequency of 42 kHz and a quality factor Q to obtain some 10 dB of band edge peaking above the high-frequency level. The gain at high frequencies is to be 6 dB. The circuit should use LM741 opamps and operate to at least 200 kHz before high-frequency roll-off becomes noticeable.

Solution

For the circuit in Fig. 5.1 we find with a choice of $C = 10$ nF

$$R = \frac{1}{\omega_0 C} = \frac{1}{2\pi \times 42\ \text{kHz} \times 10\ \text{nF}} = 379\ \Omega$$

A glance at Fig. 4.13 suggests the choice 10 dB of peaking above the level at dc is obtained for $Q = 3$. In our case we are concerned with the peaking above the level at infinity but this does not change the Q required. For $Q = 3$ we have $QR = 1.137$ kΩ. Next we need to determine the summing coefficients. We pick $d = 0$ and have $a = 2$ to implement the high-frequency gain of 6 dB. A constraint is that the usable frequency range must be larger than 200 kHz. LM741 opamps have $f_t \approx 1.5$ MHz; Eq. (5.4) requires, therefore, $1 + a + b + c < 7.5$. To realize a highpass from Eq. (5.5) we need to satisfy $[a - b(kQ)] = 0$ and $[a - ck] = 0$, that is

$$b = a/(kQ) \quad \text{and} \quad c = a/k$$

As a safety margin, let us choose $1 + a + b + c = 5$. Thus we must pick

$$1 + a + b + c = 1 + a\left[1 + \frac{1}{k}\left(1 + \frac{1}{Q}\right)\right] = 1 + 2\left(1 + \frac{4}{3k}\right) = 5$$

i.e.,

$$\frac{1}{k} = 0.75 \quad \text{and} \quad \frac{R}{k} = 0.75 \times 379\ \Omega = 284\ \Omega$$

We have then $a = 2$, $b = 0.50$, and $c = 1.5$, and with $R_0 = R_A = 10$ kΩ; the summing resistors are as given in Fig. 5.2, which shows the circuit and its tested performance.

We make a few observations: At 200 kHz (cursor) the gain is reduced to 4.97 dB, about 1 dB below specifications; the safety margin for high-frequency roll-off should be increased. The peak represents correctly $Q = 3$: the gain at that point equals $(6 + 20\ \log 3) \approx 16$ dB. There is an unspecified zero of transmission at $f \approx 1.5$ kHz. Since the gain stays below -56 dB, this zero will likely cause no problems. If continuous roll-off toward $f = 0$ Hz is required, careful adjusting (tuning) of the resistor R/k will be necessary to eliminate the constant coefficient in the numerator of $T(s)$ (experimentally $R/k = 283.7\ \Omega$ lets the gain roll off to below -100 dB). We note that this performance is very sensitive to element values because the constant coefficient $k_0 = 0$ in Eq. (5.1) is established by subtracting two (relatively) large numbers! Such difference effects ought to be avoided if possible because as a rule component tolerances will be too large in practice.

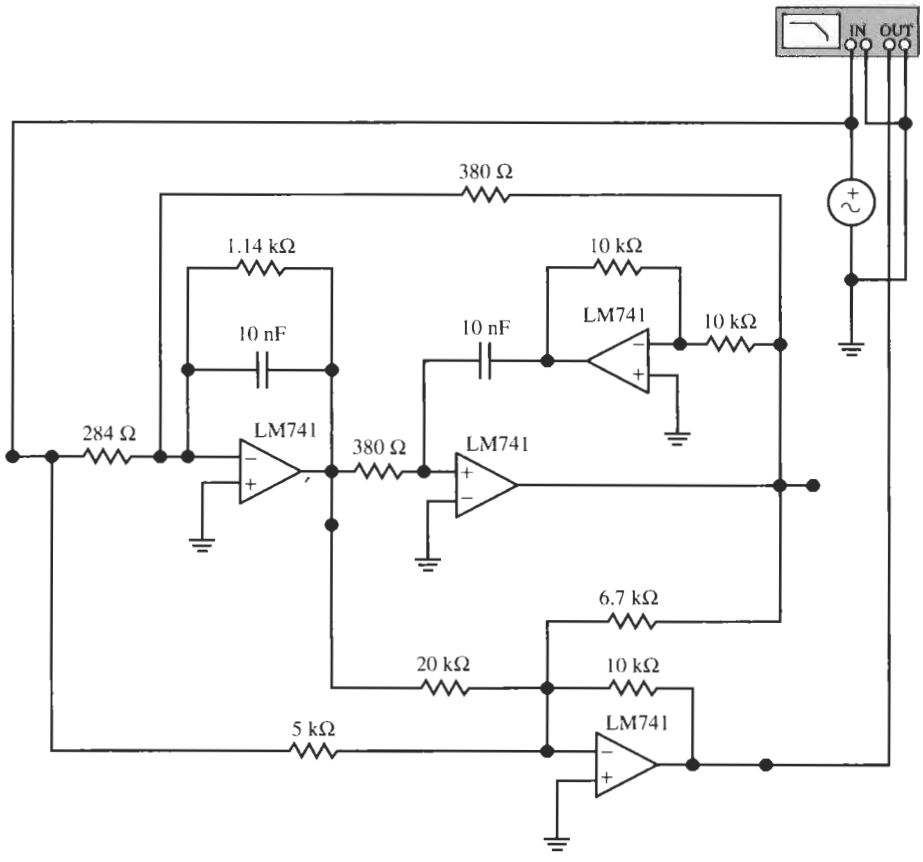

(a)

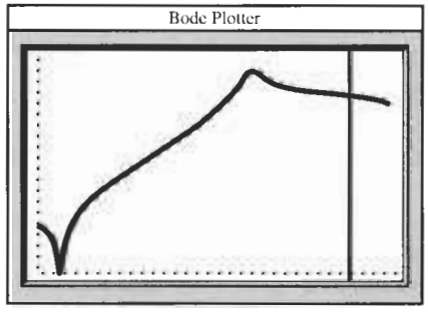

(b)

Figure 5.2 The highpass circuit of Example 5.1 and its performance. (Bode Plotter scales: 1 to 400 kHz; -80 to +20 dB; cursor at 202 kHz, 4.97 dB.)

$T(s)$ in Eq. (5.5) enables us to build second-order sections with arbitrary transmission zeros. For instance, an interesting and important filter is one with transmission zeros on the $j\omega$-axis. Note that choosing the summer coefficients such that $c = d = 0$ and $[a - b(kQ)] = 0$ results in the function

$$T_{\mathrm{BE}}(s) = \frac{V_{\mathrm{out}}}{V_{\mathrm{I}}} = \frac{N(s)}{D(s)} = -a\frac{s^2 + \omega_0^2}{s^2 + s\omega_0/Q + \omega_0^2} \tag{5.6}$$

The numerator of Eq. (5.6) has zeros at $s_{1,2} = \pm j\omega_0$, i.e., $N(j\omega_0) = 0$. The filter has no output at the frequency ω_0. Figure 5.3 shows a pole-zero diagram and a plot of the magnitude

$$|T_{\mathrm{BE}}(j\omega)| = a\frac{\omega_0^2 - \omega^2}{\sqrt{\left(\omega_0^2 - \omega^2\right)^2 + (\omega\omega_0/Q)^2}} \tag{5.7}$$

of this function for some value of Q and $a = 1$. Because of the particular shape of the magnitude the filter is known as a *notch filter*, and also as a *band elimination* or *bandreject filter*. The filter is useful in applications in which a specific frequency must be eliminated. For example, instrumentation systems require that the power-line frequency of 60 Hz be eliminated.

The notch filter reduces the magnitude of the output not at just one frequency but over a band of frequencies, and in this sense it is band elimination in nature. The width of the band, BW, over which the function $|T_{\mathrm{BE}}(j\omega)|$ is reduced to less than the gain a at 0 and ∞, say a/q with $q > 1$, is determined by Q. This band, $\mathrm{BW} = \omega_2 - \omega_1$, can be obtained by equating Eq. (5.7) to a/q:

$$a\frac{\omega_0^2 - \omega^2}{\sqrt{\left(\omega_0^2 - \omega^2\right)^2 + (\omega\omega_0/Q)^2}} = \frac{a}{q}$$

or

$$\left(\omega_0^2 - \omega^2\right)^2\left(q^2 - 1\right) = (\omega\omega_0/Q)^2 \tag{5.8}$$

This equation has four solutions; the two positive ones are ω_1 and ω_2 and their difference can be shown to be

$$\mathrm{BW} = \omega_2 - \omega_1 = \frac{\omega_0}{Q\sqrt{q^2 - 1}}$$

These two frequencies are marked in Fig. 5.3 for $q^{-1} = 0.707$, corresponding to 3-dB loss, $1/q = 10^{-3/20}$. For this value of q we have $Q = \omega_0/\mathrm{BW}$, the same as the definition in a

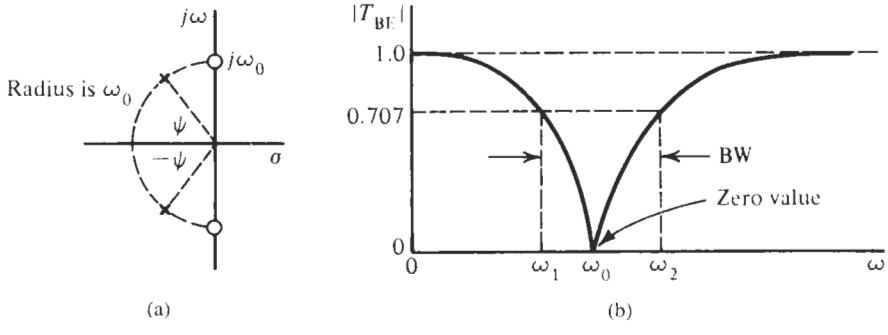

Figure 5.3 Plots of the pole-zero pattern in the s-plane (a) and of the magnitude, Eq. (5.7), (b) of a notch filter.

bandpass, Eq. (5.2b), with $BW = BW_{-3\,dB}$. Equation (5.8) lets us determine the value of Q required to meet the specified loss $1/q$ over a band Δf:

$$Q = \frac{f_0}{\Delta f \sqrt{q^2 - 1}} \tag{5.9}$$

It is also useful to note the symmetry relationships for the magnitude

$$|T_{BE}(j\omega_1)| = |T_{BE}(j\omega_2)| \tag{5.10}$$

and for the phase

$$\theta_1(j\omega_1) = -\theta_2(j\omega_2) \tag{5.11}$$

These relations hold for all frequencies that satisfy

$$\omega_1 \omega_2 = \omega_0^2 \tag{5.12}$$

EXAMPLE 5.2

Design a notch filter to eliminate the frequency component at $f_0 = 830$ Hz from a signal. The low- and high-frequency gains must be 0 dB and the attenuation must not be larger than 1 dB in a band of width $\Delta f = 100$ Hz around f_0. Use the circuit in Fig. 5.1 built with $C = 0.1$-μF capacitors and LM741 opamps.

Solution

We use the circuit in Fig. 5.1 with $a = 1$ and $c = d = 0$ to realize

$$\frac{V_{out}}{V_1} = -\frac{s^2 + s(\omega_0/Q)[1 - b(kQ)] + \omega_0^2}{s^2 + s\omega_0/Q + \omega_0^2}$$

With $C = 0.1\ \mu$F we find $R = 1/(\omega_0 C) = 1.918$ kΩ. The required loss of less than 1 dB in a band $\Delta f = 100$ Hz around f_0 results in

$$q = 10^{1/20} = 1.122$$

so that Eq. (5.9) yields

$$Q = \frac{f_0}{\Delta f \sqrt{1.2589 - 1}} = 16.3$$

This value gives $QR = 31.3$ kΩ and we find from the requirement $1 - bkQ = 0$ that we can get an implementation with the smallest number of different resistors if we choose $k = 1/Q$ and $b = 1$. The remaining resistors are arbitrary; we choose 10 kΩ. The circuit and test results are shown in Fig. 5.4. The sharp notch with attenuation -61 dB is at 828 Hz (measured a higher resolution), and the -1-dB band reaches from 780 to 880 Hz. The attenuation

can be measured to increase to −3 dB at approximately 500 kHz due to the finite bandwidth of the summer opamp. This is in agreement with Eq. (5.4) [or Eq. (2.58)]: for $a = b = 1$ and $f_t \approx 1.5$ MHz the bandwidth of the inverting summer is expected to be ≈500 kHz.

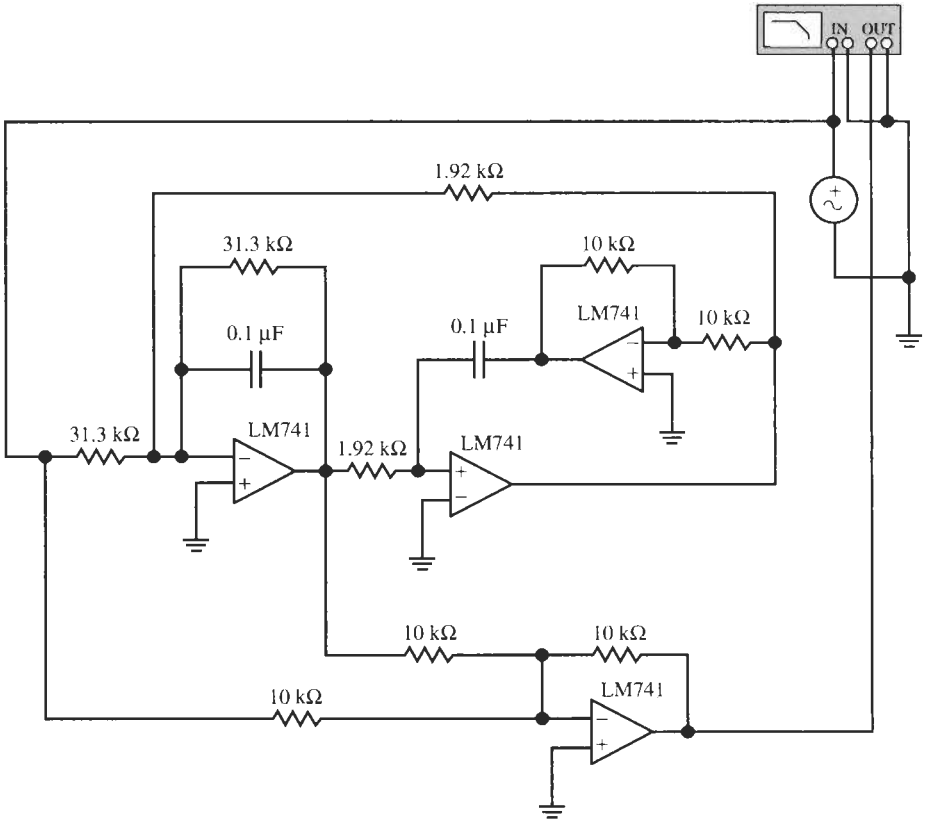

(a)

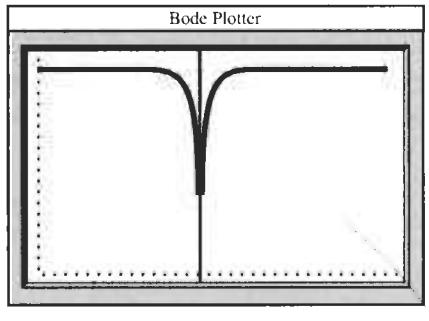

(b)

Figure 5.4 The notch filter design for Example 5.2 and test results. (Bode Plotter scales: 600Hz to 1.2 kHz; −40 to 0 dB; cursor at 827 Hz, −25.4 dB.)

The depth of the notch is very sensitive to obtaining $1 - bkQ = 0$. Inaccurate component values reduce the depth. In some applications, such as for *gain equalization* in transmission systems, a deep notch is not required but rather a *dip* in gain specifications over a limited band of frequencies. This is shown in Fig. 5.5 for a dip of 6 dB, corresponding to a gain reduction to one-half the value at dc. The transfer function to accomplish this task is Eq. (5.5) with $a = 1$ and $c = d = 0$

$$T_{eq}(s) = \frac{V_{out}}{V_1} = -\frac{s^2 + s(\omega_0/Q)[1 - b(kQ)] + \omega_0^2}{s^2 + s\omega_0/Q + \omega_0^2} = -\frac{s^2 + sp\omega_0/Q + \omega_0^2}{s^2 + s\omega_0/Q + \omega_0^2} \tag{5.13}$$

but the number $p = [1 - b(kQ)] \neq 0$. The two design parameters in addition to ω_0^2 are p and Q. They are determined as follows. From Eq. (5.13) we have

$$|T_{eq}(j\omega_0)| = |p| \tag{5.14}$$

$|p| < 1$ determines the level of the dip. Note that if a *gain boost* is specified then $|p| > 1$. As always, Q sets the bandwidth via

$$\frac{(\omega_0^2 - \omega^2)^2 + (p\omega\omega_0/Q)^2}{(\omega_0^2 - \omega^2)^2 + (\omega\omega_0/Q)^2} = \frac{1}{q^2}$$

or

$$(\omega_0^2 - \omega^2)^2 (q^2 - 1) = (\omega\omega_0/Q)^2 (1 - p^2q^2) \tag{5.15}$$

where $q^{-1} = |T(j\omega)|$ is the specified attenuation at ω_1 and ω_2; see Fig. 5.5. Solving this expression for the prescribed bandwidth yields

$$BW_q = \omega_2 - \omega_1 = \frac{\omega_0}{Q}\sqrt{\frac{1 - (pq)^2}{q^2 - 1}}$$

that is, the required quality factor equals

$$Q = \frac{f_0}{\Delta f}\sqrt{\frac{1 - (pq)^2}{q^2 - 1}} \tag{5.16}$$

Equation (5.16) is valid for a dip in gain, $|p| < 1$. For a gain boost, $|p| > 1$, the absolute value of the term under the square root in Eq. (5.16) must be taken. Equations (5.8) and (5.9) are special cases of Eqs. (5.15) and (5.16) for $p = 0$.

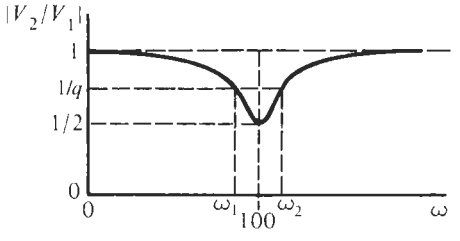

Figure 5.5 Transfer function magnitude with a gain dip for gain equalization.

EXAMPLE 5.3

Design a filter that has 0-dB gain at high and at low frequencies, but reduces the gain by a factor of 2, that is, to −6dB, at the frequency 1200 Hz. The gain reduction should equal at least 2 dB in a band $\Delta f = 400$ Hz. Use the circuit in Fig. 5.1, with $C = 0.1$-μF capacitors and LM741 opamps.

Solution

We use again the circuit in Fig. 5.1 with $a = 1$ and $c = d = 0$ to realize

$$\frac{V_{\text{out}}}{V_1} = -\frac{s^2 + s\,(\omega_0/Q)\,[1 - b(kQ)] + \omega_0^2}{s^2 + s\omega_0/Q + \omega_0^2}$$

For $f_0 = 1.2$ kHz we find $R = 1.326$ kΩ. The required > 2-dB loss in a band $\Delta f = 400$ Hz around f_0 results in

$$q = 10^{2/20} = 1.259$$

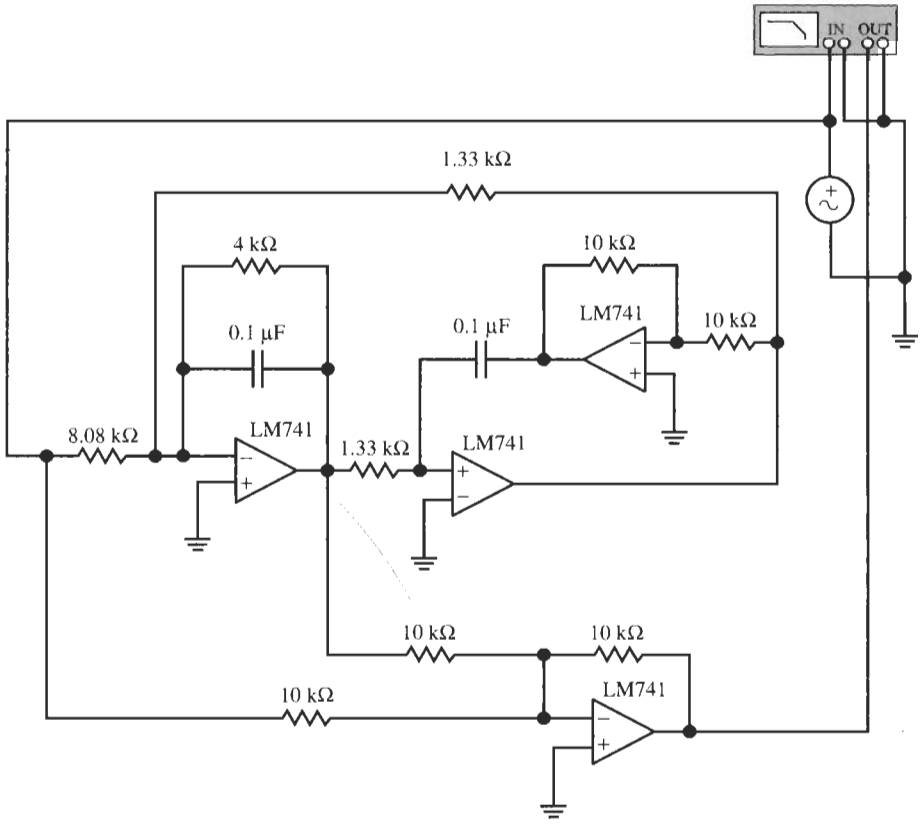

(a)

Figure 5.6 The magnitude equalizer design for Example 5.3 and test results. (Bode Plotter scales: 600 Hz to 2.3 kHz; −20 to 0 dB; cursor at 1.20 kHz, −5.94 dB.)

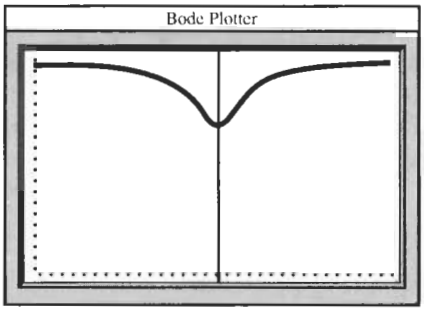

(b)

Figure 5.6 Continued

and the specified value $p = 0.5$ (corresponding to -6 dB) yields from Eq. (5.16)

$$Q = \frac{1200}{400}\sqrt{\frac{1-(0.5\times 1.259)^2}{1.585-1}} = 3.048$$

Thus, $QR = 4.04$ kΩ. Finally, from $p = 0.5 = 1 - b(kQ)$ we choose $b = 1$ so that $k = 1/(2Q)$ and $R/k = 2QR = 8.08$ kΩ. The remaining resistors are selected as 10 kΩ. Figure 5.6 shows the design and the test results. The deepest attenuation is 5.94 dB at 1.2 kHz; the -2-dB band is between 1.01 and 1.401 kHz. As in the previous example, the attenuation increases to -3 dB at approximately 500 kHz due to the finite bandwidth of the summer opamp.

The structure in Fig. 5.1 can also be configured as a second-order *allpass* filter. Allpass filters transmit signals at all frequencies equally well and change only the phase. They were discussed in Chapter 3 for first-order circuits. In the present case, the transfer function we are trying to obtain is

$$T_{AP}(s) = -\frac{s^2 - s(\omega_0/Q) + \omega_0^2}{s^2 + s(\omega_0/Q) + \omega_0^2} \tag{5.17}$$

From this equation we see that the positions of the poles and zeros differ by the sign of their real part. The pole-zero configuration is shown in Fig. 5.7. Allpass circuits are inserted into transmission systems to achieve phase or delay correction. Their phase is (including the 180° arising from the minus sign)

$$\theta_{AP}(\omega) = 180° - 2\tan^{-1}\frac{\omega\,\omega_0/Q}{\omega^2 - \omega_0^2} \tag{5.18}$$

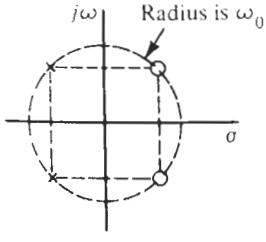

Figure 5.7 Pole-zero plot of a second-order allpass filter.

but the allpass does not affect the magnitude because on the $j\omega$-axis, T_{AP} is a ratio of two conjugate complex numbers and so its magnitude is equal to unity for all frequencies. Note that θ_{AP} is twice the phase of the lowpass function plotted in Fig. 4.13 because we add the two equal phases of numerator and denominator of $T_{AP}(j\omega)$. To obtain the function of Eq. (5.17) we use Eq. (5.5) with $a = 1, c = d = 0$, and $[1 - b(kQ)] = -1$,

$$T_{AP}(s) = -\frac{s^2 - s(\omega_0/Q)[b(kQ) - 1] + \omega_0^2}{s^2 + s\omega_0/Q + \omega_0^2} \tag{5.19}$$

We can satisfy the condition $[b(kQ) - 1] = 1$ by choosing $b = 1$ and $k = 2/Q$, i.e., $R/\text{k} = 0.5QR$ as shown in Example 5.4.

EXAMPLE 5.4

Design an allpass filter whose phase traverses the range of approximately 90° to −90° over the frequency span 30 kHz ± 3000 Hz. Use the circuit in Fig. 5.1, with C = 10-nF capacitors and LM741 opamps.

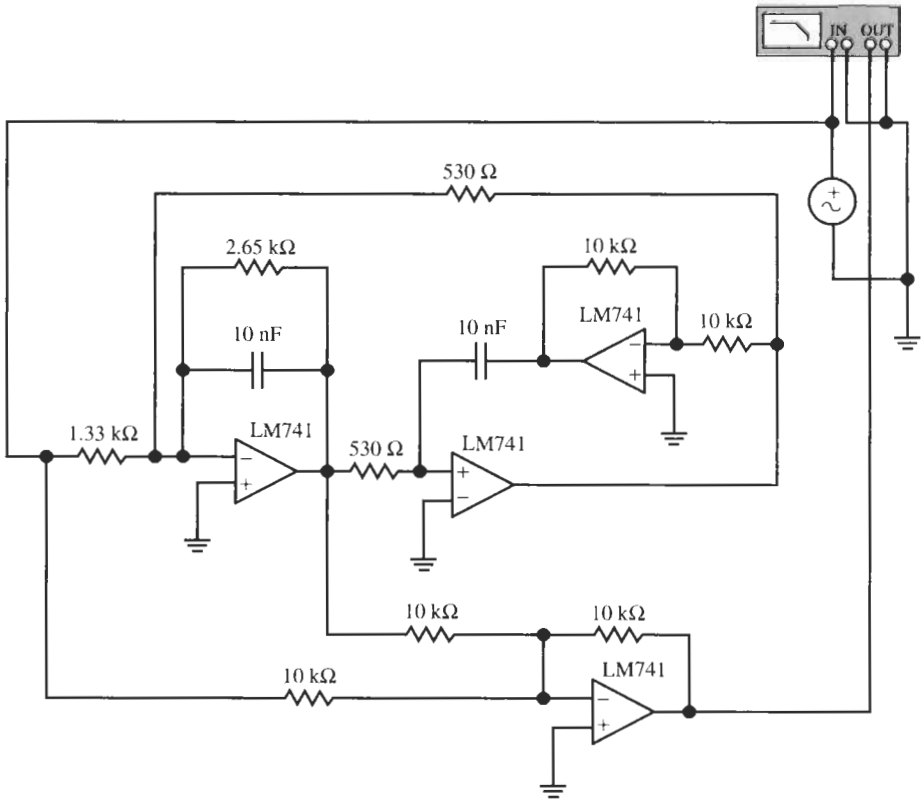

(a)

Figure 5.8 The allpass circuit for Example 5.4 and test results. (Bode Plotter scales: 10 to 80 kHz; −180° to 180°; cursor at 29.1 kHz, −1.38°.)

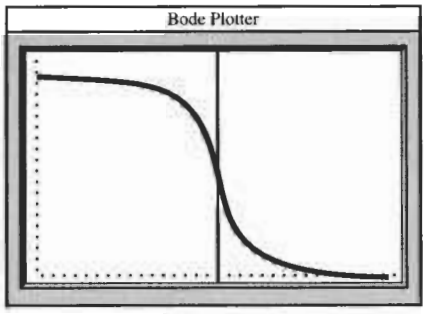

(b)

Figure 5.8 Continued

Solution

An exact analytical method for the design of such filters will be discussed in Chapter 10. For now we consult Fig. 4.13; remember that our allpass filter is inverting, i.e., it adds 180° to the plotted phase, and estimate that $Q \approx 5$ will do the job. Recall that the allpass phase is twice the lowpass phase. We use again the circuit in Fig. 5.1 with $a = b = 1, c = d = 0$, and $R/k = QR/2$ to realize Eq. (5.19). For $f_0 = 30$ kHz we find $R = 531\ \Omega$, $QR = 2.653$ kΩ, and $R/k = 1.326$ kΩ. Figure 5.8 shows circuit and test results for the phase. The magnitude is constant at 0 dB and the phase equals 0° at 29 kHz and goes from +90° to −90° in 26.2 kHz $\leq f \leq$ 32.4 kHz, that is, over a span of 6 kHz as required. Note that $\theta_{AP} \approx 0°$ at $f = f_0$. Apart from the effect of component tolerances, the test results are only approximately equal to the specifications because we started from the approximate value $Q \approx 5$.

Finally we mention that our four-opamp biquad can also implement so-called *lowpass* and *highpass notch* filters. Consulting Eq. (5.1) with $k_1 = 0$, a "lowpass notch" is defined as a notch filter with

$$T(0) = k_0/\omega_0^2 > T(\infty) = k_2$$

and a "highpass notch" has

$$T(0) = k_0/\omega_0^2 < T(\infty) = k_2$$

These filters are needed when the attenuations to the right and left of the transmission zero are unequal. To see how they are implemented we return to the general transfer function of Eq. (5.5) and notice that we need to satisfy $[a - b(kQ)] = 0$, along with $c = 0$ but $d \neq 0$ so that the coefficient k_0 is larger than $k_2 = a$; thus the lowpass notch function is

$$\frac{V_{out}}{V_1} = -\frac{as^2 + \omega_0^2(a + dk)}{s^2 + s\omega_0/Q + \omega_0^2} \tag{5.20}$$

Similarly, for the highpass notch we set $[a - b(kQ)] = 0$, along with $d = 0$ but $c \neq 0$ so that the coefficient k_0 is less than $k_2 = a$; thus the highpass notch function is

$$\frac{V_{out}}{V_1} = -\frac{as^2 + \omega_0^2(a - ck)}{s^2 + s\omega_0/Q + \omega_0^2} \tag{5.21}$$

Note that the circuit realization in Example 5.1, Fig. 5.2, inadvertently turned out to be a highpass notch because the inaccurate components resulted in a transmission zero at $f \approx 1.5$ kHz. The design of these filters is not difficult; we just need to specify Q and ω_0, and the gains at the extreme frequencies, 0 and ∞. All circuit elements can then be determined.

EXAMPLE 5.5

Design a lowpass notch to have 3 dB of low-frequency gain and −30-dB loss at high frequencies. The lowpass passband should be quite flat with the band edge at $f = 280$ Hz. Use LM741 opamps.

Solution

The function of Eq. (5.20) is needed here, with $[a - b(kQ)] = 0$ from Eq. (5.5). To satisfy the flat passband requirement, we consult Fig. 4.13 and choose $Q = 0.8$. The −30-dB high-frequency loss gives $a = 10^{-3/2} = 0.0316$; at dc the gain equals $|T(0)| = a + dk$, which is specified to equal 1.414 (+3 dB). We need to set, therefore, $dk = \sqrt{2} - a = 1.381$. The pole

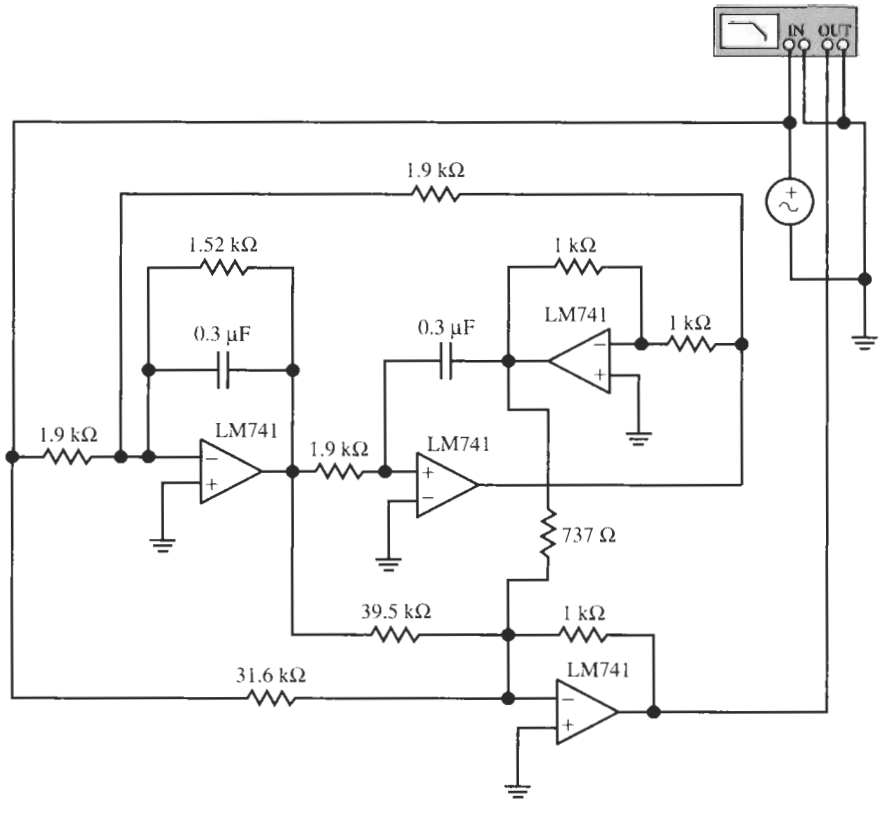

(a)

Figure 5.9 The lowpass notch filter of Example 5.5 and test results. (Bode Plotter scales: 10 Hz to 1MHz; −60 to +10 dB; cursor at 282Hz, 0.62 dB.)

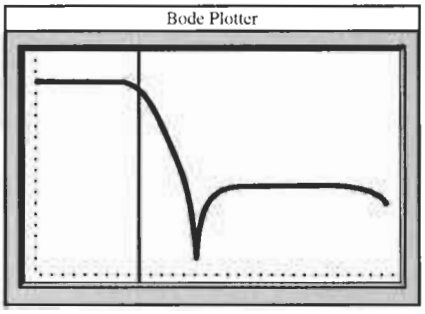

(b)

Figure 5.9 Continued

frequency is at the band edge, 280 Hz. Using $C = 0.3\ \mu$F, we find $R = 1.9$ kΩ, which we may set equal to R/k ($k = 1$) if we pick $d = 1.381$; also $QR = 1.52$ kΩ. Finally, we need to set b; from $[a - b(kQ)] = 0$ we find

$$b = a/(kQ) = 0.0316/0.8 = 0.0395$$

The lowpass notch circuit and its performance are shown in Fig. 5.9. The transmission zero is at 1.9 kHz ($= f_0\sqrt{\sqrt{2}/a}$) as expected. The summer bandwidth limitations reduce the high-frequency gain by 3 dB (to -33 dB) at approximately 650 kHz, in agreement with Eq. (5.4): $1.5\ \text{MHz}/(1 + a + b + d) = 1.5\ \text{MHz}/2.45 \approx 610$ kHz.

We now see the versatility of the four-opamp biquad circuit. Starting with the most general structure, Fig. 5.1 described by Eq. (5.5), simply disconnecting certain resistors from the circuit and reevaluating others, we can design entirely arbitrary transfer functions. In this sense the circuit in Fig. 5.1 can be considered a universal filter, easily and economically implemented using packages with four opamps (so-called *quads*) on one integrated circuit. The circuit can be tuned in a noninteractive manner for precise filter parameters. The pole frequency ω_0 is tuned by varying the resistor R at the output of the first opamp (R_4 in Fig. 4.10), Q is set by the resistor QR, and for bandpass and lowpass filters the gain is controlled by R/k. In the full biquadratic function of Eq. (5.5), the parameter a controls the high-frequency gain and c or d are chosen to set the low-frequency gain. At the same time c and/or d, of course, also determine the zero (notch) frequency, and b is adjusted to control the notch depth. We present in Table 5.1 a summary of the transfer functions that we found to be realizable with the four-opamp circuit. Next we shall discuss briefly the phase response of the circuits.

5.1.1 Phase Response of the General Biquadratic Circuit

Apart from the allpass, biquadratic circuits are normally designed for their magnitude behavior. Nevertheless, the engineer should have an understanding of the phase response of biquads. The circuits are described by Eq. (5.1). On the $j\omega$-axis we have

$$\begin{aligned} T(j\omega) &= \frac{N(j\omega)}{D(j\omega)} = \frac{N(j\omega)}{-\omega^2 + j\omega\omega_0/Q + \omega_0^2} \\ &= \frac{|N(j\omega)|\, e^{j\theta_1}}{|D(j\omega)|\, e^{j\theta_2}} = \left|\frac{N(j\omega)}{D(j\omega)}\right| e^{j(\theta_1 - \theta_2)} \end{aligned} \tag{5.22}$$

TABLE 5.1 Standard Forms of Second-Order Responses

	Frequency Response	Poles/Zeros	Name
$T_{LP} = \dfrac{\omega_0^2}{s^2 + \dfrac{\omega_0}{Q}s + \omega_0^2}$	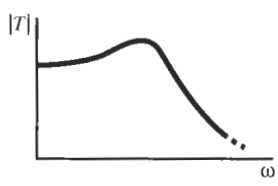	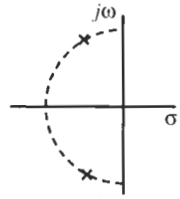	Lowpass
$T_{BP} = \dfrac{\dfrac{\omega_0}{Q}s}{s^2 + \dfrac{\omega_0}{Q}s + \omega_0^2}$	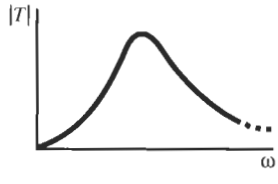	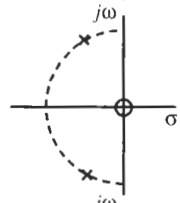	Bandpass
$T_{BE} = \dfrac{s^2 + \omega_0^2}{s^2 + \dfrac{\omega_0}{Q}s + \omega_0^2}$	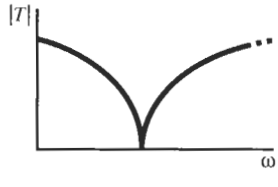	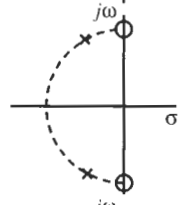	Bandstop "notch"
$T_{HP} = \dfrac{s^2}{s^2 + \dfrac{\omega_0}{Q}s + \omega_0^2}$	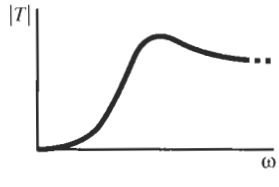	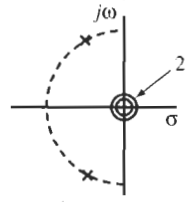	Highpass
$T_{AP} = \dfrac{s^2 - \dfrac{\omega_0}{Q}s + \omega_0^2}{s^2 + \dfrac{\omega_0}{Q}s + \omega_0^2}$	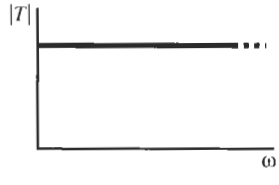	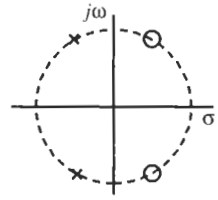	Allpass
$T_{LPN} = \dfrac{s^2 + k^2\omega_0^2}{s^2 + s\dfrac{\omega_0}{Q} + \omega_0^2}$	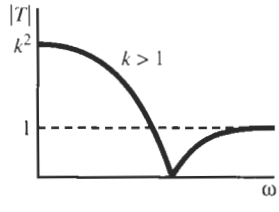	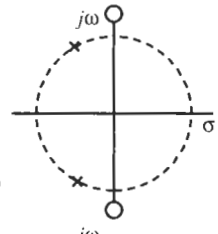	Lowpass notch
$T_{HPN} = \dfrac{s^2 + h^2\omega_0^2}{s^2 + s\dfrac{\omega_0}{Q} + \omega_0^2}$	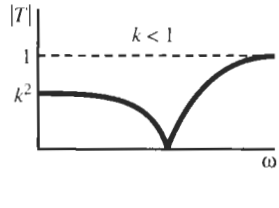	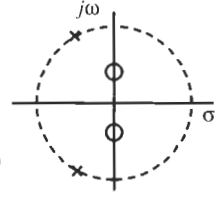	Highpass notch

We discussed in Chapters 1 and 4 that the phase of $T(j\omega)$ is obtained by subtracting the phase of the denominator from that of the numerator:

$$\phi(\omega) = \theta_1(\omega) - \theta_2(\omega) = \theta_1 - \tan^{-1}\frac{\omega\omega_0/Q}{\omega_0^2 - \omega^2} = \theta_1 - \tan^{-1}\frac{(\omega/\omega_0)(1/Q)}{1 - \omega^2/\omega_0^2} \tag{5.23}$$

We recognize

$$\theta_{LP}(\omega) = -\tan^{-1}\frac{\omega\omega_0/Q}{\omega_0^2 - \omega^2} \tag{5.24}$$

as the phase of a (noninverting) lowpass function, Eq. (4.31). It was plotted in Fig. 4.13b for various values of Q and normalized frequencies ω/ω_0. The phase of the numerator has in general the same form as $\theta_2(\omega)$ but depends, of course, on the specific transfer function. We show in Table 5.2 the most common forms of $N(s)$ and the phases of $N(j\omega)$. According to Eq. (5.23) we only have to add the phases in Table 5.2 to $\theta_2(\omega)i$ to obtain the total phase of the biquad. We note that in a lowpass, $N(j\omega) = \omega_0^2$ so it adds zero to $\theta_2(\omega)$; in a bandpass function, we have $N(j\omega) = j(\omega\omega_0/Q)$, which adds $+90°$ to $\theta_2(\omega)$, and a highpass has $N(j\omega) = -\omega^2$, which means the total phase equals $\phi(\omega) = 180° - \theta_2(\omega)$. Since the difference between the phases contributed by the different filters is only a constant, we show in Fig. 5.10 the resulting phase shifts for various values of Q plotted versus different axes. Finally we note that the phase of an allpass filter, Eq. (5.18), is simply twice that of a lowpass filter, and that the phase of the numerator of a notch filter changes abruptly at $\omega = \omega_0$ from zero to 180°. Figure 5.10 shows the result. Our discussion assumed that all filters are noninverting; if the filter is inverting, the factor (-1) simply adds 180° to the results in Fig. 5.10.

TABLE 5.2 Common Forms of $N(s)$ and Phases of $N(j\omega)$

Name	$N(s)$	$N(j\omega)$	Plot of $\theta_1(\omega)$
Lowpass	ω_0^2	ω_0^2	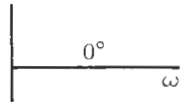
Bandpass	$\frac{\omega_0}{Q}s$	$j\frac{\omega_0\omega}{Q}$	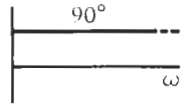
Bandstop	$s^2 + \omega_0^2$	$-\omega^2 + \omega_0^2$	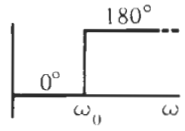
Highpass	s^2	$-\omega^2$	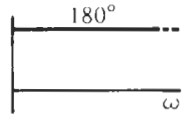

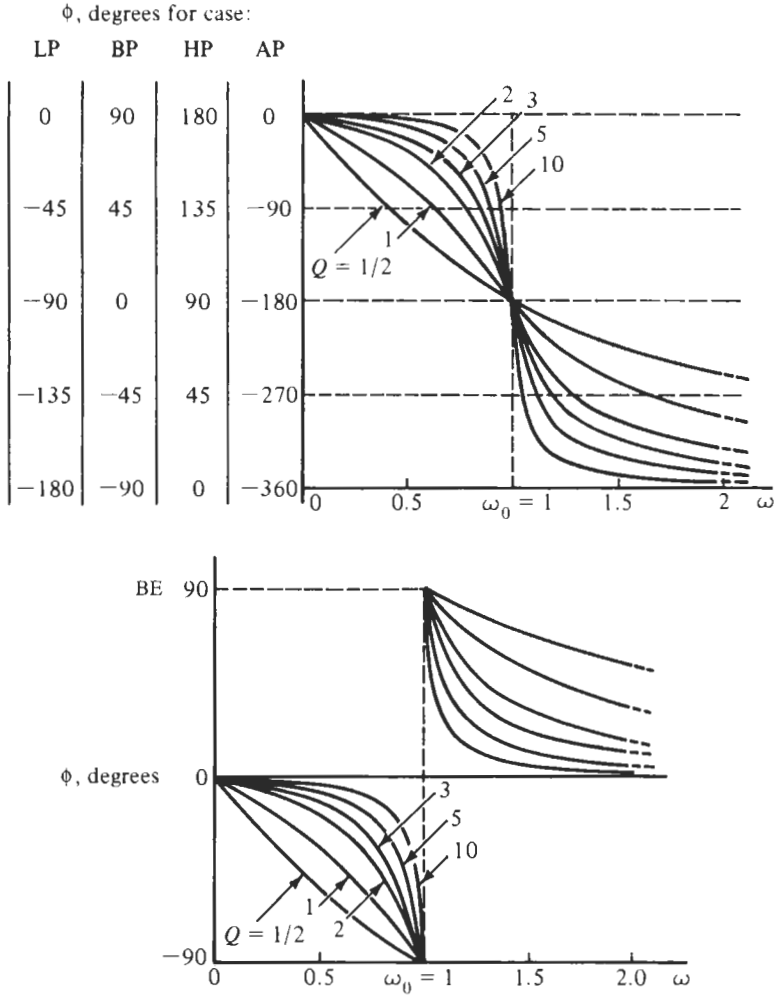

Figure 5.10 The phases of the most common second-order filters.

We next discuss the second method for the creation of transmission zeros, feeding the input signal into different nodes in the circuit.

5.2 BY VOLTAGE FEEDFORWARD

Poles are the *natural frequencies* of a system and we recall from mathematics or elementary circuits courses that the natural frequencies of a system are determined when the excitation is zero. In our situation, circuit analysis, this means all inputs are set to zero. This insight provides us with the clue on how to generate the needed inputs. For achieving some desired polynomial $N(s)$ in Eq. (5.1) without disturbing the roots of $D(s)$, the poles, we must feed the input voltages to the circuit in such a fashion that the core pole-generating circuit is restored when the inputs are set to zero. Figure 5.11 illustrates how this can be done. The figure shows a part of a circuit, with two admittances displayed explicitly. We may now *feed an input into*

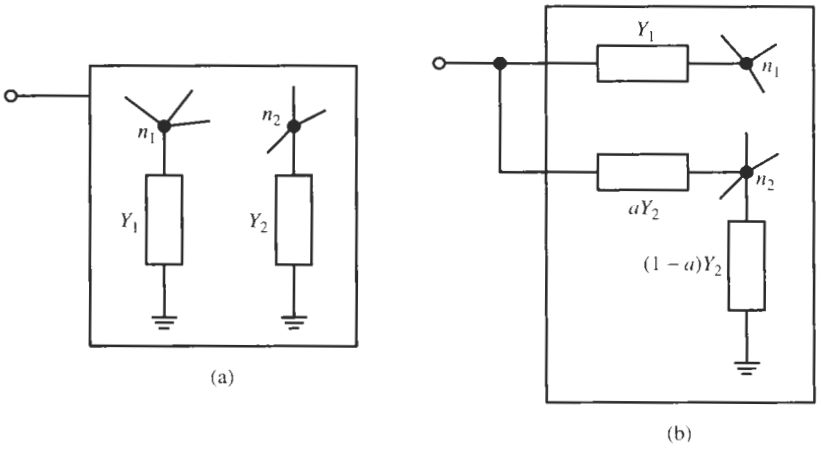

Figure 5.11 (a) Part of a zero-input pole-generating circuit with two components connected between nodes n_1 and n_2, respectively, and ground. (b) Y_1 is lifted off ground completely and connected to the input; Y_2 is lifted off ground partially and connected to the input.

the node created by lifting any element completely or partially off ground. The meaning of his statement is illustrated in Fig. 5.12 on a simple *RLC* bandpass filter circuit. The transfer function realized is

$$\frac{V_2}{V_1} = \frac{G}{sC + G + \dfrac{1}{sL}} = \frac{sLG}{s^2LC + sLG + 1} \tag{5.25}$$

and we observe that the poles are generated by the *RLC* parallel circuit in Fig. 5.12b with admittance $Y(s) = sC + 1/(sL) + G$. The bandpass circuit in Fig. 5.12a was obtained by lifting G *completely* off ground and feeding the input voltage into the resulting node. Similarly, leaving $R = 1/G$ connected to ground but lifting the capacitor and the inductor *partially* off ground with the parts aC and L/b connected to the input as shown in Fig. 5.12c, we obtain the node equation

$$(V_1 - V_2)\left(saC + \frac{b}{sL}\right) = V_2\left[s(1-a)C + \frac{1-b}{sL} + G\right] \tag{5.26}$$

It can be solved for

$$\frac{V_2}{V_1} = \frac{saC + \dfrac{b}{sL}}{sC + \dfrac{1}{sL} + G} = \frac{s^2aLC + b}{s^2LC + sLG + 1} \tag{5.27}$$

and is seen to be a band-rejection function with transmission zeros at $s = \pm j\sqrt{b/(aLC)}$. Note that both the bandpass and the band-rejection function have the same poles as the generating network, the admittance $Y(s)$ of the parallel *RLC* circuit in Fig. 5.12b. Using the same method we can generate a lowpass: select $a = 0$, that is, leave C connected to ground. The fraction b of the inductor that is connected to the input determines the dc gain.

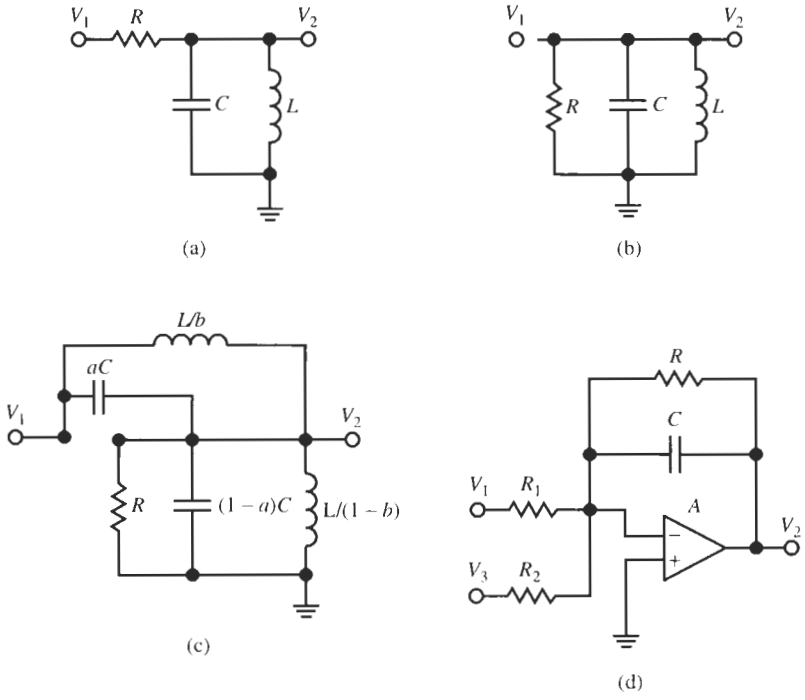

Figure 5.12 (a) *RLC* bandpass filter; (b) the pole-generating *RLC* parallel connection; (c) L and C partially lifted off ground; (d) opamp circuit.

In the circuits addressed in this book, active RC filters, an additional input is available to us that can be used without changing the poles. We may feed the input signal into the *virtual ground* node of an opamp. Assuming an ideal opamp so that the inverting input terminal voltage is zero, $V_- = 0$, the circuit in Fig. 5.12d realizes

$$V_2 = \frac{V_1 G_1 + V_3 G_2}{sC + G} \tag{5.28}$$

Clearly, whether the additional input V_3 is applied or not, the pole does not change. To summarize, the zero-generating method simply states:

In active filters new transmission zeros can be created by feeding the input into any virtual ground node or into any node created by lifting a component completely or partially off ground.

This manner of zero generation is usable for arbitrary filter structures; we will in the following present the method on the Åckerberg–Mossberg, the Delyiannis–Friend, and the GIC circuits.

Consider the circuit in Fig. 5.13. It is an Åckerberg–Mossberg filter that we endeavor to convert into a full biquad with arbitrary transmission zeros by feeding the input signal V_1 through new elements into all the virtual ground nodes in the circuit as shown. We propose to use V_2 as the output and have again assumed equal capacitors C. Also, recalling the earlier

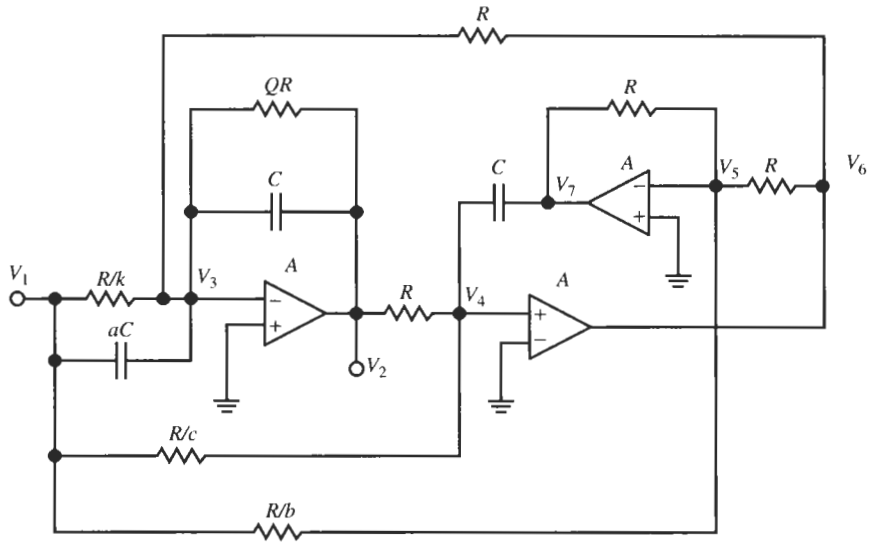

Figure 5.13 The general Åckerberg–Mossberg biquad.

discussion of the Åckerberg–Mossberg circuit, we have labeled the resistors in a manner that is convenient for the analysis without giving up any design freedom. The analysis proceeds by writing node equations at the summing nodes labeled V_3, V_4, and V_5. Assuming ideal opamps so that the voltages at these nodes are zero, we obtain

$$\begin{aligned} V_1(saC + kG) + (sC + G/Q)V_2 + GV_6 &= 0 \\ cGV_1 + GV_2 + sCV_7 &= 0 \\ GV_6 + GV_7 + bGV_1 &= 0 \end{aligned}$$

Let us still call $CR = 1/\omega_0$ and we obtain from these equations

$$(s + \omega_0/Q)\, V_2 + V_1\,(sa + k\omega_0) + \omega_0 V_6 = 0 \tag{5.29}$$

$$c\omega_0 V_1 + \omega_0 V_2 + sV_7 = 0 \tag{5.30}$$

$$V_6 + V_7 + bV_1 = 0 \tag{5.31}$$

Solving the equations for the transfer function $T(s) = V_2/V_1$ results in

$$T(s) = -\frac{as^2 + s\omega_0(k - b) + c\omega_0^2}{s^2 + s\omega_0/Q + \omega_0^2} \tag{5.32}$$

$T(s)$ is seen to be a full biquadratic function that can realize zeros anywhere in the s-plane. Specifically, we obtain the standard functions by choosing the constants k, a, b, and c as given in Table 5.3.

We see that the design of filters with the circuit in Fig. 5.13 is very straightforward. We simply determine the value of R for given capacitor C and frequency f_0, select the value of the resistor QR to realize the specified Q, and pick the parameters a, b, c, and k to realize

TABLE 5.3 Parameter Choice to Define the Filter Type for Eq. (5.32)[a]

Filter Type	a	b	c	k	Comments
Highpass	a	0	0	0	a sets the high-frequency gain
Lowpass	0	0	c	0	c sets the low-frequency gain
Bandpass	0	b	0	b	$b = 0$ if inverting bandpass $k = 0$ if noninverting bandpass
Allpass	1	$1/Q$	1	0	
Notch	1	0	1	0	
Highpass notch	a	0	$< a$	0	a sets the high-frequency gain c sets the low-frequency gain
Lowpass notch	a	0	$> a$	0	a sets the high-frequency gain c sets the low-frequency gain

[a]In all cases $R = 1/(\omega_0 C)$.

the required function type. The circuit is as versatile as the four-amplifier biquad in Fig. 5.1, uses one opamp less, and is insensitive to careful component matching and tuning for realizing the numerator coefficients as was necessary for Eq. (5.5). In practice, the opamp summer, however, has the advantage of suppressing any peaking at high frequencies caused by the frequency dependence of the amplifier gain, $A(s)$. Let us illustrate the design process with a couple of examples.

EXAMPLE 5.6

Repeat the highpass design of Example 5.1 with the circuit in Fig. 5.13. Use LM741 opamps.

Solution

The highpass filter's cut-off frequency was 42 kHz and the quality factor $Q = 3$. The gain at high frequencies was specified as 6 dB, and the circuit was required to operate to at least 200 kHz before noticeable high-frequency roll-off.

Choosing $C = 10$ nF, we have

$$R = \frac{1}{\omega_0 C} = \frac{1}{2\pi \times 42 \text{ kHz} \times 10 \text{ nF}} = 379\ \Omega$$

and $QR = 1.137$ kΩ. Next we need to determine the feed-in coefficients. With $b = c = k = 0$ and $a = 2$ to implement the high-frequency gain of 6 dB, we have the resistor and capacitor values in the circuit in Fig. 5.14, which also shows the tested performance.

We make a few observations: As done in earlier examples, we have rounded the elements to make the circuit practical. The gain is > 6 dB until approximately 660 kHz (cursor), with a 3.5-dB peaking observed at ≈ 380 kHz. This is caused by the nonideal opamps. But because no summer is used, the summer's lowpass behavior is not encountered. The peak at 16.9 dB represents $Q \approx 3.5$. If required, this value can be reduced by tuning the resistor QR. This circuit has, of course, no parasitic low-frequency transmission zero because no sensitive adjustment of resistors is required: the coefficients of s^0 and s^1 are exactly zero by setting $b = c = k = 0$. At low frequencies, the gain decreases to below −120 dB.

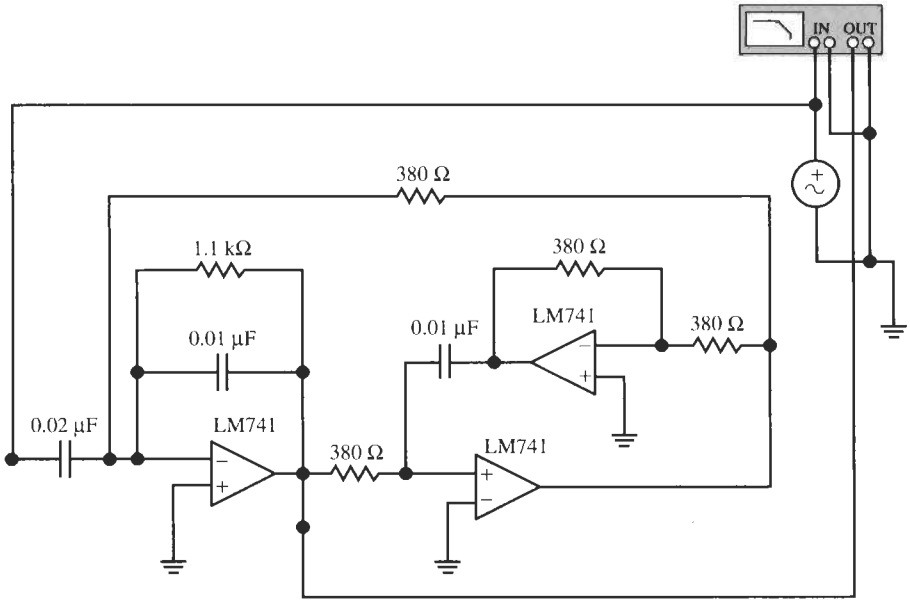

(a)

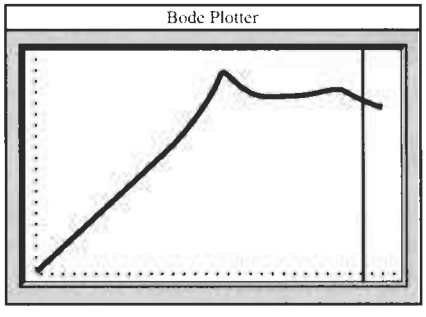

(b)

Figure 5.14 The highpass circuit of Example 5.6 and its performance. (Bode Plotter scales: 1 kHz to 1 MHz; −60 to +20 dB; cursor at 661 kHz, 6.28 dB.)

EXAMPLE 5.7

Design a lowpass notch filter to meet the specifications of Example 5.5: 3-dB low-frequency gain and −30-dB loss at high frequencies. The lowpass passband must be flat with the band edge at $f = 280$ Hz. Use LM741 opamps.

Solution

The function of Eq. (5.32) is used with $k = b = 0, a = 10^{-30/20} = 0.0316$ (corresponding to −30-dB), and $c = 1.414$ (+3 dB). To satisfy the flat passband requirement, we choose again $Q = 0.8$. The pole frequency is at the band edge, 280 Hz. Using $C = 0.3\ \mu$F, we find

$R = 1.9\ \text{k}\Omega$ and $QR_2 = 1.52\ \text{k}\Omega$. The lowpass notch circuit and its performance are shown in Fig. 5.15. The transmission zero is at 1.9 kHz ($= f_0\sqrt{c/a}$) as expected.

The design is seen to be easy; no careful matching of resistors is required and one opamp is saved compared to the circuit in Example 5.5. We notice a rise in gain at higher frequencies (beyond 30 kHz) caused by the nonideal opamps. This peaking was avoided in Example 5.5 because the lowpass behavior of the summer suppressed it.

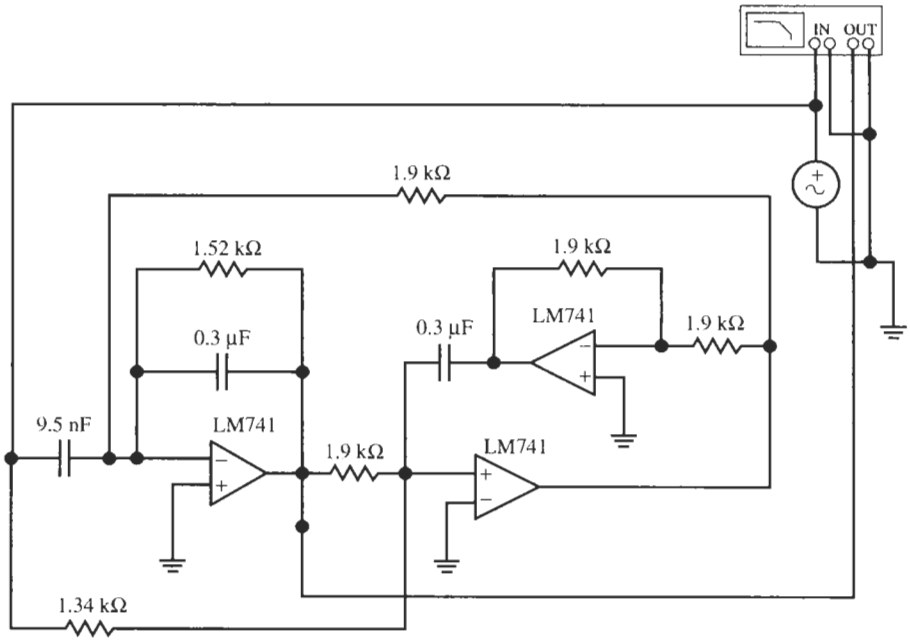

(a)

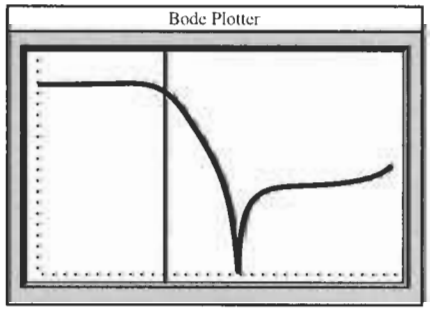

(b)

Figure 5.15 The lowpass notch filter of Example 5.7 and test results. (Bode Plotter scales: 10 Hz to 100 kHz; −60 to +10 dB; cursor at 292 kHz, 0.45 dB.)

Let us consider next whether a general biquad can be constructed from the GIC circuit in Fig. 4.41. The circuit is repeated in Fig. 5.16 with all available grounded components split into a part connected to the input and a part remaining at ground. We also have labeled all

capacitors as C and all resistors, with the exception of the one determining the quality factor, as R because we found earlier that this was the optimum choice. To analyze the circuit, we write Kirchhoff's current law at the nodes labeled V_5, V_4, and V_6 and assume ideal opamps so that $V_4 = V_5 = V_6$. We obtain

$$2GV_6 = cGV_1 + GV_2$$
$$(G + sC)V_4 = GV_2 + sCV_3$$
$$(G + G/Q + sC)V_5 = (bG/Q + asC)V_1 + GV_3$$

Calling again $\omega_0 = 1/(CR)$, and using that $V_4 = V_5 = V_6$, these equations become

$$2V_4 = cV_1 + V_2 \tag{5.33}$$
$$(\omega_0 + s)\, V_4 = \omega_0 V_2 + sV_3 \tag{5.34}$$
$$[\omega_0(1 + 1/Q) + s]V_4 = (b\omega_0/Q + as)\, V_1 + \omega_0 V_3 \tag{5.35}$$

Solving for the transfer function $T(s) = V_2/V_1$ results in

$$T(s) = \frac{V_2}{V_1} = \frac{s^2(2a - c) + s\,(\omega_0/Q)\,(2b - c) + c\omega_0^2}{s^2 + s\omega_0/Q + \omega_0^2} \tag{5.36}$$

We observe that Eq. (5.36) can realize an arbitrary transfer function with zeros anywhere in the s-plane. Table 5.4 shows the parameter values necessary.

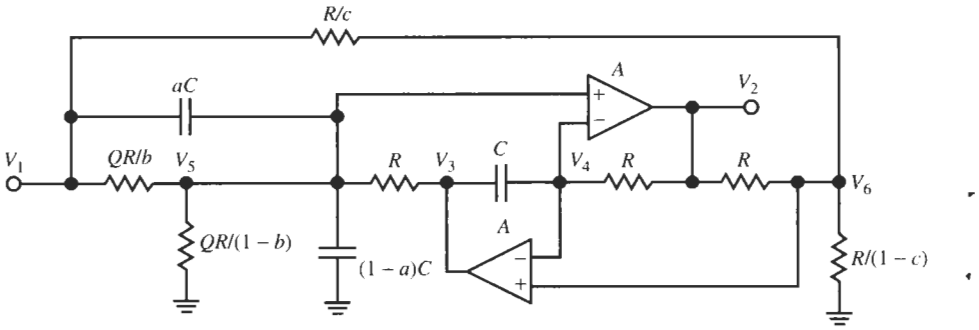

Figure 5.16 A general biquad based on the GIC circuit.

TABLE 5.4 Parameter Choice to Define the Filter Type for Eq. (5.36)[a]

Filter type	a	b	c	Comments
Highpass	a	0	0	$2a$ sets the high-frequency gain
Lowpass	$c/2$	$c/2$	c	c sets the low-frequency gain
Bandpass	0	b	0	$2b$ sets the bandpass gain
Allpass	1	0	1	
Notch	1	1/2	1	
Highpass notch	$a > c$	$c/2$	c	c sets the low-frequency gain $(2a - c)$ sets the high-frequency gain
Lowpass notch	$a < c$	$c/2$	c	c sets the low-frequency gain $(2a - c)$ sets the high-frequency gain

[a]In all cases $R = 1/(\omega_0 C)$.

EXAMPLE 5.8

Design the notch filter of Example 5.2 with the GIC biquad of Fig. 5.16. To be eliminated is the frequency component at $f_0 = 830$ Hz from a signal. The low- and high-frequency gains must be 0 dB and the attenuation must not be larger than 1 dB in a band of width 100 Hz around f_0. Use the circuit in Fig. 5.16 built with $C = 0.1$ μF capacitors and LM741 opamps.

Solution

The circuit in Fig. 5.16 with $a = c = 1$ and $b = 0.5$ realizes

$$T(s) = \frac{V_2}{V_1} = \frac{s^2 + \omega_0^2}{s^2 + s\omega_0/Q + \omega_0^2}$$

As in Example 5.2, with $C = 0.1$ μF we find $R = 1/(\omega_0 C) = 1.918$ kΩ. The required loss of less than 1 dB in a band $\Delta f = 100$ Hz around f_0 results in

$$q = 10^{1/20} = 1.122$$

so that Eq. (5.9) yields

$$Q = \frac{f_0}{\Delta f\sqrt{1.2589 - 1}} = 16.3$$

This value gives $QR = 31.3$ kΩ.

The circuit and test results are shown in Fig. 5.17. The sharp notch with attenuation -61 dB is at 828 Hz (measured at higher resolution) and the -1-dB band reaches from 781 to 882 Hz. The high-frequency gain can be measured to increase to $+3$ dB at approximately 700 kHz due to the finite bandwidth of the opamps. The gain decreases again to low levels after approximately 1 MHz.

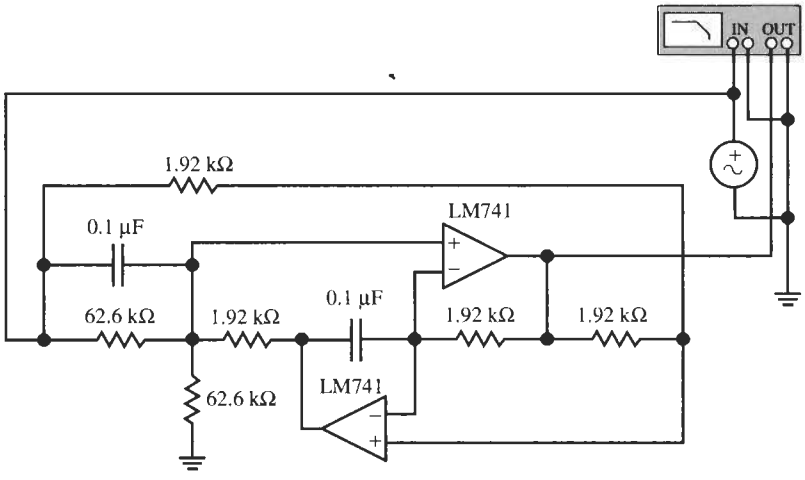

(a)

Figure 5.17 The notch filter design for Example 5.8 and test results. (Bode Plotter scales: 700 Hz to 1kHz; -40 to 0 dB; cursor at 782 Hz, -1.01 dB.)

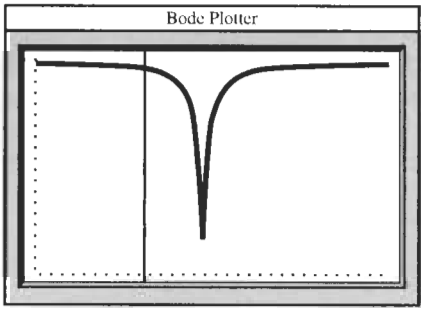

(b)

Figure 5.17 Continued

The following example serves again as a reminder that basing the design of active *RC* filters on ideal operational amplifiers can cause serious discrepancies between expectation and practice. Unless experience has proven the reliable behavior of a design, careful simulation, or better yet, experiments should be conducted to verify performance.

EXAMPLE 5.9

Use the circuit in Fig. 5.16 to design a lowpass filter with 0-dB passband gain, cut-off frequency 890 Hz, and a quality factor of 0.707.

Solution

From Table 5.4 we find the parameters $c = 1$ and $a = b = 0.5$. The transfer function to be realized is then

$$T(s) = \frac{V_2}{V_1} = \frac{\omega_0^2}{s^2 + s\omega_0/Q + \omega_0^2}$$

Using $C = 0.1\ \mu$F with two 0.05-μF capacitors in parallel to realize $a = 0.5$ results in $R = 1.788$ kΩ and $QR = 1.265$ kΩ, which is split into two 2.53-kΩ resistors in parallel to realize $b = 0.5$. Figure 5.18 shows the circuit, and simulation and test results.

We notice that under the assumption of *ideal* (or extremely fast) opamps, the circuit behaves exactly as specified (Fig. 5.18b), with an attenuation increase at 40 dB per decade. Because we are concerned about practical designs we test the circuit with real opamps (LM741, $f_t = 1.5$ MHz). We find that the 0-dB passband and the cut-off frequency are maintained, and that the attenuation increases as before for $f > 900$ Hz, but the gain increases again after only 11 kHz at the rate of 20 dB per decade (Fig. 5.18c). Recalling our discussion of Bode plots in Chapter 3, this behavior suggests a zero of multiplicity three at approximately 11 kHz. Evidently, this behavior is caused by the opamps and we need to determine the reason so that corrective measures may possibly be taken. Straightforward although laborious analysis of the circuit in Fig. 5.18a with finite opamp gain $A(s)$ leads to the complete transfer function. We shall not concern ourselves with the details, but just note that for frequencies $f \gg f_0$ the numerator is modified from ω_0^2 to $\omega_0^2 + s^2/A(s)$. Using the integrator model of the opamp, Eq. (2.18), we find, therefore, that the numerator becomes

$$N(s) \approx \omega_0^2 + s^3/\omega_t$$

that is, there is indeed a triple zero at

$$f^3 \approx f_0^3 \frac{f_t}{f_0}, \quad \text{or} \quad f \approx f_0 \sqrt[3]{|A(j\omega_0)|}$$

Unfortunately, for given opamps the designer has no control over the location of this zero; it is located a factor of $\sqrt[3]{|A(j\omega_0)|}$ beyond the specified cut-off frequency. In the present case, with $f_0 = 890$ Hz and $f_t = 1.5$ MHz, we have $f = f_0 \sqrt[3]{|A(j\omega_0)|} = 890\sqrt[3]{1500/0.89} \approx 10.6$ kHz. The test result in Fig. 5.18c is a close approximation of this value. Even a high-frequency opamp such as the HA 2542-2 with a gain-bandwidth product of 90 MHz places the triple zero to only 47 kHz, too low for most applications. We conclude that the GIC circuit is not a good choice for building lowpass filters because the factor $\sqrt[3]{|A(j\omega_0)|}$ is as a rule too small for separating parasitic behavior from the useful frequency range.

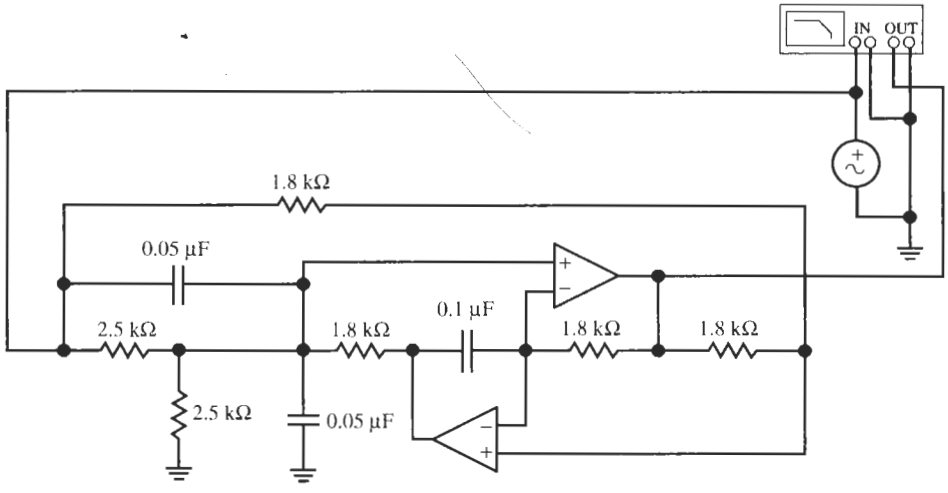

(a)

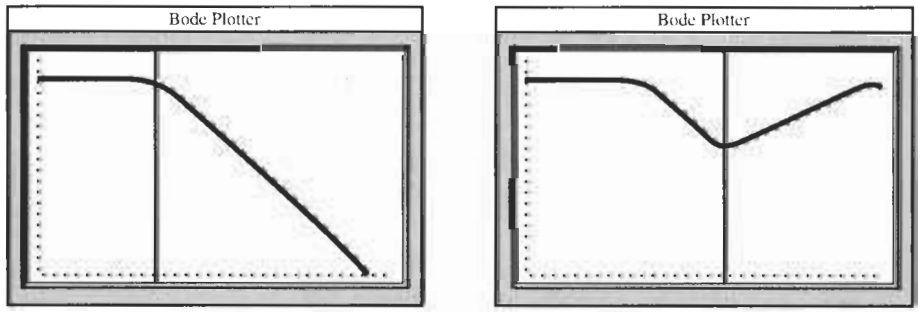

(b) (c)

Figure 5.18 (a) The lowpass filter design for Example 5.9; (b) results for operation with *ideal* opamps; (c) test results with *real* opamps. (Bode Plotter scales for b: +20 Hz to 1.5 MHz; −120 to +10 dB; cursor at 859 Hz, −2.93 dB. Bode Plotter scales for c: 20 Hz to 1.5 MHz; −120 to +10 dB; cursor at 10.7 kHz, −40.3 dB.)

Let us next consider the Delyiannis–Friend bandpass circuit of Fig. 4.37 as a general biquad. We split already the conductor G_1 into aG_1 and $(1-a)G_1$ to be able to adjust the gain; the other grounded component available to us is the resistor KR, which we split as shown in Fig. 5.19. To analyze the circuit, we write node equations and obtain

$$V_+\left(\frac{G}{1-K}+\frac{(1-b)G}{K}+\frac{bG}{K}\right)=\frac{bG}{K}V_1+\frac{G}{1-K}V_2$$

or

$$V_+ = b(1-K)V_1 + KV_2 \tag{5.37}$$

At the inverting opamp input we have

$$V_-(sC+G_2) = V_x sC + G_2 V_2 \tag{5.38}$$

and at the node marked V_x,

$$V_x[aG_1+(1-a)G_1+2sC] = aG_1V_1 + sCV_- + sCV_2 \tag{5.39}$$

Assuming that the opamp is ideal, $A=\infty$, we set $V_- = V_+$ and eliminate the internal voltage V_x from the equations. The result is

$$\begin{aligned} T(s)=\frac{V_2}{V_1} &= b\frac{s^2+s\dfrac{2G_2}{C}\left[1+\dfrac{G_1}{2G_2}\left(1-\dfrac{a/b}{1-K}\right)\right]+\dfrac{G_1G_2}{C^2}}{s^2+s\dfrac{2G_2}{C}\left(1-\dfrac{G_1}{2G_2}\dfrac{K}{1-K}\right)+\dfrac{G_1G_2}{C^2}} \\ &= b\frac{s^2+s\dfrac{\omega_0}{Q_0}\left[1+2Q_0^2\left(1-\dfrac{a/b}{1-K}\right)\right]+\omega_0^2}{s^2+s\dfrac{\omega_0}{Q_0}\left(1-2Q_0^2\dfrac{K}{1-K}\right)+\omega_0^2} \end{aligned} \tag{5.40}$$

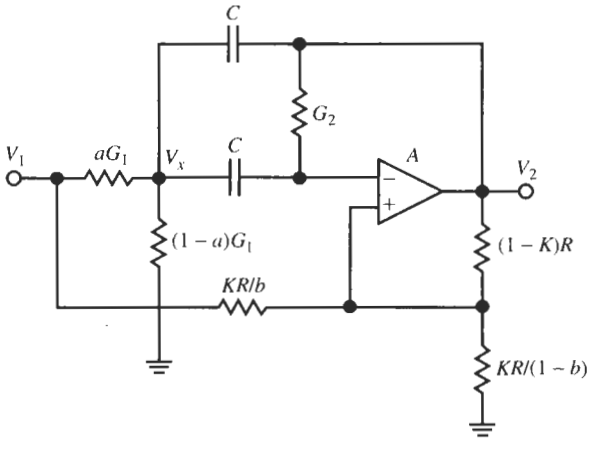

Figure 5.19 The Delyiannis–Friend circuit of Fig. 4.37 with all grounded components used to generate additional input terminals.

As a check on our algebra we note that for $b = 0$ this function is reduced to the bandpass function of Eq. (4.137) with $A = \infty$, ω_0 and Q_0 were defined in Eq. (4.130) as

$$\omega_0 = 1/\left(C\sqrt{R_1 R_2}\right) \quad \text{and} \quad Q_0 = 0.5\sqrt{R_2/R_1} \tag{5.41}$$

A nearly optimal value of Q_0 was found in Eq. (4.142) to be $Q_0 = 1.5$ so that the quality factor of the filter is

$$Q = \frac{1.5}{1 - 4.5\dfrac{K}{1-K}} \tag{5.42}$$

with K determined for a specified Q by

$$K = \frac{1}{1 + \dfrac{4.5}{1 - 1.5/Q}} < 1 \tag{5.43}$$

Because of the lack of available parameters in Eq. (5.40), lowpass and highpass functions cannot be realized with Eq. (5.40); neither can we build lowpass and highpass notch filters. But an allpass function, a notch, a gain dip, and a gain boost can be obtained depending on how the term

$$1 + 2Q_0^2\left(1 - \frac{a/b}{1-K}\right)$$

in the numerator of Eq. (5.40) is determined. If we evaluate

$$|T(j\omega_0)| = b\left|\frac{-\omega_0^2 + j\dfrac{\omega_0^2}{Q_0}\left[1 + 2Q_0^2\left(1 - \dfrac{a/b}{1-K}\right)\right] + \omega_0^2}{-\omega_0^2 + j\dfrac{\omega_0^2}{Q_0}\left(1 - 2Q_0^2\dfrac{K}{1-K}\right) + \omega_0^2}\right| = b\frac{1 + 2Q_0^2\left(1 - \dfrac{a/b}{1-K}\right)}{1 - 2Q_0^2\dfrac{K}{1-K}}$$

and set the result equal to a value p, $|T(j\omega_0)| = p$, as in Eq. (5.14), we obtain

$$\frac{p}{b} = \frac{1 + 2Q_0^2\left(1 - \dfrac{a/b}{1-K}\right)}{1 - 2Q_0^2\dfrac{K}{1-K}}$$

This equation is solved for the design parameter a:

$$a = Kp + (1-K)\left(b + \frac{b-p}{2Q_0^2}\right) \tag{5.44}$$

For given pole quality factor, p determines the linear coefficient in the numerator of Eq. (5.40). It is obtained from the following table for different filter types.

Filter Type	p	Comments
Allpass	$p/b = -1$	
Notch	$p/b = 0$	
Dip	$p/b < 1$	p is the value of the dip at $f = f_0$
Boost	$p/b > 1$	p is the value of the boost at $f = f_0$

Equation (5.44) determines what fractions a and b of the two resistors R_1 and KR are to be connected to the input. Note that only the parameter a is determined, leaving b free to set the gain. As illustrations of the design of these single-amplifier biquads, let us build a notch filter and a gain equalizing circuit having a gain boost.

EXAMPLE 5.10

Repeat the notch filter design of Example 5.8 with a single-amplifier biquad using an LM741 opamp.

Solution

The notch filter was to eliminate the frequency component at $f_0 = 830$ Hz from a signal. At $f = 0$ and $f = \infty$, a gain of 0 dB was prescribed; the attenuation had to be less than 1 dB in a band of width 100 Hz around f_0. We use the circuit in Fig. 5.19 with a/b from Eq. (5.44) and $p = 0$ to realize

$$T(s) = b\frac{s^2 + \omega_0^2}{s^2 + s\dfrac{\omega_0}{Q_0}\left(1 - 2Q_0^2\dfrac{K}{1-K}\right) + \omega_0^2}$$

$b = 1$ to realize a 0-dB gain at the extreme frequencies. With $Q_0 = 1.5$ and $C = 0.1\ \mu$F we find from Eq. (5.41)

$$R_2 = 9R_1 \quad \text{and} \quad R_1R_2 = 1/(\omega_0 C)^2 = (1.918\ \text{k}\Omega)^2$$

Thus, we have $R_1 = 639\ \Omega$ and $R_2 = 5.753\ \text{k}\Omega$. As in Example 5.2, the required loss of less than 1 dB in a band $\Delta f = 100$ Hz around f_0 results in

$$q = 10^{1/20} = 1.122$$

so that Eq. (5.9) yields

$$Q = \frac{f_0}{\Delta f\sqrt{1.2589 - 1}} = 16.3$$

We find from Eq. (5.43) and Eq. (5.44) with $p = 0$

$$K = \frac{1}{1 + \dfrac{4.5}{1 - 1.5/16.3}} = 0.1679, \quad \frac{a}{b} = (1-K)\frac{1 + 2Q_0^2}{2Q_0^2} = 1.0170$$

with $b = 1$. This is not realizable since $a \leq 1$ is required for positive resistor values. Let us deviate from the design specs, choose $a = 1$, and accept $b = 1/1.017 = 0.983$ giving us a

0.146-dB loss at $f = 0$ and ∞. We choose arbitrarily $R = 10$ kΩ. The circuit and test results are shown in Fig. 5.20. The flat loss away from the notch is about −0.15 dB as designed; the sharp notch with attenuation −55 dB is at 841 Hz (measured at higher resolution). The notch depth can be tuned by adjusting b (the 1.75-kΩ resistor), and the −1-dB band reaches from 791 to 902 Hz. The attenuation can be measured to increase from 0 to −3 dB at approximately 1.3 MHz due to the finite bandwidth of the opamp [$f_{-3\,\mathrm{dB}} \approx f_t/(1 + K)$].

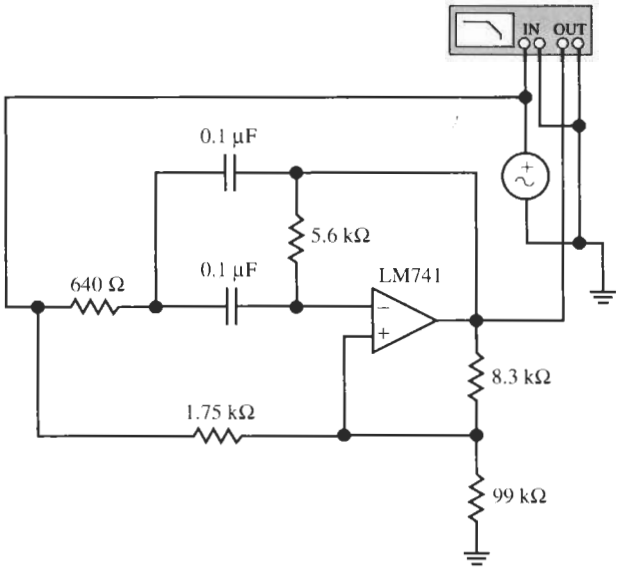

(a)

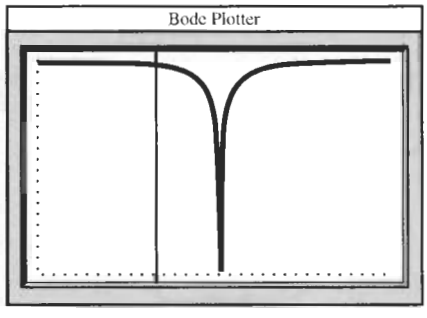

(b)

Figure 5.20 The notch filter design for Example 5.10 and test results. (Bode Plotter scales: 700 Hz to 1kHz; −60 to 0 dB; cursor at 789 Hz, −0.98 dB.)

EXAMPLE 5.11

To compensate the loss caused elsewhere in a transmission channel, a filter with 0-dB overall gain, but a gain boost of 6 dB at the frequency 12 kHz, is required to equalize the signal level. The gain boost should equal at least 2 dB in a band $\Delta f = 4$ kHz. Use the circuit in Fig. 5.19, with $C = 0.01$ μF capacitors and an LM741 opamp.

Solution

As required, we use the circuit in Fig. 5.19 realizing

$$T(s) = b\frac{s^2 + s\frac{\omega_0}{Q_0}\left[1 + 2Q_0^2\left(1 - \frac{a/b}{1-K}\right)\right] + \omega_0^2}{s^2 + s\frac{\omega_0}{Q_0}\left(1 - 2Q_0^2\frac{K}{1-K}\right) + \omega_0^2}$$

with a/b from Eq. (5.44) and $p = 2$ (corresponding to a 6-dB gain boost). According to Eq. (5.41) we have

$$R_2 = 9R_1 \quad \text{and} \quad R_1 R_2 = 1/(\omega_0 C)^2 = (1.326\ \text{k}\Omega)^2$$

Thus, $R_1 = 442\ \Omega$ and $R_2 = 3.979\ \text{k}\Omega$. The required > 2-dB gain in a band $\Delta f = 4$ kHz around f_0 results in

$$q = 10^{-2/20} = 0.7943$$

and the specified value $p = 2$ yields from Eq. (5.16)

$$Q = \frac{12}{4}\sqrt{\frac{(2 \times 0.7943)^2 - 1}{1 - 0.6310}} = 6.096$$

For this value of Q we find from Eq. (5.43)

$$K = \frac{1}{1 + \frac{4.5}{1 - 1.5/6.096}} = 0.1435$$

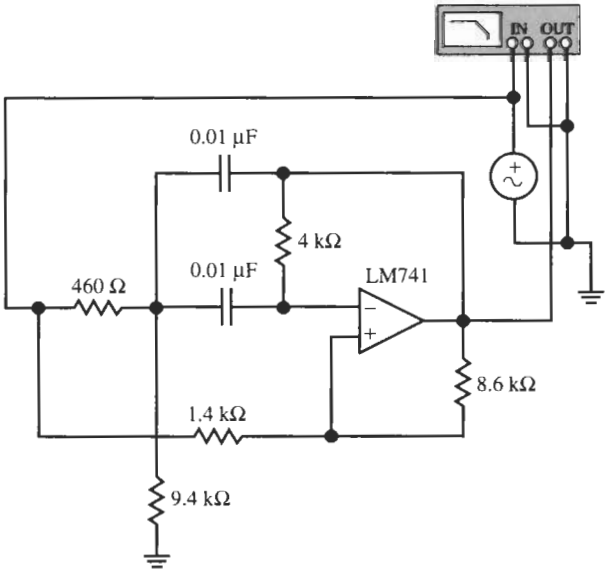

(a)

Figure 5.21 The magnitude equalizer design for Example 5.11 and test results. (Bode Plotter scales: 6 to 25 kHz; −20 to 10 dB; cursor at 11.8 kHz, 5.92 dB.)

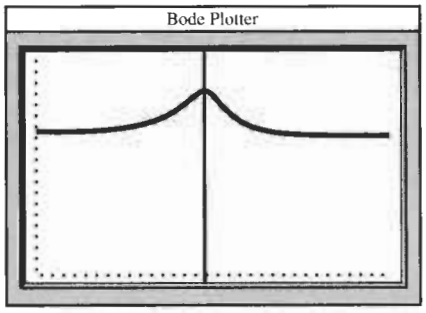

(b)

Figure 5.21 Continued

Let us set $b = 1$ (0 dB at the extreme frequencies); then we obtain from Eq. (5.44)

$$a = 2 \times 0.1435 + (1 - 0.1435)\left(1 + \frac{1-2}{4.5}\right) = 0.9532$$

R is chosen arbitrarily as 10 kΩ. The circuit and test results are shown in Fig. 5.21. The peak gain is 5.92 dB at 11.8 kHz; the 2-dB band is between 9.83 and 13.7 kHz. As in the previous example, the attenuation increases to −3 dB at approximately 1.3 MHz due to the finite bandwidth of the opamp.

We have seen that only lowpass, highpass, and lowpass and highpass notch functions can be realized via the Delyiannis–Friend circuit in Fig. 5.19 because the number of signal feed-in points was limited. To expand our options we return to the Sallen–Key filter of Fig. 4.31b where more grounded elements are available to generate possible signal inputs. The circuit is shown in Fig. 5.22. As done for the Sallen–Key circuit we write node equations for the nodes labeled V_-, V_a, and V_b to obtain

$$V_- = \frac{1}{K}V_2 + c\frac{K-1}{K}V_1 = \frac{1}{K}V_2 + c_k V_1$$

where c_k is defined as

$$c_k = c\frac{K-1}{K} \tag{5.45}$$

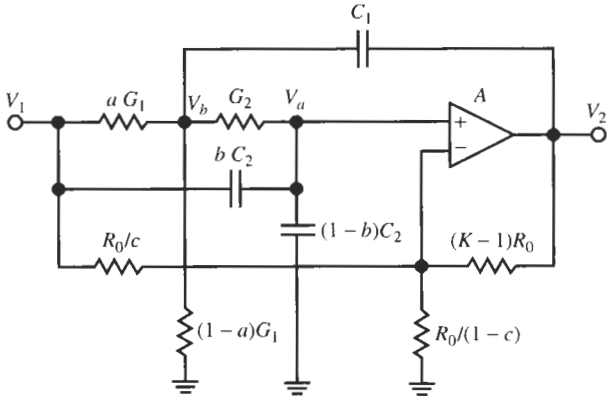

Figure 5.22 A general biquad based on the Sallen–Key filter of Fig. 4.32b.

Further

$$V_a(sC_2R_2 + 1) = V_b + bsC_2R_2V_1$$
$$V_b(sC_1R_1 + 1 + R_1G_2) = sC_1R_1V_2 + R_1G_2V_a + aV_1$$

If we assume finite opamp gain A, we have

$$V_a - V_- = V_2/A$$

Solving these equations for the transfer function yields

$$T(s) = \frac{V_2}{V_1}$$
$$= -\frac{K}{1 + K/A} \frac{s^2(c_k - b) + s\left[\dfrac{G_1 + G_2}{C_1}(c_k - b) + c_k\dfrac{G_2}{C_2}\right] + (c_k - a)\dfrac{G_1G_2}{C_1C_2}}{s^2 + s\left[\dfrac{G_1 + G_2}{C_1} + \dfrac{G_2}{C_2}\left(1 - \dfrac{K}{1 + K/A}\right)\right] + \dfrac{G_1G_2}{C_1C_2}} \tag{5.46}$$

We wrote this equation in its general form to be able to check that the denominator is identical to the one in Eq. (4.99), which means that the poles did not change. The dependence of the function on finite opamp gain is also the same as in Eq. (4.99) so that the resulting errors can be computed as in Eqs. (4.113) to (4.116). We assume in the following $|A| = \infty$. As we did for the Sallen–Key circuit in Section 4.5.1, let us now make the practically convenient choices

$$C_1 = C_2 = C, \quad \text{and} \quad R_1 = R_2 = R$$

and set

$$\omega_0 = 1/(CR), \quad Q = 1/(3 - K) \tag{5.47}$$

The transfer function then takes on the simpler form

$$T(s) = \frac{V_2}{V_1} = \frac{N(s)}{D(s)} = -K\frac{s^2(c_k - b) + s\omega_0(3c_k - 2b) + (c_k - a)\omega_0^2}{s^2 + s\omega_0/Q + \omega_0^2} \tag{5.48}$$

We observe that the circuit can implement an arbitrary biquadratic function

$$T(s) = -\frac{s^2k_2 + sk_1 + k_0}{s^2 + s\omega_0/Q + \omega_0^2}$$

by appropriate choice of the coefficients a, b, and c as shown in Table 5.5. We comment here that although all types of second-order functions can be obtained, this circuit is important only for the lowpass and highpass notch filters. The remaining functions are more easily realized with fewer components and component matching requirements from the Sallen–Key circuits of Figs. 4.31b and 4.33, or the Delyiannis–Friend circuits of Figs. 4.37 and 5.19.

Because the fractions a, b, and c must be less than or at most equal to unity, we must be aware of some restrictions on the realizable filter parameters. For instance, consider the lowpass and highpass notch filters for which we have from Table 5.5 the transfer function

$$T(s) = K\frac{c_k}{2}\frac{s^2 + 2\dfrac{a - c_k}{c_k}\omega_0^2}{s^2 + s\omega_0/Q + \omega_0^2} \tag{5.49}$$

TABLE 5.5 Parameter Choice to Define the Filter Type for Eq. (5.48)[a]

Filter type	a	b	c	$N(s)$
Highpass	c_k	$3c_k/2$	c	$s^2Kc_k/2$
Lowpass	a	0	0	$aK\omega_0^2$
Bandpass	c_k	c_k	c	$s\omega_0Kc_k$
Allpass	$c_k\dfrac{3Q+1}{2Q+1}$	$c_k\dfrac{3Q+1}{2Q+1}$	c	$K(b-c_k)[s^2-s\omega_0/Q+\omega_0^2]$
Notch	$\dfrac{3c_k}{2}$	$\dfrac{3c_k}{2}$	c	$K(c_k/2)(s^2+\omega_0^2)$
Highpass notch	a	$\dfrac{3c_k}{2}$	c	$K\dfrac{c_k}{2}(s^2+2\dfrac{a-c_k}{c_k}\omega_0^2)$
Lowpass notch	a	$\dfrac{3c_k}{2}$	c	$K\dfrac{c_k}{2}(s^2+2\dfrac{a-c_k}{c_k}\omega_0^2)$

[a]In all cases $R = 1/(\omega_0 C)$. If the fractions a, b and c are not specified in columns 1 to 3, they are [with $c_k = c(K-1)/K$ from (Eq. (5.45)] determined from the listed numerator polynomials. Note that a, b, and $c \le 1$.

If we compare this expression with the general function of Eq. (5.1) we identify

$$k_2 = Kc_k/2, \quad \text{and} \quad k_0 = K(a-c_k)\omega_0^2$$

along with $b = 3c_k/2$ to make $k_1 = 0$. Consequently we find the constraints

$$a = \frac{k_0\omega_0^{-2}+2k_2}{K} \le 1, \quad b = \frac{3k_2}{K} \le 1, \quad c = \frac{2k_2}{K-1} \le 1 \tag{5.50}$$

The most restrictive one of these conditions must be satisfied if the circuit is to be realizable with positive component values. Alternatively, often specified are the notch frequency f_N

$$f_N = \sqrt{\frac{k_0}{k_2}} = f_0\sqrt{2\frac{a-c_k}{c_k}} = f_0\sqrt{\frac{aK}{k_2}-2}$$

and the constant k_2; in that case the constraint on a in Eq. (5.50) is replaced by

$$a = \left(2+\frac{f_N^2}{f_0^2}\right)\frac{k_2}{K} \le 1 \tag{5.51}$$

EXAMPLE 5.12

Use the circuit of Fig. 5.22 to realize a lowpass notch with 24-dB high-frequency attenuation and α-dB gain at low frequencies. The passband corner is specified to be 400 Hz; there is to be no peaking. Build the circuit with LM741 opamps and maximize α.

Solution

The transfer function is given in Eq. (5.49) with $b = 3c_k/2$. Choosing $C = 0.1\ \mu$F, the passband corner of 400 Hz results in $R = 1/(\omega_0 C) = 3.979\ \text{k}\Omega$. We found earlier (Fig.

4.13a) that no peaking is measured when $Q = 0.707$, that is, with Eq. (5.47), $K = 1.586$. The specified 24-dB high-frequency attenuation corresponds to $10^{-24/20} = 0.0631 = k_2$. With these numbers we have from Eq. (5.50)

$$a = \frac{k_0\omega_0^{-2} + 2 \times 0.0631}{1.586} \leq 1, \quad b = \frac{3 \times 0.0631}{1.586} = 0.1194, \quad c = \frac{2 \times 0.0631}{0.586} = 0.2154$$

We choose $a = a_{max} = 1$, which leads to the constraint $k_0\omega_0^{-2} \leq 1.46$ corresponding to 3.29-dB low-frequency gain. Choosing finally $R_0 = 10$ kΩ leads to the circuit in Fig. 5.23. The circuit function is as specified; the notch frequency is at ≈1.9 kHz as predicted by Eq. (5.51). Gain roll-off caused by the frequency-dependent opamp gain starts at approximately 700 kHz.

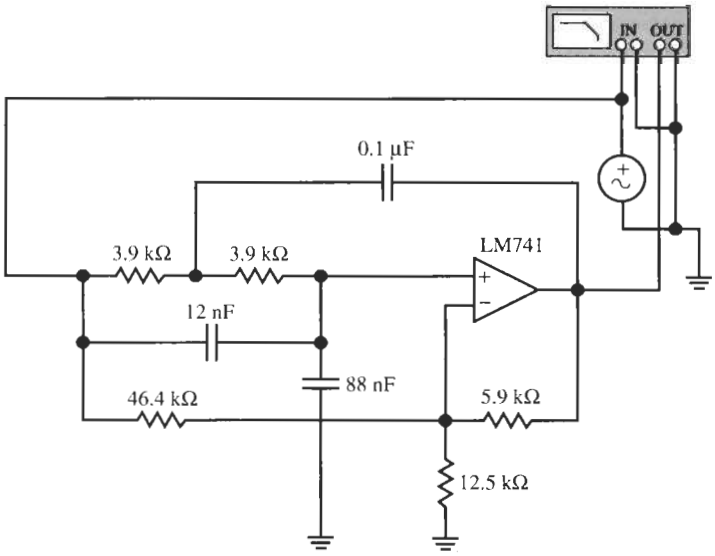

(a)

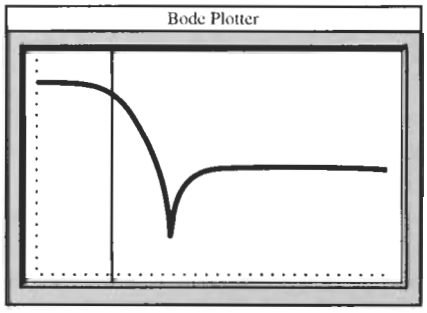

(b)

Figure 5.23 The lowpass notch filter of Example 5.12 and test results. (Bode Plotter scales: 50 Hz to 700 kHz; −60 to 10 dB; cursor at 408 Hz, 0.03 dB.)

5.3 CASCADE DESIGN REVISITED

In this chapter and in Chapter 4 we have developed a number of second-order sections $T_j(s)$ that permit us to realize arbitrary biquadratic functions. To realize more demanding specifications than are possible with second-order functions we need to be able to implement functions of higher order,

$$T(s) = \frac{V_{out}}{V_{in}} = \frac{N(s)}{D(s)} = \frac{b_{2m}s^{2m} + b_{2m-1}s^{2m-1} + \cdots + b_1 s + b_0}{s^{2n} + a_{2n-1}s^{2n-1} + \cdots + a_1 s + a_0} \tag{5.52}$$

In connection with first-order circuits we discussed in Chapter 3, Section 3.6, a method that will allow us to address this problem with the knowledge gained so far is *cascade design*. The cascade method is used widely in industry for implementing high-order specifications. It is well understood, very easy to implement, has low sensitivity to component tolerances, and is efficient in its use of circuit elements. It uses a modular approach and results in filters that for the most part show good performance in practice. One of the main advantages of cascade filters is that they are very easy to adjust (or *tune*) because each biquad is responsible for the realization of only one pole pair and zero pair: in the realizations the individual critical frequencies of the filter are *decoupled* from each other. In addition, the design method is completely general in that arbitrary transfer functions of the form of Eq. (5.52) can be realized. Naturally, to keep the circuits stable and prevent them from oscillating, this means that the poles, the roots of $D(s)$, are restricted to the left half of the complex s-plane (the coefficients a_j are positive). However, the transmission zeros, the roots of $N(s)$, can be anywhere in the s-plane. As we illustrated in the first part of this chapter, their location depends only on the structure of the second-order sections. An additional advantage is that cascade design is easy and transparent because in the design we can focus on the low-order sections $T_j(s)$, which are generally simpler to implement than the high-order function $T(s)$.

To recapitulate, in the cascade procedure we need to factor the high-order circuit requirement of Eq. (5.52), with $n \geq m$ and $n > 1$, into a number of simpler specifications that result in practical circuits and that are readily implemented. These are then connected in a chain, that is, in a *cascade circuit*, as shown in Fig. 5.24, to realize the specified requirements. The degree of the specified function was assumed in Eq. (5.52) to be even, i.e., $2n$. If it is odd, one of the blocks T_j will be of first order and can be realized as discussed in Chapter 3, Sections 3.2 or 3.4. Thus, for our consideration, $T(s)$ in Eq. (5.52) is a ratio of two polynomials $N(s)$ and $D(s)$ of degrees $2m$ and $2n$, respectively. We selected, without loss of generality, the coefficient $a_{2n} = 1$, because we can always divide numerator and denominator by a_{2n}. The filter is then realized by connecting the functions $T_j(s) = V_{oj}/V_{ij}$ such that the total transfer behavior realized by that circuit is derived to be

$$\begin{aligned} T(s) = \frac{V_{out}}{V_{in}} &= \frac{V_{o1}}{V_{in}} \times \frac{V_{o2}}{V_{o1}} \times \frac{V_{o3}}{V_{o2}} \times \ldots \times \frac{V_{o(n-1)}}{V_{o(n-2)}} \times \frac{V_{out}}{V_{o(n-1)}} \\ &= T_1(s)T_2(s)\ldots T_{n-1}(s)T_n(s) = \prod_{j=1}^{n} T_j(s) \end{aligned} \tag{5.53}$$

i.e., the total transmission specification is obtained from the *product* of the low-order blocks. Equation (5.53) holds because the connection guarantees that the input voltage of circuit block

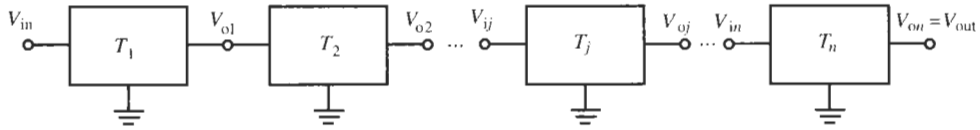

Figure 5.24 Cascade connection of second-order sections $T_j(s) = V_{oj}/V_{ij}$.

j is equal to the output voltage of block $(j-1)$, $V_{ij} = V_{o(j-1)}$. As we discussed in Section 3.6, Eq. (5.53) is valid under the assumption that the output impedance of block number j is much smaller than the input impedance of block $j+1$,

$$\left|Z_{\text{out},j}(j\omega)\right| << \left|Z_{\text{in},j+1}(j\omega)\right| \tag{5.54}$$

so that section T_{j+1} does not load T_j, i.e., two consecutive sections do not interact. Ideally $Z_{\text{out}} = 0$ and $Z_{\text{in}} = \infty$.

The goal is to realize the $2n$th-order function $T(s)$ via simpler circuits in an efficient way with low sensitivities to component tolerances. Because both $N(s)$ and $D(s)$ are even, they can be factored into the product of second-order pole-zero pairs, as expressed in the following form:

$$T(s) = \frac{N(s)}{D(s)} = \frac{\prod_{i=1}^{m} k_i\left(\alpha_{2i}s^2 + \alpha_{1i}s + \alpha_{0i}\right)}{\prod_{j=1}^{n}\left(s^2 + s\omega_{0j}/Q_j + \omega_{0j}^2\right)}$$

$$= \prod_{j=1}^{n} k_j \frac{\alpha_{2j}s^2 + \alpha_{1j}s + \alpha_{0j}}{s^2 + s\omega_{0j}/Q_j + \omega_{0j}^2} = \prod_{j=1}^{n} T_j(s) \tag{5.55}$$

The notation assumes that both N and D are of degree $2n$; if $m < n$, the numerator will contain $2(n-m)$ factors of unity. If the degree of $T(s)$ is odd, the function can always be factored into the product of even terms as shown in Eq. (5.55) and a *first-order* factor. The first-order section, realized as discussed in Chapter 3, is then added to the higher order circuit as an additional block.

As shown in Eq. (5.55), we have again expressed the denominator in terms of the usual filter parameters, the quality factor Q and the pole frequency ω_0. Our problem is then reduced to realizing the second-order sections

$$T_j(s) = k_j \frac{\alpha_{2j}s^2 + \alpha_{1j}s + \alpha_{0j}}{s^2 + s\omega_{0j}/Q_j + \omega_{0j}^2} = k_j t_j(s) \tag{5.56}$$

We have also introduced the *gain constant* k_j. It is defined, e.g., such that the leading coefficient in the numerator of the *gain-scaled* transfer function $t_j(s)$ equals unity or such that $\left|t_j(j\omega_{0j})\right| = 1$.

EXAMPLE 5.13

The transfer function of a sixth-order filter, with a normalized frequency parameter $s = j\omega/\omega_0$, is

$$T(s) = \frac{s^5 + 2.5s^4 + 0.5625s}{s^6 + 0.390s^5 + 3.067s^4 + 0.785s^3 + 3.056s^2 + 0.387s + 0.989}$$

The function specifies a bandpass filter with two transmission zeros, one to the right and one to the left of the passband, which is centered around ω_0. We shall leave the discussion of how to find such a function from prescribed requirements until Chapter 8. The filter is to be realized as a cascade circuit. Find a possible set of second-order functions.

Solution

Factoring the numerator and denominator polynomials by a suitable root-finding algorithm, we obtain

$$\begin{aligned} T(s) &= \frac{s\left(s^2 + 0.25\right)\left(s^2 + 2.25\right)}{\left(s^2 + 0.09s + 0.83\right)\left(s^2 + 0.2s + 1.01\right)\left(s^2 + 0.1s + 1.18\right)} \\ &= T_1(s)T_2(s)T_3(s) \\ &= \frac{k_1 s}{s^2 + 0.09s + 0.83} \times \frac{k_2\left(s^2 + 0.25\right)}{s^2 + 0.2s + 1.01} \times \frac{k_3\left(s^2 + 2.25\right)}{s^2 + 0.1s + 1.18} \end{aligned} \tag{5.57}$$

In this case, $n = 3$ and the numerator is odd, i.e., $N(s)$ is factored into a product of two second-order factors and a first-order term, s. For generality, we also have included three constants k_i to permit us to adjust the gain of the sections; the product of the three constants, of course, must equal unity, $k_1k_2k_3 = 1$, to meet the specified function. The denominator has three conjugate complex roots as shown in Eq. (5.57) and the function is broken into three terms according to Eq. (5.55).

Factoring a given transfer function is a simple numerical process that makes use of a suitable polynomial root finder available in many inexpensive software packages. The problem of designing the sixth-order filter is now simplified to realizing the three second-order functions $T_1(s)$, $T_2(s)$, and $T_3(s)$. We know how to handle this task: several implementation methods were discussed earlier in this chapter and in Chapter 4.

Although this process is simple and leads in a straightforward way to a possible cascade design, we still must resolve several difficulties:

1. We should determine which zero should be assigned to which pole in Eq. (5.55) when the biquadratic functions $T_j(s)$ are formed. For example, in Eq. (5.57), we could also form

$$T(s) = \frac{k_1\left(s^2 + 0.25\right)}{s^2 + 0.09s + 0.83} \times \frac{k_2 s}{s^2 + 0.2s + 1.01} \times \frac{k_3\left(s^2 + 2.25\right)}{s^2 + 0.1s + 1.18}$$

or

$$T(s) = \frac{k_1\left(s^2 + 2.25\right)}{s^2 + 0.09s + 0.83} \times \frac{k_2\left(s^2 + 0.25\right)}{s^2 + 0.2s + 1.01} \times \frac{k_3 s}{s^2 + 0.1s + 1.18}$$

There is a total of six possibilities. Since we have in general n pole pairs and n zero pairs

(counting zeros at 0 and at ∞) we can select from n factorial, $n! = 1 \times 2 \times 3 \times \ldots \times n$, possible *pole-zero pairings*.

2. We might be concerned about the order in which the biquads in Eq. (5.55) should be cascaded. The question is whether the *cascading sequence* makes a difference. For n biquads, we have $n!$ possible sequences. In Example 5.13 we have the options of choosing

$$T_1T_2T_3 \quad T_1T_3T_2 \quad T_2T_1T_3 \quad T_2T_3T_1 \quad T_3T_1T_2 \quad T_3T_2T_1$$

3. Since only the product of the gain constants k_j is prescribed, we must ask whether there is an optimum *gain distribution*. The gain constants in Eq. (5.55), of course, do not affect the frequency response, but they determine the signal level for each biquad. In Eq. (5.57) we have $k_1k_2k_3 = 1$, but the value of each k_i is not specified.

Because the total transfer function $T(s)$ is simply the product of the biquad sections, we may be led to conclude that the answers to the three questions are quite arbitrary. This is certainly a correct conclusion for a "paper design," but not in practice. We will see shortly that the main consequence of our answers to the above three points is their effect on the signal level. That is, pole-zero pairing, section ordering, and gain distribution determine the magnitude of the voltages at the internal nodes in the cascade filter. The reason why this is important is that the second- or first-order sections $T_j(s)$ in the cascade circuit use active devices, in our case opamps. We saw in Chapter 2 that the maximum undistorted signal level that the opamps can handle is limited. The opamp output voltage V_o is, of course, always restricted to be less than the power supply voltage, but more importantly, it is limited by the slew rate SR. As we saw in Eq. (2.27), this limit is set by the amplifiers used and is inversely proportional to the operating frequency, $|V_{o,max}| < SR/\omega$. We will next develop a procedure for finding a solution that will result in practical cascade filters. We emphasize that good answers to these questions do *not* just amount to minor adjustments when designing a cascade filter, but that the cascade circuit will likely not perform to specifications in practice unless correct answers to the three points are available at the design stage. The concept is not difficult to understand but we have to write a number of equations to provide us with the tools to arrive at conclusive answers.

We have to make sure that the signal level at any section output, $|V_{oj}(j\omega)|$, satisfies

$$\max |V_{oj}(j\omega)| < V_{o,max}, \quad 0 \le \omega \le \infty, \quad j = 1, \ldots, n \tag{5.58}$$

that is, the maximum of the output voltage at all opamps stays below some level $V_{o,max}$ set by power supply or slew rate limits. Note that this condition must indeed be satisfied for *all* frequencies and not only in the passband, because large signals even outside the passband must not be allowed to overload and saturate the opamps. When opamps are overdriven, their operation becomes *nonlinear* and results in higher harmonics that are generated by the nonlinear opamp behavior. The problems that arise when saturating the opamps are harmonic and intermodulation distortion of the signal, changed operating points, and ultimately deviations in filter performance.

The restriction at the other extreme is the electrical noise. We must make certain that signals stay large enough to remain above the electrical noise created by random movements of electrons. They cause the currents to fluctuate, which results in small random signals in the circuit (in the microvolt to millivolt range). Once the applied signal *in the passband* becomes

very small, it must be amplified back up to the prescribed output level, say 0 dB from input to output. If a signal is smaller than the random noise signals, it is very hard to recover: amplifying the signal to the desired output level will increase both the applied signals and the noise by the same amount—the *signal-to-noise ratio* cannot be improved by amplification. Consequently, the signal-to-noise ratio will be hurt if in the cascade filter the signal suffers excessive in-band attenuation, i.e., if it is permitted to become very small. As a consequence, the second condition we must fulfill in a successful filter design is that the minimum of the output voltages of any biquad must be made as large as possible: we must satisfy

$$\min \left|V_{oj}\left(j\omega\right)\right| \quad \rightarrow \max \quad \text{for} \quad \omega_L \leq \omega \leq \omega_U, \quad j = 1, \ldots, n \tag{5.59}$$

ω_L and ω_U are, respectively, the lower and upper corners of the passband. In this case we are, of course, concerned only with signal frequencies in the passband, because in the stopband the signal-to-noise ratio is of no interest. Note, however, that the noise spectrum of a filter section usually has the same shape as the transfer function magnitude. This means that the highest noise peaks occur at the pole frequencies with the highest Q-values. Since these are mostly found just beyond the specified corners of the passband, they would not be included in the measurement defined in Eq. (5.59). Therefore, to avoid decreased dynamic range caused by possibly large noise peaks at the passband corners, it is advisable to extend the frequency range beyond the specified passband corners, ω_L, ω_U, into the transition band.

Let us proceed then to determine what can be done with the available design freedom to optimize the *dynamic range*, that is the range between the smallest and largest signal that the circuit can process without distortion. Let us start with pole-zero pairing.

5.3.1 Pole-Zero Pairing

Our strategy for choosing pole-zero assignments should be clear: in any biquad in the cascade circuit we must avoid undue attenuation in the passband as well as unneeded gain. In other words, we must strive to keep the signal level "as flat as possible," safely above the noise floor and below the maximum that the opamps can handle without distortion. If we suppose that the overall gain of the filter is specified, then any frequency components that become too small must be amplified to the prescribed level. But this will also amplify the noise! Similarly, if a frequency component of the signal becomes too large, it must be attenuated back to the prescribed level. But this also reduces the remaining smaller signal components whose magnitude comes closer to the noise level! We conclude that keeping the signal level in the passband as flat as possible optimizes the dynamic range.

To help tackle the problem, let us assume that the largest signal in biquad j is measured at its output V_{oj}. This assumption will always be correct in single-amplifier biquads, such as in Figs. 4.31, 4.37, and 5.22, where section output and opamp output are the same. In multiamplifier biquads, such in the two-integrator loop (Fig. 4.10) or the GIC circuit (Fig. 4.46), *each* opamp output has to be evaluated and the maximum opamp output voltage in the biquad section should be used.

According to our discussion, we should choose the pole-zero pairing such that in a given biquad the signal maximum, $M_j = \max \left|V_{oj}(j\omega)\right|$, is minimized for all frequencies, and the signal minimum, $m_j = \min \left|V_{oj}(j\omega)\right|$, is maximized in the passband. In other words, using Eq. (5.56), $\left|t_j(j\omega)\right|$ *should be as flat as possible in the frequency range of interest.* Figure 5.25 illustrates the situation. Plotted is a typical magnitude of V_{oj} as a function of

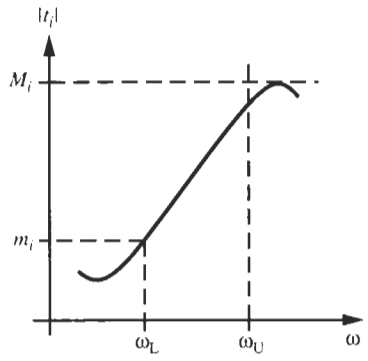

Figure 5.25 Typical biquad output voltage as a function of frequency. Notice that the maximum M_j lies just outside the upper edge ω_U of the passband and the minimum m_j lies at the lower passband corner ω_L.

frequency over the passband $\omega_L \leq \omega \leq \omega_U$, and maximum M_j and minimum m_j are indicated. Notice that M_j may lie outside and m_j at the edge of the passband; the actual minimum of the magnitude $|V_{oj}(j\omega)|$ or of $|t_j(j\omega)|$ lies, of course, in the stopband and is of no concern. Because the values of M_j and m_j change when the relative positions of the poles and the zeros of $t_j(s)$ are altered, the pole-zero assignment must be chosen such that the ratio M_j/m_j is as close to unity as possible. This means that for *each* biquad the "measure of flatness"

$$d_j = \left(\frac{M_j}{m_j} - 1\right), \quad j = 1, 2, \ldots, n \tag{5.60}$$

should be minimized. The optimal pole-zero assignment for the total $2n$th-order cascade filter is then the one that minimizes the maximum value of d_j:

$$d_{\max} = \max\{d_j\} \rightarrow \min, \quad j = 1, 2, \ldots, n \tag{5.61}$$

Algorithms that accomplish this task are available in the literature.[1] Because we have to explore $n!$ choices, the problem of pole-zero assignment is very computation intensive even in fairly simple low-order cases; it requires substantial software and computer resources.

Fortunately, a simple solution can be used that provides good suboptimal results if the appropriate computing facilities are not available. It is based on the intuitive insight that if the pole and zero pair were identical, their ratio t_j would equal unity. The circuit would, of course, provide no filtering at all, but the function would be optimally flat. Following this clue, we simply *assign each pole or pole pair to the closest zero.* On occasion, depending on system requirements, we may also preassign some pole-zero pair(s) and leave them out of the remaining pairing process. For instance, if the numerator contains a term s^2, we may prefer to factor it into $s \times s$ instead of $s^2 \times 1$, i.e., we may prefer to realize two second-order bandpass sections instead of a highpass and a lowpass because excellent bandpass circuits are available.

EXAMPLE 5.14

Determine the optimal pole-zero pairing for the transfer function of Eq. (5.57) of Example 5.13. Use the simple pole-zero assignment suggested above.

[1] See References 1–5.

Solution

The transfer function was

$$T(s) = \frac{k_1 s}{s^2 + 0.09s + 0.83} \times \frac{k_2 (s^2 + 0.25)}{s^2 + 0.2s + 1.01} \times \frac{k_3 (s^2 + 2.25)}{s^2 + 0.1s + 1.18}$$

The zeros are located at $z_1 = 0$ and $z_2 = \infty$, $z_{3,4} = \pm j0.05$, and at $z_{5,6} = \pm j1.5$, and the poles are at $p_{1,2} = -0.045 \pm j0.9099$, $p_{3,4} = -0.1 \pm j1.0$, and $p_{5,6} = -0.05 \pm j1.085$. According to the approximate assignment rule just stated, we should pair ($z_{1,2}$, $p_{3,4}$), ($z_{3,4}$, $p_{1,2}$), and ($z_{5,6}$, $p_{5,6}$). This is the choice indicated in Fig. 5.26 and in Eq. (5.62):

$$T(s) = T_1(s)T_2(s)T_3(s) = \frac{k_1 (s^2 + 0.25)}{s^2 + 0.09s + 0.83} \times \frac{k_2 s}{s^2 + 0.2s + 1.01} \times \frac{k_3 (s^2 + 2.25)}{s^2 + 0.1s + 1.18} \quad (5.62)$$

Notice that we shifted only the zeros but kept the gain constants associated with their poles.

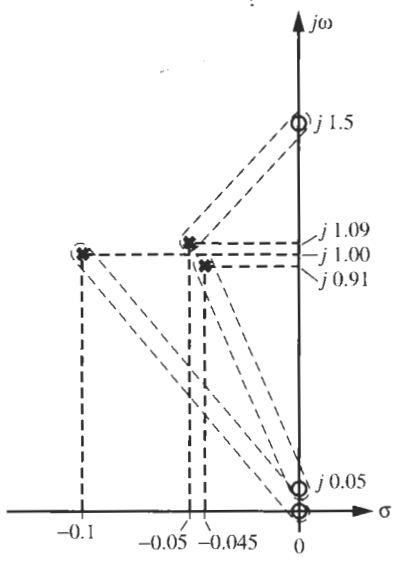

Figure 5.26 Pole-zero diagram for Example 5.14. Only the first quadrant is shown.

Having solved (at least approximately) the pole-zero assignment, we next attend to the question of section ordering

5.3.2 Section Ordering

Since we have n sections, there are $n!$ possibilities in which the biquads can be connected to form the cascade network. For example, for the sixth-order network with three sections in Example 5.13, we saw that there existed six possible ways to cascade the biquads. The best ordering sequence is the one that maximizes the dynamic range. Our task is to find that optimal sequence.

The procedure is completely analogous to the previous discussion where pole-zero pairs

were chosen to keep the transfer functions of the individual sections as flat as possible. Now the *section ordering* is chosen such that the transfer functions,

$$H_i(s) = \frac{V_{oi}}{V_{in}} = \prod_{j=1}^{i} T_j(s), \qquad i = 1, \ldots n \tag{5.63}$$

from filter input to the output of the ith intermediate biquad are as flat as possible. H_n is, of course, equal to the total transfer function $T(s)$. This choice will help ensure that the maximum signal voltages do not overdrive the opamps and that, over the passband, the smallest signal stays well above the noise floor. Consequently, relationships similar to Eqs. (5.51) and (5.52) must be satisfied: we need to make certain that for all i the circuit satisfies

$$\max |V_{oi}(j\omega)| < V_{o,max}, \quad 0 \le \omega \le \infty \tag{5.64}$$

$$\min |V_{oi}(j\omega)| \to \max \quad \text{for} \quad \omega_L \le \omega \le \omega_U \tag{5.65}$$

$V_{oi}(s)$ is the output voltage *of the cascade of the first i sections* when driven by an input signal V_{in}. With $H_i(s)$ given in Eq. (5.63), we define the maximum M_i of the transfer function from the input to the output of Section i for all ω,

$$M_i = \frac{\max |V_{oi}(j\omega)|}{|V_{in}|} = \max \left| \frac{V_{oi}(j\omega)}{V_{in}} \right| = \max |H_i(j\omega)| \quad \text{for} \quad 0 \le \omega \le \infty \tag{5.66}$$

and the minimum m_i of that function over the passband,

$$m_i = \frac{\min |V_{oi}(j\omega)|}{|V_{in}|} = \min \left| \frac{V_{oi}(j\omega)}{V_{in}} \right| = \min |H_i(j\omega)| \quad \text{for} \quad \omega_L \le \omega \le \omega_U \tag{5.67}$$

where we assumed that the input signal spectrum is constant for all frequencies. We then require again that the flatness criterion of Eq. (5.60) is minimized, now, however, *by choice of the cascading sequence*. The optimal sequence is the one that minimizes the maximum number d_i as prescribed in Eq. (5.61),

$$\max\{d_i\} = \max\left(\frac{M_i}{m_i} - 1\right) \to \min \tag{5.68}$$

Note that we do not have to consider d_n because, with all sections connected in the cascade filter, d_n is nothing but a measure of the *prescribed* passband variations.

With the problem identified, the optimum cascading sequence can be found in principle by calculating d_i for all $n!$ sequences and selecting the one that satisfies Eq. (5.68). As in the pole-zero assignment problem, a *brute-force* optimization approach involves a considerable amount of computation, and more efficient methods have been developed which use linear programming techniques, such as the "branch and bound" method, or "back track programming." The necessary computer algorithms are described in the literature.[2]

If the required software routines are not available to us, we can for most designs use a cascading sequence that, based on experience or intuition, appears to be a good choice. A selection that is often very close to the optimum is the one that chooses the section sequence in the order of increasing values of Q_i, i.e.,

[2]See References 6 and 7.

$$Q_1 < Q_2 < \cdots < Q_n \tag{5.69}$$

so that the section with the flattest transfer function magnitude (the lowest Q) comes first, the next flattest one second, and so on. The possible choices are frequently further limited by other considerations. For example, it is often desirable to have as the first section in the cascade a lowpass or a bandpass biquad so that high-frequency signal components are kept from the amplifiers in the filter in order to minimize slew-rate problems. Similarly, the designer may wish to employ a highpass or a bandpass biquad as the last section to eliminate low-frequency noise, dc offset, or power supply ripple from the filter output. If such practical constraints are important, we choose the placement of these sections first and perform the optimum sequencing only on the remaining sections. The following example will illustrate some of the steps discussed.

EXAMPLE 5.15

Continue Example 5.14 to find the optimal cascading sequence for the three second-order sections.

Solution

Since the coefficient of s in the denominators of the second-order sections of Eq. (5.62) equals ω_{0i}/Q_i, and the constant coefficient equals ω_{0i}^2, we have

$$Q_1 = \frac{\omega_{01}}{0.09} = \frac{\sqrt{0.83}}{0.09} \approx 10.12, \quad Q_2 = \frac{\sqrt{1.01}}{0.2} \approx 5.03, \quad Q_3 = \frac{\sqrt{1.18}}{0.1} \approx 10.86$$

Using the suggestion of Eq. (5.69) and continuing with the section numbering in Eq. (5.62), the optimal ordering is, therefore, $T_2T_1T_3$. If we were instead to emphasize the elimination of high-frequency signals from the filter and low-frequency noise from the output, the ordering $T_2T_3T_1$,

$$T(s) = \frac{k_2 s}{s^2 + 0.2s + 1.01} \times \frac{k_3\left(s^2 + 2.25\right)}{s^2 + 0.1s + 1.18} \times \frac{k_1\left(s^2 + 0.25\right)}{s^2 + 0.09s + 0.83} \tag{5.70}$$

would be preferable because the bandpass section, T_2, has the best high-frequency attenuation, and section T_1 provides reasonable attenuation at low frequencies ($0.25/0.83 = 0.30 \approx -10$ dB), whereas T_3/k_3 has a high-frequency gain of unity and amplifies low-frequency noise by more than $2.25/1.18 = 1.91 \approx 5.6$ dB. In our case, this suboptimal ordering gives almost identical results to the optimal one, $T_2T_1T_3$, because $Q_1 \approx Q_3$.

5.3.3 Gain Assignment

The last step we have to attend to in the realization of a cascade filter is the assignment of the gain constants k_i. Generally, the selection is again based on dynamic range concerns with the goal of keeping the signals below amplifier saturation limits. To see how we might proceed, we note that filters are linear circuits and all voltages rise in proportion to V_{in}. It is clear then that if we raise the input signal voltage we will overdrive that opamp first, which sees the largest

output voltage after the previous two steps (pole-zero assignment and section ordering) were completed. It follows that we place equal stress on all opamps and can process the maximum undistorted input signal if we choose the gain constants such that *all internal output voltages* $V_{oi}, i = 1, \ldots, n-1$, *are equal in magnitude* to the prescribed magnitude of the output voltage, V_{on}:

$$\max |V_{oi}(j\omega)| = \max |V_{on}(j\omega)| = \max |V_{\text{out}}(j\omega)|, \quad i = 1, \ldots, n-1 \tag{5.71}$$

Assuming before that the *output* voltage of the biquads (rather than an internal opamp) reaches the critical magnitude, this choice assures that for a given signal level none of the opamps in the blocks of Fig. 5.24 is overdriven sooner than any other one. Note, however, the earlier comments about precautions necessary in multiamplifier biquads.

For the analysis it is convenient to use the notation of Eqs. (5.55) and (5.56), i.e.,

$$T(s) = \prod_{j=1}^{n} T_j(s) = \prod_{j=1}^{n} k_j \prod_{j=1}^{n} t_j(s) \tag{5.72}$$

and, for the intermediate transfer functions of Eq. (5.63),

$$H_i(s) = \prod_{j=1}^{i} T_j(s) = \prod_{j=1}^{i} k_j \prod_{j=1}^{i} t_j(s) \tag{5.73}$$

Further, for convenience of notation we introduce the label K for the product of all section gain constants,

$$K = \prod_{j=1}^{n} k_j \tag{5.74}$$

Then the *prescribed* gain of the total cascade circuit is

$$\max |T(j\omega)| = \max |H_n(j\omega)| = K \max \prod_{j=1}^{n} |t_j(j\omega)| = K M_n \tag{5.75}$$

where we defined

$$M_n = \max \prod_{j=1}^{n} |t_j(j\omega)| \tag{5.76}$$

Similar to the definition of M_n, let us denote the maxima of the intermediate $n-1$ gain-scaled transfer functions by M_i, i.e.,

$$\max \prod_{j=1}^{i} |t_j(j\omega)| = M_i, \quad i = 1, \ldots, n-1 \tag{5.77}$$

We now assume that the input signal magnitude $|V_{\text{in}}|$ is constant, independent of frequency. This means that the requirement of equal voltage maxima throughout the cascade circuit,

$\max|V_{oi}(j\omega)| = \max|V_{out}(j\omega)|$, corresponds to $\max|H_i(j\omega)| = \max|H_n(j\omega)| = \max|T(j\omega)|$. Thus, with Eqs. (5.73) to (5.77) we have $\max|V_{o1}(j\omega)| = \max|V_{out}(j\omega)|$, i.e., $k_1 M_1 = K M_n$ or

$$k_1 = K\frac{M_n}{M_1} \tag{5.78}$$

Similarly, $\max|V_{o2}(j\omega)| = \max|V_{out}(j\omega)|$ results in $k_1 k_2 M_2 = K M_n$, i.e., with Eq. (5.78),

$$k_2 = \frac{M_1}{M_2} \tag{5.79}$$

Proceeding in the same manner with $\max|V_{oi}(j\omega)| = \max|V_{out}(j\omega)|$, $i = 3, \ldots, n$, yields

$$k_j = \frac{M_{j-1}}{M_j}, \quad j = 2, \ldots, n \tag{5.80}$$

Choosing the gain constants as in Eqs. (5.78) and (5.80) guarantees that all opamps see the same maximum voltage to ensure that the largest possible signal can be processed without distortion. Note that changing the total gain of the n-section cascade filter affects only K, i.e., the gain constant k_1 of the first section. The voltages in all other sections $T_i(s)$, $i = 2, \ldots, n$ increase or decrease proportionally, but their *relative* magnitudes stay the same, as determined by k_i in Eq. (5.80).

Let us summarize this somewhat involved procedure: To maximize the dynamic range in a cascade filter, we need to maximize in each filter section the minimum signal level in the passband and minimize the maximum signal level. In addition, the maxima of the output voltages of all sections should be made equal. The way to accomplish this is first choose the pole-zero pairing, next perform section ordering, and last determine the gain assignment. Specifically, if the necessary software for an optimal solution is not available, we

1. assign the zeros to the closest poles,
2. order the sections in the cascade in the order of increasing values of Q, and
3. compute the gain constants according to Eqs. (5.78) and (5.80). The values M_i needed to evaluate these equations are readily computed from the known functions $t_i(s)$ or with the help of a circuit simulator, such as SPICE or Electronics Workbench (the program used throughout this text), from an initial trial design.

EXAMPLE 5.16

Continue Example 5.15 to find the optimal gain constants for the three second-order sections so that their maximum output levels are equalized. The specified midband filter gain is 10 dB. Use the section ordering in Eq. (5.70). Realize the filter with three suitable Åckerberg–Mossberg biquads based on LM741 opamps. The center frequency is $f_0 = 15.7$ kHz.

Solution

The transfer function is

$$T(s) = \frac{k_1 s}{s^2 + 0.2s + 1.01} \times \frac{k_2\left(s^2 + 2.25\right)}{s^2 + 0.1s + 1.18} \times \frac{k_3\left(s^2 + 0.25\right)}{s^2 + 0.09s + 0.83} \tag{5.81}$$

where we have renamed the gain constants k_1, k_2, and k_3 such that their subscripts indicate the order of the sections. For the prescribed 10-dB gain we find from Eq. (5.75),

$$KM_3 = 3.16 \tag{5.82}$$

The maximum of Section 1, M_1, follows directly from the maximum Q of a bandpass function: $M_1 \approx 1/0.2 = 5$. The remaining maxima M_2 and M_3 can be computed by evaluating the functions in Eq. (5.76) with Eq. (5.81). We find

$$M_1 \approx \frac{1}{0.2} = 5, \quad M_2 \approx 46, \quad M_3 \approx 125$$

With M_i known, and using Eq. (5.82), Equations (5.78) and (5.80) give

$$k_1 = \frac{KM_3}{M_1} = \frac{3.16}{5} = 0.63, \quad k_2 = \frac{M_1}{M_2} \approx \frac{5}{46} = 0.11, \quad k_3 = \frac{M_2}{M_3} \approx \frac{46}{125} = 0.38$$

that is

$$T(s) = T_2 T_3 T_1 = \frac{0.63s}{s^2 + 0.2s + 1.01} \times \frac{0.11\left(s^2 + 2.25\right)}{s^2 + 0.1s + 1.18} \times \frac{0.38\left(s^2 + 0.25\right)}{s^2 + 0.09s + 0.83} \tag{5.83}$$

These values result in all section outputs being equal to $KM_3 = 3.16$ times the input voltage level for a uniform gain of 10 dB. If the designer were to find out later that system performance would improve for a different filter gain, say, 25 dB ($KM_3 = 17.8$) rather than 10 dB, the redesign is easy: it is necessary only to alter the first section in the cascade from $k_1 = 0.63$ to

$$k_1 = KM_3/M_1 = 17.8/5 = 3.56$$

to achieve the new circuit for which dynamic range is still optimized.

This completes the steps required to optimize the dynamic range. We next have to select the appropriate Åckerberg–Mossberg sections. The first section, T_2, is the bandpass filter of Fig. 4.29. We select $C_1 = C_2 = C = 0.01\ \mu$F so that with $f_0 = 15.7$ kHz we obtain $R_1 = 1/(\omega_0 C) = 1.013\ \text{k}\Omega$. Because $Q_2 = 5.03$ from Example 5.15, we have for the resistor QR the value 5.13 kΩ. Finally, the numerator coefficient of the first section in Eq. (5.83) equals $k_1 = 0.63$ which results in $R/k_1 = 1.61$ kΩ.

The circuit for the two notch sections is given in Fig. 5.13 with $k = b = 0$ from Eq. (5.32). We choose again $C_1 = C_2 = C = 0.01\ \mu$F so that for the second section, T_3, we have

$$R_1 = 1/\left(\sqrt{1.18} \times 2\pi \times 15700\ \text{Hz} \times 0.01\ \mu\text{F}\right) = 933\ \Omega$$

and $QR = 10.13$ kΩ. The feed-in components are

$$aC = 0.11 \times 0.01\ \mu\text{F} = 1.1\ \text{nF} \quad \text{and} \quad \frac{R}{c} = \frac{933\ \Omega}{0.11 \times 2.25/1.18} = 4.4\ \text{k}\Omega$$

For the last section, T_1, we obtain similarly $R = 1.1$ kΩ and $QR = 11.3$ kΩ. The feed-in elements are

$$aC = 3.8 \text{ nF} \quad \text{and} \quad \frac{R}{c} = \frac{933\ \Omega}{0.38 \times 0.25/0.83} = 8.16\ \text{k}\Omega$$

Figure 5.27a shows the circuit and Fig. 5.27b the test results. The filter has a flat passband at 10.6 dB gain with $f_0 = 15.6$ kHz as required, with a 1-dB gain variation (ripple) in 14.8 kHz $\leq f \leq$ 16.8 kHz. The transmission zeros are at 8.3 and 23.7 kHz, close to the specified values. Looking at all opamps, we find signal level variations over the passband to be less than 9 dB (a factor 2.8) with the maximum gain at 10.6 dB. To verify that our design indeed equalizes the maximum signal levels at the three section outputs, we show in Fig. 5.27c the simulated output voltages. Evidently, their maxima are at approximately 10 dB as specified.

To demonstrate that gain equalization is very important in cascade realizations, consider the case where equalization is *not* performed. Had the designer chosen all $k_i = 1$ in Eq. (5.81), the maximum output levels would have been 13.9 dB at V_{o1}, 31.9 dB at V_{o2}, and 41.3 dB at V_{o3}. Reducing the overall gain from 41.3 dB to the prescribed level of 10 dB by increasing the input resistor would result in a maximum level of −17 dB at V_{o1} and −7.9 dB at V_{o2}. The difference of (10 dB + 17 dB) = 27 dB, a factor of approximately 23 in opamp output voltages, would force the input voltage to be 23 times smaller than in the optimized design.

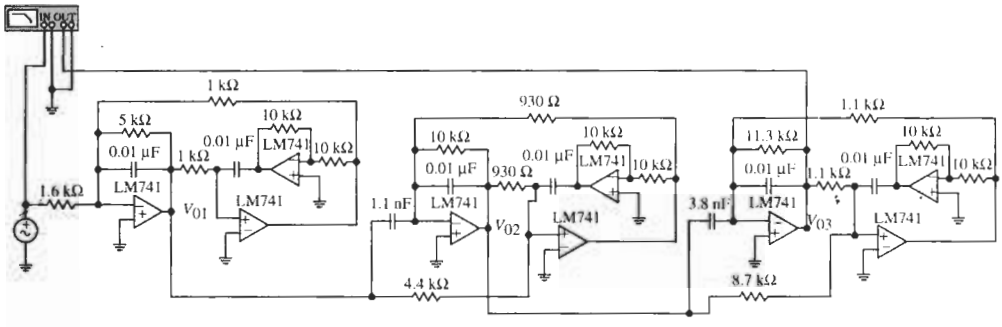

(a)

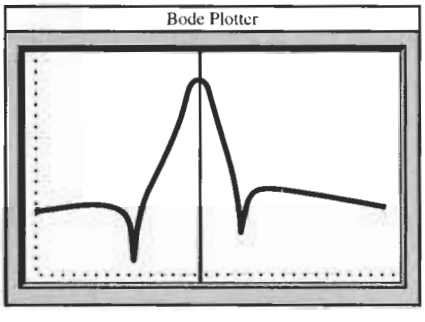

(b)

Figure 5.27 (a) The cascade circuit of Example 5.16; (b) test results; (c) simulated voltage levels. (Bode Plotter scales: 3 to 100 kHz; −80 to 20 dB; cursor at 15.61 kHz, 10.59 dB.)

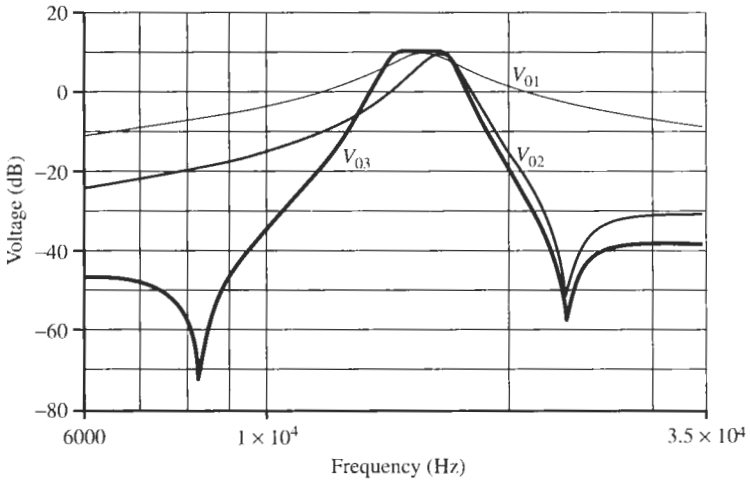

(c)

Figure 5.27 Continued

Notice that the optimal cascading routine we discussed, pole-zero pairing, section ordering, and gain assignment, is entirely general and does not depend on the transfer function or its type. It is independent of the actual implementation of the second-order building blocks. The designer may choose any convenient technology, and the circuit architecture that seems preferable from the point of view of sensitivity, element numbers, types, values and element value spreads, power consumption, or other practical considerations. As a further example consider the realization of a fifth-order lowpass filter.

EXAMPLE 5.17

Realize the filter function

$$T(s) = T_1(s)T_2(s)T_3(s) = \frac{k\left(s^2 + 29.2^2\right)\left(s^2 + 43.2^2\right)}{(s + 16.8)\left(s^2 + 19.4s + 20.01^2\right)\left(s^2 + 4.72s + 22.52^2\right)}$$

The frequency is normalized with respect to 1000 Hz and the low-frequency gain is to be 13.5 dB. Use single-amplifier biquads. This is a fifth-order elliptic lowpass filter used in telephone channel bank applications. We shall discuss the method to arrive at this function later in this book.

Solution

We have already factored $T(s)$ into three modules. Because $T(s)$ is odd, there will be one first-order term. We have

$$T(s) = T_1(s)T_2(s)T_3(s) = \frac{h_1}{s + 16.8}\,\frac{h_2\left(s^2 + 29.2^2\right)}{s^2 + 19.4s + 20.01^2}\,\frac{h_3\left(s^2 + 43.2^2\right)}{s^2 + 4.72s + 22.52^2} \tag{5.84}$$

We have labeled the three gain constants h_1, h_2, and h_3; they must be determined such that the low-frequency gain is 13.5 dB. We have from $T(0)$

$$h_1h_2h_3\frac{1}{16.8}\frac{29.2^2}{20.01^2}\frac{43.2^2}{22.52^2} = 0.4664h_1h_2h_3 = 10^{13.5/20} = 4.732 \tag{5.85}$$

i.e., $h_1h_2h_3 = 10.145$. The pole-zero pairing assigns zeros to the closest poles; this is the assignment in Eq. (5.84). To select the cascading sequence we need to find the quality factors. From Eq. (5.84) we have

$$Q_2 = 20.01/19.4 = 1.03 \quad \text{and} \quad Q_3 = 22.52/4.72 = 4.77 \tag{5.86}$$

We also try to reduce high-frequency signals from entering the filter, which suggests taking the first-order function T_1 as first section. Cascading the sections in the order of increasing values of Q results in the sequence in Eq. (5.84), which we now proceed to realize.

We shall use the first-order section of Fig. 3.24 with $C_1 = 0$. The second-order sections will be Sallen–Key circuits with additional feed-in components, Fig. 5.22. The filter calls for two lowpass notch sections described by Eq. (5.49):

$$T(s) = K\frac{c_k}{2}\frac{s^2 + 2\dfrac{a - c_k}{c_k}\omega_0^2}{s^2 + s\omega_0/Q + \omega_0^2} = k_2\frac{s^2 + \omega_N^2}{s^2 + s\omega_0/Q + \omega_0^2}$$

With k_2 and f_N specified we have to satisfy from Eqs. (5.50) and (5.51)

$$a = \left(2 + \frac{f_N^2}{f_0^2}\right)\frac{k_2}{K} \le 1, \quad b = \frac{3k_2}{K} \le 1, \quad c = \frac{2k_2}{K - 1} \le 1 \tag{5.87}$$

At this point let us recall that the Sallen–Key filter experiences a decrease in f_0 and an increase in Q when real opamps with $A \neq \infty$ are used. Let us estimate the size of these errors and see how they can be minimized in the design. Referring to Eqs. (4.113) to (4.116), we have

$$f_{0R} \approx f_0\left(1 - \frac{\varepsilon}{2}\right) \quad \text{and} \quad Q_R \approx Q\left(1 + \frac{\varepsilon}{2}\right) \tag{5.88}$$

where the error was

$$\varepsilon = \frac{\omega_0}{\omega_t}K^2 = \frac{K^2}{|A(j\omega_0)|}$$

The parameter K for each biquad is determined through Q by Eq. (4.105), $K = 3 - 1/Q$. With Q_2 and Q_3 in Eq. (5.86), we have for the two sections

$$K_2 = 3 - 1/1.03 = 2.03 \quad \text{and} \quad K_3 = 3 - 1/4.77 = 2.79$$

so that the errors in Sections 2 and 3 are

$$\frac{\varepsilon_2}{2} = \frac{2.03^2}{1500/20.01} \approx 0.0275 \quad \text{and} \quad \frac{\varepsilon_3}{2} = \frac{2.79^2}{1500/22.52} \approx 0.0584$$

By Eq. (5.88) the opamps cause f_0 and Q to decrease and increase, respectively, by $\varepsilon/2$. Let us anticipate these nominal errors and *predistort* the specified values. Predistortion means we design for a nominally larger f_0 and smaller Q so that the opamp effect restores the parameters to the required values. Thus, we design the filter section T_2 with

$$\omega_{02} = 20.01\left(1 + \frac{\varepsilon_2}{2}\right) = 20.01 \times 1.0275 = 20.57 \tag{5.89a}$$

$$Q_2 = 1.03\left(1 - \frac{\varepsilon_2}{2}\right) = 1.03 \times 0.9725 = 1.00$$

and T_3 with

$$\omega_{03} = 22.52\left(1 + \frac{\varepsilon_3}{2}\right) = 22.52 \times 1.0584 = 23.84 \tag{5.89b}$$

$$Q_3 = 4.77\left(1 - \frac{\varepsilon_3}{2}\right) = 4.77 \times 0.9416 = 4.49$$

Let us choose $C = 0.01\ \mu$F for all capacitors. Then we find for $T_2(s)$ with the predistorted parameters in Eq. (5.89a)

$$R = \frac{1}{2\pi \times 1000\text{s}^{-1} \times 20.57 \times 0.01\ \mu\text{F}} = 773.72\ \Omega \quad \text{and} \quad K = 3 - 1/Q = 2.00$$

Also, from Eq. (5.87),

$$a = \left(2 + \frac{29.2^2}{20.57^2}\right)\frac{h_2}{2.00} = 2.008h_2 \leq 1, \quad b = \frac{3h_2}{2} = 1.500h_2 \leq 1,$$

$$c = \frac{2h_2}{1.00} = 2.00h_2 \leq 1$$

This means that we must choose $h_2 \leq 1/2.008 = 0.498$. Let us pick this value of h_2 since Eq. (5.85) requires a large gain. We get

$$a = 1, \quad b = 0.747, \quad \text{and} \quad c = 0.996 \approx 1$$

Similarly, we find for $T_3(s)$ with Eq. (5.89b),

$$R = \frac{1}{2\pi \times 1000\text{s}^{-1} \times 23.84 \times 0.01\ \mu\text{F}} = 667.6\ \Omega \quad \text{and} \quad K = 2.778$$

and

$$a = \left(2 + \frac{43.2^2}{23.84^2}\right)\frac{h_3}{2.778} = 1.902h_3 \leq 1, \quad b = \frac{3h_3}{2.778} = 1.080h_3 \leq 1,$$

$$c = \frac{2h_3}{1.778} = 1.125h_3 \leq 1$$

We must choose $h_3 \leq 1/1.902 = 0.526$. Let us pick this value of h_3 to get

$$a = 1, \quad b = 0.568, \quad \text{and} \quad c = 0.592$$

With h_2 and h_3 determined, we find from Eq. (5.85) $h_1 = 38.73$. Because of the constraints

on the values of h_2 and h_3 we could not equalize the signal levels at the three opamps. We have at the output of T_1 a gain of 7.27 dB, at the output of T_2 a gain of 7.78 dB, and at the filter output, of course, the required 13.5 dB gain. The third opamp, therefore, determines the maximum signal amplitude.

The first-order section T_1 is the lossy integrator from Fig. 3.24 described by Eq. (3.70),

$$T_1(s) = \frac{G_1}{sC + G_2} = \frac{G_1/C}{s + G_2/C} \rightarrow \frac{h_1}{s + 16.8}$$

Consequently, we obtain

$$R_2 = \frac{1}{2\pi \times 1000\text{s}^{-1} \times 16.8 \times 0.01\ \mu\text{F}} = 947.35\ \Omega$$

$$R_1 = \frac{1}{h_1 \times 2000\pi\,\text{s}^{-1} \times 0.01\ \mu\text{F}} = 411\ \Omega$$

Finally, choosing $R_0 = 5\ \text{k}\Omega$ in Fig. 5.22 we have the circuit in Fig. 5.28. We notice that the filter performs as specified. In this example we had no more degrees of freedom to adjust the gain constants to equalize the signal level according to Eqs. (5.75) to (5.79). Adjusting h_2 and h_3 to their maxima is the best choice available. Of course, there is no limit on h_1.

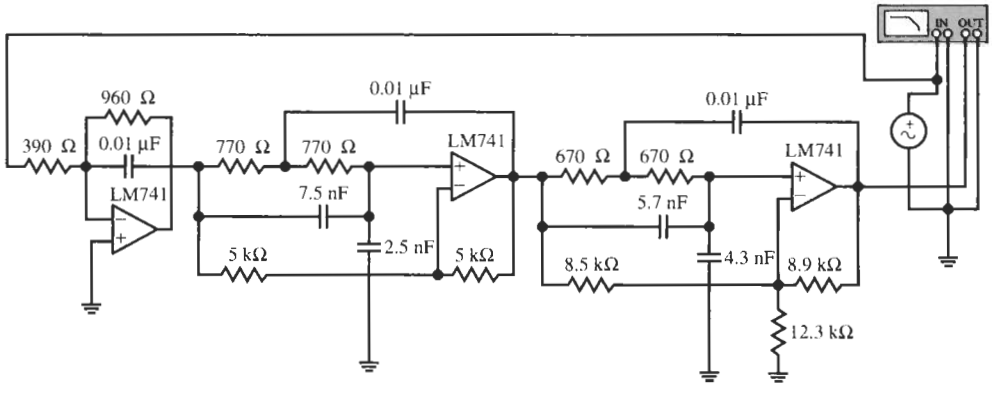

(a)

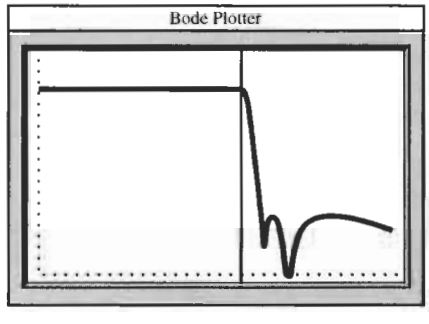

(b)

Figure 5.28 The fifth-order lowpass circuit for Example 5.17 and test results. (Bode Plotter scales: 1 to 200 kHz; −40 to 20 dB; cursor at 21.0 kHz, 12.0 dB.)

For building active filters we have now available in our arsenal a variety of first- and second-order building blocks with which we can realize poles anywhere in the left half s-plane and zeros anywhere in the s-plane. Further, with the cascade method we can connect these building blocks to implement sophisticated filters of high order. In Examples 5.16 and 5.17 we have illustrated the process of implementing a high-order transfer function. How to generate these transfer functions to satisfy some required design goal we shall explore in the following chapters, beginning with general lowpass magnitude specifications.

REFERENCES

[1] S. Halfin, "An Optimization Method for Cascaded Filters," *Bell Syst. Tech. J.*, Vol. 49, pp. 185–190, 1970.

[2] S. Halfin, "Simultaneous Determination of Ordering and Amplifications of Cascaded Subsystems," *J. Optimiz. Theory Applic.*, Vol. 6, pp. 356–360, 1970.

[3] E. Lüder, "Optimization of the Dynamic Range and the Noise Distance of RC-Active Filters by Dynamic Programming," *Int. J. Circuit Theory Applic.*, Vol. 3, pp. 365–370, 1975.

[4] G. S. Moschytz, *Linear Integrated Networks—Design*. van Nostrand Reinhold, New York, 1975.

[5] R. Schaumann, M. S. Ghausi and K. R. Laker, *Design of Analog Filters: Passive, Active RC and Switched Capacitor*. Prentice-Hall, Englewood Cliffs, NJ, 1990.

[6] A. S. Sedra and P. O. Brackett, *Filter Theory and Design: Active and Passive*. Matrix, Portland, OR, 1978.

[7] W. M. Snelgrove and A. S. Sedra, "Optimization of Dynamic Range in Cascade Active Filters," *Proc. IEEE Int. Symp. Circ. Syst.*, pp. 151–155, 1978.

PROBLEMS

5.1 In the transfer function

$$T(s) = \frac{N(s)}{D(s)} = \frac{k_2 s^2 + k_1 s + k_0}{s^2 + s(\omega_0/Q) + \omega_0^2}$$

determine the conditions the coefficients k_0, k_1, and k_2 must satisfy so that $T(s)$ is a (a) lowpass, (b) highpass, (c) bandpass, (d) allpass; (e) band-rejection function; (f) a magnitude equalizer that provides (f1) a gain dip; (f2) a gain boost.

5.2 Use the general Åckerberg–Mossberg biquad in Fig. 5.1 to realize the filters in Parts (a) through (m) below. The following abbreviations or symbols are used: HP = highpass; LP = lowpass; BP = bandpass; BE = band elimination; AP = allpass; N = notch; ME/B = magnitude equalizer with gain boost; ME/D = magnitude equalizer with gain dip; ω_0 or f_0 = pole frequency; ω_z or f_z = zero frequency; Q = pole quality factor; BW = bandwidth; H_0 = dc gain; H_M = midband gain; H_∞ = high-frequency gain. Use practical component values and LM741 or HA 2542-2 opamps as appropriate. In all cases test your designs with Electronics Workbench (EWB) and comment on any inaccuracies observed.

(a) HP with $\omega_0 = 9$ krad/s; $Q = 4.5$; $H_\infty = 0$ dB

(b) HP with $\omega_0 = 600$ krad/s; $Q = 4.5$; $H_\infty = 0$ dB

(c) BP with $\omega_0 = 6.3$ krad/s; $Q = 35$; $H_M = 24$

(d) BP with $\omega_0 = 64$ krad/s; bandwidth $= 2.2$ kHz; $H_M = 1$

(e) BE with $f_z = 24$ kHz; signal level -15 dB below dc gain in a band of 3.2 kHz; $H_\infty = H_0 = 0$ dB

(f) BE with $\omega_z = 1.2$ Mrad/s; signal level -36 dB below H_0 in a band of 60 kHz; $H_\infty = H_0 = +4$ dB

(g) LPN with $\omega_0 = 17$ krad/s; $\omega_z = 47$ krad/s; $H_\infty = 0$ dB; band edge gain peaking of 5 dB above H_0

(h) LPN with $f_0 = 2$ MHz; $H_0 = 0$ dB; $H_\infty < -30$ dB band edge gain peaking of 2 dB above H_0

(i) HPN with $f_0 = 900$ Hz; $f_z = 300$ Hz; no band edge gain peaking; $H_0 = -29$ dB; $H_\infty = +12$ dB

(j) ME/B with a 5-dB gain boost above 0 dB, centered around 700 kHz. The filter will have 0 dB gain at high and low frequencies; the bandwidth of the boost must be 35 kHz at a level of at least 3 dB above 0 dB

(k) ME/D with a dip of 8 dB below a flat 2-dB-wide-band gain. The dip should be centered at 40 kHz and must be larger than 3 dB over a band of width 2 kHz

(l) AP where the phase ranges from 45° to −45° over a frequency band of 1000 Hz centered around 8.2 kHz

(m) AP where the phase changes from +10° at $f = 1.2$ kHz to −60° at $f = 3.6$ kHz

5.3 Consider an *RLC* circuit as shown in Fig. P5.3 in which one element is varied over its range of values from 0 to ∞. Verify that the locus of the poles of $T(s) = V_2/V_1$ are those shown in the figure.

5.4 Consider the circuit in Fig. P5.4.

(a) Show that the transfer function $T(s) = V_2/V_1$ has the form

$$T(s) = \frac{s^2 + \omega_z^2}{s^2 + (\omega_0/Q)\,s + \omega_0^2}$$

(b) Express ω_0, ω_z, Q, and the low- and high-frequency asymptotic gains in terms of the element values.

(c) Determine expressions for $|T(j\omega)|$ and the phase of $T(j\omega)$.

(d) In the expressions determined for Part (c), let $\omega_0 = 1$ and $Q = 5$. Sketch the magnitude and phase as a function of frequency from $\omega = 0$ to $\omega = 5$ rad/s.

(e) Explain what happens if the inductor L is lossy. (Model the loss as a series resistor and find the transfer function.)

(f) Assume a resistive load R_L is connected to the output terminals such that $R_L >> R_2$ but that there is a nonnegligible parasitic load capacitor C_L. Find the transfer function and explain the changed behavior.

5.5 Repeat the steps (a) through (e) outlined in Problem 5.4 for the circuit in Fig. P5.5. (d) Determine the transfer function obtained if C_1 and R are partially lifted off ground.

5.6 Repeat the steps (a) through (d) outlined in Problem 5.4 for the circuit in Fig. P5.6. (e) Determine the transfer function if L_1 and R are partially lifted off ground.

5.7 Repeat the designs in Problem 5.2 with the Åckerberg–Mossberg biquad in Fig. 5.13.

5.8 Use the circuit in Fig. 5.13 to realize the functions

(a) $T(s) = \dfrac{s^2 + \omega_z^2}{s^2 + s\omega_0/Q + \omega_0^2}$ $\qquad \omega_z < \omega_0$

(b) $T(s) = \dfrac{s^2 + \omega_z^2}{s^2 + s\omega_0/Q + \omega_0^2}$ $\qquad \omega_z > \omega_0$

(c) $T(s) = \dfrac{s^2 + \omega_z^2}{s^2 + s\omega_0/Q + \omega_0^2}$ $\qquad \omega_z = \omega_0$

(d) $T(s) = \dfrac{s^2 + s\omega_0/Q_z + \omega_0^2}{s^2 + s\omega_0/Q + \omega_0^2}$

(e) $T(s) = \dfrac{s^2 - s\omega_0/Q + \omega_0^2}{s^2 + s\omega_0/Q + \omega_0^2}$

5.9 In the circuit of Fig. P5.9 the capacitors have the same value C and all resistors except one have the common value of R. Analyse the circuit to determine the transfer functions

$$T_a = \frac{V_2}{V_1}, \quad T_b = \frac{V_3}{V_1}, \quad \text{and} \quad T_c = \frac{V_4}{V_1}$$

and classify each as lowpass, bandpass, bandstop, etc. Evaluate the pole deviations (frequency and quality factor when the integrator model is used for the opamps).

5.10 Using one of the outputs described in Problem 5.9, design a bandpass filter for which $\omega_0 = 10,000$ rad/s with a bandwidth of 1000 rad/s. Scale the circuit so that all element values are in a practical range. Test your design with EWB.

5.11 Show how the noninverting integrator in Fig. P5.11 can be used to reduce the number of opamps of the Tow–Thomas biquad in Fig. 4.9 by one. Evaluate the

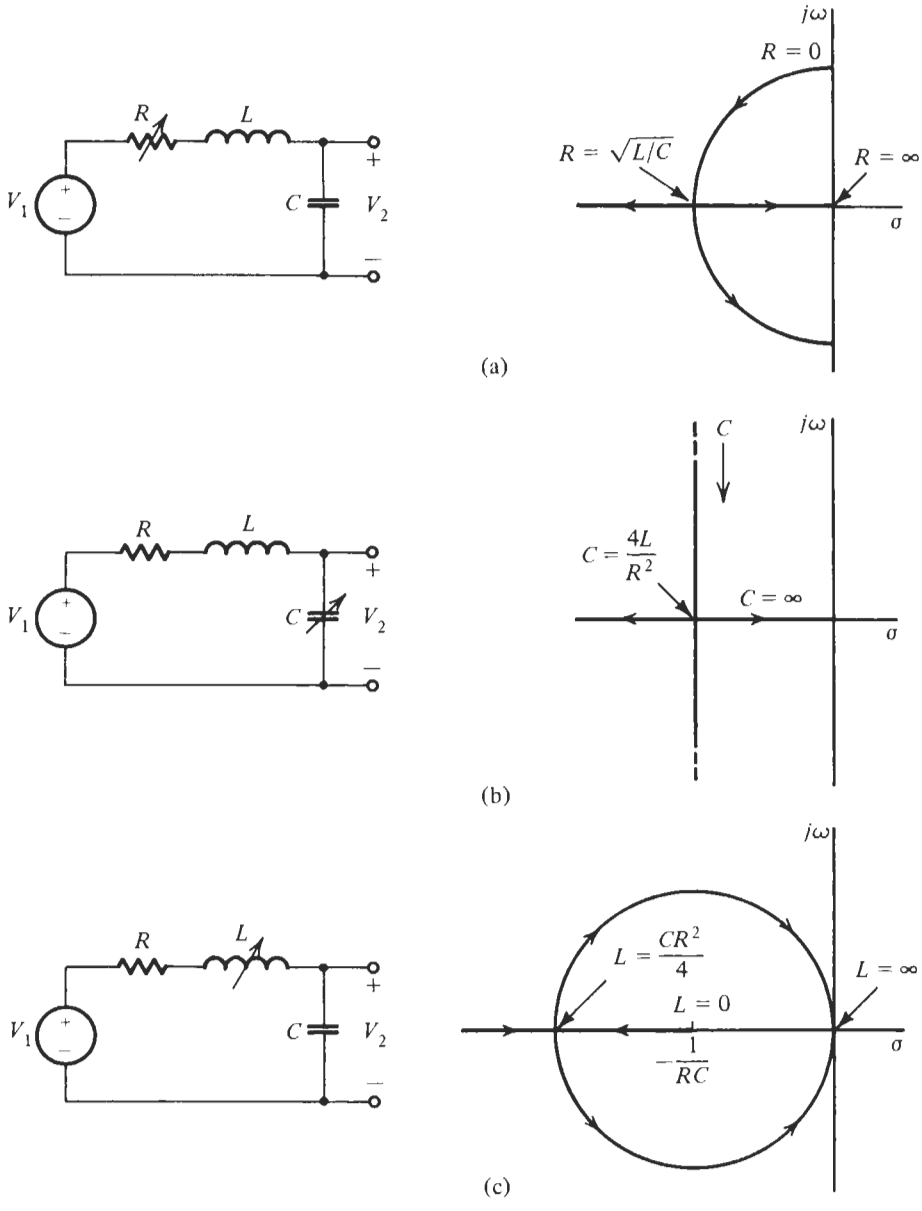

Figure P5.3

performance of this integrator for a nonideal opamp (use the integrator model). Refer also to Problem 4.16.

5.12 Consider the three-opamp circuit shown in Fig. P5.12. Writing equations at nodes x, y, and z, determine the transfer function $T = V_2/V_1$. Show that when $R_2 = R_3$, the filter becomes a notch filter, while when $R_2 = 2R_3$, the filter is an allpas one. Show that design can be accomplished by the choices $C_1 = C_2 = 1$, $R_1 = 1/Q$, and $R_2 = Q$.

5.13 Figure P5.13 shows the pole-zero plots of two transfer functions $T(s)$. Sketch the magnitudes and phases

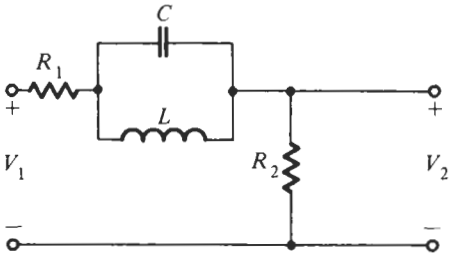

Figure P5.4

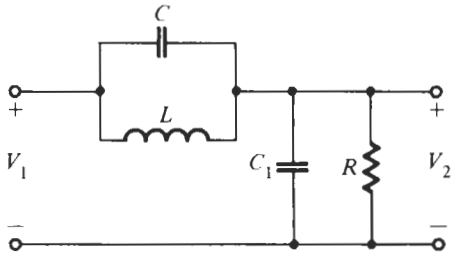

Figure P5.5

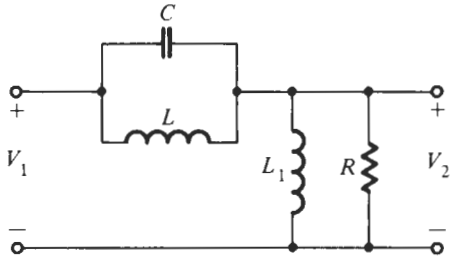

Figure P5.6

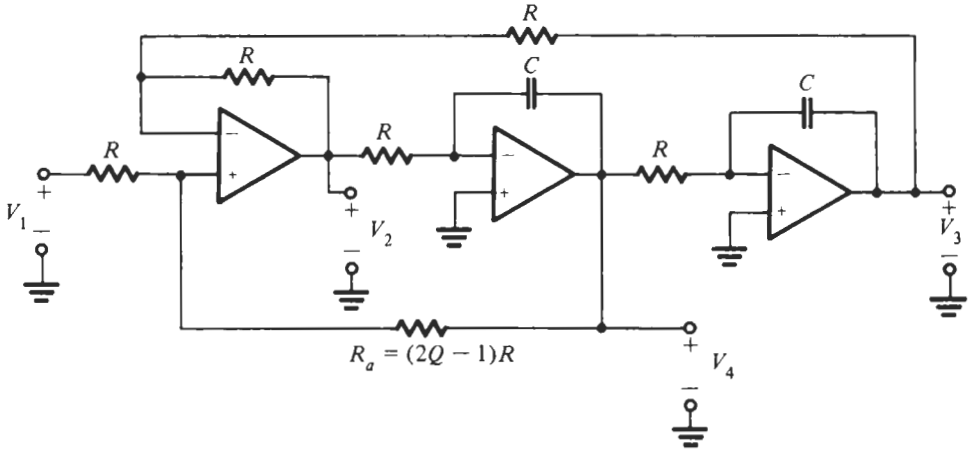

Figure P5.9

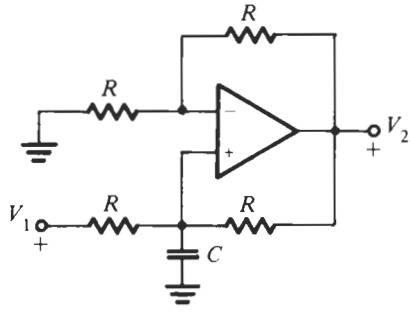

Figure P5.11

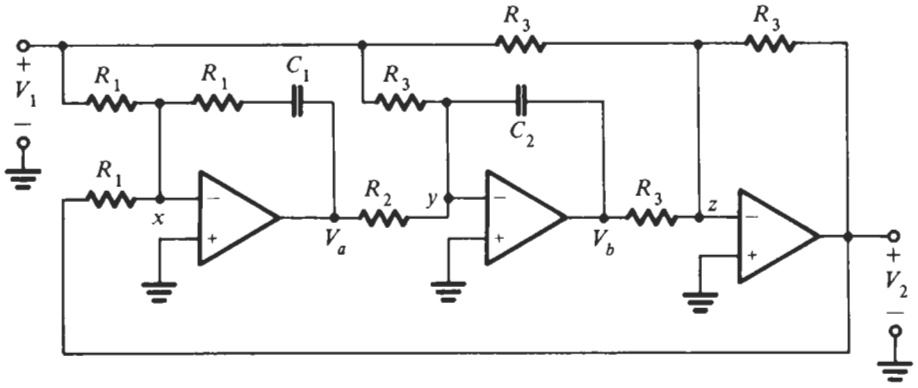

Figure P5.12

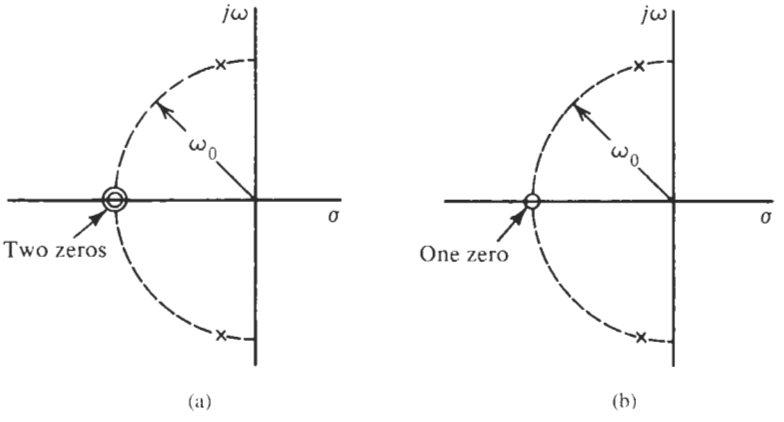

Figure P5.13

of the functions $T(j\omega)$. Make clear the values $\omega = 0$ and $\omega = \infty$ and the general shape of the responses.

5.14 Figure P5.14 shows a passive *RLC* circuit for which $C = 1/4$ F, $L = 1$ H, and $R = 1/2\ \Omega$. Design an inductorless circuit to fit in the box of Fig P5.14b, which is the analog of that shown in Fig. P5.14a with respect to ω_0 and Q. Give schematic and element values.

5.15 As far as possible, repeat Problem 5.2 with the GIC circuit of Fig. 5.16.

5.16 As far as possible, repeat Problem 5.2 with the Delyiannis–Friend circuit of Fig. 5.19.

5.17 Realize the function (it is a fifth-order Butterworth lowpass function; see Chapter 6)

$$T(s) = \frac{1}{s^5 + 3.2361s^4 + 5.2361s^3 + 3.2361s^2 + 1}$$

as a cascade of two second-order Åckerberg–Mossberg sections and one first-order active sections. The dynamic range should be maximized. The frequency is normalized by $f_0 = 680$ kHz. The maximum capacitor value is 1 nF; use practical component values and HA 2542-2 opamps, and test your design with EWB.

5.18 Realize the sixth-order bandpass function

$$T(s) = \frac{K_0 s^3}{(s^2 + 0.03755s + 1)(s^2 + 0.01936s + 1.05314)(s^2 + 0.01821s + 0.94059)}$$

as a cascade of GIC bandpass sections. The frequency is normalized by $f_0 = 5$ kHz. $T(s)$ is a sixth-order Chebyshev function (see Chapter 7) with a 0.5-dB ripple bandwidth of $\Delta f = 300$ Hz. Optimize the

dynamic range with the procedure discussed in the text and use practical elements and LM741 opamps. Test your design with EWB.

5.19 Realize the transfer function

$$T(s) = \frac{H_M s\left(s^2 + 1\right)}{\left(s^2 + 0.2s + 0.87\right)\left(s^2 + 0.5s + 1\right)}$$

as a cascade connection of two appropriate single-amplifier biquads. The frequency is normalized with respect to $\omega_0 = 2\pi \cdot 3.6$ krad/s. Choose equal capacitors, practical resistor values, and LM741 opamps in your design. Select any free parameters to minimize sensitivities. Maximize the dynamic range. Test the design with EWB.

5.20 Realize the (fourth-order Chebyshev) transfer function

$$T(s) = \frac{0.1250}{\left(s^2 + 0.41044s + 0.19579\right)\left(s^2 + 0.17001s + 0.90290\right)}$$

as a cascade of two Sallen–Key sections. The cutoff frequency is $f_0 = 8.6$ kHz. The gain constant should be realized correctly. Maximize the dynamic range, use practical element values and LM741 opamps, and test your design with EWB.

5.21 Realize the function of Example 5.17, but use Åckerberg–Mossberg sections. The cutoff frequency is 2.8 MHz. Use practical component values and HA 2542-2 opamps. Test the design with EWB.

5.22 Realize the function of Example 5.16 but use single-amplifier biquads. Be sure to use practical component values and use LM7421 opamps. Test your design with EWB.

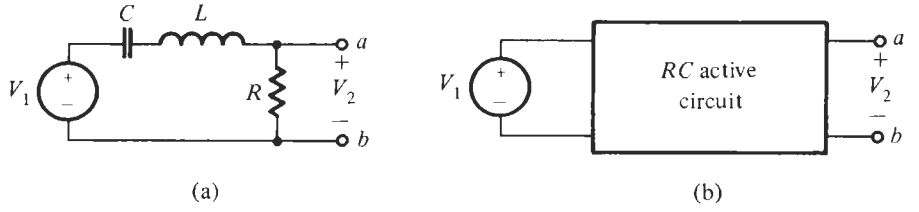

(a) (b)

Figure P5.14

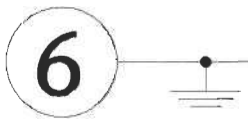

LOWPASS FILTERS WITH MAXIMALLY FLAT MAGNITUDE

This chapter is concerned with the design of lowpass filters of order greater than two so that we can implement filters with tougher requirements than can be realized with second-order functions. Some of the general concepts were discussed in Chapter 1, which the student may wish to review at this time. We will show first how the high-order function can be derived that meets practical filtering specifications and we will then realize this function by connecting first- and second-order sections in cascade. We shall focus in this chapter on functions that *approximate* the ideal lowpass specifications in a *maximally flat* sense.

6.1 THE IDEAL LOWPASS FILTER

The input voltage v_1 shown in Fig. 6.1 contains a low-frequency signal plus unwanted high-frequency signals, such as shrill tones, scratching sounds, or chirps. To remove these, leaving only the low-frequency signal, requires that we have a lowpass filter capable of passing low frequencies and rejecting high frequencies. Had the voltage v_1 contained several low-frequency signal components, we would like the filter design to be such that each was transmitted without change in amplitude. It is clear then, that the ideal filter characteristic we seek is that shown in Fig. 6.2. Below the normalized frequency of $\omega = 1$, the magnitude of $T(j\omega)$ is constant; above that frequency the value of T is 0. The passband and stopband are clearly separated at $\omega = 1$. Because of its shape, this ideal lowpass filter characteristic is called a *brick wall* response. Although we recognize that we will not be able to achieve this ideal because no rational function of finite degree n can have such

abrupt changes, it provides a basis on which we can rate an approximation. As shown in Fig. 6.3a, we desire that $|T_n|$ be as nearly constant as possible in the passband. In the stopband we require an n-pole roll-off. We have added the subscript n to the transfer function T to indicate that we wish generally to consider a function of order n. For most useful cases, we want the transition from passband to stopband to be as abrupt as possible. The degree n is then a large number, in contrast to $n = 2$, as was the case of second-order sections.

The method we will use in our approach to this problem is illustrated in Fig. 6.4. Suppose we use a cascade connection of circuits as was discussed in Section 5.3, Fig. 5. 24. Assume three sections with transfer functions T_1, T_2, and T_3 as indicated in Fig. 6.4 so that their gains multiply. The dashed line in Fig. 6.4 shows the product that is of the form required in Fig. 6.3a. The large values of $|T_1|$ are just overcome by the small values of $|T_2|$ and $|T_3|$ to achieve the approximation to the brick wall characteristic. The transfer functions have the same cut-off frequency, but different values of Q. How to determine the required values of Q will be our first objective.

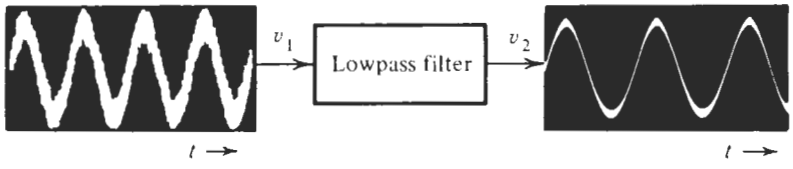

Figure 6.1 The function of a lowpass filter.

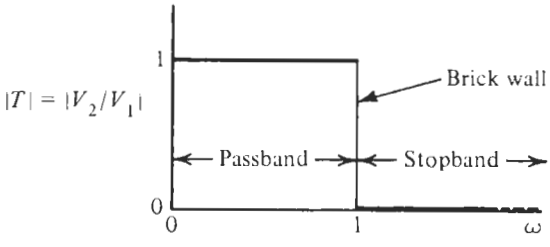

Figure 6.2 Ideal lowpass response: the "brick wall."

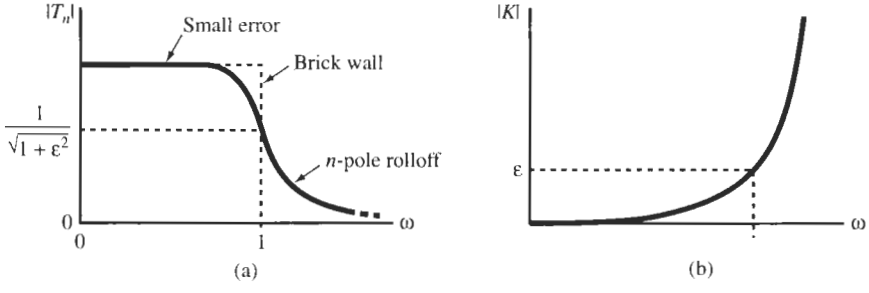

Figure 6.3 Lowpass magnitude: (a) transfer function; (b) characteristic function.

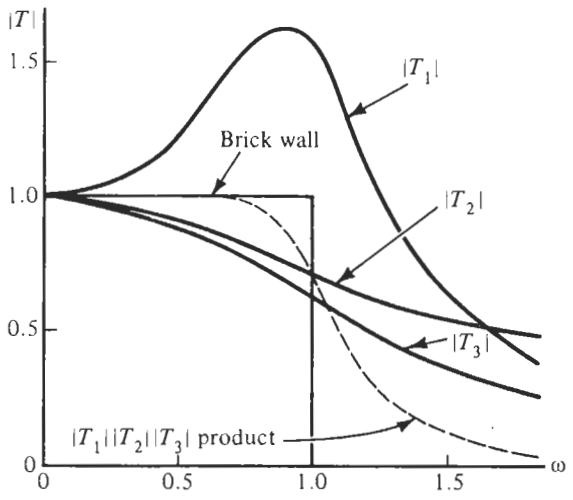

Figure 6.4 Generating an approximation for the brick wall lowpass by multiplying (cascading) three second-order functions.

6.2 BUTTERWORTH RESPONSE

We first review a topic in the algebra of complex numbers. If we denote the real and imaginary parts of the complex transfer function as

$$T(j\omega) = \text{Re } T(j\omega) + j \text{ Im } T(j\omega) \tag{6.1}$$

then we may enumerate some of the properties of $T(j\omega)$. Now the real part of Eq. (6.1) is an *even* function, while the imaginary part is an *odd* function. This means that replacing $j\omega$ by $-j\omega$ will change the sign of the imaginary part, but not that of the real part. Hence

$$T(-j\omega) = \text{Re } T(j\omega) - j \text{ Im } T(j\omega) \tag{6.2}$$

This function is known as the *conjugate* of $T(j\omega)$, so that

$$T(-j\omega) = T^*(j\omega) \tag{6.3}$$

Since

$$T(j\omega)T^*(j\omega) = (\text{Re } T)^2 + (\text{Im } T)^2 = |T(j\omega)|^2 \tag{6.4}$$

we have the important relationship

$$|T(j\omega)|^2 = T(j\omega)T(-j\omega) \tag{6.5}$$

In the past we have frequently replaced s by $j\omega$ or $j\omega$ by s, so that

$$|T(j\omega)|^2 = T(s)T(-s)|_{s=j\omega} \tag{6.6}$$

which is an important relationship in our study. Now the magnitude-squared function is an even function in that $|T(j\omega)|^2 = |T(-j\omega)|^2$. If we represent the magnitude-squared function

as a quotient of polynomials, then both the numerator and the denominator polynomial must be even. Let this quotient be

$$|T_n(j\omega)|^2 = \frac{|N_n(j\omega)|^2}{|D_n(j\omega)|^2} = \frac{A(\omega^2)}{B(\omega^2)} \tag{6.7}$$

The frequency ω is suitably normalized and the subscript n indicates that $T_n(s)$ is of degree n. Filter designers have found it convenient to introduce a *characteristic function* $K(s)$ that describes the deviation of $|T_n(j\omega)|$ from unity. With $K(s)$, $T_n(s)$ is written as

$$|T_n(j\omega)|^2 = \frac{1}{1 + |K(j\omega)|^2} \tag{6.8}$$

i.e., K is defined through $|K(j\omega)|^2 = |T_n(j\omega)|^{-2} - 1$; specifically for the notation in Eq. (6.7) we have

$$|K(j\omega)|^2 = \frac{B(\omega^2)}{A(\omega^2)} - 1 = \frac{B(\omega^2) - A(\omega^2)}{A(\omega^2)} \tag{6.9}$$

Figure 6.3b shows a sketch of $|K|$ corresponding to $|T_n|$ in Fig. 6.3a. We note that $|K|$ must be very small (ideally zero) in the passband and become increasingly large (ideally infinite) for frequencies in the stopband.

We choose for now a simple form for the polynomial $A(\omega^2)$, letting it be a constant $A_0 = 1$, i.e., we assume that there are no transmission zeros at finite values of ω. Then we obtain

$$|T_n(j\omega)|^2 = \frac{1}{1 + B_2\omega^2 + B_4\omega^4 + B_6\omega^6 + \cdots + B_{2n}\omega^{2n}} \tag{6.10}$$

We have set $A_0 = B_0 = 1$ so that $|T_n(j0)|^2 = 1$ as required for the ideal lowpass according to Fig. 6.2. With Eq. (6.10) we have from Eq. (6.9)

$$|K(j\omega)|^2 = B_2\omega^2 + B_4\omega^4 + B_6\omega^6 + \cdots + B_{2n}\omega^{2n} \tag{6.11}$$

that is, the squared magnitude of the characteristic function is a polynomial. Let us now require that the function $|K(j\omega)|$ approximates zero in the passband in the *maximally flat* sense, that is we require that as many derivatives as possible are zero at $\omega = 0$,

$$\left.\frac{d^k\left(|K(j\omega)|^2\right)}{d\left(\omega^2\right)^k}\right|_{\omega=0} = 0, \qquad \text{for } k = 1, 2, \ldots, n-1 \tag{6.12}$$

This shows that we need to set $B_2 = B_4 = \ldots = B_{2(n-1)} = 0$. ($k = n - 1$ is as far as we can go, because, for $k = n$, $|K(j\omega)|$ would become identically zero.) Consequently, we have the desired functions

$$|K(j\omega)|^2 = B_{2n}\omega^{2n} = \varepsilon^2\omega^{2n} \tag{6.13}$$

and

$$|T_n(j\omega)|^2 = \frac{1}{1 + B_{2n}\omega^{2n}} = \frac{1}{1 + \varepsilon^2\omega^{2n}} \tag{6.14a}$$

where we have introduced the notation $B_{2n} = \varepsilon^2$ because it will be convenient in our later development. The meaning of ε is clear from Fig. 6.3. If we still set $\varepsilon^2 = 1$, the function of Eq. (6.14a) is known as the *Butterworth response*:

$$|T_n(j\omega)|^2 = \frac{1}{1 + \omega^{2n}} \tag{6.14b}$$

From this equation we observe some interesting properties of the Butterworth response:

1. The Butterworth filter is an *all-pole* filter; it has zeros only at infinity ($\omega \to \infty$).
2. $|T_n(j0)| = 1$ for all n. This is a consequence of normalization.
3. $|T_n(j1)| = 1/\sqrt{2} \approx 0.707$ for all n, corresponding to -3 dB.
4. For large ω, $|T_n(j\omega)|$ exhibits n-pole roll-off, that is the attenuation increases by $20n$ dB per decade.

Figure 6.5 illustrates the magnitudes of Butterworth filters of orders 1 through 10.

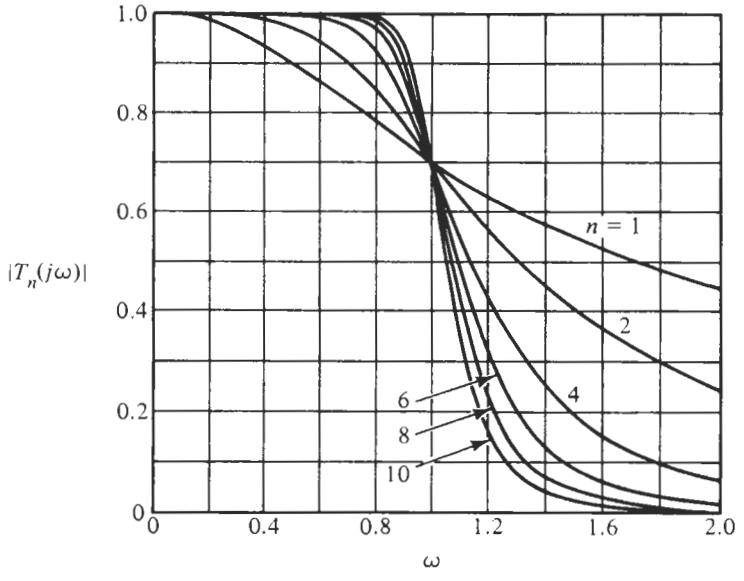

Figure 6.5 Butterworth magnitude of orders 1 to 10.

6.3 BUTTERWORTH POLE LOCATIONS

Our next objective is to determine the location of the poles for the transfer function with a Butterworth response. We begin by combining Eq. (6.6) with Eq. (6.14b) modified by letting $\omega = s/j$:

$$T_n(s)T_n(-s) = \frac{1}{1 + (s/j)^{2n}} \tag{6.15}$$

$$= \frac{1}{1 + (-1)^n s^{2n}} \tag{6.16}$$

The poles of Eq. (6.16) are the roots of the equation

$$B_n(s)B_n(-s) = 1 + (-1)^n s^{2n} = 0 \tag{6.17}$$

where B_n has been introduced to designate the *Butterworth polynomial.*

We will illustrate the solution of Eq. (6.17) by considering several examples. Let $n = 1$ so that

$$1 - s^2 = (1 + s)(1 - s) = 0 \tag{6.18}$$

Thus the poles are located as $s = \pm 1$, as shown in Fig. 6.6a. The pole in the right half-plane corresponds to an unstable system, and so we select the pole in the left half-plane to associate with B_1 and T_1. Then

$$B_1 = s + 1 \qquad \text{and} \qquad T_1 = \frac{1}{s + 1} \tag{6.19}$$

If we let $n = 2$, then Eq. (6.17) becomes

$$s^4 + 1 = 0 \qquad \text{or} \qquad s^4 = -1 \tag{6.20}$$

This equation has four solutions. If we write $-1 + j0$ in the polar form,

$$-1 = 1\angle(180° + k360°) \tag{6.21}$$

$k = 0, 1, 2, 3$, then we see that the angles of this equation are

$$\theta_k = \frac{180° + k360°}{4} = 45°, 135°, 225°, 315° \tag{6.22}$$

as shown in Fig. 6.6b. As we did for the $n = 1$ case, we select the roots in the left half-plane to assign to $T_s(s)$.

$$B_2(s) = (s + 0.707 + j0.707)(s + 0.707 - j0.707) = s^2 + \sqrt{2}s + 1 \tag{6.23}$$

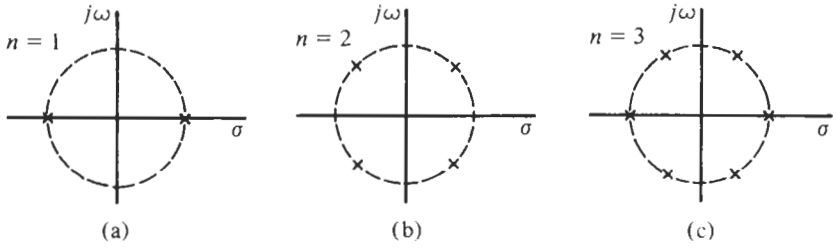

Figure 6.6 Zeros of $B_n(s)B_n(-S)$ for $n = 1, 2$, and 3.

and

$$T_2 = \frac{1}{s^2 + \sqrt{2}s + 1} \tag{6.24}$$

For $n = 3$ the form of Eq. (6.17) is

$$1 - s^6 = 0 \qquad \text{or} \qquad s^6 = 1 \tag{6.25}$$

The angles corresponding to Eq. (6.22) are

$$\theta_k = \frac{k360^\circ}{6} = 0^\circ, 60^\circ, 120^\circ, 180^\circ, 240^\circ, 300^\circ \tag{6.26}$$

and all roots of Eq. (6.25) are on a unit circle (Fig. 6.6c). If we generalize the two angle relationships of Eqs. (6.22) and (6.26), we have

$$\theta_k = 90^\circ \left(\frac{2k + n - 1}{n} \right) \qquad k = 1, 2, \ldots, 2n \tag{6.27}$$

We will seldom use this, since a different form is better suited to our needs.

All the poles of $T_n(s)$ are located on the unit circle because of the frequency normalization in which we set $\omega_0 = 1$. In addition, we will always select the poles in the left half-plane, since only these correspond to a stable circuit. Now θ_k in Eq. (6.27) is the angle measured from the positive real axis. Since our concern is in the left half-plane, let us measure the angle with respect to the negative real axis, designating it as ψ_k as in Fig. 4.2. Using this approach, we return to the case $n = 3$ and Eq. (6.25) and see that the angles of the three poles are

$$\psi_k = 0^\circ, +60^\circ, -60^\circ \tag{6.28}$$

Knowing the sine and cosine of 60°, we see that

$$B_3(s) = (s + 1)\left(s + \frac{1}{2} + j\frac{\sqrt{3}}{2}\right)\left(s + \frac{1}{2} - j\frac{\sqrt{3}}{2}\right) = (s + 1)(s^2 + s + 1) \tag{6.29}$$

This form is better suited to our needs, especially if we use the form of Eq. (6.29), from which

$$B_n = \begin{matrix} 1 \\ \text{or} \\ (s + 1) \end{matrix} \times \prod_k (s^2 + 2 \cos \psi_k s + 1) \tag{6.30}$$

Two simple rules permit us to determine ψ_k:

1. If n is odd, then there is a pole at $\psi = 0^\circ$; if n is even, then there are poles at $\psi = \pm 90^\circ/n$.
2. Poles are separated by $\psi = 180^\circ/n$.

The consequences of these rules are that there are never poles on the imaginary axis, and there

is always symmetry with respect to both the real and the imaginary axes when the poles for both $T_n(s)$ and $T_n(-s)$ are included.

There are various ways in which information about the Butterworth response can be presented. The angles for each value of n can be presented, as is done in Fig. 6.7, as derived from the rules given following Eq. (6.30). Table 6.1 tabulates the pole locations for $n = 2$ to $n = 10$, and Table 6.2 gives the coefficients of the Butterworth polynomials $B_n(s)$. The value of Q for each of the pole locations is routinely found using the result given in Eq. (4.13) and apparent in Eq. (6.30), since $\omega_0 = 1$,

$$Q = \frac{1}{2 \cos \psi} \tag{6.31}$$

Such values are given in Table 6.3. Finally, once $B_n(s)$ is known, the phase angle associated with the Butterworth response is found as

$$\theta_B = -\tan^{-1} \frac{\text{Im } B_n(j\omega)}{\text{Re } B_n(j\omega)} \tag{6.32}$$

These angles for $n = 1$ to $n = 10$ are given in Fig. 6.8.

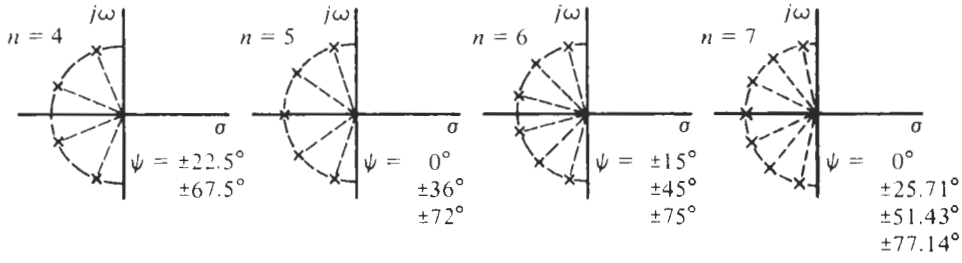

Figure 6.7 Poles of Butterworth filters of orders 4 to 7.

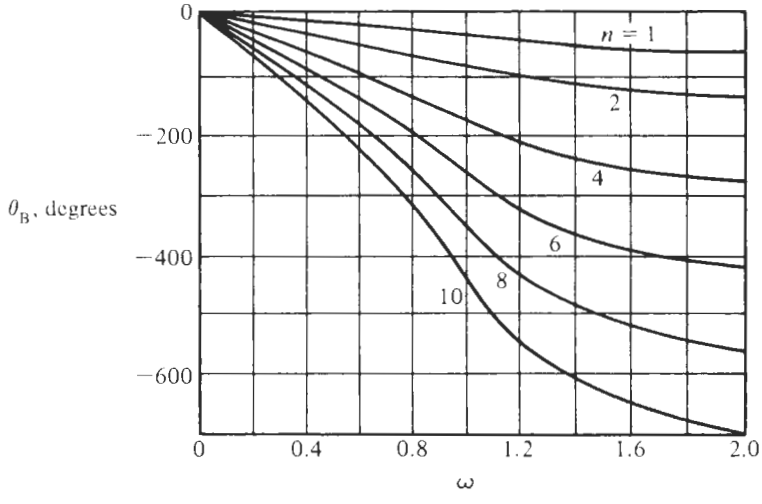

Figure 6.8 Butterworth phase for $n = 1$ to 10.

TABLE 6.1 Pole Locations for Butterworth Responses

$n=2$	$n=3$	$n=4$	$n=5$	$n=6$	$n=7$	$n=8$	$n=9$	$n=10$
-0.7071068	-0.5000000	-0.3826834	-0.8090170	-0.2588190	-0.9009689	-0.1950903	-0.9396926	-0.1564345
$\pm j0.7071068$	$\pm j0.8660254$	$\pm j0.9238795$	$\pm j0.5877852$	$\pm j0.9659258$	$\pm j0.4338837$	$\pm j0.9807853$	$\pm j0.3420201$	$\pm j0.9876883$
	-1.0000000	-0.9238795	-0.3090170	-0.7071068	-0.2225209	0.5555702	-0.1736482	-0.4539905
		$\pm j0.3826834$	$\pm j0.9510565$	$\pm j0.7071068$	$\pm j0.9649279$	$\pm j0.8314696$	$\pm j0.9848078$	$\pm j0.8910065$
			-1.0000000	-0.9659258	0.6234898	-0.8314696	-0.5000000	-0.7071068
				$\pm j0.2588190$	$\pm j0.7818315$	$\pm j0.5555702$	$\pm j0.8660254$	$\pm j0.7071068$
					-1.0000000	-0.9807853	-0.7660444	-0.8910065
						$\pm j0.1950903$	$\pm j0.6427876$	$\pm j0.4539905$
							-1.0000000	-0.9876883
								$\pm j0.1564345$

TABLE 6.2 Coefficients of the Butterworth Polynomial $B_n(s) = s^n + \sum_{i=0}^{n-1} a_i s^i$

n	a_0	a_1	a_2	a_3	a_4	a_5	a_6	a_7	a_8	a_9
2	1.0000000	1.4142136								
3	1.0000000	2.0000000	2.0000000							
4	1.0000000	2.6131259	3.4142136	2.6131259						
5	1.0000000	3.2360680	5.2360680	5.2360680	3.2360680					
6	1.0000000	3.8637033	7.4641016	9.1416202	7.4641016	3.8637033				
7	1.0000000	4.4939592	10.0978347	14.5917939	14.5917939	10.0978347	4.4939592			
8	1.0000000	5.1258309	13.1370712	21.8461510	25.6883559	21.8461510	13.1370712	5.1258309		
9	1.0000000	5.7587705	16.5817187	31.1634375	41.9863857	41.9863857	31.1634375	16.5817187	5.7587705	
10	1.0000000	6.3924532	20.4317291	42.8020611	64.8823963	74.2334292	64.8823963	42.8020611	20.4317291	6.3924532

TABLE 6.3 Q of Butterworth Poles

n even								n odd[a]						
2	**4**	**6**	**8**	**10**	**12**	**14**	**16**	**3**	**5**	**7**	**9**	**11**	**13**	**15**
0.71	0.54	0.52	0.51	0.51	0.50	0.50	0.50	1.00	0.62	0.55	0.53	0.52	0.51	0.51
	1.31	0.71	0.60	0.56	0.54	0.53	0.52		1.62	0.80	0.65	0.59	0.56	0.55
		1.93	0.90	0.71	0.63	0.59	0.57			2.24	1.00	0.76	0.67	0.62
			2.56	1.10	0.82	0.71	0.65				2.88	1.20	0.88	0.75
				3.20	1.31	0.94	0.79					3.51	1.41	1.00
					3.83	1.51	1.06						4.15	1.62
						4.47	1.72							4.78
							5.10							

[a] For n odd there is also a real pole for which $Q = 0.5$.

EXAMPLE 6.1

We wish to tabulate information concerning the fifth-order Butterworth response and calculate the phase angle at the frequency $\omega = 1$.

Solution

Since $n = 5$ indicates an odd Butterworth function, we know that one pole is located at $\psi = 0$ and that the others are separated from it by multiples of $180°/5 = 36°$. Thus

$$\psi_k = 0°, \pm 36°, \pm 72° \tag{6.33}$$

The pole locations are

$$p_i, p_i^* = -\cos\ \psi \pm j\ \sin\ \psi \tag{6.34}$$

They are then at

$$-1.0000000$$
$$-0.3090170 \pm j\ 0.9510565$$
$$-0.8090170 \pm j\ 0.5877852$$

The values of Q for the poles are found from Eq. (6.31) as 0.500, 0.618 and 1.618. The fifth-order Butterworth function is

$$B_5(s) = (s+1)(s^2 + 2\ \cos\ 36°\ s + 1)(s^2 + 2\ \cos\ 72°\ s + 1) \tag{6.35}$$

which can be compared with values tabulated in Table 6.2. The phase angle at $\omega = 1$ can be calculated from Eq. (6.35) by simply determining the phase of each of the terms. Here we see that

$$\theta_B(j1) = 45° + 90° + 90° = 225° \tag{6.36}$$

which agrees with an estimated value taken from Fig. 6.8.

6.4 LOWPASS FILTER SPECIFICATIONS

We have defined in Eq. (1.10) the attenuation of a filter as a function of frequency as

$$\alpha\ (\omega) = -20\ \log |T_n\ (\omega)| \tag{6.37}$$

measured in dB, which makes

$$|T_n\ (\omega)| = 10^{-\alpha(\omega)/20} \tag{6.38}$$

on a linear scale. Note that in this notation $\alpha(\omega)$ is a positive number because $|T_n(\omega)| \leq 1$ is assumed in the passband and, especially, in the stopband; see Fig. 6.3a. The Butterworth response in Fig. 6.5 was shown on linear coordinates. The corresponding plot of α in decibels as a function of linear ω is shown in Fig. 6.9 for the passband and Fig. 6.10 for the stopband. Such plots are useful for visualizing magnitudes, but actual design values are always found using a computer or calculator.

The manner in which specifications of a lowpass filter are given to the engineer is illustrated in Fig. 6.11. For the passband extending from $\omega = 0$ to $\omega = \omega_p$ the attenuation should not be larger than α_{max}. From ω_p to ω_s we have a transition band. Then the specifications indicate that from ω_s on for all higher frequencies the attenuation should not be less than α_{min}. It is customary to define the passband corner at $\omega = 1$, i.e., ω_p is the normalizing frequency and

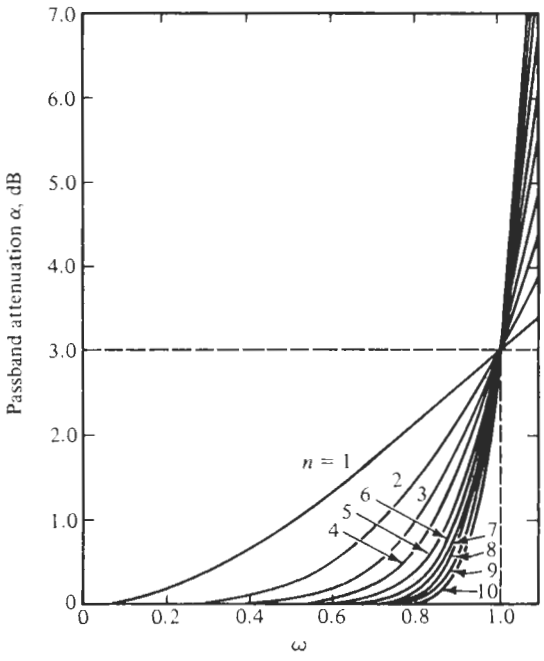

Figure 6.9 Passband attenuation of a Butterworth filter.

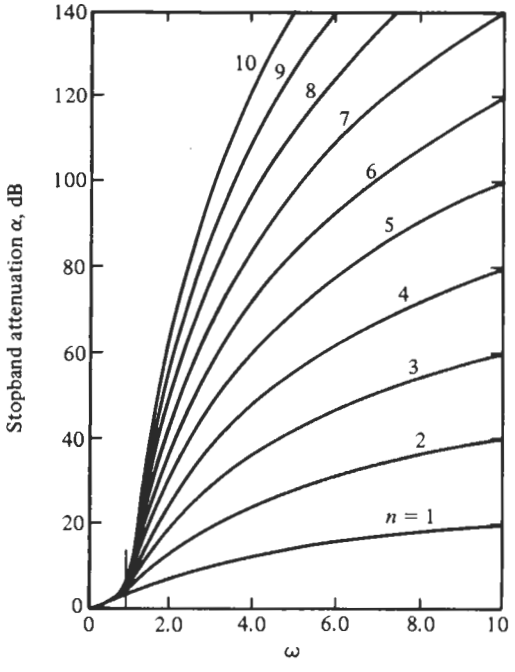

Figure 6.10 Stopband attenuation of a Butterworth filter.

we label $\omega_p = 1$. Given this information we need to find the two available parameters, the coefficient ε^2 and the degree n, of the maximally flat transfer function $|T_n(j\omega)|$ in Eq. (6.14a), where $|T_n(j1)| = 1/\sqrt{1+\varepsilon^2}$. With Eq. (6.37), we have at the passband corner,

$$\alpha_{max} = 10 \log\left(1 + \varepsilon^2\right) \tag{6.39}$$

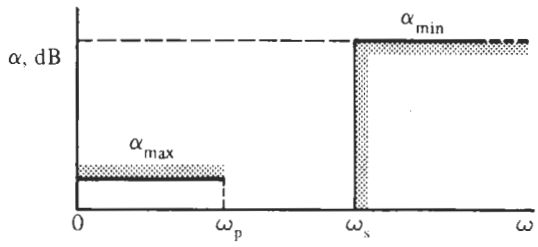

Figure 6.11 Lowpass filter specifications.

which is solved for

$$\varepsilon^2 = 10^{0.1\alpha_{max}} - 1 \tag{6.40}$$

At the stopband corner,[1] $\omega = \omega_s$, the specification is

$$\alpha_{min} = 10 \log\left(1 + \varepsilon^2 \omega_s^{2n}\right) \tag{6.41}$$

into which we insert Eq. (6.40)

$$\alpha_{min} = 10 \log\left[1 + \left(10^{0.1\alpha_{max}} - 1\right)\omega_s^{2n}\right] \tag{6.42}$$

This gives

$$\omega_s^{2n} = \frac{10^{0.1\alpha_{min}} - 1}{10^{0.1\alpha_{max}} - 1} \tag{6.43}$$

Taking the logarithm of this equation and solving for the degree n yields

$$n = \frac{\log[\left(10^{0.1\alpha_{min}} - 1\right) / \left(10^{0.1\alpha_{max}} - 1\right)]}{2 \log \omega_s} \tag{6.44}$$

We can readily evaluate this equation is by computer or calculator. The degree n must be, of course, an integer. But since the result of Eq. (6.44) is not ordinarily an integer, we *round up* to the next *larger* integer value and assign it to n. With n and ε known from Eqs. (6.40) and (6.44), the function

$$|T_n(j\omega)|^2 = \frac{1}{1 + \varepsilon^2 \left(\omega/\omega_p\right)^{2n}} \tag{6.45}$$

is completely determined. We have also shown the frequency ω_p that normalizes all frequency parameters.

The design procedure is carried out in two steps.

1. Using Eq. (6.40) determine the parameter ε. It sets the maximum attenuation in the passband, often referred to as the *ripple* width.
2. Use Eq. (6.44) to calculate the degree n, rounded up to the next larger integer.

[1]Remember that ω_s is normalized to the passband corner because we set $\omega_p = 1$.

Equation (6.45) is strictly speaking *not* a Butterworth filter function unless $\varepsilon = 1$. In the definition of a Butterworth lowpass filter, Eq. (6.14b), we have the passband edge at $\omega = 1$ and the attenuation at that frequency equal to 3 dB, i.e., $\varepsilon = 1$ is assumed. It is very helpful to start from this definition because a large number of design tables with poles, transfer functions, Q values, and even element values are available for such normalized Butterworth filters. Let us still rewrite Eq. (6.45) in a way that lets us take advantage of this information as far as possible. We bring $|T_n(j\omega)|^2$ into the form

$$|T_n(j\omega)|^2 = \frac{1}{1 + [\varepsilon^{1/n}(\omega/\omega_p)]^{2n}} = \frac{1}{1 + [\omega/(\varepsilon^{-1/n}\omega_p)]^{2n}} \tag{6.46}$$

and label $\varepsilon^{-1/n}\omega_p$ a new normalizing frequency $\omega_B > \omega_p$ where B stands for Butterworth,

$$\omega_B = \varepsilon^{-1/n}\omega_p \tag{6.47}$$

Equation (6.46) has the form of a standard Butterworth squared magnitude that, at $\omega = \omega_B$, has 3-dB attenuation but at $\omega = \omega_p < \omega_B$ has the smaller attenuation α_{max} as required in Fig. 6.11. Using this notation, we can make use of all tables and other data available in the literature on Butterworth filters; we only need to use ω_B as the denormalizing frequency in the final design.

EXAMPLE 6.2

Suppose that we are required to realize the following specifications with a maximally flat magnitude response:

$$\alpha_{max} = 0.5 \text{ dB} \qquad \alpha_{min} = 20 \text{ dB}$$
$$\omega_p = 1000 \text{ rad/s} \qquad \omega_s = 2000 \text{ rad/s}$$

Solution

To determine the transfer function that can be realized we find ε and n. Equations (6.40) and (6.44) yield, with $\omega_s/\omega_p = 2$,

$$\varepsilon^2 = 10^{0.05} - 1 = 0.12202 \qquad n = \frac{\log[(10^2 - 1)/(10^{0.05} - 1)]}{2 \log 2} = 4.83$$

We round n to $n = 5$. To be able to use Butterworth tables we next use Eq. (6.47) to find the denormalizing frequency

$$\omega_B = 0.349^{-1/5} \times 1000 \text{ rad/s} = 1234.1 \text{ rad/s}$$

that is to be used in the final design. The fifth-order Butterworth filter function is then from Table 6.1

$$T(s) = \frac{N(s)}{D(s)} = \frac{1}{(s+1)(s^2 + 1.6180s + 1)(s^2 + 0.6180s + 1)} \tag{6.48}$$

where $s = s/\omega_B$. This function can be realized as a cascade of one first-order and two second-order lowpass circuits, similar to Example 5.17 but with no finite transmission zeros.

To proceed, let us design a circuit for Eq. (6.48) using LM741 opamps in a cascade of the first-order section in Fig. 3.24 which realizes, by Eq. (3.70) with $C_1 = 0$ and $C_2 = C$,

$$T_1(s) = \frac{G_1}{sC + G_2} = \frac{G_1/C}{s + G_2/C}$$

and two Sallen–Key second-order lowpass sections from Fig. 4.31b, which each realize, by Eq. (4.111),

$$T(s) = \frac{aKG_1G_2}{s^2C_1C_2 + s[C_2(G_1 + G_2) + C_1G_2(1 - K)] + G_1G_2}$$

We break the transfer function into three sections,

$$T(s) = T_1T_2T_3 = \frac{k_1}{s + 1}\frac{k_2}{s^2 + 1.6180s + 1}\frac{k_3}{s^2 + 0.6180s + 1}$$

where we have assigned three gain constants k_1, k_2, and k_3 whose product must equal 1. The sections are arranged in the order of increasing values of Q as Eq. (5.69) recommends ($Q_1 = 0.5 < Q_2 = 0.618 < Q_3 = 1.618$). To compute the gain assignment we have by inspection the maximum of section T_1, $M_1 = 1$ at $\omega = 0$, the maximum of the cascade of T_1 and T_2, $M_2 = 1$ also at $\omega = 0$, and the maximum of the cascade of all three sections, $M_3 = 1$, to satisfy the design requirement. Thus, from Eqs. (5.78) and (5.80) we must choose $k_1 = k_2 = k_3 = 1$. For the first-order module we have

$$T_1(s) = \frac{G_1/C}{s + G_2/C} = \frac{1}{s + 1}$$

We choose $C = 0.1\ \mu$F so that for $\omega_B = 1234.1$ rad/s we obtain

$$R_1 = R_2 = \frac{1}{\omega_B C} = 8.103\ \text{k}\Omega$$

For the second-order sections we choose again $C_1 = C_2 = C$ and $G_1 = G_2 = G = 1/R$ to obtain

$$T(s) = \frac{aK\omega_0^2}{s^2 + s\omega_0/Q + \omega_0^2}$$

where $\omega_0 = 1/(RC)$ and $Q = 1/(3 - K)$. Then we set

$$T_2(s) = \frac{aK\omega_0^2}{s^2 + s\omega_0/Q + \omega_0^2} = \frac{1}{s^2 + 1.6180s + 1}$$

to obtain with $C = 0.1\ \mu$F and $\omega_B = 1234.1$ rad/s

$$R = \frac{1}{\omega_B C} = 8.103\ \text{k}\Omega, \quad K = 3 - Q^{-1} = 1.382, \quad a = 1/K = 0.724$$

Similarly for Section 3,

$$T_3(s) = \frac{aK\omega_0^2}{s^2 + s\omega_0/Q + \omega_0^2} = \frac{1}{s^2 + 0.6180s + 1}$$

we find

$$R = \frac{1}{\omega_B C} = 8.103\ \text{k}\Omega, \quad K = 3 - Q^{-1} = 2.382, \quad \text{and} \quad a = 1/K = 0.420$$

Because the design specified very low frequencies and values of Q, we need not be concerned with predistortion to correct the errors predicted by Eq. (4.125); the errors are of the order of 0.2%, likely less than the errors in the available components. Figure 6.12 shows the circuit and its performance, using as always LM741 opamps. The cut-off frequency is (approximately) as designed and the circuit provides ≈20-dB attenuation at 318 Hz (2000 rad/s). The gain rolls off at $20n = 100$ dB per decade. The −3-dB point is at ≈200 Hz (at ω_B). Higher accuracy can be obtained if required by using more accurate components in the realized circuit. A critical component is the 13-kΩ resistor in the third section; it adjusts Q_3 and thereby varies the 0.5-dB cut-off frequency as is apparent from studying Fig. 6.4.

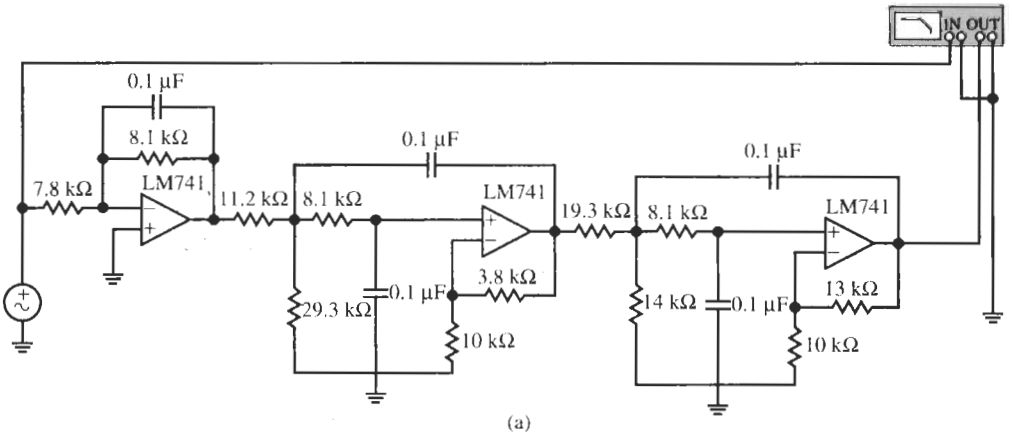

(a)

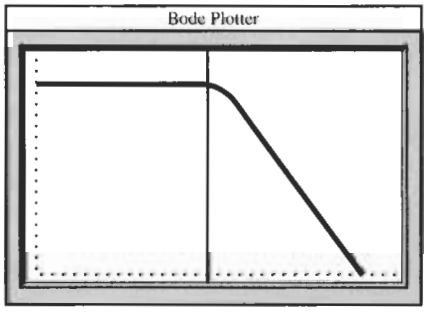

(b)

Figure 6.12 Fifth-order all-pole lowpass filter for Example 6.2 and test result. (Bode Plotter scales: 5 Hz to 5 kHz; −120 to 10 dB; cursor at 142.4 Hz, −0.687 dB.)

6.5 ARBITRARY TRANSMISSION ZEROS

As their name suggests, maximally flat *all-pole* lowpass filters have no finite transmission zeros; all their zeros are at $f = \infty$. If the engineer can place finite transmission zeros onto the $j\omega$ axis close to the edge of the stopband rather than needing to rely on a monotonic attenuation increase, the gain roll-off through the transition band is faster. This is illustrated by comparing the test results in Examples 5.7 and 6.2. The cost of inserting finite transmission zeros into a transfer function is reduced attenuation increase at high frequencies: Note that $T(s)$ in Eq. (1.12) for high frequencies behaves like $s^{(m-n)}$ so that the attenuation increases at $20(n-m)$ dB per decade rather than at $20n$ dB/decade as in an all-pole function. Since, as a rule, a narrow transition band is desirable, rapid attenuation increase through the transition band is more important than faster roll-off at high frequencies. Let us investigate, therefore, whether we can develop a filter with finite transmission zeros and maximally flat passband performance.

Return to Eq. (6.9) where we defined the characteristic function $K(s)$ via its magnitude

$$|K(j\omega)|^2 = \frac{B(\omega^2)}{A(\omega^2)} - 1 = \frac{B(\omega^2) - A(\omega^2)}{A(\omega^2)} = \frac{E(\omega^2)}{A(\omega^2)} \tag{6.49}$$

We have defined the even polynomial

$$\begin{aligned} E(\omega^2) &= E_0 + E_2\omega^2 + E_4\omega^4 + \cdots + E_{2n}\omega^{2n} \\ &= (1-1) + (B_2 - A_2)\omega^2 + (B_4 - A_4)\omega^4 + \cdots \\ &\quad + (B_{2(n-1)} - A_{2(n-1)})\omega^{2(n-1)} + B_{2n}\omega^{2n} \end{aligned} \tag{6.50}$$

i.e., $E_0 = B_0 - A_0 = 1 - 1 = 0$ resulting in $|K(j1)| = 0$ and $|T_n(j1)| = 1$. Because we are developing a lowpass and would like to reject infinite frequencies, it is obvious from Eq. (6.7) that the degree of the denominator $B(\omega^2)$ must be at least two higher than the degree of $A(\omega^2)$. This is reflected in Eq. (6.50) where $E_{2n} = B_{2n}$. For our earlier discussion of all-pole functions, we assumed that $A = A_0 = \text{const}$ so that there are no zeros in $|T_n(j\omega)|^2$ of Eq. (6.7). In that case Eq. (6.50) reduces to Eq. (6.11). If now A is a function of ω, that is $A = A(\omega^2)$, and we still aim at a maximally flat transfer function, we need to satisfy again Eq. (6.12)

$$\left.\frac{d^k\left(|K(j\omega)|^2\right)}{d\left(\omega^2\right)^k}\right|_{\omega=0} = \left.\frac{d^k}{d\left(\omega^2\right)^k}\left(E(\omega^2)\frac{1}{A(\omega^2)}\right)\right|_{\omega=0} = 0 \tag{6.51}$$

for as many values of k as possible. Using the chain rule of differentiation, we obtain for $k = 1$,

$$\left.\frac{d}{d(\omega^2)}\left[E(\omega^2)\frac{1}{A(\omega^2)}\right]\right|_{\omega=0} = \left.\left[E'\frac{1}{A} + E\left(\frac{1}{A}\right)'\right]\right|_{\omega=0} = \frac{B_2 - A_2}{A_0} = 0$$

i.e., $B_2 = A_2$. For convenience, we represented $d/d(\omega^2)$ by a prime. Similarly, for $k = 2$,

$$\left.\frac{d^2}{d(\omega^2)^2}\left[E(\omega^2)\frac{1}{A(\omega^2)}\right]\right|_{\omega=0} = \left.\left[E''\frac{1}{A} + 2E'\left(\frac{1}{A}\right)' + E\left(\frac{1}{A}\right)''\right]\right|_{\omega=0} = \frac{2(B_4 - A_4)}{A_0} = 0$$

i.e., $B_4 = A_4$. Proceeding in this manner for $k = 3, 4, \ldots, n-1$, we obtain the condition

$$B_{2i} = A_{2i}, \quad i = 0, 1, \ldots, n-1 \tag{6.52}$$

that must be satisfied if the squared magnitude $|T_n(j\omega)|^2$ is that of a transfer function $T_n(s)$ with a maximally flat passband. Thus, in Eq. (6.7) we pick a suitable numerator polynomial $A(\omega^2)$ that has the desired transmission zeros and then form the denominator by adding to $A(\omega^2)$ one high-order term:

$$|T_n(j\omega)|^2 = \frac{|N(j\omega)|^2}{|D(j\omega)|^2} = \frac{A(\omega^2)}{B(\omega^2)} = \frac{A(\omega^2)}{A(\omega^2) + B_{2n}\omega^{2n}} \tag{6.53}$$

Clearly, our earlier choice $A(\omega^2) = A_0 = 1$ leading to Eq. (6.14a) is a special case of Eq. (6.53). The parameter B_{2n} determines the maximum passband attenuation according to

$$|T_n(j1)|^2 = \frac{1}{1+\varepsilon^2} = \frac{1}{1 + B_{2n}/A(1)}$$

that is,

$$B_{2n} = \varepsilon^2 A(1) \tag{6.54}$$

This equation is in agreement with $B_{2n} = \varepsilon^2$ introduced in Eq. (6.13) where we had $A(1) = 1$. The difference between n and the degree of $A(s)$ determines the high-frequency roll-off. This was pointed out in the beginning of this section. To find the actual transfer function $T_n(s)$, we consult Eqs. (6.5) and (6.6) and write Eq. (6.53) as

$$T_n(j\omega)\, T_n(-j\omega)|_{j\omega=s} = \frac{N_n(s)}{D_n(s)} \frac{N_n(-s)}{D_n(-s)} = \frac{A(-s^2)}{A(-s^2) + (-1)^n B_{2n} s^{2n}} \tag{6.55}$$

Numerator and denominator of this function are even in s and can be factored into their roots which are symmetrical to the origin in the s-plane. Because the denominator $D_n(s)$ of

$$T_n(s) = \frac{N_n(s)}{D_n(s)} \tag{6.56}$$

is a Hurwitz polynomial with roots only in the left half s-plane, we collect all left half-plane roots into $D_n(s)$ and the right half-plane roots into $D_n(-s)$. $A(s)$ is also even, but the distribution of its roots to $N_n(s)$ and $N_n(-s)$ is not unique because the transmission zeros of $T_n(s)$ may be anywhere in the s-plane. We just have to make certain that conjugate complex roots stay together because all coefficients of $A(s)$ and of $N_n(s)$ are real.

A complete design example will illustrate the points made and will demonstrate how the final cascade circuit is obtained.

EXAMPLE 6.3

Design a lowpass filter to meet the following requirements:

1. Maximally flat passband with $\alpha_{\max} = 2$ dB in 0 Hz $= f =$ 18 kHz.
2. dc gain equal to $T_n(0) = 1$.

3. Transmission zeros at $f_1 = 36$ kHz and $f_2 = 72$ kHz.
4. At high frequencies the attenuation must increase at least 40 dB per decade.

Use LM741 opamps, suitable capacitor sizes, and Åckerberg–Mossberg biquads for the realization.

Solution

To make the passband corner equal to 1, we choose $f_p = 18$ kHz as the normalizing frequency. Then, with $\omega_0 = 2\pi f_p = 113.1$ krad/s we have the transfer function

$$|T_n(j\omega)|^2 = \frac{(\omega^2/4-1)^2(\omega^2/16-1)^2}{(\omega^2/4-1)^2(\omega^2/16-1)^2 + B_{2n}\omega^{2n}} \tag{6.57}$$

ω is the normalized frequency. The function has transmission zeros at $2f_p$ and $4f_p$ as specified, and its dc gain is unity. We next need to determine the order n. Since the numerator is of degree four, the specified high-frequency roll-off of 40 dB/decade means the degree of the denominator must be 2 higher, that is, $n = 6$. In addition we need to determine the value of B_{2n}, i.e., B_{12}, to meet the $\alpha_{max} = 2$ dB requirement. Since a maximally flat function has its maximum passband attenuation at $\omega = 1$, we have from Eq. (6.57)

$$|T_6(j1)|^2 = \frac{1}{1+\dfrac{B_{12}}{(1/4-1)^2(1/16-1)^2}} = \frac{1}{1+\left(\dfrac{64}{45}\right)^2 B_{12}} = 10^{-0.2} = 0.631$$

Solving for B_{12} yields $B_{12} = 0.28916$. Thus, after replacing ω by s/j, the function $T_6(s)$ to be realized is obtained from

$$T_6(s)T_6(-s) = \frac{N_4(s)N_4(-s)}{D_6(s)D_6(-s)} = \frac{(s^2/4+1)^2(s^2/16+1)^2}{(s^2/4+1)^2(s^2/16+1)^2 + 0.28916s^{12}}$$

Clearly, factoring the numerator results in $N_4(s) = (s^2/4+1)(s^2/16+1)$. Factoring the 12th-order denominator requires a root-finding algorithm; one obtains the 12 roots at

$$p_{1-4} = \pm 1.1218953 \pm j0.3392977 \qquad p_{5-8} = \pm 0.7324634 \pm j0.8328554$$
$$p_{9-12} = \pm 0.2387817 \pm j1.0214683$$

Note that the roots are located in quads symmetrically to the origin in the s-plane as was shown in Fig. 6.6b for the case $n = 2$. The left half-plane roots are the poles of $T_6(s)$. We find

$$T(s) = \frac{1.85964(s^2/4+1)(s^2/16+1)}{(s^2+2.24379s+1.37377)(s^2+1.46493s+1.23015)(s^2+0.47756s+1.10041)} \tag{6.58}$$

The constant coefficient in the numerator arises from $1/\sqrt{B_{12}} = 1/\sqrt{0.28916}$ because in the last equation we set the coefficient of s^6 equal to unity. Note that $T_6(j0) = 1$ as required.

This completes the derivation of the transfer function to meet the specifications set in the problem statement. To realize the function as a cascade circuit of three second-order sections we factor Eq. (6.58) into the product $T_1T_2T_3$ and assign the poles to the closest zeros. Since the zeros are on the $j\omega$ axis, at $\pm j2$ and at $\pm j4$ this assignment can be performed by inspection of Eq. (6.58): we find

$$T_6(s) = T_1T_2T_3 = \frac{k_1}{s^2 + 2.24379s + 1.37377} \times \frac{k_2\left(s^2/16 + 1\right)}{s^2 + 1.46493s + 1.23015} \frac{k_3\left(s^2/4 + 1\right)}{s^2 + 0.47756s + 1.10041} \tag{6.59}$$

where the product of the three gain constants $k_1k_2k_3$ must be equal to $K = 1.85964$. Computing the quality factors, we have

$$Q_1 = \frac{\sqrt{1.37377}}{2.24379} = 0.522, \quad Q_2 = 0.757, \quad \text{and} \quad Q_3 = 2.197$$

so that the sequence in Eq. (6.59) in the order of increasing values of Q is the one to be chosen for the realization.

The gain assignment proceeds by evaluating the voltage maxima at the outputs of the gain-scaled functions t_1, t_1t_2, and $t_1t_2t_3$. These values can readily be obtained with a computer, but a little insight into the functions will let us solve the task more easily: We have a lowpass requirement and $|T_1|$ and $|T_2|$ whose quality factors are less than 0.707 decrease over the passband. We can deduce, therefore, that their maxima as well as the maximum of their product occur at the origin. Thus, we have

$$\max|t_1| = M_1 = 1/1.37 = 0.73, \quad M_2 = \max|t_1t_2| = \frac{1}{1.37}\frac{1}{1.23} = 0.59$$

Finally, $\max|t_1t_2t_3| = M_3$ is obtained by noting that the transfer function is monotonically decreasing over the passband, that is, its maximum occurs also at zero. Thus,

$$M_3 = \max|t_1t_2t_3| = \frac{1}{1.373}\frac{1}{1.230}\frac{1}{1.00} \approx 0.54$$

Consequently, we have from Eqs. (4.78) to (4.80)

$$k_1 \approx 1.86\frac{0.54}{0.73} \approx 1.38, \quad k_2 = \frac{0.73}{0.59} = 1.24, \quad k_3 = \frac{0.59}{0.54} = 1.1$$

The three modules are then

$$T_6(s) = T_1T_2T_3 = \frac{1.38}{s^2 + 2.24379s + 1.37377} \times \frac{-1.24\left(s^2/16 + 1\right)}{s^2 + 1.46493s + 1.23015} \frac{-1.1\left(s^2/4 + 1\right)}{s^2 + 0.47756s + 1.10041} \tag{6.60}$$

They are realized by cascading three of the four-amplifier biquads shown in Fig. 5.1, one configured as a lowpass and two as lowpass notch filters. We have multiplied T_2 and T_3 by (-1) because by Eq. (5.5) the circuit realizes an inverting gain,

$$\frac{V_{\text{out}}}{V_{\text{I}}} = -\frac{as^2 + s(\omega_0/Q)[a - b(kQ)] + \omega_0^2[a + dk]}{s^2 + s\omega_0/Q + \omega_0^2} \tag{6.61}$$

where $\omega_0 = 1/(RC)$ and we set $c = 0$.

For the lowpass we dispense with the summing amplifier and use the circuit in Fig. 4.29 directly. With the elements identified in Fig. 5.1, it realizes Eq. (4.27a),

$$T_1(s) = \frac{k\omega_0^2}{s^2 + s\omega_0/Q + \omega_0^2} = \frac{1.38}{s^2 + 2.2438s + 1.3738} = \frac{(1.38/1.3738)1.3738}{s^2 + 2.2438s + 1.3738} \tag{6.62}$$

On the right-hand side of Eq. (6.62) we have brought T_1 into a form that helps us identify the filter parameters. If we pick the capacitors as $C = 0.01\ \mu$F, the resistor level will be of the order of $1/(\omega_0 C) \approx 880\ \Omega$. Resistors in the k$\Omega$ range are preferred. Thus we pick all capacitors as $C = 0.001\ \mu\text{F} = 1$ nF. Then we compute for T_1:

$$R = \frac{1}{2\pi \times 1.3738 \times 18000s^{-1} \times 10^{-9}\text{F}} = 6.44\text{k}\Omega, \quad Q_1 R = 0.522 \times 6.44\text{k}\Omega = 3.36\ \text{k}\Omega$$

Equation (6.62) shows that $k = 1.38/1.374 \approx 1.0$, thus we have

$$R/k = 6.44/1.0\ \text{k}\Omega = 6.44\text{k}\Omega$$

To be able to identify the parameters of T_2 easily, we bring the function into the form

$$T_2(s) = \frac{0.0775s^2 + 1.24}{s^2 + 1.46493s + 1.23015} = \frac{as^2 + \omega_0^2(a + dk)}{s^2 + s\omega_0/Q + \omega_0^2}$$

Also, we need to remember that $a = bkQ$ to create the zero in Eq. (6.61). We have

$$R = \frac{1}{1.2302\omega_0 \times 10^{-9}\text{F}} = 7.19\text{k}\Omega, \quad Q_2 R = 0.757 \times 7.19\ \Omega = 5.44\text{k}\Omega$$

The prescribed numerator coefficients result in $a = 0.0775$ and

$$1.24 = 1.23(a + dk) = 0.0953 + 1.23dk, \quad \text{and} \quad 0.0775 = 0.757bk$$

giving $dk = 0.9307$ and $bk = 0.1024$. Let us choose $k = 1$; then we have $d = 0.931$ and $b = 0.102$.

Proceeding in a similar fashion for T_3, we obtain

$$T_3(s) = \frac{0.275s^2 + 1.10}{s^2 + 0.47756s + 1.10041} = \frac{as^2 + \omega_0^2(a + dk)}{s^2 + s\omega_0/Q + \omega_0^2}$$

the element values

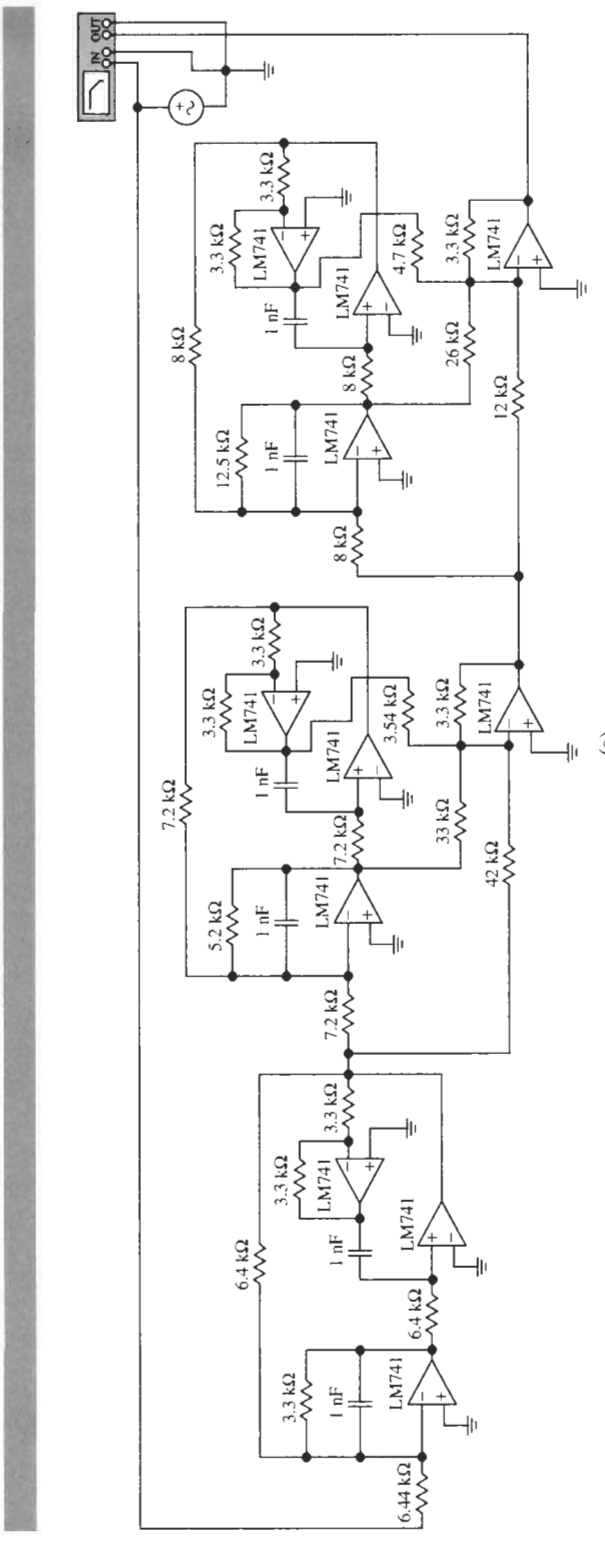

(a)

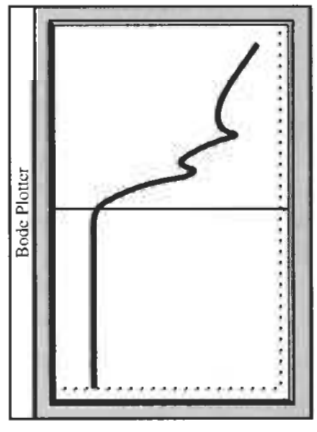

(b)

Figure 6.13 Sixth-order cascade lowpass circuit for Example 6.3 and test results. (Bode Plotter scales: 500 Hz to 500kHz; −100 to 10 dB; cursor at 18.13 kHz, −2.547 dB.)

$$R = \frac{1}{1.1004\omega_0 \times 10^{-9}\text{F}} = 8.04\text{k}\Omega, \quad Q_3 R = 2.197 \times 8.04\text{k}\Omega = 17.65\ \text{k}\Omega$$

and the numerator coefficients

$$a = 0.275, 0.275 + dk \approx 1, 0.275 = 2.197bk$$

We set again $k = 1$ to get $d = 0.725$ and $b = 0.125$ along with $c = 0$.

The resulting circuit together with test results is shown in Fig. 6.13. The circuit performed as designed except for an ≈1.5-dB peaking at the passband edge that requires tuning. It is an advantage of cascade design that tuning is accomplished easily because the second-order stages are isolated. Hence the performance of any module is not affected by any other module. In this case, the observed peaking is corrected readily by reducing the Q-determining resistor on Module 3 (which peaks closest to the bandedge) from 17.5 to 12.5 kΩ as done in the figure. The test results show clearly the two transmission zeros, the 2-dB bandedge at 18 kHz (cursor) and the 40-dB/decade roll-off at high frequencies in contrast to 100 dB/decade that would be obtained for an all-pole design.

In this chapter we have developed a method for finding a realizable transfer function that satisfies the design constraints in Fig. 6.11. We did this by finding a function that approximates zero attenuation in the passband in the maximally flat sense so that the error is as small as possible at $\omega = 0$ and then gradually increases toward the maximum allowed value $\alpha_{\max}$ at the end of the passband, ω_p. The degree n was then determined such that the transfer function clears the corner $\alpha_{\min}$ at the edge of the stopband, ω_s. This situation is shown in Fig. 6.14a. Now, since the specifications permit $\alpha_{\max}$ to be reached throughout the passband we may ask whether "greater efficiency" in the approximation can be obtained if we allow the error to be distributed more evenly throughout the passband as is sketched in Fig. 6.14b. Greater efficiency would result in a function of lower order n that can be realized with fewer components and lower cost. Such a transfer function with ripples in the passband may be obtained if we change the requirement of maximal flatness that resulted in the condition that all coefficients B_i in Eq. (6.11) are zero with the exception of B_{2n}. We shall discuss the derivation of such a function in the next chapter.

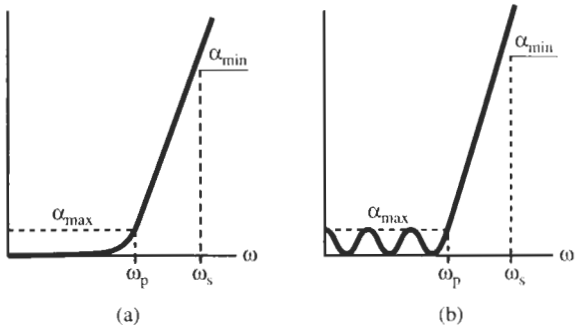

Figure 6.14 Different strategies for approximating a lowpass specification: (a) maximally flat function; (b) equiripple approximation.

PROBLEMS

6.1 Show that the real part of the transfer function

$$T(s) = \frac{s^2 + \omega_z^2}{s^2 + s\omega_0/Q + \omega_0^2}$$

is even, that its imaginary part is odd and that $|T(j\omega)|^2 = T(j\omega)T(-j\omega)$.

6.2 Use Eqs. (6.26) and (6.30) to find the roots of the fifth- and sixth-order Butterworth polynomials. The polynomial coefficients are listed in Table 6.2. Compare your answers with the ones in Table 6.1.

6.3 Figure P6.3 shows an *RCL* circuit in which $R_2 = 1$ and L_1 and C_2 are to be determined so that V_2/V_1 gives a Butterworth frequency response.

6.4 Figure P6.4 shows an *RLC* circuit driven by a current source I_1. It is given that $R_2 = 1$. You are to find the values of C_1 and L_2 such that V_2/I_1 gives a Butterworth frequency response.

6.5 A maximally flat magnitude transfer function is characterized by the parameters $\varepsilon = 0.075$ and $n = 7$. Determine the minimum attenuation at the stopband frequency $\omega_s = 1.85\omega_p$. Assume $f_p = 980$ Hz. Find the transfer function and its poles, relying on Butterworth tables. Design a test a Sallen–Key filter using suitable opamps.

6.6 A maximally flat magnitude transfer function is to be derived such that $\alpha_{max} = 0.02$ dB in $0 \le \omega \le 1$ and $\alpha_{min} = 48$ dB for $\omega \ge 2.2$. Find the parameters n and ε, and use Butterworth tables to the function. Design a test Sallen–Key filter using suitable opamps.

6.7 A Butterworth transfer function is characterized by $n = 7$. Determine ε and the attenuation at $\omega = 12$ ($\omega_p = 1$). What is the phase angle at $f = 0.8$?

6.8 A maximally flat magnitude transfer function is characterized by α_{min}, α_{max}, and $n = 5$. The frequency is normalized to the passband corner. Determine the lowest frequency ω_s at which α_{min} is encountered.

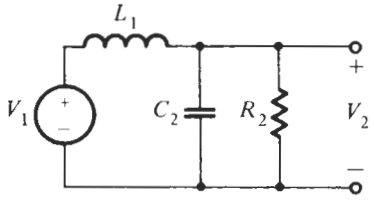

Figure P6.3

6.9 A maximally flat magnitude transfer function is characterized by α_{min}, α_{max}, and $\omega_s = 1.25$. The frequency is normalized to the passband corner. Determine the degree n. Find the function.

6.10 Consider the following three sets of specifications:

	α_{max} dB	α_{min} dB	ω_p, rad/s	ω_s, rad/s
(a)	0.25	15	10,000	14,000
(b)	0.50	30	750	1,750
(c)	1.00	25	1,250	4,375

For each of the three cases do the following:
(i) Determine n, the required order of the LP filter with maximally flat magintude.
(ii) Determine the actual attenuation at the edge of the passband and the edge of the stop band, $\alpha(\omega_p)$ and $\alpha(\omega_s)$.
(iii) Determine the attenuation at the frequencies $2 \times \omega_s$ and $10 \times \omega_s$.

6.11 Repeat Problem 6.4 for the following three specifications:

	α_{max}, dB	α_{min}, dB	f_p, Hz	f_s, Hz
(a)	0.25	18	1000	1400
(b)	0.50	20	2000	2800
(c)	0.50	30	1000	1400

6.12 A fifth-order lowpass maximally flat-magnitude filter characteristic has the values $\omega_p = 1000$ rad/s and $\alpha_{max} = 0.35$ dB. What will be the attenuation of the response when $\omega = 2000$ rad/s?

6.13 In the following series of problems a lowpass filter is to be designed having the loss specifications as shown in Fig. P6.13. For each specification do the following:

(a) Determine the degree n of the required maximally flat magnitude response.

(b) Determine the location of the poles in the s-plane and the quality factor of each pole.

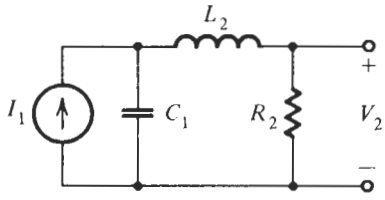

Figure P6.4

(c) Determine the actual loss $\alpha_{min}(\omega_p)$ and $\alpha_{max}(\omega_s)$ at the passband and stopband corners.

(d) Design the filter and test the performance.

	α_{max}, dB	α_{min}, dB	f_p, Hz	f_s, Hz
(i)	0.5	30	1000	2330
(ii)	0.5	20	1000	2000
(iii)	1.0	35	1000	3500
(iv)	0.5	20	1000	1725

6.14 We wish to design a lowpass filter to satisfy the loss specifications shown in Fig. P6.14. Thus we wish a filter with a flat loss of α_1 dB and a max. flat response specified by α_2, α_3, ω_1, and ω_2. Our final design might better be described as a filter attenuator. For uniformity, we will specify that the Sallen–Key circuit of Fig. 4.31a be used and that the capacitors in the realization should have the value of 1 μF.

	α_1, dB	α_2, dB	α_3, dB	ω_1, rad/s	ω_2, rad/s
(i)	8	9	23	1000	2300
(ii)	6	8	32	1000	3000
(iii)	10	10.5	40	100	800

6.15 Derive a lowpass transfer function with maximally flat magnitude to have $\alpha_{max} = 0.5$ dB passband attenuation in $f \leq 1.2$ MHz and attenuation increase of 40 dB per decade at high frequencies. The function must have infinite attenuation at $f = 6$ MHz. Using suitable opamps, realize and test the transfer function.

6.16 A maximally flat magnitude transfer function is characterized by the parameters $\varepsilon = 0.05$ and $n = 8$. The stopband corner is prescribed to be $\omega_s = 1.65$. There are two transmission zeros on the normalized frequency axis at $\omega = 2.4$ and 4.0. Determine the transfer function, the maximum attenuation α_{min} in the passband, and the rate of attenuation increase at very high frequencies.

6.17 To be designed is an amplifier filter with two Sallen–Key stages. The gain at dc is to be $\alpha = 20$ dB and the gain must be $\alpha = 17$ dB at $\omega = 10$ krad/s. Design and test the filter. Use LM741 opamps and be sure to use practical component values.

6.18 Design a lowpass filter with a maximally flat response to meet the specifications: $\alpha_{max} = 0.50$ dB, $\alpha_{min} = 30$ dB, $\omega_p = 750$ rad, $\omega_s = 1750$ rad/s.

(a) Make use of Sallen–Key circuits with $K = 14$, and magnitude scale to obtain elements in a practical range.

(b) To the filter designed in Part (a), we wish to add gain enhancement of 20 dB (flat for all frequencies). Modify the design of Part (a) to accomplish this objective.

6.19 Design an Åckerberg–Mossberg circuit with two equal capacitors. Choose the resistors such that the circuit has a Butterworth response with dc gain equal to K.

6.20 Consider the RC opamp circuit shown in Fig. P6.20. What value of R_1 and R_2 will give the transfer function

$$T(s) = \frac{s^2}{s^2 + (1/Q)s + 1}$$

6.21 A highpass filter is required to meet the specifications shown in Fig. P6.21. Make use of the RC–CR transformation of Section 4.5.1. to design the filter, and scale so that all capacitors have the value of $C = 0.1$ μF

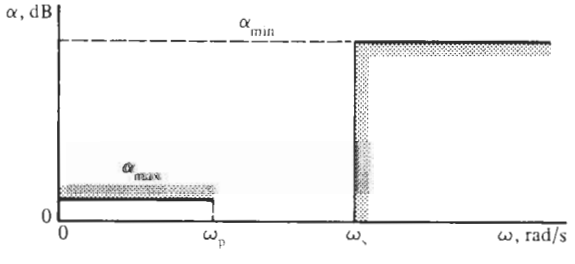

Figure P6.13

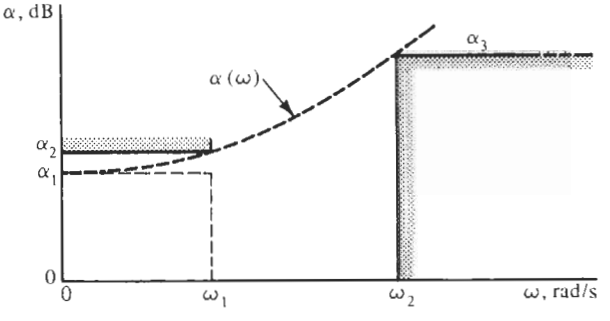

Figure P6.14

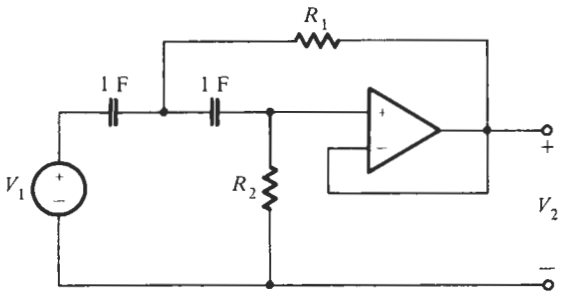

Figure P6.20

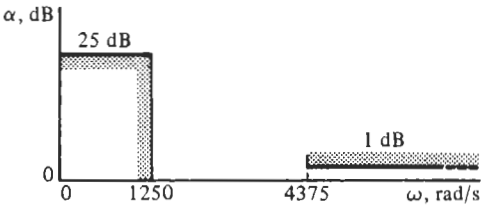

Figure P6.21

7 LOWPASS FILTERS WITH EQUAL-RIPPLE (CHEBYSHEV) MAGNITUDE RESPONSE

The preceding chapter has dealt with the maximally flat approximation of a given lowpass requirement. The function we dealt with was Eq. (6.8),

$$|T_n(j\omega)|^2 = \frac{1}{1 + |K_n(j\omega)|^2} \tag{7.1}$$

For an all-pole transfer function $T_n(s)$ we had

$$|K_n(j\omega)|^2 = (\varepsilon\omega^n)^2 \tag{7.2}$$

We have introduced the subscript n to denote specifically the order of the function. Recall that for a Butterworth response we had $\varepsilon = 1$, and that for all-pole transfer functions, $|K_n(j\omega)|$ must be a *polynomial*. The polynomial $\varepsilon\omega^n$ in Eq. (7.2) is monotonically increasing, which implies that the error of $|T_n(j\omega)|$ is monotonically increasing toward the corner of the passband, $\omega = 1$. Note that we again normalized the passband corner to 1 as is customary in the literature on filters. We now will find a different function $|K_n(j\omega)|$ that will go uniformly back and forth over the range $\alpha \leq \alpha_{\max}$ in $\omega \leq \omega_p = 1$ and lets us make better use of the attenuation constraints over the whole passband.

7.1 THE CHEBYSHEV POLYNOMIAL

Suppose that we wish the response function to be confined to the cross-hatched strip shown in Fig. 7.1a where the strip's width, defined by ε, may be made as narrow as we wish by choosing

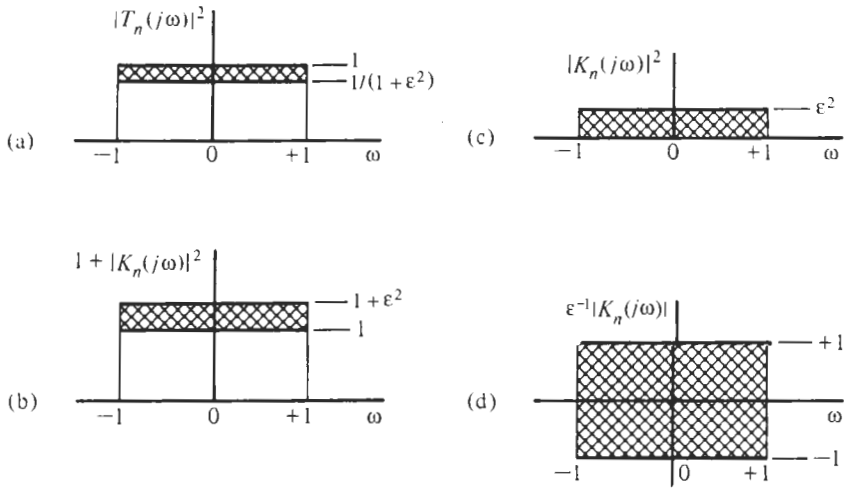

Figure 7.1 Defining the passband area for the function $|K_n(j\omega)|$.

a small value for e. Our task is then to find a function $|K_n(j\omega)|$ that will result in $|T_n(j\omega)|$ in Eq. (7.1) to satisfy the specified constraints. The graphic construction in Fig. 7.1 provides us with an approach. In Fig. 7.1b we show the corresponding cross-hatched area covered by the denominator of Eq. (7.1). We then subtract 1 from the figure to obtain the required limits of $|K_n(j\omega)|$ shown in Fig. 7.1c. Finally, we extract the square root and scale the magnitude by ε to obtain the cross-hatched strip in Fig. 7.1d. It has the dimension of a square; the limits of amplitude are ± 1 and the limits in ω are ± 1. We seek now a function $|K_n(j\omega)|$ that may be scaled to fit in this box. Once it is found, the response $|T_n(j\omega)|$ in Eq. (7.1) will result; it turns out to be of great importance in the design of filters. The result is attributed to the Russian engineer P. L. Chebyshev,[1] who used the functions in studying the construction of steam engines.

One function that is known to go back and forth in ± 1 is known to be the sinusoid,

$$y(x) = \cos nx \tag{7.3}$$

where n is an integer. This function will oscillate forever for all x in $-\infty < x < +\infty$; to limit the range to $|x| \leq \pm 1$, we introduce the transformation of variable

$$x = \cos^{-1}\omega \tag{7.4}$$

so that we have the result

$$y = \cos\left(n \cos^{-1}\omega\right) = C_n(\omega) \quad \text{for} \quad |\omega| \leq 1 \tag{7.5}$$

Although it does not look like one, the function $C_n(\omega)$ in Eq. (7.5) is a polynomial: We can show this by using a well-known trigonometric identity to write

[1]Pafnuti L. Chebyshev (1821–1894). His paper was published in *Oevres*, Vol. I, St. Petersburg, 1899. Some authors also use the German transliteration Tschebyscheff.

$$\cos n\theta = 2^{n-1}\cos^n\theta - \frac{n}{1!}2^{n-3}\cos^{n-2}\theta + \frac{n(n-3)}{2!}2^{n-5}\cos^{n-4}\theta - \frac{n(n-3)(n-5)}{3!}2^{n-7}\cos^{n-6}\theta + \cdots$$

This expression is recognized as a polynomial in ω by inserting $\theta = \cos^{-1}\omega$. We find

$$C_n(\omega) = 2^{n-1}\omega^n - \frac{n}{1!}2^{n-3}\omega^{n-2} + \frac{n(n-3)}{2!}2^{n-5}\omega^{n-4} - \frac{n(n-3)(n-5)}{3!}2^{n-7}\omega^{n-6} + \cdots \tag{7.6}$$

$C_n(\omega)$ are the *Chebyshev polynomials* of order n. The first few of these polynomials are given in Table 7.1. We also have listed a recursion formula that follows directly from the trigonometric identity

$$\cos n\theta = 2\cos\theta\cos(n-1)\theta - \cos(n-2)\theta \tag{7.7}$$

The first four of the polynomials are plotted in Fig. 7.2a over the range $|\omega| \leq 1$. Notice that in some sense these functions are distorted cosine waves, bunched toward $\omega = \pm 1$. It is clear that $C_n(\omega)$ and its square, shown for $n = 4$ in Fig. 7.2b, when scaled appropriately, satisfy the requirements to fit into the boxes we imposed in Fig. 7.1d and c, respectively. Furthermore, the ripples within the boxes are always equal, ± 1 for C_n and between $+1$ and 0 for C_n^2. For this reason, the functions are also called *equal-ripple* (or sometimes, *equiripple*) functions.

TABLE 7.1 The First Four Chebyshev Polynomials and Recursion Formula

$C_0(\omega) = 1$
$C_1(\omega) = \omega$
$C_2(\omega) = 2\omega^2 - 1$
$C_3(\omega) = 4\omega^3 - 3\omega$
$C_n(\omega) = 2\omega C_{n-1}(\omega) - C_{n-2}(\omega)$

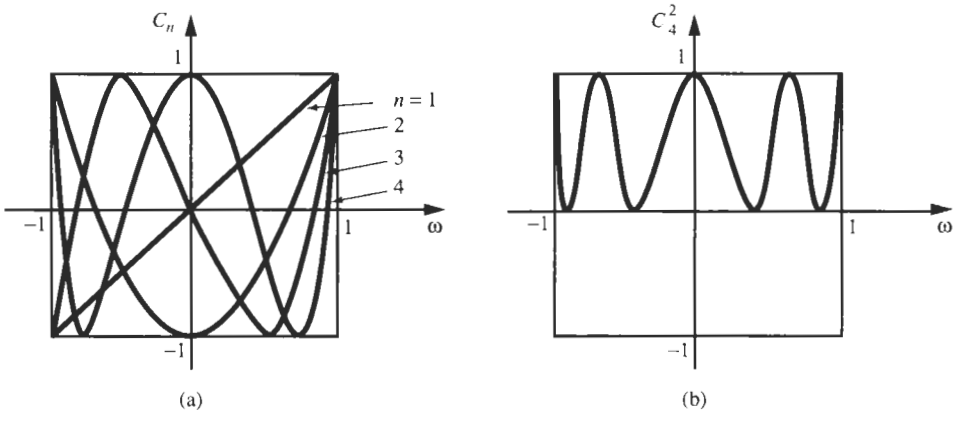

Figure 7.2 (a) The first four Chebyshev polynomials; (b) the square of the functions $C_4(\omega)$.

7.2 THE CHEBYSHEV MAGNITUDE RESPONSE

$C_n(\omega)$ is useful for the function $|K_n(j\omega)|$ we sought for Eq. (7.1). Thus, after squaring C_n and setting $|K_n(j\omega)| = \varepsilon C_n(\omega)$, we have the *Chebyshev magnitude response* from Eq. (7.1),

$$|T_n(j\omega)|^2 = \frac{1}{1 + \varepsilon^2 C_n^2(\omega)} \tag{7.8}$$

where $C_n(\omega)$ is given in Eq. (7.5). Note that as given in Eq. (7.5), C_n is defined only for $|\omega| \leq 1$. Thus, this function satisfies the requirements cited earlier, valid for the frequency range $-1 \leq \omega \leq +1$. We know that Eq. (7.8) must also apply for ω larger than 1, and so we do have the problem of determining how to interpret the cosine function and its inverse for $|\omega| > 1$. There are two approaches to resolve this problem. One is to recognize that C_n is a polynomial, as we saw in Eq. (7.6), which is valid for any ω. The other possibility that is more convenient for our purpose is to observe that for $|\omega| = 1$ the inverse cosine becomes imaginary (R. W. Daniels, 1974). Thus,

$$\cos^{-1}\omega = jz \quad \text{or} \quad \omega = \cos jz \tag{7.9}$$

From the exponential form of the cosine function,

$$\omega = \cos jz = \frac{e^{j(jz)} + e^{-j(jz)}}{2} = \cosh z$$

that is, $z = \cosh^{-1}\omega$, we have

$$\cos^{-1}\omega = j\cosh^{-1}\omega \tag{7.10}$$

Finally, we substitute this result into Eq. (7.5) to obtain

$$C_n(\omega) = \cos\left(nj\cosh^{-1}\omega\right) = \cosh\left(n\cosh^{-1}\omega\right) \quad \text{for} \quad |\omega| \geq 1 \tag{7.11}$$

With Eqs. (7.5) and (7.11), the transfer function magnitude in Eq. (7.8) is determined for all values of ω. The function is plotted in Fig. 7.3 for $n = 6$. We see the following:

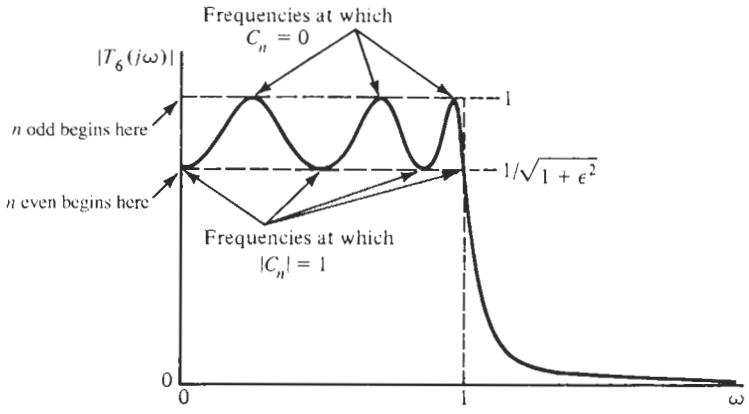

Figure 7.3 Sixth-order Chebyshev transfer function magnitude.

1. Behavior at $\omega = 0$: Since $C_n(0) = 0$ for n odd and $C_n(0) = 1$ for n even: then

$$|T_n(j0)| = 1 \quad \text{for } n \text{ odd}, \qquad |T_n(j0)| = \frac{1}{\sqrt{1+\varepsilon^2}} \quad \text{for } n \text{ even} \tag{7.12}$$

2. Similarly, the behavior at $\omega = 1$ follows from the fact that $C_n(1) = 1$; thus

$$|T_n(j1)| = \frac{1}{\sqrt{1+\varepsilon^2}} \quad \text{for all } n \tag{7.13}$$

This is shown for $n = 6$ in Fig. 7.3. Notice that the minima of $|T_n(j\omega)|$ will occur when $C_n^2(\omega) = 1$, and the maxima when $C_n^2(\omega) = 0$. These points are also indicated in Fig. 7.3. We also note that in the frequency range from $\omega = -1$ to $\omega = +1$, there are n ripples. Since the magnitude function is even, there will be n half-ripples or half-cycles (from minimum to maximum or maximum to minimum) in the range from $\omega = 0$ to $\omega = +1$. In general, there will be n maxima in the range $\omega = -1$ to $\omega = +1$, and $n + 1$ minima.

Consider now the attenuation of Chebyshev filters. The definition of attenuation is for our case

$$\alpha_n = -10 \log |T_n(j\omega)|^2 = 10 \log \left|1 + \varepsilon^2 C_n^2(\omega)\right| \quad \text{dB} \tag{7.14}$$

A plot of this response for $n = 7$ is given in Fig. 7.4. It shows the rippling nature of the Chebyshev response in the passband ($\omega \leq 1$) and the rapid rise to large values of attenuation when $\omega > 1$.

To evaluate the Chebyshev response in the stopband where $\omega > 1$, we use Eq. (7.11) in Eq. (7.14). We get

$$\alpha_n = 10 \log[1 + \varepsilon^2 C_n^2(\omega)] = 10 \log[1 + \varepsilon^2 \cosh^2(n \cosh^{-1} \omega)] \quad \text{dB} \tag{7.15}$$

Figure 7.5 shows these attenuation curves for $n = 2$ through 10 for the case $\varepsilon = 0.1526$ (0.1-dB passband ripple). It is instructive to compare the attenuation increase in a Chebyshev filter with that of the maximally flat response that was given in Fig. 6.10. Notice that the equal-ripple attenuation increases far more rapidly for the same value of n and that the transition band is much narrower. For example, a lowpass filter with $\alpha_{\min} = 60$ dB at $\omega_s = 2$ requires by Fig. 7.5 a Chebyshev function of order $n = 7$, whereas Fig. 6.10 indicates that a filter with maximally flat magnitude would need the order $n = 10$.

Two values are of special interest to us. One is the maximum value of attenuation, $\alpha_{\max}$, in the passband; it occurs when $C_n^2 = 1$. In that case, Eq. (7.14) simplifies to the form

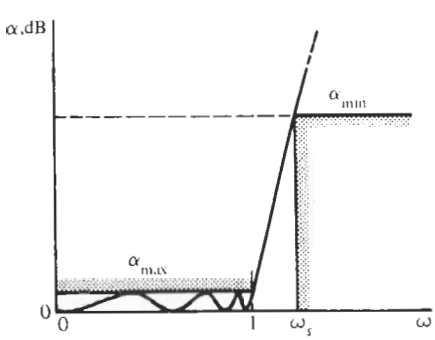

Figure 7.4 Attenuation for a seventh-order Chebyshev lowpass filter as a function of ω.

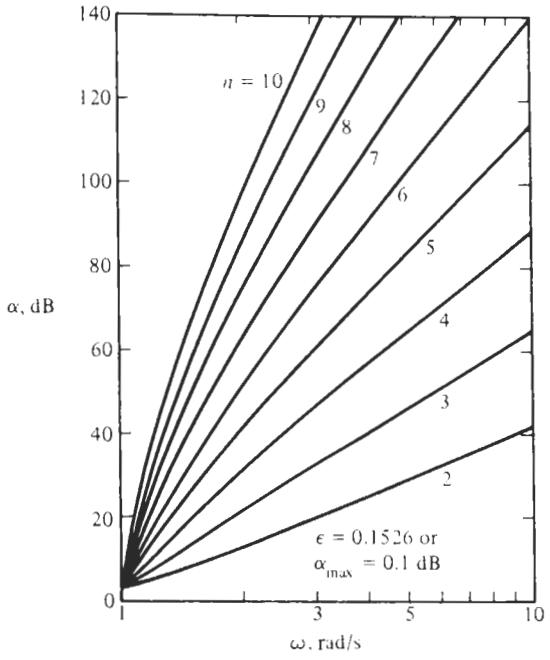

Figure 7.5 Stopband behavior of Chebyshev filters of orders 2 to 10 for a 0.1-dB passband ripple.

$$\alpha_{\max} = 10 \log\left(1 + \varepsilon^2\right) \tag{7.16}$$

which may be solved for prescribed passband attenuation to give ε as

$$\varepsilon = \sqrt{10^{\alpha_{\max}/10} - 1} \tag{7.17}$$

This is the same expression as Eq. (6.40) for the maximally flat approximation. For example, the case $\alpha_{\max} = 0.1$ dB results in $\varepsilon = \sqrt{10^{0.01} - 1} = 0.15262$, the value used in Fig. 7.5. The second point of interest is the frequency ω_s where the attenuation reaches for the first time the prescribed minimum value $\alpha_{\min}$. Consulting Fig. 7.4, we can readily compute this from Eq. (7.15) as

$$\alpha_{\min} = 10 \log[1 + \varepsilon^2 \cosh^2\left(n \cosh^{-1} \omega_s\right)] \quad \text{dB} \tag{7.18}$$

Let us return to Fig. 7.4 and examine more carefully the requirements of a filter with a Chebyshev response. We note that we may specify the maximum passband attenuation, $\alpha_{\max}$, the minimum stopband attenuation, $\alpha_{\min}$, and the transition bandwidth between passband and stopband. As always, we normalize the passband corner frequency to $\omega_p = 1$ so that the transition bandwidth is given by the desired stopband corner, ω_s, where the value $\alpha_{\min}$ is reached for the first time. We wish next to compute the degree n of the filter that realizes these specifications. We begin the calculations with $\alpha_{\min}$ from Eq. (7.18). If we divide both sides of Eq. (7.18) by 10, take the antilogarithm, and subtract 1 from both sides, we have

$$\varepsilon^2 \cosh^2\left(n \cosh^{-1} \omega_s\right) = 10^{\alpha_{\min}/10} - 1 \tag{7.19}$$

where ε was given in Eq. (7.17) in terms of specified filter requirements. If we combine these two equations we find

$$\cosh\left(n \cosh^{-1} \omega_s\right) = \left(\frac{10^{\alpha_{min}/10} - 1}{10^{\alpha_{max}/10} - 1}\right)^{1/2}$$

which is solved for the degree n:

$$n = \frac{\cosh^{-1}\left[\left(10^{0.1\alpha_{min}} - 1\right) / \left(10^{0.1\alpha_{max}} - 1\right)\right]^{1/2}}{\cosh^{-1} \omega_s} \tag{7.20a}$$

This equation can readily be evaluated. A more convenient approximate form for use with a calculator may be derived as

$$n \approx \frac{\ln \sqrt{4\left(10^{0.1\alpha_{min}} - 1\right) / \left(10^{0.1\alpha_{max}} - 1\right)}}{\ln\left(\omega_s + \sqrt{\omega_s^2 - 1}\right)} \tag{7.20b}$$

An example will illustrate the computations.

EXAMPLE 7.1

The following specifications are given for a Chebyshev lowpass filter:

$$\omega_p = 1, \quad \omega_s = 2.33, \quad \alpha_{max} = 0.5 \text{ dB}, \quad \alpha_{min} = 22 \text{ dB}$$

Solution

We compute the degree of the function directly from Eq. 7.20b,

$$n \approx \frac{\ln \sqrt{4\left(10^{2.2} - 1\right) / \left(10^{0.05} - 1\right)}}{\ln\left(2.33 + \sqrt{2.33^2 - 1}\right)} = \frac{\ln 71.4}{\ln 4.43} = 2.87$$

which we round up to $n = 3$.

It is interesting to compare the degree that would be required for a maximally flat filter with the same specifications. From Eq. (6.44) we find

$$n = \frac{\log\left[\left(10^{2.2} - 1\right) / \left(10^{0.05} - 1\right)\right]}{2 \log 2.33} = \frac{\log 1290.7}{2 \log 2.33} = 4.23$$

which we need to round up to 5. Hence, a fifth-order maximally flat filter is required to meet the specifications that led to a third-order Chebyshev filter. The example illustrates the greater efficiency (lower order) of the equal-ripple approximation compared with the maximally flat function. We will further compare these functions in Section 7.4.

7.3 LOCATION OF CHEBYSHEV POLES

In Chapter 6 we found that the poles of the function with a maximally flat magnitude were located on a circle of radius ω_0, at angles with respect to the negative real axis that were easy to determine. We next undertake a similar determination of pole locations for the Chebyshev case. Our starting place is to replace ω by s/j in Eq. (7.8) and then recall from Chapter 6 that

$$|T_n(j\omega)|^2\big|_{\omega=s/j} = T(s)T(-s)$$

so that

$$T(s)T(-s) = \frac{1}{1+\varepsilon^2 C_n^2(s/j)} \tag{7.21}$$

The pole locations are determined by setting the denominator of this equation to zero, and then solving the equation. This requires that

$$C_n\left(\frac{s}{j}\right) = 0 \pm j\frac{1}{\varepsilon} \tag{7.22}$$

For $\omega < 1$,

$$C_n\left(\frac{s}{j}\right) = \cos\left[n\cos^{-1}\left(\frac{s}{j}\right)\right] = \cos nw \tag{7.23}$$

where w is a complex number:

$$\cos^{-1}\left(\frac{s}{j}\right) = w = u + jv \tag{7.24}$$

We next calculate $\cos nw$ so that this may be equated to Eq. (7.22). Then

$$\begin{aligned}\cos nw &= \cos(nu + jnv) \\ &= \cos nu \cosh nv - j \sin nu \sinh nv \\ &= 0 \pm j\frac{1}{\varepsilon}\end{aligned} \tag{7.25}$$

Equating the real and imaginary parts of these equations gives two relationships:

$$\cos nu \cosh nv = 0 \tag{7.26}$$

$$\sin nu \sinh nv = \pm\frac{1}{\varepsilon} \tag{7.27}$$

From the first of these equations we observe that because $\cosh uv$ can never be zero since its smallest value is 1, it is necessary that $\cos nu$ be zero. The values of u for which this is true are

$$u_k = \frac{\pi}{2n}, \frac{3\pi}{2n}, \frac{5\pi}{2n}, \cdots \tag{7.28}$$

or generally,

$$u_k = \frac{\pi}{2n}(2k-1) \quad k+1, 2, \ldots, 2n \tag{7.29}$$

For these values of u_k

$$\sin nu_k = \pm 1 \tag{7.30}$$

so that

$$v_k = \pm\frac{1}{n}\sinh^{-1}\left(\frac{1}{\varepsilon}\right) = \pm a \tag{7.31}$$

Having determined the necessary values of u_k and v_k, we return to Eq. (7.24), $w = \cos^{-1}(s/j)$. For each value of $w_k = u_k + jv_k$ the corresponding value of s is

$$s_k = j\cos w_k = j\cos\left[\frac{\pi}{2n}(2k-1) + ja\right] \tag{7.32}$$

Then if $s_k = \sigma_k + j\omega_k$, we have from this equation

$$\sigma_k = \pm\sinh a \sin\frac{2k-1}{2n}\pi, \quad \omega_k = \cosh a \cos\frac{2k-1}{2n}\pi \tag{7.33}$$

which completes our solution, for these are the s-plane locations of the poles $s_k = \sigma_k + j\omega_k$ of $T(s)T(-s)$. We can routinely assign those in the left half-plane to $T(s)$, as we did for the maximally flat magnitude case. They are

$$\sigma_k = -\sinh a \sin\frac{2k-1}{2n}\pi, \quad \omega_k = \cosh a \cos\frac{2k-1}{2n}\pi, \quad k = 1, 2, \ldots, n \tag{7.34}$$

We gain insight into the pole locations if we square Eqs. (7.33) and add the results. Since $\sin^2 x + \cos^2 x = 1$ for any x we obtain

$$\left(\frac{\sigma_k}{\sinh a}\right)^2 + \left(\frac{\omega_k}{\cosh a}\right)^2 = 1 \tag{7.35}$$

If we drop the index k and let σ and ω have any values, then we recognize this to be the equation of an ellipse for which the major semiaxis is $\cosh a$, the minor semiaxis is $\sinh a$, and the foci are $\pm j1$. These features are illustrated in Fig. 7.6.

Equation (7.34) is an important result, for it gives us the pole locations of a Chebyshev filter and allows us to determine the pole frequencies and pole quality factors we need for design. If α_{max}, α_{min}, $\omega_p = 1$, and ω_s are given, we may follow these steps in determining these parameters:

1. From Eqs. (7.17) and (7.20) find ε and the degree n.
2. Determine

$$a = \frac{1}{n}\sinh^{-1}\frac{1}{\varepsilon} = \frac{1}{n}\ln\left(\frac{1}{\varepsilon} + \sqrt{\frac{1}{\varepsilon^2}+1}\right) \tag{7.36}$$

3. Compute sinh a and cosh a.
4. Find the Chebyshev poles from Eq. (7.34).
5. The pole frequencies and pole quality factors of the Chebyshev filter are

$$\omega_{0k} = \sqrt{\sigma_k^2 + \omega_k^2}, \quad Q_k = \frac{\omega_{0k}}{2\sigma_k} \tag{7.37}$$

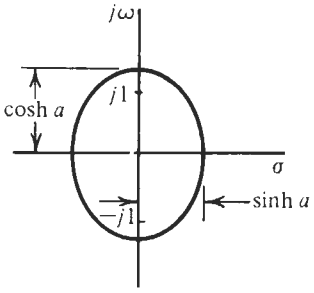

Figure 7.6 Locus of the roots of Chebyshev polynomials in the s-plane.

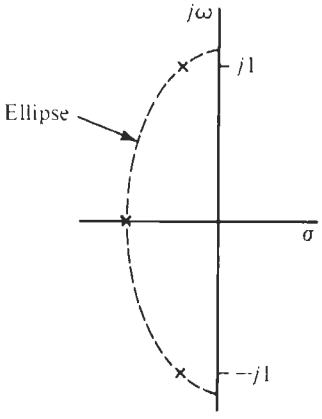

Figure 7.7 Poles of a third-order Chebyshev filter with 1-dB passband ripple.

EXAMPLE 7.2

We wish to determine the location of the Chebyshev poles for $n = 3$ and $\alpha_{\max} = 1$ dB.

Solution

We first find a from Eq. (7.36):

$$a = \frac{1}{3}\sinh^{-1}\left(10^{1/10} - 1\right)^{-1/2} = 0.476$$

From this, sinh $a = 0.494$ and cosh $a = 1.115$. The poles are found from Eq. (7.34) to be

$$s_1 = -0.494 \quad \text{and} \quad s_2, s_3 = -0.247 \pm j0.966$$

These are shown in Fig. 7.7. Their locus is an ellipse that passes through these points. The polynomial corresponding to these poles, the denominator polynomial of $T_3(s)$, is

$$D_3(s) = (s + 0.494)\left(s^2 + 0.494s + 0.994\right)$$

For the second-order factor, we see that $\omega_0 = 0.999$ and $Q = 2.02$. These values are useful for finding a circuit realization.

EXAMPLE 7.3

For this example we shall find a Chebyshev transfer function to meet the requirements $n = 5$ and $\alpha_{max} = 0.5$ dB in $0 \leq \omega \leq 1000$ rad/s. The passband gain is 0 dB. Note that these passband specifications and the degree are the same as the ones in Example 6.2 where a maximally flat transfer functions was found and implemented.

Solution

From Eq. (7.17) we compute $\varepsilon^2 = 0.12202 = 0.3493^2$ as in Example 6.2 and use $n = 5$ as specified. Then we have from Eq. (7.36) $a = 0.35484$ and $\cosh a = 1.06362$, $\sinh a = 0.36232$. With $k = 1, 2, 3, 4$, and 5 we get from Eq. (7.34)

$$s_1 = -0.11196 + j1.01156, \quad s_2 = -0.29312 + j0.62518$$
$$s_3 = -0.36232$$
$$s_4 = -0.29312 - j0.62518, \quad s_5 = -0.11196 - j1.01156$$

Note that these pole frequencies are normalized. The transfer function $T_5(s)$ equals

$$T_5(s) = \frac{0.1789}{(s + 0.3623)\left(s^2 + 0.5862s + 0.4768\right)\left(s^2 + 0.2239s + 1.0358\right)} \tag{7.38}$$

The numerator arises from the fact that by Eq. (7.6) the coefficient of s^5 is $2^4 = 16$ and by Eq. (7.8) C_5 is multiplied by ε in $|T_n(j\omega)|^2$. Thus, we transported a factor $1/(16\varepsilon)$ into the numerator because the coefficient of s^5 is unity in the denominator of Eq. (7.38). Note also that for an odd-order Chebyshev filter the dc gain is 0 dB; thus, $0.1789 = 0.3623 \times 0.4768 \times 1.0358$ as is required.

Extensive tables are available giving the pole locations of Chebyshev filters for a number of values of α_{max} and n. Table 7.2 shows the poles for $\alpha_{max} = 0.5$, 1, 2, and 3 dB for orders 1 through 10. For other values of α_{max} the corresponding pole location can readily be found with the help of Eqs. (7.34) and (7.36).

7.4 COMPARISON OF MAXIMALLY FLAT AND EQUAL-RIPPLE RESPONSES

We have now two response functions from which to choose when designing a filter: maximally flat with Butterworth as a special case and equal ripple or Chebyshev. Further responses will be introduced in later chapters. How shall we make a choice of the response to be used? We first observe that to make a comparison we should identify frequencies

TABLE 7.2 Chebyshev Pole Locations[a]

	$\alpha_{max} = 0.5$ dB		$\alpha_{max} = 1$ dB		$\alpha_{max} = 2$ dB		$\alpha_{max} = 3$ dB	
n	α	β	α	β	α	β	α	β
1	2.8628	0	1.9625	0	1.3076	0	1.0024	0
2	0.7128	1.0040	0.5489	0.8951	0.4019	0.8133	0.3224	0.7772
3	0.3132	1.0219	0.2471	0.9660	0.1845	0.9231	0.1493	0.9038
	0.6265	0	0.4942	0	0.3689	0	0.2986	0
4	0.1754	1.0163	0.1395	0.9834	0.1049	0.9580	0.0852	0.9465
	0.4233	0.4209	0.3369	0.4073	0.2532	0.3968	0.2056	0.3920
5	0.1120	1.0116	0.0895	0.9901	0.0675	0.9735	0.0549	0.9659
	0.2931	0.6252	0.2342	0.6119	0.1766	0.6016	0.1436	0.5970
	0.3623	0	0.2895	0	0.2183	0	0.1775	0
6	0.0777	1.0085	0.0622	0.9934	0.0470	0.9817	0.0382	0.9764
	0.2121	0.7382	0.1699	0.7272	0.1283	0.7187	0.1044	0.7148
	0.2898	0.2702	0.2321	0.2662	0.1753	0.2630	0.1427	0.2616
7	0.0570	1.0064	0.0457	0.9953	0.0346	0.9866	0.0281	0.9827
	0.1597	0.8071	0.1281	0.7982	0.0969	0.7912	0.0789	0.7881
	0.2308	0.4479	0.1851	0.4429	0.1400	0.4391	0.1140	0.4373
	0.2562	0	0.2054	0	0.1553	0	0.1265	0
8	0.0436	1.0050	0.0350	0.9965	0.0625	0.9898	0.0216	0.9868
	0.1242	0.8520	0.0997	0.5448	0.0754	0.8391	0.0614	0.8365
	0.1859	0.5693	0.1492	0.5644	0.1129	0.5607	0.0920	0.5590
	0.2193	0.1999	0.1760	0.1982	0.1332	0.1969	0.1055	0.1962
9	0.0345	1.0040	0.0277	0.9972	0.0209	0.9919	0.0171	0.9896
	0.0992	0.8829	0.0797	0.8769	0.0603	0.8723	0.0491	0.8702
	0.1520	0.6553	0.1221	0.6509	0.0924	0.6474	0.0753	0.6459
	0.1864	0.3487	0.1497	0.3463	0.1134	0.3445	0.0923	0.3437
	0.1984	0	0.1593	0	0.1206	0	0.0983	0
10	0.0279	1.0033	0.0224	0.9978	0.0170	0.9935	0.0138	0.9915
	0.0810	0.9051	0.1013	0.7143	0.0767	0.7113	0.0401	0.8945
	0.1261	0.7183	0.0650	0.9001	0.0493	0.8962	0.0625	0.7099
	0.1589	0.4612	0.1277	0.4586	0.0967	0.4567	0.0788	0.4558
	0.1761	0.1589	0.1415	0.1580	0.1072	0.1574	0.0873	0.1570

[a]In terms of the α and β values given, the second-order factor is $s^2 + 2\alpha s + \alpha^2 + \beta^2$, and $\omega_0 = \sqrt{\alpha^2 + \beta^2}$, $Q = \sqrt{\alpha^2 + \beta^2}/(2\alpha)$.

that have the same significance in the two responses. We do this by taking the maximally flat function defined in Eq. (6.14a) and comparing its performance with the function of Eq. (7.8),

$$|T_B(j\omega)|^2 = \frac{1}{1+\varepsilon^2\omega^{2n}} \leftrightarrow |T_C(j\omega)|^2 = \frac{1}{1+\varepsilon^2 C_n^2(\omega)} \tag{7.39}$$

where we have used the subscripts B and C, respectively, to label the maximally flat (or Butterworth) and the Chebyshev functions. Comparing these two expressions makes sense because both have the same specifications over the passband: $\alpha_{max} = 10\log(1+\varepsilon^2)$ in $0 \le \omega \le 1$. A plot of the two functions is shown in Fig. 7.8. Observe now that at high frequencies we find from Eq. (7.39)

$$\alpha_B = 10\log\left(1+\varepsilon^2\omega^{2n}\right) \quad \text{and} \quad \alpha_C \approx 10\log\left[1+\left(2^{n-1}\varepsilon\omega^n\right)^2\right] \tag{7.40}$$

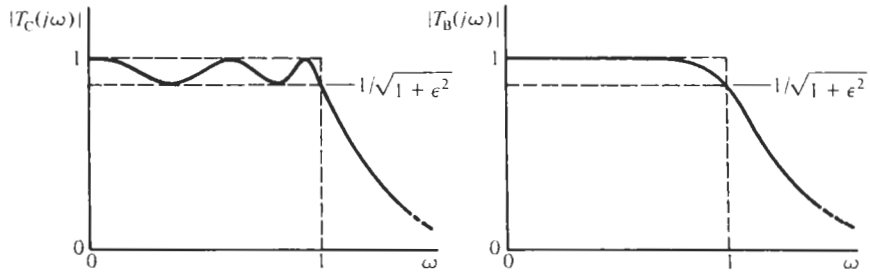

Figure 7.8 Maximally flat and Chebyshev filters formulated to provide the same passband attenuation specifications.

where we have used that by Eq. (7.6) C_n approaches the value $C_n(\omega) \approx 2^{n-1}\omega^n$ for $\omega \to \infty$. Let us further assume $\varepsilon^2\omega^2 \gg 1$. Then we find

$$\alpha_B \approx 20 \log (\varepsilon\omega^n) \quad \text{and}$$
$$\alpha_C \approx 20 \log (2^{n-1}\varepsilon\omega^n) = 20\,(n-1) \log 2 + 20 \log (\varepsilon\omega^n) \tag{7.41}$$

that is, for large ω,

$$\alpha_C = 6.02\,(n-1) + \alpha_B \tag{7.42}$$

This is a substantial increase in stopband attenuation over the maximally flat approximation. For example, for a fifth-order filter the Chebyshev attenuation is 24 dB larger than in the maximally flat case.

What price do we pay for this increased attenuation in a circuit of the same order and complexity? Part of the answer is that the pole Qs are larger. In a maximally flat function we found the Q value in Eq. (6.31), which, after referencing the angle to the *negative* real axis, becomes

$$Q_B = \frac{1}{2 \sin \dfrac{2k-1}{2n}\pi} = \frac{1}{2 \sin \theta_k} \tag{7.43}$$

Here we have called $(2k-1)\pi/(2n) = \theta_k$. For the Chebyshev case we found from Eq. (7.37)

$$Q_C = \frac{\omega_{0k}}{2\sigma_k} = \frac{\sqrt{\sigma_k^2 + \omega_k^2}}{2\sigma_k} \tag{7.44}$$

which, after substituting Eq. (7.34), becomes

$$Q_C = \frac{\omega_{0k}}{2\sigma_k} = \frac{\sqrt{(\sinh a \sin\theta_k)^2 + (\cosh a \cos\theta_k)^2}}{2 \sinh a \sin\theta_k} = \frac{1}{2}\sqrt{1 + \frac{1}{\tanh^2 a \tan^2 \theta_k}} \tag{7.45}$$

with a from Eq. (7.36). ($\tanh a$ is the hyperbolic tangent function, $\tanh a = \sinh a / \cosh a$.) After some manipulation this equation can be recast into the form

$$Q_C = \frac{1}{2\sin\theta_k}\sqrt{1+\frac{\cos^2\theta_k}{\sinh^2 a}} = Q_B\sqrt{1+\frac{\cos^2\theta_k}{\sinh^2 a}} \tag{7.46}$$

which says that Q_C is always larger than Q_B. For example, in Example 6.2 we had the quality factors 0.618 and 1.618 in the two second-order modules of the fifth-order maximally flat filter. Using Eq. (7.46) we find that the quality factors for the fifth-order 0.5-dB ripple Chebyshev case are $0.618 \times 1.905 = 1.177$ and $1.618 \times 2.808 = 4.543$; these are the values calculated in Example 7.3.

It is a simple matter to compute the Chebyshev Qs from Eq. (7.45) for given α_{max} and n. For example, for $\alpha_{max} = 0.5$ dB, the following table is easily found:

n	2	3	4	5	6	7	8	9	10
Q	0.86	1.71	0.71	1.18	0.68	1.09	0.68	1.06	0.67
			2.94	4.54	1.81	2.58	1.61	2.21	1.53
					6.51	8.84	3.47	4.48	2.89
							11.53	14.58	5.61
									17.99

The values $Q = 1/2$ for poles on the negative real axis have not been included in the table. As a practical matter it is important to note that it is often more difficult to adjust filter stages with high values of Q.

Another price we pay for the increased attenuation in the Chebyshev case is a phase characteristic of increased nonlinearity. The phase $\theta(\omega)$ of $T(j\omega)$ and the derivative of θ with respect to ω will be studied in detail in Chapter 10. Until then, we show for comparison the two graphs of phase θ for the Butterworth and Chebyshev cases in Fig. 7.9. We notice that the phase in the passband from $\omega = 0$ to $\omega = 1$ is more nearly linear in the Butterworth case than

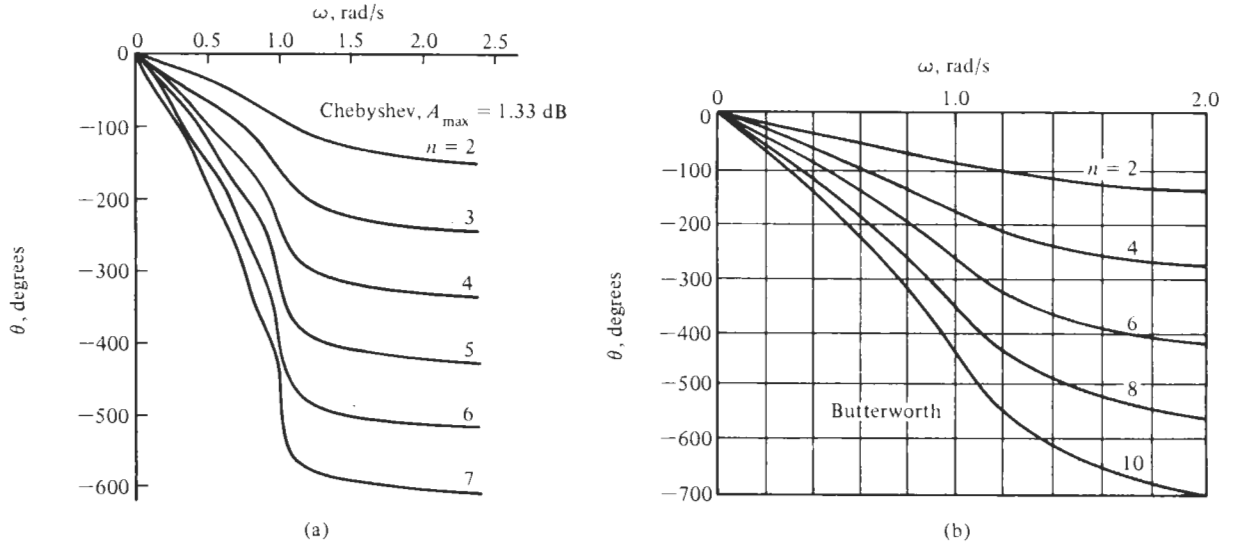

Figure 7.9 Chebyshev (a) and Butterworth (b) phase responses.

in the Chebyshev case. We shall show later that a more nonlinear phase will result in delay distortion.

In summary, the choice between a maximally flat magnitude and a Chebyshev response requires trade-off between the conflicting requirements of (1) high attenuation in the stopband and steeper roll-off near the cut-off frequency, and (2) higher values of Q leading to more difficult circuit realizations and less linear phase characteristics. The actual choice will depend on the weight that the designer assigns to each of the conflicting requirements.

7.5 CHEBYSHEV FILTER DESIGN

We are now prepared to go through step-by-step procedures for designing lowpass Chebyshev filters. This will be done with examples. Table 7.3 lists the steps and compares them with those required for maximally flat magnitude filters. The specifications for a required filter are always the maximum passband attenuation (the ripple), α_{max}, the minimum stopband attenuation, α_{min}, and the transition bandwidth, ω_s (assuming the passband corner, ω_p, is normalized to 1).

TABLE 7.3 Comparison of Steps for Maximally Flat and Chebyshev Cases

Maximally Flat	Step	Chebyshev
$n = \dfrac{\log[(10^{\alpha_{min}/10} - 1)/(10^{\alpha_{max}/10} - 1)]}{2 \log \omega_s}$ Round up to an integer	1. Find n	$n = \dfrac{\cosh^{-1}[(10^{\alpha_{min}/10} - 1)/(10^{\alpha_{max}/10} - 1)]^{1/2}}{\cosh^{-1} \omega_s}$ Round up to an integer
$\varepsilon = (10^{\alpha_{max}/10} - 1)^{1/2}$	2. Find ε	$\varepsilon = (10^{\alpha_{max}/10} - 1)^{1/2}$
a. If n is odd,	3. Find pole locations	a. Find θ_k for Butterworth case
$\theta_k = 0°, \quad \pm k\dfrac{180°}{n}$, k is an integer	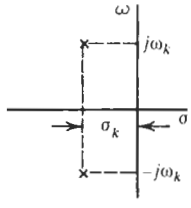	b. Find $a = \dfrac{1}{n} \sinh^{-1}\left(\dfrac{1}{\varepsilon}\right)$
b. If n is even,		c. Then
$\theta_k = \pm \dfrac{180°}{2n}, \quad \pm k\dfrac{180°}{n} \pm \dfrac{180}{2n}$		$-\sigma_k = \sin \theta_k \sinh a$
Radius $= \Omega_0$ $-\sigma_k = \Omega_0 \cos \theta_k, \quad \pm\omega_k = \Omega_0 \sin \theta_k$		$\pm\omega_k = \cos \theta_k \cosh a$

EXAMPLE 7.4

We require a lowpass filter to satisfy the specifications in Fig. 7.10. The loss in the passband to 10 kHz is to be 0.3 dB or less, and beyond 24.58 kHz the loss is to be at least 22 dB. Normalized frequencies are also shown in the figure with the end of the ripple band normalized to $\omega = 1$ as is customary.

Solution

We first compute the degree of the required approximation using Eq. (7.20)

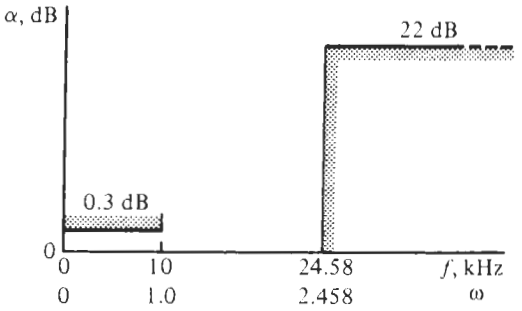

Figure 7.10 Specifications for Example 7.4.

$$n = \frac{\cosh^{-1}[(10^{2.2} - 1)/(10^{0.05} - 1)]^{1/2}}{\cosh^{-1} 2.548} = 2.933$$

which we round up to 3. This rounding to the next higher integer (rather than using the fractional degree calculated) will help in clearing the prescribed stopband corner in Fig. 7.10. Next we compute a using Eq. (7.36):

$$a = \frac{1}{3} \sinh^{-1} (10^{0.05} - 1)^{-1/2} = 0.6765$$

from which we find $\cosh a = 1.2377$ and $\sinh a = 0.7293$. The location of the poles is given by Eq. (7.34) from which we find

$$p_1, p_2 = 0.3646 \pm j1.072, \quad p_3 = 0.7293 \tag{7.47}$$

For the complex pair of poles, we use Eq. (7.37) to find that $Q = 1.553$ and $\omega_0 = 1.1323$. The attenuation actually realized at the stopband is found using Eq. (7.18):

$$\alpha_n (2.458) = 10 \log[1 + \varepsilon^2 \cosh^2 (3 \cosh^{-1} 2.458)] = 22.89 \quad \text{dB}$$

The circuit will be realized made as a cascade connection of two stages having the properties summarized in Fig. 7.11. Also shown in Fig. 7.11 are the simple RC voltage divider we propose to use for the first-order section, and the Sallen–Key circuit of Fig. 4.31b, Eq. (4.111), to realize the second-order section. This circuit is matched to the requirements of the complex pair of poles given in Eq, (7.47).

The design equation for the first-order stage is

$$\sigma_0 = \frac{1}{RC} = 0.7293$$

If we select $C = 10$ nF and recall that frequencies were normalized so that $2\pi \times 10$ kHz scales to 1, then we obtain $R = 2.18\,\text{k}\Omega$. Using the circuit sketched in Fig. 7.11, we calculate for the second stage

$$R_1 = \frac{1}{\omega_0 C} = 1.40\,\text{k}\Omega, \quad K = 3 - \frac{1}{Q} = 2.356, \quad \text{and} \quad a = \frac{1}{K} = 0.4244$$

The value of a results in the dc gain being equal to 0 dB. The resistor R in this stage we choose as $R = 5\,\text{k}\Omega$. Finally, we must remember that these two stages cannot be cascaded directly because the first stage cannot be loaded without affecting its performance. We solve the

problem by using an opamp buffer and get the circuit in Fig. 7.12. The 0.3-dB ripple is visible and the measured −3-dB gain is at $f = 12.3$ kHz. Figure 7.13 illustrates how the cascade connection of the two sections multiplies the individual gains to realize the total prescribed gain.

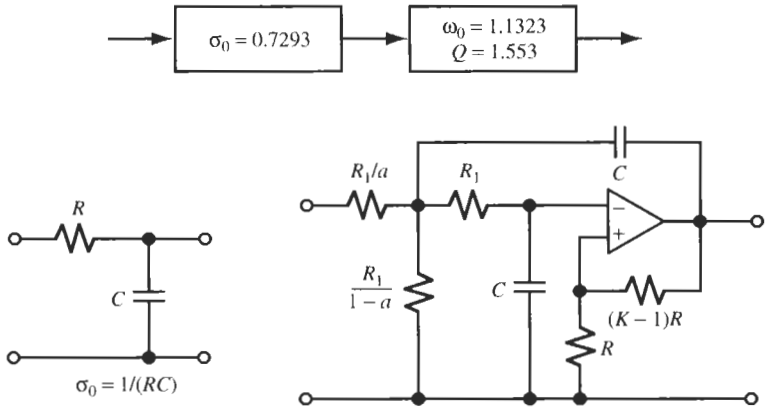

Figure 7.11 Block diagram of circuit models for Example 7.4.

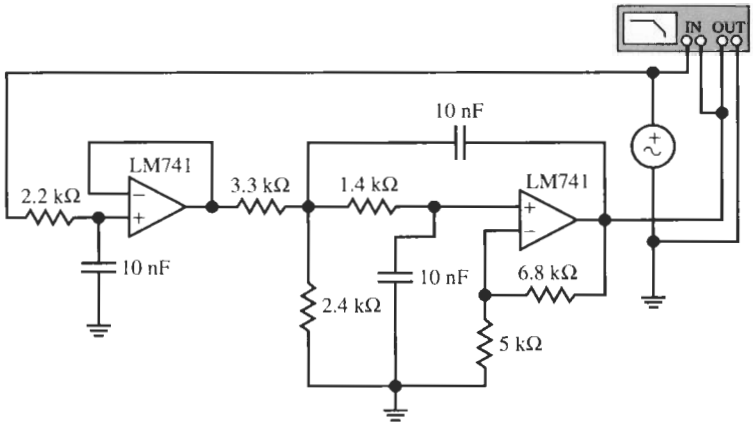

(a)

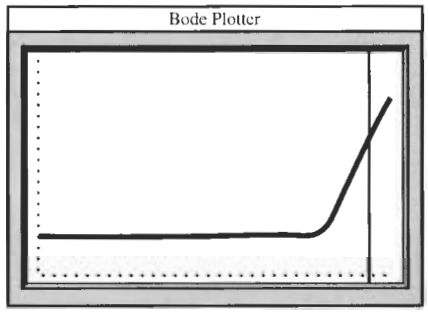

(b)

Figure 7.12 Third-order Chebyshev filter for Example 7.4 and test results showing attenuation $\alpha(\omega)$. (Bode Plotter scales: 100 Hz to 35 kHz; 10 to −40 dB; cursor at 24.25 kHz, −22.89 dB.)

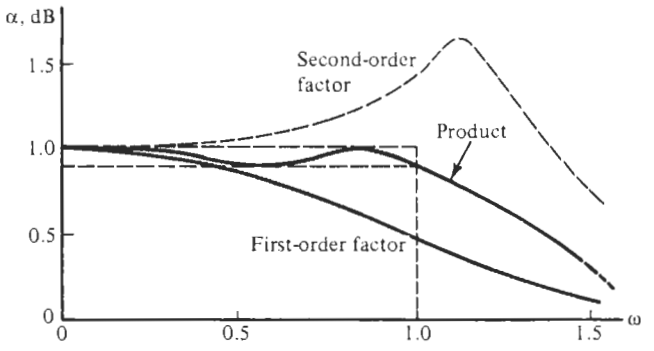

Figure 7.13 The gain in dB of the two sections in Fig. 7.11.

EXAMPLE 7.5

Realize a circuit to implement the fifth-order Chebyshev lowpass transfer function we found in Example 7.3. The function was given in Eq. (7.38). Realize this function as a cascade of the same sections as in Example 6.2 and compare the performance.

Solution

We form three sections to be connected in the order of increasing values of Q; thus, because

$$Q_1 = 0.5, \quad Q_2 = 1.178, \quad \text{and} \quad Q_3 = 4.55$$

we connect the modules in the sequence

$$T_5(s) = T_1T_2T_3 = \frac{k_1}{s + 0.3623}\,\frac{k_2}{s^2 + 0.5862s + 0.4768}\,\frac{k_3}{s^2 + 0.2239s + 1.0358}$$

with $k_1k_2k_3 = K = 0.1789$. Using Eq. (5.77), we compute, as in Example 6.2, $M_1 = 2.760$, $M_2 \approx 5.8$, and, because the total gain is 0 dB, $M_3 = 1/K = 5.590$. Then we get

$$k_1 = \frac{KM_3}{M_1} = \frac{0.1789 \times 5.590}{2.760} = 0.362, \quad k_2 = \frac{2.760}{5.8} = 0.476, \quad k_3 = \frac{5.8}{5.59} = 1.03 \approx 1$$

Thus,

$$T(s) = T_1T_2T_3 = \frac{0.362}{s + 0.3623}\,\frac{0.476}{s^2 + 0.5862s + 0.4768}\,\frac{1.0}{s^2 + 0.2239s + 1.0358}$$

For the first-order module we have

$$T_1(s) = \frac{G_1/C}{s + G_2/C} = \frac{0.362}{s + 0.3623}$$

We choose $C = 0.1\ \mu$F so that for $\omega_{01} = 362.3$ rad/s we obtain

$$R_1 = R_2 = \frac{1}{\omega_{01}C} = 27.6\,\text{k}\Omega$$

For the second-order sections we choose again $C_1 = C_2 = C$ and $G_1 = G_2 = G = 1/R$ to obtain

$$T(s) = \frac{aK\omega_0^2}{s^2 + s\omega_0/Q + \omega_0^2}$$

where $\omega_0 = 1/(RC)$ and $Q = 1/(3 - K)$. Then we set

$$T_2(s) = \frac{aK\omega_{02}^2}{s^2 + s\omega_{02}/Q_2 + \omega_{02}^2} = \frac{0.476}{s^2 + 0.5862s + 0.4768}$$

to obtain with $C = 0.1\,\mu$F and $\omega_{02} = 476.8$ rad/s

$$R = \frac{1}{\omega_{02}C} = 20.97\text{k}\Omega, \quad K = 3 - Q_2^{-1} = 2.151, \quad a = \frac{0.476}{0.4768 \times 2.151} = 0.464$$

Similarly, for Section 3,

$$T_3(s) = \frac{aK\omega_{03}^2}{s^2 + s\omega_{03}/Q_3 + \omega_{03}^2} = \frac{1.0}{s^2 + 0.2239s + 1.0358}$$

we find with $\omega_{03} = 1.017$ krad/s

$$R = \frac{1}{\omega_{03}C} = 9.82\text{k}\Omega, \quad K = 3 - Q_3^{-1} = 2.780, \quad \text{and} \quad a = \frac{1.0}{1.017 \times 2.78} = 0.35$$

As in Example 6.2, we need not be concerned with predistortion to correct the errors predicted by Eq. (4.113). Figure 7.14 shows the circuit and its performance with LM741 opamps. The cut-off frequency is as designed at 160 Hz and the circuit provides ≈100 dB attenuation at 1 kHz, whereas the maximally flat design in Example 6.2 had only 73-dB attenuation at 1 kHz, a difference of approximately 24 dB as predicted by Eq. (7.42). We

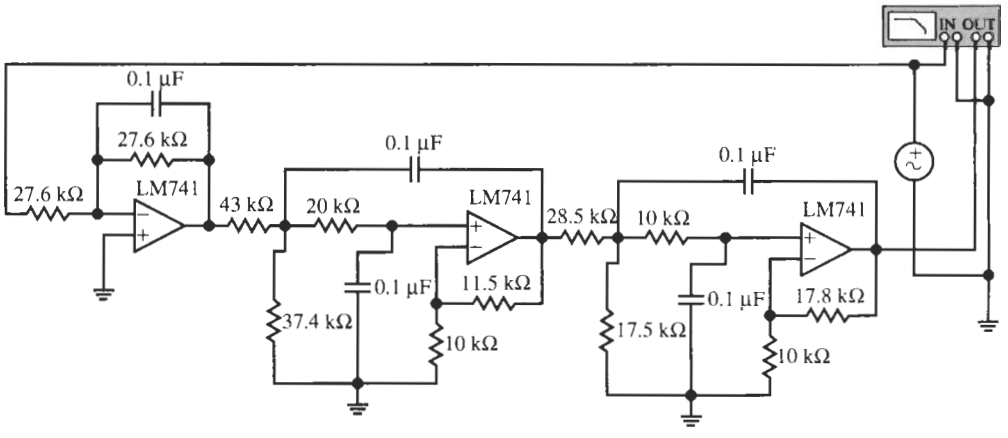

(a)

Figure 7.14 Fifth-order Chebyshev lowpass filter for Example 7.5 and test result. (Bode Plotter scales: 5 Hz to 5 kHz; −120 to 10 dB; cursor at 152.7 Hz, −1.898 dB.)

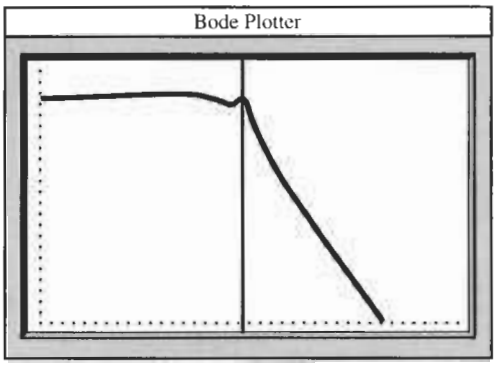

(b)

Figure 7.14 Continued

notice the ripples at the passband edge, but the ripple width is ≈3.5 dB as we move toward the bandedge, far larger than specified. As we noted earlier, the precise realization is very sensitive to f_{0i} and Q_I. If higher accuracy is required more accurate components must be used.

We now have several methods available to us for deriving realizable lowpass transfer functions from which circuits can be implemented that meet prescribed attenuation specifications. We shall next investigate a simple and elegant technique that will enable us to use our knowledge of lowpass transfer functions for deriving other filter types, such as highpass, bandpass, or band-rejection filters. This will be accomplished by a technique referred to as *frequency transformation.*

REFERENCES

R. W. Daniels, *Approximation Methods for Electronic Filter Design*. McGraw-Hill, New York, 1974, p. 33.

PROBLEMS

7.1 A Chebyshev lowpass filter is required to provide $\alpha_{\min} = 48$ dB of attenuation at $f_s \geq 9.6$ kHz with maximum passband attenuation of $\alpha_{\max} = 0.4$ dB in $0 \leq f \leq 3.2$ kHz. Find ε and the degree n_C of the function. Repeat the problem for a filter with maximally flat magnitude. Compare the results with respect to degree and Q values.

7.2 Repeat Problem 7.1 for Chebyshev and maximally flat magnitude functions with the same value for $\alpha_{\max}$ but with

(a) $f_s = 7$ kHz, $\alpha_{\min} = 48$ dB

(b) $f_s = 48$ kHz, $\alpha_{\min} = 24$ dB

(c) $f_s = 48$ kHz, $\alpha_{\min} = 72$ dB

What conclusions can be drawn about the efficiency of the two approximation functions and about its dependence on stopband attenuation and transition bandwidth?

7.3 Find the pole positions of the Chebyshev function derived in Problem 7.2c and determine ω_0 and Q for each pole pair. Find the corresponding transfer function. What is the attenuation increase at high frequencies?

7.4 From Table 7.2, find the transfer function and the ω_0, and Q values corresponding to

(a) $\alpha_{\max} = 0.5$ dB, $n = 6$

(b) $\alpha_{\max} = 0.5$ dB, $n = 8$

(c) $\alpha_{\max} = 2$ dB, $n = 6$

7.5 Verify Eq. (7.46), which states that for a given filter order a Chebyshev realization has always larger quality factors than a maximally flat magnitude function with the same specifications.

7.6 Consider the attenuation characteristic shown in Fig. P7.6 where $\alpha_{max} = 0.5$ dB. Find the attenuation, α, at the frequency that is twice the frequency at the end of the ripple band, $\omega = 2000$ rad/s.

7.7 Design a lowpass filter with a Chebyshev response satisfying the following specifications: $\alpha_{max} = 0.25$ dB, $\alpha_{min} = 18$ dB, $\omega_p = 1000$ rad/s, $\omega_s = 1400$ rad/s. Adjust the gain so the minimum value of $\alpha(\omega)$ is 0 dB. Magnitude scale so that the element values in your circuit realization are in a practical range (Fig. P7.7).

Design and build the circuit with Sallen–Key biquads and first-order sections if needed. Test the performance of your design with Electronics Workbench (EWB).

7.8 Repeat Problem 7.7 for the specifications: $\alpha_{max} = 0.5$ dB, $\alpha_{min} = 25$ dB, $\omega_p = 1000$ rad/s, $\omega_s = 1800$ rad/s.

7.9 Repeat the lowpass filter design described in Problem 7.8 for the following specifications: $\alpha_{max} = 1.0$ dB, $\alpha_{min} = 60$ dB, $\omega_p = 1000$ rad/s, $\omega_s = 3000$ rad/s.

7.10 Design a lowpass filter with equal ripple passband for the following specifications:

(a) Stopband: $\alpha_{min} = 65$ dB at $f_s = 10.4$ kHz

(b) Passband: $\alpha_{max} = 0.5$ dB, $f_c = 4.5$ kHz

Use Åckerberg–Mossberg sections and first-order sections as needed to realize the filter. Be sure to use practical component values and LM741 opamps.

7.11 By Eq. (7.39), the degree of the filter in Problem 7.10 is $n_C = 6.23$. The passband ripple is fixed. Explore which specification should be relaxed to be able to realize the function with only three second-order sections. Investigate alternatives.

7.12 Repeat Problem 7.10 but for a filter with maximally flat magnitude. Compare degrees and Q values for the two realizations.

7.13 Design a Chebyshev lowpass filter for the following specifications:

(a) Stopband: $\alpha_{min} = 48$ dB at $f_s = 1.07$ MHz

(b) Passband: $\alpha_{max} = 1$ dB, $f_c = 500$ kHz

Use Sallen–Key sections and first-order sections as needed to realize the filter. Be sure to use practical component values and HA2542-2 opamps. Test the design with EWB and comment on any errors.

7.14 Design a Chebyshev lowpass filter with a passband in $0 \le f \le 65$ kHz and $\alpha_{max} = 0.5$ dB; the stopband is in $f \ge 135$ kHz with a minimum attenuation of $\alpha_{min} = 30$ dB. The preferred capacitors are 1 nF. Realize the function with Åckerberg–Mossberg sections; test the circuit with EWB and comment on any deviations in your design for the following cases:

(a) using fast opamps such as the HA2542-2

(b) using LM741 opamps and employing predistortion to compensate for the expected errors caused by the slower and less expensive opamps.

7.15 Consider a specification requiring a sixth-order Chebyshev lowpass to achieve the desired high-frequency attenuation increase of 120 dB/decade. Assume that the designer has the option of using various ripple widths for the passband performance. From Table 7.2, compute the quality factors for the design options of $\alpha_{max} = 0.5$, 1, 2, and 3 dB and determine a relationship between ripple width and quality factor. Make a judgment as to which option is preferable and why.

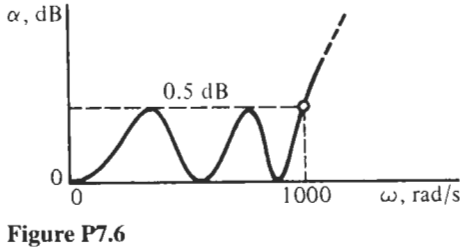

Figure P7.6

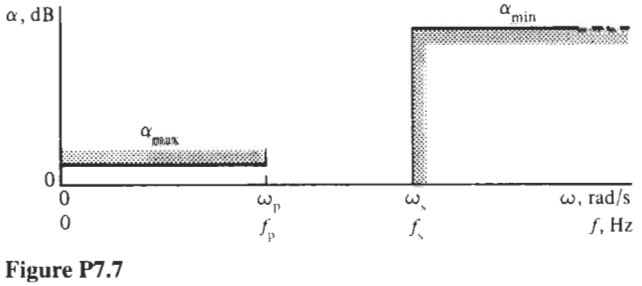

Figure P7.7

8 INVERSE CHEBYSHEV AND CAUER FILTERS

We have in the previous two chapters discussed two methods for arriving at lowpass responses. Our development started from the squared magnitude of the transfer function, Eq. (6.8),

$$|T_n(j\omega)|^2 = \frac{1}{1 + |K(j\omega)|^2}$$

where $K(s)$ is the characteristic function. In both the maximally flat (Butterworth) approximation in Chapter 6 and the equal-ripple (Chebyshev) approximation in Chapter 7, $K(s)$ is a polynomial, which means that the filters have all-pole responses with all transmission zeros at infinity. We also saw, however, that finite transmission zeros could be prescribed for a response with maximally flat passband without destroying the maximal flat property. Example 6.3 gave an illustration of such a design in which two transmission zeros were assigned to achieve a faster roll-off to some prescribed level of attenuation. Specifically, we chose zeros at $f_1 = 36$ kHz and $f_2 = 72$ kHz and saw that in the stopband the attenuation stayed below 45 dB. The first minimum attenuation of 47.8 dB was reached

between f_1 and f_2 at 43.5 kHz and a second minimum of 66 dB at 110 kHz between f_2 and $f = \infty$.

There remain two open questions for us to answer: If a certain level of attenuation (45 dB in Example 6.3) is adequate in the stopband, can we achieve a better design by placing the transmission zeros such that all attenuation minima reach the same level? In other words, can we find a placement of zeros such that the attenuation has equal minima in the stopband? Figure 8.1a shows such a response. The second question is how to find the degree of the transfer function with finite transmission zeros in some methodical manner from prescribed values of α_{max} and α_{min}. Both questions will be answered by the *inverse Chebyshev* response discussed in Section 8.1. We encountered an illustration of such a design already in Example 5.17.

Another point about which we might be curious concerns the optimal efficiency of a lowpass approximation. In the equal-ripple response we exploited the allowed tolerance α_{max} uniformly over the passband whereas in the maximally flat approach we accepted an increasing error toward the passband corner by concentrating all our efforts at $\omega = 0$. The result was that for given attenuation specifications the equal-ripple approach using Chebyshev polynomials was more efficient (meaning of lower order) than the maximally flat approach using Butterworth polynomials. In the stopband, the attenuation of both Butterworth and Chebyshev responses increases monotonically beyond the prescribed minimum α_{min} at the stopband corner. We should then ask the following question: If Chebyshev polynomials give a more efficient approximation of a lowpass response, meaning they are of lower order, than Butterworth polynomials, could even higher efficiency, meaning functions of even lower order, be achieved by finding an approximation method that has an equal-ripple response in both passband and stopband, as illustrated in Fig. 8.1b? This is indeed the case. The resulting filters use elliptic functions and are referred to as *Elliptic Filters* (or Cauer filters after Wilhelm Cauer, who did much of the theoretical de-

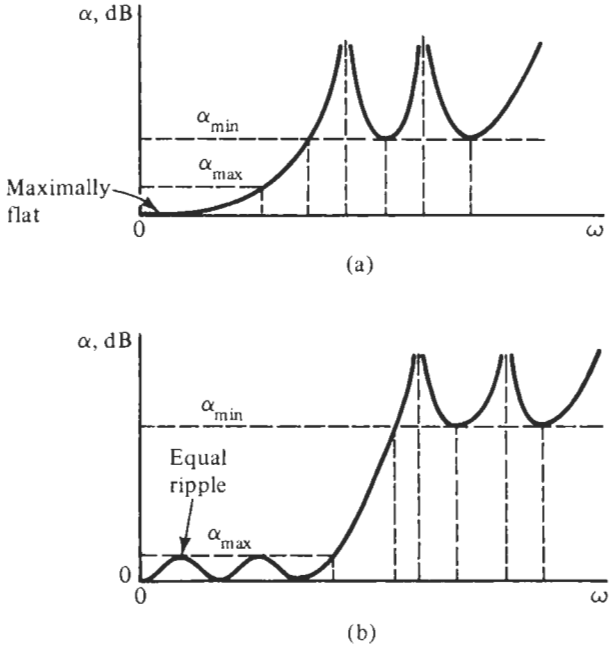

Figure 8.1 Lowpass attenuation requirements with (a) maximally flat passband and equal-ripple stopband, and (b) equal-ripple passband and stopband.

velopment in the 1930s and 1940s in Germany). We will present Cauer filters in Section 8.3.

8.1 THE INVERSE CHEBYSHEV RESPONSE

All forms of lowpass responses are competitive in the sense that the designer may choose one or another depending on its advantages or disadvantages. Many designers prefer the inverse Chebyshev response for filter design. One of the objectives of our study will be to discover why this might be.

We first show that the inverse Chebyshev response function may be generated in three steps. As shown in Fig 8.2, we begin with the lowpass Chebyshev response of Chapter 7, which is

$$|T_C(j\omega)|^2 = \frac{1}{1 + \varepsilon^2 C_n^2(\omega)} \tag{8.1}$$

It is shown in Fig 8.2a. We next subtract this function from 1, giving

$$1 - |T_C(j\omega)|^2 = \frac{\varepsilon^2 C_n^2(\omega)}{1 + \varepsilon^2 C_n^2(\omega)} \tag{8.2}$$

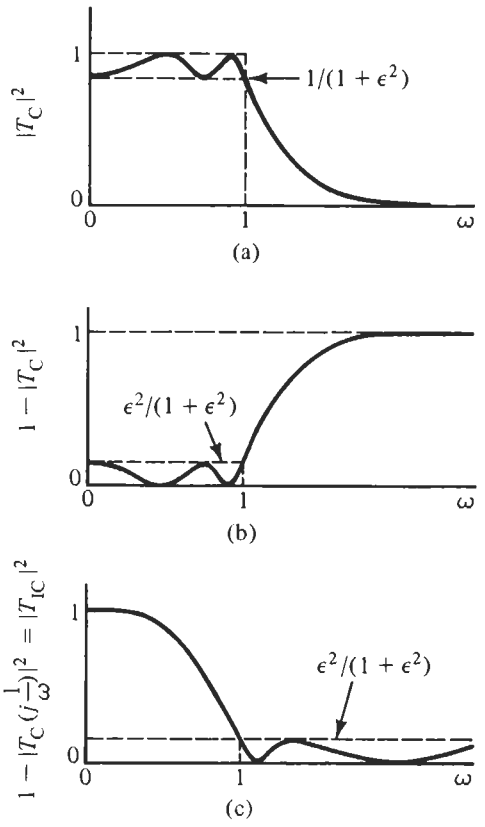

Figure 8.2 Derivation of the inverse Chebyshev response.

which is the response shown in Fig 8.2b. Finally we invert frequency by replacing ω with $1/\omega$, giving the inverse Chebyshev response in Fig. 8.2c:

$$|T_{\mathrm{IC}}(j\omega)|^2 = \frac{\varepsilon^2 C_n^2(1/\omega)}{1 + \varepsilon^2 C_n^2(1/\omega)} \tag{8.3}$$

Given this response, we have a number of questions to answer: (1) What are the characteristics of the response? (2) Where are the poles and zeros of $T_{\mathrm{IC}}(s)$ located in the s-plane? (3) How does the form of the response relate to specifications? We first drop the subscript IC and then proceed.

Notice that $\omega = 1$ is the edge of the stopband. We direct special attention to the frequency $\omega = 1$. Since $C_n(1) = 1$ for all n, then from Eq. (8.3),

$$|T(j1)|^2 = \frac{\varepsilon^2}{1 + \varepsilon^2} \tag{8.4}$$

Referring to Fig 8.2a, we see that the ripple band that extends from 0 to 1 for the Chebyshev response corresponds to the range of 1 to ∞ for the inverse Chebyshev response of Fig 8.2c. Thus the upper limit of $|T(j\omega)^2|$ in the stopband of the inverse Chebyshev response is the same as that for $\omega = 1$, that is, the value given by Eq. (8.4). In terms of the attenuation give by

$$\alpha = -10 \log |T(j\omega)|^2 \tag{8.5}$$

the minimum value of the attenuation in the stopband is, from Eq. (8.4),

$$\alpha_{\min} = -10 \log |T(j1)|^2 = 10 \log \left(1 + \frac{1}{\varepsilon^2}\right) \text{ dB} \tag{8.6}$$

Solving this equation for ε gives

$$\varepsilon = \left(10^{\alpha_{\min}/10} - 1\right)^{-1/2} \tag{8.7}$$

If Eq. (8.3) is written in the form found by dividing the denominator by the numerator,

$$|T(j\omega)|^2 = \frac{1}{1 + 1/[\varepsilon^2 C_n^2(1/\omega)]} \tag{8.8}$$

then we may make use of Eq. (8.5) to determine an expression for the attenuation

$$\alpha = -10 \log \left[1 + \frac{1}{\varepsilon^2 C_n^2(1/\omega)}\right] \text{ dB} \tag{8.9}$$

This is the general form of the inverse Chebyshev response, and a typical plot of this response is shown in Fig. 8.3 for both $|T|^2$ and α. We are especially interested in the behavior of $|T|^2$ and α in the stopband, that is for frequencies in excess of 1. At the frequency $\omega = 1$ the attenuation is $\alpha_{\min}$, and this corresponds to the value $\varepsilon^2/(1 + \varepsilon^2)$ for $|T|^2$. The equal-ripple nature of $|T|^2$ as shown in Fig. 8.3a indicates oscillations between this value and 0. From Eq. (8.3) the limits of the ripples correspond to

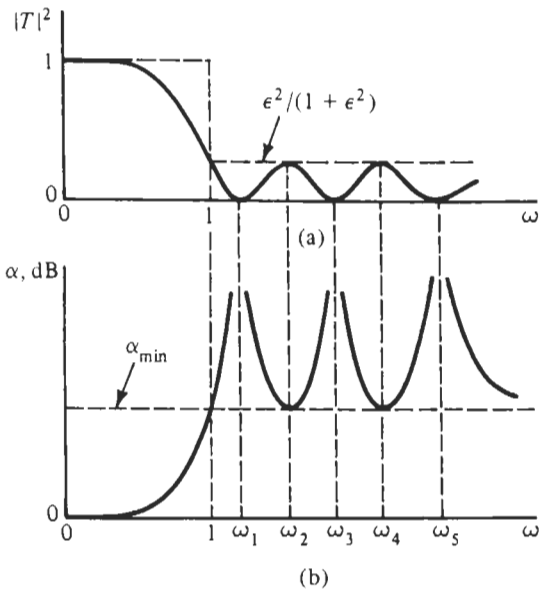

Figure 8.3 Typical magnitude-squared (a) and attenuation (b) of inverse Chebyshev filters.

$$C_n^2\left(\frac{1}{\omega_k}\right) = 0, \quad k = 1, 3, 5, \ldots \quad \text{and} \quad C_n^2\left(\frac{1}{\omega_k}\right) = 1, \quad k = 2, 4, 6, \ldots \tag{8.10}$$

We wish to solve for these frequencies. Evidently they correspond to

$$\cos\, n\, \cos^{-1}\left(\frac{1}{\omega_k}\right) = \begin{cases} 0 \\ \pm 1 \end{cases} \tag{8.11}$$

since the Chebyshev function is expressed in terms of trigonometric functions in the range of ω from 1 to ∞. Let $\theta_k = \cos^{-1}(1/\omega_k)$ and observe that

$$\cos\, n\theta_k = 0 \quad \text{when} \quad n\theta_k = k\frac{\pi}{2} \quad \text{for } k \text{ odd} \tag{8.12}$$

$$\cos\, n\theta_k = 1 \quad \text{when} \quad n\theta_k = k\frac{\pi}{2} \quad \text{for } k \text{ even} \tag{8.13}$$

Thus all frequencies for maxima and minima are given by one equation:

$$\cos^{-1}\left(\frac{1}{\omega_k}\right) = \theta_k = \frac{k\pi}{2n} \tag{8.14}$$

or

$$\omega_k = \sec\frac{k\pi}{2n} \tag{8.15}$$

where odd values of k correspond to $|T|^2 = 0$ and even values of k to the value $|T|^2 = \varepsilon^2/(1+\varepsilon^2)$, as shown in Fig. 8.3a. In terms of the attenuation plot, $\alpha = \infty$ for k odd and $\alpha = \alpha_{\min}$ for $\omega = 1$ and k even. The oscillations in Fig. 8.3 have been shown as almost sinusoidal for clarity. In reality the oscillations are bunched near $\omega = 1$, as shown for $n = 9$ in Fig. 8.4.

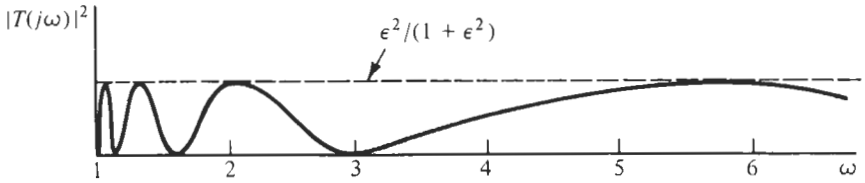

Figure 8.4 Stopband ripples of a ninth-order inverse Chebyshev filter.

From Figs. 8.3 and 8.4 it is seen that the stopband begins at the frequency $\omega = 1$. It is crucial that frequency scaling be done such that this is the case. This is shown in Fig. 8.5. Another frequency ω_p is also defined as being the end of the passband. This frequency must be a value that results from the scaling of the stopband frequency to $\omega_s = 1$.

So much for the features of the stopband. To observe the interesting characteristic of the passband, we note that the asymptotic form of the Chebyshev function for large ω is, by Eq. (7.6),

$$C_n(\omega) \cong 2^{n-1}\omega^n, \quad \omega \gg 1 \tag{8.16}$$

Hence we know that near $\omega = 0$

$$C_n\left(\frac{1}{\omega}\right) \cong 2^{n-1}\left(\frac{1}{\omega}\right)^n, \quad \omega \ll 1 \tag{8.17}$$

If we substitute this approximate form into Eq. (8.8), there results

$$|T|^2 \cong \frac{1}{1 + 1/\varepsilon^2[2^{n-1}(1/\omega^n)]^2} \tag{8.18}$$

$$= \frac{1}{1 + \omega^{2n}/(\varepsilon^2 2^{2n-1})} = \frac{1}{1 + (\omega/\omega_k)^{2n}} \tag{8.19}$$

where

$$\omega_k = \left(\varepsilon^2 2^{2n-2}\right)^{1/2n} = \left(\varepsilon 2^{n-1}\right)^{1/n} \tag{8.20}$$

Since Eq. (8.19) has the form of the equation for the maximally flat response, Eq. (6.46), we may conclude that for small ω the inverse Chebyshev response is maximally flat. We will show later that if ω_k given by Eq. (8.20) is larger than 1, then this response is "flatter" than a maximally flat response of equal degree.

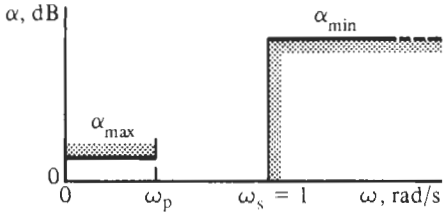

Figure 8.5 Lowpass attenuation specifications.

8.2 FROM SPECIFICATIONS TO POLE AND ZERO LOCATIONS

As was done for the maximally flat and Chebyshev lowpass responses, we determine the value of n that will satisfy specific $\alpha_{\min}$ and $\alpha_{\max}$. We begin with Eq. (8.9) and apply the specifications shown in Fig. 8.5. In that figure we see that the end of the passband, where the attenuation is less than $\alpha_{\max}$, is ω_p and the stopband starts at $\omega_s = 1$. Then

$$\alpha_{\max} = 10 \log \left[1 + \frac{1}{\varepsilon^2 C_n^2(1/\omega_p)} \right] \tag{8.21}$$

If we substitue the value of ε^2 found in Eq. (8.7) into this equation, we may solve for $C_n^2(1/\omega_p)$:

$$C_n^2\left(\frac{1}{\omega_p}\right) = \frac{10^{\alpha_{\min}/10} - 1}{10^{\alpha_{\max}/10} - 1} \tag{8.22}$$

This equation applies to the passband for which $\omega < 1$, where the Chebyshev function is expressed in terms of hyperbolic functions. If we extract the square root of Eq. (8.22), then it may be written

$$\cosh\left[n \cosh^{-1}\left(\frac{1}{\omega_p}\right)\right] = \left[\frac{10^{\alpha_{\min}/10} - 1}{10^{\alpha_{\max}/10} - 1}\right]^{1/2} \tag{8.23}$$

Solving this equation for n, we obtain finally

$$n = \frac{\cosh^{-1}\left[(10^{\alpha_{\min}/10} - 1)/(10^{\alpha_{\max}/10} - 1)\right]^{1/2}}{\cosh^{-1}(1/\omega_p)} \tag{8.24}$$

This equation may be compared to that found by the Chebyshev response, Eq. (7.20a). They are seen to be identical except that Eq. (8.34) is scaled such that $\omega_s = 1$, while Eq. (7.20a) is scaled such that $\omega_p = 1$. Thus if written in terms of ω_s/ω_p, the two equations are the same. We conclude that the Chebyshev and the inverse Chebyshev responses require the same value of n to satisfy the general specifications.

$$\alpha_{\max}, \quad \alpha_{\min}, \quad \omega_p, \quad \omega_s$$

Having found the value of n that will satisfy the specifications of Fig. 8.5 we may now determine the location of the poles and zeros. For the magnitude-squared function we may identify numerator and denominator as

$$|T|^2 = \left.\frac{p(s)p(-s)}{q(s)q(-s)}\right|_{s=j\omega} \tag{8.25}$$

Equating this result to Eq. (8.3), we make the identifications

$$p(s)p(-s)|_{s=j\omega} = \varepsilon^2 C_n^2\left(\frac{1}{\omega}\right) \tag{8.26}$$

from which the zero locations for $T(s)$ will be found, and

$$q(s)q(-s)|_{s=j\omega} = 1 + \varepsilon^2 C_n^2\left(\frac{1}{\omega}\right) \tag{8.27}$$

for the poles. Now the only values of ω in Eq. (8.26) that will cause the function to become zero are in the range $\omega > 1$ when the Chebyshev function is expressed in terms of trigonometric functions. Thus, zeros are those values ω_k where

$$C_n^2\left(\frac{1}{\omega_k}\right) = 0 \tag{8.28}$$

This is identical to Eq. (8.10), and the solution to this requirement was given by Eq. (8.15) for k odd,

$$\omega_k = \sec\left(\frac{k\pi}{2n}\right), \quad k = 1, 3, 5, \ldots, n \tag{8.29}$$

Equation (8.27), which defines the poles of the inverse Chebyshev response, has the same form as the denominator of Eq. (7.8), except that ω was replaced by $1/\omega$. Since we have already determined the locations of the Chebyshev poles in Section 7.3, the poles for the inverse Chebyshev response may be found by a simple procedure: find the Chebyshev poles as in Eq. (7.34) and take their reciprocals. Note that when using Eq. (7.34) for inverse Chebyshev filters ε must be determined from the inverse-Chebyshev equation (8.6) involving $\alpha_{\min}$ in the stopband, *not* from the Chebyshev equation (7.17) involving $\alpha_{\max}$ of the passband. Under this provision, if a Chebyshev pole is found at $s_k = \sigma_k + j\omega_k$ with the magnitude (its distance from the origin) and quality factor

$$\omega_{0k} = \sqrt{\sigma_k^2 + \omega_k^2} \quad \text{and} \quad Q_{Ck} = \frac{\omega_{0k}}{2\sigma_k} \tag{8.30}$$

then the pole location $p_k = \alpha_k + j\beta_k$ of the inverse Chebyshev response is at

$$p_k = \frac{1}{s_k} = \frac{\sigma_k - j\omega_k}{\sigma_k^2 + \omega_k^2} = \frac{\sigma_k}{\omega_{0k}^2} - j\frac{\omega_k}{\omega_{0k}^2} = \alpha_k + j\beta_k \tag{8.31}$$

with magnitude and quality factor

$$|p_k| = \sqrt{\alpha_k^2 + \beta_k^2} = \frac{1}{\omega_{0k}} \quad \text{and} \quad Q_{ICk} = \frac{|p_k|}{2\alpha_k} = \frac{1/\omega_{0k}}{2\sigma_k/\omega_{0k}^2} = \frac{\omega_{0k}}{2\sigma_k} = Q_{Ck} \tag{8.32}$$

The situation is shown in Fig. 8.6a. Observe that the pole is mirrored at the unit circle and that Chebyshev and inverse Chebyshev filters have the same quality factors. Thus, a characteristic pole and zero location pattern for the inverse Chebyshev response is that shown in Fig. 8.6b for the case $n = 9$. We will now illustrate this general procedure in terms of an example.

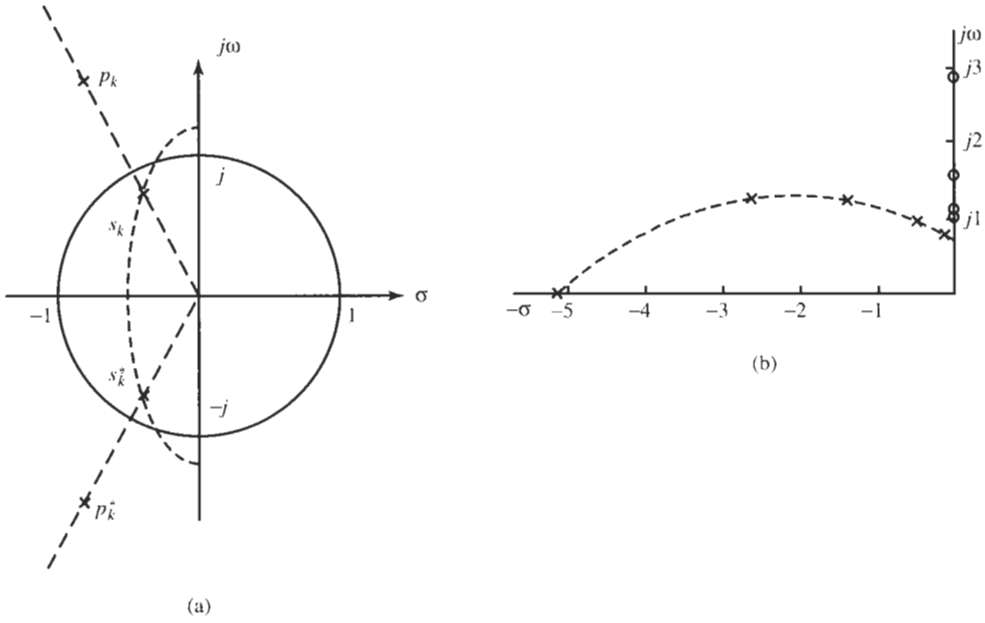

Figure 8.6 (a) Pole reciprocation in an inverse Chebyshev filter; since the poles of the Chebyshev and the inverse Chebyshev filter lie on the same radial line, they have the same pole Q. (b) Location of poles and zeros of a ninth-order inverse Chebyshev filter.

EXAMPLE 8.1

The specifications for an inverse Chebyshev filter are given in terms of the notation in Fig. 8.5 as

$$\alpha_{\min} = 18\text{dB}, \quad \alpha_{\max} = 0.25\text{ dB}, \quad \omega_s = 140\text{ krad/s (22.3 kHz)},$$
$$\omega_p = 100\text{ krad/s (15.9 kHz)}$$

Solution

The required value of n is found using Eq. (7.20b):

$$n = \frac{\ln\sqrt{4\left(10^{1.8}-1\right)/\left(10^{0.025}-1\right)}}{\ln\left(1.4+\sqrt{1.4^2-1}\right)} = 4.81$$

which we round up to $n = 5$. With n known, we next determine the location of the inverse Chebyshev poles. We find first ε from Eq. (8.6):

$$\varepsilon = \frac{1}{\sqrt{10^{0.1\alpha_{\min}}-1}} = \frac{1}{\sqrt{10^{1.8}-1}} = 0.1269$$

Then, from Eq. (7.36)

$$a = \frac{1}{5}\sinh^{-1}\left(\frac{1}{0.1269}\right) = 0.5523$$

This lets us calculate the Chebyshev pole positions, using Eq. (7.34) with $k = 1, 2, 3$. We will also make use of Eq. (8.32). The resulting values are in the table below.

k	σ_k	ω_k	ω_{0k}	Q_k
1	−0.1795	$\pm j1.0998$	1.1144	3.104
2	−0.4699	$\pm j0.6797$	0.8263	0.8792
3	−0.5808	0	0.5808	0.5

To determine the positions of the inverse Chebyshev poles and zeros, we find the reciprocal of ω_{0k}, labeled w_{0k}, but keep the same values of Q_k, and use Eq. (8.31) for the zeros ω_{zk}. The required values are as follows:

k	w_{0k}	Q_k	$\alpha_k \pm j\beta_k$	ω_{zk}
1	0.8973	3.104	$+0.1445 \pm j0.8856$	1.0515
2	1.2102	0.8792	$-0.6882 \pm j0.9954$	1.7013
3	1.7218	0.5	$-1.7218 \pm j0$	∞

The calculated poles and zeros are shown in Fig. 8.7 for the upper half-plane. These locations are based on the assumption that $\omega_s = 1$, but since the specified ω_s was 140 krad/s, frequency scaling by 140 krad/s is required.

To continue the example, let us find a circuit to realize the poles p_k and zeros ω_{zk} of Fig. 8.7. We use Åckerberg–Mossberg biquads for the realization because they allow us to achieve

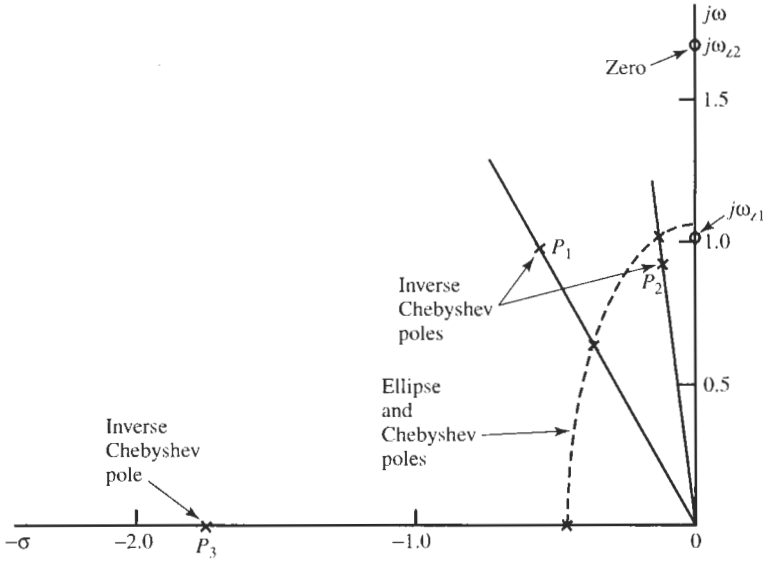

Figure 8.7 Pole and zero positions for Example 8.1.

arbitrary gain, and we pick suitable capacitor sizes. As always, we use LM741 opamps. Let us aim for a low-frequency gain of 13 dB.

First we pair off the poles as shown in Fig. 8.8a so that the zeros are associated with the closest poles; we need two lowpass notch circuits and one additional first-order module. The total transfer function is

$$T(s) = T_1T_2T_3 = \frac{k_1}{s + 1.7218}\,\frac{k_2\left(s^2 + 2.8944\right)}{s^2 + 1.3764s + 1.4646}\,\frac{k_3\left(s^2 + 1.1057\right)}{s^2 + 0.2890s + 0.8052} \tag{8.33}$$

where $k_1k_2k_3 = K$, with $KM_3 = 4.47$, corresponding to the prescribed 13-dB gain. We choose the sequence of the modules in the order of increasing Q as shown in Eq. (8.33). Following the procedure in Section 5.3, we compute from the voltage levels at the origin

$$M_1 = \frac{1}{1.72} = 0.58, \quad M_2 = \frac{2.89}{1.46 \times 1.72} = 1.15, \quad \text{and} \quad M_3 = \frac{2.89 \times 1.10}{1.46 \times 1.72 \times 0.81} = 1.57$$

to give

$$k_1 = K\frac{M_3}{M_1} = \frac{4.47}{0.58} = 7.71, \quad k_2 = \frac{M_1}{M_2} = 0.50, \quad k_3 = \frac{M_2}{M_3} = 0.73$$

Note that these constants are determined to make the dc gain of T_2 and T_3 equal to 1 and that all the required passband gain is assigned to T_1. To make the *stop*band corner equal to unity, we choose $\omega_s = 140$ krad/s as the normalizing frequency.

We build the filter by taking the first-order section of Fig. 3.24, which realizes, with $C_2 = 0$,

$$T(s) = \frac{G_1}{sC_2 + G_2}$$

and cascade it with two of the four-amplifier biquads shown in Fig. 5.1, both configured as lowpass notch filters. We have multiplied T_2 and T_3 by (-1) because by Eq. (5.5) the circuit is inverting,

$$T(s) = -\frac{as^2 + \omega_0^2\,(a + d)}{s^2 + s\omega_0/Q + \omega_0^2}$$

with $\omega_0 = 1/(RC)$ and where we set $c = 0$, $k = 1$, and $a = bkQ$. All parameters are defined in Fig. 5.1.

The first-order lowpass results in

$$T_1(s) = \frac{G_1/C_2}{s + G_2/C_2} = \frac{7.71}{s + 1.7218}$$

We choose $C_2 = 1$ nF to yield

$$R_1 = \frac{1}{7.71\omega_sC_2} = 926\ \Omega \quad \text{and} \quad R_2 = \frac{1}{1.722\omega_sC_2} = 4.15\ \text{k}\Omega$$

For T_2 we have

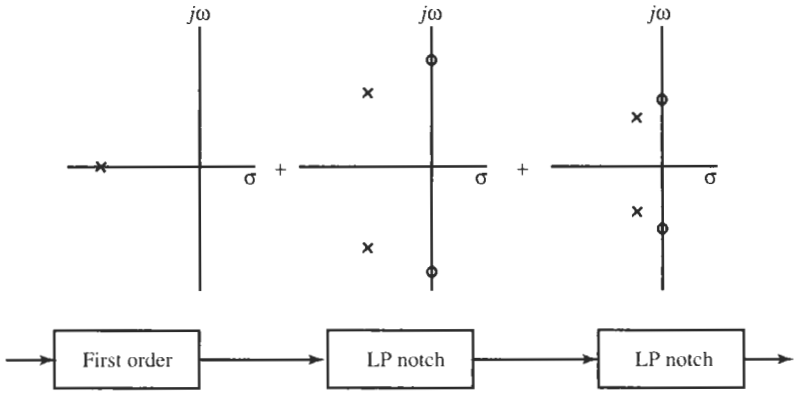

(a)

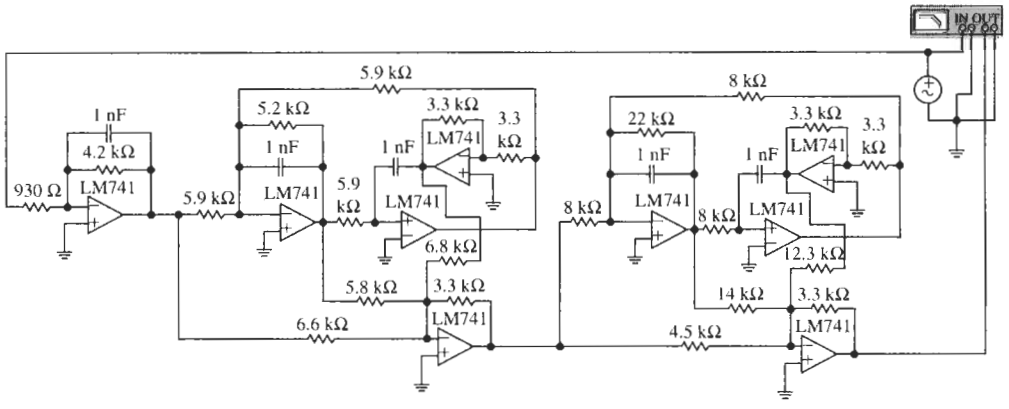

(b)

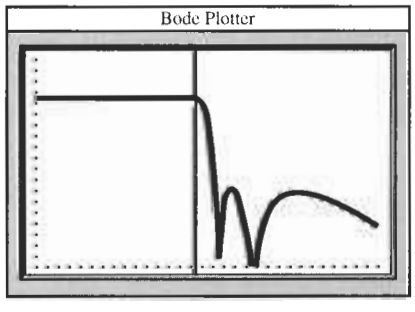

(c)

Figure 8.8 Fifth-order inverse Chebyshev lowpass circuit for Example 8.1; (a) pole-zero assignment and section ordering; (b) circuit diagram; (c) test results. (Bode Plotter scales: 2 to 290 kHz; −20 to 20 dB; cursor at 16.64 kHz, 12.75 dB.)

$$T_2(s) = -\frac{as^2 + \omega_0^2(a+d)}{s^2 + s\omega_0/Q + \omega_0^2} = -\frac{0.50\,(s^2 + 2.8944)}{s^2 + 1.3764s + 1.4646}$$

With $C = 1$ nF and $Q = 0.879$ we find

$$R = \frac{1}{\sqrt{1.465}\omega_s C} = 5.90\ \text{k}\Omega, \quad QR = 5.19\text{k}\Omega$$

Also, $a = 0.50$ and $a + d = 0.50 \times 2.8944/1.4646 = 0.988$, and we get $d = 0.488$ and $b = a/Q_2 = 0.569$.

Similarly, we have for T_3

$$T_3(s) = -\frac{as^2 + \omega_0^2(a+d)}{s^2 + s\omega_0/Q + \omega_0^2} = -\frac{0.73\,(s^2 + 1.1057)}{s^2 + 0.2890s + 0.8052} \tag{8.34}$$

and $Q = 3.10$; we choose again $C = 1$ nF to give

$$R = \frac{1}{\sqrt{0.805}\omega_s C} = 7.96\ \text{k}\Omega \quad \text{and} \quad QR = 24.68\ \text{k}\Omega$$

In addition, Eq. (8.34) requires $a = 0.73$, which gives $b = a/Q_3 = 0.236$. Further, $d = 0.268$.

The resulting circuit together with test results is shown in Fig. 8.8b and c. The circuit performs correctly; the passband corner (cursor) is at 16.6 kHz where the gain is 0.25 dB down from its dc level of 13 dB. The initially observed 0.4-dB peaking at the passband edge was corrected easily by reducing the resistor QR in T_3 from the computed 24.7 kΩ to 22 kΩ. As we have seen in earlier examples, this simple tuning procedure is an advantage of cascade design where all second-order stages are isolated so that their influence on filter performance is readily identified. The test results show clearly the two transmission zeros; the measured stopband with gain of −4.8 dB (≈18 dB below the 13-dB passband gain) starts at 21.8 kHz. The two attenuation peaks in the stopband are seen to be equal (at −4.8 dB) as required.

The example has shown that the pole and zero locations for the inverse Chebyshev response can be determined by a simple step-by-step procedure. If computer aids are not available, each step can be accomplished readily with a calculator.

8.3 CAUER MAGNITUDE RESPONSE

A comparison of the three responses shown in Fig. 8.9 provides us with a rationale for introducing yet another response. We recall from Chapter 6 that the maximally flat response was derived with the objective of reducing the error between the response and the brick-wall response as much as possible for frequencies near $\omega = 0$, and this resulted in a maximally flat magnitude characteristic. The Chebyshev response of Chapter 7 distributed this error over the entire passband, and this resulted in an equal-ripple response. The result was that the size of the frequency band between the end of the passband and the beginning of the stopband, $\omega_s - \omega_p$, was reduced for a given order n. We will call this the *transition band*, and speak of a small transition band as a *sharp cut-off* characteristic. In both the maximally flat and

the Chebyshev cases the way we meet the attenuation specifications α_{max} and α_{min} in the transition band is to control the size of n. We found that for given specifications the Chebyshev response required a smaller value of n than the maximally flat case. The inverse Chebyshev response provided an approach similar to the maximally flat case with finite transmission zeros discussed in Section 6.5. By introducing zeros of $T(s)$ on the imaginary axis beyond ω_s, we gave up the asymptotic increase in attenuation at higher frequencies. However this is seldom important since our objective is to obtain a specified α_{min} at the frequency ω_s and at all higher frequencies. Thus an increase of 0 dB per octave would be satisfactory, even though this cannot be achieved. Again referring to Fig. 8.9 (see also Fig. 8.20a), we see that the maximally flat and the Chebyshev responses can be regarded as inefficient in the stopband in the sense that they provide more attenuation than is needed. With the introduction of zeros in the inverse Chebyshev response, not only does the attenuation increase faster through the transition band, but by selecting the zero locations carefully we strive to distribute the attenuation more evenly over the stopband.

In a similar manner we can reason that the maximally flat and the inverse Chebyshev responses are inefficient in the passband because they provide less attenuation than the acceptable value α_{max}, whereas the Chebyshev function fully exploits the permitted α_{max} over the whole passband. This suggests that a new response with equal ripples in both passband and stopband would be superior to even the inverse Chebyshev response. We shall show that indeed this is the case as was first demonstrated by Wilhelm Cauer. Unfortunately, the treatment leads to equations with elliptic functions that are less well known and harder to solve. But because of the importance of Cauer (or *elliptic*) filters numerous tables and design curves are available to the engineer. To illustrate the substantial gains to be made, consider some numbers: if we take as requirements that $\omega_s/\omega_p = 1.5$, $\alpha_{min} = 50$ dB, and $\alpha_{max} = 0.5$ dB, then for a maximally flat response it is necessary that $n = 17$, and for a Chebyshev response that $n = 8$. For a Cauer response, it is necessary only that $n = 5$. This is a significant improvement.

Cauer first used his new theory in solving a filter problem for the German telephone industry. His new design achieved specifications with one less inductor than had ever been done before. The world first learned of the Cauer method not through scholarly publication but through a patent disclosure, which eventually reached the Bell Laboratories. Legend has it that the entire Mathematics Department of Bell Laboratories spent the next 2 weeks at the New York Public Library studying elliptic functions. Cauer had studied mathematics under Hilbert at Göttingen, and so elliptic functions and their applications were familiar to him.

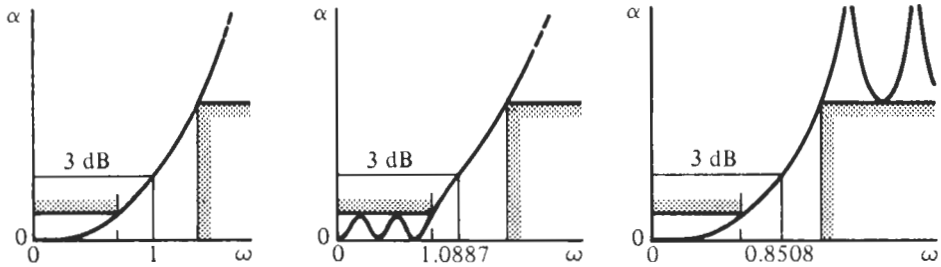

Figure 8.9 Filter magnitude response: (a) maximally flat; (b) Chebyshev; (c) inverse Chebyshev.

Given the objective of attaining a response that is equal ripple in both the passband and the stopband, what are the problems to be considered in determining $T(s)$? As shown in Fig. 8.10, the poles of $T(s)$ must be placed in such a way that we have equal ripple in the passband. In our study of the Chebyshev response these poles were located on an ellipse. Given that we must have zeros of $T(s)$ on the imaginary axis, we wish to locate them such that equal ripple is achieved in the stopband, which requires that $\alpha_1 = \alpha_2 = \alpha_{\min}$.

Let us review the previous approximation methods to get an indication on how we might want to proceed. In all cases, the squared magnitude of the lowpass transfer function was expressed as in Eq. (6.8) as

$$|T(j\omega)|^2 = \frac{1}{1 + |K(j\omega)|^2} \tag{8.35}$$

where $K(s)$ was the characteristic function. The transfer function $T(s)$ has its passband where $K(s)$ is small; in particular, transmission is perfect ($T = 1$) at the zeros of $K(s)$. The stopband of T is in the range where K is large: specifically, the transmission zeros ($T = 0$) occur where K has its poles. For the maximally flat approximation, $K(s)$ is a polynomial, εs^n, with all its zeros at the origin and poles at infinity corresponding to maximally flat behavior at these frequencies. For the equal-ripple approximations, $K(s)$ is again given via a polynomial, the Chebyshev polynomial $C_n(s)$, $K = \varepsilon C_n(s)$. In this case, the zeros are carefully chosen to achieve equal ripples between 0 dB and $\alpha_{\max}$ throughout the passband, but all poles and hence transmission zeros are at infinity. We found in Section 6.5 that we could assign arbitrary transmission zeros to the stopband of a filter with maximally flat passband by choosing $K(s) = \varepsilon s^n / A(s)$. Here, K still has all its zeros at the origin for a maximally flat passband but has poles at the roots of the denominator polynomial $A(s)$, which are placed on the $j\omega$-axis at those frequencies where we wanted to have transmission zeros. With inverse Chebyshev filters, Eq. (8.8), we refined this approach by finding a method to place all poles of $K(s)$ such that all attenuation minima in the stopband were at the same level $\alpha_{\min}$. It should be apparent then that in the present case we

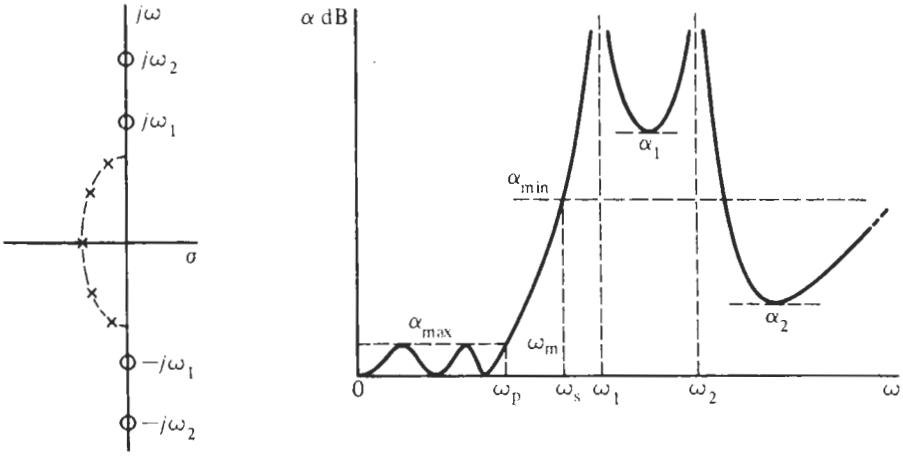

Figure 8.10 Transfer function with equal-ripple passband and finite stopband transmission zeros (loss poles).

need again a ratio of polynomials for $K(s)$ where poles *and* zeros are chosen on the $j\omega$-axis to achieve equal ripples in *both* passband and stopband. In some sense we need to combine the Chebyshev with the inverse Chebyshev responses.

Suppose then that we set $K(s)$ equal to a new function $R_n(s)$ of order n, which is a quotient of polynomials:

$$R_n(s) = \frac{P(s)}{Q(s)} \quad \text{or} \quad |R_n(j\omega)|^2 = \frac{P(j\omega)\,P(-j\omega)}{Q(j\omega)\,Q(-j\omega)} = R_n^2(\omega) \tag{8.36}$$

We have used the simplified notation $|R_n(j\omega)| = R_n(\omega)$. Following previous developments, we multiply R_n by the parameter ε. Then the new function replacing Eq. (8.35) will be

$$|T(j\omega)|^2 = \frac{1}{1 + \varepsilon^2 R_n^2(\omega)} \tag{8.37}$$

or

$$|T(j\omega)|^2 = \frac{Q(j\omega)\,Q(-j\omega)}{Q(j\omega)\,Q(-j\omega) + \varepsilon^2 P(j\omega)\,P(-j\omega)} \tag{8.38}$$

From this we see that the poles of R_n will be the required zeros of T. The attenuation corresponding to Eq. (8.37) is

$$\alpha = 10\,\log[1 + \varepsilon^2 R_n^2(\omega)] \tag{8.39}$$

Before studying this equation further let us make the decision that the end of the ripple band will be the normalized frequency $\omega_p = 1$, and further that we will set $R_n(1) = 1$. Then from the last equation,

$$\alpha(1) = \alpha_{\max} = 10\,\log\left(1 + \varepsilon^2\right) \tag{8.40}$$

or

$$\varepsilon = \sqrt{10^{\alpha_{\max}/10} - 1} \tag{8.41}$$

This is the same expression we found for the Chebyshev and maximally flat approximation functions. Now referring to Fig. 8.10 and the requirement that $\alpha_1 = \alpha_2 = \alpha_{\min}$ we shall require that $|R_n| = \pm L$ at the frequencies at which α has a minimum value in the stopband, as well as at ω_s. This will require that

$$\alpha_{\min} = 10\,\log(1 + \varepsilon^2 L^2) \tag{8.42}$$

or that

$$L^2 = \frac{10^{\alpha_{\min}/10} - 1}{10^{\alpha_{\max}/10} - 1} \tag{8.43}$$

This quotient has appeared before in the expression for n for both the maximally flat and the Chebyshev responses. We see that from the usual specifications we may determine ε and L. To go further, we must know more about our new function R_n. This we do in the next section.

8.4 CHEBYSHEV RATIONAL FUNCTIONS

It should be no surprise that $R_n(\omega, L)$, the *Chebyshev rational functions*, exactly meet the requirements outlined in the last section. The behavior of such functions is illustrated for the case $n = 4$ in Fig. 8.11. From that figure we see the following properties of $R_n(\omega, L)$:

1. In the frequency range $-1 < \omega < 1$ there are four zeros and an equal-ripple response with

$$|R_n(\omega, L)| \leqq 1 \tag{8.44}$$

2. At the frequency that we have chosen to be the end of the passband, $\omega = \pm 1$, we see that $R_n(\pm 1) = 1$, but in general

$$R_n(1) = 1 \quad \text{and} \quad R_n(-1) = (-1)^n \tag{8.45}$$

$R_n(\omega)$ is even for n even and odd for n odd as was the case for the Chebyshev functions C_n.

3. For $|\omega| > 1$ there are four poles and the lower limit of the function is L.

$$|R_n(\omega, L)| \geq L \tag{8.46}$$

This special case $n = 4$ generalizes as shown in Fig. 8.12, which tabulates $R_n(\omega, L)$ for $n = 2$ to $n = 5$, and also compares these functions to the corresponding Chebyshev functions $C_n(\omega)$.

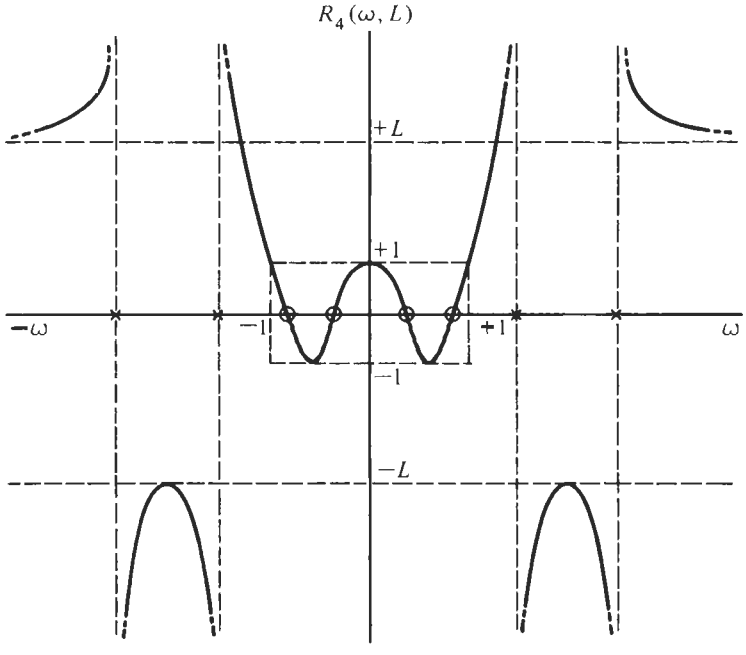

Figure 8.11 Chebyshev rational function of order $n = 4$.

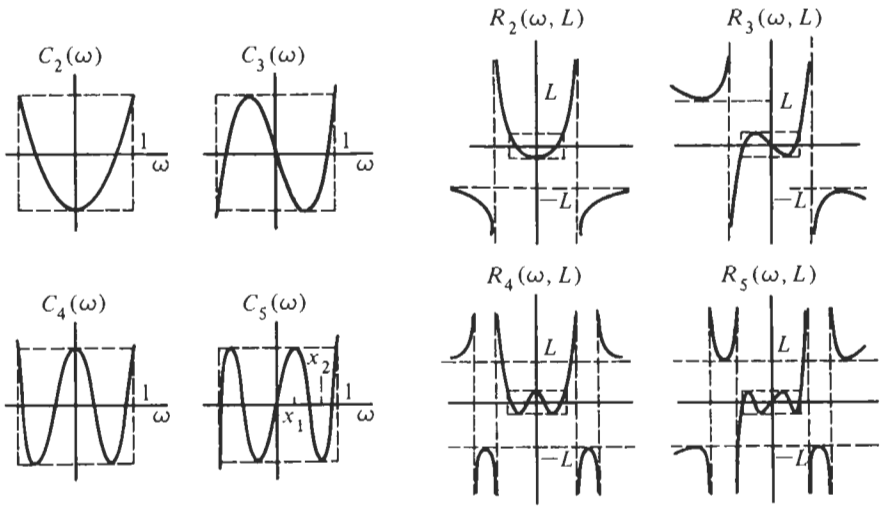

Characteristics

$C_n(\omega)$	$R_n(\omega, L)$
1. $C_n(\omega)$ is even (odd) if n is even (odd)	1. $R_n(\omega, L)$ is even (odd) if n is even (odd)
2. $C_n(\omega)$ has all zeros in $\lvert\omega\rvert < 1$	2. $R_n(\omega, L)$ has all zeros in the range $\lvert\omega\rvert < 1$ and all its poles in the range $\lvert\omega\rvert > 1$
3. $C_n(\omega)$ oscillates between ± 1 in the passband	3. $R_n(\omega, L)$ oscillates between ± 1 in the passband
4. $C_n(\omega) = 1$ at $\omega = 1$	4. $R_n(\omega, L) = 1$ at $\omega = 1$
5. $C_n(\omega) = 1$ increases monotonically for $\lvert\omega\rvert > 1$ (in the stopband)	5. $R_n(\omega, L) = 1$ increases between $\pm L$ and ∞ in the stopband

Figure 8.12 (a) Chebyshev polynomial and (b) Chebyshev rational function.

The Chebyshev rational functions may be constructed from the poles and zeros illustrated in Fig. 8.12. For $n = 4$.

$$R_4(s, L) = C_4 \frac{(s^2 + \omega_{z1}^2)(s^2 + \omega_{z2}^2)}{(s^2 + \omega_{p1}^2)(s^2 + \omega_{p2}^2)} \tag{8.47}$$

and for $n = 5$,

$$R_5(s, L) = C_5 s \frac{(s^2 + \omega_{z1}^2)(s^2 + \omega_{z2}^2)}{(s^2 + \omega_{p1}^2)(s^2 + \omega_{p2}^2)} \tag{8.48}$$

The corresponding pole-zero locations for these two cases are shown in Fig 8.13. Clearly, C_4 and C_5 are constants that depend on L.

With this knowledge of $R_n(\omega, L)$ we may turn to the Cauer magnitude function

$$|T(j\omega)|^2 = \frac{1}{1 + \varepsilon^2 R_n^2(\omega, L)} \tag{8.49}$$

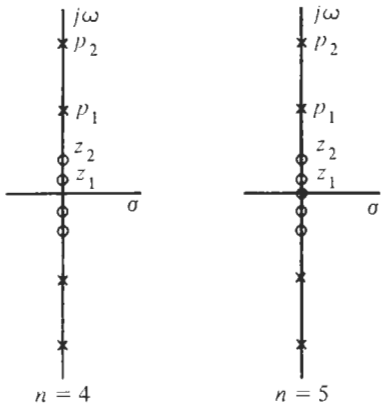

Figure 8.13 Poles and zeros of Chebyshev rational functions of orders $n = 4$ and $n = 5$.

and pay special attention to the frequencies at which the response is either a maximum or minimum. A typical response is shown in Fig. 8.14. In terms of this response, we make the following observations:

1. The zeros of $R(\omega, L)$, designated ω_{zv}, correspond to the equation $|T(j\omega)|^2 = 1$. These are seen to be located in the passband.
2. The poles of $R_n(\omega, L)$, designated ω_{pv}, correspond to the frequencies at which $|T(j\omega)|^2 = 0$. These are shown in Fig. 8.14 in the stopband.

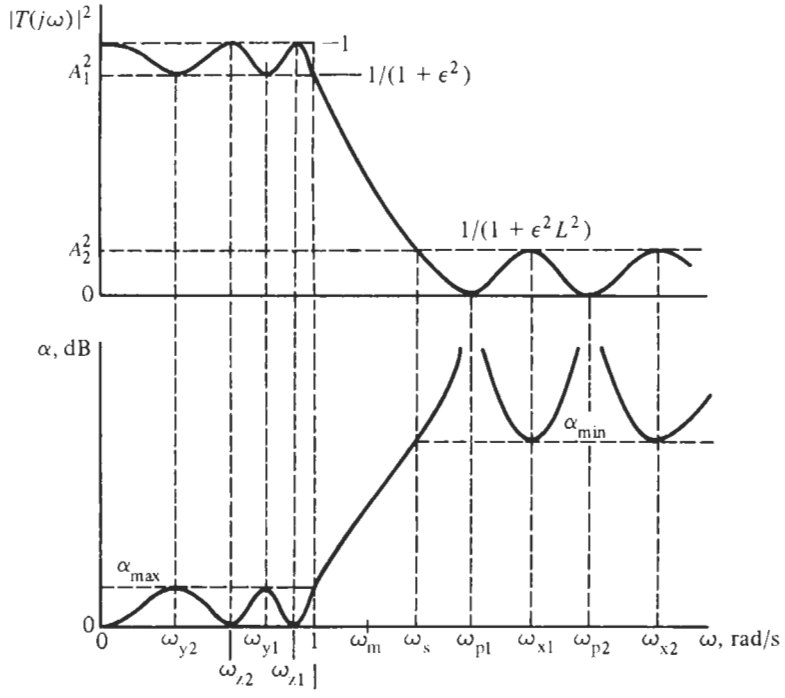

Figure 8.14 Typical Cauer filter response.

3. When $R_n(\omega, L) = 1$, we define the attenuation $\alpha_{\max}$ which occurs at $\omega = 1$ and various other freqencies in the passband. Under this condition,

$$|T(j\omega)|^2 = \frac{1}{1+\varepsilon^2} \tag{8.50}$$

4. Similarly, we are interested in frequencies at which $R_n(\omega, L) = \pm L$, where

$$|T(j\omega)|^2 = \frac{1}{1+\varepsilon^2 L^2} \tag{8.51}$$

These relate to the attenuation having the value $\alpha_{\min}$.

This information is summarized in Table 8.1.

By examining our new function $R_n(\omega)$ deeper, one can show that an interesting relationship exists between the zeros ω_{zv} and the poles ω_{pv} of R_n. It is obvious, of course, that the expression $\omega_p\omega_s = \omega_m^2$ must be valid between the frequencies at the passband corner ω_p and the stopband corner ω_s, where ω_m is a frequency in the transition band (see Fig. 8.10 or Fig. 8.14). Now recall that we chose to normalize the frequency axis such that the passband corner is $\omega_p = 1$. Thus, for the normalized frequencies we have $\omega_m = \sqrt{\omega_s}$, and one can prove that

$$\omega_{zv} = \frac{\omega_m^2}{\omega_{pv}} = \frac{\omega_s}{\omega_{pv}} \tag{8.52}$$

that is, poles and zeros of R_n are reciprocal with respect to a frequency in the transition band. The various parameters are identified in Fig. 8.14. The sketch is somewhat distorted in the interest of clarity of the definitions of the frequencies. An actual response for a Cauer filter of order $n = 5$ is given in Fig. 8.15, which shows the characteristic bunching of the ripples near $\omega = 1$ in the passband, and even more so in the stopband.

With this information we can write explicit expressions for the Chebyshev rational function $R_n(\omega)$. The functions must have all poles and zeros on the ω-axis related by Eq. (8.52), i.e.,

$$R_n(\omega, L) = k\prod_{v=1}^{n/2}\frac{\omega^2 - \left(\omega_s^2/\omega_{pv}^2\right)}{\omega^2 - \omega_{pv}^2} \quad \text{for } n \text{ even} \tag{8.53a}$$

$$R_n(\omega, L) = k\omega\prod_{v=1}^{(n-1)/2}\frac{\omega^2 - \left(\omega_s^2/\omega_{pv}^2\right)}{\omega^2 - \omega_{pv}^2} \quad \text{for } n \text{ odd} \tag{8.53b}$$

TABLE 8.1 Cauer Magnitude Response Characteristics

Band	$\lvert T(j\omega)\rvert^2$	Attenuation α	$R_n(\omega, L)$	Frequency Notation	Frequency Name
Pass	1	$\alpha = 0$	0	ω_{zv}	Attenuation zeros, zeros of R_n
	$\frac{1}{1+\varepsilon^2}$	$\alpha = \alpha_{\max}$	± 1	ω_{yv}	
Stop	0	$\alpha = \infty$	∞	ω_{pv}	Attenuation poles, transmission zeros
	$\frac{1}{1+\varepsilon^2 L^2}$	$\alpha = \alpha_{\min}$	$\pm L$	ω_{xv}	

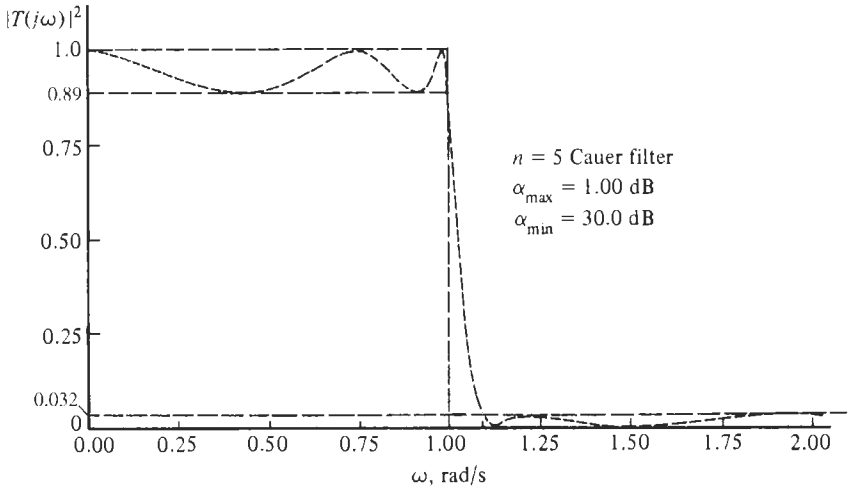

Figure 8.15 Fifth-order Cauer magnitude response.

where k is determined such that the ripple maxima in the passband are equal to unity to satisfy Eq. (8.50), and the degree must be found so that the minima in the stopband are equal to L as required by Eq. (8.51). This result can be shown to have far-reaching consequences: it means that if we can find the poles ω_{pv} of R_n, such that the stopband has equal ripples, then the passband will also have equal ripples if we choose the zeros of R_n by Eq. (8.52). ω_{pv} are the *attenuation poles* or transmission zeros of the transfer function $T(s)$. They often form the first specification in a design.

8.5 CAUER FILTER DESIGN

We come now to the task of determining the Cauer transfer function $T(s)$ from Eq. (8.38) so that the circuit can be designed. Unfortunately this is not as simple as it was for the maximally flat and the Chebyshev responses. Cauer found a systematic procedure for calculating this information, later published in his textbook (Cauer, 1958; Daniels, 1974). It is rather involved, making use of elliptic functions, which were first studied by Jacobi in 1826. Engineers who design Cauer (or elliptic) filters generally do so by the use of extensive tables, design curves, and computer-based algorithms.

As always, our design process starts from the prescribed specifications

$$\alpha_{max}, \quad \alpha_{min}, \quad \omega_s \quad (\text{or } \omega_s/\omega_p) \tag{8.54}$$

from which the degree n must be found. Actually, of the four parameters n, α_{max}, α_{min}, and ω_s any three may be prescribed and the fourth can be determined, but as a rule we need to find n. We can do this, in principle, by solving Eq. (8.37) for n. This job leads again to elliptic functions, but since a precise solution is not necessary (we need only to find an integer), we shall use a simple graphic process. Consider Eq. (8.37) and rewrite the expression to compute the attenuation at the corner of the stopband,

$$\alpha_{min} = 10 \log \left[1 + \varepsilon^2 R_n^2 (\omega_s)\right] \tag{8.55}$$

Remember that for Cauer filters $\alpha_{\min}$ is constant over the stopband so we may as well evaluate the expression at ω_s. For reasonable filter requirements, we can safely assume $1 << \varepsilon^2 R_n^2(\omega)$ in the stopband so the 1 can be neglected. Thus we have

$$\alpha_{\min} \approx 10 \log \left[\varepsilon^2 R_n^2(\omega_s)\right] = 20 \log \varepsilon + 20 \log R_n(\omega_s)$$

or

$$\alpha_{\min} + 20 \log \frac{1}{\varepsilon} \approx 20 \log R_n(\omega_s) \tag{8.56}$$

With the aid of a computer, $20 \log R_n(\omega)$ can be plotted as a function of ω_s for various values of n, leading to a family of design curves as shown in Fig. 8.16. Once we calculate $\varepsilon = \sqrt{10^{0.1\alpha_{\max}} - 1}$ from Eq. (8.41), the left-hand-side values of Eq. (8.56) can be marked on the ordinate and the intersection of the vertical line ω_s and the horizontal line $\alpha_{\min} + 20 \log (1/\varepsilon)$ gives the degree n of the Cauer filter that meets the specifications. Naturally, if the intersection of the two lines falls in between two n-curves, the larger value of n should be chosen. For example, $\alpha_{\min} = 50$ dB at $\omega_s = 1.5$ and a 0.5-dB passband ripple lead to $n = 5$ as is shown in the figure. The case in Fig. 8.15, $\alpha_{\min} = 30$ dB, $\omega_s = 1.1$, and $\alpha_{\max} = 1$ dB, also requires $n = 5$.

Before we proceed to find the Cauer transfer function, let us pause for moment to make two important observations that are true for all the filters discussed and that the filter designer should bear in mind.

1. There is a trade-off between passband ripple ε (or $\alpha_{\max}$) and stopband attenuation $\alpha_{\min}$, as Eq. (8.56) indicates:

$$\alpha_{\min} + 20 \log \frac{1}{\varepsilon} \approx 20 \log R_n(\omega_s) \quad \text{for Cauer} \tag{8.57a}$$

The narrower the passband ripple a designer requires the larger becomes the number $20 \log (1/\varepsilon)$ and, hence, the sum $\alpha_{\min} + 20 \log (1/\varepsilon)$. For given n, smaller passband ripple can be traded against increased stopband attenuation and vice versa; it is

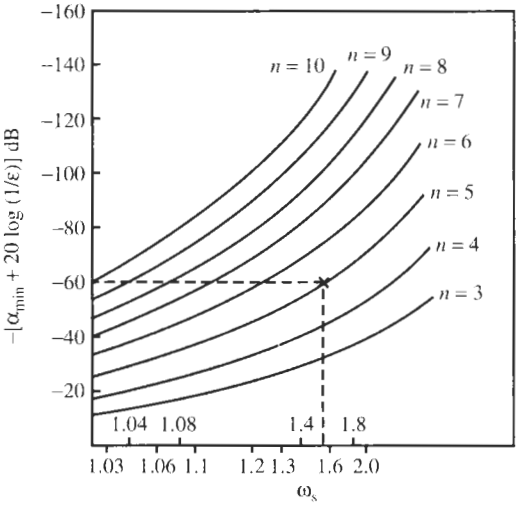

Figure 8.16 Design curves for determining the order n of an elliptic filter from given minimum stopband attenuation $\alpha_{\min}$, transition bandwidth ω_s, and passband ripple ε. Note the passband corner is normalized to $\omega_p = 1$. [From Sedra and Bracket (1978), with permission.]

the sum $\alpha_{\min} + 20 \log (1/\varepsilon)$, which sets the degree n. This observation is not true just for Cauer filters, but is valid for maximally flat and Chebyshev filters as well. We did not write down the explicit expressions because closed-form solutions for n are available in those cases. Note that from Eq. (6.14a) for the maximally flat function and from Eq. (7.15) for the Chebyshev filter, respectively, we can express the attenuation as

$$\alpha_{\min} + 20 \log (1/\varepsilon) \approx 20 \log \omega_s^n \quad \text{for maximally flat} \tag{8.57b}$$

$$\alpha_{\min} + 20 \log (1/\varepsilon) \approx 20 \log \cosh \left(n \cosh^{-1} \omega_s\right) \quad \text{for Chebyshev} \tag{8.57c}$$

Design curves for maximally flat and Chebyshev filters can be drawn analogous to those in Fig. 8.16, and the trade-off between $\alpha_{\min}$ and $\alpha_{\max}$ is apparent (see Fig. 8.19).

2. Figure 8.16 shows that n increases rapidly as the transition band narrows. The transition band should, therefore, not be chosen narrower than necessary if filter order is of concern.

Let us return now to finding the transfer function of a Cauer filter. We have developed an easy method to determine n from given filter attenuation requirements. From this information the transfer function with coefficients and its poles and zeros can be determined by a number of steps that involve elliptic functions. Rather than exploring the unfamiliar mathematics, we shall resort to any one of the numerous available design tables. There is no single or even standard method to present the information. Since transfer function data have to be matched to four parameters, $\alpha_{\max}$, $\alpha_{\min}$, ω_s, and n, the tables can be arranged in different ways and tend to be too voluminous to be included in this book. Many excellent references with design tables are available in the literature.[1] Also, there is no unique way to enter the tables with given filter specifications. We present in the following a few of the possibilities to make access to the literature simpler. Our goal is to find the transfer function

$$T(s) = \frac{N(s)}{D(s)} = \frac{C \prod_{i=1}^{m} \left(s^2 + a_i\right)}{s^n + b_{n-1} s^{n-1} + b_{n-2} s^{n-2} + \cdots + b_1 s + b_0} \tag{8.58}$$

where C is a constant determined such that

$$|T(j\omega)|_{\max} = 1$$

We can factor the denominator polynomial $D(s)$ into

$$D(s) = \left(s^2 + b_{11} s + b_{10}\right)\left(s^2 + b_{21} s + b_{20}\right)\left(s^2 + b_{31} s + b_{30}\right) \cdots \tag{8.59a}$$

if n is even, or into

$$D(s) = (s + p)\left(s^2 + b_{11} s + b_{10}\right)\left(s^2 + b_{21} s + b_{20}\right) \cdots \tag{8.59b}$$

if n is odd. The tables will provide us with the coefficients a_i, p, b_{i1}, b_{i0}, and C, but they ask for input in various different ways.

[1] See References 4, 6, and 7.

Table 8.2 shows one way of organizing the data in a matrix. Each "page" gives $T(s)$ for one value of α_{max}; the page is subdivided by values of the parameter ω_s/ω_p, and further into rows according to n. The corresponding values of α_{min} and C are listed for convenience, although they can be computed from the known α_{max}, ω_s/ω_p, and n. Together with Fig. 8.16, such a table is very easy to use.

TABLE 8.2 Cauer Parameters for $\alpha_{max} = 0.5$ dB

n	α_{min}	Constant C	Numerator of $T(s)$	Denominator $T(s)$
			(A) $\omega_s/\omega_p = 1.5$	
2	8.3	0.38540	$s^2 + 3.92705$	$s^2 + 1.03153 + 1.60319$
3	21.9	0.31410	$s^2 + 2.80601$	$(s^2 + 0.45286s + 1.14917)(s + 0.766952)$
4	36.3	0.015397	$(s^2 + 2.53555)(s^2 + 12.09931)$	$(s^2 + 0.25496s + 1.06044)(s^2 + 0.92001s + 0.47183)$
5	50.6	0.019197	$(s^2 + 2.42551)(s^2 + 5.43764)$	$(s^2 + 0.16346s + 1.03189)(s^2 + 0.57023s + 0.57601)(s + 0.42597)$
			(B) $\omega_s/\omega_p = 2.0$	
2	13.9	0.20133	$s^2 + 7.4641$	$s^2 + 1.24504 + 1.59179$
3	31.2	0.15424	$s^2 + 5.15321$	$(s^2 + 0.53787s + 1.14849)(s + 0.69212)$
4	48.6	0.0036987	$(s^2 + 4.59326)(s^2 + 23.22720)$	$(s^2 + 0.30116s + 1.06258)(s^2 + 0.88456s + 0.41032)$
5	66.1	0.0046205	$(s^2 + 4.36495)(s^2 + 10.56773)$	$(s^2 + 0.19255s + 1.03402)(s^2 + 0.58054s + 0.52500)(s + 0.392612$
			(C) $\omega_s/\omega_p = 3.0$	
2	21.5	0.083974	$s^2 + 17.48528$	$s^2 + 1.35715 + 1.55532$
3	42.8	0.063211	$s^2 + 11.82781$	$(s^2 + 0.58942s + 1.14559)(s + 0.65263)$
4	64.1	0.00062046	$(s^2 + 10.4554)(s^2 + 58.471)$	$(s^2 + 0.32979s + 1.063281)(s^2 + 0.86258s + 0.37787)$
5	85.5	0.00077547	$(s^2 + 9.8955)(s^2 + 25.0769)$	$(s^2 + 0.21066s + 1.0351)(s^2 + 0.58441s + 0.496388)(s + 0.37452$

EXAMPLE 8.2

Find an elliptic filter that has $\alpha_{max} = 0.5$ dB, $\alpha_{min} = 65$ dB, $\omega_p = 1000$ rad/s, and $\omega_s = 2$krad/s.

Solution

We compute $\omega_s/\omega_p = 2$ and

$$\alpha_{min} + 20 \log (1/\varepsilon) = \alpha_{min} + 20 \log \frac{1}{\sqrt{10^{0.1\alpha_{max}} - 1}} = 65\text{dB} + 9.14\text{ dB} = 74.14dB$$

to obtain $n = 5$. Table 8.2 gives

$$T(s) = \frac{0.39261}{s + 0.39261} \times \frac{0.12028\left(s^2 + 4.36495\right)}{s^2 + 0.58054s + 0.52500} \times \frac{0.097847\left(s^2 + 10.56773\right)}{s^2 + 0.19255s + 1.03402}$$

We arranged the modules in the order of increasing Q (0.5–1.25–5.27), and split the gain constant 0.0046205 from the table into three factors as shown, such that each of the factors satisfies $|T(j\omega)|_{max} = T(0) = 1$ in preparation for a cascade design.

The degree n is clear enough in most tables, as is the transition bandwidth ω_s (for $\omega_p = 1$). Occasionally, n is given only indirectly by the number of poles listed in the table and ω_s is sometimes represented as an angle, known as the modular angle

$$\theta = \sin^{-1}\left(\frac{\omega_p}{\omega_s}\right) \tag{8.60}$$

Some tables are given in terms of parameters that have their origin in transmission-line theory. In that case the *reflection coefficient* may be called for, usually expressed as a percentage. If the reflection coefficient has a magnitude $|\rho|$, then it is related to the passband attenuation limit and to ε by the equation

$$\alpha_{max} = -10 \log\left(1 - |\rho|^2\right) \quad \text{or} \quad |\rho| = \sqrt{1 - 10^{-0.1\alpha_{max}}} = \sqrt{\frac{\varepsilon^2}{1+\varepsilon^2}} \tag{8.61}$$

The tables by Christian and Eisenmann (1977) are a case in point. Other tables ask for the minimum value A_1 of the desired magnitude in the passband: by Eq. (8.50),

$$A_1 = |T(j\omega)|_{min} = \frac{1}{\sqrt{1+\varepsilon^2}} = 10^{-0.05\alpha_{max}} \tag{8.62a}$$

and for the maximum value A_2 of the magnitude in the stopband: by Eq. (8.51),

$$A_2 = |T(j\omega)|_{max} = \frac{1}{\sqrt{1+\varepsilon^2 L^2}} = 10^{-0.05\alpha_{min}} \tag{8.62b}$$

Refer to Fig. 8.14 for the meaning of A_1 and A_2. Tables 8.3, 8.4. and 8.5 give examples for Cauer filters of order 2, 3, and 4.

EXAMPLE 8.3

Find an elliptic filter transfer function with $\alpha_{max} = 0.45$ dB, $\alpha_{min} = 17$ dB, and a sharp cut-off so that $\omega_s/\omega_p = 1.1$.

Solution

We find from Eqs. (8.62a) and (8.62b)

$$A_1 = 10^{-0.05\alpha_{max}} = 0.9495 \quad \text{and} \quad A_2 = 10^{-0.05\alpha_{min}} = 0.1413$$

Also, from Fig. 8.16 with $\alpha_{min} + 20 \log(1/\varepsilon) = 17\,\text{dB} + 9.62\,\text{dB} \approx 26.62\,\text{dB}$ we have $n = 4$. Table 8.5 gives the coefficients for the fourth-order case. From the framed box we obtain

$$T(s) = \frac{0.1399\left(s^2 + 1.2909\right)\left(s^2 + 4.3497\right)}{\left(s^2 + 1.0274s + 0.7858\right)\left(s^2 + 0.1264s + 1.0520\right)}$$

Note that the term labeled H in Tables 8.3, 8.4, and 8.5 is equal to C in Eq. (8.58).

TABLE 8.3 Second-Order Elliptic Function Parameters[a]

$$H(s) = \frac{H(s^2 + a_0)}{s^2 + b_1 s + b_0}$$

	A_1						
ω_s	**0.7**	**0.75**	**0.8**	**0.85**	**0.9**	**0.95**	**0.99**
2.0	0.597566	0.672335	0.761953	0.87093	1.09079	1.28475	1.70530
	0.748566	0.807532	0.889100	1.01055	1.21614	1.67671	3.39116
	7.46410	7.46393	7.46393	7.46393	7.46410	7.46394	7.46437
	0.070208	0.081143	0.095295	0.115081	0.146639	0.213409	0.449766
1.8	0.586497	0.658788	0.744765	0.852101	0.996903	1.22172	1.49664
	0.761473	0.821030	0.903240	1.02526	1.23061	1.68388	3.25137
	5.93375	5.93375	5.933773	5.93377	5.93399	5.93377	5.93385
	0.089828	0.121755	0.146865	0.146865	0.186645	0.269588	0.542449
1.6	0.568640	0.636848	0.716947	0.814969	0.942467	1.12264	1.21673
	0.780727	0.840896	0.923621	1.04564	1.24863	1.68414	3.01139
	4.55831	4.55832	4.55842	4.55832	4.55832	4.55832	4.55836
	0.119892	0.138356	0.162086	0.194981	0.246530	0.350990	0.654022
1.4	0.535956	0.596787	0.666375	0.747996	0.845981	0.956021	0.859430
	0.811695	0.872098	0.954382	1.07401	1.26798	1.65069	2.61881
	3.33173	3.33166	3.33173	3.33167	3.33172	3.33167	3.33171
	0.170533	0.196320	0.229155	0.274010	0.342509	0.473248	0.778164
1.3	0.507505	0.562111	0.622959	0.691325	0.766598	0.829058	0.658076
	0.835122	0.894952	0.975687	1.09135	1.27415	1.62319	2.34888
	2.76980	2.76979	2.76981	2.76979	2.76982	2.76890	2.76972
	0.211054	0.242333	0.281803	0.334915	0.414008	0.556729	0.839569
1.2	0.461178	0.506162	0.553873	0.603117	0.647985	0.656811	0.450447
	0.867973	0.925546	1.00200	1.10866	1.26987	1.55118	2.02342
	2.23597	2.23595	2.23597	2.23595	2.23591	2.23595	2.23595
	0.271698	0.310453	0.358503	0.421457	0.511141	0.659054	0.896281
1.1	0.372652	0.401509	0.428498	0.450238	0.457760	0.420582	0.244714
	0.916613	0.967014	1.03128	1.11609	1.23375	1.41020	1.63605
	1.71409	1.71408	1.71409	1.71405	1.71408	1.71409	1.71394
	0.374317	0.423125	0.481308	0.553478	0.647782	0.781571	0.945011
1.05	0.285907	0.302274	0.314810	0.320161	0.310931	0.266561	0.142026
	0.951232	0.991713	1.04130	1.10322	1.18267	1.28875	1.40382
	1.43865	1.43866	1.43866	1.43866	1.43867	1.43867	1.43868
	0.462837	0.516984	0.579033	0.651806	0.739845	0.850992	0.966006

From Sticht and Huelsman (1973). Copyright 1973. Pergamon Press Ltd.

[a] Coefficients in each group from top to bottom, are b_1, b_0, a_0, and $H(= A_2)$.

The available information, α_{max}, α_{min}, ω_s/ω_p always leads to the degree n and the relevant coefficients of $T(s)$. When designing a filter, we need only to "translate" the specifications into the quantities called for in the table at hand, and must be careful to make sure of the definitions used in the table. The result is a transfer function that can be realized by the same procedures we encountered earlier. Since we are interested in lowpass filters with finite transmission zeros, we require for the implementation second-order lowpass-notch sections that were discussed in Chapter 5. The realization of a fifth-order elliptic filter was presented in Example 5.17. An additional example will illustrate the process further.

TABLE 8.4 Third-Order Elliptic Function Parameters[a]

$$H(s) = \frac{H(s^2 + a_1)}{(s + p)(s^2 + b_{11}s + b_{10})}$$

	ω_s						
A_1	**1.05**	**1.10**	**1.15**	**1.20**	**1.30**	**1.40**	**1.60**
0.99	3.00155	2.38167	2.04962	1.84049	1.59035	1.44703	1.29096
	0.085439	0.164793	0.239930	0.308389	0.423881	0.514156	0.641363
	1.17110	1.27550	1.35412	1.41484	1.50033	1.55605	1.62210
	1.20541	1.37031	1.53363	1.69962	2.04551	2.41363	3.22359
	2.91611	2.21688	1.80968	1.53210	1.16647	0.932875	0.649595
	0.835656	0.702859	0.585336	0.488077	0.346305	0.254634	0.150824
0.95	1.39312	1.16920	1.05328	0.978047	0.887854	0.834076	0.773178
	0.128759	0.208146	0.267535	0.313860	0.382084	0.429629	0.491552
	1.09401	1.126378	1.14386	1.15422	1.16538	1.17039	1.17419
	1.20541	1.37031	1.53359	1.69962	2.04548	2.41363	3.22359
	1.26436	0.961054	0.784827	0.664187	0.505756	0.404446	0.281626
	0.550613	0.393746	0.298822	0.235598	0.158103	0.113422	0.066000
0.90	0.989843	0.850207	0.776613	0.729373	0.671004	0.635840	0.595349
	0.131719	0.197936	0.243978	0.278588	0.327809	0.361387	0.414241
	1.04501	1.05130	1.05182	1.05044	1.04612	1.04183	1.03480
	1.20541	1.37031	1.53360	1.69962	2.04550	2.41363	3.22359
	0.858124	0.652271	0.532635	0.450785	0.343166	0.274453	0.191108
	0.408593	0.279160	0.207846	0.162349	0.108001	0.077236	0.044840
0.85	0.796463	0.692067	0.636652	0.600774	0.556216	0.529099	0.497668
	0.125887	0.182370	0.220415	0.248520	0.287999	0.314599	0.348306
	1.01490	1.00922	1.00267	0.966551	0.986391	0.978507	0.967482
	1.20541	1.37031	1.53361	1.69962	2.04549	2.41362	3.22359
	0.670582	0.509696	0.416235	0.352254	0.268216	0.214500	0.149361
	0.330211	0.221527	0.163808	0.127519	0.084606	0.060434	0.035059
0.80	0.672056	0.588202	0.543408	0.514269	0.477902	0.455659	0.429765
	0.117935	0.167009	0.199450	0.223182	0.256259	0.278406	0.306340
	0.993886	0.981243	0.970727	0.962023	0.948671	0.938912	0.925798
	1.20541	1.37031	1.53361	1.69962	2.04549	2.41362	3.22359
	0.554123	0.421193	0.343958	0.291087	0.221642	0.177253	0.123426
	0.277706	0.184503	0.135945	0.105649	0.069994	0.049969	0.028976
0.75	0.580701	0.510790	0.473303	0.448768	0.418123	0.399259	0.377272
	0.109462	0.152592	0.180768	0.201218	0.229618	0.248517	0.272306
	0.978189	0.960951	0.947897	0.937548	0.922206	0.011278	0.896878
	1.20541	1.37031	1.53361	1.69962	2.04549	2.41362	3.22359
	0.471237	0.358197	0.292535	0.247550	0.188505	0.150742	0.104965
	0.238762	0.157652	0.115915	0.089987	0.059570	0.042510	0.024646
0.70	0.508377	0.448812	0.416747	0.395725	0.369369	0.353124	0.334131
	0.100986	0.139154	0.163859	0.181717	0.206412	0.222806	0.243387
	0.965965	0.945461	0.930629	0.919159	0.902442	0.089734	0.875469
	1.20541	1.37033	1.53361	1.69962	2.04549	2.41362	3.22360
	0.407390	0.309657	0.252888	0.214008	0.162958	0.130318	0.090743
	0.207883	0.136715	0.100376	0.077873	0.051520	0.036758	0.021308

From Sticht and Huelsman (1973). Copyright 1973. Pergamon Press Ltd.

[a] Coefficients in each group from top to bottom, are p, b_{11}, b_{10}, a_1, H, and A_2.

TABLE 8.5 Fourth-Order Elliptic Function Parameters[a]

$$H(s) = \frac{H(s^2 + a_1)(s^2 + a_2)}{(s^2 + b_{11}s + b_{10})(s^2 + b_{21}s + b_{20})}$$

	ω_s						
A_1	**1.05**	**1.075**	**1.1**	**1.15**	**1.20**	**1.25**	**1.30**
0.99	1.24184	1.36998	1.43445	1.48461	1.49416	1.48916	1.48067
	1.76639	1.64271	1.52732	1.35343	1.23106	1.14128	1.07349
	1.15362	1.22234	1.29092	1.42978	1.57242	1.71971	1.87203
	0.073511	0.104589	0.132384	0.179552	0.218090	0.250180	0.277321
	1.09961	1.12737	1.14901	1.18196	1.20610	1.22469	1.23958
	3.31266	3.84083	4.34993	5.29789	6.22434	7.15325	8.09589
	0.503140	0.389504	0.306376	0.209067	0.150187	0.112478	0.086921
0.97	1.11694	1.15719	1.17084	1.17132	1.16143	1.14961	1.13807
	1.17034	1.05721	0.974214	0.860463	0.785950	0.733037	0.693369
	1.15363	1.22235	1.29093	1.42979	1.57244	1.71971	1.87203
	0.082382	0.109829	0.132841	0.169869	0.198774	0.222152	0.241517
	1.06041	1.07297	1.08228	1.09550	1.10463	1.11140	1.11664
	3.31252	3.85097	4.34995	5.29782	6.22442	7.15325	8.09588
	0.315149	0.233744	0.182127	0.120698	0.086036	0.064240	0.049553
0.95	1.00616	1.02456	1.02740	1.01897	1.00707	0.994981	0.983063
	0.949099	0.853237	0.785841	0.695368	0.637238	0.595833	0.563827
	1.15362	1.22235	1.29090	1.42980	1.57240	1.71971	1.87203
	0.081657	0.106240	0.126428	0.158254	0.182889	0.202523	0.218409
	1.04043	1.04722	1.05200	1.05833	1.06243	1.06526	0.06699
	3.31238	3.85097	4.34973	5.29772	6.22421	7.15328	8.09613
	0.245492	0.180326	0.139862	0.092248	0.065716	0.049015	0.037702
0.925	0.903747	0.911065	0.909212	0.897844	0.885261	0.873655	0.863732
	0.800608	0.718662	0.662419	0.587723	0.539585	0.505447	0.480059
	1.15363	1.22235	1.29093	1.42979	1.57243	1.71971	1.87204
	0.078638	0.100616	0.118456	0.146316	0.167498	0.184309	0.198090
	1.02465	1.02747	1.02921	1.03102	1.03182	1.03207	1.03216
	3.31249	3.85095	4.34992	5.29794	6.22440	7.15331	8.09589
	0.198567	0.145089	0.112302	0.073994	0.052617	0.039221	0.030239
0.9	0.825168	0.827693	0.822969	0.811096	0.799091	0.788335	0.779239
	0.709059	0.636774	0.587138	0.521773	0.479903	0.450211	0.428090
	1.15363	1.22235	1.29041	1.42981	1.57240	1.71971	1.87203
	0.075144	0.095172	0.111155	0.136283	0.155159	0.170095	0.182294
	1.01374	1.01413	1.01394	1.01299	1.01180	1.01058	1.00947
	3.31240	3.85096	4.34581	5.29794	6.22422	7.15326	8.09589
	0.169268	0.123463	0.095443	0.062763	0.044651	0.033285	0.025661
0.85	0.708408	0.706199	0.700475	0.688058	0.676966	0.667721	0.659911
	0.598882	0.537875	0.496416	0.442241	0.407509	0.383057	0.364750
	1.15363	1.22235	1.29092	1.42978	1.57243	1.71971	1.87203
	0.068333	0.085454	0.099089	0.120059	0.135776	0.148163	0.158248
	0.999163	0.996486	0.993986	0.989660	0.986076	0.983077	0.980558
	3.31250	3.85096	4.34987	5.29786	6.22434	7.15335	8.09589
	0.133093	0.096781	0.074682	0.049106	0.034894	0.026019	0.020059
0.8	0.621079	0.617140	0.611017	0.599431	0.589557	0.581212	0.574306
	0.532447	0.478486	0.442216	0.394408	0.363967	0.342428	0.326332
	1.15363	1.22235	1.29041	1.42982	1.57240	1.71971	1.87204
	0.062131	0.077101	0.088880	0.107103	0.120623	0.131234	0.139842
	0.989514	0.984974	0.981121	0.974761	0.969765	0.965686	0.962302

Continued

TABLE 8.5 Continued

	ω_s						
A_1	**1.05**	**1.075**	**1.1**	**1.15**	**1.20**	**1.25**	**1.30**
	3.31250	3.85096	4.34613	5.29772	6.22423	7.15327	8.09589
	0.110293	0.080095	0.061824	0.040580	0.028851	0.021504	0.016576
0.75	0.550687	0.546069	0.540306	0.529453	0.520419	0.513005	0.506861
	0.487251	0.438112	0.405011	0.361820	0.334160	0.314640	0.300027
	1.15363	1.22235	1.29093	1.42979	1.57243	1.71971	1.87204
	0.056514	0.069762	0.080214	0.096136	0.107970	0.117237	0.124738
	0.982530	0.976711	0.971880	0.964177	0.958218	0.953427	0.949476
	3.31251	3.85096	4.34992	5.29791	6.22439	7.15327	8.09589
	0.093955	0.068176	0.052571	0.034540	0.024536	0.018289	0.014096
0.7	0.491207	0.486393	0.480919	0.470946	0.462799	0.456159	0.450655
	0.454281	0.408647	0.377979	0.337967	0.312352	0.294272	0.280747
	1.15363	1.22235	1.29092	1.42979	1.57244	1.71972	1.87203
	0.051378	0.063179	0.072459	0.086558	0.097012	0.105183	0.111795
	0.977203	0.970443	0.964919	0.956218	0.949563	0.944251	0.939898
	3.31247	3.85102	4.34989	5.29795	6.22448	7.15335	8.09607
	0.081317	0.058963	0.045465	0.029861	0.21211	0.015810	0.012188

From Sticht and Huelsman (1973). Copyright 1973, Pergamon Press Ltd.

[a] Coefficients in each group from top to bottom, are $b_{11}, b_{10}, a_1, b_{21}, b_{20}, a_2$, and $H(= A_2)$.

EXAMPLE 8.4

Design a circuit to realize the filter of Example 5.3. The cut-off frequency is 2.4 kHz. Use the GIC biquad of Fig. 5.16.

Solution

The function realized by the GIC biquad was given in Eq. (5.34), with all parameters identified in Fig. 5.16. We set $b = c/2$ to realize the notch; the resulting function to realize the two modules is

$$T_i(s) = \frac{s^2(2a - c) + c\omega_0^2}{s^2 + s\omega_0/Q + \omega_0^2}$$

where $\omega_0 = 1/(RC)$. We factor the fourth-order transfer function of Example 8.3 into

$$T(s) = T_1 T_2 = \frac{0.5934\left(s^2 + 1.2909\right)}{s^2 + 1.0274s + 0.7858} \frac{0.2358\left(s^2 + 4.3497\right)}{s^2 + 0.1264s + 1.0520}$$

$$= \frac{0.5934s^2 + 0.7660}{s^2 + 1.0274s + 0.7858} \frac{0.2358s^2 + 1.0257}{s^2 + 0.1264s + 1.0520}$$

with $Q_1 = 0.863$ and $Q_2 = 8.115$. The gain constant is divided such that both sections have equal maxima of 0 dB and are at -0.225 dB at the origin. Also we choose $C = 10$ nF for the capacitors in both modules.

For T_1 we obtain $c = 0.766/0.7858 = 0.975$, $b = 0.488$, and $a = 0.5\,(c + 0.5934) = 0.784$. Further,

$$R = \frac{1}{2\pi\sqrt{0.7858} \times 24000 \times 10^{-9}}\text{k}\Omega = 7.48\ \text{k}\Omega \quad \text{and} \quad Q_1 R = 6.456\ \text{k}\Omega$$

In the same way, for T_2 we have $c = 1.0257/1.052 = 0.975$, $b = 0.488$, $a = 0.5\,(c + 0.2358) = 0.605$, and

$$R = \frac{1}{2\pi\sqrt{1.0520} \times 24000 \times 10^{-9}}\text{k}\Omega = 6.464\text{k}\Omega \quad \text{and} \quad Q_2 R = 52.47\text{k}\Omega$$

The circuit and test performance are given in Fig. 8.17. The design realizes the expected ripple of 0.45 dB and has a flat loss of approximately 0.17 dB; the passband corner is at 2.35 kHz and the −17-dB stopband starts at 2.62 kHz (a factor 1.11 above the passband corner). The gain rises above −17 dB in the stopband for frequencies above about 120 kHz. It is caused by the nonideal opamps and can be explained by finite ω_t effects, as in Example 5.9. Different biquad modules must be used if this reduced high-frequency attenuation gives rise to problems in the system using the filter.

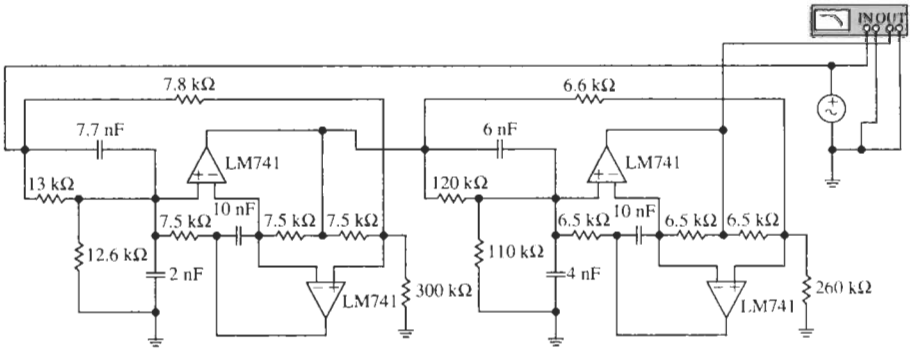

(a)

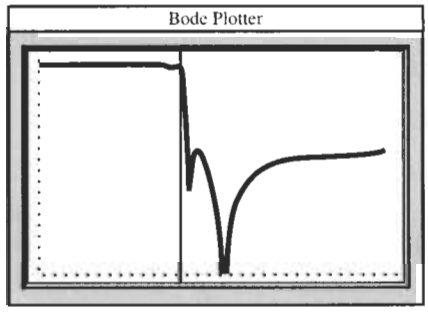

(b)

Figure 8.17 Circuit and test performance for Example 8.4. (Bode Plotter scales: 200 Hz to 100 kHz; −40 to 0 dB; cursor at 2.344 kHz, −0.634 dB.)

8.6 COMPARISON OF THE CLASSICAL FILTER RESPONSES

When developing a lowpass filter, the designer needs to have comparative information about which of the various design possibilities is best for the application. Therefore, we next address the following question: how do the Cauer and inverse Chebyshev responses compare with those found previously for the lowpass filter in Chapters 6 and 7? The quantities we will compare are (1) the degree, (2) the passband response, (3) the stopband response, (4) the transition from passband to stopband, (5) the values of Q required, (6) the time delay, and (7) circuits for the realization of the responses. To be able to be concrete, we shall make the comparisons using a specific case, the specifications of Example 8.1 and the maximally flat, Chebyshev, inverse Chebyshev, and Cauer or elliptic responses that meet these requirements.

We need to decide, first, how to bring the functions into a form that makes sensible comparisons possible. We must make sure that the comparison is based on functions that meet the same requirements. Thus, we specify that each response satisfies the conditions

$$0 < \alpha \leq \alpha_{\max} \quad \text{in } 0 \leq \omega \leq \omega_p \quad \text{and} \quad \alpha_{\min} < \alpha \quad \text{in } \omega_s \leq \omega < \infty \tag{8.63}$$

We shall do this by scaling the frequency such that all responses have $\omega_p = 1$ as the passband corner frequency. This choice is not unique; we could have chosen, for example, to let all responses have the same half-power frequency, but as the -3-dB point is normally in the transition band, it is either not known to the designer without further computations or may even be of little interest. A further problem that makes comparisons problematic is that different types of responses satisfying the conditions of Eq. (8.63) will have different degrees. We know that to satisfy a given set of requirements yields the lowest order in an elliptic filter, Chebyshev and inverse Chebyshev responses have the same degree but are of higher order, and maximally flat response functions are least efficient and need to be of higher order yet. Nevertheless, let us assemble the necessary equations and consider how the responses satisfying the requirements in Example 8.1,

$$\begin{aligned} 0 < \alpha \leq \alpha_{\max} = 0.25 \text{ dB} \quad &\text{in} \quad \omega \leq \omega_p = 100\text{krad/s} \\ \alpha_{\min} = 18 \text{ dB} < \alpha \quad &\text{in} \quad \omega_s = 140\text{krad/s} \leq \omega < \infty \end{aligned} \tag{8.64}$$

would compare.

Let us start by determining the required degrees. The degree of the maximally flat response was given in Eq. (6.44) as

$$n_{MF} = \frac{\log[(10^{0.1\alpha_{min}} - 1)/(10^{0.1\alpha_{max}} - 1)]}{2\log(\omega_s/\omega_p)} \tag{8.65}$$

where the frequency axis is usually normalized such that $\omega_p = 1$. If $\alpha_{max} = 3$ dB, $n_{MF} = n_B$, the degree of the Butterworth response. For the given specifications we obtain $n_{MF} = 10.33$, so that we need to work with $n_{MF} = 11$. The degree of the Chebyshev response was given in Eq. (7.20),

$$n_{Ch} = \frac{\cosh^{-1}[(10^{0.1\alpha_{min}} - 1)/(10^{0.1\alpha_{max}} - 1)]}{\cosh^{-1}(\omega_s/\omega_p)}$$

$$\approx \frac{\ln \sqrt{4\left(10^{0.1\alpha_{\min}}-1\right)/\left(10^{0.1\alpha_{\max}}-1\right)}}{\ln\left(\omega_s/\omega_p+\sqrt{\left(\omega_s/\omega_p\right)^2-1}\right)} \tag{8.66}$$

Again, ω may be normalized such that $\omega_p = 1$. We found that the degree of the inverse Chebyshev filter is the same as that of the Chebyshev filter, but now the frequency is normalized such that $\omega_s = 1$. From Example 8.1, the required degree is $n_{Ch} = 5$. There is no easy closed-form expression for the degree n_E of the elliptic filter; we shall rely on Fig. 8.16 to find n_E. For the requirements of Example 8.4, $n_E = 4$.

The maximally flat and the Chebyshev transfer function magnitudes were found in Eqs. (6.14a) and (7.8) to equal

$$|T_{MF}(j\omega)|^2 = \frac{1}{1+\varepsilon^2\omega^{2n}} \quad \text{and} \quad |T_C(j\omega)|^2 = \frac{1}{1+\varepsilon^2 C_n^2(\omega)} \tag{8.67}$$

where $C_n(\omega) = \cos\left(n\cos^{-1}\omega\right)$ in the passband ($\omega \le 1$) and $C_n(\omega) = \cosh\left(n\cosh^{-1}\omega\right)$ in the stopband and transition band ($\omega > 1$). For both cases, as well as for the elliptic function, ε is given by the maximum acceptable passband attenuation,

$$\varepsilon = \sqrt{10^{0.1\alpha_{\max}}-1} \tag{8.68}$$

according to Eqs. (6.40), (7.17), and (8.41). In our case we find $\varepsilon^2 = 0.2434^2 = 0.05925$. For the inverse Chebyshev filter, by Eq. (8.8) the transfer function magnitude is

$$|T_{IC}(j\omega)|^2 = \frac{1}{1+\dfrac{1}{\varepsilon^2 C_n^2(1/\omega)}} \tag{8.69}$$

where, however, from Eq. (8.7) ε is now given by the smallest acceptable stopband attenuation:

$$\varepsilon = 1/\sqrt{10^{0.1\alpha_{\min}}-1} \tag{8.70}$$

For our case we have $\varepsilon^2 = 0.1269^2 = 0.01610$.

We intend to compare the attenuation for the three cases; from Eqs. (6.41) with (8.70) we obtain

$$\alpha_{MF} = 10\log\left[1+\left(10^{0.1\alpha_{\max}}-1\right)\omega^{2n}\right] \tag{8.71}$$

$$\alpha_C = 10\log\left[1+\left(10^{0.1\alpha_{\max}}-1\right)C_n^2(\omega)\right] \tag{8.72}$$

which for our numbers become

$$\alpha_{MF} = 10\log[1+0.05925\omega^{22}] \tag{8.73}$$

and

$$\alpha_C = 10\log[1+0.05925\cos^2\left(5\cos^{-1}\omega\right)] \tag{8.74}$$

In addition we have from Eqs. (8.69) and (8.70) the attenuation of the inverse Chebyshev filter

$$\alpha_{IC} = 10 \log \left[1 + \frac{1}{\left(10^{0.1\alpha_{min}} - 1\right)^{-1} C_n^2 (1/\omega)} \right] \tag{8.75}$$

where we must remember that $\omega = 1$ is the *stop*band corner. To be able to plot all attenuation functions versus one ω-axis where the passband corner is at 1 as in the maximally flat and the Chebyshev cases, we need to determine the 0.25-dB passband corner in the inverse Chebyshev case and rescale the frequency axis. From Eq. (8.75) we find

$$\alpha_{IC} = 0.25 = 10 \log \left\{ 1 + \frac{1}{0.01610 \cosh^2 \left[(5 \cosh^{-1} (1/\omega_p) \right]} \right\}$$

which we solve[2] for $1/\omega_p$:

$$\frac{1}{\omega_p} = \cosh \left[\frac{1}{5} \cosh^{-1} \frac{1}{0.1269\sqrt{10^{0.025} - 1}} \right] = 0.7308$$

This value should be used to scale the ω-axis for the inverse Chebyshev filter so that ω_p becomes 1. If we do this in Eq. (8.75), we obtain

$$\alpha_{IC} = 10 \log \left\{ 1 + \frac{1}{0.01610 \cosh^2 [5 \cosh^{-1} (1.3585/\omega)]} \right\} \tag{8.76}$$

Equations (8.73), (8.74), and (8.76) are the expressions, along with the attenuation of a fourth-order Cauer filter meeting the requirements of Eq. (8.64), on which we can base the comparison. The corresponding curves are plotted in Fig. 8.18.

Figure 8.18a shows the attenuation in $0 \leq \omega \leq 2.5$ and Fig. 8.18b shows the passband response in $0 \leq \omega \leq 1$. We notice that all four curves satisfy the requirements of Eq. (8.64). A discussion follows.

8.6.1 Degree

As predicted, the elliptic (Cauer) filter needs the lowest order to meet the specifications. Even for these relatively simple requirements, the maximally flat function has more than twice the degree of the Chebyshev response and 2.5 times that of a Cauer filter. Note that by design all functions meet the passband requirements exactly; the main difference is found in the stopband approximation. To make the difference in efficiency between Chebyshev and maximally flat approximations more apparent we have plotted in Fig. 8.19 curves for Eqs. (8.57b) and (8.57c) on the same coordinates as in Fig. 8.16. Notice how rapidly the degree of the maximally flat functions increases as the transition band becomes narrower. This figure can be used to find the degree for maximally flat (Butterworth) and equal-ripple (Chebyshev and inverse Chebyshev) filters in the same manner as Fig. 8.16 for elliptic (Cauer) filters.

[2] This value $1/\omega_p$ is a little less than $1/1.4$ because we had to pick an integer degree, $n = 5$, instead of ω the theoretical smaller value of 4.81.

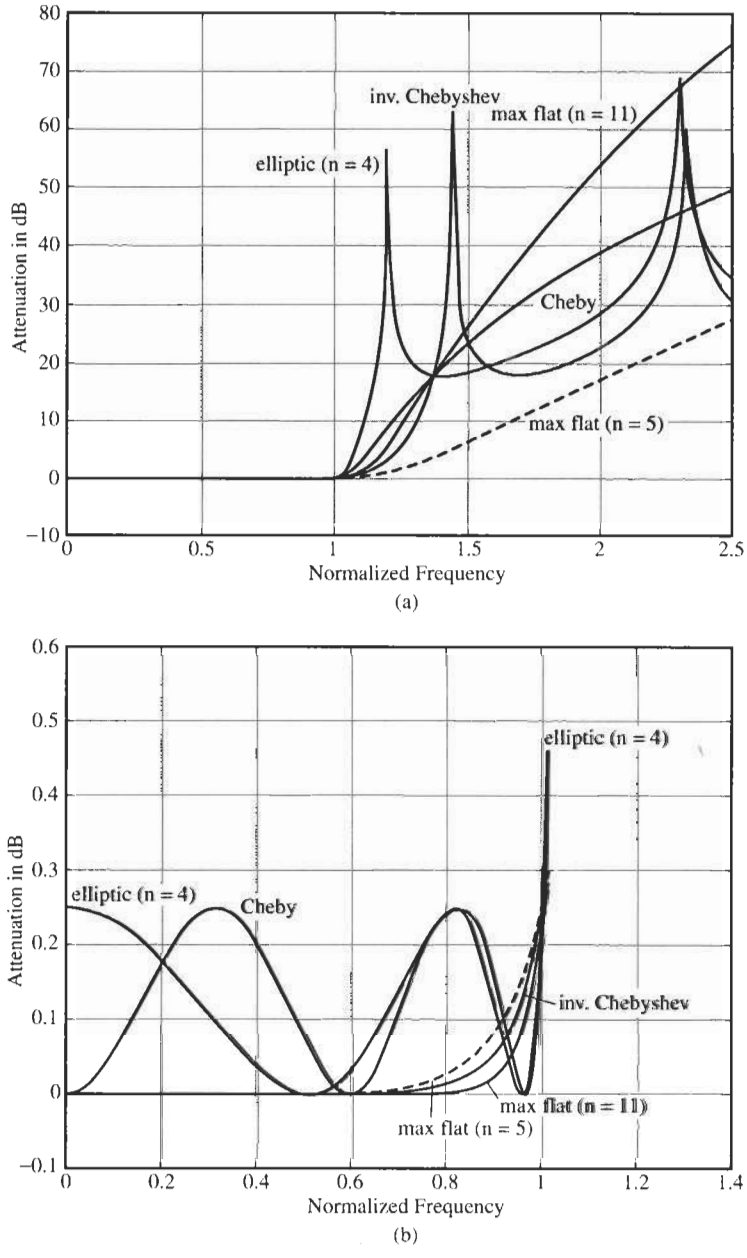

Figure 8.18 (a) Response curves comparing maximally flat ($n = 11$ and $n = 5$), Chebyshev ($n = 5$), inverse Chebyshev ($n = 5$), and Cauer ($n = 4$) responses to meet the same attenuation specifications; (b) passband response.

8.6.2 Passband Response

As Fig. 8.18b demonstrates, the inverse Chebyshev, the eleventh-order maximally flat, and even the fifth-order maximally flat responses are better than the Chebyshev and Cauer responses

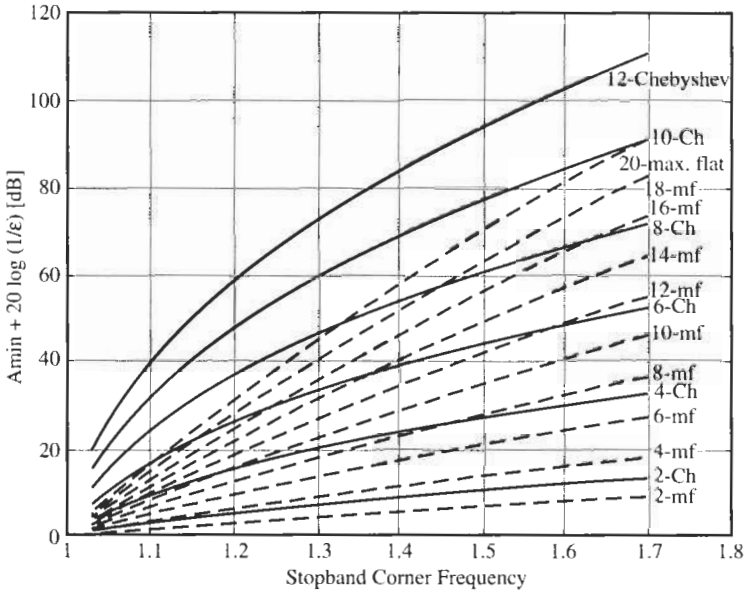

Figure 8.19 Design curves to find the degree of maximally flat and equal-ripple approximations as functions of passband ripple width α_{max}, stopband attenuation α_{min}, and stopband corner frequency ω_s. The passband corner is normalized to $\omega_p = 1$. The ordinate is labeled in $\alpha_{min} + 20 \log (1/\varepsilon)$ [dB], the abscissa is ω_s. Curves for Chebyshev filters of orders $2, 4, \ldots, 12$, and for maximally flat filters of orders $2, 4, 6, \ldots, 20$ are shown.

over the whole passband; they offer substantially lower attenuation everywhere, except at ω close to 1. Not surprisingly, the eleventh-order maximally flat function has the best passband performance, at the severe cost of more than twice the order, but the inverse Chebyshev filter is a close second, without incurring any additional expenses in degree. Observe that the fifth-order inverse Chebyshev response is "flatter" than the fifth-order maximally flat one. It is an often-claimed advantage of inverse Chebyshev approximations that they have a "flatter" passband than maximally flat approximations *of equal degree*; however, we must remember that the latter functions do not meet the stopband requirements so that the comparison is generally not meaningful. If the specified attenuation requirements could be met with the low-order maximally flat function, they would, of course, also be met by an inverse Chebyshev function of even lower order!

8.6.3 Stopband Response

The all-pole maximally flat and Chebyshev responses have higher attenuation than the inverse Chebyshev and Cauer responses at higher values of frequency. This is normally not significant if α_{min} is the minimum attenuation required over the entire stopband. Note, though, that we are comparing the performance of a eleventh-order maximally flat filter with fifth-order Chebyshev and inverse Chebyshev filters because we insisted that all functions meet the same attenuation specifications. The eleventh-order maximally flat response has a superior stopband performance, again at the high cost of doubling the degree. For comparison purposes we have also drawn (dotted) the fifth-order maximally flat response in Fig. 8.18a. Although per

design it meets the passband specifications exactly, as expected, it misses the required stopband performance by a wide margin—although even this function exceeds the inverse Chebyshev and elliptic attenuations when the frequency is large enough (larger than $\omega \approx 2.1$ in the example). Also by design, the fourth-order elliptic filter function meets the stopband exactly.

8.6.4 Transition Band

As seen from Fig. 8.18a, among the functions compared the fourth-order Cauer filter has by far the narrowest transition band: it reaches the prescribed stopband attenuation already at $\omega_s \approx 1.15$ rather than at the required value $\omega_s \approx 1.4$.[3] Narrow transition bands are a particular strong point of elliptic approximations. It would take a maximally flat function of order 25 and a Chebyshev filter of order 8 to achieve the same narrow transition band.

Among the remaining functions, the Chebyshev response rises the fastest initially and then slows down, the opposite behavior of the inverse Chebyshev response, but per design, all functions reach the prescribed point (18 dB, 140 krad/s) simultaneously. In the transition band, the eleventh-order maximally flat response lies between the Chebyshev and inverse Chebyshev responses.

8.6.5 The Q Values Required

As shown in Eq. (8.32), the Q values of the inverse Chebyshev response are the same as those of the Chebyshev response, but this is correct only *for the same value of* ε. Typically, an inverse Chebyshev filter has lower Q values than a Chebyshev filter meeting the same attenuation specifications α_{max} and α_{min}. To see this, we return to the expression for the Chebyshev quality factors, Eq. (7.45),

$$Q = \frac{1}{2}\sqrt{1 + \frac{1}{\tanh^2 a \, \tan^2 \theta_k}} \tag{8.77}$$

where θ_k are fixed angles defined in Eq. (6.27) and a was given in Eq. (7.36),

$$a = \frac{1}{n} \sinh^{-1} \frac{1}{\varepsilon} \tag{8.78}$$

Note that a decreases with increasing ε. The important point is that Q is a function of ε. To be able to distinguish between the two cases, let us assign subscripts: IC for the inverse Chebyshev case and C for Chebyshev. Thus we have from Eq. (8.68),

$$\varepsilon_C = \sqrt{10^{0.1\alpha_{max}} - 1} \quad \text{to lead to } Q_C \tag{8.79}$$

and from Eq. (8.70),

$$\varepsilon_{IC} = \frac{1}{\sqrt{10^{0.1\alpha_{min}} - 1}} \quad \text{to lead to } Q_{IC} \tag{8.80}$$

[3] The approximating power of the Cauer filter is even stronger than this example indicates: the elliptic filter would require a degree of only 3.5, which we rounded up to 4.

Consider now the ratio $\varepsilon_C/\varepsilon_{IC}$. We intend to show that this ratio is usually (but not always) larger than 1. We obtain

$$\left(\frac{\varepsilon_C}{\varepsilon_{IC}}\right)^2 = \left(10^{0.1\alpha_{max}} - 1\right)\left(10^{0.1\alpha_{min}} - 1\right) = 10^{0.1\alpha_{max}}\,10^{0.1\alpha_{min}} - 10^{0.1\alpha_{min}} - 10^{0.1\alpha_{max}} + 1$$

which we rewrite as

$$\left(\frac{\varepsilon_C}{\varepsilon_{IC}}\right)^2 - 1 = 10^{0.1\alpha_{max}}\left(10^{0.1\alpha_{min}} - 1\right) - 10^{0.1\alpha_{min}} \tag{8.81}$$

For typical, even modest, attenuation requirements, such as for instance $\alpha_{min} = 25$ dB and $\alpha_{max} = 0.2$ dB, the right-hand side of Eq. (8.81) is positive, which means $\varepsilon_C > \varepsilon_{IC}$. It follows from Eq. (8.78) that $a_C < a_{IC}$. Let us return to Eq. (8.77), which we write as

$$4Q^2 - 1 = \frac{1}{\tanh^2 a\ \tan^2 \theta_k}$$

$\tan^2 \theta_k$ is the same for both Chebyshev and inverse Chebyshev responses because the angles θ_k are independent of ε and the poles of the two filters are obtained by reciprocation as we saw earlier in Fig. 8.6a. Thus, we obtain

$$\frac{4Q_C^2 - 1}{4Q_{IC}^2 - 1} = \frac{\tanh^2 a_{IC}}{\tanh^2 a_C} > 1 \tag{8.82}$$

As $\tanh a$ is a monotonically increasing function of a and $a_C < a_{IC}$, the right-hand side of Eq. (8.82) is larger than 1 and hence $Q_C > Q_{IC}$, meaning that Chebyshev filters have normally higher Q values than inverse Chebyshev filters.

As an example consider the modest design requirement with the specifications of Example 8.1, i.e., $\alpha_{min} = 18$ dB, $\alpha_{max} = 0.25$ dB, and $n = 5$. This gives $\varepsilon_C = 0.2434$, $\varepsilon_{IC} = 0.1269$ and, from Eq. (8.78), $a_C = 0.4241$ and $a_{IC} = 0.5523$. With these numbers we find from Eq. (8.82)

$$Q_C^2 = 1.5736 Q_{IC}^2 - 0.1434$$

The circuit was realized as a fifth-order inverse Chebyshev filter with quality factors in the table below. Had we realized the specifications with a Chebyshev filter, also of fifth order, the quality factors would have been larger as predicted by Eq. (8.82); they are also shown in the table and can be verified by direct computation using the results of Chapter 7.

Inverse Chebyshev Q_{IC} ($n = 5$)	3.10	0.88	0.5
Chebyshev Q_C ($n = 5$)	3.87	1.04	0.5

Note that the quality factor of a negative real pole equals 0.5 and does not change. Although the example demonstrates that Q_C is larger than Q_{IC} for the same specifications, in this case the increase is only moderate because of the modest requirements. For filters with more demanding

specifications, the increase in Q can be substantial; for instance, for $\alpha_{max} = 0.1$ dB in the passband ($\omega \leq 1$) and $\alpha_{min} = 70$ dB in the stopband at $\omega \geq 1.9$, we find from Eq. (8.66) $n = 9$ and from Eq. (8.82)

$$Q_C^2 = 7.2256 Q_{IC}^2 - 1.5569$$

This equation indicates an increase by approximately a factor 2.7. For example, a realization with an inverse Chebyshev filter with a $Q_{IC} = 9.5$ would need a Chebyshev filter with $Q_C = 25.5$.

This result, $Q_C > Q_{IC}$, is among the main reasons why inverse Chebyshev filters are well liked by designers, because

1. lower values of Q are easier to implement and the realization is less sensitive to component tolerances, and
2. as we shall discuss below and in Chapter 10, filters with lower Q values have better delay performance.

For completeness, we also list in the table below the Q values of the remaining two designs although comparisons are not meaningful because the functions have different degrees.

Elliptic Q_E ($n = 4$)	6.17	0.76	—	—	—	—
Maximally flat Q_{MF} ($n = 11$)	3.51	1.20	0.87	0.52	0.59	0.5

The table serves only to point out that the elliptic response has the highest Q values and the largest Q values of the maximally flat and the inverse Chebyshev responses are comparable. We saw in Section 4.3, Fig. 4.13, that attenuation changes more rapidly with frequency as Q increases. This is consistent with our observations in the present comparison: the most rapid change of attenuation across the transition band occurs for the elliptic filter, which has the largest pole quality factor; next is the Chebyshev filter, followed by the inverse Chebyshev and the maximally flat responses. We may conclude that, in general, steep cut-off regions with narrow transition bands require functions with high Q poles. Alternatively, as the comparison with the Cauer and the maximally flat responses indicates, functions of high order are necessary for steep cut-off.

8.6.6 Time Delay

Filter delay will be discussed in detail in Chapter 10. Ideally, a response function ought to provide a delay that is constant, or nearly so, over the frequency range of interest, typically the passband. If the delay is more constant, signal components over a wide frequency band are delayed equally so that distortion is minimized. This is particularly important for the transmission of pulses in data communication networks.

Since delay is defined as the (negative) slope of the phase versus frequency, we can expect from the steep phase slope in Fig. 4.13b that responses with high Q values have a "poor" delay performance, which is a strong function of frequency. In this sense we find in the literature the statement that maximally flat response functions have the best delay, followed in order by the inverse Chebyshev, the Chebyshev, and the elliptic response. Figure 8.20 demonstrates the meaning of this statement. For the comparison we have plotted the

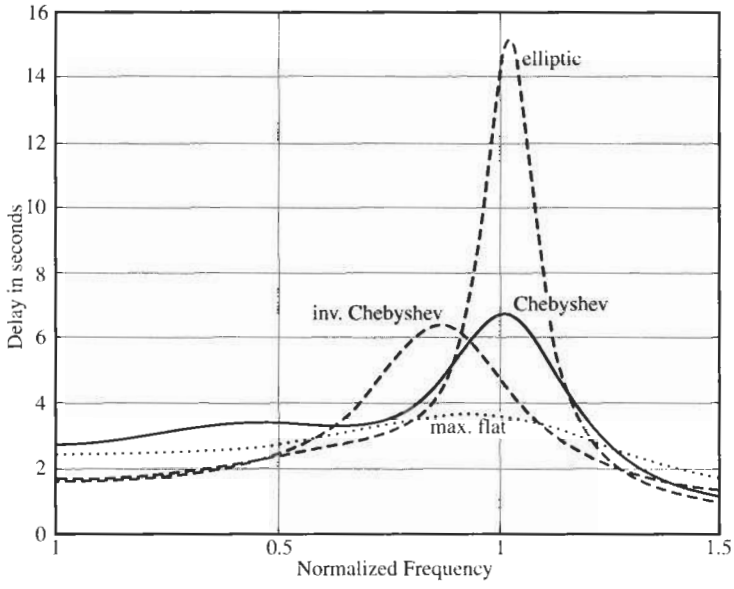

Figure 8.20 Delay performance of fourth-order Cauer, Chebyshev, inverse Chebyshev, and maximally flat responses. The common specification is $\alpha_{max} = 0.5$-dB passband attenuation.

delays of four fourth-order functions that all meet a 0.5-dB ripple passband requirement.[4] We observe that the "most constant" delay that varies least with frequency is provided by the maximally flat response, and the least constant by the elliptic function. Chebyshev and inverse Chebyshev responses are in between the two extremes, with the inverse Chebyshev function slightly better.

We must be aware, though, that any general statement, such as "maximally flat responses have the best delay, elliptic filters are worst, with (inverse) Chebyshev responses in the middle" is as a rule quite meaningless or at least misleading because it does not take into account any differences in degree. Recall that the functions were developed for the purpose of approximating a brick-wall lowpass *magnitude* with no attention being paid to the delay performance. Since the functions are very different in the degree necessary to satisfy a given attenuation specification, a comparison makes sense in practice only if all functions meet the prescribed magnitude requirements. With this practical restriction in mind we have plotted in Fig. 8.21a the delay performance of four filters whose degree is computed to satisfy the same attenuation requirements ($\alpha_{max} = 0.5$ dB, $\alpha_{min} = 24$ dB, $\omega_s = 1.25$). The necessary filter orders are $n_{max.flat} = 17$, $n_{Cheb} = n_{inv.Cheb} = 7$, and $n_{ellip} = 4$. We notice that the comparison now leads to different conclusions. The Chebyshev response has the least constant delay, the inverse Chebyshev response is noticeably better with both a lower peak delay and fewer ripples in the passband, and the maximally flat function is only slightly better than the inverse Chebyshev response. Surprisingly, the elliptic response in this

[4] Note that the functions are somewhat arbitrary because stopband and transition band requirements are not stated; thus only the maximally flat response is completely defined.

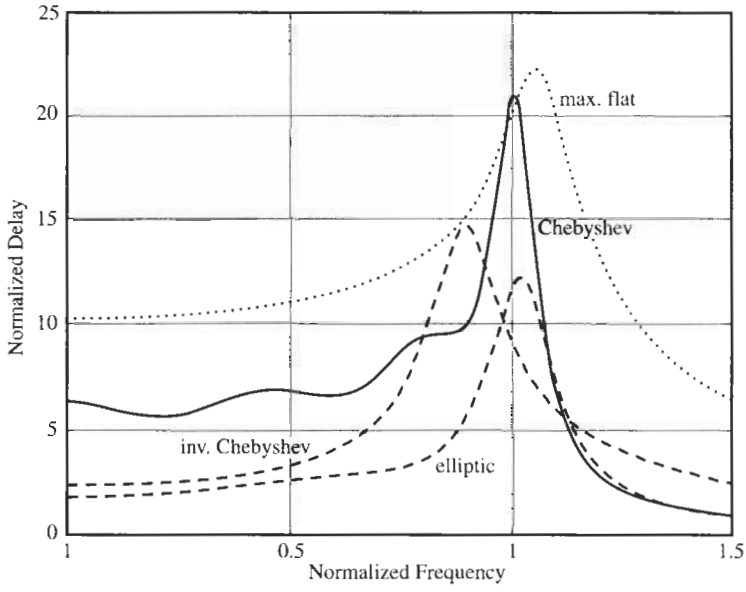

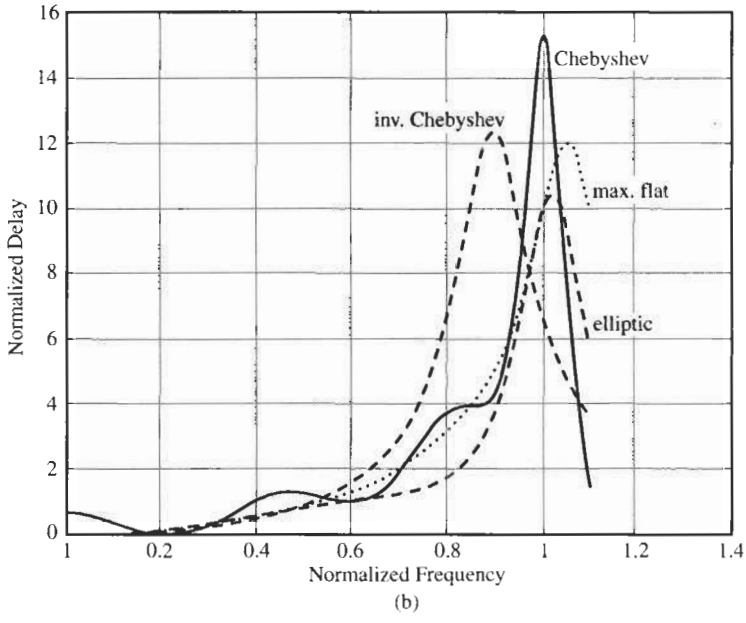

Figure 8.21 (a) Delay performance of fourth-order Cauer, seventh-order Chebyshev and inverse Chebyshev, and seventeenth-order maximally flat responses. All functions meet the same attenuation requirements $\alpha_{max} = 0.5$ dB, $\alpha_{min} = 24$ dB, $\omega_s = 1.25$; (b) curves scaled to the same minimum to simplify the comparison.

example shows the least variable delay performance. Because *absolute delay* is normally of less concern than *delay variation*, we have repeated the plot in Fig. 8.21b after subtracting from each delay curve its minimum so that the delay variation across the passband can be directly compared. The "flatter" delay performance of the inverse Chebyshev filter is a direct consequence of the lower Q values. Chebyshev responses are ordinarily much inferior due to their higher Qs. Although maximally flat (Butterworth) filters have even lower Qs, they suffer in the delay comparison because of the higher degree needed to satisfy the attenuation specifications. On the other hand, Cauer filters have larger Q values, which hurts their delay performance, but they gain in the comparison because of their substantially lower degree. Our example indicates that the delays of the various types of filter functions are indeed different, dictated by their unequal quality factors, but that the differences are not as large as might first be expected after the different degree requirements are taken into account.

8.6.7 Circuit Realization

For the realization, the difference between maximally flat, Chebyshev, inverse Chebyshev, and Cauer filters is that the latter two have finite transmission zeros, which makes the realization in principle somewhat more difficult. The difference in difficulty or cost per module is quite small, though. We have presented in Chapter 5 a number of one-, two-, three-, and four-amplifier circuit modules that can realize finite transmission zeros. The additional cost over the all-pole modules in Chapter 4 lies usually in two or three additional resistors or capacitors, a minimal expense. The extra design effort is negligible, particularly in view of numerous computer aids that are available. More important for the cost of any realization is the difference in filter order, which translates directly into the expense of components and the size of the final circuit. For instance for the requirements underlying Fig. 8.21, it would be unreasonable to attempt to build a seventeenth-order all-pole maximally flat filter at about four times the cost of a fourth-order Cauer filter.

Inverse Chebyshev filters have several practical advantages, among them low order, modest Q values, good delay performance, and minimal passband attenuation. Unless the transition band is very narrow and drives up the degree of the required function, these advantages, with almost no additional costs over Chebyshev designs, recommend their use over competing approaches. Designers are well advised to keep this filter type in mind for their applications.

REFERENCES

[1] W. Cauer, *Synthesis of Linear Communication Networks*. McGraw-Hill, New York, 1958, App. 3.

[2] E. Christian and E. Eisenmann, *Filter Design Tables and Graphs*. Transmission Networks International, Inc., Knightsbridge, NC, 1977.

[3] R. W. Daniels, *Approximation Methods for Electronic Filter Design*. McGraw-Hill, New York, 1974, Chap. 5.

[4] R. Saal, *Handbook of Filter Design*. AEG-Telefunken, Berlin, 1979.

[5] A. S. Sedra, and P. O. Brackett, *Filter Theory and Design: Active and Passive*. Matrix, Portland, OR, 1978.

[6] D. S. Sticht and L. P. Huelsman, "Direct Determination of Elliptic Network Functions," *Int. J. Comput. Elec. Eng.*, Vol. 1, pp. 272–280, 1973.

[7] A. L. Zverev, *Handbook of Filter Synthesis*. Wiley, New York, 1967.

PROBLEMS

8.1 For this problem, we wish to study an inverse Chebyshev lowpass filter characteristic that meets the following specifications: $\alpha_{max} = 0.25$ dB, $\alpha_{min} = 18$ dB, $\omega_p = 1000$ rad/s, $\omega_s = 1650$ rad/s. Verify the frequencies identified in Fig. P8.1 for infinite attenuation and satisfying α_{min}.

8.2 Design an inverse Chebyshev lowpass filter that satisfies the specifications given in Problem 8.1. Choose suitable first- and second-order sections and build the filter as a cascade circuit. Use LM741 opamps and test your design with Electronics Workbench (EWB).

8.3 Design an inverse Chebyshev lowpass filter that satisfies the specifications given in Problem 6.13.d.i. Build the filter as a cascade circuit with suitable first- and second-order sections. Choose appropriate opamps and test your design with EWB.

8.4 Design an inverse Chebyshev lowpass filter that satisfies the specifications given in Problem 6.13.d.ii. Build the filter as a cascade circuit with suitable first- and second-order sections. Choose appropriate opamps and test your design with EWB.

8.5 Table 7.2 lists the poles of Chebyshev filters for various degrees and specifications. From this table construct a table for the poles of the inverse Chebyshev filter of degrees $n = 3$ and $n = 4$ for $\alpha_{max} = 0.5$ dB and $\alpha_{max} = 1.0$ dB.

8.6 Design an inverse Chebyshev lowpass filter that satisfies the specifications given in Problem 7.9. Build the filter as a cascade circuit with suitable first- and second-order sections. Choose appropriate opamps and test your design with EWB.

8.7 Design an inverse Chebyshev lowpass filter that satisfies the specifications given in Problem 7.10. Build the filter as a cascade circuit with suitable first- and second-order sections. Choose appropriate opamps and test your design with EWB.

8.8 The *LC* circuit shown in Fig. P8.8 is the normalized ladder realization of a Cauer (elliptic) lowpass filter.

(a) Determine the degree of the transfer function.

(b) Sketch $|T(j\omega)|^2$ and $\alpha(\omega)$ as in Fig. 8.14.

(c) Identify the frequencies of infinite attenuation on the sketches made in (b). Label the frequency values.

8.9 Repeat Problem 8.7 for the circuit in Fig. P8.9.

8.10 Use Figs. 8.16 and 8.19 to determine (estimate) the degrees necessary for a maximally flat, Chebyshev, inverse Chebyshev, and Cauer (elliptic) filter to meet the following requirements. If the data are outside the design curves, use the appropriate equation to determine the needed degree.

	α_{max} [dB]	α_{min} [dB]	ω_p[rad/s]	ω_s[rad/s]
(a)	0.1	62	900	1500
(b)	0.05	45	12 k	15 k
(c)	1.2	42	4200	5880
(d)	0.5	28	1 M	1.65 M
(e)	0.5	25	15 k	16.5 k

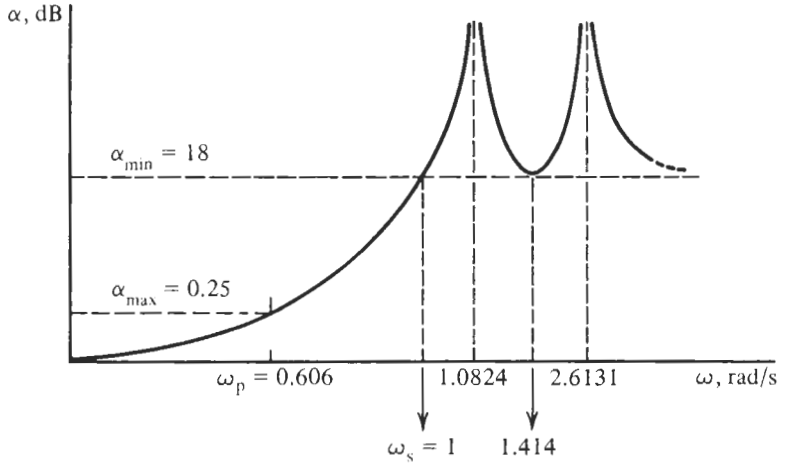

Figure P8.1

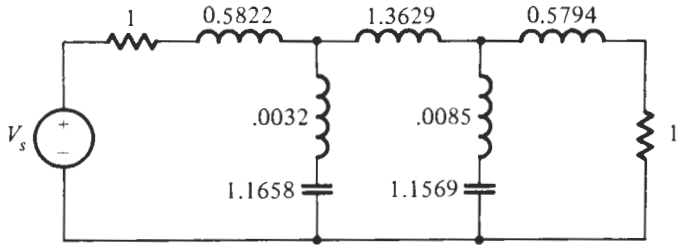

Figure P8.8

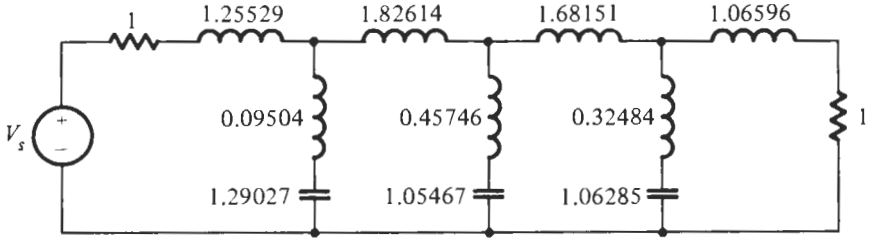

Figure P8.9

8.11 For the following set of values, $\alpha_{max} = 0.177$ dB, $\alpha_{min} = 40.2$ dB, $\omega_s/\omega_p = 1.37$, a table of Cauer (elliptic) filter parameters indicates the following pole and zero positions:

Poles $-0.59676, -0.09225 \pm j1.0423, -0.3629 \pm j0.7737$
Zeros $\pm j1.4149, \pm j2.0732$

Outline a step-by-step procedure in going from these data to a filter realization.

8.12–8.20 When designing Cauer filters using tables it is necessary to try out various possibilities and make compromises to satisfy specifications approximately. The following problems are constructed such that the specifications given in Table 8.2 are matched exactly. Thus the problems are intended to concentrate on finding a circuit that satisfies the specifications. For each of the following nine problems design a circuit with suitable first- or second-order sections, and appropriate opamps, and test the performance of your design.

Problem	Frequency Ratio from Table 8.2	n	ω_p
8.12	$\omega_s/\omega_p = 1.5$	3	1000 rad/s
8.13	$\omega_s/\omega_p = 1.5$	4	100 krad/s
8.14	$\omega_s/\omega_p = 1.5$	5	24 krad/s
8.15	$\omega_s/\omega_p = 2.0$	3	3 krad/s
8.16	$\omega_s/\omega_p = 2.0$	4	1 Mrad/s
8.17	$\omega_s/\omega_p = 2.0$	5	13 krad/s
8.18	$\omega_s/\omega_p = 3.0$	3	130 krad/s
8.19	$\omega_s/\omega_p = 3.0$	4	10 Mrad/s
8.20	$\omega_s/\omega_p = 3.0$	5	100 rad/s

8.21 Use Tables 8.3 to 8.5 to find the Cauer transfer function satisfying the following requirements. For each case assume $f_p = 14.6$ kHz, choose suitable filter sections, LM741 opamps, and realize and test the circuit implementing the specifications.

(a) $\alpha_{max} = 2.0$ dB, $A_2 = 0.35$, $\omega_s = 1.2$

(b) $A_1 = 0.80$, $\alpha_{min} = 23$ dB, $\omega_s = 1.3$

(c) $A_1 = 0.95$, $A_2 = 0.58$, $\omega_s = 1.1$

(d) $\alpha_{max} = 1.5$ dB, $\alpha_{min} = 34$ dB, $\omega_s = 1.3$

9 FREQUENCY TRANSFORMATION

We discussed in the previous three chapters a number of methods for deriving a lowpass transfer function that satisfies a set of given attenuation specifications, such as $\alpha_{\max}$ and $\alpha_{\min}$, over prescribed intervals along the frequency axis. We shall show in this chapter how these same methods can be used to derive realizable transfer functions that approximate the behavior of different types of filters, such as bandpass, highpass, band-rejection, or other kinds of filter specifications. The approach we use is to employ *frequency transformations* that convert the required behavior of the "target" filter (bandpass, highpass, etc.) into the equivalent specifications of a so-called *lowpass prototype*. The approximation problem is then solved on the lowpass prototype by the methods discussed in the previous chapters, and the resulting lowpass transfer function is translated back into the domain of the target filter, which can be realized by a suitable method. Frequency transformation is an important concept in filter design because it permits us to utilize the vast literature and numerous tables that exist for the design of lowpass filters.

To avoid confusion between different frequency axes in our development, we will label the frequency parameter for the lowpass prototype filter with capital letters, $S = \Sigma + j\Omega$, and use the usual lower-case notation, $s = \sigma + j\omega$, for the frequency variable of the target filter function, the highpass, bandpass, band-rejection function, etc. With this notation, we start our discussion from the magnitude $|T_L(j\Omega)|$ of a lowpass transfer function $T_L(S)$ that meets certain specifications, such as, for example, a third-order Chebyshev response. To transform $|T_L(j\Omega)|$ into the magnitudes of a highpass $T_H(s)$, bandpass $T_B(s)$, band-elimination $T_{BE}(s)$, or other type of filter, we now seek a function

$$\Omega = X(\omega) \tag{9.1}$$

that accomplishes the desired transformation along the $j\omega$-axis. For instance, for a lowpass-to-bandpass transformation, we need to find the function X such that $|T_L(jX(\omega))| \Rightarrow |T_B(j\omega)|$.

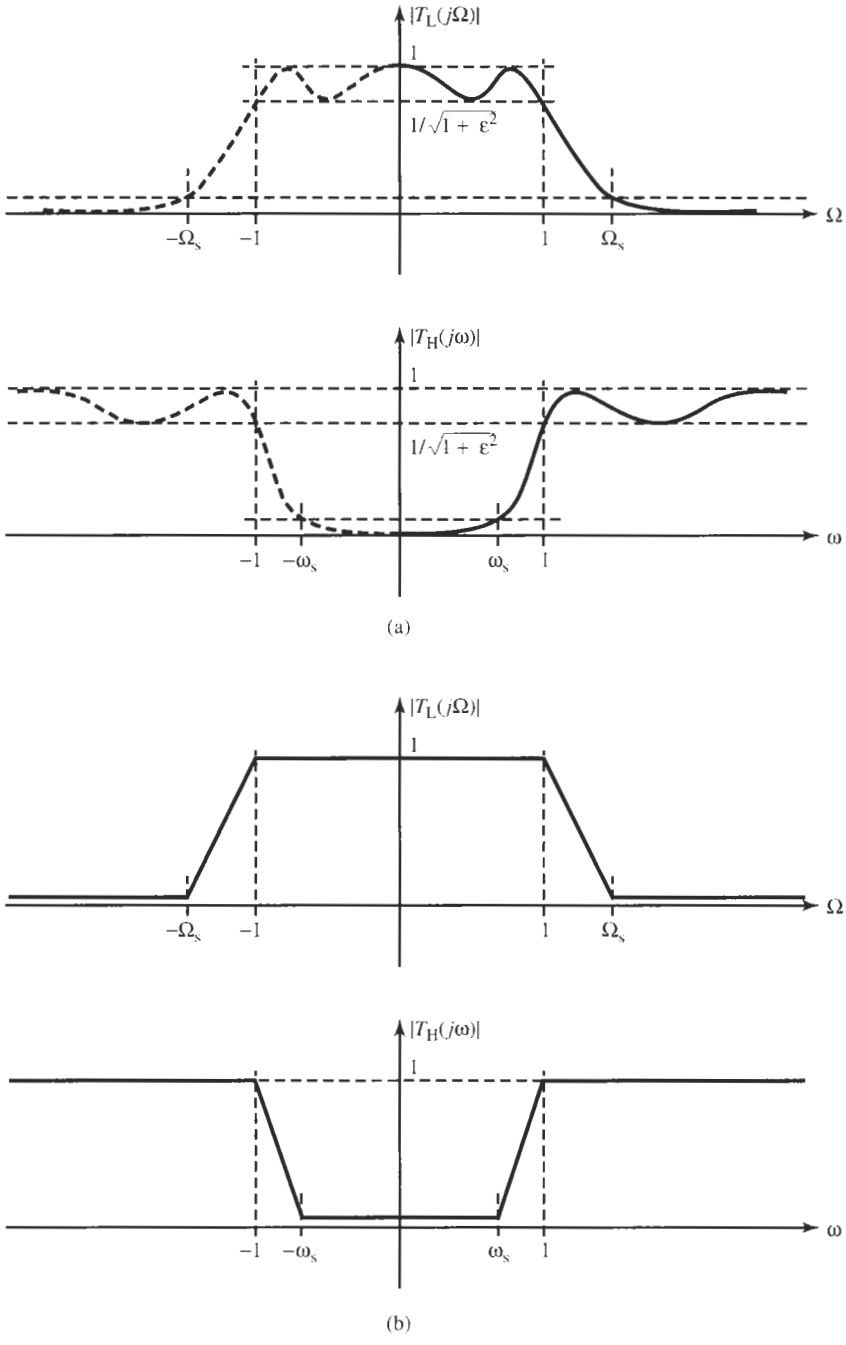

Figure 9.1 Magnitudes of a lowpass and a highpass transfer function plotted versus frequency from $-\infty$ to $+\infty$. (a) A third-order Chebyshev approximation is assumed and the passband corner is normalized to $\Omega = 1$ as is customary. Values of $|T|$ for negative frequencies are shown by dashed lines. (b) Simplified schematic representation of the transformation.

It aids our understanding in the following development to remember that magnitudes are *even* functions of frequency [see, e.g., Eqs. (6.45) and (7.8)], so that $|T_L(j\Omega)| = |T_L(-j\Omega)|$, and similarly for other transfer functions. This is illustrated in Fig. 9.1 for a lowpass and a highpass function. We shall for the most part plot $|T|$ only for positive values of ω, but keep the even nature of the functions and their symmetry in mind. Note also that by Eq. (9.1) we are transforming only the independent variable Ω of $|T_L(j\Omega)|$, that is, the horizontal axis. Dimensions along the vertical axis do not get changed. For example, if the lowpass has a passband whose magnitude varies with equal ripples in $1 \geq |T_L(j\Omega)| \geq 1/\sqrt{1+\varepsilon^2}$, then this lowpass function would be transformed into a highpass whose passband magnitude also varies along the ω-axis in the Chebyshev sense between 1 and $1/\sqrt{1+\varepsilon^2}$ (seen in Fig. 9.1a). Because of this fact we shall use in the following discussion the simplified representation shown in Fig. 9.1b.

9.1 LOWPASS-TO-HIGHPASS TRANSFORMATION

There are many signal-processing situations in which low-frequency components of a signal must be eliminated. This is illustrated in Fig. 9.2 where a high-frequency signal is distorted by low-frequency oscillations. To clean the signal, we then need to find a suitable highpass transfer function with high attenuation, $\alpha_{\min}$, at low frequencies (the stopband) and low attenuation, $\alpha_{\max}$, at high frequencies (the passband). To see how this can be accomplished, consider the task of transforming a lowpass function into the highpass function, i.e., we seek the functional relationship of Eq. (9.1) such that

$$|T_L(j\Omega)| = |T_L(jX(\omega))| = |T_H(j\omega)| \tag{9.2}$$

This equation says that we need to substitute a function $X(\omega)$ for Ω in the lowpass function such that a highpass function is obtained. Our task is accomplished easily if we reason from Fig. 9.1 that the frequencies of the lowpass passband, $-1 \leq \Omega \leq +1$, and highpass passband, $+1 \leq \omega \leq -1$, are transformed into each other by the function

$$\Omega = -\frac{1}{\omega} \tag{9.3}$$

It helps our understanding to visualize "infinity" ($+\infty$ or $-\infty$) to be *one* point on the continuous frequency axis, so that in the highpass function the passband starts from $\omega = 1$, goes along increasing values of ω to $\omega = \infty$, then wraps around to negative values of ω and continues from $-\infty$ to $\omega = -1$. Similarly, on the lowpass axis $\Omega = \infty$ is a point on the $j\Omega$-axis and the stopband, $\Omega_s \leq \Omega \leq -\Omega_s$, is transformed into the highpass stopband $-\omega_s \leq \omega \leq +\omega_s$ by the same function (9.3). In making the transformation, we identified $\Omega_s = -1/\omega_s$. Following

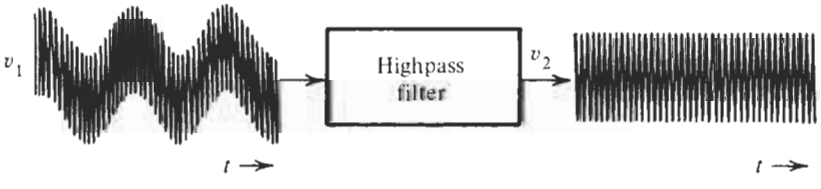

Figure 9.2 Illustration of the function of a highpass filter: low-frequency components of a signal are eliminated from the output.

this interpretation, each of the lowpass and highpass functions has only one passband and one stopband. They are separated by the transition bands $1 \leq \Omega \leq \Omega_s$ and $-\Omega_s \leq \Omega \leq -1$ in the lowpass and $\omega_s \leq \omega \leq 1$ and $-1 \leq \omega \leq -\omega_s$ in the highpass function. Figure 9.3 shows a sketch of Eq. (9.3). As is indicated by the arrows, it shows quite clearly that any value in the lowpass passband, $-1 \leq \Omega \leq +1$, is transformed into the highpass passband $+1 \leq \omega \leq -1$. Similarly, the values in the lowpass stopband, $\Omega_s \leq \Omega \leq -\Omega_s$, transform into the highpass stopband, $-\omega_s \leq \omega \leq +\omega_s$.

Before we can realize the transfer functions we need to return from the imaginary axes to the complex plane, i.e., we need to replace $j\Omega$ by S and $j\omega$ by s. This is done by multiplying Eq. (9.3) by j,

$$j\Omega = -\frac{j}{\omega} = \frac{1}{j\omega}$$

that is, the lowpass-to-highpass transformation we were seeking in Eq. (9.2) is

$$S = Z(s) = \frac{1}{s} \tag{9.4}$$

where we have labeled $jX(s/j) = Z(s)$. Let us still note that the minus sign in Eq. (9.3) is not important because the magnitude functions into which the transformation is to be inserted are even. We have elected to use the minus sign for consistency with our later derivations and to obtain the plus sign in Eq. (9.4) after expanding Eq. (9.3) into the complex plane.

We can make an important point about the frequency transformation $X(\omega)$ in Eq. (9.3) or $Z(s)$ in Eq. (9.4): Frequency transformation transforms the passband of the lowpass, centered

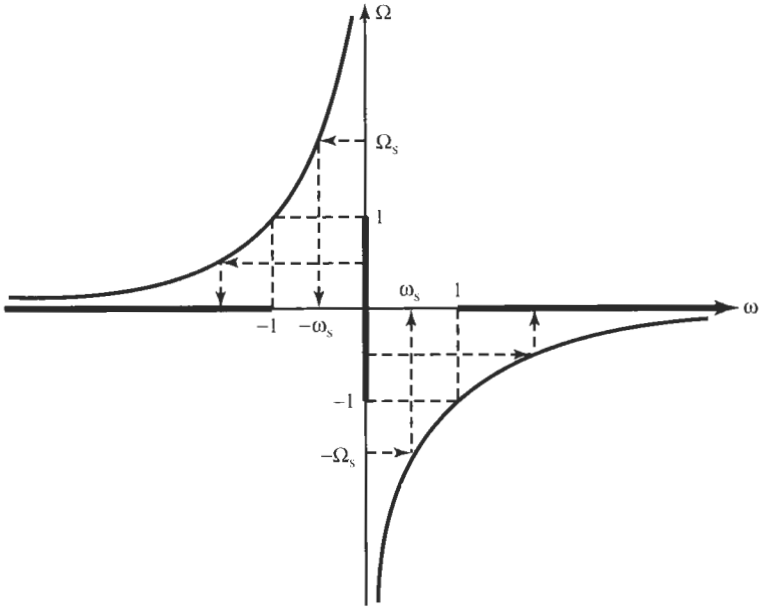

Figure 9.3 Plot of the function (9.3) showing how the transformation of the lowpass interval on the Ω-axis (thick line segment) is transformed into the highpass interval of the ω-axis (thick line segments).

around $\Omega = 0$, into that of the highpass, centered around $\omega = \infty$. Similarly, it transforms the lowpass stopband that is centered around $\Omega = \infty$ into that of the highpass, centered around $\omega = 0$. Consequently, referring to Fig. 9.3 we observe that the frequency transformation functions $X(\omega)$ and $Z(s)$ have a zero "in the center of" the passband of the highpass (at $\omega = \infty$) and have a pole "in the center of" the highpass stopband (at $\omega = 0$). We shall see that this is generally true of the frequency transformation. At "the centers of" the passbands of the *target filters* (highpass, bandpass, band-rejection, or other types) the frequency transformation has zeros; at "the center of" the stopbands of the target filters the frequency transformation has poles. We will define the meaning of "the center of" passbands and stopbands as we progress in our study of frequency transformation.

Consider then how we can transform a highpass attenuation specification into that of a prototype lowpass filter where we know how to find the transfer function, such as with a maximally flat or equal-ripple approximation. A realistic highpass attenuation characteristic, the dashed curve $\alpha(\omega) = -20 \log |T_H(j\omega)|$ in dB, is shown in Fig. 9.4a, along with the specifications α_{min} and α_{max}. Figure 9.4b illustrates the transformation from the highpass attenuation specifications to those of the lowpass.

The sequence of steps in designing a highpass filter with specified requirements by use of frequency transformation can be summarized as follows:

1. Divide the frequency axis of the highpass filter by the passband corner frequency ω_p so that the passband is in $\omega \geq 1$. In all remaining steps the frequency is then normalized. (Because the functions are even, only positive frequencies need to be considered.)
2. Use Eq. (9.3), $\Omega = 1/\omega$, to determine the stopband corner frequency of the prototype lowpass: $\Omega_s = 1/\omega_s$. As mentioned, we may disregard the minus sign in Eq. (9.3).
3. Find the degree n of the lowpass filter required to meet the constraints $\alpha \leq \alpha_{max}$ in $0 \leq \Omega \leq 1$ and $\alpha \geq \alpha_{min}$ for $\Omega \geq \Omega_s$. Use Eq. (6.44) if a maximally flat passband is specified and Eq. (7.20) for an equal-ripple approximation. Consult Fig. 8.16 for the degree of a Cauer filter.
4. Compute (or use tables to determine) the lowpass transfer function $T_L(S)$ as demonstrated in the previous three chapters.
5. Use Eq. (9.4) to find the highpass function $T_H(s)$ by replacing S by $1/s$ in $T_L(S)$.
6. Realize $T_H(s)$.

An example will illustrate the process.

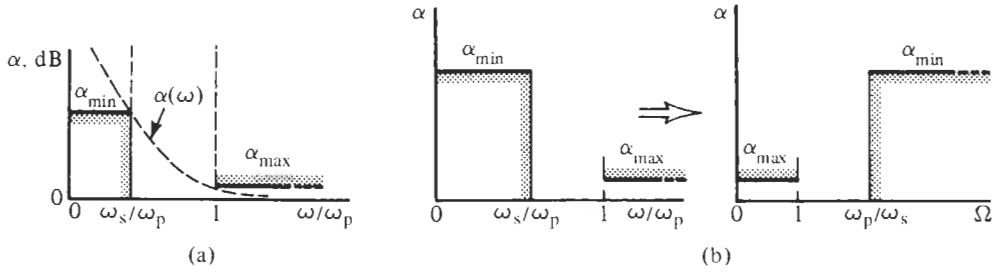

Figure 9.4 (a) Typical highpass attenuation specifications $\alpha(\omega)$ in dB; (b) highpass attenuation specifications transformed to those of a lowpass. The frequency axis for all plots is normalized by the passband corner frequency, such that the passband edge is at unity.

EXAMPLE 9.1

A 200-mV, 45-kHz signal is corrupted by a 2-V, 12-kHz sine wave. Design a highpass filter to remove the 2-V sine wave such that its remaining magnitude is no larger than 2% of 200 mV. The high-frequency gain should be 0 dB, and passband attenuation $\alpha_{\max} \leq 1$ dB will be sufficient.

Solution

Let us develop a highpass circuit with passband starting at 43.75 kHz and stopband between dc and 12.5 kHz. These two corner frequencies will give us a small safety margin to be certain that the frequencies specified in the problem are met. We need to calculate next the required stopband attenuation: 2% of 200 mV is 4 mV; to reduce 2 V to less than 4 mV requires an attenuation of at least $-20 \log(0.004/2) = 53.98$ dB. Let us pick 55 dB as a safety margin for our design. We normalize the frequency axis by dividing it by $\omega_p = 2\pi \times 43.75 = 274.89$ krad/s. The stopband corner is at $\omega_s = 12.5/43.75 = 1/3.5$, and Eq. (9.3) gives $\Omega_p = 1$ and $\Omega_s = 3.5$. Attempting a maximally flat passband, we compute from Eq. (6.44) $n = 5.95$, that is, a sixth-order filter is necessary to do the job. In an effort to obtain a less expensive solution, we may try a Chebyshev design. From Eq. (7.20) we find

$$n = \frac{\ln \sqrt{4\left(10^{5.5} - 1\right) / \left(10^{0.1} - 1\right)}}{\ln\left(3.5 + \sqrt{3.5^2 - 1}\right)} = 4.0008$$

Since we designed already with a safety margin of 1 dB, we take this value and round down to $n = 4$ and in the process save one biquad compared to a design with a maximally flat passband. From Table 7.2 we find for $n = 4$ and $\alpha_{\max} = 1$ dB the Chebyshev lowpass function

$$T_L(S) = \frac{0.2457}{\left(S^2 + 0.2690S + 0.9866\right)\left(S^2 + 0.6738S + 0.2794\right)} \tag{9.5}$$

The numerator coefficient equals $1/(2^3\varepsilon)$ and results in $T_L(0) = 0.8913$, i.e., -1 dB, as specified. Using Eq. (9.4), i.e., replacing S by $1/s$ results in the desired highpass function

$$\begin{aligned} T_H(s) &= \frac{0.2457s^4}{\left(1 + 0.2690s + 0.9866s^2\right)\left(1 + 0.6738s + 0.2794s^2\right)} \\ &= \frac{0.8913s^4}{\left(s^2 + 0.2727s + 1.0136\right)\left(s^2 + 2.412s + 3.579\right)} \end{aligned} \tag{9.6}$$

This we factor into

$$T = T_1 T_2 = \frac{k_1 s^2}{s^2 + 2.412s + 3.579} \frac{k_2 s^2}{s^2 + 0.2727s + 1.0136}$$

in preparation for a cascade design. Observe that $T_H(\infty)$ is at -1 dB as we require. The product of the gain constants must be $k_1 k_2 = K_0 = 0.8913$ and the sequence of the modules T_1 and T_2 is in the order of increasing values of Q, $Q_1 = 0.78$ and $Q_2 = 3.69$. To find the optimum gain constants for equalizing the signal level in the cascade circuit we need to determine the values M_1 and M_2 according to the discussion in Chapter 5, Section 5.3. We find $M_1 = 1$ (at $s = \infty$) and $M_2 K_0 = 1$ because 0-dB high-frequency gain is prescribed for the total filter;

thus $M_2 = 1/K_0$. Thus, by Eqs. (5.78) and (5.79), $k_1 = 1$ and $k_2 = K_0 = 0.8913$, and we must realize the two modules

$$T_1(s) = \frac{s^2}{s^2 + 2.412s + 3.579} \quad \text{and} \quad T_2(s) = \frac{0.8913s^2}{s^2 + 0.2727s + 1.0136}$$

This we can do with the circuit in Fig. 4.33 that realizes the function

$$T(s) = \frac{K\omega_0^2 s^2}{s^2 + s\omega_0(3 - K) + \omega_0^2}$$

We choose $C = 1$ nF to get for T_1,

$$R = 1/(\omega_{p1}C) = 1\Big/\left(\sqrt{3.579} \times 2.749 \times 10^{-4}\right)\ \Omega = 1.923\ \text{k}\Omega, \quad K = 3 - Q_1^{-1} = 1.718$$

Similarly, for Module 2, we obtain

$$R = 1/(\omega_{p2}C) = 1\Big/\left(\sqrt{1.0136} \times 2.749 \times 10^{-4}\right)\ \Omega = 3.61\ \text{k}\Omega, \quad K = 3 - Q_2^{-1} = 2.729$$

Let us choose the resistor level in the K-determining divider in both modules as $R = 5$ kΩ. Now, since $K_1 = 1.72$ results in 4.7-dB gain rather than 0 dB as required, we split the feed-in capacitor of Module 1 into 0.6 and 0.4 nF for a voltage divider ratio of $0.6 \approx 1/K_1$. Similarly, the gain of Module 2 is $K_2 = 2.73$ (= 8.7 dB) so that the input capacitor of Module 2 is split into 0.39 and 0.6 nF for a divider ratio of $0.394 \approx 1/K_2$. The maximum signal level of the two modules is then equal to approximately 0 dB, as is the total filter gain.

Figure 9.5 shows the circuit and its performance. After some fine-tuning of Q_2 (via the

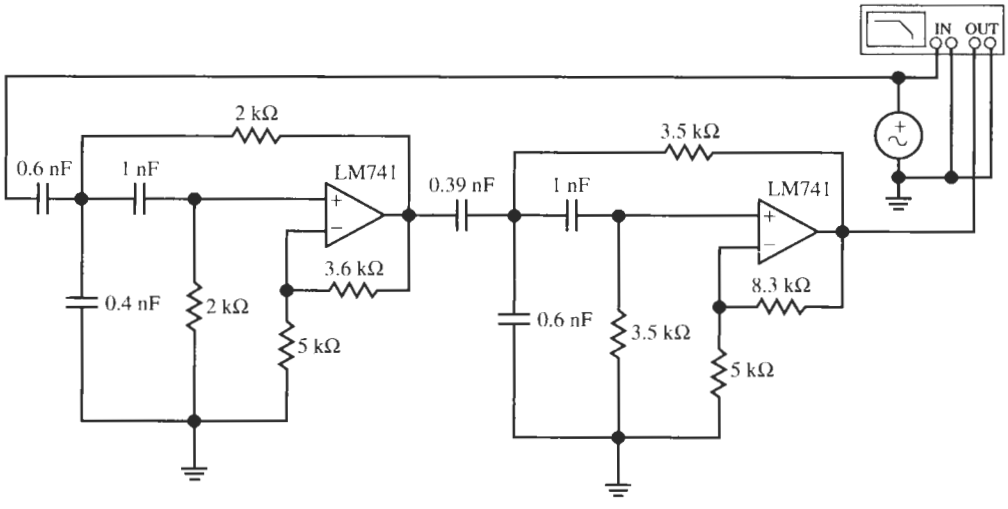

(a)

Figure 9.5 (a) The Chebyshev highpass filter of Example 9.1; (b) its frequency response measured on the Bode Plotter; (c) input (upper trace) and output (lower trace) signals seen on an oscilloscope. Note the different scales on the oscilloscope traces. (Bode plotter scales: 1 to 500 kHz; −120 to 0 dB; cursor at 44.53 kHz, −0.964 dB; oscilloscope scales: horizontal (time base): 0.05 ms/div; vertical: upper trace: 2 V/div; lower trace: 200 mV/div.)

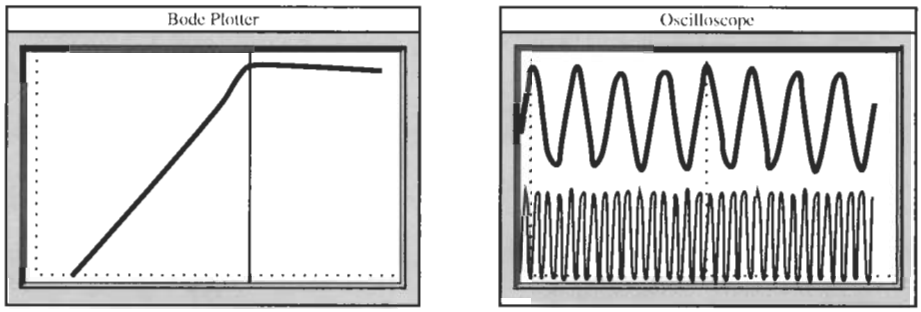

(b) (c)

Figure 9.5 Continued

8.3-kΩ resistor in Module 2) the circuit's frequency response is as designed. The oscilloscope display (compare also with Fig. 9.2) shows the filter output (lower trace) when driven by the specified input signal (upper trace—a sum of a 200-mV, 45-kHz and a 2-V, 12-kHz sinusoid). Notice that the filter removes the 12-kHz signal almost completely from the output. The 55-dB attenuation (a factor of 0.0018) achieved at the stopband corner is adequate for the task of cleaning the high-frequency sinusoid.

Let us make a few observations about the pole locations in a filter obtained via a lowpass-to-highpass transformation. A lowpass transfer function in general has the form

$$T(S) = \frac{K\,(S + z_1)\,(S + z_2)\cdots(S + z_m)}{(S + p_1)\,(S + p_2)\,(S + p_3)\cdots(S + p_n)} \tag{9.7}$$

where $n > m$. We derived functions of this type in Section 6.5. The lowpass-to-highpass transformation, Eq. (9.4), replaces S by $1/s$, so that the function becomes

$$\begin{aligned} T(1/s) &= \frac{K\,(1/s + z_1)\,(1/s + z_2)\cdots(1/s + z_m)}{(1/s + p_1)\,(1/s + p_2)\,(1/s + p_3)\cdots(1/s + p_n)} \\ &= \frac{K s^{n-m}\,(1 + sz_1)\,(1 + sz_2)\cdots(1 + sz_m)}{(1 + sp_1)\,(1 + sp_2)\,(1 + sp_3)\cdots(1 + sp_n)} \end{aligned} \tag{9.8}$$

Note that the dc gain of the lowpass, $K(z_1 z_2 \cdots z_m)/(p_1 p_2 \cdots p_n)$, becomes the gain at infinity of the highpass response. The lowpass with m finite zeros and n finite poles in addition to $n - m$ zeros at infinity is converted to a highpass with $n - m$ zeros at the origin and poles and zeros located at $sz_j + 1 = 0$ and $sp_i + 1 = 0$, respectively, i.e., at

$$s = \frac{1}{z_j} \qquad \text{and} \qquad s = \frac{1}{p_i} \tag{9.9}$$

This is referred to as *reciprocation*. If we express a complex pole position of the lowpass in polar form,

$$p_i = r_i e^{j\alpha_i}$$

then the pole in the highpass function becomes

$$\frac{1}{p_i} = \frac{1}{r_i} e^{-j\alpha_i} \tag{9.10}$$

The analogous equation can be written for the zeros. Reciprocation is illustrated in Fig. 9.6a for a complex pole p_1, in Fig 9.6b for its conjugate p_2, which, of course, will always be there since poles must occur in conjugate complex pairs, and in Fig. 9.6c for a pole p_3 on the negative real axis. Zeros occur as a rule on the $j\omega$-axis; in Fig. 9.6c we have also shown such a zero z_1 and its reciprocated position in the highpass. We see that a pole p_1 inside the unit circle in the second quadrant goes outside the unit circle to $1/p_1$ in the third quadrant and its conjugate p_2 in the third quadrant becomes $1/p_2$ in the second quadrant. We can say that poles are mirrored at the unit circle. Thus, conjugate complex poles inside the unit circle become conjugate complex poles outside the unit circle and vice versa; ω_0 is changed to $1/\omega_0$ but Q is not altered. This was demonstrated in Example 9.1 in Eqs. (9.5) and (9.6).

The application of pole reciprocation for the Butterworth response is very direct. Since all poles are on the unit circle and bearing in mind that poles occur in conjugate pairs, reciprocation does not change their positions at all—neither ω_0 nor Q changes. The poles of an nth-order Butterworth lowpass response become the poles of the Butterworth highpass response and n zeros are added at the origin; see Fig. 9.7.

This simplicity of reciprocation for Butterworth filters does not extend to other types of responses, such as the Chebyshev case, as we saw in Example 9.1, Eqs. (9.5) and (9.6). For the Chebyshev response we found that the poles are located on an ellipse. Equation (9.10) is, of course, still valid for the reciprocated poles, but their locus is not an ellipse.

Reciprocation of poles and zeros is demonstrated in the following example, which also shows that the lowpass-to-highpass transformation is not restricted to all-pole filters, but is valid for arbitrary lowpass functions.

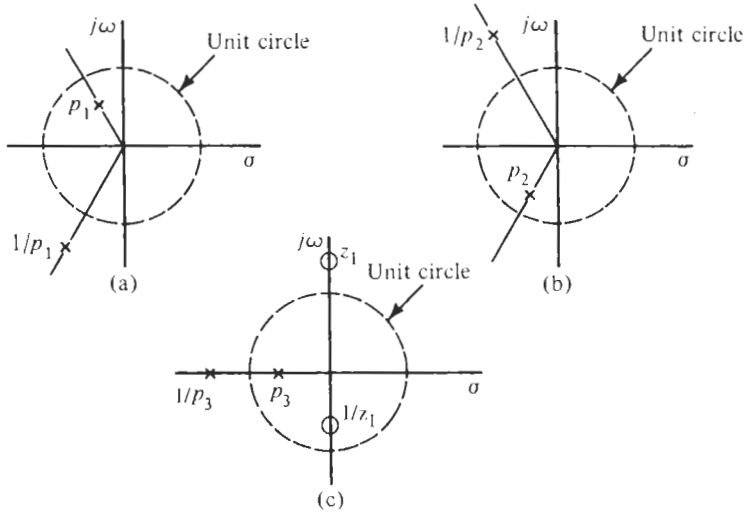

Figure 9.6 Reciprocation of pole positions in the lowpass-to-highpass transformation.

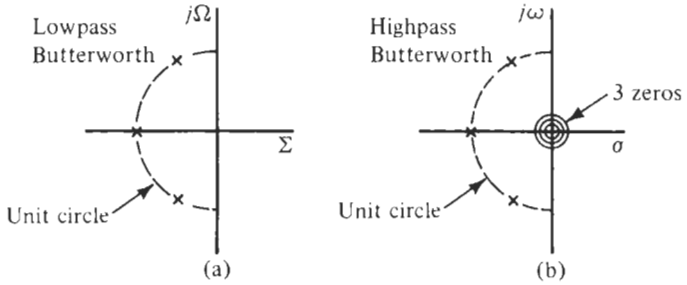

Figure 9.7 Pole reciprocation in Butterworth functions.

EXAMPLE 9.2

Convert the lowpass circuit of Example 6.3 to a highpass filter.

Solution

The transfer function with maximally flat magnitude was given in Eq. (6.60)

$$T(S) = T_1T_2T_3 = \frac{1.38}{S^2 + 2.24379S + 1.37377} \times \frac{-1.24\left(S^2/16 + 1\right)}{S^2 + 1.46493S + 1.23015} \frac{-1.1\left(S^2/4 + 1\right)}{S^2 + 0.47756S + 1.10041} \tag{9.11}$$

Using Eq. (9.4), the highpass function becomes

$$T(s) = T_1T_2T_3 = \frac{1.38s^2}{1 + 2.24379s + 1.37377s^2} \times \frac{-1.24\left(1/16 + s^2\right)}{1 + 1.46493s + 1.23015s^2} \frac{-1.1\left(1/4 + s^2\right)}{1 + 0.47756s + 1.10041s^2}$$

which we bring into the form

$$T(s) = T_1T_2T_3 = \frac{1.00s^2}{s^2 + 1.63331s + 0.72792} \times \frac{-1.00\left(1/16 + s^2\right)}{s^2 + 1.19085s + 0.81291} \frac{-1.00\left(1/4 + s^2\right)}{s^2 + 0.43398s + 0.90875} \tag{9.12}$$

You can show that the three pole quality factors, $Q_1 = 0.522$, $Q_2 = 0.757$, and $Q_3 = 2.197$, have not changed, as expected, but the three pole frequencies ω_i are converted into $1/\omega_i$, $i = 1, 2, 3$. We do not have to be concerned with the optimum gain assignment because the lowpass-to-highpass transformation does not distort the vertical axis, the attenuation, of the filter modules.

The implementation then proceeds precisely as in Example 6.3. We realize the three sections by the four-amplifier biquad of Fig. 5.1; it realizes the transfer function

$$\frac{V_{\text{out}}}{V_{\text{I}}} = -\frac{as^2 + s\omega_0/Q[a - b(kQ)] + \omega_0^2[a - ck]}{s^2 + s\omega_0/Q + \omega_0^2}$$

where we set $d = 0$ in Eq. (5.5) to ensure positive components. We require a realization with $a - b(kQ) = 0$ for T_2 and T_3, and $a - b(kQ) = 0$ and $a - ck = 0$ for T_1. Using again $C = 1$ nF we obtain for Module 1

$$R = \frac{1}{2\pi \times 0.85318 \times 18{,}000\ \text{s}^{-1} \times 10^{-9}\text{F}} = 10.36\ \text{k}\Omega,$$
$$Q_1 R = 0.522 \times 10.36\ \text{k}\Omega = 5.41\ \text{k}\Omega$$

along with $k = 1$, $a = 1$, $b = 1/Q_1 = 1.9157$, and $c = 1$. For Module 2 we have

$$R = \frac{1}{2\pi \times 0.90162 \times 18{,}000\ \text{s}^{-1} \times 10^{-9}\text{F}} = 9.806\ \text{k}\Omega,$$
$$Q_2 R = 0.757 \times 9.806\ \text{k}\Omega = 7.424\ \text{k}\Omega$$

along with $a = 1$, $k = 1$, $b = 1/Q_2 = 1.321$, and $c = 1 - 1/16 = 0.9375$. Finally, for Module 3 we obtain

$$R = \frac{1}{2\pi \times 0.95328 \times 18{,}000\ \text{s}^{-1} \times 10^{-9}\text{F}} = 9.275\ \text{k}\Omega,$$
$$Q_3 R = 2.197 \times 9.275\ \text{k}\Omega = 20.378\ \text{k}\Omega$$

and with $a = 1$, $k = 1$, $b = 1/Q_3 = 0.455$, and $c = 1 - 1/4 = 0.75$.

Figure 9.8 shows the circuit and test results. The resistor $Q_3 R$ had to be reduced to 19 kΩ to avoid slight peaking caused by Q enhancement due to finite opamp bandwidth. The cut-off frequency is at 18 kHz (cursor) and the passband gain is 0 dB as specified. The transmission zeros are at 4.35 kHz (≈18 kHz/4) and 9.6 kHz (≈18 kHz/2) as expected from the transfer function. These values are (approximately) equal to the reciprocated lowpass zeros: [1/(36/18)] × 18 kHz = 9 kHz and [1/(72/18)] × 18 kHz = 4.5 kHz. Their positions can be fine-tuned if desired by adjusting the resistors R_0/c in the second and third modules. We

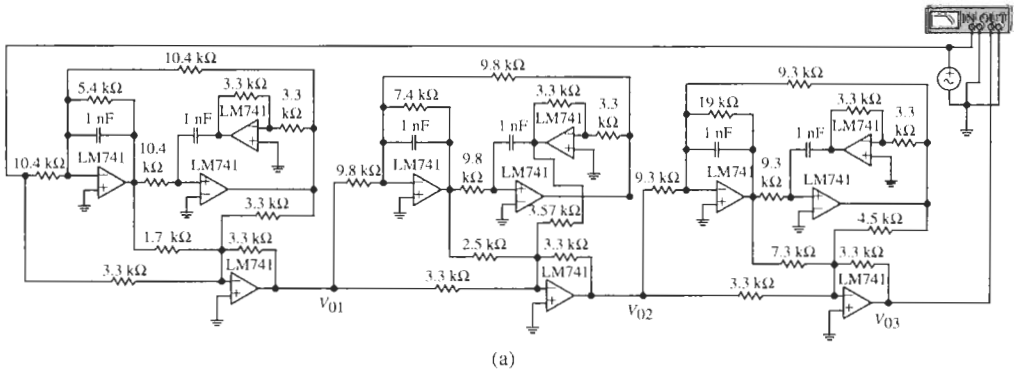

(a)

Figure 9.8 Results for Example 9.2. (a) Circuit; (b) test results; (c) simulation results from the three section outputs. (Bode Plotter scales: 500 Hz to 500 kHz; −100 to 10 dB; cursor at 18.82 kHz, 0.120 dB.)

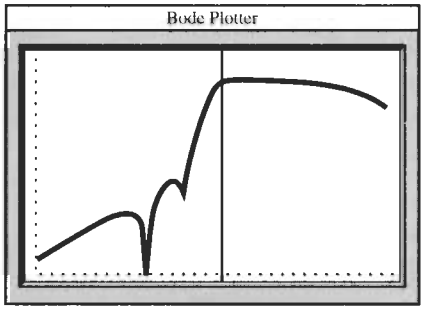

(b)

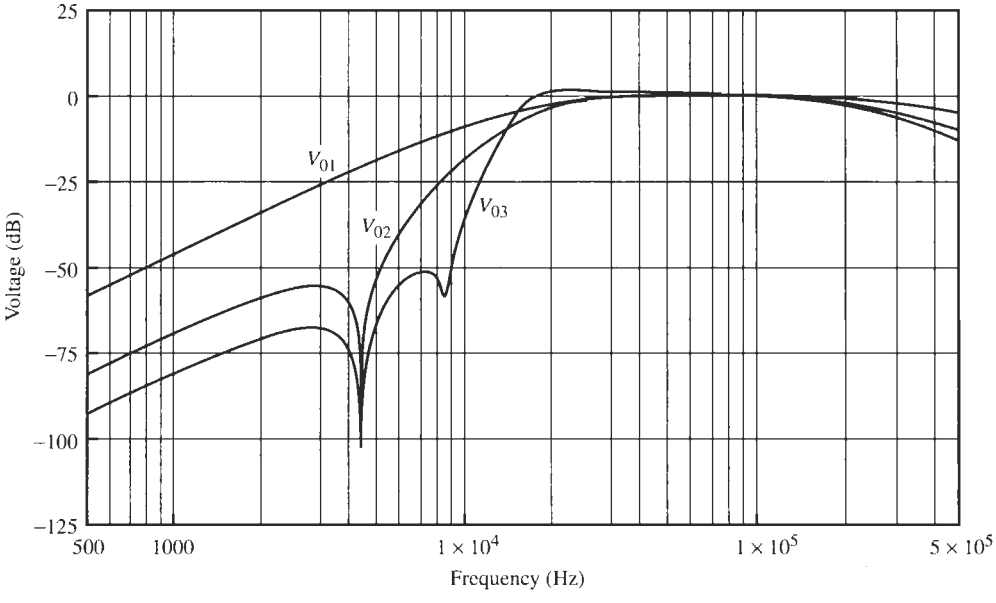

(c)

Figure 9.8 Continued

notice the gain roll-off, starting at $\approx$ 150 kHz, that is caused by the 1.5-MHz bandwidth of the LM741 opamps. Figure 9.8c contains the simulated response at the outputs of the three sections. It shows how the filter function is obtained by multiplying the three transfer functions and also that all section outputs have the same maximum signal level.

9.2 LOWPASS-TO-BANDPASS TRANSFORMATION

To transform a lowpass function to a bandpass function we need an equation $\Omega = X(\omega)$ as in Eq. (9.1) that converts the lowpass into a bandpass

$$|T_L(j\Omega)| = |T_L(jX(\omega)| = |T_B(j\omega)|$$

Specifically, we convert the lowpass passband into the bandpass passbands and the lowpass stopband into the bandpass stopbands. To understand the functional relationship required, we draw a diagram of the two filter types, similar to the one in Fig. 9.1b. Figure 9.9 shows the

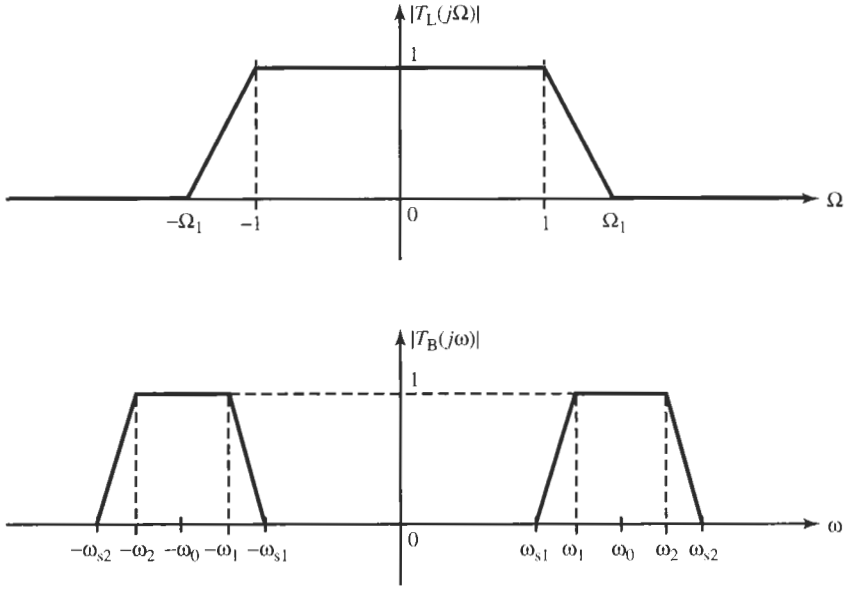

Figure 9.9 The positions of lowpass and bandpass responses on the frequency axes.

simplified lowpass magnitude in $-\infty \leq \Omega \leq +\infty$ as well as the bandpass magnitude in $-\infty \leq \omega \leq +\infty$. We have identified passbands, transition bands, and stopbands, and we have again normalized the lowpass passband to lie in $-1 \leq \Omega \leq +1$. The bandpass passband (for positive frequencies) is in the range $\omega_1 \leq \omega \leq \omega_2$. Figure 9.10 shows a diagram of Ω versus ω with the intended passbands identified on both axes by thick line segments. As in the highpass case in Fig. 9.3, the arrows indicate how the lowpass and the bandpass passbands are mapped into each other. To determine the function $X(\omega)$, we recall from our discussion in the lowpass-to-highpass transformation that $X(\omega)$ should have a zero in the center of the passbands and a pole in the center of the stopbands the target filter. Thus, as Fig. 9.10 indicates, we should have poles of $X(\omega)$ at $\omega = 0$ and at $\omega = \infty$ and zeros at frequencies labeled $\omega = \pm\omega_0$. Such a function is

$$\Omega = X(\omega) = \frac{1}{B}\frac{(\omega - \omega_0)(\omega + \omega_0)}{\omega} = \frac{1}{B}\frac{\omega^2 - \omega_0^2}{\omega} \tag{9.13}$$

It has zeros at $\omega = \pm\omega_0$ as required and becomes infinite at $\omega = 0$ and $\omega = \infty$. We have allowed for a multiplying constant, labeled $1/B$, to be able to adjust the slope of the function. Now observe from the sketch in Fig. 9.10 that $X(\omega)$ is to be determined such that the corner of the lowpass passband, $\Omega = 1$, is transformed into the two values $\omega = -\omega_1$ and $\omega = +\omega_2$, which specify the corners of the passband in the bandpass filter. Thus setting $\Omega = 1$ in Eq. (9.13), we obtain the quadratic equation

$$\omega^2 - B\omega - \omega_0^2 = 0 \tag{9.14}$$

which must have the solutions $-\omega_1$ and ω_2, i.e.,

$$(\omega + \omega_1)(\omega - \omega_2) = \omega^2 - (\omega_2 - \omega_1)\omega - \omega_1\omega_2 = 0 \tag{9.15}$$

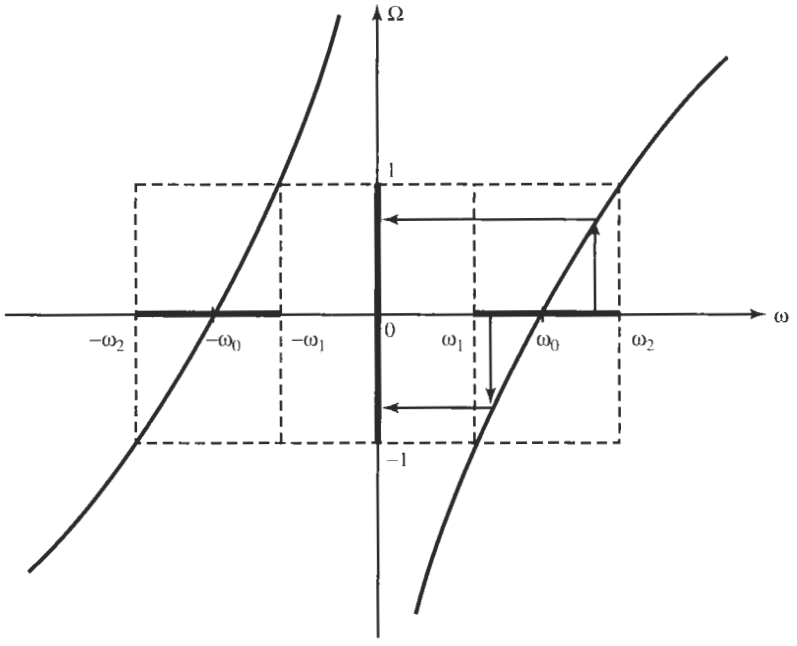

Figure 9.10 The function $X(\omega)$ to convert a lowpass magnitude into a bandpass magnitude.

Comparing Eqs. (9.14) and (9.15), we identify the quantities

$$\omega_0^2 = \omega_1\omega_2 \qquad \text{and} \qquad B = \omega_2 - \omega_1 \tag{9.16}$$

Evidently, the parameter B is the bandwidth of the bandpass filter and ω_0, referred to as "the center of the passband," is recognized as the geometric mean of the two band edges. Since all quantities in Eq. (9.13) are determined, we may now multiply the expression by j to extend the validity of Eq. (9.13) from the imaginary axes into the complex plane:

$$j\Omega = jX(\omega) = \frac{j}{B}\frac{\omega^2 - \omega_0^2}{\omega} = -\frac{1}{B}\frac{\omega^2 - \omega_0^2}{j\omega} \tag{9.17}$$

With $S = j\Omega$ and $s = j\omega$, Eq. (9.17) can be rewritten as

$$S = Z(s) = \frac{1}{B}\frac{s^2 + \omega_0^2}{s} \tag{9.18a}$$

or as

$$S = \frac{\omega_0}{B}\frac{s^2 + \omega_0^2}{\omega_0 s} = Q\left(\frac{s}{\omega_0} + \frac{\omega_0}{s}\right) \tag{9.18b}$$

Typically, the bandpass frequency s is normalized with respect to the value of the bandpass center frequency ω_0 so that the transformation function with normalized frequency becomes

$$S = Q\frac{s^2+1}{s} = Q\left(s + \frac{1}{s}\right) \tag{9.18c}$$

The new quantity Q, defined as center frequency of the bandpass filter divided by its bandwidth,

$$Q = \frac{\omega_0}{B} = \frac{1}{\omega_2/\omega_0 - \omega_1/\omega_0} \tag{9.19}$$

is referred to as the *quality factor* of the bandpass filter.

Equation (9.18) is the lowpass-to-bandpass transformation we were seeking. If we substitute Eq. (9.18) into a lowpass function $T_L(S)$ we obtain a bandpass function $T_B(s)$. Note that if the lowpass function is of degree n, the bandpass will be of degree $2n$; for example, a fourth-order lowpass filter converts into an eighth-order bandpass filter.

It is of interest to ascertain the pole locations of the bandpass function, when the lowpass is given. Consider initially a first-order lowpass,

$$T_L(S) = \frac{1}{S + \Sigma_1} \tag{9.20}$$

The situation is depicted in Fig. 9.11a. Assuming that s is normalized so that the frequency $\omega_0 = 1$, the bandpass function will have the denominator

$$S + \Sigma_1 = Q\frac{s^2+1}{s} + \Sigma_1 = 0 \tag{9.21}$$

which has roots where

$$s^2 + \frac{\Sigma_1}{Q}s + 1 = 0$$

that is, the negative real pole at $S = -\Sigma_1$ is converted to two complex poles at

$$p_1, p_2 = -\frac{\Sigma_1}{2Q} \pm j\sqrt{1 - \left(\frac{\Sigma_1}{2Q}\right)^2} \tag{9.22}$$

where we assumed that $2Q > \Sigma_1$, so that the roots are complex. The first-order lowpass of Eq. (9.20) becomes a second-order bandpass

$$T_B(s) = \frac{1}{Q\left(s^2+1\right)/s + \Sigma_1} = \frac{s}{s^2 + s\Sigma_1/Q + 1} \tag{9.23}$$

The more interesting case is that of complex poles in the lowpass function, that is, the lowpass has a denominator term $S^2 + aS + b$ with complex roots (Fig. 9.11b):

$$T_L(S) = \frac{1}{S^2 + aS + b} \tag{9.24}$$

The lowpass-to-bandpass transformation results in the equation

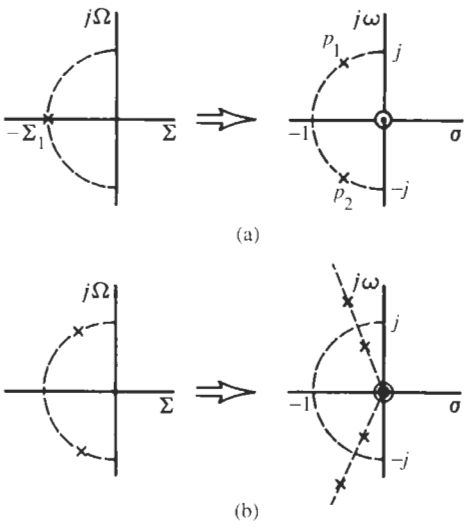

Figure 9.11 Pole transformation for (a) a first-order lowpass; (b) a second-order lowpass.

$$\left(Q\frac{s^2+1}{s}\right)^2 + aQ\frac{s^2+1}{s} + b = 0$$

for the bandpass poles. This gives the fourth-order polynomial

$$s^4 + \frac{a}{Q}s^3 + \left(2 + \frac{b}{Q^2}\right)s^2 + \frac{a}{Q}s + 1 = 0 \tag{9.25}$$

Since a, b, and Q are known, this polynomial can always be factored by a suitable computer algorithm, but solutions in closed form can be obtained readily because of the special relationship between the roots: We note that Eq. (9.25) has four roots that must appear in conjugate complex pairs,

$$\left(s^2 + \frac{\omega_{01}}{q_1}s + \omega_{01}^2\right)\left(s^2 + \frac{\omega_{02}}{q_2}s + \omega_{02}^2\right) = 0 \tag{9.26}$$

where ω_{01} and q_1 are the pole frequency and pole quality factor of the one pole pair and ω_{02} and q_2 are those of the other pair. If we multiply these two factors, we obtain

$$s^4 + \left(\frac{\omega_{01}}{q_1} + \frac{\omega_{02}}{q_2}\right)s^3 + \left(\omega_{01}^2 + \omega_{02}^2 + \frac{\omega_{01}}{q_1}\frac{\omega_{02}}{q_2}\right)s^2 + \left(\frac{\omega_{01}\omega_{02}^2}{q_1} + \frac{\omega_{01}^2\omega_{02}}{q_2}\right)s + \omega_{01}^2\omega_{02}^2 = 0 \tag{9.27}$$

and can now compare coefficients between this result and Eq. (9.25). From the constant coefficient we observe directly that

$$\omega_{01}\omega_{02} = 1, \qquad \text{i.e.,} \qquad \omega_{01} = \frac{1}{\omega_{02}} \tag{9.28}$$

We see that the two pole frequencies are reciprocals of each other, symmetrical around $\omega_0 = 1$. Further, from comparing the coefficients of s^3 and s we find

$$\frac{\omega_{01}}{q_1} + \frac{\omega_{02}}{q_2} = \frac{\omega_{01}\omega_{02}^2}{q_1} + \frac{\omega_{01}^2\omega_{02}}{q_2} = \frac{a}{Q} \tag{9.29}$$

which with Eq. (9.28) yields

$$\frac{\omega_{02} - \omega_{01}}{q_2} = \frac{\omega_{02} - \omega_{01}}{q_1}, \qquad \text{i.e.,} \qquad q_1 = q_2 = q \tag{9.30}$$

This is an important result; it says that the two bandpass pole pairs have the same quality factors. Equations (9.28) and (9.30) allow us to sketch the locations of the bandpass poles arising from a second-order lowpass as is shown in Fig. 11b. Further, from Eq. (9.29) we then obtain

$$\omega_{01} + \omega_{02} = \omega_{02} + \frac{1}{\omega_{02}} = q\frac{a}{Q} \tag{9.31}$$

By comparing the two s^2 coefficients in Eqs. (9.25) and (9.27) and using Eqs. (9.28) and (9.30), we have

$$\omega_{01}^2 + \omega_{02}^2 + \frac{1}{q^2} = 2 + \frac{b}{Q^2} \tag{9.32a}$$

or

$$\omega_{02}^2 - 2 + \frac{1}{\omega_{02}^2} = \left(\omega_{02} - \frac{1}{\omega_{02}}\right)^2 = \frac{b}{Q^2} - \frac{1}{q^2} \tag{9.32b}$$

Taking next the square root of Eq. (9.32b) and adding the result to Eq. (9.31), we obtain

$$\omega_{02} = \frac{aq}{2Q} + \frac{1}{2}\sqrt{\frac{b}{Q^2} - \frac{1}{q^2}} = \frac{1}{\omega_{01}} \tag{9.33}$$

which can be solved for the pole frequencies as soon as we find q. Since the right-hand side of Eq. (9.32b) is equal to a complete square and, therefore, positive, we note that

$$q^2 \geq Q^2/b \tag{9.34}$$

is required. We can compute q by adding 2 on each side of Eq. (9.32a)

$$\omega_{01}^2 + 2 + \omega_{02}^2 = \left(\omega_{02} + \frac{1}{\omega_{02}}\right)^2 = 4 + \frac{b}{Q^2} - \frac{1}{q^2}$$

and equating the result to the square of Eq. (9.31). This gives the equation

$$\left(q\frac{a}{Q}\right)^2 = 4 + \frac{b}{Q^2} - \frac{1}{q^2}$$

that is, q is determined by the fourth-order equation

$$\left(\frac{aq^2}{Q}\right)^2 - \left(\frac{4Q}{a} + \frac{b}{aQ}\right)\left(\frac{aq^2}{Q}\right) + 1 = 0 \tag{9.35}$$

which is solved readily because it is actually a second-order equation in q^2:

$$q^2 = \frac{Q}{a}\left[\left(\frac{2Q}{a} + \frac{b}{2aQ}\right) \pm \sqrt{\left(\frac{2Q}{a} + \frac{b}{2aQ}\right)^2 - 1}\right] \tag{9.36}$$

We must choose the plus sign of the square root so that the restriction (9.34) is satisfied and a positive value of ω_{02} is obtained in Eq. (9.33). An example will illustrate the calculations.

EXAMPLE 9.3

A lowpass function has poles at $\Sigma \pm j\Omega = 0.5 \pm j0.866$, i.e., the transfer function is that of Eq. (9.24) with $a = b = 1$:

$$T_L(S) = \frac{1}{S^2 + S + 1}$$

Let the prescribed bandwidth of the bandpass be $B = 1$ and, of course, $\omega_0 = 1$.

Solution

The quality factor is $Q = \sqrt{1}/1 = 1$. The lowpass-to-bandpass transformation of Eq. (9.18c) results in the bandpass function

$$T_B(s) = \frac{1}{Q^2\left(\dfrac{s^2+1}{s}\right)^2 + Q\dfrac{s^2+1}{s} + 1} = \frac{s^2}{s^4 + s^3 + 3s^2 + s + 1} \tag{9.37}$$

To find the positions of the four poles of the bandpass, we use Eq. (9.36) with $a = b = Q = 1$ to get

$$q^2 = \left(2 + \frac{1}{2}\right) + \sqrt{\left(2 + \frac{1}{2}\right)^2 - 1} = 2.5 + \sqrt{5.25} = 4.7913$$

that is, $q = 2.1889$. We find from Eq. (9.33),

$$\omega_{02} = \frac{q}{2} + \frac{1}{2}\sqrt{1 - \frac{1}{q^2}} = \frac{2.1889 + \sqrt{0.7913}}{2} = 1.5392, \qquad \omega_{01} = 0.6497$$

With these numbers, the poles are from Eq. (9.26),

$$s_{1,2} = -\omega_{01}\left(\frac{1}{2q} \pm j\sqrt{1 - \frac{1}{4q^2}}\right) = -0.1484 \pm j0.6325, \qquad s_{3,4} = -0.3516 \pm j1.4985$$

which yields the transfer function in Eq. (9.37).

The lowpass-to-bandpass transformation can be applied to arbitrary lowpass functions, such as Eq. (6.58). If there are finite transmission zeros (they are normally on the $j\Omega$-axis), these are also transformed into the bandpass domain by Eq. (9.13): a zero at $j\Omega_z$ is converted by the equation $\Omega_z = Q(\omega^2 - 1)/\omega$ into two zeros on the $j\omega$-axis as follows:

$$\omega^2 - \frac{\Omega_z}{Q}\omega - 1 = (\omega + \omega_{z1})(\omega - \omega_{z2}) = 0$$

that is, into

$$\omega_{z1} = \sqrt{\frac{\Omega_z^2}{4Q^2} + 1} - \frac{\Omega_z}{2Q} \qquad \text{and} \qquad \omega_{z2} = \sqrt{\frac{\Omega_z^2}{4Q^2} + 1} + \frac{\Omega_z}{2Q} \tag{9.38}$$

Note that $\omega_{z1}\omega_{z2} = 1$. This means that the two transformed zeros, ω_{z1} and ω_{z2}, are also on the $j\omega$-axis and are geometrically symmetrical around $\omega_0 = 1$. Figure 9.12 illustrates how to transform such a case.

The sequence of steps in designing a bandpass filter with specified requirements by use of frequency transformation can be summarized as follows; the situation is illustrated in Fig. 9.13.

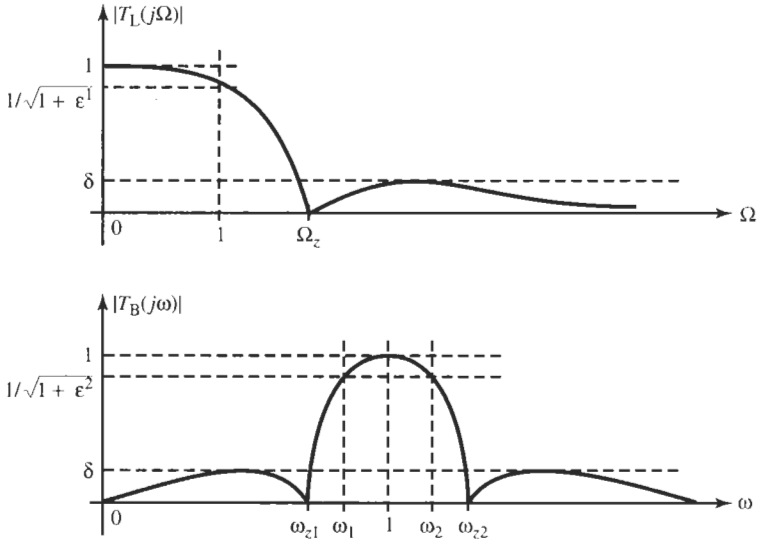

Figure 9.12 A lowpass with a finite transmission zero transformed into a bandpass and vice versa. Only positive values of frequency are shown.

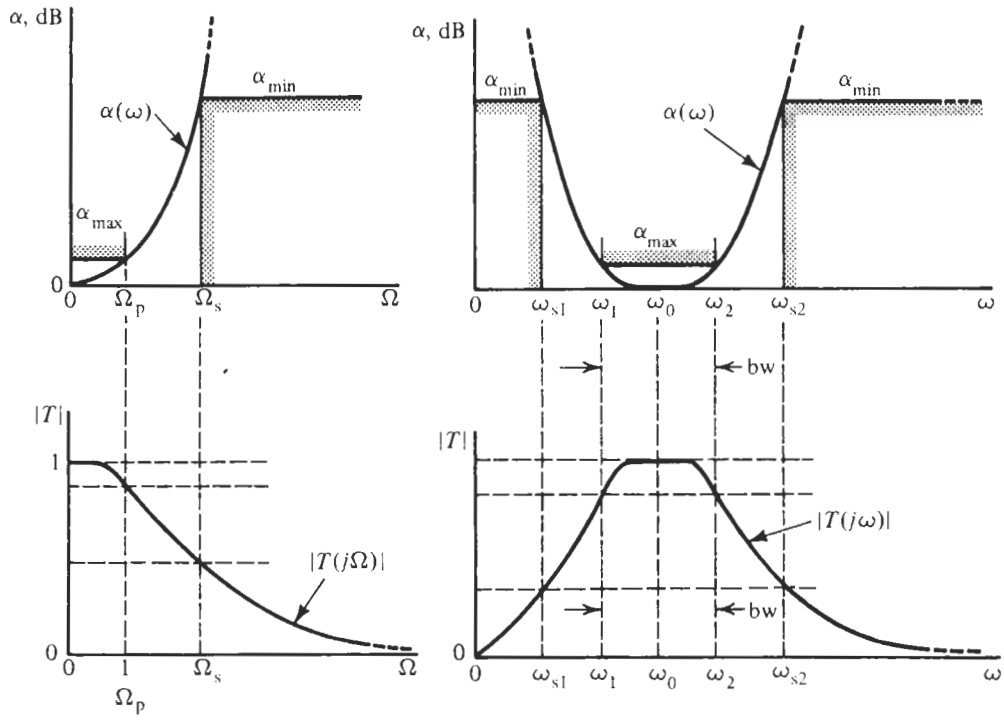

Figure 9.13 The relationship between parameters and variables in the lowpass-to-bandpass transformation. The lowpass characteristic (left) is converted into the bandpass characteristic (right) and vice versa.

1. Compute $\omega_0 = \sqrt{\omega_1 \omega_2}$ and $Q = \omega_0/(\omega_2 - \omega_1)$ from the specified bandwidth of the bandpass filter.
2. Divide the frequency axis of the bandpass frequency by ω_0 so that the center frequency of the bandpass filter is normalized to unity.
3. Use Eq. (9.18c), $\Omega = Q(\omega^2 - 1)/\omega$, to determine the stopband corner frequency of the prototype lowpass from the stopband corner of the bandpass: $\Omega_s = Q(\omega_s^2 - 1)/\omega_s$. If $\omega_{s1}\omega_{s2} = 1$ and α_{min} are the same in upper and lower stopbands, ω_{s1} and ω_{s2} result in the same value $|\Omega_s|$. If $\omega_{s1}\omega_{s2} \neq 1$ and α_{min} are different in upper and lower stopbands, perform this computation for both the upper and the lower stopband corners of the bandpass. Two values of Ω_s will result and Ω_s arising from the lower stopband corner will be negative; disregard the minus sign because $|T_L|$ is an even function.
4. If specified, calculate the transmission zeros Ω_{zi}, $i = 1, \ldots,$ of the lowpass prototype function, from those of the bandpass: $\Omega_{zi} = Q(\omega_{zi}^2 - 1)/\omega_{zi}$ (see Fig. 9.12).
5. Find the degree n of the lowpass filter required to meet the constraints $\alpha \leq \alpha_{max}$ in $0 \leq \Omega \leq 1$ and $\alpha \geq \alpha_{min}$ for $\Omega \geq \Omega_s$. Use Eq. (6.44) if a maximally flat passband is specified and Eq. (7.20) for an equal-ripple approximation. Use Fig. 8.16 for an elliptic approximation. If different values of α_{min} are specified for different values of Ω_s, take the one that results in the highest value of n, since one value n must satisfy all constraints.
6. Compute (or use tables to determine) the lowpass transfer function $T_L(S)$ as demonstrated in the previous three chapters.

7. Use Eq. (9.18c) to find the bandpass function $T_B(s)$ by replacing S by $Q(s^2 + 1)/s$ in $T_L(S)$.
8. Realize $T_B(s)$.

We will work through a couple of examples to illustrate the complete steps required in designing a bandpass, starting from specifications and ending with the circuit.

EXAMPLE 9.4

Design a bandpass filter to meet the following specifications:

Passband: 1-dB equal ripple in 12 kHz $\leq f \leq$ 36 kHz; the gain must be 0 dB

Stopbands: at least 30 dB in $f \leq f_{s1} = 4.8$ kHz and at least 25 dB in $f \geq f_{s2} =$ 72 kHz

Use LM741 opamps and realize the circuit with GIC sections. The largest signal expected in the application is 500 mV, the smallest about 20 mV; it is, therefore, important to pay attention to the dynamic range.

Solution

Let us follow the suggested eight steps to complete this problem. We first compute

$$f_0 = \sqrt{12 \times 36}\,\text{kHz} = 20.78\,\text{kHz} \qquad \text{and} \qquad Q_B = \frac{20.78}{36 - 12} = 0.8660$$

The *normalized* passband corners are then $f_1 = 0.5774$ and $f_2 = 1.7321$. Note that $f_1 f_2 = 1$. These two values transform into $\Omega = \pm 1$ on the lowpass frequency axis as can readily be verified. The stopband corners are at $\omega_{s1} = 0.2309$ and $\omega_{s2} = 3.4641$; note that their product is not equal to 1, i.e., they are not geometrically symmetrical. In the lowpass domain these frequencies become

$$\Omega_{s1} = Q(0.2309^2 - 1)/0.2309 = -3.55 \qquad \text{and} \qquad \Omega_{s2} = Q(3.4641^2 - 1)/3.4641 = 2.75$$

The lowpass problem we have at this point is depicted in Fig. 9.14. We are now at Step 5. From Eq. (7.20b) we have

$$n = \frac{\ln \sqrt{4\left(10^{0.1\alpha_{min}} - 1\right)/\left(10^{0.1\alpha_{max}} - 1\right)}}{\ln\left(\Omega_s + \sqrt{\Omega_s^2 - 1}\right)}$$

which for Ω_{s1} and Ω_{s2} gives

$$n_1 = \frac{\ln \sqrt{4\left(10^3 - 1\right)/\left(10^{0.1} - 1\right)}}{\ln\left(3.55 + \sqrt{3.55^2 - 1}\right)} = 2.49 \qquad \text{and}$$

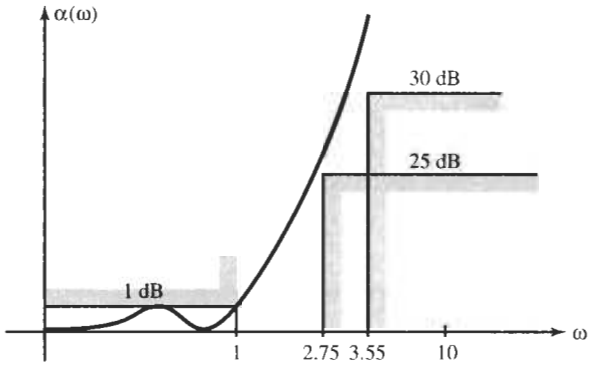

Figure 9.14 The lowpass prototype specification for Example 9.4. The gain function $\alpha(\omega)$ must clear both corners, (2.75, 25 dB) and (3.55, 30 dB), for the same value n. By design, $\alpha(\omega)$ always goes through the point (1, 1 dB) at the passband corner.

$$n_2 = \frac{\ln \sqrt{4\left(10^{2.5}-1\right)/\left(10^{0.1}-1\right)}}{\ln(2.75+\sqrt{2.75^2-1})} = 2.54$$

It follows that $n = 3$ meets both stopband constraints and is, therefore, the degree we must use for our design. The lowpass prototype function is obtained from Table 7.2:

$$T_L(S) = \frac{0.491}{(S+0.4941)\left(S^2+0.4941S+0.9942\right)}$$

where the numerator term 0.491 arises from the requirement that an odd-order Chebyshev filter at the origin has a gain of unity.

Next we use Eq. (9.18c) to find the bandpass function $T_B(s)$ by replacing S by $0.866(s^2+1)/s$. The first-order factor contributes the pole pair

$$0.866\frac{s^2+1}{s}+0.4941 \qquad \text{or} \qquad s^2+0.57055s+1$$

Similarly we obtain the remaining terms, using a root-finding program or the algorithm discussed previously. The result is

$$T_B(s) = \frac{0.756s^3}{\left(s^2+0.57055s+1\right)\left(s^2+0.42156s+2.92240\right)\left(s^2+0.14426s+0.34218\right)}$$

For a cascade filter, we factor the transfer function into three second-order bandpass sections,

$$T_B(s) = T_1T_2T_3 = \frac{k_1s}{s^2+0.57055s+1}\,\frac{k_2s}{s^2+0.42156s+2.92240}\,\frac{k_3s}{s^2+0.14426s+0.34218}$$

where $k_1k_2k_3 = K = 0.756$. We connect the three modules in the sequence $T_1T_2T_3$ in the order of increasing values of Q: $Q_1 = 1.753$, $Q_2 = 4.055$, $Q_3 = 4.055$. Note from the preceding discussion that the last two pole terms have the same quality factor as is expected from Eq. (9.30). We next need to evaluate the maxima of the intermediate transfer functions, Eq. (5.76). Using a mathematics package or manual evaluations we find

$$M_1 = \max|t_1(j\omega)| = \frac{1}{0.571} = 1.75, \quad M_2 = \max|t_1 t_2| \approx 1.92,$$

$$M_3 = \max|t_1 t_2 t_3| = \frac{1}{K} = 1.32$$

Then we have from Eqs. (5.78) and (5.80)

$$k_1 = K\frac{M_3}{M_1} = 0.756\frac{1.32}{1.75} = 0.57, \quad k_2 = \frac{M_1}{M_2} = \frac{1.75}{1.92} = 0.91, \quad k_3 = \frac{M_2}{M_3} = \frac{1.92}{1.32} = 1.45$$

For the filter implementation, GIC modules of Fig. 4.46b were prescribed. We may need to make use of the input voltage divider because our gain constants are not equal to 2. The circuit realizes

$$T(s) = \frac{2as\omega_0/Q}{s^2 + s\omega_0/Q + \omega_0^2}$$

with $\omega_0 = 1/(RC)$. In Fig. 4.46b we labeled $C_1 = C_2 = C$, $R_1 = R_3 = R_4 = R_5 = R_0$, and $R = QR_0$. Let us choose $C = 1$ nF. Then we obtain for T_1:

$$T_1(s) = \frac{2as\omega_{01}/Q_1}{s^2 + s\omega_{01}/Q_1 + \omega_{01}^2} = \frac{k_1 s}{s^2 + 0.57055s + 1}$$

Since $\omega_{01} = 2\pi \times 20780$ rad/s $= 130.57$ krad/s and $Q_1 = 1.753$, we have

$$R = 1/(\omega_{01}C) = 1/\left(130.57 \times 10^{-6}\right)\Omega = 7.66\ \text{k}\Omega,$$

$$Q_1 R_0 = 1.753 \times 7.66\ \text{k}\Omega = 13.45\ \text{k}\Omega$$

and

$$a = \frac{k_1}{2 \times 0.571} = 0.50$$

Similarly for Module 2,

$$T_2(s) = \frac{2as\omega_{02}/Q_2}{s^2 + s\omega_{02}/Q_2 + \omega_{02}^2} = \frac{k_2 s}{s^2 + 0.42156s + 2.92240}$$

with $\omega_{02} = 2\pi\sqrt{2.9224} \times 20780$ rad/s $= 223.2$ krad/s and $Q_2 = 4.055$

$$R = 1/\left(223.2 \times 10^{-6}\right)\Omega = 4.48\ \text{k}\Omega$$

$$Q_2 R_0 = 4.055 \times 4.48\ \text{k}\Omega = 18.17\ \text{k}\Omega$$

and

$$a = \frac{k_2}{2 \times 0.42156} = 1.08$$

Of course, we must have $a \leq 1$. Let us for simplicity set $a = 1$ and accept an 8% gain error. Finally, for Module 3,

$$T_3(s) = \frac{2as\omega_{03}/Q_3}{s^2 + s\omega_{03}/Q_3 + \omega_{03}^2} = \frac{k_3 s}{s^2 + 0.14426s + 0.34218}$$

with $\omega_{03} = 2\pi\sqrt{0.34218} \times 20780$ rad/s $= 76.375$ krad/s and $Q_3 = 4.055$,

$$R = 1/\left(76.375 \times 10^{-6}\right)\Omega = 13.09\ \text{k}\Omega$$

$$Q_3 R_0 = 53.1\ \text{k}\Omega$$

$$a = \frac{k_3}{2 \times 0.14426} = 5.02$$

We have now several options concerning dynamic range in completing the design. Let us discuss the alternatives in some detail to illustrate the trade-offs the filter designer has to face. Since positive components require $a \leq 1$, we can set $a = 1$ and accept unequal signal levels in the filter. $a = 1$ results in $k_3 = 0.1443 \times 2 = 0.2886$ rather than $k_3 = 1.45$, for a 14-dB difference in signal level between Module 3 and Modules 1 and 2. This would bring the smallest signals throughout the passband to 20 mV/5 = 4 mV, uncomfortably close to the noise level. We can elect to deviate from the optimal gain $H = 2$ of the GIC filter stage, design Module 3 for a gain of five, and accept the less than optimal performance as discussed in Section 4.5.3. This is not a good option. In addition, if 0-dB passband gain is a firm requirement, there is always the possibility of adding a finite-gain amplifier to the cascade at the input of Module 3, at the cost of an additional opamp and two resistors. This amplifier simply multiplies the voltage at the output of Section 2 by five (14 dB) and thereby raises the output of the total filter gain to the required 0 dB. A difficulty in this choice is that the output of Section 2 has its maximum voltage at the 0-dB level so that the opamp of the gain stage sees a maximum voltage of five times 500 mV. By Eq. (2.27), 2.5 V at 40 kHz is just below the slew rate of 741-type opamps so that no distortion problems should occur over the entire passband.

To decide between the three choices requires some engineering judgment: The 14-dB gain error in the filter reduces the dynamic range by 14 dB because the signals in Section 3 are that much closer to the noise level. Deviating from $H = 2$ causes errors frequency and Q that should be avoided. Since we need three second-order GIC sections, six opamps are required; a likely implementation will use two quad-opamp chips with two opamps to spare. Therefore, the cost of an additional opamp will be negligible, and that is the design choice we make. The amplifier we use is the noninverting stage of Fig. 2.11 with $R_1 = 1\ \text{k}\Omega$ and $R_2 = 4.2\ \text{k}\Omega$ for the required gain of $1.45/0.2886 \approx 5$. This step equalizes the signal levels throughout the filter at 0 dB, except that we are accepting that the opamp of the 14-dB gain stage has an output voltage larger than that of the remaining opamps in the filter by 14 dB. In principle, this amplifier with flat (frequency-independent) gain of five could be placed anywhere in the cascade; the difference between the smallest and largest voltage will always be 14 dB as long as we wish to retain the optimal design of the GIC stage with $H = 2$.

Figure 9.15 shows the circuit and test performance. All specified requirements are met, as the passband detail (Fig. 9.15b) and overall response curves (Fig. 9.15c) demonstrate. The passband gain is at 0 dB; the ripple is measured at 0.9 dB. The response curves at the outputs of the three modules have their maxima at 0 dB and the gain stage has a maximum at +14 dB as is shown in the simulation plots in Fig. 9.15d.

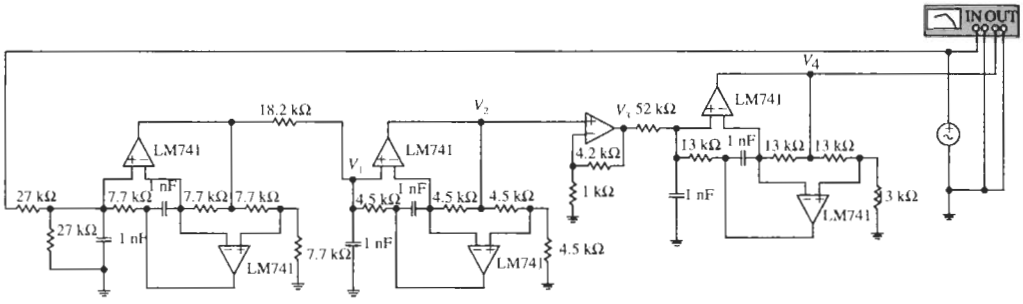

(a)

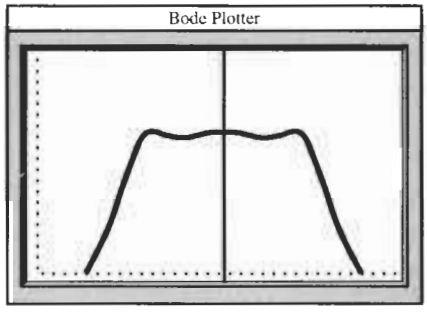

(b)

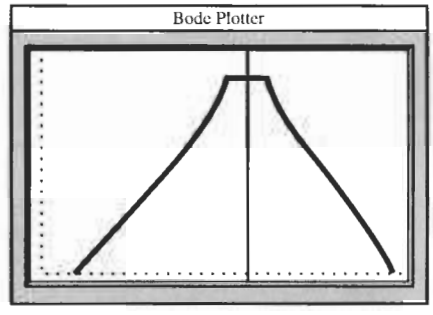

(c)

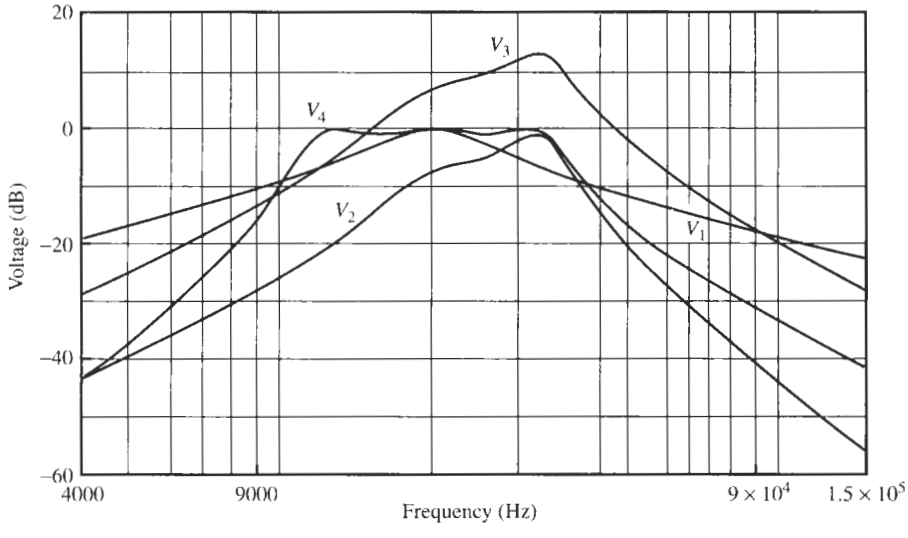

(d)

Figure 9.15 Circuit and test performance for Example 9.4: (a) filter circuit; (b) passband detail; (c) overall performance; (d) simulated responses at the section and amplifier outputs. [Bode Plotter scales: (b) 6 to 60 kHz; −20 to 10 dB; cursor at 20.32 kHz, 0.019 dB; (c) 100 Hz to 1 MHz; −120 to 10 dB; cursor at 20.89 kHz, 0.465 dB.]

The following example illustrates how bandpass transmission zeros are transformed into the lowpass domain where we know how to handle typical specifications, such as degree and type of function.

EXAMPLE 9.5

A bandpass filter is needed with a 3-dB passband in 35 kHz $\leq f \leq$ 85 kHz. There are strong interference signals at 14 and 200 kHz that must be attenuated by a minimum of 40 dB. As these are very close to the specified passband and would necessitate an expensive and hard to design high-order filter, it is proposed to increase the roll-off by employing transmission zeros near $f_{z1} = 14$ kHz and $f_{z2} = 200$ kHz. To keep costs down, low values of quality factor are desired: a maximally flat transfer function magnitude in the passband should be used. The degree $n = 6$ is known to provide adequate attenuation in the stopband. Design the filter.

Solution

We start by computing $f_0 = \sqrt{35 \times 85}$ kHz $= 54.544$ kHz and $Q = 54.544/50 = 1.091$. The two transmission zeros are then at $f_{z1} = 14/54.544 = 0.2567$ and $f_{z2} = 200/54.544 = 3.667$. In the lowpass domain, the transmission zeros are at

$$\Omega_{z1} = Q\frac{\omega_{z1}^2 - 1}{\omega_{z1}} = 1.09\frac{0.2567^2 - 1}{0.2567} = -3.9664 \quad \text{and} \quad \Omega_{z2} = 1.09\frac{3.667^2 - 1}{3.667} = 3.700$$

As mentioned previously, we may disregard the minus sign because magnitude functions are even. Since the values of $|\Omega_{z1}|$ and Ω_{z2} are very close and the problem states that transmission zeros *near* these points are needed, we simplify the design by choosing in the lowpass prototype only *one* zero at $\Omega_z = 3.8$. By Eq. (9.38), in the bandpass this zero translates into the two values

$$\omega_{z1,2} = \sqrt{\frac{3.8^2}{4 \times 1.09^2} + 1} \mp \frac{3.8}{2 \times 1.09} \approx 0.27, 3.75 \tag{9.39}$$

corresponding to 14.7 and 204 kHz, certainly close enough to the specifications.

To determine mathematically the form of the transfer function with maximally flat magnitude and one transmission zero, we now go to the lowpass domain where we know how to approach the problem. According to our discussion in Section 6.5, Eq. (6.53), a maximally flat lowpass function with $\alpha_{max} = 3$ dB and $n = 3$ (a sixth-order bandpass results in a third-order lowpass function) is obtained from

$$|T_L(j\Omega)|^2 = \frac{\left(\Omega^2 - 3.8^2\right)^2}{\left(\Omega^2 - 3.8^2\right)^2 + B_6\Omega^6}$$

where B_6 is determined so that $|T_L(j\Omega)|^2 = 0.5$ at the passband corner $\Omega = 1$. We get $B_6 = (1 - 3.8^2)^2 = 180.63$. Thus, after replacing Ω by S/j the expression becomes

$$T_L(S)T_L(-S) = \frac{\left(S^2 + 3.8^2\right)^2}{\left(S^2 + 3.8^2\right)^2 - 180.63S^6}$$

Using a root finder, the equation can be factored as:

$$T_L(S) = \frac{0.0196\left(S^2 + 3.8^2\right)}{(S + 0.7445)\left(S^2 + 0.4592S + 0.3798\right)}$$

The coefficient 0.0196 is inserted to make $T_L(0) = 1$. Next we use the lowpass-to-bandpass transformation to establish the transfer function that we need to realize. Using Eq. (9.18c) in $T(S)$, we obtain

$$T_B(s) = \frac{0.0196\left[\left(1.091\dfrac{s^2+1}{s}\right)^2 + 3.8^2\right]}{\left(1.091\dfrac{s^2+1}{s} + 0.7445\right)\left[\left(1.091\dfrac{s^2+1}{s}\right)^2 + 0.4592\left(1.091\dfrac{s^2+1}{s}\right) + 0.3798\right]}$$

After a little algebra and with the help of a root finder, this results in

$$T_B(s) = \frac{0.01797s\left(s^4 + 14.1316s^2 + 1\right)}{\left(s^2 + 0.6824s + 1\right)\left(s^4 + 0.4209s^3 + 2.3191s^2 + 0.4209s + 1\right)}$$

$$= \frac{0.01797s\left(s^2 + 0.2667^2\right)\left(s^2 + 3.7497^2\right)}{\left(s^2 + 0.6824s + 1\right)\left(s^2 + 0.1568s + 0.5938\right)\left(s^2 + 0.2640s + 1.6839\right)}$$

Notice that the bandpass function is of order six, has one zero at the origin, one at infinity, and the others as specified in Eq. (9.39). For a three-module cascade circuit we again factor the function into

$$T_B(s) = T_1T_2T_3 = \frac{k_1 s}{s^2 + 0.6824s + 1}\,\frac{k_2\left(s^2 + 0.2667^2\right)}{s^2 + 0.1568s + 0.5938}\,\frac{k_3\left(s^2 + 3.7497^2\right)}{s^2 + 0.2640s + 1.6839}$$

where $k_1k_2k_3 = K = 0.018$. Each of the zeros is associated with the closest pole, and the modules are sequenced in the order of increasing Q values: $Q_1 = 1.47$, $Q_2 = Q_3 = 4.91$. Notice that $Q_2 = Q_3$ as expected. This completes the approximation problem, the bandpass transfer function $T_B(s)$ is known, and we may proceed with the design.

Next we need to find the gain constants: from T_1 we see directly that $M_1 = 1/0.68 \approx 1.47$. Also, since a total gain of 0 dB is prescribed, we have $M_3 = 1/(k_1k_2k_3) = 55.6$. To find M_2 we need to determine the maximum of $|t_1t_2|$. If suitable software is not available, we can estimate $M_2 \approx 5$ by evaluating the expression "a little to the right of" $\sqrt{0.59}$, i.e., moving toward the peak of T_1 and away from the peak value of T_2. Therefore, by Eqs. (5.78) and (5.80), the gain constants are

$$k_1 \approx 0.018 \times 55.6/1.47 \approx 0.68, \quad k_2 \approx 1.47/5 \approx 0.294, \quad \text{and} \quad k_3 \approx 5/55.6 \approx 0.09$$

Let us implement this filter also with GIC biquads, one bandpass section as in Fig. 4.46b and two sections with transmission zeros. That circuit was introduced in Fig. 5.16 and realizes the function in Eq. (5.36):

$$T(s) = \frac{V_2}{V_1} = \frac{s^2(2a - c) + s\,(\omega_0/Q)\,(2b - c) + c\omega_0^2}{s^2 + s\omega_0/Q + \omega_0^2} \tag{9.40}$$

where $\omega_0 = 1/(RC)$ and all other parameters are defined in Fig. 5.16. The bandpass module T_1 must realize

$$T_1(s) = \frac{2as\omega_0/Q}{s^2 + s\omega_0/Q + \omega_0^2} \Rightarrow \frac{0.68s}{s^2 + 0.6824s + 1}$$

with $\omega_{01} = 342.71$ krad/s and $Q_1 = 1.47$. Choosing $C = 1$ nF, we obtain the element values

$$R = 1/(342.71 \text{ krad/s} \times 1 \text{ nF}) = 2.918 \text{ k}\Omega \quad \text{and} \quad QR = 4.29 \text{ k}\Omega$$

Also, since the gain constant equals 0.68, we have $2a = 0.68/0.682$ or $a \approx 1/2$. Modules 2 and 3 have transmission zeros that require from Eq. (9.40) that $c = 2b$; the function is, therefore,

$$T(s) = \frac{(2a - c)s^2 + c\omega_0^2}{s^2 + s\omega_0/Q + \omega_0^2}$$

In the following steps, remember that positive components require the parameters a, b, and c to be less than or at most equal to 1. To realize Module 2 we need

$$T_2(s) = \frac{(2a - c)s^2 + c\omega_0^2}{s^2 + s\omega_0/Q + \omega_0^2} \Rightarrow \frac{0.29\left(s^2 + 0.2667^2\right)}{s^2 + 0.1568s + 0.5938}$$

With $C = 1$ nF, $\omega_{02} = \sqrt{0.594}\omega_0 = 264.1$ krad/s, and $Q_2 = 4.91$, we calculate

$$R = 1/(264.1 \text{ krad/s} \times 1 \text{ nF}) = 3.786 \text{ k}\Omega \quad \text{and} \quad QR = 18.59 \text{ k}\Omega$$

Because a, b, and $c \leq 1$, we compute the parameters as follows: To establish the position of the zero we require from the value $T_2(0)$

$$\frac{c}{2a - c} = \frac{0.2667^2}{0.5938} = 0.120, \quad \text{i.e.,} \quad 1.12c = 0.24a$$

also $2a - c = 0.294$. These two equations have the solutions

$$a = 0.165, \quad c = 0.035, \quad \text{and} \quad b = c/2 = 0.0175$$

Lastly, we find for Module 3,

$$T_3(s) = \frac{(2a - c)s^2 + c\omega_0^2}{s^2 + s\omega_0/Q + \omega_0^2} \Rightarrow \frac{0.09\left(s^2 + 3.7497^2\right)}{s^2 + 0.2640s + 1.6839}$$

with $\omega_{03} = 444.7$ krad/s and $Q_3 = 4.91$. As before, we compute

$$R = 1/(444.7 \text{ krad/s} \times 1\text{nF}) = 2.248 \text{ k}\Omega \quad \text{and} \quad QR = 11.04 \text{ k}\Omega$$

For the remaining parameters we obtain:

$$\frac{c}{2a - c} = \frac{3.7497^2}{1.6839} = 8.350 \quad \text{or} \quad 9.35c = 16.7a$$

to establish the position of the zero. In addition $2a - c = 0.09$ must be satisfied. These two equations have no roots that are ≤ 1. So we choose the maximum for c, $c = 1$, and obtain $a = 0.56$ and $b = c/2 = 0.5$. This choice gives an error in filter gain of $\approx +2.5$ dB $[(2a - c)/0.09 = 0.12/0.09 = 1.33]$. With this computation, all components are determined and the final circuit is shown in Fig. 9.16a.

It is of interest to study the performance of this circuit more carefully to gain further insight into the performance of cascade designs. We see that the filter behaves essentially as desired. The 3-dB passband is in 37 kHz $\leq f \leq$ 76 kHz, close to but somewhat narrower than the specification, and the stopband attenuation at the critical frequencies (14 and 200 kHz) is larger than 45 dB. Notice on the network analyzer ("Bode Plotter," Fig. 9.16b) in the circuit with "real" components that the zero at lower frequencies, 14 kHz, is realized correctly, but

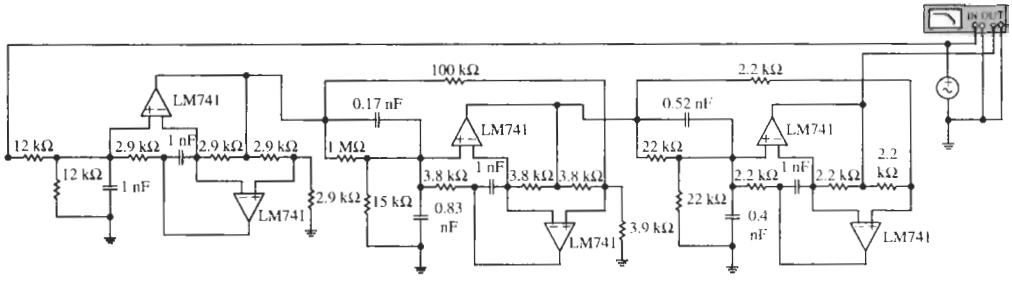

(a)

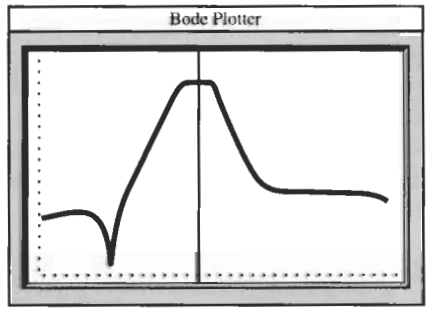

(b)

Figure 9.16 Circuit and test results for Example 9.5; (a) final circuit; (b) test response; (c) simulation results. (Bode Plotter scales: 5 kHz to 1 MHz; −80 to 10 dB; cursor at 54.40 kHz, 0.693 dB.)

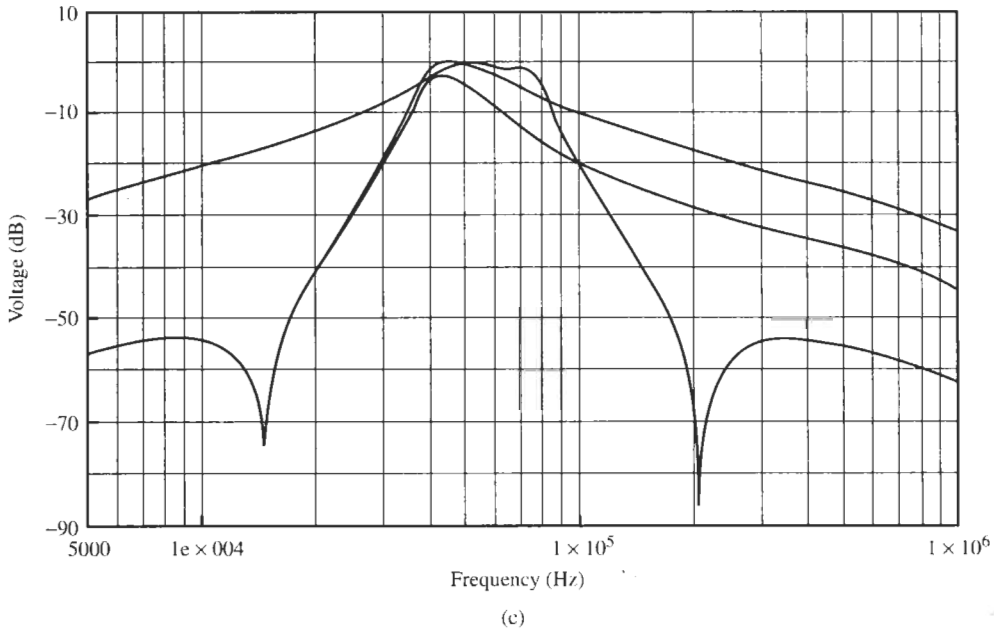

Figure 9.16 Continued

the one at 200 kHz appears absent. Nevertheless, the attenuation is adequately high for our purpose. We note that there is no error in our design. We based the design on ideal opamps and *if ideal opamps are used* in the *third* module that realizes the 200-kHz transmission zero, the zero at 204 kHz is indeed present. This is demonstrated readily by simulating the circuit (Fig. 9.16c) where the opamps in the third module are replaced by ideal ones. In this figure we also show the outputs of the first and second module to verify that their maximum values differ by less than 1.5 dB: Dynamic range maximization was performed correctly. Evidently, the *real* opamps caused the quality factor of the transmission zero at 200 kHz to be so low that the zero is effectively absent. This should have come as no great surprise because, as the student may by now expect, 200 kHz is too high a frequency range to be realized accurately with 741-type opamps. Lastly, we note the effect of the values of Q_1, Q_2, and Q_3. As is clear from the design and is verified by the simulation in Fig. 9.16c, the second and third sections with their peaking responses ($Q_2 = Q_3 = 4.91$) set the transfer function level at the band edges, whereas the first section "fills in" the center of the passband. Recognizing this behavior makes it obvious how to fine-tune the response, if needed. For instance, initial testing showed that the passband was insufficiently flat; it had peaks at the corners and a valley in the center. A simple increase of the Q-setting resistor of Module 1 from the computed 4.29 to 6 kΩ (split in Fig. 9.16a into two 12-kΩ resistors in parallel) flattened out the passband response (Fig. 9.16b).

9.3 LOWPASS-TO-BAND-ELIMINATION TRANSFORMATION

We will next investigate how a lowpass function can be transformed into a *band-elimination* function, also referred to as *bandstop* or *band-rejection* function. A band-rejection filter has a transfer characteristic as sketched in Fig. 9.17. In contrast to bandpass filters where signal components in a limited frequency range were to be preserved and all others rejected, a band-

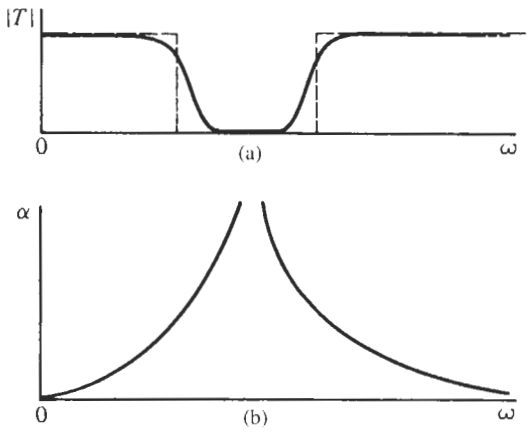

Figure 9.17 (a) Transfer characteristic and (b) attenuation of a bandstop filter.

elimination filter is designed to have high attenuation for the signals in a given frequency range, but transmit all others with no or minimal loss. Examples for the need of bandstop filters are shown in Fig. 9.18, where a bandstop filter is used to remove an intermediate frequency, leaving intact all others (Fig. 9.18a) and for cleaning an electrocardiogram signal from 60-Hz interference (Fig. 9.18b).

Similar to our approach in the previous two sections, we are looking for a transformation equation $\Omega = X(\omega)$ that converts the lowpass into a band-elimination function,

$$|T_L(j\Omega)| = |T_L(jX(\omega)| = |T_{BE}(j\omega)|$$

Specifically, we convert again the passband and stopbands of the lowpass function into the passbands and stopbands of the band-rejection function. We do this along the whole frequency axis from minus to plus infinity, keeping in mind that the functions are even. The diagram of the two filter types in Fig. 9.19 will help our understanding of the needed conversion. The figure shows the lowpass magnitude in $-\infty \leq \Omega \leq +\infty$ and the band-elimination magnitude in $-\infty \leq \omega \leq +\infty$. We have identified passbands, transition bands, and stopbands, and as always have normalized the lowpass passband to lie in $-1 \leq \Omega \leq +1$. The passbands of the band-elimination filter (for positive frequencies) are in the ranges $0 \leq \omega \leq \omega_1$ and $\omega_2 \leq \omega \leq \infty$. Similar to our earlier sketches, we show in Fig. 9.20 the

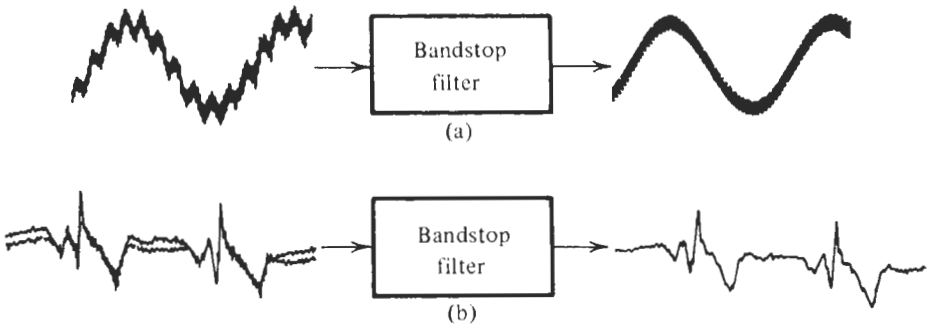

Figure 9.18 (a) Elimination of an intermediate frequency from a signal; (b) cleaning an electrocardiogram from 60-Hz noise.

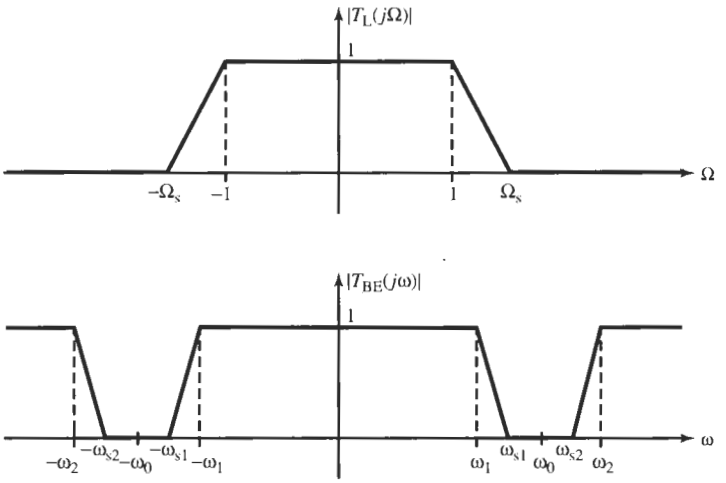

Figure 9.19 The positions of lowpass and band-elimination responses on the frequency axes.

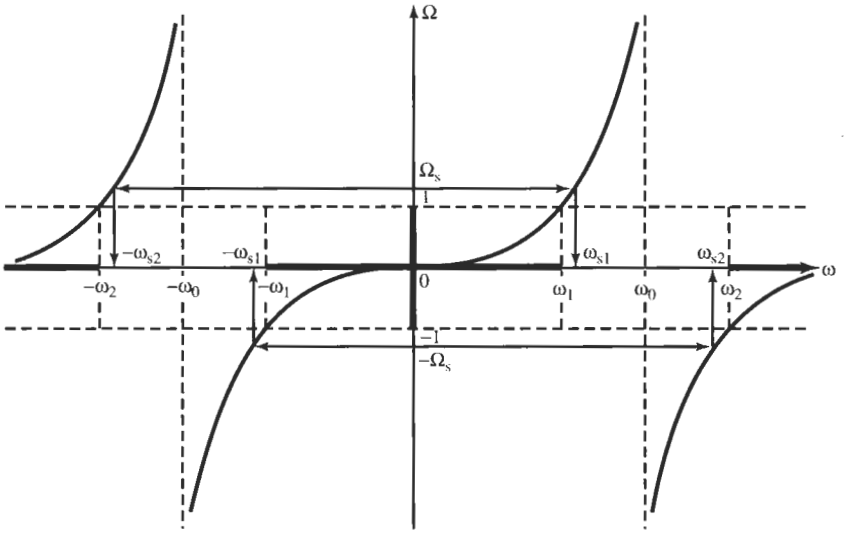

Figure 9.20 The function $X(\omega)$ to convert a lowpass magnitude into a bandstop magnitude.

function $X = \Omega(\omega)$ with the passbands identified on both axes by thick line segments. The function X is readily computed if we recall from our earlier discussion that $X(\omega)$ should have a zero in the center of each passband and a pole in the center of each stopband of the target band-elimination filter. Thus, as Fig. 9.20 indicates, we should have zeros of $X(\omega)$ at $\omega = 0$ and at $\omega = \infty$ and poles at frequencies labeled $\omega = \pm\omega_0$. Such a function is

$$\Omega = X(\omega) = -B\frac{\omega}{(\omega - \omega_0)(\omega + \omega_0)} = -B\frac{\omega}{\omega^2 - \omega_0^2} \tag{9.41}$$

It has the required poles at $\omega = \pm\omega_0$ and is zero at $\omega = 0$ and $\omega = \infty$. As in the bandpass case, we have introduced a multiplying constant, labeled B, to be able to adjust the slope of the function. Now observe from the sketch in Fig. 9.20 that $X(\omega)$ transforms the corner of the lowpass passband, $\Omega = 1$, into the two values $\omega = \omega_1$ and $\omega = -\omega_2$ that specify the corners of the passbands in the band-elimination filter. Thus setting $\Omega = 1$ in Eq. (9.41), we obtain the quadratic equation

$$\omega^2 + B\omega - \omega_0^2 = 0 \tag{9.42}$$

which has the solutions ω_1 and $-\omega_2$, i.e.,

$$(\omega - \omega_1)(\omega + \omega_2) = \omega^2 + (\omega_2 - \omega_1)\omega - \omega_1\omega_2 = 0 \tag{9.43}$$

Proceeding as we did for the bandpass case, we compare Eqs. (9.42) and (9.43) and identify the quantities

$$\omega_0^2 = \omega_1\omega_2 \quad \text{and} \quad B = \omega_2 - \omega_1 \tag{9.44}$$

The parameter B is the difference between the two passband corners of the band-rejection filter and ω_0 is recognized as the geometric mean of the two band edges. Next we multiply Eq. (9.41) by j to extend the validity of the expression from the imaginary axis into the complex plane:

$$j\Omega = jX(\omega) = -jB\frac{\omega}{\omega^2 - \omega_0^2} = B\frac{j\omega}{-\omega^2 + \omega_0^2} \tag{9.45}$$

With $S = j\Omega$ and $s = j\omega$, Eq. (9.45) can be rewritten as

$$S = Z(s) = B\frac{s}{s^2 + \omega_0^2} = \frac{B}{\omega_0}\frac{\omega_0 s}{s^2 + \omega_0^2} = \frac{1}{Q}\left(\frac{1}{s/\omega_0 + \omega_0/s}\right) \tag{9.46a}$$

As is customary, this becomes

$$S = Z(s) = \frac{1}{Q}\frac{s}{s^2 + 1} = \frac{1}{Q}\left(\frac{1}{s + 1/s}\right) \tag{9.46b}$$

when the bandstop frequency s is normalized with respect to $\omega_0 = \sqrt{\omega_1\omega_2}$. We shall refer to the quantity Q,

$$Q = \frac{\omega_0}{B} = \frac{1}{\omega_2/\omega_0 - \omega_1/\omega_0} \tag{9.47}$$

again as the *quality factor* of the band-elimination filter, although this definition is no longer intuitively meaningful because ω_0 is in the center of the stopband in this filter and $\omega_2 - \omega_1$ is the difference of the two passbands corners.[1] Nevertheless, Q tells us how narrow a band of

[1] The *pass*band "bandwidth" in a band-rejection filter is really infinite because the passband extends from ω_2 through infinity to $-\omega_2$ and then from $-\omega_1$ to $+\omega_1$.

frequencies, $\omega_2 - \omega_1$, the filter eliminates around the frequency ω_0: the higher Q the narrower the band over which the attenuation is large. Figure 9.21 illustrates the meaning of Q in a bandstop filter.

Equation (9.46) is the lowpass-to-bandstop transformation we were seeking. Note that it is the reciprocal of the lowpass-to-bandpass transformation of Eq. (9.18). If we substitute Eq. (9.46) into a lowpass function $T_L(S)$ of order n we obtain a band-elimination function $T_{BE}(s)$ or order $2n$. It has $2n$ poles as discussed next, and n zero factors $(s^2 + 1)$:

$$T_L(S) = \frac{1}{n\text{th-order polynomial in } S} \Leftrightarrow T_{BE}(s) = \frac{(s^2+1)^n}{2n\text{th-order polynomial in } s} \tag{9.48}$$

In Fig. 9.22 we have sketched the transformation for the case $n = 3$.

The pole locations of the bandstop function derived from a given lowpass are computed in a manner analogous to the one we discussed for the bandpass. For a first-order lowpass,

$$T_L(S) = \frac{1}{S + \Sigma_1} \tag{9.49}$$

we get with Eq. (9.46b) the denominator of the band-elimination function

$$S + \Sigma_1 = \frac{1}{Q}\frac{s}{s^2+1} + \Sigma_1 = 0 \tag{9.50}$$

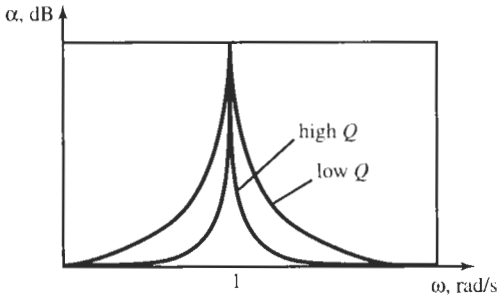

Figure 9.21 The meaning of Q in band-rejection filters.

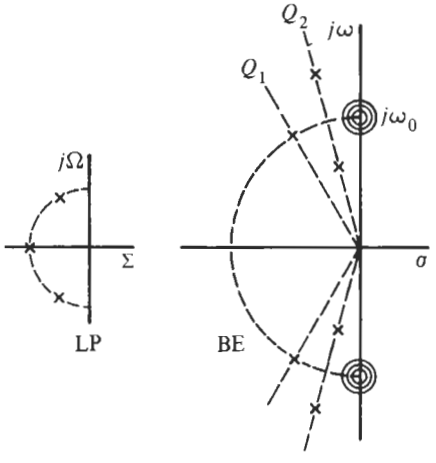

Figure 9.22 Poles and zeros of a sixth-order band-elimination filter obtained from a third-order lowpass. Notice that all transmission zeros are located at the same frequency, ω_0. As in the bandpass case, a negative real pole becomes normally a complex pole pair, and the two pole frequencies generated from a lowpass pole pair are the reciprocal of each other, Eq. (9.58), and the pole pairs have the same Q factor, Eq. (9.59).

It has roots where

$$s^2 + \frac{1}{Q\Sigma_1}s + 1 = 0 \tag{9.51}$$

that is, the negative real pole at $S = -\Sigma_1$ is converted to the two poles

$$p_1, p_2 = -\frac{1}{2Q\Sigma_1} \pm j\sqrt{1 - \left(\frac{1}{2Q\Sigma_1}\right)^2} \tag{9.52}$$

as is shown in Fig. 9.22 where we assumed that $2\Sigma_1 Q > 1$, so that the poles are complex. The first-order lowpass of Eq. (9.49) becomes a second-order band-elimination or notch filter

$$T_{BE}(s) = \frac{1}{(1/Q)s/(s^2+1) + \Sigma_1} = \frac{(1/\Sigma_1)(s^2+1)}{s^2 + s/(\Sigma_1 Q) + 1} \tag{9.53}$$

Similar to the bandpass case shown in Fig. 9.11 a real pole is transformed to a pair of conjugate complex poles. In addition, a pair of $j\omega$-axis transmission zeros is created. We can realize the second-order notch sections of Eq. (9.53) with the notch filters we discussed in Chapter 5 (see Table 5.1). Figure 9.23 reminds us of the shape of the magnitude of a notch filter.

More important is the case of complex poles in the lowpass function:

$$T_L(S) = \frac{1}{S^2 + aS + b} \tag{9.54}$$

With Eq. (9.46) it leads to the equation

$$\left(\frac{1}{Q}\frac{s}{s^2+1}\right)^2 + a\frac{1}{Q}\frac{s}{s^2+1} + b = 0 \tag{9.55}$$

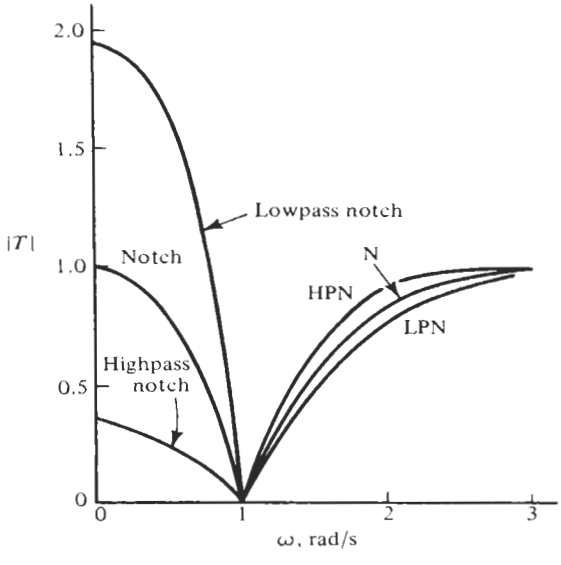

Figure 9.23 Magnitudes of second-order notch, lowpass notch, and highpass notch filters. As a rule, all three kinds of notch modules are needed in the design of band-elimination filters.

for the poles of the band-rejection filter. As in the bandpass case, they are determined from a fourth-order polynomial,

$$s^4 + \frac{a}{bQ}s^3 + \left(2 + \frac{1}{bQ^2}\right)s^2 + \frac{a}{bQ}s + 1 = 0 \tag{9.56}$$

which can be factored by a suitable computer algorithm. Comparing this polynomial with that of the bandpass case, Eq. (9.25), we notice that the two expressions are of the same form. Closed-form solutions can, therefore, be obtained if we just replace the parameters a by a/b and b by $1/b$ in Eqs. (9.33) and (9.36). Thus, the lowpass function of Eq. (9.54) is transformed into a band-elimination function

$$T_{\mathrm{BE}}(s) = \frac{\frac{1}{b}\left(s^2 + 1\right)^2}{\left(s^2 + \frac{\omega_{01}}{q_1}s + \omega_{01}^2\right)\left(s^2 + \frac{\omega_{02}}{q_2}s + \omega_{02}^2\right)} \tag{9.57}$$

with

$$\omega_{01}\omega_{02} = 1, \quad \text{i.e.,} \quad \omega_{01} = \frac{1}{\omega_{02}} \tag{9.58}$$

and

$$q_1 = q_2 = q \tag{9.59}$$

as before; refer to Eq. (9.48) and Fig. 9.22. The pole frequencies are obtained from

$$\omega_{02} = \frac{aq}{2bQ} + \frac{1}{2}\sqrt{\frac{1}{bQ^2} - \frac{1}{q^2}} = \frac{1}{\omega_{01}} \tag{9.60}$$

with $q^2 \geq bQ$, and q is computed from

$$q^2 = \frac{bQ}{a}\left[\left(\frac{2bQ}{a} + \frac{1}{2aQ}\right) + \sqrt{\left(\frac{2bQ}{a} + \frac{1}{2aQ}\right)^2 - 1}\right] \tag{9.61}$$

For instance, in Example 9.3 we had $a = b = 1$; the lowpass $T_{\mathrm{L}}(S) = 1/(S^2 + S + 1)$ with $a = b = 1$ would, therefore, be transformed into the band-rejection function

$$T_{\mathrm{BE}}(s) = \frac{\left(s^2 + 1\right)^2}{s^4 + s^3 + 3s^2 + s + 1} \tag{9.62}$$

with the same poles as the bandpass in Eq. (9.37) but with transmission zeros at $\pm j1$.

To realize functions of the form of Eq. (9.57) requires both a lowpass notch and a highpass notch module. This can be seen from the fact that by Eq. (9.58) one of the two frequencies ω_{01} and ω_{02} is less than ω_0 resulting in a lowpass notch, LPN, where $\omega_{\mathrm{pole}} < \omega_0$, and the other is

larger than ω_0 requiring a highpass notch, HPN, where $\omega_{\text{pole}} > \omega_0$; see Fig. 9.23. For example, factoring Eq. (9.62) with the aid of Eqs. (9.58) to (9.61) or with the help of a computer routine results in

$$T_{\text{BE}}(s) = T_{\text{LPN}} T_{\text{HPN}} = \frac{s^2 + 1}{s^2 + 0.2968 + 0.4221} \frac{s^2 + 1}{s^2 + 0.7032 + 2.3691}$$

If the prototype lowpass function is odd, that is, it has one negative real pole as in Eq. (9.52), the resulting second-order module is a notch section as in Eq. (9.53) with $\omega_{\text{pole}} = \omega_0$. Thus, in general all three kinds of notch modules are needed for the design of band-elimination filters.

The lowpass-to-bandstop transformation can, of course, also be applied to lowpass functions with one or more finite transmission zeros $\pm j\Omega_{zi}$. Using Eq. (9.46), $\Omega_{zi} = -(\omega/Q)/(\omega^2 - 1)$, this zero is transformed into two zeros ω_{z1} and ω_{z2} on the $j\omega$-axis:

$$\omega^2 + \frac{\omega}{\Omega_{zi} Q} - 1 = (\omega - \omega_{z1})(\omega + \omega_{z2}) = 0$$

Note that $|\omega_{z1}\omega_{z2}| = 1$, which means that the two transformed zeros are geometrically symmetrical around $\omega_0 = 1$. Figure 9.24b illustrates how to transform such a case.

The sequence of steps used in designing a band-elimination filter with specified requirements by use of frequency transformation can be summarized as follows (refer also to Fig. 9.24).

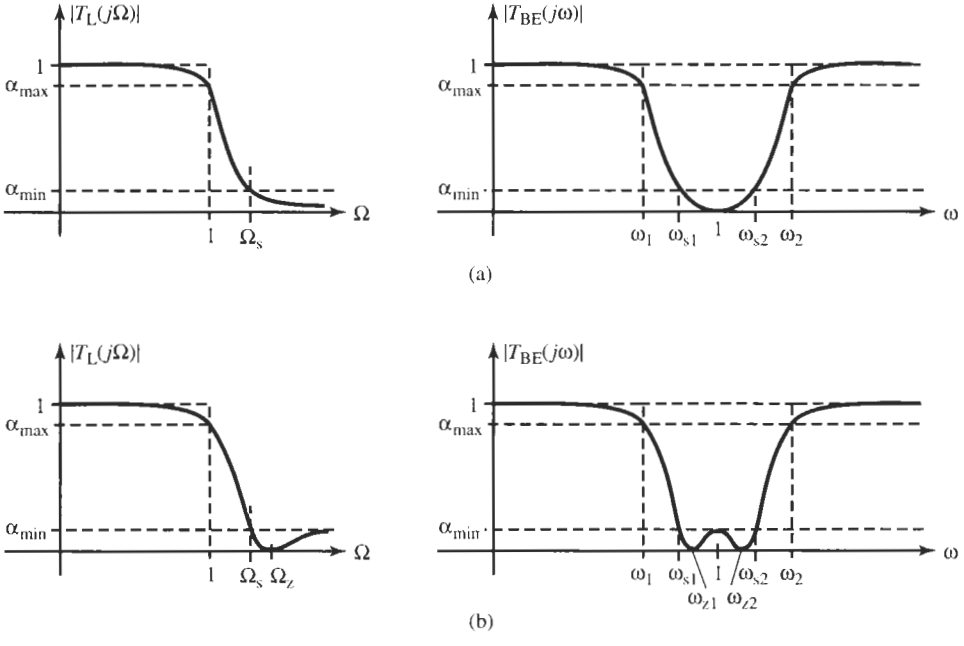

Figure 9.24 Relationship between the parameters of lowpass and band-elimination filters: (a) all-pole lowpass functions; (b) lowpass function with a finite transmission zero. Only positive values of frequency are shown.

1. Compute $\omega_0 = \sqrt{\omega_1 \omega_2}$ and $Q = \omega_0/(\omega_2 - \omega_1)$ from the specifications of the band-elimination filter.
2. Divide the frequency axis of the band-elimination filter by ω_0 so that the frequency in the center of the stopband of the filter is normalized to 1.
3. Use Eq. (9.46b), $\Omega = -(\omega/Q)/(\omega^2 - 1)$, to determine the stopband corner frequency of the prototype lowpass from the stopband corners of the band-elimination filter: $\Omega_s = -(\omega_s/Q)/(\omega_s^2 - 1)$. If $\omega_{s1}\omega_{s2} = 1$ and α_{min} is the same in upper and lower stopbands, ω_{s1} and ω_{s2} result in the same value $|\Omega_s|$. If $\omega_{s1}\omega_{s2} \neq 1$ and α_{min} is different in upper and lower stopbands, perform this computation for both the upper and the lower stopband corners of the band-rejection filter. Two values of Ω_s will result and Ω_s arising from the lower stopband corner will be negative; disregard the minus sign because $|T_L|$ is an even function.
4. If specified, calculate the transmission zeros Ω_{zi}, $i = 1, \ldots,$ of the lowpass prototype function, from those of the bandstop filter: $\Omega_{zi} = -(\omega_{zi}/Q)/(\omega_{zi}^2 - 1)$.
5. Find the required degree n of the lowpass filter to meet the constraints $\alpha \leq \alpha_{max}$ in $0 \leq \Omega \leq 1$ and $\alpha \geq \alpha_{min}$ for $\Omega \geq \Omega_s$. For elliptic filters, consult Fig. 8.16. Use Eq. (6.44) if a maximally flat passband is specified and Eq. (7.20) for an equal-ripple approximation. If different values of α_{min} are specified for different values of Ω_s, take the one that results in the highest value of n, since one value n must satisfy all constraints.
6. Compute (or use tables to determine) the lowpass transfer function $T_L(S)$ as demonstrated in the previous three chapters.
7. Use Eq. (9.46) to find the band-elimination function $T_{BE}(s)$ by replacing in $T_L(S)$ S by $(s/Q)/(s^2 + 1)$.
8. Realize $T_{BE}(s)$.

The following example will guide us through a complete design process for a band-rejection filter:

EXAMPLE 9.6

We wish to design a bandstop filter with the following specifications:

Maximally flat passbands in $0 \leq f \leq 3.6$ kHz and 9.1 kHz $\leq f < \infty$;

Passband gain equal to 0 dB; $\alpha_{max} = 1.5$ dB; and

Stopband in 5.45 kHz $\leq f \leq 5.90$ kHz; $\alpha_{min} = 38$ dB.

Solution

We compute $f_0 = \sqrt{3.6 \times 9.1}$ kHz $= 5.724$ kHz and $\sqrt{f_{s1} f_{s2}} = \sqrt{5.45 \times 5.90}$ kHz $= 5.67$ kHz and observe that the specifications are nearly geometrically symmetrical. Also $Q = 5.724/(9.1 - 3.6) = 1.041$. The lowpass-to-bandstop transformation, Eq. (9.46), is then

$$S = \frac{1}{Q}\frac{1}{s + 1/s} = \frac{0.961}{s + 1/s} \tag{9.63}$$

or, on the imaginary axis, $\Omega = -0.961\omega/(\omega^2 - 1)$. We can verify that this equation transforms 3.6 kHz to -1 and 9.1 kHz to $+1$ on the Ω-axis. The lower stopband frequency, 5.45 kHz, is transformed into $\Omega = -9.79$, and 5.90 kHz goes into $\Omega = +15.85$. These prototype lowpass requirements are shown in Fig. 9.25.

Since a maximally flat passband is prescribed we compute n from Eq. (6.44):

$$n = \frac{\log[(10^{0.1\alpha_{\min}} - 1)/(10^{0.1\alpha_{\max}} - 1)]}{2 \log \omega_s} = \frac{\log[(10^{3.8} - 1)/(10^{0.15} - 1)]}{2 \log 9.79} = 2.11$$

The next larger integer value, $n = 3$, should be taken; however, since n is very close to two we will choose a trial design with $n = 2$ and see how the circuit performs.

A second-order Butterworth function is, from Table 6.2,

$$T_L(S) = \frac{1}{S^2 + \sqrt{2}S + 1} \tag{9.64}$$

where $\Omega = 1$ is the 3-dB frequency. Since the specified passband edge is, however, the 1.5-dB frequency, by Eq. (6.44) we need to scale Ω by

$$\varepsilon^{1/2} = (10^{0.15} - 1)^{1/4} = 0.8014$$

This gives the transformation, with Eq. (9.63),

$$\frac{S}{\sqrt{\varepsilon}} = \frac{S}{0.8014} = \frac{0.961}{s + 1/s} \quad \text{or} \quad S = \frac{0.770s}{s^2 + 1}$$

Substituting this expression into the second-order lowpass function, Eq. (9.64), and factoring the resulting fourth-order polynomial results in

$$T_{BE}(s) = T_1 T_2 = \frac{s^2 + 1}{s^2 + 0.6922s + 1.7452} \frac{s^2 + 1}{s^2 + 0.3966s + 0.5730} \tag{9.65}$$

Both quality factors are $q = 1.909$ so that we do not have to be concerned with section ordering or pole-zero assignment. Remember that s is normalized with respect to ω_0.

For the design of the two biquads let us use the four-amplifier Åckerberg–Mossberg circuit of Fig. 5.1, which realizes Eq. (5.5). For our case, the equation becomes

$$\frac{V_{out}}{V_1} = -\frac{s^2 + \omega_0^2(1 - c + d)}{s^2 + s\omega_0/q + \omega_0^2}$$

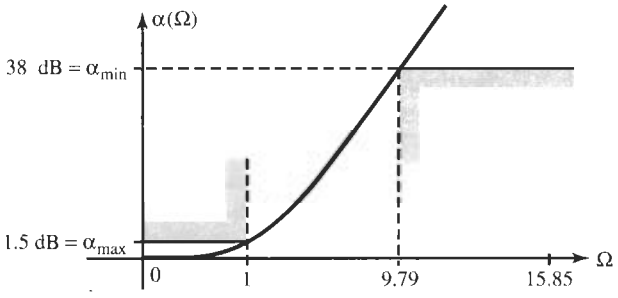

Figure 9.25 The prototype lowpass specifications for Example 9.6.

where we chose $a = k = 1$ and note that in the notation in this example the quality factor is q. To realize the transmission zero we also set $a - b(kq) = 1 - 1.909b = 0$ in Eq. (5.5) to give $b = 0.524$. All parameters were identified in Fig. 5.1 and $\omega_0 = 1/(RC)$. From Eq. (9.65) we find with $d = 0$,

$$T_1(s) = -\frac{s^2 + \omega_{01}^2(1-c)}{s^2 + s\omega_{01}/q + \omega_{01}^2} = -\frac{s^2 + \omega_0^2}{s^2 + 0.6922s\omega_0 + 1.7452\omega_0^2} \tag{9.66}$$

We have with $C = 10$ nF and $\omega_{01} = 2\pi \times \sqrt{1.7452} \times 5724$ rad/s $= 47.51$ krad/s

$$R = \frac{1}{\omega_{01}C} = 2.105\ \text{k}\Omega \quad \text{and} \quad QR = 1.909 \times 2.105\ \text{k}\Omega = 4.018\ \text{k}\Omega$$

Also, $1 - c = 1/1.745 = 0.573$ results in $c = 0.427$. Similarly, for T_2 we have

$$T_2(s) = -\frac{s^2 + \omega_{02}^2(1+d)}{s^2 + s\omega_{02}/q + \omega_{02}^2} = -\frac{s^2 + \omega_0^2}{s^2 + 0.3966s\omega_0 + 0.5730\omega_0^2} \tag{9.67}$$

where $c = 0$. With $C = 10$ nF and $\omega_{02} = 2\pi \times \sqrt{0.573} \times 5724$rad/s $= 27.22$ krad/s we find

$$R = \frac{1}{\omega_{02}C} = 3.673\ \text{k}\Omega \quad \text{and} \quad QR = 1.909 \times 3.673\ \text{k}\Omega = 7.012\ \text{k}\Omega$$

and $1 + d = 1/0.573 = 1.745$, that is, $d = 0.745$.

The circuit and its performance are shown in Fig. 9.26. The circuit behaves nearly as specified; the -1.5-dB points are 3.6 kHz (cursor) and 9.9 kHz, and the attenuation is ≥ 38 dB in 5.43 kHz $\leq f \leq$ 5.91 kHz (measured at higher resolution on the network analyzer). The transmission zero is at $f_0 = 5.67$ kHz and the passband gain is 0 dB. The gain begins to roll off at approximately 95 kHz due to finite opamp bandwidth. As expected, the stopband attenuation is nearly, but not quite, met because we chose $n = 2$ although "a degree of 2.11"

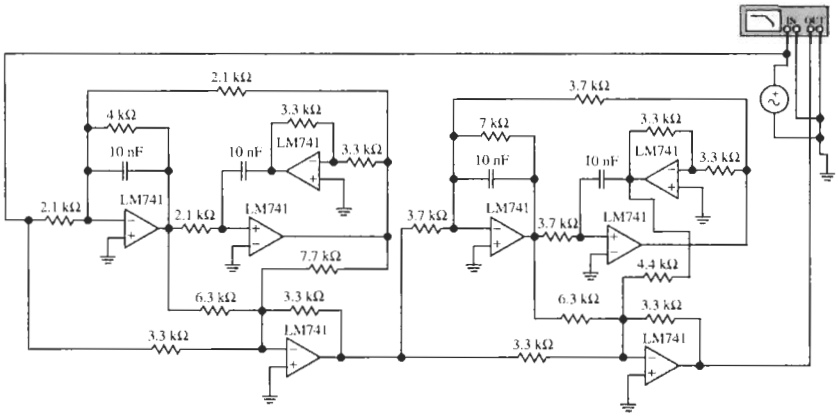

(a)

Figure 9.26 Design and test performance of the circuit of Example 9.6. (Bode Plotter scales: 1 to 200 kHz; −60 to 10 dB; cursor at 3.615 kHz, −1.547 dB.)

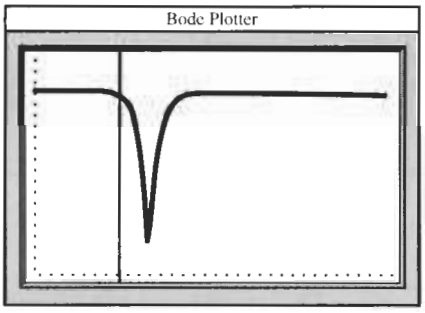

(b)

Figure 9.26 Continued

was required. We shall consider the circuit adequate because of the considerable cost savings: $n = 3$ would have required one additional biquad in the realization for a 50% higher cost!

The circuit in Example 9.6 we designed with no error margin for the rejection bandwidth. In practice, this approach is generally not recommended because unavoidable component tolerances will likely cause the manufactured circuit to deviate from the specified performance. For a practical design, we need to study the circuit and try to find ways to better its performance. In Problem P9.34, the reader is encouraged to demonstrate that the circuit can be improved and even a small error margin can be provided at no extra cost. It is necessary only to reduce the values of the 4.4-kΩ and 7.7-kΩ resistors in the circuit in Fig. 9.26 so that the two transmission zeros no longer coincide at $\omega = \omega_0$. This step broadens the rejection band, but also reduces its depth.

9.4 LOWPASS-TO-MULTIPLE PASSBAND TRANSFORMATION

Although the responses that we will most often need for the solution of filter design problems are those that we have considered thus far (lowpass, bandpass, highpass, bandstop), the concept of frequency transformation is more general. It can be applied to problems that meet more than the simple requirements of the cases treated earlier in this chapter, a single passband surrounded by stopbands. Rather, we may use the transformation to handle requirements of multiple passbands and stopbands. As in the previous cases, these are then referred to a lowpass where we know how to treat the approximation problem and derive a maximally flat, equal-ripple, or other type of transfer function.

Consider, for example, a requirement in which a band-elimination filter as discussed in the previous section must in addition strongly attenuate components at high frequencies to reduce the total noise power. In that case we need to have two passbands and two stopbands as is illustrated in Fig. 9.27. In general, we may have several passbands, all of which are, of course, separated by stopbands. Obviously, passbands and stopband always alternate along the frequency axis. Let us also suppose that all passbands have an identical attenuation requirement, namely the same passband gain, normalized to unity, i.e., 0 dB, and the same passband and stopband tolerances α_{max} and α_{min} as sketched in Fig. 9.27. Our task is then to determine a suitable transformation function $\Omega = X(\omega)$ that maps passbands and stopbands from the ω-axis onto passband and stopband, respectively, on the Ω-axis.

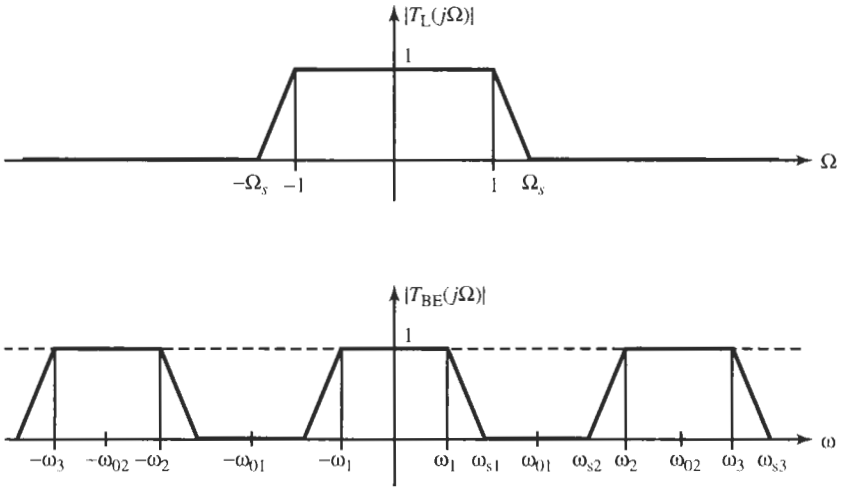

Figure 9.27 Magnitude requirement of a band-rejection filter with an additional stopband at high frequencies.

This new transformation equation is obtained readily by using the same approach that served us well previously: we place a pole into "the center" of each stopband and a zero into "the center" of each passband, remembering that poles and zeros occur symmetrical to the origin. We shall discuss presently how to find "the center." The function to achieve the transformation appropriate for Fig. 9.27 is then

$$\Omega = X(\omega) = \frac{1}{B}\frac{\omega(\omega-\omega_{02})(\omega+\omega_{02})}{(\omega-\omega_{01})(\omega+\omega_{01})} = \frac{1}{B}\frac{\omega\left(\omega^2-\omega_{02}^2\right)}{\left(\omega^2-\omega_{01}^2\right)} \tag{9.68}$$

$\Omega(\omega)$ is plotted in Fig. 9.28. The function has a zeros at $\omega = 0$ and at $\pm\omega_{02}$ in the frequency range in which passbands are prescribed. Poles are at $\pm\omega_{01}$ in the range in which stopbands are located; in addition, there is automatically a pole at infinity, in the second stopband, because the numerator of $\Omega(\omega)$ is of order one higher than the denominator. As always, we allowed for a multiplying constant, $1/B$, to be able to have a sufficient number of parameters to adjust the function $\Omega(\omega)$ to the specified requirements. To make Eq. (9.68) dimensionally correct, B must be a frequency; it will shortly be seen to be the total width of the passbands of the target filter. To determine the unknown parameters B, ω_{01}, and ω_{02} we notice from Fig. 9.28 that for $\Omega = 1$ the function has the values ω_1, $-\omega_2$, and ω_3, the three frequencies that set the corners of the passbands. Thus, setting $\Omega = 1$ in Eq. (9.68) we obtain the third-order polynomial

$$\omega^3 - B\omega^2 - \omega\omega_{02}^2 + B\omega_{01}^2 = 0 \tag{9.69}$$

According to our discussion, this polynomial can be factored as

$$(\omega-\omega_1)(\omega+\omega_2)(\omega-\omega_3) =$$
$$\omega^3 - \omega^2(\omega_3+\omega_1-\omega_2) - \omega[\omega_1\omega_2+(\omega_2-\omega_1)\omega_3] + \omega_1\omega_2\omega_3 = 0 \tag{9.70}$$

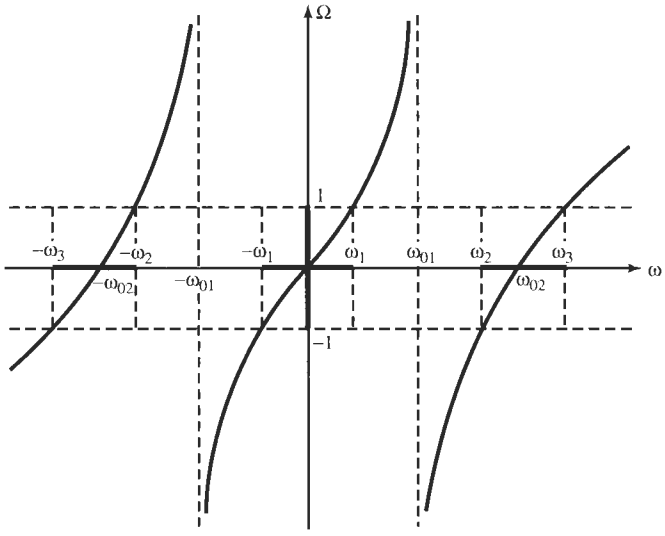

Figure 9.28 The function $\Omega(\omega)$ of Eq. (9.68) to transform a target filter with two passbands and two stopbands into a prototype lowpass.

Comparing coefficients between Eqs. (9.69) and (9.70), we obtain three equations for the three unknown parameters in terms of the prescribed passband corner frequencies:

$$B = \omega_1 + (\omega_3 - \omega_2)\,, \quad \omega_{01}^2 = \frac{\omega_1\omega_2\omega_3}{\omega_1 + (\omega_3 - \omega_2)}, \quad \omega_{02}^2 = \omega_1\omega_2 + (\omega_2 - \omega_1)\,\omega_3 \tag{9.71}$$

All parameters are positive and, as predicted, B is the total width of the passbands. Also, we can show readily that $\omega_1 < \omega_{01} < \omega_2$, i.e., ω_{01} is in the first stopband, and $\omega_2 < \omega_{02} < \omega_3$, i.e., ω_{02} is in the upper passband as Fig. 9.28 demands. Further, $0 < \omega_{01} < \omega_{02} < \infty$, that is, the poles and zeros of the transformation equation (9.68) are simple and alternate along the ω-axis. Next we proceed as in our previous discussions and multiply Eq. (9.68) by j to extend the function into the s-plane:

$$j\Omega = jX(\omega) = \frac{1}{B}\frac{j\omega\left(-\omega^2 + \omega_{02}^2\right)}{\left(-\omega^2 + \omega_{01}^2\right)}$$

Using $S = j\Omega$ and $s = j\omega$ leads to the wanted frequency transformation

$$S = Z(s) = \frac{1}{B}\frac{s\left(s^2 + \omega_{02}^2\right)}{\left(s^2 + \omega_{01}^2\right)} \tag{9.72}$$

with B, ω_{01}, and ω_{02} given in Eq. (9.71). The poles and zeros of $Z(s)$ are shown in Fig. 9.29.

Observe that $Z(s)$ is a third-order equation. Consequently, an nth-order lowpass prototype function is transformed into a target filter transfer function of order $3n$. Thus, a second-order section T_{L} results in a sixth-order filter T_{T}, which can be realized, for example, as a cascade of three biquads:

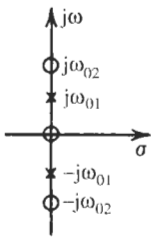

Figure 9.29 Pole-zero pattern of the frequency transformation function $Z(s)$ of Eq. (9.72).

$$T_{\mathrm{L}}(S) = \frac{1}{S^2 + aS + b} \Leftrightarrow T_{\mathrm{T}}(s) = \frac{1}{\left[\frac{1}{B}\frac{s\left(s^2+\omega_{02}^2\right)}{\left(s^2+\omega_{01}^2\right)}\right]^2 + a\left[\frac{1}{B}\frac{s\left(s^2+\omega_{02}^2\right)}{\left(s^2+\omega_{01}^2\right)}\right] + b}$$

$$= \frac{B^2\left(s^2+\omega_{01}^2\right)^2}{\begin{array}{l} s^6 + aBs^5 + \left(2\omega_{02}^2 + bB^2\right)s^4 + aB\left(\omega_{01}^2+\omega_{02}^2\right)s^3 \\ + \left(2\omega_{01}^2 bB^2 + \omega_{02}^4\right)s^2 + aB\omega_{01}^2\omega_{02}^2 s + bB^2\omega_{01}^4 \end{array}}$$

Notice that this equation has two transmission zeros each at $\pm j\omega_{01}$ just as we found in the band-rejection function of Eq. (9.57), but in contrast to Eq. (9.57) we also now have two zeros at $\omega = \infty$ as expected from Figs. 9.27 and 9.28.

Let us illustrate the computations with a simple example.

EXAMPLE 9.7

On some normalized frequency axis, we desire passbands in $0 \leq \omega \leq \omega_1 = 1$ and $\omega_2 = 3 \leq \omega \leq 5 = \omega_3$. Figure 9.30 shows the situation with brick-wall-type filters with the lowpass filter magnitude plot turned by 90° to show clearly the relationship between the target filter T_{T} and the lowpass prototype T_{L}. Find the frequency transformation and the transfer function of the filter. Assume a second-order 0.5-dB Chebyshev lowpass function satisfies the attenuation requirement.

Solution

From Table 7.2, the lowpass transfer function is

$$T_{\mathrm{L}}(S) = \frac{1.4313}{S^2 + 1.4256S + 1.5161}$$

Notice that $T(0)$ corresponds to -0.5 dB. The parameters of the frequency transformation are, from Eq. (9.71)

$$B = 1 + (5-3) = 3, \quad \omega_{01} = \sqrt{\frac{15}{3}} = \sqrt{5} = 2.2361, \quad \omega_{02} = \sqrt{13} = 3.6156$$

so that the transformation, Eq. (9.72), is

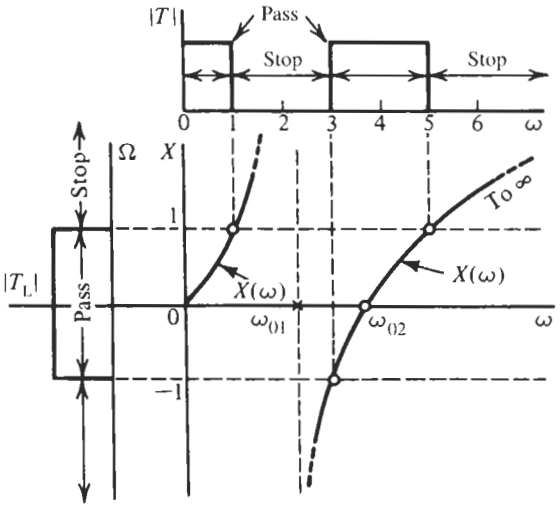

Figure 9.30 The frequency transformation for Example 9.7.

$$S = \frac{s}{3}\frac{s^2+13}{s^2+5}$$

Substituting S in $T_L(S)$ results in

$$T_T(s) = \frac{1.4313}{\left(\frac{s}{3}\frac{s^2+13}{s^2+5}\right)^2 + 1.4256\left(\frac{s}{3}\frac{s^2+13}{s^2+5}\right) + 1.5161}$$

$$= \frac{12.8817\,(s^2+5)^2}{s^6 + 4.2768s^5 + 39.6449s^4 + 76.9824s^3 + 305.4490s^2 + 277.9920s + 341.1225}$$

Using a computer, this function can be factored into

$$T_T(s) = \frac{k_1}{s^2+2.7464s+24.7245}\,\frac{k_2\,(s^2+5)}{s^2+0.4934s+8.6019}\,\frac{k_3\,(s^2+5)}{s^2+1.0370s+1.6040}$$

where $k_1k_2k_3 = 12.8817$ and we have assigned the zeros to the closest poles. Notice that there are three second-order modules; the second and third one, a highpass notch and a lowpass notch, realize the stopband around $\omega_{01} = \sqrt{5}$, and the second-order lowpass, Module 1, realizes the high-frequency stopband at $\omega \to \infty$.

In the following example we provide a further illustration of how to derive a frequency transformation function. It should help clarify the procedure that we may adopt in a more general situation.

EXAMPLE 9.8

A band-elimination filter is to be realized whose attenuation is specified in Fig. 9.31. It must reject low-frequency signals up to ω_{s1} and signals in an intermediate frequency range

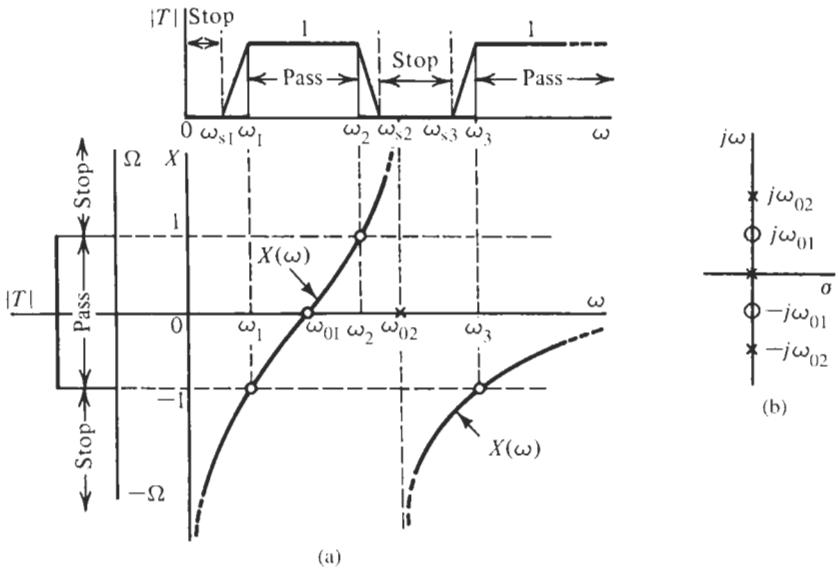

Figure 9.31 (a) The attenuation requirement for Example 9.8 and the frequency transformation; (b) pole-zero plot of the reactance function $\Omega(\omega) = X(\omega)$.

$\omega_{s2} \leq \omega \leq \omega_{s3}$. Its passbands are in $\omega_1 \leq \omega \leq \omega_2$ and $\omega \geq \omega_3$. Find a suitable frequency transformation that maps this requirement onto a prototype lowpass function where the approximation problem may be solved by the methods presented in previous chapters.

Solution

To solve the problem we need only to identify stopbands and passbands so that poles and zeros of the function $\Omega = X(\omega)$ can be identified. We have stopbands around the origin of the ω-axis and in $\omega_{s2} \leq \omega \leq \omega_{s3}$. Passbands are found in $\omega_1 \leq \omega \leq \omega_2$ and "around ∞." Proceeding with the method of placing *zeros* of Ω in passbands (where the attenuation is *small*) and *poles* in stopbands (where we need *large* attenuation), we have immediately

$$\Omega(\omega) = X(\omega) = -B\frac{\omega^2 - \omega_{01}^2}{\omega\left(\omega^2 - \omega_{02}^2\right)} \tag{9.73}$$

with $\omega_1 \leq \omega_{01} \leq \omega_2$ and $\omega_{s2} \leq \omega_{02} \leq \omega_{s3}$. Notice the pole at $\omega = 0$ and the zero at $\omega = \infty$. As we have seen before, the sign of Eq. (9.73) must be negative because we have a factor ω in the denominator (a pole at $\omega = 0$). When multiplying X by j we obtain the term $-j/\omega$, which becomes $1/(j\omega) = 1/s$ when we expand Eq. (9.73) into the complex plane. Figure 9.31 shows that $\Omega = 1$ at $-\omega_1$, ω_2, and $-\omega_3$. We can, therefore, set Eq. (9.73) equal to 1 and solve it for its three roots,

$$\begin{aligned}\omega^3 + B\omega^2 - \omega_{02}^2\omega - B\omega_{01}^2 &= (\omega+\omega_1)(\omega-\omega_2)(\omega+\omega_3)\\ &= \omega^3 + (\omega_3 - \omega_2 + \omega_1)\omega^2 - [\omega_3(\omega_2 - \omega_1) + \omega_1\omega_2]\omega - \omega_1\omega_2\omega_3\\ &= 0\end{aligned}$$

Comparing coefficients, we obtain the result

$$B = (\omega_3 - \omega_2) + \omega_1, \quad \omega_{01}^2 = \frac{\omega_1\omega_2\omega_3}{\omega_1 + (\omega_3 - \omega_2)}, \quad \omega_{02}^2 = \omega_3(\omega_2 - \omega_1) + \omega_1\omega_2 \tag{9.74}$$

as in Eq. (9.71). Alternatively we could proceed and insert the three passband corner frequencies into Eq. (9.73) to find (refer to Fig. 9.31)

$$\begin{aligned} X(\omega_1) &= -B\frac{\omega_1^2 - \omega_{01}^2}{\omega_1\left(\omega_1^2 - \omega_{02}^2\right)} = -1 \\ X(\omega_2) &= -B\frac{\omega_2^2 - \omega_{01}^2}{\omega_2\left(\omega_2^2 - \omega_{02}^2\right)} = +1 \\ X(\omega_3) &= -B\frac{\omega_3^2 - \omega_{01}^2}{\omega_3\left(\omega_3^2 - \omega_{02}^2\right)} = -1 \end{aligned} \tag{9.75}$$

These are three simultaneous equations for the three unknowns that can be solved to give the same result as in Eq. (9.74). The parameters of the frequency transformation are then determined and we form the transformation function

$$Z(s) = jX(\omega)|_{\omega=s/j} = B\frac{s^2 + \omega_{01}^2}{s\left(s^2 + \omega_{02}^2\right)} \tag{9.76}$$

Let us finish the example with numerical values: Assume the normalized values $\omega_1 = 1$, $\omega_2 = 2$, and $\omega_3 = 3$. From Eq. (9.74) we find

$$B = 3 - 2 + 1 = 2, \quad \omega_{01}^2 = \frac{6}{1 + (3 - 2)} = 3, \quad \omega_{02}^2 = 3(2 - 1) + 2 = 5$$

The same result is obtained from Eqs. (9.75) to give

$$Z(s) = 2\frac{s^2 + 3}{s\left(s^2 + 5\right)}$$

9.5 THE FOSTER REACTANCE FUNCTION

We should now be able to recognize a pattern in the different frequency transformation functions we derived for going from the lowpass frequency S to the frequency parameter s of the other types of filters. Starting from the simplest trivial transformation

$$S = Z(s) = Ks \tag{9.77}$$

which converts a lowpass into a lowpass with a rescaled frequency, we proceed to the lowpass-to-highpass transformation of Eq. (9.4),

$$S = Z(s) = K\frac{1}{s} \tag{9.78}$$

the lowpass-to-bandpass transformation, Eq. (9.21a),

$$S = Z(s) = K\frac{s^2 + \omega_0^2}{s} \tag{9.79}$$

the lowpass-to-band-elimination transformation, Eq. (9.46a),

$$S = Z(s) = K\frac{s}{s^2 + \omega_0^2} \tag{9.80}$$

and the multipassband transformations of Eqs. (9.74) and (9.76)

$$S = Z(s) = K\frac{s\left(s^2 + \omega_{02}^2\right)}{\left(s^2 + \omega_{01}^2\right)} \tag{9.81}$$

$$S = Z(s) = K\frac{s^2 + \omega_{01}^2}{s\left(s^2 + \omega_{02}^2\right)} \tag{9.82}$$

The parameters $K, \omega_0^2, \omega_{01}^2$, and ω_{02}^2 are positive constants to be determined from the prescribed passband corners of the target filter. We observe that the transformations $Z(s)$ are rational functions, $Z(s) = Kn(s)/d(s)$, where $n(s)$ and $d(s)$ are polynomials. Z is constructed such that its imaginary part

$$\Omega(\omega) = X(\omega) = \frac{Z(j\omega)}{j} = K\frac{1}{j}\frac{n(j\omega)}{d(j\omega)}$$

has zeros where the specified target filter has passbands and poles where it has stopbands:

$$\Omega(\omega) = X(\omega) = K\frac{\left(\omega^2 - \omega_{01}^2\right)\left(\omega^2 - \omega_{03}^2\right)\cdots\left(\omega^2 - \omega_{0(2n-1)}^2\right)}{\omega\left(\omega^2 - \omega_{02}^2\right)\left(\omega^2 - \omega_{04}^2\right)\cdots\left(\omega^2 - \omega_{0(2n)}^2\right)} \tag{9.83}$$

Thus we obtain

$$Z(s) = K\frac{n(s)}{d(s)} = K\frac{\left(s^2 + \omega_{01}^2\right)\left(s^2 + \omega_{03}^2\right)\cdots\left(s^2 + \omega_{0(2n-1)}^2\right)}{s\left(s^2 + \omega_{02}^2\right)\left(s^2 + \omega_{04}^2\right)\cdots\left(s^2 + \omega_{0(2n)}^2\right)} \tag{9.84}$$

For example, the lowpass-to-bandpass transformation of Eq. (9.79) is a special case with only one passband, $\omega_{01} = \omega_0$, and all other ω_{0i} terms, $i = 2, 3, \ldots, 2n$, absent. Similarly, the lowpass-to-bandstop transformation of Eq. (9.80) is a special case with $\omega_{01} = 0$, $\omega_{02} = \omega_0$, and all other ω_{0i} terms, $i = 3, 4, \ldots, 2n$, absent.

Figure 9.32 shows the general shape of $\Omega(\omega) = X(\omega)$. From its construction with alternating passbands and stopbands, we observe the following:

1. $\Omega(\omega) = X(\omega)$ has simple poles and zeros that alternate on the $j\omega$-axis:

$$0 < \omega_{01} < \omega_{02} < \omega_{03} < \cdots < \omega_{0(2n-1)} < \omega_{0(2n)} < \infty$$

2. $\Omega(\omega)$ is an odd function, i.e., $\Omega(+\omega) = -\Omega(-\omega)$. Because the function is odd, that is $\Omega(\omega)/\omega$ is even, the pole and zero terms appear as $(\omega - \omega_{0i})(\omega + \omega_{0i}) = \omega^2 - \omega_{0i}^2$.

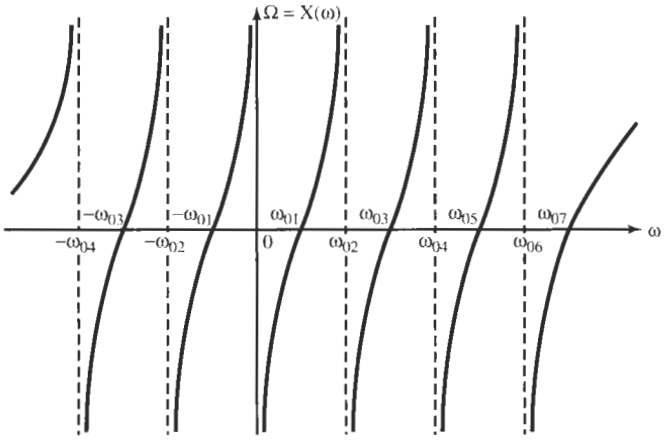

Figure 9.32 The general Foster reactance function $\Omega(\omega) = X(\omega)$.

3. At the origin $\Omega(\omega)$ has either a simple pole or a simple zero because at $\omega = 0$ it must be either a passband or a stopband; the same is true at ∞. This means that the difference in degrees of numerator and denominator is exactly 1.
4. The slope of $\Omega(\omega)$ versus ω is always positive: $d\Omega/d\omega > 0$.

Applying these properties to $Z(s)$ in Eq. (9.84), we note that either $n(s)$ is even and $d(s)$ is odd, or vice versa, that is, either $n(s)$ or $d(s)$, but not both, will have a multiplier s. The constant K is positive and the zero and pole terms for finite values of ω_{0i} are $(s^2 + \omega_{0i}^2)$.

The functions $X(\omega)$ we just described are called the *Foster reactance functions* in recognition of R. M. Foster's work in 1924. The name arises from the fact that an inductor of value $L = 1$ has a reactance $\Omega L = X(\omega)$. Its impedance $SL = S = Z(s)$ is a physically realizable function as we shall demonstrate next, and this is the reason for our impedance notation "Z" in Eqs. (9.77) through (9.84). Also, the inverse of Z, the admittance $Y = 1/Z$, is a realizable function; Z and Y lead to dual circuits.

To be concrete in the following discussion, let us use the frequency transformations on an inductive impedance SL and use the definitions for K, ω_0^2, and the remaining constants that we developed in the earlier parts of this chapter. For Eq. (9.77) K is given by the cut-off frequency ω_c, $K = 1/\omega_c$. Observe then that SL in Eq. (9.77) is a (normalized) inductor of value L/ω_c. For Eq. (9.78) $K = \omega_c$ and SL becomes a (normalized) capacitor of value $1/(L\omega_c)$. Note that we assumed that the impedance level is still normalized: to obtain the actual element values, we must multiply the inductor by the normalizing resistor R and divide the capacitor by R.

Staying with such normalized elements, for the lowpass-to-bandpass transformation of Eq. (9.79) we had $K = 1/B$. B was the bandwidth of the bandpass filter and ω_0 was its center frequency. SL can be then be written as

$$SL = \frac{L}{B}\frac{s^2 + \omega_0^2}{s} = \frac{L}{B}s + \frac{\omega_0^2 L/B}{s} \tag{9.85}$$

If we express this equation as $Z'(s) = sL' + 1/(sC')$ we recognize that $Z'(s)$ represents a series connection of an inductor $L' = L/B$ and a capacitor of value $C' = B/(\omega_0^2 L)$.

Similarly, for Eq. (9.80) we had $K = B$ and we obtain

$$SL = BL\frac{s}{s^2+\omega_0^2} = \frac{1}{\dfrac{s}{BL} + \dfrac{\omega_0^2/BL}{s}} \tag{9.86}$$

This equation represents the parallel connection of a capacitor $1/(BL)$ and inductor BL/ω_0^2, both with normalized impedance level.

In an analogous fashion we rewrite Eq. (9.81) with $K = 1/B$ as

$$SL = \frac{L}{B}\frac{s\left(s^2+\omega_{02}^2\right)}{\left(s^2+\omega_{01}^2\right)} = \frac{L}{B}s + \frac{s\,(L\Delta/B)}{s^2+\omega_{01}^2} = \frac{L}{B}s + \frac{1}{\dfrac{s}{L\Delta/B} + \dfrac{\omega_{01}^2 B/(L\Delta)}{s}} \tag{9.87}$$

where we have called $\omega_{02}^2 - \omega_{01}^2 = \Delta > 0$. The parameters B, ω_{01}^2, and ω_{02}^2 were defined in Eq. (9.71). Evidently, Eq. (9.87) represents an inductor L/B in series with a parallel connection of a capacitor $B/(L\Delta)$ and an inductor $L\Delta/(B\omega_{01}^2)$.

Finally, from Eq. (9.82) we have with $K = B$,

$$SL = BL\frac{s^2+\omega_{01}^2}{s\left(s^2+\omega_{02}^2\right)} = BL\frac{\omega_{01}^2/\omega_{02}^2}{s} + \frac{1}{\dfrac{s}{LB\Delta/\omega_{02}^2} + \dfrac{\omega_{02}^2}{LB\Delta/\omega_{02}^2}\dfrac{1}{s}} \tag{9.88}$$

which represents a capacitor $\omega_{02}^2/(LB\omega_{01}^2)$ in series with a parallel connection of an inductor $LB\Delta/\omega_{02}^4$ and a capacitor $\omega_{02}^2/(LB\Delta)$. Again, $\Delta = \omega_{02}^2 - \omega_{01}^2$ and the parameters B, ω_{01}^2, and ω_{02}^2 for this transformation were defined in Eq. (9.74). The LC realizations of all these impedances are summarized in Fig. 13.16, as are their duals, the admittances obtained by replacing the impedance SL by the admittance SC.

We shall have much more to say about reactance functions and the (LC) impedances $Z(s)$ in Chapter 13 when we discuss the realization of LC ladder filters. For now we will only note the following:

1. All terms in Eqs. (9.85) to (9.88) are positive and, hence, are realizable elements.
2. The expressions on the right-hand sides of Eqs. (9.85) to (9.88) were obtained mathematically by forming *partial fraction expansions* of the impedances $Z(s)$.
3. The general case of Eq. (9.84) can be treated in the same fashion. The impedance $Z(s)$ and its inverse, the admittance $Y(s) = 1/Z(s)$, can be shown to lead to circuits consisting of interconnections of positive components.
4. The functions $\Omega(\omega)$ can also be interpreted as the imaginary parts, the susceptances $B(\omega)$, of admittances $Y(s)$. We can convince ourselves readily that in this case in the discussion relating to Eqs. (9.85) to (9.88) the following replacements should be made:

$Z(s)$	replace by	$Y(s)$
Reactance $X(\omega)$		Susceptance $B(\omega)$
Capacitance		Inductance
Inductance		Capacitance
Series		Parallel
Parallel		Series

This interpretation will also be seen in Fig. 13.16.

REFERENCES

R. M. Foster, "A Reactance Theorem," *Bell Syst. Tech. J.*, Vol. 3, pp. 259–267, 1924.

PROBLEMS

9.1 Design a highpass filter with a maximally flat response to meet the attenuation specification given in Fig. P9.1. Determine the attenuation your filter realizes at the two frequencies $\omega = 1.2$ krad/s and $\omega = 800$ rad/s. Use Åckerberg–Mossberg sections, LM741 opamps, and test your design with Electronics Workbench (EWB).

9.2 Repeat Problem 9.1 but design the filter for a Chebyshev magnitude response.

9.3 A highpass filter with a maximally flat response with the specifications shown in Fig. P9.3 is to be designed.

(a) Use a cascade connection of Sallen–Key circuits and a first-order section if needed to realize the filter and test your design with EWB.

(b) Modify the circuit to provide a gain enhancement of 10 dB (flat for all frequencies) without using additional opamps.

9.4 A highpass filter with a Chebyshev passband is required. The specifications are those in Fig. P9.4.

(a) Design the filter based on Sallen–Key sections and test your design with EWB.

(b) Determine the loss actually realized by your design at $\omega = 1100$ rad/s and at $\omega = 900$ rad/s.

9.5 Repeat Problem 9.4 for the specifications in Fig. P9.5.

9.6 Repeat Problem 9.5 for a highpass filter with maximally flat passband response.

9.7 Repeat Problem 9.5 for a highpass filter with an inverse Chebyshev passband response.

9.8 For the bandpass specifications shown in Fig. P9.8, a maximally flat magnitude response is required. As an intermediate stage in the design, we are required to find the number of poles and the radius of the circle

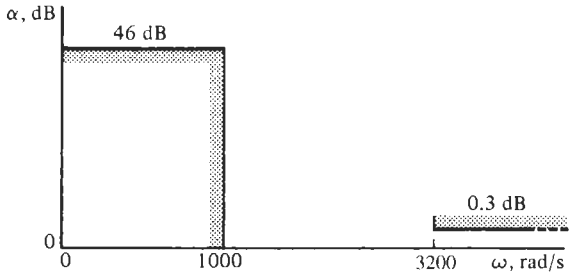

Figure P9.1

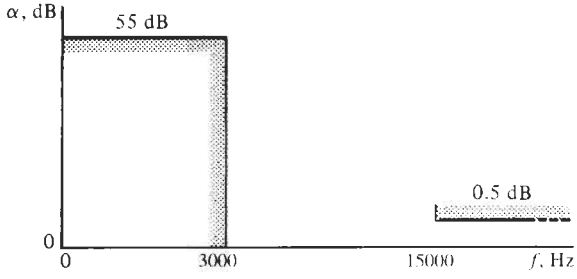

Figure P9.3

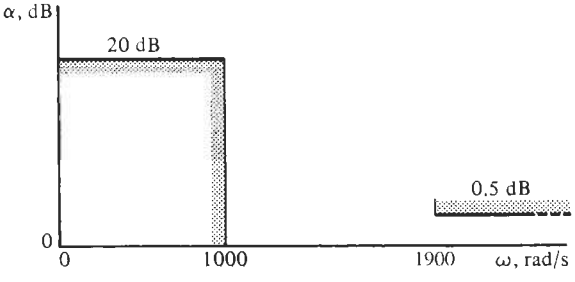

Figure P9.4

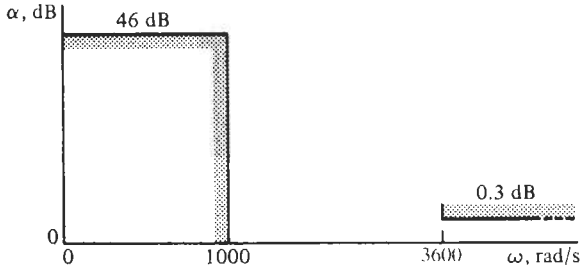

Figure P9.5

on which the lowpass prototype poles are located. Design the circuit as a cascade connection of GIC sections and test the performance with EWB.

9.9 A filter with a maximally flat passband response must satisfy the attenuation specified in Fig. P9.9.

(a) Find the pole locations that correspond to this response.

(b) Design the filter with suitable first- and second-order blocks and test the performance. Be certain that appropriate opamps and practical component values are used.

9.10 Design a bandpass filter to meet the specifications shown in Fig. P9.10, with the added requirement that the response be Butterworth. It is required that $\alpha(2000) = 0$ dB. In your final design, all capacitors should have the value of 0.1 nF. Build the circuit with suitable first- and second-order sections, HA2542-2 opamps, and test your design with EWB.

9.11 Figure P9.11 shows a required response that is maximally flat in the passband. It is given that $\alpha(500) = \alpha(1000) = 1$ dB. It is also given that the filter realization may use only two opamps to minimize power consumption. Determine the largest loss (attenuation) that can be obtained at a frequency of $\omega = 3000$ rad/s.

9.12 As shown in Fig. P9.12, a bandpass transfer function is specified to have 12 dB of attenuation in the two stopbands. To obtain the smallest passband attenuation as small as possible, the Chebyshev approximation is employed. Only two opamps are permitted for the filter and only 0.01-μF capacitors may be used. Design a filter to meet the specifications and indicate the value of α_{max} that your design achieves. Test the

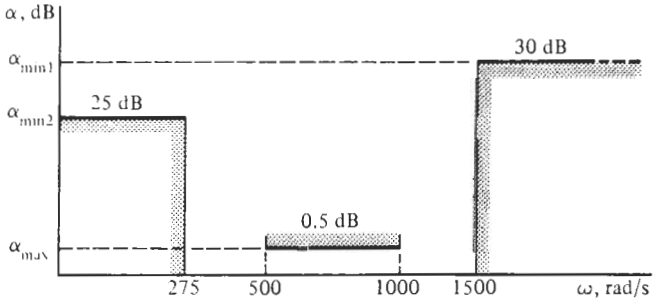

Figure P9.8

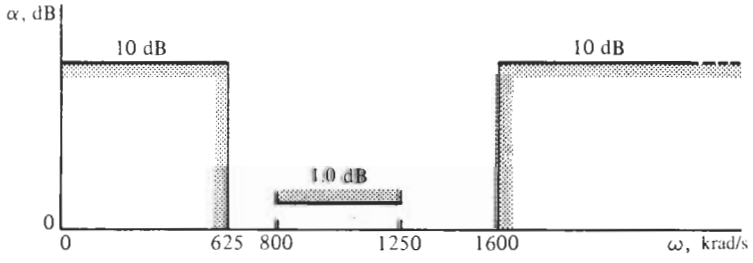

Figure P9.9

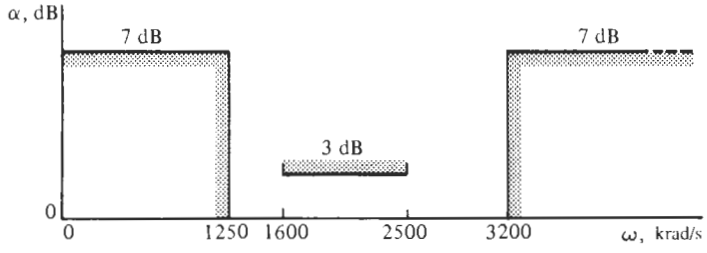

Figure P9.10

circuit with EWB. Compare the achieved α_{max} with the computed value.

9.13 Design a filter with maximally flat magnitude to satisfy the bandpass specifications shown in Fig. P9.13. Adjust the gain of the filter such that the midband gain equals 0 dB, and use only 0.1-μF capacitors in your realization. Use GIC sections with suitable opamps and test your design with EWB.

9.14 Reconsider Problem 9.13. The specification is changed to have a Chebyshev passband response rather than a maximally flat one. Design a filter to meet the new specification and test your circuit with EWB. Magnitude scale your element sizes so that they are in a practical range.

9.15 Repeat Problem 9.12, but use an elliptic approximation for your design. Compare the achieved α_{max} with the one obtained in Problem 9.12.

9.16 Design a bandstop filter with a maximally flat magnitude response having the frequency characteristic shown in Fig. P9.16. Calculate the attenuation your design actually achieves at $f = 800$ Hz and $f = 850$ Hz. Use magnitude scaling so that element values are in a practical range. If possible use all identical capacitors and no more than four opamps (a "quad"). Test your design.

9.17 Design a bandstop filter with a Chebyshev passband having the frequency response shown in Fig. P9.17. Scale the impedance level so that element values are in a practical range. Build the circuit with suitable filter sections and opamps and test your design with EWB.

9.18 Repeat Problem 9.16 for the frequency response shown in Fig. P9.18, but employ the inverse Chebyshev approximation.

9.19 From the specifications given in Fig. P9.19, design a filter with a maximally flat passband such that the midband gain equals 0 dB. All capacitors in the filter should have the same value; scale the magnitude so that practical component values are obtained. Build the filter with Åckerberg–Mossberg sections and LM741 opamps, and test the circuit's performance.

9.20 From the specifications given in Fig. P9.20, design a filter with maximally flat passband response. The gain should be adjusted such that $\alpha(707) = 0$ dB. Use magnitude scaling so that practical component values are obtained and all capacitors in the filter

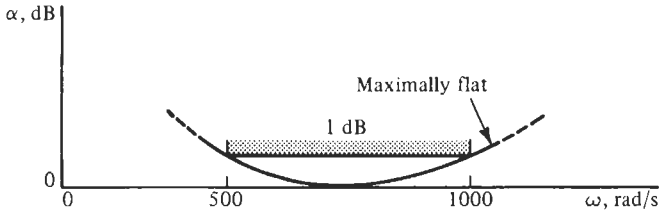

Figure P9.11

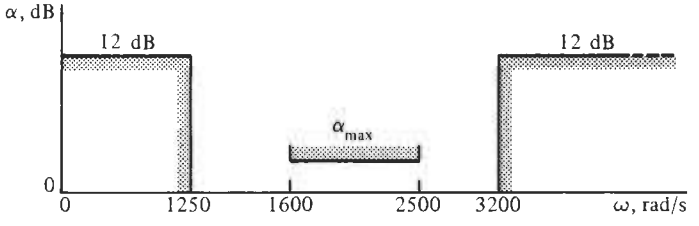

Figure P9.12

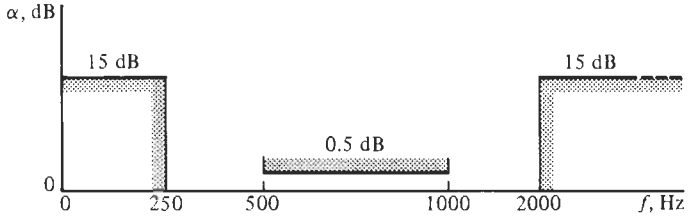

Figure P9.13

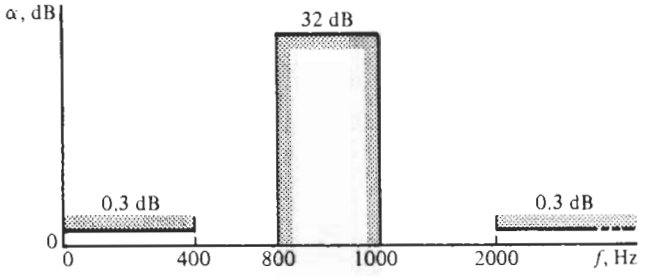

Figure P9.16

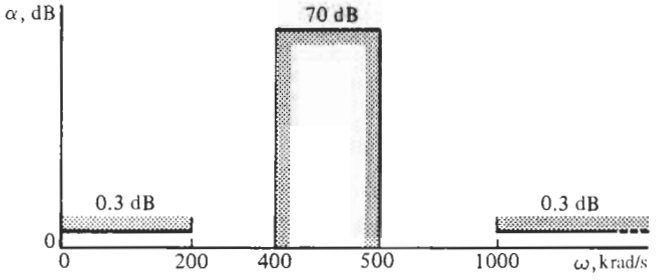

Figure P9.17

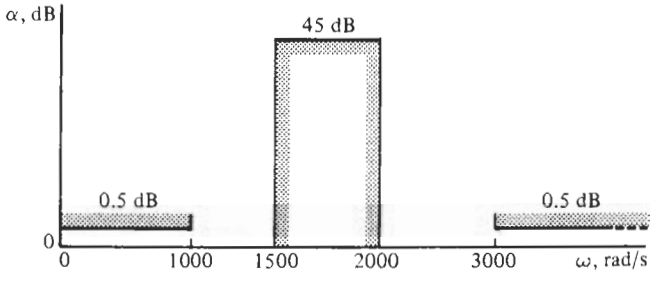

Figure P9.18

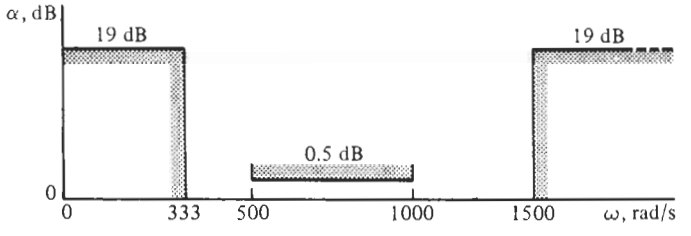

Figure P9.19

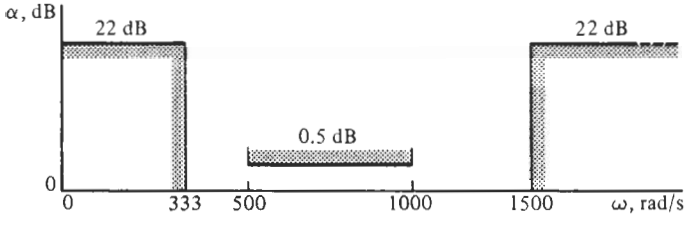

Figure P9.20

have the same value. Build and test the circuit using LM741 opamps.

9.21 When asked to reengineer some old equipment, a student intern comes across the passive RLC circuit in Fig. P9.21a with the components $C = 0.01\mu$F, $L = 0.2$ mH, and $R = 60\Omega$. An electronic circuit must be designed without inductors to replace the passive RLC filter, i.e., a circuit must be found to put in the box in Fig. P9.21b that is the analog of that in Fig. P9.21a with respect to ω_0, Q, and $|T(j\omega)|$. Build the circuit and test your design.

9.22 With the switch open, the circuit shown in Fig. P9.22 is found to have the voltage-ratio transfer function

$$\frac{V_2}{V_1} = \frac{-k_1 s}{s^2 + (k_2/C_1)s + (k_3/C_1)}$$

where k_1, k_2, and k_3 are constants. The switch is then closed connecting the capacitor into the circuit.

(a) Write expressions for ω_0, BW, $|V_2/V_1|_{\max}$ and indicate whether connecting C_2 into the circuit causes them to increase or decrease.

(b) The capacitor C_2 is adjusted to a specific value C_0, and then to a second value $2C_0$. Using the results of part (a), sketch $|V_2/V_1|$ as a function of ω for the two cases.

9.23 The circuit of Fig. P9.23 is the Delyiannis–Friend biquad (Fig. 4.35) with the capacitors ganged (connected) together so that when tuning C they change together. Give an algorithm for the orthogonal tuning of ω_0 and the bandwidth $BW = \omega_0/Q$.

9.24 In the circuit of Fig. P9.24, the capacitor C_1 is tuned. What is the effect of C_1 on ω_0 and the bandwidth $BW = \omega_0/Q$?

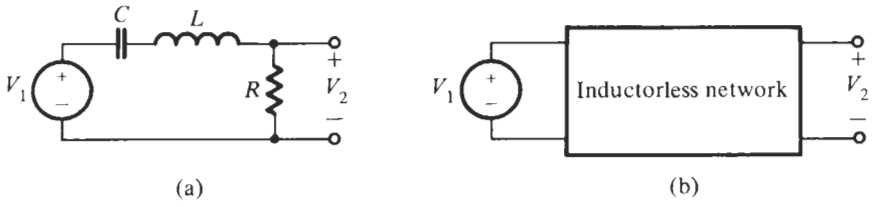

Figure P9.21

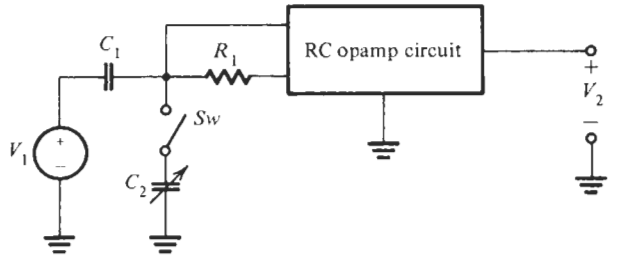

Figure P9.22

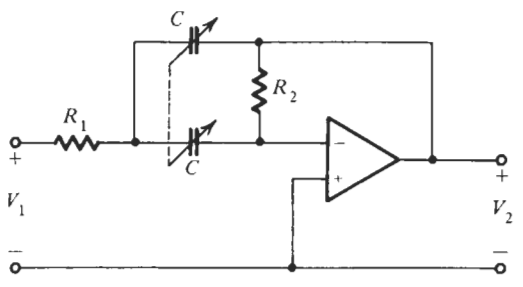

Figure P9.23

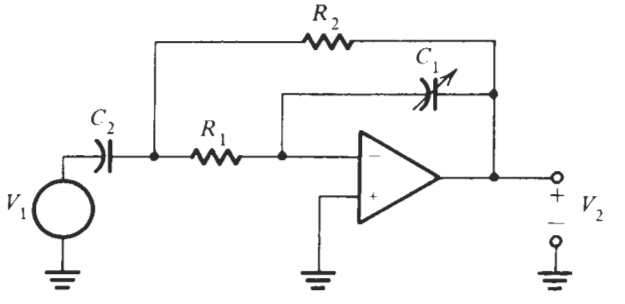

Figure P9.24

9.25 Design a filter with an elliptic magnitude response that satisfies the specifications given in Fig. P9.25. Adjust the gain such that the attenuation is always positive, and magnitude scale so that element sizes are in a practical range. Build and test your design.

9.26 Find the order n of the maximally flat and Chebyshev responses needed to meet the specifications given in Fig. P9.26.

9.27 You are required to design a bandstop filter with a Cauer magnitude satisfying the specifications shown in Fig. P9.27. Use magnitude scaling to give practical element values, use LM741 opamps, and design and test the circuit.

9.28 For this problem, we are studying the frequency transformation $X(\omega)$ that transforms the lowpass prototype characteristic into the frequency characteristic shown in Fig. P9.28.

(a) Sketch $X(\omega)$ and identify pole and zero frequencies.

(b) Write the frequency transformation $Z(s)$ in its general form.

9.29 Repeat Problem 9.28 for the frequency characteristic shown in Fig. P9.29.

9.30 Repeat Problem 9.28 for the frequency characteristic shown in Fig. P9.30.

9.31 Repeat Problem 9.28 for the frequency characteristic shown in Fig. P9.31.

9.32 Figure P9.32 shows a double passband frequency characteristic for which we wish to find a prototype lowpass. For the numerical values given:

(a) Show that the frequency transformation function $Z(s)$ equals

$$Z(s) = 0.5\frac{(s^2 + 2.23)(s^2 + 10.77)}{s(s^2 + 7)}$$

(b) Construct a column that might fit into Fig. 13.16.

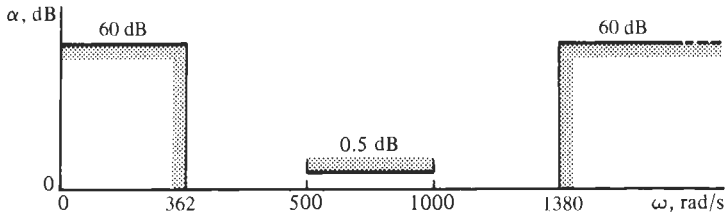

Figure P9.25

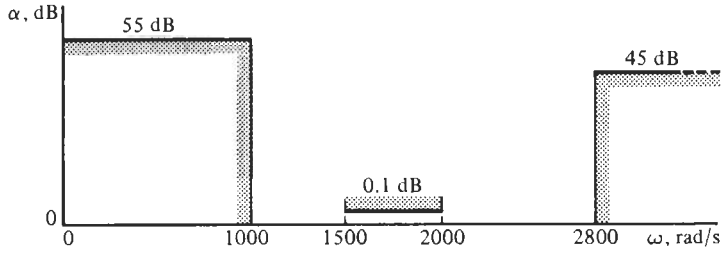

Figure P9.26

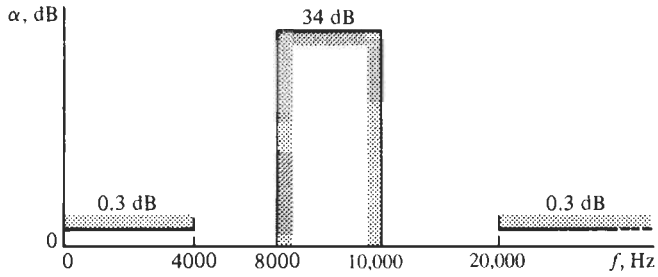

Figure P9.27

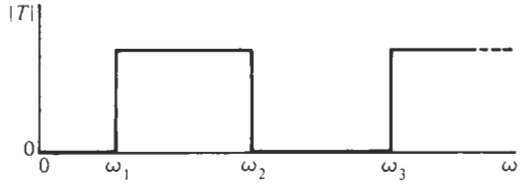

Figure P9.28

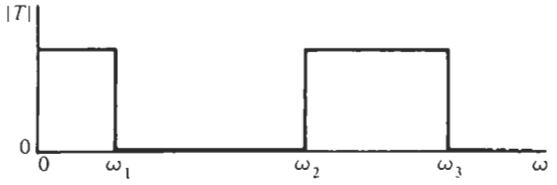

Figure P9.29

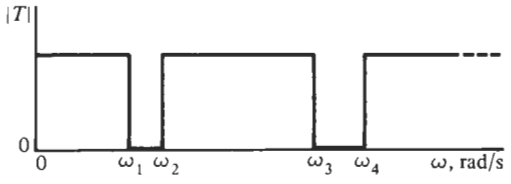

Figure P9.30

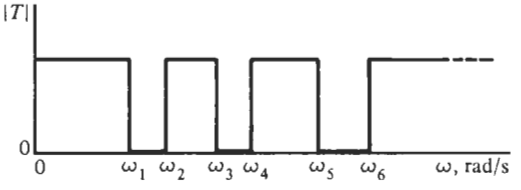

Figure P9.31

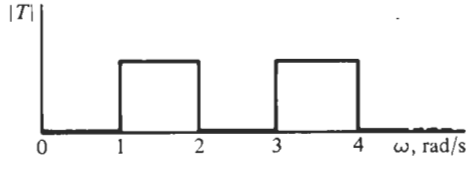

Figure P9.32

9.33 For the double notch filter in Fig. P9.30, with $\omega_1 = 100$ rad/s, $\omega_2 = 200$ rad/s, $\omega_3 = 300$ rad/s, and $\omega_4 = 400$ rad/s, perform the following:

(a) Determine the frequency transformation $Z(s)$.

(b) Design ladder branches to fit Fig. 13.16.

9.34 The design in Example 9.6 had the minimum order, $n = 4$, and left no margin for error in the width of the -38-dB stopband. In the circuit of Example 9.6, we used the standard design of a band-rejection filter and placed all transmission zeros into the center of the stopband by selecting the parameters b and c according to

$$\omega_{01}^2(1 - c) = \omega_{02}^2(1 + d) = \omega_0^2$$

Show that by deviating from this process and permitting the transmission zeros to be "off center," the error margin can be improved with no extra cost. In practice, this means only that the values of the 4.4-kΩ and 7.7-kΩ resistors must be changed (reduced) so that the notch frequencies of the two biquads shift away from the ω_0 toward the stopband corners. Redesign the circuit found in Example 9.6 accordingly and test its performance with EWB. Be sure that the stopband attenuation remains at the prescribed minimum of -38 dB. For your design, determine the new -38-dB stopband bandwidth.

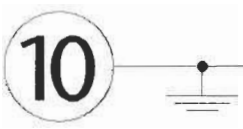

DELAY FILTERS

In Chapters 6, 7, and 8 we have derived transfer functions that allow us to realize a specified lowpass magnitude response. In doing so we paid no attention to the phase of the functions or, more importantly, to the delay that a signal will experience when being processed by the filter. Delay is one of the basic and natural attributes of signal processing: a signal cannot appear at the output of a system earlier than or even at the same time as it is applied at the input. Delay occurs naturally in the transmission of signals through a circuit, a system, or, generally, through space, such as in a coaxial cable or optical fiber. We will deal in this chapter with the design of delay filters that approximate the operation of a pure delay, without changing the magnitude or shape of the input signal.

10.1 TIME-DELAY AND TRANSFER FUNCTIONS

Delay is a time-domain quantity, but filters are designed from frequency-domain specifications such as magnitude and phase. Hence it is necessary to relate the two quantities. We begin with the input signal v_1 shown in Fig. 10.1a. This signal is introduced into a circuit that provides a delay of D seconds. The output is a delayed replica of the input signal and is shown in Fig. 10.1c as v_2. In equation form we are given $v_1(t)$, and we require that

$$v_2(t) = v_1(t - D) \tag{10.1}$$

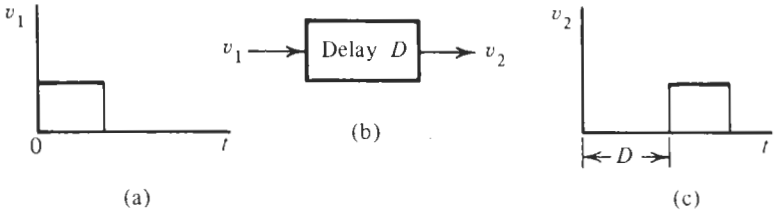

Figure 10.1 A conceptual system to provide an ideal delay.

From Fourier analysis we know that any signal can be decomposed into an infinite summation of sinusoidal signals. Let one of these be

$$v_1 = A \sin(\omega t + \phi) \tag{10.2}$$

Then from Eq. (10.1) the output will be

$$v_2 = A \sin[\omega(t - D) + \phi] \tag{10.3}$$

or

$$v_2 = A \sin(\omega t - \omega D + \phi) \tag{10.4}$$

Then we see that the input and output signals differ only by a phase angle, which is

$$\theta = -\omega D \tag{10.5}$$

If all Fourier components of the input signal are delayed by the same amount D and not changed in amplitude, then the output will indeed be a delayed replica of the input.

Now the phasor representation of Eq. (10.2) is

$$V_1 = A\angle\phi \tag{10.6}$$

while that for Eq. (10.4) is

$$V_2 = A\angle(\phi - \omega D) \tag{10.7}$$

Hence the ratio V_2/V_1 is

$$\frac{V_2}{V_1} = 1\angle -\omega D$$

or in exponential form

$$T(j\omega) = \frac{V_2(j\omega)}{V_1(j\omega)} = 1e^{-j\omega D} = 1e^{-j\omega/(1/D)} \tag{10.8}$$

It is usual to employ frequency scaling and in this case a convenient normalizing frequency is the reciprocal of the delay we want to implement:

$$\omega_c = \frac{1}{D} \tag{10.9}$$

Then $T(j\omega) = e^{-j\omega/\omega_c} = e^{-j\omega_n}$. We generalize by going to the s-plane, i.e., we set $j\omega_n = s_n$. In the following discussion we drop the subscript n and remember that in all subsequent treatment s is a normalized frequency. Then the transfer function of Eq. (10.8) becomes

$$T(s) = \frac{V_2(s)}{V_1(s)} = e^{-s} \tag{10.10}$$

In effect we are approximating an ideal delay function with $D = 1$. The magnitude and phase of this function are shown in Fig. 10.2. It tells us that the phase is linear with negative slope, the magnitude is constant, and the delay is constant at the value 1. Under such circumstances a signal will be delayed without distortion.

Unfortunately, it is not possible to realize the transfer function $T(s) = -e^{-s}$ with a finite number of lumped elements. The best we can do is to approximate Eq. (10.10) with a rational quotient of polynomials,

$$T(s) = N(s)/D(s) \tag{10.11}$$

the polynomials $N(s)$ and $D(s)$ being of relatively small degree, perhaps between 2 and 10. Our next task is to find such a polynomial quotient and then to study how well it does approximate the requirement of Eq. (10.10).

If we let $s = j\omega$ in Eq. (10.11), then $T(j\omega)$ becomes complex and may be written

$$T(j\omega) = R(\omega) + jX(\omega) \tag{10.12}$$

The phase of $T(j\omega)$ is

$$\theta = \tan^{-1}\left[\frac{X(\omega)}{R(\omega)}\right] \tag{10.13}$$

Substituting this into Eq. (10.5), and solving for the delay, gives

$$D = \frac{-1}{\omega}\tan^{-1}\left(\frac{X}{R}\right) \tag{10.14}$$

This is a transcendental function and, for the most part, not well suited to our needs when designing a delay filter. Equation (10.14) represents the delay, also called the *phase delay*, at one

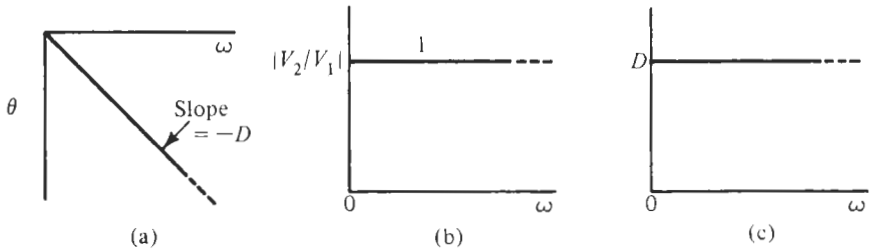

Figure 10.2 Definition of the operation of an ideal delay filter.

particular frequency. We saw earlier that to avoid distortion a circuit needs to provide a constant delay, so what we need is a method that lets us describe and design a constant delay. Mathematically we can approach that problem if we define delay as the negative derivative of the phase

$$D(\omega) = -\frac{d\theta(\omega)}{d\omega} \tag{10.15}$$

In Eq. (10.5) where $\theta(\omega)$ changes linearly with frequency this gives us the delay D as required. In general, the phase as expressed in Eq. (10.13) is not linear, but we can use the definition of Eq. (10.15) to derive a function $T(s)$ such that its phase in linear, that is, its negative slope D is constant, over some specified frequency range. All signal components in that frequency range are then delayed by the same amount, signifying a constant delay. Thus, we may differentiate Eq. (10.13) to obtain

$$D(\omega) = \frac{-RdX/d\omega + XdR/d\omega}{R^2 + X^2} \tag{10.16}$$

This is a rational function, a quotient of polynomials in ω, and involves the real and imaginary parts of the transfer function T we are trying to find. Fortunately, techniques have been developed that make time delay as defined by Eq. (10.15) easy to measure (Temes and LaPatra, 1977), and so it is the definition most often used. To distinguish the two, delay as defined by Eq. (10.5) is known as *phase delay*, while that defined by Eq. (10.15) is known as *group delay* or sometimes as *signal delay* or *envelope delay*. In the remainder of our discussion we will make use of the definition of Eq. (10.15) exclusively, and so will refer to it simply as *delay*.

10.2 BESSEL–THOMSON RESPONSE

Our objective is to find a family of lowpass transfer functions $T_j(s)$ that will give approximately constant time delay for as large a range of ω as possible. The strategy to be followed is to (1) assume a form for the transfer function, (2) compute the corresponding delay, (3) expand it in the form of a Taylor series about $\omega = 0$, and (4) find the conditions that will cause as many coefficients in the series expansion to vanish as possible. These conditions will then be used to determine the required form of the transfer function. One of the first to use this approach was W. E. Thomson of the British Post Office Research Station (Thomson, 1949; see also Huggins, 1949, Kiyasu, 1943). It turns out that the coefficients of the polynomials in $T(s)$ are closely related to Bessel polynomials. For this reason we will call the response that results the *Bessel–Thomson response*, although it is called either the Thomson or Bessel response in the literature.

We will illustrate the procedure just described in terms of an all-pole second-order transfer function:

$$T_2(s) = \frac{a_0}{s^2 + a_1 s + a_0} \tag{10.17}$$

For this function the phase is

$$\theta = -\tan^{-1}\left(\frac{a_1\omega}{a_0 - \omega^2}\right) \tag{10.18}$$

Differentiating with respect to ω gives

$$D = -\frac{d\theta}{d\omega} = \frac{a_1}{a_0}\frac{1 + \omega^2/a_0}{1 + (a_1^2/a_0^2 - 2/a_0)\omega^2 + \omega^4/a_0^2} \tag{10.19}$$

Simple division of the numerator by the denominator gives a result in Taylor series form:

$$D = \frac{a_1}{a_0}\left[1 + \left(\frac{1}{a_0} - \frac{a_1^2}{a_0^2} + \frac{2}{a_0}\right)\omega^2 + \cdots\right] \tag{10.20}$$

For the second term to vanish we require that

$$\frac{a_1^2}{a_0^2} = \frac{3}{a_0} \tag{10.21}$$

or

$$a_1^2 = 3a_0 \tag{10.22}$$

To normalize D so that it will have the value of $D = 1$ that we require, we set $a_0 = a_1$, which, from Eq. (10.22), requires that $a_0 = a_1 = 3$. Then we have determined the form of the transfer function

$$T_2 = \frac{3}{s^2 + 3s + 3} \tag{10.23}$$

The corresponding delay is given by Eq. (10.19):

$$D_2(\omega) = \frac{3\omega^2 + 9}{\omega^4 + 3\omega^2 + 9} \tag{10.24}$$

Such calculations, though laborious, are routine. A similar analysis for a third-order all-pole function gives the transfer function

$$T_3 = \frac{15}{s^3 + 6s^2 + 15s + 15} \tag{10.25}$$

for which the delay is

$$D_3 = \frac{6\omega^4 + 45\omega^2 + 225}{\omega^6 + 6\omega^4 + 45\omega^2 + 225} \tag{10.26}$$

After having found two transfer functions with approximately constant delay, we should ask ourselves what type of approximations they represent. The derivation was based on selecting the coefficients of the transfer function such that as many coefficients as possible of the Taylor series expansion of the delay are zero. We can conclude, therefore, that the approximation is *maximally flat*. This conclusion is supported by the forms of D_2 and D_3 in Eqs. (10.24) and (10.26): the denominator of each of the two expressions is obtained by adding one high-order term to the corresponding numerator. This should remind us of our discussion of the maximal flat magnitude in Chapter 6, specifically Eq. (6.53), where we determined that this was the condition to be satisfied by a rational function to approximate

a constant in the maximally flat sense.[1] Applying this rule to Eq. (10.19) results in the equation

$$1/a_0 = a_1^2/a_0^2 - 2/a_0$$

which is identical to Eq. (10.21) and so leads to the same solution.

A clever method that is computationally simpler and more direct is due to Storch (1954). It starts from Eq. (10.10), the transfer function for an ideal time delay:

$$T(s) = e^{-s} = \frac{1}{e^s} \tag{10.27}$$

and makes use of the hyperbolic function identity

$$e^s = \sinh\ s + \cosh\ s \tag{10.28}$$

Then the transfer function becomes

$$T(s) = \frac{1}{e^s} = \frac{1}{\sinh\ s + \cosh\ s} = \frac{1/\sinh\ s}{1 + \coth\ s} \tag{10.29}$$

The series expansions of the hyperbolic functions of concern are

$$\cosh\ s = 1 + \frac{s^2}{2!} + \frac{s^4}{4!} + \frac{s^6}{6!} + \cdots \tag{10.30}$$

$$\sinh\ s = s + \frac{s^3}{3!} + \frac{s^5}{5!} + \frac{s^7}{7!} + \cdots \tag{10.31}$$

Dividing the first by the second, inverting, repeating the division, and continuing this process, we obtain the infinite continued fraction expansion of the coth s function:

$$\coth\ s = \frac{1}{s} + \cfrac{1}{\frac{3}{s} + \cfrac{1}{\frac{5}{s} + \cfrac{1}{\frac{7}{s} + \cdots}}} \tag{10.32}$$

In the Storch approach the continued fraction is simply truncated after n terms. The result is a quotient of polynomials where the numerator is identified with cosh s and the denominator with sinh s. The sum of the numerator and denominator polynomials is thus the approximation to e^s in Eq. (10.29). Storch showed that this truncation gave maximally flat delay at $\omega = 0$, no matter where the continued fraction is truncated. Further, he was first to associate the denominator polynomial thus obtained with a class of Bessel polynomials.

To show the simplicity of the Storch approach, we let $n = 2$ and then $n = 3$. For $n = 2$, Eq. (10.32) becomes

[1] Note that maximal flatness is a mathematical property of a rational function. Whether this function represents physically a magnitude or a delay is immaterial.

$$\coth s = \frac{1}{s} + \frac{1}{3/s} = \frac{3 + s^2}{3s} \tag{10.33}$$

Adding numerator and denominator, we obtain

$$\mathcal{B}_2 = s^2 + 3s + 3 \tag{10.34}$$

which is identical to the denominator of Eq. (10.23), which we obtained with great difficulty. For $n = 3$,

$$\coth s = \frac{1}{s} + \frac{1}{3/s + 1/(5/s)} = \frac{6s^2 + 15}{s^3 + 15s} \tag{10.35}$$

Again adding numerator and denominator gives

$$\mathcal{B}_3 = s^3 + 6s^2 + 15s + 15 \tag{10.36}$$

which is the same as the denominator of Eq. (10.25). We may use this procedure to generate all denominator polynomials. As an alternative, we may make use of the following recursion formula[2]:

$$\mathcal{B}_n = (2n - 1)\mathcal{B}_{n-1} + s^2\, \mathcal{B}_{n-2} \tag{10.37}$$

and so generate the Bessel polynomial for any value of n. In forming the Bessel–Thomson function, the numerator of $T(s)$ is always chosen so that $T_n(j0) = 1$. Thus the general form of the function is

$$T_n(s) = \frac{\mathcal{B}_n(0)}{\mathcal{B}_n(s)} \tag{10.38}$$

We will be interested in properties of the Bessel polynomial $\mathcal{B}_n(s)$. But before we undertake this study, let us see how we have fared in making $D_n(\omega)$ maximally flat. For each $T_n(s)$ of Eq. (10.38) we can calculate the corresponding $D_n(\omega)$, by use of Eq. (10.16), just as was done in finding $D_2(\omega)$ in Eq. (10.24) and $D_3(\omega)$ in Eq. (10.26). The result of plotting each $D_n(\omega)$ as a function of ω is shown in Fig. 10.3. Sure enough, $D_n(\omega) \cong 1$ for small ω, and the delay is flat over a range of ω, with larger values of n giving a wider band of frequencies for flat response. Thus we have attained our objective of approximating the flat delay shown in Fig. 10.2c.

Because the Bessel–Thomson approximation leads to lowpass filters, we are concerned with the lowpass magnitude characteristic of the function:

$$|T_n(j\omega)| = \left| \frac{\mathcal{B}_n(0)}{\mathcal{B}_n(j\omega)} \right| \tag{10.39}$$

The magnitude of the Bessel–Thomson filter is plotted for orders 4 and 8 in Fig. 10.4. We notice a very gradual transition from passband to stopband that is characteristic for all n. Corresponding plots for Butterworth responses of orders 4 and 8 are shown for comparison.

[2] We use the script $\mathcal{B}$ to avoid confusion with the Butterworth polynomial.

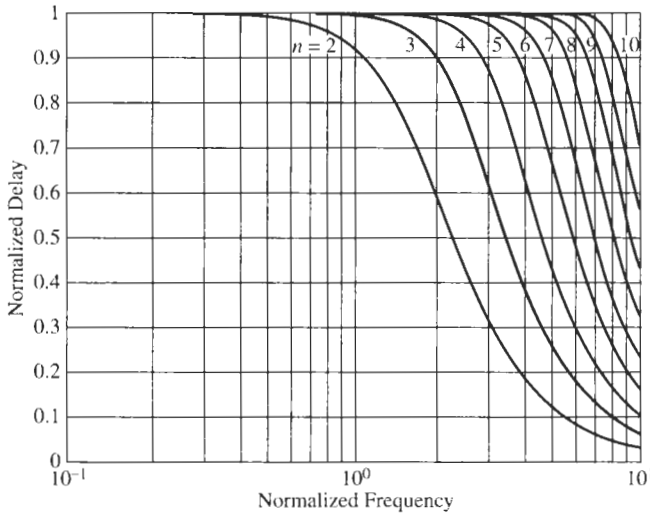

Figure 10.3 Delay of Bessel–Thomson filters of orders 2 through 10.

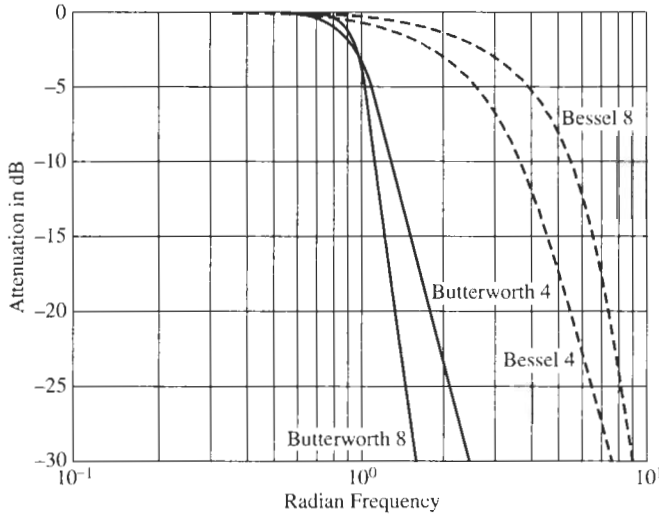

Figure 10.4 Comparison of Bessel–Thomson and Butterworth responses of orders 4 and 8.

The attenuation of both responses increases for high frequencies at the same rate as any all-pole lowpass filter, namely as ω^n, i.e., $20n$ dB/decade. But note that the magnitude of the Bessel–Thomson filter is neither constant over a wide range of ω through the passband, nor does it have sharp cut-off in the transition region. In this respect it performs worse than even the Butterworth response (to say nothing of the Chebyshev or Cauer responses). We will see shortly that Bessel–Thomson filters have smaller pole quality factors, and from our earlier discussions we expect this to result in a more gradual roll-off, as illustrated in Fig. 10.4. In Section 10.4 we compare the Bessel–Thomson response with others in more detail.

10.3 BESSEL POLYNOMIALS

The procedure for generating Bessel polynomials described in the last section can be extended to any value of n. The result is the family of polynomials that begins

$$\begin{aligned}
\mathcal{B}_0 &= 1 \\
\mathcal{B}_1 &= s + 1 \\
\mathcal{B}_2 &= s^2 + 3s + 3 \\
\mathcal{B}_3 &= s^3 + 6s^2 + 15s + 15 \\
\mathcal{B}_4 &= s^4 + 10s^3 + 45s^2 + 105s + 105 \\
&\vdots \quad \vdots
\end{aligned} \tag{10.40}$$

If we write the polynomials in the general form

$$\mathcal{B}_n = s^n + a_{n-1}s^{n-1} + \cdots + a_1 s + a_0 = \sum_{j=0}^{n} a_j s^j \qquad a_n = 1 \tag{10.41}$$

Then the coefficients can be tabulated as shown in Table 10.1, which gives values to $n = 8$, but could be routinely extended to higher n using the recursion relationship of Eq. (10.37).

Unlike the Butterworth and Chebyshev responses, there is no simple rule to determine the roots of $\mathcal{B}_n(s) = 0$, which are the poles of the Bessel–Thomson response. But the roots can be routinely found by computer methods; they are tabulated up to $n = 8$ in Table 10.2; the poles in the s plane are shown in Fig. 10.5 and tabulated in Table 10.3. It was shown by Henderson and Kautz (1958) that the poles of the Bessel–Thomson response very nearly lie on eccentric circles. The centers for the circles for successive values of n are equally spaced along the positive real axis, and the radii of successive circles differ by equal amounts.

Filters are designed from ω_0 and Q specifications that may be found from pole locations. If the pole is located at $-\alpha \pm j\beta$, then, as we found in Eq. (7.37),

$$\omega_0 = (\alpha^2 + \beta^2)^{1/2} \tag{10.42}$$

and

$$Q = \frac{1}{2\alpha}(\alpha^2 + \beta^2)^{1/2} \tag{10.43}$$

TABLE 10.1 Coefficients of $\mathcal{B}_n(s) = s^n + a_{n-1}s^{n-1} + \cdots + a_1 s + a_0$

n	a_0	a_1	a_2	a_3	a_4	a_5	a_6	a_7
1	1							
2	3	3						
3	15	15	6					
4	105	105	45	10				
5	945	945	420	105	15			
6	10,395	10,395	4,725	1,260	210	21		
7	135,135	135,135	62,370	17,325	3,150	378	28	
8	2,027,025	2,027,025	945,945	270,270	51,975	6,930	630	36

TABLE 10.2 Roots of $\mathcal{B}_n(s) = 0$ for $n = 1$ to $n = 8$ [Poles of $T_n(s)$ for Bessel–Thomson Response]

n								
1	-1.0000000							
2	-1.5000000	$\pm j0.8660254$						
3	-2.3221854;	-1.8389073	$\pm j1.7543810$					
4	-2.8962106	$\pm j0.8672341$;	-2.1037894	$\pm j2.6574180$				
5	-3.6467386;	-3.3519564	$\pm j1.7426614$;	-2.3246743	$\pm j3.5710229$			
6	-4.2483594	$\pm j0.8675097$;	-3.7357084	$\pm j2.6262723$;	-2.5159322	$\pm j4.4926730$		
7	-4.9717869;	-4.7582905	$\pm j1.7392861$;	-4.0701392	$\pm j3.5171740$;	-2.6856769	$\pm j5.4206941$	
8	-5.5878860	$\pm j0.8676144$;	-2.8389840	$\pm j6.3539113$;	-4.3682892	$\pm j4.4144425$;	-5.2048408	$\pm j2.6161751$

TABLE 10.3 $\mathcal{B}_n(s)$ in Factored Form for $n = 1$ to $n = 8$

n	$\mathcal{B}_n(s)$	$\mathcal{B}_n(0)$
1	$s + 1$	1
2	$s^2 + 3s + 3$	3
3	$(s^2 + 3.67782s + 6.45944)(s + 232219)$	15
4	$(s^2 + 5.79242s + 9.14013)(s^2 + 4.20758s + 11.4878)$	105
5	$(s^2 + 6.70391s + 14.2725)(s^2 + 4.64934s + 18.15631)(s + 3.64674)$	945
6	$(s^2 + 8.49672s + 18.80113)(s^2 + 7.47142s + 20.85282)(s^2 + 5.03186s + 26.51402)$	10,395
7	$(s^2 + 5.37135s + 36.59678)(s^2 + 8.14029s + 28.93655)(s^2 + 9.51658s + 25.66644)(s + 4.97179)$	135,135
8	$(s^2 + 5.67797s + 48.43202)(s^2 + 1.22567s + 8.73658)(s^2 + 8.736578s + 38.56925)(s^2 + 10.40968s + 33.93474)(s^2 + 11.17577s + 31.97723)$	2,027,025

From these relationships the values of ω_0 and Q for $n = 2$ to $n = 8$ are tabulated in Table 10.4.

The relationship of the Bessel–Thomson poles to those previously found for the Butterworth and Chebyshev cases is of special interest. The general form of these relationships is illustrated by specific example. Let us consider the case $n = 3$, $\alpha_{\max} = 0.1$ dB for the Chebyshev response. To reach a meaningful comparison, let us scale the frequency so that all responses have the same half-power value of 0.707. The transfer function of the Bessel–Thomson filter is

$$T_3(s) = \frac{15}{s^3 + 6s^2 + 15s + 15} \tag{10.44}$$

and the corresponding magnitude function with $s = j\omega$ is

TABLE 10.4 Poles of $T_n(s)$ in Terms of Q, ω_0, and σ

n	ω_0; Q Are Ordered Pairs; $-\sigma$ Is One Entry				$\mathcal{B}_n(0)$
2	1.732; 0.577				3
3	2.542; 0.691	2.322			15
4	3.023; 0.522	3.389; 0.806			105
5	3.778; 0.564	4.261; 0.916	3.647		945
6	4.336; 0.510	4.566; 0.611	5.149; 1.023		10,395
7	5.066; 0.532	5.379; 0.661	6.050; 1.126	4.971	135,135
8	5.655; 0.506	5.825; 0.560	6.210; 0.711	6.959; 1.226	2,027,025

$\mathcal{B}_n(0) = \prod_{i=1}^{n-1} \text{or } {}^{n} \omega_i^2 \times \begin{cases} 1, & n \text{ even} \\ \sigma_l, & n \text{ odd.} \end{cases}$

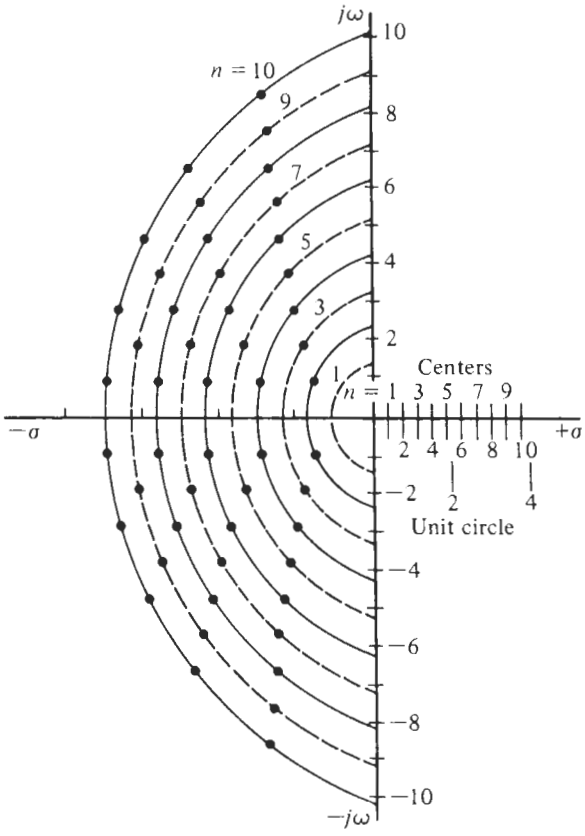

Figure 10.5 Pole locations of Bessel–Thomson filters.

$$|T_3(j\omega)| = \frac{15}{[(15 - 6\omega^2)^2 + (15\omega - \omega^3)^2]^{1/2}} \tag{10.45}$$

From this we determine that T_3 has a value of 0.707 when $\omega = 1.755666$. If we scale the $n = 3$ poles given in Table 10.2 by this amount, we obtain the scaled pole location as

$$-1.32268 \qquad \text{and} \qquad -1.04741 \pm j0.99926 \tag{10.46}$$

The Butterworth poles lie on the unit circle shown in Fig. 10.6, and the Chebyshev poles are on an ellipse that is inside the unit circle. The Bessel–Thomson poles lie outside the unit circle. This is an interesting demonstration, which shows that moving the poles of $T(s)$ a small distance in the s-plane changes the form of response achieved.

Specifically we note that shifting the poles further to the left, away from the $j\omega$ axis, means that these poles have lower quality factors. Consequently, as we know already from our earlier discussion, Bessel–Thomson filters cannot provide steep cut-off behavior in the transition band in addition to the flat delay for which they were designed. Considering the Bessel–Thomson delay in Fig. 10.3 and comparing it with Fig. 8.21, the delay performances of the other lowpass responses discussed in Chapters 6 to 8, we see that there is a trade-off between the requirements of flat delay and steep attenuation increase. Since flat attenuation requires low-Q poles and

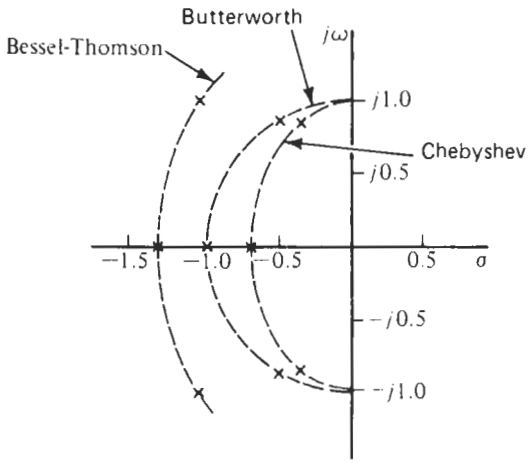

Figure 10.6 Pole locations of third-order Bessel, Butterworth, and Chebyshev responses.

steep roll-off depends on high-Q poles, the requirements are in conflict and cannot be realized with the same transfer function. The incompatibility of the requirements arises from the fact that our transfer functions have their zeros on the $j\omega$-axis (including ∞); as soon as we allow zeros to be in the right half-plane, at $z_i = \sigma_i \pm j\omega_i$ with $\sigma_i > 0$, we can realize filters that have both flat delay and sharp cut-off specifications. We will treat this situation in Chapter 11.

10.4 FURTHER COMPARISONS OF RESPONSES

We should remind ourselves that the Bessel–Thomson response resulted from imposing the requirements that

$$\frac{dD_n(\omega)}{d\omega}\Big|_{\omega=0} = 0 \qquad \text{and} \qquad D_n(0) = 1 \tag{10.47}$$

and that the delay be maximally flat at $\omega = 0$. From this we determined the required coefficients of $T_n(s)$ and the pole positions we have just discussed. We merely accepted the magnitude response that resulted and found that $|T_n(j\omega)| = 1$ only at low frequencies. In contrast, the Butterworth, Chebyshev, and Cauer responses were derived without reference to delay. But $D_n(\omega)$ can be found for any transfer function by simply determining the phase function $\theta(\omega)$ and then differentiating with respect to ω. We next inquire as to the delay responses associated with the Butterworth and Chebyshev transfer functions.

The Butterworth response was derived from the requirement that the magnitude function be maximally flat for small ω. If we determine the delay characteristics by the method just described, the result is as shown in Fig. 10.7 for $n = 2$ to $n = 10$. We see that the delay has a peak value, especially for larger values of n, at the normalized frequency $\omega = 1$. This may be contrasted to the Bessel–Thomson response shown in Fig. 10.3, which achieves the maximally flat response form. The reason for the peaking delay of the Butterworth response is found in the higher pole quality factors resulting in sharper cut-off and less linear phase.

The delay response for Chebyshev filters is more complicated. They were derived from the requirement of equal-ripple attenuation in the passband, and this resulted in a phase response that was much less linear than the phase of a filter with maximally flat magnitude. In the Chebyshev case, the transfer functions are determined by the ripple width $\alpha_{\max}$ as well as

by their order n, and so are the delays. Figure 10.8 shows the delay characteristic of the Chebyshev responses for $n = 3, 5, 7$, and 9. We have plotted the Chebyshev delay for 0.5-dB and 2-dB ripple, and notice that the delay gets worse, i.e., less constant, not only with increasing degree but also that larger ripple results in worse delay performance. The reason is again the larger quality factor: Q increases with increasing ripple as can be verified from Table 7.2. Chebyshev delay responses will likely cause considerable delay distortion and the problem is worse with elliptic filters because of their larger Q values. But in making this statement we are again cautioned that the degree of the total filter must be kept in mind as we pointed out in Section 8.6.

Another distinguishing characteristic of the Bessel–Thomson filter is the time-domain response to a step input, the so-called *step response*. When a step voltage is applied to a filter, as shown in Fig. 10.9, the resulting response is usually characterized by two quantities. The

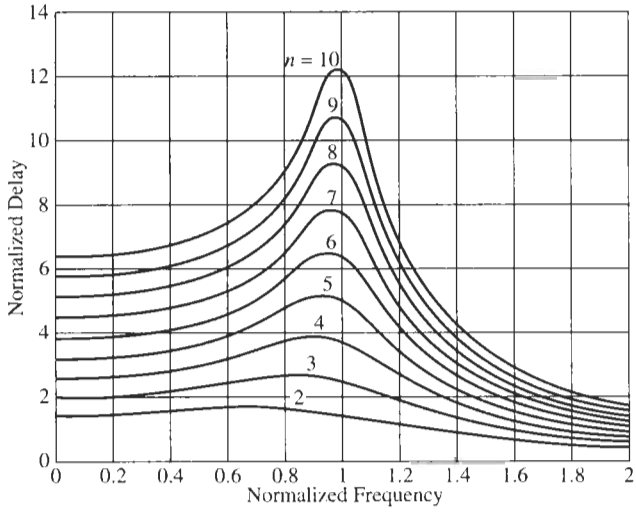

Figure 10.7 Delay of Butterworth filters of orders 2 through 10.

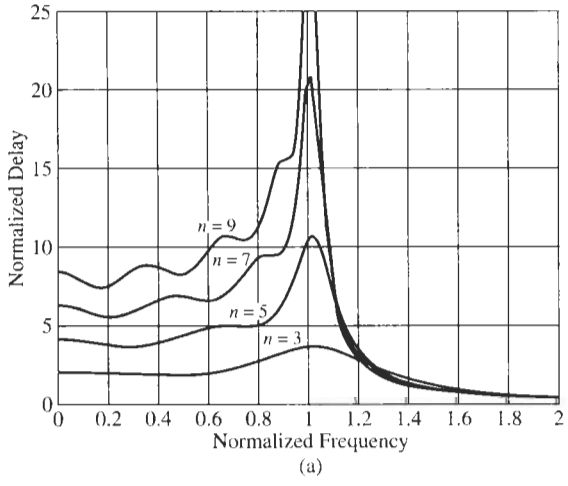

(a)

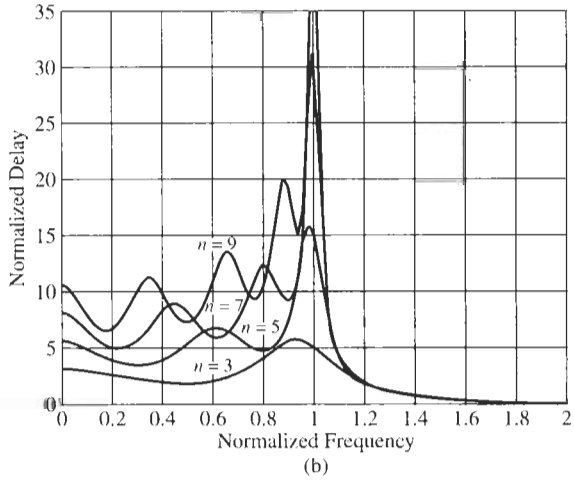

(b)

Figure 10.8 Delay of Chebyshev filters of orders 3, 5, 7, and 9: (a) 0.5-dB ripple; (b) 2-dB ripple.

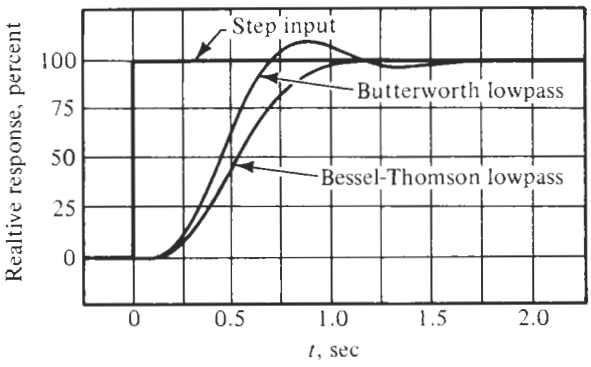

Figure 10.9 Step response of Butterworth and Bessel–Thomson filters ($n = 4$).

first is the *overshoot*, defined as

$$\% \text{ overshoot} = \frac{v_{2\max} - v_{2\text{final}}}{v_{2\text{final}}} \times 100\% \tag{10.48}$$

The second quantity is the *rise time*, usually defined as the time for the response $v_2(t)$ to go from 10 to 90% of its final value. The two responses shown in Fig. 10.9 are for the case $n = 4$. The Butterworth response has considerable overshoot, while the Bessel–Thomson response does not. Also the Butterworth response has a smaller rise time than the Bessel–Thomson response. These same characteristics are shown in Fig. 10.10 for a pulse input and for $n = 8$ Butterworth and Bessel–Thomson filters. This absence of overshoot and ringing is a distinguishing characteristic of Bessel–Thomson filters and is sometimes the reason for their selection for a given application.

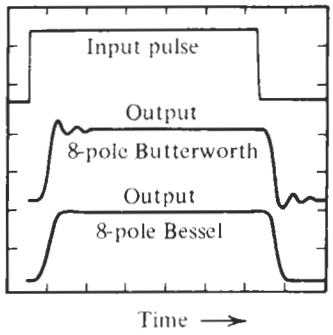

Figure 10.10 Pulse response of eighth-order Butterworth and Bessel–Thomson filters.

10.5 DESIGN OF BESSEL–THOMSON FILTERS

At this point in our development of a design procedure for the Butterworth, Cauer, and Chebyshev filters we showed that the specification of attenuations $\alpha_{\min}$ and $\alpha_{\max}$ together with related frequencies determined n, the order of the filter response. There is no such direct analysis available for Bessel–Thomson filters, and there is no formula for n. Consequently we make use of design curves to help us find the smallest degree necessary. Figure 10.11 explains the definitions used. Design is accomplished using guidelines often derived from prior experience.

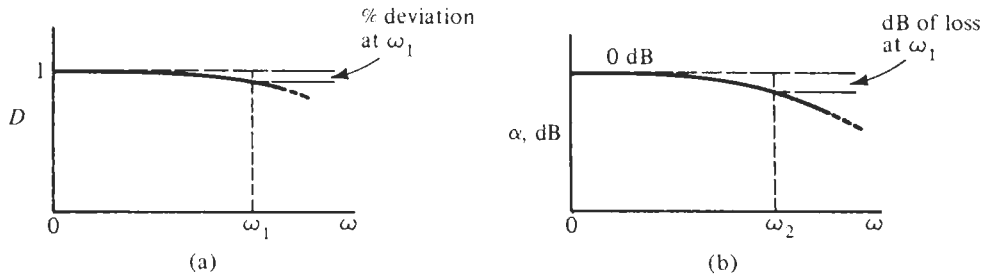

Figure 10.11 Definitions of delay error and passband attenuation in Bessel–Thomson filters.

1. As shown in Fig. 10.11a we define an error in percent by which the filter's delay deviates from the ideal $D = 1$. Since D is a function of frequency, we need to specify at which frequency ω_1 the maximally acceptable delay error occurs.
2. In an analogous fashion, Fig. 10.11b shows how the Bessel–Thomson lowpass passband attenuation differs from the ideal, 0 dB. Again we need to specify at which frequency ω_2 the maximally acceptable loss occurs.

This information is used in Fig. 10.12 to determine the required degree of the Bessel–Thomson filter. In Fig. 10.12a we have plotted the passband attenuation error as a function of filter degree and frequency. For instance, if a 2-dB passband loss is acceptable until $\omega_1 = 1.7$, the intersection of the horizontal line at 2 dB and the vertical line at 1.7 results in $n \approx 4.2$. As always, we round up to use $n = 5$. Analogously, Fig. 10.12b contains design curves that relate the delay error to degree and frequency. A prescribed maximum delay error of 3% up to a frequency of 3.3 leads to $n \approx 5.3$, i.e., $n = 6$ must be taken. If *both* requirements are to be met by *the same* filter, we have to use the larger of the two degrees: $n = 6$.

3. Finally, in some occasions the delay filter serves a secondary function of acting as a

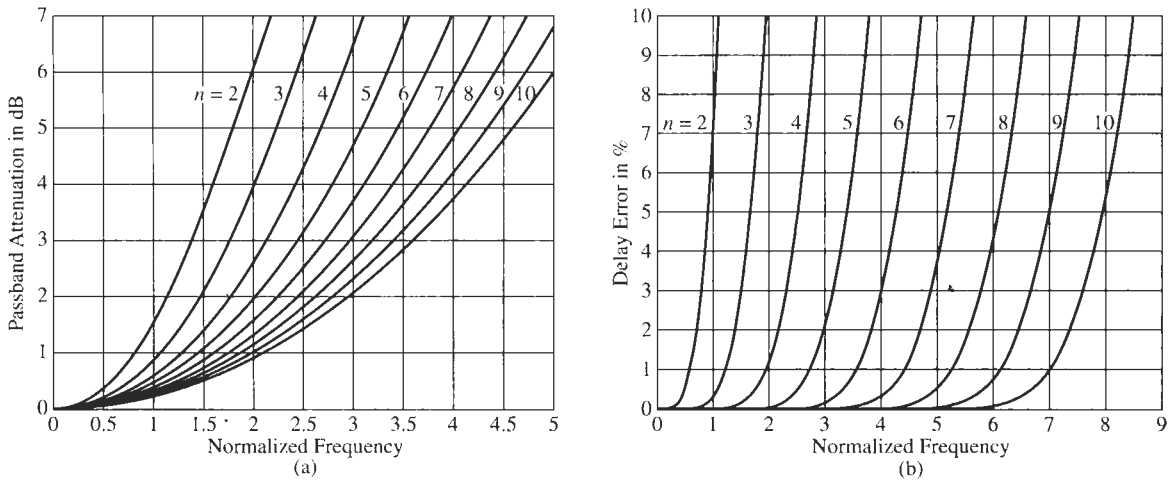

Figure 10.12 Design curves for determining the degree n of the Bessel–Thompson filter to meet (a) the acceptable loss and (b) the maximum delay error.

lowpass filter. Then it is required to determine the loss it provides at some frequency ω_3 in the stopband,

$$\alpha(\omega_3) = 20 \log |T(j\omega_3)| = 20 \log \left| \frac{\mathcal{B}_n(0)}{\mathcal{B}_n(j\omega)} \right| \text{ dB} \tag{10.49}$$

Because closed-form solutions for the degree n are not available we use again a set of design curves. Figure 10.13 shows a plot of the stopband attenuation of Bessel–Thomson filters of order n, which helps to find the necessary degree. For example, if 18-dB attenuation is needed at $\omega_3 = 6.5$, the figure indicates that $n = 7$ will be required. Since only one parameter, the degree n, is available to the designer, the largest degree must be chosen so that all specifications can be met. Note that if substantial stopband attenuation is required coupled with good delay performance, a delay filter of very high order would be necessary. In these cases alternative techniques are preferred that use delay equalizers together with maximally flat or inverse Chebyshev responses. We will leave the discussion of these approaches to Chapter 11.

Let us next illustrate the design of a Bessel–Thomson filter by an example.

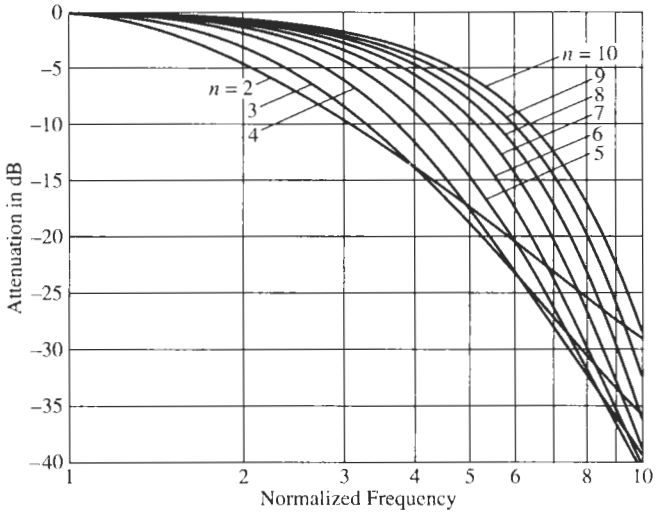

Figure 10.13 Transition and stopband attenuation of Bessel–Thomson filters.

EXAMPLE 10.1

To be designed is a delay filter to provide $D = 100\ \mu$s delay with a delay deviation of at most 10% at the frequency $\omega_1 = 25$ krad/s and at most 1-dB loss at a frequency $\omega_2 = 10$ krad/s.

Solution

We first have to determine the normalizing frequency ω_c so that we know how to interpret the normalized frequency axes in Fig. 10.12. According to Eq. (10.9) we have $\omega_c = 1/D = 1/100\ \mu\text{s} = 10$ krad/s. Therefore, ω_1 corresponds to 2.5 and ω_2 to 1. From Fig. 10.12b we

find that the 10% deviation requirement is satisfied by $n = 4$. From Fig. 10.12a we require $n = 3$ to keep the loss at less than 1 dB. Clearly, a Bessel–Thomson filter of order $n = 4$ is required.

From Table 10.3, the transfer function is

$$T_4(s) = \frac{9.14013}{s^2 + 5.79242s + 9.14013} \frac{11.4878}{s^2 + 4.20758 + 11.4878}$$

As an alternative we may consult Table 10.4, from which Q and ω_0 of the two sections are seen to be

$$\omega_1 = 3.023, \quad Q_1 = 0.522, \quad \omega_2 = 3.389, \quad Q_2 = 0.809$$

We have split the numerator factor 105 into $105 = 9.14013 \times 11.4878$ so that each module realizes 0 dB at $\omega = 0$. Thus the filter function is fully specified. For the circuit we select the Sallen–Key module of Fig. 4.31a, which realizes, by Eq. (4.100) with $K = 1$:

$$T(s) = \frac{G_1 G_2/(C_1 C_2)}{s^2 + \dfrac{G_1 + G_2}{C_1} s + \dfrac{G_1 G_2}{C_1 C_2}} = \frac{\omega_0^2}{s^2 + \dfrac{\omega_0}{Q} s + \omega_0^2}$$

We have set $K = 1$ because 0 dB gain is specified for each module. To solve for the element values we compute

$$G_1 + G_2 = \frac{\omega_0 C_1}{Q} \quad \text{and} \quad G_2 = \frac{\omega_0^2 C_1 C_2}{G_1}$$

Inserting the second equation into the first one results in

$$G_1^2 - \frac{\omega_0 C_1}{Q} G_1 + \omega_0^2 C_1 C_2 = 0 \quad \text{or} \quad \left(\frac{G_1}{\omega_0 C_1}\right)^2 - \frac{1}{Q}\left(\frac{G_1}{\omega_0 C_1}\right) + \frac{C_2}{C_1} = 0$$

This quadratic equation has no real solutions if we choose, as we usually do, two equal capacitors. Consequently, let us try to find the constraint on the capacitor ratio. Solving the quadratic equation, we find

$$\frac{G_1}{\omega_0 C_1} = \frac{1}{2Q} \pm \sqrt{\frac{1}{4Q^2} - \frac{C_2}{C_1}}$$

This equation requires $C_2/C_1 < 0.9175$ for Module 1 and $C_2/C_1 < 0.3820$ for Module 2. Selecting readily available capacitor values, let us in Module 1 choose $C_1 = 2$ nF, $C_2 = 1$ nF and in Module 2, $C_1 = 5$ nF, $C_2 = 1$ nF. Then we obtain

$$\frac{G_1}{\omega_0 C_1} = 1.6040 \text{ in Module 1}, \quad \frac{G_1}{\omega_0 C_1} = 1.0446 \text{ in Module 2}$$

Using further that $\omega_{01} = 3.023 \times 10$ krad/s and $\omega_{02} = 3.389 \times 10$ krad/s, we use our equations to compute

$$R_{11} = 10.31 \text{ k}\Omega, \quad R_{21} = 53.0 \text{ k}\Omega, \quad R_{12} = 5.65 \text{ k}\Omega, \quad R_{22} = 30.8 \text{ k}\Omega$$

With this we have determined all elements; the final circuit and its experimental performance are shown in Fig. 10.14. Not many instruments permit measuring the delay directly, but only the phase; we have shown in Fig. 10.14b the phase versus a linear frequency scale. Notice that the phase is almost perfectly linear over the specified range of frequencies. More detailed curves of magnitude and phase responses are contained in Fig. 10.18c.

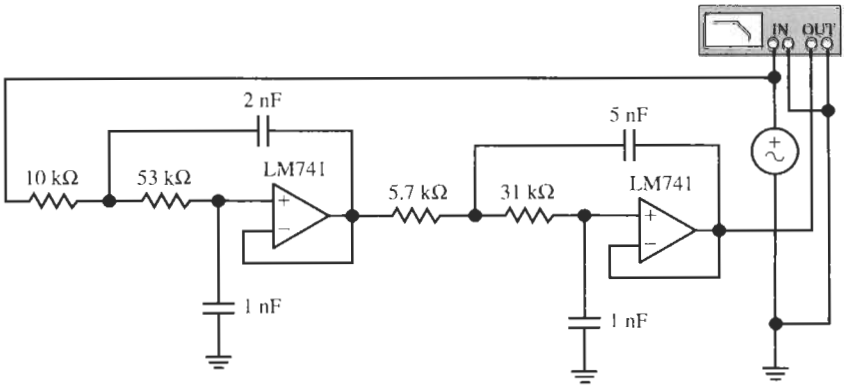

(a)

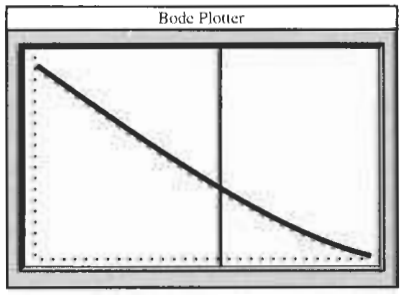

(b)

Figure 10.14 Circuit and test results for Example 10.1: (a) circuit, (b) test results. (Bode Plotter scales: 100 mHz to 7 kHz; −225 to 0°; cursor at 3.920 kHz, −140.3°.)

10.6 EQUAL-RIPPLE DELAY RESPONSE

When we discussed the Chebyshev approximation of a magnitude function in Chapter 7, we saw that we could gain advantages by distributing the permitted magnitude error uniformly over the passband rather than letting it increase monotonically toward the corner of the passband as in the maximally flat response in Chapter 6. When considering delay approximations in this chapter we might ask ourselves whether similar advantages might not be obtained if we develop a filter with an equiripple delay, rather than the maximally flat (Bessel–Thomson) approximation. Figure 10.15 illustrates the performance we would hope to obtain: for a desired specified delay, normalized in the figure to $D(0) = 1$, we would like to achieve some combination of smaller delay error and wider bandwidth. The approach we take follows the previous treatment, that is, we start from a lowpass transfer function $T_E(s)$ with a new denominator polynomial $\mathcal{E}(s)$

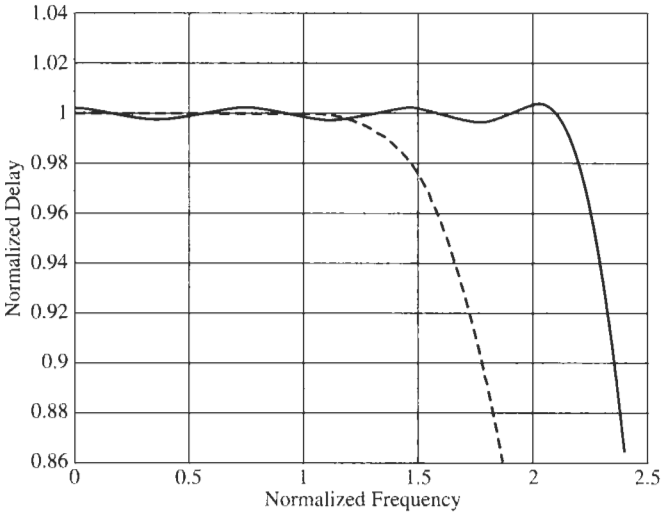

Figure 10.15 Equiripple delay versus Bessel–Thomson (dashed curve) delay performance. Both curves are normalized to provide $D(0) = 1$, and assume functions of order $n = 7$.

$$T_{\mathcal{E}}(s) = \frac{\mathcal{E}(0)}{\mathcal{E}(s)} = \frac{a_0}{s^n + a_{n-1}s^{n-1} + \cdots + a_1 s + a_0} \tag{10.50}$$

and then form an expression for the delay as in Eq. (10.16). Similar to the Bessel–Thomson case where we required the delay to approximate a constant ($D = 1$) in the maximally flat sense, we now impose the condition that the delay approximate the constant with uniform error over the desired bandwidth. As depicted in Fig. 10.15, for a given delay error the useful bandwidth of the equiripple delay approximation is expected to be wider than that of a maximally flat delay approximation of the same order.

Unfortunately, in contrast to the maximally flat case or the equiripple magnitude response, closed-form solutions for an equiripple delay transfer function have not been found. Numerical routines must be employed. A way to determine the n coefficients of the nth-order transfer function $T_{\mathcal{E}}(s)$ is as follows: Since a constant delay implies a linear phase, we may start the numerical approach from a required linear phase and assume a sinusoidal ripple for ease of treatment,

$$\theta(\omega) = -D_0\omega - \Delta\theta \sin(\omega T) \tag{10.51}$$

The delay is then computed as

$$D_{\mathcal{E}}(\omega) = -\frac{d\theta}{d\omega} = D_0 + \Delta\theta \times \pi/180^\circ \times T \times \cos(\omega T) \tag{10.52}$$

where we have converted $\Delta\theta$ into radians. T is the period of the ripple; it is (very) approximately equal to the constant delay bandwidth divided by $n/2$, n being the degree of the function $T_{\mathcal{E}}(s)$. Just as in the maximally flat case, we choose a normalizing frequency $\omega_c = 1/D_0$ in the design of the delay filter. To determine the polynomial $\mathcal{E}(s)$ a differential equation can be set up that specifies that the phase of Eq. (10.50) has exactly n locations where the slope equals D_0; using an optimization routine, for given values $\Delta\theta$ this differential equation can be solved

numerically for the coefficients of $\mathcal{E}(s)$. We shall not discuss the algorithms that might achieve the task of finding $\mathcal{E}(s)$ but just list a couple of results. Table 10.5[3] contains the polynomials for $\Delta\theta = 0.05°$ and $\Delta\theta = 0.5°$, and Fig. 10.16 contains plots of the delay and magnitude of $T_{\mathcal{E}}(s)$ for $\Delta\theta = 0.05°$ and orders 2 through 10. Plots for $\Delta\theta = 0.5°$ can be found in Zverev (1967). The constant-delay bandwidth of the 0.5° filter is slightly wider than that of the 0.05° response, and the attenuation is slightly larger, and steeper in the transition band. Note that the normalized delay implemented by the function $T_{\mathcal{E}}(s)$ is not $D_0 = 1$ at the origin. Rather, D_0 as well as the constant-delay bandwidth $\omega_{\mathcal{E}}$ are functions of n. The exact values are usually unimportant; approximate numbers are given in Table 10.6.

The more interesting specification is the delay error; it is twice the ripple width,

$$\Delta D = 2T\Delta\theta \times \frac{\pi}{180°} \tag{10.53}$$

and is independent of n because the functions were designed to provide exactly the specified ripple. The delay error is, of course, proportional to the phase error as indicated by Eq. (10.53). For $\Delta\theta = 0.05°$ the error is $\Delta D \approx 0.015$ and for $\Delta\theta = 0.5°$ it is $\Delta D \approx 0.15$. However, the bandwidth $\omega_{\mathcal{E}}$ over which the delay error ΔD stays within the design specifications increases with n; it is also given in Table 10.6.

Note that the delay, the delay error, and $\omega_{\mathcal{E}}$ are normalized by the frequency $\omega_c = 1/D$ that is given by the desired delay D of the filter. Thus, the denormalized physical values are D/ω_c, $\Delta D/\omega_c$, and $\omega = \omega_c\omega_{\mathcal{E}}$. When performing the denormalization we must remember though that equiripple delay filters have $D_0 \neq 1$ (see Table 10.6), whereas Bessel–Thomson filters approximate $D_0 = 1$. Since the denormalizing frequency $\omega_c = 1/D$ is determined from the desired delay D of the filter, we need to change the denormalizing frequency to $\omega_c = D_0 \times (1/D)$ so that the intrinsic delay D_0 of the equiripple delay filters is accounted for.

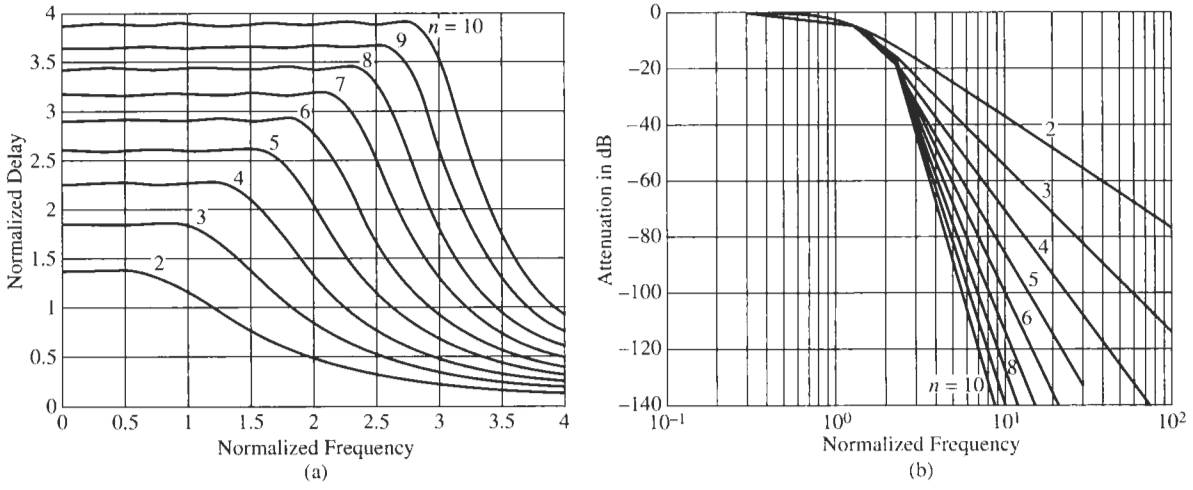

Figure 10.16 (a) Equiripple delay for orders 2 through 10 for 0.05° phase error. (b) Attenuation curves for the 0.05° ripple case.

[3] The functions were reconstructed from data given in A. I. Sverev, *Handbook of Filter Synthesis*.

TABLE 10.5 Equiripple Delay Polynomials and Their Factors[a]

n	$\mathcal{E}(s)$ for $\Delta\theta = 0.05°$
2	$s^2 + 2.0175s + 1.4638$
3	$s^3 + 2.7542s^2 + 3.6664s + 1.9660 = (s + 1.0459)(s^2 + 1.7082s + 1.8797)$
4	$s^4 + 3.4188s^3 + 6.5467s^2 + 6.5781s + 2.9098 = (s^2 + 1.4894s + 2.5170)(s^2 + 1.9294s + 1.1561)$
5	$s^5 + 4.0722s^4 + 10.2813s^3 + 15.0219s^2 + 12.8995s + 4.9527 =$ $(s + 0.9429)(s^2 + 1.3465s + 3.3726)(s^2 + 1.7828s + 1.5575)$
6	$s^6 + 4.6578s^5 + 14.5748s^4 + 27.6303s^3 + 34.8174s^2 + 25.9327s + 8.9446 =$ $(s^2 + 1.2301s + 4.3029)(s^2 + 1.6465s + 2.1607)(s^2 + 1.7811s + 0.9621)$
7	$s^7 + 5.2339s^6 + 19.7000s^5 + 45.9244s^4 + 76.5219s^3 + 84.0877s^2 + 57.1076s + 17.9801$ $= (s + 0.8613)(s^2 + 1.1456s + 5.3703)(s^2 + 1.5420s + 2.9514)(s^2 + 1.6850s + 1.3170)$
8	$s^8 + 5.7343s^7 + 25.119s^6 + 68.773s^5 + 141.60s^4 + 203.386s^3 + 203.617s^2 + 125.414s + 36.5917$ $= (s^2 + 1.0686s + 6.4160)(s^2 + 1.4432s + 3.8117)(s^2 + 1.5847s + 1.8509)(s^2 + 1.6379s + 0.8084)$
9	$s^9 + 6.2587s^8 + 31.569s^7 + 99.720s^6 + 246.287s^5 + 438.42s^4 + 582.20s^3 + 532.669s^2 + 308.05s + 84.108$ $= (s + 0.7939)(s^2 + 1.0115s + 7.6186)(s^2 + 1.3700s + 4.8149)(s^2 + 1.5122s + 2.5672)(s^2 +$ $1.5712s + 1.1250)$
10	$s^{10} + 6.6928s^9 + 37.9672s^8 + 134.350s^7 + 384.195s^6 + 807.263s^5 + 1324.078s^4 + 1588.383s^3 +$ $1357.028s^2 + 727.618s + 187.178$ $= (s^2 + 0.9565s + 8.7122)(s^2 + 1.2963s + 5.8059)(s^2 + 1.4304s + 3.3496)(s^2 + 1.4918s +$ $1.5957)(s^2 + 1.5178s + 0.6923)$
n	$\mathcal{E}(s)$ for $\Delta\theta = 0.5°$
2	$s^2 + 1.7179s + 1.2251$
3	$s^3 + 2.2194s^2 + 2.9172s + 1.4585 = (s + 0.8257)(s^2 + 1.3937s + 1.7664)$
4	$s^4 + 2.6972s^3 + 5.2265s^2 + 4.8753s + 2.1352 = (s^2 + 1.2075s + 2.6095)(s^2 + 1.4896s + 0.8182)$
5	$s^5 + 3.1428s^4 + 8.1546s^3 + 10.9062s^2 + 9.3599s + 3.4350 =$ $(s + 0.7056)(s^2 + 1.0823s + 3.6258)(s^2 + 1.3549s + 1.3427)$
6	$s^6 + 3.5157s^5 + 11.4100s^4 + 19.4175s^3 + 24.5344s^2 + 17.2433s + 5.8956 =$ $(s^2 + 0.9787s + 4.6423)(s^2 + 1.2332s + 2.0607)(s^2 + 1.3038s + 0.6163)$
7	$s^7 + 3.9483s^6 + 15.8251s^5 + 33.0994s^4 + 56.4783s^3 + 58.8283s^2 + 40.3332s + 12.3134$ $= (s + 0.6283)(s^2 + 0.9196s + 5.9694)(s^2 + 1.1626s + 3.0449)(s^2 + 1.2378s + 1.0782)$
8	$s^8 + 4.1884s^7 + 19.3554s^6 + 45.9464s^5 + 95.5431s^4 + 126.1854s^3 + 125.4300s^2 + 72.8840s + 20.9485$ $= (s^2 + 0.8370s + 6.8217)(s^2 + 1.0604s + 3.8587)(s^2 + 1.1331s + 1.6445)(s^2 + 1.1579s + 0.4839)$
9	$s^9 + 4.6717s^8 + 25.9466s^7 + 72.4476s^6 + 187.884s^5 + 314.508s^4 + 429.991s^3 + 380.601s^2 +$ $224.492s + 60.1767$ $= (s + 0.5729)(s^2 + 0.8158s + 8.5927)(s^2 + 1.0355s + 5.2528)(s^2 + 1.1095s + 2.5840)(s^2 +$ $1.1380s + 0.9006)$
10	$s^{10} + 4.7816s^9 + 29.1123s^8 + 86.8714s^7 + 253.433s^6 + 478.789s^5 + 783.666s^4 + 871.575s^3 +$ $734.966s^2 + 371.405s + 93.741$ $= (s^2 + 0.7414s + 9.1004)(s^2 + 0.9420s + 5.9103)(s^2 + 1.0099s + 3.2341)(s^2 + 1.0386s +$ $1.3573)(s^2 + 1.0497s + 0.3970)$

[a]The functions are reconstructed from data given in Zverev (1967).

TABLE 10.6 D_0 and Constant-Delay Bandwidth $\omega_{\mathcal{E}}$ for the Equiripple Delay Functions

	$\Delta\theta = 0.05°$, $\Delta D \approx 0.015$		$\Delta\theta = 0.5°$, $\Delta D \approx 0.15$	
n	D_0	$\omega_{\mathcal{E}}$	D_0	$\omega_{\mathcal{E}}$
2	1.39	0.58	1.45	0.80
3	1.86	0.92	1.94	1.25
4	2.27	1.25	2.34	1.66
5	2.60	1.54	2.67	1.83
6	2.91	1.67	3.00	2.20
7	3.17	2.15	3.21	2.42
8	3.43	2.35	3.54	2.71
9	3.66	2.59	3.66	2.93
10	3.89	2.83	4.04	3.06

EXAMPLE 10.2

A circuit is to realize the delay $D = 200\ \mu s$ over a frequency band of 3 kHz. The delay error must be less than 4%. Find the appropriate normalizing frequency.

Solution

For a Bessel–Thomson design, we pick $\omega_c = 1/200\ \mu s = 5$ krad/s and consult Fig. 10.12b: at the normalized frequency $2\pi \times 3000/5000 = 3.77$ we find that $n = 6$ is required.

For an equiripple delay design, we now face an uncertainty in picking the degree. Let us start by choosing a fourth-order 0.05° phase error response; if $n = 4$ is insufficient we repeat these steps for a larger n. We note from Table 10.6 that the constant-delay error is $\Delta D/D_0 = 0.015/2.27 = 0.66\%$, more than adequate. The constant-delay bandwidth for a fourth-order filter is

$$\frac{2.27 \times 5 \text{ krad/s}}{2\pi} 1.25 = 2.26 \text{ kHz}$$

too small by 25%. Thus, taking the next larger value of n, $n = 5$, we find the bandwidth to be

$$\frac{2.6 \times 5 \text{ krad/s}}{2\pi} 1.54 = 3.18 \text{ kHz}$$

which meets the specifications.

We shall still look at a comparison of the performance of the delay filters to help us decide which one to choose for an application. We have plotted in Fig. 10.17a the delay response of Bessel–Thomson, and of 0.05°- and 0.5°-equiripple delay filters of orders 4 and 7. All delays are normalized to $D = 1$ to facilitate the comparison. We observe that for a given delay, both equiripple delay responses have a wider constant-delay bandwidth than Bessel–

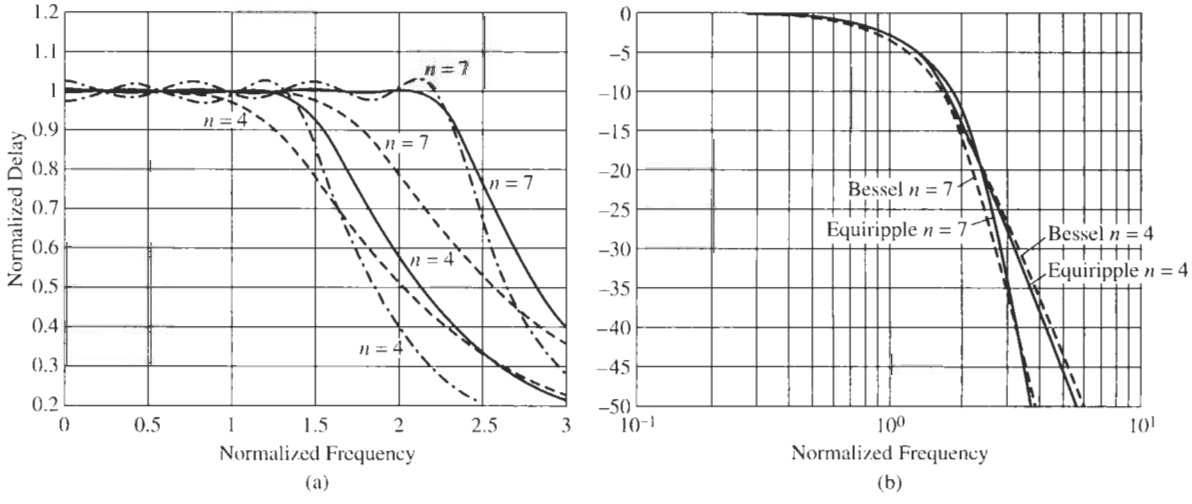

Figure 10.17 Comparison of delay filters: (a) fourth- and seventh-order Bessel–Thomson (dashed curves) and equiripple responses originating from linear phases with 0.05° (solid curves) and 0.5° phase errors; (b) attenuation of Bessel–Thomson and 0.05° equiripple delay responses.

Thomson filters. Figure 10.17b compares the attenuation performance of the Bessel–Thomson and 0.05° equiripple phase filters in pass- and stopbands. We see that the equiripple attenuation response is somewhat better than the maximally flat response, in that it provides a little sharper cut-off, though the differences are not large. (The 0.5°-phase equiripple delay response has a marginally wider bandwidth and a slightly larger attenuation than the 0.05° curves.) This comparison indicates that equiripple delay responses are generally preferable over Bessel–Thomson responses, especially since the advantages come at no cost: for the same degree, circuit structures for Bessel–Thomson filters are the same as the ones for equiripple delay filters, only the component values change. In addition, the equiripple design may require fewer circuit modules than a Bessel–Thomson filter. Normally the 0.05° case is chosen because of the smaller delay error.

Let us consider an example to see how the circuits compare for the same specifications; we shall repeat the requirements of Example 10.1 but design an equiripple delay filter.

EXAMPLE 10.3

Design a delay filter for the requirements given in Example 10.1: $\leq 10\%$ deviation in delay at frequencies $\leq \omega_1 = 25$ krad/s, and ≤ 1 dB loss at frequencies $\leq \omega_2 = 10$ krad/s. The filter is to provide $D = 100\ \mu$s delay. Use an equiripple delay filter with 0.05° phase error.

Solution

We choose again a fourth-order filter; according to Table 10.6, we have to account for the intrinsic delay of $D_0 = 2.27$. The normalizing frequency ω_c is then $\omega_c = 2.27/D = 2.27/100\ \mu\text{s} = 22.7$ krad/s. The delay error is $0.015/2.27 = 0.66\%$ as we saw in Example 10.2, and the constant-delay bandwidth is $(1.25 \times 22.7)/(2\pi) = 4.51$ kHz, higher than required. Since the equiripple delay filter provides better attenuation performance, i.e., lower passband loss (see Fig. 10.17b), than the Bessel–Thomson response in Example 10.1, we do not need to be concerned with the loss performance.

From Table 10.5, the transfer function is

$$T_4(s) = \frac{2.5170}{s^2 + 1.4894s + 2.5170} \frac{1.1561}{s^2 + 1.9294s + 1.1561}$$

from which the Q and ω_0 specifications of the two sections are seen to be

$$\omega_1 = 1.5865, \quad Q_1 = 1.065, \quad \omega_2 = 1.0752, \quad Q_2 = 0.5573$$

We observe that the quality factors of the equiripple delay filter are a little higher than those of the equivalent Bessel–Thomson circuit (see Example 10.1). We have assigned two numerator factors so that each module realizes 0 dB at $\omega = 0$. For the circuit we can again select the Sallen–Key module of Fig. 4.31a, which realizes with $K = 1$:

$$T(s) = \frac{G_1G_2/(C_1C_2)}{s^2 + \dfrac{G_1 + G_2}{C_1}s + \dfrac{G_1G_2}{C_1C_2}} = \frac{\omega_0^2}{s^2 + \dfrac{\omega_0}{Q}s + \omega_0^2}$$

As in Example 10.1, because of the required 0-dB gain we cannot use equal capacitors. To solve for the element values we compute

$$G_1 + G_2 = \frac{\omega_0 C_1}{Q} \quad \text{and} \quad G_2 = \frac{\omega_0^2 C_1 C_2}{G_1}$$

along with

$$\frac{G_1}{\omega_0 C_1} = \frac{1}{2Q} \pm \sqrt{\frac{1}{4Q^2} - \frac{C_2}{C_1}}$$

To have real solutions, we require $C_2/C_1 < 0.2204$ for Module 1 and $C_2/C_1 < 0.8049$ for Module 2. Selecting readily available capacitor values, let us in Module 1 choose $C_1 = 5$ nF, $C_2 = 1$ nF and in Module 2, $C_1 = 2$ nF, $C_2 = 1$ nF. Then we obtain

$$\frac{G_1}{\omega_0 C_1} = 0.6124 \text{ in Module 1}, \quad \frac{G_1}{\omega_0 C_1} = 1.449 \text{ in Module 2}$$

Using further that $\omega_{01} = 1.5865 \times 22.7$ krad/s $= 36.0$ krad/s and $\omega_{02} = 1.0752 \times 22.7$ krad/s $= 24.408$ krad/s, we use our equations to compute

$$R_{11} = 9.155\ \text{k}\Omega, \quad R_{21} = 17.15\ \text{k}\Omega, \quad R_{12} = 14.32\ \text{k}\Omega, \quad R_{22} = 59.36\ \text{k}\Omega$$

The circuit and its experimental performance are shown in Fig. 10.18. We have measured again the phase versus a linear frequency scale as is shown in Fig. 10.18b. Within the measurement resolution, the phase is seen to be "exactly" linear until ≈ 5.1 kHz, far better than the design requirements. The magnitude error is a little lower than 1 dB as can be expected from Fig. 10.17b. On the more detailed simulation plot in Fig. 10.18c, which shows the Bessel–Thomson response of the design in Example 10.1 for comparison, we notice that the loss of the equiripple response is lower than that of the Bessel–Thomson filter until about 7.9 kHz and thereafter increases faster. The phase is almost exactly linear to provide 100 μs until 5.1

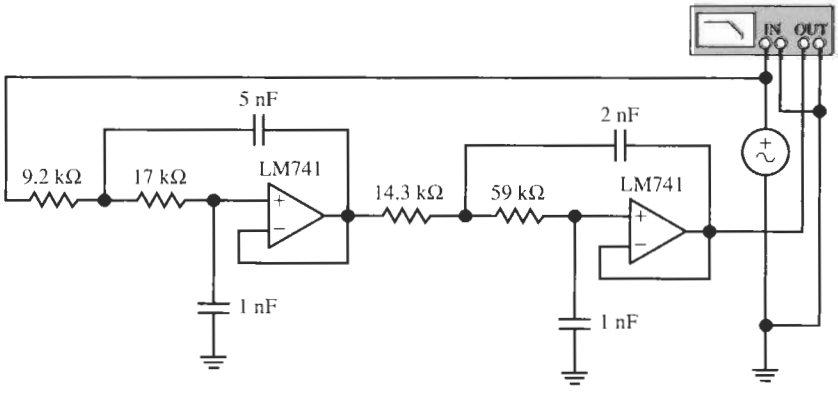

(a)

Figure 10.18 Circuit and test results for Example 10.3: (a) circuit, (b) test, and (c) simulation results. (Bode Plotter scales: 1 Hz to 10 kHz; −315 to 0°; cursor at 5.800 kHz, −208.2°.)

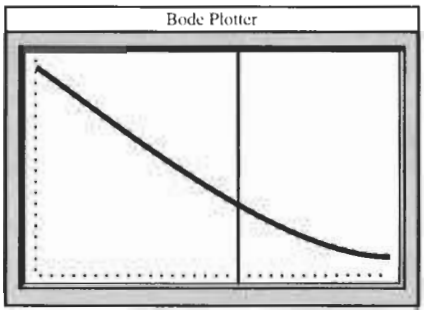

(b)

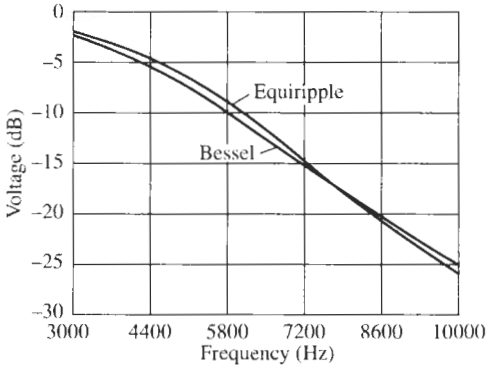

(c)

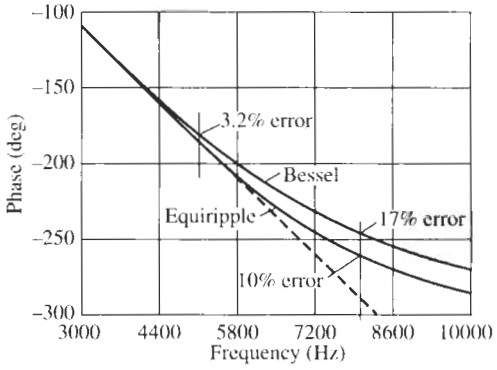

(d)

Figure 10.18 Continued

kHz (where the Bessel–Thomson filter already shows a 3.2% delay error); the allowed 10% delay error does not occur until $\approx$ 8.1 kHz (where the Bessel filter's delay error is 17%). These results demonstrate the superiority of the equiripple-delay design that we alluded to in our earlier discussion. A straight line with slope -100 μs is also shown in the phase plot of Fig. 10.18c.

10.7 APPROXIMATING AN IDEAL DELAY FUNCTION

So far in this chapter we have developed rational transfer functions $T(s) = N(s)/D(s)$ to approximate the exponential function of Eq. (10.10),

$$T(s) = \frac{V_2(s)}{V_1(s)} \approx e^{-s}$$

with the goal of obtaining a filter that realizes the ideal magnitude $|T(j\omega)| \equiv 1$ and the ideal delay $D \equiv 1$. The two approaches we used led to lowpass filters

$$T(s) = \frac{K}{D(s)} \tag{10.54}$$

where K is a constant and the polynomial $D(s)$ is designed to let $T(s)$ approximate a constant delay in either a maximally flat or an equiripple format. We saw that the frequency range over which the delay is constant within some specified error depends on the degree n of the approximation. Since the functions $T(s)$ in Eq. (10.54) are lowpass functions, it is clear that errors in magnitude from the ideal $|T(j\omega)| \equiv 1$ will grow as frequencies increase. In many applications this is acceptable or even desirable because the lowpass behavior of the "delay" function helps to eliminate unwanted high-frequency noise. However, since high-frequency components of the signal are attenuated as well, we must expect that sharp corners of signals, $v(t)$, in the time domain become rounded because the higher harmonics of the Fourier expansion of $v(t)$ are eliminated or at least reduced. If the signal shape must be preserved, it may be desirable to be able to delay the signal without limiting its frequency band. Let us briefly discuss how a circuit can be designed that provides a "pure" delay.

The reason why we obtained a bandlimiting transfer function is that we started the approximation procedure from a lowpass function, Eq. (10.54). We did not attempt to make any use of a potential numerator polynomial $N(s)$. Thus, rather than assuming that the numerator is a constant, $N(s) = K$, let us start from the general expression $T(s) = N(s)/D(s)$, or, on the $j\omega$-axis:

$$T(j\omega) = \frac{N(j\omega)}{D(j\omega)} = \frac{|N(j\omega)|\, e^{j\theta_N(\omega)}}{|D(j\omega)|\, e^{j\theta_D(\omega)}} = \frac{|N(j\omega)|}{|D(j\omega)|} e^{j[\theta_N(\omega) - \theta_D(\omega)]} \tag{10.55}$$

Using Eq. (10.15), the delay is then

$$D(\omega) = -\frac{d[\theta_N(\omega) - \theta_D(\omega)]}{d\omega} \tag{10.56}$$

Our concern here is with the magnitude,

$$|T(j\omega)| = \frac{|N(j\omega)|}{|D(j\omega)|} = \left|\frac{N(j\omega)}{D(j\omega)}\right| \tag{10.57}$$

which should be equal to a frequency-independent constant K, preferably $K = 1$. To make the ratio of the magnitudes of the two complex numbers $N(j\omega)$ and $D(j\omega)$ equal to unity for all frequencies, $N(j\omega)$ and $D(j\omega)$ must be conjugate complex, that is $N(j\omega) = D(-j\omega)$, or in the s-plane, $N(s) = D(-s)$. The transfer function is then

$$T(s) = \frac{D(-s)}{D(s)} \tag{10.58}$$

We encountered such functions in Chapter 3 for third order and in Chapter 5 for fourth order. They were labeled *allpass functions* because with $|T(j\omega)| \equiv 1$ they pass all frequency components of a signal equally well.

We know that the phase angles of conjugate complex numbers are equal in magnitude but opposite in sign. Consequently, from Eqs. (10.55) and (10.56) the phase angle and delay of an allpass filter are

$$\theta_{AP}(\omega) = \theta_N(\omega) - \theta_D(\omega) = -2\theta_D(\omega) \tag{10.59}$$

and

$$D_{AP}(\omega) = -2\frac{d\theta_D(\omega)}{d\omega} \tag{10.60}$$

In other words, phase and delay have twice the value that is contributed by the denominator of the allpass function alone.

With the question of a constant frequency-independent magnitude solved, we now need to concern ourselves with how to find a denominator polynomial with linear phase so that the filter has a constant delay. But this is precisely the problem we addressed and solved in Section 10.2 for the maximally flat delay (Bessel–Thomson) response and in Section 10.6 for the equiripple delay response. To be able to use this information, the tables and curves for the allpass design, we only need to remember that the allpass filter has twice the delay of an all-pole lowpass filter of equal degree. The design procedure for a Bessel–Thomson delay filter with constant magnitude is, therefore, as follows:

1. From Fig. 10.12b find the degree n necessary so that the delay error is within prescribed bounds. Remember that the allpass filter has twice the delay D of the lowpass; thus, the denormalizing frequency should be $\omega_0 = 1/(D/2) = 2/D$.
2. From Tables 10.1 through 10.4 find the coefficients, roots, factors, or quality factors and pole frequencies of the Bessel–Thomson polynomial $\mathcal{B}_n(s)$ as required.
3. Form the allpass function $T(s) = \mathcal{B}_n(-s)/\mathcal{B}_n(s)$.
4. Realize $T(s)$ by a cascade connection of the appropriate first- or second-order sections from Chapters 3 and 5.

If an equiripple delay is preferred over a maximally flat one, use the analogous procedure but find the relevant polynomials $\mathcal{E}_n(s)$ in Table 10.5.

EXAMPLE 10.4

A 1-kHz triangular waveform with a 30% duty cycle (the rising edge is three times steeper than the falling edge; see the oscilloscope display Fig. 10.20b) must be delayed by $D = 100\ \mu$s. Design a filter with constant magnitude and maximally flat delay, such that the first seven harmonics of the Fourier expansion of the signal are transmitted without distortion.

Solution

To cover the first seven harmonics, we assume the delay error must not be larger than 1% until 7 kHz (seven times 1 kHz). We recall first that the allpass function has twice the delay of a Bessel–Thomson filter; to be able to use the design tables and curves of the Bessel–Thomson case, we divide D by two and take as normalizing frequency $\omega_0 = 2/D = 20$ krad/s. The end of the delay band, 7 kHz, corresponds to 44 krad/s. The $\leq 1\%$ delay error must, therefore, be maintained until the normalized frequency $44/20 = 2.2$. Figure 10.12b shows that $n = 5$ is the required degree of the allpass filter. From Table 10.3 with Eq. (10.58) it has the transfer function

$$T_{AP}(s) = T_1T_2T_3 = \frac{s - 3.6467}{s + 3.6467}\frac{s^2 - 4.6493s + 18.1563}{s^2 + 4.6493s + 18.1563}\frac{s^2 - 6.7039s + 14.2725}{s^2 + 6.7039s + 14.2725} \tag{10.61}$$

which we have already expressed in factored form. The design parameters are

$$\sigma_1 = 3.6467, \quad \omega_{02} = 4.261, \quad Q_2 = 0.916, \quad \omega_{03} = 3.778, \quad Q_2 = 0.564$$

It remains for us to design the three allpass sections indicated in Eq. (10.61).

For the first-order allpass we can use the active implementation of Section 3.4.3, Fig. 3.34a, repeated as Fig. 10.19a. The circuit realizes

$$T_1(s) = \frac{s - 1/(RC)}{s + 1/(RC)} \tag{10.62}$$

Evidently, we must select components such that $RC = 1/(3.6467\omega_0)$. Choosing $C = 1$ nF results in $R = 13.71$ kΩ.

As second-order section we choose the GIC section of Fig. 5.16, redrawn in Fig. 10.19b. With $a = c = 1$ and $b = 0$ (Table 5.4), the circuit realizes Eq. (5.36), repeated here as Eq. (10.63):

$$T(s) = \frac{V_2}{V_1} = \frac{D(-s)}{D(s)} = \frac{s^2 - s\omega_0/Q + \omega_0^2}{s^2 + s\omega_0/Q + \omega_0^2} \tag{10.63}$$

where $R = 1/(\omega_0 C)$. Note that the GIC section provides a very good allpass filter with no elements that must be carefully adjusted to achieve the correct numerator. We can, therefore, use low-tolerance components.

For the allpass stage T_2 we have $Q_2 = 0.916$ and $\omega_{02} = 4.261$. With $C = 1$ nF, this yields $R = 1/(4.621 \times 2 \times 10^4 \times 10^{-9})\ \Omega = 11.734$ kΩ. Similarly we have for T_3 with $\omega_{03} = 3.778$ and $C = 1$ nF: $R = 1/(3.7781 \times 2 \times 10^4 \times 10^{-9})\ \Omega = 13.23$ kΩ and $Q_3 = 0.564$.

The complete circuit is shown in Fig. 10.20a along with a measurement setup. The circuit's input signal is the 1 kHz–100 mV triangular wave with 30% duty cycle; the oscilloscope, Fig. 10.20b, shows the input waveform (left trace) and output waveform (right trace). Notice that the output wave shape is equal to that of the input, but delayed by 100 μs as required. The fact that no distortion is visible in the shape of the output signal verifies that all important harmonics of the signal are transmitted properly. We also display the frequency response of the allpass filter in Fig. 10.20c; it shows that the gain is flat at 0 dB until about 860 kHz before the attenuation increases due to the finite bandwidth of the opamps.

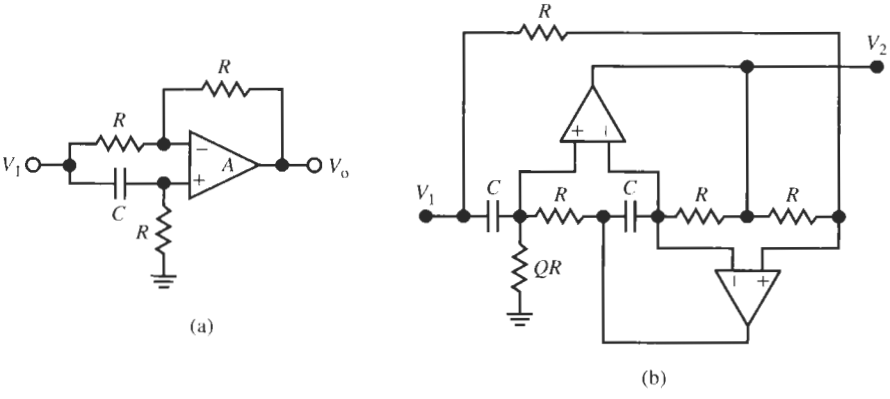

Figure 10.19 Two active allpass circuits: (a) first order; (b) second order.

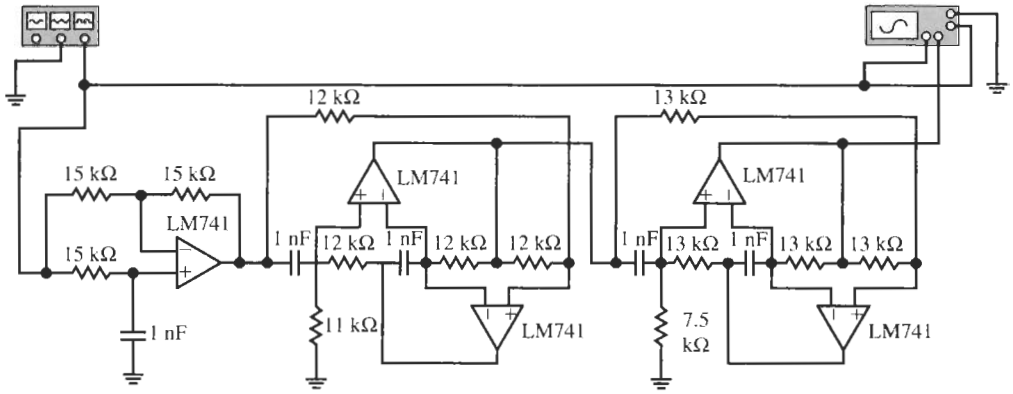

(a)

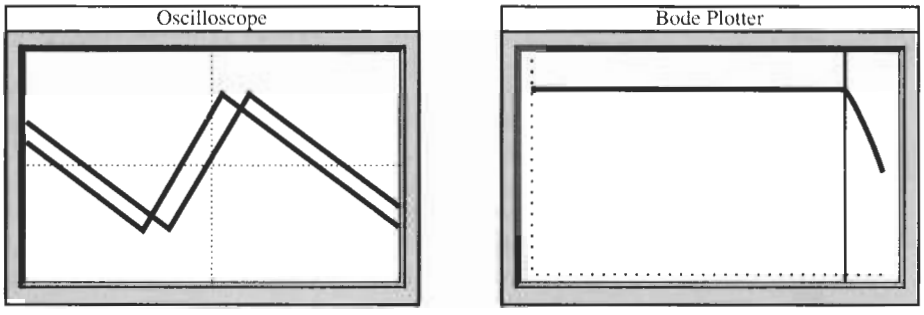

(b) (c)

Figure 10.20 Circuit and test results for Example 10.4: (a) circuit; (b, c) front panels of test equipment (oscilloscope, network analyzer) and test results. (Bode Plotter scales: 1 Hz to 5 MHz; −80 to 10 dB; cursor at 857.7 kHz, 0.355 dB; oscilloscope scales: time base: 0.1 ms/div; both channels: 50 mV/div.)

10.8 IMPROVING HIGH-FREQUENCY ATTENUATION GENERATING GAIN BOOSTS

We will next discuss a problem which in a sense is the opposite of the one addressed in Section 10.7. From Fig. 10.13 for maximally flat delay and Fig. 10.16c for equiripple delay we see that the attenuation increase of delay filters developed from a lowpass function is only modest. In some applications one wishes to provide constant delay but also reject out-of-band noise or other signals so that a delay filter of high order is necessary. The question is, therefore, whether a method for a more efficient design can be found.

Once again we return to the lowpass function of Eq. (10.54) with a constant numerator $N(s) = K$ and ask ourselves what modifications are available to achieve our goal. We saw in our earlier work that transmission zeros will improve the stopband attenuation, but in the present circumstances they must be chosen such that the delay will not change. Now note that a transmission zero at ω_z and its conjugate at $-\omega_z$ on the $j\omega$-axis cause a numerator factor of the form $(s^2 + \omega_z^2)$. On the $j\omega$-axis this factor becomes $(-\omega^2 + \omega_z^2)$ and we observe that it is a real number for all frequencies and does not contribute to the delay. We conclude that

we may always augment the delay filter function with numerator factors that give $j\omega$-axis zeros in suitable locations without changing the delay. Summarizing the design procedure for a Bessel–Thomson delay filter with finite transmission zeros, we obtain the following:

1. From Fig. 10.12b find the degree n necessary so that the delay error is within prescribed bounds.
2. From Tables 10.1 through 10.4 find the coefficients, roots, factors, or quality factors and pole frequencies of the Bessel–Thomson polynomial $\mathcal{B}_n(s)$ as required.
3. Form the delay function, with $m \leq n/2$,

$$T(s) = \frac{\mathcal{B}_0 \left(s^2/\omega_{z1}^2 + 1\right) \cdots \left(s^2/\omega_{zm}^2 + 1\right)}{\mathcal{B}_n(s)} \tag{10.64}$$

   with as many transmission zeros as may be required to achieve the desired attenuation. $\mathcal{B}_0$ is the constant coefficient of the polynomial $\mathcal{B}_n(s)$ so that $T(0) = 1$. Placing the transmission zeros correctly may require careful analysis or simulation of the circuit.
4. Realize $T(s)$ by a cascade connection of the appropriate first- or second-order sections from Chapters 3 and 5.

The result of this approach is illustrated in Fig. 10.21 for a seventh-order all-pole Bessel–Thomson filter. The figure shows the attenuation for the all-pole Bessel–Thomson filter and for the all-pole filter augmented by one or two transmission zeros. We note that by placing suitable transmission zeros into the stopband, a substantially faster attenuation increase can be achieved without affecting the delay. The roll-off is faster as the zero is moved closer to the passband corner (to $\omega = 1$ in this case) but the attenuation minimum to the right of the zero also increases. If the attenuation for frequencies above the zero is still too low, a second zero or even further transmission zeros may be placed as is shown in Fig. 10.21. Notice that

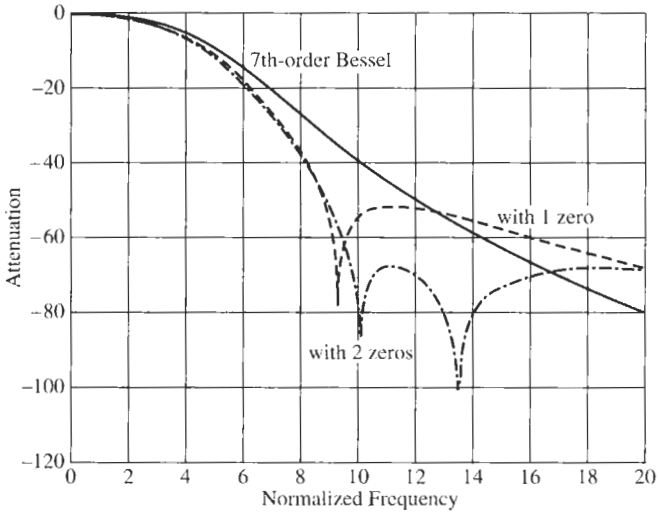

Figure 10.21 Attenuation of Bessel–Thomson filter with and without finite $j\omega$-axis transmission zeros for the case of a single zero at $\omega_{z1} = 9.2$, and for the case of two zeros at $\omega_{z1} = 10$ and $\omega_{z2} = 13.6$.

the attenuation increase toward the transmission zeros is not very steep, that is, the notch is not narrow, because of the low pole Qs of the Bessel–Thomson denominator. Consequently, a small effect on the loss is seen in the passband as well (see Fig. 10.21). This situation is somewhat better for equiripple delay filters because of their higher pole quality factors.

To keep the delay unaffected by the transmission zeros in Eq. (10.64), it is critical that the designer selects good notch sections with large zero quality factors Q_{zi} so that the numerator terms do not contribute to the filter's phase. Notice that whereas an ideal notch factor $(s^2/\omega_{zi}^2 + 1)$ is purely real on the $j\omega$-axis, in practice the notch will have finite depth so that the realized factor takes the form $(s^2/\omega_{zi}^2 + Q_{zi}^{-1}s/\omega_{zi} + 1)$ with finite values of Q_{zi}. The phase and delay contributions then become

$$\theta_{zi} = \tan^{-1}\left(\frac{1}{Q_{zi}}\frac{\omega/\omega_{zi}}{1-\omega^2/\omega_{zi}^2}\right) \text{ and } D_{zi} = -\frac{1}{\omega_{zi}Q_{zi}}\frac{1+(\omega/\omega_{zi})^2}{(\omega^2/\omega_{zi}^2-1)^2+[\omega/(\omega_{zi}Q_{zi})]^2} \quad (10.65)$$

From this equation we see that large zero-quality factors are essential if we wish to prevent the delay of the filter from being altered by the transmission zeros and to maintain small values of D_{zi}. In most circuits, $Q_{zi} = \infty$ depends on careful adjustment (tuning) of the component values. Examples are the four-amplifier biquad in Fig. 5.1 that realizes Eq. (5.5) and demands that $a = bkQ$ for a notch, and both the general Delyiannis–Friend and Sallen–Key biquads in Figs. 5.19 and 5.22, which require that complicated expressions are set to zero to realize a notch [see Eqs. (5.40) and (5.46)]. Far better choices are the GIC biquad in Fig. 5.16, which requires only that a resistor ratio of 1/2 be maintained (see Table 5.4) and especially the three-amplifier biquad in Fig. 5.13, which obtains a notch by removing a resistor (setting it to ∞, see Table 5.3).[4]

Transmission channels normally have lowpass behavior that depresses the amplitude of signal components close to the bandedge. To compensate for this loss, a filter is needed that provides a localized boost in gain near the end of the passband with little or no additional gain as ω goes to zero. In particular for data channels, the signal must often be further lowpass filtered to achieve additional attenuation of high-frequency noise, but the delay must remain constant to minimize phase distortion. The question arises, therefore, whether we can devise a circuit to achieve simultaneously a constant delay, the needed gain boost, and additional stopband attenuation.

We have seen that constant delay with moderate stopband attenuation is obtained from the pole positions, by selecting a Bessel–Thomson or equiripple delay polynomial for the denominator of the transfer function. The attenuation can be improved without disturbing the delay by constructing a numerator with conjugate complex zeros as in Eq. (10.64) because, on the $j\omega$-axis, the numerator will then be a real number that does not contribute to the delay. Bearing in mind that the denominator must not be altered to retain the constant delay, we can achieve a boost only from further numerator factors that are real numbers when evaluated on the $j\omega$-axis. Such factors are formed from zeros on the *real* axis, at $\pm\sigma_z$, symmetrical to the origin: $(s/\sigma_z + 1)(s/\sigma_z - 1) = (s^2/\sigma_z^2 - 1)$. On the $j\omega$-axis, the term $|\omega^2/\sigma_z^2 + 1|$ is larger than 1 so that a frequency-dependent increase in gain can be expected. The transfer function is constructed analogous to the one in Eq. (10.64).

[4] Often the parameter Q_z is also affected by the opamps' gain-bandwidth products so that for very accurate design requirements functional tuning of the circuit will be necessary.

$$T(s) = \frac{\mathcal{B}_0(s^2/\sigma_z^2 - 1)}{\mathcal{B}_n(s)} \tag{10.66}$$

and can, of course, be further supplemented by one or more transmission zeros on the $j\omega$-axis if the attenuation needs to be increased:

$$T(s) = \frac{\mathcal{B}_0(s^2/\sigma_z^2 - 1)(s^2/\omega_{z1}^2 + 1)\cdots(s^2/\omega_{zm}^2 + 1)}{\mathcal{B}_n(s)} \tag{10.67}$$

Clearly, on the $j\omega$-axis the numerators in these equations are real numbers so that phase and delay are determined only by the denominator $\mathcal{B}_n(s)$. We are cautioned that Eq. (10.65) also applies here: in practice the factor $(s^2/\sigma_z^2 - 1)$ may contain a linear term, $(s^2/\sigma_z^2 + Q_z^{-1}s/\sigma_z - 1)$, so that delay errors can be expected. If equiripple delays are preferred, we only need to replace $\mathcal{B}_n(s)$ by the equiripple polynomial $\mathcal{E}_n(s)$ of Section 10.6.

Figure 10.22 illustrates the behavior of these functions for the Bessel–Thomson case. We have shown in Fig. 10.22a the attenuation of a seventh-order Bessel–Thomson filter and three curves with boosts corresponding to zeros at, respectively, ± 2, ± 3, and ± 5 on the real axis. The designer can adjust the amount of boost $B(\omega)$ by varying σ_z. Since the only change in the transfer function that the boost factor causes is the term $(s^2/\sigma_z^2 - 1)$, the height of $B(\omega)$ in dB as a function of frequency is computed from

$$B(\omega) = 20\,\log(1 + \omega^2/\sigma_z^2) \tag{10.68}$$

For example $\sigma_z = 2$ results in a boost of 1.94 dB at $\omega = 1$ and of 6 dB at $\omega = 2$ over the function with no boost. Equation (10.68) makes it clear that decreasing σ_z, that is, a smaller distance between the two real zeros $\pm\sigma_z$, gives more boost as is also shown in Fig. 10.22a.

As pointed out in Eq. (10.67), nothing prevents us from shaping the stopband further with zeros on the imaginary axis. We have shown this with a zero at $\pm j9$ in Fig. 10.22b for two curves (dashed–dotted) with boosts corresponding to zeros at ± 3 and ± 5. Since according to

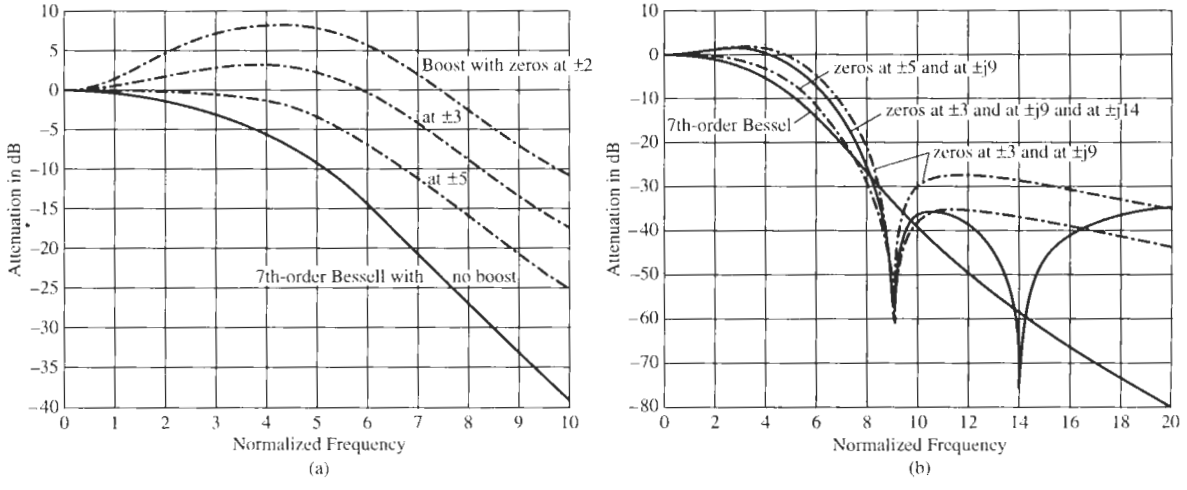

Figure 10.22 (a) Attenuation behavior of a seventh-order Bessel–Thomson filter with boost; (b) the effect of transmission zeros on the performance.

Eq. (10.68) the boost reduces the attenuation at all frequencies, including the stopband (by ≈ 28 dB at $\omega = 10$ for $\sigma_z = 2$; see Fig. 10.22a), additional transmission zeros may be employed to increase attenuation to the required level. To demonstrate this fact, we have used a second zero at $\omega_{z2} = 14$ in Fig. 10.22b to increase the loss of the ($\sigma_z = 3 - \omega_{z1} = 9$) curve. Observe that additional zeros reduce the gain of the boost throughout, even at low frequencies, so that iterative adjustments may be necessary to maintain the boost at the required level in the passband.

REFERENCES

K. W. Henderson and W. H. Kautz, "Transient Responses of Conventional Filters," *IRE Trans. Circuit Theory*, Vol. CT-5, pp. 333–347, 1958.

W. H. Huggins, "Network Approximation in the Time Domain," Rep E 5048A, Air Force Cambridge Research Labs, Cambridge, MA, October 1949.

Z. Kiyasu, "On a Design Method of Delay Networks," *J. Inst. Elec. Commun. Eng. Jpn.*, Vol. 26, pp. 598–610, 1943.

L. Storch, "Synthesis of Constant-Time-Delay Ladder Networks Using Bessel Polynomials," *Proc. IRE*, Vol. 42, pp. 1666-1675, 1954.

G. C. Temes and J. W. LaPatra, *Introduction to Circuit Synthesis and Design*. McGraw-Hill, New York, 1977, p. 567.

W. E. Thomson, "Delay Networks Having Maximally Flat Frequency Characteristics," *Proc. IEE*, pt. 3, Vol. 96, pp. 487–490, 1949.

A. I. Zverev, *Handbook of Filter Synthesis*. New York: Wiley, 1967.

PROBLEMS

10.1 For the circuit in Fig. P10.1, determine the values of L and C such that the delay is maximally flat at $\omega = 0$ and the half-power frequency of $|T(j\omega)|$ occurs at $\omega = 1$. Repeat for an equiripple delay. Compare the quality factors of the two cases.

10.2 Use the recursion equation, Eq. (10.37), to verify $\mathcal{B}_4$ in Eq. (10.40) and the entries in Table 10.1 for $n = 5$, 6, and 7.

10.3 Accepting the factored polynomial in Table 10.3 for $n = 6$, verify the entries in Table 10.4 for $n = 6$.

10.4 Design a fourth-order Bessel–Thomson filter to provide 100-μs delay. What are the filter's attenuation error and the delay error in the frequency band $0 \leq f \leq 2.6$ kHz? Realize the circuit as a cascade of two biquads of your choice. Be certain to use practical component values and implement and test your design with Electronics Workbench (EWB).

10.5 Repeat Problem 10.4 for a fourth-order equiripple delay filter.

10.6 Compute the delay provided by a sixth-order Butterworth filter. Repeat for a sixth-order Chebyshev filter. Evaluate both delays at the normalized frequency $\omega = 1.2$.

10.7 Design a Bessel–Thomson filter to provide 65-μs delay. The attenuation error must not be larger than 2 dB up to $f = 4$ kHz and the delay error in $f < 8.5$ kHz must stay below 6%. Realize the delay filter as a cascade topology. Be certain to use practical component values and implement and test your design with EWB.

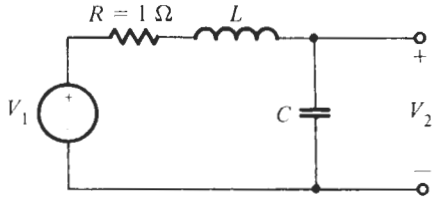

Figure P10.1

10.8 Repeat Problem 10.7 for an equiripple delay approximation.

10.9 A Bessel–Thomson filter is to be designed to provide 125-μs delay. The delay error must be less than 7.5 μs in $f \leq 5$ kHz. Realize the delay filter as a cascade topology. Be certain to use practical component values and implement and test your design with EWB. What is the attenuation that this filter provides in the passband below 5 kHz? Does it agree with expectations?

10.10 Repeat Problem 10.9 for an equiripple delay approximation.

10.11 A Bessel–Thomson approximation function is to be flat within 5% of its delay at dc of 1 ms up to the frequency 1800 rad/s.

(a) Determine the appropriate Bessel–Thomson function.

(b) What is the attenuation of the function at 1800 rad/s and at 14,000 rad/s?

10.12 Design a Bessel–Thomson delay filter having at most a 10% deviation in delay at the normalized frequency $\omega = 3.0$ and at most a 1-dB deviation at $\omega = 1.35$. The filter is to provide 200-μs delay. Complete the design with practical element values and LM741 opamps, and test the performance.

10.13 A Bessel–Thomson delay filter must at most have a 3.0% deviation in delay at the normalized frequency $\omega = 4.0$ and at most 1-dB deviation at $\omega = 1.7$. The filter is to provide 60-μs delay. Complete the design with practical element values and suitable opamps, and test the performance.

10.14 Repeat Problem 10.13 for an equiripple delay lowpass function.

10.15 Design a seventh-order delay filter with a 0.05° linear phase. The delay should equal 55 μs.

(a) Give an approximate value for delay error realized in the passband. (The passband is the frequency range where the delay is approximately constant.)

(b) Determine the attenuation at the passband corner.

(c) Realize the circuit and test its performance.

10.16 Design a 0.05° equiripple delay filter to have 30-μs delay over a frequency band of 56 kHz. The delay error should be less than 100 ns. Realize the circuit with suitable active *RC* sections and test its performance.

10.17 Build a filter (an allpass circuit) that implements a pure delay of 20 μs based on

(a) Bessel–Thomson approximation,

(b) an equiripple delay approximation.

The delay must be constant over the band $0 \leq f \leq 45$ kHz with an error of no higher than 2%. Realize the circuit with active filter sections of your choice and test its performance.

10.18 A 25-kHz trigger pulse $v_1(t)$ and its delayed copy $v_2(t)$ are applied to a control system. To ensure safe operation of the system, v_2 must be delayed by 2.5 ms. It is important that the waveforms of v_1 and v_2 are "exact" copies of each other. You may assume that the copies are adequate if the first nine harmonics are transmitted with no attenuation. Design and test a circuit to perform the required function. State clearly any assumption you make in developing the circuit.

10.19 A Gaussian magnitude response is given by the equation

$$|T(j\omega)| = e^{-\omega^2/2}$$

and a second-order approximation of this response is

$$|T(j\omega)|^2 \approx \frac{1}{1 + \omega^2 + 0.5\omega^4}$$

(a) Determine $T(s)$.

(b) Find the poles of $T(s)$.

(c) What is the half-power frequency?

(d) Compare the delay performance of the Bessel–Thomson and the Gaussian second-order transfer functions.

(e) Assume the frequency is normalized with respect to 8 kHz. Build and test a circuit to realize the function found in (b).

10.20 The Bessel–Thomson delay filter derived in Problem 10.13 is to be augmented by a transmission zero at eight times the constant delay frequency $\omega = 4.0$. Design the filter and compare its experimental performance with the design in Problem 10.13.

10.21 The Bessel–Thomson filter of Problem 10.9 is to be redesigned such that the attenuation is at least 20 dB larger than the Bessel–Thomson design of Problem 10.9 in the frequency range $6 \leq \omega \leq 12$, where ω is the normalized design frequency. Build and test the circuit.

10.22 The filter designed in Problem 10.9 requires a gain boost of approximately 4 dB at 4 kHz. Build and test the redesigned filter.

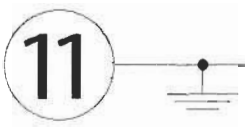

DELAY EQUALIZATION

We have in the earlier parts of this book dealt with filters that were specifically designed to provide some desired magnitude response. We paid no attention to the phase or delay that was realized—as a matter of fact, once the magnitude was identified, we had to accept whatever phase and delay response the filters provided. We encountered the opposite situation in Chapter 10: there we designed a lowpass transfer function specifically to provide a linear phase, that is, a constant delay, but after the degree was fixed we had no control over the attenuation. These filter responses are widely used because they satisfy many practical requirements, but there are applications in which not only a required magnitude response must be realized but a constant delay is necessary as well. One example is a signal that has sharp transitions in the time domain, such as a train of pulses. As we know from Fourier analysis, such a signal contains many components of different magnitudes and phases over a band of frequencies. To reconstitute a pulse with little or no distortion at the filter output the delay must be constant over the frequency band, otherwise severe distortion in the shape of the pulse will result. In this chapter we will address the question of how to design a filter that has a specified magnitude, such as a maximally flat or an inverse Chebyshev response, and that at the same time provides a constant delay over the filter's passband. The process is referred to as *delay equalization*.

An example of an application is the signal filtering requirement in Fig. 11.1 where a triangular signal is corrupted by some high-frequency "noise" that must be removed. To eliminate the noise, a lowpass filter is required, for example with a fifth-order Butterworth response, that passes all important frequency components that make up the triangular signal in the time domain. But the filter must not distort the components' relative phases so that the signal shape is not changed. Thus, as is shown in Fig. 11.1, at the output we clearly recognize the shape of the input signal; it is essentially undisturbed, although sharp corners, such as the peak, are rounded because the lowpass filter removed the highest frequencies. Figure 11.2 shows the delay requirement and the correction needed.

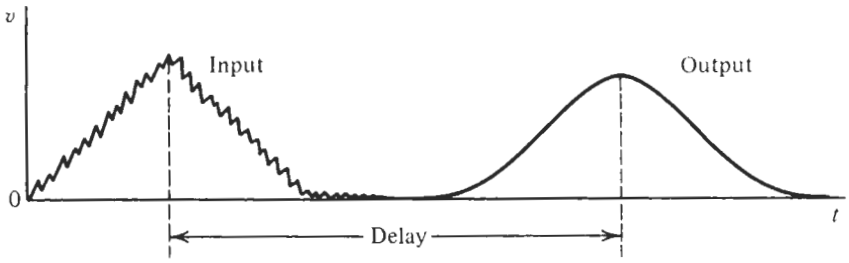

Figure 11.1 Desired filtering process of a signal in the time domain.

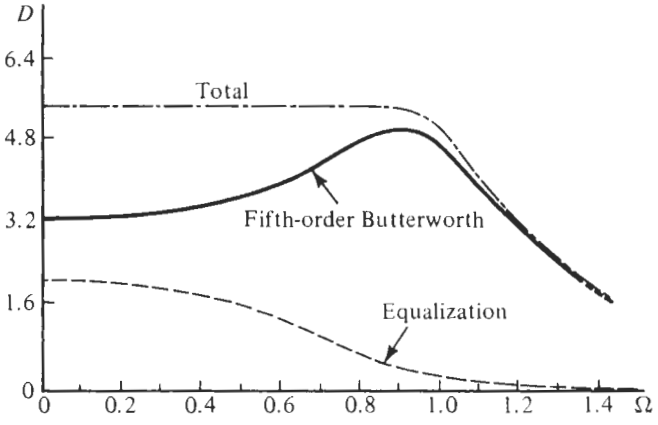

Figure 11.2 Delay of a fifth-order Butterworth filter, desired total delay, and necessary delay to be added to that of the Butterworth filter for equalization.

11.1 EQUALIZATION PROCEDURES

We saw in our study so far that designing a filter for a certain magnitude response gave us a circuit in which we had no control over the phase, because after choosing the type of magnitude response, such as Chebyshev or Butterworth, all poles and zeros are determined, and there remains no degree of freedom to meet any additional filter specifications. Our only option was to select an approximation that gave the "least objectionable" phase or delay. We addressed this issue in Section 8.6 (refer to Figs. 8.20 and 8.21). We observed there that delay variations are reduced by choosing a filter with low Q values, and that Butterworth and inverse Chebyshev functions are generally preferable over the Chebyshev case. Also, we noted that the delay is a strong function of the filter order n, so that in some situations even the elliptic response may provide the best, meaning the least variable delay.

If the obtained delay varies too much for the signal-processing requirement at hand, we can only modify the transfer function. But we must do this in such a way that the filter's magnitude response is not destroyed. A solution to the problem is suggested in Fig. 11.3. We propose to connect the filter T_M with the desired magnitude response, $|T_M(j\omega)|$,

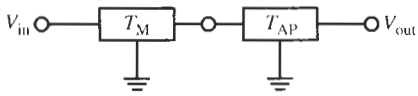

Figure 11.3 Cascade connection of a filter $T_M(s)$ with the desired magnitude response and an allpass filter $T_{AP}(s)$ to equalize the delay. In general, $T_{AP}(s)$ itself will consist of a cascade connection of several first- or second-order allpass sections.

in cascade with a circuit T_{AP} whose magnitude response is equal to unity, $|T_{AP}(j\omega)| \equiv 1$, but whose phase varies with frequency. We encountered such so-called *allpass* filters before: for first-order in Chapter 3, Figs. 3.13 and 3.34, and in Chapter 5, where the elements of several second-order circuits could be adjusted to provide an allpass response $T_{AP}(s)$. The transfer function of the cascade configuration in Fig. 11.3 is $T(s) = T_M(s)T_{AP}(s)$, or on the $j\omega$-axis:

$$\begin{aligned} T(j\omega) &= T_M(j\omega)T_{AP}(j\omega) \\ &= |T_M(j\omega)|\,|T_{AP}(j\omega)|\,e^{-j\theta_M(\omega)}e^{-j\theta_{AP}(\omega)} = |T_M(j\omega)|\,e^{-j[\theta_M(\omega)+\theta_{AP}(\omega)]} \end{aligned} \tag{11.1}$$

We see that the magnitudes multiply with no contribution from the allpass module because $|T_{AP}(j\omega)| \equiv 1$, and that the phases add. Since the delay is obtained from the negative derivative of the phase, the delays D_M and D_{AP} add as well:

$$D(\omega) = -\frac{d[\theta_M(\omega) + \theta_{AP}(\omega)]}{d\omega} = -\frac{d\theta_M(\omega)}{d\omega} - \frac{d\theta_{AP}(\omega)}{d\omega} = D_M(\omega) + D_{AP}(\omega) \tag{11.2}$$

Note that the total delay D in this process will increase because D is larger than either D_M or D_{AP}. In principle then, our task is clear: if $D(\omega) = D_0$ is to be constant over some specified frequency range, and $D_M(\omega)$ is known from the transfer function that provides the desired magnitude response, we must find an allpass function to provide

$$D_{AP}(\omega) = D_0 - D_M(\omega) \tag{11.3}$$

This equation can, in general, not be satisfied exactly for all frequencies, but can only be approximated for frequencies in a finite interval. We shall see that the wider the frequency range of interest and the smaller the permitted delay error are, the more expensive the solution becomes because it requires allpass filters of increasingly high order.

To provide a magnitude that is equal to unity for all frequencies, we saw in Chapter 10, Eq. (10.58), that we need a transfer function

$$T_{AP}(s) = \frac{N(s)}{D(s)} = \frac{D(-s)}{D(s)} \tag{11.4}$$

in which the numerator is obtained from the denominator by replacing s by $-s$. The pole-zero patterns of such allpass functions, for $n = 1$ to 4, are shown in Fig. 11.4. The pattern in Fig. 11.4a belongs to a first-order allpass with one pole and one zero at equal distances from the origin. That shown in Fig. 11.4b for a second-order allpass has two poles and two zeros in quadrantal symmetry. Figure 11.4c for a third-order allpass can be thought of as the superposition of the previous two patterns; the fourth-order allpass pattern in Fig. 11.4d follows from two second-order ones, and so on.

The design of a filter with constant delay (over a limited frequency range) is accomplished in two steps:

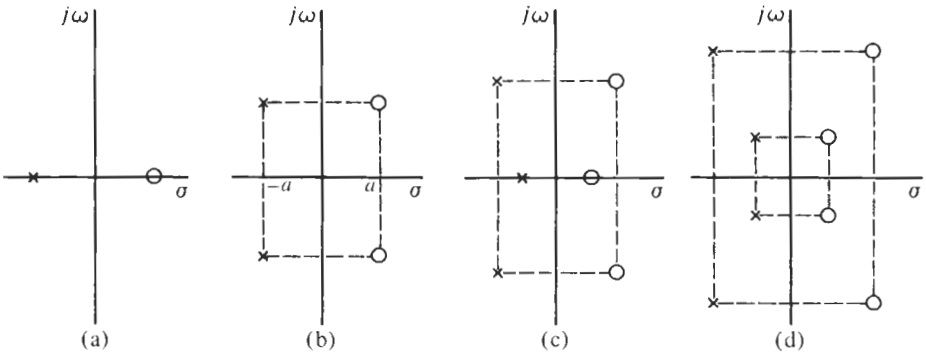

Figure 11.4 Typical pole-zero patterns of allpass filters of orders 1, 2, 3, and 4.

1. Design the filter with the required magnitude response $|T_M(j\omega)|$.
2. Calculate the delay $D_M(\omega)$ that the filter provides and supplement it by the delays of cascaded first- or second-order allpass modules such that the total delay, the sum of $D_M(\omega)$ and $D_{AP}(\omega)$, is approximately constant over the prescribed frequency range. This step is formalized in Eq. (11.3) and illustrated in Fig. 11.2.

Since phase or delay equalization makes use of first- and second-order allpass circuits, let us study more closely the delay they contribute to a filter.

11.2 EQUALIZATION WITH FIRST-ORDER MODULES

Consider the first-order allpass function

$$T_1(s) = K\frac{s-\sigma_1}{s+\sigma_1} \tag{11.5}$$

corresponding to the pole-zero pattern in Fig. 11.4a. Its magnitude and phase equal

$$|T_1(j\omega)| = K \quad \text{and} \quad \theta_1 = \theta_{\text{numerator}} - \theta_{\text{denominator}} = -2\tan^{-1}\left(\frac{\omega}{\sigma_1}\right) \tag{11.6}$$

Observe that in an allpass numerator and denominator have the same phase so that the allpass phase is simply twice the denominator phase. The delay is computed as

$$D_1(\omega) = -\frac{d\theta}{d\omega} = \frac{2/\sigma_1}{1+(\omega/\sigma_1)^2} \tag{11.7}$$

This function is plotted in Fig. 11.5; we note that the delay decreases with increasing frequency. Its maximum is at $\omega = 0$ and has the value

$$D_{1,\max} = D_1(0) = 2/\sigma_1 \tag{11.8}$$

For the realization of the first-order allpass function, we review the active circuits of Section 3.4.3, Fig. 3.34, repeated here in Fig. 11.6. Both circuits realize $T_1(s)$ as in Eq. (11.5) with $\sigma_1 = 1/(RC)$:

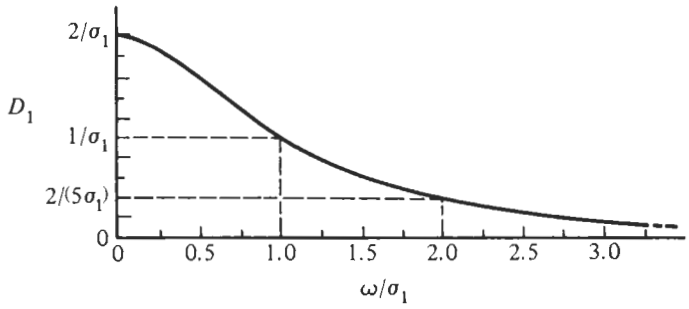

Figure 11.5 Delay of a first-order allpass filter.

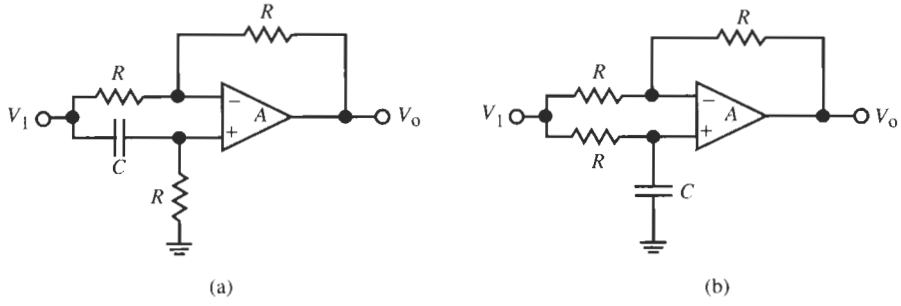

Figure 11.6 Two first-order active allpass circuits to realize $T_1(s)$ in Eq. (11.9): (a) non-inverting, $K = 1$; (b) inverting, $K = -1$.

$$T_1(s) = \pm\frac{s - 1/(RC)}{s + 1/(RC)} \tag{11.9}$$

The circuit in Fig. 11.6a has $K = +1$; the one in Fig. 11.6b is inverting, i.e., it gives $K = -1$. It is clear that the two modules realize the same delay, but their phases differ by 180°.

Now that we have an expression for the delay $D_1(\omega)$ in Eq. (11.7) let us consider how to use it to equalize the delay of a given function $T_M(s)$. Normally we make use of one first-order allpass only to achieve some minimal delay equalization in simple cases. The second-order allpass modules discussed in Section 11.3 are preferred for more complicated requirements. In the present case we have only one parameter, $\sigma_1 = 1/(RC)$, which must be optimally adjusted to achieve our goal. Example 11.1 will illustrate the procedure.

EXAMPLE 11.1

The delay of a third-order Butterworth filter with the parameters $\alpha_{max} = 3$dB in $f_c = 2$ kHz must be equalized as best as possible with one first-order active allpass module. Determine the appropriate components R and C, the final delay D_1 realized, as well as ΔD_1 over the passband before and after equalization.

Solution

Let us normalize the frequency axis by $\omega_c = 4\pi$ krad/s so that the cut-off frequency is at $\omega_n = 1$. Note that $\omega_n = \omega/\omega_c$ is a normalized frequency. We shall use here the subscript n

to identify the normalized frequency because it will help us to keep track of the normalizing frequency ω_c that determines the actual delay. The Butterworth transfer function is then

$$T_B(s_n) = \frac{1}{s_n^3 + 2s_n^2 + 2s_n + 1}$$

whose phase and delay are given by

$$\theta_B(\omega_n) = -\tan^{-1}\frac{2\omega_n - \omega_n^3}{1 - \omega_n^2}$$

$$D_B(\omega_n) = -\frac{d\theta_B(\omega_n)}{d\omega} = -\frac{d\theta_B(\omega_n)}{d\omega_n} \times \frac{d\omega_n}{d\omega} = \left[\frac{d}{d\omega_n}\left(\tan^{-1}\frac{2\omega_n - \omega_n^3}{1 - \omega_n^2}\right)\right] \times \frac{1}{\omega_c} \tag{11.10}$$

We multiply the function $T_B(s)$ by the first-order allpass

$$T_1(s) = \frac{s_n - \sigma_1}{s_n + \sigma_1}$$

Its phase and delay are

$$\theta_1(\omega) = -2\tan^{-1}\frac{\omega_n}{\sigma_1} \quad \text{and} \quad D_1(\omega_n) = 2\frac{d}{d\omega_n}\left(\tan^{-1}\frac{\omega_n}{\sigma_1}\right) \times \frac{1}{\omega_c}$$
$$= \frac{1}{\omega_c}\left[\frac{2/\sigma_1}{1 + (\omega_n/\sigma_1)^2}\right] \tag{11.11}$$

where $\sigma_1 = 1/(RC)$ is also a normalized frequency. Carrying out the differentiation steps explicitly, making use of the chain rule, clarifies how the normalizing frequency ω_c enters the actual delay (with units of time): the normalized delay is denormalized by dividing it by ω_c.

The normalized delay contributed by T_B, the term in brackets in Eq. (11.10), is plotted in Fig. 11.7. We notice that in the frequency range of interest D_B varies from a minimum of $D_B(0) = 2$ to a maximum of $D_B(0.81) \approx 2.75$, a spread of $\Delta D_B = 0.75$. Our objective is to reduce this difference by use of the allpass T_1, which requires us to find some optimum value of σ_1. Considering the shape of the function D_1 plotted in Fig. 11.5 we see that by adding D_1 to D_B some measure of equalization can be achieved: we increase the delay at $\omega_n = 0$ more than at $\omega_n = 0.81$.

As a trial, we choose $\sigma_1 = 1.2$ and show the resulting normalized equalizer delay, the term in brackets in Eq. (11.11), also in Fig. 11.7. It is labeled "equalizer delay—1.2." From Eq. (11.8), it adds $2/1.2 = 1.67$ to the delay at $\omega_n = 0$ but only approximately 1.15 at $\omega_n = 0.81$, so that the spread of $D_{max} - D(0)$ of the combined delay (the curve labeled "total delay—1.2") equals $3.9 - 3.67 = 0.23$, a noticeable reduction from the value 0.75 of the Butterworth filter. However, observe from Fig. 11.7 that the smallest *total* delay $D_{min} = D(1) = 3.5$ in the passband for this case occurs at the passband edge, $\omega_n = 1$, so that the spread is $3.9 - 3.5 = 0.40$. The engineer must now decide whether flat delay is important up to the -3-dB passband edge, and then use experience or further trials to fine-tune the performance. Assuming that we must go to the bandedge $\omega_n = 1$, we may try to equalize the delays at $\omega_n = 0$ and at $\omega_n = 1$: choosing $\sigma_1 = 1.4$ would result in the curve labeled "total delay—1.4" in Fig. 11.7 where the spread is now $3.78 - 3.45 = 0.33$, a 17.5% improvement over 0.40. In

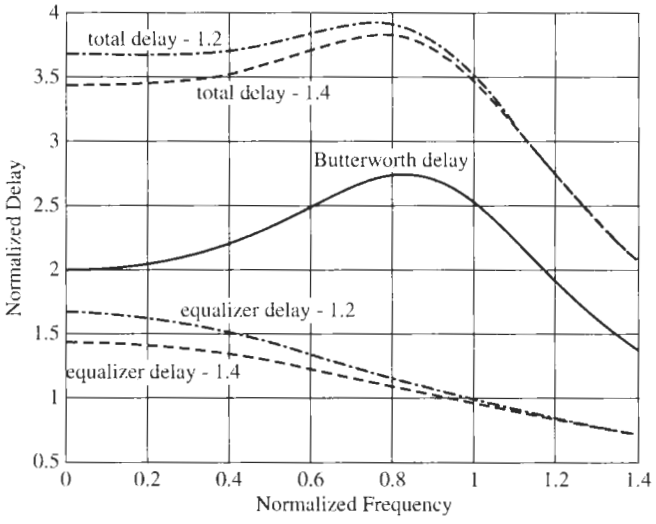

Figure 11.7 Normalized delay curves for Example 11.1. Equalizer delays 1.2 and 1.4 are for the parameter $\sigma_1 = 1.2$ and 1.4, respectively. The total delay is the sum of the delays contributed by the Butterworth filter, D_B, and the equalizer allpass.

any event, we observe visually from Fig. 11.7 that the delay of the Butterworth-allpass cascade varies less over the passband than that of the unequalized Butterworth filter.

The average delay of the equalized filter is approximately 3.65, which is denormalized to $D = 3.65/\omega_c = 3.65/4\pi$ krad/s $= 290$ μs; the maximum delay variation equals $\Delta D = (3.78 - 3.45)/\omega_c = 0.33/4\pi$ krad/s ≈ 26 μs. Without equalization, the average delay is smaller and the delay variation larger: $D = 2.3/4\pi$ krad/s $= 183$ μs and $\Delta D = (2.75 - 2)/\omega_c = 0.75/4\pi$ krad/s ≈ 60 μs. The total delay is as a rule not critical, but the delay variation is important. We see that the addition of the simple first-order allpass reduced the delay variation over the passband from approximately 33 to about 9%.

As the last step of the allpass design we determine the components: Having selected $\sigma_1 = 1.4$, we have the relationship $RC = 1/(\sigma_1\omega_c) = 56.84$ μs; we choose $C = 10$ nF to get the resistors $R = 5.68$ kΩ. Either of the two circuits in Fig. 11.6 may be taken as far as the delay equalization is concerned. If a phase inversion is not permitted for the application and the implementation of the Butterworth filter is inverting, we choose the allpass in Fig. 11.6b; otherwise we choose the circuit in Fig. 11.6a.

In our example we strove to minimize the delay variations over the frequency band of interest because this will often be of most concern. There are, of course, many other criteria that may be selected to arrive at an optimized delay. For example, it may be desirable to construct the filter such that the delay will be maximally flat at the origin or be of equal ripple nature over the passband. In general, computer routines are needed to solve such requirements, but in some simple cases closed-form solutions are available. For example, if $T_M(s)$ is a Butterworth filter of order n and equalization is to be achieved with one first-order allpass such that the delay is maximally flat at $\omega = 0$, the single available parameter σ_1 of Eq. (11.5) is determined (Blinchikoff and Zverev, 1976, p. 217 ff) as

$$\sigma_1 = \left(2 \sin \frac{3\pi}{2n}\right)^{1/3} \tag{11.12}$$

and the delay at the origin is equal to

$$D(0) = \frac{1}{\sin[\pi/(2n)]} + \frac{2}{\sigma_1} \tag{11.13}$$

The third-order Butterworth filter of Example 11.1 would yield $\sigma_1 = 1.26$ and $D(0) = 2 + 1.59 = 3.59$, two values very close the those in Example 11.1.

11.3 EQUALIZATION WITH SECOND-ORDER MODULES

Second-order allpass functions were given in Eq. (5.17), repeated in Eq. (11.14a) for convenience:

$$T_2(s) = K_0 \frac{s^2 - s\omega_0/Q + \omega_0^2}{s^2 + s\omega_0/Q + \omega_0^2} \tag{11.14a}$$

Ideally, the gain constant K_0 should be equal to 1. Second-order allpass stages have the advantage of giving us two design parameters per module, the pole frequency ω_0 and the quality factor Q, which can be adjusted for optimal delay equalization. In other respects the procedure follows the one for first-order allpass filters. Let us again use the normalized frequency, $s_n = s/\omega_0$, to work with the allpass function

$$T_2(s_n) = K_0 \frac{s_n^2 - s_n/Q + 1}{s_n^2 + s_n/Q + 1} \tag{11.14b}$$

We then compute the phase of $T_2(j\omega_n)$,

$$\theta_2(\omega_n) = -2 \tan^{-1}\left(\frac{\omega_n/Q}{1 - \omega_n^2}\right) \tag{11.15}$$

and the delay,

$$D_2(\omega_n) = -\frac{d\theta_2(\omega_n)}{d\omega} = -\frac{d\theta_2(\omega_n)}{d\omega_n} \times \frac{d\omega_n}{d\omega} = \frac{d}{d\omega_n}\left[2 \tan^{-1}\left(\frac{\omega_n/Q}{1 - \omega_n^2}\right)\right] \times \frac{1}{\omega_0}$$

that is,

$$D_2(\omega_n) = \frac{1}{\omega_0}\left[\frac{(2/Q)\left(1 + \omega_n^2\right)}{\left(1 - \omega_n^2\right)^2 + (\omega_n/Q)^2}\right] \tag{11.16}$$

D_2 is the delay that each cascaded second-order allpass section adds to the total filter, and our goal is to determine the two parameters ω_0 and Q such that the total delay is as constant as required over the specified frequency range. To help in this task we plot a set of design curves in Fig. 11.8. They show the normalized delays, the expression in brackets in Eq. (11.16), as

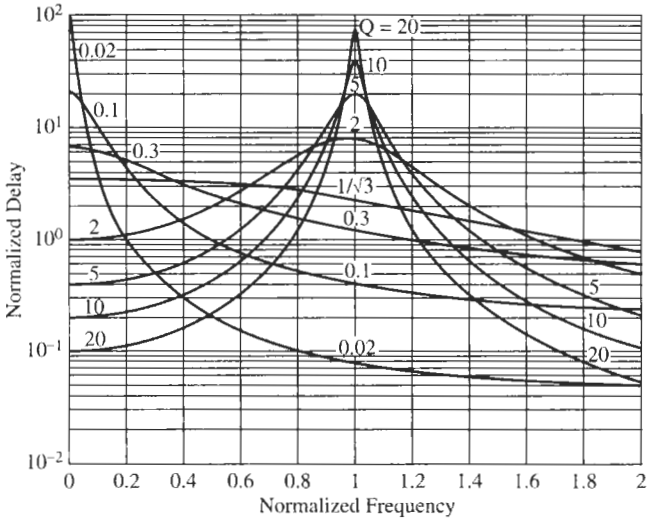

Figure 11.8 The normalized delay $\omega_0 D_2(\omega_n)$ of a second-order allpass filter as function of Q.

functions of Q. Figure 11.8 supports our earlier assertion that delay variations will be larger as the quality factor increases. From Eq (11.16) it is clear that

$$D_2(0) = \frac{1}{\omega_0}\frac{2}{Q} \tag{11.17}$$

and that D_2 goes to zero as $1/\omega_n^2$ for large frequencies. The maximum of the delay curves can be found by taking the derivative of Eq. (11.16) and setting it to zero. The result is the quadratic equation in ω_n^2,

$$\left(\omega_n^2\right)^2 + 2\omega_n^2 + \left(Q^{-2} - 3\right) = 0$$

which is solved for ω_n:

$$\omega_{n,\max} = \sqrt{-1 + \sqrt{4 - Q^{-2}}} \tag{11.18}$$

From this equation we see that $\omega_{n,\max} \approx 1$ for $Q > 1$. For $\omega_n \approx 1$ we find from Eq. (11.16) that the peak value of the delay equals

$$D_{2,\max} \approx \frac{4Q}{\omega_0} \tag{11.19}$$

This equation can also be written as

$$D_{2,\max} = \frac{2}{\omega_0/(2Q)} = \frac{2}{\alpha} \tag{11.20}$$

where $\pm\alpha$ is the real part of the poles and zeros of the allpass function (Fig. 11.4b). It indicates that for $Q > 1$, $D_{\max}$ is determined by the real part of the poles (and zeros). By Eq. (11.18) the

largest value of Q for which the delay has a maximum for positive ω_n is $Q = 1/\sqrt{3} = 0.5774$; from Eq. (11.17) this maximum is $D_2 = 3.464/\omega_0$ at $\omega_n = 0$. Note that for $Q = 1/\sqrt{3}$ the delay becomes

$$D_2(\omega_n) = \frac{2\sqrt{3}}{\omega_0}\left(\frac{1+\omega_n^2}{1+\omega_n^2+\omega_n^4}\right) \tag{11.21}$$

which, according to Eq. (6.53), means that it is maximally flat (see the $1/\sqrt{3}$ curve in Fig. 11.8).

As we stated earlier, our objective is now to connect one or more second-order allpass modules in cascade with the filter T_M. T_M was designed to satisfy the attenuation requirements and the cascaded allpass sections are then designed such that the delay of the total transmission path is constant over the frequency band of interest. Each delay module will have its own values of ω_0 and Q and the delays are simply added. For undemanding equalization problems, it will be possible to use cut-and-try methods (to "eyeball" the design), but for complicated equalization tasks, or those with rigid specifications, computer optimization programs will be necessary (see Section 11.4).

Once the allpass sections are found, they can be realized by any one of several general biquad modules we discussed in Chapter 5. For example, the four-amplifier Åckerberg–Mossberg section of Fig. 5.1 realizes Eq. (5.5). It becomes an allpass filter if we set $(a - bkQ)/a = -1$. Alternatively, the GIC module of Fig. 5.16 is an allpass filter, if in Eq. (5.36) we set $a = c = 1$ and $b = 0$. If only a single opamp per biquad may be used, the Delyiannis–Friend circuit in Fig. 5.19 or the Sallen–Key module in Fig. 5.22 is available. We should bear in mind that the degree of the allpass may be odd, that is, one module may be of first order. Let us work through an example to illustrate the design process; we shall attempt to equalize the delay of a Chebyshev filter, which, from our previous work, we know has poor delay performance (see Fig. 8.20).

EXAMPLE 11.2

For a fifth-order Chebyshev lowpass filter with 0.5-dB passband ripple and passband corner at $f_0 = 3.7$ kHz ($\omega_0 = 23.246$ krad/s), we wish to design a delay equalizer. Cost constraints dictate that at most three first- or second-order equalizer sections may be used.

Solution

From Table 7.2 we find the transfer function:

$$T_{CH}(s_n) = \frac{0.1789}{(s_n^2 + 0.2239s_n + 1.0358)(s_n^2 + 0.5862s_n + 0.4768)(s_n + 0.3623)}$$

The frequency parameter s_n is normalized by ω_0. The delay of this filter can be computed and plotted; the result is shown as the curve "CH 5" in Fig. 11.9a. The objective is now to find three delay sections to equalize the delay as best as possible. We observe that $\Delta D = D_{max} - D_{min} \approx 11 - 3.7 = 7.3$ in the unequalized Chebyshev filter, which means the delay variation is $\Delta D_{CH} \approx 7.3/\omega_0 = 314\ \mu$s after denormalization.

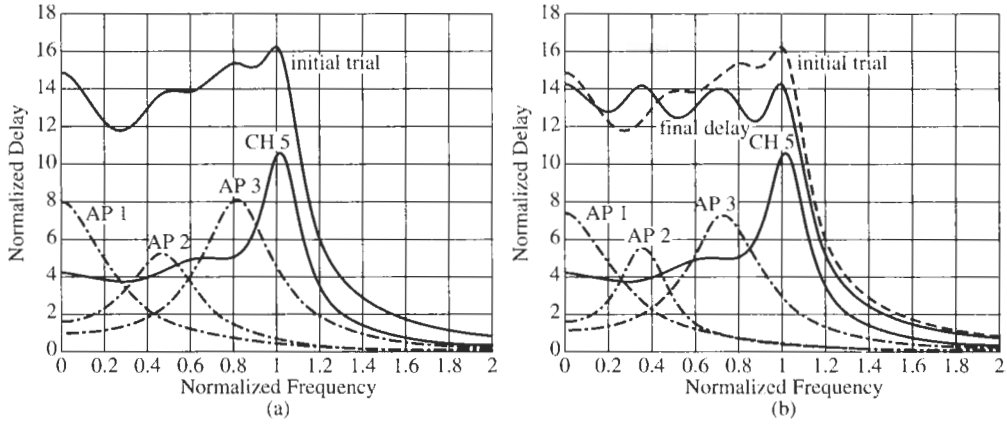

Figure 11.9 The allpass responses for equalizing the delay of the fifth-order Chebyshev filter of Example 11.2: (a) initial result; (b) final equalizer response.

With no optimization program available, we resort to a trial-and-error method[1] with help of the design curves in Figs. 11.5 and 11.8. The equalized delay will be larger than the peak delay, $D = 11$, of the Chebyshev filter. Let us guess at the final average delay being $D = 13$. This means we need to increase the delay at the origin by about $D = 8$; we use as first stage a first-order section, called "Allpass 1 (AP 1)" with $\sigma_1 = 2/8 = 0.25$ by Eq. (11.8). We proceed to "fill the remaining delay valley" with one or two second-order stages. At $\omega_n = 0.5$, the sum of the delays of AP 1 and CH 5 comes to approximately 6.5: we try to equalize by a second-order stage (AP 2) with a peak of 5 at $\omega_n = 0.5$; Eq. (11.19) yields $Q_2 \approx 1.25$. As a quick sketch will show, a third section (AP 3) is required with a peak of approximately 8 at $\omega_n = 0.8$, resulting in $Q_3 = 2$. Inserting these parameters into Eqs. (11.7) and (11.16) and plotting the resulting functions and their sum with the Chebyshev delay CH 5 results in the curve labeled "initial trial" in Fig. 11.9a. We note that our "eyeballing" procedure brought us closer to the desired constant delay, but that further fine-tuning is necessary.

To guide us, we observe from the "initial trial" curve that the peak of Stage 2 is too far to the right and too low; we correct it by choosing $Q_2 = 1.34$ and shifting its peak from $\omega_n = 0.5$ to $\omega_n = 0.38$. Next we note that that the delay at the origin is a little too high; we reduce it by increasing σ_1 from 0.25 to 0.27. Lastly, we shift the peak of Stage 3 from $\omega_n = 0.8$ to $\omega_n = 0.76$ and reduce Q_3 to 1.79. The resulting curves AP 1, AP 2, AP 3 are shown in Fig. 11.9b; their sum with CH 5 is the "final delay" curve shown in the figure. The "initial trial" curve is included in dashed form for comparison.

The final delay has an equal-ripple nature with a ripple width of about $\Delta D = 1.8$. The figure shows clearly how the allpass sections make up the ripples. It helps to understand the individual contributions of the allpass stages when deciding which stage is to be adjusted experimentally or by a computer algorithm for further fine-tuning. To reduce the ripple width substantially would require a higher degree, that is, additional delay modules. We shall look

[1] These trial-and-error procedures are quite easily completed with some computer aids; for this example MATLAB was used. The "eyeballing" and "fine-tuning" procedures are greatly helped by the designer's experience.

at this issue in Section 11.4. The realized average delay is approximately $D \approx 13.5/\omega_0 = 13.5/(2\pi \times 3.7 \text{ krad/s}) = 580\ \mu\text{s}$ with a ripple width $\Delta D \approx 1.8/\omega_0 = 77\ \mu\text{s}$, a substantial improvement over $\Delta D_{\text{CH}} = 314\ \mu\text{s}$ in the unequalized filter. To realize the allpass filter we use the first-order stage of Fig. 11.6a followed by two second-order Sallen–Key stages of Fig. 5.22. The components of the first-order circuit, AP 1, are obtained from $RC = 1/(\sigma_1\omega_0) = 159\ \mu\text{s}$, which with $C = 10$ nF results in $R = 15.9\ \text{k}\Omega$.

The Sallen–Key blocks with $C_1 = C_2 = C$ and $R_1 = R_2 = R$, $\omega_0 = 1/(CR)$, and $Q = 1/(3 - K)$ realize Eq. (5.48), repeated here as Eq. (11.22):

$$T(s) = \frac{V_2}{V_1} = \frac{N(s)}{D(s)} = -K\frac{s^2(c_k - b) + s\omega_0(3c_k - 2b) + (c_k - a)\omega_0^2}{s^2 + s\omega_0/Q + \omega_0^2} \tag{11.22}$$

With Table 5.5 and the notation used there,

$$a = b = \frac{3Q + 1}{3Q - 1} \times \frac{2Q - 1}{2Q + 1}$$

and $c_k = 1$, Eq. (11.22) simplifies to

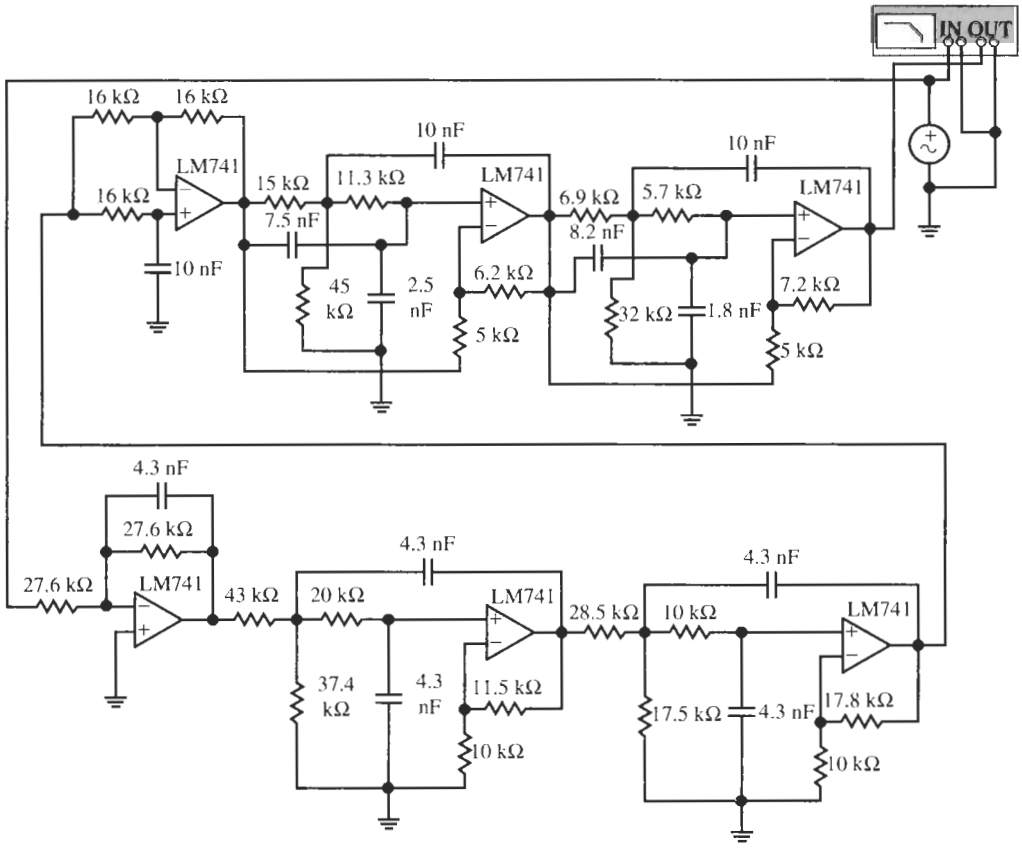

(a)

Figure 11.10 (a) Circuit for Example 11.2, (b) test and (c) simulation results. (Bode Plotter scales: 10 Hz to 100 kHz; −80 to 10 dB; cursor at 3.425 kHz, −14.76 dB.)

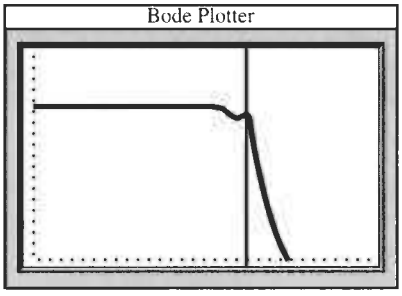

(b)

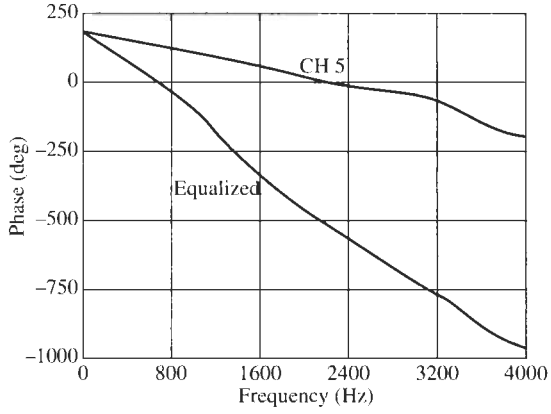

(c)

Figure 11.10 Continued

$$T(s) = K\,(b - c_k)\,\frac{s^2 - s\omega_0/Q + \omega_0^2}{s^2 + s\omega_0/Q + \omega_0^2} = \left(\frac{2Q-1}{2Q+1}\right)\frac{s^2 - s\omega_0/Q + \omega_0^2}{s^2 + s\omega_0/Q + \omega_0^2} \tag{11.23}$$

For the allpass stage AP 2 we had $Q_2 = 1.34$ and $\omega_n = 0.38$. With $C = 10$ nF, this results in $R = 1/(0.38 \times 2\pi \times 3700 \times 10^{-8})\ \Omega = 11.3\ \text{k}\Omega$; $Q_2 = 1.34$ gives $K = 2.25$ and $a = b = 0.76$. Similarly we have for AP 3 with $\omega_n = 0.76$, $C = 10$ nF, and $Q_3 = 1.79$: $R = 1/(0.76 \times 2\pi \times 3700 \times 10^{-8})\ \Omega = 5.66\ \text{k}\Omega$, $K = 2.44$, and $a = b = 0.82$. For the fifth-order Chebyshev filter we use the design of Example 7.5 and rescale the frequency from $\omega = 1000$ rad/s to $\omega = 23.24$ krad/s (change the 100 nF capacitors into $100/23.24 = 4.3$ nF capacitors). The complete tenth-order circuit is shown in Fig. 11.10a, with LM741 opamps and realistic element values. The lower three sections are the Chebyshev filter and the upper three are the allpass equalizer. Figure 11.10b shows the magnitude response. Apart from a flat loss of approximately 12 dB caused by the gain constants in Eq. (11.23), it is identical to that in Fig. 7.14 because the allpass has no other effect on the magnitude. Figure 11.10c shows that the phase stays linear beyond the passband corner where the Chebyshev delay has the large peak.

The student may wonder why the phase of the unequalized filter, CH 5 (the upper phase curve in Fig. 11.10c), is more linear than that of the equalized one over much of the passband. The explanation of this behavior is not difficult and can be expected from the delay variations of CH 5 in Fig. 11.9b, which for $\omega_n < 0.9$ (3.33 kHz) are actually less than those of the "final delay." Our main effort in equalizing the delay went into eliminating the delay peak of CH 5 at $\omega_n = 1$. This goal was reached: note the substantial change in phase slope of the Chebyshev filter CH 5 at about 3.3 kHz, whereas the equalized phase slope stays reasonably constant until beyond 3.7 kHz.

11.4 STRATEGIES FOR EQUALIZER DESIGN

We have developed in Section 11.3 a trial-and-error strategy with which arbitrary delay characteristics may be equalized by a cascade connection of a number of first- and second-order allpass sections. This method is adequate for relatively simple requirements, but because

closed-form solutions are not available, computer optimization methods are normally used for complex problems. Software packages have been developed for this task.

When designing an equalizer, it is helpful to get first an initial estimate of the number of stages that will be required. To understand the approach to obtaining an estimate, we return to Example 11.2. We can interpret Fig. 11.9b as indicating that the purpose of the equalizer is to "add the missing delay" to the delay of the filter CH 5 that provided the specified magnitude response. This we do in such a way that a constant level of delay is reached, $D = 13$ in the example. This is illustrated in Fig. 11.11, where we have shown the delay of CH 5 along with a curve obtained by subtracting CH 5 from the constant value $D = 13$. The area A_{Eq} below the equalizer response, the "13 − CH 5" curve, must be filled by the delay of the allpass stages to be found. The number n of first- and second-order sections that are needed for this purpose depends on the amount of peaking of the magnitude filter and on the acceptable delay error ΔD. A very rough estimate that works reasonably well for modest demands on the equalizer can be shown to be

$$n \approx A_{\text{Eq}}/\pi \tag{11.24}$$

For instance, in the case of Example 11.2, the area under the "13 − CH 5" curve in Fig. 11.11 can be estimated quite simply by counting the number of the (2×0.1) rectangles. We count approximately 41 rectangles for a total area of about $2 \times 0.1 \times 41 = 8.2$. Dividing this number by π gives 2.61, which we round up to 3. The estimate is in agreement with our use of two second-order plus one first-order stage in Example 11.2.

A more serious weakness of the crude estimate in Eq. (11.24) is that it does not include information on the maximum *delay deviation* ΔD. We saw in Fig. 11.9 that each allpass stage adds one peak to the equalized delay response, and that more and smaller ripples require more stages. Intuitively we expect that an equalizer of higher degree will reduce the delay variations and, of course, increase the average delay because more stages add to the delay. Figure 11.12 illustrates this statement. Plotted are the delay response of the fifth-order 0.5-dB-ripple Chebyshev lowpass filter CH 5 of Example 11.2, and the equalized delay responses after cascading CH 5 with a fourth-order allpass, the fifth-order allpass of Example 11.2, and

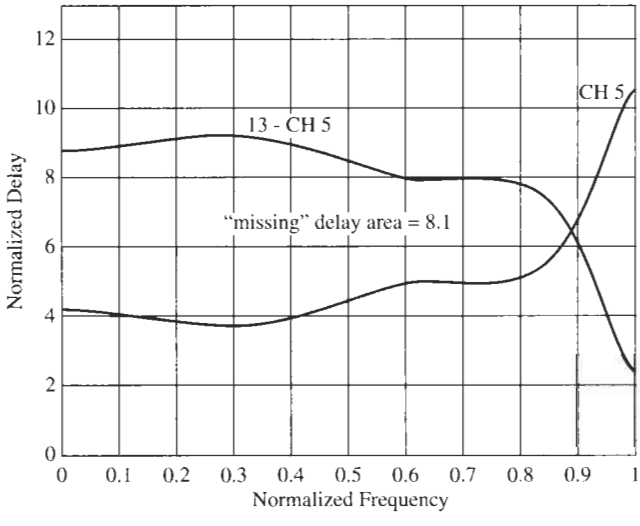

Figure 11.11 Illustrating the method of estimating the number of allpass sections needed to design a delay equalizer: The allpass stages provide the "missing" delay, the area under the equalizer response. It is obtained by subtracting the delay of the magnitude filter (here CH 5) from the desired delay (here 13).

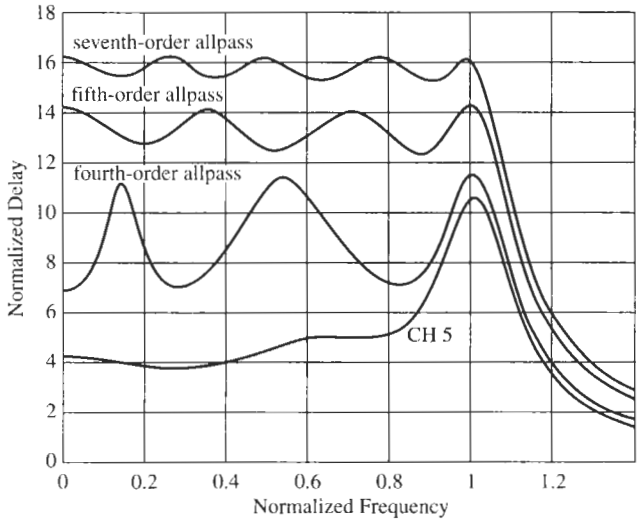

Figure 11.12 Delay responses of a fifth-order 0.5-dB-ripple Chebyshev lowpass filter with no equalization (CH 5), and with fourth-, fifth-, and seventh-order allpass equalizers. The equalizer parameters are adjusted to achieve an equal-ripple delay response over the passband.

a seventh-order allpass. Table 11.1 contains the allpass-section parameters for these designs. Observe that the fourth-order equalizer is not a good solution because the ripple width ΔD is barely less than the delay variations of the original CH 5 filter. We notice from the figure that the average delay increases with equalizer order, as does the number of ripples. The reduced delay variation ΔD with increasing degree is apparent. Unfortunately, no closed-form solutions are available to let us estimate the degree required as a function of the specified delay error ΔD; cut-and-try methods or, if available, computer optimization routines must be used.

Once we have arrived at an initial estimate of the number n of allpass sections needed we can select suitable criteria for optimizing the design. Optimization criteria are usually expressed in terms of a number that may be the difference between the desired delay D_d and the available delay D_a, expressed as an average error, a mean-squared error, or a peak error. If minimizing a mean-squared error is selected, standard procedures (Blinchikoff and Zverev, 1976, pp. 103–106, 233–235) may be followed. Let D_d be the desired delay over the range of frequencies ω_1 to ω_2. We then start from the estimated number n of first- and second-order sections to be used and compute their characterizing parameters σ_1, ω_0, and Q, from the least-square error defined as

$$\varepsilon = \int_{\omega_1}^{\omega_2} [D_d(\omega) - D_a(\omega)]^2 d\omega \tag{11.25}$$

For example, we may require D_d to be a constant, D_0, and the available delay D_a is the delay D_M of a given magnitude filter that is augmented by the delay of an allpass with complexity

TABLE 11.1 Allpass-Stage Parameters for Fig. 11.12

Stage	First-order	Second-order		Second-order		Second-order	
	σ_1	ω_0	Q	ω_0	Q	ω_0	Q
Fourth-order	—	0.154	1.40	0.556	1.60	—	—
Fifth-order	0.27	0.385	1.34	0.763	1.79	—	—
Seventh-order	0.25	0.294	1.15	0.513	1.50	0.820	2.07

given by n. The term in brackets then equals $D_0 - (D_M + D_{AP})$ and Eq. (11.25) represents an error that is to be minimized by choice of the allpass parameters. We then require that

$$\frac{\partial \varepsilon}{\partial \sigma_1} = 0, \quad \frac{\partial \varepsilon}{\partial \omega_{0i}} = 0, \quad \frac{\partial \varepsilon}{\partial Q_i} = 0$$

The simultaneous solution of these differential equations gives the optimal values of all available parameters σ_i, ω_{0i}, and Q_i. From these solutions, the response can be calculated. If the result is not acceptable, the computations are repeated for a larger value of n. The method is analogous to the trial-and-error approach that we used in Example 11.2 for determining an allpass specified via Eq. (11.3), but the efficiency and speed of a computer make it possible for the designer to try many possibilities until deciding which design to use.

REFERENCES

H. J. Blinchikoff and A. I. Zverev, *Filtering in the Time and Frequency Domains*. Wiley, New York, 1976.

PROBLEMS

11.1 Figure P11.1 shows the Delyiannis–Friend circuit of Fig. 4.35, modified by the addition of a second opamp summing circuit. Determine the values for k_1 and k_2 such that the transfer function $T = V_2/V_1$ is a second-order allpass function.

11.2 Use the circuit of Fig. P11.1 to design an allpass with the parameters $\omega_0 = 46$ krad/s and Q chosen to give a peak normalized delay of $D \approx 8$. Choose appropriate opamps to build the circuit and test its performance.

11.3 Repeat Problem 11.2, but for the frequency $\omega_0 = 46$ Mrad/s.

11.4 In Fig. P11.4, let the output voltages of the highpass and the lowpass blocks be V_{2LP} and V_{2HP}, respectively, and let these filters be third-order Butterworth lowpass and highpass modules. Consider the function

$$T(s) = \frac{V_{2LP} \pm V_{2HP}}{V_s}$$

and show that the plus sign results in a second-order allpass function, while the minus sign results in a first-order allpass function.

11.5 Twenty-five identical first-order allpass section are connected in cascade. What is the resulting value of σ_0 if the overall delay at $\omega = 10^4$ rad/s is 2 ms.

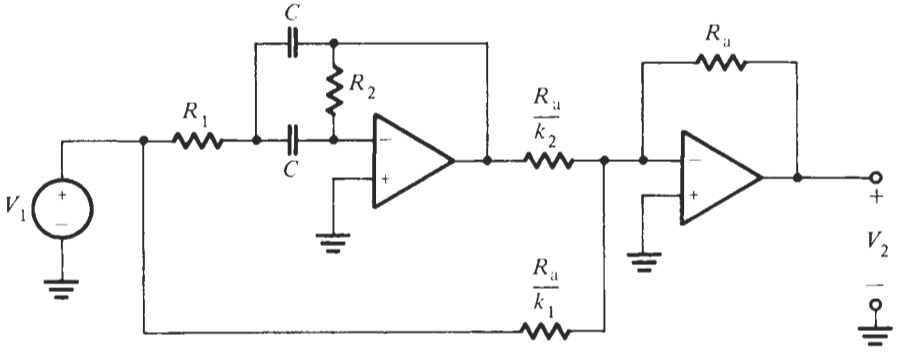

Figure P11.1

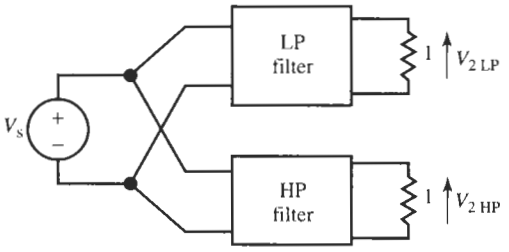

Figure P11.4

and the delay at $1.5x\,10^4$ rad/s is 1 ms? Note that the delays of all the sections add; see Eq. (11.2).

11.6 Measurement of the delay introduced by communications equipment is shown in Fig. P11.6 with normalized delay D_n. We wish to design a first-order circuit to provide delay equalization so that the total delay is approximately constant from $\omega = 0.1$ to $\omega = 1.0$. Denormalize the frequency by $\omega = 20$ krad/s and design a circuit that will provide the required delay equalization.

11.7 The measurement of the delay in a certain transmission channel provides the curve shown in Fig. P11.7. We wish to introduce delay equalization so that the total delay is approximately constant from $\omega = 0$ to $\omega = 1$. Find the required transfer function and realize the circuit to provide the desired equalization. Denormalize the frequency by $f = 8.5$ kHz, build the circuit, and test the performance of your design.

11.8 The measured normalized delay D_n introduced by some communication equipment is shown in Fig. P11.8. Delay equalization must be provided so that the total delay is approximately constant over the range of frequencies shown in the figure.

(a) Find the transfer function and design a circuit that will provide the required equalization.

(b) Scale the circuit so that the delay $D_n = 1$ becomes $D = 1\ \mu$s.

11.9 It is required to design an allpass filter satisfying the given linear delay

$$D(\omega) = -0.48\omega + 4.6 \quad 1 \le \omega \le 6$$

A computer optimization program provides the needed parameters as follows: one first-order section with $\sigma = 3.5$ and four second-order sections each having a Q of 0.5 and frequencies 3.2, 3.8, 4.5, and 4.8.

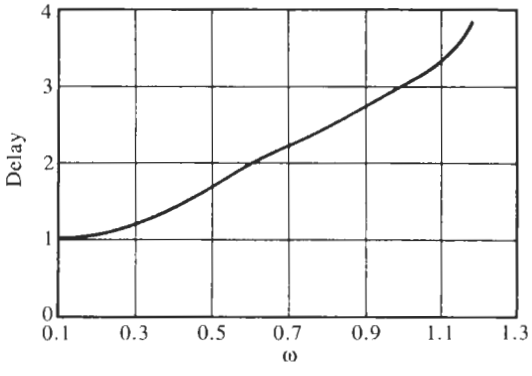

Figure P11.6

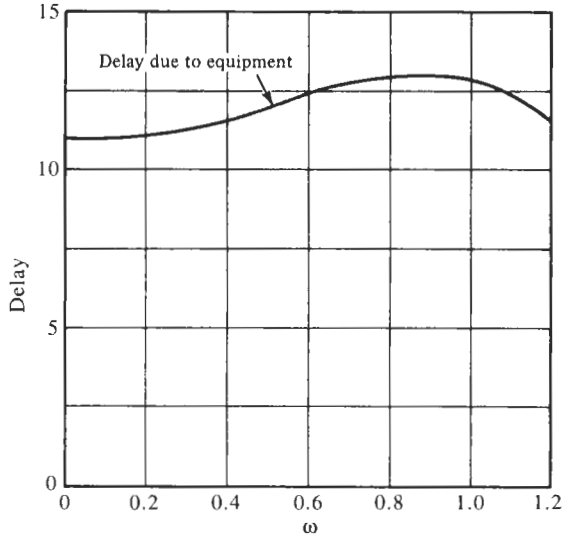

Figure P11.7

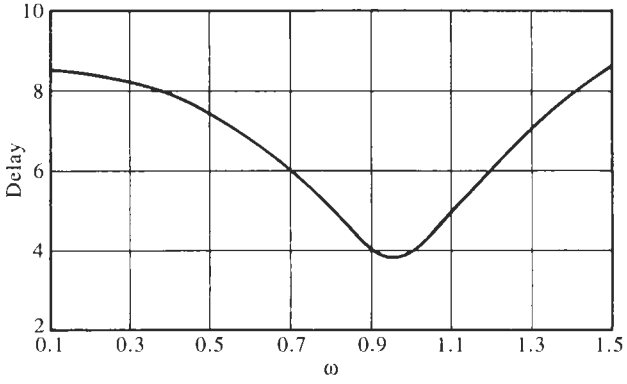

Figure P11.8

(a) Design the normalized circuit to satisfy the computed parameters.

(b) Frequency scale so that $\omega = 1$ becomes $\omega = 1000$ rad/s, and determine the practical element values for the circuit designed in part (a). Use LM741 opamps and test your design.

11.10 The delay of a sixth-order Butterworth lowpass filter (see Fig. 10.7) must be equalized over the passband $0 \leq \omega \leq 1$ by a number of cascaded allpass sections. Estimate the number of allpass modules needed for the task. Remember that the total delay of the cascade connection will be larger than the peak delay of the Butterworth filter.

11.11 For high-frequency equalization, it is often necessary to use passive circuits. A passive allpass can be designed as the balanced so-called *constant-resistance* lattice shown in Fig. P11.11 (see also Section 13.6). If $Z_a Z_b = R_0^2$, show

(a) that the transfer function is

$$T(s) = \frac{V_2}{V_1} = \frac{1 - Z_a/R_0}{1 + Z_a/R_0}$$

From this result it follows that if Z_a on the $j\omega$-axis is purely imaginary then $T(j\omega)$ is a ratio of two conjugate complex numbers and its magnitude is unity: $|T(j\omega)| \equiv 1$. The functions $Z_a(s)$ that satisfy this condition are of the form of Eq. (9.84), with special cases given in Eqs. (9.77) to (9.82). They are so-called *Foster reactance functions* discussed in Section 9.5, and are realizable as LC impedances as we saw in the examples in Fig. 9.33. Consequently, the lattice network in Fig. P11.11 is an allpass circuit under the condition $Z_a Z_b = R_0^2$.

(b) that the input impedance is $Z_{in}(s) = V_1/I_1 = R_0$.

(c) Verify that the result of (b) permits the passive allpass circuits in Fig. P11.11 to be cascaded with no need for buffering.

11.12 Apply the results of Problem 11.11 to the circuit shown in Fig. P11.12, and show that the transfer function represents a first-order allpass circuit with a pole at $-\sigma_0$ and a zero at $+\sigma_0$. Obtain design equations for L and C in terms of σ_0.

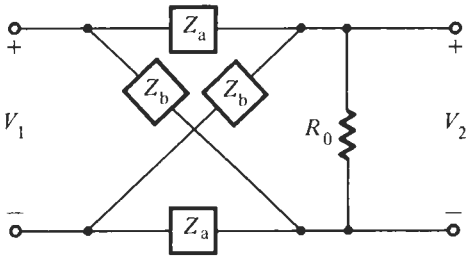

Figure P11.11

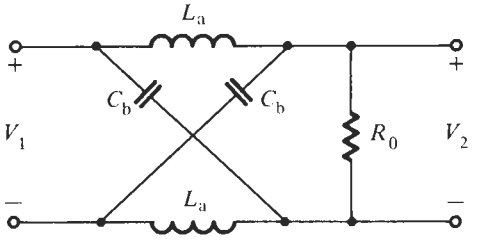

Figure P11.12

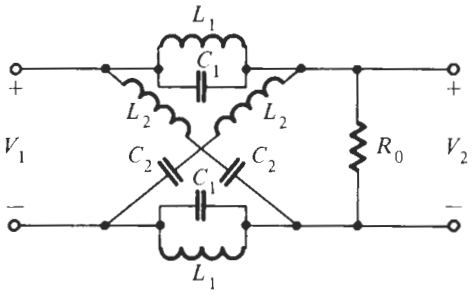

Figure P11.13

11.13 Apply the results of Problem 11.11 to the circuit given in Fig. P11.13 and show that the transfer function is a second-order allpass function. Determine design equations for the inductors and capacitors in terms of specified allpass parameters ω_0 and Q.

11.14 Use the results of Problems 11.12 and 11.13 to design a passive three-section delay equalizer for a communications channel. The required parameters were computed to be

Section	f_0	Q
I	58.1 MHz	2.815
II	71.8 MHz	3.272
III	85.2 MHz	4.209

Realize the circuit with practical component values and test its performance with EWB.

SENSITIVITY

In all our examples and discussions in earlier chapters we have made an effort to present realistic designs. We have constructed the circuits with real amplifiers (LM741), and resistors and capacitors with realistic values, rounded to one, two, or at most three decimals. The simulation and test results indicated that the design equations we developed along the way are correct, and our circuits worked as required. Nevertheless, in practice we still have to be concerned with a problem: components with exact design values will generally not be available, so that the assumption that the circuits are built with exact components is unrealistic. We can certainly go into the laboratory and carefully select components with the desired values or tune them until the circuit behaves as specified, but in manufacture this will generally not be possible or be too expensive.

To illustrate the problem we show in Fig. 12.1 circuits and test results of two second-order bandpass filters designed to realize a center frequency of 10 kHz, a 3-dB bandwidth of 333 Hz ($Q = 30$), and midband gain of 6 dB. The circuits we chose are the Q-enhanced Delyiannis–Friend module of Fig. 4.38 and the GIC module of Fig. 4.46a. The two designs and the test arrangement are shown in Fig. 12.1a, and the responses for nominal component values in Fig. 12.1b. The slight variance in the magnitude responses results from our rounding of component values and the different effect of the opamps' gain-bandwidth product in the two circuits. This was discussed in Chapter 4. The difference of 180° in phase between the two designs reflects the fact that the Delyiannis–Friend circuit is inverting [see Eq. (4.129)]. The differences in performance are negligible, and both modules realize the specified filter design parameters. If we now send the designs to be manufactured, specifying component tolerances of 1%, and then take 20 random samples to retest their performance, we obtain for the Delyiannis–Friend circuit the responses in Fig. 12.1c. The results are somewhat disconcerting: the center frequency varies from a low of 9.64 kHz to a high of 10.10 kHz, a span of 4.6% of the nominal value of 10 kHz. Since the required bandwidth is only 3.3% of the center frequency, we can label the performance as unacceptable because the

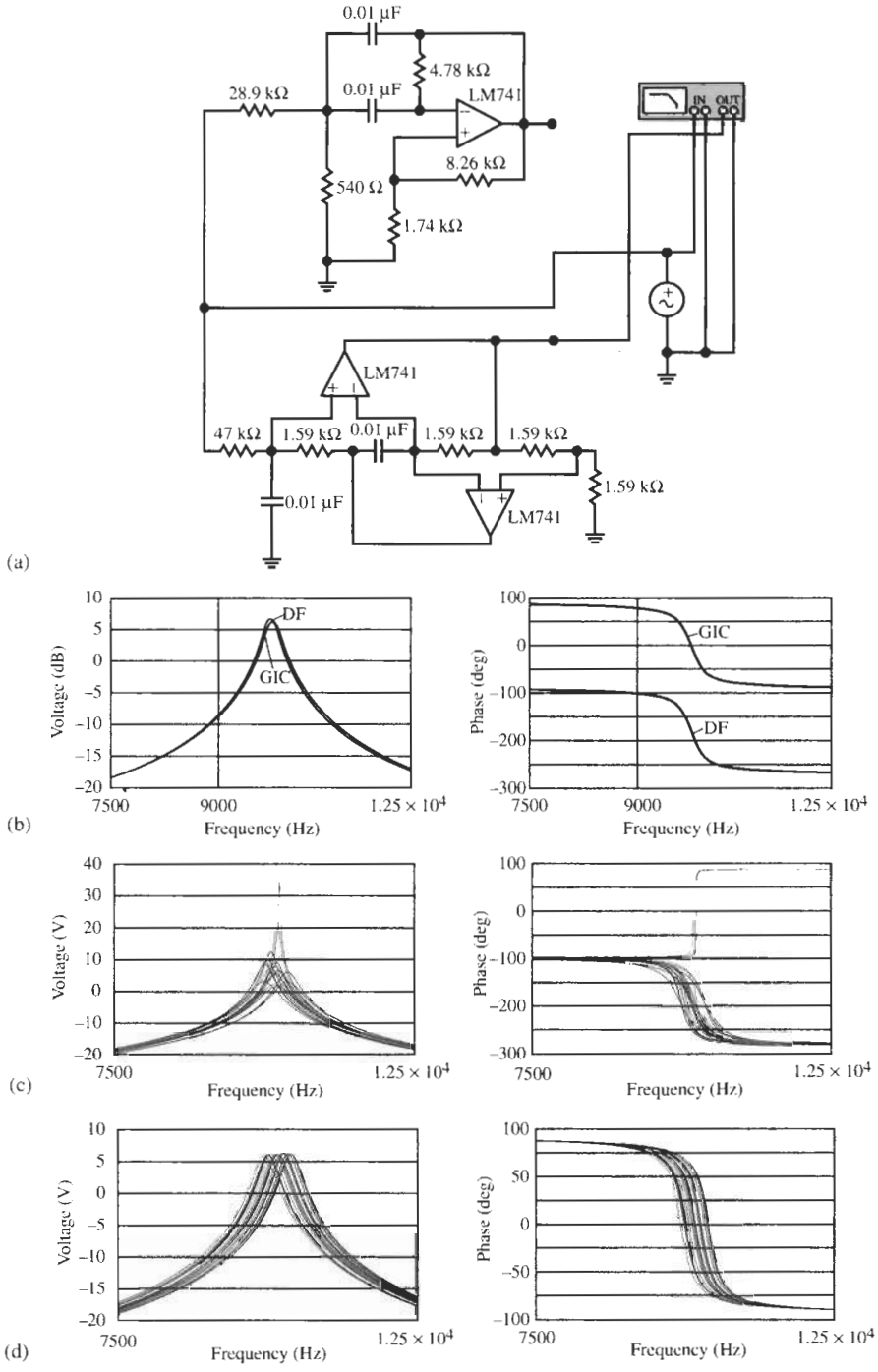

Figure 12.1 Design and performance of two bandpass sections; (a) second-order Delyiannis–Friend (DF) and GIC modules; (b) nominal performance; (c) 20 random responses for the Delyiannis–Friend circuit; (d) 20 random responses of the GIC circuit. Both are assumed to be built with components of 1% tolerances and Gaussian distribution.

center of the passband will be shifted to the outside of the prescribed bandwidth. Q values vary from a low of about 20 to over 100. As a matter of fact, for the responses with the highest peaks the circuit oscillates, i.e., we have negative[1] Qs, as indicated by the positive values of phase. Hoping for better results with the GIC circuit, we test 20 random samples and obtain the responses in Fig. 12.1d. Indeed, the results are better: Q and gain are fairly constant, but again the center frequency varies from a low of 9.64 kHz to a high of 10.10 kHz. Visually, the results in Fig. 12.1d appear more predictable than the ones in Fig. 12.1c.

Clearly, we need to investigate these problems. We must develop a measure to let the engineer predict the expected variations, as well as deviations of performance of different circuits. We should be able to answer the following questions:

How do component tolerances affect a circuit's response?

How do such changes relate to filter specifications, such as ω_0, Q, and gain?

How do the responses of different circuits reflect the component tolerances?

How do such changes relate to our preference of one circuit over another?

One answer to these questions is provided by the measure of *sensitivity*, first introduced by Bode in 1940, which we study in this chapter. We will find that sensitivity calculations are quite straightforward but often somewhat laborious. They are necessary, however, for any complete design because the sensitivity of a circuit is a very important criterion. It lets us decide on the likelihood of a successful design, gives us information on the quality, and cost, of the components required. It also permits us to make estimates on how many parts of a manufacturing run of a design are likely to be acceptable, i.e., to answer the question of *yield*.

12.1 DEFINITION OF BODE SENSITIVITY

Transfer functions and circuit parameters are functions of the elements from which the circuit is constructed, and changes must be expected, of course, if the element values change. Thus, poles may shift and transfer function magnitudes and shapes may be altered, as shown in Fig. 12.2. If a circuit has a component, say a resistor R, that is expected to vary, and we pull out R for study, we may represent the situation as shown in Fig. 12.3. We can write the dependence for the transfer function and its parameters, such as pole frequency and quality factor, formally as

$$\frac{V_2}{V_1} = T(s, R), \quad \omega_0 = \omega_0(R), \quad Q = Q(R)$$

Using this representation, a well-known way of determining small changes of the transfer function and its parameters when R varies is via a Taylor series expansion around the nominal value R_0,

[1] If we consult Eq. (4.129) and compute the phase for negative values of Q_0, it becomes clear that the phase becomes positive for $\omega > \omega_0$. Negative Q results in right half-plane poles and an unstable circuit. Negative Q can in general not be detected from the magnitude response alone because it depends on Q^2 [see Eq. (4.30)].

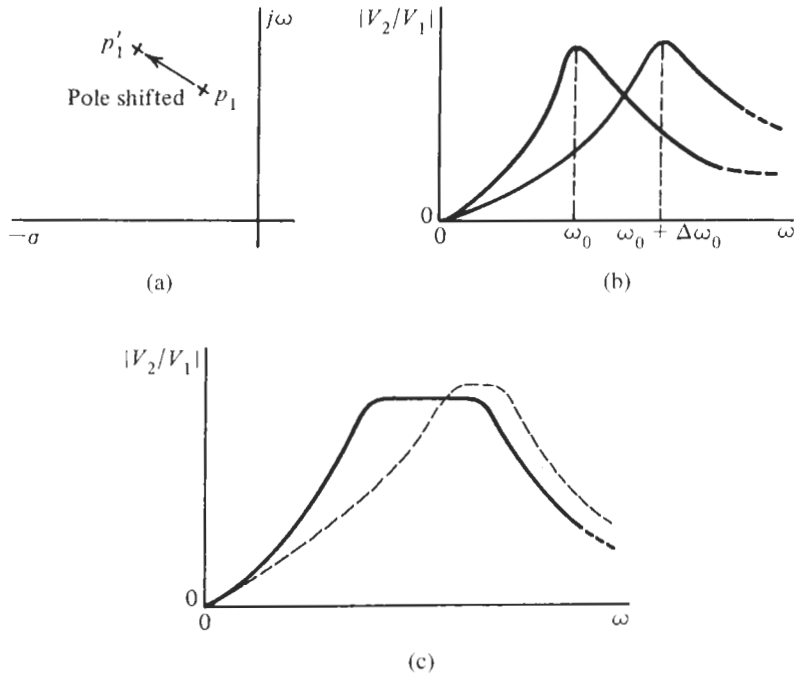

Figure 12.2 Typical changes caused by changing circuit components: (a) shifts of the poles; (b, c) shifts of the complete transfer function.

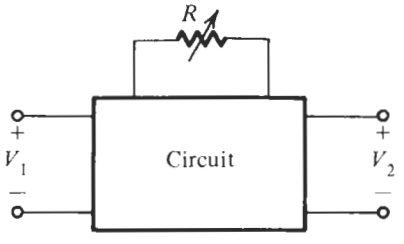

Figure 12.3 A circuit with one resistor shown extracted for studying sensitivity.

$$T(s, R) = T(s, R_0) + \left(\frac{\partial T(s, R)}{\partial R} \bigg|_{R=R_0} \right) dR + \cdots = T(s, R_0) + \Delta T(s, R_0) \tag{12.1a}$$

$$\omega_0(R) = \omega_0(R_0) + \left(\frac{\partial \omega_0(R)}{\partial R} \bigg|_{R=R_0} \right) dR + \cdots = \omega_0(R_0) + \Delta\omega_0(R_0) \tag{12.1b}$$

and similarly for Q. It is important to observe that we terminated the Taylor series after the linear term. It means that we assume *small changes* in the component R. The situation is sketched in Fig. 12.4. We have used partial derivatives because the circuit depends on more than one component. Equation (12.1a) indicates that we calculate the transfer function change as

$$\Delta T(s, R_0) = \frac{\partial T(s, R)}{\partial R} \bigg|_{R=R_0} dR \tag{12.2a}$$

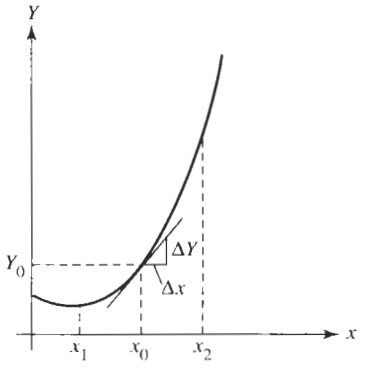

Figure 12.4 Determining the small change of a function $Y(x)$ via the derivative $\partial Y/\partial x$ at the nominal point x_0. Note that sensitivity is a small-change measure; good results ∂Y cannot be expected for large changes ∂x because of the increasing difference between the function and its tangent. At the point x_1, the slope is zero and so is the sensitivity; at the point x_2 the slope and the sensitivity are larger.

and similarly for the changes in its parameters

$$\Delta\omega_0 = \frac{\partial\omega_0}{\partial R}dR \quad \text{and} \quad \Delta Q = \frac{\partial Q}{\partial R}dR \tag{12.2b}$$

All derivatives are evaluated at the nominal point, R_0. For example, according to Eq.(12.2b) a change ∂R in component value results in a changes in ω_0 and Q of $\partial\omega_0/\partial R$ and $\partial Q/\partial R$, respectively, times dR (see Fig. 12.4).

Absolute component tolerances are rarely meaningful or even known. Clearly, when a resistor R changes by 10 Ω, we expect the effect of this change to be less if the resistor's nominal value is 10 kΩ rather than 100 Ω, that is, the effects depend on whether the change is 0.1 or 10%. Thus, we normally deal with relative changes, measured in percent; for example,

$$\%\text{ change in } Q = \partial Q/Q \times 100\%$$
$$\%\text{ change in } R = \partial R/R \times 100\%$$

We then rewrite Eq. (12.2a) as

$$\frac{\Delta T}{T} = \left(\frac{R}{T}\frac{\partial T}{\partial R}\right)\frac{dR}{R} = S_R^T\frac{dR}{R} \tag{12.3}$$

and label the quantity

$$S_R^{T(s)} = \frac{R}{T(s)}\frac{\partial T(s)}{\partial R} = \frac{\partial T(s)/T(s)}{\partial R/R} \tag{12.4a}$$

the *sensitivity* of T with respect to R: sensitivity is the ratio of the relative error of the function $T(s)$ to the relative component error. For small but finite differences, i.e., $\partial R \to \Delta R$ and $\partial T \to \Delta T$, Eq. (12.3) can be written as

$$\frac{\Delta T}{T} \approx S_R^T\frac{\Delta R}{R} \tag{12.5}$$

It says that the relative change in R results in a relative change in T that is S_R^T times as large. The relative change $\Delta T(s)/T(s)$ is also referred to as *variability*, so that we can say the variability of T equals the sensitivity times the variability of the component R. This suggests that small

values of sensitivity are desirable, whereas circuits with large sensitivities ought to be avoided. Analogous expressions are true for the parameters of the transfer function:

$$S_R^Q = \frac{\partial Q/Q}{\partial R/R}, \quad S_R^{\omega_0} = \frac{\partial \omega_0/\omega_0}{\partial R/R} \tag{12.4b,c}$$

These equations are general; let us for the purpose of a general discussion of sensitivity label the function or parameter in question Y and the component x (see Fig. 12.4). Then the sensitivity expression becomes

$$S_x^Y = \frac{\partial Y/Y}{\partial x/x} = \frac{x}{Y}\frac{\partial Y}{\partial x} \tag{12.6}$$

Recall from differential calculus that

$$d(\ln u) = \frac{du}{u} \tag{12.7}$$

Then we may rewrite the sensitivity also as

$$S_x^Y = \frac{x}{Y}\frac{\partial Y}{\partial x} = \frac{\partial \ln Y}{\partial \ln x} \tag{12.8}$$

Two important observations may be made at this point. First we note that since sensitivity is computed from the slope of the function Y, we need to be consistent on our understanding of where the slope is measured: the derivative is evaluated at the *nominal* component value (at x_0 in Fig. 12.4). Second, we note from Eq. (12.4a) that in general sensitivity is a function of frequency if Y depends on frequency. For example, the sensitivity of a transfer function magnitude to a component R at the nominal value R_0 equals

$$S_R^{|T(j\omega, R_0)|} = \frac{R}{|T(j\omega, R)|}\left.\frac{\partial |T(j\omega, R)|}{\partial R}\right|_{R=R_0} \tag{12.9}$$

Clearly, it depends on frequency. So we must make certain that we agree at which frequency it is measured and evaluate the sensitivity at or close to the operating frequency. It is as a rule of little relevance that one's design has very low sensitivities at dc when the circuit is to operate in the range of a few hundred kHz.

The problem of interest to Bode when he introduced the concept of sensitivity (Bode, 1945) was the change in a transfer function T when one of the elements in the transmission system, an amplifier, was likely to suffer large changes. If the system is represented as in Fig. 12.5a where T_2 represents the amplifier, the overall transfer function is

$$T = T_1 T_2 \tag{12.10}$$

It is clear that T_2 directly affects the transmission; its sensitivity to T_2 is

$$S_{T_2}^T = \frac{T_2}{T}\frac{\partial T}{\partial T_2} = \frac{T_2}{T}T_1 = \frac{T_1 T_2}{T_1 T_2} = 1 \tag{12.11}$$

From this we see that a 1% change in T_2 results in a 1% change in T as anticipated. If feedback is introduced as in Fig. 12.5b then, as studied in Chapter 2, Eq. (2.77),

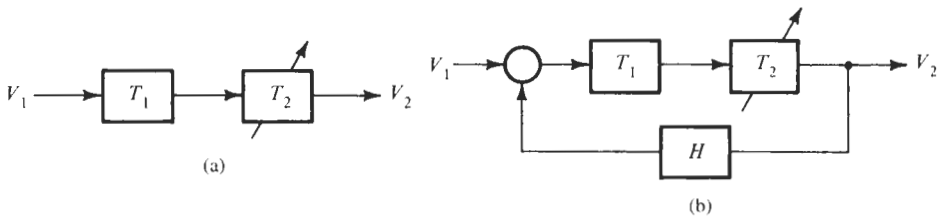

Figure 12.5 A transmission system: (a) without feedback; (b) with feedback.

$$T = \frac{T_1 T_2}{1 + HT_1 T_2} \tag{12.12}$$

and the sensitivity function is found by applying Eq. (12.8),

$$S_{T_2}^T = \frac{T_2}{T}\frac{\partial T}{\partial T_2} = \frac{T_2}{T}\frac{T_1(1 + HT_1T_2) - T_1T_2HT_1}{(1 + HT_1T_2)^2} = \frac{1}{1 + HT_1T_2} \tag{12.13}$$

Now if we select the parameters such that the *loop gain* $HT_1T_2 \gg 1$, the transfer function is

$$T \approx \frac{1}{H}$$

and the sensitivity becomes

$$S_{T_2}^T \approx \frac{1}{HT_1T_2} \ll 1$$

For example, if the loop gain is 1000, the sensitivity is 10^{-3} compared to the value 1 for the open-loop system. The result of this analysis led to the widespread use of feedback in transmission systems.

EXAMPLE 12.1

Apply sensitivity analysis to the inverting amplifier of Chapter 2, shown for convenience in Fig. 12.6.

Solution

We have from Eq. (2.55),

$$T = \frac{V_2}{V_1} = -\frac{R_2/R_1}{1 + (1 + R_2/R_1)/A} = -\frac{G_0}{1 + (1 + G_0)/A}$$

where we have labeled the amplifier's low-frequency gain G_0. The sensitivity of T with respect to R_1 is

$$S_{R_1}^T = \frac{R_1}{T}\frac{\partial T}{\partial R_1} = \frac{R_1}{T}\frac{\partial}{\partial R_1}\left[\frac{-R_2}{R_1 + (R_1 + R_2)/A}\right] = -\frac{R_1}{T}\frac{-R_2(1 + 1/A)}{[R_1 + (R_1 + R_2)/A]^2}$$

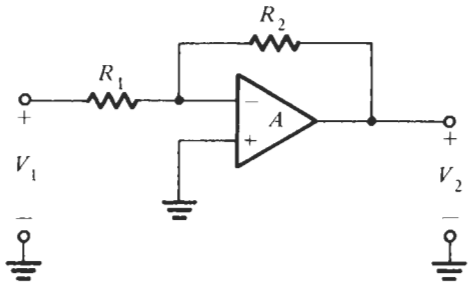

Figure 12.6 Inverting amplifier based on an opamp.

which we evaluate at $A \to \infty$:

$$S_{R_1}^T = \left. \frac{R_1(1 + 1/A)}{R_1 + (R_1 + R_2)/A} \right|_{A \to \infty} = -1$$

Similarly, we obtain

$$S_{R_2}^T = \frac{R_2}{T} \frac{\partial T}{\partial R_2} = \frac{R_2}{T} \frac{R_1 + (R_1 + R_2)/A - R_2/A}{[R_1 + (R_1 + R_2)/A]^2} = \left. \frac{R_1 + R_1/A}{[R_1 + (R_1 + R_2)/A]} \right|_{A \to \infty} = 1$$

These results show that a 1% change in the resistors R_1 and R_2 causes, respectively, a -1% or $+1\%$ change in G_0. Since accurate and stable resistors are available, this value of sensitivity is acceptable. To evaluate the sensitivity to the opamp gain A, we compute

$$S_A^T = \frac{A}{T} \frac{\partial}{\partial A} \left[\frac{-G_0}{1 + (1 + G_0)/A} \right] = \frac{-(1 + G_0)}{(A + 1 + G_0)}$$

Since usually $A \gg 1 + G_0$ in the frequency range of interest, the sensitivity is approximately

$$S_A^T \approx \frac{1}{A}(1 + G_0)$$

This is a very small number for large A. It demonstrates that the amplifier gain is approximately equal to $G_0 = -R_2/R_1$, independent of A, as long as the opamp gain A is large. However, if R_2 is removed ($R_2 = \infty$) so that there is no feedback, the sensitivity becomes

$$S_A^T = \left. \frac{R_1 + R_2}{(A + 1)R_1 + R_2} \right|_{R_2 \to \infty} \approx 1$$

and changes in A translate directly into changes of G_0. Whereas sensitivities of the order of unity are acceptable for passive components, they are normally far too large for opamp gains, because the active parameters in a circuit must be expected to vary widely. Recall from our discussion in Chapter 2 that the opamp's gain-bandwidth product ω_t can be expected to vary by 30% to over 100% in processing, in addition to being dependent on operating conditions, such as temperature and bias.

We will next derive some general formulas that follow from Eq. (12.8); they will be useful when computing sensitivities of the filter circuits in this book. We will again assume that Y is a function of a parameter x, or of several parameters $x_1, x_2, x_3, \ldots$. If Y is independent of

x, then $S_x^Y = 0$, obviously, because the derivative is zero. If Y is proportional to x, that is, $Y = kx$, where k is a constant independent of x, then $S_x^Y = 1$:

$$Y = kx \quad \Rightarrow \quad S_x^Y = 1 \tag{12.14a}$$

Often, we will encounter the form $Y = kx^a$ where a and k are constants. From Eq. (12.8) we find directly $S_{x_1}^Y = a$:

$$Y = kx^a \quad \Rightarrow \quad S_x^Y = a \tag{12.14b}$$

If Y is a product of two (or more) functions, $Y = Y_1 Y_2 Y_3 \cdots$, each of which depends on x, we have, with $\ln Y = \ln Y_1 + \ln Y_2 + \cdots$:

$$\frac{\partial \ln (Y_1 Y_2 Y_3 \cdots)}{\partial \ln x} = \frac{\partial \ln Y_1}{\partial \ln x} + \frac{\partial \ln Y_2}{\partial \ln x} + \frac{\partial \ln Y_3}{\partial \ln x} + \cdots$$

The result is:

$$Y = Y_1 Y_2 Y_3 \cdots \Rightarrow S_x^Y = S_x^{Y_1} + S_x^{Y_2} + \cdots \tag{12.14c}$$

i.e., the sensitivities of all functions Y_i add. In like manner, if Y is a quotient, $Y = Y_1/Y_2$, we find

$$Y = Y_1/Y_2 \Rightarrow S_x^Y = S_x^{Y_1} - S_x^{Y_2} \tag{12.14d}$$

from which it follows directly that

$$S_x^{1/Y} = \frac{\partial \ln(1/Y)}{\partial \ln x} = -\frac{\partial \ln Y}{\partial \ln x} = -S_x^Y \tag{12.14e}$$

A further very powerful relationship makes use of the chain rule of differentiation: if Y is a function of x, which in turn is a function of a variable t, we differentiate $\partial Y/\partial t = (\partial Y/\partial x) \times (\partial x/\partial t)$. The sensitivity is then computed as

$$Y = Y[x(t)] \quad \Rightarrow \quad S_t^Y = \frac{t}{Y}\frac{\partial Y}{\partial x}\frac{\partial x}{\partial t} \times \frac{x}{x} = \frac{x}{Y}\frac{\partial Y}{\partial x} \times \frac{t}{x}\frac{\partial x}{\partial t}$$

or

$$Y = Y[x(t)] \quad \Rightarrow \quad S_t^Y = S_x^Y S_t^x \tag{12.14f}$$

that is, we multiply the sensitivity of the function Y to the component x by the sensitivity of the component x to the variable t. This relationship is convenient to use, for example, when a filter parameter, say Q, is a function of a resistor R, which depends on temperature T. Then we compute $S_T^Q = S_R^Q S_T^R$. Or when we wish to determine how sensitive a transfer function $T(s)$ is to the gain-bandwidth product ω_t of an opamp A, we compute $S_{\omega_t}^{T(s)} = S_A^{T(s)} S_{\omega_t}^A$.

It is not sufficient, as a rule, to compute sensitivities to a single parameter, because the variations in all the circuit's components add to cause performance deviations. Thus, *single-parameter sensitivities* give only incomplete predictions of the variations to be expected. Conclusions based on single-parameter sensitivity results should be treated with caution. When

a function depends on several elements, $Y = Y(x_1, x_2, \ldots, x_n)$, as all our filters do, and we wish to find the likely total change when *all* the elements are expected to vary, we make use again of differential calculus to find the total derivative. Assuming n components, we have

$$dY = dY(x_1, x_2, \ldots, x_n) = \frac{\partial Y}{\partial x_1}dx_1 + \frac{\partial Y}{\partial x_2}dx_2 + \cdots + \frac{\partial Y}{\partial x_n}dx_n$$

This equation is recast in the form

$$\begin{aligned}\frac{dY}{Y} &= \frac{x_1}{Y}\frac{\partial Y}{\partial x_1}\frac{dx_1}{x_1} + \frac{x_2}{Y}\frac{\partial Y}{\partial x_2}\frac{dx_2}{x_2} + \cdots + \frac{x_n}{Y}\frac{\partial Y}{\partial x_n}\frac{dx_n}{x_n} \\ &= S_{x_1}^{Y}\frac{dx_1}{x_1} + S_{x_2}^{Y}\frac{dx_2}{x_2} + \cdots + S_{x_n}^{Y}\frac{dx_n}{x_n}\end{aligned} \tag{12.14g}$$

It says that the total percentage change of Y is the sum of all their respective sensitivities multiplied by the percentage changes of the components.

Equation (12.14g) gives a quick estimate of the expected circuit performance. More accurate *multiparameter sensitivity* results may be obtained from a *Monte Carlo* analysis. In a Monte Carlo analysis we vary most or all components of a circuit randomly over a specified tolerance range, such as 1%, with given statistical distributions, such as uniform or Gaussian, to simulate the manufacturing process. We then perform analyses of the circuit for its response for each set of element values. Clearly, computer analysis with appropriate circuit-simulation software is necessary for that purpose because normally several hundred analyses are required to yield valid statistical results. The plots in Fig. 12.1 were obtained in this manner.

EXAMPLE 12.2

Calculate the sensitivity expressions for pole-frequency and quality factor of the *RLC* lowpass filter in Fig. 12.7.

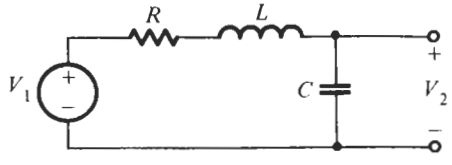

Figure 12.7 Passive *LC* lowpass filter.

Solution

The transfer function is

$$T(s) = \frac{V_2}{V_1} = \frac{1}{s^2LC + sCR + 1} = \frac{1}{LC}\frac{1}{s^2 + sR/L + 1/(LC)}$$

Clearly, we have

$$\omega_0 = \frac{1}{\sqrt{LC}} = L^{-1/2}C^{-1/2} \quad \text{and} \quad Q = \frac{1}{R}\sqrt{\frac{L}{C}} = R^{-1}L^{1/2}C^{-1/2} \tag{12.15}$$

We obtain immediately from Eq. (12.14b)

$$S_L^{\omega_0} = -\frac{1}{2}, \quad S_C^{\omega_0} = -\frac{1}{2}, \quad S_R^{\omega_0} = 0$$

and

$$S_L^{Q} = +\frac{1}{2}, \quad S_C^{Q} = -\frac{1}{2}, \quad S_R^{Q} = -1$$

This analysis shows that a +1% change in L or C causes a 0.5% change in ω_0 and Q, and changing R by 1% causes no change in ω_0 but a −1% change in Q. The sign in each case indicates whether the change is increasing or decreasing. These sensitivities are considered low. The circuit is an example of an LC ladder filter; we shall find out in Chapter 13 that LC ladders in general tend to have very low sensitivities.

The total changes are computed with Eq. (12.14g) as

$$\frac{d\omega_0}{\omega_0} = S_L^{\omega_0}\frac{dL}{L} + S_C^{\omega_0}\frac{dC}{C} + S_R^{\omega_0}\frac{dR}{R} = -\frac{1}{2}\left(\frac{dL}{L} + \frac{dC}{C}\right) \tag{12.16a}$$

$$\frac{dQ}{Q} = S_L^{Q}\frac{dL}{L} + S_C^{Q}\frac{dC}{C} + S_R^{Q}\frac{dR}{R} = \frac{1}{2}\left(\frac{dL}{L} - \frac{dC}{C}\right) - \frac{dR}{R} \tag{12.16b}$$

We still make an important observation. If the relative changes in L and C are in the same direction, they add to changes in ω_0, but subtract in their contribution to changes in Q. This conclusion is intuitively obvious from Eq. (12.15): if both L and C increase, their effects on ω_0 add because ω_0 depends on a *product* of the two elements; but the errors tend to cancel in Q, which depends on a *ratio* of the components. An increase in R, i.e., larger losses, results in a decrease in Q, but does not affect ω_0.

The explanation at the end of Example 12.2 may need a more formal justification: Consider two components in a circuit, and let us take resistors R_1 and R_2 to be specific. If these components suffer tolerances ΔR_1 and ΔR_2, the elements in the circuit are not the nominal values R_{10} and R_{20}, but rather

$$R_1 = R_{10} + \Delta R_1 = R_{10}\left(1 + \frac{\Delta R_1}{R_{10}}\right) \quad \text{and} \quad R_2 = R_{20} + \Delta R_2 = R_{20}\left(1 + \frac{\Delta R_2}{R_{20}}\right)$$

where $\Delta R_1/R_{10}$ and $\Delta R_2/R_{20}$ are the relative errors. If a circuit is now a function of the *product* of the two components, the dependence is on

$$R_1 \times R_2 = R_{10}R_{20}\left(1 + \frac{\Delta R_1}{R_{10}}\right)\left(1 + \frac{\Delta R_2}{R_{20}}\right) = R_{10}R_{20}\left(1 + \frac{\Delta R_1}{R_{10}} + \frac{\Delta R_2}{R_{20}} + \frac{\Delta R_1}{R_{10}}\frac{\Delta R_2}{R_{20}}\right)$$

or, after neglecting the product of the errors as small,

$$R_1 \times R_2 \approx R_{10}R_{20}\left(1 + \frac{\Delta R_1}{R_{10}} + \frac{\Delta R_2}{R_{20}}\right) \tag{12.17a}$$

We notice that for a dependence on a *product*, the errors *add*. This is the situation with L and C in ω_0 in Eq. (12.15) and is reflected in the plus sign in Eq. (12.16a) between

$\Delta L/L$ and $\Delta C/C$. If, however, the circuit is a function of a ratio of R_1 and R_2 we have the dependence on

$$\frac{R_1}{R_2} = \frac{R_{10}(1+\Delta R_1/R_{10})}{R_{20}(1+\Delta R_2/R_{20})} \approx \frac{R_{10}}{R_{20}}\left(1+\frac{\Delta R_1}{R_{10}}\right)\left(1-\frac{\Delta R_2}{R_{20}}\right)$$
$$= \frac{R_{10}}{R_{20}}\left(1+\frac{\Delta R_1}{R_{10}}-\frac{\Delta R_2}{R_{20}}-\frac{\Delta R_1}{R_{10}}\frac{\Delta R_2}{R_{20}}\right) \approx \frac{R_{10}}{R_{20}}\left(1+\frac{\Delta R_1}{R_{10}}-\frac{\Delta R_2}{R_{20}}\right) \qquad (12.17b)$$

In writing the previous equation we used that $1/(1+x) \approx 1-x$ for small x and again neglected the product of error terms. Evidently then, in the dependence on a *ratio* the errors *subtract*. We have this situation with L and C in the parameter Q in Eq. (12.15), which is reflected in the minus sign in Eq. (12.16b) between $\Delta L/L$ and $\Delta C/C$.

In the next example let us try to explain some of our observations in Fig. 12.1 and attempt to find design guidelines that lead to a more acceptable circuit. It also serves as an illustration for the use of the sensitivity equations (12.14a) through (12.14g).

EXAMPLE 12.3

Compute the total deviations of pole frequency and pole quality factor of the GIC circuit and the Q-enhanced Delyiannis–Friend circuit. Assume 1% component errors to verify the results in Fig. 12.1. Based on the results, make design choices appropriate for the specifications and the circuits.

Solution

The GIC circuit was given in Fig. 4.46a and the parameters of interest are from Eq. (4.169a) with unequal capacitors:

$$\omega_0 = \sqrt{\frac{R_4}{C_1C_2R_1R_3R_5}} \quad \text{and} \quad Q = R\sqrt{\frac{C_1}{C_2}}\sqrt{\frac{R_4}{R_1R_3R_5}} \qquad (12.18)$$

A comment is appropriate at this point: It is generally not permissible in sensitivity calculations to assume that different components are equal, such as in our case $C_1 = C_2$ or $R_1 = R_3 = R_4 = R_5$, even if in the GIC design we make that selection. As long as these components are different elements with their own tolerances, their individual contributions must be considered; choosing their *nominal* values equal in a design does not necessarily imply that their tolerances or changes are equal as well.

We find from Eq. (12.18) with Eq. (12.14b) that

$$S_k^{\omega_0} = +\frac{1}{2} \quad \text{or} \quad -\frac{1}{2}, \quad S_k^Q = +\frac{1}{2} \quad \text{or} \quad -\frac{1}{2}, \quad \text{and} \quad S_R^Q = 1$$

because of the square-root dependence; k stands for any of the components (except R) and the plus sign or minus sign, respectively, reflects whether k is in the numerator or denominator. We notice that a 1% error in any component contributes a positive or negative 0.5% error to ω_0 or Q as in Example 12.2. We could have expected this similar behavior because the GIC

circuit was obtained from the passive LC lowpass by simulating the behavior of the inductor; refer to Section 4.5.3. To compute the total error we obtain from Eq. (12.14g)

$$\begin{aligned}\frac{d\omega_0}{\omega_0} &= S_{R_1}^{\omega_0}\frac{dR_1}{R_1} + S_{R_3}^{\omega_0}\frac{dR_3}{R_3} + S_{R_4}^{\omega_0}\frac{dR_4}{R_4} + S_{R_5}^{\omega_0}\frac{dR_5}{R_5} + S_{C_1}^{\omega_0}\frac{dC_1}{C_1} + S_{C_2}^{\omega_0}\frac{dC_2}{C_2} \\ &= -\frac{1}{2}\left(\frac{dC_1}{C_1} + \frac{dC_2}{C_2} + \frac{dR_1}{R_1} + \frac{dR_3}{R_3} + \frac{dR_5}{R_5} - \frac{dR_4}{R_4}\right) \end{aligned} \tag{12.19a}$$

If all components vary by 1% and we assume that all errors add, i.e., *all* component deviations are positive except those of R_4, we find from this equation that

$$\frac{d\omega_0}{\omega_0} = -\frac{1}{2}(0.01 + 0.01 + 0.01 + 0.01 + 0.01 + 0.01) = -0.03$$

signifying that ω_0 is reduced by 3%, a -3% error. Similarly, if all component errors go in the opposite direction we find that $d\omega_0/\omega_0 = +3\%$. For this pessimistic *worst-case* assumption, $d\omega_0/\omega_0$ would vary by $\pm 3\%$ for a total of 6%. In reality, component changes will not all be in the same direction; some will increase and others decrease, so that random cancellations in Eq. (12.19a) can be expected. For example, if we assume that both R_4 and R_5 increase so that their effects cancel [see Eq. (12.17b)], the $d\omega_0/\omega_0$ error would be $\pm 2\%$ for a total of 4%. These results explain our findings in Fig. 12.1d: we observed ω_0 tolerances of 4.6%, with most of the variations being smaller.

Consider next Q tolerances. Similar to the computations just completed, we find

$$\begin{aligned}\frac{dQ}{Q} &= S_R^Q\frac{dR}{R} + S_{C_1}^Q\frac{dC_1}{C_1} + S_{C_2}^Q\frac{dC_2}{C_2} + S_{R_4}^Q\frac{dR_4}{R_4} + S_{R_1}^Q\frac{dR_1}{R_1} + S_{R_3}^Q\frac{dR_3}{R_3} + S_{R_5}^Q\frac{dR_5}{R_5} \\ &= \frac{dR}{R} + \frac{1}{2}\left(\frac{dC_1}{C_1} - \frac{dC_2}{C_2}\right) + \frac{1}{2}\left(\frac{dR_4}{R_4} - \frac{dR_1}{R_1} - \frac{dR_3}{R_3} - \frac{dR_5}{R_5}\right) \end{aligned} \tag{12.19b}$$

From this equation we can again estimate the worst-case error by assuming that all component errors have signs such that their contribution add in the same direction, e.g., $dC_1/C_1 > 0$ and $dC_2/C_2 < 0$. Instead, let us be more realistic and assume that cancellations will occur. Referring to the discussion leading to Eqs. (12.17a) and (12.17b), we note that typically, the capacitor errors will tend to cancel, at least partially, if we can assume that the components come from the same processing batch: they will all be positive ($dC_1/C_1 > 0$ and $dC_2/C_2 > 0$) or all negative ($dC_1/C_1 < 0$ and $dC_2/C_2 < 0$) by the same percentage so that their *ratio* stays unaffected. As a consequence, the first term in parentheses in Eq. (12.19b) will be zero or at least very small. The same argument can be made for the resistors; thus R_4 errors will compensate one of the others in the last parentheses in Eq. (12.19b). The remaining two errors will add to a maximum value of -1%, which helps to compensate the $+1\%$ error in R. As a result, if we can make these not unrealistic assumptions about ratios of like components, the relative error in Q will be very small. Indeed, this was our observation for the 20 sample tests in Fig. 12.1d.

We next ask ourselves how we can use these sensitivity results to arrive at better design guidelines for the GIC circuit, to meet the ($f_0 = 10$ kHz, $Q = 30$) requirement. We saw that with reasonably realistic assumptions the circuit realizes the specified values of Q and midband gain. However, if the bandwidth is 333 Hz, i.e., 3.33% of 10 kHz for $Q = 30$, then we cannot tolerate that the center frequency f_0 varies by 3 to 6% as our estimate in Eq. (12.19a)

indicated and as was confirmed by the results in Fig. 12.1d. The reason is that the passband shifts outside the specified range (see Fig. 12.2b). Let us demand that f_0 shifts by no more than 10% of the specified bandwidth, that is, by ≈ 33 Hz. This means we must require that $\Delta f_0/f_0 \leq 0.0033 = 0.33\%$, so that from Eq. (12.19a) the design requirement is

$$\frac{\Delta f_0}{f_0} \leq \frac{1}{2}\left(6 \times \frac{\Delta k}{k}\right) = 3\frac{\Delta k}{k}$$

if all elements, labeled k, have the same tolerances. The constraint $\Delta f_0/f_0 \leq 0.0033$ means that $\Delta k/k \leq 0.001$ is required, i.e., more expensive 0.1% components are necessary for the design. This choice assumes that all component errors have adding effects and is, of course, again a pessimistic worst-case design. In reality, random cancellations will occur so that we will likely be able to work with larger component tolerances. But if all circuits must meet the specifications, we have to use 0.1% components. Figure 12.8 shows the results of 20 random samples with 0.1% element tolerances. We observe that our predictions were correct. Nearly all sampled circuits meet the design specifications.

Let us next deal with the Delyiannis–Friend circuit in Fig. 4.37; the relevant equations are found in Section 4.5.2, Eqs. (4.130) and (4.140), repeated here for convenience:

$$\omega_0 = \sqrt{\frac{1}{C_1 C_2 R_1 R_2}}, \quad Q = \frac{Q_0}{1 - 2\alpha Q_0^2} \tag{12.20}$$

with

$$Q_0 = \frac{1}{2}\sqrt{\frac{C_1}{C_2}}\sqrt{\frac{R_2}{R_1}} \quad \text{and} \quad \alpha = \frac{K}{1-K}$$

K is the resistor ratio identified in Fig. 4.37. For the ω_0 sensitivities we find as before with Eqs. (12.14b) and (12.14g),

$$\frac{d\omega_0}{\omega_0} = S_{C_1}^{\omega_0}\frac{dC_1}{C_1} + S_{C_2}^{\omega_0}\frac{dC_2}{C_2} + S_{R_4}^{\omega_0}\frac{dR_1}{R_1} + S_{R_1}^{\omega_0}\frac{dR_2}{R_2} = -\frac{1}{2}\left(\frac{dC_1}{C_1} + \frac{dC_2}{C_2} + \frac{dR_1}{R_1} + \frac{dR_2}{R_2}\right) \tag{12.21}$$

resulting in $d\omega_0/\omega_0$ deviations of the same order as for the GIC module. The 20 sample tests of Fig. 12.1c verify this finding.

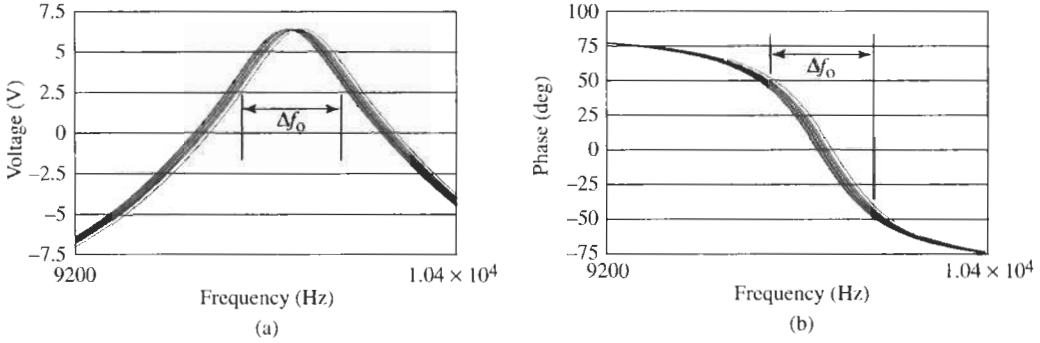

Figure 12.8 Test results for the GIC circuit of Fig. 12.1 built with 0.1% components. The marked bandwidth Δf_0 is in 9.73 kHz $\leq f \leq$ 10.05 kHz; the measured f_0 is at 9.89 kHz.

To compute the Q sensitivities is more involved but will be made relatively simple by careful use of the sensitivity equations (12.14). Let us start by observing from Eq. (12.20) that Q is a function of Q_0 and α : $Q = Q(Q_0, \alpha)$. Similarly $Q_0 = Q_0(C_1, C_2, R_1, R_2)$ and $\alpha = \alpha(K)$.[2] Then we obtain with Eqs. (12.14f) and (12.14g)

$$\begin{aligned}\frac{dQ}{Q} &= S_{Q_0}^{Q} S_{C_1}^{Q_0} \frac{dC_1}{C_1} + S_{Q_0}^{Q} S_{C_2}^{Q_0} \frac{dC_2}{C_2} + S_{Q_0}^{Q} S_{R_1}^{Q_0} \frac{dR_1}{R_1} + S_{Q_0}^{Q} S_{R_2}^{Q_0} \frac{dR_2}{R_2} + S_{\alpha}^{Q} S_{K}^{\alpha} \frac{dK}{K} \\ &= S_{Q_0}^{Q} \left(S_{C_1}^{Q_0} \frac{dC_1}{C_1} + S_{C_2}^{Q_0} \frac{dC_2}{C_2} + S_{R_1}^{Q_0} \frac{dR_1}{R_1} + S_{R_2}^{Q_0} \frac{dR_2}{R_2} \right) + S_{\alpha}^{Q} S_{K}^{\alpha} \frac{dK}{K} \end{aligned} \tag{12.22}$$

and we note that $S_{C_1}^{Q_0} = S_{R_2}^{Q_0} = 0.5$ and $S_{C_2}^{Q_0} = S_{R_1}^{Q_0} = -0.5$. Also we calculate

$$\begin{aligned} S_{Q_0}^{Q} &= \frac{Q_0}{Q} \frac{\partial}{\partial Q_0} \left(\frac{Q_0}{1 - 2\alpha Q_0^2} \right) = \frac{Q_0}{Q} \frac{1 - 2\alpha Q_0^2 + 4\alpha Q_0^2}{(1 - 2\alpha Q_0^2)^2} = \frac{1 + 2\alpha Q_0^2}{1 - 2\alpha Q_0^2} \\ &= \frac{Q}{Q_0} \left[2 - (1 - 2\alpha Q_0^2) \right] = 2\frac{Q}{Q_0} - 1 \\ S_{\alpha}^{Q} &= \frac{\alpha}{Q} \frac{\partial}{\partial \alpha} \left(\frac{Q_0}{1 - 2\alpha Q_0^2} \right) = -\frac{2\alpha Q_0^2}{1 - 2\alpha Q_0^2} = -2\alpha Q_0 Q \\ S_{K}^{\alpha} &= \frac{K}{\alpha} \frac{\partial}{\partial K} \left(\frac{K}{1 - K} \right) = \frac{K}{\alpha} \frac{1}{(1 - K)^2} = \frac{1}{1 - K} = \frac{\alpha}{K} \end{aligned}$$

Inserting these expressions into Eq. (12.22) gives us the desired equation:

$$\frac{dQ}{Q} = \left(\frac{Q}{Q_0} - \frac{1}{2} \right) \left[\left(\frac{dC_1}{C_1} - \frac{dC_2}{C_2} \right) + \left(\frac{dR_2}{R_2} - \frac{dR_1}{R_1} \right) \right] - 2\alpha Q_0 Q \frac{1}{1 - K} \frac{dK}{K} \tag{12.23}$$

After our discussion in connection with Eq. (12.17b), we observe that the form of the brackets in this expression indicates that Q depends on the ratios C_1/C_2 and R_2/R_1. Note from Eq. (12.23) that dQ/Q is nearly proportional to Q so that the errors may be expected to be larger. For our design we have, nominally, $Q_0 = 1.5$, $Q = 30$; thus, from Eqs. (4.143) and (4.144),

$$\alpha = \frac{1 - Q_0/Q}{2Q_0^2} = 0.211, \qquad K = \frac{\alpha}{1 + \alpha} = 0.174$$

The Q deviations are then

$$\frac{dQ}{Q} = 19.5 \left(\frac{dC_1}{C_1} - \frac{dC_2}{C_2} - \frac{dR_1}{R_1} + \frac{dR_2}{R_2} \right) - 23.00 \frac{dK}{K} \tag{12.24}$$

For component tolerances of 1%, the first term may be as large as 0.78 and the second one 0.23. In the worst case, if these two terms add we find $dQ/Q \approx 1$, i.e., we have a total of 100%

[2] We have combined the two resistors that determine K into the one parameter K because only the tap position matters. If this voltage divider is built from two separate resistors, both must be accounted for separately.

error in both directions. If we may assume that the component *ratios* C_1/C_2 and R_2/R_1 stay approximately constant with varying elements, the term in parentheses will be zero or at least small [see Eq. (12.17b)], but the second term results in 23 times the error in K. This explains the observed large Q deviations in Fig. 12.1c, and confirms the discussion in Chapter 4 of the sensitive adjustments needed for Q in the single-amplifier biquad.

We also observed in Fig. 12.1c two responses, which based on the measured phase appeared to be oscillations. Oscillations are always a threat in active filters with high values of Q because the poles are close to the imaginary axis and component tolerances may push the pole locations into the right half-plane. In the present case, notice from Eq. (12.20) that Q will become negative, causing instability, if $2\alpha Q_0^2 > 1$. For our suggested design choice of $Q_0 = 1.5$ [see Eq. (4.142)], $Q = 30$ results in $2\alpha Q_0^2 = 2 \times 0.2111 \times 2.25 = 0.95$. Notice that a 3% increase in that value raises Q to 70 and an increase of 4% results in $Q = 125$. An additional increase by 1% yields $Q = 819$ and, of course, a total increase of approximately 5.25% gives $Q = \infty$ and causes instability. Among the 20 samples considered in Fig. 12.1, apparently there were two to violate the stability constraint. The numbers indicate that Q is very sensitive to component tolerances as Q becomes large. The situation we have here is depicted in Fig. 12.4 where the slope of the curve becomes rapidly steeper as Y, here Q, increases.

These simple sensitivity calculations give us considerable insight into circuit behavior. They show that *for large* values of Q the GIC circuit is preferable over the Q-enhanced Delyiannis–Friend biquad because it avoids the hard to control variations of Q. In both circuits we expect approximately the same ω_0 tolerances, but the larger Q sensitivities of the Delyiannis–Friend circuit make it difficult to manufacture without careful adjustments or expensive small-tolerance components. We may argue that the Delyiannis–Friend circuit without Q enhancement in Fig. 4.35 could be taken instead because it has low Q sensitivities: by Eq. (4.130) we find $S_{R_2}^{Q_0} = -S_{R_1}^{Q_0} = 0.5$. However, this is coupled with resistor ratios of Q_0^2, which may pose a manufacturing problem if Q_0 is large.

12.2 SECOND-ORDER SECTIONS

We spent a large part of our work so far in this book on the derivation and design of second-order sections. We have seen that second-order modules are used in their own right to build simple filters; in addition, they are connected in cascade for the design of high-order transfer functions to permit the realization of more complex requirements. Let us next study the sensitivity of biquads to gain further insight into their performance and learn what some of the critical issues are that we need to pay attention to when selecting and designing reliable practical circuits.

A second-order transfer function is written as

$$T_2(s) = \frac{N(s)}{D(s)} = \frac{N(s)}{s^2 + s\omega_0/Q + \omega_0^2} \tag{12.25}$$

For all cases of importance we may assume that $Q > 0.5$, so that the poles are complex; if the denominator is factored to show the two poles, p_1 and its conjugate $p_2 = p_1^*$,

$$s^2 + s\omega_0/Q + \omega_0^2 = (s - p_1)(s - p_2) = (s - p_1)(s - p_1^*)$$

we find

$$p_1 = -\omega_0\left(\frac{1}{2Q} - j\sqrt{1-\frac{1}{4Q^2}}\right), \quad p_2 = -\omega_0\left(\frac{1}{2Q} + j\sqrt{1-\frac{1}{4Q^2}}\right) \tag{12.26}$$

If ω_0 and Q depend on the variable component x we can compute the variation in p_1 from the derivative. Using the product rule we find from Eq. (12.26)

$$\frac{\partial p_1}{\partial x} = -\frac{\partial \omega_0}{\partial x}\left(\frac{1}{2Q} - j\sqrt{1-\frac{1}{4Q^2}}\right) - \omega_0\frac{\partial}{\partial x}\left(\frac{1}{2Q} - j\sqrt{1-\frac{1}{4Q^2}}\right)$$

or

$$x\frac{\partial p_1}{\partial x} = -\frac{x}{\omega_0}\frac{\partial \omega_0}{\partial x}\omega_0\left(\frac{1}{2Q} - j\sqrt{1-\frac{1}{4Q^2}}\right) - \omega_0\left(\frac{-1}{2Q^2} - j\frac{\frac{1}{2Q^3}}{2\sqrt{1-\frac{1}{4Q^2}}}\right)x\frac{\partial Q}{\partial x} \tag{12.27}$$

Using Eq. (12.26), we can bring this expression into the form

$$\frac{x}{\partial x}\frac{\partial p_1}{p_1} = S_x^{p_1} = S_x^{\omega_0} - j\frac{S_x^Q}{\sqrt{4Q^2-1}} \tag{12.28a}$$

and similarly

$$S_x^{p_2} = \left(S_x^{p_1}\right)^* = S_x^{\omega_0} + j\frac{S_x^Q}{\sqrt{4Q^2-1}} \tag{12.28b}$$

As we might have expected, these equations show that the sensitivity of the pole depends on the sensitivities of both ω_0 and Q. But the important observation is that the position of p_1 is $\sqrt{4Q^2-1} \approx 2Q$ times more sensitive to variations in ω_0 than to variations in Q. We saw in our earlier study that the pole locations determine the shape of the passband, such as maximally flat or equal-ripple. Accurate pole positions are important, and the designer is well advised to pay special attention to low ω_0 sensitivities when selecting a biquad.

All circuits suggested in this book have the lowest possible magnitude of the sensitivity of ω_0 to component values, namely $|1/2|$. It is not difficult to show that $\left|S_x^{\omega_0}\right| = 1/2$ is the minimum we can expect to reach: note that ω_0 has units of 1/time; in second-order circuits with two capacitors, ω_0 must be formed, therefore, as the inverse of the square root of two RC time constants,

$$\omega_0 = \frac{k}{\sqrt{R_1C_1R_2C_2}} \tag{12.29}$$

so that $S_x^{\omega_0} = -1/2$ for all components x. k is a dimensionless quantity; typically $k = 1$ as, for instance, in the Delyiannis–Friend circuit, Eq. (4.130); alternatively, k may be given, e.g., by a ratio of two resistors as in the GIC biquad, Eq. (4.169a).[3] As a rule it is not advisable to

[3] It does not violate our argument that these equations depend on $1/\sqrt{C^2} = 1/C$; this form arises from our labeling two separate components by the same name: $C_1 = C_2 = C$.

select a module where ω_0 depends on opamp parameters because these are poorly controlled and will result in large ω_0 deviations.

Let us return to Eq. (12.25) and look at sensitivity effects in a different way. Specifically, we want to establish the frequency dependence of transfer function deviations. We know that a transfer function can be expressed in terms of magnitude and phase, $T(j\omega) = |T(j\omega)|\, e^{j\theta(\omega)}$. Using this notation we find with Eq. (12.8)

$$S_x^{T(j\omega)} = \frac{\partial \ln T(j\omega)}{\partial \ln x} = \frac{\partial \ln |T(j\omega)|}{\partial \ln x} + jx\frac{\partial \theta(\omega)}{\partial x} = S_x^{|T(j\omega)|} + j\theta(\omega) S_x^{\theta(\omega)} \tag{12.30}$$

The varying component is again labeled x. Equation (12.30) provides us an easy way of separating magnitude and phase sensitivities: the real part of the sensitivity of $T(j\omega)$ gives important information on the sensitivity of the magnitude,

$$S_x^{|T(j\omega,x)|} = \mathrm{Re}\left[S_x^{T(j\omega,x)}\right] \tag{12.31a}$$

and the imaginary part tells us about the changes in phase:

$$x\frac{\partial \theta(\omega, x)}{\partial x} = \mathrm{Im}\left[S_x^{T(j\omega,x)}\right] \tag{12.31b}$$

Let us turn our attention next to the effect of poles and zeros on the sensitivity of second-order modules. Generally, we obtain from $T(s) = N(s)/D(s)$ with Eq. (12.8)

$$S_x^{T(s)} = \frac{\partial \ln[N(s)/D(s)]}{\partial \ln x} = \frac{\partial \ln N(s)}{\partial \ln x} - \frac{\partial \ln D(s)}{\partial \ln x} = \frac{x}{\partial x}\frac{\partial N(s)}{N(s)} - \frac{x}{\partial x}\frac{\partial D(s)}{D(s)} \tag{12.32}$$

This equation shows that near a pole or a zero where $D(s)$ or $N(s)$ become small, the sensitivities are large. We saw in our previous work that poles tend to cluster near the passband corners of a filter. The equation alerts us to the fact that filter deviations are largest close to the edges of the passband. Indeed, this is observed in practice.

Poles are in the vicinity of the passband and are dominant in their effects on the passband, whereas zeros are in the stopband and generally have much less influence on the passband behavior. Let us concentrate in the following on second-order sections where $D(s)$ is of the form $D(s) = s^2 + s\omega_0/Q + \omega_0^2$, and assume $N(s) = s$ so that $\partial N/\partial x = 0$. For this second-order bandpass function $T_2(s)$ we obtain from Eq. (12.32)

$$\begin{aligned} S_x^{T_2(s)} &= 0 - x\frac{\left(\dfrac{s}{Q} + 2\omega_0\right)\dfrac{\partial \omega_0}{\partial x} - \dfrac{s\omega_0}{Q^2}\dfrac{\partial Q}{\partial x}}{s^2 + s\omega_0/Q + \omega_0^2} \\ &= -\frac{\left(\dfrac{s\omega_0}{Q} + 2\omega_0^2\right)\dfrac{x}{\omega_0}\dfrac{\partial \omega_0}{\partial x} - \dfrac{s\omega_0}{Q}\dfrac{x}{Q}\dfrac{\partial Q}{\partial x}}{s^2 + s\omega_0/Q + \omega_0^2} \\ &= -\frac{\left(\dfrac{s\omega_0}{Q} + 2\omega_0^2\right) S_x^{\omega_0} - \dfrac{s\omega_0}{Q} S_x^Q}{s^2 + s\omega_0/Q + \omega_0^2} = -\frac{\left(\dfrac{s_n}{Q} + 2\right) S_x^{\omega_0} - \dfrac{s_n}{Q} S_x^Q}{s_n^2 + s_n/Q + 1} \end{aligned} \tag{12.33}$$

In the last part of this equation we have divided numerator and denominator by ω_0^2 to be able to deal with the normalized frequency $s_n = s/\omega_0$ and to arrive at a simpler expression. In practice, when designing filters we are concerned mostly with magnitude specifications. A more meaningful expression for our needs can, therefore, be gained from Eq. (12.33) by extracting the magnitude sensitivity. To be able to use Eq. (12.31), we evaluate Eq. (12.33) on the $j\omega$-axis, multiply numerator and denominator by the conjugate of the denominator, $(1 - \omega_n^2 - j\omega_n/Q)$, and get the result:

$$S_x^{T_2(j\omega)} = -\frac{\left(\frac{j\omega_n}{Q} + 2\right)\left(1 - \omega_n^2 - j\omega_n/Q\right) S_x^{\omega_0} - \frac{j\omega_n}{Q}\left(1 - \omega_n^2 - j\omega_n/Q\right) S_x^Q}{\left(1 - \omega_n^2\right)^2 + (\omega_n/Q)^2}$$

This equation we split into real and imaginary parts:

$$\begin{aligned} S_x^{T_2(j\omega)} = & -\frac{\left[(\omega_n/Q)^2 + 2\left(1 - \omega_n^2\right)\right] S_x^{\omega_0} - (\omega_n/Q)^2 S_x^Q}{\left(1 - \omega_n^2\right)^2 + (\omega_n/Q)^2} \\ & + j\frac{\omega_n}{Q}\frac{\left(1 + \omega_n^2\right) S_x^{\omega_0} + \left(1 - \omega_n^2\right) S_x^Q}{\left(1 - \omega_n^2\right)^2 + (\omega_n/Q)^2} \end{aligned} \tag{12.34}$$

According to Eq. (12.31a) the real part is the magnitude sensitivity,

$$S_x^{|T_2(j\omega)|} = -\frac{2\left(1 - \omega_n^2\right) + (\omega_n/Q)^2}{\left(1 - \omega_n^2\right)^2 + (\omega_n/Q)^2} S_x^{\omega_0} + \frac{(\omega_n/Q)^2}{\left(1 - \omega_n^2\right)^2 + (\omega_{n'}/Q)^2} S_x^Q \tag{12.35a}$$

which we write in the form

$$S_x^{|T_2(j\omega)|} = S_{\omega_0}^{|T_2(j\omega)|} S_x^{\omega_0} + S_Q^{|T_2(j\omega)|} S_x^Q \tag{12.36}$$

At the same time, the imaginary part of Eq. (12.34) provides us with the phase deviations to be expected:

$$x\frac{\partial\theta(\omega)}{\partial x} = \frac{\left(1 + \omega_n^2\right)(\omega_n/Q)}{\left(1 - \omega_n^2\right)^2 + (\omega_n/Q)^2} S_x^{\omega_0} + \frac{\left(1 - \omega_n^2\right)(\omega_n/Q)}{\left(1 - \omega_n^2\right)^2 + (\omega_n/Q)^2} S_x^Q \tag{12.35b}$$

In comparing Eqs. (12.35a) and (12.36) we have identified the sensitivities of the magnitude of the second-order function $T_2(j\omega)$ with respect to ω_0 and to Q:

$$S_{\omega_0}^{|T_2(j\omega)|} = -\frac{2\left(1 - \omega_n^2\right) + (\omega_n/Q)^2}{\left(1 - \omega_n^2\right)^2 + (\omega_n/Q)^2} \tag{12.37a}$$

$$S_Q^{|T_2(j\omega)|} = \frac{(\omega_n/Q)^2}{\left(1 - \omega_n^2\right)^2 + (\omega_n/Q)^2} \tag{12.37b}$$

To get a better understanding of these functions, they are plotted in Fig. 12.9. First, we notice that

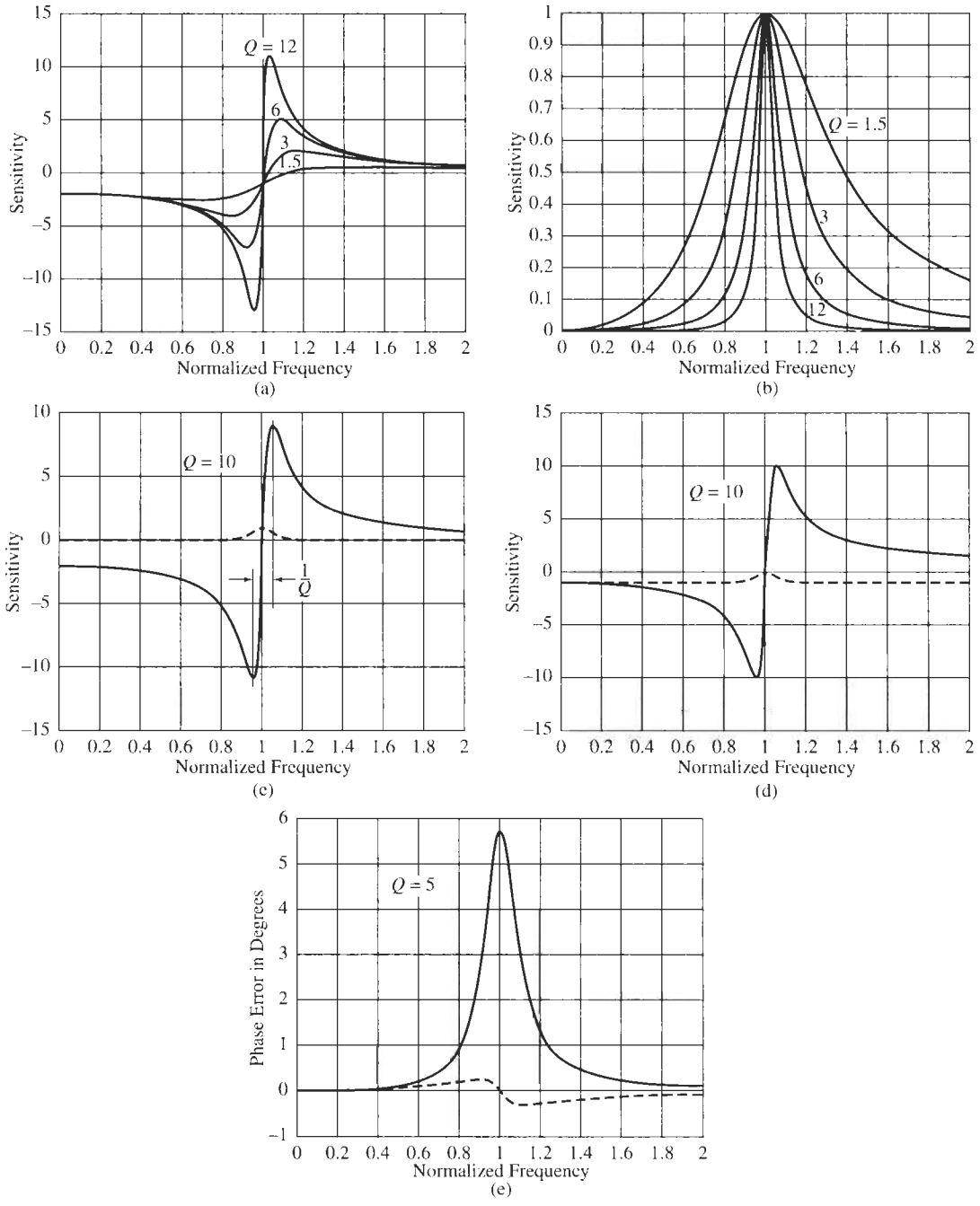

Figure 12.9 Sensitivity of the transfer function magnitude and phase functions of normalized frequency ω_n, plotted for different values of Q: (a) $S_{\omega_0}^{|T_2(j\omega)|}$; (b) $S_Q^{|T_2(j\omega)|}$. Note the different scales. (c) Both sensitivities plotted on the same scale for $Q = 10$: solid line: $S_{\omega_0}^{|T_2(j\omega)|}$; dashed line: $S_Q^{|T_2(j\omega)|}$; (d) added effects of a bandpass numerator per Eqs. (12.41) and (12.42); (e) phase deviations for $Q = 5$; the scale is $(180°/\pi)/100 \times d\theta$ in degrees per percent error of ω_0 and Q. Solid line for ω_0 errors; dashed line for Q errors.

$$\max S_Q^{|T_2(j\omega)|} = 1 \quad \text{at} \quad \omega_n = 1 \tag{12.38}$$

for all values of Q. The change in sensitivity versus Q is more rapid as Q increases. As a matter of fact, the shape of $S_Q^{|T_2(j\omega)|}$ looks like the response curve of a bandpass with midband gain equal to unity as Fig. 12.9b shows. The shape of $S_{\omega_0}^{|T_2(j\omega)|}$ is more complicated. We can compute from Eq. (12.37a) that, for large values of Q,

$$\max S_{\omega_0}^{|T_2(j\omega)|} \approx Q - 1 \quad \text{at} \quad \omega_{n2} \approx 1 + \frac{1}{2Q} \tag{12.39a}$$

$$\min S_{\omega_0}^{|T_2(j\omega)|} \approx -Q - 1 \quad \text{at} \quad \omega_{n1} \approx 1 - \frac{1}{2Q} \tag{12.39b}$$

Figure 12.9a shows the behavior for several values of Q. We notice that $S_{\omega_0}^{|T_2(j\omega)|}$ has a span from its maximum to its minimum of approximately $2Q$, which is $2Q$ times wider than that of $S_Q^{|T_2(j\omega)|}$, Fig. 12.9b. Since $S_{\omega_0}^{|T_2(j\omega)|}$ multiplies $S_x^{\omega_0}$, this result confirms the one reached from Eq. (12.28): the importance of low values of $S_x^{\omega_0}$. To emphasize this important point further, we show in Fig. 12.9c curves for $S_{\omega_0}^{|T_2(j\omega)|}$ and $S_Q^{|T_2(j\omega)|}$ for $Q = 10$, plotted on the same scale. Observe that the peak values of $S_{\omega_0}^{|T_2(j\omega)|}$ occur at the corners ω_{n1} and ω_{n2} of the bandpass passband where $\omega_{n2} - \omega_{n1} \approx 1/Q$ by Eq. (12.39). Corresponding plots can be constructed for deviations in phase. For the plot of phase deviations in Fig. 12.9e for $Q = 5$ we have multiplied Eq. (12.35b) by $(180°/\pi)/100$ to convert radians to degrees and scale the ordinate by 1%. Then it yields the phase deviation when multiplied by the error in ω_0 or Q in percent. For example, an ω_0 error of 2% results in the corresponding peak phase deviation (at $\omega = 1$) of $2 \times 5.7° = 11.4°$. Observe that the difference in size of phase errors contributed by ω_0 and Q deviations further emphasizes the importance of low ω_0 errors.

Our discussion has assumed that the numerator $N(s)$ of Eq. (12.25) is independent of the component x so that no terms are contributed by $\partial N/\partial x$ in Eq. (12.32). In general, of course, the numerator may be a complete second-order polynomial as is the case for the modules discussed in Chapter 5. If any of the numerator coefficients depend on the component x in question, our analysis proceeds just as before, but the corresponding sensitivity terms must be added to those we derived in Eq. (12.34). The most frequent situations are

$$N(s) = K\omega_0^2 \quad \text{or} \quad N(s) = Ks\omega_0/Q$$

i.e., we deal with a lowpass or a bandpass filter where the numerator terms are set by the same elements as the corresponding denominator coefficients. Examples are the Sallen–Key lowpass, Eq. (4.100), the Delyiannis–Friend bandpass, Eq. (4.128), and the GIC bandpass, Eq. (4.168a). Let us assume for simplicity that the gain constant K does not depend on x. Then we obtain as additional terms in Eq. (12.34) for a lowpass function

$$\frac{x}{N(s)}\frac{\partial N(s)}{\partial x} = \frac{x}{K\omega_0^2}\frac{\partial\left(K\omega_0^2\right)}{\partial x} = \frac{x}{\omega_0^2}2\omega_0\frac{\partial\omega_0}{\partial x} = 2S_x^{\omega_0} \tag{12.40}$$

and for the bandpass case

$$\frac{x}{N(s)}\frac{\partial N(s)}{\partial x} = \frac{x}{Ks\omega_0/Q}\frac{\partial\left(Ks\omega_0/Q\right)}{\partial x} = \frac{x}{\omega_0/Q}\left(\frac{1}{Q}\frac{\partial\omega_0}{\partial x} - \frac{\omega_0}{Q^2}\frac{\partial Q}{\partial x}\right) = S_x^{\omega_0} - S_x^Q \tag{12.41}$$

Since all the terms are real, they add only to Eq. (12.35a) and have no effect on the phase deviations. For instance, for the bandpass case we obtain with Eqs. (12.35a) and (12.41) the total sensitivity:

$$S_x^{|T_2(j\omega)|} = \left[1 - \frac{2\left(1-\omega_n^2\right)+(\omega_n/Q)^2}{\left(1-\omega_n^2\right)^2+(\omega_n/Q)^2}\right] S_x^{\omega_0} + \left[\frac{(\omega_n/Q)^2}{\left(1-\omega_n^2\right)^2+(\omega_n/Q)^2} - 1\right] S_x^Q \tag{12.42}$$

The effect of the contribution is not large; it raises the $S_{\omega_0}^{|T_2(j\omega)|}$ curve by 1 so that the positive and negative excursions are symmetrical, and lowers the $S_Q^{|T_2(j\omega)|}$ curve by 1 so that $S_Q^{|T_2(j\omega)|} = 0$ at $\omega_n = 1$ and approaches -1 for small and large frequencies. Figure 12.9d shows the result corresponding to Fig. 12.9c when the numerator effects are added to those of the poles in Fig. 12.9c.

Our discussion demonstrates clearly that small variations of pole frequency are far more important than small changes in quality factor. Also observe that the errors increase with Q. It follows that low-Q filters are easier to design with less accurate components than high-Q filters. Figure 12.9 shows that sensitivities are strong functions of frequency and that the passband *edges* are very critical, whereas much smaller deviations can be expected away from the passband corners.

12.3 HIGH-ORDER FILTERS

We have seen in Section 12.2 how sensitivity analysis of a general second-order module gave us much insight into biquad performance and provided directions for the selection of superior second-order modules. In this section we will consider sensitivity analysis of high-order filter functions in a similar fashion to develop guidelines for their design. We start from the nth-order transfer function of Eq. (1.12)

$$T(s) = \frac{N(s)}{D(s)} = \frac{b_m s^m + b_{m-1}s^{m-1} + \ldots + b_1 s + b_0}{a_n s^n + a_{n-1}s^{n-1} + \ldots + a_1 s + a_0} \tag{12.43}$$

and factor numerator and denominator polynomials into their roots, the zeros z_i and poles p_j,

$$T(s) = \frac{N(s)}{D(s)} = K\frac{(s-z_1)(s-z_2)(s-z_3)\cdots(s-z_m)}{(s-p_1)(s-p_2)(s-p_3)\cdots(s-p_n)} \tag{12.44}$$

where $K = b_m/a_n$. To calculate the sensitivities to an element x we use Eq. (12.32) and obtain

$$\begin{aligned} S_x^{T(s)} &= \frac{\partial \ln N(s)}{\partial \ln x} - \frac{\partial \ln D(s)}{\partial \ln x} \\ &= S_x^K + x\frac{\partial}{\partial x}\{[\ln(s-z_1)+\cdots+\ln(s-z_m)] - [\ln(s-p_1)+\cdots+\ln(s-p_n)]\} \\ &= S_x^K - \left[\frac{x\dfrac{\partial z_1}{\partial x}}{s-z_1} + \cdots + \frac{x\dfrac{\partial z_m}{\partial x}}{s-z_m}\right] + \left[\frac{x\dfrac{\partial p_1}{\partial x}}{s-p_1} + \cdots + \frac{x\dfrac{\partial p_n}{\partial x}}{s-p_n}\right] \end{aligned}$$

Using the definition of sensitivity in Eq (12.6) we can finally bring this expression into the form

$$S_x^{T(s)} = S_x^K - \left[\frac{z_1 S_x^{z_1}}{s - z_1} + \cdots + \frac{z_m S_x^{z_m}}{s - z_m}\right] + \left[\frac{p_1 S_x^{p_1}}{s - p_1} + \cdots + \frac{p_n S_x^{p_n}}{s - p_n}\right] \tag{12.45}$$

In deriving Eq. (12.45) we assumed that all zeros and poles are functions of the component x of concern; if this is not the case, i.e., if any z_i or p_j is independent of x, we simply set the corresponding sensitivity term to zero. As a rule, though, in a high-order circuit all poles and zeros will be functions of most or all components unless we take special measures to avoid it.

The first term in Eq. (12.45) is the sensitivity of the gain constant K; it is normally not important for filter performance. More critical are the remaining terms in the brackets. We observe that the sensitivity becomes large near all the zeros and all the poles. When $s = j\omega$ and we move along the $j\omega$-axis, we must expect that $S_x^{T(j\omega)}$ becomes large each time we move past a zero or pole because the denominator terms $s - z_I$ and $s - p_j$ become small. This is especially serious for the poles that are in the vicinity of the passband of the filter. We learned in our previous study that the transfer function zeros are normally in the stopband; consequently we need to be less concerned with the zeros. Throughout the passband, then, we are most interested in the poles that have the dominant effect on sensitivity in the filter's passband. Neglecting all remaining terms, we have

$$S_x^{T(s)} \approx \frac{p_1 S_x^{p_1}}{s - p_1} + \cdots + \frac{p_n S_x^{p_n}}{s - p_n} \tag{12.46}$$

or on the $j\omega$-axis:

$$S_x^{T(j\omega)} \approx \frac{p_1 S_x^{p_1}}{j\omega - p_1} + \cdots + \frac{p_n S_x^{p_n}}{j\omega - p_n} \tag{12.47}$$

The numerator terms in Eq. (12.47) are determined by the pole sensitivities in Eq. (12.28); they are in general not zero. The denominator terms, $j\omega - p_j$, $j = 1, \ldots, n$, are the distances of the poles from the $j\omega$-axis as the frequency moves through the passband, in case of a lowpass filter, from $\omega = 0$ to $\omega = 1$. Figure 12.10 shows a plot of the upper half-plane pole positions for a thirteenth-order 2-dB-ripple Chebyshev filter where we have indicated the magnitudes

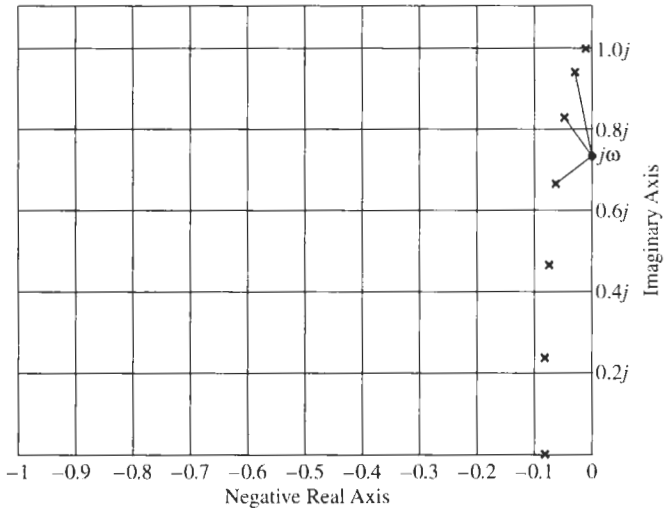

Figure 12.10 Upper half s-plane pole positions of a thirteenth-order 2-dB Chebyshev filter.

of three of these denominators, $|j\omega - p_j|$. As the figure illustrates, for high-order filters with large quality factors, the terms $|j\omega - p_j|$ tend to be small and, furthermore, become smaller as ω moves toward the edge of the passband, $\omega = 1$. This observation further supports the fact that sensitivities are normally largest at the passband corner.

12.3.1 Cascade Design

Our observation about large sensitivities appears to indicate that the design of high-order filters requires expensive very-low-tolerance components *unless* we can somehow overcome the predictions of Eq. (12.47). Because it is not possible to make *all* poles independent of x and hence their sensitivities zero, the best we can do is to make all pole sensitivities equal to zero with the exception of the one of a single pole, say p_1 (and, of course, its conjugate, p_1^*). In a circuit this means that the element x affects only one conjugate complex pole pair, and all remaining poles of the high-order filter are isolated from any variations of x. In that case the sensitivity of T to x is from Eq. (12.47)

$$S_x^{T(j\omega)} = -\left(\frac{p_1 S_x^{p_1}}{j\omega - p_1} + \frac{p_1^* S_x^{p_n^*}}{j\omega - p_1^*}\right) = -\frac{p_1 S_x^{p_1}\left(j\omega - p_1^*\right) + p_1^* S_x^{p_n^*}\left(j\omega - p_1\right)}{(j\omega)^2 - \left(p_1 + p_1^*\right) j\omega + |p_1|^2} \tag{12.48}$$

It should not be surprising that with Eqs. (12.26) and (12.28), this expression can be shown to equal Eq. (12.33), because a filter with only one complex pole pair is of second order. To have all other pole pairs separated from the element x we must isolate them from that component. The reader will perceive that this separation is accomplished by the *cascade design* that we used frequently in previous chapters because it resulted in convenient and transparent design methods. We recognize now that it is not just convenience, but that for high-order filters sensitivity considerations make cascade design almost unavoidable if the circuit is to perform well in practice.

We discussed cascade design in detail in Section 5.3, where we saw, Eq. (5.50), that the transfer function $T(s)$ was factored into a product of first- and second-order modules,

$$T(s) = T_1(s)T_2(s)\ldots T_k(s)\ldots T_{n-1}(s)T_n(s) = \prod_{j=1}^{n} T_j(s) \tag{12.49}$$

Assuming now that the component x is part of Module k, we compute from this equation the sensitivity

$$S_x^{T(s)} = \frac{\partial \ln\left(T_1 T_2 \cdots T_k \cdots T_{n-1} T_n\right)}{\partial \ln x} = \frac{\partial \ln(T_1)}{\partial \ln x} + \cdots + \frac{\partial \ln(T_k)}{\partial \ln x} + \cdots \frac{\partial \ln(T_n)}{\partial \ln x} = S_x^{T_k(s)}$$

and observe that the sensitivity $S_x^{T(s)}$ of the total transfer function $T(s)$ equals the sensitivity $S_x^{T_k(s)}$ of Module k that contains x:

$$S_x^{T(s)} = S_x^{T_k(s)} \tag{12.50}$$

The sensitivities of all other T_i are zero, of course, because the sections T_i, $i \neq k$, are independent of x. So, if we select a good low-sensitivity second-order module T_k, the total filter has the same low sensitivity to element tolerances. In previous chapters we encountered many examples for such cascade designs.

12.3.2 *LC* Ladders

There is one other method that has long been known by filter designers to lead to excellent circuits with very low sensitivity to component tolerances: the lossless ladder filter. A *lossless ladder* is a circuit structure as shown in Fig. 12.11 where all components apart from source and load resistors, R_1 and R_2, are lossless, that is, they are capacitors and inductors that dissipate no energy. We will discuss some aspects of *LC* filter design in the following chapters.

Before we discuss the sensitivity of *LC* filters, let us try to achieve an intuitive understanding of the reason behind the observed low sensitivities of these circuits. To do this we take a small detour and recall a few simple power relations from elementary circuit analysis courses: In the circuit in Fig. 12.11, the power delivered by the source V_S to the filter, that is, to the right of terminals 1–1′, is

$$P_1 = |I_1(j\omega)|^2 \,\mathrm{Re}Z_{\mathrm{in}}(j\omega) \tag{12.51}$$

where I_1 is the current flowing to the right through R_1 and $Z_{\mathrm{in}}(s)$ is the impedance seen into the filter at terminals 1–1′. The maximum value that this power P_1 can have is obtained when $Z_{\mathrm{in}}(j\omega)$ is *matched* to the source resistor R_1, i.e., when $Z_{\mathrm{in}}(j\omega) = R_1$. Under that condition, the voltage V_1 equals $V_S/2$ and $P_{1,\max}$ becomes

$$P_{1,\max} = \frac{|V_S(j\omega)|^2}{4R_1} \tag{12.52}$$

Next consider the power delivered to the load R_2. It is

$$P_2 = \frac{|V_2(j\omega)|^2}{R_2} \tag{12.53}$$

Now note that $P_1 = P_2$ because no power is lost in our *lossless LC* circuit between the ports, terminals 1–1′ and 2–2′. Thus, $|P_2| \le |P_1, \max|$, and if we take the ratio of the two power expressions in Eqs. (12.52) and (12.53), we obtain

$$|H(j\omega)|^2 = \frac{P_2}{P_{1,\max}} = \frac{4R_1}{R_2}\left|\frac{V_2(j\omega)}{V_S(j\omega)}\right|^2 \le 1 \tag{12.54}$$

Note that this power ratio $|H(j\omega)|^2$, i.e., $H(s)$, is related by the multiplying factor $2\sqrt{R_1/R_2}$ to our normal transfer function that was defined as the voltage ratio $T(s) = V_2/V_S$:

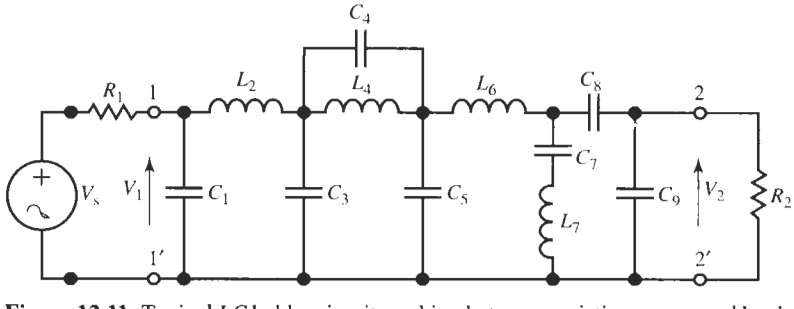

Figure 12.11 Typical *LC* ladder circuit working between resistive source and load terminations.

$$|H(j\omega)|^2 = \frac{P_2}{P_{1,\max}} = \frac{4R_1}{R_2}\left|\frac{V_2(j\omega)}{V_S(j\omega)}\right|^2 = \frac{4R_1}{R_2}|T(j\omega)|^2$$

or, after taking the square root and replacing $j\omega$ by s,

$$H(s) = \frac{N(s)}{D(s)} = 2\sqrt{\frac{R_1}{R_2}}\frac{V_2(s)}{V_S(s)} = 2\sqrt{\frac{R_1}{R_2}}T(s) \tag{12.55}$$

The two functions have the same frequency dependence, but differ by a constant set by the termination resistors. It is important to observe that, clearly, the ratio $|H(j\omega)|^2$ must be less than or at most equal to unity.

Equation (12.55) defines a transfer function constructed for maximum power transfer. Per Eq. (12.54), it satisfies $|H(j\omega)| \leq 1$ for all frequencies *and* all element values because, since the filter is *passive* and cannot provide gain, physically, we can of course not extract more power from the filter at V_2 than is delivered to it by the source at V_1. If we use $H(s)$ as defined in Eq. (12.55) as our transfer function in Eq. (12.43), it follows that the attenuation is nonnegative:

$$\alpha(\omega, x) = 20 \log \frac{1}{|H(j\omega)|} \geq 0\text{dB} \tag{12.56}$$

We have labeled α as $\alpha(\omega, x)$ to signify that this statement must be true for all frequencies *and components*. Stated differently, we can say that the attenuation $\alpha(\omega, x)$ can only *increase* from 0 dB if any component changes its value. This is obvious physically because the filter in Fig. 12.11 is passive, i.e., it cannot provide gain, which would mean $\alpha < 0$ for the notation of Eq. (12.56). Consequently, the dependence of $|H(j\omega)|$ and of α on x must be quadratic as shown in Fig. 12.12a at any point where the circuit provides its maximum gain (or minimum loss) of 0 dB. For the fifth-order Chebyshev filter sketched in Fig. 12.12b, for example, such points are at the frequencies $\omega_r = 0$, 0.59, and 0.95.

Figure 12.12a provides the explanation we were seeking. Since the slopes of $|H(j\omega_r, x)|$ and of $\alpha(\omega_r, x)$ are zero at the nominal design point x_0 we conclude that the sensitivities at these points are not just small, *but zero*. By going more deeply into the theory of *LC* filters, it can be shown that the sensitivities away from the points ω_r throughout the passband are small, although not zero (Sedra and Brackett, 1978; Schaumann et al., 1990).

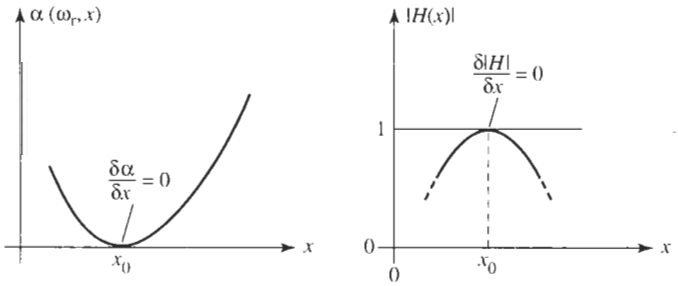

Figure 12.12 (a) Quadratic dependence of attenuation $|H(j\omega_r, x)|$ and $\alpha(\omega_r, x)$ on a component x at a nominal design point x_0; (b) passband behavior of a fifth-order Chebyshev lowpass filter.

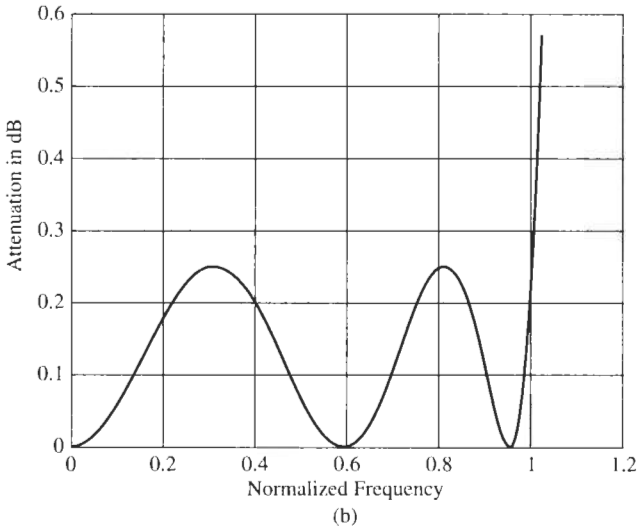

Figure 12.12 Continued

The realization (Orchard, 1966) that such excellent sensitivity behavior can be expected from lossless ladders filters, and that these passive structures have an intrinsic advantage over active filters, has motivated a search for methods to simulate the design of *LC* filters with active components. The reason is that conveniently sized inductors are not available for miniaturized electronic systems. It will also serve as motivation for us to study in the following chapters ways to simulate the behavior of *LC* ladders with active filters. We already encountered a successful result of this effort in the GIC biquad in Fig. 4.46a. As we saw in Section 4.5.3, by replacing the inductor in the *LC* lowpass filter of Fig. 4.39 by a gyrator-*C* combination, an active equivalent was found; it simulates the function of the *LC* circuit and shows excellent performance. Since sensitivity is only a mathematical property of the transfer function and the network configuration, we will be studying methods to simulate the form of the circuit equations or the circuit configuration. This must be accomplished such that the low sensitivities of *LC* filters are maintained in the active circuit, even if the simple physical argument, that the loss can only be positive, is not valid in the active realization.

REFERENCES

H. W. Bode, *Network Analysis and Feedback Amplifier Design*. Van Nostrand Reinhold, New York, 1945.

H. J. Orchard, "Inductorless Filters," *Electron. Lett.*, Vol. 2, pp. 224–225, September 1966.

R. Schaumann, M. S. Ghausi, and K. R. Laker, *Design of Analog Filters: Passive, Active RC and Switched Capacitor*, Chapter 2. Prentice Hall, Englewood Cliffs, NJ, 1990.

A. S. Sedra and P. O. Brackett, *Filter Theory and Design: Active and Passive*. Matrix, Portland, OR, 1978.

PROBLEMS

12.1 For the circuit given in Fig. P12.1, derive the transfer function V_2/V_1, and show that it is a lowpass filter. Determine expressions for Q and ω_0. From this information, compute the sensitivity function S_x^y where

$y = Q, \omega_0$, and $x = L, C, R_1$, and R_2.

12.2 Repeat Problem 12.1 for the bandpass filter shown in Fig. P12.2.

12.3 Repeat Problem 12.1 for the highpass filter given in Fig. P12.3.

12.4 Repeat Problem 12.1 for the bandstop filter given in Fig. P12.4.

12.5 In Section 4.5.1 we discussed the Sallen–Key filter. The circuit is shown again in Fig. P12.5. The transfer function was given in Eq. (4.101) under the assumption of ideal opamps.

(a) Calculate the sensitivities of ω_0 and Q to all the components.

(b) Compute the variation of ω_0 when the tolerances of R_1, R_2 are $\pm 3\%$ and those of C_1, C_2 are $\pm 10\%$. Is there a difference in performance when the components can be expected to track in their variations in contrast to nontracking elements?

(c) Compute the variations in Q when the component tolerances are the ones given in (b). Discuss the performance difference in two circuits built with tracking and nontracking elements, respectively.

(d) Discuss the sensitivity of Q to the component ratio K as a function of Q.

12.6 If the opamp of the Sallen–Key filter in Fig. P12.5 is not ideal, i.e., the amplifier gain A is finite, the transfer function is given in Eq. (4.99). Neglecting the frequency dependence of A, i.e., assuming that A is constant, determine the sensitivities of ω_0 and Q to the amplifier gain A.

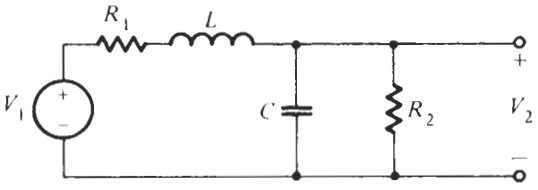

Figure P12.1

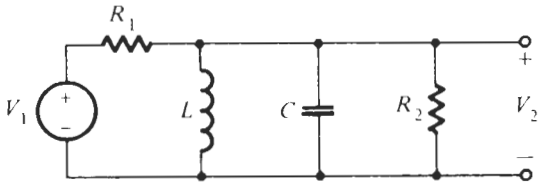

Figure P12.2

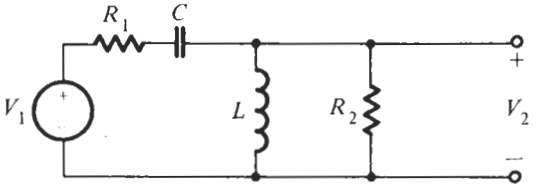

Figure P12.3

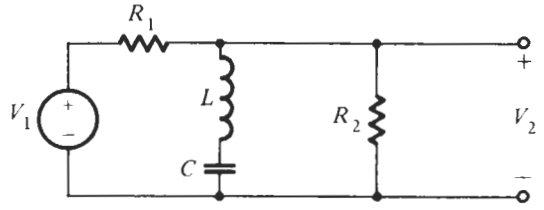

Figure P12.4

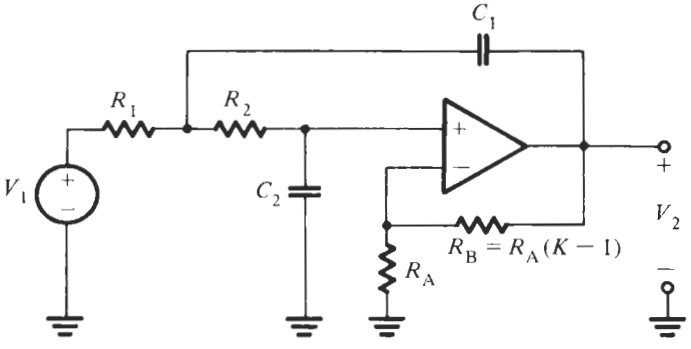

Figure P12.5

12.7 Using Eq. (12.8), prove the following relationships (Y is a function of x; k and n are constants)

$$S_x^{1/Y} = S_{1/x}^Y = -S_x^Y \qquad S_x^{kY} = S_x^Y$$

$$S_x^{kx^n} = n \qquad S_x^{Y^n} = nS_x^Y$$

$$S_x^{k+Y} = \frac{Y}{k+Y} S_x^Y$$

12.8 The Delyiannis–Friend bandpass circuit of Fig. 4.37 has the transfer function given in Eq. (4.127).

(a) Assuming the operational amplifier is ideal, compute the sensitivities of ω_0 and Q and gain H to the resistors and capacitors.

(b) Answer questions 12.5b and 12.5c for the Delyiannis–Friend circuit.

(c) Repeat Part (a) for the case when the opamp is not ideal, i.e., find the sensitivities to the opamp gain A.

12.9 Find the sensitivities of ω_0 and Q of the GIC bandpass in Fig. 4.46a, described by the function of Eq. (4.168a). Answer questions 12.5b and 12.5c for the GIC circuit.

12.10 Often sensitivities can be improved significantly by choosing the right nominal design values for the components. This problem will illustrate this fact. Three Sallen–Key designs are shown in Figs. P12.10a, b, and c for different choices of the feedback parameter K.

(a) Prepare a table for all three circuits containing the sensitivities of Q to all the component values, including K.

(b) Evaluate your results for $Q = 10$.

12.11 A GIC bandpass filter is built with temperature-dependent resistors $R_i = R_{0i}[1+\alpha(T-T_r)]$ where α is the temperature coefficient. The resistors are fabricated from the same material and you may assume that α is the same for all resistors.

(a) Derive an expression for the variations that may be expected in ω_0.

(b) Use sensitivity analysis to estimate the expected variations and compare the results of (a) and (b).

(c) Derive an expression for the variations that may be expected in Q.

(d) Use sensitivity analysis to estimate the expected variations and compare the results of (c) and (d).

12.12 The sensitivity analysis of two similar circuit designs gives the following table for Q sensitivities:

Sensitivity	Design 1	Design 2
$S_{R_1}^Q$	$-1/2 + Q\sqrt{C_2/C_1}$	$-1/2 + Q\sqrt{C_2/C_1}$
$S_{R_2}^Q$	$-1/2 + Q\sqrt{C_2/C_1}$	$-1/2 + Q(\sqrt{C_2/C_1} - \sqrt{C_1/C_2})$
$S_{C_1}^Q$	$-1/2 + 2Q\sqrt{C_2/C_1}$	$-1/2 + 2Q\sqrt{C_2/C_1}$
$S_{C_2}^Q$	$-1/2$	$-1/2 - Q\sqrt{C_1/C_2}$

We wish to compare the two designs to see if one has an advantage over the other.

(a) Consider the three possibilities, $C_1 = C_2$, $C_1 < C_2$, and $C_1 > C_2$ for some typical value of Q. Which design would you select?

(b) Consider the special case $\sqrt{C_2/C_1} = 1/Q$. Which design would you select?

12.13 In the Sallen–Key filter of Fig. P12.5, the resistors are functions of temperature. Use sensitivity results to compute the dependence of the transfer function magnitude on temperature. Assume that the temperature dependence of the resistors can be modeled as $R_i = R_{0i}[1 + \alpha(T - T_r)]$. Equations (12.14f) and (12.36) are helpful for this problem.

12.14 (a) For the circuit given in Fig. P12.14, show that

$$\frac{V_2}{V_1} = \frac{-(G_1/C_1)s}{s^2 + s(G_1+G_2)/C_2 + G_1G_2/(C_1C_2)}$$

(b) From the result found in Part (a), determine expressions for the sensitivity function S_x^y where $y = Q$, the bandwidth BW, and ω_0, and where $x = R_1$, R_2, C_1, and C_2.

12.15 (a) Given the circuit of Fig. P12.15, show that

$$T(s) = -\frac{\frac{R_2}{R_3}\frac{1}{R_1R_2C_1C_2}}{s^2 + \frac{R_1+R_2+R_1R_2/R_3}{R_1R_2C_2}s + \frac{1}{R_1R_2C_1C_2}}$$

(b) Determine the ω_0 and Q sensitivities for changes in R_1, R_2, C_1, and C_2.

12.16 An RC opamp circuit is described by the transfer function

$$T(s) = -\frac{G_1G_2/(C_1C_2)}{s^2 + [G_1/C_1 + (G_2/C_2)(1-1/A)]s + G_1G_2/(C_1C_2)}$$

In this equation, A is the opamp gain that is assumed to be a constant.

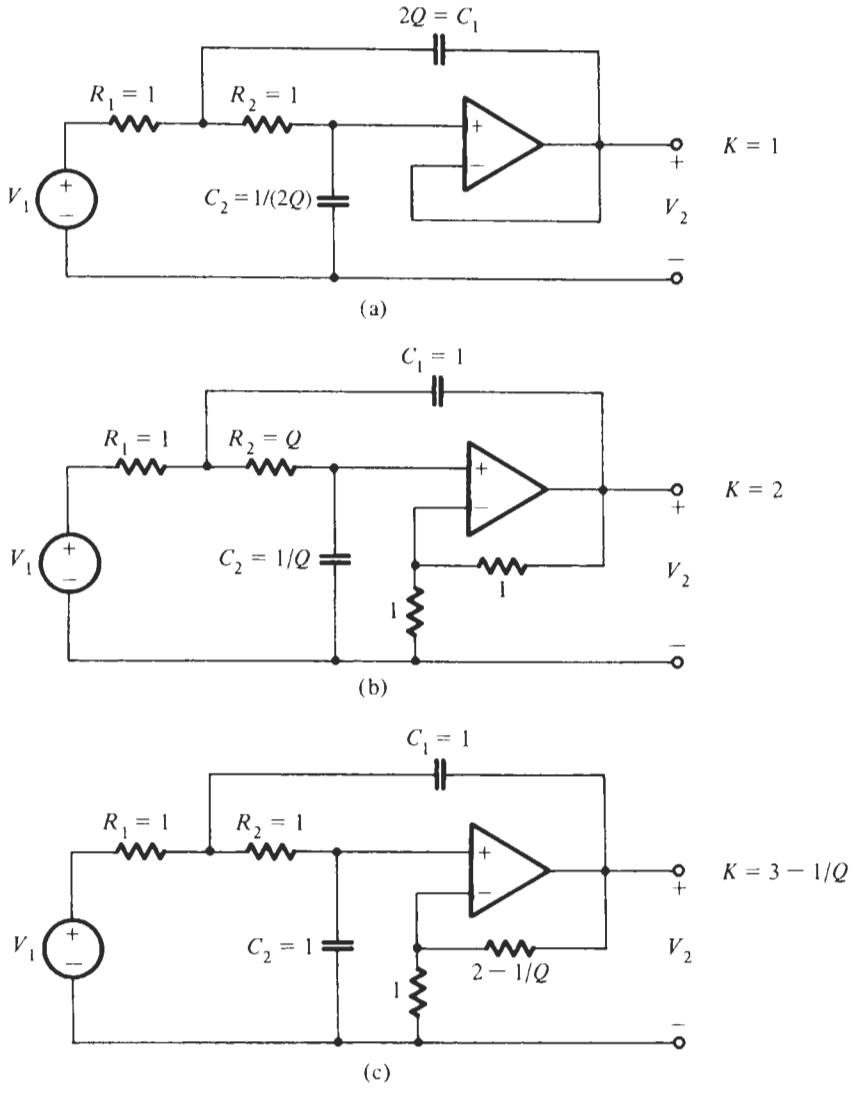

Figure P12.10

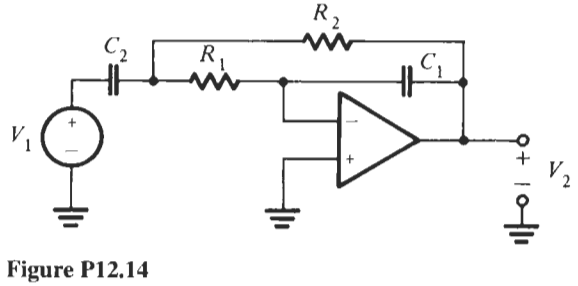

Figure P12.14

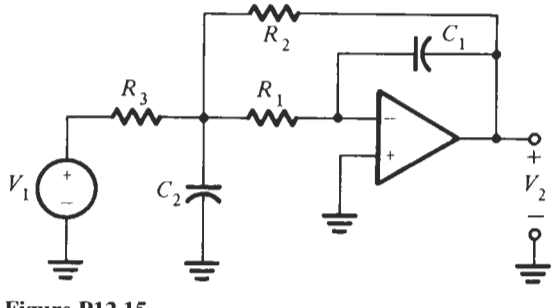

Figure P12.15

(a) Find the sensitivity of ω_0 and Q with respect to the gain A.

(b) For the batch of opamps available to the engineer, the fabrication tolerances are ±85%. Discuss the reliability of the sensitivity results obtained in (a).

12.17 Consider the following design equations for the normalized components of the Sallen–Key lowpass filter (they are due to W. Saraga): $C_2 = 1$, $C_1 = 3Q$, $R_2 = 1/(\sqrt{3}\omega_0)$, $R_1 = 1/(Q\omega_0)$, and $K = 4/3$. Compute the Q sensitivities and prepare entries for the table constructed in Problem 12.10. Compare the sensitivities to those previously determined in Problem 12.10.

12.18 The circuit shown in Fig. P12.18 is known as a twin-T filter.

(a) Show that $T = V_2/V_1$ has a zero at $\omega_z = 1/(RC)$.

(b) Find the sensitivity of ω_z to the circuit elements R_1, R_2, R_3, C_1, C_2, and C_3.

(c) What is the worst-case variability of ω_z when all components vary by 3%?

(d) What change in ω_z can be expected if like components can be assumed to track in their variations?

12.19 Design an Åckerberg–Mossberg bandpass section for the specifications in Fig. 12.1. Use Electronics Workbench (EWB) to perform a Monte Carlo analysis of this circuit. Assume components with 1% tolerances and perform about 20 runs. Compare the results with the ones of the Delyiannis–Friend and the GIC circuits in Fig. 12.1.

12.20 Equation (12.45) assumes that the poles and zeros of $T(s)$ in Eq. (12.43) are simple. Derive a result analogous to Eq. (12.45) for the case of multiple poles and zeros. This can be done easily by use of Eq. (12.8).

12.21 It can be shown that a network function $T(s)$ is a *bilinear* function of any of its components x, that is, it can be written as

$$T(s) = \frac{a(s) + xb(s)}{c(s) + xd(s)}$$

where a, b, c, and d are functions of frequency but *not* of the component x. This implies that any network polynomial, say the denominator of a transfer function, is a linear function of any of the components: $D(s) = c(s) + xd(s)$. Assume now that $D(s)$ has a root p of multiplicity $m > 1$, that is, D has a factor $(s - p)^m$. Assume p depends on the components x. Use the results presented in the beginning of this problem to show that when x changes to $x + \Delta x$, the multiple root p changes into m simple roots. *Hint*: Bring $D(s, x) = c(s) + (x + \Delta x)d(s) = 0$ into the form

$$1 + \frac{\Delta x}{x}\left(\frac{xd(s)}{D(s, x)}\right) = 0$$

and expand $xd(s)/D(s, x)$ into partial fractions, containing a high-order term $(s - p)^{-m}$. The result indicates that the m roots are approximately on a circle around the point p.

12.22 An eighth-order Butterworth bandpass transfer function is implemented as a cascade connection of four Åckerberg–Mossberg biquads. The circuit is constructed with ±5% capacitors and ±1% resistors. The operating frequency is low enough to be able to assume the opamps are ideal. We can also assume that the components track in their variations, that is, all capacitors are either too large or too small, and the same is true for resistors. This would be the case, for instance, if the filter were implemented as an integrated circuit where mask dimensions determine the relative tolerances of components. Based on these assumptions, use sensitivity calculations to estimate

(a) the deviation in center frequency of each biquad and

(b) the deviation that must be expected in the eighth-order filter.

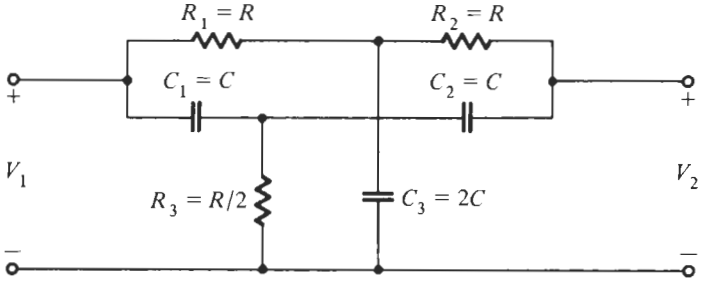

Figure P12.18

13 *LC* LADDER FILTERS

Although the subject of this book is the design of active filters, that is, filters that use active devices to provide *gain*, such as operational amplifiers, we shall discuss in this chapter some details concerning the design of *passive LC* filters. The motivation for diverting our attention temporarily from active filters was given in Section 12.3, where we saw that passive *LC* ladders have an inherent advantage over active filters in terms of their sensitivity to component tolerances. To recapitulate, we show in Fig. 12.12b the typical attenuation characteristic for a Chebyshev lowpass filter. For such filters the passband attenuation $\alpha_{\max}$ is often small, perhaps 0.1 dB, and at several frequencies $\alpha = 0$, so that there is no loss due to the filter. These frequencies are identified as $\omega_r = 0$, 0.59, and 0.95 in the figure. The corresponding transfer function magnitude response $|H(j\omega)|$ is defined in Eq. (12.55). It has the value $|H(j\omega)| = 1$ at the frequencies for which $\alpha = 0$.

At any frequency at which the attenuation vanishes, we consider the change in attenuation caused by any element x that changes from its nominal or design value x_0. Whether the element value increases or decreases, the attenuation must increase. This was illustrated in Fig. 12.12a. At the design value of the element it is clear that

$$\frac{\partial \alpha\,(\omega_r, x)}{\partial x} = 0 \quad \text{and} \quad \frac{\partial H\,(\omega_r, x)}{\partial x} = 0 \tag{13.1}$$

By Eq. (12.2a) it follows from this equation that the sensitivity functions are indeed zero at frequencies at which $\alpha = 0$ and $|H(j\omega)| = 1$. The sensitivity functions of interest are, with $x = L_k$, and $x = C_k$,

$$S_{L_k}^{|H|} = \frac{L_k}{|H|}\frac{\partial |H|}{\partial L_k}, \quad S_{C_k}^{|H|} = \frac{C_k}{|H|}\frac{\partial |H|}{\partial C_k} \tag{13.2}$$

Since the values of $\alpha_{\max}$ remain small throughout the passband, sensitivities can be shown to remain small over the passband. It is true that the sensitivities may become large in the stopband, but this is normally of less concern to the designer since requirements on loss are less stringent in the stopband in most filter applications.

It was pointed out by Orchard (1966) that the conclusions reached for the doubly terminated lossless filter do not apply to singly terminated circuits, and thus these circuits are inherently more sensitive.

Because of the low sensitivity to component values that characterizes the doubly terminated *LC* ladders, these circuits are commonly used in filter applications. As we will learn in the next chapter, this also means that the *LC* ladder is used as a model for circuits that use active elements to simulate inductors, resistors, and other elements.

The oldest electrical filters, built in the 1800s and the early 1900s, were made with inductors and capacitors arranged in ladder form, as shown in Fig. 12.11. To achieve transfer of signal power, the ladder has a source V_S, as a rule with a source resistor R_1, and is terminated by a load resistor R_2 that dissipates the output signal energy and where the output signal is measured. We will be interested in lossless ladders for a number of reasons:

1. Even though the design of *LC* filters has its roots in antiquity, lossless ladders remain widely used to this day for high-frequency applications or when no power is available to drive the active devices.
2. *LC* ladder filters form prototype models that are simulated by active circuits, both with discrete components and in fully integrated form on an integrated circuit chip. The goal is, of course, to develop the active circuit in such a way that the simulation inherits the excellent sensitivity properties of lossless *passive* ladders even if the intuitive power transfer argument on which Fig. 12.12a is based no longer holds for the *active* circuit.
3. Finally if we succeed in developing an active simulation of the passive ladder, we will be able to make use of the huge volume of design information and tables that are available for *LC* ladders.

A detailed study of lossless ladders and their design goes beyond this text. Many texts can be consulted which have sections about *LC* filters or are entirely devoted to that subject (see References 1–10). We shall just present sufficient detail to permit us to undertake simple ladder designs and to understand the origins of the active simulations that have been found convenient and useful in practice.

13.1 SOME PROPERTIES OF LOSSLESS LADDERS

Consider the general diagram in Fig. 13.1a and assume the lossless ladder has the simple form in Fig. 13.1b. Since the signal is supplied to the ladder by a resistive source and the load is resistive as well, the ladder is said to be *doubly terminated*. The low-sensitivity property we are interested in is valid for doubly terminated ladders; as mentioned, sensitivities can be shown to be worse when either one or both terminations are absent, such as, e.g., $R_1 = 0$ and/or $R_2 = \infty$. We will, therefore, be concerned only with ladders working between two resistors.

We notice intuitively that the ladder in Fig. 13.1b is a lowpass filter: at low frequencies all inductors tend to be small impedances (short circuits at dc) and all capacitors large impedances

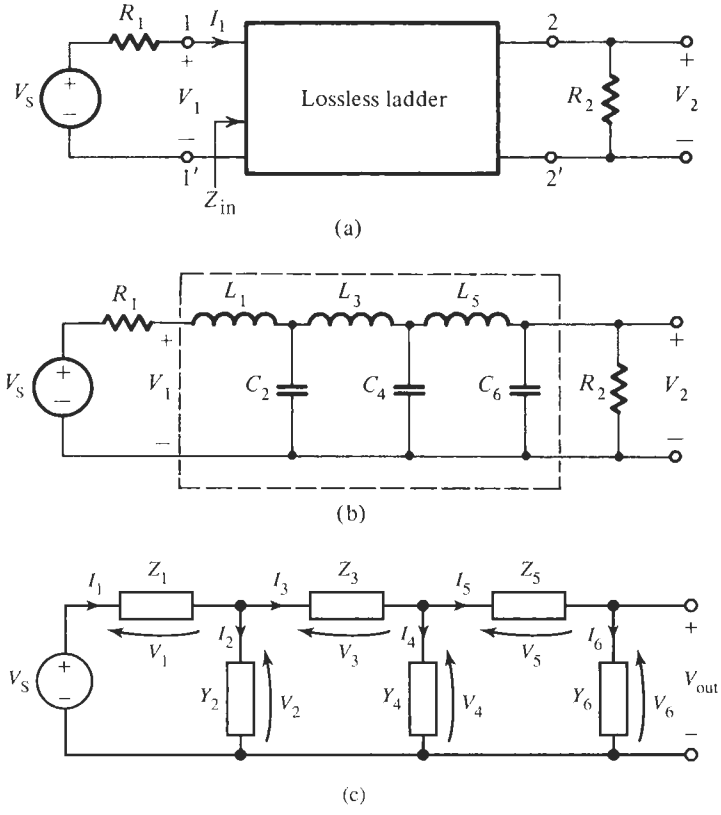

Figure 13.1 Circuit diagram for a doubly terminated lossless ladder: (a) general representation; (b) sixth-order all-pole lowpass ladder; (c) the ladder with series impedances and shunt admittances.

(open circuits at dc). Thus, at dc the filter reduces to two parallel wires and the voltage transfer function is given simply by the resistive voltage divider:

$$T(0) = \frac{V_2}{V_S} = \frac{R_2}{R_1 + R_2} \tag{13.3a}$$

In terms of the power ratio $H(s)$ defined in Eq. (12.55) we would have

$$H(0) = 2\sqrt{\frac{R_1}{R_2}}T(0) = 2\frac{\sqrt{R_1 R_2}}{R_1 + R_2} \tag{13.3b}$$

At high frequencies on the other hand, inductors tend to become open circuits and capacitors short circuits, which means that no electrical signal can reach the output and

$$T(\infty) = \frac{V_2}{V_S} = 0 \tag{13.4}$$

To see more precisely how the circuit behaves we need to analyze it. Let us introduce the notation Y_j for the shunt branches and Z_i for the series branches as shown in Fig. 13.1c:

$Y_6(s) = sC_6 + G_2$, $Z_5(s) = sL_5$, $Y_4 = sC_4$, $Z_3 = sL_3$, $Y_2 = sC_2$, $Z_1 = sL_1 + R_1$. Then we can write Kirchhoff's laws, KCL and KVL, and Ohm's law starting at the output node, assuming that no current flows from the output terminals. We obtain consecutively from

$$
\begin{aligned}
&\text{KCL:} && I_5 = I_6 + 0 = Y_6 V_6 \\
&\text{Ohm's Law:} && V_5 = I_5 Z_5 = Z_5 Y_6 V_6 \\
&\text{KVL:} && V_4 = V_5 + V_6 = (1 + Z_5 Y_6) V_6 \\
&\text{KCL:} && I_3 = I_4 + I_5 = V_4 Y_4 + I_5 = [Y_4(1 + Z_5 Y_6) + Y_6] V_6 \\
&\text{Ohm's Law:} && V_3 = Z_3 I_3 = Z_3[Y_4(1 + Z_5 Y_6) + Y_6] V_6 \\
&\text{KVL:} && V_2 = V_3 + V_4 = \{Z_3[Y_4(1 + Z_5 Y_6) + Y_6] + (1 + Z_5 Y_6)\} V_6 \\
& && \quad = \{(1 + Z_3 Y_4)(1 + Z_5 Y_6) + Z_3 Y_6\} V_6 \\
&\text{KCL:} && I_1 = I_2 + I_3 = Y_2 V_2 + [Y_4(1 + Z_5 Y_6) + Y_6] V_6 \\
& && \quad = \{[Y_4 + Y_2(1 + Z_3 Y_4)](1 + Z_5 Y_6) + Y_2 Z_3 Y_6 + Y_6\} V_6 \\
&\text{Ohm's Law:} && V_1 = Z_1 I_1 = Z_1\{[Y_4 + Y_2(1 + Z_3 Y_4)](1 + Z_5 Y_6) + Y_2 Z_3 Y_6 + Y_6\} V_6 \\
&\text{KVL:} && V_S = V_1 + V_2 = \{[Z_1 Y_4 + Z_1 Y_2(1 + Z_3 Y_4)](1 + Z_5 Y_6) + Z_1 Y_2 Z_3 Y_6 \\
& && \qquad + Z_1 Y_6 + (1 + Z_3 Y_4)(1 + Z_5 Y_6) + Z_3 Y_6\} V_6 \\
& && \quad = \{1 + Z_1(Y_2 + Y_4 + Y_6) + Z_3(Y_4 + Y_6) + Z_5 Y_6 + Z_1 Y_2 Z_3(Y_4 + Y_6) \\
& && \qquad + (Z_1 Y_2 + Z_1 Y_4 + Z_3 Y_4) Z_5 Y_6 + Z_1 Y_2 Z_3 Y_4 Z_5 Y_6\} V_6 = Q(s) V_6
\end{aligned}
\tag{13.5}
$$

Let us label temporarily the output voltage V_6 as V_{out} rather than using our usual notation V_2 to be able to distinguish it from the voltage V_2 across the admittance Y_2. Then the exact transfer function of the ladder in Fig. 13.1c is

$$T(s) = \frac{V_6}{V_S} = \frac{V_{\text{out}}}{V_S} = \frac{1}{Q(s)} \tag{13.6}$$

where $Q(s)$ is the expression in braces identified in Eq. (13.5). For an all-pole LC lowpass filter where apart from R_1 and R_2 each of the admittances and impedances in the ladder is one capacitor or inductor, respectively, $Q(s)$ is a polynomial. In the more general case, where some or all of the Z_i and Y_j contain several capacitors and inductors as shown in Fig. 12.11, $Q(s)$ is a rational function and so is $T(s)$. Specifically, in the circuit in Fig. 12.11 we have for the impedance of Branch 4 and the admittance of Branch 7

$$Z_4(s) = \frac{sL_4}{1 + s^2 L_4 C_4}, \quad Y_7(s) = \frac{sC_7}{1 + s^2 L_7 C_7} \tag{13.7}$$

Since by Eq. (13.5) $Q(s)$ consists of a sum of products of Z_i and Y_j, it is clear that $Q(s)$ for Fig. 12.11 is a rational function whose denominator is $(1 + s^2 L_4 C_4)(1 + s^2 L_7 C_7)$. Thus,

$$T(s) = \frac{V_{\text{out}}}{V_S} = \frac{1}{Q(s)} = \frac{N(s)}{D(s)} = \frac{\left(1 + s^2 L_4 C_4\right)\left(1 + s^2 L_7 C_7\right)}{D(s)} \tag{13.8}$$

where $D(s)$ is a polynomial. We observe that in this case $T(s)$ has finite transmission zeros at $\omega_4 = 1/\sqrt{L_4 C_4}$ and $\omega_7 = 1/\sqrt{L_7 C_7}$. Intuitively, we should expect this result from Fig. 12.11 because Branch 4 is an open circuit at the parallel resonance of L_4 and C_4, and output and

input of the filter are disconnected for $\omega = \omega_4$. Similarly, at the series resonance of L_7 and C_7 Branch 7 is a short circuit placed across the filter so that, again, a signal at the frequency ω_7 cannot reach the output.

For the ladder in Fig. 13.1b, $Q(s)$ is a sixth-order polynomial because we have six reactances (inductors and capacitors) so that $Z_1Y_2Z_5Y_6Z_3Y_4$ contributes the high-order term $s^6L_1L_3L_5C_2C_4C_6$. We see, therefore, that $T(\infty)$ becomes

$$T(s)|_{s\to\infty} = \frac{V_{\text{out}}}{V_S} = \left.\frac{1}{s^6L_1L_3L_5C_2C_4C_6}\right|_{s\to\infty} = 0 \tag{13.9}$$

as we predicted in Eq. (13.4). In general, if the ladder has n branches with one inductor in each series branch and one capacitor in each shunt branch, the function $Q(s)$ is an nth-order polynomial $D(s)$ and the transfer function is of order n,

$$T(s) = \frac{V_{\text{out}}}{V_S} = \frac{K}{D(s)} = \frac{K}{s^n + a_{n-1}s^{n-1} + \cdots + a_1s + a_0} \tag{13.10}$$

At dc and at high frequencies, we have

$$T(0) = \frac{K}{a_0} = \frac{R_2}{R_1 + R_2} \quad \text{and} \quad T(s)|_{s\to\infty} = \left.\frac{K}{s^n}\right|_{s\to\infty} = 0 \tag{13.11}$$

This means that from its high value at dc, $T(0) = K/a_0$, the transfer function magnitude decreases at the rate $-6n$ dB per octave or $-20n$ dB per decade as $s \to \infty$. Clearly the function represents a lowpass filter.

Two specific examples of the general form of the ladder in Fig. 13.1b are shown in Fig. 13.2. We can calculate the transfer function by direct analysis, or, alternatively, we can use Eq. (13.5) and substitute the specific values for these two circuits. For Fig. 13.2a we have from Eq. (13.5) with $Z_1 = sL_1 + R_1$ and $Y_2 = sC_2 + G_2$ and all other reactances absent (set to zero)

$$\begin{aligned} T(s) = \frac{V_{\text{out}}}{V_S} &= \frac{1}{1 + Z_1Y_2} = \frac{1}{1 + (sL_1 + R_1)(sC_2 + G_2)} \\ &= \frac{1}{s^2L_1C_2 + s(C_2R_1 + L_1G_2) + 1 + R_1G_2} = \frac{1}{s^2 + 2s + 2} \end{aligned} \tag{13.12}$$

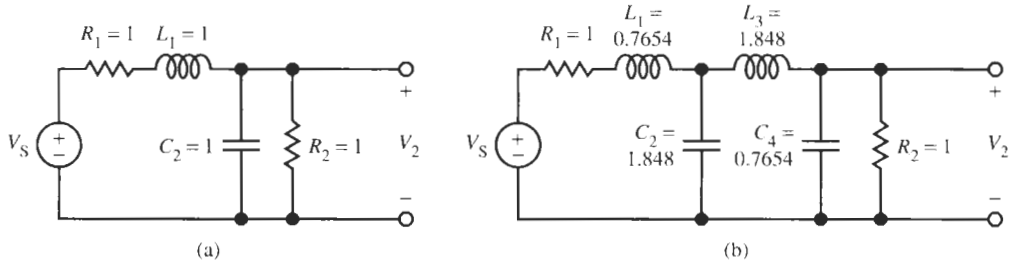

Figure 13.2 Lossless networks with normalized component values: (a) second-order *LC* coupling network; (b) fourth-order *LC* Butterworth lowpass filter with normalized impedance values and cut-off frequency $\omega = 1$.

Similarly, for Fig. 13.2b we obtain with $Z_1 = sL_1 + R_1$, $Y_2 = sC_2$, $Z_3 = sL_3$, and $Y_4 = sC_4 + G_2$, and again all other reactances absent:

$$T(s) = \frac{V_{out}}{V_S} = \frac{1}{1 + Z_1(Y_2 + Y_4) + (1 + Z_1Y_2)Z_3Y_4}$$

$$= \frac{1}{1+(sL_1+R_1)(sC_2+sC_4+G_2)+sL_3(sC_4+G_2)+s^2L_3C_2(sL_1+R_1)(sC_4+G_2)}$$

Inserting the element values in Fig. 13.2b we obtain

$$T(s) = \frac{1}{2}\frac{1}{s^4 + 2.613s^3 + 3.414s^2 + 2.613s + 1} \tag{13.13a}$$

which is recognized as the fourth-order Butterworth function (see Table 6.2) with a factor 1/2 to account for the voltage division between two equal resistors at dc. Note that by Eq. (12.55) $T(s) = H(s)/2$ so that

$$H(s) = \frac{1}{s^4 + 2.613s^3 + 3.414s^2 + 2.613s + 1} \tag{13.13b}$$

Thus, the *LC* circuit in Fig. 13.2b is a fourth-order Butterworth filter.

We can make an interesting interpretation of this circuit's operation that will help our understanding of the development to follow: The fourth-order Butterworth function has four transmission zeros, all at $\omega = \infty$. Now observe that L_1 and L_3 become open circuits at $\omega = \infty$ and C_2 and C_4 become short circuits, creating four transmission zeros at infinity. This is completely analogous to the way Z_4 and Y_7 in Eq. (13.7) are creating the two transmission zeros at ω_4 and ω_7 in $T(s)$ of Eq. (13.8). We shall see that one of the aims of the ladder development we will discuss is to realize the prescribed transmission zeros via series impedance poles and shunt impedance zeros.

An important property of the transfer function of Eq. (13.10) is that the denominator polynomial $D(s)$ must be a *Hurwitz polynomial*, that is, all its zeros are in the left half-plane for reasons of stability. This means that the denominator polynomial must have all its coefficients positive (and *not* zero). For example, the denominator of Eq. (13.13) can be factored so that

$$T(s) = \frac{1}{2}\frac{1}{(s^2 + 0.7654s + 1)(s^2 + 1.8478s + 1)} \tag{13.14}$$

has four left half-plane roots at $-0.3827 \pm j0.9239$ and $-0.9239 \pm j0.3827$ (see Table 6.1).

In arriving at Eqs. (13.5), (13.12), and (13.13) we analyzed the circuits and obtained the transfer function $T(s)$. For the synthesis or design problem, we have the inverse situation. Given the values R_1 and R_2 and the prescribed form of the transfer function $T(s)$, we are required to find the element values of the lossless ladder; for example, if we are given Eq. (13.13) we are asked to find the circuit in Fig. 13.2b.

13.2 A SYNTHESIS STRATEGY

In the doubly terminated circuit in Fig. 13.1a, we have identified the current from the source, I_1, and its reference direction, and Z_{in} as the input impedance of the *RLC* circuit made up

of the lossless ladder terminated by R_2. We assume that the circuit is operating in sinusoidal steady state. The input impedance has both a real and an imaginary component

$$Z_{\text{in}} = R_{\text{in}} + jX_{\text{in}} \tag{13.15}$$

and the current at the input is

$$I_1 = \frac{V_S}{R_1 + Z_{\text{in}}} \tag{13.16}$$

Now since the *LC* circuit is lossless, we may equate the average power into the circuit, P_1, Eq. (12.51), to that in the load. Thus,

$$P_1 = R_{\text{in}} |I_1(j\omega)|^2 = \frac{|V_2(j\omega)|^2}{R_2} \tag{13.17}$$

Substituting Eq. (13.16) for I_1 into this equation gives us

$$\frac{R_{\text{in}} |V_S(j\omega)|^2}{|R_1 + Z_{\text{in}}|^2} = \frac{|V_2(j\omega)|^2}{R_2} \tag{13.18}$$

From this equation we determine the magnitude squared of the desired transfer function

$$\left| \frac{V_2(j\omega)}{V_S(j\omega)} \right|^2 = |T(j\omega)|^2 = \frac{R_2 R_{\text{in}}}{|R_1 + Z_{\text{in}}|^2} \tag{13.19}$$

To relate this expression to the transfer function $H(s)$ that we proposed to use for *LC* filters and that was defined in Eqs. (12.54) and (12.55), we multiply Eq. (13.19) by $4R_1/R_2$ and obtain

$$|H(j\omega)|^2 = \frac{4R_1}{R_2} \left| \frac{V_2(j\omega)}{V_S(j\omega)} \right|^2 = \frac{4R_1 R_{\text{in}}}{|R_1 + Z_{\text{in}}|^2} \leq 1 \tag{13.20}$$

With Eq. (13.15) we can bring this equation into the form

$$|H(j\omega)|^2 = 1 - \frac{|R_1 - Z_{\text{in}}|^2}{|R_1 + Z_{\text{in}}|^2} = 1 - |\rho(j\omega)|^2 \tag{13.21}$$

where the auxiliary function $\rho(s)$ is known as the *reflection coefficient*. $\rho(s)$ is a measure of how well R_1 and Z_{in} are matched; we have always $|\rho(j\omega)|^2 \leq 1$ and for perfect matching $\rho(s) = 0$. Evidently, $\rho(s)$ is defined as

$$|\rho(j\omega)|^2 = |\rho(s)|\,|\rho(-s)||_{s=j\omega} = \frac{|R_1 - Z_{\text{in}}(j\omega)|^2}{|R_1 + Z_{\text{in}}(j\omega)|^2} \tag{13.22}$$

From this equation we see that $\rho(s)$ may be separated from $\rho(-s)$ to give

$$\rho(s) = \pm \frac{R_1 - Z_{\text{in}}(s)}{R_1 + Z_{\text{in}}(s)} \tag{13.23}$$

Clearly, this equation may be solved for Z_{in} in terms of $\rho(s)$ and R_1. The result is

$$Z_{in} = R_1 \frac{1 - \rho(s)}{1 + \rho(s)} \tag{13.24}$$

or

$$Z_{in} = R_1 \frac{1 + \rho(s)}{1 - \rho(s)} \tag{13.25}$$

Observe that these expressions give us two reciprocal impedances. Now, since ρ is determined by the prescribed transfer function H, we have reduced the problem to determining a lossless circuit terminated in a resistor R_2 from a specified Z_{in}. Sidney Darlington (1939) showed in his classic paper that this was always possible, and so the circuit may be found. To illustrate the application of the strategy, consider the problem of determining circuits having a Butterworth response for which there are equal terminations with $R_1 = R_2 = 1$, a normalized value that may later be magnitude scaled.

The Butterworth response is

$$|H(j\omega)|^2 = \frac{1}{1 + \omega^{2n}} \tag{13.26}$$

Note that this magnitude-squared function is less than or equal to unity and so satisfies the condition of Eq. (13.20). Since the magnitude-squared function is

$$|H(j\omega)|^2 = H(s)H(-s)|_{s=j\omega} \tag{13.27}$$

then from Eq. (13.10) we have

$$|H(j\omega)|^2 = \frac{K_H}{|D(j\omega)|^2} = \left| \frac{K_H}{D(s)D(-s)} \right|_{s=j\omega} \tag{13.28}$$

The constant K_H is related to the constant K in Eq. (13.10) by $K_H = 2\sqrt{R_1/R_2}K$, and $D(s)$ is known from our study of the Butterworth functions in Chapter 6. The polynomials $D(s)$ are shown in the following table for $n = 1, 2$, and 3:

Order	$\lvert D(j\omega)\rvert^2$	$D(s)$
1	$1 + \omega^2$	$s + 1$
2	$1 + \omega^4$	$s^2 + \sqrt{2}s + 1$
3	$1 + \omega^6$	$s^3 + 2s^2 + 2s + 1$

So we see that a_0 in Eq. (13.11) is 1 for all n, and with equal terminations it is then necessary that $K = 0.5$ so that $K_H = 1$. Thus, $H(s)$ is determined. With that accomplished, we may determine from Eq. (13.21) the auxiliary function of Eq. (13.23). We have

$$|\rho(j\omega)|^2 = 1 - \frac{1}{1 + \omega^{2n}} = \frac{\omega^{2n}}{1 + \omega^{2n}} \tag{13.29}$$

Since

$$\omega^{2n}\big|_{\omega^2=-s^2} = s^n(-s)^n \tag{13.30}$$

we see that

$$\rho(s) = \frac{s^n}{D(s)} \tag{13.31}$$

Substituting this value of $\rho(s)$ into Eqs. (13.24) and (13.25), we obtain

$$Z_{in} = R_1\left[\frac{1-\rho(s)}{1+\rho(s)}\right]^{\pm 1} = R_1\left[\frac{D(s)-s^n}{D(s)+s^n}\right]^{\pm 1} \tag{13.32}$$

It is convenient to normalize the impedance level of the circuit by setting $R_1 = 1$. If we do that in the last equation, and then let n have several values, we will see the pattern that is followed in obtaining the circuits. Consider the cases for $n = 1$, $n = 2$, and $n = 3$:

***n* = 1**: For $n = 1$, $D = s + 1$ and $\rho(s) = s/(s+1)$. Hence the impedance Z_{in} is either

$$Z_{in} = \frac{1 - s/(s+1)}{1 + s/(s+1)} = \frac{1}{2s+1} \tag{13.33}$$

or

$$Z_{in} = 2s + 1 \tag{13.34}$$

The circuit realizations of these two Z_{in} functions are shown in Fig. 13.3 with the section enclosed by the dashed lines being the lossless coupling circuit. In this case the element values are evident from direct inspection of the expressions for Z_{in}.

***n* = 2**: As already tabulated, $D = s^2 + \sqrt{2}s + 1$ for the case $n = 2$ and hence

$$\rho(s) = \frac{s^2}{s^2 + \sqrt{2}s + 1} \tag{13.35}$$

Then we find that Z_{in} is

$$Z_{\text{in}} = \frac{\sqrt{2}s + 1}{2s^2 + \sqrt{2}s + 1} \tag{13.36}$$

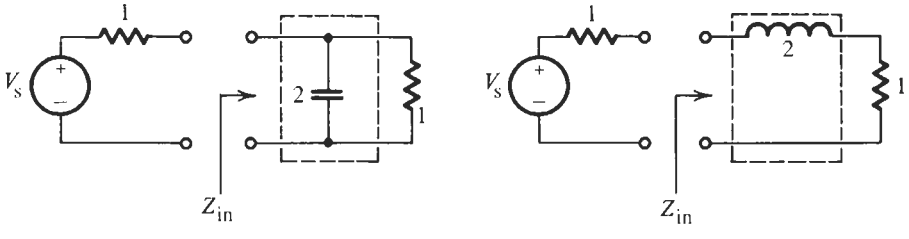

Figure 13.3 Realization of first-order Butterworth filters obtained from Z_{in} in Eqs. (13.33) and (13.34).

or the reciprocal of this quantity. This time we cannot determine the circuit by this Z_{in} directly by inspection. Instead, we expand this function, or its reciprocal, as a continued fraction. This is always done by dividing the polynomial of higher degree by the polynomial of lower degree. The continued fraction is carried out by synthetic division in these steps:

$$\begin{array}{r} \sqrt{2}\,s+1)2s^2+\sqrt{2}\,s+1(\sqrt{2}\,s \leftarrow C_1 s \\ \underline{2s^2+\sqrt{2}\,s} \\ 1)\sqrt{2}\,s+1(\sqrt{2}\,s \leftarrow L_2 s \\ \underline{\sqrt{2}\,s} \\ 1)\,1\,(1 \leftarrow R_2 \\ \underline{1} \\ 0 \end{array} \tag{13.37}$$

Thus, Z_{in} is expanded into a continued fraction as follows:

$$Z_{in}=\frac{\sqrt{2}s+1}{2s^2+\sqrt{2}s+1}=\cfrac{1}{\sqrt{2}s+\cfrac{1}{\sqrt{2}s+\cfrac{1}{1}}}=\cfrac{1}{sC_1+\cfrac{1}{sL_2+\cfrac{1}{G_2}}} \tag{13.38a}$$

Similarly, for the reciprocal of Eq. (13.36) we have

$$Z_{in}=\frac{2s^2+\sqrt{2}s+1}{\sqrt{2}s+1}=\sqrt{2}s+\cfrac{1}{\sqrt{2}s+\cfrac{1}{1}}=sL_1+\cfrac{1}{sC_2+\cfrac{1}{R_2}} \tag{13.38b}$$

The two circuits that have been found by this process are shown in Figs. 13.4a and b, respectively. We observe that the two partial fraction expansions are identical, but in Eq. (13.38b) it is treated as an impedance whereas in Eq. (13.38a) it is an admittance. Accordingly, the admittances in Fig. 13.4a are replaced by impedances in Fig. 13.4b of the same numerical value; the two circuits so obtained are said to be *duals*.

***n* = 3**: For $n = 3$ we found that $D(s) = s^3 + 2s^2 + 2s + 1$ so $\rho(s)$ is obtained directly from Eq. (13.31) as

$$\rho(s)=\frac{s^3}{s^3+2s^2+2s+1} \tag{13.39}$$

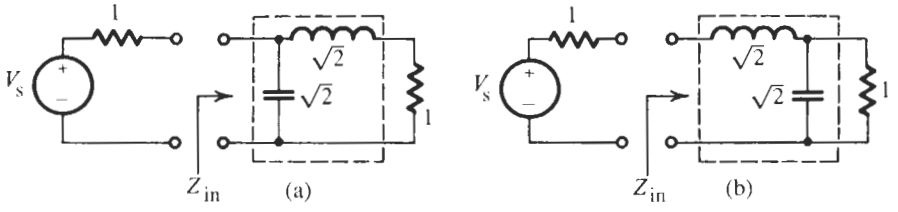

Figure 13.4 Second-order Butterworth filters obtained from Z_{in} in Eq. (13.38).

and we find Z_{in}:

$$Z_{\text{in}} = \frac{2s^2 + 2s + 1}{s^3 + 2s^2 + 2s + 1} \tag{13.40}$$

and from that its reciprocal. We next expand Z_{in} in a continued fraction by dividing the denominator polynomial by the numerator polynomial in the pattern of dividing one step, inverting, dividing one step, inverting, and so on. Thus

$$\begin{array}{llllll}
2s^2 + 2s + 1 \;)\; 2s^3 + 2s^2 + 2s + 1 \;(\; s \leftarrow L_1 s & & & & & \\
\qquad\qquad\quad \underline{2s^3 + 2s^2 + \; s\qquad} & & & & & \\
 & s + 1\;)2s^2 + 2s + 1 \;(\; 2s \leftarrow C_2 s & & & & \\
 & \qquad\quad \underline{2s^2 + 2s\qquad} & & & & \\
 & & 1\;) \quad s + 1 \;(\; s \leftarrow L_3 s & & & \\
 & & \qquad \underline{s\qquad} & & & \\
 & & \qquad\quad 1\;)\;1\;(\;1 \leftarrow R_2 & & & \\
 & & \qquad\qquad\;\; \underline{1} & & & \\
 & & \qquad\qquad\;\; 0) & & &
\end{array}$$

or

$$Z_{in} = \cfrac{1}{s + \cfrac{1}{2s + \cfrac{1}{s + \cfrac{1}{1}}}} \tag{13.41}$$

From this continued fraction expansion, and from its reciprocal, we recognize the two dual circuits in Fig. 13.5, each consisting of a lossless coupling circuit terminated in 1-Ω resistors. The steps are summarized in Fig. 13.6. Recalling our comment about transmission zeros being realized by series impedance poles and shunt impedance zeros we observe that the circuits in Figs. 13.3, 13.4, and 13.5 realize, respectively, one, two, and three transmission zeros at $\omega = \infty$.

The circuits we have found and their elements are listed in Table 13.1 for the cases $n = 2$ and $n = 3$ that we have just studied. If this process is continued until $n = 10$, then all the values in the table are obtained. For example, Fig. 13.2b contains the case $n = 4$. Notice that

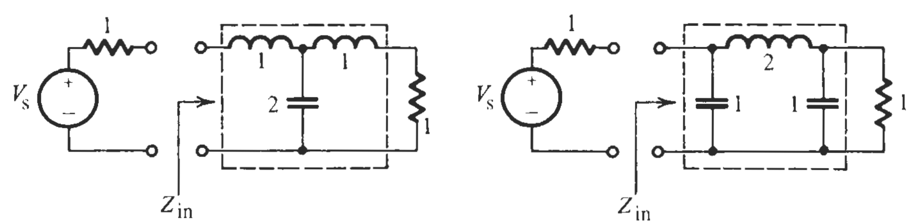

Figure 13.5 Realization of third-order Butterworth filters from Eq. (13.40).

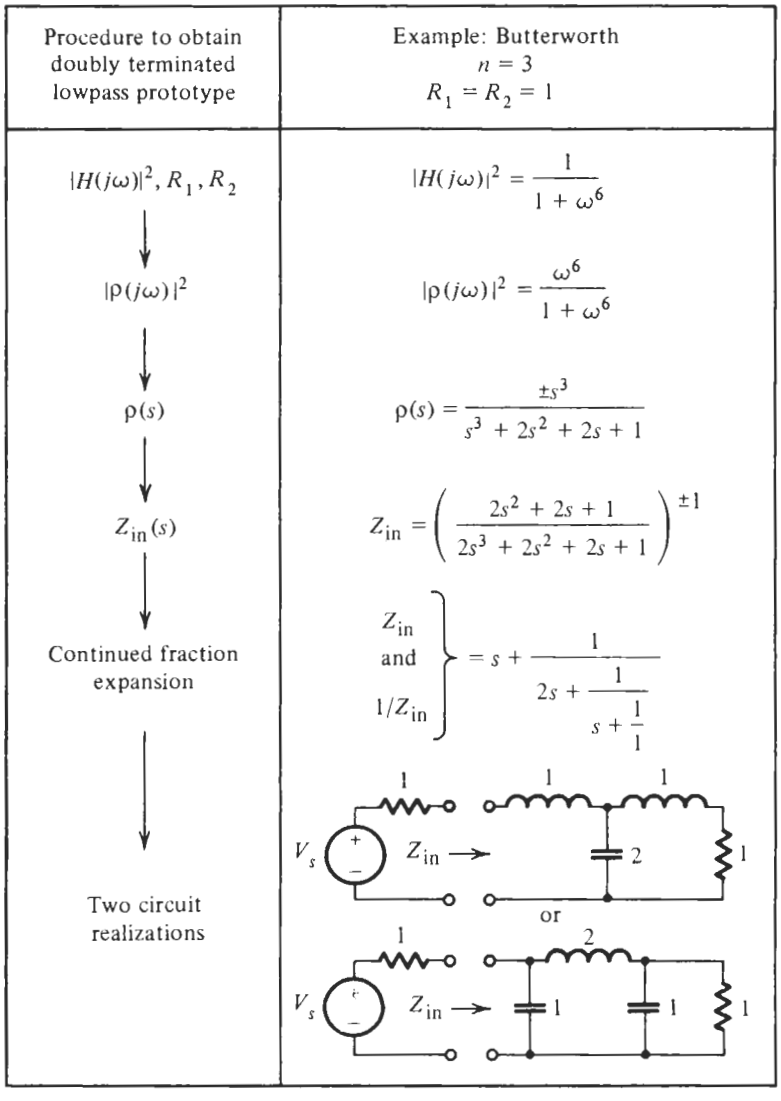

Figure 13.6 Synthesis process for all-pole lowpass filters.

the realization of the nth-order transfer function requires exactly n reactances, one for each degree of freedom; such a realization is referred to as *canonic*. The realization of all-pole lowpass filters is always canonic, but this is not the case for *LC* ladders in general. When using Table 13.1, remember that it assumes that the two terminating resistors are *equal* and that the elements are normalized both with respect to the impedance level in that $R_1 = R_2 = 1$, and with respect to the frequency that is assumed to be the 3-dB frequency, $\omega_p = 1$. If $\alpha_{max} \neq 3$dB, we have to use a different frequency to denormalize the elements as was discussed in Section 6.4, Eq. (6.47):

$$\omega_B = \varepsilon^{-1/n} \omega_p \tag{13.42}$$

TABLE 13.1 Table of Element Values for Doubly Terminated Butterworth Filters for $n = 2$ to $n = 10$ Normalized to Half-Power Frequency of 1 rad/s

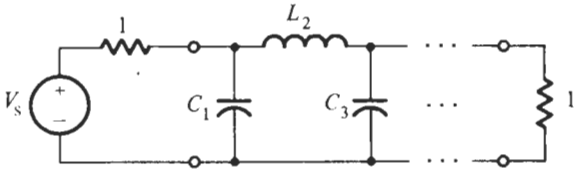

n	C_1	L_2	C_3	L_4	C_5	L_6	C_7	L_8	C_9	L_{10}
2	1.414	1.414								
3	1.000	2.000	1.000							
4	0.7654	1.848	1.848	0.7654						
5	0.6180	1.618	2.000	1.618	0.6180					
6	0.5176	1.414	1.932	1.932	1.414	0.5176				
7	0.4450	1.247	1.802	2.000	1.802	1.247	0.4450			
8	0.3902	1.111	1.663	1.962	1.962	1.663	1.111	0.3902		
9	0.3473	1.000	1.532	1.879	2.000	1.879	1.532	1.000	0.3473	
10	0.3129	0.9080	1.414	1.782	1.975	1.975	1.782	1.414	0.9080	0.3129

n	L_1	C_2	L_3	C_4	L_5	C_6	L_7	C_8	L_9	C_{10}

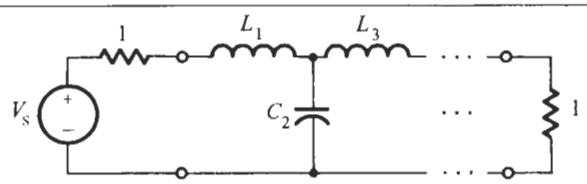

EXAMPLE 13.1

To be designed is a fifth-order *LC* filter having a maximally flat passband with $\alpha_{max} = 0.7$ dB in $f \leq f_p = 460$ kHz. Source and load resistors are 50 Ω.

Solution

Let us choose a minimum-inductance ladder so that the first and last elements are capacitors.[1] From Table 13.1 we find the circuit in Fig. 13.7a. From Eq. (6.40) we obtain $\varepsilon = \sqrt{10^{0.07} - 1} = 0.4182$ so that

$$\omega_B = \varepsilon^{-1/5}\omega_p = 1.191 \times 2\pi \times 4.6 \times 10^5 = 3.44 \text{ Mrad/s}$$

[1]This is, as a rule, a good choice to make quite apart from reducing the number of bulky, expensive, and less than ideal inductors (inductors are more lossy than capacitors), because it places capacitors at the input and output nodes where they can be used to "absorb" parasitic capacitors associated with source and load connections.

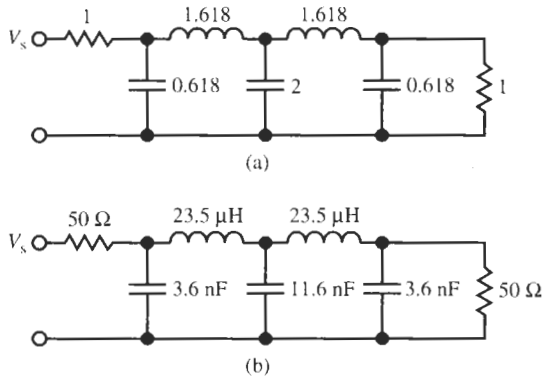

Figure 13.7 The normalized (a) and denormalized (b) fifth-order *LC* lowpass filter of Example 13.1.

With these numbers, we denormalize the resistors by multiplying by 50 Ω, and the inductors and the capacitors, respectively, by multiplying by

$$50\ \Omega/3.44\ \text{Mrad/s} = 14.5\ \mu\text{H} \quad \text{and} \quad 1/(50\ \Omega \times 3.44\ \text{Mrad/s}) = 5.81\ \text{nF}$$

Figure 13.7b shows the final circuit.

Comparing the two coupling circuits of Fig. 13.5 we notice again that the impedances of the two circuits have reciprocal relationships and are said to be duals of each other. Observe that one has two inductors and one capacitor and the other has one inductor and two capacitors. Since the two realizations are completely equivalent, there may be some basis for choice depending on whether inductors or capacitors are most easily obtained. One is called the minimum-capacitance realization and the other the minimum-inductance realization. These properties hold in general as illustrated by Table 13.2. The last elements are different, depending on whether n is even or odd. Of the two realizations, one will always be minimum inductance and the other minimum capacitance.

There are many other interesting properties of ladder circuits that are discussed in advanced treatises on the subject. The general problem of finding a ladder realization is not as simple as

TABLE 13.2 Doubly Terminated Lossless Ladders

	Minimum Inductance	Minimum Capacitance
n even	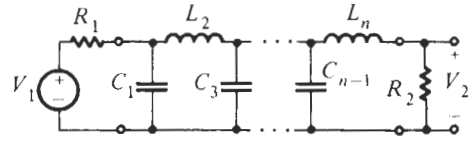	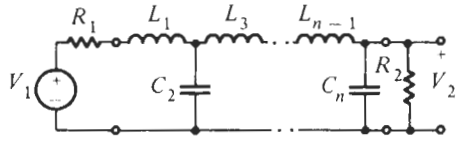
n odd	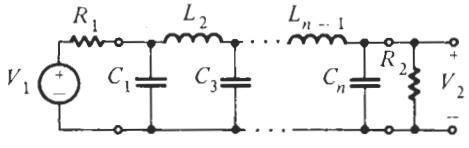	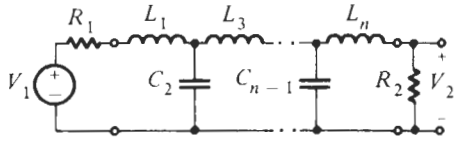

might be suggested by the special case of Butterworth filters. We will discuss the main aspects of the topic in Section 13.4. Also in some cases the lossless terminated circuit is found only by including ideal transformers in the realization. Often it is possible to realize different values of R_1 and R_2, and sometimes it is not possible to find a circuit with equal terminations without an ideal transformer. The next example will illustrate the case of unequal termination.

EXAMPLE 13.2

Consider the realization of a filter with a Butterworth response for which $n = 3$, $R_1 = 1$, and $R_2 = 2$. ·

Solution

From Eq. (13.3b) we see that

$$H^2(0) = 4 \times \frac{2}{9} = \frac{8}{9}$$

Then we have

$$|\rho(j\omega)|^2 = 1 - \frac{8/9}{1+\omega^6} = \frac{\omega^6 + 1/9}{1+\omega^6}$$

and

$$\rho(s)\rho(-s) = \frac{(s^3 + 1/3)(-s^3 + 1/3)}{(s^3 + 2s^2 + 2s + 1)(-s^3 + 2s^2 - 2s + 1)}$$

so that

$$\rho(s) = \frac{s^3 + 1/3}{s^3 + 2s^2 + 2s + 1}$$

From this we find with Eq. (13.24):

$$Z_{\text{in}}(s) = \frac{2s^2 + 2s + 2/3}{2s^3 + 2s^2 + 2s + 4/3}$$

The continued fraction expansion of this function gives

$$Z_{\text{in}} = \cfrac{1}{s + \cfrac{1}{1.5s + \cfrac{1}{2s + \cfrac{1}{0.5}}}} \tag{13.43}$$

The circuit realizations of this impedance and its reciprocal are shown in Fig. 13.8. The circuit in Fig. 13.8a must be taken because $R_2 = 2$ was prescribed.

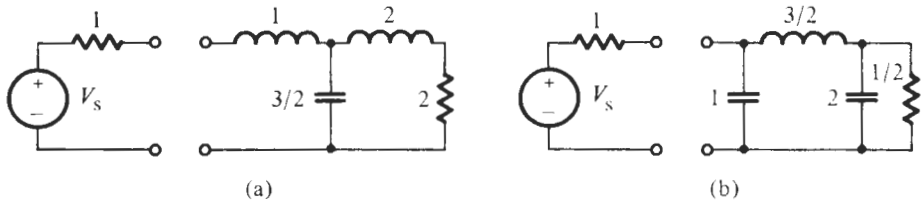

Figure 13.8 (a, b) The two possible realizations of Eq. (13.43). Here (a) must be taken because the problem prescribes $R_2 = 2$.

13.3 TABLES FOR OTHER RESPONSES

In the last section we introduced the notion of generating tables for the *LC* filter elements. We did this for the Butterworth response to arrive at Table 13.1 for degrees $n = 2$ to $n = 10$; tables for larger values of n can be found in the literature (Zverev, 1967). Table 13.1 was derived for equal terminating resistors $R_1 = R_2 = 1$ and the half-power frequency $\omega = 1$, where the magnitude was normalized such that $|H(j0)| = 1$ or $\alpha(0) = 0$ dB. After appropriate scaling of impedance level and frequency [see Eq. (13.42)], Table 13.1 can be used not just for the design of Butterworth filters, but for any filter with maximally flat magnitude response.

The development was based on the availability of the magnitude-squared $|H(j\omega)|^2$ of an all-pole transfer function $H(s)$, and since $|H(j\omega)|^2$ is available for many other types of all-pole responses, the general procedure of the previous section can be applied to any of them. Thus, we can determine the *LC* ladder for many different types of magnitude responses. For example, we know the transfer functions for maximally flat or equal-ripple delay filters from Chapter 10, and tables with the inductors and capacitors of lossless Bessel and equal-ripple delay filters of order n are obtained in precisely the same way as for Butterworth responses. They are available for the design of lossless delay filters. Also, we know from Chapter 7 that the Chebyshev response has the form[2]

$$|H(j\omega)|^2 = \frac{1}{1 + \varepsilon^2 C_n^2(\omega)} \tag{13.44}$$

and falls into this category. Whereas for Butterworth and Bessel–Thomson filters we had just one parameter, the degree n, to be concerned with, Eq. (13.44) reminds us that the Chebyshev response must be tabulated not only for different values of n, but also for some factor that is equivalent to ε, usually $\alpha_{\max}$. This makes tabulating the information for Chebyshev filters more complex than it was for the maximally flat response where the information about $\alpha_{\max}$ could simply be taken care of by frequency scaling, Eq. (13.42). Table 13.3 is typical of Chebyshev response tables: the passband ripple $\alpha_{\max} = 0.1$ dB is used with n ranging from 2 to 8, and $\alpha_{\max} = 0.5$ and 1.0 dB for $n = 3$, 5, and 7. Observe that $R_2 \neq 1$ for even values of n because $H(0)$ is given by the specified ripple width, and $H(0) \neq 1$ if n is even. It can be shown (Sedra and Brackett, 1978; Schaumann et al., 1990) that in this case

$$R_2 = \left(1 + 2\varepsilon^2 \pm 2\varepsilon\sqrt{1 + \varepsilon^2}\right) R_1 \tag{13.45}$$

[2] Recall that the difference between $H(s)$ and the voltage transfer function $T(s)$ we used earlier is only a constant multiplier with no other effect on the frequency response.

TABLE 13.3 Chebyshev Lowpass Element Values (1-rad/s Bandwidth)

n	C_1	L_2	C_3	L_4	C_5	L_6	C_7	L_8	R_2
				(A) Ripple Width = 0.1 dB					
2	0.84304	0.62201							0.73781
3	1.03156	1.14740	1.03156						1.00000
4	1.10879	1.30618	1.77035	0.81807					0.73781
5	1.14681	1.37121	1.97500	1.37121	1.14681				1.00000
6	1.16811	1.40397	2.05621	1.51709	1.90280	0.86184			0.73781
7	1.18118	1.42281	2.09667	1.57340	2.09667	1.42281	1.18118		1.00000
8	1.18975	1.43465	2.11990	1.60101	2.16995	1.58408	1.94447	0.87781	0.73781
				(B) Ripple Width = 0.5 dB					
3	1.5963	1.0967	1.5963						1.0000
5	1.7058	1.2296	2.5408	1.2296	1.7058				1.0000
7	1.7373	1.2582	2.6383	1.3443	2.6383	1.2582	1.7373		1.0000
				(C) Ripple Width = 1.0 dB					
3	2.0236	0.9941	2.0236						1.0000
5	2.1349	1.0911	3.0009	1.0911	2.1349				1.0000
7	2.1666	1.1115	3.0936	1.1735	3.0936	1.1115	2.1666		1.0000
n	L_1'	C_2'	L_3'	C_4'	L_5'	C_6'	L_7'		R_2

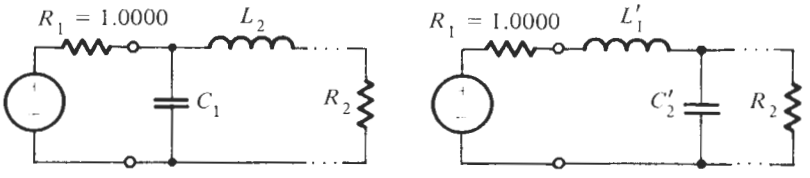

where the two values R_{21} and R_{22} for the two signs are related by $R_{21}R_{22} = R_1^2$. Either one of the values may be taken in the design.

If the needed filter parameters are not listed in the table, such as, e.g., $\alpha_{max} = 0.3$ dB, or $n = 6$ for $\alpha_{max} = 0.5$ dB, we can follow the procedures outlined for the Butterworth response to derive the required circuit elements. Another alternative is to make use of explicit formulas that have been developed for the Butterworth and the Chebyshev cases (Sedra and Brackett, 1978; Schaumann et al., 1990). These formulas may be used to expand existing tables or to derive new ones.

We saw early in our study of filter functions that more efficient realizations of attenuation requirements could be achieved by placing transmission zeros at finite frequencies in the stopband, rather than using all-pole filters with zeros only at infinity. For instance, in Chapter 8 we learned that the Cauer (or elliptic) form of response was significantly more efficient, meaning of lower degree, in realizing a desired magnitude than alternative approaches. The Cauer filter allows us to specify independently three of the four parameters, maximum passband attenuation α_{max} (or ε), minimum stopband attenuation α_{min}, the degree n, and the width of the transition band. Consequently, tables for the design of Cauer filters are more difficult to develop and are far more complex because a filter must be identified by three parameters. Nevertheless, design algorithms have been devised, making extensive use of the computer, and tables are available for the designer to consult when developing lossless Cauer filters (Saal, 1974; Zverev, 1969).

13.4 GENERAL LADDER DESIGN METHODS

In this book we will not study in detail the design strategies leading to Cauer filters, or generally to *LC* ladder filters with finite transmission zeros, but we shall briefly point out the principal steps involved in the process. This will facilitate our access to the literature and help us understand the design tables. Also, it will allow us to undertake simple designs ourselves when an appropriate table is not available. The procedure through which general ladder filters are generated is known as the *Cauer ladder development*. Significant features of Cauer circuits are illustrated in Fig. 13.9. The circuits are developed in such a way that parallel resonance circuits in a series branch, as shown in Fig. 13.9a, or series resonant circuit in a shunt branch, as shown in Fig. 13.9b, produce the required zeros of transmission at prescribed frequencies, marked ω_{z1} and ω_{z2} in the figure. Such impedances and admittances take the form of Eq. (13.7) and lead to transmission zeros as was shown in Eq. (13.8). The challenge is to find a ladder realization that generates these resonant circuits at the specified frequencies.

With all-pole transfer functions, $H(s) = K/D(s)$, the procedure discussed in Section 13.2 led to a function that we could expand into a continued fraction to obtain the element values of an impedance Z_{in} with a single resistor at the output. We now have a transfer function that is a ratio of polynomials, $H(s) = N(s)/D(s)$. Although in this case the synthesis process is more involved, it starts in the same way as for the all-pole case in Section 13.2. The method is not difficult but involves considerable algebraic detail. We will explain it next.

We need to find the reflection coefficient $\rho(s)$ that was determined from the specified transfer function in Eq. (13.21):

$$|\rho(j\omega)|^2 = 1 - |H(j\omega)|^2 = 1 - \frac{|N(j\omega)|^2}{|D(j\omega)|^2} \tag{13.46}$$

This expression we bring on a common denominator:

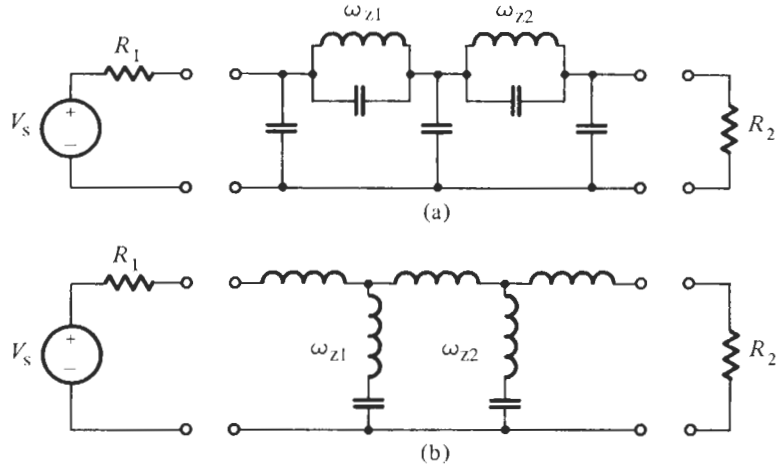

Figure 13.9 Cauer ladders: transmission zeros realized by (a) impedance poles in the series branches; (b) impedance zeros in the shunt branches.

$$|\rho(j\omega)|^2 = \frac{|D(j\omega)|^2 - |N(j\omega)|^2}{|D(j\omega)|^2} = \frac{|F(j\omega)|^2}{|D(j\omega)|^2} \tag{13.47}$$

and observe first that $\rho(s)$ has the same denominator $D(s)$ as the transfer function $H(s)$. We have given the even polynomial $|D(j\omega)|^2 - |N(j\omega)|^2$ the new name $|F(j\omega)|^2$. Finally, as we did a number of times in the past, we extend the expression from the $j\omega$-axis onto the s-plane and factor the result:

$$|\rho(j\omega)|^2\big|_{j\omega=s} = \rho(s)\rho(-s) = \left.\frac{|F(j\omega)|^2}{|D(j\omega)|^2}\right|_{j\omega=s} = \frac{F(s)F(-s)}{D(s)D(-s)} \tag{13.48}$$

Thus, we have obtained the reflection coefficient

$$\rho(s) = \pm\frac{F(s)}{D(s)} \tag{13.49}$$

$F(s)$, the so-called *reflection zero* polynomial, has roots where the reflection coefficient $\rho(s)$ is zero. By Eq. (13.46) these zeros are at the points of perfect transmission where $|H(j\omega)| = 1$, i.e., on the $j\omega$-axis in the passband. Therefore, apart from the $(\pm)$ uncertainty in sign, $F(s)$ is uniquely determined from the *even* polynomial $|F(j\omega)|^2$. Also, $D(s)$ is uniquely determined, either from the known denominator of $H(s)$ or by collecting all the left half-plane roots of $|D(j\omega)|^2$. Since $\rho(s)$ is known, we can determine the impedance Z_{in}. This was accomplished in Eqs. (13.24) and (13.25):

$$Z_{\text{in}}(s) = R_1\left[\frac{1-\rho(s)}{1+\rho(s)}\right]^{\pm 1} \tag{13.50}$$

or, with Eq. (13.49):

$$Z_{\text{in}}(s) = R_1\frac{D(s) \mp F(s)}{D(s) \pm F(s)} \tag{13.51}$$

Z_{in} is the input impedance of the *LC* ladder terminated in the resistor R_2. Our next goal is to find the circuit elements of the ladder structure such that the prescribed transfer function $H(s)$ is realized and the input impedance is Z_{in}. We will understand readily that the simple continued-fraction expansion employed in Section 13.2 will generally not be useful: it generates only individual capacitors and inductors in the shunt and series branches of the ladder, but not the resonance circuits with resonances at specified transmission zero frequencies as in Fig. 13.9. Another approach is called for.

13.4.1 The Twoport Parameters

To proceed, it is helpful first to separate the resistive terminations so that we can deal with only the lossless elements of the *LC* coupling network. To do this, we describe the lossless ladder in Fig. 13.10 by its two-port parameters, the *open-circuit impedance parameters*,

$$V_1 = z_{11}(s)I_1 + z_{12}(s)I_2 \tag{13.52}$$

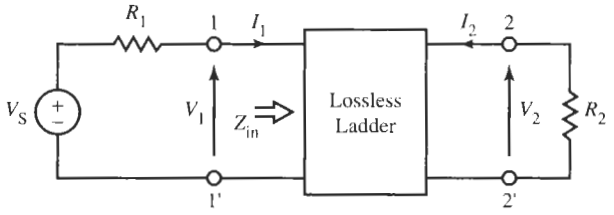

Figure 13.10 Lossless twoport with input and output voltages and currents identified.

$$V_2 = z_{21}(s)I_1 + z_{22}(s)I_2 \tag{13.53}$$

or the *short-circuit admittance parameters*

$$I_1 = y_{11}(s)V_1 + y_{12}(s)V_2 \tag{13.54}$$

$$I_2 = y_{21}(s)V_1 + y_{22}(s)V_2 \tag{13.55}$$

From elementary circuits courses we recall that

$z_{11}(s) = (V_1/I_1)|_{I_2=0}$ is the open-circuit input impedance at port 1–1′, that is, the impedance measured into the input terminals 1–1′ when the output 2–2′ is an open circuit, i.e., $I_2 = 0$.

$z_{12}(s) = (V_1/I_2)|_{I_1=0}$ is the backward open-circuit transfer impedance; it tells us which voltage V_1 is generated at the open-circuited ($I_1 = 0$) terminals 1–1′ by an input current I_2 at the terminals 2–2′.

$z_{21}(s) = (V_2/I_1)|_{I_2=0}$ is the forward open-circuit transfer impedance; it tells us which voltage V_2 is generated at the open-circuited ($I_2 = 0$) terminals 2–2′ by an input current I_1 at the terminals 1–1′.

$z_{22}(s) = (V_2/I_2)|_{I_1=0}$ is the open-circuit input impedance at port 2–2′, that is, the impedance measured into the terminals 2–2′ when the terminals 1–1′ are an open circuit, i.e., $I_1 = 0$.

The currents I_1 and I_2 are assumed to flow *into* the lossless twoport as shown in Fig. 13.10. We still remark that for passive circuits $z_{12} = z_{21}$. Note that the input impedance Z_{in} identified in Fig. 13.10 includes the termination resistor R_2 and, therefore, is *not* the same as z_{11} for which the output terminals are open.

The analogous definitions hold for the short-circuit admittance parameters, e.g.,

$y_{11}(s) = (I_1/V_1)|_{V_2=0}$ is the short-circuit input admittance at port 1–1′, that is, the admittance measured into the input terminals 1–1′ when the output 2–2′ is a short circuit, i.e., $V_2 = 0$.

and similarly for the other terms. Again, $y_{12} = y_{21}$ for passive circuits. Finally note that $y_{11} \neq 1/z_{11}$ because the output is a short circuit for y_{11} whereas it is an open circuit for z_{11}. Thus, the two parameters are derived from two different circuits.

Let us deal with the z-parameters in the following. To find the voltage transfer function we compute from Fig. 13.10 with Eqs. (13.52) and (13.53):

$$V_S = R_1 I_1 + V_1 = (R_1 + z_{11})\, I_1 + z_{12} I_2 \quad \text{and} \quad V_2 = -R_2 I_2 = z_{12} I_1 + z_{22} I_2$$

From these two equations we find after a few steps the voltage ratio

$$T(s) = \frac{V_2}{V_S} = \frac{z_{12}R_2}{(R_1 + z_{11})(R_2 + z_{22}) - z_{12}^2} \tag{13.56}$$

or, by Eq. (12.55),

$$H(s) = \frac{N(s)}{D(s)} = 2\sqrt{\frac{R_1}{R_2}}\frac{V_2}{V_S} = \frac{\sqrt{4R_1R_2}z_{12}}{(R_1 + z_{11})(R_2 + z_{22}) - z_{12}^2} \tag{13.57}$$

Also, the input impedance can be obtained from Eqs. (13.52) and (13.53) as

$$Z_{\text{in}} = \frac{V_1}{I_1} = \frac{z_{11}R_2 + z_{11}z_{22} - z_{12}^2}{z_{22} + R_2} \tag{13.58}$$

We have now determined the transfer function and the input impedance as functions of the termination resistors and the z-parameters of the *LC* circuit. Our aim is the inverse of these relationships: we wish to identify a realizable set of z-parameters from the specified transfer function $H(s) = N(s)/D(s)$ (and the prescribed termination resistors R_1 and R_2). To accomplish this goal we follow a method due to S. Darlington (1939).

By Eq. (13.51), numerator and denominator polynomials of Z_{in} are determined from the known transfer function, and we next split them into their even parts, m_i, and odd parts, n_i, $i = 1, 2$. Taking the upper sign[3] in Eq. (13.51) we obtain

$$Z_{\text{in}}(s) = R_1\frac{D(s) - F(s)}{D(s) + F(s)} = R_1\frac{m_1(s) + n_1(s)}{m_2(s) + n_2(s)} \tag{13.59}$$

This result we equate with Eq. (13.58),

$$Z_{\text{in}}(s) = R_1\frac{m_1 + n_1}{m_2 + n_2} = \frac{z_{11}R_2 + z_{11}z_{22} - z_{12}^2}{z_{22} + R_2} \tag{13.60}$$

From this equation we need to identify the parameters z_{ij}, $i, j = 1, 2$, that describe the lossless twoport. To help in this task we bring Eq. (13.60) into the form

$$Z_{\text{in}}(s) = R_1\frac{m_1}{n_2}\frac{1 + n_1/m_1}{1 + m_2/n_2} = z_{11}\frac{1 + \left(z_{11}z_{22} - z_{12}^2\right)/(R_2z_{11})}{1 + z_{22}/R_2} \tag{13.61}$$

After this step we can formally identify

$$z_{11} = R_1\frac{m_1}{n_2}, \quad z_{22} = R_2\frac{m_2}{n_2}, \quad \text{and} \quad \frac{z_{11}z_{22} - z_{12}^2}{z_{11}} = R_2\frac{n_1}{m_1}$$

If we insert the first two of these equations into the last one, we obtain

$$z_{12} = \sqrt{R_1R_2}\frac{\sqrt{m_2m_1 - n_1n_2}}{n_2}$$

[3] The lower sign results simply in the reciprocal impedance.

Finally, note from Eq. (13.57) that the transmission zeros of the transfer function $H(s)$, that is the roots of $N(s)$, should also be the zeros of $z_{12}(s)$. Indeed, if we substitute the equations for z_{11}, z_{22}, and z_{12} into Eq. (13.57) we obtain $N(s) = \sqrt{m_2 m_1 - n_1 n_2}$. Consequently, our job of identifying the z-parameters of the lossless network is complete:

$$z_{11} = R_1 \frac{m_1}{n_2}, \quad z_{22} = R_2 \frac{m_2}{n_2}, \quad z_{12} = \sqrt{R_1 R_2}\frac{N(s)}{n_2} \tag{13.62}$$

A few comments are necessary concerning the properties of z-parameters. We will only state them and leave the proofs for more advanced treatises.

1. It is reassuring that all three z-parameters have the same denominator polynomial $n_2(s)$ because, being network functions of the same circuit, they must, of course, have the same poles.
2. $z_{11}(s)$ and $z_{22}(s)$ are *odd* rational functions; as a matter of fact it is possible to prove that they are *reactance functions* of the type discussed in Section 9.5 and, therefore, are realizable *LC* impedances.
3. For Eq. (13.62) to represent a physically realizable set of z-parameters, $z_{12}(s)$ must also be an *odd* rational function. This implies that the transmission zero polynomial $N(s)$ must be even [as, e.g., in Eq. (13.8)].

Point 3 suggests that we need to find a solution for the case when $N(s)$ is odd. Fortunately, the problem is solved easily by bringing Eq. (13.60) into the form

$$Z_{\text{in}}(s) = R_1 \frac{n_1}{m_2}\frac{1 + m_1/n_1}{1 + n_2/m_2} = z_{11}\frac{1 + \left(z_{11}z_{22} - z_{12}^2\right)/\left(R_2 z_{11}\right)}{1 + z_{22}/R_2} \tag{13.63}$$

instead of that of Eq (13.61). In complete analogy to Eq. (13.62) we then obtain by the same process as before

$$z_{11} = R_1 \frac{n_1}{m_2}, \quad z_{22} = R_2 \frac{n_2}{m_2}, \quad z_{12} = \sqrt{R_1 R_2}\frac{N(s)}{m_2} \tag{13.64}$$

and we see that all the parameters are odd rational functions and have the same poles. Darlington has shown that the parameters derived in Eqs. (13.62) and (13.64) are realizable sets of z-parameters.

Starting from equations that express the transfer function H and the input impedance Z_{in} in terms of the short-circuit admittance parameters, we can readily show that a completely analogous procedure leads to a realizable set of y-parameters. All parameters are given in Table 13.4.

TABLE 13.4 z- and y-Parameters of a Lossless Coupling Network Describing the Input Impedance $Z_{\text{in}} = (m_1 + n_1)/(m_2 + n_2)$; m_i Is Even, n_i Is Odd

$N(s)$	z_{11}/R_1	z_{22}/R_2	$z_{12}/\sqrt{R_1 R_2}$	$y_{11}R_1$	$y_{22}R_2$	$-y_{12}\sqrt{R_1 R_2}$
Even	m_1/n_2	m_2/n_2	N/n_2	m_2/n_1	m_1/n_1	N/n_1
Odd	n_1/m_2	n_2/m_2	N/m_2	n_2/m_1	n_1/m_1	N/m_1

It remains for us to find a realization procedure for the lossless twoport coupling network. Before doing that, let us present an example that illustrates how to derive the z- and y-parameters from a given transfer function.

EXAMPLE 13.3

To be realized is the transfer function

$$|H(j\omega)|^2 = \frac{(3.2^2 - \omega^2)^2}{(3.2^2 - \omega^2)^2 + 10.4176\omega^6} \tag{13.65}$$

as an *LC* filter terminated in two equal resistors $R_1 = R_2 = R = 1.2$ kΩ. The frequency is normalized with respect to 60 kHz. We wish to find the open-circuit impedance parameters.

Solution

First we observe that Eq. (13.65) describes a lowpass filter with a transmission zero at $f_z = 3.2 \times 60$ kHz $= 182$ kHz. According to Eq. (6.54), the filter has a maximally flat magnitude with $\alpha_{max} = 0.5$ dB as can be seen by evaluating $H(j1)$.

Next we convert the leading coefficient in the denominator of $|H(j\omega)|^2$ to unity for convenience in the following development,

$$|H(j\omega)|^2 = \frac{0.0960\,(3.2^2 - \omega^2)^2}{\omega^6 + 0.0960\,(3.2^2 - \omega^2)^2} \tag{13.66}$$

and obtain from Eq. (13.46),

$$|\rho(j\omega)|^2 = 1 - |H(j\omega)|^2 = 1 - \frac{0.0960\,(3.2^2 - \omega^2)^2}{\omega^6 + 0.0960\,(3.2^2 - \omega^2)^2}$$

$$= \frac{\omega^6}{\omega^6 + 0.0960\,(3.2^2 - \omega^2)^2}$$

and, with $\omega^2 = -s^2$,

$$\rho(s)\rho(-s) = \frac{-s^6}{-s^6 + 0.0960\,(3.2^2 + s^2)^2}$$

We next employ a root finder, and group the left half-plane poles into $\rho(s)$. Using the plus sign in Eq. (13.49), we have

$$\rho(s) = \frac{F(s)}{D(s)} = \frac{s^3}{s^3 + 2.8507s^2 + 4.0152s + 3.1725}$$

and from Eq. (13.51) the desired input impedance:

$$Z_{\text{in}}(s) = R_1 \frac{D(s) - F(s)}{D(s) + F(s)} = R_1 \frac{2.8507s^2 + 4.0152s + 3.1725}{2s^3 + 2.8507s^2 + 4.0152s + 3.1725}$$

Proceeding with Eq. (13.60) we have

$$Z_{\text{in}}(s) = R_1 \frac{m_1 + n_1}{m_2 + n_2} = R_1 \frac{2.8507s^2 + 4.0152s + 3.1725}{2s^3 + 2.8507s^2 + 4.0152s + 3.1725}$$

that is,

$$m_1 = 2.8507s^2 + 3.1725, \quad n_1 = 4.0152s$$
$$m_2 = 2.8507s^2 + 3.1725, \quad n_2 = 2s^3 + 4.0152s$$

From Table 13.4, this gives us the z- and y-parameters. Notice that $m_1 = m_2$ so that $z_{11} = z_{22}$: the network is symmetrical. We note also from Eq. (13.66) that $N(s) = 0.3098(s^2 + 3.2^2)$ is even, so that from Table 13.4 we obtain with $R_1 = R_2 = R$,

$$\frac{z_{11}}{R} = \frac{z_{22}}{R} = \frac{2.8507s^2 + 3.1725}{2s^3 + 4.0152s} = \frac{1.4254\left(s^2 + 1.0549^2\right)}{s\left(s^2 + 1.4169^2\right)} \tag{13.67a}$$

and, with Eq. (13.66):

$$\frac{z_{12}}{R} = \frac{N(s)}{n_2} = \frac{0.3098\left(s^2 + 3.2^2\right)}{2s^3 + 4.0152s} = \frac{0.1549\left(s^2 + 3.2^2\right)}{s\left(s^2 + 1.4169^2\right)} \tag{13.67b}$$

Similarly, we find from Table 13.4:

$$y_{11}R = y_{22}R = \frac{2.8507s^2 + 3.1725}{4.0152s} = 0.7100\frac{s^2 + 1.0549^2}{s} \tag{13.68a}$$

$$-y_{12}R = \frac{0.3098\left(s^2 + 3.2^2\right)}{4.0152s} = 0.07716\frac{s^2 + 3.2^2}{s} \tag{13.68b}$$

Observe that z_{11}, z_{22}, y_{11}, and y_{22} each has alternating poles and zeros as in Fig. 9.32. z_{12} and y_{12} are transfer functions, not impedances or admittances, and their poles and zeros need not alternate, although the functions must be odd.

13.4.2 Immittance Synthesis

To understand how we might proceed with designing the *LC* ladder let us first discuss how an *LC* impedance or admittance is realized. A common name that refers to both impedance and admittance is *immittance*. Because the algebra for the design becomes quite involved, let us consider a low-order case, specifically the third-order admittance

$$Y(s) = \frac{ks\left(s^2 + \beta^2\right)}{s^2 + \alpha^2} \tag{13.69}$$

where $0 < \alpha < \beta$ because poles and zeros must alternate. This simple case will be sufficient for showing us what to do; higher order functions are treated analogously, but the aid of a computer will generally be necessary as the order increases. We learned earlier that such a

function can be expanded into a continued fraction as in Eq. (13.41) to identify the elements. An alternative method expands the function into *partial fractions*:

$$Y(s) = \frac{ks\left(s^2+\beta^2\right)}{s^2+\alpha^2} = ks + \frac{k\left(\beta^2-\alpha^2\right)s}{s^2+\alpha^2} = ks + \frac{k_0 s}{s^2+\alpha^2} \tag{13.70}$$

We introduced the abbreviation $k_0 = k(\beta^2 - \alpha^2)$. Note that $k_0 > 0$ because $\beta > \alpha$. A partial fraction expansion shows explicitly all the poles of the immittance; in this case there is a pole at infinity contributing the term ks, and the pair of poles at $\pm j\alpha$. The coefficients k and k_0 are called the *residues* of the poles.

The circuit realization of Eq. (13.70) is shown in Fig. 13.11: Y consists of a capacitor $C_1 = k$ connected in parallel with a series resonant circuit comprising a capacitor $C_2 = k_0/\alpha^2$ and an inductor $L_2 = 1/k_0$. Evidently, we have created a resonant circuit whose resonance is at $\alpha = 1/\sqrt{L_2 C_2}$. If we place this resonant circuit across the signal path in the ladder, just as Y_7 in Fig. 12.11, signals at the frequency α would be blocked.

LC impedances and their reciprocals, *LC* admittances, satisfy the same properties, so either one can be used for the realization. To realize an immittance means we need to find positive elements and their interconnections so that the circuit can be built. As a general rule, when realizing an *LC* immittance, always expand the function around the poles, which are then subtracted or *removed* from the function to leave a simpler remainder. Once all poles have been removed, the remainder is zero and the realization is complete. An example will illustrate the process and the different ways with which an *LC* impedance can be realized. It is important for us to understand these methods before we undertake ladder design.

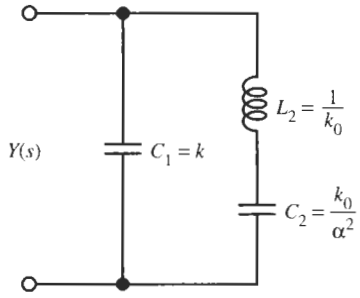

Figure 13.11 Circuit realization of Eq. (13.70).

EXAMPLE 13.4

Realize the *LC* admittance

$$Y(s) = \frac{\left(s^2+1\right)\left(s^2+9\right)\left(s^2+25\right)}{s\left(s^2+4\right)\left(s^2+16\right)} \tag{13.71}$$

Solution

Note that the function is odd and that poles (at $0, \pm j2, \pm j4, \infty$) and zeros (at $\pm j1, \pm j3, \pm j5$) are simple and alternate along the $j\omega$-axis as depicted in Fig. 9.32. Clearly, the analogous observations can be made about the impedance

$$Z(s) = \frac{1}{Y(s)} = \frac{s\left(s^2+4\right)\left(s^2+16\right)}{\left(s^2+1\right)\left(s^2+9\right)\left(s^2+25\right)} \tag{13.72}$$

which, therefore, is also realizable. Since these functions are odd, at $\omega = 0$ and at $\omega = \infty$ there will always be either a pole or a zero.

Consider first the expansion of Y of Eq. (13.71) in partial fractions: we have to consider a term for each pole, keeping conjugate complex poles together,

$$Y(s) = k_\infty s + \frac{k_0}{s} + \frac{k_1 s}{s^2+4} + \frac{k_2 s}{s^2+16} \tag{13.73}$$

To determine the value k_∞ we divide Eq. (13.73) by s and let $s \to \infty$. Then the last three terms on the right-hand side of Eq. (13.73) go to zero and we have

$$k_\infty = \left.\frac{Y(s)}{s}\right|_{s\to\infty} = \left.\frac{\left(s^2+1\right)\left(s^2+9\right)\left(s^2+25\right)}{s^2\left(s^2+4\right)\left(s^2+16\right)}\right|_{s\to\infty} = 1$$

To find k_0 we multiply Eq. (13.73) by s and let $s \to 0$ to obtain

$$sY(s)|_{s=0} = k_0 = \frac{1\times 9\times 25}{4\times 16} = 3.5156$$

To find k_1 we perform

$$\left.\frac{\left(s^2+4\right)Y(s)}{s}\right|_{s^2=-4} = k_1 = \frac{(-4+1)(-4+9)(-4+25)}{-4(-4+16)} = 6.5625$$

Finally, k_2 is computed from

$$\left.\frac{\left(s^2+16\right)Y(s)}{s}\right|_{s^2=-16} = k_2 = \frac{(-16+1)(-16+9)(-16+25)}{-16(-16+4)} = 4.9219$$

Then we have generated the expansion

$$\begin{aligned} Y(s) &= s + \frac{3.5156}{s} + \frac{6.5625s}{s^2+4} + \frac{4.9219s}{s^2+16} \\ &= s + \frac{1}{0.2844s} + \frac{1}{0.1525s + \dfrac{1}{1.6406s}} + \frac{1}{0.2032s + \dfrac{1}{0.3076s}} \end{aligned} \tag{13.74}$$

Figure 13.12a shows the realization. It is obtained by observing that admittances in parallel add and that $1/Y$ is an impedance and impedances in series add.

Treating next the impedance of Eq. (13.72) we form a partial fraction expansion in a similar fashion

$$Z(s) = \frac{1}{Y(s)} = \frac{s\left(s^2+4\right)\left(s^2+16\right)}{\left(s^2+1\right)\left(s^2+9\right)\left(s^2+25\right)} = \frac{k_1 s}{s^2+1} + \frac{k_2 s}{s^2+9} + \frac{k_3 s}{s^2+25}$$

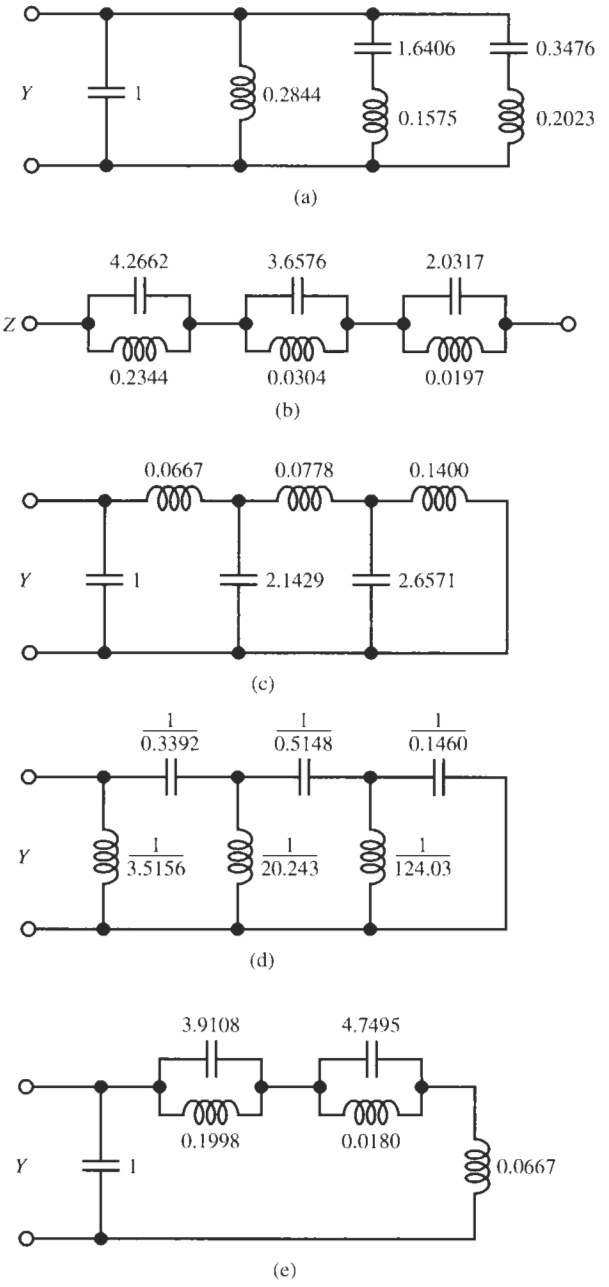

Figure 13.12 Five (a–e) equivalent realizations of the admittance of Eq. (13.71).

We obtain k_1 from

$$k_1 = \frac{s^2 + 1}{s} Z(s)|_{s^2=-1} = \frac{3 \times 15}{8 \times 24} = 0.2344$$

and similarly for k_2 and k_3. The result is the expansion

$$Z(s) = \frac{0.2344s}{s^2+1} + \frac{0.2734s}{s^2+9} + \frac{0.4922s}{s^2+25}$$

$$= \cfrac{1}{4.2662s + \cfrac{1}{0.2344s}} + \cfrac{1}{3.6576s + \cfrac{1}{0.0304s}} + \cfrac{1}{2.0317s + \cfrac{1}{0.0197s}} \tag{13.75}$$

The circuit is given in Fig. 13.12b; it shows explicitly all impedance poles where $Z = \infty$, i.e., the network becomes an open circuit, whereas the realization in Fig. 13.12a showed the admittance poles, $Y = \infty$, where the network is a short circuit.

We can also express the admittance in Eq. (13.71) as a ratio of polynomials,

$$Y(s) = \frac{(s^2+1)(s^2+9)(s^2+25)}{s(s^2+4)(s^2+16)} = \frac{s^6+35s^4+259s^2+225}{s^5+20s^3+64s} \tag{13.76}$$

and subtract (or "remove") the pole at infinity, then invert the remainder, remove the pole at $\omega = \infty$, invert the remainder, and so forth, until all poles are removed and the remaining function is zero. This leads to

$$Y(s) = s + \cfrac{1}{\cfrac{s^5+20s^3+64s}{15s^4+195s^2+225}} = s + \cfrac{1}{0.0667s + \cfrac{1}{\cfrac{15s^4+195s^2+225}{7s^3+49s}}}$$

$$= s + \cfrac{1}{0.0667s + \cfrac{1}{2.1429s + \cfrac{1}{\cfrac{7s^3+49s}{90s^2+225}}}}$$

and so on, until

$$Y(s) = s + \cfrac{1}{0.0667s + \cfrac{1}{2.1429s + \cfrac{1}{0.0778s + \cfrac{1}{2.6571s + \cfrac{1}{0.1400s}}}}} \tag{13.77}$$

We recognize this expression as the continued fraction expansion we dealt with before: it is obtained by long division of the polynomial of higher order by the polynomial of lower order, starting the division from the highest powers. The circuit is shown in Fig. 13.12c.

Alternatively, we could remove the pole at $\omega = 0$, invert the remainder, remove the pole at $\omega = 0$, invert the remainder, etc., until the process is completed. This is accomplished by a continued long division starting from the lowest order terms and results in

$$Y(s) = \frac{225+259s^2+35s^4+s^6}{64s+20s^3+s^5} = \frac{3.5156}{s} + \cfrac{1}{\cfrac{64s+20s^3+s^5}{188.69s^2+31.4844s^4+s^6}}$$

$$= \frac{3.5156}{s} + \cfrac{1}{\cfrac{0.3392}{s} + \cfrac{1}{\cfrac{188.69s^2 + 31.4844s^4 + s^6}{9.3211s^3 + s^5}}}$$

and so on, until finally we have

$$Y(s) = \frac{3.5156}{s} + \cfrac{1}{\cfrac{0.3392}{s} + \cfrac{1}{\cfrac{20.2433}{s} + \cfrac{1}{\cfrac{0.5148}{s} + \cfrac{1}{\cfrac{124.025}{s} + \cfrac{1}{\cfrac{0.1460}{s}}}}}} \quad (13.78)$$

Figure 13.12d shows this circuit. Similar expansions can be obtained for the impedance in Eq. (13.72) giving us two more circuits to realize the same V/I ratio or I/V ratio. All these circuits are equivalent, in that they realize the same voltage-to-current relationship at the input terminals.

Naturally, if desired we may mix the realization procedures. For example, starting from the admittance in Eq. (13.76) we can expand the function as

$$Y(s) = s + \frac{1}{\dfrac{s^5 + 20s^3 + 64s}{15s^4 + 195s^2 + 225}} = s + \frac{1}{\dfrac{s\left(s^2 + 4\right)\left(s^2 + 16\right)}{15\left(s^2 + 1.2798\right)\left(s^2 + 11.7204\right)}}$$

$$= s + \cfrac{1}{\cfrac{0.2557s}{s^2 + 1.2798} + \cfrac{0.0667s^3 + 0.9923s}{s^2 + 11.7204}}$$

$$= s + \cfrac{1}{\cfrac{0.2557s}{s^2 + 1.2798} + \cfrac{0.2105s}{s^2 + 11.7204} + 0.0667s}$$

$$= s + \cfrac{1}{\cfrac{1}{3.9108s + \cfrac{1}{0.1998s}} + \cfrac{1}{4.7495s + \cfrac{1}{0.0180s}} + 0.0667s}$$

This realization is shown in Fig. 13.12e. Notice that all circuits have the same number of elements, six, and the same number of inductors, three each, and capacitors, three each. The number of elements is equal to the degree of the function; the realizations are said to be *canonic*. Note that although the implementations realize the same immittance, with the same number of components, the element values are different so there may be practical reasons to choose one over the other, for example, to obtain smaller component ratios C_{max}/C_{min} or L_{max}/L_{min}.

Summarizing the synthesis of *LC* immittances, we observe that regardless of the algorithms used, continued fraction expansion, partial fraction expansion, or a mixture of the two, the process always concentrates on the poles, removing one pole or pole-pair at a time until the remaining function is zero and the realization is complete.

13.4.3 Ladder Development

We are now ready to employ this realization procedure to design the lossless ladder, starting from the z- or y-parameters. We shall illustrate the method on the parameters derived in Example 13.3, but a number of questions arise that must be answered first:

1. We derived both the z- and the y-parameters describing the circuit. Which ones should we take to realize the ladder? The short answer is: Take the set that has the higher degree. The reasoning for this choice can be found in Schaumann et al. (1990). In Example 13.3, we take the z-parameters in Eq. (13.67).
2. We know by now how to realize an input immittance of an LC circuit so we know how to handle z_{11} or z_{22}. But in the LC ladder design procedure we need to realize all three prescribed parameters, z_{11}, z_{22}, and z_{12}, simultaneously. How can this be done? The answer is: We realize z_{11} *or* z_{22}, whichever is of higher degree, and pay attention that the specified transmission zeros, i.e., the factors of the numerator of z_{12}, are realized in the process. The method proceeds by following a sequence of *partial pole removal–zero shifting–complete pole removal*, which will be discussed next. If the algorithm is carried out correctly, the third parameter, say z_{22} after we realized z_{11} and z_{12}, is realized automatically as prescribed.
3. We know that transmission zeros ω_{zi} in a ladder are obtained from parallel resonance circuits in the series branches of the ladder or series resonance circuits in shunt branches, but z_{11} (or z_{22}) have no information on the prescribed locations ω_{zi}. How can z_{11} (or z_{22}) be realized such that these transmission zeros are obtained? The answer again is the *partial pole removal–zero shifting–complete pole removal* procedure to be discussed next.

To understand the process, let us return to the low-order case of Eq. (13.70) and consider the imaginary part $B(\omega)$ of the admittance $Y(j\omega) = G(\omega) + jB(\omega)$. We know that the real part is zero because the function is odd, so we have

$$jB(\omega) = \frac{j\omega k\left(\beta^2 - \omega^2\right)}{\alpha^2 - \omega^2} = j\left(k\omega + \frac{k_0\omega}{\alpha^2 - \omega^2}\right) \tag{13.79}$$

In this equation, we had $k_0 = k(\beta^2 - \alpha^2)$. Figure 13.13 contains a plot of $B(\omega)$ versus ω, showing the zeros at 0 and β and the poles at α and at ∞. By removing the pole at $\omega = \infty$ *completely*, that is, by subtracting the term $k\omega$ from Eq. (13.79), we are left with the remainder

$$B_1(\omega) = B(\omega) - k\omega = \frac{k_0\omega}{\alpha^2 - \omega^2} \tag{13.80}$$

We can make some important observations: the function B_1 no longer has a pole at $\omega = \infty$: after all, we removed the pole *completely*, so instead B_1 has a zero at $\omega = \infty$ because at $\omega = \infty$ there must be either a pole or a zero. Also we note that the pole at α has not changed, neither has the zero at the origin, but the zero at β disappeared along with the pole at infinity.

Now note what happens when we remove the pole only *partially*. By *partial pole removal* we mean that a term $k'\omega$ with $k' < k$ is subtracted from Eq. (13.79). Figure 13.13 shows that in that case the function still has a pole at $\omega = \infty$, in addition to the unchanged pole at α and the zero at 0, but the zero at β has *shifted* to a new location closer to infinity, the point from where we removed the pole partially. If we express this operation mathematically, we obtain the equation

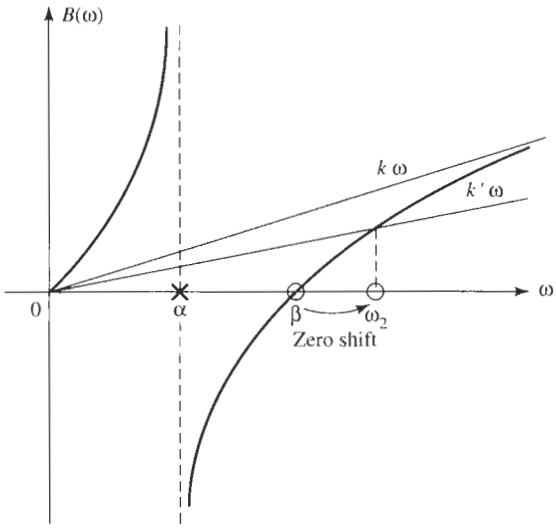

Figure 13.13 Plot of the imaginary part $B(\omega)$, Eq. (13.79), of the third-order admittance of Eq. (13.70). Subtracting the asymptotic line $k\omega$ from $B(\omega)$ corresponds to a *complete* pole removal. Subtracting the line $k'\omega$ with $k' < k$ removes the pole only *partially* and leaves a remainder function of the same degree, but with the zero shifted from β to ω_z.

$$B_2(\omega) = B(\omega) - k'\omega = (k - k')\omega + \frac{k_0\omega}{\alpha^2 - \omega^2}$$
$$= \frac{\omega(k - k')\left(\alpha^2 + \dfrac{k_0}{k - k'} - \omega^2\right)}{\alpha^2 - \omega^2} \tag{13.81}$$

Evidently, the function B_2 is still of third order, has poles at infinity and at α, a zero at the origin, and the zero at β shifted to the new location

$$\omega_z = \sqrt{\alpha^2 + \frac{k_0}{k - k'}} = \sqrt{\alpha^2 + k\frac{\beta^2 - \alpha^2}{k - k'}} = \sqrt{\beta^2 + \frac{k'}{k - k'}\left(\beta^2 - \alpha^2\right)} \tag{13.82}$$

From this equation we see clearly that ω_z increases as the value of k' comes closer to k, i.e., as an increasing fraction of the residue k is removed. Specifically, $\omega_z > \beta$ if $k' > 0$ and $\omega_z \to \infty$ as $k' \to k$, the case of complete pole removal. Because zeros and poles must alternate along the $j\omega$-axis and the poles (here, one at α) do not move, we may conclude that a *zero cannot shift across a pole.*

This behavior is our clue on how to make progress with the ladder synthesis. We proceed as follows: If, say, z_{11} has a pole at $\omega = \infty$, that is $z_{11}(s)|_{s\to\infty} = ks$, we remove that pole *partially*, $z_{11}(s) - k's$, to generate a zero at the prescribed location ω_z. The necessary algebra is simple: we only need to make the equation $z_{11}(s) - k's = 0$ at $\omega = \omega_z$, that is, we obtain k' from the equation

$$k' = \left.\frac{z_{11}(s)}{s}\right|_{s^2=-\omega_z^2} \tag{13.83}$$

Then the remaining function $z_1 = z_{11} - k's$ will have zeros at $\pm j\omega_z$. Next, we take the inverse $1/z_1$ to create poles at $\pm j\omega_z$. Realizing these poles *completely* generates a resonant circuit whose resonance frequency results in the desired transmission zero.

An important observation is called for at this point: for the process to work properly the pole or poles that were removed *partially* to generate specified zeros *must* in the end be removed *completely*. This will guarantee that the immittance parameter at the other port, say z_{22} if we started the realization with z_{11}, is automatically realized correctly.

This procedure, as stated with partial pole removals at $s = \infty$, will work for those cases in which an immittance zero must be shifted to higher frequencies. Recall that a zero shifts toward the location from where the pole was partially removed. If a zero must be shifted to lower frequencies, the procedure is analogous, but is modified by removing a pole partially *at the origin*, $s = 0$. Indeed, it can be shown that it is always possible to shift zeros of an immittance to the specified transmission zeros so that the procedure is general. Let us continue Example 13.3 by completing the synthesis procedure of the immittance parameters of a desired *LC* ladder. It will illustrate the steps involved in the realization.

EXAMPLE 13.5

Find the lossless twoport specified in Example 13.3.

Solution

We mentioned already that the twoport parameters of higher order must be used. For our case, they are the impedance parameters of Eq. (13.67). Let us choose $R = 1$ and worry about the denormalization later. We have:

$$z_{11} = z_{22} = \frac{2.8507s^2 + 3.1725}{2s^3 + 4.0152s} = \frac{1.4254(s^2 + 1.0549^2)}{s(s^2 + 1.4169^2)} \tag{13.84a}$$

$$z_{12} = \frac{s^2 + 3.2^2}{2s^3 + 4.0152s} = \frac{0.1549(s^2 + 3.2^2)}{s(s^2 + 1.4169^2)} \tag{13.84b}$$

We will find it very helpful to generate a sketch of the pole-zero patterns of all the functions involved in the design process, and to mark on this plot the partial and complete pole removals and the shifting of zeros. It generates a "road map" to guide us through the synthesis problem step by step. Figure 13.14a shows the pole-zero diagrams for the z-parameters in Eq. (13.84). The top line is the pole-zero diagram[4] for z_{12} showing in particular the transmission zero at 3.2 we are required to realize; the next line is the corresponding diagram for z_{11} with the same poles as the ones of z_{12} but with poles and zeros alternating as required. Since the zero at 1.05 cannot be shifted across the pole location at 1.42, we are apparently stuck. However, we recall from the presentation in Example 13.4 that we may choose to realize either the impedance or the admittance without affecting the circuit's behavior. Let us, therefore, consider implementing the admittance $y_1 = 1/z_{11}$. Its pole-zero diagram is in the third line in Fig. 13.14a, where the positions of poles and zeros are simply interchanged from the z_{11}-line. We see that now the

[4]Sketched is the positive ω-axis only with a pole at $+1.42$ and a zero at $+3.2$. The functions are odd so that the negative ω-axis with a pole at -1.42 and a zero at -3.2 contains no new information. Removal of an "internal" pole at ω_0 with $0 < \omega_0 < \infty$ is, therefore, considered as removing the two poles at $\pm\omega_0$.

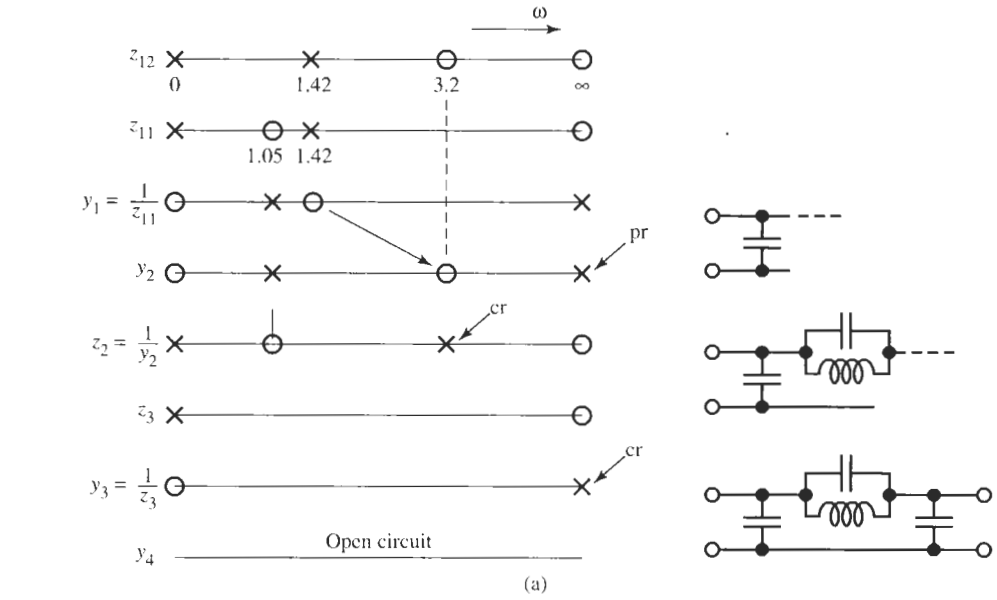

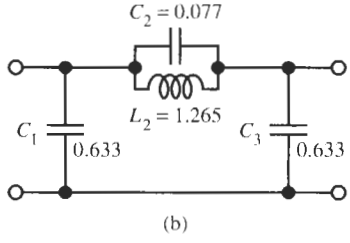

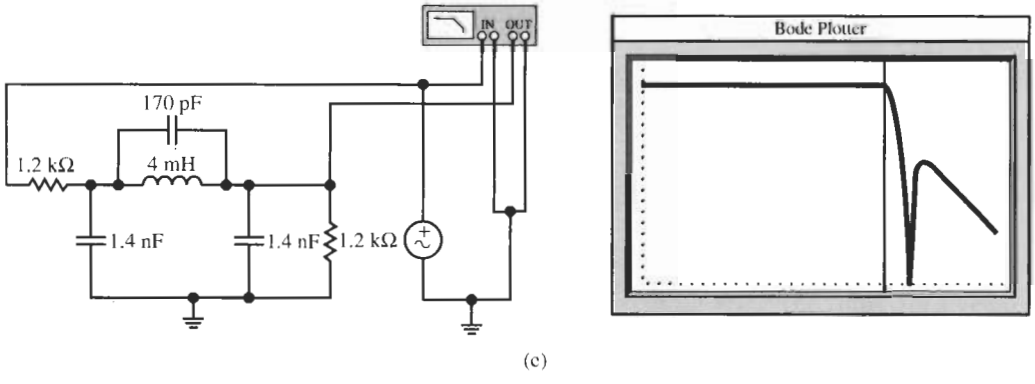

Figure 13.14 (a) Pole-zero diagrams for the z-parameters in Eq. (13.84) and for all immittances that occur during the realization process (cr, complete removal; pr, partial removal). The right shows how the circuit develops as more poles are removed. (b) Normalized circuit. (c) Final lossless ladder and test performance. (Bode Plotter scales: 1 Hz to 10 MHz; −80 to 0 dB; cursor at 61.05 kHz, −6.553 dB.)

zero at 1.42 can be shifted to the required location at 3.2 if we remove the pole at $\omega = \infty$ partially by an appropriate amount. To do this we form according to Eq. (13.83),

$$k' = \left.\frac{y_1(s)}{s}\right|_{s^2=-3.2^2} = \frac{-3.2^2 + 1.4169^2}{1.4254\left(-3.2^2 + 1.0549^2\right)} = 0.6330$$

and subtract $0.6330s$ from $y_1(s) = 1/z_{11}(s)$. This gives us the first element, a shunt capacitor $C_1 = 0.633$, and results in the remainder function y_2:

$$y_2 = y_1 - 0.6330s = \frac{0.0688s\left(s^2 + 3.2^2\right)}{s^2 + 1.0549^2}$$

Notice that we obtained the zeros at $\pm j3.2$ as intended. Next we invert y_2 into $z_2 = 1/y_2$ to create poles at $\pm j3.2$ and find the partial fraction expansion as explained in Example 13.4:

$$z_2 = \frac{s^2 + 1.0549^2}{0.0688s\left(s^2 + 3.2^2\right)} = \frac{12.955s}{s^2 + 3.2^2} + \frac{1}{0.6330s} = z + \frac{1}{0.6330s}$$

This expansion shows both the poles at $\pm j3.2$ at the pole at 0. We then remove the poles at $\pm j3.2$ completely by subtracting z from z_2. The parallel resonance circuit

$$z = \frac{12.955s}{s^2 + 3.2^2} = \frac{1}{0.0772s + \dfrac{1}{1.2651s}}$$

consists of a capacitor $C_2 = 0.077$ and an inductor $L_2 = 1.265$ (see Fig. 13.14a, line 5). The remainder, $z_3 = 1/(0.6330s)$, has a pole at the origin and a zero at infinity.

Since we still have to realize the second transmission zero (at $\omega = \infty$), but we have no immittance pole at that frequency, we have to invert z_3 to generate a pole at infinity,

$$y_3 = 1/z_3 = 0.6330s$$

and remove this pole completely to realize the zero as required (Fig. 13.14a, line 7). This step completes the realization because the remaining function is a zero admittance, i.e., an open circuit. Notice that for this last step no partial pole removal–zero shifting was required because we had already a pole at the right location. This last complete pole removal also satisfies the requirement of a complete pole removal at $\omega = \infty$ to complement the earlier partial removal of that pole in Step 1 of our synthesis process. Figure 13.14b shows the final circuit. Note that the circuit is symmetrical, so that $z_{11} = z_{22}$, as specified. This verifies that z_{22} was realized correctly.

Lastly, we need to denormalize the elements to meet the specifications in Example 13.3. We multiply the capacitors by $1/(1.2\ \text{k}\Omega \times 2\pi \times 60\ \text{krad/s}) = 2.21$ nF, the inductor by $1.2\ \text{k}\Omega/(2\pi \times 60\ \text{krad/s}) = 3.183$ mH, and the resistors by 1.2 kΩ. The denormalized LC filter and test results are shown in Fig. 13.14c.

Let us address two additional concerns:

1. Since z_{12} is a function of the same network as z_{11}, it is clear that both functions have the same poles, and we also made sure that z_{12} has the correct zeros. But a polynomial is not completely specified by its zeros; there is also a constant multiplier that must be realized.

For instance, the function z_{12} in our example had the numerator $0.1549(s^2 + 3.2^2)$ and we paid no attention to the factor 0.1549 that determines the gain realized by the circuit. So the gain constant may not be accurate. Indeed, this observation is correct, and the procedure described, in general, may not realize a prescribed gain correctly. Although this is generally not a large problem since incorrect frequency-independent gain can always be corrected with an amplifier, the engineer will certainly want to know the value of the gain constant that was realized.

Because we are concerned only with a frequency-independent gain constant, the realized gain can easily be computed by evaluating the obtained circuit at one convenient frequency, usually $\omega = 0$ or $\omega = \infty$, and then comparing the result with the prescribed gain in z_{12}. In our case, a simple evaluation is performed at $\omega = 0$: we have from Eq. (13.84b)

$$\text{prescribed: } z_{12}|_{s\to 0} = \left.\frac{0.1549\,(s^2 + 3.2^2)}{s\,(s^2 + 1.4169^2)}\right|_{s\to 0} = \frac{0.1549\,(3.2^2)}{s\,(1.4169^2)} = \frac{1}{1.266s}$$

For $s \to 0$ the inductor L_2 in the realized circuit in Fig. 13.14b shorts out the series capacitor C_2 so that the two capacitors C_1 and C_3 of value 0.633 remain in parallel, for a total capacitor $C = 1.266$ across the ladder. This gives

$$\text{realized: } z_{12}|_{s\to 0} = \left.\frac{V_1}{I_2}\right|_{s\to 0} = \frac{1}{s\,(C_1 + C_3)} = \frac{1}{1.266s}$$

So, since realized and prescribed z_{12} are the same in our example, the realization is exact, including the gain constant.

2. Notice that our realization is not canonic: it used four components for a third-order transfer function. The reason is that we removed a pole first partially, costing us one component, and then completely, at the expense of a second component for the same pole. As can be seen readily, the general *LC* ladder development is not canonic; it costs one additional element for each partial pole removal.

   However, even if four elements were used in our realization, it is of course not of fourth order. Notice that it has three capacitors in a loop so that one capacitor voltage does not add a degree of freedom in the circuit: the voltages are constrained by $V_{C1} + V_{C2} + V_{C3} = 0$ and, therefore, are not independent.

A summary of the design process for lossless ladders is contained in Table 13.5. The procedure will work for almost all filter requirements of practical importance. The resulting circuit has one of the two structures shown in Fig. 13.9, possibly a combination of the two. The ladder development for all-pole functions in Section 13.2 is a special case of the general design procedure given here: since in the all-pole case, transmission zeros are at infinity, they are realized directly by series inductors or shunt capacitors; no partial pole removals are necessary and the realization is canonic.

We have emphasized in Table 13.5 that transmission zeros are realized only by complete pole removals, whereas partial removals do not contribute to the generation of zeros. Considering the circuit in Fig. 13.14b, this point may need an explanation because at

TABLE 13.5 *LC* Ladder Design Procedure

1. From design tables or by solving the approximation problem, find the transfer function $H(s)$ or its magnitude $|H(j\omega)|$.
2. Compute the reflection coefficient $\rho(s)$ by Eqs. (13.46) to (13.49):

$$|\rho(j\omega)|^2 = 1 - |H(j\omega)|^2 = \frac{|F(j\omega)|^2}{|D(j\omega)|^2}$$

$$\rho(s) = \pm\frac{F(s)}{D(s)}$$

3. Find the input impedance $Z_{in}(s)$ of the doubly terminated *LC* ladder by Eq. (13.51) with specified termination resistors. Determine the even and odd parts of the numerator and denominator polynomials of $Z_{in}(s)$, Eq. (13.59):

$$Z_{in}(s) = R_1\frac{D(s) - F(s)}{D(s) + F(s)} = R_1\frac{m_1(s) + n_1(s)}{m_2(s) + n_2(s)}$$

4. Use Table 13.4 to determine the z- or y-parameters. Select the set that is of higher order, and in the chosen set select the immittance function that has the highest degree.
5. Draw a pole-zero diagram of the chosen immittance parameters. Realize the input immittance of highest degree (z_{11} or z_{22}, or as the case may be, y_{11} or y_{22}) such that the transmission zeros are implemented by partial pole removal—zero shifting—complete pole removal. Refer to Example 13.5 for details. Note that a transmission zero is *not* realized by a partial pole removal, but only by a complete pole removal. Complete the realization of one transmission zero at a time until all the required zeros are implemented; note that *all* the zeros of a case of multiple zeros must be realized.[a] Be certain that any partially removed pole is later removed completely.
6. Check the realized gain constant, if required, by evaluating the final circuit at a convenient frequency, usually $\omega = 0$ or $\omega = \infty$.

[a] For example, a third-order Butterworth filter has three transmission zeros at infinity. Thus, a zero at infinity must be realized three times, see Eq. (13.41) and Fig. 13.5, where the series inductor and the two shunt capacitors each realizes one of these zeros.

$\omega = \infty$ both C_1 and C_3 create a short circuit across the signal path and appear to block signals from reaching the output. There is, however, a fundamental difference between the action of these two capacitors: C_1 removes the pole at $\omega = \infty$ only *partially* whereas C_3 removes it *completely*. Figure 13.15 illustrates the difference. The circuit to the right of C_1 is still a short circuit (has an admittance pole) at $\omega = \infty$ so that the input current I_0 at node n_1 splits between two short circuits and $I_2 \neq 0$. We have in effect a capacitive current divider: labeling as Y_1 and Y_2, respectively, the admittances in the paths of I_1 and I_2,

$$Y_1 = sC_1, \quad Y_2 = \frac{1}{Z_2} = \frac{1}{1/sC_2 + 1/(sC_3 + G_2)}$$

we obtain by current division

$$\frac{I_2}{I_0} = \frac{Y_2}{Y_1 + Y_2} = \frac{1}{1 + Y_1Z_2} = \frac{1}{1 + sC_1\,[1/sC_2 + 1/\,(sC_3 + G_2)]}$$

which for $s \to \infty$ is not zero:

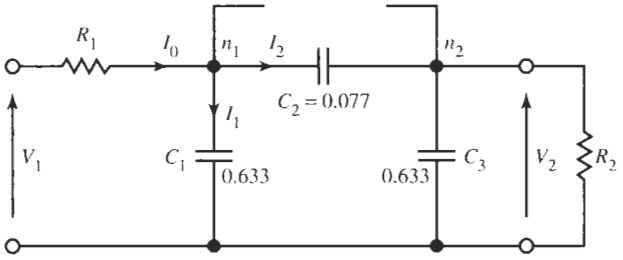

Figure 13.15 The asymptotic ladder of Fig. 13.14b for $\omega \to \infty$. (The inductor L_2 is an open circuit at infinite frequencies.)

$$I_2 = \frac{C_2C_3}{C_2C_3 + C_1(C_3 + C_2)} I_0 = 0.0978 I_0$$

This fraction of the input current I_0 flows toward the output node n_2 and generates the voltage

$$V_2 = \frac{0.0978}{sC_3 + G_2} I_0$$

and $V_2(\infty) = 0$. By completely removing of the pole at infinity, C_3 creates the specified zero at $\omega = \infty$.

13.5 FREQUENCY TRANSFORMATION

We studied the concept of frequency transformation in considerable detail in Chapter 9, so that our treatment here can be brief. In Chapter 9 we outlined the main use for such transformations, the conversion of one transfer function type into another. Normally, we transform a bandpass, highpass, band-rejection, or other filter requirement into a lowpass prototype specification where simple formulas and/or design tables are available to facilitate the derivation of the lowpass prototype function. This function is then transformed back into the other type of transfer function (bandpass, highpass, etc.) where the circuit design is completed. Since in this chapter we are interested in transforming *LC* filters, let us concentrate on the relevant ideas and design solutions.

Exactly as in Chapter 9, we can transform the required filter specifications from the bandpass, highpass, or other type of transfer characteristic, the "target filter," into a lowpass prototype specification where the transfer function can be found. In our study of active filters, we then transformed the lowpass function $T_L(S)$ from the S-domain into the function of the target filter $T(s)$, i.e., of the highpass, bandpass, or other type of function. We did this by replacing the lowpass frequency S by the appropriate transformation equation, $Z(s)$ of Eqs. (9.77) to (9.84), which we derived in Chapter 9 for different types of target filters. $T(s)$ is then realized by any of the methods we studied so far.

In contrast to this approach that had to be used for active filters, a simpler method is available for *LC* filters. We do not need to construct the transfer function $T(s)$ of the target filter, but can complete the design process of the *LC* filter in the lowpass domain, S, as discussed in earlier sections of this chapter. This results in the inductors L_i with the impedances SL_i and the capacitors C_j whose admittances are SC_j, and their interconnections. In the normalized lowpass prototype circuit, we then replace the element immittances

$$Z_L = SL \quad \text{by} \quad LZ(s) \quad \text{and} \quad Y_C = SC \quad \text{by} \quad CZ(s) \tag{13.85}$$

Since we saw that the function $Z(s)$ is realizable as an LC impedance or as an LC admittance, both Z_L and Y_C are LC immittances in the s domain and our task is complete. We can interpret this operation as transforming the realized circuit from a lowpass filter to the target filter, rather than transforming the lowpass function into the target function, which only then is realized. The transformations of the normalized components L and C are given in Fig. 13.16. With the entries of this figure, the design of different types of transmission requirements becomes very straightforward as we shall show with the help of a couple of examples.

Eq.	9.81	9.82	9.89	9.90	9.91	9.92
	LP	HP	BP	BE	Double Passband	Double Passband
Z	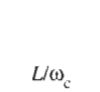		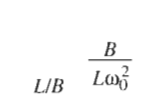	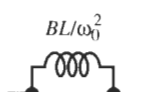		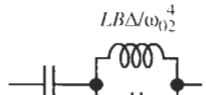
Y	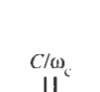		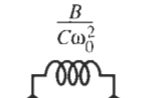	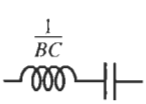	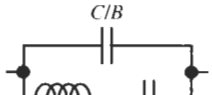	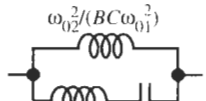

Figure 13.16 Transformations of the lowpass immittances L and C to ladder arms for highpass, bandpass, band-reject, and multiple-passband filters. The components are normalized with respect to $R = 1\ \Omega$. *Note:* $\Delta = \omega_{02}^2 - \omega_{01}^2$.

EXAMPLE 13.6

To be designed is a highpass filter as a lossless ladder. The magnitude must have a Butterworth response with a 3-dB cut-off frequency of $\omega_c = 3.3$ Mrad/s ($f_c = 525$ kHz). The attenuation increase toward low frequencies should be at least 60 dB per decade. Source and load resistors are $R = 300\Omega$.

Solution

The roll-off of 60 dB per decade requires $n = 3$. The components of a third-order Butterworth lowpass filter are available in Table 13.1 (or we may go directly to Fig. 13.5). Because the lowpass-to-highpass transformation converts Ls to Cs and vice versa, let us take the minimum-capacitance ladder so that after the transformation we obtain a minimum-inductance ladder. The circuit is repeated in Fig. 13.17a. This is the normalized lowpass filter, with cut-off frequency $\omega = 1$ and $R_1 = R_2 = 1$. From Fig. 13.16, column HP, after including the impedance-level

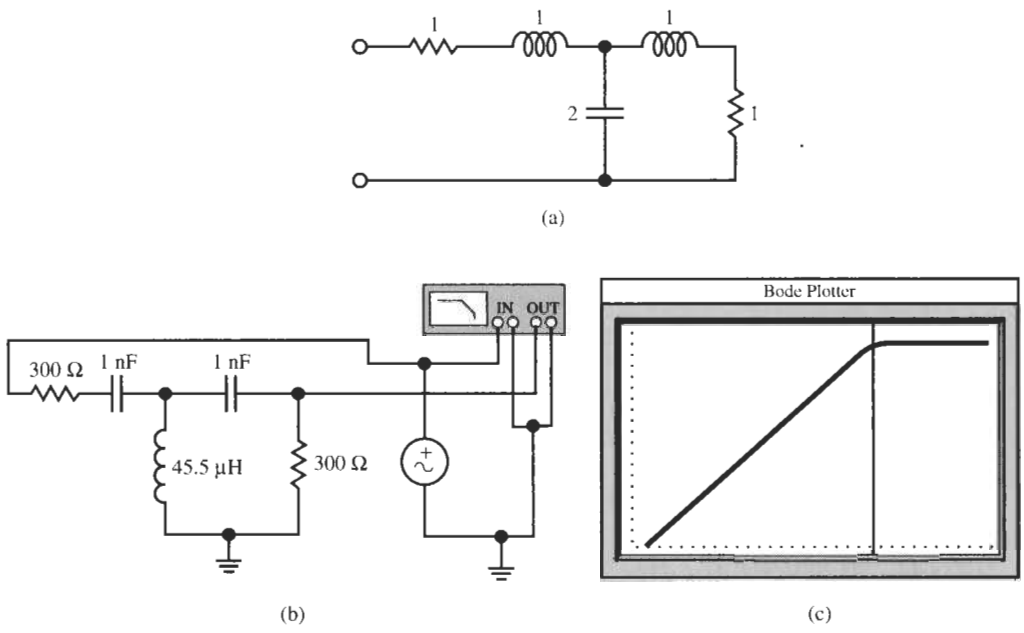

Figure 13.17 (a) Third-order Butterworth lowpass prototype *LC* ladder; (b) third-order highpass filter and test performance. (Bode Plotter scales: 1 kHz to 10 MHz; −160 to 0 dB; cursor at 524.8 kHz, −9.077 dB.)

denormalization, we learn that the following replacements must be made to transform the prototype lowpass:

$$L_{1,\mathrm{LP}} = L_{3,\mathrm{LP}} = 1 \Rightarrow C_{1,\mathrm{HP}} = C_{3,\mathrm{HP}} = \frac{1}{RL_{1,\mathrm{LP}}\omega_c} = \frac{1}{300\ \Omega \times 1 \times 3.3\mathrm{Mrad/s}} = 1.01\mathrm{nF}$$

$$C_{2,\mathrm{LP}} = 2 \Rightarrow L_{2,\mathrm{HP}} = \frac{R}{C_{2,\mathrm{LP}}\omega_c} = \frac{300\ \Omega}{2 \times 3.3\mathrm{Mrad/s}} = 45.45\mu\mathrm{H}$$

The highpass circuit and test results are shown in Fig. 13.17b. Notice the cut-off frequency is at $f_c = 525$ kHz as specified. (The gain at f_c is −9 dB because the doubly terminated *LC* filter has an intrinsic attenuation of 6 dB.) The roll-off toward low frequencies is −60 dB per decade.

EXAMPLE 13.7

Design an *LC* bandpass ladder filter for the following specifications:

Source and load resistors: 50 Ω

Attenuation increase at high frequencies: 20 dB per decade

Passband center frequency: 230 kHz

Maximally flat passband with 0.5-dB bandwidth of 28 kHz

Transmission zero at 279 kHz

Solution

First we determine the frequency transformation to convert the bandpass specifications into those of a prototype lowpass. Let us normalize the frequency axis by $\omega_n = 2\pi$ krad/s; then we have from Eq. (9.18a) the transformation

$$S = \frac{1}{B}\frac{s^2 + \omega_0^2}{s} = \frac{1}{28}\frac{s^2 + 230^2}{s} \tag{13.86}$$

Because the frequency transformation results in a geometrically symmetrical filter, with $f_1 f_2 = 230^2$ and $f_2 - f_1 = 28$ we find the passband corners at $f_1 = 216.43$ and $f_2 = 244.43$. These two bandedges are transformed into the points $\Omega = -1$ and $\Omega = +1$ on the lowpass frequency axis:

$$\frac{1}{28}\frac{216.43^2 - 230^2}{216.43} = -1, \quad \frac{1}{28}\frac{244.43^2 - 230^2}{244.43} = +1$$

The transmission zero at 279 kHz is transformed into the point $\Omega = 3.2$. Because of the symmetry, the filter will produce a second transmission zero at $230^2/279 = 189.6$, which becomes $\Omega = -3.2$ on the lowpass frequency axis.

Since the numerator of the lowpass prototype has a factor $(S^2 + 3.2^2)$ and the high-frequency attenuation increase is specified as 20 dB per decade, the degree of the lowpass function must be $n = 3$. The required third-order maximally flat lowpass function with $\alpha_{\max} = 0.5$ dB we encountered in Example 13.3, Eq. (13.66):

$$|H(j\Omega)|^2 = \frac{0.0960\left(3.2^2 - \Omega^2\right)^2}{\Omega^6 + 0.0960\left(3.2^2 - \Omega^2\right)^2} \tag{13.87}$$

so that the realization is known from Example 13.5: the normalized lowpass prototype circuit was given in Fig. 13.14b. It is repeated for ease of reference in Fig. 13.18a.

We next have to apply the frequency transformation of Eq. (13.86) for which we consult Fig. 13.16, column BP. Accordingly, using Eq. (9.85), we need to replace capacitors C_1 and C_3 by parallel LC resonance circuits:

$$C_1 = C_3 = 0.633 \;\Rightarrow\; SC_1 = \frac{C_1}{B}\frac{s^2 + \omega_0^2}{s} = \frac{C_1}{B}s + \frac{\omega_0^2 C_1/B}{s} \tag{13.88}$$

Thus, we have the capacitors and inductors in branches 1 and 3:

$$C_{11} = C_{31} = \frac{C_1}{B} \times \frac{1}{R} = \frac{0.633}{2\pi \times 28000} \times \frac{1}{50\ \Omega} = 71.96\text{nF}$$

$$L_{11} = L_{31} = \frac{B}{\omega_0^2 C_1} \times R = \frac{28 \times 50\ \Omega\text{s}}{230 \times 2\pi \times 230000 \times 0.633} = 6.654\ \mu\text{H}$$

Note that by Eq. (13.86) all LC branches have the same resonance frequency ω_0. Therefore, these two components resonate at the passband center: 230 kHz. Similarly we obtain for the series capacitor C_2 the parallel LC circuit with the elements

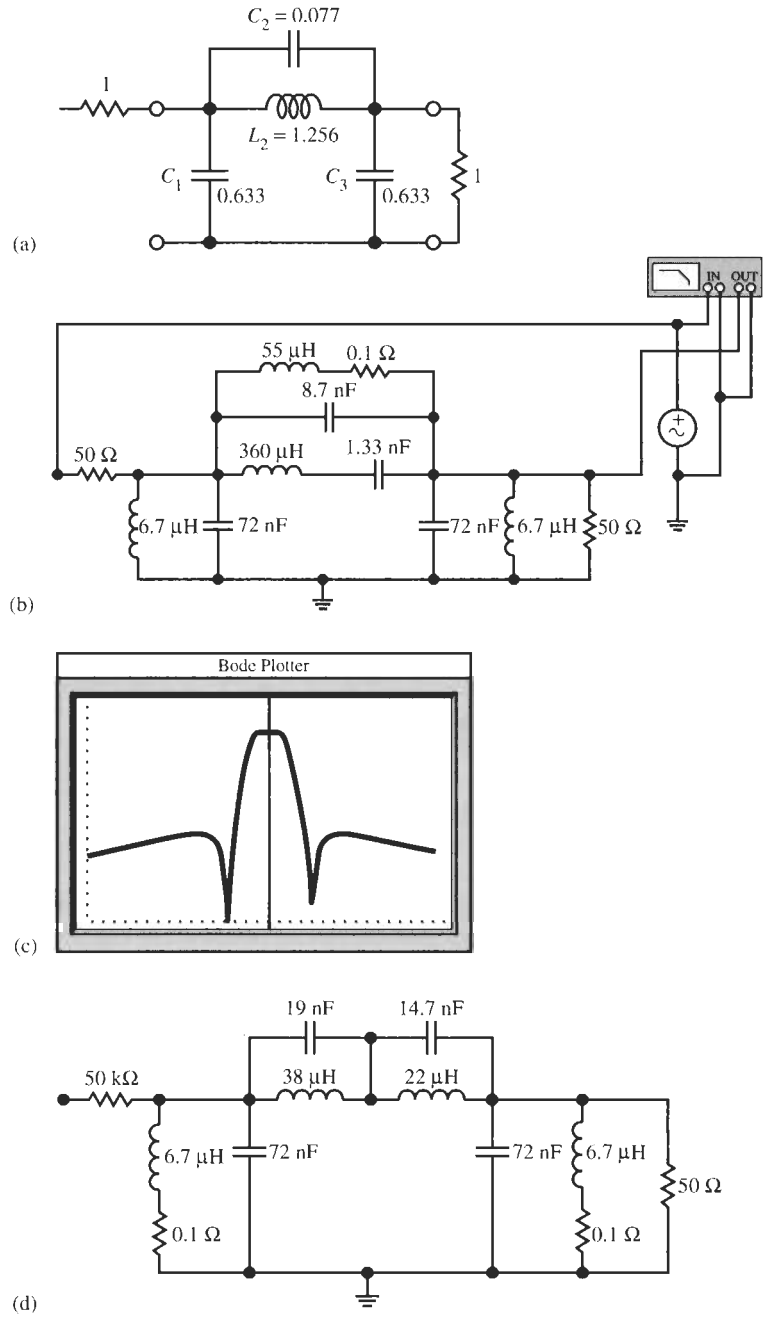

Figure 13.18 (a) Lowpass prototype circuit; (b) bandpass circuit and test set-up; (c) test results; (d) redesigned bandpass circuit. (Bode Plotter scales: 100 to 500 kHz; −60 to 0 dB; cursor at 229.7 kHz, −6.027 dB.)

$$C_{21} = \frac{C_2}{B} \times \frac{1}{R} = \frac{0.077}{2\pi \times 28000} \times \frac{1}{50\ \Omega} = 8.754\ \text{nF}$$

$$L_{21} = \frac{B}{\omega_0^2 C_2} \times R = \frac{28 \times 50\ \Omega}{230 \times 2\pi \times 230000 \times 0.077} = 54.70\ \mu\text{H}$$

As a check we calculate that these two components resonate also at 230 kHz. Finally, we convert the series inductor L_2 into a series resonance circuit

$$L_2 = 1.265 \quad \Rightarrow \quad SL_2 = \frac{L_2}{B}\frac{s^2 + \omega_0^2}{s} = \frac{L_2}{B}s + \frac{\omega_0^2 L_2/B}{s}$$

with the elements

$$L_{22} = \frac{L_2}{B} \times R = \frac{1.265 \times 50\ \Omega}{2\pi \times 28000} = 359.5\ \mu\text{H}$$

$$C_{22} = \frac{B}{\omega_0^2 L_2} \times \frac{1}{R} = \frac{28}{230 \times 2\pi \times 230000 \times 1.265 \times 50\ \Omega} = 1.332\ \text{nF}$$

L_{22} and C_{22} resonate at 230 kHz as well.

The final circuit[5] and test results are shown in Fig. 13.18b and c. The passband center frequency is at 230 kHz (cursor) where the gain is −6 dB as expected. Bandwidth and the two transmission zeros are as designed.

There is an additional matter that the designer may wish to attend to for practical reasons. Observe that the series branch in Fig. 13.18b, consisting of two capacitors and two inductors, must realize the two transmission zeros at 279 and 189.6 kHz: there must be two parallel resonances at these frequencies. But the circuit in the realized form cannot be adjusted easily because all four elements contribute to the transmission zeros. To improve the circuit and arrive at a more practical and tunable design, the series branch should be redesigned. This can be done in the following manner.

The fourth-order LC impedance of the series branch was obtained by transforming the impedance SL_2 in parallel with the admittance SC_2 of Fig. 13.18a by Eq. (13.86). The total admittance of the series branch is, therefore,

$$Y = SC_2 + \frac{1}{SL_2} = \frac{C_2}{B}\frac{s^2 + \omega_0^2}{s} + \frac{B}{L_2}\frac{s}{s^2 + \omega_0^2}$$

and the impedance

$$Z = \frac{1}{Y} = \frac{B}{C_2}\frac{s\left(s^2 + \omega_0^2\right)}{\left(s^2 + \omega_0^2\right)^2 + B^2/(LC)s^2} = \frac{B}{C_2}\frac{s\left(s^2 + \omega_0^2\right)}{s^4 + s^2[2\omega_0^2 + B^2/(LC)] + \omega_0^4}$$

[5]The student may disregard the 0.10-Ω resistor in series with the 55-μH inductor. It is inserted to break the inductive loop in the simulation underlying the "test" results. This resistor is, of course, not needed in a physical circuit; in addition, real inductors are lossy in any event because of wire resistance.

As just mentioned, this impedance must have two poles at $\omega_{p1} = 2\pi \times 189.6$ krad/s and at $\omega_{p2} = 2\pi \times 279$ krad/s. Thus, it must be of the form

$$Z = \frac{B}{C_2} \frac{s\left(s^2 + \omega_0^2\right)}{\left(s^2 + \omega_{p1}^2\right)\left(s^2 + \omega_{p2}^2\right)} = \frac{k_1 s}{s^2 + \omega_{p1}^2} + \frac{k_2 s}{s^2 + \omega_{p2}^2}$$

As we predicted, the impedance contains two parallel resonance circuits in series. If we perform the partial fraction expansion as discussed in Example 13.4 for the numbers in Example 13.7, we obtain

$$Z = \frac{172s}{s^2 + 189^2} + \frac{216s}{s^2 + 279^2}$$

where all frequencies are again normalized with respect to $\omega_n = 2\pi$ krad/s. The resulting circuit is shown in Fig. 13.18d. Observe that now we can tune the two transmission zeros separately and independently; in addition, the spread in component values is smaller, resulting in an improved circuit.

13.6 DESIGN OF PASSIVE EQUALIZERS

We covered allpass filters in detail in Chapter 11, when we discussed equalizers that have the transfer function

$$T(s) = \frac{V_2}{V_1} = \frac{D(-s)}{D(s)} \tag{13.89}$$

Since allpass functions have transmission zeros at the roots of $D(-s)$, which are not on the $j\omega$-axis, these filters cannot be realized as ladders whose transmission zeros, as we saw, are restricted to the imaginary axis. Therefore, alternative structures are needed.

The symmetrical *lattice* topology in Fig. 13.19 is such a circuit. It can realize the functions of Eq. (13.89) if we choose the impedances such that

$$Z_1(s)Z_2(s) = R_0^2 \tag{13.90}$$

i.e., the impedances are inverses:

$$\frac{Z_1(s)}{R_0} = \frac{R_0}{Z_2(s)}$$

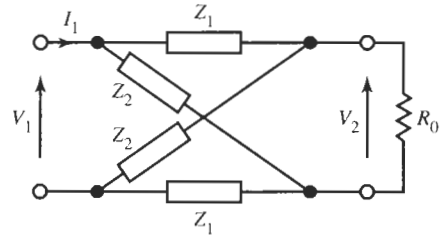

Figure 13.19 The constant-resistance symmetrical lattice.

Since our aim is a lossless circuit, we deal with *LC* impedances and we know already that if Z_1 is realizable then so is Z_2. We can analyze the circuit directly to find the transfer function

$$T(s) = \frac{V_2}{V_1} = \frac{1 - Z_1/R_0}{1 + Z_1/R_0} = \frac{Z_2/R_0 - 1}{Z_2/R_0 + 1} \tag{13.91}$$

and the input impedance

$$Z_{\text{in}}(s) = \frac{V_1}{I_1} = R_0 \tag{13.92}$$

Equation (13.92) is an interesting result. It says that when the symmetrical lossless lattice is terminated by the resistor R_0 then its input impedance is also a resistor R_0. It is a so-called *constant-resistance lattice* and implies that we can cascade these constant-resistance lattices just like active circuits with no need for buffering. Similarly, we can connect a constant-resistance lattice in cascade with a lossless ladder filter because from the point of view of the ladder the lattice looks just like a resistor. Figure 13.20 shows these applications.

We will discuss next a design strategy for such lattices. Since we just proved that lattices can be cascaded, we need to be concerned only with first- and second-order circuits because higher-order functions can be obtained from lower-order ones by cascading. Consider then a first-order function for Eq. (13.89) and equate it to Eq. (13.91). This gives

$$T(s) = \frac{\sigma - s}{\sigma + s} = \frac{1 - s/\sigma}{1 + s/\sigma} = \frac{1 - Z_1/R_0}{1 + Z_1/R_0} \tag{13.93}$$

Consequently the two *LC* impedances are an inductor R_0/σ and a capacitor $1/(\sigma R_0)$:

$$Z_1 = R_0 \frac{s}{\sigma}, \quad \text{and} \quad Z_2 = R_0 \frac{\sigma}{s} \tag{13.94}$$

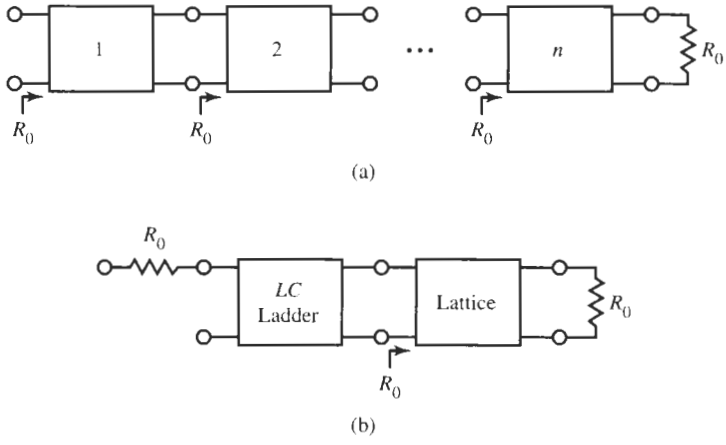

Figure 13.20 Constant-resistance lattices (a) in a cascade connection to build high-order circuits; (b) as a phase-correction circuit for a lossless ladder.

as Fig. 13.21a shows. Similarly, we obtain for second-order circuits with complex poles

$$T(s) = \frac{s^2 - s\omega_0/Q + \omega_0^2}{s^2 + s\omega_0/Q + \omega_0^2} = \frac{1 - \dfrac{s\omega_0/Q}{s^2 + \omega_0^2}}{1 + \dfrac{s\omega_0/Q}{s^2 + \omega_0^2}} = \frac{1 - Z_1/R_0}{1 + Z_1/R_0} \tag{13.95}$$

so that the two impedances are

$$Z_1 = R_0 \frac{s\omega_0/Q}{s^2 + \omega_0^2} = \frac{1}{\dfrac{Q}{R_0}\left(\dfrac{s}{\omega_0} + \dfrac{\omega_0}{s}\right)}, \quad Z_2 = R_0 \frac{s^2 + \omega_0^2}{s\omega_0/Q} = R_0 Q \left(\frac{s}{\omega_0} + \frac{\omega_0}{s}\right) \tag{13.96}$$

Z_1 is a parallel *LC* circuit and Z_2 is a series *LC* circuit as shown in Fig. 13.21b.

Notice that these realizations are expensive: the first-order allpass circuit requires two capacitors and two inductors, and the second-order allpass is realized with eight reactances, four capacitors and four inductors. More economical solutions can be devised if transformers are permitted. These are also shown in Fig. 13.21. We leave it to the problems to verify that the

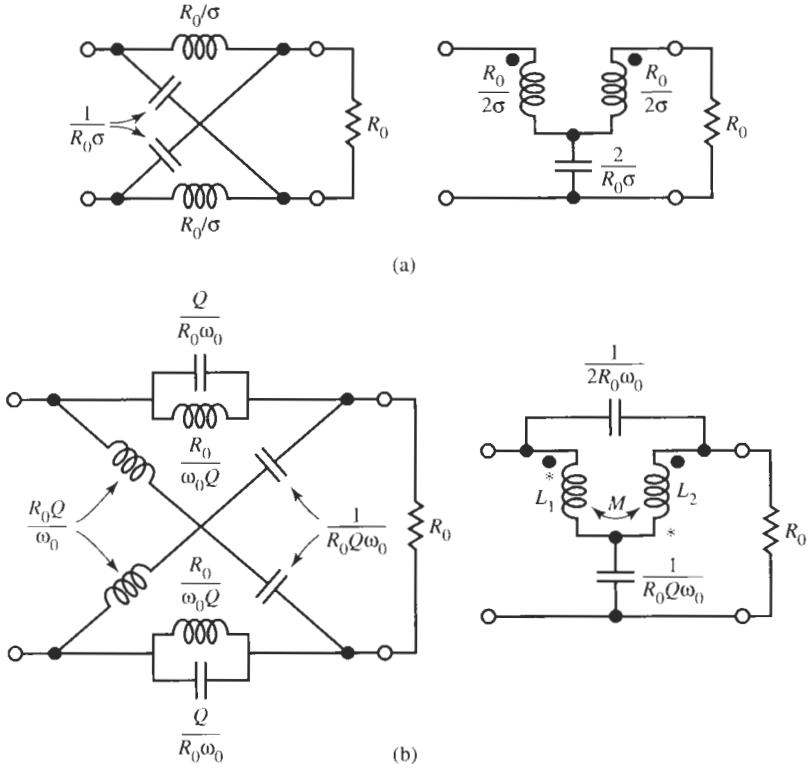

Figure 13.21 Constant resistance allpass lattices and equivalent transformers; (a) first-order; (b) second-order; the transformer components are $L_1 = L_2 = [QR_0/(2\omega_0)](1 + 1/Q^2)$, $M = [QR_0/(2\omega_0)](1 - 1/(Q^2)$; the winding direction is indicated by dots (•) if $M > 0$ and asterisks (*): if $M < 0$.

transformer circuits perform the same transfer and input impedance functions as those without transformers.

The derivation of allpass circuits to meet prescribed equalizer or constant delay requirements was covered in Chapter 11. Here we will only present an example to demonstrate the simple design process for lossless allpass filters.

EXAMPLE 13.8

Assume a fourth-order equalizer must be designed to correct the delay error of an LC ladder filter. The ladder's termination resistors are $R = 300\Omega$. The equalizer transfer function was determined to be

$$T(s) = \frac{s^2 - 4.5s + 1}{s^2 + 4.5s + 1}\frac{s^2 - 0.39s + 1}{s^2 + 0.39s + 1}$$

The frequency is scaled by $f_c = 1.2$ MHz.

Solution

We realize the allpass with two second-order sections. To obtain the elements we form

$$T(s) = T_1T_2 = \frac{1 - \dfrac{4.5s}{s^2+1}}{1 + \dfrac{4.5s}{s^2+1}}\frac{1 - \dfrac{0.39s}{s^2+1}}{1 + \dfrac{0.39s}{s^2+1}}$$

and we find for T_1:

$$Z_{11} = R\frac{4.5s}{s^2+1} = \frac{1}{\dfrac{0.222}{R}s + \dfrac{1}{4.5Rs}}, \quad Z_{12} = R\frac{s^2+1}{4.5s} = 0.222Rs + \frac{1}{(4.5/R)s}$$

Thus, Z_{11} consists of

$$C_{11} = \frac{0.222}{R\omega_c} = \frac{0.222}{300 \times 7.54}\text{ pF} = 98.14\text{ pF} \quad \text{and} \quad L_{11} = \frac{4.5R}{\omega_c} = 179.05\ \mu\text{H}$$

in parallel, and Z_{12} of

$$L_{12} = \frac{0.222R}{\omega_c} = 8.833\ \mu\text{H} \quad \text{and} \quad C_{12} = \frac{4.5}{R\omega_c} = 1.989\text{ nF}$$

in series. Because the ladder required a 300-Ω load resistor, we chose, of course, $R = 300\Omega$ for our normalizing resistor so that the equalizer input resistance is 300 Ω. With $Q_1 = 0.2222$, we find for the transformer's primary and secondary inductances, L_1, and the mutual inductance, M_1:

$$L_1 = \frac{Q_1R_0}{2\omega_0}\left(1 + \frac{1}{Q_1^2}\right) = \frac{0.2222 \times 300\ \Omega}{2 \times 7.54 \times 10^6}\left(1 + \frac{1}{0.2222^2}\right) = 93.95\ \mu\text{H}$$

$$M_1 = \frac{Q_1 R_0}{2\omega_0}\left(1 - \frac{1}{Q_1^2}\right) = -85.1\ \mu\text{H}$$

Note that M is negative. Similarly for T_2 we obtain

$$Z_{21} = R\frac{0.39s}{s^2+1} = \frac{1}{\dfrac{2.564}{R}s + \dfrac{1}{0.39Rs}}, \quad Z_{22} = R\frac{s^2+1}{0.39s} = 2.564Rs + \frac{1}{(0.39/R)s}$$

and we have for Z_{21} the parallel connection of

$$C_{21} = \frac{2.564}{R\omega_c} = 1.134\ \text{nF} \quad \text{and} \quad L_{21} = \frac{0.39R}{\omega_c} = 15.52\ \mu\text{H}$$

and for Z_{22} a series connection of

$$L_{22} = \frac{2.564R}{\omega_c} = 102.0\ \mu\text{H} \quad \text{and} \quad C_{21} = \frac{0.39}{R\omega_c} = 172.4\ \text{pF}$$

In this section we have $Q_2 = 2.564$ so that we obtain for the transformer:

$$L_2 = 58.77\ \mu\text{H} \quad \text{and} \quad M_2 = 43.25\ \mu\text{H}$$

Figure 13.22 shows the resulting circuit and its transformer equivalent.

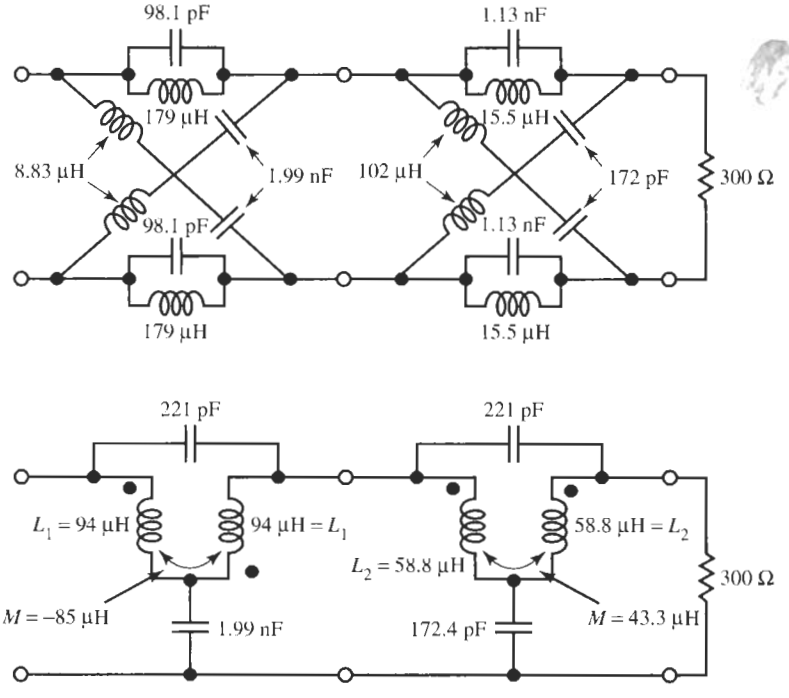

Figure 13.22 Fourth-order delay equalizer for Example 13.8.

transformer circuits perform the same transfer and input impedance functions as those without transformers.

The derivation of allpass circuits to meet prescribed equalizer or constant delay requirements was covered in Chapter 11. Here we will only present an example to demonstrate the simple design process for lossless allpass filters.

EXAMPLE 13.8

Assume a fourth-order equalizer must be designed to correct the delay error of an LC ladder filter. The ladder's termination resistors are $R = 300\Omega$. The equalizer transfer function was determined to be

$$T(s) = \frac{s^2 - 4.5s + 1}{s^2 + 4.5s + 1}\frac{s^2 - 0.39s + 1}{s^2 + 0.39s + 1}$$

The frequency is scaled by $f_c = 1.2$ MHz.

Solution

We realize the allpass with two second-order sections. To obtain the elements we form

$$T(s) = T_1T_2 = \frac{1 - \dfrac{4.5s}{s^2+1}}{1 + \dfrac{4.5s}{s^2+1}}\frac{1 - \dfrac{0.39s}{s^2+1}}{1 + \dfrac{0.39s}{s^2+1}}$$

and we find for T_1:

$$Z_{11} = R\frac{4.5s}{s^2+1} = \frac{1}{\dfrac{0.222}{R}s + \dfrac{1}{4.5Rs}}, \quad Z_{12} = R\frac{s^2+1}{4.5s} = 0.222Rs + \frac{1}{(4.5/R)s}$$

Thus, Z_{11} consists of

$$C_{11} = \frac{0.222}{R\omega_c} = \frac{0.222}{300 \times 7.54}\text{ pF} = 98.14\text{ pF} \quad \text{and} \quad L_{11} = \frac{4.5R}{\omega_c} = 179.05\ \mu\text{H}$$

in parallel, and Z_{12} of

$$L_{12} = \frac{0.222R}{\omega_c} = 8.833\ \mu\text{H} \quad \text{and} \quad C_{12} = \frac{4.5}{R\omega_c} = 1.989\text{ nF}$$

in series. Because the ladder required a 300-Ω load resistor, we chose, of course, $R = 300\Omega$ for our normalizing resistor so that the equalizer input resistance is 300 Ω. With $Q_1 = 0.2222$, we find for the transformer's primary and secondary inductances, L_1, and the mutual inductance, M_1:

$$L_1 = \frac{Q_1R_0}{2\omega_0}\left(1 + \frac{1}{Q_1^2}\right) = \frac{0.2222 \times 300\ \Omega}{2 \times 7.54 \times 10^6}\left(1 + \frac{1}{0.2222^2}\right) = 93.95\ \mu\text{H}$$

$$M_1 = \frac{Q_1 R_0}{2\omega_0}\left(1 - \frac{1}{Q_1^2}\right) = -85.1\ \mu\text{H}$$

Note that M is negative. Similarly for T_2 we obtain

$$Z_{21} = R\frac{0.39s}{s^2+1} = \frac{1}{\dfrac{2.564}{R}s + \dfrac{1}{0.39Rs}}, \quad Z_{22} = R\frac{s^2+1}{0.39s} = 2.564Rs + \frac{1}{(0.39/R)s}$$

and we have for Z_{21} the parallel connection of

$$C_{21} = \frac{2.564}{R\omega_c} = 1.134\ \text{nF} \quad \text{and} \quad L_{21} = \frac{0.39R}{\omega_c} = 15.52\ \mu\text{H}$$

and for Z_{22} a series connection of

$$L_{22} = \frac{2.564R}{\omega_c} = 102.0\ \mu\text{H} \quad \text{and} \quad C_{21} = \frac{0.39}{R\omega_c} = 172.4\ \text{pF}$$

In this section we have $Q_2 = 2.564$ so that we obtain for the transformer:

$$L_2 = 58.77\ \mu\text{H} \quad \text{and} \quad M_2 = 43.25\ \mu\text{H}$$

Figure 13.22 shows the resulting circuit and its transformer equivalent.

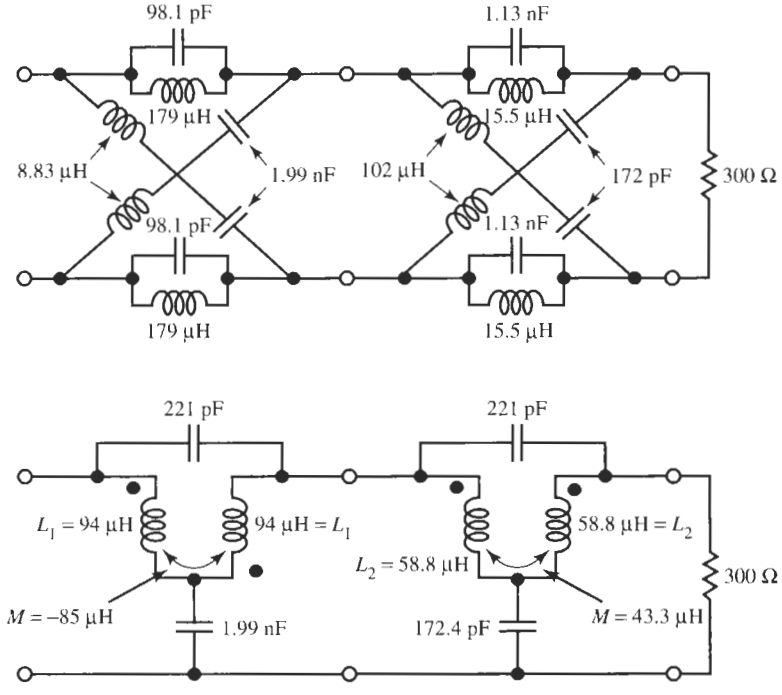

Figure 13.22 Fourth-order delay equalizer for Example 13.8.

REFERENCES

[1] N. Balabanian, *Network Synthesis*. Prentice Hall, Englewood Cliffs, NJ, 1958.

[2] W.-K. Chen, *Passive and Active Filters—Theory and Implementation*. Wiley, New York, 1986.

[3] S. Darlington, "Synthesis of Reactance 4-Poles Which Produce Prescribed Insertion Loss Characteristics." *J. Math. Phys.*, pp. 257–353, 1939.

[4] W. Heinlein and H. Holmes, *Active Filters for Integrated Circuits*. Oldenbourg Verlag, Vienna, 1974.

[5] H. J. Orchard, "Inductorless Filters." *Electron. Lett.*, Vol. 2, pp. 224–225, September 1966.

[6] R. Saal. *Handbook of Filter Design*. AEG-Telefunken AG Publishing Department, Frankfurt am Main, Germany, 1979.

[7] R. Schaumann, M. S. Ghausi, and K. R. Laker, *Design of Analog Filters: Passive, Active RC and Switched Capacitor*. Prentice Hall, Englewood Cliffs, NJ, 1990.

[8] A. S. Sedra and P. O. Brackett, *Filter Theory and Design: Active and Passive*. Matrix, Portland, OR, 1978.

[9] G. C. Temes and J. W. Lapatra, *Introduction to Circuit Synthesis and Design*. McGraw-Hill, New York, 1977.

[10] A. I. Zverev, *Handbook of Filter Synthesis*. Wiley, New York, 1967.

PROBLEMS

13.1 Realize the following *LC* admittance in the four canonic forms. In the function the impedance level is normalized by $R_0 = 1.2$ kΩ and the frequency by $\omega_0 = 650$ krad/s. Give the final circuits with denormalized components.

$$Y(s) = \frac{s\left(s^2+2\right)\left(s^2+4\right)}{\left(s^2+1\right)\left(s^2+3\right)}$$

13.2 Verify that the admittance in Eq. (13.71) can be expressed as

(a) Eq. (13.75)

(b) Eq. (13.77)

(c) Eq. (13.78)

13.3 Realize the impedance of Example 13.4 in the form pictured in Fig. P13.3.

13.4 Realize a Butterworth filter as a lossless ladder. The specifications are $\alpha_{\min} = 20$ dB at $\omega_s = 1.41$. The passband corner must be at $f_p = 185$ kHz.

13.5 A lossless lowpass ladder filter is to be realized with the following specifications:

Maximally flat magnitude with $\alpha_{\max} = 0.5$ dB in $0 \leq f \leq 120$ kHz

$\alpha_{\min} = 18$ dB in $f \geq 600$ kHz

Source and load resistors $R = 300\Omega$

Design the circuit and test its performance.

13.6 Repeat Problem 13.5 for a filter with an equal-ripple passband.

13.7 A lowpass filter is needed to provide a delay of 40 μs. The delay error must be less than 2% and the attenuation less than 3 dB in $f \leq 10$ kHz. Build the circuit as a lossless ladder.

13.8 Design a sixth-order lossless ladder with an equal-ripple constant delay of $D = 68$ μs.

13.9 Use Table 13.1 to design a seventh-order minimum-inductance ladder to have a maximally flat passband with $\alpha_{\max} = 0.1$ dB in $f \leq 230$ kHz. Source and load resistors are 75 Ω. Test your design with Electronics Workbench (EWB).

13.10 Use Table 13.3 to design a seventh-order Chebyshev lowpass ladder with 0.5-dB ripple in $f < 68$ kHz. Source and load resistors are 120 Ω.

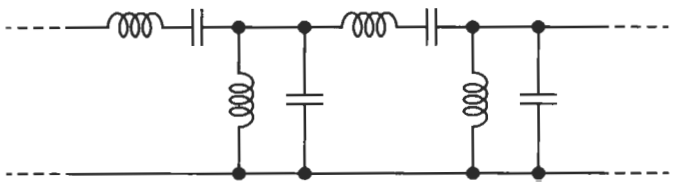

Figure P13.3

13.11 Use Table 13.3 to design a sixth-order Chebyshev lowpass ladder with $\alpha_{max} = 0.1$ dB. The load resistor is prescribed to be 100 Ω.

13.12 This problem is concerned with the application of frequency-transformation techniques to obtain a given frequency response from a lowpass prototype. Assume that the prototype is a third-order Butterworth doubly terminated lossless circuit. Determine the element values in the frequency-transformed circuit and sketch $|T(j\Omega)|$ as a function of frequency, if the transformation is that specified in Fig. 13.16:

(a) Column HP

(b) Column BP

(c) Column BE

(d) Column Double Passband with Eq. (9.87)

(e) Column Double Passband with Eq. (9.88)

13.13 Repeat Problem 13.12 if the lowpass prototype is that given in Fig. P13.13.

13.14 Use frequency transformation methods to convert

(a) the lowpass of Problem 13.4 into a highpass.

(b) the lowpass of Problem 13.5 into a highpass.

(c) the lowpass of Problem 13.5 into a bandpass.

(d) the lowpass of Problem 13.8 into a highpass.

(e) the lowpass of Problem 13.8 into a bandpass.

(f) the lowpass of Problem 13.8 into a band-rejection filter.

(g) the lowpass of Problem 13.9 into a highpass.

(h) the lowpass of Problem 13.9 into a bandpass.

(i) the lowpass of Problem 13.9 into a band-rejection filter.

(j) the lowpass of Problem 13.10 into a highpass.

(k) the lowpass of Problem 13.10 into a bandpass.

(l) the lowpass of Problem 13.10 into a band-rejection filter.

13.15 (a) In this problem, you are given $\rho(s)$ derived from Eq. (13.21) and asked to find the two doubly terminated lossless realizations with $R_1 = 1\ \Omega$. The function is

$$\rho(s) = \frac{s^2 + 1.35s + 0.35}{s^2 + 3s + 1}$$

In working the problem, ignore small numerical differences that might have resulted from improper rounding.

(b) Build the circuits, denormalize them with $R_0 = 1000\ \Omega$ and $f_0 = 100$ kHz, and test the performance.

13.16 Repeat Problem 13.15 for the function

$$\rho(s) = \frac{(s^2 + 0.6934s + 0.4808)(s + 0.6934)}{s^3 + 2s^2 + 2s + 1}$$

13.17 For the doubly terminated lossless realization shown in Fig. P13.13:

(a) Find another doubly terminated circuit that meets the same specifications.

(b) Find $\rho(s)$ that describes the circuit.

13.18 Repeat Problem 13.17 for the circuit given in Fig. P13.18.

13.19 (a) The specification function for a doubly terminated lossless network is

$$|T(j\omega)|^2 = \frac{K}{1 + \omega^8}$$

It indicates a fourth-order Butterworth filter. Find two circuit realizations. Carry through the steps of determining $\rho(s)$ and z_{11} to find the circuits. You may wish to check your result in an appropriate table.

(b) Denormalize the circuits with $R_0 = 1.2\ \text{k}\Omega$ and $\omega_p = 55$ krad/s and test their performance with EWB.

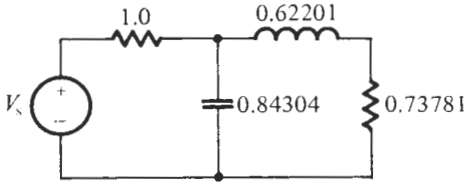

Figure P13.13

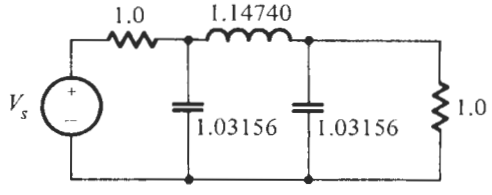

Figure P13.18

13.20 Repeat Problem 13.19 for a fifth-order Butterworth filter where

$$|T(j\omega)|^2 = \frac{K}{1+\omega^{10}}$$

13.21 The specification function for a doubly terminated lossless filter has the form

$$|T(j\omega)|^2 = \frac{K}{1+\omega^6}$$

indicating a third-order Butterworth response.

(a) Find two realizations if it is required that $R_1 = 1$ and $R_2 = 2$.

(b) Repeat (a) if it is required that $R_1 = 1$ and $R_2 = 3$.

13.22 In the text, the entries for z_{ij} in Table 13.4 were derived for $N(s)$ even. Verify

(a) the entries for z_{ij} for N odd and

(b) the entries for y_{ij}.

13.23 The magnitude squared of a lowpass transfer function with normalized frequency is given as

$$|H(j\omega)|^2 = \frac{\left(1-\omega^2/4\right)^2}{\left(1-\omega^2/4\right)^2 + 0.14565\omega^6}$$

(a) Identify the type of approximation this function represents.

(b) What is the attenuation at the passband corner $\omega = 1$?

(c) Find the z- and y-parameters that describe the LC ladder and realize $H(s)$ with source and load resistors $R_S = R_L = 1$.

(d) Denormalize the circuit so that $f = 300$ kHz is the passband edge and source and load are 300 Ω. Test the performance of your design with EWB.

13.24 The transfer function

$$H(s) = \frac{0.01714\left(s^2+6.5^2\right)}{s^3+1.2498s^2+1.5337s+0.7243}$$

is that of a third-order lowpass prototype with equal-ripple passband, $\alpha_{max} = 0.5$ dB, and $\alpha_{min} = 38$ dB stopband attenuation in $\omega_s \geq 4$. The originally specified bandpass has a passband in 9 MHz $\leq f \leq$ 12 MHz and a transmission zero at $f_z = 4.5$ MHz. Source and load are 50 Ω. Find an LC ladder realization for the bandpass and test the performance of your design with EWB.

13.25 A sixth-order bandpass filter is to be built to satisfy the following specifications:

Geometrically symmetrical transfer characteristic

Maximally flat passband in 50 kHz $\leq f <$ 70 kHz, $\alpha_{max} \leq 1$ dB

Stopband with $\alpha_{min} \geq 20$ dB in $f \geq 80$ kHz

A transmission zero at f_z in the upper stopband

Source and load termination 600 Ω

Find the location of f_z and design and test the circuit.

13.26 Realize a Bessel–Thomson filter as a lossless ladder to satisfy

30-μs delay with $\leq 1\%$ error up to 13 kHz

Attenuation not larger than 2 dB up to 110 kHz

Source and load 120 Ω

13.27 This problem relates to the speaker crossover system shown in Fig. P13.27. For this system, find the average power in both the lowpass load and the highpass load, and show that the sum of these two powers is a constant.

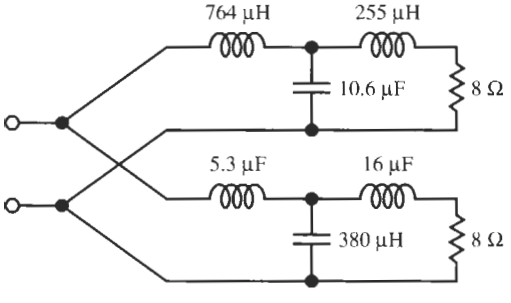

Figure P13.27

13.28 Prove that the symmetrical lattice in Fig. 13.19 is described by Eq. (13.91) provided that the condition in Eq. (13.90) holds.

13.29 Verify that the transformer circuits in Fig. 13.22 are equivalent to the corresponding symmetrical constant-resistance lattices in the figure.

13.30 Design an *LC* allpass filter to meet the following specifications

maximally flat delay $D(0) = 70\ \mu$s with delay error $\leq 0.8\%$ in $f \leq 35$ kHz

load resistor is $R = 1.3\ \text{k}\Omega$.

13.31 Design a fifth-order *LC* allpass filter with an equal-ripple delay of $D(0) = 36\ \mu$s. The circuit's input impedance must appear like a 300-Ω resistor for all frequencies. Design an appropriate circuit.

13.32 This problem has the objective of eliminating interference from a television set. From a spectrum analyzer, it is found that reception will be improved if the following attenuation can be obtained by a filter:

f (MHz)	α (dB)
48	$\geq$ 20
60	$\leq$ 2
66	$\geq$ 20

Design a passive filter to put on the front end of a television receiver to match a 50-Ω transmission line. Test the performance of your design with EWB.

14 LADDER SIMULATIONS BY ELEMENT REPLACEMENT

In the last chapter we extolled the virtues of the doubly terminated lossless ladder: among the advantages are low sensitivity to component tolerances, and voluminous design information and design tables that are available to the filter engineer. It is helpful also that the frequency transformation can be applied directly to a finished lowpass prototype circuit so that other types of filter requirements can be obtained with little need for redesign. The price paid for these advantages is high. Inductors are hard to construct, being heavy and bulky. Except for applications at the highest frequencies where inductor values of the order of nanohenries (10^{-9} H) are used, *LC* filters have the disadvantage that they cannot be implemented in microelectronic form and are difficult to adapt to integrated-circuit (IC) realization. We shall discuss methods for designing analog filters in IC form in Chapters 16 and 17; for now let us investigate how we may build active *RC* filters in a way that inherits the positive properties of lossless *LC* filters. Our main objective is to eliminate the need for inductors. Two approaches are helpful: (1) element replacement and (2) operational simulation. In this chapter we will study the element replacement method and leave operational simulation until Chapter 15.

14.1 THE GENERAL IMPEDANCE CONVERTER

If an *LC* filter is known, such as the circuits in Figs. 13.8 or 13.9, we need to ask how they can be replaced by active inductorless structures. One method that promises success is to replace the inductors by some active electronic circuit whose input impedance looks inductive. As we did throughout this book, for our active devices we will again use operational amplifiers so

that the frequency range for which the inductor simulation is valid is, of course, limited, but we will strive to achieve useful designs over at least several tens of kilohertz[1] so that our new circuits can compete and be compared with the active filters we designed so far.

We encountered the concept of inductor simulation in Section 4.5.3 where we introduced the gyrator as a twoport whose input impedance is inversely proportional to the load impedance. As a reminder, Fig. 14.1 shows the principle, a circuit that is described by the equations

$$I_1 = -g_m V_2 \quad \text{and} \quad I_2 = g_m V_1 \tag{14.1}$$

To keep with common practice we have labeled the constant g_m, a *transconductance*, with physical units of 1/Ohm or Siemens [S]. A transconductance is the ratio of the current at one port and the voltage at the other port. The input impedance is then given by

$$Z_{in}(s) = \frac{1}{g_m^2}\left(-\frac{I_2}{V_2}\right) = \frac{1}{g_m^2}\frac{1}{Z_L(s)} \tag{14.2}$$

If we now terminate this gyrator by a capacitor C, i.e., $Z_L(s) = 1/(sC)$, the input impedance is the desired inductor L:

$$Z_{in}(s) = s\frac{1}{g_m^2}C = sL \tag{14.3}$$

with L given by $L = C/g_m^2$. Observe also that $Z_{in} = \infty$ if the output terminals are shorted, $Z_L = 0$.

It is clear from the filters we are trying to implement without inductors that we need to find ways to realize both grounded inductors as in Fig. 14.1 and floating inductors. In a floating inductor, the two terminals are at different voltages, neither equal to zero (or grounded) as in Fig. 14.2a. Any circuit we propose to replace the inductor must satisfy the following tests: (1) if terminals 2–2′ are shorted then $Z_{11'} = sL$, and if terminals 1–1′ are shorted, then $Z_{22'} = sL$. These conditions are illustrated in Fig. 14.2b. Because short-circuiting one port of a gyrator creates an open circuit at the other port, we may connect a gyrator on either side of a grounded capacitor to realize such a floating inductor. This is shown in Fig. 14.3. Clearly, if we short

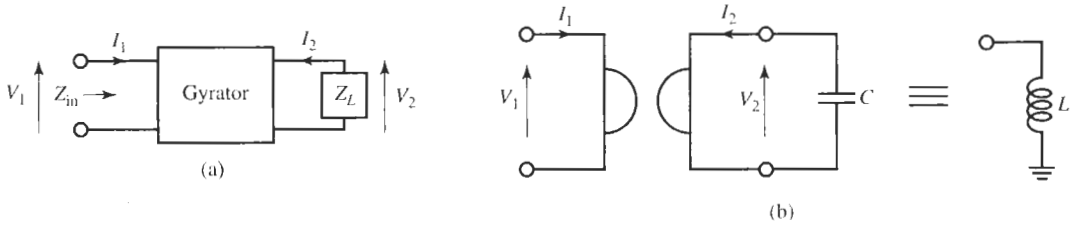

Figure 14.1 (a) Twoport used to realize an input impedance inversely proportional to the load impedance, $Z_{in} = k/Z_L$; (b) gyrator symbol; the gyrator is used to realize an inductor.

[1] This range is limited by the opamp bandwidth; we will use LM741 opamps to facilitate comparisons with other design methods in this book. If opamps with wider bandwidth are used, the frequency range is, of course, larger.

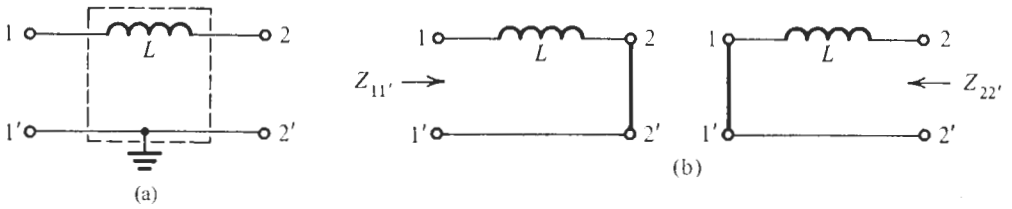

Figure 14.2 (a) Floating inductor; (b) conditions for simulating a floating inductor.

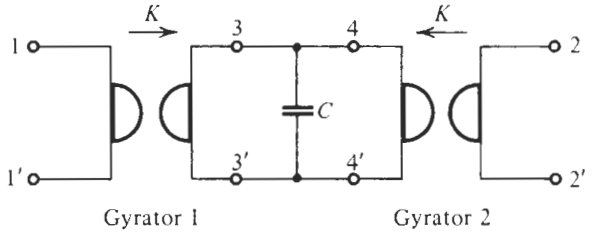

Figure 14.3 Simulating a floating inductor by means of two gyrators.

terminals 2–2′, terminals 4–4′ are an open circuit and the input impedance is $Z_{11'} = sC/g_m^2$. The same argument works in reverse, of course, since by Eq. (14.2) $Z_L = 1/(g_m^2 Z_{in})$, so that the criterion illustrated in Fig. 14.2b is satisfied.

Thus, we have now methods to simulate both grounded and floating inductors, and simple very successful electronic circuits whose input impedance looks inductive are built this way. We shall discuss them in Chapter 16. For now we have to confront first a difficulty with implementing gyrators by using operational amplifiers. It is clear from Eq. (14.1) that fundamentally a gyrator consists of two voltage-controlled current sources. Figure 14.4 shows the concept. However, opamps are voltage-controlled voltage sources and no simple opamp circuits to build true gyrators[2] with good performance have been found. We will pursue a different track, also encountered earlier, to arrive at the desired inductance simulation.

Recall from Section 4.5.3 the discussion of the general impedance converter (GIC) (Antoniou, 1969). The input impedance of the GIC in Fig. 4.45b is inductive and the GIC was used to build excellent second-order filters by simulating the behavior of the inductor. The circuit is repeated in Fig. 14.5a with general impedances; its analysis was performed in Section 4.5.3 and we saw that, for ideal opamps, the GIC has the input impedance

$$Z_{11'} = \frac{Z_1 Z_3}{Z_2 Z_4} Z_5 \tag{14.4}$$

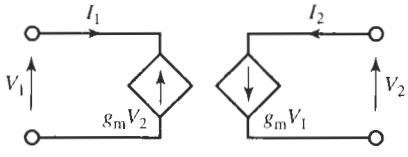

Figure 14.4 A gyrator circuit constructed from two voltage-controlled current sources.

[2] A true gyrator has an *input* impedance that is inversely proportional to the *load* impedance as indicated in Eq. (14.2).

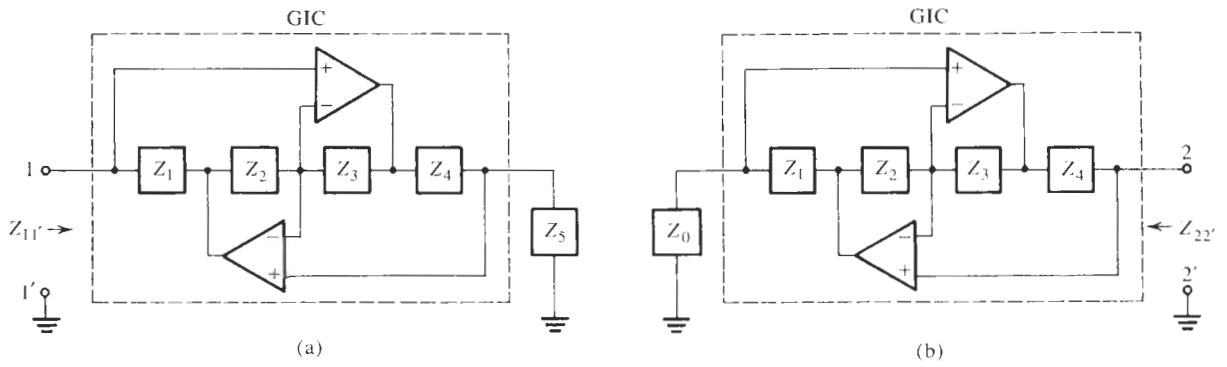

Figure 14.5 The general impedance converter (GIC) circuit: (a) forward direction; (b) reverse direction.

We can repeat the analysis to find the impedance $Z_{22'}$ at the other end of the GIC when its input is terminated by an impedance Z_0. The result is

$$Z_{22'} = \frac{Z_2 Z_4}{Z_1 Z_3} Z_0 \tag{14.5}$$

We have in Fig. 14.5 enclosed the GIC circuit in a dashed box to identify the input and the load impedances. Note that the circuit is not a gyrator because the input impedance is proportional rather than inversely proportional to the load impedance. However, referring to Eq. (14.4), we can still obtain an inductive input by choosing $Z_i = R_i, i = 1, 3, 4, 5$, and $Z_2 = 1/(sC_2)$. Then we have $Z_{11'} = sC_2R_1R_3R_5/R_4$. We referred to this circuit as GIC I in Section 4.5.3 and used it to build the GIC biquads. Alternatively, we can choose $Z_i = R_i, i = 1, 2, 3, 5$, and $Z_4 = 1/(sC_4)$ so that

$$Z_{11'} = sL_0 = s\left(C_4\frac{R_1R_3}{R_2}\right)R_5 = sTR_5 \tag{14.6}$$

Notice that this equation can be interpreted as indicating that the load resistor is converted into an inductor by multiplying the resistor by s and a time constant T. Looking at the GIC in this manner will be helpful in our derivations below.

We declared in Section 4.5.3 that this circuit, the GIC II, would be used in connection with simulating inductors in LC ladders. Having arrived at this point, we must now investigate how good the inductor $L_0 = C_4R_1R_3R_5/R_2$ is.

14.2 OPTIMAL DESIGN OF THE GIC

Judging by Eq. (14.6) that is derived for ideal opamps, the inductor is ideal. But we know already from the discussion of the GIC circuit in Section 4.5.3 that using real operational amplifiers will result in nonideal performance. To investigate these deviations from the ideal, we analyze the GIC (Sedra and Brackett, 1978) in Fig. 14.5a with the integrator model $A(s) \approx \omega_t/s$ for the opamps. We set $Z_i = R_i, i = 1, 2, 3, 5, Z_4 = 1/(sC_4)$, and neglect terms proportional to $1/(A_1A_2)$, implying that for all frequencies of interest $\omega^2 \ll \omega_{t1}\omega_{t2}$. Analogous to the discussion in Section 4.5.3 we then obtain for the input impedance

$$Z_{\text{in}}(s) \approx sL_0 \frac{1 + \left(\frac{1}{A_2}\frac{G_3}{G_2} + \frac{1}{A_1}\right)\left(1 + \frac{G_5}{sC_4}\right)}{1 + \left(\frac{1}{A_2} + \frac{1}{A_1}\frac{G_2}{G_3}\right)\left(1 + \frac{sC_4}{G_5}\right)} \tag{14.7}$$

where L_0 was defined in Eq. (14.6). We next approximate $1/(1+x)$ as $1-x$ for small x,

$$Z_{\text{in}}(s) \approx sL_0 \left[1 + \left(\frac{1}{A_2}\frac{G_3}{G_2} + \frac{1}{A_1}\right)\left(1 + \frac{G_5}{sC_4}\right)\right]\left[1 - \left(\frac{1}{A_2} + \frac{1}{A_1}\frac{G_2}{G_3}\right)\left(1 + \frac{sC_4}{G_5}\right)\right]$$

and obtain, for $s = j\omega$,

$$Z_{\text{in}}(j\omega) \approx j\omega L_0 \left[1 - \left(\frac{j\omega}{\omega_{t2}} + \frac{j\omega}{\omega_{t1}}\frac{G_2}{G_3}\right)\left(1 + \frac{j\omega C_4}{G_5}\right) + \left(\frac{j\omega}{\omega_{t2}}\frac{G_3}{G_2} + \frac{j\omega}{\omega_{t1}}\right)\left(1 + \frac{G_5}{j\omega C_4}\right)\right] \tag{14.8}$$

having again neglected $|A_1 A_2|$ as small. Finally, we partition this equation into its real and imaginary parts,

$$Z_{\text{in}}(j\omega) = j\omega\,(L_0 + \Delta L) + R_{\text{loss}}$$

to determine the inductor error ΔL and the losses represented by a series resistor R_{loss}. We find

$$R_{\text{loss}} = \omega^2 L_0 \left(1 - \frac{G_3}{G_2}\right)\left(\frac{1}{\omega_{t2}} + \frac{1}{\omega_{t1}}\frac{G_2}{G_3}\right) \tag{14.9}$$

This is an important result; it indicates that the inductor is lossless if we choose $R_2 = R_3$:

$$R_{\text{loss}} = \infty \quad \text{if} \quad R_2 = R_3 \tag{14.10}$$

Note that this result is independent of ω_{t1} and ω_{t2}, whereas for the GIC I the opamps had to be matched to yield a lossless inductor [refer to Eq. (4.174)]. Choosing, therefore, $R_2 = R_3$ we obtain from Eq. (14.8) the inductor error

$$\Delta L = L_0 \frac{\omega}{\omega_{t2}}\left(1 + \frac{\omega_{t2}}{\omega_{t1}}\right)\left(\frac{\omega C_4}{G_5} + \frac{G_5}{\omega C_4}\right) \tag{14.11}$$

ΔL is minimized by selecting in the design

$$G_5 = \omega_c C_4 \tag{14.12}$$

where ω_c is some critical frequency. Assuming further that $\omega_{t1} \approx \omega_{t2}$ and noting that $|A(j\omega)| = \omega_t/\omega$, we have from Eq. (14.11) the remaining inductor error

$$\frac{\Delta L}{L_0} \approx \frac{4}{|A(j\omega)|} \tag{14.13}$$

as in Eq. (4.177). We try to minimize the inductor error at a point where the sensitivity is largest; thus, we usually choose ω_c in Eq. (14.12) at the passband corner. The inductor is given by

$$L_0 = C_4 R_1 R_5 \tag{14.14}$$

By Eq. (14.12) this determines the resistor R_1 as

$$R_1 = \omega_c L_0 \tag{14.15}$$

Figure 14.6 shows the circuit we just analyzed for simulating a grounded inductor.

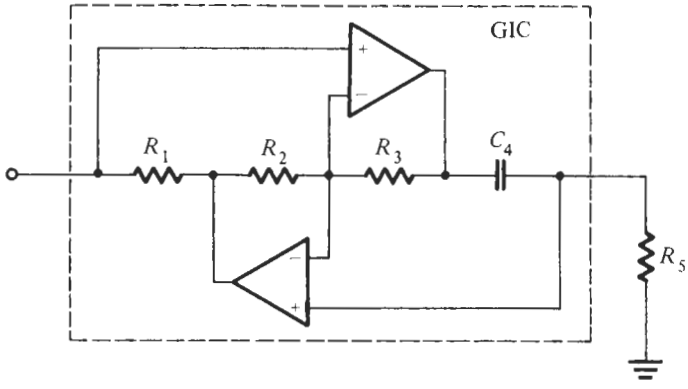

Figure 14.6 General impedance converter to simulate a grounded inductor $L_0 = C_4 R_1 R_3 R_5 / R_2$. The optimal component choice is $R_2 = R_3$, and $G_5 = \omega_c C_4$ where ω_c is some frequency that is critical in the design.

EXAMPLE 14.1

To get an idea of the quality of our simulated inductor let us perform an experiment. To this end we construct a series LC resonant circuit Z_{LC} and form a voltage divider between it and a 50-Ω resistor. The divider voltage V_2 should then have a zero at the resonance frequency $\omega_0 = 1/\sqrt{LC}$. Let the resonance frequency be 15 kHz and the capacitor $C = 0.01$ μF. We then need to construct an inductor of value $L = 11.26$ mH.

Solution

Let us choose the critical frequency for our design as $\omega_c = \omega_0$, the notch frequency; then we have for the simulated inductor $R_1 = 1.061$ kΩ by Eq. (14.15); selecting $C_4 = 0.01$ μF, we find from Eq. (14.12) $R_5 = 1/(\omega_0 C_4) = R_1$. The remaining two resistors, $R_2 = R_3$, we choose equal to 1.00 kΩ.

The resulting circuit is shown in Fig. 14.7a. The test results indicate the realized zero frequency is $f_R = 14.69$ kHz, an error of −2.0%. From Eq. (14.13) the inductor error is expected to be approximately

$$\frac{\Delta L}{L_0} \approx \frac{4}{|A(j\omega)|} = \frac{4}{1000/15} = 0.06 = 6\%$$

from which we compute that f_R is reduced by approximately 3% from the design value f_0:

$$\frac{f_R}{f_0} = \sqrt{\frac{L_0 C}{(L_0 + \Delta L)\, C}} = \sqrt{\frac{1}{1 + \Delta L / L_0}} \approx \sqrt{1 - \frac{\Delta L}{L_0}} \approx 1 - \frac{\Delta L}{2L_0} = 0.97$$

Considering the approximations made in deriving Eq. (14.13), the agreement with the measured value is reasonable. Figure 14.7b indicates that the notch depth is at 33.9 dB. At the resonance frequency, the voltage V_2 of the circuit is obtained by voltage division as $V_2/V_1 = R_{\text{loss}}/(50\ \Omega + R_{\text{loss}}) = 10^{-33.9/20} \approx 0.02$, which permits us to compute the loss resistor of the simulated inductor: $R_{\text{loss}} \approx 1\ \Omega$. It follows that the inductor has a quality factor of $\omega_0 L_0/R_{\text{loss}} = 1060/1 \approx 1000$, and demonstrates that excellent inductor simulation is attainable with a GIC.

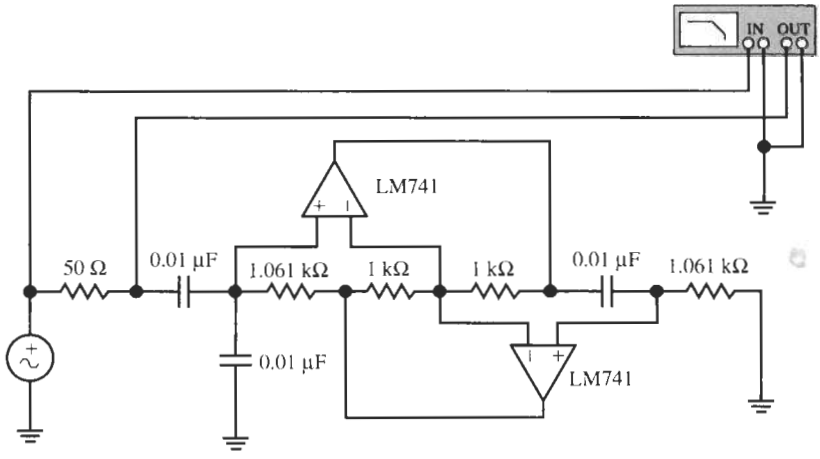

(a)

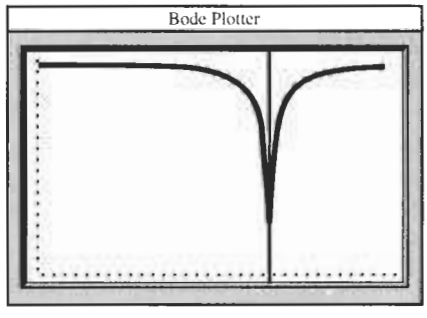

(b)

Figure 14.7 Resonance circuits with (a) a simulated inductor and (b) test results. (Bode Plotter scales: 12.5 to 16 kHz; −40 to 0 dB; cursor at 14.69 kHz, −33.94 dB.)

To obtain a floating inductor, we use again the conditions depicted in Fig. 14.2 and note from Eq. (14.4) that $Z_{11'} = 0$ if $Z_5 = 0$, that is, a short circuit at the GIC output results in a short circuit at its input. Similarly, by Eq. (14.5), $Z_{22'} = 0$ if $Z_0 = 0$. Thus, we can connect two GICs back to back with a resistor in the center as is shown in Fig. 14.8.

When assembling the GIC-based circuitry to realize a floating inductor as in Fig. 14.8, we must be careful that the active devices receive the necessary bias currents. For instance, observe that the two noninverting input terminals of the opamps A_2 are blocked by capacitors; there is no dc path to these terminals and their dc input currents are zero. This causes incorrect

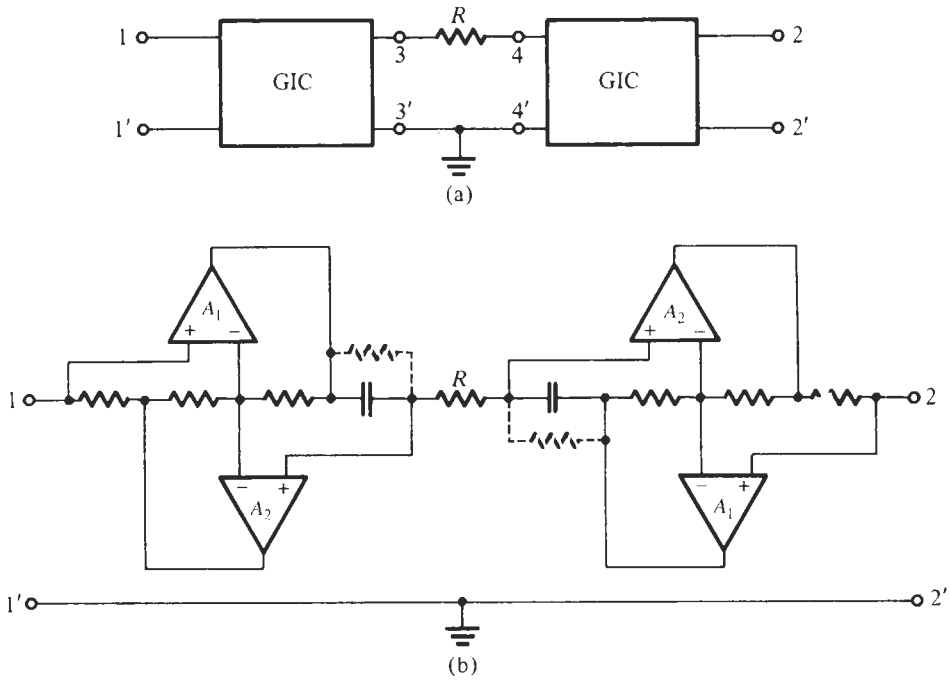

Figure 14.8 Creating a floating inductor with general impedance converters: (a) principal configuration; (b) actual GIC circuits. Note that a dc path, if needed, must be provided for the input terminal of amplifiers A_2; the two resistors shown as the dashed connection perform this function.

operation in, for example, bipolar amplifiers by blocking the dc base currents of the input stage.[3] Unless the capacitors are lossy and permit a small dc current to flow, we must solve the problem by connecting large resistors in parallel to the capacitors. The effect of this circuit modification on the simulated inductor can be assessed quite easily from Eq. (14.4): we substitute for Z_4 the admittance $Y_4 = 1/Z_4$, which is now not just the capacitor C_4 but C_4 in parallel with the additional resistor $R_4 = 1/G_4$. We find the input impedance

$$Z_{11'}(s) = (sC_4 + G_4)\, R_1 R_5 = sC_4 R_1 R_5 + G_4 R_1 R_5 = sL_0 + R_{\text{loss}} \qquad (14.16)$$

where we set, of course, $R_2 = R_3$ by Eq. (14.10). Thus the inductor becomes lossy. For instance, for the numbers in Example 14.1 a parallel resistor of $R_4 = 1\ \text{M}\Omega$ would result in a series loss resistor of $R_{\text{loss}} = 1\ \Omega$.

14.3 REALIZING SIMPLE LADDERS

With the inductor simulations we presented, the design of an active simulation of a complete *LC* ladder is accomplished easily. We only have to design the passive *LC* ladder by the methods presented in the previous chapter, or by use of tables or other design information, and then

[3] It also causes difficulties when simulating the design with, for instance, SPICE, because no dc path exists to these nodes.

replace the grounded and floating inductors by the methods discussed in the preceding section, Figs. 14.6 and 14.8. Two examples will illustrate the method.

EXAMPLE 14.2

To eliminate low-frequency noise from a system, we require a third-order highpass filter with a maximally flat passband and a half-power frequency of 75 Hz. If we were to construct the circuit as a passive *LC* filter, large rather heavy inductors would be required. So we propose to use an active implementation with simulated inductors. Source and load terminations are $R_0 = 1.2\ \text{k}\Omega$.

Solution

We start the solution from a third-order Butterworth lowpass filter. In normalized form it is given in Fig. 14.9a. The lowpass–highpass transformation replaces *L*s by *C*s and vice versa to arrive

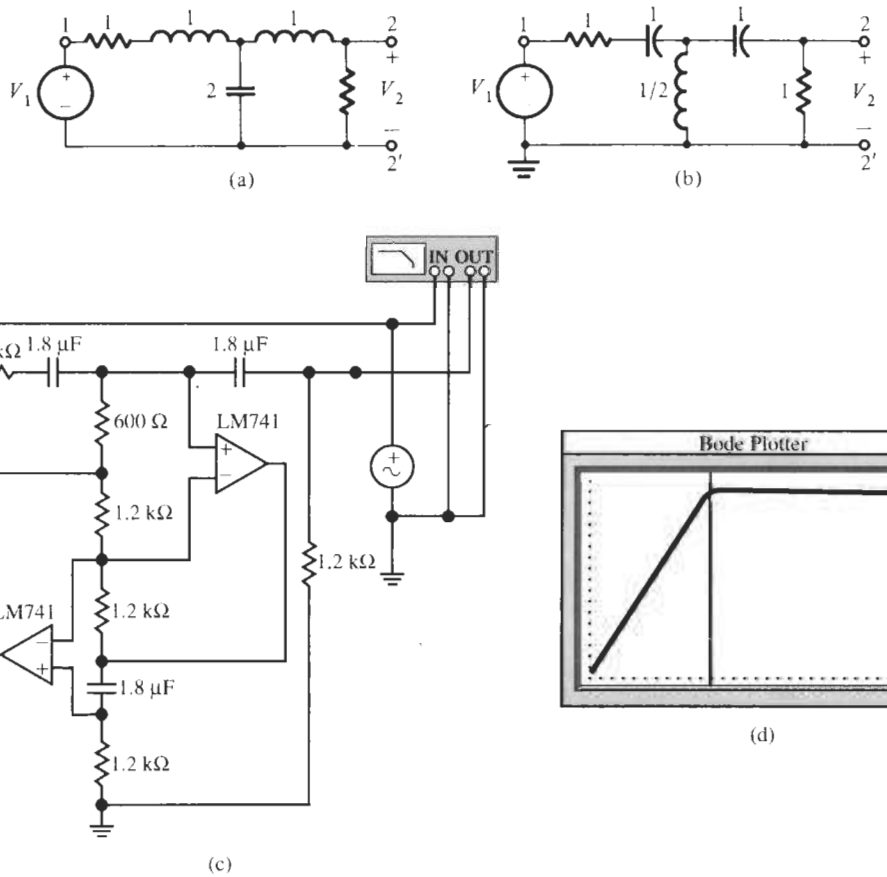

Figure 14.9 (a) Third-order Butterworth prototype lowpass filter; (b) the corresponding highpass filter; (c, d) the final circuit and test results. (Bode Plotter scales: 0.5 Hz to 400 kHz; −140 to 0 dB; cursor at 75.07 Hz, −8.794 dB.)

at the highpass circuit in Fig. 14.9b. We need to simulate an inductor of value $L = 0.5$, i.e., $L = 0.5 = C_4 R_1 R_5$. To minimize the number of different capacitors, we choose all capacitors equal at $C_4 = 1$. The cut-off frequency is still normalized to unity so that by Eq. (14.12) $R_5 = 1$ and by Eq. (14.14) $R_1 = 0.5$. Finally, we need to denormalize the components. We multiply the resistors by 1.2 kΩ and the capacitors by $1/(2\pi \times 75 \text{ rad/s} \times 1200\ \Omega) = 1.768\ \mu\text{F}$.

The final circuit and test results are contained in Fig. 14.9c and d. We observe that the circuit behaves practically as the ideal filter. The performance is as specified until about 230 kHz where the opamps' finite bandwidth causes a decline in gain. The cut-off frequency is at 75 Hz; note that passband gain is −6 dB because the circuit is based on a doubly terminated *LC* ladder with an inherent factor 1/2 caused by the voltage division between the equal input and load resistors. The fact that there is essentially a zero of transmission at the origin shows that the simulated inductor [of the relatively large value $0.5 \times 1200\ \Omega/(2\pi \times 75 \text{ rad/s}) = 1.27$ H] is almost perfect with a negligible loss resistor.

Our next example will realize an *LC* filter with a floating inductor to permit us to assess its performance. We will redesign the circuit in Fig. 13.14c, which will give us a comparison between the passive and active realizations.

EXAMPLE 14.3

We wish to implement an active realization of the *LC* filter in Fig. 13.14c. The circuit is a third-order lowpass filter with a 0.5-dB cut-off frequency of 60 kHz and a transmission zero at 182 kHz. The specified frequency range is very high for an active filter built with LM741 opamps; it will be a serious test for the active simulation.

Solution

As is indicated in Fig. 13.14c we need to realize only the active simulation of a 4-mH floating inductor. The remaining circuitry stays unchanged. We use the GIC circuit in Fig. 14.8b with $C_4 = 10$ nF and choose the passband corner frequency, 60 kHz, as the critical frequency f_c. Thus, we have by Eqs. (14.12) and (14.15):

$$R_5 = \frac{1}{\omega_c C_4} = \frac{1}{120{,}000\pi \times 10^{-8}}\ \Omega = 265.3\ \Omega \quad \text{and} \quad R_1 = \frac{L}{C_4 R_5} = \omega_c L = 1.508\ \text{k}\Omega$$

To provide bias currents to the amplifiers, we connect a 1-MΩ resistor in parallel with each capacitor C_4. By Eq. (14.16) this will add a series loss resistor of 0.4 Ω to the inductor.

The final circuit and its test performance are shown in Fig. 14.10. We observe that the passband is correctly realized; the transmission zero is at 173 kHz, too low by about 5%. This deviation is caused by the opamps' finite gain-bandwidth product. (Simulating the performance for ideal opamps places the zero at 183 kHz.) Note though that the circuit behaves essentially as specified until the megahertz range; the high-frequency roll-off normally seen at frequencies above 300 kHz is not visible here because it is masked by the filter's stopband attenuation.

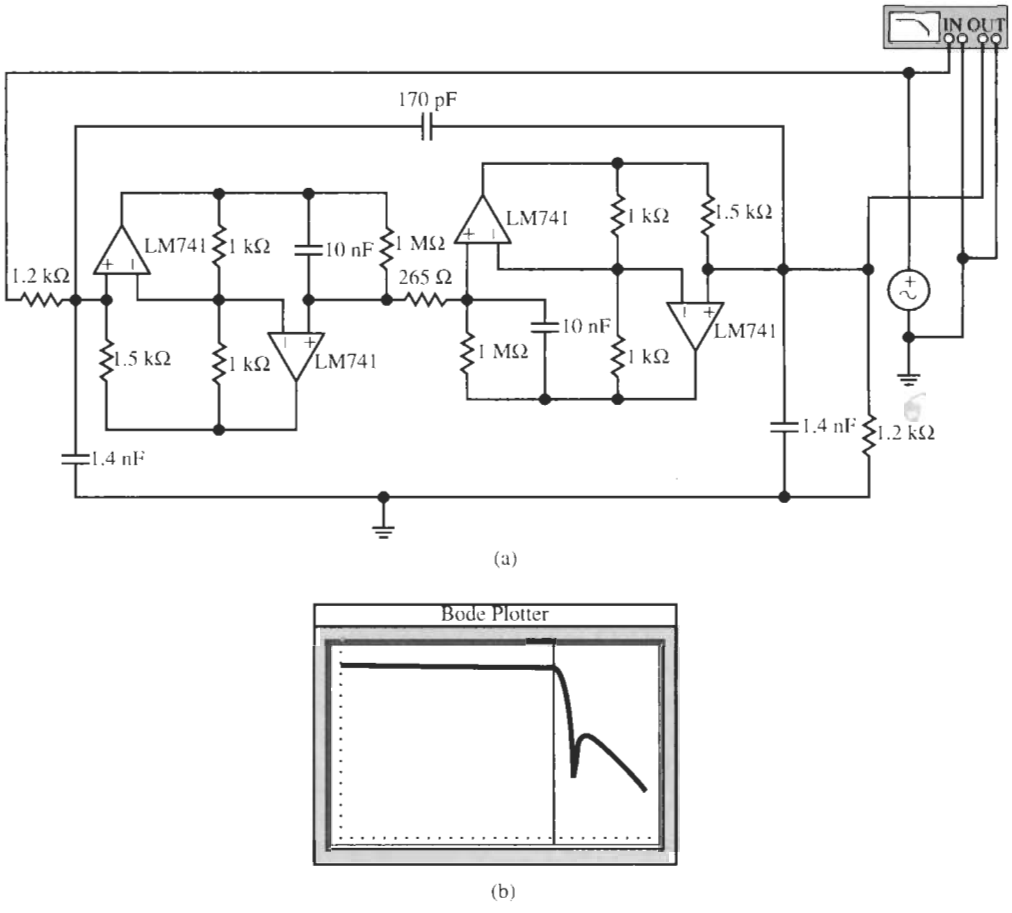

Figure 14.10 The *LC* simulation of the ladder of Fig. 13.14c and test performance. (Bode Plotter scales: 0.5 Hz to 10 MHz; −80 to 0 dB; cursor at 59.69 kHz, −7.000 dB.)

The two examples have shown that designing an active ladder from an existing *LC* circuit with GIC-based simulated inductors is a very simple procedure. It requires only an element replacement, using one or two GICs depending on whether the inductor is grounded or floating, respectively. Although the method is simple, we note that the realization potentially uses a large number of operational amplifiers if many floating inductors are needed: four opamps per floating inductor. This is always the case for lowpass filters where normally no grounded inductors are used. It is worthwhile, therefore, to explore whether more efficient methods can be found that result in savings of components, especially opamps. We will discuss two approaches in the following two sections: the first is Gorski-Popiel's procedure, which generalizes the method we discussed in Section 14.2, Fig. 14.8; the second is Bruton's FDNR method, which transforms the ladder so that inductors are eliminated and replaced by resistors.

14.4 GORSKI-POPIEL'S EMBEDDING TECHNIQUE

The technique (Gorski-Popiel, 1967) we are about to discuss is a generalization of the inductor simulation method by use of the general impedance converters of Fig. 14.6, described by Eq. (14.4). Consider the special case of the GIC of Fig. 14.11 with $Z_i = R_i, i = 1, 2, 3, Y_4 = 1/Z_4 = sC_4$, and $R_2 = R_3$ to obtain infinite Q by Eq. (14.10). With the notation in Fig. 14.11a we obtain from the circuit

$$\frac{V_1}{I_1} = sC_4R_1\frac{V_2}{I_2} = sT\frac{V_2}{I_2} \tag{14.17}$$

T is the time constant C_4R_1 that is a characteristic of the GIC. Assuming the opamps are ideal, the voltages V_1 and V_2 are equal because their difference is forced to zero, $V_1 - V = 0$, by the opamp inputs. Thus, the relationship between the currents and the voltages of the GIC input and output ports is

$$V_1 = V_2 \quad \text{and} \quad I_2 = sTI_1 \tag{14.18}$$

Since we will have ample need to use this GIC block in our circuits, let us adopt the simplified representation in Fig. 14.11b. Consider now how we can use this block to eliminate inductors in a ladder and instead simulate their behavior.

In Figs. 14.12 and 14.13 we show the principle of the approach. Figure 14.12 contains a resistive circuit (consisting here of just one resistor R) and we connect a GIC into the input branch. If we label the input current and voltage of the resistive circuit as I_{1R} and V_{1R}, the voltage and current at the input of the GIC are

$$V_1 = V_{1R} \quad \text{and} \quad I_{1R} = sTI_1 \tag{14.19}$$

where, of course, $V_{1R} = RI_{1R}$. Consequently the circuit is described by

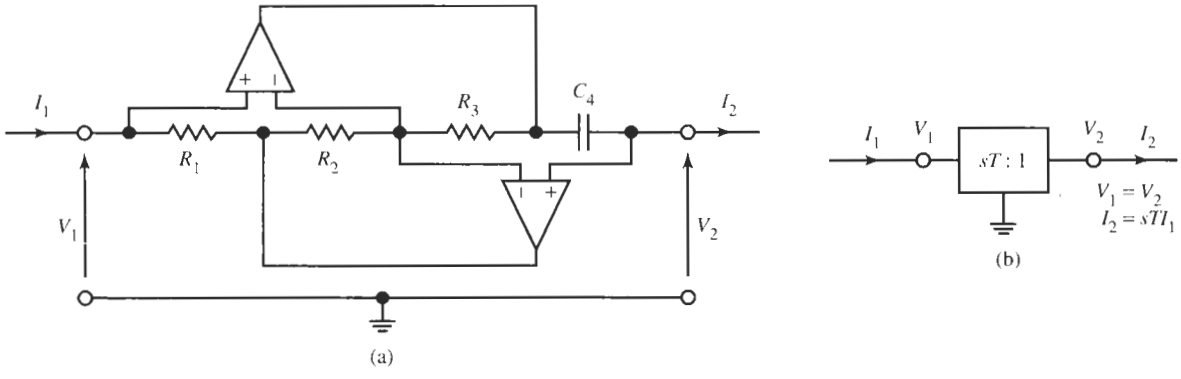

Figure 14.11 (a) The general impedance converter (GIC); (b) simplified representation of the GIC.

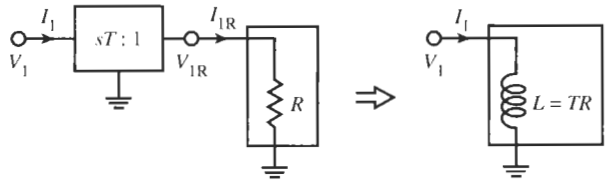

Figure 14.12 Converting a resistor R to an inductor TR.

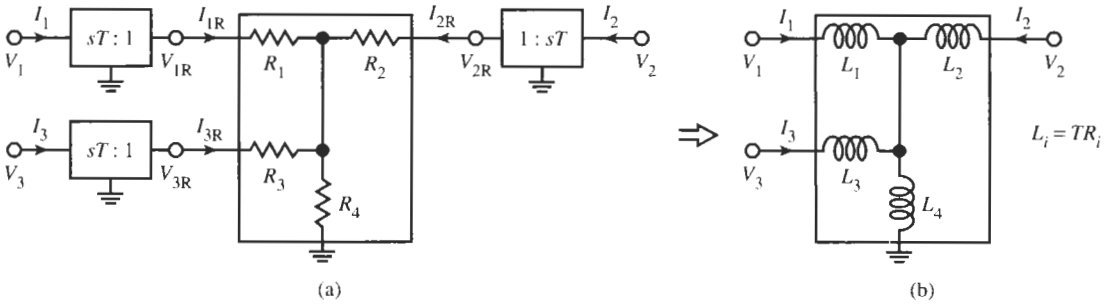

Figure 14.13 A threeport resistor network (a) embedded in GICs becomes a threeport inductor network (b).

$$V_1 = V_{1R} = RI_{1R} = sTRI_1 \quad \text{or} \quad \frac{V_1}{I_1} = Z_{in} = sTR = sL \tag{14.20}$$

We see that inserting the GIC into the input branch of the single-resistor network makes the resistor R in the combined network look like an inductor $L = TR$. This result is not surprising because it is precisely what we did in Fig. 14.6 to arrive at Eq. (14.14). The circuit in Fig. 14.8b, where a floating inductor was realized from a resistor with the help of two GICs, is a further special case of this transformation.

To demonstrate that this process is not limited to single resistors or even to twoport networks, consider the resistive threeport in Fig 14.13a. It is described by

$$V_{1R} = (R_1 + R_4)\, I_{1R} + R_4 I_{2R} + R_4 I_{3R} \tag{14.21a}$$

$$V_{2R} = R_4 I_{1R} + (R_2 + R_4)\, I_{2R} + R_4 I_{3R} \tag{14.21b}$$

$$V_{3R} = R_4 I_{1R} + R_4 I_{2R} + (R_3 + R_4)\, I_{3R} \tag{14.21c}$$

After embedding this network in GICs as shown in Fig. 14.13a and using Eq. (14.19), we have the equations

$$V_1 = sT(R_1 + R_4)I_1 + sTR_4 I_2 + sTR_4 I_3 \tag{14.22a}$$

$$V_2 = sTR_4 I_1 + sT(R_2 + R_4)I_2 + sTR_4 I_3 \tag{14.22b}$$

$$V_3 = sTR_4 I_1 + sTR_4 I_{2R} + sT(R_3 + R_4)I_3 \tag{14.22c}$$

that describe the inductor circuit in Fig. 14.13b. We can generalize this process by writing Eqs. (14.21) and (14.22) in matrix format. This gives

$$\begin{pmatrix} V_{1R} \\ V_{2R} \\ V_{3R} \end{pmatrix} = \mathbf{R} \begin{pmatrix} I_{1R} \\ I_{2R} \\ I_{3R} \end{pmatrix} = \begin{bmatrix} R_1 + R_4 & R_4 & R_4 \\ R_4 & R_2 + R_4 & R_4 \\ R_4 & R_4 & R_3 + R_4 \end{bmatrix} \begin{pmatrix} I_{1R} \\ I_{2R} \\ I_{3R} \end{pmatrix} \tag{14.23a}$$

or

$$\mathbf{V}_R = \mathbf{R}\mathbf{I}_R \tag{14.23b}$$

where $\mathbf{V}_R$ and $\mathbf{I}_R$ are the voltage and current column vectors and $\mathbf{R}$ is the resistor matrix indicated in Eq. (14.23a). The GIC embedding process yields with $\mathbf{V}_R = \mathbf{V}$ and $\mathbf{I}_R = sT\mathbf{I}$

$$\begin{pmatrix} V_1 \\ V_2 \\ V_3 \end{pmatrix} = \mathbf{R} \begin{pmatrix} sTI_1 \\ sTI_2 \\ sTI_3 \end{pmatrix}, \quad \text{i.e.,} \quad \mathbf{V} = \mathbf{RI}_R = s(T\mathbf{R})\mathbf{I} = s\mathbf{LI} \tag{14.24}$$

where $\mathbf{L} = T\mathbf{R}$ is the inductor matrix

$$\mathbf{L} = T\mathbf{R} = \begin{bmatrix} L_1 + L_4 & L_4 & L_4 \\ L_4 & L_2 + L_4 & L_4 \\ L_4 & L_4 & L_3 + L_4 \end{bmatrix} \tag{14.25}$$

with $L_i = TR_i, i = 1, 2, 3, 4$. It should be clear to the student that this method is readily extended to more complex inductor networks and to inductor n-ports. We simply connect a GIC into each wire (except ground) leading into the inductor network with the GIC output port V_2–I_2 (the right side in Fig. 14.11a) facing the inductors, and replace each inductor by a resistor of value $R = L/T$.

The utility of this transformation for building simulated LC filters lies in making it possible with GICs to convert complete inductive subnetworks into resistive subnetworks rather than having to treat each individual inductor separately. A number of GICs may be saved in the process. The method is as follows: In an LC ladder, we identify all inductor subnetworks containing the inductors L_i, and cut them from the remaining circuit. Each cut we reconnect by a general impedance converter of the form in Fig. 14.11 and replace all inductors by resistors

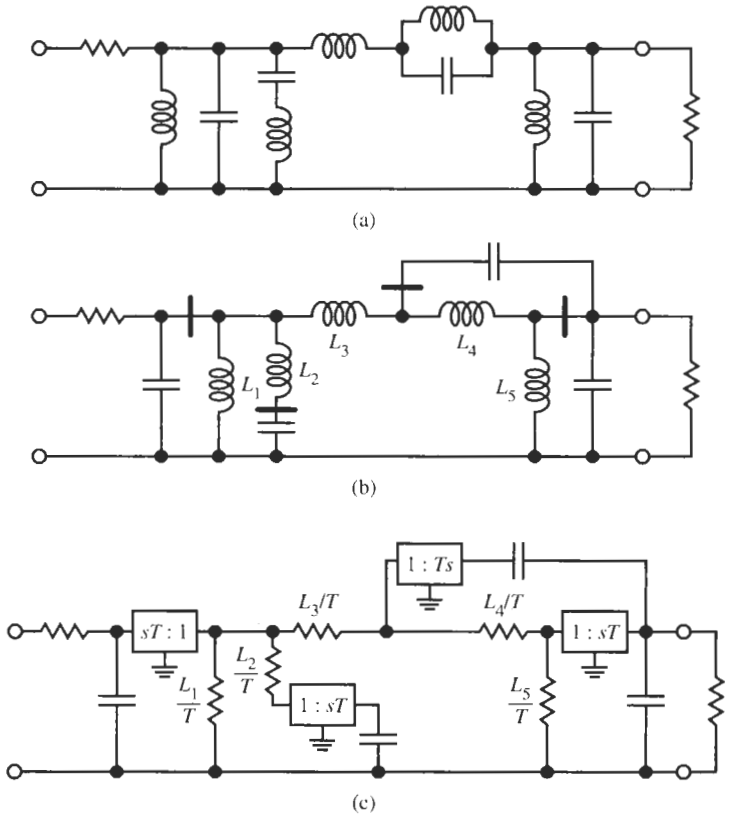

Figure 14.14 Gorski-Popiel's embedding technique for building LC ladders with simulated inductors. (a) Original ladder; (b) ladder redrawn to identify the inductor subnetworks and the necessary cuts; (c) final implementation with resistors and GICs.

of value $R_i = L_i / T$. Apart from nonidealities caused by opamp limitations, the performance of the new circuit will be identical to the original LC ladder. Figure 14.14 illustrates the embedding technique on a given LC circuit. Note that three GICs were saved by the embedding method compared to the approach that treats each inductor separately.

EXAMPLE 14.4

To illustrate the embedding technique let us design the LC ladder of Fig. 13.18d in active form with simulated inductors. Reduce the midband frequency to 23 kHz.

Solution

The circuit was a sixth-order bandpass filter with two transmission zeros, a maximally flat passband with $\alpha_{max} = 0.5$ dB and passband center at 230 kHz. The performance of the LC filter was shown in Fig. 13.18c. Attempting to design a bandpass active filter with 741-type opamps at such high frequencies and large Q values is not realistic.[4] We are asked to reduce the center frequency of the bandpass by a factor of 10 to 23 kHz to have some assurance of a successful design. In the ladder this is accomplished easily by increasing the capacitor and inductor values by a factor of 10. In the interest of realistic component values for the active filter let us also scale source and load resistors up to 1 kΩ, that is, we increase the impedance level by a factor of 20. The resulting circuit is shown in Fig. 14.15a, drawn to show the inductor subnetwork. We have also indicated the position of the three cuts necessary to isolate the subnetwork. For this purpose we consider the 0.1-Ω resistors to be short circuits because the troubling inductor loops will disappear in the active implementation.

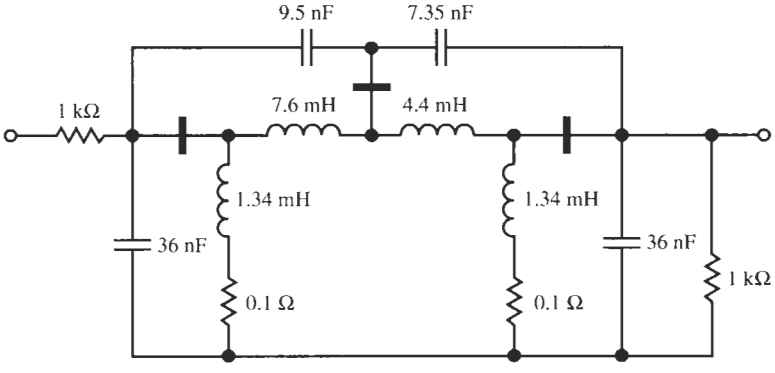

(a)

Figure 14.15 Circuits and test results for Example 14.4. (a) The LC filter redrawn to show the inductor subnetwork and the three required cuts; (b) test set-up for the final circuit; (c) the GIC; (d) test results. (Bode Plotter scales 10 to 50 kHz; −60 to 0 dB; cursor at 22.24 kHz, −5.690 dB.)

[4]In a design with 741-type opamps at such high frequencies, severe deviations must be expected due to the finite $\omega_t \approx 2\pi \times 10^6$ rad/s. However, with faster amplifiers, such as, for example, the HA-2542-2 introduced in Chapter 2, with a unity-gain frequency of 90 MHz, the higher frequency specifications can be implemented with little error.

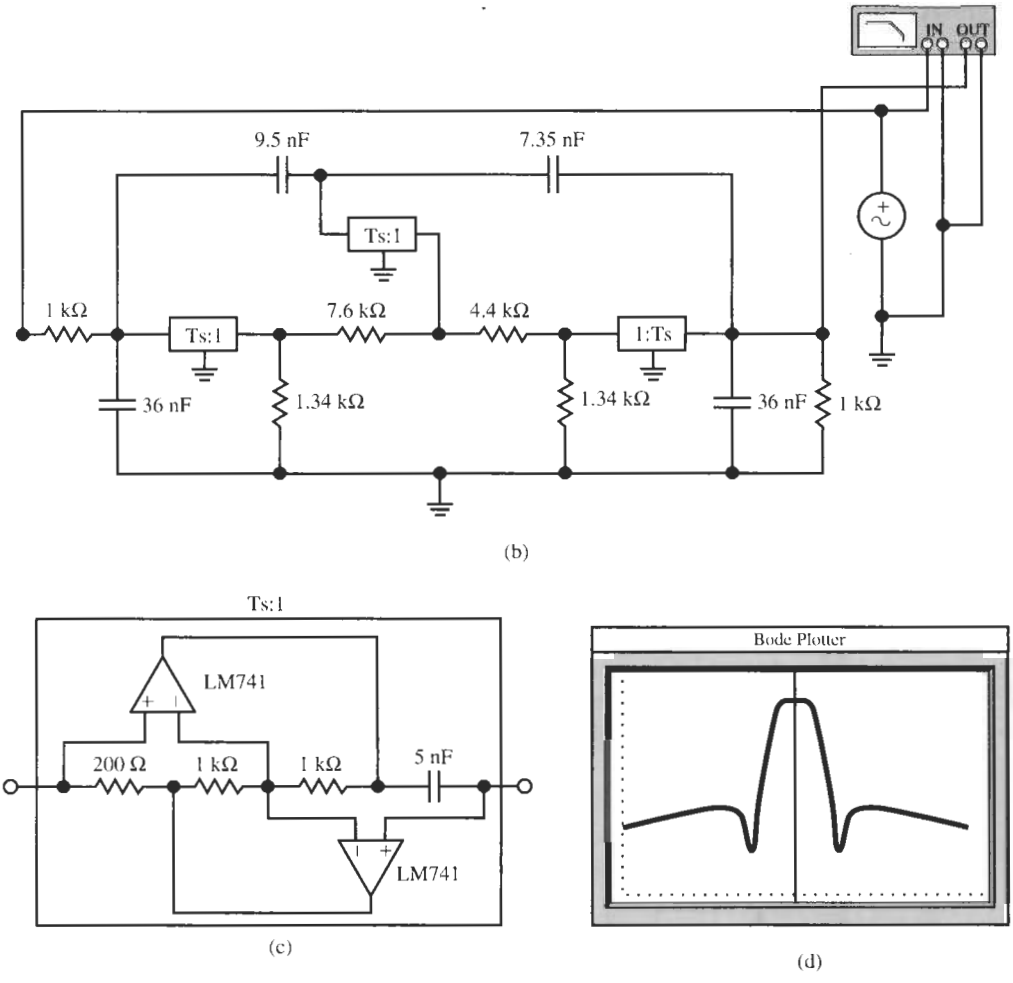

Figure 14.15 Continued

The cuts are then bridged by GICs as in Fig. 14.14c and the inductor subnetwork becomes a resistor subnetwork with the elements $R_i = L_i/T$. Although it is not necessary to keep all time constants, T, the same throughout the design, it is convenient to do so because it results in identical GIC circuits. Let us choose in the GIC $C_4 = 5$ nF and $R_1 = 200\ \Omega$, then $T = 1\ \mu$s and the inductor values in millihenries become resistor values in kiloohms. The final filter is shown in Fig. 14.15b and the sT:1-GIC block is shown in Fig. 14.15c. The 1:sT-GIC block is the same circuit, but turned around so the end nearest the capacitor C_4 faces the resistor subnetwork. The test performance is displayed in Fig. 14.15d. We observe that the performance is as specified but with a small frequency shift to the left because the simulated inductors are slightly increased [see Eq. (14.13)].

Note that we used only three GICs with a total of six opamps whereas we would have required six GICs with 12 opamps had we simulated the two floating and two grounded inductors individually.

The discussion and examples demonstrate that *LC* ladder simulation using Gorski–Popiel's embedding technique is both simple and powerful. We saw that a few well-defined steps lead from the lossless ladder to the active circuit, and that the active circuit can indeed compete with the performance of the passive *LC* filter if we use sufficiently fast amplifiers. Next, as promised, we introduce a further method to simulate an *LC* ladder with active components: Bruton's use of the *frequency-dependent negative resistor* (FDNR).

14.5 BRUTON'S FDNR TECHNIQUE

In an attempt to eliminate inductors from an *LC* ladder, L. Bruton (1969) had the idea to scale *all* the impedances of the ladder by the frequency-dependent factor $1/s$. Such an impedance-level scaling operation should certainly be legal because this operation does not affect the transfer function. The motivation behind this scaling operation is that scaling an inductive impedance sL by $1/s$ leaves us with a resistor of the same value, $R = L$, and the inductor is eliminated. However, so as not to change the transfer function in the scaling operation, *all* components must be scaled by the same factor. Thus, scaling the three passive elements in a ladder

$$Z_R = R, \quad Z_L = sL, \quad Z_C = \frac{1}{sC} \tag{14.26}$$

by $1/s$ gives the new components

$$Z'_R = \frac{R}{s}, \quad Z'_L = L, \quad Z'_C = \frac{1}{s^2 C} \tag{14.27}$$

Thus, we notice that such scaling actually results in a transformation of the elements: For normalized values, we find that a resistor R becomes a capacitor of value $1/R$, an inductor L becomes a resistor of value L, and a capacitor C becomes a new element that we have not encountered before. On the $j\omega$-axis the element is

$$Z'_C(j\omega) = -\frac{1}{\omega^2 C} \tag{14.28}$$

which is seen to be real, frequency dependent, and negative. Appropriately, it is called a *frequency-dependent negative resistor* or FDNR. Sometimes it is also referred to as a supercapacitor, but we shall use the more common name FDNR. It has been given the label D, i.e., $D = C$; its circuit symbol is four parallel lines, a "double capacitor," as shown in Fig. 14.16.

Notice in particular that none of the impedances obtained in the Bruton transformation describes an inductor. Thus, inductors are successfully eliminated but the price paid is the introduction of the peculiar new element D, whose impedance is negative and inversely proportional to the square of the frequency. Unless we find a way to realize this component, the transformation will be of little practical use.

Consider again the general impedance converter in Fig. 14.6, which for ideal opamps realized the input impedance of Eq. (14.4),

$$Z_{11'} = \frac{Z_1 Z_3 Z_5}{Z_2 Z_4} = \frac{Y_2 Y_4}{Y_1 Y_3 Y_5} \tag{14.29}$$

Element	Bruton transformed element
R	$1/R = C$
L	$R = L$
C	$D = C$

Figure 14.16 Passive components obtained from the Bruton transformation.

If we now choose $Y_1 = sC_1$, $Y_5 = sC_5$ and resistors for the other three elements, we obtain

$$Z_{11'} = \frac{G_2G_4}{s^2C_1C_5G_3} = \frac{R_3}{s^2C_1C_5R_2R_4} = \frac{1}{s^2D} \tag{14.30}$$

Nothing can be gained by choosing two unequal capacitors; so we let $C_1 = C_5 = C$. Further, as we can demonstrate by methods analogous to the ones we used in Sections 4.5.3 or 14.2, the optimal choice is $R_2 = R_3$. Then we have for our new component

$$Z_{11'}(j\omega) = -\frac{1}{\omega^2C^2R_4} = -\frac{1}{\omega^2D} \tag{14.31}$$

where D is identified as $D = C^2R_4$ with units of [As^2/V] or [Fs]. Similarly to the earlier GIC-based circuits, we can show that for $R_2 = R_3$ and $R_4 = 1/(\omega_cC)$, $Q_D = \infty$ and the error in D equals

$$\frac{\Delta D}{D} \approx -\frac{4}{|A(j\omega)|} \tag{14.32}$$

ω_c is a critical frequency in the design, such as the passband corner. Figure 14.17 shows how we can implement the FDNR element.

We still observe that the FDNR procedure is particularly useful for lowpass filters where all capacitors are grounded. The reason is that FDNRs have one terminal at ground and capacitors are transformed into FDNRs. Floating FDNRs can be conceived, but their operation has not been found to be satisfactory in practice.

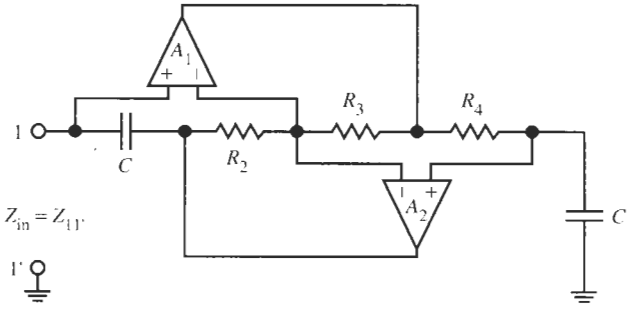

Figure 14.17 The frequency-dependent negative resistor (FDNR). For the optimal choice $R_2 = R_3$, $Z_{in}(j\omega) = -1/(\omega^2D)$ with $D = C^2R_4$.

An example will illustrate the design procedure and help us identify two practical difficulties that must be addressed.

EXAMPLE 14.5

Consider designing a fourth-order Butterworth filter with half-power frequency of $\omega_0 = 200{,}000$ rad/s (31.8 kHz); source and load are $R = 3$ kΩ. The design should make use of FDNRs.

Solution

As each capacitor results in one FDNR element it is more economical and advisable to use an minimum-capacitance ladder. From Table 13.1 we obtain the normalized circuit in Fig. 14.18a and, using the transformations of Fig. 14.16, the transformed circuit in Fig. 14.18b. Let us use a normalizing frequency $\omega_n = 100$ krad/s so that passbands corner is at $\omega = 2$.

Proceeding to the FDNR element, we use the circuit in Fig. 14.17 that realizes $Z_{in}(j\omega) = -1/(\omega^2 D)$, with $D = C^2 R_4$ and, by Eq. (14.31), $R_4 = 1/(\omega_c C)$. Thus, we have for the two FDNRs:

$$\text{FDNR1:} \quad 1.8485 = C^2 R_4 = \frac{C}{\omega_c}, \quad \text{i.e.,} \quad C = 1.8485\omega_c$$

$$\text{FDNR2:} \quad 0.7654 = C^2 R_4 = \frac{C}{\omega_c}, \quad \text{i.e.,} \quad C = 0.7654\omega_c$$

A natural choice for ω_c is $\omega_c = \omega_0 = 200{,}000$ rad/s, or normalized $\omega_c = 2$. With these numbers we have

$$\text{FDNR1:} \quad C = 2 \times 1.8485 = 3.697 \quad \text{with} \quad R_4 = \frac{1}{\omega_c C} = \frac{1}{7.394} = 0.135$$

$$\text{FDNR2:} \quad C = 2 \times 0.7654 = 1.531 \quad \text{with} \quad R_4 = \frac{1}{\omega_c C} = \frac{1}{3.042} = 0.3287$$

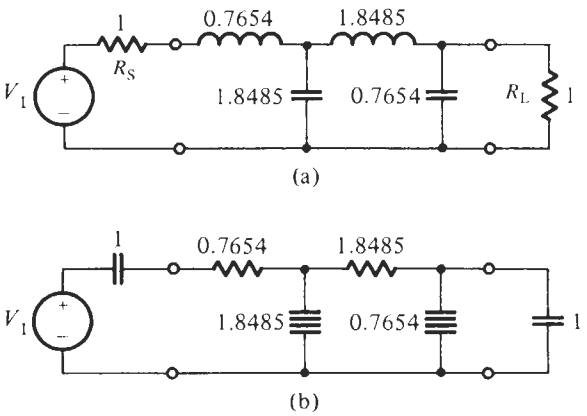

Figure 14.18 (a) Minimum-capacitance ladder and (b) Bruton transformation.

Finally we need to denormalize all the elements. We note that the transformed circuit has lost its source and load resistors: they were converted to capacitors. The normalizing resistor R_n is, therefore, arbitrary and can be chosen at will to achieve convenient components values. Let us choose $R_n = 5\ \text{k}\Omega$, then the resistors are multiplied by 5 kΩ, and the capacitors by $1/(\omega_0 R_0) = 1$ nF. Figure 14.19a shows the circuit with normalized elements and Fig 14.19b the final filter with denormalized components.

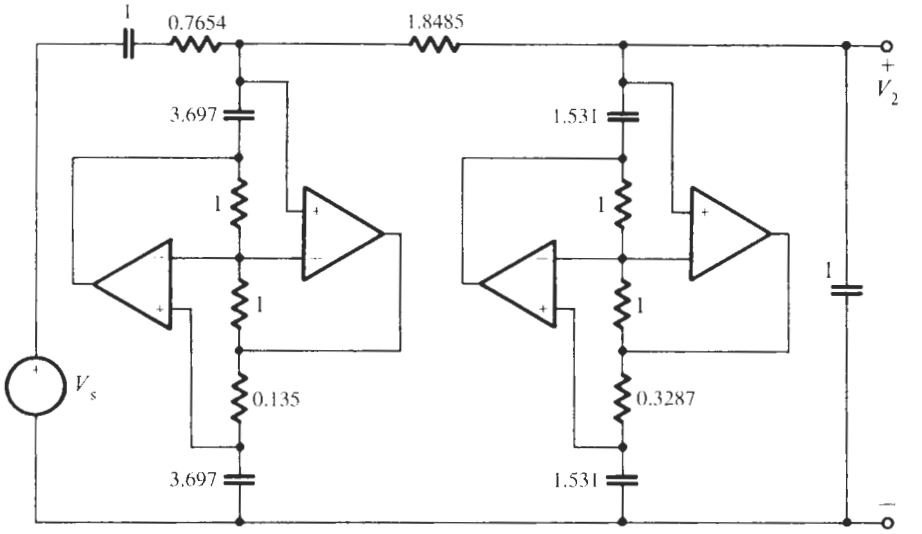

Figure 14.19 The filter designed in Example 14.5: (a) normalized circuit; (b) with denormalized elements.

The realization in Fig. 14.19b is completely equivalent to the original ladder in Fig. 14.18a and shows excellent performance with low sensitivities. However, before testing our design we need to attend to a couple of difficulties.

1. Since the *whole* filter needs to be transformed in Bruton's procedure, including the source and load resistors that become capacitors, the resistive source and load terminations disappear. If these terminations are prescribed external to the filter, we need to reinsert them without destroying the filter. This can be accomplished by use of unity-gain buffers as is shown in the final version in Fig. 14.20b. Also, the buffer provides an output node from which the filter output voltage can be taken without affecting the filter.
2. In the circuit as drawn (see Fig. 14.19), any dc path to the noninverting input terminals of the upper opamps is blocked by capacitors so that the opamps cannot draw any bias currents. This problem is similar to the one already encountered in certain GIC configurations in the previous section. We can solve it by bypassing the first capacitor after the input, C_1 in Fig. 14.20b, by a large resistor R_a. Naturally, this insertion will cause low-frequency gain errors in the filter's performance because a resistor in the transformed domain corresponds to an inductor in the original *LC* filter: in effect, the source resistor is bypassed by a large inductor (refer to Fig. 14.20a).

A better solution is to bypass also the output capacitor C_2 by a resistor R_b and then determine the values of R_a and R_b such that the dc performance of the FDNR design,

$$\frac{V_2}{V_1} = \frac{R_b}{R_a + R_{11} + R_{12} + R_b} \tag{14.33}$$

matches that of the prototype *LC* ladder,

$$\frac{V_2}{V_1} = \frac{R_L}{R_S + R_L} \tag{14.34}$$

From Eqs. (14.33) and (14.34), we obtain the result

$$\frac{R_b}{R_a} = \frac{R_L}{R_S}\left(1 + \frac{R_{11} + R_{12}}{R_a}\right) = \frac{R_L}{R_S}\left(1 + \frac{1}{R_a}\sum_i R_{1i}\right) \tag{14.35}$$

The equation lets us compute R_b once R_a is chosen. Nevertheless, the two resistors R_a and R_b still correspond to inductors shunting the source and load terminations in the *LC* prototype ladder (Fig. 14.20a). To minimize their effect we need to choose R_a and R_b much larger than the sum of all the series resistors: $R_a, R_b \gg \sum R_{1i}$ in the FDNR design.

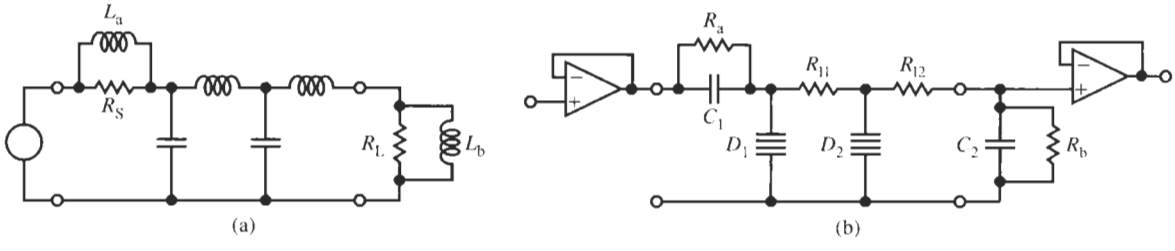

Figure 14.20 (a) The *LC* ladder with parasitic shunt inductors caused by the necessity to provide bias currents; (b) Bruton transformation including bypass resistors and buffers.

EXAMPLE 14.6

Let us complete the design of Example 14.5 and test the resulting circuit.

Solution

We had $R_{l1} = 3.827$ kΩ and $R_{l2} = 9.243$ kΩ and $R_S = R_L$ in the *LC* prototype ladder. Thus, $R_{l1} + R_{l1} = 13$ kΩ and $R_a = R_b = 1$ MΩ seems sufficiently large to achieve a correct design. The final circuit and its test performance are shown in Fig. 14.21. Observe that the circuit behaves as desired starting at very low frequencies, that is, the bypass resistors have no apparent effect. Buffers at input and output permit us to connect the specified 3-kΩ source and load resistors. We notice at about 230 kHz an unspecified transmission zero. This zero is caused by opamp nonidealities (it is absent in a simulation with ideal opamps), but since the zero is in the stopband and is beneficial in helping to narrow the transition region, we shall not attempt to determine exactly how it is generated.

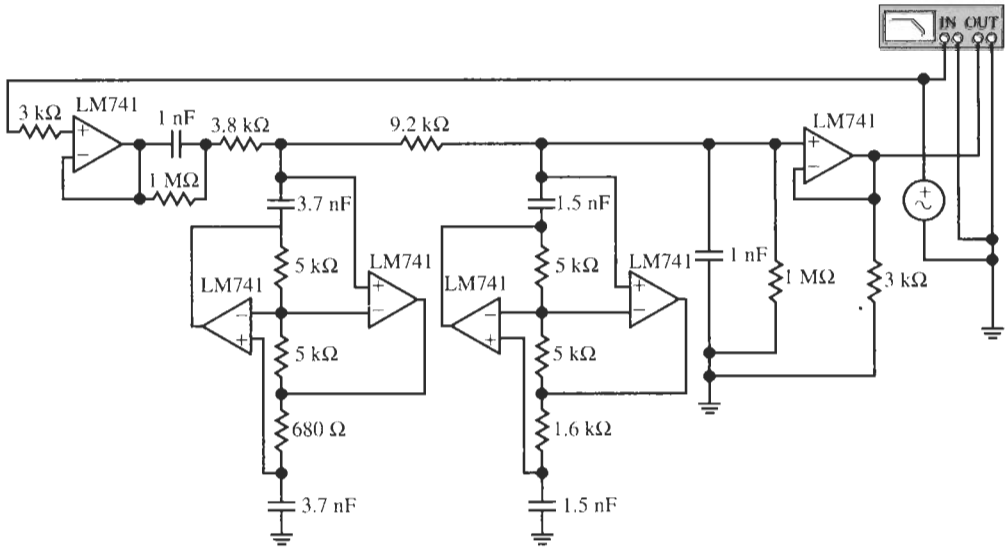

(a)

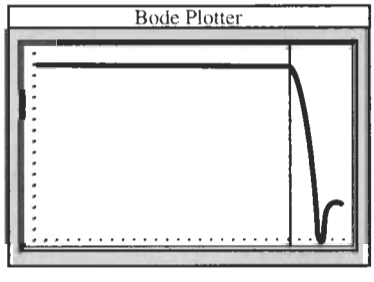

(b)

Figure 14.21 (a) Final FDNR design for Example 14.5 with bypass resistors, buffers, and specified load resistors; (b) test performance. (Bode Plotter scales: 1 mHz to 1 MHz; −100 to 0 dB; cursor at 28.48 kHz, −8.167 dB.)

Let us present an additional example to illustrate the steps that should be taken to arrive at a cost-effective design of an active ladder with the FDNR technique.

EXAMPLE 14.7

A lowpass filter is to be designed with a maximally flat passband in $0 \leq f \leq 6$ kHz and $\alpha_{max} \leq 2$ dB. There must be transmission zeros at $f_1 = 12$ kHz and at $f_2 = 24$ kHz. Also, we require an attenuation increase at high frequencies of at least 40 dB per decade. Source and load resistors are 1.0 kΩ.

Solution

We discussed in earlier chapters how such a transfer function can be determined and we saw in Chapter 13 how a lossless ladder filter is derived once the transfer function is known. Because we wish to concentrate on the FDNR process in this example, let us proceed directly to the resulting lowpass prototype circuit. It is shown in Fig. 14.22a. The circuit has three floating inductors that would require six GICs and would make the GIC-based implementation expensive. However, since the circuit has only three floating inductors and five capacitors, the dual topology will have three grounded capacitors and five inductors. This will permit us a realization with three FDNRs; the five inductors will be converted to five resistors. The method of converting a circuit into its dual is discussed in elementary circuits courses; the resulting dual circuit is shown in Fig. 14.22b. Notice that this structure is also a good candidate for the Gorski-Popiel embedding technique: only four GICs would be needed to isolate the inductor subnetwork from the remainder of the filter. However, since we have only three grounded capacitors, the realization with three FDNRs is possible. Let us proceed with that approach.

The Bruton transformation of the filter results in the structure depicted in Fig. 14.22c. We require three FDNRs from which we find

$$\text{FDNR 1:} \quad 1.0217 = C^2 R_4 = \frac{C}{\omega_c}, \quad \text{i.e.,} \quad C = 1.0217\omega_c \quad \text{and} \quad R_4 = \frac{1}{\omega_c C}$$

A logical choice for ω_c is the passband edge, i.e., $\omega_c = 2\pi \times 6000$ rad/s. Let us normalize the frequency by $\omega_n = 2\pi \times 1000$ rad/s so that we deal with the normalized bandedge $\omega_{cn} = 6$. Then we have for the normalized capacitors in FDNR 1: $C = 6.1302$ and we will attempt to denormalize by multiplying the capacitors with 1 nF. Since it will be easier to locate a 6-nF capacitor in the parts bin than a 6.13-nF capacitor, let us deviate slightly from the optimal value of $\omega_{cn} = 6$ and choose instead $\omega_{cn} = C/1.0217 = 6/1.0217 = 5.8726$. Then we have

$$R_4 = \frac{1}{\omega_c C} = \frac{1}{5.8726 \times 6} = 0.02838$$

We mentioned that we wish to denormalize the capacitors by multiplying them by $C_n = 1$ nF. Thus the normalizing resistor is equal to

$$R_n = \frac{1}{2\pi \times 6000 \times 10^{-9}} \Omega = 26.526 \text{ k}\Omega \tag{14.36}$$

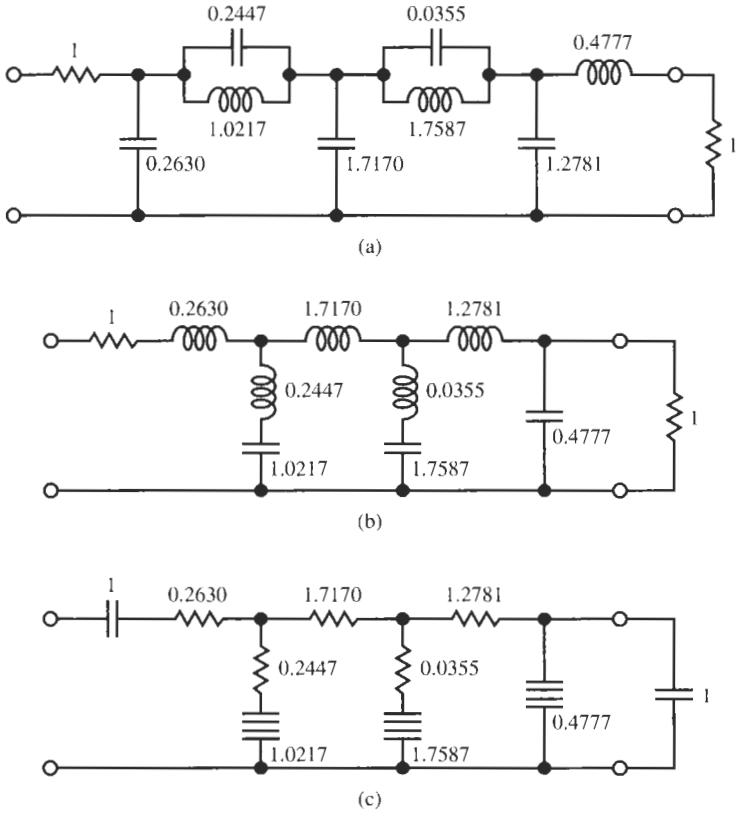

Figure 14.22
(a) Sixth-order minimum-inductance ladder; the realization would require six GICs; (b) the dual minimum-capacitance ladder; its realization would require four GICs; (c) the Bruton transformation of the ladder in (b), which requires three[5] FDNRs.

it will be used to denormalize *all* resistors in the filter. In a similar fashion we obtain for

$$\text{FDNR 2:} \quad 1.7587 = C^2 R_4 = \frac{C}{\omega_c}, \quad \text{i.e.,} \quad C = 1.7587\omega_c \quad \text{and} \quad R_4 = \frac{1}{\omega_c C}$$

Here a convenient value is $C = 10$ nF; this requires us to choose instead of the optimal value $\omega_{cn} = 6$ the frequency $\omega_{cn} = C/1.7587 = 10/1.7587 = 5.6860$. R_4 is then

$$R_4 = \frac{1}{\omega_c C} = \frac{1}{5.6860 \times 10} = 0.017587$$

Lastly we have for

$$\text{FDNR 3:} \quad 0.4777 = C^2 R_4 = \frac{C}{\omega_c}, \quad \text{i.e.,} \quad C = 0.4777\omega_c \quad \text{and} \quad R_4 = \frac{1}{\omega_c C}$$

Let us choose 3 nF as a convenient capacitor value, which means we pick as the "edge frequency" $\omega_{cn} = C/0.4777 = 3/0.4777 = 6.2801$ rather that the optimal $\omega_{cn} = 6$, and

[5]Note though that the FDNR realization may require two additional opamps at input and output for buffering.

$$R_4 = \frac{1}{\omega_c C} = \frac{1}{6.2801 \times 3} = 0.05308$$

It was recommended earlier that ω_c should be a frequency close to the passband corner. In choosing frequencies ω_{cn} for the three FDNRs different from the exact value $\omega_{cn} = 6$ but close to it, we have traded a theoretically slightly larger error ΔD for the practical advantage of more easily found capacitor values.

The circuit can now be completed. We denormalize all resistors by $R_n = 26.526\ \text{k}\Omega$ from Eq. (14.36) and obtain the result in Fig. 14.23a. Figure 14.23b shows the test result. The 2-dB passband corner is at 6 kHz and we see clearly the two transmission zeros at 12 and 24 kHz. Just as in the previous example we note a parasitic zero at approximately 170 kHz, which arises from the finite gain-bandwidth product of the opamps. Again, this parasitic zero is far away from the passband and is beneficial in improving the stopband attenuation; we shall not investigate the origin of this zero.

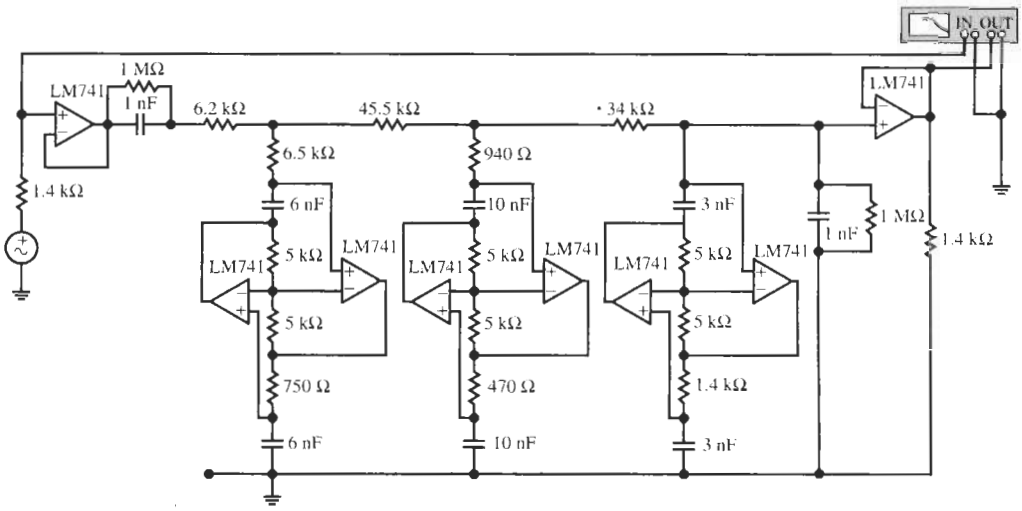

(a)

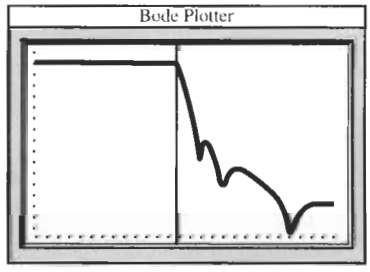

(b)

Figure 14.23 (a) FDNR realization for Example 14.7; (b) test performance. (Bode Plotter scales: 100 Hz to 600 kHz; −120 to 0 dB; cursor at 5.878 kHz, −8.192 dB.)

Note that changing the termination resistors in an *LC* ladder requires rescaling all the component values, whereas in the FDNR realization the termination resistors are isolated from the filter by the buffers and have no effect on the performance. We have chosen arbitrarily $R = 1.4$ kΩ for the FDNR design in Fig. 14.23a to demonstrate that these values have no effect.

14.6 CREATING NEGATIVE COMPONENTS

Negative circuit elements are useful for a variety of applications. It would be desirable, therefore, to have available some method that permits us to implement negative components. For example, we may wish to eliminate the losses of reactive circuit components to obtain, e.g., an ideal inductor. This can be achieved by placing a negative resistor in series or parallel with the component. There are in the literature on filters a number of filter transformations with promising properties, but they entail negative components. Also we may recall from elementary circuits courses that in the equivalent circuit of an ordinary transformer the mutual inductance is often negative. Naturally, we cannot buy, say, a negative resistor or negative inductor, but by the use of active devices we can construct an electronic circuit whose input impedance simulates a negative element. The approach we take is to design a twoport, a *negative impedance converter* (NIC), such that the input impedance is proportional to the negative of the load impedance, $Z_{in}(s) = -kZ_L(s)$. Figure 14.24a illustrates this case. The circuit to achieve this result is surprisingly simple and effective.

Consider the circuit in Fig. 14.24b. It contains two resistors and one operational amplifier in addition to the to-be-converted impedance Z_L. To understand intuitively why this simple circuit provides a negative impedance at its input, notice that the current flowing through Z_L equals V_1/Z_L because the opamp forces the voltage V^+ to be equal to $V^- = V_1$. Consequently the opamp's output voltage V_o equals $V_o = V_1 + R_2(V_1/Z_L)$ and the input current, $I_{in} = G_1(V_1 - V_o) = -R_2(V_1/Z_L)G_1$, flows *into* the source terminals, implying a negative input admittance $Y_{in} = I_{in}/V_1 = -G_1R_2/Z_L$. We can verify this intuitive result by using formal nodal analysis. We find at the opamp input nodes in Fig. 14.24b

$$I_{in} = G_1(V_1 - V_o), \quad V_+(Y_L + G_2) = V_oG_2 \tag{14.37}$$

If we assume the opamp is ideal, that is $V_+ = V_1$, we obtain the two equations

$$\frac{I_{in}}{V_1} = Y_{in} = G_1\left(1 - \frac{V_o}{V_1}\right), \quad \frac{V_o}{V_1} = 1 + \frac{Y_L}{G_2}$$

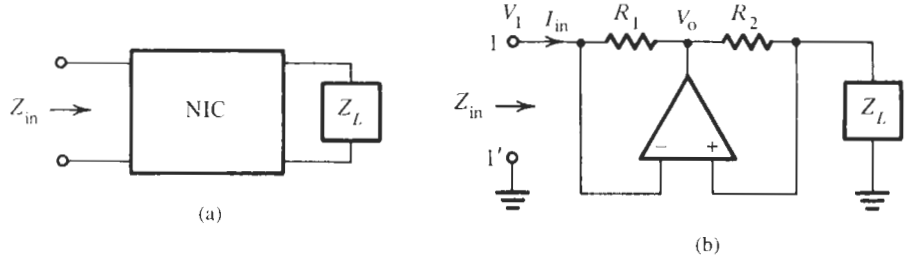

Figure 14.24 (a) The negative impedance converter realizing $Z_{in}(s) = -kZ_L(s)$; (b) a simple opamp NIC circuit.

They may be combined to yield the expected result

$$Y_{\text{in}} = -\frac{G_1}{G_2} Y_{\text{L}} \quad \text{or} \quad Z_{\text{in}} = -\frac{R_1}{R_2} Z_{\text{L}} \tag{14.38}$$

From this we see that the circuit realizes a negative impedance. Specifically, it is the negative of the load impedance multiplied by a scaling factor set by two resistors.

To understand the limitations of the simple general impedance converter in Fig. 14.24b, we need to investigate its performance with real opamps. As always, the operational amplifier is described by $(V_+ - V_-)A = V_o$ and we will use the integrator model, $A(s) \approx \omega_t/s$. Introducing this model in Eqs. (14.37), we find

$$Y_{\text{in}}(s) = -G_1 \left[\frac{Y_{\text{L}} + G_2}{G_2 - (Y_{\text{L}} + G_2)/A(s)} - 1 \right]$$

or

$$Z_{\text{in}}(s) = -\frac{R_1}{R_2} Z_{\text{L}} \times \frac{1 - (1 + Y_{\text{L}} R_2)/A(s)}{1 + (1 + Z_{\text{L}} G_2)/A(s)} \tag{14.39}$$

For $A = \infty$, Eq. (14.39) reduces, of course, to Eq. (14.38), but for finite-gain opamps Eq. (14.39) permits us to assess the frequency range over which the element is valid and useful, and any errors we may expect in the simulated negative impedance.

Let us use an example to verify that these mysterious negative elements actually function as predicted by the theory, and at the same time investigate the useful frequency range for a given opamp.

EXAMPLE 14.8

Use a 2-kΩ and a −1-kΩ resistor and form a voltage divider. Test the output voltage and verify that the circuit works as predicted. Use a high-frequency opamp (the 90-MHz HA 2542-2 we encountered earlier) and determine the useful frequency range. The circuit is given in Fig. 14.25a.

Solution

The ideal transfer function is

$$\frac{V_2}{V_1} = \frac{-1\ \text{k}\Omega}{2\ \text{k}\Omega - 1\ \text{k}\Omega} = -1 \tag{14.40}$$

so we can expect 0-dB gain and 180° phase shift. The question to be answered is over which frequency range this result is valid.

With all resistors equal to 1 kΩ and the integrator model for the opamp, the "negative resistor" is from Eq. (14.39)

$$Z_{\text{in}}(s) = -1\ \text{k}\Omega \left(\frac{1 - 2s/\omega_t}{1 + 2s/\omega_t} \right)$$

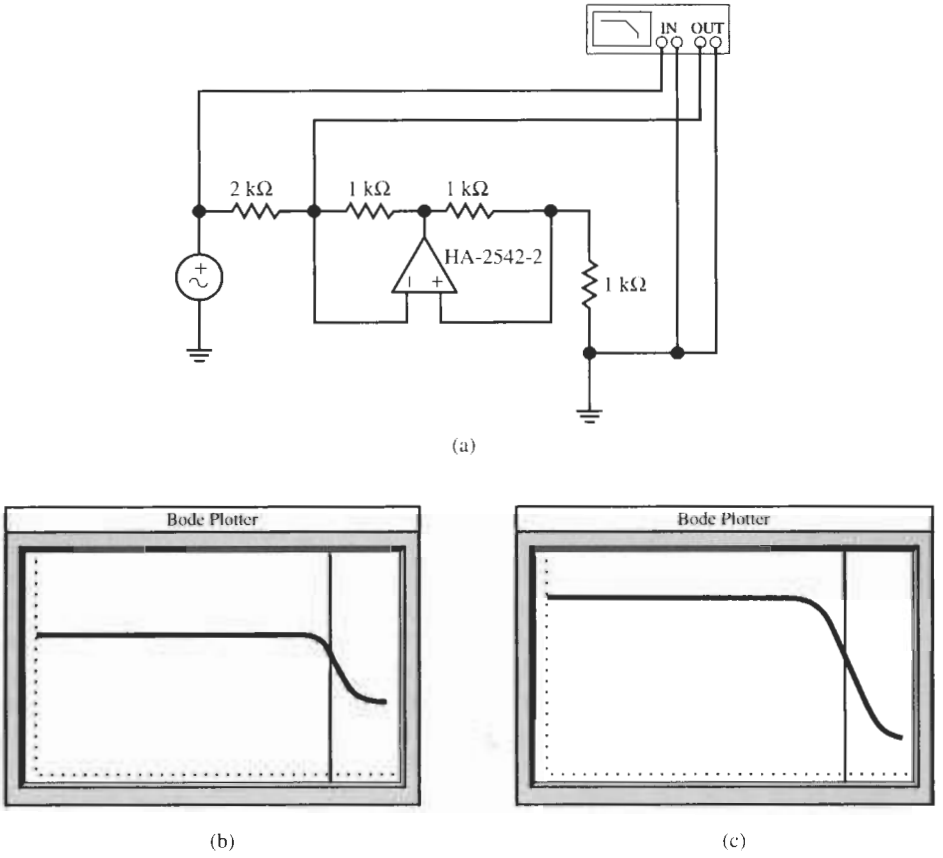

Figure 14.25 Circuit and experimental performance of a negative impedance converter realizing a −1-kΩ resistor. The opamp is a HA-2542-2. (a) Circuit; (b) magnitude response; (c) phase response. (Bode Plotter scales: 10 mHz to 1 GHz; (b) −20 to 10 dB; cursor at 16.68 MHz, −3.001 dB; (c) −45° to 225°; cursor at 16.68 MHz, −110.9°.)

This is an interesting result that could have been anticipated from Eq. (14.39): the input impedance is the expected 1-$k\Omega$ resistor, but it is multiplied by a first-order allpass function; the only error is, therefore, the phase

$$\phi(\omega) = -2\tan^{-1}\frac{\omega}{\omega_t/2}$$

This means that the realized impedance is a negative "resistor" whose phase is −90° at one-half the gain-bandwidth product of the opamp.

To see how this result translates into the performance of the voltage divider, we form

$$T(s) = \frac{V_2}{V_1} = \frac{Z_{in}(s)}{2\text{ k}\Omega + Z_{in}(s)} = \frac{1}{2\text{ k}\Omega/Z_{in}(s) + 1}$$
$$= \frac{1}{1 - 2\dfrac{1 + 2s/\omega_t}{1 - 2s/\omega_t}} = -\frac{1 - 2s/\omega_t}{1 + 6s/\omega_t}$$

We note that for low frequencies $T(s)$ equals -1 as predicted in Eq. (14.40), but it has a pole at $\omega_t/6$, i.e., at $\approx$ 15 MHz for an HA 2542-2 opamp. At this frequency the gain begins to decrease from 0 dB as we saw in Section 3.3 when we studied Bode plots; then there is a zero at $\omega_t/2$ (at $\approx$ 45 MHz) where the gain curve flattens out at the level of $20 \log(2/6) \approx -9.5$ dB.

At the same time the phase is at 180° for lower frequencies, reflecting the value $T = -1$, and is $\approx 135°$ at the 3-dB point, i.e., at approximately 15 MHz. These are the observed results shown in Figs. 14.25b and 14.25c.

We conclude that the negative impedance converter works as predicted.

There is a variety of other uses for negative impedances, apart from the one occurring in filter transformations. Let us illustrate them with a further example. For instance, frequently in the design of *LC* filters we will have to make use of transformers and it would be interesting to find out whether transformers can also be simulated with active components so that the whole *LC* filter can be built in microelectronic form. Our next example will demonstrate that this is indeed possible.

EXAMPLE 14.9

We wish to design an electronic circuit that behaves like a unity-coupled transformer. The transformer turns-ratio must equal 4 and it must be inverting, that is, its voltage ratio is $V_2/V_1 = -4$.

Solution

To approach this problem we recall from elementary circuits courses that the transformer in Fig. 14.26a can be represented by the inductive-T model in Fig. 14.26b. L_1 and L_2 are the primary and secondary inductances, respectively, and M is the mutual inductance. The dots in Fig. 14.26a indicate that we specified a voltage ratio of *minus* 4, a requirement that also leads to the mutual inductance M being negative. Since we know how to implement an inductive-T circuit from Section 14.4, we need only be concerned with the negative inductor $-M$, which is the subject of the discussion in this section.

We have to write a few transformer equations, which we derive readily from the circuit in Fig. 14.26b. We find

$$V_1 = sL_1I_1 - sMI_2, \quad V_2 = -sMI_1 + sL_2I_2 \tag{14.41}$$

Further, $V_2/I_2 = -R_L$. If we combine these equations, we can compute the voltage ratio

$$\frac{V_1}{V_2} = -\left(\frac{L_1}{M} + s\frac{L_1L_2 - M^2}{M}\frac{1}{R_L}\right) \tag{14.42}$$

where $M = k\sqrt{L_1L_2}$ and k is the coefficient of coupling. Ideally, $k = 1$ for unity coupling; in practice, real transformers have $k < 1$, but $k \approx 1$.

Let us try to realize a unity-coupled transformer as specified in the problem statement. This means that we require $M = \sqrt{L_1L_2}$ and $L_1L_2 - M^2 = 0$. Then we have from Eq (14.42)

$$\frac{V_1}{V_2} = -\frac{L_1}{M} = -\frac{L_1}{\sqrt{L_1 L_2}} = -\sqrt{\frac{L_1}{L_2}} = -\frac{n_1}{n_2} \tag{14.43}$$

Here we have used that the inductances are proportional to the square of the number of turns in their windings.

For our problem we need $n_2/n_1 = 4$. To get some guidance in determining the transformer elements, we calculate from Eqs. (14.41) the input impedance

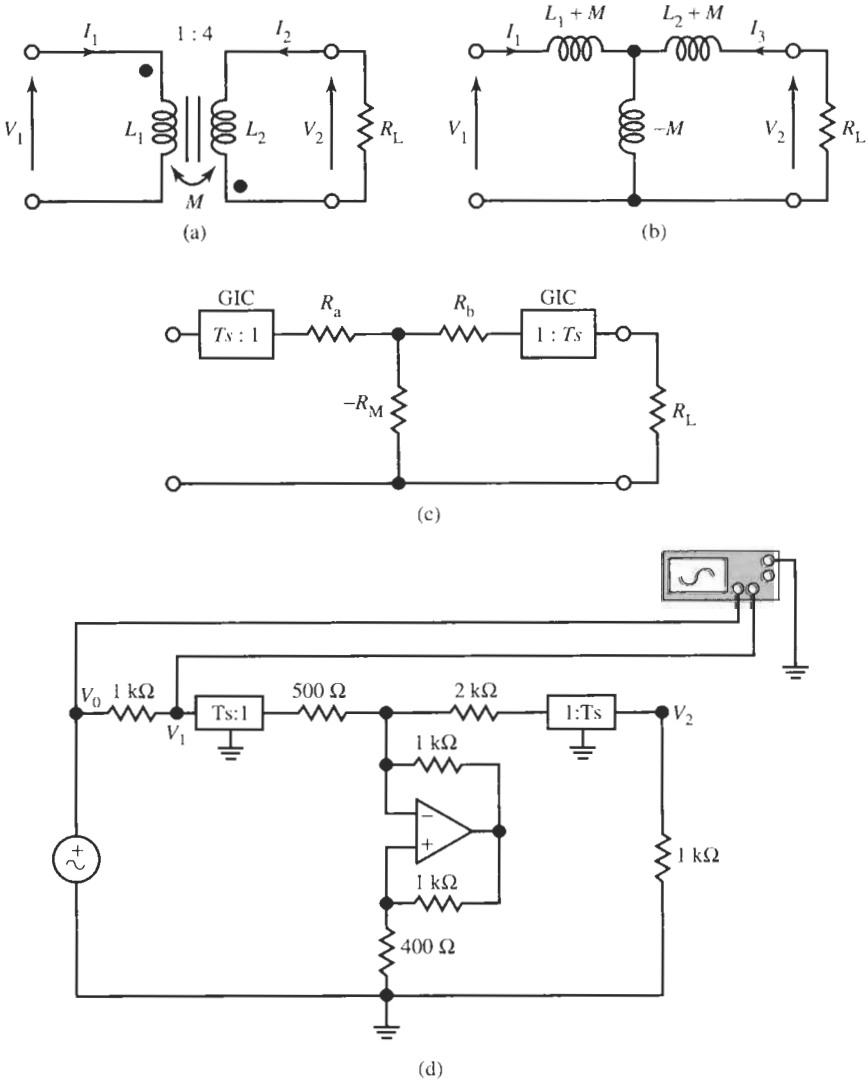

Figure 14.26 Implementation of an electronic transformer. (a) Transformer symbol; (b) inductive-T equivalent circuit; (c) resistive-T embedded between two GICs; (d) final transformer circuit using five opamps; (e, f) test results. [oscilloscope scales: horizontal (time base) 0.05-ms/div, vertical: (e) Channel A (V_1): 5mV/div, Channel B (V_2): 10 mV/div. (f) Ch. A (V_0): 50 mV/div, Ch. B (V_1): 5 mV/div]

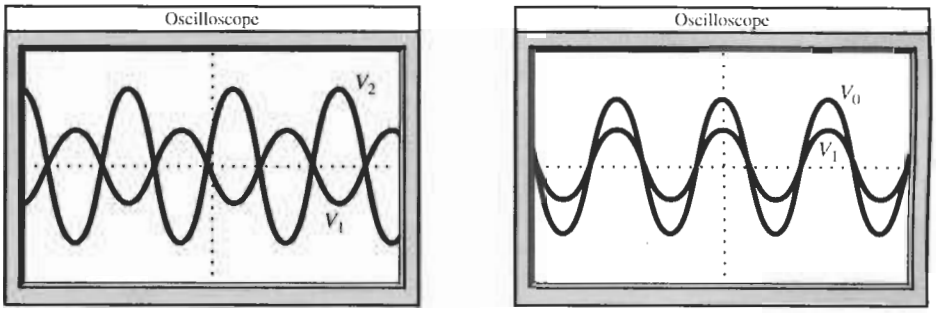

(e) (f)

Figure 14.26 Continued

$$Z_{\text{in}} = \frac{V_1}{I_1} = sL_1 - \left.\frac{s^2M^2/R_L}{1 + sL_2/R_L}\right|_{M^2=L_1L_2} = \frac{sL_1}{1 + sL_2/R_L} \tag{14.44}$$

Ideally we select $\omega L_2 \gg R_L$ so that

$$Z_{\text{in}} = \frac{L_1}{L_2}R_L = \left(\frac{n_1}{n_2}\right)^2 R_L \tag{14.45}$$

a well-known result. In our case, let us assume that $R_L = 1$ kΩ and that the frequency of interest is 5 kHz. Then we should select $L_2 \gg 1000/(2\pi \times 5000)$ H ≈ 32 mH. Let us choose $L_2 = 1.6$ H, a factor of 50 larger than 32 mH. By Eq. (14.43), this gives $L_1 = 0.1$ H to get $L_2/L_1 = 16$ for the required voltage ratio of 4, and $M = \sqrt{L_1L_2} = 0.4$ H.

With this step the transformer parameters are determined and we proceed to the resistive T section embedded between two GICs. Figure 14.26c shows the circuit. The inductors are implemented as $L = R/T$ where T is given by Eq. (14.17): $T = C_4R_1$. Let us choose the two components of the GIC (Fig. 14.11) as $R_1 = 10$ kΩ and $C_4 = 0.1$ μF so that $T = 1$ ms. We also used $R_2 = R_3 = 1$ kΩ and LM741 opamps in the GICs. In Fig. 14.26c we have

$$R_a = \frac{L_1 + M}{T} = \frac{(0.1 + 0.4)\text{H}}{10^{-3}\text{s}} = 500\ \Omega$$

$$R_b = \frac{1.6 + 0.4}{10^{-3}}\ \Omega = 2\ \text{k}\Omega$$

$$R_M = \frac{|-0.4|}{10^{-3}}\ \Omega = 400\ \Omega$$

Figure 14.26d is the final circuit, with test results given in Figs. 14.26e and 14.26f. The two voltages V_1 and V_2 are measured on the oscilloscope. Notice that, as specified, V_2 is approximately four times as large as V_1 and is 180° out of phase with V_1.

If we measure the voltages at V_0 and V_1, we find from the oscilloscope display in Fig. 14.26f, $V_1/V_0 \approx 11$ mV/200 mV $= 0.055$. Since the input resistance of the transformer is

$1\ \text{k}\Omega/4^2 = 62.5\ \Omega$, the voltage divider ratio should be $62.5\ \Omega/(1062.5\ \Omega) = 0.059$, in good agreement with the observation.

We may conclude that the circuit in Fig. 14.26d is a good and practical simulation of a transformer. Observe that very large inductors can be simulated with ease, but note that the circuit is relatively expensive in using five operational amplifiers.

REFERENCES

A. Antoniou, "Realization of Gyrators Using Operational Amplifiers and Their Use in Active *RC* Network Synthesis," Proc. IEE, Vol. 116, pp. 1838–1850, 1969.

L. T. Bruton, "Network Transfer Functions Using the Concept of Frequency-Dependent Negative Resistance," *IEEE Trans. Circuit Theory*, Vol. CT-16, pp. 406–408, 1969.

J. Gorski-Popiel, "RC-Active Synthesis Using Positive-Immittance Converters." *Electron. Lett.*, Vol. 3, pp. 381–382, August 1967.

A. S. Sedra and P. O. Brackett, *Filter Theory and Design: Active and Passive*. Matrix Publishers, Portland, OR, 1978, Sec. 8.4.

PROBLEMS

14.1 Derive Eq. (14.5) for the GIC operating in reverse.

14.2 Derive Eq. (14.7) that expresses the deviations in the simulated inductor that must be expected because of finite opamp bandwidth.

14.3 Design and test a parallel *R–L–C* resonant circuit with a simulated inductor. The resonance frequency must be 16 kHz; the impedance of the circuit at resonance must be larger than 100 kΩ, and the technology limits the largest capacitor to $C = 35$ pF.

14.4 For a particular filtering problem, the prototype shown in Fig. P14.4 is chosen. This is a singly terminated fourth-order Chebyshev lowpass filter having a ripple width of 0.9 dB and a bandwidth of 1 rad/s. For the final design, the filter is to be frequency scaled by a factor of 10,000 and magnitude scaled to give practical element sizes. Design and test the filter using Electronics Workbench (EWB). The methods to be employed are

(a) direct inductor replacement

(b) Gorski-Popiel's method

(c) Bruton's FDNR technique

14.5 A filtering problem is found to require a fourth-order lowpass Butterworth filter as the prototype. The filter is to have a half-power frequency of 1000 Hz. Magnitude scale to give practical element sizes. Design the filter and test its performance with EWB. Make use of

(a) direct inductor replacement

(b) Gorski-Popiel's method

(c) Bruton's FDNR technique

14.6 Using simulated inductors, design a doubly terminated highpass filter based on a fourth-order Butterworth prototype. The half-power frequency of the filter is to be 5 kHz and the terminating resistors are 100 Ω each. Build the circuit and test your design.

14.7 The specifications for a highpass filter are shown in Fig. P14.7. It is further specified that the response be maximally flat. Using the methods from this chapter, find a filter realization and magnitude scale to give element values in a practical range. Test your design.

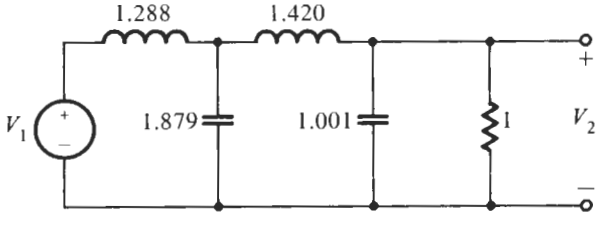

Figure P14.4

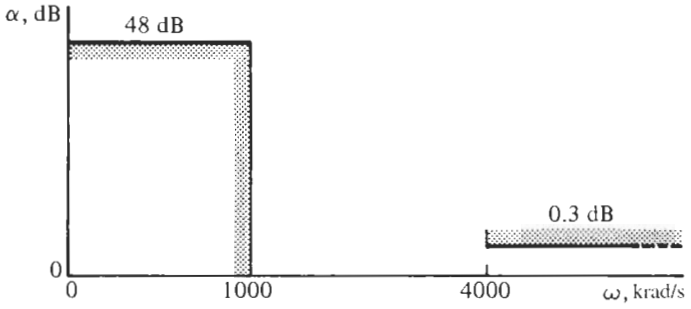

Figure P14.7

14.8 A Chebyshev highpass filter is required to satisfy the specifications given in Fig. P14.8. Using

(a) Gorski-Popiel's method

(b) Bruton's FDNR technique

find a filter realization. Magnitude scale to obtain practical element values and test your circuit's performance.

14.9 While reengineering some old equipment the circuit shown in Fig. P14.9 is found. The design calculations have been lost, but the component's values were measured as given in the figure, and the nameplate indicates

$f_0 = 1218$ Hz; half-power frequencies:

$f_L = 752.8$ Hz and $f_H = 1970.8$ Hz

As an engineer, you are assigned to replace this filter with a new one using active filter techniques. Of course you may not use any inductors, and you are restricted to use no more than two quad-opamp chips. Among the options discussed in this chapter, use a suitable method; justify your choice. Design the circuit with practical element values, and measure the attenuation characteristics you achieve.

14.10 The following specifications are made on a bandpass filter that is to have a Butterworth response. The prototype is to be third order, $f_0 = 1$ kHz, and the two half-power frequencies are 1250 and 800 Hz. The terminating resistors are $R_1 = R_2 = 1$ kΩ. Design the filter using a suitable method from those discussed in this chapter; be sure you use elements in a practical range, and test your design.

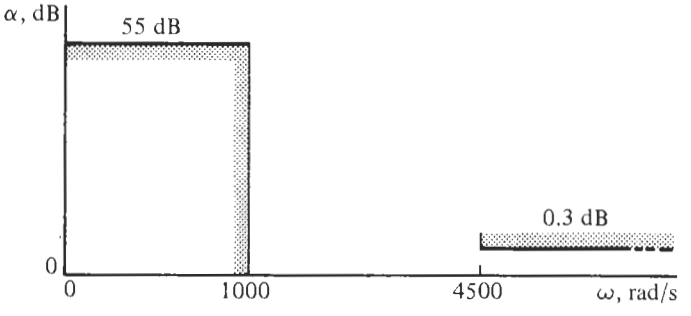

Figure P14.8

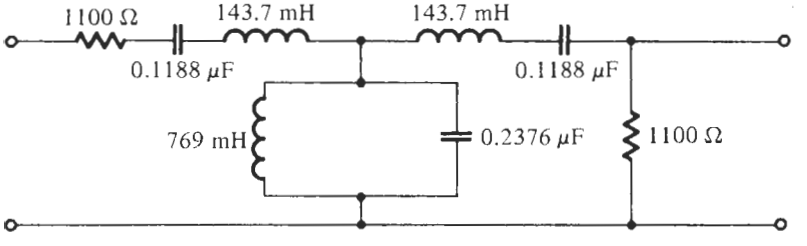

Figure P14.9

14.11 The prototype for a filter is second-order Butterworth lowpass. A bandpass characteristic is required in which $\omega_0 = 14{,}500$ rad/s and the half-power bandwidth is 1800 rad/s. Using the methods from this chapter, design and test the bandpass filter.

14.12 This problem requires the design of a bandpass filter to meet the specifications set for Problem 9.19. In contrast to the earlier design methods, this design is to be made using element simulation based on doubly terminated ladder filters. Choose a suitable technique, justify your choice, and build and test your circuit.

14.13 The starting point for this problem is the normalized circuit given in Problem 8.8. It is a lowpass Cauer (elliptic) filter. Denormalize the components such that the passband edge frequency is $f_c = 22.6$ kHz and source and load resistors are 600 Ω. Find a realization that is equivalent to the passive filter using a suitable method presented in this chapter. Make sure you use practical element sizes in your design and test its performance.

14.14 Repeat Problem 14.13 for the circuit in Fig. P8.9. The passband corner is $\omega_p = 10$ krad/s; source and load resistors are 1 kΩ.

14.15 Design a bandstop filter that satisfies the attenuation specifications of Fig. P14.15. Use a Butterworth prototype in your design and make use of a suitable method from this chapter in completing your design. The number of opamps must be minimized. The use of 1-kΩ terminating resistors is suggested. Build and test your design.

14.16 A required bandpass design leads to the prototype shown in Fig. P14.16. It is a fifth-order Chebyshev lowpass filter with a 0.5-dB ripple, normalized so that the 3-dB bandwidth is 1.0 rad/s. The bandpass filter must have $\omega_0 = 1000$ rad/s and a 3-dB bandwidth of 1000 rad/s. The filter is driven by a voltage source with a source resistor of 1 kΩ. Build a suitable active circuit, using the methods from this chapter, and test your design.

14.17 Repeat Problem 15.14 using the seventh-order prototype shown in Fig. P14.17. This prototype has a Chebyshev lowpass response with a ripple width of 0.5 dB, normalized such that the 3-dB bandwidth is 1.0 rad/s.

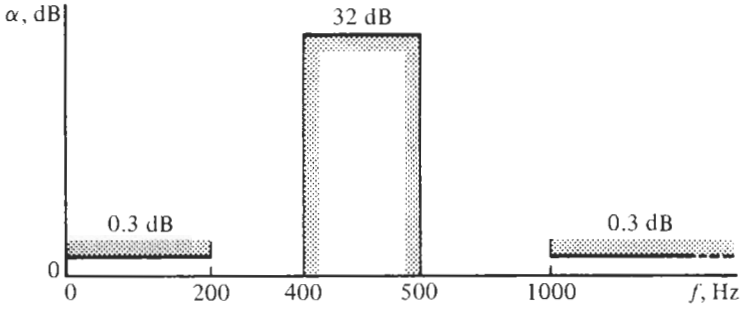

Figure P14.15

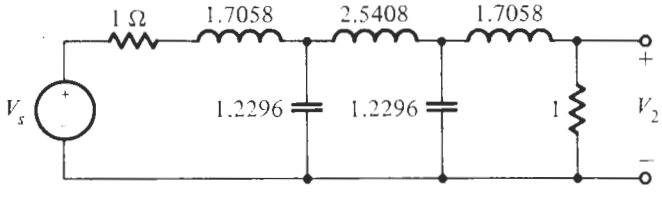

Figure P14.16

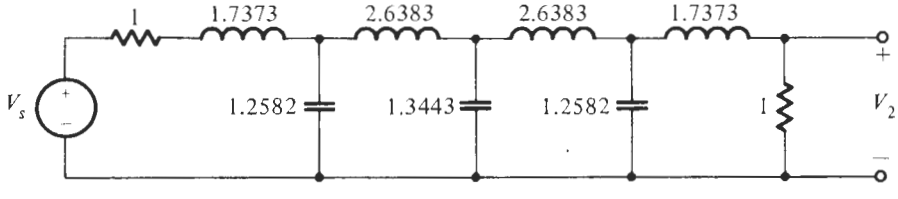

Figure P14.17

14.18 Repeat Problem 14.16 using as the prototype a sixth-order Butterworth lowpass. The 3-dB bandwidth is $f_c = 3.6$ kHz; the load resistor is prescribed to be 7 kΩ. Realize the filter and test your design. *Hint:* Consult Table 13.1.

14.19 Realize the circuit of Example 14.8 by Gorski-Popiel's ladder embedding technique.

14.20 Repeat Problem 14.16 using as prototype the entry in Table 13.1 for $n = 7$.

14.21 Realize a bandpass filter based on a third-order Chebyshev filter with 0.1-dB passband ripple. The bandpass center is at 19 kHz, BW = 4.5 kHz, and the load resistor is 3.2 kΩ. Design and test the circuit using a suitable active ladder technique.

14.22 Convert the lowpass prototype of Problem 14.21 to a band-rejection circuit. The center of the rejected band is at $f_0 = 28$ kHz and $Q_{BR} = 3$. The termination resistors are as in Problem 14.21. Use a suitable inductor replacement method and test your design.

14.23 To optimize the performance of some equipment, the loss of an inductor L, modeled as a series loss-resistor $R_L = 195\ \Omega$, must be eliminated. For the operation it is very important that the effective inductor is "lossless" over as wide a frequency range as possible. The equipment must be very inexpensive; LM741 opamps should be used. Using the information in Section 14.6, the student engineer assigned to the task designs a negative resistor to be placed in series with L. Making use of Eq. (14.44), optimize the negative-resistor circuit so that the finite opamp ω_t has as little effect as possible.

14.24 What passive circuit has the same input impedance as the circuit given in Fig. P14.24?

14.25 A poorly packaged and badly wound inductor of value $L = 0.34$ H is found to have a self-resonance frequency of only $f_0 = 11$ kHz. This implies that the parasitic capacitor that appears in parallel to L is approximately 600 pF. Since the inductor cannot be changed, it is proposed to reduce the parasitic capacitor so that the self-resonance frequency is at least equal to 200 kHz. Design and test an appropriate circuit to accomplish this goal.

14.26 The circuit shown in Fig. P14.26 is a model for a tunnel diode. We wish to simulate this circuit for an experiment using the concepts of Section 14.6. It is specified that the simulation circuit must not contain inductors nor, of course, negative resistors. Find an equivalent circuit meeting these specifications and having the same Z_{in}.

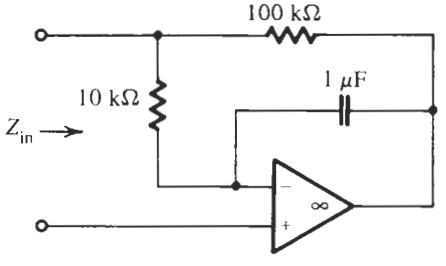

Figure P14.24

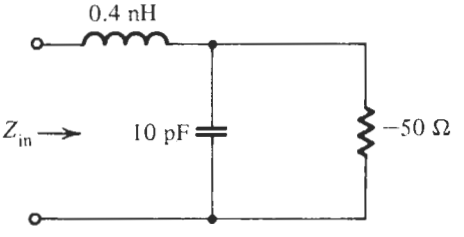

Figure P14.26

OPERATIONAL SIMULATION OF LADDERS

In the last chapter we introduced an innovation in the design of ladders: we showed that it is possible to realize an *LC* ladder by using synthetic elements, such as simulated inductors or negative components. To accomplish this goal we used gyrators or, more precisely, general impedance converters, to implement an electronic circuit whose input impedance looks inductive. Another approach we employed was to transform the complete ladder; this led to the frequency-dependent negative resistor. The fact that this peculiar element, the FDNR, has no physical equivalent, does not detract from its usefulness, because we can readily find an electronic circuit to simulate its behavior.

The method we introduce in this chapter takes a different approach: by modeling all circuit equations and the voltage–current relationships of the elements, it simulates the operation of the ladder rather than its components. The method dates back to an era in which analog computers were widely used. To use an analog computer to study a system—be it an electric circuit, a mechanical system such as the automobile, or a chemical processing plant—that system is modeled by writing equations based on conservation laws. Then the equations are represented by block diagrams or signal-flow graphs. Each block represents some analog operation, such as summation, differentiation, or integration. When the blocks are properly patched together, the resulting circuit, the analog computer, is a model of the system under study. The method we introduce in this chapter uses the analog computer itself as the filter. Although this appears to be a roundabout and impractical way, the resulting circuits are easy to design and are very competitive with the ones we studied in previous chapters. In many ways they behave better. Let us proceed, therefore, and find a method that realizes the ladder by simulating the operation of its equations and components.

15.1 SIMULATION OF LOWPASS LADDERS

To clarify the previous statement, consider the sixth-order all-pole lowpass ladder in Fig. 15.1. It is described by Kirchhoff's laws, i.e., by the equations

$$V_1 = V_0 - V_2, \quad V_3 = V_2 - V_4, \quad V_5 = V_4 - V_6 \tag{15.1}$$

$$I_2 = I_1 - I_3, \quad I_4 = I_3 - I_5, \quad I_6 = I_5 - I_7 = I_5 \tag{15.2}$$

where we assumed that $I_7 = 0$. In addition, we need the V–I relationships for the series and shunt branches of the ladder:

$$I_1 = \frac{V_1}{sL_1 + R_S}, \quad I_3 = \frac{V_3}{sL_3}, \quad I_5 = \frac{V_5}{sL_5} \tag{15.3}$$

$$V_2 = \frac{I_2}{sC_2}, \quad V_4 = \frac{I_4}{sC_4}, \quad V_6 = \frac{I_6}{sC_6 + G_L} \tag{15.4}$$

We see then that to simulate the operation we need circuits, which form the difference of two voltages or currents, Eqs. (15.1) and (15.2), and those that perform lossy or lossless integration, Eqs. (15.3) and (15.4). We encountered such circuits before in our study: we performed the operations of addition or subtraction by the modules discussed in Section 2.7, and we presented circuits that integrate a signal in Section 4.4. If we take such circuits and connect them appropriately, all the equations will be realized and the resulting total structure should realize the prescribed LC filter.

To see how we can develop this process in a methodical manner so that the results become generally valid, consider the general ladder in Fig. 15.2. We have labeled the components in the series branches by admittances Y_i and those in the shunt branches by impedances Z_j. The ladder is described by the equations

$$I_1 = Y_1 (V_0 - V_2) \tag{15.5}$$

$$V_2 = Z_2 (I_1 - I_3) \tag{15.6}$$

$$I_3 = Y_3 (V_2 - V_4) \tag{15.7}$$

$$V_4 = Z_4 (I_3 - I_5) \tag{15.8}$$

$$I_5 = Y_5 (V_4 - V_6) \tag{15.9}$$

$$V_6 = Z_6 (I_5 - I_7) = Z_6 I_5 \tag{15.10}$$

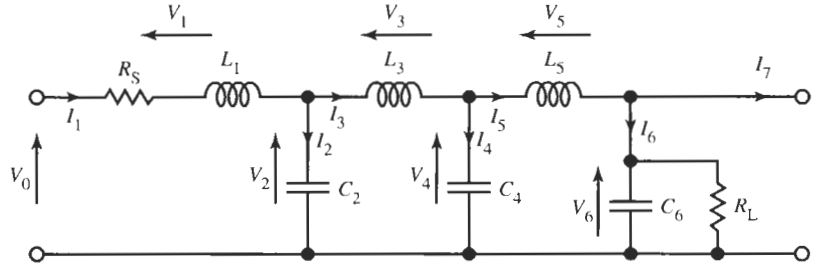

Figure 15.1 A sixth-order LC lowpass ladder.

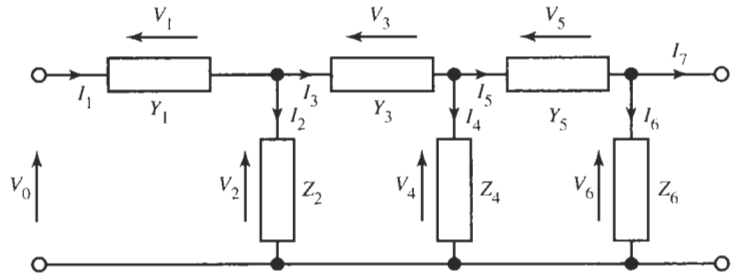

Figure 15.2 The ladder of Fig. 15.1 with general immittances in the ladder arms.

We have to deal next with two issues that complicate a direct realization of these equations with opamp circuits:

1. Both the inputs and the outputs of our opamp-based circuits are voltages and not currents.
2. It is much easier to realize opamp circuits that sum signals than ones that take their difference.

The first problem we can solve easily by scaling the equations by a resistor R_p. We obtain from Eq. (15.5):

$$R_p I_1 = R_p Y_1 (V_0 - V_2) \quad \rightarrow \quad v_{I1} = t_{Y1} (v_0 - v_2) \tag{15.11}$$

In the right equation we labeled $R_p I_1$ (which is now a voltage) by the lower-case symbol v_{I1} and retained the subscript I to remind ourselves that this voltage was derived from a current in the circuit. For consistency of notation we label all voltages in the normalized circuit by lower-case v. The dimensionless quantity $R_p Y_1$ we labeled t_{Y1} because it is now a transfer function $t_{Y1} = v_{I1}/(v_0 - v_2)$. In a similar fashion we obtain from Eqs. (15.6) to (15.10)

$$V_2 = \frac{Z_2}{R_p} (R_p I_1 - R_p I_3) \quad \rightarrow \quad v_2 = t_{Z2} (v_{I1} - v_{I3}) \tag{15.12}$$

$$R_p I_3 = R_p Y_3 (V_2 - V_4) \quad \rightarrow \quad v_{I3} = t_{Y3} (v_2 - v_4) \tag{15.13}$$

$$V_4 = \frac{Z_4}{R_p} (R_p I_3 - R_p I_5) \quad \rightarrow \quad v_4 = t_{Z4} (v_{I3} - v_{I5}) \tag{15.14}$$

$$R_p I_5 = R_p Y_5 (V_4 - V_6) \quad \rightarrow \quad v_{I5} = t_{Y5} (v_4 - v_6) \tag{15.15}$$

$$V_6 = \frac{Z_6}{R_p} R_p I_5 \quad \rightarrow \quad v_6 = t_{Z6} v_{I5} \tag{15.16}$$

At this time we have converted all quantities to voltages and have solved the first difficulty.

The second issue we need to address is that of performing sums rather than taking differences, that is, we prefer to deal with the six equations

$$v_{I1} = t_{Y1} [v_0 + (-v_2)], \quad v_2 = t_{Z2} [v_{I1} + (-v_{I3})], \quad v_{I3} = t_{Y3} [v_2 + (-v_4)] \tag{15.17}$$

$$v_4 = t_{Z4} [v_{I3} + (-v_{I5})], \quad v_{I5} = t_{Y5} [v_4 + (-v_6)], \quad v_6 = t_{Z6} v_{I5} \tag{15.18}$$

where we *sum* v_0 to $(-v_2)$, v_{I1} to $(-v_{I3})$, and so on. To accomplish this without the need for an inverter for each voltage, we choose to use those transfer functions that arise from the impedances Z_j as inverting, that is, we replace t_{Zj} by $-t_{Zj}$. Performing this step and keeping track of the minus signs, we obtain from Eqs. (15.17) and (15.18):

$$v_{I1} = t_{Y1}[v_0 + (-v_2)],\ (-v_2) = -t_{Z2}[v_{I1} + (-v_{I3})],\ (-v_{I3}) = t_{Y3}[(-v_2) + v_4] \quad (15.19)$$

$$v_4 = -t_{Z4}[(-v_{I3}) + v_{I5}],\ v_{I5} = t_{Y5}[v_4 + (-v_6)],\ (-v_6) = -t_{Z6}v_{I5} \quad (15.20)$$

The operations needed to construct a block diagram are summarized in Fig. 15.3. Using the symbolism in Fig. 15.3a, we can construct the diagram in Fig. 15.4a to realize Eqs. (15.19) and (15.20). Observe that now the voltages v_2, v_{I3}, and v_6 in all equations are negative so that only summers are needed in the block diagram representation of Fig. 15.4a.

Alternatively, we could also have selected the transfer functions t_{Yj} as inverting, i.e., t_{Yj} is replaced by $-t_{Yj}$, to obtain instead of Eqs. (15.19) and (15.20)

$$-v_{I1} = -t_{Y1}[v_0 + (-v_2)],\quad -v_2 = t_{Z2}[(-v_{I1}) + v_{I3}],\quad v_{I3} = -t_{Y3}[(-v_2) + v_4] \quad (15.21)$$

$$v_4 = t_{Z4}[v_{I3} + (-v_{I5})],\quad -v_{I5} = -t_{Y5}[v_4 + (-v_6)],\quad -v_6 = t_{Z6}(-v_{I5}) \quad (15.22)$$

Now the voltages v_{I1}, v_2, v_{I5}, and v_6 have minus signs appropriate for summing as shown in Fig. 15.4b. As is customary we have placed all signals arising from currents into the upper line of the block diagrams. The price paid for saving the inverters is a possible sign inversion (a 180° phase shift) in the total filter; this is normally unimportant. The diagrams can also be drawn as in Fig. 15.5 or generally as in Fig. 15.6, which gave rise to the name *leapfrog* filter. Observe that in each block diagram the loops consist of an inverting and a noninverting block so that the gain around each loop is negative as required for stability. For example, the gain in Loop 1 of Fig. 15.4a is $t_{Y1}(-t_{Z2})$, that in Loop 2 is $(-t_{Z2})t_{Y3}$, and so forth.

We are now ready to consider the actual implementation of the circuit. Let us return to Eqs. (15.3) and (15.4) where we had

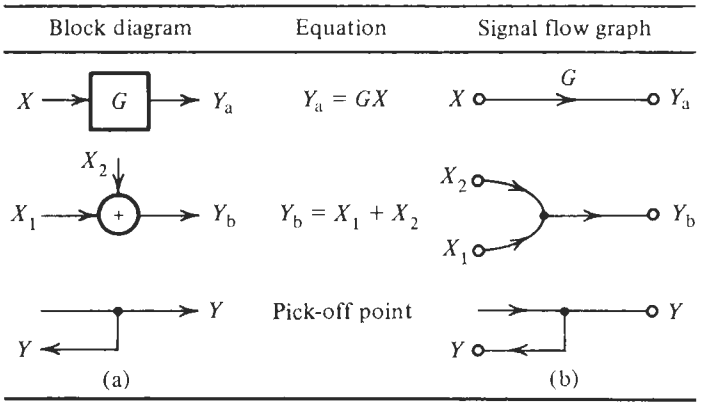

Figure 15.3 Block diagram symbols (a) and signal flow graph notation (b) of the elements necessary to implement Eqs. (15.19) and (15.20).

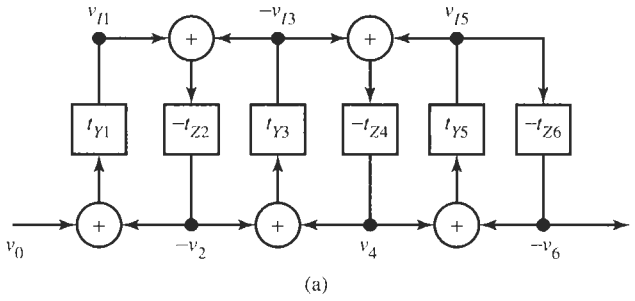

Figure 15.4 Block diagrams realizing (a) Eqs. (15.19) and (15.20) and (b) Eqs. (15.21) and (15.22).

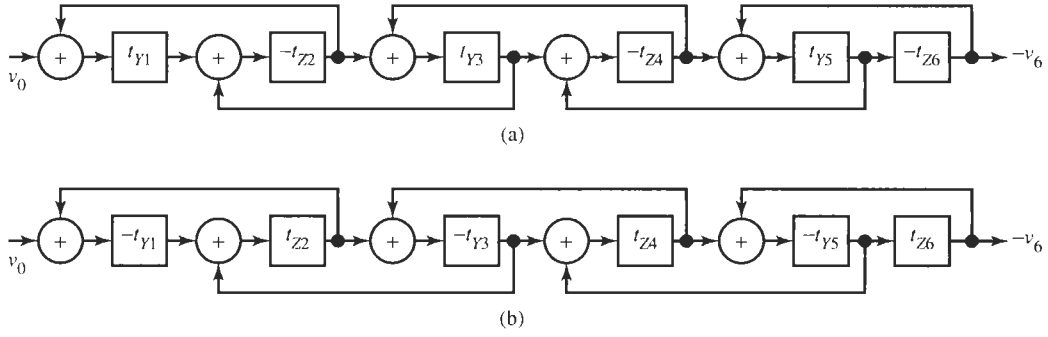

Figure 15.5 Block diagrams redrawn from Figs. 15.4a and b.

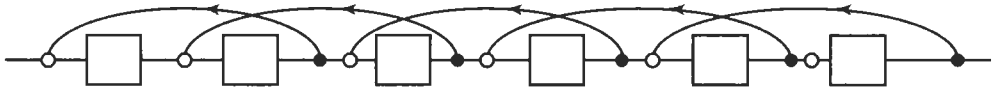

Figure 15.6 Block diagrams of Fig. 15.5 drawn as a leapfrog structure.

$$Y_1 = \frac{1}{sL_1 + R_S}, \quad Z_2 = \frac{1}{sC_2}, \quad Y_3 = \frac{1}{sL_3},$$
$$Z_4 = \frac{1}{sC_4}, \quad Y_5 = \frac{1}{sL_5}, Z_6 = \frac{1}{sC_6 + G_L} \tag{15.23}$$

To obtain the transfer functions for the signal-flow graph with the signs agreed to for Eqs. (15.19) and (15.20) we scaled all impedances by some resistor R_p and multiplied Z_2, Z_4, and

Z_6 by -1. The subscript, p, in R_p signifies that this resistor scales the *passive* ladder. The result is

$$t_{Y1} = R_p Y_1 = \frac{R_p}{sL_1 + R_S} = \frac{1}{sL_1/R_p + R_S/R_p} = \frac{1}{s\tau_1 + q_S} \tag{15.24}$$

$$t_{Z2} = -\frac{Z_2}{R_p} = -\frac{1}{sC_2R_p} = -\frac{1}{s\tau_2} \tag{15.25}$$

$$t_{Y3} = \frac{1}{sL_3/R_p} = \frac{1}{s\tau_3} \tag{15.26}$$

$$t_{Z4} = -\frac{1}{sC_4R_p} = -\frac{1}{s\tau_4} \tag{15.27}$$

$$t_{Y5} = \frac{1}{sL_5/R_p} = \frac{1}{s\tau_5} \tag{15.28}$$

$$t_{Z6} = -\frac{1}{sC_6R_p + G_LR_p} = -\frac{1}{s\tau_6 + q_L} \tag{15.29}$$

Observe that we require four ideal (lossless) integrators and two lossy integrators, and that inverting and noninverting integrators alternate as we progress through the ladder (see Fig. 15.4). The integrators have the time constants τ_i, $i = 1, \ldots, 6$; the two loss terms q_S and q_L identified in Eqs. (15.24) and (15.29) reflect the source and load resistors. Internal to the ladder all components are lossless and so are the integrators.

Lossy and lossless integrators were discussed in Section 4.4, specifically Eqs. (4.64) and (4.67). The inverting integrator was shown in Fig. 4.23a and the best among the noninverting integrators in Fig. 4.26. Both have only one input, but observe from Eqs. (15.19) through (15.22) that we need to integrate the sum of two voltages. An additional opamp to realize a summer, Fig. 2.29a, appears to be needed for each integrator. A much more economical solution is obtained by merging the operations of summation and integration. Note that the Miller integrator in Fig. 4.23a may have a second input as is shown in Fig. 15.7a with an additional feedback resistor R_F to make the integrator lossy. Equivalently, we can obtain a two-input (lossy) integrator if in the summer of Fig. 2.29a we place a capacitor C in parallel with the feedback resistor R_F. We explored the effects of nonideal opamps in Chapter 4; assuming now the opamp is ideal, we obtain from Eq. (2.90) immediately

$$V_o = -\frac{1}{sC + G_F}\left(\frac{V_1}{R_1} + \frac{V_2}{R_2}\right) = -\frac{1}{sCR_a + G_FR_a}\left(\frac{R_a}{R_1}V_1 + \frac{R_a}{R_2}V_2\right) \tag{15.30a}$$

or

$$V_o = -\frac{1}{s\tau + q}(a_1V_1 + a_2V_2) \tag{15.30b}$$

Analogously, we may provide two inputs through R_1 and R_2 and a loss resistor R_F to the noninverting integrator of Fig. 4.26 as is shown in Fig. 15.7b. Direct analysis or making the appropriate changes in notation in Eq. (4.81) results in

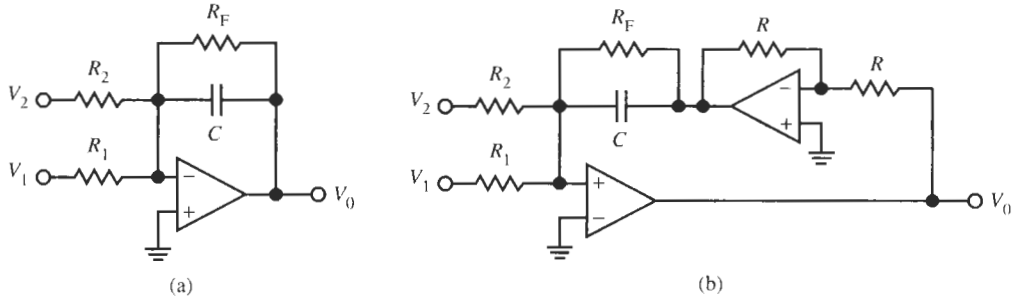

Figure 15.7 Inverting (a) and noninverting (b) summing lossy integrators for the realization of Eqs. (15.24) through (15.29).

$$V_o = +\frac{1}{sC + G_F}\left(\frac{V_1}{R_1} + \frac{V_2}{R_2}\right) = +\frac{1}{sCR_a + G_F R_a}\left(\frac{R_a}{R_1}V_1 + \frac{R_a}{R_2}V_2\right) \tag{15.31a}$$

or

$$V_o = +\frac{1}{s\tau + q}(a_1 V_1 + a_2 V_2) \tag{15.31b}$$

For the active integrators we have used a scaling resistor R_a; the subscript, a, signifies that the resistor R_a scales the *active* network. Thus, the circuits in Fig. 15.7 scale two voltages by two different coefficients,[1] add them, and perform an inverting or noninverting lossy integration of the sum with an integration constant τ, exactly as required for our case. Naturally, if we set $R_F = \infty$ and $R_2 = \infty$, we obtain lossless integrators with a single input.

Combining our results, we have from Eqs. (15.19), (15.20), and (15.24) to (15.29)

$$\begin{aligned} v_{I1} &= \frac{1}{sL_1/R_p + R_S/R_p}[v_0 + (-v_2)] = \frac{v_0 + (-v_2)}{s\tau_1 + q_S} \\ (-v_{I3}) &= \frac{1}{sL_3/R_p}[(-v_2) + v_4] = \frac{(-v_2) + v_4}{s\tau_3} \\ v_{I5} &= \frac{1}{sL_5/R_p}[v_4 + (-v_6)] = \frac{v_4 + (-v_6)}{s\tau_5} \end{aligned} \tag{15.32}$$

which can be realized by the noninverting integrator in Fig. 5.7b, and

$$\begin{aligned} (-v_2) &= -\frac{1}{sC_2R_p}[v_{I1} + (-v_{I3})] = -\frac{v_{I1} + (-v_{I3})}{s\tau_2} \\ v_4 &= -\frac{1}{sC_4R_p}[(-v_{I3}) + v_{I5}] = -\frac{(-v_{I3}) + v_{I5}}{s\tau_4} \end{aligned} \tag{15.33}$$

[1] The two factors a_1 and a_2 scale the voltages if needed. This is a useful feature if the dynamic range of the filter is to be optimized. For the discussion in this book we shall not deal with dynamic range optimization and have $a_1 = a_2 = 1$.

$$(-v_6) = -\frac{1}{sC_6R_p + G_LR_p}v_{I5} = -\frac{v_{I5}}{s\tau_6 + q_L}$$

which are realized by the inverting integrator in Fig. 15.7a. The resulting circuit is shown in Fig. 15.8; it interconnects all integrators for our filter of Fig. 15.1 as in Fig. 15.4a.

Let us still make an observation about our choice of integrators and the expected performance of the simulated ladder when the opamps are not ideal. Without having to perform any lengthy analysis of the effects, we may use the results we derived in Section 4.4. Notice that each loop consists of an inverting Miller integrator with a negative q factor, Eq. (4.70a), and a noninverting integrator with a positive q factor of equal magnitude, Eq. (4.82) (see Table 4.1). Each loop in Fig. 15.8 looks just like the Åckerberg–Mossberg biquad of Fig. 4.29 so that in every loop of the simulated ladder the deviations caused by nonideal opamps cancel! This is an interesting and very useful result that justifies our choice of pairing the Miller integrator in Fig. 15.7a with the particular noninverting integrator in Fig. 15.7b.

In summary, operational simulation or leapfrog design of lowpass filters is accomplished in the following steps:

1. From the specifications for the lowpass filter determine a suitable LC lowpass prototype. Normally a doubly terminated LC ladder is employed, but other types, such as singly terminated ladders, may be used as well.
2. Identify the various impedances and admittances as in Fig. 15.2.
3. Scale the immittances by a suitable resistor value. This will convert the immittances of the ladder into transfer functions for the signal-flow block diagram of the operational simulation and the currents into voltages.
4. Select the leapfrog block diagrams to simulate the circuit. These are given in Fig. 15.4. Either one of the two forms can be taken for the realization. Since the two

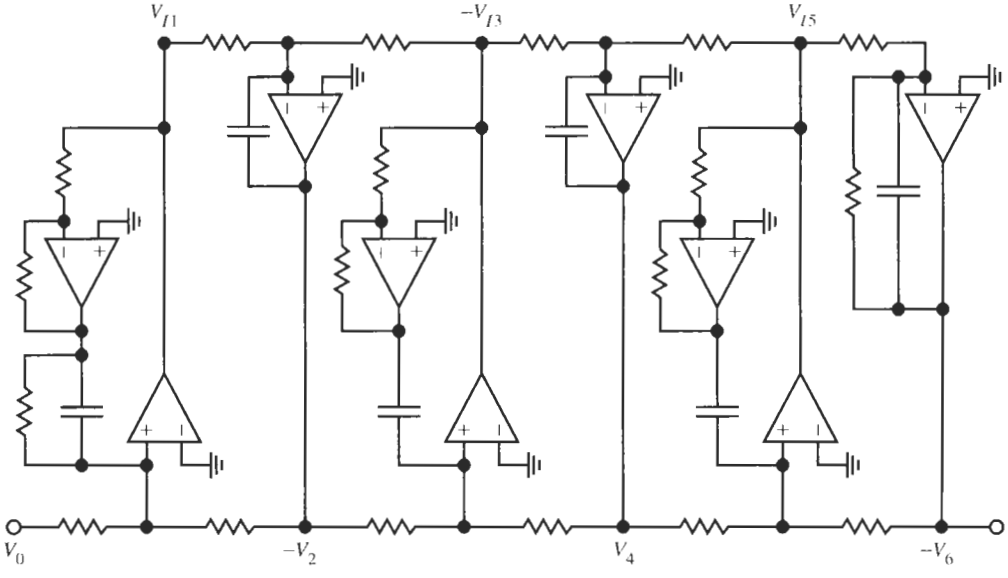

Figure 15.8 Active realization of the lowpass ladder of Fig. 15.1.

transfer functions t_{Zi} and t_{Yj} are normally integrators, and noninverting integrators use more opamps for their implementation, it is preferable to use the structure with the fewest noninverting integrators. The advantage is slight, though: because inverting and noninverting integrators are paired to maintain negative loop gains throughout the filter, the difference in their numbers is one at most.

5. Find active summing integrators to realize each of the blocks. Good choices are the integrators in Fig. 15.7. Be certain to alternate inverting and noninverting integrators to keep the loop gains negative.

6. Interconnect the integrators as required by the block diagram selected in Fig. 15.4.

An example will illustrate the procedure.

EXAMPLE 15.1

Use the operational simulation discussed to implement a sixth-order Chebyshev lowpass with 0.1-dB passband ripple. The passband bandwidth is 340 krad/s and the source resistor R_S equals 1.2 kΩ.

Solution

Let us take the ladder topology in Fig. 15.1; the normalized elements for the cut-off frequency $\omega_c = 1$ and the normalized source resistor $R_1 = 1$ are obtained from Table 13.3 as

$$L_1 = 1.1681 \quad C_2 = 1.4040 \quad L_3 = 2.0562 \quad C_4 = 1.5171 \quad L_5 = 1.9028 \quad C_6 = 0.8618$$

The normalized load resistor is $R_2 = 0.7378 = 1/1.3554$ per Table 13.3. The denormalized LC filter inductors and capacitors are $L_i R_S/\omega_c$ and $C_j/(R_S\omega_c)$, and the resistors are $R_S = 1.2$ kΩ and $R_L = 885.4$ Ω (see Fig. 15.9a). Then we have from Eqs. (15.24) to (15.29)

$$\begin{aligned}
t_{Y1} &= \frac{1}{sL_1/R_p + R_1/R_p} = \frac{1}{s1.1681/R_p + 1/R_p} \\
t_{Z2} &= -\frac{1}{sC_2R_p} = -\frac{1}{s1.4040R_p} \\
t_{Y3} &= \frac{1}{sL_3/R_p} = \frac{1}{s2.0562/R_p} \\
t_{Z4} &= -\frac{1}{sC_4R_p} = -\frac{1}{s1.5171R_p} \\
t_{Y5} &= \frac{1}{sL_5/R_p} = \frac{1}{s1.9028/R_p} \\
t_{Z6} &= -\frac{1}{sC_6R_p + G_2R_p} = -\frac{1}{s0.8618R_p + 1.3554R_p}
\end{aligned} \tag{15.34}$$

These integrators we now use in Eqs. (15.32) and (15.33) and compare the results with the active integrators of Eq. (15.30a) or (15.31a), respectively, depending on whether the integration is inverting or not. In the following equations we may refer to Fig. 15.8 to help identify the input and output voltages of the integrators. For the first one of Eqs. (15.34), we get

$$v_{I1} = \frac{1}{s1.1681/R_p + 1/R_p}[v_0 + (-v_2)] \quad \rightarrow$$

$$V_{I1} = \frac{1}{sCR_a + G_F R_a}\left[\frac{R_a}{R_1}V_0 + \frac{R_a}{R_2}(-V_2)\right] \tag{15.35}$$

Since v_0 and $(-v_2)$ have scale factors of 1, we select $R_1 = R_2 = R_a$. By comparing coefficients in the two integrator functions themselves, i.e.,

$$\frac{1}{s1.1681/R_p + 1/R_p} \quad \rightarrow \quad \frac{1}{sCR_a + G_F R_a}$$

we obtain after denormalizing the passive ladder elements

$$CR_a = \frac{1.1681 \times (R_S/\omega_c)}{R_p} \quad \text{and} \quad \frac{R_a}{R_F} = \frac{R_S}{R_p} \tag{15.36}$$

Here we have a great deal of choice for the component values of the active implementation. For example, we may choose $R_a = R_p$, but this choice would eliminate the freedom of selecting convenient and practical capacitor values. Instead we choose first a practical value for C and keep it the same for all integrators; let us pick $C = 0.5$ nF. Then we find from Eq. (15.36)

$$R_a R_p = \frac{1.1681 \times (R_S/\omega_c)}{C} = \frac{1.1681 \times 1.2\ \text{k}\Omega}{340\ \text{krad/s} \times 0.5\ \text{nF}} = (2.871\ \text{k}\Omega)^2$$

and

$$R_F = \frac{R_a R_p}{R_S} = \frac{(2.871\ \text{k}\Omega)^2}{1.2\ \text{k}\Omega} = 6.871\ \text{k}\Omega$$

Let us select $R_a = 2\ \text{k}\Omega = R_1 = R_2$ to give $R_p = 4.123\ \text{k}\Omega$. This determines all components of the first active integrator circuit.

For the second integration, with $R_F = \infty$, we obtain

$$(-v_2) = -\frac{1}{s1.4040R_p}[v_{I1} + (-v_{I3})] \quad \rightarrow \quad (-V_2) = -\frac{1}{sCR_a}\left[\frac{R_a}{R_1}V_{I1} + \frac{R_a}{R_2}(-V_{I3})\right]$$

where we set again $R_1 = R_2 = R_a$ because the scale factors are equal to 1. As in the previous case we find by equating the two integrator functions

$$CR_a = \frac{1.4040R_p}{R_S\omega_c}$$

that is, with $C = 0.5$ nF,

$$\frac{R_a}{R_p} = \frac{1.4040}{\omega_c C R_S} = \frac{1.4040}{340\text{krad/s} \times 0.5\ \text{nF} \times 1.2\ \text{k}\Omega} = 8.2588$$

It is important to note that we may select a different resistor R_a for each active integrator because the integrators perform independently of each other, but that *all* components in

the passive ladder must be scaled by the *same* resistor; therefore, only one passive scaling resistor R_p is available. We have from the first integrator $R_p = 4.123\ \text{k}\Omega$, which leads to $R_a = R_1 = R_2 = 34.05\ \text{k}\Omega$. This completes the design of integrator number two.

Proceeding with the third integration, we find

$$(-v_{I3}) = \frac{1}{s2.0562/R_p}[(-v_2) + v_4] \quad \rightarrow \quad (-V_{I3}) = \frac{1}{sCR_a}\left[\frac{R_a}{R_1}(-V_2) + \frac{R_a}{R_2}V_4\right] \tag{15.37}$$

and by comparing the integrators

$$CR_a = \frac{2.0562 \times (R_S/\omega_c)}{R_p}$$

or

$$R_a = \frac{2.0562R_S}{\omega_c C R_p} = \frac{2.0562 \times 1.2\ \text{k}\Omega}{340\ \text{krad/s} \times 0.5\ \text{nF} \times 4.123\ \text{k}\Omega} = 3.520\ \text{k}\Omega = R_1 = R_2$$

Integrators number 4 and 5 result in

$$v_4 = -\frac{1}{s1.5171R_p}[(-v_{I3}) + v_{I5}] \quad \rightarrow \quad V_4 = -\frac{1}{sCR_a}\left[\frac{R_a}{R_1}(-V_{I3}) + \frac{R_a}{R_2}V_{I5}\right]$$

that is,

$$CR_a = \frac{1.5171R_p}{R_S\omega_c} \quad \text{or} \quad R_a = \frac{1.5171R_p}{R_S\omega_c C} = 30.66\ \text{k}\Omega = R_1 = R_2$$

and

$$v_{I5} = \frac{1}{s1.9028/R_p}[v_4 + (-v_6)] \quad \rightarrow \quad V_{I5} = \frac{1}{sCR_a}\left[\frac{R_a}{R_1}V_4 + \frac{R_a}{R_2}(-V_6)\right]$$

that is,

$$CR_a = \frac{1.9028 \times (R_S/\omega_c)}{R_p} \quad \text{or} \quad R_a = \frac{1.9028R_S}{\omega_c C R_p} = 3.258\ \text{k}\Omega = R_1 = R_2$$

Finally, we have for the last integrator

$$(-v_6) = -\frac{1}{s0.8618R_p + 1.3554R_p}v_{I5} \quad \rightarrow \quad (-V_6) = \frac{1}{sCR_a + G_F R_a}\left(\frac{R_a}{R_1}V_{I5}\right)$$

which gives us the equations

$$CR_a = \frac{0.8618R_p}{\omega_c R_S} \quad \text{and} \quad G_F R_S R_a = 1.3554R_p$$

or

$$R_a = \frac{0.8618R_p}{\omega_c C R_S} = 17.418\ \text{k}\Omega \quad \text{and} \quad R_F = \frac{R_a R_S}{1.3554R_p} = 3.74\ \text{k}\Omega$$

With this step we have determined all components of the active circuit. Its implementation with LM741 opamps is shown in Fig. 15.9a, along with the test set-up. The *LC* prototype is shown above the active ladder to demonstrate the correspondence between the active and passive realizations. The performance is seen in Fig 15.9b. There is about a 6% shift in cut-off frequency due to the finite opamp bandwidth, otherwise the circuit behaves precisely as designed until well above 500 kHz where the effects of the finite opamp bandwidth become noticeable. (The attenuation levels off at ≈ -180 dB, whereas the attenuation of the ideal *LC* ladder increases indefinitely.) Having paired integrators with positive and negative quality factors in the feedback loops of the filter, the finite value of ω_t of the operational amplifiers has only minimal effects at lower frequencies so that the response curves of the active and passive ladders are virtually identical. Notice that even with the components rounded to one or two digits, the test performance is nearly ideal; this verifies that the active circuit has indeed the very low sensitivities of the passive *LC* ladder. We may conclude that the operational simulation of a ladder is an excellent method of building filters.

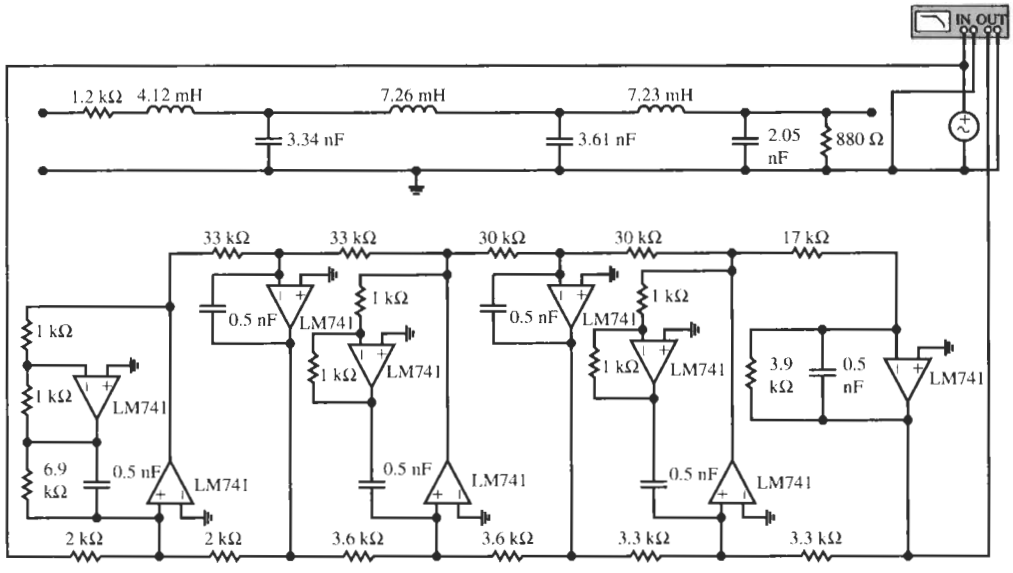

(a)

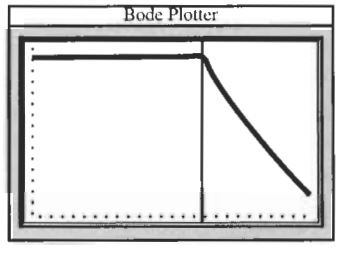

(b)

Figure 15.9 (a) The passive *LC* lowpass ladder and the active simulation circuit of Example 15.1; (b) test performance. (Bode Plotter scales: 1 to 600 kHz; −160 to 0 dB; cursor at 49.48 kHz, −7.239 dB.)

15.2 DESIGN OF GENERAL LADDERS

We saw in the previous section that the method of operational simulation led to active lowpass ladders with superb performance. In this section we shall extend this method to general ladders, that is, to ladders whose series and shunt arms, Fig. 15.2, have arbitrary LC immittances along with possibly a resistor. Examples of what we wish to be able to realize were given in Figs. 12.11, 13.9, 13.4, and 13.18d. In general, therefore, we must be able to handle LC ladders whose series and shunt branches are shown in Fig. 15.10a and b, respectively. The series arm in Fig. 15.10a implements the impedance

$$Z(s) = R_1 + sL_1 + \frac{1}{sC_{p1}} + \frac{1}{sC_{p2} + \dfrac{1}{sL_2}}$$

or, since we agreed to label the series arms by admittances,

$$Y(s) = \frac{1}{Z(s)} = \frac{1}{R_l + sL_1 + \dfrac{1}{sC_{p1}} + \dfrac{1}{sC_{p2} + \dfrac{1}{sL_2}}} \tag{15.38}$$

We have included a resistor R_L because just as the lowpass ladder discussed previously, a general doubly-terminated lossless ladder will at input and output have resistors that we need to include in the active simulation. We have given the capacitors a subscript, p, to indicate that these capacitors come from the *passive* ladder and to distinguish them from the capacitors used in the active simulations. In a similar fashion we obtain for the shunt immittances in Fig. 15.10b

$$Z(s) = \frac{1}{G_1 + sC_{p1} + \dfrac{1}{sL_1} + \dfrac{1}{sL_2 + \dfrac{1}{sC_{p2}}}} \tag{15.39}$$

All the ladders we encountered so far in this book have branches that are special cases of the ones shown in Fig. 15.10. After we have identified the immittances of the general series and shunt ladder arms, we can now proceed in exactly the same manner as in the previous section for the lowpass ladder. But the question we will need to answer first is how to simulate an immittance of the form shown in Eqs. (15.38) or (15.39). In our discussion of LC filters we labeled this form a continued fraction expansion.

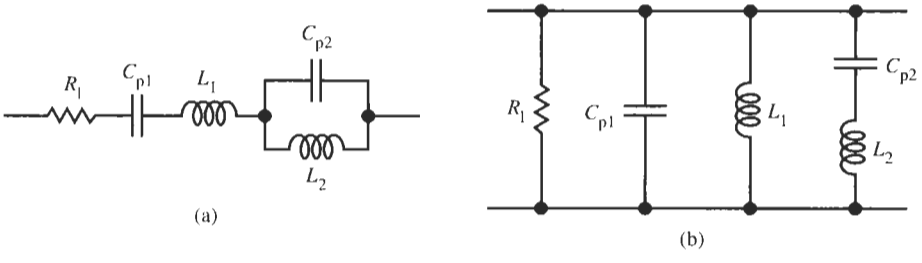

Figure 15.10 (a) Series arm and (b) shunt arm of a general lossless ladder.

A series branch generates a current $I_i = Y[V_{i-1} + (-V_{i+1})]$ (see Fig. 15.2), which after the procedure of the last section we convert into a voltage via scaling by a resistor R_p: $I_i R_p = Y R_p[V_{i-1} + (-V_{i+1})]$. The admittance of Eq. (15.38) then acts effectively as a transfer function,

$$R_p Y(s) = \cfrac{1}{\cfrac{R_1}{R_p} + s\cfrac{L_1}{R_p} + \cfrac{1}{sC_{p1}R_p} + \cfrac{1}{sC_{p2}R_p + \cfrac{1}{sL_2/R_p}}}$$

For consistent notation, we again label $R_p Y(s) = t_Y$ and all normalized quantities by lowercase symbols:

$$t_Y(s) = \cfrac{1}{r_1 + sl_1 + \cfrac{1}{sc_{p1}} + \cfrac{1}{sc_{p2} + \cfrac{1}{sl_2}}} \tag{15.40}$$

The impedance of a shunt arm, Eq. (15.39), is used to generate a voltage, $V_i = Z[I_{i-1} + (-I_{i+1})]$ (see Fig. 15.2), which we treat the same way,

$$\frac{Z(s)}{R_p} = \cfrac{1}{G_1 R_p + sC_{p1}R_p + \cfrac{1}{sL_1/R_p} + \cfrac{1}{s\cfrac{L_2}{R_p} + \cfrac{1}{sC_{p2}R_p}}}$$

and, following our agreement to make the shunt arms inverting so that the realization requires only summers, we have

$$-\frac{Z(s)}{R_p} = -t_Z(s) = -\cfrac{1}{g_1 + sc_{p1} + \cfrac{1}{sl_1} + \cfrac{1}{sl_2 + \cfrac{1}{sc_{p2}}}} \tag{15.41}$$

Recall that this process converts the currents into voltages so that all signals in the simulated ladder are voltages and only summers are needed. As soon as we know how to realize t_Z and t_Y we can interconnect them as is indicated in Fig. 15.4a and the design is complete.

The general approach to a realization of Eqs. (15.40) and (15.41) makes use of the fact that a network in the feedback branch of an operational amplifier becomes inverted. We encountered special cases of this throughout our study of active filters; here let us consider specifically the circuits in Fig. 15.11, which have two inputs because we will again have to sum two signals before processing them in t_Y or t_Z. The block labeled $-T$ in Fig. 15.11a is a transfer function $T(s) = -V_3/V_0$ whose input is assumed to be located at the arrow head, that is, it is driven by the opamp output. Assuming the amplifier is ideal, we analyze the circuit by writing a node equation at the noninverting input node to obtain

$$V_1 G_{i1} + V_2 G_{i2} + Y V_3 = 0 \quad \text{with} \quad V_3 = -T V_0 \tag{15.42}$$

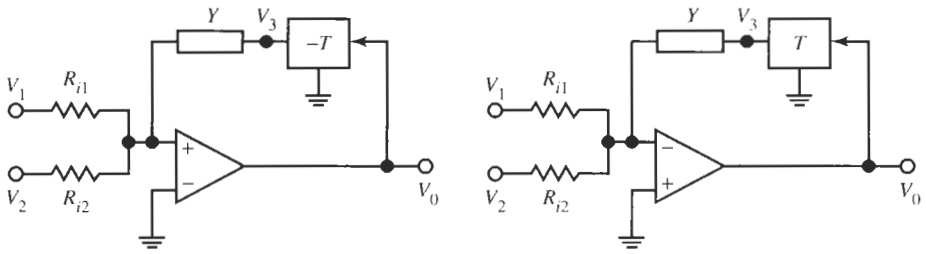

Figure 15.11 Realizing a transfer function inversely proportional to $Y(s)T(s)$: (a) noninverting; (b) inverting.

If we combine these two equations and eliminate V_3 we obtain

$$V_0 = +\frac{1}{YT}(V_1 G_{i1} + V_2 G_{i2}) = +\frac{G_a}{YT}\left(\frac{G_{i1}}{G_a}V_1 + \frac{G_{i2}}{G_a}V_2\right) \tag{15.43a}$$

where $R_a = 1/G_a$ is a scaling resistor for the *active* circuit. A similar analysis of the circuit in Fig. 15.11b results in

$$V_0 = -\frac{1}{YT}(V_1 G_{i1} + V_2 G_{i2}) = -\frac{G_a}{YT}\left(\frac{G_{i1}}{G_a}V_1 + \frac{G_{i2}}{G_a}V_2\right) \tag{15.43b}$$

Observe that T in Fig. 15.11a is inverting to maintain negative feedback to the noninverting input node of the opamp. Notice the similarity of the last two equations to Eqs. (15.30) and (15.31), and note that if $T = 1$ (a straight-though connection from V_0 to V_3) and Y is a capacitor in parallel with a resistor, $Y = sC + G_F$, the circuit in Fig. 15.11b is our inverting summing lossy integrator of Fig. 15.7a. Similarly, if $Y = sC + G_F$ and T is an inverter, $T = -1$. Figure 15.11a represents the noninverting summing lossy integrator of Fig. 15.7b. It follows that the discussion in the previous section is a special case of the present more general approach.

The power of the concept presented in Fig. 15.11 is that T may be a function of s and that we may connect several feedback branches in parallel so that the functions $G_a/(YT)$ can be quite arbitrary. Concentrate specifically on our need to implement the noninverting function of Eq. (15.40) and consider the circuit in Fig. 15.12a. Assuming the opamps are ideal, we can write node equations at the opamp input nodes; we find by routine analysis for the amplifier A_1

$$G_{i1}V_1 + G_{i2}V_2 + Y_0 V_{t0} + Y_1 V_{t1} + Y_2 V_{t2} + G_3 V_3 = 0$$

with

$$V_{t0} = -T_0 V_0, \quad V_{t1} = -T_1 V_0, \quad V_{t2} = -T_2 V_0$$

so that

$$G_{i1}V_1 + G_{i2}V_2 = (Y_0 T_0 + Y_1 T_1 + Y_2 T_2)\, V_0 - G_3 V_3 \tag{15.44}$$

Further, for the amplifier A_2

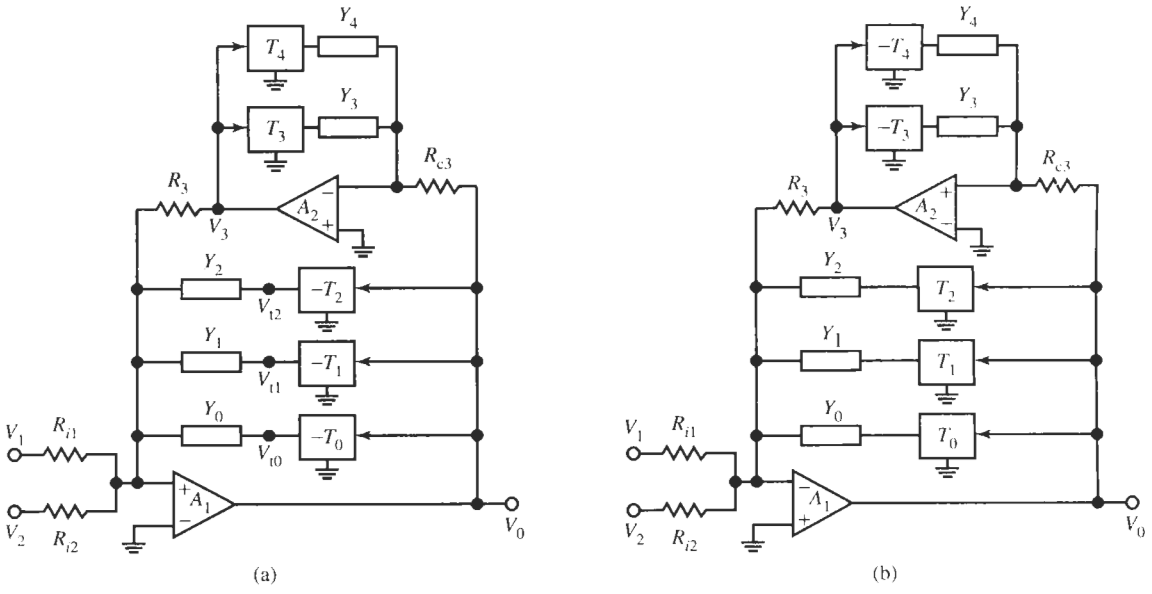

Figure 15.12 A general configuration for realizing Eqs. (15.40) and (15.41): (a) noninverting; (b) inverting.

$$G_{c3}V_0 + (Y_3T_3 + Y_4T_4)\,V_3 = 0, \quad \text{i.e.,} \quad V_3 = -\frac{G_{c3}}{Y_3T_3 + Y_4T_4}V_0 \tag{15.45}$$

Combining Eqs. (15.44) and (15.45) results in

$$V_0 = +\frac{1}{Y_0\,T_0 + Y_1T_1 + Y_2T_2 + \dfrac{G_3G_{c3}}{Y_3T_3 + Y_4T_4}}(G_{i1}V_1 + G_{12}V_2) \tag{15.46}$$

Next we scale the impedance level of the circuit by R_a to obtain

$$V_0 = +\frac{1}{R_aY_0\,T_0 + R_aY_1T_1 + R_aY_2T_2 + \dfrac{1}{\dfrac{Y_3T_3}{R_aG_3G_{c3}} + \dfrac{Y_4T_4}{R_aG_3G_{c3}}}}\left(\frac{R_a}{R_{i1}}V_1 + \frac{R_a}{R_{12}}V_2\right) \tag{15.47}$$

Let us now compare the multiplier of this sum of the two scaled voltages with the function t_Y of Eq. (15.40):

$$\frac{1}{R_aY_0\,T_0 + R_aY_1T_1 + R_aY_2T_2 + \dfrac{1}{\dfrac{Y_3T_3}{R_aG_3G_{c3}} + \dfrac{Y_4T_4}{R_aG_3G_{c3}}}} \rightarrow \frac{1}{r_1 + sl_1 + \dfrac{1}{sc_{p1}} + \dfrac{1}{sc_{p2} + \dfrac{1}{sl_2}}} \tag{15.48}$$

We can then readily determine the components of the active circuit so that we obtain the correct realization of the series arm of the ladder: we choose $Y_0 = G_0$ and $T_0 = 1$ to have

$$r_1 = \frac{R_1}{R_p} = \frac{R_a}{R_0}, \quad \text{i.e.,} \quad R_0 = \frac{R_a R_p}{R_1} \tag{15.49}$$

Similarly, we recognize that $Y_1 = sC_1$ and $T_1 = 1$ results in

$$sl_1 = s\frac{L_1}{R_p} = R_a sC_1, \quad \text{i.e.,} \quad C_1 = \frac{L_1}{R_a R_p} \tag{15.50}$$

Further, setting $Y_2 = G_2$ and replacing $-T_2$ by an inverting integrator, $-T_2 = -1/(sC_2R_{c2})$, results in

$$\frac{1}{sc_{p1}} = \frac{1}{sC_{p1}R_p} = R_a G_2 \frac{1}{sC_2 R_{c2}}, \quad \text{i.e.,} \quad C_2 = C_{p1}\frac{R_a R_p}{R_2 R_{c2}} \tag{15.51}$$

To complete the comparison of the two functions in Eq. (15.48) we need to equate the remaining two terms:

$$sc_{p2} = sC_{p2}R_p = \frac{Y_3 T_3}{R_a G_3 G_{c3}} \quad \text{and} \quad \frac{1}{sl_2} = \frac{1}{sL_2/R_p} = \frac{Y_4 T_4}{R_a G_3 G_{c3}}$$

For the first of these two equations we set $Y_3 = sC_3$ and $T_3 = 1$ to obtain

$$C_3 = C_{p2}\frac{R_a R_p}{R_3 R_{c3}} \tag{15.52}$$

and for the second one we set $Y_4 = G_4$ and make T_4 a noninverting integrator, $T_4 = +1/(sC_4R_{c4})$; the result is

$$C_4 = \frac{L_2}{R_{c4}R_4}\frac{R_3 R_{c3}}{R_a R_p} \tag{15.53}$$

In Eqs. (15.49) through (15.53) we still have considerable freedom in choosing the various resistor values. We exploit this freedom first to select a convenient value C for all capacitors in the active realization: $C_1 = C_2 = C_3 = C_4 = C$. Then we have from Eqs. (15.49) to (15.53):

$$\frac{L_1}{C} = R_a R_p = r^2, \quad R_0 = \frac{r^2}{R_1}, \tag{15.54}$$

$$R_2 R_{c2} = \frac{C_{p1}}{C}r^2, \quad R_3 R_{c3} = \frac{C_{p2}}{C}r^2, \quad R_4 R_{c4} = \frac{L_2}{C}\frac{R_3 R_{c3}}{r^2} = \frac{L_2 C_{p2}}{C^2}$$

The first of these equations determines the product of R_a and R_p, which we labeled $R_a R_p = r^2$, and the last three equations determine the products $R_k R_{ck}$, $k = 2, 3, 4$. As we saw already in Example 15.1, all components in the passive circuit must, of course, be scaled by the same resistor. This means that there is only one value R_p. But every branch of the active simulation of the ladder may have a different value R_a that can be used for scaling to obtain convenient component values.

With this, all components of the block $Y(s)$ are determined; it remains to find values for the two feed-in resistors R_{i1} and R_{i2} in Fig. 15.12a. By Eq. (15.47) they set the scale factors R_a/R_{i1} and R_a/R_{i2} of the input voltages V_1 and V_2, respectively. For an optimal design these two resistors are used for maximizing the dynamic range. As we discussed in connection with cascade circuits in Section 5.3, to maximize the dynamic range we equalize the signal levels at all operational amplifier outputs. In our case this can be done by appropriately selecting the scale factors a_i for equalizing the signal level throughout the filter. Also the individual resistors in the products in Eq. (15.54) can be determined uniquely if we design the active circuit such that the dynamic range is maximized. Using the available freedom to choose the resistors appropriately lets us scale the voltage levels throughout the simulated ladder and allows us to equalize the maxima of the opamp output voltages. We shall not discuss the details in this book but refer the interested student to the literature (Schaumann et al., 1990). For the discussion in this book the scale factors R_a/R_{i1} and R_a/R_{i2} are equal to unity so that we have

$$R_{i1} = R_{i2} = R_a \tag{15.55}$$

For simplicity, we choose

$$R_k = R_{ck} \tag{15.56}$$

The corresponding circuit to realize t_Y is shown in Fig. 15.13a along with the passive series branch of the ladder to point out the one-to-one correspondence between the two.

The development of the shunt arm follows precisely the same method: we analyze the circuit in Fig. 15.12b to obtain

$$V_0 = -\frac{1}{R_a Y_0 T_0 + R_a Y_1 T_1 + R_a Y_2 T_2 + \dfrac{1}{\dfrac{Y_3 T_3}{R_a G_3 G_{c3}} + \dfrac{Y_4 T_4}{R_a G_3 G_{c3}}}} \left(\frac{R_a}{R_{i1}} V_1 + \frac{R_a}{R_{12}} V_2\right) \tag{15.57}$$

and compare the result with t_Z of Eq. (15.41):

$$-\frac{1}{R_a Y_0 T_0 + R_a Y_1 T_1 + R_a Y_2 T_2 + \dfrac{1}{\dfrac{Y_3 T_3}{R_a G_3 G_{c3}} + \dfrac{Y_4 T_4}{R_a G_3 G_{c3}}}} \rightarrow$$

$$-\frac{1}{g_1 + sc_{p1} + \dfrac{1}{sl_1} + \dfrac{1}{sl_2 + \dfrac{1}{sc_{p2}}}}$$

If we now repeat the steps taken for the series branch for the inverting block (the shunt arm), comparing the corresponding terms on both sides of the arrow, and choose

$$T_0 = T_1 = 1, \quad T_2 = \frac{1}{sC_2 R_{c2}}, \quad T_3 = 1, \quad T_4 = \frac{1}{sC_4 R_4},$$
$$Y_2 = G_2, \quad Y_3 = sC_3, \quad Y_4 = G_4$$

we find the component values of the active simulation of the passive shunt arm as

$$\frac{C_{p1}}{C} = \frac{R_a}{R_p} = m, \quad R_0 = mR_1, \tag{15.58}$$

$$R_2R_{c2} = m\frac{L_1}{C}, \quad R_3R_{c3} = m\frac{L_2}{C}, \quad R_4R_{c4} = \frac{C_{p2}}{C}\frac{1}{m}R_3R_{c3} = \frac{L_2C_{p2}}{C^2}$$

where we labeled the ratio $R_a/R_p = m$ and set all capacitors equal to C. Equations (15.55) and (15.56) hold here as well.

This circuit and the passive shunt branch of the ladder are shown in Fig. 15.13b; we notice again the one-to-one correspondence of the branches and components. For example, if R_1 is absent ($R_1 = \infty$), also $R_0 = \infty$; if $C_{p1} = 0$ so is C_1; if the inductor L_1 is absent ($L_1 = \infty$), the branch containing C_2 is not used, and so forth. On the other hand, if a ladder arm contains components that are not included in Fig. 15.13, it is a simple step to add them to the design. For instance, if a ladder series arm contains two resonant circuits, such as shown in Fig. 13.18d, we can arrive at a methodical implementation by simply adding to the parallel connection of the active circuit in Fig. 15.13a an additional branch like the one containing the resistors R_3 and R_{c3}. This will realize the two required parallel resonant circuits in series. In any case, the individual resistors in the products in Eq. (15.58) can be determined uniquely if we maximize the dynamic range of the active ladder (Schaumann et al., 1990).

We have established the circuit configuration and all components as functions of the *LC* prototype and a few scaling resistors so that we are ready to design the active ladder by operational simulation. We expect, of course, that the all-pole lowpass design of the previous section must be a special case of the general ladder; comparing the circuits in Fig. 15.13 with the ones in Fig. 15.7 verifies this fact. Thus, the six steps we presented in Section 15.1 must be valid for the general case as well after a modification appropriate for the new notation:

1. From the filter specifications, determine a suitable *LC* lowpass prototype. Normally a doubly terminated *LC* ladder is employed, but other types, such as singly terminated ladders, may be used as well.
2. Identify the various impedances and admittances as in Figs. 15.2 and 15.10.
3. Using the frequency transformation, convert the lowpass prototype into the desired filter type as discussed in Section 13.5.
4. Scale the immittances by a suitable resistor value, R_p. This will convert the ladder immittances into transfer functions for the operational simulation, and the currents into voltages.
5. Select the leapfrog block diagram to simulate the circuit. These are given in Fig. 15.4. Either one of the two forms can be taken for the realization. Choose the form with the fewest noninverting integrators. The advantage is slight, though, because inverting and noninverting integrators are paired to maintain negative loop gains throughout the filter.
6. Find the active circuits in Fig. 15.13 to realize each t_Z and t_Y. For every absent component in the passive *LC* prototype ladder the corresponding branch in the active simulation is also absent. For instance, if there is no parallel resonant circuit, L_2C_{p2}, in $Y(s)$, Fig. 15.13a, the branch containing R_3R_{c3} is not used. Or if there is no shunt inductor L_1 in $Z(s)$, Fig. 15.13b, the branch containing R_2R_{c2} is also absent. Be certain to alternate inverting and noninverting blocks to keep the loop gains negative.
7. Interconnect the active branches as required by the block diagram selected in Fig. 15.4.

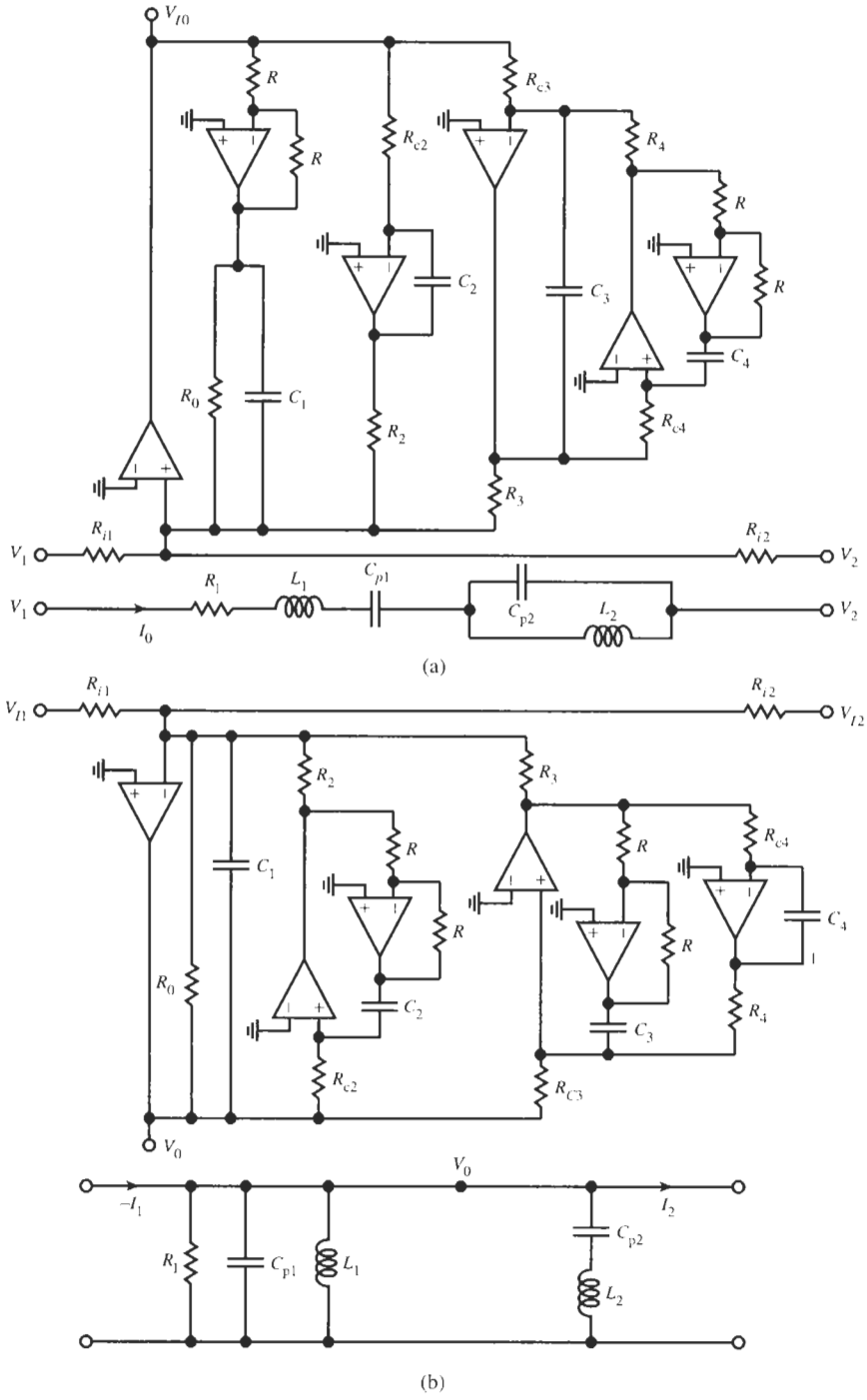

Figure 15.13 Realizations of (a) a series ladder arm and (b) a shunt ladder arm. The circuits are interconnected as shown in the block diagram in Fig. 15.4a. As for the lowpass case of the previous section, the signs of all signals are correct so that a direct interconnection is possible. Normally, we choose all identical capacitors: $C_i = C$.

Table 15.1 summarizes the necessary equations for the design. We start by selecting a convenient practical capacitor value C, and then determine the numbers $r^2 = R_a R_p$ for each series arm and $m = R_a/R_p$ for each shunt arm of the ladder, as specified in the table. Remember that R_p has the same value for the whole filter, but that R_a may be different for each ladder arm. If the components L_1 and/or C_{p1} are absent. The parameters r^2 and m, respectively, can be chosen freely, but there is still only one value R_p. The remaining components of the active simulation are then computed as shown in Table 15.1. The multipliers included in the table after the "×" signs are used to denormalize the elements; the factors assume that the components of the prototype LC ladder are normalized, such that the source resistor R_S and the cut-off frequency ω_c equal 1, but that the value of C we chose is *not* normalized. If the LC ladder elements used for the design are not normalized, the multipliers after the "×" sign equal 1.

An example will illustrate the design process.

TABLE 15.1 Design Equations for the Active Branches of a General LC Ladder Simulation

	Choose a Convenient Value for C	
	Series Branch Fig. 15.13a	Shunt Branch Fig. 15.13b
Determine	$R_a R_p = r^2 = \frac{L_1}{C} \times \frac{R_S}{\omega_c}$ If $L_1 = 0$, choose any convenient value for r^2.	$\frac{R_a}{R_p} = m = \frac{C_{p1}}{C} \times \frac{1}{R_S \omega_c}$ If $C_{p1} = 0$, choose any convenient value for m.
Then find		
$R_0 =$	$\frac{r^2}{R_1}$	$m R_1$
$R_2 = R_{c2} =$	$\sqrt{\frac{C_{p1}}{C} r^2 \times \frac{1}{R_S \omega_c}}$	$\sqrt{m \frac{L_1}{C} \times \frac{R_S}{\omega_c}}$
$R_3 = R_{c3} =$	$\sqrt{\frac{C_{p2}}{C} r^2 \times \frac{1}{R_S \omega_c}}$	$\sqrt{m \frac{L_2}{C} \times \frac{R_S}{\omega_c}}$
$R_4 = R_{c4} =$	$\sqrt{\frac{L_2 C_{p2}}{C^2} \times \frac{1}{\omega_c^2}}$	$\sqrt{\frac{L_2 C_{p2}}{C^2} \times \frac{1}{\omega_c^2}}$

Note: Select $R_{i1} = R_{i2} = R_a$; keep R_p constant throughout the design.

EXAMPLE 15.2

Realize the LC ladder of Example 13.5 by the operational method. The normalized passive circuit is given in Fig. 13.14b. In contrast to the passive ladder that has an intrinsic loss of 6 dB, it is desired to realize the active filter with 12-dB passband gain. The two 1.2-kΩ source and load resistors specified in Example 13.5 are part of the external system in which the filter operates and must be available in the final circuit.

Solution

To reduce the number of ladder arms, we perform first a source transformation as shown in Fig. 15.14a; this leads to the operational block diagram in Fig. 15.14b. The blocks in this diagram realize

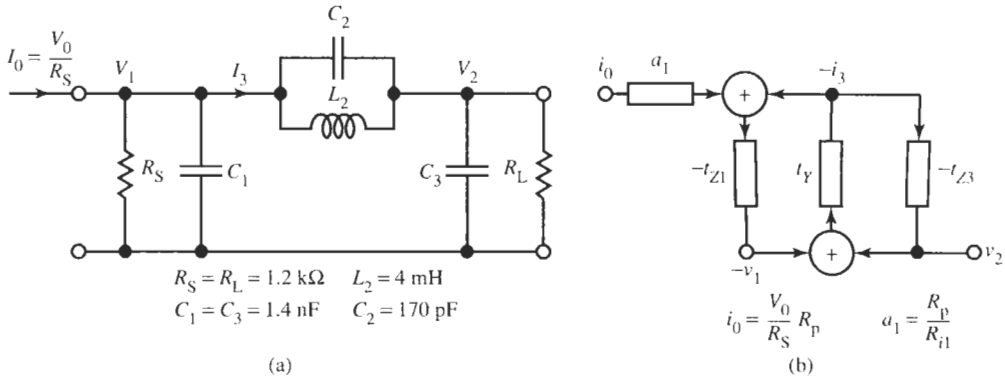

Figure 15.14 (a) The ladder of Fig. 13.14b after source transformation; (b) the operational block diagram.

$$-v_1 = -\frac{Z_1}{R_p}[a_1 i_0 + (-i_3)] = -t_{Z_1}[a_1 i_0 + (-i_3)] = -\frac{a_1 i_0 + (-i_3)}{sC_1 R_p + G_S R_p}$$

$$-i_3 = Y_2 R_p(-v_1 + v_2) = t_Y(-v_1 + v_2) = \left(sC_2 R_p + \frac{R_p}{sL_2}\right)(-v_1 + v_2) = \frac{-v_1 + v_2}{\dfrac{1}{sC_2 R_p + \dfrac{R_p}{sL_2}}}$$

$$v_2 = -\frac{Z_3}{R_p}(-i_3) = -t_{Z_3}(-i_3) = -\frac{(-i_3)}{sC_3 R_p + G_L R_p}$$

We brought t_Y into a form to match Eq. (15.40). All summer coefficients are equal to unity but we have shown explicitly the coefficient $a_1 = R_a/R_{i1}$ in the first block for later use in gain scaling. Let us pick $C = 1$ nF for all capacitors in the active circuit. Next we consult Table 15.1 and obtain for the block $-t_{Z_1}$: $m = C_1/C = 1.4$, $R_{0S} = mR_S = 1.4 \times 1.2\ \text{k}\Omega = 1.68\ \text{k}\Omega$. Since there in no inductor L_1, we may choose r^2. We select $r^2 = R_a R_p = (1.2\ \text{k}\Omega)^2$. Then we find for the block t_Y:

$$R_3 R_{c3} = \frac{C_2}{C} r^2 = \frac{170\ \text{pF}}{1\ \text{nF}}(1.2\ \text{k}\Omega)^2 = (494.77\ \Omega)^2; \qquad \text{we choose } R_3 = R_{c3} = 494.77\ \Omega$$

$$R_4 R_{c4} = \frac{L_2 C_2}{C^2} = (824.62\ \Omega)^2; \qquad \text{we choose } R_4 = R_{c4} = 824.62\ \Omega$$

Finally for the block $-t_{Z_3}$ we have: $m = C_3/C = 1.4$, and $R_{0L} = mR_L = 1.4 \times 1.2\ \text{k}\Omega = 1.68\ \text{k}\Omega$.

It remains for us to determine the coupling resistors between the three blocks. To do this, we observe from Fig. 15.14b that the "voltages" $-I_3 R_p = -i_3$, $-v_1$, and v_2 add in the summers with unity coefficients, but $(V_0/R_S)R_p = i_0$ adds with the coefficient a_1 that we need to determine for the prescribed gain of 12 dB. We follow Eq. (15.55) and pick all coupling resistors equal; let us choose them as 1.2 kΩ; this implies that $R_a = 1.2\ \text{k}\Omega$ and, in turn, determines $R_p = 1.2\ \text{k}\Omega$ because r^2 is fixed at $R_a R_p$ in block t_Y. The value of R_a in the shunt branches $-t_{Z_1}$ and $-t_{Z_3}$ is unimportant as long as we have the correct ratio $m = 1.4$. Because the value of $R_p = 1.2\ \text{k}\Omega$ must be the same throughout the filter, R_a for the first stage

equals $mR_p = 1.68$ kΩ (see Table 15.1). By Fig. 15.14b the input voltage is multiplied by $a_1 = R_a/R_{i1} = 1.68/1.2 = m = 1.4$. $a_1 = 1$ means that the filter realizes a −6-dB loss as in the passive ladder. Therefore, in our case, we realize a gain that is 20 log 1.4 ≈ 3 dB higher, that is, the filter gain is (−6 + 3) dB = 3 dB. Our task is to realize a 12-dB gain; this means we have to add 15 dB, that is, increase a_1 by a factor 5.62. This is accomplished if we reduce R_{i1} by a factor 5.62 from 1.2 kΩ to $R_{i1} = 213$ Ω.

The last design specification we need to satisfy is that there must be 1.2-kΩ resistors available at input and output. This is taken care of easily by scaling the impedance level of the input integrator by a factor 1200/213 = 5.62, and splitting the loss resistor of the last integrator into 500 Ω + 1.2 kΩ. The final circuit and the test set-up are shown in Fig. 15.15. Note that because of the low sensitivities of the ladder design, we could build the circuit with all standard-value components. Testing the performance showed substantial peaking in the stopband near the transmission zero; experimentation revealed quickly the cause to be the main LM741 opamp of the block t_Y. A faster opamp is required for the relatively high frequencies of concern in this example. The difficulty is remedied by employing an HA 2542-2 with 90-MHz unity-gain bandwidth. The test results in Fig. 15.15 verify the good passband sensitivity property. The lowpass cut-off frequency and the passband gain are as specified, as is the transmission zero. Overall, the performance is comparable to that of the passive ladder in Fig. 13.14c, and we have obtained the desired 12-dB gain that the passive ladder would not be able to implement without the use of an amplifier. We note still that the filter is tunable as easily as the *LC* prototype where fine adjustments can be accomplished readily by tuning the *LC* resonant circuit (the notch): in the active simulation the notch is tuned by adjusting one or both of the two 830-Ω resistors.

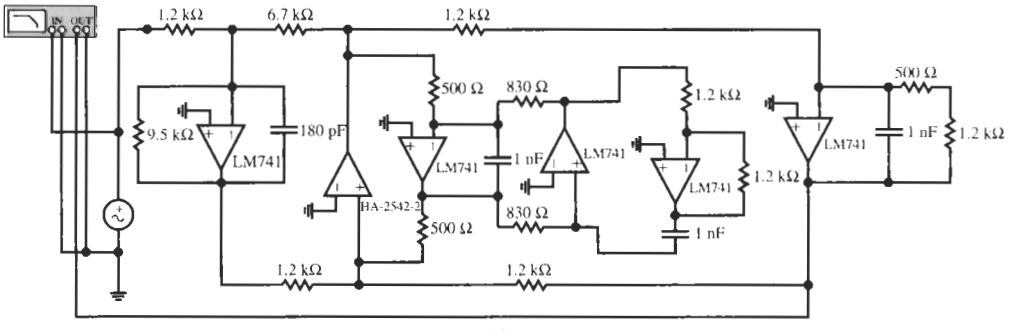

(a)

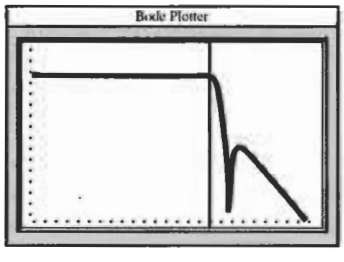

(b)

Figure 15.15 (a) Final circuit for Example 15.2; (b) test results. (Bode Plotter scales: 10 Hz to 10 MHz; −40 to 20 dB; cursor at 59.1 kHz, 11.69 dB.)

Notice that the filter behaves almost as well as the *LC* ladder in spite of the use of many low-frequency opamps. Observe specifically the sharp roll-off and deep notch. The main reason is that in this design procedure we also are pairing inverting phase-lead integrators ($Q < 0$) with noninverting phase-lag integrators ($Q > 0$) so that their two phase errors cancel in all loops. (In the circuit in Fig. 15.14b this happens in t_Y where the transmission zero is implemented.)

It can be shown that the simulation of the general ladders discussed in this section is very insensitive to opamp phase errors as long as we pair in each loop of the implementation inverting integrators with negative Q factors and noninverting integrators with positive Q factors.

15.3 ALL-POLE BANDPASS LADDERS

The design of bandpass ladders is, of course, a special case and can always be handled by the process discussed in the previous section. However, for the design of all-pole bandpass functions there are shortcuts available that the designer may make use of and that may lead to a simpler and more economical circuit. Let us briefly present them. Our goal is to implement each of the bandpass ladder arms by a simpler biquad if possible, and in the process save on operational amplifiers.

The design of all-pole bandpass filters is customarily based on the lowpass-to-bandpass frequency transformation $S = Q(s^2+1)/s$, where s is the bandpass frequency normalized to the band-center ω_0 and $Q = \omega_0/\Delta\omega$ is determined by the desired bandwidth $\Delta\omega$ of the bandpass. This transformation results in the series or shunt *LC* (or *RLC* for the end branches) ladder arms shown in Fig. 15.16. The lowpass-to-bandpass transformation converts a normalized lossy inductor L_{LP} of the lowpass prototype into a series *RLC* resonance circuit,

$$R + SL_{LP} \rightarrow R + L_{LP}Q\frac{s^2+1}{s} = R + sL_{LP}Q + \frac{1}{s/(L_{LP}Q)}$$
$$= R + sL_{BP} + \frac{1}{sC_{BP}} \tag{15.59}$$

A normalized lossy capacitor C_{LP} is transformed into as parallel *RLC* resonance circuit:

$$G + SC_{LP} \rightarrow G + C_{LP}Q\frac{s^2+1}{s} = G + sC_{LP}Q + \frac{1}{s/(C_{LP}Q)}$$
$$= G + sC_{BP} + \frac{1}{sL_{BP}} \tag{15.60}$$

Thus, after the lowpass-to-bandpass transformation we have ladders of the form shown in Fig. 15.16a with bandpass ladder arms displayed in Fig. 15.16b.

A bandpass series ladder admittance takes the form

$$Y(s) = \frac{1}{R + sL_{BP} + \dfrac{1}{sC_{BP}}} = \frac{s/L_{BP}}{s^2 + sR/L_{BP} + 1/(L_{BP}C_{LP})} \tag{15.61}$$

and a shunt impedance,

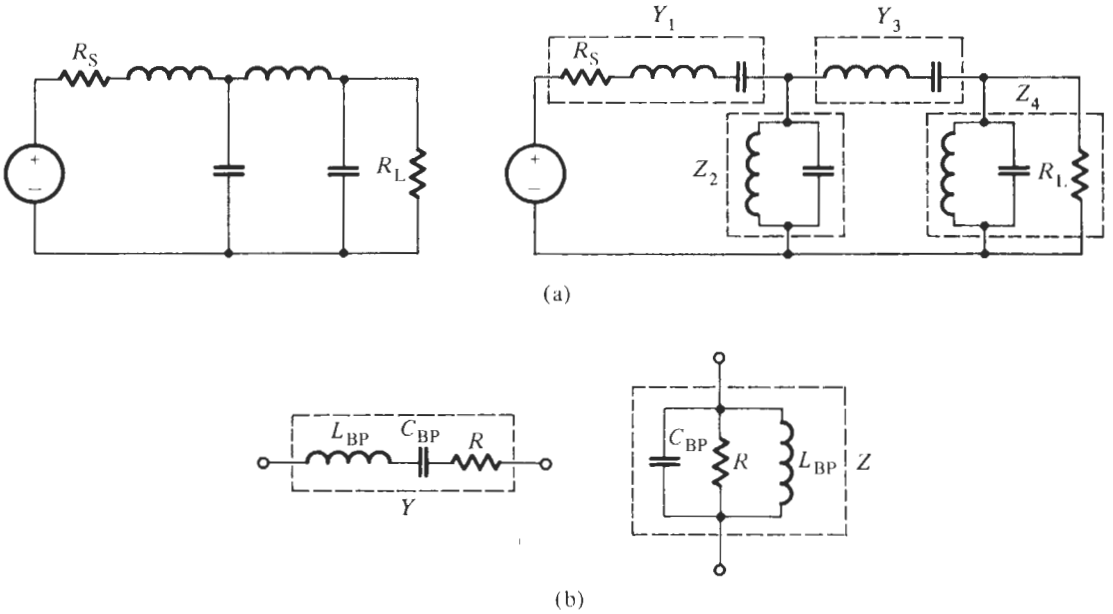

Figure 15.16 (a) Typical lowpass ladder converted to bandpass ladder; (b) general lossy ladder arms for the operational simulation. Note that the immittances in (b) are special cases of the general ladder arms in Fig. 15.13.

$$Z(s) = \frac{1}{G + sC_{BP} + \dfrac{1}{sL_{BP}}} = \frac{s/C_{BP}}{s^2 + sG/C_{BP} + 1/(L_{LP}C_{BP})} \tag{15.62}$$

As expected, these two immittances are special cases of Eqs. (15.38) and (15.39), respectively, and both of them have the form of bandpass functions. We can make this more obvious by using a scaling resistor R_p as we did before, and also, as we agreed, make the transfer function arising from the shunt arms, Z, inverting (see Fig. 15.4a):

$$t_Y(s) = Y(s)R_p = \frac{s\left(R_p/L_{BP}\right)}{s^2 + sR/L_{BP} + 1/(L_{BP}C_{LP})} = \frac{\left(R_p/R\right)s\omega_0/Q}{s^2 + s\omega_0/Q + \omega_0^2} \tag{15.63}$$

$$t_Z(s) = -\frac{Z(s)}{R_p} = -\frac{s\left(G_p/C_{BP}\right)}{s^2 + sG/C_{BP} + 1/(L_{LP}C_{BP})} = -\frac{\left(G_p/G\right)s\omega_0/Q}{s^2 + s\omega_0/Q + \omega_0^2} \tag{15.64}$$

In both cases the second-order section is lossless ($Q = \infty$) if the resistor R is absent. This will be the case for all internal ladder arms, whereas the first and last arms are lossy because they include the source and load resistor, respectively. We see, therefore, that operationally the ladder arms generated from a lowpass-to-bandpass transformation are equivalent to inverting and noninverting second-order bandpass filters. For the realization we may take any convenient second-order bandpass sections at our disposal as long as they can

1. implement infinite Q values,
2. be inverting and noninverting, and
3. have two inputs.

These bandpass circuits are then interconnected as implied in Fig. 15.4, where we have to pay attention that inverting and noninverting modules alternate along the simulated ladder. As we saw before, there is no need to concern ourselves with the signs of the signals; by alternating inverting and noninverting branches we are assured that the signals add at the branch inputs with the correct signs.[2]

Seeing now that we really need only a second-order bandpass filter rather than two individual integrators for each ladder arm, we can attempt to achieve a more direct solution by using the results of Chapter 4, and possibly a more economical implementation with single-amplifier bandpass biquads. Returning to active realizations in Fig. 15.13, we recognize that we implemented the simple bandpass branches (Fig. 15.16b) by the three-amplifier Åckerberg–Mossberg circuit discussed in Chapter 4, Fig. 4.29. The circuit was found to have excellent performance. The inverting and noninverting circuits are redrawn in Fig. 15.17 for ease of reference.

We encountered a suitable single-amplifier inverting bandpass module in the Delyiannis–Friend circuit of Fig. 4.37. It is shown in Fig. 15.18a with two inputs and somewhat different notation. Using standard procedures, we analyze the circuit to find

$$V_0 = -\frac{1}{1-K}\,\frac{s\dfrac{1}{C}\left(G_{i1}V_1 + G_{i2}V_2\right)}{s^2 + s\dfrac{G_1}{C}\left(2 - \dfrac{G_2}{G_1}\dfrac{K}{1-K}\right) + \dfrac{G_1 G_2}{C^2}} \tag{15.65}$$

where we labeled $G_{i1} + G_{i2} + G_3 = G_2$. We assumed ideal opamps in the analysis; any errors resulting from this assumption were discussed in detail in Chapter 4. We should now compare Eq. (15.65) realized by the circuit in Fig. 15.18a with t_Z in Eq. (15.64). Before we do this, let us for simplicity set $R_{i1} = R_{i2} = R_i$ and select $R_1 = R_2$. This results in

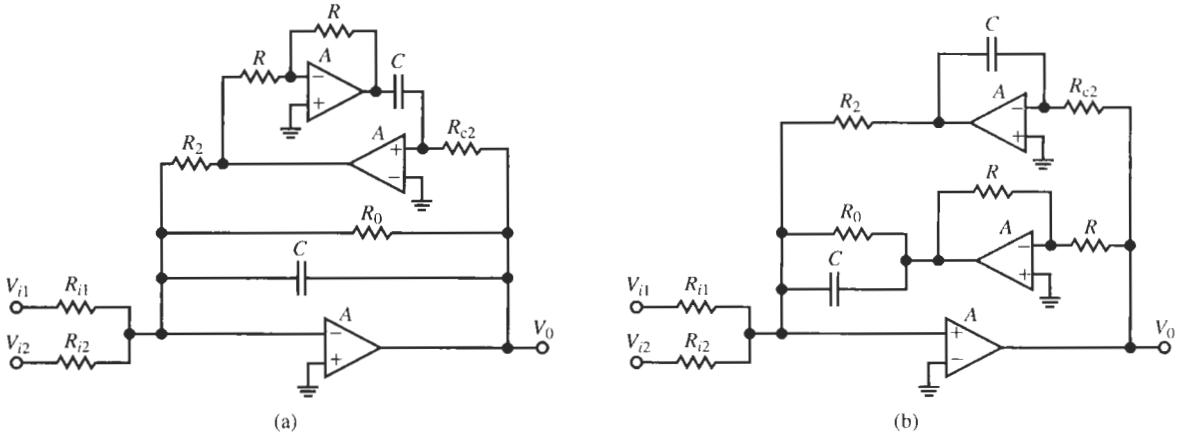

Figure 15.17 Two forms of the Åckerberg–Mossberg bandpass circuit with two inputs: (a) inverting; (b) noninverting. Note that the circuits can realize $Q = \infty$ by removing R_0 ($R_0 = \infty$).

[2] The realization may implement the negative of the prescribed functions; this is as a rule of no concern because it is simply a 180° shift in phase.

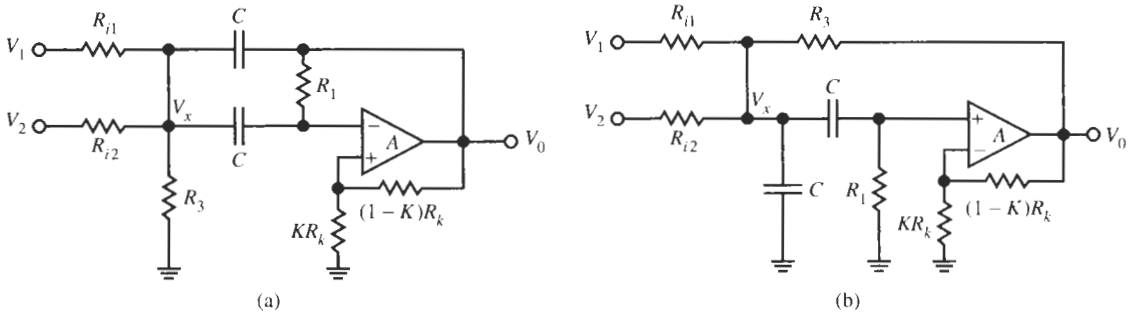

Figure 15.18 Single-amplifier bandpass modules to realize (a) a shunt arm (inverting); (b) a series arm (noninverting).

$$V_0 = -\frac{s\dfrac{1}{R_i C}\dfrac{1}{1-K}}{s^2 + s\dfrac{G_1}{C}\left(2 - \dfrac{K}{1-K}\right) + \dfrac{G_1^2}{C^2}}(V_1 + V_2) = -t_Z(s)\,(V_1 + V_2) \tag{15.66}$$

Thus, we need to compare the two forms

$$-\frac{s\dfrac{1}{R_i C}\dfrac{1}{1-K}}{s^2 + s\dfrac{G_1}{C}\left(2 - \dfrac{K}{1-K}\right) + \dfrac{G_1^2}{C^2}} \leftrightarrow -\frac{s\,(G_p/C_{BP})}{s^2 + sG/C_{BP} + 1/(L_{BP}C_{LP})} \tag{15.67}$$

Evidently, by comparing coefficients between the two expressions we have

$$\omega_0 = \frac{1}{CR_1} = \frac{1}{\sqrt{L_{BP}C_{bp}}}, \quad \frac{G_1}{C}\left(2 - \frac{K}{1-K}\right) = \frac{G}{C_{BP}}, \quad \frac{1}{R_i C}\frac{1}{1-K} = \frac{G_p}{C_{BP}}$$

From these three equations we find the components of the inverting active bandpass biquad for given values R, L_{BP}, and C_{BP}. Taking first the case of the lossy end sections of the ladder, we have

$$R_1 = \frac{1}{\omega_0 C} = \frac{\sqrt{L_{BP}C_{bp}}}{C}, \quad K = \frac{2\omega_0 C_{BP}R - 1}{3\omega_0 C_{BP}R - 1} = \frac{2Q-1}{3Q-1}, \tag{15.68}$$

$$R_i = \frac{1}{1-K}\frac{C_{BP}}{C}R_p$$

The parameter $Q = \omega_0 C_{BP}R$ is the quality factor of the ladder arm; for the internal lossless blocks we obtain from Eq. (15.68) with $R = \infty$, i.e., $Q = \infty$,

$$R_1 = \frac{1}{\omega_0 C} = \frac{\sqrt{L_{BP}C_{bp}}}{C}, \quad K = \frac{2}{3} \quad \text{and} \quad R_i = 3\frac{C_{BP}}{C}R_p \tag{15.69}$$

To realize the *non*inverting bandpass, we use a circuit that we did not encounter before. It can be considered a modification of the Sallen–Key module of Section 4.5.1 and is shown in Fig. 15.18b. Assuming again $A = \infty$ for analyzing the structure, we find

$$V_0 = \frac{s\dfrac{1}{KC}(G_{i1}V_1 + G_{i2}V_2)}{s^2 + s\dfrac{G_1}{C}\left[2 + \dfrac{G_2}{G_1} - \dfrac{G_3}{KG_1}\right] + \dfrac{G_1G_2}{C^2}} \tag{15.70}$$

where we labeled again $G_{i1} + G_{i2} + G_3 = G_2$. We compare this function with t_Y in Eq. (15.63), again set $R_{i1} = R_{i2} = R_1$, and, further, select $G_2 = G_1$. This results in

$$V_0 = +\frac{s\dfrac{1}{KCR_i}}{s^2 + s\dfrac{G_1}{C}\left[3 - \dfrac{G_3}{KG_1}\right] + \dfrac{G_1^2}{C^2}}(V_1 + V_2) = +t_Y(s)(V_1 + V_2)$$

Specifically, we compare coefficients between the expressions

$$\frac{s\dfrac{1}{KCR_i}}{s^2 + s\dfrac{G_1}{C}\left[3 - \dfrac{G_3}{KG_1}\right] + \dfrac{G_1^2}{C^2}} \leftrightarrow \frac{s\left(R_p/L_{BP}\right)}{s^2 + sR/L_{BP} + 1/(L_{LP}C_{BP})} \tag{15.71}$$

We obtain just as for the noninverting module:

$$\omega_0 = \frac{1}{CR_1} = \frac{1}{\sqrt{L_{BP}C_{BP}}}, \quad \frac{1}{R_1C}\left[3 - \frac{G_3}{KG_1}\right] = \frac{R}{L_{BP}}, \quad KCR_i = \frac{L_{BP}}{R_p} \tag{15.72}$$

For the end sections of the ladder where $Q = \omega_0 L_{BP}/R$ is finite, the components of the active noninverting bandpass biquad for given values R, L_{BP}, and C_{BP} are

$$R_1 = \frac{1}{\omega_0 C} = \frac{\sqrt{L_{BP}C_{BP}}}{C}, \quad K = \frac{R_1/R_3}{3 - R/(\omega_0 L_{BP})} = \frac{Q}{3Q-1}\frac{R_1}{R_3}, \quad R_i = \frac{L_{BP}}{R_pKC} \tag{15.73}$$

where $R_1 = R_2$ was assumed. For the internal lossless blocks with infinite Q, i.e., $R = 0$, we have

$$R_1 = \frac{1}{\omega_0 C} = \frac{\sqrt{L_{BP}C_{BP}}}{C}, \quad K = \frac{1}{3}\frac{R_1}{R_3}, \quad R_i = 3\frac{1}{R_p}\frac{R_3}{R_1}\frac{L_{BP}}{C} \tag{15.74}$$

With this step we have completed the design of the two single-amplifier biquads (SABs) for simulating an *LC* doubly-terminated bandpass ladder. The design formulas are summarized in Table 15.2. Building the circuit with SABs gives, of course, a more economical result than using two-integrator loops with three-opamp Åckerberg–Mossberg (ÅM) circuits. However, we must expect a more sensitive circuit with larger deviations. Recall from the analysis and the comparisons discussed in Chapter 4 that the finite gain-bandwidth product ω_t of the opamps causes larger frequency errors in SABs than in ÅM modules and that the quality factor in SABs is *very* sensitive to component tolerances. This last issue is particularly critical because we need to build second-order bandpass sections with large and even infinite Q values when simulating *LC* ladders. The SAB design method is recommended, therefore, only for less critical specifications. To demonstrate the design process and the larger sensitivities, let us design a bandpass with single-amplifier and ÅM modules.

TABLE 15.2 Design Equations for the Biquads in Fig. 15.18 for Realizing a Bandpass Ladder with Series and Shunt Branches Containing L_{BP}, C_{BP}, and R

In Fig. 15.18 Choose $R_{i1} = R_{i2} = R_1$, $R_1 = R_2$, and C; Then Compute	
For the Inverting Shunt Arm Fig. 15.18a	For the Noninverting Series Arm Fig. 15.18b
$R_1 = \dfrac{1}{\omega_0 C} = \dfrac{\sqrt{L_{BP}C_{BP}}}{C}$	$R_1 = \dfrac{1}{\omega_0 C} = \dfrac{\sqrt{L_{BP}C_{BP}}}{C}$
$K = \dfrac{2\omega_0 C_{BP}R - 1}{3\omega_0 C_{BP}R - 1} = \dfrac{2Q-1}{3Q-1}$	$K = \dfrac{R_1/R_3}{3 - R/(\omega_0 L_{BP})} = \dfrac{Q}{3Q-1}\dfrac{R_1}{R_3}$
with $Q = \omega_0 C_{BP} R = \dfrac{R}{\omega_0 L_{BP}}$	with $Q = \dfrac{1}{\omega_0 C_{BP} R} = \dfrac{\omega_0 L_{BP}}{R}$
$\left(K = \dfrac{2}{3} \text{ if } Q = \infty\right)$	$\left(K = \dfrac{1}{3}\dfrac{R_1}{R_3} \text{ if } Q = \infty\right)$
$R_i = \dfrac{1}{1-K}\dfrac{C_{BP}}{C}R_p$	$R_i = \dfrac{L_{BP}}{R_p K C}$
Condition to Be Satisfied: $2G_i + G_3 = G_2$, **Which Means**	
$2(1-K)\dfrac{C}{C_{BP}}\dfrac{1}{R_p} + G_3 = G_2$	$\left(\dfrac{2Q}{3Q-1}\omega_0 C_{BP} R_p + 1\right) G_3 = G_2$

In these equations choose a convenient value for R_p and compute R_3. Note: R_p is the same for the whole circuit!

EXAMPLE 15.3

We wish to implement an operational simulation of a sixth-order all-pole LC bandpass filter with 1-dB passband ripple. The desired center frequency is 32 kHz and the bandwidth 3 kHz. Source and load resistors are 800 Ω. The LC bandpass filter is shown in Fig. 15.19a. Design an active simulation using ÅM and, for comparison, single-amplifier biquads.

Solution

Let us pick $C = 10$ nF for the capacitors of the active circuit. Then we have for the first block by Table 15.1

$$\frac{C_1}{C} = \frac{135}{10} = m = 13.5 \quad \text{and} \quad R_0 = 13.5 \times 800\ \Omega = 10.8\ \text{k}\Omega$$

Further,

$$R_2 R_{c2} = m\frac{L_1}{C} = 13.5\frac{185\ \mu\text{H}}{10\ \text{nF}} = (499.8\ \Omega)^2$$

We pick $R_2 = R_{c2} = 500\ \Omega$ and, arbitrarily, $R_p = 348.2\ \Omega$. Because $m = 13.5$, this implies $R_a = R_{i1} = R_{i2} = 4.7\ \text{k}\Omega$.

For the second block we have

$$r^2 = \frac{L_1}{C} = \frac{42.2\text{mH}}{10\text{nF}} = (2054\Omega)^2 \quad \text{and} \quad R_2 R_{c2} = r^2\frac{C_1}{C} = (499\ \Omega)^2$$

Since we selected R_p, we have now $R_a = r^2/R_p = 12.116\ \text{k}\Omega = R_{i1} = R_{i2}$. We pick again $R_2 = R_{c2} = 500\ \Omega$.

The third block is identical to the first one. Observe that all three block have zeros at $f = (2\pi \times 500 \times 10^{-8})^{-1} = 31.8\ \text{kHz} \approx 32\ \text{kHz}$ as we expected.

With these components the midband gain is about 0 dB. If we want to reduce the gain by a factor 1/2 (−6 dB) to that of the passive ladder we need to reduce G_{i1} by 1/2 by doubling the value of R_{i1}. The final circuit and the test performance are shown in Fig. 15.19a. If we simulate the active circuit with ideal opamps (or measure the performance with a high-frequency opamp, such as the HA 2542-2), we find that the performance of the active and passive ladders is almost identical, but the effect of the finite ω_t of the LM741 opamps is to reduce the center frequency by ≈ 1 kHz (3.2%) and increase the ripple width from 1 to about 2.6 dB.

To design the three single-amplifier biquads we need the *LC* components:
Blocks 1 and 3:

$$L_{BP} = 0.185\ \text{mH}, \quad C_{BP} = 135\ \text{nF}, \quad R = 800\ \Omega$$

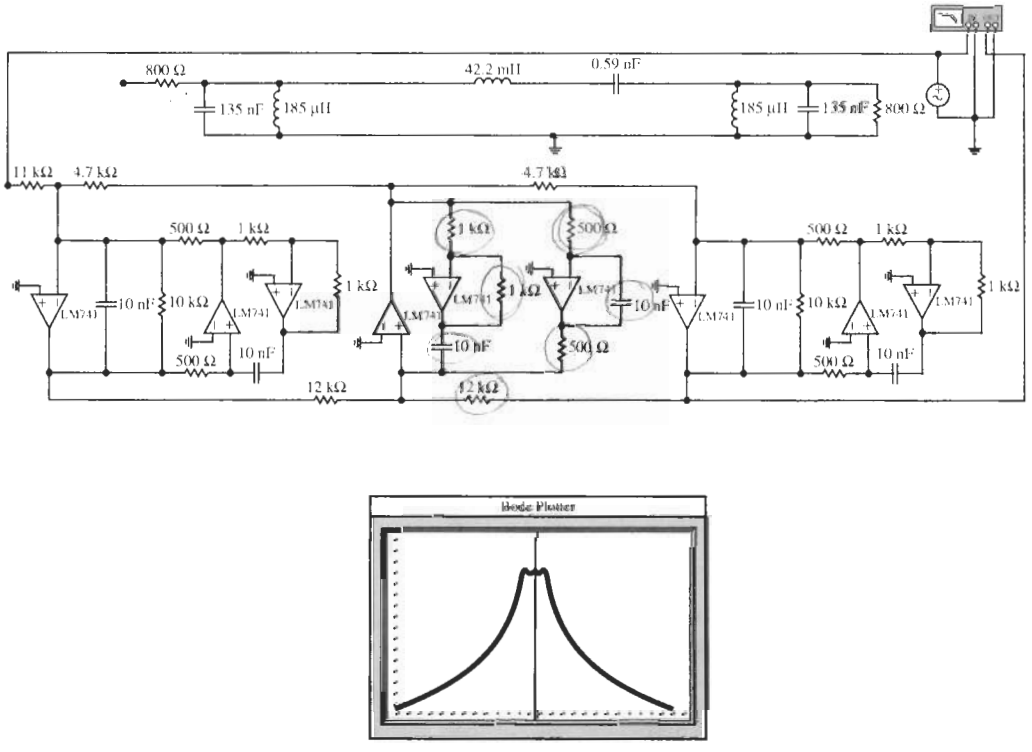

(a)

Figure 15.19 Circuits and test results for the bandpass design of Example 15.3: (a) *LC* bandpass, ÅM stimulation, and test performance of the circuit based on ÅM modules; (b) circuit and test result based on SABs. [(a) (Bode Plotter scales: 18 to 55 kHz; −80 to 10 dB; cursor at 30.96 kHz, −5.032 dB; (b) Bode Plotter scales: 15 to 80 kHz; −80 to 0 dB; cursor at 28.79 kHz, −6.025 dB.)

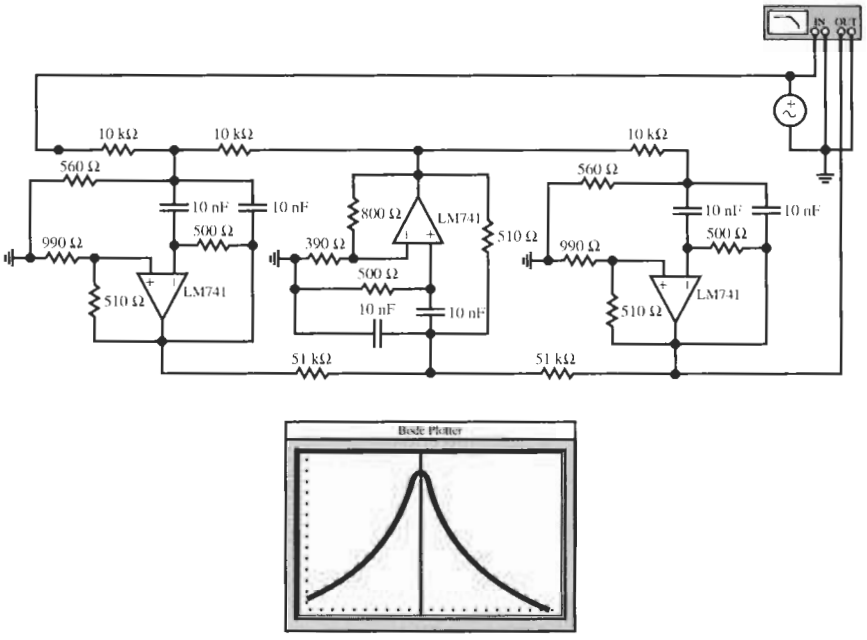

(b)

Figure 15.19 Continued

Block 2:

$$L_{BP} = 42.2 \text{ mH}, \quad C_{BP} = 0.59 \text{ nF}, R = \infty$$

Choosing $C = 10$ nF, we then calculate from Table 15.2 for all three blocks:

$$R_1 = \frac{\sqrt{L_{BP}C_{BP}}}{C} = 499.8\ \Omega$$

and for Blocks 1 and 3:

$$K = 0.6629, \quad R_i = 40.0R_p, \quad \text{and} \quad \frac{2}{40.05}\frac{1}{R_p} + \frac{1}{R_3} = \frac{1}{R_2}$$

Let us choose $R_p = 250\ \Omega$,[3] then $R_3 = 555\ \Omega$ and $R_i = 10.0\ \text{k}\Omega$.

For Block 2 we have

$$K = \frac{1}{3}\frac{R_1}{R_3} = \frac{166.7\ \Omega}{R_3}, \quad R_i = 3\frac{R_3}{R_1}\frac{L_{BP}}{R_pC} = 3\frac{R_3}{500\ \Omega}\frac{42.2\text{ mH}}{250\ \Omega\ \times 10\text{ nF}} = 101.3R_3$$

[3]Any convenient value can be chosen for R_p that leads to reasonable component values. R_p is only a scale factor for the LC ladder; it is no component itself.

and we have to satisfy $(\frac{2}{3}\omega_0 C_{BP} R_p + 1)G_3 = G_2$ which, with $R_1 = R_2$, results in

$$R_3 = R_1\left(\tfrac{2}{3}\omega_0 C_{BP} R_p + 1\right)\Omega = 1.013 \times 500\ \Omega = 507\ \Omega$$

and $R_i = 51.46\ \text{k}\Omega$, $K = 0.328$.

The circuit and a test set-up are shown in Fig. 15.19b. We notice that the filter uses significantly fewer components than the implementation in Fig. 15.19a and that it realizes the prescribed bandpass fairly closely. But considering the passband more carefully, we notice that the center frequency is too low by 10% (at ≈ 28.8 kHz rather than at 32 kHz) and that the bandwidth is too narrow by approximately 35% (at 1.95 kHz instead of the specified 3 kHz). These deviations can be reduced by carefully selecting components. If we use a high-frequency opamp (such as the HA 2542-2) the 10% passband shift nearly disappears, but the bandwidth is still too narrow (at 2.3 kHz). The observed deviations are only partially due to the finite value of ω_t; serious errors are contributed by component tolerances because of the large sensitivities of these circuit modules. Although the SAB-based circuit in this example (Fig. 15.19b) serves to illustrate the design process, the design specifications are too demanding for a realization with single-amplifier biquads to be practical.

REFERENCE

R. Schaumann, M. S. Ghausi, and K. R. Laker, *Design of Analog Filters: Passive, Active RC and Switched Capacitor*, Chapter 6. Prentice Hall, Englewood Cliffs, NJ, 1990.

PROBLEMS

15.1 Design a lowpass filter using the operational simulation method. The prototype for this problem is a fifth-order Butterworth filter as described in Table 13.1. The half-power frequency is to be 10,000 rad/s and source and load resistors are 3 kΩ. Be sure to design your circuit to give elements in a practical range of values. Use LM741 opamps and test the performance of your design with Electronics Workbench (EWB).

15.2 Repeat Problem 15.1 if the prototype is changed to a sixth-order Butterworth filter as described in Table 13.1, but other conditions remain unchanged.

15.3 Repeat Problem 15.1 if the prototype is changed to a fifth-order Chebyshev lowpass filter having a ripple width of 0.1 dB as described in Table 13.3.

15.4 This problem requires that a lowpass filter be designed to have the appearance of the structure shown in Fig. 15.8. The prototype is a fifth-order Chebyshev filter with 0.1-dB ripple width that is described in Table 13.3. The passband corner frequency is 240 kHz; the required terminations can be chosen but must be of the order of 1 kΩ. Use appropriate opamps and components of practical sizes, and build and test your design.

15.5 Use operational simulation to design an eighth-order Chebyshev lowpass with $\alpha_{max} = 0.1$-dB passband ripple in $0 \leq f \leq 128$ kHz. The prescribed load resistor is 1450 Ω. Use LM741 opamps and test your design with EWB.

15.6 Repeat Problem 14.5 for the methods discussed in this chapter.

15.7 Repeat Problem 14.7 for the methods discussed in this chapter.

15.8 The *LC* ladder implementation of a Bessel-Thomson filter with $D = 30\ \mu$s delay and $\leq 1\%$ delay error of 13 kHz is shown in Fig. P15.8. The filter has less than 2-dB attenuation in $f \leq 110$ kHz. Realize the circuit by the operational simulation method; use LM741 opamps and test your design.

15.9 This problem requires the design of a bandpass filter making use of the operational simulation method. The prototype lowpass is a third-order Butterworth

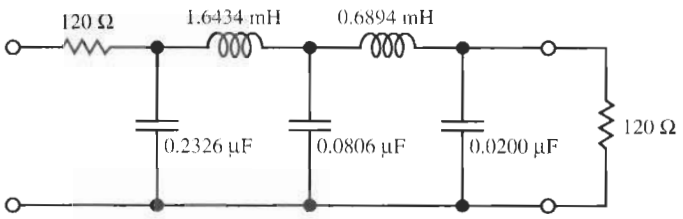

Figure P15.8

filter. The two half-power frequencies of the bandpass filter are 1960 and 2040 Hz. Source and load resistors are 1.8 kΩ. Consider whether the simplified circuitry in Section 15.3 can be used. Use LM741 opamps, practical element values, and test your design.

15.10 Using the methods discussed in this chapter, design a bandpass filter for which the prototype is a fourth-order Butterworth filter. For the filter, $f_0 = 60$ kHz and the lower 3-dB frequency is 48 kHz. The filter is driven by a voltage source with a 300-Ω source resistor. You may choose the load termination; it is not prescribed. Preferred are 1-nF capacitors. Use appropriate opamps for the design and test its performance.

15.11 Repeat Problem 14.9 with the design methods discussed in this chapter.

15.12 Design a bandpass filter with $f_0 = 9$ kHz and the 3-dB bandwidth of 980 Hz. The prototype is a fourth-order filter with a maximally flat passband magnitude. The circuit must use LM741 opamps. Use any design freedom to obtain practical element values. Decide which bandpass design method to use, discuss trade-offs, and test your design with EWB.

15.13 Repeat Problem 15.9 with the prototype changed to a fifth-order Chebyshev filter with a 0.1-dB ripple width as obtained from Table 13.3.

15.14 Repeat Problem 15.9 if the prototype is changed to the seventh-order Chebyshev filter with a 0.1-dB ripple width described in Table 13.3.

15.15 Design a filter that has a bandpass characteristic by the operational-simulation (leapfrog) method. For this problem, the prototype is the third-order Chebyshev filter with a 0.5-dB ripple width obtained from Table 13.3. Design for the center frequency of $\omega_0 = 3000$ rad/s, with a 0.5-dB bandwidth of 500 Hz. Use the method of Section 15.3, practical component values, and LM741 opamps. Test your design.

15.16 The circuit in Fig. P15.16 is the *LC* ladder implementation of a bandpass filter with a 1.7-dB equal-ripple passband in 10 kHz $\leq f \leq$ 18 kHz. The stopband attenuation $\alpha_{\min} > 42$ dB in $f > 26$ kHz. Realize the circuit with the operational simulation method and test your design.

15.17 Verify that Eqs. (15.46) and (15.57) describe the operation of the circuits in Fig. 15.12.

15.18 Verify that Eqs. (15.58) are the design equations for the components of the shunt branch in Fig. 15.13b.

15.19 A bandreject filter is required to provide an equal-ripple passband with $\alpha_{\max} = 1$ dB in $f \leq 80$ kHz and $f \geq 180$ kHz and $\alpha_{\min} \geq 20$ dB in 100 kHz $\leq f \leq$ 150 kHz. The *LC* realization is shown in Fig. P15.19. Implement the circuit by the operational simulation. Test your design.

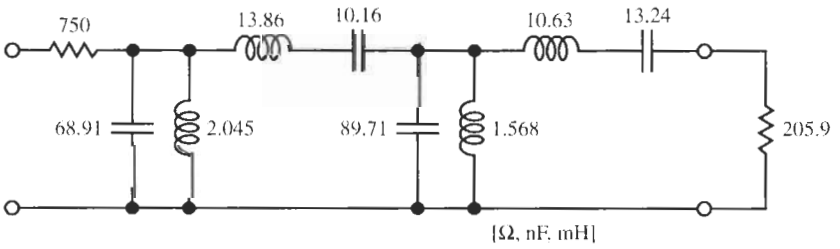

Figure P15.16

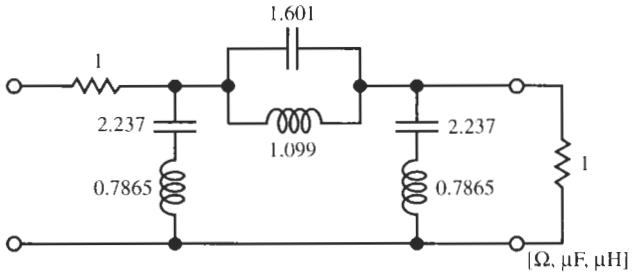

Figure P15.19

15.20 Design a lowpass filter based on a fifth-order inverse Chebyshev approximation with $\alpha_{max} = 1$ dB in $0 \leq f \leq 6.9$ kHz and two equal termination resistors of value 2.7 kΩ. Use LM741 opamps for the circuit and test your design with EWB.

15.21 Repeat the design of the Cauer filter of Problem 14.13 with the methods discussed in this chapter.

15.22 Repeat Problem 14.15 with the operational simulation method discussed in this chapter.

15.23 A bandpass ladder is shown in Fig. P15.23 with element values in Ω, μH, μF. Redesign the circuit with the methods of this chapter. Test your result with EWB.

15.24 A highpass filter is required to have a passband in $f \geq 68$ kHz with $\alpha_{max} \leq 0.3$ dB; the stopband must be in $f \leq 55$ kHz with $\alpha_{min} \geq 53$ dB. The termination resistors are 1.2 kΩ. The resulting *LC* implementation is shown in Fig. P15.24. Realize the circuit by the methods presented in this chapter and test your design.

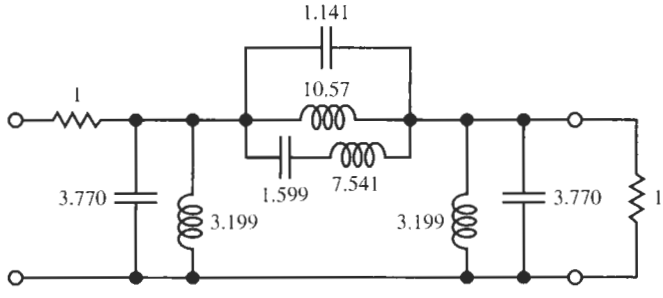

Figure P15.23

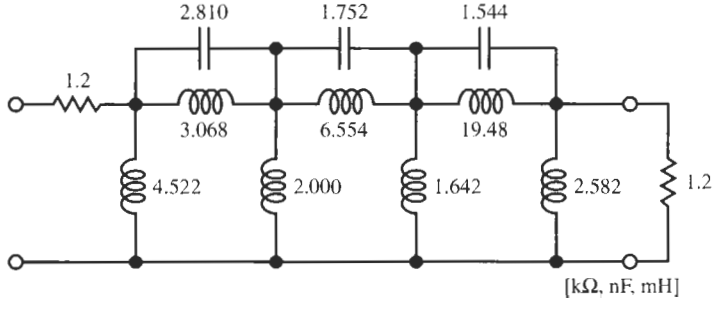

Figure P15.24

15.25 A normalized inverse Chebyshev lowpass circuit is shown in Fig. P15.25. Denormalize the circuit such that the termination resistors are 1.5 kΩ and the passband corner equals 7.3 kHz. Realize the resulting filter by the methods of this chapter and test the circuit with EWB.

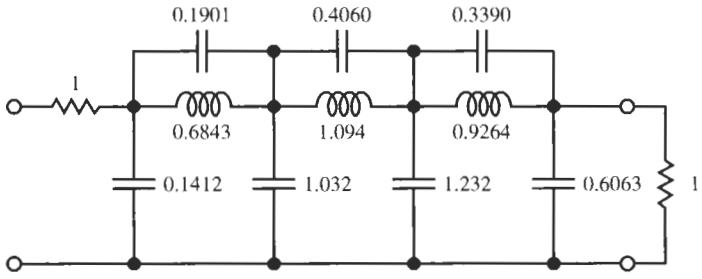

Figure P15.25

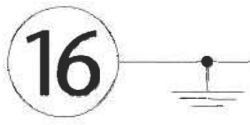

TRANSCONDUCTANCE-C FILTERS

We have previously discussed a variety of powerful and practical techniques for designing active filters. All the methods were based on embedding one or more operational amplifiers into a passive RC network such that the resulting feedback system realizes the required transfer function. We have seen repeatedly in our study that the use of opamps generally limits the frequency range over which our designs could be employed with predictable results. Recall that the errors introduced into the filter parameters, such as pole frequencies and quality factors, increase as the application frequencies rise relative to the opamp's gain-bandwidth product ω_t. Thus, to achieve a predictable design it is generally not recommended that these active RC circuits be employed at frequencies much above 5 or 10% of ω_t.

For improved reliability and reduced cost, the industry increasingly strives to place complete signal-processing systems on one integrated circuit (IC), including any continuous-time analog filters that may be needed. For purposes of bandlimiting, antialiasing, and reconstruction (Haddad and Parsons, 1991), even in predominantly digital systems continuous-time filters can be required to interface with the real world, where signals are in continuous-time format. Also, even internal to a digital transmission system, analog filters are used for bandlimiting to achieve noise reduction, and for equalizing gain or delay. In the read/write channel of a disk drive, for example, an analog lowpass filter that provides a constant delay (refer to Chapter 10) over a frequency range up to tens of megahertz is normally found. At the same time, the filter often needs to supply gain equalization (a gain boost) to compensate for losses in the transmission channel. As this example suggests, the modern communications industry needs integrated filters in the range of tens to hundreds of megahertz, and applications in the gigahertz range, such as in wireless communication systems, are becoming increasingly important. It should be clear that to be able to arrive at a predictable circuit performance at these frequencies, normal active *RC* filters are not useful. Apart from being incompatible or only poorly compatible with the dominant IC technology, CMOS (where resistors are not normally available), we need amplifiers with very large bandwidth coupled with high gain, which makes them hard to design and, in discrete form, less available and expensive. At the other extreme is the demand for analog integrated filters in the low audio range, for instance, for the telephone system where low cost coupled with high accuracy are at a premium.

Several approaches have emerged to solve the stated problems. For low-frequency integrated filters, a widely employed practical solution uses *switched-capacitor* (SC) *filters*. The design of SC filters follows fundamentally the active *RC* methods we presented in this book but avoids the use of resistors that are hard to implement accurately in MOS technology. It relies on the fact that a rapidly switched capacitor behaves like a resistor so that *RC* time constants are determined by ratios of capacitors and by the clock frequency with which the capacitors are switched. We will discuss this method in the next chapter. Also available for the design of low-to-intermediate frequency integrated filters is the *MOSFET-C* method. The MOSFET-*C* method, in principle, again follows techniques for standard active *RC* design and also avoids the use of resistors. Instead, it employs MOSFET transistors biased in the triode region where they behave like nonlinear resistors. The resulting signal nonlinearities are eliminated in the filter by designing the circuit carefully in fully balanced differential form where the nonlinearities can be shown to cancel between the positive and the negative signal paths. MOSFET-*C* filters have also been reported for successful high-frequency designs where they make use of special purpose on-chip amplifiers with bandwidths as high as a gigahertz. We will not discuss MOSFET-*C* filters in this book, but refer the interested reader to the references (Johns and Martin, 1998; Tsividis and Voorman, 1992).

The last method that is also usable from the low audio range, but extends to applications at hundreds of megahertz, avoids operational amplifiers altogether and instead obtains the required gain from *transconductance amplifiers*. Whereas operational amplifiers, as we know, are voltage-controlled voltage sources, transconductance amplifiers are voltage-controlled *current* sources, $I_{out} = g_m V_{in}$. This design method generally uses only transconductance amplifiers and capacitors and is referred to, therefore, as the *transconductance-C* (or g_m-*C*) *method*. It is the subject of this chapter. g_m-*C* filters are aimed specifically at high-frequency integrated filters and are at this time (2000) the dominant circuits for these applications. A recent concise overview of much of the material in this chapter can be found in Sánchez-Sinencio and Silva-Martínez (2000).

Although high-frequency filters are the main aim of this design method, g_m-C circuits can be used as well for integrated filters at low frequencies. The small bandwidth of opamps would cause no difficulties in this case and opamps can, of course, be integrated. But a problem arises with low-frequency opamp-based active RC filters because integrated capacitors are limited to around 30 pF. Much larger values consume too much silicon area on the integrated circuit chip. As a consequence, the design calls for huge resistors that also consume too much area and cause considerable noise. To see the problem, recall that the critical frequencies, such as the cut-off frequency of a lowpass filter, are set by an RC product. For example, $\omega_c = 10$ krad/s ($f_c = 1.59$ kHz) together with a maximum capacitor size of $C = 20$ pF results in a resistor $R = 5$ MΩ, which is impossible or at least very difficult to realize with any kind of accuracy. We shall see that in transconductance-C filters on the other hand, the frequency parameters are set by g_m/C ratios so that $g_m = 0.2\ \mu$ A/V will be needed together with $C = 20$ pF to set $\omega_c = 10$ krad/s. A transconductance value this small or even smaller is readily obtained with normal processing and biasing.

16.1 TRANSCONDUCTANCE CELLS

We can obtain some motivation for using transconductance-based circuits for our high-frequency active filters by recalling that individual transistors are fundamentally voltage-to-current converters characterized by their transconductance parameter. Figure 16.1 shows bipolar and MOS transistor symbols[1] and a simple generic small-signal model, Fig. 16.1c. We shall now proceed to find the parameters of the model; it will help us understand the behavior of a transconductance cell. In developing a model, we will restrict ourselves to MOS technology because we wish the filters to be compatible with digital circuitry; in other words, our analog integrated filters should be able to reside together with digital circuits on the same integrated circuit.

In the saturation region, an MOS transistor device is governed by the equation

$$i_D = \frac{1}{2}\mu C_{ox}\frac{W}{L}(v_{GS} - V_t)^2 \tag{16.1}$$

Here, the model's output current $i_O = i_D$ is the total drain current, i.e., the dc bias current I_D and the ac current $i_d(t)$: $i_D = I_D + i_d(t)$. The input voltage $v_I = v_{GS} = V_{GS} + v_{gs}(t)$ is the total gate-to-source voltage, μ is the carrier mobility, C_{ox} is the oxide capacitance per unit area of the channel (typical value: 1.5 fF/μm^2), and V_t is the threshold voltage. Using derivatives, the transconductance parameter is defined as

$$g_m = \frac{i_d}{v_{gs}} = \frac{\partial i_D}{\partial v_{GS}}\bigg|_{I_D, V_{GS}} = \frac{2I_D}{(v_{GS} - V_t)} = \sqrt{2}\sqrt{\mu C_{ox}\frac{W}{L}}\sqrt{I_D} \tag{16.2}$$

We note that g_m can be adjusted by the width-to-length ratio, W/L, of the gate and is proportional to the square root of the bias current I_D. A typical value for the parameter

[1] It is not the objective of this chapter to delve in detail into transistor operation; we will list only a few equations relevant for our purpose. For an in-depth treatment see, for example, Sedra and Smith (1998), Chapters 4 and 5.

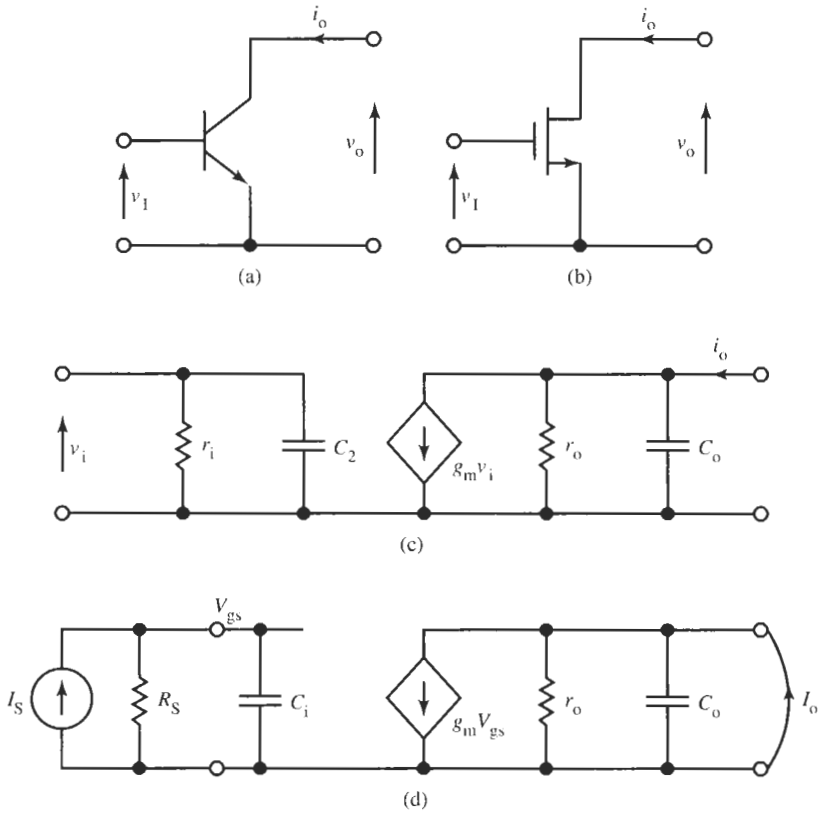

Figure 16.1 (a) Bipolar and (b) MOS transistors; (c) generic small-signal model; (d) small-signal model driven by a current source.

μC_{ox} is 100 μA/V^2 so that for a square device ($W = L$) biased at 100 μA we obtain[2] $g_m \approx 140\ \mu A/V = 140\ \mu S$. For the remaining components of the small-signal model in Fig. 16.1c we obtain

$$r_o = \frac{1}{g_o} = \frac{V_A}{I_D} \tag{16.3}$$

where V_A is the Early voltage for the MOS device, and the effective input capacitor C_i in the saturation region is approximately $C_i \approx 0.75 C_{ox} WL$. Note that in contrast to bipolar transistors the input resistor r_i in an MOS device is infinite because the transistor gate is an open circuit at dc. The output capacitor C_o depends on device size, connections, and layout and is of the order of 0.01 pF or less. The important parameter for our purpose is the bandwidth. We use the circuit in Fig. 16.1d, that is, we assume the source is a current I_s because often a transconductance cell is driven by another transconductance cell. The short-circuit output current I_o is obtained from Fig. 16.1d by direct analysis as

[2] Although, of course, the g_m values can be increased by choosing a large ratio W/L, a comparison with the BJT shows that for the same bias conditions bipolar transistors tend to have a larger transconductance than MOS devices.

$$I_o = g_m V_{gs} = g_m \frac{1}{sC_i + G_S} I_s$$

Let us assume the previous numbers for a small MOS transistor with $W = 5\,\mu$m and $L = 1\,\mu$m, and let us assume that $R_S = 50\,\text{k}\Omega$. Then we have $g_m \approx 315\,\mu$S, $C_i = 5.6 \times 10^{15}$F $= 5.6$ fF and the bandwidth is $1/(C_i R_S) = 3.55$ Grad/s or 566 MHz. If the current source is ideal ($G_S = 0$) we have unity current gain, $I_o/I_s = 1$, at $\omega_T = g_m/C_i = 56$ Grad/s or $f_T \approx 9$ GHz.

To summarize this little review, remember the following important points:

- Bipolar and MOS transistors are fundamentally voltage-controlled current sources characterized by transconductances.
- Bipolar transistors have larger transconductance values than MOS devices and are generally faster.
- The bandwidth of either device type is in the hundreds of megahertz and can reach gigahertz values.

In addition we note that the equations are based on derivatives of the nonlinear transistor characteristics; they are valid for small signals and significant nonlinearities must be expected when signals are larger than a few tens of millivolts.

To develop active filters built with transconductors, we need to investigate how to build practical transconductors or, as they are often labeled, *operational transconductance amplifiers* (OTAs) that retain the high-frequency properties of the transistors with which they are constructed. Although in a few cases individual transistors have been used, as a rule, the requirements are more difficult and demand, e.g., differential input and output, higher output impedance, or larger signals, so that more complex stages are needed. As it is not our intent to consider designs of component-level electronic circuits, we leave this discussion to other references that explain the design of analog integrated circuit in great detail (Gray and Meyer, 1993; Johns and Martin, 1998; Sedra and Smith, 1998). Numerous transconductors have been developed in recent years; their designs and the resulting circuits are available in the literature. However, since transconductors are less prevalent and less well known than operational amplifiers, let us look at some fundamental circuit concepts, and then construct a suitable model on which to base our high-frequency filters.

We did encounter transconductance cells once before in our study: the input stages of operational amplifiers are transconductors. Refer to Fig. 2.2a, where we labeled the part of the circuit consisting of transistors $Q1$ to $Q8$ and resistors $R1$ to $R3$ as g_m. This transconductance cell is represented by the input stage symbol in Fig. 2.3a; it generates an output current I proportional to the differential input voltage $V_+ - V_-$, $I = g_m(V_+ - V_-)$, as stated in Eq. (2.4). The equivalent configuration can be designed in complementary MOS (CMOS). If we reduce the circuit to its essential features, shown in Fig. 16.2a, we have a differential input pair $M1$, $M2$, a current-mirror active load $M3$, $M4$, and a constant current I_B for biasing, derived from $M5$. The output current for this case is

$$I_o = \frac{I_B}{(V_{GS} - V_t)} V_i = g_m V_i \tag{16.4}$$

where the transconductance g_m is reduced from the value in Eq. (16.2) because only one-half of the bias current flows on each side of the differential circuit. We note that the output current is taken from a node between two drains so that the output resistor of this cell equals $r_{o2} || r_{o4}$ and the input capacitance has one-half the value of input capacitance of an input transistor because two C_i are in series.

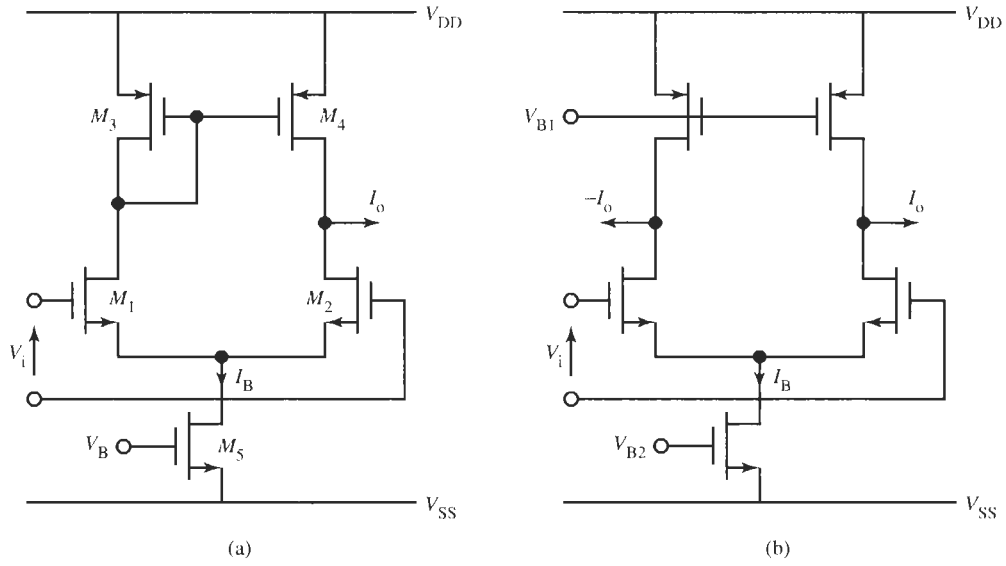

Figure 16.2 Basic CMOS transconductance stages: (a) single-ended output; (b) differential output.

This fundamental stage needs improving in various ways to arrive at practical OTAs. One weak property is the relatively low dc gain. Note that the low-frequency open-circuit voltage gain of the CMOS stage for the typical parameters $g_m = 200\,\mu$A/V, $V_A = 50V$, $I_B = 100\,\mu$ A, i.e., $r_o = 500$ kΩ, is only

$$\frac{V_o}{V_i} = g_m\,(r_{o2}||r_{o4}) \approx 50 \approx 34\text{dB}$$

Improved values of gains of 50 to 80 dB can be obtained by increasing r_o, without raising I_B and consuming more power to increase g_m. This is accomplished by improved current mirrors and, especially, by using cascode design. Another shortcoming is the limited signal range before nonlinearities become unacceptable. Again a number of solutions have been proposed; among them are source degeneration and cross-coupling of input pairs, so that good transconductance stages can process signals in the range of 1 V with nonlinearities of no more than 1% or so. These improvements add to the complexity of the basic stage in Fig. 16.2a, but we emphasize that the resulting circuits remain very simple, using only 12 to 15 transistors.

An additional modification is often necessary for practical transconductors: In analog integrated circuits it is preferable to process signals differentially because, among other advantages, it improves noise performance and reduces distortion. There are two reasons:

1. Voltages or currents that tend to corrupt the main signal, such as switching noise in the system, power supply ripple, or other extraneous signals, tend to appear in common mode for both positive and negative signal paths and cancel in differential processing.
2. Active devices cause nonlinearities. This is true, for example, in the MOS transistor that is essentially a square-law device [see Eq. (16.1)]. In that case, a voltage signal $v(t)$ leads to the drain current with second-order nonlinearities:

$$i_d = g_1 v + g_2 v^2$$

g_2 and g_3 are coefficients expressing the nonlinearity. However, applying the signal differentially as $v_+ = +v$ and $v_- = -v$ and taking the current differentially as well, we have

$$i_{d+} = g_1(+v) + g_2(+v)^2 \quad \text{and} \quad i_{d-} = g_1(-v) + g_2(-v)^2$$

If we now form the output by taking the difference,

$$i_d = i_{d+} - i_{d-} = \left(g_1 v + g_2 v^2\right) - \left(-g_1 v + g_2 v^2\right) = 2g_1 v$$

we not only cancel the nonlinearity but we double the linear part of the signal for a 6-dB gain.

In our basic circuit in Fig. 16.2a we already have a differential input. To achieve the differential output, we may simply dispense with the current mirror and take the output from both sides, after applying an appropriate bias so that the transistors $M3$ and $M4$ act as current sources. This is shown in Fig. 16.2b. Observe that the advantages of differential operation are obtained at no cost in circuit complexity, but the price paid is a halving of the transconductance because we no longer add the two currents from both sides of the differential pair by means of the mirror.

As we progress in this chapter, we will soon learn that it is convenient to have transconductors with more than one input; two inputs are sufficient for most situations. We can achieve this requirement quite simply by connecting the output terminals of two g_m cells so that the currents add. This is shown in Fig. 16.3 with the transconductor symbol we used in Fig. 2.3. Observe that adding currents requires no special circuitry but "needs only a node" where by Kirchhoff's current law we have $I_o = I_{o1} + I_{o2}$. Some savings in circuitry can be obtained by doubling only the input differential pair and adding their output currents.

Let us point out again that the circuits are very simple and small in area. As a matter of fact this simplicity of the transconductance circuit, compared with the ones of most operational amplifiers, is one of the main reasons for using them for integrated filter design. Not only do they consume less silicon area, but the simple circuitry is at the base of their good high-frequency response. Note that in the basic stages in Fig. 16.2 there is no internal node between the input and output terminals.[3] Thus there are no nodes, especially no high-

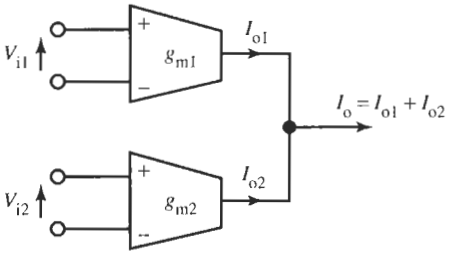

Figure 16.3 Connecting the outputs of two transconductors to achieve the effect of one transconductor with two inputs.

[3] An internal node is one with no connections to either input or output.

impedance nodes, where parasitic capacitors can result in long time constants that limit the bandwidth. Consequently, these cells are essentially as fast as the transistors out of which they are constructed. The literature contains many transconductors with bandwidths in the hundreds of megahertz; even CMOS designs with bandwidth of over 1 GHz have been reported.

16.1.1 A Model

Having seen now that transconductors, compared with operational amplifiers, are relatively simple analog integrated circuits that are designed readily for very wide bandwidth, we are at last ready to develop the model[4] on which we will base the design of filters. The model we use is essentially the one for the MOS transistor in Fig. 16.1c, repeated with slightly changed notation in Fig. 16.4. Figure 16.4a contains the single-ended transconductor model, with the transconductor symbol shown on the right. Figure 16.4b shows the fully differential model with its symbol seen on the right. The notation we adopt for the transconductance symbols is such that the current $I_o = g_m V_i$ enters the terminal marked by the minus sign and leaves the terminal marked by the plus sign; in other words, the minus terminal sinks current and the plus terminal sources current. The model adopted in *Electronics Workbench* (EWB) is a rectangular box labeled "OTA" (refer to Fig. 16.5) but with unmarked connectors; the four terminals correspond to those in Fig 16.4b: the upper input terminal and lower output terminal are designated "+."

As we intend to use this model for the designs in this chapter, let us have a closer look at its performance. Figure 16.5a shows the test set-up. The OTA is driven by a 100-mV voltage source with a 100-Ω source resistor. The 100-Ω resistor is largely irrelevant, of course, because the OTA input is essentially an open circuit so that no current flows. Only at the highest frequencies does the time constant created by the source resistor and the 0.1-pF input capacitor have a small effect on magnitude and phase. For the first test, the OTA output is an open circuit. Figure 16.5b shows the frequency response. We notice that the low-frequency gain is 60 dB as expected because $g_m r_o = 200\ \mu S \times 5\ M\Omega = 1000 = 60$ dB. The −3-dB frequency should be at $1/(2\pi C_o r_o) \approx 128$ kHz, which is what we measure (cursor in Fig. 16.5b). Following the transfer characteristic toward higher frequencies, we come to the point which the gain is unity (0 dB); this unity-gain frequency is 128 MHz. The signal generator in Fig. 16.5a was set to that frequency so that on the oscilloscope we should observe two equal signals. Figure 16.5c shows the oscilloscope display verifying the prediction. The phase shift between the two signals is nearly −270° (or +90°). This is also as expected because the gain of the OTA connection used is inverting, accounting for −180° phase shift, and, by Fig. 16.5b, the circuit looks like an integrator (the OTA loaded by its parasitic output capacitor!), adding the remaining −90° phase.

---

[4] For verification of our designs and for simulation and test results, we use in this text the commercial program Electronics Workbench. Among others, EWB has models for numerous commercial operational amplifiers, built in for ready use and realistic simulations of circuit performance. Thus, there is no need to use our own opamp models. Commercial transconductors are still much less available, and unfortunately EWB contains no transconductor models. To be able to proceed with the practical flavor of the material and test our designs, we implement in EWB the simplified, but realistic, model in Fig. 16.4.

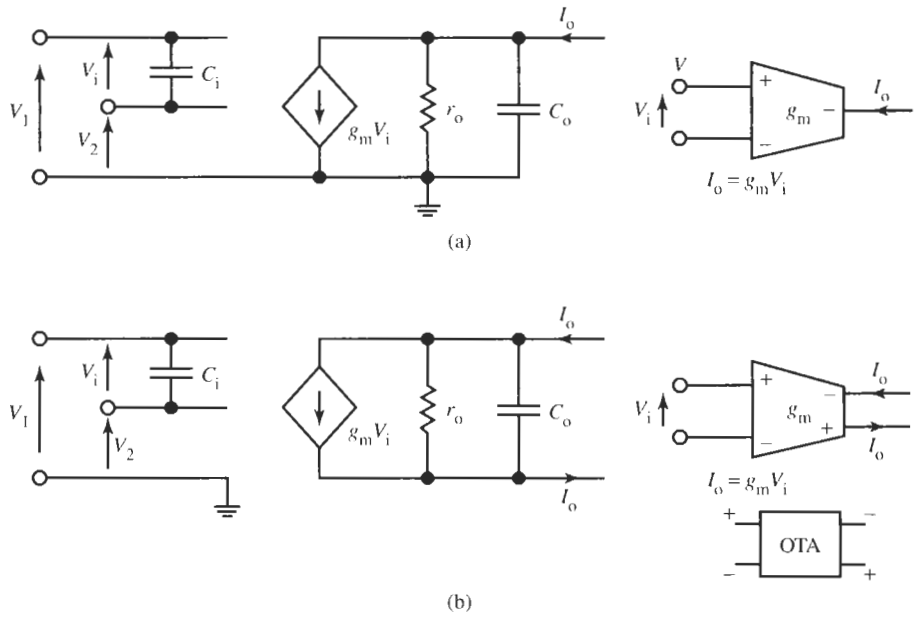

Figure 16.4 Small-signal model for a transconductor and its symbols: (a) single-ended circuit; (b) differential circuit. In both cases $I_o = g_m V_i$. The *Electronics Workbench* model is labeled OTA. The four connectors correspond to those of the fully differential transconductor. The model values we will use are $g_m = 200\ \mu A/V = 200\ \mu S$, $C_i = 0.1$ pF, $C_o = 0.25$ pF, $r_o = 5\ M\Omega$; g_m is designed to have a second pole at ≈ 650 MHz.

Further, if we look carefully at Fig. 16.5b, we notice a break in the slope of the magnitude at around 600 MHz. To determine whether this observation is real, we need to eliminate the pole at $1/(2\pi C_o r_o) \approx 128$ kHz because it masks the effect of the higher pole. We can do this by measuring the short-circuit output current. Because a current at 600 MHz is too difficult to measure, we approximate a short circuit by a 50-Ω resistor and measure the voltage instead. Connecting the "unattached" 50-Ω resistor in Fig. 16.5a to the circuit's output terminals, we observe the voltage gain in Fig. 16.5d; it is at $I_o \times 50\ \Omega = -40$ dB, corresponding to $I_o = 200\ \mu A$ as we would expect from the model parameters. Figure 16.5d also shows that the current gain itself, apart from any output capacitor C_o and resistor r_o, has a pole at 560 MHz. It supports the observation made earlier concerning the break in magnitude-slope at "around 600 MHz." Finally it is of interest to observe the phase of the current gain corresponding to the magnitude in Fig. 16.5d. It is shown in Fig. 16.5e: we expect 180° because the OTA connection used the inverting output. Indeed, we measure 180° for low frequencies but there is a 5° phase error at 52 MHz, and the phase becomes, of course, $\approx 135°$ at 560 MHz, the location of the pole.

In summary, we may conclude that the frequency response of our theoretical model, which is a very close representation of many published transistor-level transconductor circuits, behaves in a predictable fashion and will be useful for testing the transconductor-C circuits to be derived in the following sections.

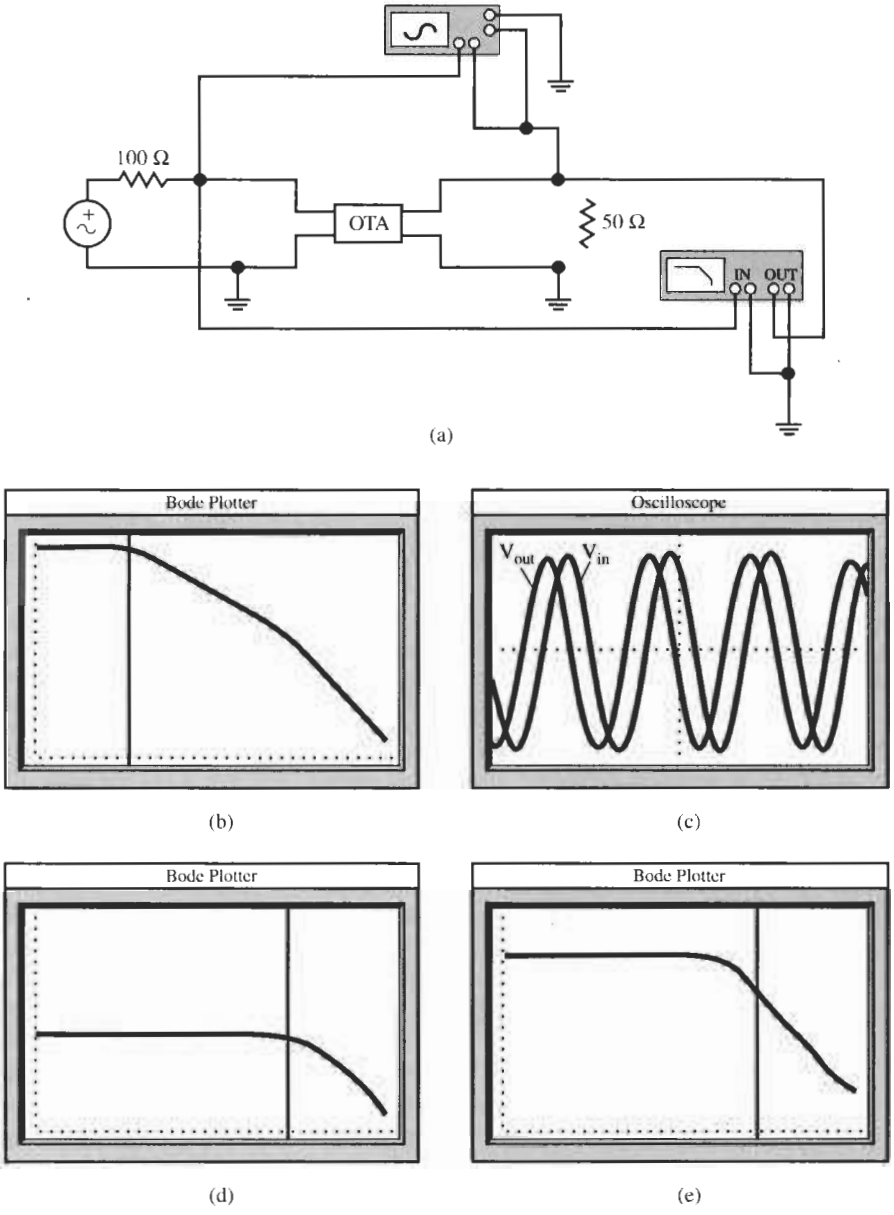

Figure 16.5 Testing the OTA: (a) test circuit; (b) open-circuit transfer characteristic; (c) input and output voltages at the unity-gain frequency; (d) the short-circuit transconductor current magnitude; (e) the short-circuit transconductor current phase. [(b) Bode Plotter scales: 1 kHz to 100 GHz; −120 to 60 dB; cursor at 121.2 kHz, 57.2 dB (c) oscilloscope scales: time base: 2 ns/div; vertical scale: 50 mV/div; (d) Bode Plotter scales: 1 kHz to 100 GHz; −120 to 50 dB; cursor at 562.3 MHz, −43.28 dB; (e) Bode Plotter scales: 1 kHz to 100 GHz; −45° to 225°; cursor at 562.3 MHz, 130.8+.]

16.2 ELEMENTARY TRANSCONDUCTOR BUILDING BLOCKS

Just as was the case with opamp-based active *RC* filters, here, with g_m-C filters we need a variety of elementary building blocks with which the filters are constructed. As the name "g_m-C filters" suggests, we wish to employ only transconductors and capacitors as basic components. In addition, we will find it helpful to have a way to realize or simulate resistors because these are difficult to implement with sufficient accuracy and over an adequate range of values. Further, as we know from our previous study, a very important building block is the integrator, so we shall investigate how these are built in g_m-C form. Lastly, for realizing simulated *LC* ladders, we found it most convenient to have available a method for building electronic inductors. In addition, because they are simple to construct and are useful components to have available generally in analog electronics, we will have a look at the design of summers and amplifiers with transconductors. Being mindful of our preference of differential configurations, we shall design all fundamental blocks in differential form, but we will always start with a single-ended structure because keeping track of only one signal path makes them easier to understand.

16.2.1 Resistors

We shall see that there is generally little need for resistors in the area of g_m-C filters with the notable exception of source and load resistors in doubly terminated *LC* ladders. We saw in Chapter 13 that we need at least two resistors in a lossless ladder: for low-sensitivity design, source and load resistors should be incorporated into the design strategy. Thus, let us begin the development by designing a g_m-based resistor.

Consider the configuration in Fig. 16.6a. It shows a transconductor with its negative output terminal connected back to its positive input terminal. Since the transconductor input is (ideally) an open circuit, the input current I_i is equal to the transconductance output current $I_o = g_m V_i$, thus

$$I_i = I_o = g_m V_i \tag{16.5}$$

Consequently, the circuit represents a resistor:

$$R = \frac{V_i}{I_i} = \frac{1}{g_m} \tag{16.6}$$

Note that this is a *grounded* resistor because V_i is referenced to ground and the inverting input of the OTA is at ground. To realize a floating resistor, we take the differential transconductance,

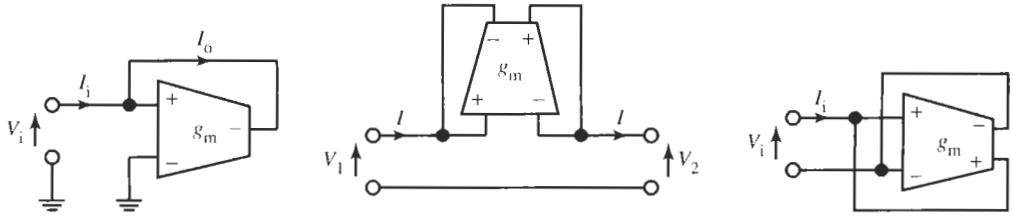

Figure 16.6 Resistor simulations with transconductors: (a) grounded; (b) floating; (c) negative and differential.

connect the two inputs to two different voltages, and feed the outputs back to the inputs as shown in Fig. 16.6b. Always paying attention that feedback is negative, we obtain the two equations,

$$I_i = I_o = I = g_m (V_1 - V_2) \tag{16.7}$$

Thus, the resistor is

$$R = \frac{V_1 - V_2}{I} = \frac{1}{g_m} \tag{16.8}$$

We pointed out that we should be certain to maintain negative feedback when forming the g_m-based resistor. If the feedback connection becomes positive, we simulate a *negative resistor*, $V_i/I_i = -R = -1/g_m$, as shown in Fig. 16.6c, in differential form. Such a negative resistor is used, for instance, to compensate transconductor losses (r_o in Fig. 16.4) or to eliminate inductor losses when very small but real spiral-wound inductors are used on ICs for filters at the highest frequencies.

The student may object that these resistor simulations are too complicated a method for obtaining "just a resistor." But note that apart from requiring a power supply that the active circuit contains in any event, the 10 to 15 small transistors likely use less silicon real estate on the IC than a real resistor. An additional advantage of the $1/g_m$ resistors that we will become to appreciate as we progress in this chapter is that the resistors are electronically variable because they depend on a bias current (or voltage). A traditional integrated resistor, implemented, say, as a diffused or a deposited layer, does not offer this possibility. Finally, as we shall see shortly, it is most helpful in g_m-C filter design to have the "resistors" technologically match and track the active devices, here transconductors, in their behavior. We shall address this issue in Example 16.1 and again at the end of Section 16.4. The following example will illustrate the performance of a simulated resistor.

EXAMPLE 16.1

Build and test a 1:2 voltage divider with two equal "resistors," once with a real resistor and a simulated one, and once with two simulated resistors.

Solution

Figure 16.7a shows the circuit along with the test set-up for measuring the performance of the voltage divider consisting of a 5-kΩ resistor and a simulated resistor of value $1/g_m = 1/200\ \mu S = 5\ k\Omega$. Figure 16.7b shows the magnitude of the transfer characteristic: the gain equals −6 dB until higher than 200 MHz, corresponding to the ratio 1/2. The oscilloscope display in Fig. 16.7c shows the 100-mV_{rms}–150-MHz input signal and the 50-mV_{rms} output signal at approximately a 42° phase shift. The gain roll-off and the phase shift are caused by OTA parasitics.

To eliminate the effect of parasitics, we replace the 5-kΩ resistor by the simulated floating resistor of Fig. 16.6b with value $1/g_m = 1/200\ \mu S = 5\ k\Omega$, shown not connected above the 5-kΩ resistor in Fig. 16.7a. We now observe the transfer ratio of 0.5 with no roll-off visible for

all test frequencies (see Fig. 16.7d) and no phase shift (Fig. 16.7e). The explanation is that the two "resistors" now have identical small-signal models as is shown in Fig. 16.7f. The transfer ratio is

$$\frac{V_2}{V_1} = \frac{Z_2}{Z_1 + Z_2} = \frac{1}{1 + Z_1/Z_2} = \frac{1}{2}$$

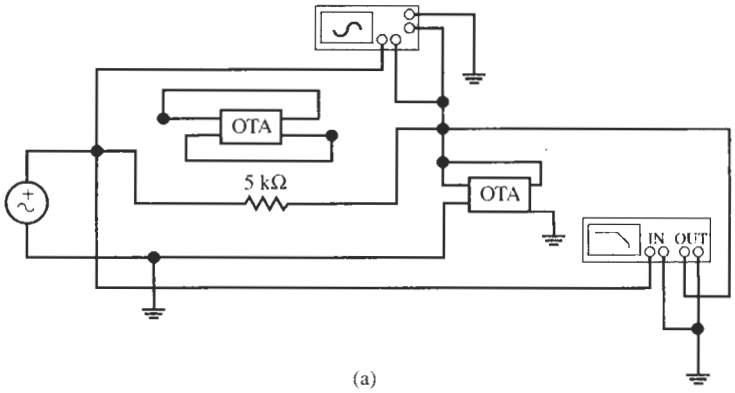

(a)

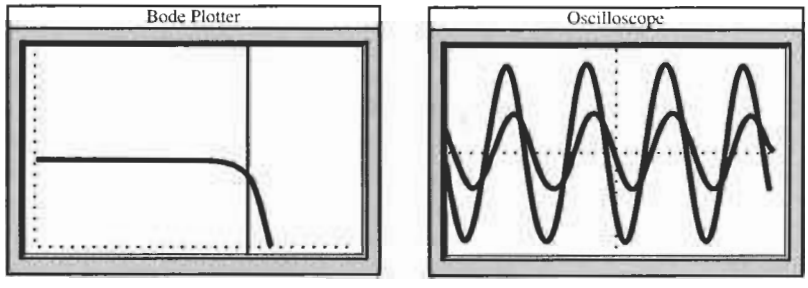

(b) (c)

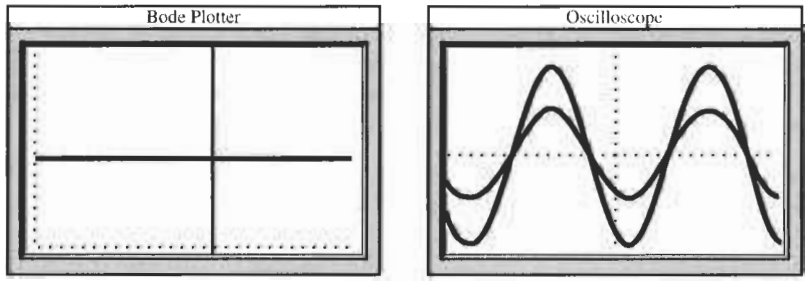

(d) (e)

Figure 16.7 Building a voltage divider with simulated resistors: (a) circuit and test system; (b) measured gain is 1/2 until $f \approx 200$ MHz; (c) input and output signals at 150 MHz; (d) frequency-independent magnitude equal to 1/2 for two simulated resistors; (e) input and output signals at 150 MHz with no phase shift; (f) small-signal model for the circuit with two simulated resistors. [(b) Bode Plotter scales: 1 kHz to 100 GHz; −20 dB to 10 dB; cursor at 215.4 MHz, −8.558 dB; (c) oscilloscope scales: 2 ns/div, 50 mV/div; (d) Bode Plotter scales: 1 kHz to 100 GHz; −20 to 10 dB; cursor at 29.87 kHz, −6.021 dB; (e) oscilloscope scales: 1 ns/div, 50 mV/div.]

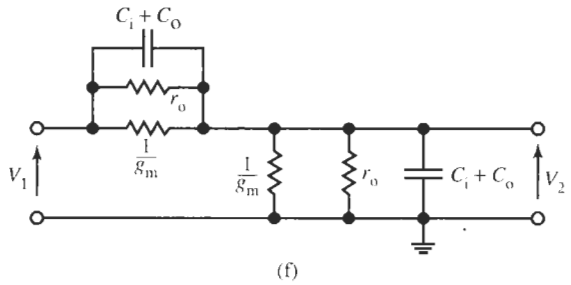

Figure 16.7 Continued

where all parasitic effects caused by C_i, C_o, and even by the frequency dependence of g_m cancel because $Z_1 = Z_2$. It is a clear demonstration of the advantages of having components match in their frequency response.

16.2.2 Integrators

Let us turn our attention next to the implementation of an integrator. The fundamental circuit is obtained by loading a transconductor by an impedance $Z(s)$ as is shown in Fig. 16.8. The circuit realizes

$$V_2 = g_m Z(s)\left(V_1^+ - V_1^-\right) = \frac{g_m}{Y(s)}\left(V_1^+ - V_1^-\right) \tag{16.9}$$

Clearly, if we use a capacitor C for the impedance, Eq. (16.9) becomes

$$V_2 = \frac{g_m}{sC}\left(V_1^+ - V_1^-\right) \tag{16.10}$$

and we have obtained the fundamental building block of g_m-C filters: the g_m-C integrator in Fig. 16.9a. Note that the integrator has differential inputs, that is, if we may realize inverting or noninverting integrators with the same circuit simply by using V_1^- or V_1^+, respectively, as the input. No separate inverter is required. Observe that the integrator is ideal if we can assume that the transconductor is ideal. In reality, the voltage-controlled current source g_m in Fig. 16.4 is also loaded by C_o and $r_o = 1/g_o$, which appear in parallel with the integrating capacitor C. Thus, with the small-signal model in Fig. 16.9b and assuming $V_1^- = 0$, the complete transfer function becomes

$$\frac{V_2}{V_1^+} = \frac{g_m}{s(C + C_o) + g_o} \tag{16.11}$$

It follows that in a real g_m-C integrator the integration capacitor C is increased to $C + C_o$ by the parasitic output capacitance of the g_m cell. Also, the integrator is lossy; it has finite dc gain,

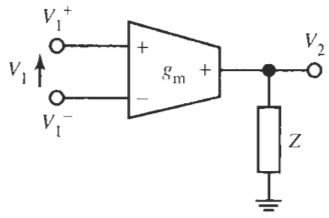

Figure 16.8 A transconductor loaded by an impedance Z.

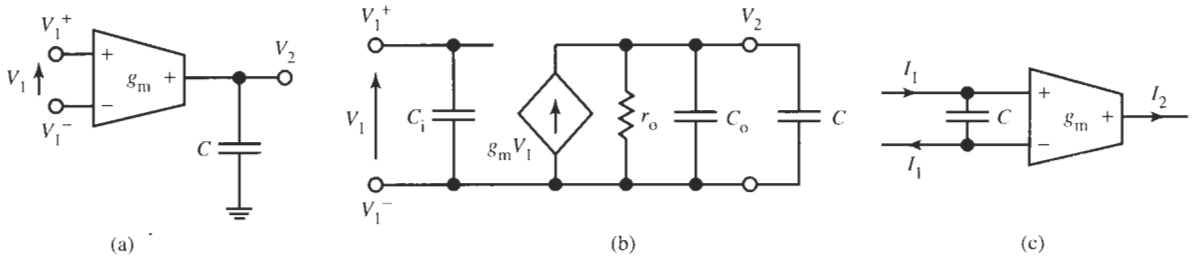

Figure 16.9 (a) single-ended voltage-mode g_m–C integrator; (b) small-signal model; (c) single-ended current-mode integrator.

$g_m/g_o = g_m r_o$, with the 3-dB frequency equal to $\omega_1 = g_o/(C + C_o)$. We see here the reason for wishing to have as large an output resistor as possible in a transconductor. Also, we note that the output capacitor C_o (0.25 pF in our model) may not be negligible and must be accounted for in integrator design when, as we shall see, for high-frequency filters the integrating capacitors C become very small; values can be as low as 1 pF or even less.

A remark is appropriate at this point about the integrators. Notice that we may arrange the integrator in the order "transconductor–capacitor" as is shown in Fig. 16.9a, or as "capacitor–transconductor" as in Fig. 16.9c. The former works by converting the voltage $V_1 = V_1^+ - V_1^-$ into a current by the transconductor; the current is then integrated on C to generate the voltage $V_2 = (g_m/sC)V_1$. This type of circuit, as well as the filters built with it, are termed "voltage mode." They are the structures we use in this book. The other type, Fig. 16.9c, works by integrating first the current I_1 on C to generate a voltage, which is then converted again to a current $I_2 = (g_m/sC)I_1$ by the transconductor. Filters built with this type of integrator are termed "current mode." Evidently the two integrating functions are the same; there is little if any difference between the performances of the two types of design.

We learned earlier (Chapter 4) that for filters based on two-integrator loops one of the integrators must be lossy. If we wish to make a g_m-C integrator lossy on purpose, we need only to connect a resistor in parallel with the capacitor C. The earlier discussion on resistors tells us that this can be done conveniently by use of a second transconductor. Figure 16.10 shows the circuit for an inverting integrator with the ideal transfer function

$$\frac{V_2}{V_1} = -\frac{g_{m1}}{sC + g_{m2}} \tag{16.12}$$

A study of the circuit will convince the student that now there are more parasitics with which to be concerned. In parallel with the integrator capacitor C we have $2C_o$ and $2r_o$ from the two transconductors as well as one C_i from g_{m2}. The actual transfer function becomes, therefore,

$$\frac{V_2}{V_1} = -\frac{g_{m1}}{s(C + 2C_o + C_i) + g_{m2} + 2g_o} \tag{16.13}$$

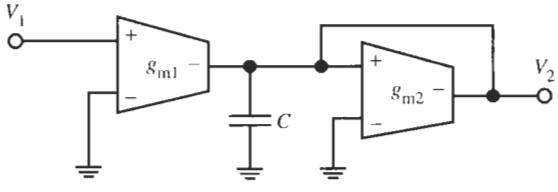

Figure 16.10 Lossy g_m-C integrator or first-order lowpass filter.

Notice that this equation determines the smallest integrating capacitor that can reasonably be used (for our model we have $2C_o + C_i = 0.6$ pF) and also places an upper limit on the dc gain: $0.5g_m r_o$ (for our model: $0.5g_m r_o = 500 \approx 54$ dB).

To design a *differential* integrator, one with differential input and differential output, let us start by considering the circuit conceptually as two single-ended integrators, one each in the positive and negative signal paths. This is illustrated in Fig. 16.11a. The integration does not change the sign if we invert *both* the input and the output connections of the transconductors. We have, therefore, interchanged the $+/-$ designation on all terminals in the bottom part of the figure compared with those of the top part. The transfer function remains $g_{m1}/(sC + g_{m2})$ in either part. The reason for taking this modification will become apparent shortly. Now notice that in the top and bottom parts none of the grounded transconductor terminals is needed and so can be dispensed with. Having changed the $+/-$ signs appropriately, we can then merge the corresponding transconductors in the two paths each into one fully differential transconductor; Fig. 16.11b shows the result. Notice that by merging the two transconductors we have doubled their input voltages: for example, on g_{m1} in Fig. 16.11a from $V_i - 0$ and $0 - V_i$, respectively, to $V_i - (-V_i) = 2V_i$ in Fig. 16.11b. This means that the currents I_o are also doubled and we have

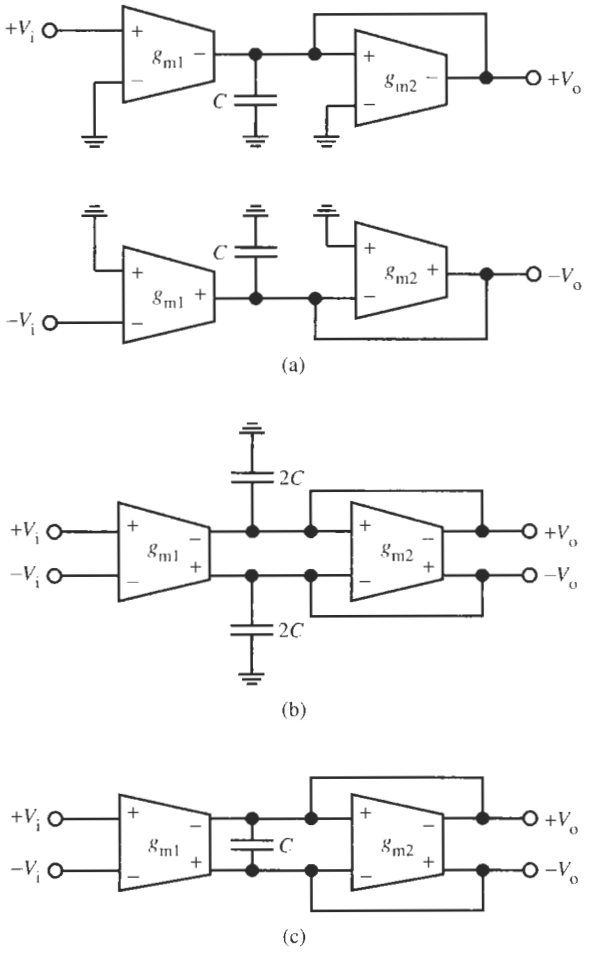

Figure 16.11 Converting a single-ended g_m-C integrator to a fully differential one: (a) concept of a differential integrator; (b) fully differential realization with two grounded capacitors; (c) fully differential realization with one floating capacitor.

to double the capacitors, as is illustrated in Fig. 16.11b, to leave the output voltage unchanged. To confirm that these steps lead to the correct differential integrator we shall analyze the circuit by writing the node equations at the two capacitor nodes. We obtain

$$V_o^+ 2sC + \left(V_i^+ - V_i^-\right) g_{m1} + \left(V_o^+ - V_o^-\right) g_{m2} = 0 \tag{16.14a}$$

and

$$V_o^- 2sC - \left(V_i^+ - V_i^-\right) g_{m1} - \left(V_o^+ - V_o^-\right) g_{m2} = 0 \tag{16.14b}$$

If we subtract Eq. (16.14b) from Eq. (16.14a) we find

$$\left(V_o^+ - V_o^-\right) 2sC = -2g_{m1}\left(V_i^+ - V_i^-\right) - 2g_{m2}\left(V_o^+ - V_o^-\right)$$

The factor 2 cancels and we obtain the inverting differential integrator function

$$\frac{V_o^+ - V_o^-}{V_i^+ - V_i^-} = \frac{2V_o}{2V_i} = \frac{V_o}{V_i} = -\frac{g_{m1}}{sC + g_{m2}} \tag{16.15}$$

We can also connect the integration capacitors differentially and take them off ground. In that case the two capacitors of value $2C$ are in series, Fig. 16.12a, and the remaining differentially connected capacitor has the value C as is shown in Fig. 16.11c. Writing node equations, we find for both sides of the differential circuit

$$g_{m1}\left(V_i^+ - V_i^-\right) + g_{m2}\left(V_o^+ - V_o^-\right) + \left(V_o^+ - V_o^-\right) sC = 0$$

a result that is identical to that of Eq. (16.15). For an implementation of differential integrators this means that connecting the capacitor differentially saves three-quarters of the capacitor area ($1C$ versus $4C$). On the other hand, the differential connection has a disadvantage. In the fabrication of integrated capacitors, the bottom plate, the one located next to the substrate of the IC, is connected to the substrate by a nonnegligible parasitic capacitor whose size is of the order of 10% of the capacitor's value. In Fig. 16.12b we have identified the capacitor's bottom plate rounded, and have indicated the capacitor C_g to ground. (The substrate is ac ground because

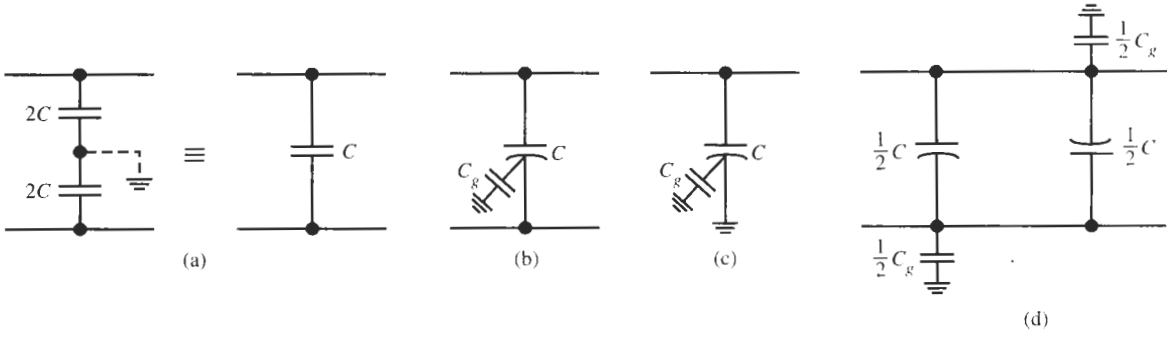

Figure 16.12 (a) Conversion of the capacitors in a differential circuit; (b) picturing parasitic bottom-plate-to-ground capacitors; (c) C_g is shorted in a correctly connected grounded capacitor; (d) suggested connection of a floating capacitor of value C.

it is connected either to ground directly or to some dc bias voltage.) As far as the integrator or a complete filter is concerned, these bottom-plate-to-ground capacitors are real capacitors that influence the circuit's behavior. C_g is shorted out and has no effect if the capacitor C has its bottom plate connected to ground (Fig. 16.12c). If differentially connected capacitors must be used to save silicon area, the IC designer may wish to connect two capacitors of value $C/2$ in parallel with bottom plates inverted as in Fig. 14.12d; the capacitors $C_g/2$ are still present, but the circuit's symmetry and balance are maintained. Our "experiments" and simulations do not deal with real integrated circuits, so bottom-plate-to-ground capacitors and their consequences will be disregarded; in effect we assume in the following $C_g = 0$.

From our discussion we can identify a set of steps for converting single-ended circuits to fully differential ones:

STEP 1: Mirror the single-ended circuit at ground.

STEP 2: Change the polarities of all inputs and outputs of the active devices.

STEP 3: Double the values of all grounded capacitors. Leave unchanged the value of any capacitor that should be connected differentially.

STEP 4: Discarding any input that may be grounded, merge the corresponding active devices into fully differential ones.

The following example will help us understand the performance of the integrator.

EXAMPLE 16.2

Design a noninverting differential integrator to have a unity-gain frequency of 6 MHz and test its performance.

Solution

We have $\omega_T = g_m/C = 2\pi \times 6$ Mrad/s; let us choose again a transconductor with $g_m = 200\ \mu$ A/V. Accounting for the parasitic C_o, we obtain $C + C_o = 5.30$ pF. Because $C_o = 0.25$ pF, let us choose $C = 5$ pF for the integrating capacitor. We can now either connect $C = 5$ pF differentially across the OTA output terminals or connect $2C = 10$ pF from either side to ground; the result is the same.

A typical practical test problem we have to address now is that almost all instruments have single-ended inputs and outputs but the integrator is fully differential. The problem is usually solved by two 1:1 transformers: one at the input to convert the single-ended source voltage to differential form and one at the output to convert the differential signal back to single-ended form for the test instrument, in our case the network analyzer (Bode Plotter).[5] We shall take typical high-frequency transformers with a bandwidth of 100 Hz to 300 MHz.

[5]We will not deal here with the issue that high-frequency instruments and cables should be terminated in 50 Ω. Also we shall assume that wires and instruments are ideal; in reality, cables that are used to connect the IC to test instruments look like a 50-Ω load in parallel with, depending on cable length, a capacitor of 30 to 50 pF. It is very important, therefore, when testing the integrator or, generally, an integrated circuit that the circuit output is buffered, otherwise the (50-Ω||30 pF) load will likely completely alter the circuit performance. Simple emitter or source followers with large devices usually provide adequate buffering.

The resulting complete test set-up is shown in Fig. 16.13a; note that we inverted the OTA output terminals to change the direction of the current through the capacitor. This realizes the specified noninverting integrator. The transfer function magnitude is seen in Fig. 16.13b. The low-frequency roll-off caused by the transformers is just visible. We have approximately 0 dB at 6 MHz (cursor) as specified and the oscilloscope display in Fig. 16.13c shows that the 6-MHz input and output signals have equal magnitude (unity gain) with a 90° phase shift coming from the integrator. The low-frequency integrator gain is $g_m r_o = 2 \times 10^{-4} \times 5 \times 10^6 = 1000 = 60$ dB as predicted by Eq. (16.11) and the measured −3-dB frequency is at approximately 6 kHz in agreement with the expectation: $g_o/(C + C_o) = 1/(5\ \text{M}\Omega \times 5.25\ \text{pF}) = 2\pi \times 6$ kHz. Evidently, the integrator performs predictably and as specified.

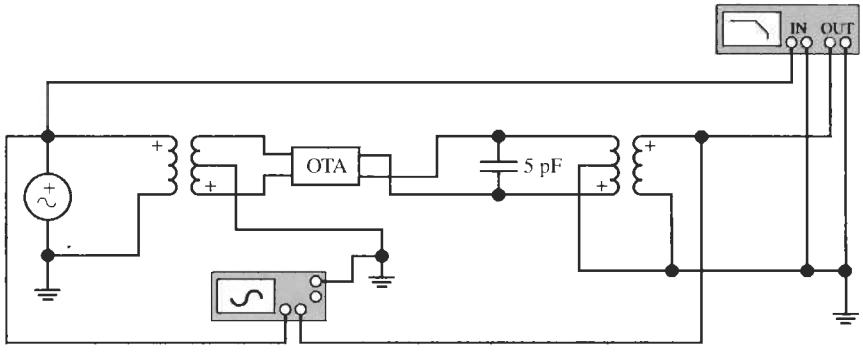

(a)

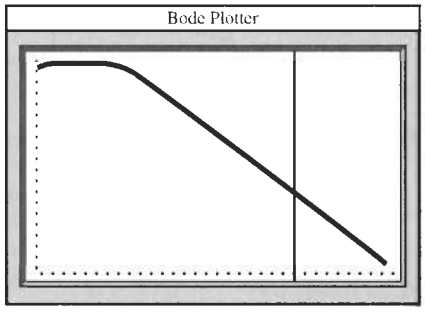

(b)

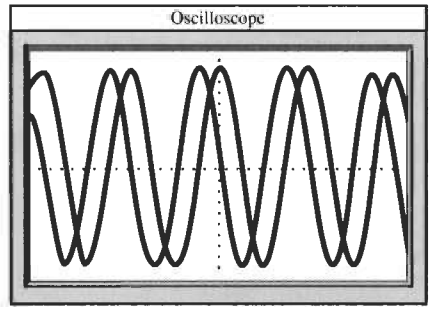

(c)

Figure 16.13 Design of a fully differential OTA-C integrator and test circuitry: (a) circuit; (b) transfer function magnitude (Bode plot); (c) input and output signal at the unity-gain frequency (6 MHz). (Bode Plotter scales: 200 Hz to 300 MHz; −40 to 60 dB; cursor at 6.325 MHz, −0.368 dB; oscilloscope scales: 0.05 μs/div; 5 mV/div.)

16.2.3 Amplifiers

To build a voltage amplifier with transconductors is a very simple task. Consulting Eq. (16.9), we see that a gain stage is constructed if we load a transconductor g_{m1} by a resistor $R = 1/g_{m2}$ to obtain

$$\frac{V_2}{V_1} = g_{m1}R = \frac{g_{m1}}{g_{m2}} \tag{16.16}$$

This equation describes an amplifier with gain g_{m1}/g_{m2}. Figure 16.14 contains the circuit. Note the crossed wires in Fig. 16.14b to achieve positive gain. Because in differential circuits we always have signals of both polarities available, changing the sign of a function is as simple as crossing wires. No special inverter circuits are necessary.

16.2.4 Summers

To build summers in this technology is a similarly simple matter. As we mentioned before, to *add currents* requires only a node where Kirchhoff's current law sums the currents. If we must *add voltages*, we convert them into currents by means of transconductors, add the resulting currents at a node, and, if the result must be another voltage, use a current-to-voltage converter to obtain the output voltage. A current-to-voltage converter is, of course, a resistor. Figure 16.15 contains the circuit. It realizes

$$V_o = \frac{g_{m1}}{g_{m0}}V_1 + \frac{g_{m2}}{g_{m0}}V_2 - \frac{g_{m3}}{g_{m0}}V_3 + \frac{g_{m4}}{g_{m0}}V_4 \tag{16.17}$$

Each voltage is multiplied by a coefficient set by a ratio of two transconductances. Notice that subtraction as with the voltage V_3 is accomplished easily by taking the corresponding current from a transconductor output terminal with different polarity.

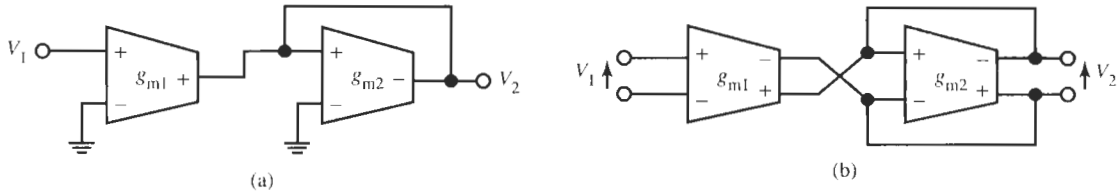

Figure 16.14 Design of (a) single-ended and (b) fully differential OTA-based amplifiers.

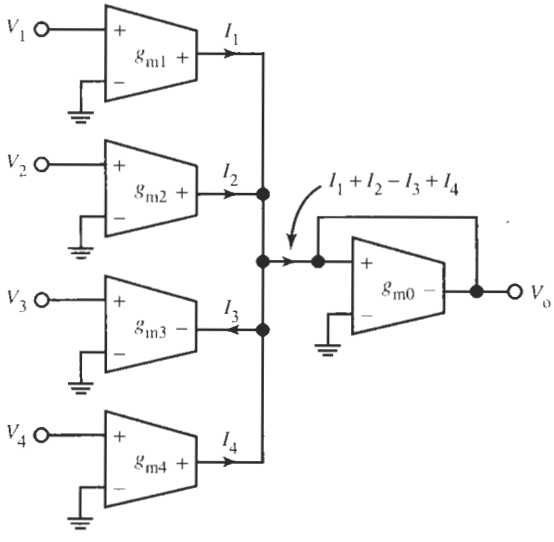

Figure 16.15 A circuit based on transconductors for summing voltages.

16.2.5 Gyrators

We found earlier in our study (Section 14.1), that a gyrator, a twoport whose input impedance is inversely proportional to the load impedance, is a useful element because it allows us to convert a capacitor into an inductor. We discovered there that it is not easy to realize a good gyrator with operational amplifiers; instead, to accomplish the conversion from C to L we used general impedance converters (GICs). But because a gyrator is fundamentally a connection of an inverting and a noninverting voltage-controlled current source [see Eq. (14.1) and Fig. 14.4] we asserted that the design of gyrators would be very easy with transconductors. Indeed, if we recall from Section 14.1 that, for the current polarities in Fig. 16.16, a gyrator is characterized by the equations

$$I_1 = g_{m2} V_2 \quad \text{and} \quad I_2 = g_{m1} V_1 \tag{16.18}$$

the gyrator construction is already accomplished. From these two equations we derive

$$\frac{V_1}{I_1} = \frac{1}{g_{m1} g_{m2}} \frac{I_2}{V_2} \quad \text{or} \quad Z_1 = \frac{1}{g_{m1} g_{m2}} Y_2 \tag{16.19}$$

If Y_2 is a capacitor C, Z_1 is an inductor $L = C/(g_{m1} g_{m2})$. For ideal transconductors this circuit behaves like an ideal inductor, but as we know by now there are a number of parasitics to detract from the ideal performance. To study their effects, examine the circuit in Fig. 16.16a and mentally replace each transconductor by its model of Fig. 16.4. We see then that in parallel with the input we have from g_{m2} the components r_o and C_o and from g_{m1} the capacitor C_i. Similarly, in parallel with C we find C_i from the transconductor g_{m2} and the elements r_o and C_o from g_{m1}. The resulting small-signal gyrator model is shown in Fig. 16.16b. Analyzing this circuit with the aid of Eq. (16.19) we find the input admittance

$$\begin{aligned} Y_{in}(s) &= g_o + s(C_i + C_o) + \frac{g_{m1} g_{m2}}{s(C + C_i + C_o) + g_o} \\ &= g_o + s(C_i + C_o) + \cfrac{1}{s\dfrac{C + C_i + C_o}{g_{m1} g_{m2}} + \dfrac{g_o}{g_{m1} g_{m2}}} \end{aligned} \tag{16.20}$$

This equation is easy to interpret: we have the desired inductor $L = (C + C_i + C_o)/(g_{m1} g_{m2})$, but with C increased to $C + C_i + C_o$ by the parasitic capacitors. Further, L is in series with a loss resistor $R_L = g_o/(g_{m1} g_{m2})$, which points out again the need for transconductors with large output resistance (low output conductance). Finally, the series connection of L and R_L is in parallel with a loss resistor $1/g_o$ and a parasitic capacitor $C_i + C_o$. This model for the inductor is shown in Fig. 16.16c; except for r_o, it is the same as the model for any physical wire-wound inductor.

Let us still consider our need for floating inductors and, lastly, for differential versions of grounded and floating inductors. We saw in Section 14.1 that connecting two impedance converters or gyrators back to back would result in a floating component. Figure 16.17 shows this for two gyrators and a capacitor; assuming all transconductors have the same value g_m, we should obtain the floating inductor $L = C/g_m^2$. To verify this result we analyze the circuit; a node equation at node V gives $sCV = g_m V_1 - g_m V_2$ and the two terminal currents are $I_1 = I_2 = g_m V$. Combining these equations and eliminating V results in the equation of a floating inductor between the two voltages V_1 and V_2,

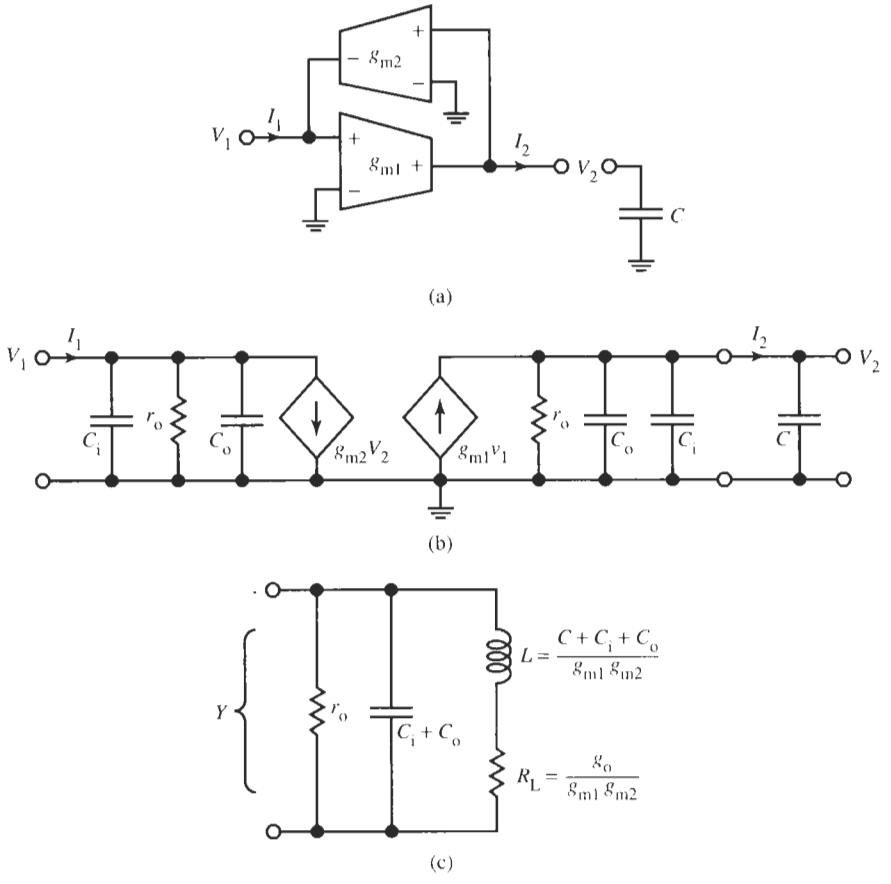

Figure 16.16 A gyrator based on transconductors: (a) generic circuit; (b) small-signal model; (c) passive model for the realized inductor.

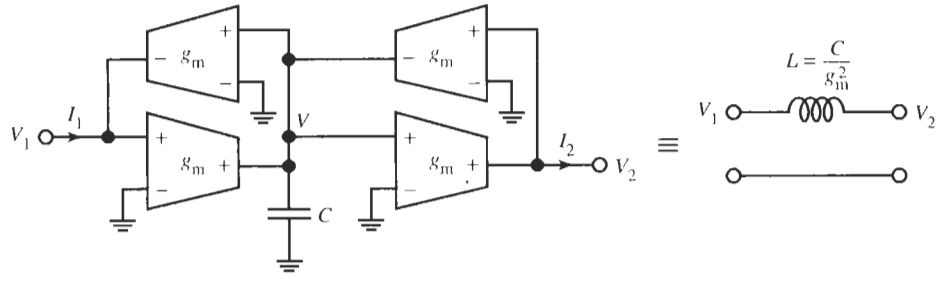

Figure 16.17 A floating inductor realized by a capacitor embedded between two gyrators.

$$I_1 = I_2 = \frac{g_m^2}{sC}(V_1 - V_2) = \frac{1}{sL}(V_1 - V_2) \tag{16.21}$$

Finally, let us consider the differential circuits for gyrator-C inductor simulations. We can do this most easily by using the mentioned four steps for single-ended-to-differential

conversion: Starting with the grounded inductor of Fig. 16.16a we draw the diagram in Fig. 16.18a where we have stretched out the gyrator rather than using the folded configuration of Fig. 16.16a. This will make it easier to follow the conversion process. Applying the four steps leads directly to the differential circuit in Fig. 16.18b. Developing the circuit for the differential realization of a floating inductor also follows the four steps mentioned above, starting from a stretched-out diagram of the floating grounded inductor of Fig. 16.17. Figure 16.19 shows the result. Let us still try to verify the behavior of a gyrator-C inductor by designing such a circuit and testing its performance. We also demonstrate how a negative resistor is used to cancel a positive one and thereby simplify the interpretation of the measurement results. Example 16.3 will guide us through the design and test steps.

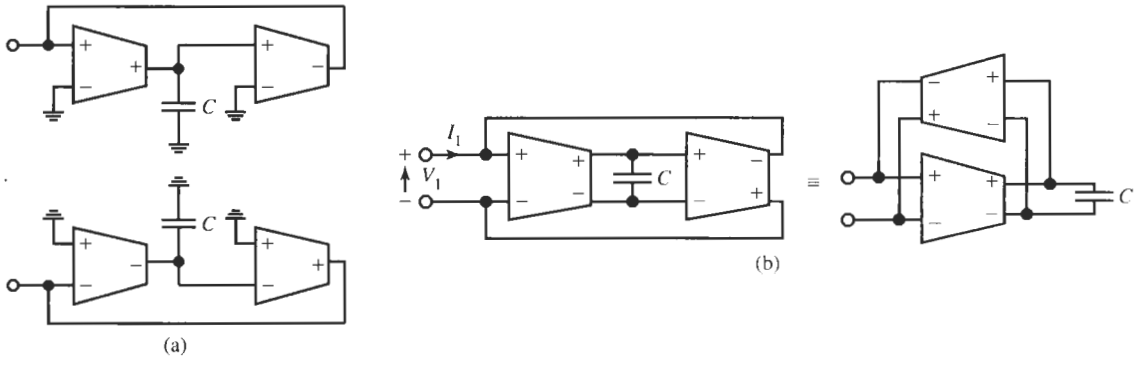

Figure 16.18 Differential realization of a grounded inductor. (a) conceptual implementation; (b) final implementation.

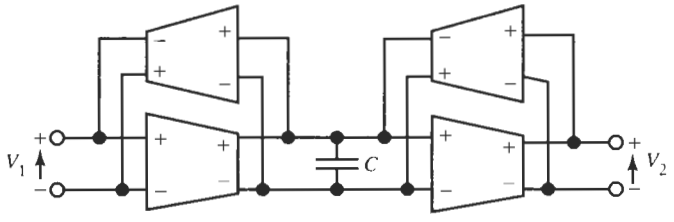

Figure 16.19 Differential realization of a floating inductor.

EXAMPLE 16.3

For a high-frequency filter in the range of 6–8 MHz, an engineer needs to design an electronic grounded inductor of value $L = 90\ \mu$H. The final circuit should be tested and the parasitics, such as loss and capacitors, if any, should be determined if possible.

Solution

For reasons of economy, the engineer decides to build the circuit with two identical transconductors of value $g_m = 0.2$ mS; the inductor becomes then $L = C/g_m^2 = 90\ \mu$H, which leads to the integrator capacitor $C + C_{\text{parasitic}} = 3.6$ pF. From the data sheet the engineer knows that

$C_{\text{parasitic}} = C_i + C_o = (0.1 + 0.25)\ \text{pF} = 0.35\ \text{pF}$. Therefore, the selected capacitor is 3.25 pF. At this point the inductor design is complete.

To test the inductor and extract the loss and the small parasitic elements appears difficult, but the measurement can be made easy by making use of a negative resistor. The simple voltage divider in Fig. 16.20a with the inductive impedance modeled as in Fig. 16.16c will help. The circuit in Fig. 16.20a has the transfer function

$$T(s) = \frac{V_2}{V_1} = \frac{G}{G + 1/(sL) - G_N} = s\frac{L}{R} \tag{16.22}$$

It indicates that if we choose $R_N = -R$, $T(s)$ is directly proportional to the inductor L, scaled by the known resistor R. The OTA circuit implementation is also shown in Fig. 16.20a. The

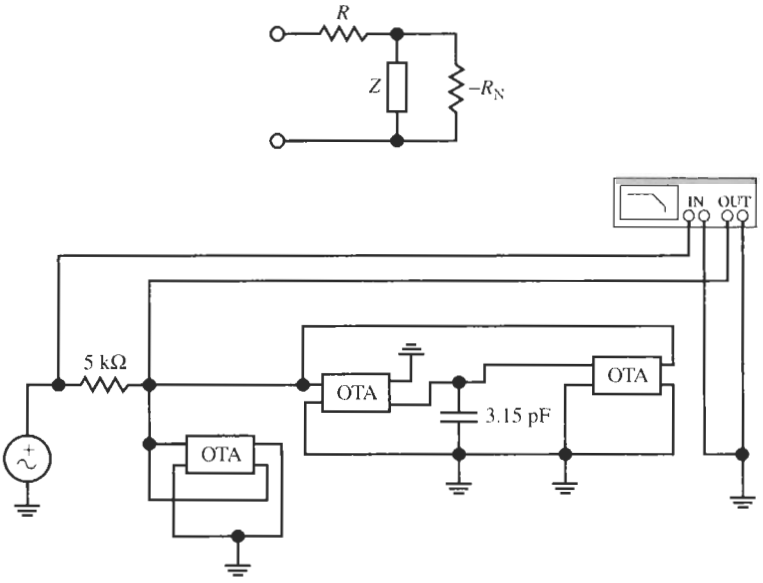

(a)

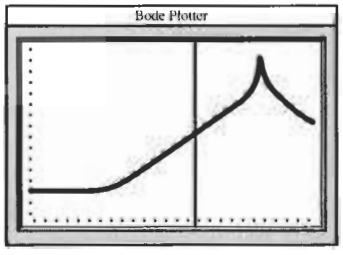

(b)

Figure 16.20 (a) A voltage divider for measuring an inductor simulated with an OTA-based gyrator; the −5-kΩ negative resistor eliminates the 5-kΩ resistor from the voltage divider; (b) the measured transfer function is directly proportional to the inductor. (Bode Plotter scales: 100 Hz to 300 MHz; −80 to 30 dB; cursor at 607.7 kHz, −23.51 dB.)

negative resistor is the left-most OTA with positive output fed back to positive input as in Fig. 16.6c. Measuring the response on a network analyzer results in the Bode plot in Fig. 16.20b. To be able to extract the parasitic components from the transfer function, we need a model for the inductive impedance. Equation (16.20) contains all relevant components and should be adequate. If we insert this equation into Eq. (16.22), we obtain

$$T(s) = \frac{G}{1/sL} = \frac{G}{g_o + s\,(C_i + C_o) + \dfrac{1}{s\dfrac{C + C_i + C_o}{g_m^2} + \dfrac{g_o}{g_m^2}}}$$

It is the magnitude of this function that is displayed in the analyzer (Fig. 16.20b). From the equation we see the following:

1. The equivalent parallel resistor is obtained from the behavior at the origin:

$$T(0) = \frac{G}{g_o + g_m^2/g_o} \approx \frac{Gg_o}{g_m^2}, \quad \text{i.e.,} \quad r_o = \frac{1}{T(0)Rg_m^2}$$

With $T(0) = -60$ dB $= 0.001$, $g_m = 0.2$ mS, and $R = 5$ kΩ, we find $r_o = 5$ MΩ, in agreement with our model.

Further, in parallel with r_o is the parasitic capacitor $C_i + C_o$. Next we observe that in parallel with these two branches is the inductor $L = (C + C_i + C_o)/g_m^2$ in series with the loss resistor $R_L = g_o/g_m^2$. Figure 16.16c shows the circuit diagram. This circuit indicates that all components are extracted readily by evaluating the measured Bode plot at a few fixed frequencies.

2. Somewhere "in the middle of" the rising slope at some frequency ω_2 where L dominates, we have

$$|T(j\omega_2)| = \omega_2 \frac{C + C_i + C_o}{g_{m1}g_{m2}R} = \omega_2 \frac{L}{R}, \quad \text{i.e.,} \quad L = |T(j\omega_2)|\,\frac{R}{\omega_2}$$

This measurement corresponds to the position of the cursor in Fig. 16.20b. With $|T| = 23.5$ dB at 607.7 kHz, we find $L = 87.6$ μH, close enough to our design goal.

3. Somewhere on the downward slope away from the peak the capacitor dominates and we have

$$|T\,(j\omega_4)| = \frac{1}{\omega_4\,(C_i + C_o)\,R}, \quad \text{i.e.,} \quad C_i + C_o = \frac{1}{\omega_4 R\,|T\,(j\omega_4)|}$$

We choose the point [−12.85 dB; 184 MHz]; this gives us $C_i + C_o = 0.76$ pF, about twice the expected 0.35 pF. A 100% error in parasitics estimation is too large, so there must be another reason. A glance at the circuit reveals the cause: the OTA of the negative resistor adds one C_i and one C_o for another 0.35 pF nominally. Thus, the test result is correct.

4. As a check we use that the resonance frequency equals $f_3 = 1/[2\pi L(C_i + C_o)]$. Inserting the numbers from the *measured* capacitor value gives $f_3 = 19.5$ MHz, which is exactly the location of the self-resonant peak!

5. Lastly, at the low-frequency 3-dB point we have $|T(j\omega_1)| = \omega_1 L/R_L$, i.e., the 3-dB frequency must be $\omega_1 = R_L/L$, where we had $R_L = g_o/g_m^2 = 5\ \Omega$. We find $f_1 = 9$ kHz, which again agrees perfectly with the test result.

A final comment about the inductor. The measured self-resonance frequency, $f_3 = 19.5$ MHz, is that of the test set-up. The inductor has nothing to do with the parasitic capacitors of the negative resistor and has only 0.35 pF with which to resonate. The real self-resonance frequency is, therefore, approximately 29 MHz. This puts the resonance point far enough away from the intended frequency range, 6–8 MHz, of the proposed filter specified in the problem.

16.3 FIRST- AND SECOND-ORDER FILTERS

Filters using the transconductance-C technique employ fundamentally the same methods that we are familiar with from our previous study of active RC circuits, but they are for the most part intended to be implemented in integrated circuit (IC) technology. Together with the fact that transconductance-C filters are normally designed for operation at much higher frequencies than circuits built with operational amplifiers, this entails some subtle differences from our previous approaches. These differences, as well as some design guidelines, are listed:

1. No resistors are used, at least not in CMOS technology. As a consequence, time constants are set as C/g_m ratios rather than as RC products.
2. Capacitors are much smaller, of the order of a few picofarad or even less. Thus, great attention must be paid to account for the parasitic capacitors in the circuit.
3. Cost considerations in discrete active RC designs prompted us to use only capacitors with standard values and, if possible, only identical capacitors. In integrated circuit design, however, capacitor sizes are determined by processing-mask dimensions so that the number of different capacitors is unimportant as a long as their values are limited to a few picofarad. Also, capacitor *ratios* should be moderate. The reason for this requirement is that many dimensionless filter parameters, such as gain or quality factor Q, are determined by capacitor ratios (and by g_m ratios), and small ratios can be realized more accurately than large ones.
4. Filter engineers will not normally design their own transconductance cells; rather transconductors will be available in the company's IC design library, together with opamps, gain stages, pad drivers, peak detectors, buffers, switches, and other analog building blocks. The filter should be designed with available values of g_m if feasible. Also, as we shall discover, important advantages for filter operation, such as better matching and tracking, can be achieved if all g_m cells are identical. Although not always possible, we shall try to design our filters with identical transconductance cells.
5. Tolerances of active and passive components in integrated circuits can be as large as 10–20%. But to obtain accurate filters, we need accurate components. In discrete circuits, we can resort to measuring the elements before assembly and to adjust or trim their values before or after the design to tune the filter's performance. None of this is possible, obviously, in integrated circuits. In integrated filters, use is made of the excellent low tolerances, as low as 0.1%, of component *ratios*, and tuning must take place by adjusting bias voltages or currents. We will say more about this issue in Section 16.5.

Let us begin our discussion of filter design with elementary first- and second-order filter blocks. Just as in the active *RC* case, several suitable blocks are available, but we will discuss only one universal first-order and one universal second-order section. We shall see that these modules can be configured to implement any arbitrary first- or second-order transfer function, respectively.

16.3.1 A First-Order Section

A universal first-order filter can be based on the lossy integrator in Fig. 16.10. We augment this integrator by a capacitor to generate a general first-order numerator. The method was discussed in Section 5.2, Fig. 5.11. Figure 16.21a shows the single-ended circuit. We lifted the fraction aC of the integrator capacitor C off ground and used it to feed a portion of the input signal directly to C. Kirchhoff's current law at the output node gives the equation

$$V_2\,(sC + g_{m2}) = V_1\,(g_{m1} + asC)$$

that is solved for the transfer function of the first-order filter:

$$\frac{V_2}{V_1} = \frac{asC + g_{m1}}{sC + g_{m2}} \tag{16.23a}$$

Using the single-ended-to-differential conversion technique we discussed in Section 16.2 results in the fully differential module in Fig. 16.21b, which is described by the same function. The two capacitors valued $2(1-a)C$ can, of course, be replaced by a single one of value $(1-a)C$ connected differentially between the voltages V_2 and $-V_2$. Now observe with reference to Fig. 16.21b, that

g_{m1} may be zero by removing that transconductor from the circuit. This results in a first-order highpass filter.

g_{m1} may be negative by removing the crossed wires and connecting the inverting output of g_{m1} to the upper capacitors and the noninverting output to the lower ones.

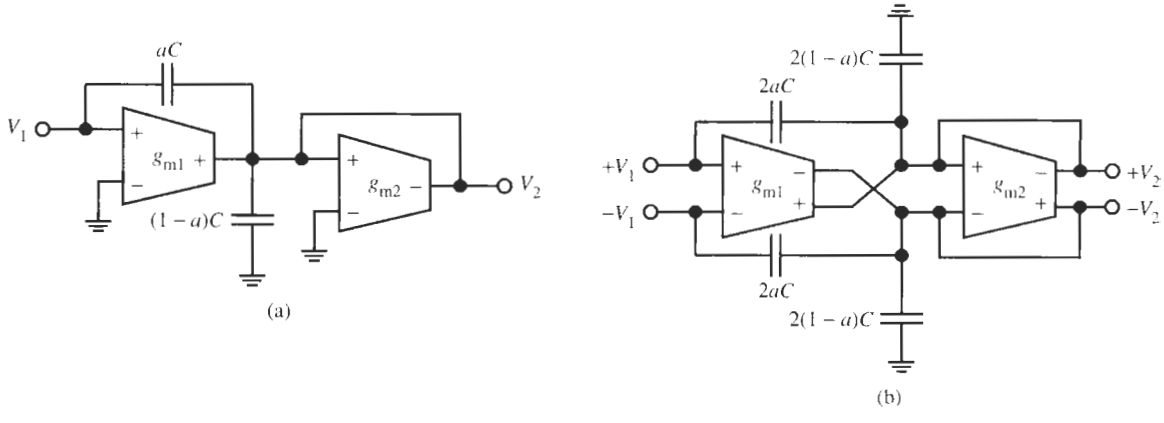

Figure 16.21 Universal first-order transconductance-*C* filter: (a) single ended; (b) differential implementation.

The fraction a can be anywhere in the range $0 \leq a \leq 1$, permitting us to adjust the coefficient of s in the numerator. It follows that the zeros of Eq. (16.23a) can be anywhere on the real axis.

g_{m2} can be removed, thus making $g_{m2} = 0$ and placing the pole at the origin for ideal integration.

Choosing $g_{m1} = -g_{m2}$ and $a = 1$ results in a first-order allpass function that can be used for phase correction.

By interchanging the $+/-$ connections of the capacitors $2aC$ at the input of g_{m1} we can change the sign of Eq. (16.23a) and make the section inverting.

Evidently then, the circuit of Fig. 16.21 is a general first-order module with a variety of applications for odd-order filters.

Before we proceed to the second-order section let us briefly consider the effects of transconductor parasitics in the first-order stage. We see from Fig. 16.21a that in parallel with the capacitor $(1-a)C$ we have the parasitic capacitors $2C_o$ and C_i as well as two output resistors. If we include these components into the analysis, we obtain instead of equation (16.23a) the following complete transfer function, which includes the effect of parasitic components:

$$\frac{V_2}{V_1} = \frac{asC_{eff} + g_{m1}}{sC_{eff} + g_{m2} + 2g_o} \tag{16.23b}$$

We labeled the effective capacitor $C + C_i + 2C_o = C_{eff}$. We note that the dc gain is lowered compared with the ideal case, and the 3-dB frequency has changed from g_{m2}/C to $(g_{m2} + 2g_o)/C_{eff}$. Whether the parasitics must be considered depends on the size of g_{m2} and C. The value of g_{m2} will normally be in the range of a few hundred μA/V so that $2g_o$, being of the order of 1 μS, can be neglected. But note that in low-frequency designs where g_m can be as small as 1μA/V or even a fraction of 1μA/V, the effect of the loss resistors is important. Such small values of g_m normally call for very low bias currents so that by Eq. (16.3) g_o also decreases. Nevertheless the effect of g_o may not be negligible. Because the design capacitor C is normally of the order of a few picofarad, the parasitic capacitors should always be included in the design. This is done conveniently by *predistorting* the value of C. By *predistortion* we mean that the expected parasitics are subtracted from the required capacitor C, that is, we choose for the circuit a capacitor C_c determined as $C_c = C - C_i - 2C_o$ so that the effective capacitor in the circuit, which includes the parasitics, equals C.

16.3.2 A Second-Order Section

As we did for the GIC biquad in Section 4.5.3, to build a second-order block, we start from the passive *RLC* circuit in Fig. 16.22a and perform a source transformation to get the circuit in Fig. 16.22b. We then recognize that a transconductance-C implementation takes the form in Fig. 16.22c:[6] g_{m1} converts the input voltage to a current, g_{m2} represents the

[6] Although we used a gyrator to derive this circuit from the passive *RLC* ladder in Fig. 16.22b, in the literature the structure is frequently referred to as a two-integrator loop, analogous to the block diagram in Fig. 4.7. The lossless $[g_{m3}/(sC_2)]$ and lossy $[g_{m4}/(sC_1 + g_{m2})]$ integrators are easily recognized in Fig. 16.22c by shifting the resistor $1/g_{m2}$ and the capacitor C_1 to the output of g_{m4}.

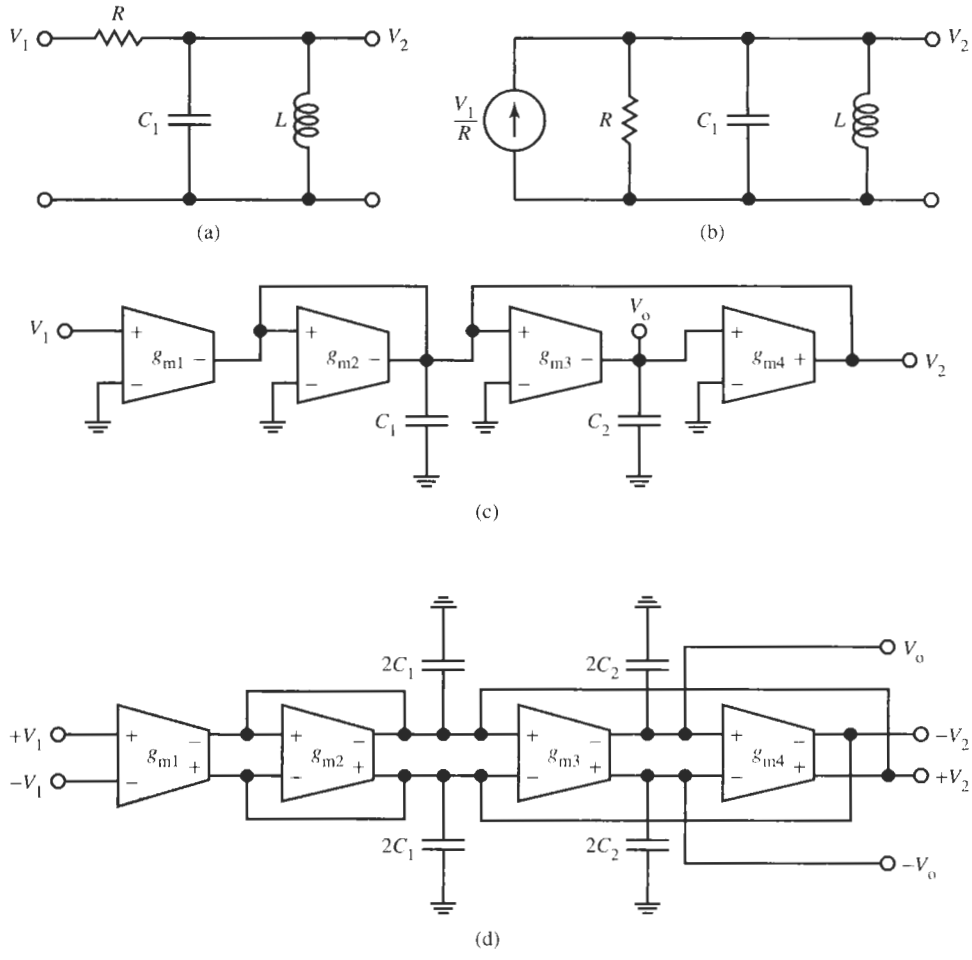

Figure 16.22 Second-order bandpass and lowpass filters: (a) passive *RLC* prototype; (b) the circuit of (a) after a source transformation; (c) the single-ended transconductor-*C* realization; (d) the differential transconductor-*C* realization.

resistor R, the capacitor C_1 is unchanged, and g_{m3} and g_{m4} form a gyrator,[7] which together with the capacitor C_2 implements the inductor $L = C_2/(g_{m3}g_{m4})$. We can then analyze the circuit, or for simplicity we can use the one-to-one correspondence with the passive prototype,

$$\frac{V_2}{V_1} = \frac{G}{G + sC_1 + \dfrac{1}{sL}}$$

and obtain the transfer function

[7] Notice that compared with Fig. 16.16a we have inverted the polarities of the two transconductors. This choice is immaterial since only their product enters Eqs. (16.24) and (16.25).

$$\frac{V_2}{V_1} = -\frac{g_{m1}}{g_{m2} + sC_1 + \dfrac{g_{m3}g_{m4}}{sC_2}} = -\frac{sC_2g_{m1}}{s^2C_1C_2 + sC_2g_{m2} + g_{m3}g_{m4}} \tag{16.24}$$

The minus sign comes from the polarity chosen for g_{m1}. It is of interest also to note that the voltage V_o is obtained from V_2 by integration,

$$V_o = -\frac{g_{m3}}{sC_2}V_2$$

so that at V_o we have a lowpass output:

$$\frac{V_o}{V_1} = -\frac{g_{m3}}{sC_2}\frac{V_2}{V_1} = \frac{g_{m1}g_{m3}}{s^2C_1C_2 + sC_2g_{m2} + g_{m3}g_{m4}} \tag{16.25a}$$

The differential version of the bandpass/lowpass filter is shown in Fig. 16.22d, obtained from Fig. 16.22c by the four-step conversion method we discussed. Let us again consider the effect of parasitic components. From Fig. 16.22c we see that C_1 is in parallel with $3g_o$, $3C_o$, and $2C_i$, and the capacitor C_2 is in parallel with g_o, C_o, and C_i. Thus, to include their effects we must replace in Eqs. (16.24) and (16.25a) the capacitive admittances sC_1 and sC_2 as follows:

$$\begin{aligned} sC_1 &\rightarrow s(C_1 + 3C_o + 2C_i) + 3g_o = sC_{1\text{eff}} + 3g_o \\ sC_2 &\rightarrow s(C_2 + C_o + C_i) + g_o = sC_{2\text{eff}} + g_o \end{aligned} \tag{16.26}$$

Thus, the capacitors C_1 and C_2 including their parasitics are replaced by $C_{1\text{eff}} = C_1 + 3C_o + 2C_i$ and $C_{2\text{eff}} = C_2 + C_o + C_i$, and the capacitors become lossy. Inserting this modification into Eq. (16.25a) results in

$$\frac{V_o}{V_1} = \frac{g_{m1}g_{m3}}{s^2C_{1\text{eff}}C_{2\text{eff}} + s[C_{2\text{eff}}(g_{m2} + 3g_o) + C_{1\text{eff}}g_o] + g_{m3}g_{m4} + g_{m2}g_o + 3g_o^2} \tag{16.25b}$$

Comments similar to the ones made for the first-order circuit after Eq. (16.23b) apply also here. All transfer function coefficients change, and, therefore, poles and zeros are altered. Whether g_o must be considered in the design depends on the ratio of the output conductance to the transconductance, g_o/g_m, but C_o and C_i should always be included because circuit capacitors will normally be in the low picofarad range.

To realize arbitrary transmission zeros we use again the feedforward technique of Section 5.2 and connect two capacitors to new inputs V_3 and V_4. To give us greater design flexibility, we leave open for now which of the voltages V_1, V_3, and V_4 are assigned as the input V_i. Figure 16.23a shows the circuit.

Observe that all internal nodes in the circuit are loaded by a circuit capacitor. This is an important property of this biquad because it means that all parasitic capacitors are in parallel with the circuit capacitors C_1 or C_2. Thus, the presence of parasitic capacitors will not change the degree of the filter: it will stay of second order [see Eqs. (16.25b) and (16.28)], and no extraneous parasitic poles or zeros with their resulting magnitude and phase errors are created.

Writing the node equation at V_2 gives

$$V_2(sC_1 + g_{m2}) + g_{m1}V_1 = g_{m4}V_o + saC_1V_3$$

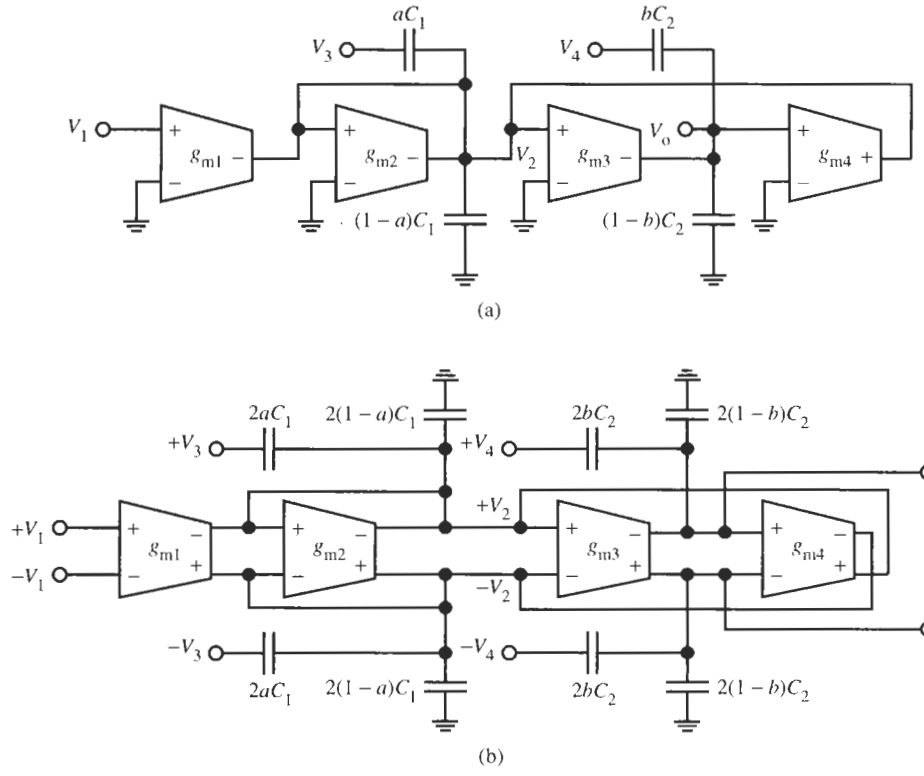

Figure 16.23 A transconductor-C biquad with arbitrary zeros: (a) single ended; (b) differential implementation.

where V_o is obtained from the node equation at V_o:

$$sC_2V_o = -g_{m3}V_2 + sbC_2V_4$$

If we eliminate V_2 from these two equations we obtain the transfer function

$$T(s) = \frac{V_o}{V_i} = \frac{s^2bC_1C_2\dfrac{V_4}{V_i} + s\left(bC_2g_{m2}\dfrac{V_4}{V_i} - aC_1g_{m3}\dfrac{V_3}{V_i}\right) + g_{m1}g_{m3}\dfrac{V_1}{V_i}}{s^2C_1C_2 + sC_2g_{m2} + g_{m3}g_{m4}} \tag{16.27}$$

where the voltage ratios in the numerator will be determined as ± 1 or 0. The conversion of the circuit to fully differential form is elementary; using the four conversion steps discussed earlier, we obtain the biquad in Fig. 16.23b. Again, the two capacitors $2(1-a)C_1$ and the two capacitors $2(1-b)C_2$ are replaced by one capacitor $(1-a)C_1$ and $(1-b)C_2$, respectively, if we choose to connect them differentially rather than as grounded components.

If the parasitic capacitors C_o, C_i and the output conductance g_o of the g_m cells cannot be neglected, we must base the design on Eq. (16.27) where sC_1 and sC_2 are replaced by the expressions in Eq. (16.26). Making the substitution yields an equation for V_o/V_i whose

denominator is equal to that of Eq. (16.25b) and whose numerator, after dividing by C_1C_2/V_i, can be shown to equal

$$s^2bV_4 + s\left[b\left(\frac{g_{m2}}{C_{1eff}} + \frac{g_o}{C_{2eff}} + \frac{3g_o}{C_{1eff}}\right)V_4 - a\frac{g_{m3}}{C_{2eff}}V_3\right] + \frac{g_{m1}g_{m3}V_1 + bg_o(3g_o + g_{m2})V_4 - 3ag_og_{m3}V_3}{C_{1eff}C_{2eff}} \tag{16.28}$$

We note that arbitrary zero pairs can still be obtained when parasitic effects cannot be neglected, but determining the design parameters a and b is considerably more complicated.

Evidently, $T(s)$ in Eq. (16.27) is a full biquadratic function that can have zeros anywhere in the s-plane, depending on how the voltage ratios are chosen. Let us first rewrite $T(s)$ in more standard format. Then we can decide which of the voltages V_1, V_3, and V_4 to use as input, V_i, and how the components should be selected to realize a desired transfer function. We shall keep with our earlier discussion and choose $g_{m2} = g_{m3} = g_{m4} = g_m$ without losing any significant design freedom. Dividing also numerator and denominator of Eq. (16.27) by C_1C_2 results in

$$T(s) = \frac{V_o}{V_i} = \frac{s^2\left(b\frac{V_4}{V_i}\right) + s\left(b\frac{g_m}{C_1}\frac{V_4}{V_i} - a\frac{g_m}{C_2}\frac{V_3}{V_i}\right) + \left(\frac{g_{m1}}{g_m}\frac{V_1}{V_i}\right)\frac{g_m^2}{C_1C_2}}{s^2 + s\frac{g_m}{C_1} + \frac{g_m^2}{C_1C_2}}$$

$$= \frac{\alpha s^2 + \beta s + \omega_z^2}{s^2 + s\omega_0/Q + \omega_0^2} \tag{16.29}$$

with

$$\omega_0 = \frac{g_m}{\sqrt{C_1C_2}}, \quad Q = \sqrt{\frac{C_1}{C_2}}, \quad \omega_z = \sqrt{\frac{g_{m1}}{g_m}\frac{V_1}{V_i}}\omega_0 \tag{16.30}$$

We must permit g_{m1} to be adjustable separately to permit $\omega_z \neq \omega_0$ as Eq. (16.30) shows. Notice that the capacitor ratio equals Q^2, which may result in some implementation difficulties if Q is large. From Eq. (16.30), we find the design equations for the two capacitors:

$$C_1 = \frac{g_m}{\omega_0}Q, \quad C_2 = \frac{g_m}{\omega_0}\frac{1}{Q} \tag{16.31}$$

Substituting these expressions into Eq. (16.29) yields

$$T(s) = \frac{V_o}{V_i} = \frac{s^2\left(b\frac{V_4}{V_i}\right) + s\left(b\frac{V_4}{V_i} - aQ^2\frac{V_3}{V_i}\right)\frac{\omega_0}{Q} + \left(\frac{g_{m1}}{g_m}\frac{V_1}{V_i}\right)\omega_0^2}{s^2 + s\frac{\omega_0}{Q} + \omega_0^2} \tag{16.32}$$

We can now construct Table 16.1 to help us design the required biquad.

To illustrate the design of these filters we will use a third-order design example that employs a cascade connection of a first-order and a second-order section.

TABLE 16.1 Design Parameters for the Biquad in Fig. 16.23, Eq. (16.32)[a]

Filter Type	V_1	V_3	V_4	a	b	g_{m1}	$H(0)$	$H(\infty)$
LP[b]	V_i	0	0	0	0	$H(0)g_m$	g_{m1}/g_m	0
BP[c]	0	V_i	0	H_M/Q^2	0	0 (absent)	0	0
HP	0	V_i	V_i	a	aQ^2	0 (absent)	0	$b = aQ^2$
BR[d]	V_i	V_i	V_i	a	aQ^2	$H(0)g_m$	g_{m1}/g_m	$b = aQ^2$
AP	V_i	V_i	V_i	$2/Q^2$	1	g_m	1	$b = 1$

[a] ω_0, Q, and ω_z are given in Eq. (16.30); $a \leq 1$; $b \leq 1$; $g_{m2} = g_{m3} = g_{m4} = g_m$. V_3 and/or V_4 may be set equal to $-V_i$ for some additional freedom in selecting the signs of the coefficients.

[b] LP is the same circuit as the one in Fig. 16.22d.

[c] H_M is the midband gain. We can also use the bandpass circuit of Fig. 16.22d with the output at V_2.

[d] We obtain a notch if $g_{m1}/g_m = b$, a lowpass notch if $g_{m1}/g_m > b$, a highpass notch if $g_{m1}/g_m < b$.

EXAMPLE 16.4

Design a lowpass filter with a cut-off frequency of $f_0 = 12$ MHz. To eliminate a strong interference signal at around three times f_0, there must be a transmission zero near $f_z = 36$ MHz. The passband gain should be 0 dB, but there must be a gain peak of 15–20 dB at the passband corner to compensate for losses in the transmission medium. At high frequencies, the attenuation should increase at 20 dB/decade.

Solution

To solve this problem we need a second-order lowpass notch (LPN) with a transmission zero at f_z and the pole frequency at f_0. Because numerator and denominator of an LPN filter are of degree 2, there is no attenuation increase at high frequencies. The required roll-off of 20 dB/decade implies an additional pole, which we obtain by cascading a first-order section with the LPN. We propose to make the bandwidth of the first-order stage wide enough so that its effect on the LPN transfer function is minimized. This is not a necessary requirement, of course, but it simplifies the design.

Let us begin with the design of the lowpass notch stage. According to our discussion we choose $g_{m2} = g_{m3} = g_{m4} = g_m$ in the LPN section, which by Table 16.1 has $V_3 = V_4 = V_1 = V_i$, and from Eq. (16.32) $b = aQ^2$. The transfer function is

$$\frac{V_o}{V_i} = \frac{s^2 b + (g_{m1}/g_m)\,\omega_0^2}{s^2 + s\omega_0/Q + \omega_0^2} = \frac{b\left[s^2 + (g_{m1}/g_m)\omega_0^2/b\right]}{s^2 + s\omega_0/Q + \omega_0^2}$$

where we must have $a \leq 1$ and $b \leq 1$ for positive capacitors. Let us try $b = 1$, which saves two capacitors (see Fig. 16.23). Because the transmission zero is prescribed to be three times f_0, by Eq. (16.30) we need $g_{m1}/g_m = 9$ or $g_{m1} = 9g_m$. Let us choose again for the transconductance $g_m = 0.2$ mS, that is $g_{m1} = 1.8$ mS. From Eq. (16.31) we obtain the nominal capacitors

$$C_{10} = \frac{200\ \mu\text{S}}{24\pi\ \text{Mrad/s}}\,Q = 2.653Q\ \text{pF} \quad \text{and} \quad C_{20} = 2.653\frac{1}{Q}\ \text{pF} \tag{16.33}$$

These values of C_{10} and C_{20} did not take into considerations any parasitic capacitors yet. Next we need to determine the quality factor: Q is found from the desired 15- to 20-dB peak at the bandedge. From the transfer function we obtain

$$\left|\frac{V_o}{V_i}\right|_{s^2=-\omega_0^2} = |-1+9|\,Q = 8Q$$

Let us aim for 20-dB gain at the passband corner; this means the $8Q = 10$ or $Q = 1.25$ and, from Table 16.1, $a = 1Q^2 = 0.64$. From Eq. (16.33) we then have the nominal capacitors

$$C_{10} = 2.653Q \text{ pF} = 3.316 \text{ pF}, \quad C_{20} = 2.653\frac{1}{Q} = 2.1224 \text{ pF}$$

C_{10} and C_{20} are the values of the effective capacitors; they are fairly small so that parasitics are likely to play an important role. So, we consider next carefully the circuit in Fig. 16.23b, or use Eq. (16.26), to ascertain the parasitic capacitors with which we have to contend. In parallel with C_{20}, across the differential output of g_{m3}, we have $C_i + C_o$ and in parallel with C_1, across the differential output of g_{m2}, we have $3C_o$ (one each from g_{m1}, g_{m2}, and g_{m4}) and $2C_i$ (one from g_{m2} and one from g_{m3}). Let us stay with the previous numbers: the differentially connected parasitic capacitors are $C_i = 0.1$ pF and $C_o = 0.25$ pF, and let us use the filter topology with grounded capacitors as shown in Fig. 16.23. According to our discussion (see Fig. 16.12) all these values must be doubled: using predistortion we have for the circuit capacitors

$$C_2 = 2\,(C_{20} - C_i - C_o) = 2(2.1224 - 0.1 - 0.25) = 3.546 \text{ pF}$$
$$C_1 = 2\,(C_{10} - 2C_i - 3C_o) = 2(3.316 - 0.2 - 0.75) = 4.732 \text{ pF}$$

and

$$aC_1 = 0.64 \times 2 \times 3.316 \text{ pF} = 4.244 \text{ pF}, \quad (1-a)C_1 = 0.36 \times 6.632 \text{ pF} = 2.388 \text{ pF}$$

Also prescribed was a 0-dB dc gain. The LPN stage contributes $g_{m1}/g_m = 9 = 19$ dB, which we need to reduce.

Let us attend now to the first-order lowpass stage. The transfer function is Eq. (16.23) with $a = 0$:

$$\frac{V_2}{V_1} = \frac{g_{m1}}{sC_0 + g_{m2}}$$

The dc gain is equal to g_{m1}/g_{m2}. Clearly, if we select $g_{m1}/g_{m2} = 1/9$, the 0-dB overall gain will have been achieved: we choose $g_{m1} = 0.2$ mS and $g_{m2} = 1.8$ mS, the same transconductance values used already in the LPN. C_0 is again the nominal capacitor without regarding parasitics. To maintain constant gain over the passband of the LPN circuit, we need to select $\omega_0 C_0 \ll g_{m2}$, so that the effect of C_0 can be neglected over the frequency range of interest. Thus

$$C_0 \ll g_{m2}/\omega_0 = 1.8 \text{ mS}/24\pi \text{ Mrad/s} \approx 24 \text{ pF}$$

Let us predistort this value, i.e., reduce it by the parasitics at the terminals of C_0 that arise from *both* the first-order section *and* the load offered by the LPN. We subtract $2C_i + 2C_o = 0.7$ pF to get $C_0 \ll 23.3$ pF, and we take $C_0 = 1.5$ pF for our design, this time connecting the capacitor differentially.

Figure 16.24a shows the circuit with test instruments; we used two transformers to be able to drive the filter differentially. Note that we did not use buffers to isolate the filter from the test set-up in line with our assumption that the connecting wires, transformers, and instruments are ideal. In a real test of an integrated filter on an IC chip, buffers (source followers, for example) would have to be inserted between filter and the IC output pads. IC pads add between 1 and 2 pF, not to mention the 50Ω and 20 pF or more added by the test equipment and connecting cables. This would load the unbuffered filter so heavily as to destroy its performance!

The blocks labeled OTA are 200-μS transconductors; OTA1 are 1.8-mS units. The test result in Fig. 16.24b verifies that the circuit performs as designed: dc gain is 0 dB, the cursor is at the passband edge ($\approx$ 12 MHz), the peak reaches $\approx$ 15 dB, and the notch is at 35.6 MHz. The increasing roll-off at high frequencies is clearly visible.

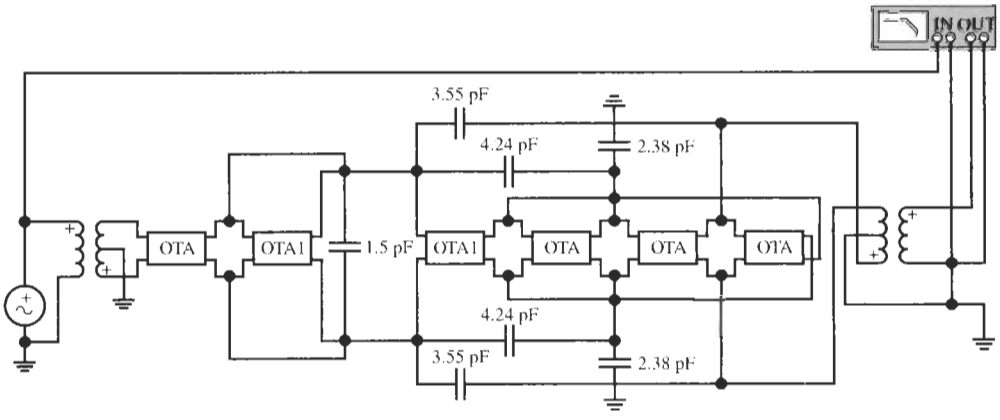

(a)

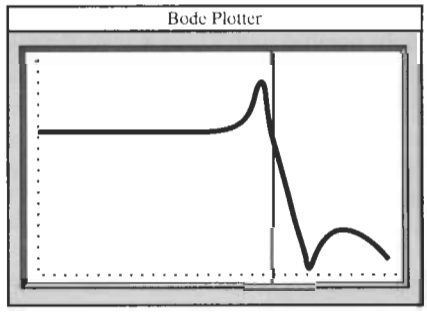

(b)

Figure 16.24 (a) Cascade connection of a first- and a second-order transconductance-C section to realize the specifications of Example 16.4; (b) test results. (Bode Plotter scales: 10 kHz to 400 MHz; −40 to 20 dB; cursor at 11.90 MHz, −1.337 dB.)

16.4 HIGH-ORDER FILTERS

The design of high-order transconductance-C filters proceeds essentially along the same lines as the design of opamp-based high-order filters. The two fundamental methods we have available are the cascade approach and the simulation of lossless ladders. We discussed the cascade method in Section 5.3 and lossless ladders and their simulation in Chapters 13, 14, and 15. The reader is encouraged to review the material at this time. In the present section we will only briefly review a few important concepts and see how they apply to the transconductance-C method.

16.4.1 Cascade Design

We saw in Section 5.3 that to design a high-order filter as a cascade of several low-order, usually first- and second-order, modules requires only that we factor numerator and denominator of the given transfer function so that the pole and zero pairs are identified. We then assign zeros to appropriate pole pairs and realize the resulting first- or second-order modules by an active filter block with the desired properties. Pole-zero pairing, section ordering, and gain assignment discussed in Section 5.3 apply here in the same manner as in opamp-based circuits. The fundamental reasons behind cascade realization were lower sensitivities to component tolerances, and the simplicity and flexibility of the design of low-order modules rather than of the complete high-order filter. The only condition to be satisfied for the approach to be valid was that the cascaded stages do not load each other so that they do not interact. For this to be valid the input impedance of the loading stage must be much larger than the output impedance of the driving stage, $|Z_{in2}| \gg |Z_{out1}|$. This condition is always satisfied in active RC filters where the filter output is taken at an opamp output and opamps are (nearly) ideal voltage sources whose output impedance is very small.

In our present case, where the active devices are transconductances whose output is a high-impedance current source, it is not immediately obvious that the cascading condition is satisfied. However, note from Figs. 16.22 or 16.23 that the input of a section is a transconductor whose input, ideally, presents an open circuit. In practice, the preceding stage is loaded only by the impedance of the parasitic input capacitor C_i that is normally small enough to form a negligible load. Note that for our model where $C_i = 0.1$ pF, even at 100 MHz the input impedance is still 16 kΩ. Furthermore, in most cases C_i is readily absorbed in the previous stage by predistortion: notice in Fig. 16.22 that a capacitor across the output terminals V_o or V_2 appears in parallel with C_2 or C_1, respectively. This means that the effect of loading the stage by C_i is easily accounted for by replacing the design values C_1 or C_2 by $C_1 - C_i$ or $C_2 - C_i$. We can, therefore, be confident that cascading works for transconductance-C filters as well. Indeed, without worrying about the validity of the approach, we used cascading in Example 16.4 in the preceding section where we absorbed C_i of the second-stage LPN in C_0 of the first-stage lowpass section.

16.4.2 Ladder Design

For the design of simulated ladders we used the signal-flow graph technique, which is based on the fact that capacitors and inductors function like integrators. Alternatively, if a lossless ladder design was available we could employ element replacement and simulate the inductors by use of general impedance converters and resistors (or gyrators and capacitors). We will

demonstrate next that completely analogous methods are available for transconductance-C design. We shall show the steps on a third-order ladder; it will give us sufficient information to allow extensions to more general ladders of higher degree.

Element Replacement

Since with transconductors, we have available simple gyrators with excellent performance (see Figs. 16.16 to 16.19), we can use them along with capacitors to replace any inductors in the lossless ladder. Figure 16.25 shows the procedure for a third-order elliptic ladder filter where we have also indicated the source transformation and the replacement of the two grounded resistors by transconductors. We notice that the implementation uses seven transconductors, numbered 1 through 7: one for the source transformation, two for the resistors, and four for the floating inductor. A differential implementation of the resulting circuit can be obtained easily by using the four conversion steps discussed in Section 16.2; we shall present an example of the procedure below.

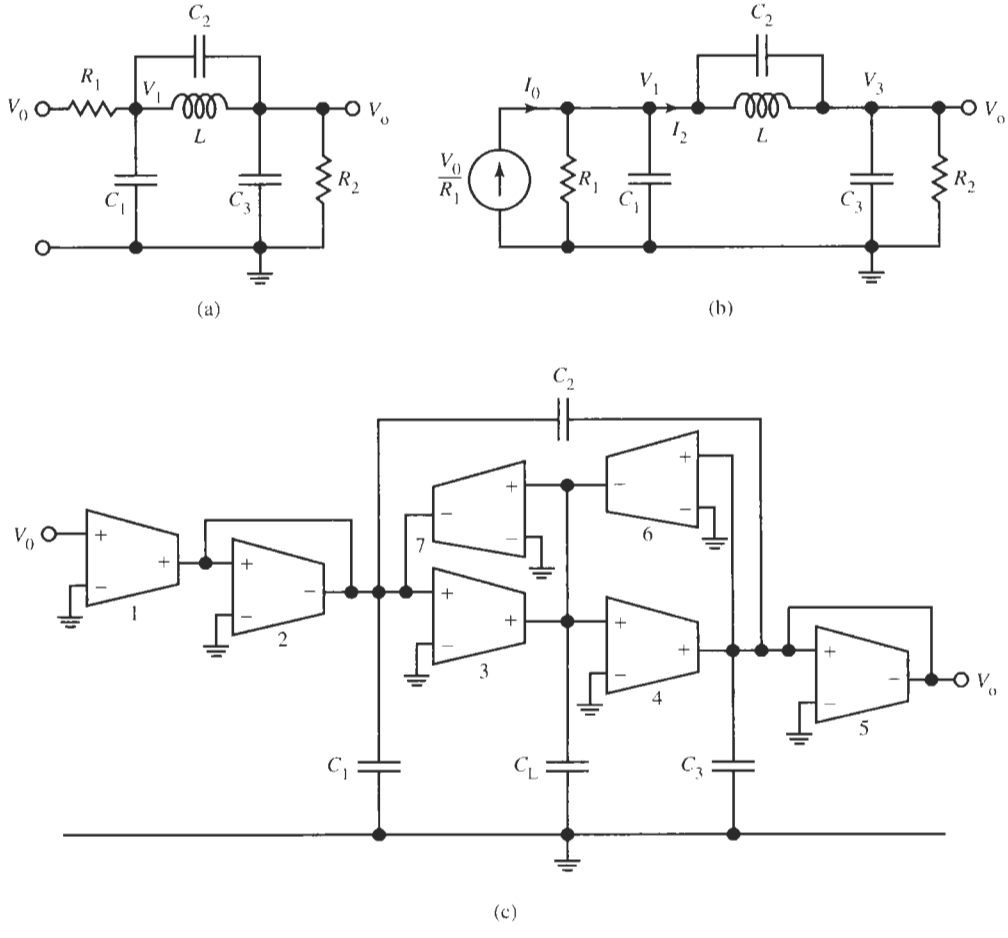

Figure 16.25 (a) LC ladder; (b) conversion to a form that is appropriate for active simulation; (c) transconductance-C equivalent.

Operational Simulation

Let us start from the same third-order ladder and disregard initially the floating capacitor C_2; we shall see shortly how to take care of C_2 without having to pull this component through the equations and the full process. The remaining ladder in Fig. 16.25b is described by the equations

$$V_1 = \frac{I_0 - I_2}{sC_1 + G_1} \qquad I_2 = \frac{V_1 - V_3}{sL} \qquad V_3 = \frac{I_2}{sC_3 + G_2} \tag{16.34}$$

Recall from Chapter 15 that for the operational simulation or signal-flow graph (SFG) method we treat all currents and voltages as voltage signals; to accomplish this we scale the equations by a resistor,

$$V_1 = \frac{RI_0 - RI_2}{sC_1R + RG_1} \quad \rightarrow \quad v_1 = \frac{v_{I0} - v_{I2}}{sc_1 + g_1} \tag{16.35a}$$

where we labeled again the scaled quantities for the signal-flow graph by lower-case symbols and retained the subscript I for the signals originating from currents. Similarly,

$$RI_2 = \frac{V_1 - V_3}{sL/R} \quad \rightarrow \quad v_{I2} = \frac{v_1 - v_3}{sl} \tag{16.35b}$$

$$V_3 = \frac{RI_2}{sC_3R + RG_2} \quad \rightarrow \quad v_3 = \frac{v_{I2}}{sc_3 + g_2} \tag{16.35c}$$

Recalling the lossless and lossy transconductance-C integrators (Figs. 16.9 and 16.10), we arrive directly from these equations at the circuit in Fig. 16.26a. Notice that we again used seven transconductors.[8] We still need to attend to the floating capacitor C_2 that was not included

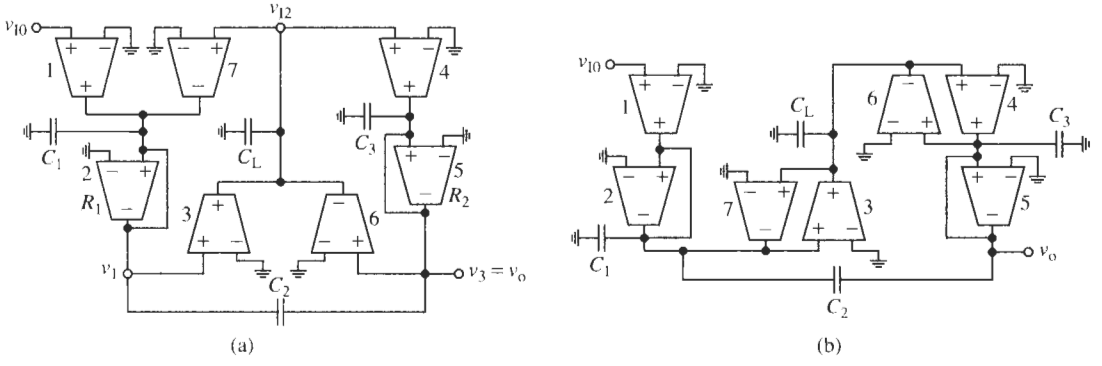

Figure 16.26 (a) Signal-flow graph implementation; (b) the circuit of (a) redrawn to show the equivalence with Fig. 16.25c.

[8] The two transconductors used to implement the two differential integrators in Eqs. (16.35a) and (16.35b) could, of course, be merged into a single differential-input transconductor. We have not done that to keep the active devices the same in all realizations and because it makes the following conversion to fully differential form easier to understand.

in the SFG method as presented. This capacitor is connected to the nodes labeled V_1 and V_3 in the original ladder and carries the current $(V_1 - V_3)sC_2$. As these two nodes are available in the circuit of Fig. 16.26a, we can complete the realization of the ladder simply by connecting C_2 to these nodes as shown in the figure.

An interesting observation can be made on the circuit structure in Fig. 16.26a: notice that the output terminal of transconductor 7 is at the input node of transconductor 3, and the input of 7 is at the output node of 3. Thus, transconductors 7 and 3 are connected in parallel, pointing in opposite directions. Similarly we see that transconductor 6 is connected in parallel with transconductor 4, also pointing in opposite directions. In Fig. 16.26b the circuit is redrawn to show these facts more clearly, and we recognize that the circuit is identical to the one in Fig. 16.25c, obtained by element replacement. This brings us to the insight that the element replacement and the operational simulation, or signal-flow graph, method lead to identical circuits! It can be shown quite easily that the equivalence of the methods of ladder realization is not limited to the third-order example we are discussing; it is valid for lossless ladders with arbitrary ladder arms (Schaumann, 1998). Consequently, we may use the method most appropriate and easiest for the situation at hand. Usually, the passive ladder with topology and component values is known, for example from a table or a synthesis program, so that the element replacement method using grounded or floating gyrators will be the simplest approach. On the other hand, if only circuit equations are given, such as those in Eq. (16.34), there is no need to synthesize the passive ladder first; rather we can use the signal-flow graph method from these equations to develop the active filter. The final circuit will be same regardless of the method used.

Let us consider a simple example to demonstrate the procedure and see the final active circuit.

EXAMPLE 16.5

We wish to design the third-order elliptic active lowpass filter shown in Fig. 16.25c. The passband gain must be 0 dB with $\alpha_{max} \leq 0.9$ dB in $0 \leq f \leq 17$ MHz and $\alpha_{min} \geq 22$ dB in $f > 28$ MHz. Source and load resistors should be 2.4 kΩ. The final realization should be a differential circuit.

Solution

The design is a doubly terminated lossless ladder; we disregard for the moment that a lossless ladder will have 6-dB loss in the passband contrary to the 0 dB specified. Because our concern in this chapter is the transconductance-C equivalent of the LC ladder, we will start directly from the result in Fig. 16.27a. The ladder design is developed easily by the procedures studied in Chapter 13; the steps follow Example 13.5 exactly. The single-ended active realization, Fig. 16.27b, is drawn directly below the passive ladder to show the correspondence between the two, and the differential implementation embedded between two transformers is shown in Fig. 16.27c.

Consider now the details of Fig. 16.27b. Since source and load resistors were prescribed to be 2.4 kΩ, and we wish to realize them with transconductors as in Fig. 16.6a so that $R = 1/g_m$, it follows that we must choose $g_m = 1/R = 416.7$ μS. This element is close to 400 μS, a value we used previously, so that minor adjusting of bias current will be sufficient. We shall use this component throughout our design.

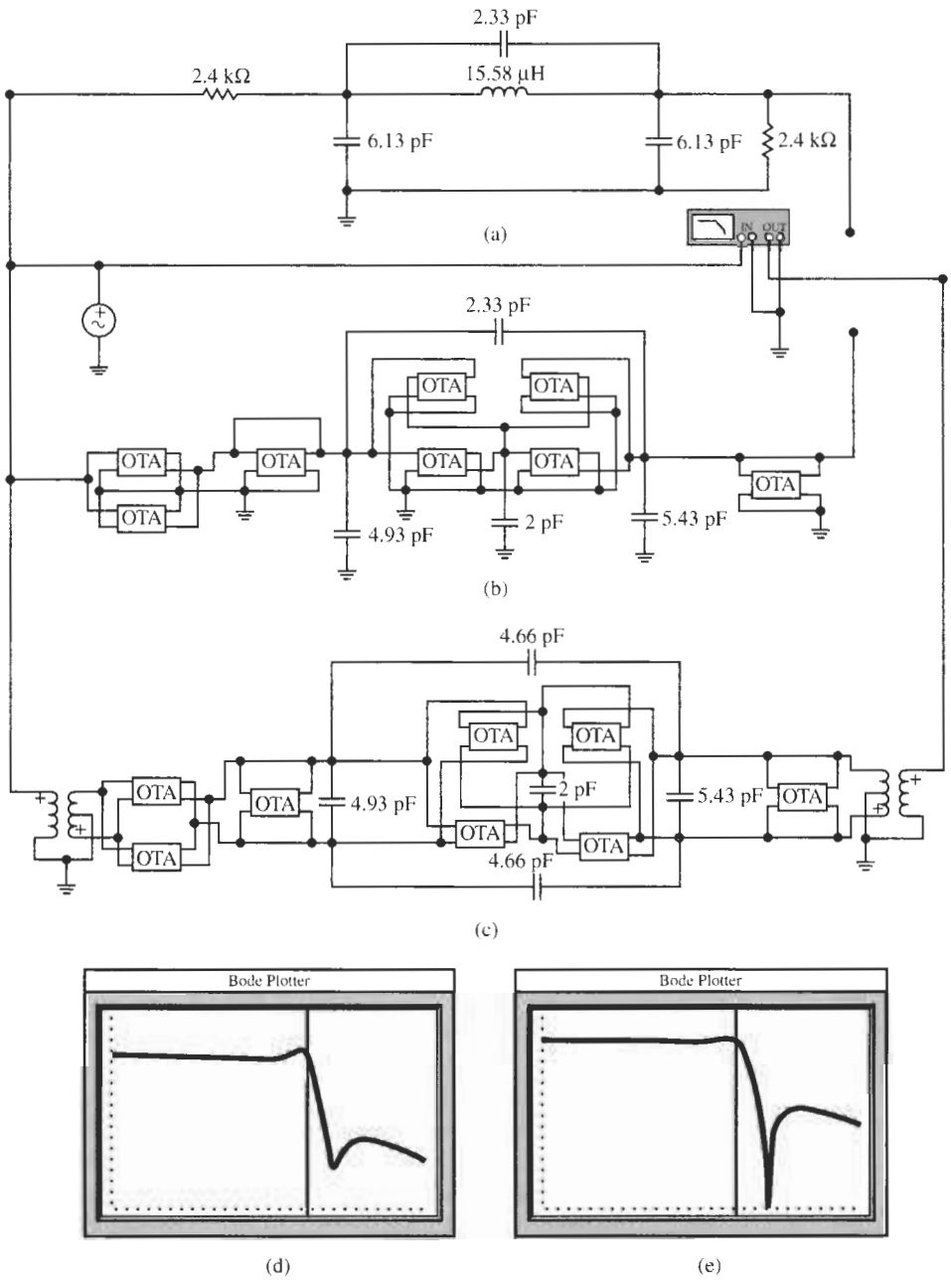

Figure 16.27 (a) The passive ladder; (b) single-ended transconductance-*C* realization of the circuit in (a); (c) the circuit of (b) in differential form; (d) test results for the active circuit (differential and single ended are identical) and, for comparison, of the passive ladder (e). [(d) Bode Plotter scales: 1 to 100 MHz; −40 to 10 dB; cursor at 17.68 MHz, 0.005 dB; (e) Bode Plotter scales: 1 to 100 MHz; −60 to 0 dB; cursor at 16.89 MHz, −6.877 dB.]

The passive ladder is driven by a voltage source; the first step in the design is a source transformation (see Figs. 16.25a and b) to convert the voltage source into a current source $I = V/R = Vg_m$ so that the series source resistor is placed in shunt, parallel to the first capacitor. The passive ladder realizes a 6-dB loss; to correct this loss in the active circuit we need to multiply the signal by a factor of 2. The correction is accomplished easily by connecting the voltage source to two g_m cells in parallel so that the input current becomes $2g_mV = 2I$. This is shown at the input of the active circuit in Fig. 16.27b. Finally we need to replace the floating inductor by a capacitor between two gyrators as is also indicated in Fig. 16.27b. The nominal capacitor value is $C_L = Lg_m^2 = 15.59\ \mu H \times (417\ \mu S)^2 = 2.711$ pF. The remaining capacitors stay unchanged in value as well as in their circuit connections; in the element replacement method we replace only the inductor.

Since the capacitor values are fairly small, we will next consider predistortion. Note that C_L is in parallel with $2C_i + 2C_o$ from the four OTAs of the gyrators. Staying with the values $C_i = 0.1$ pF and $C_o = 0.25$ pF, we reduce C_L by 0.7 pF to 2 pF. The 6.13-pF capacitor at the input is shunted by $C_i + C_o$ from the gyrator, $C_i + C_o$ from the active implementation of the input resistor, and $2C_o$ from the double OTA of the source transformation. Thus, the input capacitor should be reduced by $2C_i + 4C_o = 1.2$ pF to 4.93 pF. Finally, the 6.13-pF capacitor at the output is reduced by $C_i + C_o$ from the gyrator and $C_i + C_o$ from the load resistor to give $(6.13 - 0.7)$ pF $= 5.43$ pF. These values are shown in Fig. 16.27b.

Because a differential implementation is specified, as the last step we need to convert the single-ended filter into differential form. It is accomplished readily by use of the four steps introduced in Section 16.2. The result is seen in Fig. 16.27c. Because our OTA is already a differential-input–differential-output device some of whose terminals we did not use by connecting them to ground, the conversion is free of cost: we simply make use of the previously grounded terminals and do some minor rewiring. Remember that capacitors not connected between the differential signal paths must be doubled in value: the two floating capacitors increase from 2.33 to 4.66 pF.

Figure 16.27d displays the test result of the active circuit with the performance of the passive circuit also indicated for comparison. The differential and the single-ended circuit have identical performance but, as we discussed previously, the differential circuit has twice the signal voltage for a 6-dB gain in dynamic range and has less distortion. We note that the passive lossless ladder has a deeper notch, whereas the gyrator imperfections caused by the OTA's output conductance g_o of our model result in the expected finite notch depth. The passband gain is 0 dB as specified. The small peaking at the passband corner is caused by other parasitics and phase shifts in the transconductor.

Let us again point out the interesting property of filters derived from the topology of an *LC* ladder. Examining the circuit diagram in Fig. 16.25, and even the one in Fig. 16.23 for the second-order section that was derived from a simple ladder, we notice that all parasitic capacitors appear in parallel with actual circuit capacitors and, therefore, can be absorbed by them through predistortion. This is an important attribute of ladder-based filters. The significance of this feature lies in the facts that

1. a simple change of the nominal capacitor values can account for parasitics by predistortion, and
2. g_m-*C* filters based on ladders retain their order. This means that the degree of the filter

stays equal to the one prescribed and designed, even in the face of numerous parasitic capacitors

Consequently, the parasitic components cause no parasitic poles and zeros to disturb the transfer function, resulting in phase errors, oscillations, or other undesirable behavior: ladder simulations are more likely than other structures to perform as designed.

We turn next to the importance of simulating resistors in integrated filters by transconductors. When we introduced simulated resistors in Section 16.2, we stated that there are a number of benefits in implementing resistors via transconductors even if the IC technology permits real resistors to be fabricated. As a matter of fact, an integrated filter will not normally exhibit satisfactory behavior unless we use resistors simulated with the same transconductors as are used for the remaining design. Let us demonstrate this fact with the help of the circuit in Fig. 16.25b. Using that $R_1 = R_2 = R = 1/G$, we can derive the transfer function of this lowpass filter as

$$\frac{V_o}{I_0} = \frac{s^2LC_2+1}{s^3L\,(C_1C_2+C_1C_3+C_2C_3)+s^2LG\,(C_1+2C_2+C_3)+s\left(C_1+C_3+LG^2\right)+2G} \tag{16.36}$$

Evidently, we have a third-order lowpass function with transmission zeros at $\pm j/\sqrt{LC_2}$ and at infinity. In the *active* ladder we doubled the input current from $I_0 = g_m V_0$ to $I_0 = 2g_m V_0$, resulting in a factor of $2g_m$ in the numerator, and we replaced the inductor L by C_L/g_m^2. This yields the function

$$\frac{V_o}{V_0} = \frac{2g_m\left(s^2\dfrac{C_L}{g_m^2}C_2+1\right)}{s^3\dfrac{C_L}{g_m^2}\,(C_1C_2+C_1C_3+C_2C_3)+s^2\dfrac{C_L}{g_m^2}\,(C_1+2C_2+C_3)\,G+s\left(C_1+C_3+\dfrac{C_L}{g_m^2}G^2\right)+2G} \tag{16.37}$$

Notice that for the ideal value $g_m = G$ the dc gain is 0 dB. The most critical and least well-controlled component is the transconductor and we must assume that g_m is not only prone to suffer from fabrication tolerances but also that it varies with power supply and temperature fluctuations. We observe then that almost all the filter coefficients will be altered with changing g_m and the filter will not perform correctly. However, the situation is much improved and the mentioned difficulty disappears if we implement the resistors as $R = 1/G = 1/g_m$. Equation (16.37) then becomes

$$\frac{V_o}{V_0} = \frac{2\left(\dfrac{s^2}{g_m^2}C_LC_2+1\right)}{\dfrac{s^3}{g_m^3}C_L\,(C_1C_2+C_1C_3+C_2C_3)+\dfrac{s^2}{g_m^2}C_L\,(C_1+2C_2+C_3)+\dfrac{s}{g_m}\,(C_1+C_3+C_L)+2} \tag{16.38}$$

and we notice that g_m appears just as a frequency scaling factor. The benefit will be seen more clearly if we introduce a unit capacitor C_U, such as, e.g., $C_U = 1$ pF, relative to which

all capacitors can be measured, that is, important are the *ratios* C_k/C_U, $k = 1, 2, 3, L$. We reformat Eq. (16.38) as follows:

$$\frac{V_o}{V_0} = \frac{2\left(\dfrac{s^2C_U^2}{g_m^2}\dfrac{C_LC_2}{C_U^2}+1\right)}{\dfrac{s^3C_U^3}{g_m^3}\dfrac{C_L(C_1C_2+C_1C_3+C_2C_3)}{C_U^3}+\dfrac{s^2C_U^2}{g_m^2}\dfrac{C_L(C_1+2C_2+C_3)}{C_U^2}+\dfrac{sC_U}{g_m}\dfrac{C_1+C_3+C_L}{C_U}+2}$$

$$= \frac{2\left(a_2s_n^2+1\right)}{b_3s_n^3+b_2s_n^2+b_1s_n+b_0} \tag{16.39}$$

We now see that all the coefficients, a_i and b_j, in the filter transfer function are ratios of capacitors and s is normalized by a frequency scaling factor $\omega_c = g_m/C_U$, that is $s_n = s/\omega_c$. We pointed out before that capacitor ratios are very well controlled and are designable with small tolerances in integrated circuit technology so that we can rely on the coefficients to be realized correctly. If now g_m changes for any reason, the effect is to scale the frequency parameter by a different number, that is, the transfer characteristic just shifts along the frequency axis with no change in magnitude or phase performance.

To illustrate the effects, consider the three curves in Fig. 16.28. Shown is the performance of the differential filter of Fig. 16.27c when g_m changes and when the load resistors are not simulated as $1/g_m$ but are replaced by real resistors. We assumed here that due to fabrication tolerances or temperature changes g_m varies by +50% from 417 μS in Example 16.5 to 600 μS. Curve (1) is the nominal performance for 417 μS as in Example 16.5, Curve (2) is the performance of the filter with g_m increased to 600 μS, and Curve (3) is the filter's performance with $g_m = 600$ μS and the $1/g_m$ source and load resistors replaced by real 2.4-kΩ resistors. We observe that as predicted, by increasing g_m from 417 to 600 μS the transfer

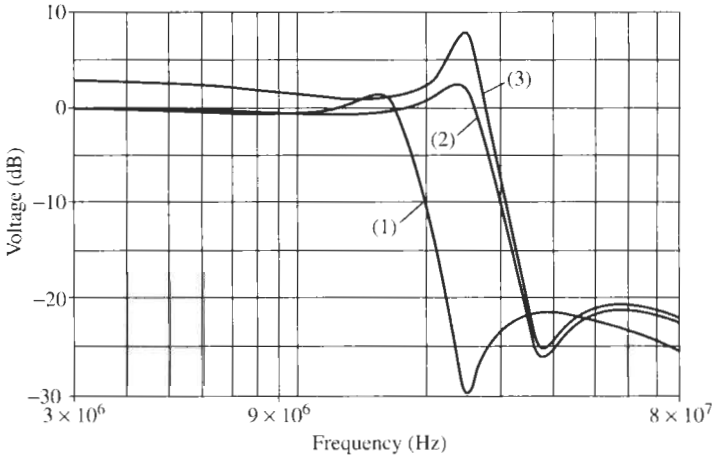

Figure 16.28 Performance of the third-order lowpass filter of Example 16.5 when g_m varies: (1) nominal performance; (2) g_m increased by 50%; (3) g_m increased by 50% and the simulated source and load terminations replaced by real 2.4-kΩ resistors.

characteristic essentially is simply shifted by 50% (from the cut-off frequency of $\approx$ 17 MHz to $\approx$ 26 MHz). The small increase in peaking at the passband corner and the reduced notch depth for the 600-μS case are caused by the small phase error of the transconductance that has a larger effect at higher frequencies. The frequency shift is easily repaired, for example, by changing the bias current of *all* transconductances until the transfer characteristic is shifted back to the specified location. If we had implemented the resistors by real 2.4-kΩ resistors instead of simulating them as $1/g_m$, the performance of the filter with $g_m = 417$ μS does not change, but more serious deviations in transfer function behavior are visible when g_m increases to 600 μS. It is less important that the passband gain is raised from 0 dB to approximately 3 dB,

$$\frac{2g_m}{2G} = g_m R = 600\ \mu\text{S} \times 2400\ \Omega = 1.44 = 3.16\ \text{dB}$$

but the changed denominator coefficients are critical: they result in large peaking at the passband corner, reflecting an increased Q. This distortion of the transfer function shape is very difficult if not impossible to correct because, even if we could devise a method to adjust elements on the integrated circuit, it is not at all obvious which component or components should be varied to bring about the needed change. It becomes clear then that simulating resistors as $1/g_m$ is highly advisable in the design of g_m-C filters.

16.5 AUTOMATIC TUNING

It has been emphasized throughout this book that analog filters must be designed with accurate component values if they are to perform as specified. The reasons should be clear: a transfer function depends on pole and zero frequencies, pole quality factors, as well as gain constants, and these parameters in turn depend on accurate element values. Thus, critical frequencies with units of 1/time are set by RC products, and their accuracy relies on the absolute values of resistors and capacitors. Similarly, the dimensionless quantities, quality factors and gain constants, are determined by ratios of like components, such as resistor ratios and capacitor ratios. In discrete circuits, any major tolerance problems in a design can be corrected by adjusting the elements: by *tuning*. Two possibilities exist: we may perform *functional tuning* where a component, usually a resistor, is adjusted or trimmed *after* completion of the design until the circuit functions as specified. For example, when a time constant T is realized by two elements, a resistor R and a capacitor C, $T = RC$, the realized value of T can be measured, and adjusted by trimming the resistor until the specified value T_0 is reached. The method permits us to use, for example, low-tolerance capacitors, $C + \Delta C$, where ΔC does not even have to be known, and then still arrive at T_0 with arbitrarily narrow tolerances by trimming R. We simply measure T while trimming R and stop at the desired value T_0. The resulting resistor will have the value

$$R = \frac{T_0}{C + \Delta C} \tag{16.40}$$

Naturally, we assume that the resistor can be varied over the necessary range.

A more difficult tuning method, labeled *deterministic tuning*, chooses to adjust some elements to their computed values *before* the design. These values are obtained from the circuit equations after accurate modeling of all relevant effects that influence the circuit performance

and after all untuned elements are carefully measured. Since the coefficients of circuit equations are normally highly nonlinear functions of the elements, the method relies heavily on computing power to arrive at results. As a trivial linear example consider determining R for the time constant after the capacitor C is measured to have the value $C + \Delta C$: Eq. (16.40) then yields the resistor value necessary for any given time constant. But examine, for instance, the effort involved in extracting ω_0, Q, and gain as a function of all components, including the operational amplifier, from the transfer function describing the Sallen–Key filter in Eq. (4.99), repeated here as Eq. (16.41),

$$T(s) = \frac{V_2}{V_1} = \frac{KG_1G_2\dfrac{1}{1+K/A}}{s^2C_1C_2 + s\left[C_2(G_1+G_2) + C_1G_2\left(1 - K\dfrac{1}{1+K/A}\right)\right] + G_1G_2} \tag{16.41}$$

Computing then the values of, say, R_1 and R_2 that are necessary to obtain the correct coefficients if C_1, C_2, and the opamp parameters are measured and known is not an easy task without carefully worked-out computer algorithms.

In any event, this discussion assumes that we have access to the circuit elements and can change them to achieve tuning. In an integrated circuit chip this assumption is clearly not valid. In spite of very careful modeling and simulation, the actual element values are not known accurately before manufacture because fabrication tolerances will lead to potentially large component errors. Twenty percent or larger errors in the absolute values of resistors and capacitors can be expected. Similarly, tolerances in opamp parameters of 50% are not uncommon and transconductance parameters can have similarly large variations. As a consequence, it is unlikely that an integrated filter will perform to specifications without any postdesign and postfabrication tuning steps. The question we will address in this section is how this can be accomplished.

To get a handle on the problem, let us note first that integrated circuit fabrication does yield very accurate *component ratios*. For example, for moderate ratios and careful layout, capacitor ratios can be as accurate as 0.1% or better. Resistor-ratio accuracies are similar. Of course, it is assumed that both components are fabricated with the same technology: for example, both capacitors are polysilicon-oxide–polysilicon; the ratio of a diffusion-oxide–metal capacitor and a polysilicon-oxide–polysilicon capacitor will have much wider tolerances. With careful design and layout, also complete functional blocks can lead to low-tolerance ratios: the ratio of two transconductances, g_{m1} and g_{m2}, of two identical transconductor cells, processed side by side on an IC chip, will be equal to unity within 1% or so. On the other hand, *absolute values* of components are not accurate at all and are prone to large tolerances in IC fabrication. As we mentioned earlier, values of 20% or larger must be expected.

We may conclude from these facts that time constants, whether implemented as RC products or as C/g_m ratios, will have large processing errors and need tuning because a time constant depends on absolute values of C and R or g_m. The frequency ω_0 in Eq. (16.30) for the biquad in Fig. 16.23 is a case in point, but the *ratio* of two frequencies, as, for example, ω_z/ω_0 in Eq. (16.30), will be realized fairly accurately. If a gain constant is determined as a ratio of two transconductances, its realization will also be fairly accurate as long as the gain is moderate. In these cases it is best if the gain can be expressed as a ratio of two integers, N/M, so that it may be implemented as the ratio of N transconductors and M transconductors as illustrated in Fig. 16.29. Also, in that case the ratio will track well with

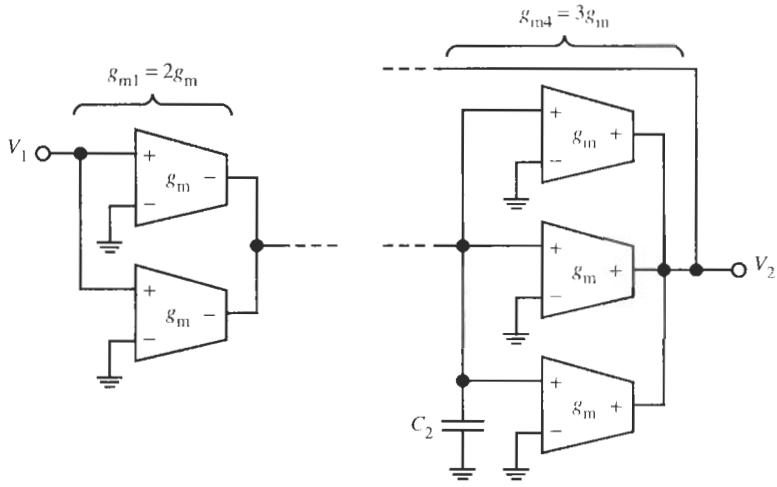

Figure 16.29 Realizing the dc gain in the circuit of Fig. 16.23, $H_0 = g_{m1}/g_{m4} = N/M$, as a ratio of transconductances; here $N/M = 2/3$.

changing operating conditions, such as bias or temperature. Similarly, if a quality factor is determined by a capacitor ratio as in Eq. (16.30) for the biquad in Fig. 16.23, we can assume that the implementation is accurate if the capacitors are designed as multiples of unit capacitors C_U, such as $C_1/C_2 = nC_U/mC_U = n/m$.

Because some tuning is unavoidable, but tuning by varying components in the conventional sense is as a rule impossible, a solution is found in devising an on-chip electronic control loop by which the integrated filter tunes itself automatically. To be able to accomplish this, electronically variable elements must be available. In our case these are the transconductors whose transconductance parameters are determined by a bias current or voltage. We then provide a signal to the integrated circuit to which the filter is referenced. Any error in filter performance is measured and the parameters are changed until the error is zero, or sufficiently small to be acceptable. A variety of approaches based on phase-locked loops, adaptive signal processing, or magnitude-locked loops have been proposed and are used (Johns and Martin; Tsividis and Voorman, 1993). We shall present the magnitude-locked-loop technique below; it relies on peak detection and is fairly easy to understand and implement.

16.5.1 Frequency Tuning

Let us return to Eq. (16.39). There we demonstrated that all filter parameters are determined by capacitor ratios and the coefficient of s^i is multiplied by $(C_U/g_m)^i$ where C_U is a unit capacitor. The main problem to be addressed by tuning is, therefore, the accurate implementation of the time constant C_U/g_m, or expressed differently, the accurate realization of the frequency parameter g_m/C_U. Let us examine then how we can tune this time constant automatically by varying g_m. Consider the circuit concept in Fig. 16.30. It shows a transconductor of value g_M loaded by a capacitor C_U. The two components form an integrator. Let us apply a reference voltage $v_1(t) = \hat{V}_1 \sin \omega_{ref} t$ to the circuit with accurate frequency f_{ref} set to the desired value $f_{ref} = g_m/(2\pi C_U)$. If we assume that f_{ref} is much larger than the integrator's 3-dB frequency so that any integrator losses can be neglected, the output of the integrator is

$$v_2(t) = -\hat{V}_1 \frac{g_M}{\omega_{ref} C_U} \cos \omega_{ref} t = -\hat{V}_2 \cos \omega_{ref} t \tag{16.42}$$

From this equation we see that $\hat{V}_1 = \hat{V}_2$ if

$$\frac{g_M}{C_U} = \omega_{ref} = 2\pi f_{ref} \tag{16.43}$$

It follows that the time constant is set accurately to $1/\omega_{ref}$ when the gain of the integrator equals unity.

To perform this operation, we need to adjust g_M until the unity-gain frequency of the integrator is f_{ref}. In a possible circuit solution we apply the reference signal to the input of the integrator and send both input and output signals through two identical peak detectors PD. The two dc outputs $\hat{V}_1$ and $\hat{V}_2$ are compared in a transconductor g_{mF} that generates a current $I_0 = g_{mF}(\hat{V}_1 - \hat{V}_2)$. The current I_0 is integrated on a capacitor C_F to generate a bias voltage V_F. The values g_{mF} and C_F are not critical. V_F is buffered and applied to the tuning terminal of the transconductor where it causes a bias current I_F to flow. The feedback loop must be closed such that feedback is negative and a stable point can be reached: let us assume that g_M is proportional to I_F so that g_M increases with rising V_F. If now $\hat{V}_1 > \hat{V}_2$, g_M is too small, I_0 is positive, and V_F increases to generate a larger bias current I_F. If $\hat{V}_1 < \hat{V}_2$, g_M is too large, I_0 is negative, and V_F decreases to reduce the bias current. As soon as $\hat{V}_1 = \hat{V}_2$, we have $I_0 = 0$,

$$I_0 = g_{mF}\left(\hat{V}_1 - \hat{V}_1 \frac{g_M}{\omega_{ref} C_U}\right) = g_{mF} \hat{V}_1 \left(1 - \frac{g_M}{\omega_{ref} C_U}\right) = 0 \tag{16.44}$$

that is, $\omega_{ref} = g_M/C_U$. At this point the bias current is adjusted such that the *master transconductor* g_M is tuned so that the time constant is correct.

To tune the filter we rely on matching of components on the integrated circuit. Clearly, it is advantageous for our assumption of matching if all transconductors are identical or if they differ by only a small integer multiple as we outlined in connection with Fig. 16.29. Since capacitor ratios are realized accurately on the IC, we can assume that the ratio of any capacitor C_i to the unit capacitor C_U, C_i/C_U, is implemented with only very small errors. We then tune all transconductors in the filter by applying the buffered V_F to all the bias terminals of the filter transconductors so that they are tuned automatically to the value g_M. This scheme is shown in Fig. 16.30 and is referred to as *master–slave tuning*: g_M is the *master* transconductor and g_m are the *slaves* that adjust their values to g_M.

By slaving the frequency parameter g_M/C_U to a reference frequency f_{ref} we have built a tracking filter that shifts its transfer function along the frequency axis as we illustrated for two points in Fig. 16.28. For example, if we design a lowpass with cut-off frequency equal to the reference frequency, the width of the lowpass passband can be set by f_{ref}. Let us emphasize again that to ensure the correct performance of such a tracking filter it is important to implement also the resistors as $1/g_M$. Otherwise, as we have seen in Section 16.4, severe distortion of the transfer function shape must be expected. Also we should note that any dc offset voltage in the transconductance g_M translates into an incorrect peak value $\hat{V}_2$. This is interpreted by the comparator as an incorrect value of g_M and will result in mistuning. Careful offset cancellation is necessary, therefore, and differential design is beneficial so that offset voltages are subtracted out.

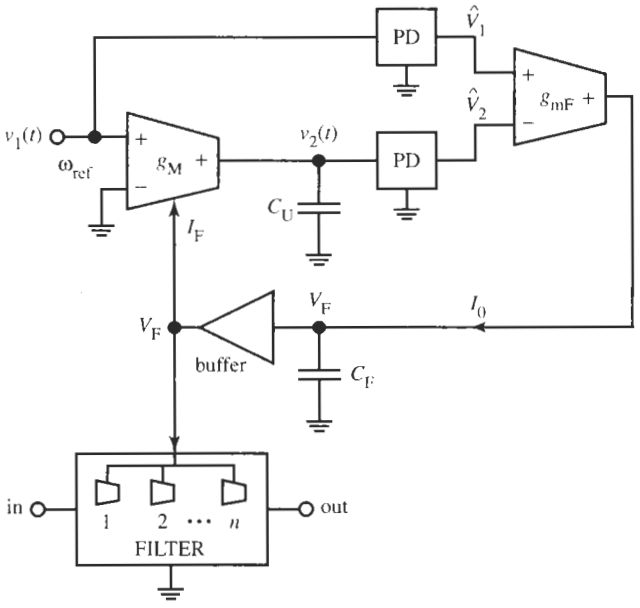

Figure 16.30 Control loop for tuning the value g_M/C_U to ω_{ref}.

16.5.2 Q-Tuning

We demonstrated several times throughout our study of filters that the quality factor is a dimensionless parameter and as such is determined by ratios of like components. A recent example was given in Eq. (16.30) for the circuit in Fig. 16.23. We are led to believe, therefore, that in integrated circuit design Q is determined accurately during fabrication with little need for further adjustment. However, we must be aware that various parasitic effects and components may cause Q to deviate unacceptably from its nominal design value. Depending on the size of these deviations, further tuning will be called for. Consider, for example, Eq. (16.25b), where we included the effects of parasitic capacitors and the output conductance of the transconductors on the coefficients of the second-order transfer function. We found that

$$\frac{\omega_0}{Q} = \frac{C_{2\text{eff}}\,(g_{m2} + 3g_o) + C_{1\text{eff}}g_o}{C_{1\text{eff}}C_{2\text{eff}}} \quad \text{and} \quad \omega_0^2 = \frac{g_{m3}g_{m4} + g_{m2}g_o + g_o^2}{C_{1\text{eff}}C_{2\text{eff}}}$$

From these two equations the quality factor can be shown to be

$$Q = \frac{\sqrt{g_{m3}g_{m4}}}{g_{m2}}\sqrt{\frac{C_1}{C_2}} \times \sqrt{\frac{1+3\dfrac{C_o}{C_1}+2\dfrac{C_i}{C_1}}{1+\dfrac{C_o}{C_2}+\dfrac{C_i}{C_2}}} \sqrt{\frac{1+\dfrac{g_{m2}g_o}{g_{m3}g_{m4}}+\dfrac{g_o^2}{g_{m3}g_{m4}}}{1+3\dfrac{g_o}{g_{m2}}+\dfrac{C_{1\text{eff}}}{C_{2\text{eff}}}\dfrac{g_o}{g_{m2}}}} = Q_0 \times \left(1+\frac{\Delta Q}{Q_0}\right) \quad (16.45)$$

We see that the quality factor is equal to the nominal value obtained from Eq. (16.27), or for equal g_m, as given in Eq. (16.30), multiplied by an error term that is determined by parasitics. To understand the error better, let us make the reasonable assumption that all ratios in the error term in Eq. (16.45) are small numbers. We then can make the approximations $\sqrt{1+x} \approx 1 + x/2$

and $1/\sqrt{1+x} \approx 1 - x/2$ for small x, and neglect all products of small terms. Assuming that $g_{m2} = g_{m3} = g_{m3} = g_m$, we obtain from Eq. (16.45)

$$Q \approx \sqrt{\frac{C_1}{C_2}} \times \left[1 + \frac{3C_o + 2C_i}{2C_1} - \frac{C_o + C_i}{2C_2} - \left(2.5 + \frac{C_{1eff}}{C_{2eff}}\right)\frac{g_o}{g_m}\right] = Q_0\left(1 + \frac{\Delta Q}{Q_0}\right) \quad (16.46)$$

Whether the error term can be neglected depends on the nominal circuit components and on the relative sizes of the parasitic elements; even whether the error is positive or negative cannot in general be anticipated. We also see that although the parasitic capacitors do not result in additional poles or zeros, they nevertheless cause errors in ω_0 and Q. Examining the term ΔQ carefully, we see that the parasitic capacitors may result in an increase or a decrease in Q that depends on the size of Q_0. On the other hand, parasitic losses g_o always cause the quality factor to be reduced. Noting that $Q_0^2 = C_1/C_2$, we can further simplify Eq. (16.46) for the case of interest, large Q, i.e., $C_1 \gg C_2$: The approximate relative Q error is

$$\frac{\Delta Q}{Q_0} \approx -\frac{C_o + C_i}{2C_2} - Q_0^2\frac{g_o}{g_m}$$

It is always negative, meaning Q is reduced by the parasitic elements; most likely, ΔQ will be dominated by g_o.

At this time, most applications of integrated filters have low-quality factors as, for example, delay filters with Bessel–Thomson transfer functions (see Chapter 10). Only few filters make use of Q tuning because of the additional circuitry required, which tends to consume too much silicon area and power, and may cause signals from the tuning operation to leak into the filter, causing unwanted interference. Nevertheless, the increasing need for integrated high-frequency communications demands very selective filters with large quality factors where the errors must be corrected. It becomes apparent then that an automatic Q-tuning method for high-Q filters is desirable and we shall discuss briefly how Q tuning can be performed.

In a bandpass function, the quality factor is defined as center frequency divided by the 3-dB bandwidth: $Q = \omega_0/\Delta\omega$. This implies that to measure Q we need to measure at least two frequencies and two voltage levels, say at midband and at the 3-dB point, and this should be done automatically and with reasonably simple circuitry. Fortunately, an easier method is available for some circuits, of which the biquad in Fig. 16.22 is one example. Taking the lowpass output V_o, Eq. (16.25a), and choosing all transconductors identical, we obtain

$$\frac{V_o}{V_1} = \frac{\dfrac{g_m^2}{C_1C_2}}{s^2 + s\dfrac{g_m}{C_1} + \dfrac{g_m^2}{C_1C_2}} = \frac{\omega_0^2}{s^2 + s\dfrac{\omega_0}{Q} + \omega_0^2} \quad (16.47)$$

Evaluating Eq. (16.47) at the pole frequency ω_0, which is also the center frequency of the bandpass, the realized gain is equal to Q:

$$|V_o/V_1|_{j\omega_0} = Q \quad (16.48)$$

Thus, if we just measure $|V_o/V_1|$ at $f = f_0$, we can deduce whether or not the quality factor is realized correctly. Again, the circuitry can be based on peak detection. Figure 16.31

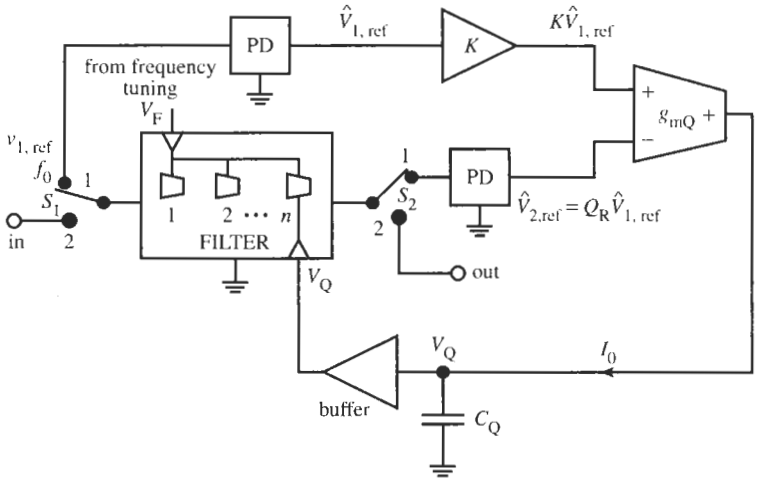

Figure 16.31 Control loop for tuning the quality factor. The switches S_1 and S_2 are in Position 1 for Q tuning and in Position 2 for filtering.

shows the concept. We must assume for the method to work properly that the frequency f_0 is correct, that is, the frequency tuning loop we discussed previously has been activated for the filter. The switches S_1 and S_2 are in Position 1, which is the filter operation for tuning the quality factor. We apply a reference signal $v_{1,\text{ref}}$ with amplitude $\hat{V}_{1,\text{ref}}$ and frequency $f = f_0$ to the filter. According to Eq. (16.48) the output is then $\hat{V}_{2,\text{ref}} = Q_R\hat{V}_{1,\text{ref}}$ where we labeled the *realized* quality factor as Q_R. We use again two matched peak detectors to form the peak value of this output, $\hat{V}_{2,\text{ref}}$, and the peak value of the input, $\hat{V}_{1,\text{ref}}$, multiplied by a gain factor K. Notice that the amplifier K is at the output of the peak detector and, thus, is a dc or low-frequency amplifier whose gain can be realized accurately by a resistor or capacitor ratio. K is set equal to the specified value $Q = Q_0$. As in the frequency-tuning loop, the two voltages are compared in a transconductor g_{mQ} and the resulting current,

$$I_0 = g_{mQ}(K - Q_R)\hat{V}_{1,\text{ref}} \tag{16.49}$$

is integrated on a capacitor C_Q. The bias voltage V_Q is then applied to a suitable component to adjust Q_R. For the circuit in Fig. 16.22, for instance, the quality factor is inversely proportional to the transconductance g_{m2}, see Eq. (16.45); we can, therefore, adjust g_{m2} to vary Q without affecting any other filter parameter. As soon as $Q = K = Q_0$, the current I_0 is reduced to zero and the final tuning voltage V_Q is obtained. At this point the switches S_1 and S_2 are thrown to Position 2 for normal filtering operation. The final voltage V_Q is held on the capacitor C_Q to maintain tuning. When the system detects a need to upgrade V_Q, for instance because Q may have drifted due to a change in temperature, filter operation must be interrupted and the filter is switched back to Q tuning. Since the method locks the filter magnitude to the magnitude $K\hat{V}_{1,\text{ref}}$ of a reference signal, it is referred to as a *magnitude-locked loop*. Our earlier remarks about dc offset apply here as well: offset cancellation is important to reduce systematic tuning errors. More details on this Q-tuning concept and specific circuitry can be found in the literature (Karsilayan and Schaumann, 2000; Tsiridis and Voorman, 1993).

16.5.3 On-Line–Off-Line Operation

Depending on the complexity of the filter and the dynamics of the tuning loops, the time required for tuning the filter will be anywhere from a few microseconds to a few milliseconds. As we illustrated in Fig. 16.31, during this time the filter cannot be in use for the intended signal processing task because we applied a reference voltage $v_{1,\text{ref}}$ to the filter input. Applying the working input signal, v_{in}, to filter during tuning results in two problems.

1. The signal v_{in} and the reference voltage $v_{1,\text{ref}}$ will interfere with each other through crosstalk, intermodulation, and other effects and result in distortion in the output signal v_{out}.
2. The relevant information on Q will be difficult to extract from the output if it is some combination of the filtered input signal and the reference voltage.

Consequently, the tuning system as discussed must be activated when the input signal v_{in} is OFF, an operation referred to as *off-line*. For master–slave frequency tuning on the other hand, no reference voltage is applied to the filter so that the frequency can be tuned while the input signal v_{in} is ON and the filter performs its intended signal processing task. This operation is termed *on-line*. The fundamental difference between the two cases is that for frequency tuning we have a separate *master* block that is tuned and sees the reference voltage, whereas the filter is just *slaved* to the master, relying on good matching of components across the integrated circuit. In the Q-tuning method we tune the filter itself, no matching needs to be assumed, but the reference voltage has to be applied to the filter, which must be taken out of service for the tuning interval.

In most filtering tasks there will be periods when the filter does not need to be active and can be taken out of operation for tuning. For instance, an integrated filter in a mobile phone can be tuned by the system in a few milliseconds as soon as ringing is detected or as soon as the receiver is turned on. Similarly, a filter in the read/write channel of a computer disk drive will have sufficient idle times that can be used for tuning. If, however, the filter cannot be taken off-line, we have to construct a *master block* for Q tuning as well. The performance of this master must model any Q deviations of the filter just as the integrator models any relevant frequency deviations in the frequency-tuning method we discussed. For instance, this master block could be a second-order section or even a complete duplicate of the filter. The price paid for this approach is larger silicon area and power consumption, in addition to raising concerns about signal integrity because tuning voltages may leak into the main filter.

REFERENCES

P. R. Gray and R. G. Meyer, *Analysis and Design of Analog Integrated Circuits*, 3rd ed., John Wiley, New York, 1993.

R. A. Haddad and T. W. Parsons, *Digital Signal Processing: Theory, Applications, Hardware*, Computer Science Press, W. H. Freeman & Company, New York, 1991.

D. A. Johns and K. Martin, *Analog Integrated Circuit Design*, John Wiley, New York, 1998.

A. I. Karsilayan and R. Schaumann, "A mixed-mode automatic tuning scheme for high-Q continuous-time filters," *IEEE Proceedings—Circuits, Devices, and Systems*, Vol. 147, No. 1, pp. 57–64, Feb. 2000.

E. Sanchez-Sinencio and J. Silva-Martinez, "CMOS transconductance amplifiers, architectures and active filters: a tutorial," *IEE Proceedings, Circuits, Devices and System*, pp. 3–12, Vol. 147, Feb. 2000.

R. Schaumann, "Simulating Lossless Ladders with Transconductance-C Circuits," *IEEE Trans. Circuits Syst. II*, Vol. 45, No. 3, pp. 407–410, March 1998.

A. S. Sedra and K. C. Smith, *Microelectronic Circuits*, 4th ed., Chapters 6 and 10. Oxford University Press, New York, 1998.

Y. Tsividis and J. O. Voorman, eds., *Integrated Continuous-Time Filters: Principles, Design and Applications*. IEEE Press, New York, 1992.

PROBLEMS

16.1 A g_m-C integrator must be designed for a unity-gain frequency of 9 MHz. The available transconductor is known to have the parameters $g_m = 200\ \mu S$, $C_i = 0.05$ pF, and $C_o = 0.19$ pF. The dc gain must be at least 68 dB.

(a) Determine the required load capacitor.

(b) Determine the minimum value of output resistance r_o the OTA must have.

(c) What is the phase at the unity-gain frequency?

(d) What are the 3-dB frequency and the phase at the 3-dB frequency?

(e) What is the highest unity-gain frequency that an integrator with this OTA can have?

(f) Implement the circuit in single-ended and differential form and test your designs with Electronics Workbench (EWB).

16.2 A g_m-C integrator is designed with an OTA with $g_m = 160\ \mu S$ and a capacitor $C = 2$ pF. The unity-gain frequency f_u is measured to be 11.85 MHz. The low-frequency gain of the integrator is 55 dB.

(a) What is the OTA's parasitic output capacitance?

(b) What is the OTA's parasitic output resistor?

(c) If the g_m value of the OTA can be varied in the range $120\ \mu S \leq g_m =\leq 240\ \mu S$ by changing the bias current, determine the range over which f_C can change.

16.3 The OTA of Problem 16.1 with g_m adjusted to the value 195 μS is used to implement a resistor in the circuit of Fig. P16.3.

(a) What is the gain of the circuit at 100 kHz?

(b) What is the expected 3-dB frequency?

(c) The 3-dB frequency must be increased substantially but no additional OTA is available on the IC to make the divider frequency independent as suggested in Example 16.1. Recommend a method that would achieve the desired increased bandwidth.

(d) Implement the circuit and test your design EWB.

16.4 A very large inductor has a series loss resistor of 240 Ω. Use the concept of Fig. 16.6c to design a negative floating resistor to be placed in series with the inductor so that the losses are canceled. What value of g_m is needed? Build and test your design with EWB.

16.5 Design a g_m-C integrator as in Fig. 16.9c with an OTA of value $g_{m1} = 300\ \mu S$ and $C = 2.2$ pF. The OTA's output resistor is only 60 kΩ resulting in low dc gain and poor phase performance of the integrator at lower frequencies. An engineer proposes to use a second OTA of appropriate value to cancel the losses with a negative resistor. Design a circuit to achieve such a lossless integrator, even in the face of lossy OTAs.

(a) What must be the value of g_{m2} of the second OTA to achieve a lossless integrator?

(b) What will be the realized dc gain if the value of g_{m2} is incorrect by 8%?

(c) What is the value of the unity-gain frequency of your design if the two OTAs are known to have the parasitic capacitors $C_{i1} = 0.08$ pF, $C_{o1} = 0.2$ pF, $C_{i2} = 0.04$ pF, $C_{o2} = 0.09$ pF?

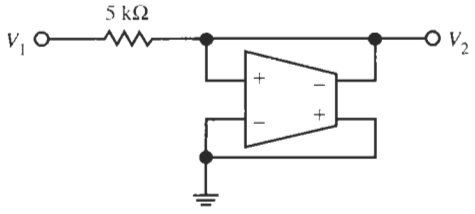

Figure P16.3

16.6 A single-ended floating inductor can be built from the simulated differential inductor circuit in Fig. 16.18b. The process is analogous to the one leading to the single-ended floating resistor in Fig. 16.6.

(a) Use OTAs with $g_m = 200\ \mu S$ and $C = 1$ nF to obtain $L \approx 25$ mH and construct a parallel resonance circuit with a second 1-nF capacitor.

(b) Use EWB to test the performance of your circuit built with LM741 opamps.

(c) Is the performance as expected?

(d) The inductor is lossy, of course; try to determine the loss resistor from your test results.

(e) How would you alter the experiment to try to get an estimate of the parasitic capacitors at the input and output of the OTAs?

16.7 Design and test a first-order lowpass filter built with a transconductance amplifier with $g_m = 200\ \mu S$ so that the following specifications are met:

dc gain: $A(0) = 68$ dB
Unity-gain frequency: $f_U = 9$ MHz

Implement and test your designs.

16.8 Repeat Problem 16.7 for the following specifications:

3-dB frequency: $f_c = 26$ kHz
Unity-gain frequency: $f_U = 6.8$ MHz

Show both single-ended and differential structures and test your designs with EWB.

16.9 Use transconductance amplifiers with the model of Fig. 16.4 to design a 5-mH inductor. Use EWB to test your design and find all parasitic components so that a passive model as in Fig. 16.16 can be drawn. *Note: You may wish to save the transconductor model for use in later problems.*

16.10 Repeat Problem 16.9 but for a differential design of $L = 300\ \mu H$.

16.11 Design and test a second-order g_m-C filter to meet the following requirements. Unspecified parameters may be selected.

(a) lowpass, $\omega_0 = 260$ krad/s, $Q = 0.9$, dc gain $H_0 = 0$ dB

(b) lowpass, $f_0 = 36$ MHz, $Q = 1.9$, dc gain $H_0 = 0$ dB

(c) highpass, $f_0 = 120$ kHz, $Q = 2.4$, high-frequency gain $H_\infty = 0$ dB

(d) highpass, $\omega_0 = 1$ Mrad/s, $Q = 0.8$, high-frequency gain $H_\infty = 2$ dB

(e) bandpass, $\omega_0 = 12$ Mrad/s, $Q = 8$, midband gain $H_M = 0$ dB

(f) bandpass, $f_0 = 800$ kHz, $Q = 15$, midband gain $H_M = 12$ dB

(g) band-rejection filter, $\omega_0 = 12$ Mrad/s, $\omega_z = 6$ Mrad/s, $Q_p = 1.2$, $Q_z = 10$, $H_\infty = 6$ dB

(h) band-rejection filter, $f_0 = 620$ kHz, $f_z = 6$ MHz, $Q_p = 3$, $Q_z = 15$, $H_\infty = 0$ dB

(i) notch filter, $f_0 = f_z = 3.6$ MHz, $Q_p = 3$, $H_\infty = 3$ dB

(j) gain boost filter, 6 dB boost at $f = 900$ kHz, $H_0 = H_\infty = -2$ dB, $\omega_0 = 5$ Mrad/s

16.12 Employ the cascade g_m-C methods with the OTA of Fig. 16.4 to design and test a cascade circuit to realize

(a) a third-order lowpass filter with maximally flat magnitude for the requirements $\alpha_{max} = 3$ dB, $\omega_p = 15$ Mrad/s, $H(0) = 34$;

(b) a third-order cascade lowpass filter with maximally flat magnitude for the requirements $\alpha_{max} = 0.5$ dB, $f_p = 1.2$ MHz, $H(0) = 0$ dB;

(c) a fifth-order cascade lowpass filter with equal-ripple magnitude for the requirements $\alpha_{max} = 0.1$ dB, $f_p = 850$ kHz, $H(0) = 0$ dB;

(d) a Chebyshev lowpass filter for the requirements $\alpha_{max} = 0.3$ dB in $0 \le f \le 10$ MHz, $\alpha_{min} = 22$ dB in $f \ge 24.6$ MHz, $H_0 = 0$ dB;

(e) a seventh-order Chebyshev highpass filter for the requirements $\alpha_{max} = 1$ dB, $f_p = 15$ MHz, $H_\infty = 4.5$ dB;

(f) a seventh-order lowpass filter with an equal-ripple delay, lowpass bandwidth $f_p = 13$ MHz;

(g) a fifth-order bandpass filter with a Chebyshev magnitude for the requirements $\alpha_{max} = 0.1$ dB, $f_p = 850$ kHz, 0.1-dB bandwidth of 70 kHz, $H_M = 25$ dB;

(h) a bandpass filter with a Chebyshev magnitude for the requirements $\alpha_{max} = 1$ dB in 12 MHz $\le f \le 39$ MHz, $\alpha_{min} \ge 30$ dB in $f \le 4.8$ MHz, and $\alpha_{min} \ge 25$ dB in $f \ge 72$ MHz, $H_M = 0$ dB (refer to Example 9.4).

16.13 Realize the fifth-order elliptic lowpass filter function of Example 5.17,

$$T(s) = T_1(s)T_2(s)T_3(s) = \frac{k\left(s^2 + 29.2^2\right)\left(s^2 + 43.2^2\right)}{(s + 16.8)\left(s^2 + 19.4s + 20.01^2\right)\left(s^2 + 4.72s + 22.52^2\right)}$$

as a cascade connection of g_m-C sections. The frequency parameter s in $T(s)$ is normalized with respect to 1 MHz. Test your design with EWB.

16.14 Realize the sixth-order lowpass function of Example 6.3,

$$T(s) = T_1T_2T_3 = \frac{k_1}{s^2 + 2.24379s + 1.37377} \times \frac{k_2\left(s^2/16 + 1\right)}{s^2 + 1.46493s + 1.23015} \frac{k_3\left(s^2/4 + 1\right)}{s^2 + 0.47756s + 1.10041}$$

as a cascade connection of three g_m-C biquads. The normalizing frequency is $f_n = 1.8$ MHz. Test your design with EWB.

16.15 Realize a lowpass filter for the specifications

$$\alpha_{max} = 0.25 \text{ dB} \qquad \alpha_{min} = 18 \text{ dB}$$
$$f_p = 16 \text{ MHz} \qquad f_s = 23 \text{ MHz}$$

with g_m-C sections. Use an inverse Chebyshev approximation and the cascade topology (refer to Example 8.1). Test your design with EWB.

16.16 Realize the elliptic lowpass function displayed in Fig. 8.15 with the frequency axis labeled in Mrad/s. Use a cascade of g_m-C sections and test your design with EWB.

16.17 Use the cascade g_m-C method to realize the lowpass filter of Example 8.4 where the cut-off frequency is rescaled to 24 MHz and test your design with EWB.

16.18 Use the cascade g_m-C method to realize the bandpass filter specified in Example 9.6, except that the frequencies are increased by a factor 100, and test your design with EWB.

16.19 Use the cascade g_m-C method of this chapter to realize the bandpass filter specified in Example 9.6, except that the frequencies are increased by a factor 1000, and test your design with EWB.

16.20 Use a cascade g_m-C filter to design a bandpass filter for the specifications in Problem 9.9 and test your design with EWB.

16.21 Use any of the methods of this chapter to design a bandstop filter for the specifications in Problem 9.16 and test your design with EWB. The frequency axis is rescaled to kHz.

16.22 Repeat Problem 16.12 but use ladder filters (element replacement or operational simulation). Test your designs with EWB.

16.23 Scale the normalized LC ladder of Fig. 13.14b such that passband corner $f_p = 13.8$ MHz and source and load terminations are 300 Ω. Realize the circuit as a g_m-C ladder and test the designs with EWB.

(a) Use element replacement.

(b) Use operational simulation.

(c) Compare the two designs. The circuits should be the same.

16.24 Design a g_m-C ladder to realize the highpass specifications of Example 9.1. Test your design with EWB.

16.25 Rescale the impedance level of Fig. 13.18d such that source and load terminations are to 750 Ω. Design a g_m-C ladder in differential form to implement the resulting circuit and test the design with EWB:

(a) By use of the element-replacement method.

(b) By use of the signal-flow graph (operational simulation) method.

(c) Compare the two methods and convince yourself that the two circuits are the same.

16.26 Denormalize the lowpass ladder shown in Fig. P14.16 so that the passband corner frequency is $f_p = 26.8$ MHz and the termination resistors are 1.2 kΩ. Build and test the resulting filter with the g_m-C element replacement method.

16.27 Scale the load resistors in the ladder of Fig. P15.19 to 1 kΩ and realize the resulting circuit as a g_m-C ladder. Your design should be in differential form; test its performance with EWB.

16.28 Repeat Problem 16.27 for the ladder in Fig. P15.23.

16.29 Repeat Problem 16.27 for the ladder in Fig. P15.25.

16.30 An LC lowpass ladder and its test performance are shown in Fig. P16.30. Realize the filter as an OTA-C ladder with simulated inductors and test the circuit's performance. Compare the two test results and comment on any differences.

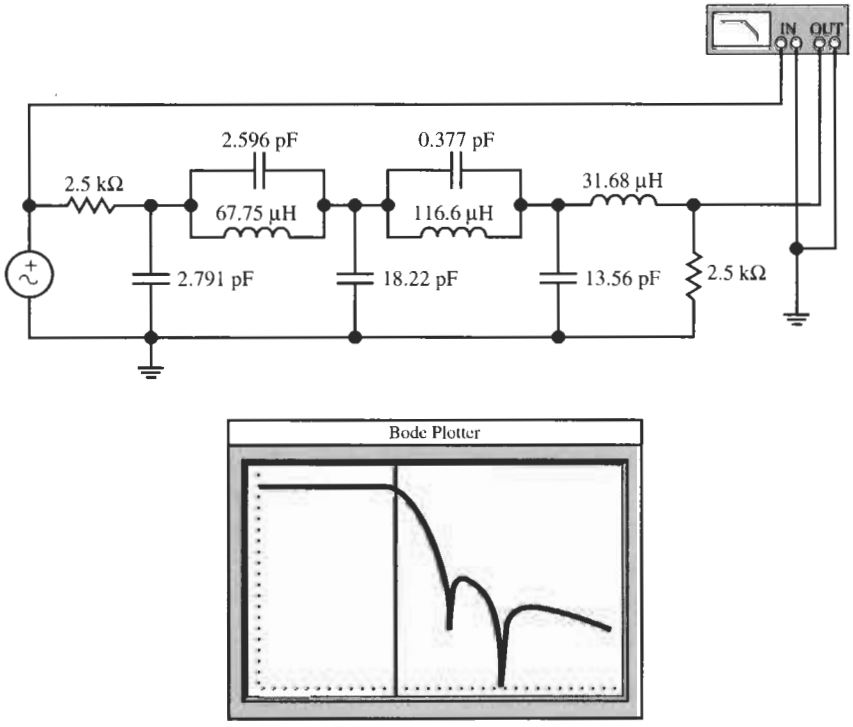

Figure P16.30 Bode Plotter Scales: 1 to 100 MHz; −120 dB to 0 dB; cursor at 6.026 kHz, −8.113 dB.

SWITCHED-CAPACITOR FILTERS

Switched-capacitor circuits were developed to be able to design accurate analog filters at voice-band frequencies economically in fully integrated form. Furthermore, for reduced power, compact design, and compatibility with digital systems, the filters had to be realized in MOS (metal-oxide semiconductor) technology. In this technology we can implement switches for the digital circuits and, as we saw in the previous chapter, we can implement capacitors, transconductance or voltage amplifiers, but not, at least not easily, good resistors. The problem to be addressed, then, is how to realize accurate RC time constants without the use of resistors. Also, we wish to avoid the need for the complicated tuning schemes discussed in the previous chapter. The solution was found in the recognition that if a capacitor is rapidly charged and discharged to two different voltages V_1 and V_2, the charge packages could be averaged over time to a current that is equivalent to that of a resistor connected to those two voltages. In other words, a resistor is simulated by a suitable combination of a capacitor and switches.

The resulting *switched-capacitor filters* have been proven to be very reliable and are used in numerous commercially successful products. After a brief look at the MOS switch, we shall in this chapter introduce the fundamentals of switched-capacitor (SC) filters.

17.1 THE MOS SWITCH

Figure 17.1a shows an MOS transistor. If this transistor is to be used as a switch, the voltage between source and gate is either zero, $V_{GS} = 0$, so that the transistor is OFF and no current flows, or it is much larger than the threshold voltage V_t, and the transistor is ON so that current can flow.

The path of interest is between source S and drain D, having the resistance R_{DS}. When the transistor is in OFF mode, R_{DS} is large, perhaps 100–1000 MΩ. When the transistor is in ON mode, R_{DS} is much smaller, perhaps between 5 and 10 kΩ, depending on transistor size. Thus the ratio between the two states is of the order of 10^5 or 100 dB. These facts are summarized in Fig. 17.1b along with a simplified model of the switch: either a short circuit or an open circuit. An alternative representation of the switch operation is depicted in Fig. 17.1c; the switch is open or closed depending on the value of v_{GS}: open when v_{GS} is low, closed when v_{GS} is high. The voltage waveform that is used to activate the switch is shown in Fig. 17.2. We have changed the notation from v_{GS} to ϕ to keep with common usage. $\phi(t)$ alternates between a low value (less than the threshold voltage to keep the switch OFF) and a high state (near V_{DD}, say 5 V for n-channel devices, to turn the switch ON). Thereby it controls the state of the switch; the waveform of $\phi(t)$ is a pulse train with period T, the clock period; $1/T = f_c$ is the *clock frequency*. It is convenient to count the period from the falling edge of the waveform.

In switched-capacitor (SC) circuits we need to operate at least two sets of switches whose ON–OFF states alternate: one set is ON when the other is OFF and vice versa. This is accomplished by a *two-phase clock*, ϕ_1 and ϕ_2, pictured in Fig. 17.3. It is required that ϕ_1 and ϕ_2 have the same frequency and also that they are *nonoverlapping*, that is, ϕ_1 and ϕ_2 are

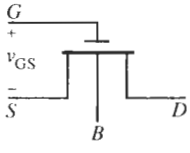

(a)

Condition	State	Equivalent Resistor	Model
$v_{GS} \gg V_t$	On	10 kΩ	Short
$v_{GS} < V_t$	Off	100 MΩ	Open

(b)

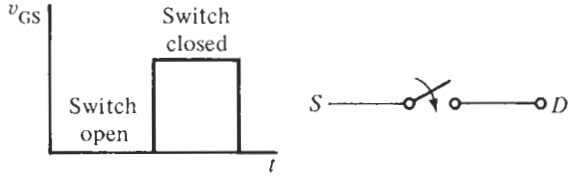

(c)

Figure 17.1 The MOS transistor: (a) schematic; (b) switch operation and model; (c) switch operation as a function of the gate-to-source voltage.

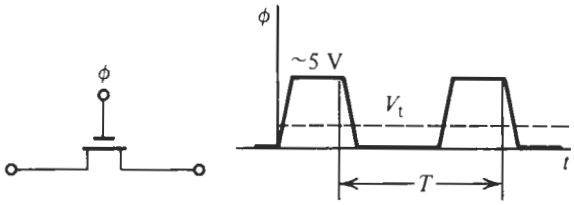

Figure 17.2 Clock waveform to activate the switch.

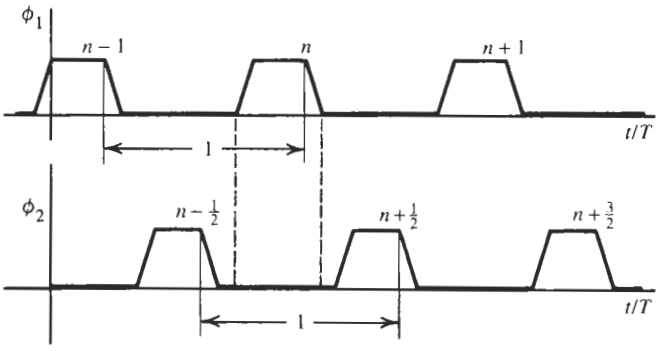

Figure 17.3 A two-phase nonoverlapping clock.

not high at the same time. It is customary to normalize the time axis by the clock period, t/T, and to denote the position of the pulses only by an integer as is shown in Fig. 17.3. For the notation of the pulse positions for ϕ_1 at $n-1$, n, $n+1$, etc., the pulse positions for ϕ_2 are at $n-1/2$, $n+1/2$, $n+3/2$, etc. When two MOS switches that are controlled by ϕ_1 and ϕ_2 are connected in series as in Fig. 17.4a, the capacitor C_R is connected to node 1 during ϕ_1 (when ϕ_1 is high) and to node 2 during ϕ_2 (i.e., when ϕ_2 is high), but at no time are nodes 1 and 2 directly connected through the two switches because one of them is always open. This situation is represented symbolically in Fig. 17.4b, or perhaps more clearly, in Fig. 17.4c.

A useful extension of this scheme is shown in Fig. 17.5. During ϕ_1 the capacitor is connected to nodes 1 and 2, during ϕ_2 to nodes 3 and 4. As an application of this configuration consider the circuit in Fig. 17.5b. During ϕ_1 the switches are in position a and the capacitor C_R charges to the value $v_C = v_{1a} - v_{1b}$. When ϕ_2 is high and the switches are thrown to position b, the voltage v_2 equals v_C,

$$v_2 = v_{1a} - v_{1b}$$

that is, v_2 is the *difference* between the two input voltages. If we set the input v_{1a} to zero and label $v_{1b} = v_1$, we find that the output is the negative of the input,

$$v_2 = -v_1$$

and we have realized an *inversion* using only switches and a capacitor.

Along with opamps and unswitched capacitors, the configuration in Fig. 17.4 is the fundamental building block of an SC filter: the SC resistor. We will examine its behavior in the next section and see how it helps us to realize accurate large time constants to obtain low-frequency poles and zeros.

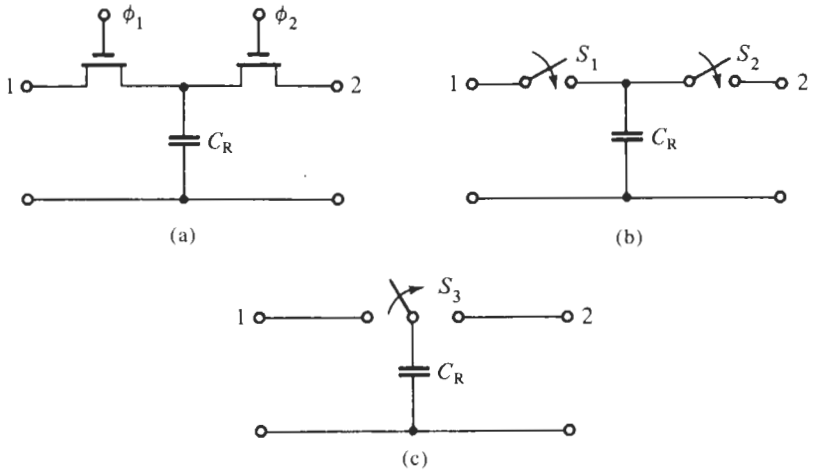

Figure 17.4 A capacitor with two MOS switches driven by a two-phase clock: (a) circuit; (b) and (c) symbolic representations.

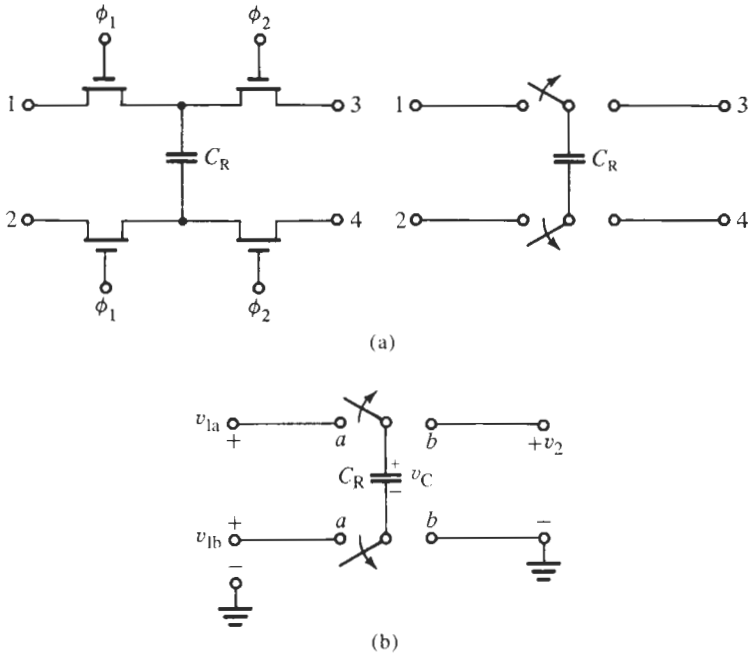

Figure 17.5 A capacitor between four MOS switches driven by a two-phase clock: (a) circuit; (b) circuit to form a voltage difference.

17.2 THE SWITCHED CAPACITOR

Consider again the circuit in Fig. 17.4, where the capacitor[1] C_R is connected to the voltage v_1 during phase ϕ_1; it stores the charge $q_1 = C_R v_1$. If we connect C_R thereafter in phase ϕ_2 to the voltage v_2, the capacitor recharges to $q_2 = C_R v_2$. The charge packet transferred from v_1 to v_2 is, therefore,

$$\Delta q = q_1 - q_2 = C_R (v_1 - v_2) \tag{17.1}$$

Let now the switch S be flipped periodically, with clock period T, such that the clock frequency $f_c = 1/T$ is so large compared to the signal frequency $\omega = 2\pi f$ of the two voltage "sources" v_1 and v_2,

$$f_c \gg \omega = 2\pi f \tag{17.2}$$

that these two signals can be assumed to be constant over the period T. Since the charge packets get transferred between the two nodes during each clock interval, we can consider the average of the transferred charge packets as a current

$$i \approx \frac{\Delta q}{T} = \Delta q f_c = f_c C_R (v_1 - v_2) \tag{17.3}$$

This equation tells us that as long as the condition (17.2) is valid, the *switched capacitor* in Fig. 17.6a behaves *approximately* like the equivalent resistor

$$R_{equ} \approx \frac{v_1 - v_2}{i} = \frac{1}{f_c C_R} \tag{17.4}$$

as shown in Fig. 17.6b, because both circuits would draw the same current i.

Let us point out here that this method of implementing a resistor solves the three main difficulties in building a low-frequency analog integrated filter:

1. Frequency parameters, i.e., RC time constants, do not depend on *absolute* values of resistors and capacitors but are set by *ratios* of MOS capacitors and by a *clock frequency:*

$$\tau = R_{equ} C = \frac{1}{f_c C_R} C = \frac{1}{f_c} \frac{C}{C_R}$$

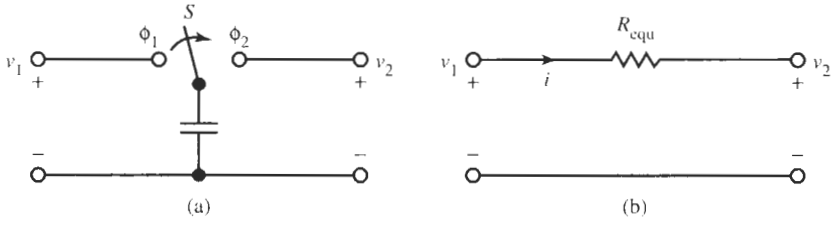

Figure 17.6 (a) A switched capacitor and (b) its resistor equivalent.

[1] The subscript R is to indicate that this switched capacitor will be used to represent a resistor.

As we discussed in the previous chapter, ratios of MOS capacitors can be implemented repeatably with an accuracy of about 0.1% or better; further, clock frequencies are obtained from a crystal-controlled clock generator and are very precise and stable.

2. It follows that accurate frequency parameters can be *designed* and *realized*, and *no postdesign tuning* is required.
3. Large time constants can be obtained on a very small silicon area: by Eq. (17.4), a 1-pF capacitor clocked at 100 kHz results in $R_{equ} = 10$ MΩ. The required silicon area is of the order of only $(50\ \mu m)^2$. Because capacitors with values as small as a fraction of 1 pF can be designed routinely, large SC "resistors" can be built on a very small silicon area. This permits us to design voice-band filters: using, for example, $C = 5$ pF for the integrator capacitor, the resulting RC time constant is $\tau = 50\ \mu s$, corresponding to a frequency of approximately 3.2 kHz, appropriate for the telephone base band.

Based on these initial considerations we are led to conclude that the SC method looks promising for the design of integrated filters at low frequencies, if we can develop suitable filter circuits. By following the simple equivalence of a resistor and a switched capacitor that is expressed in Eq. (17.4), we ought to be able to take any resistor R in the active RC filters developed earlier in our study and replace R by a capacitor $C_R = 1/(Rf_c)$. We assume, of course, that we choose a clock frequency f_c that is much larger than the signal frequency as was required by Eq (17.2). To support our motivation further let us take, e.g., an integrating summer, Fig. 17.7a, that was identified as a fundamental active filter building block. The active RC circuit in Fig. 17.7a realizes

$$V_{out} = -\frac{1}{sC_F}(G_1V_1 + G_2V_2) - \frac{C_3}{C_F}V_3 \tag{17.5}$$

Using our approximate resistor equivalent, this basic circuit is readily implemented in the SC approach as is illustrated in Fig. 17.7b: we replace the resistors by switched capacitors, $G_i = f_cC_i, i = 1, 2$, and assume the switches are clocked at f_c with $f_c \gg 2\pi f$. On the $j\omega$-axis, the describing equation is then:

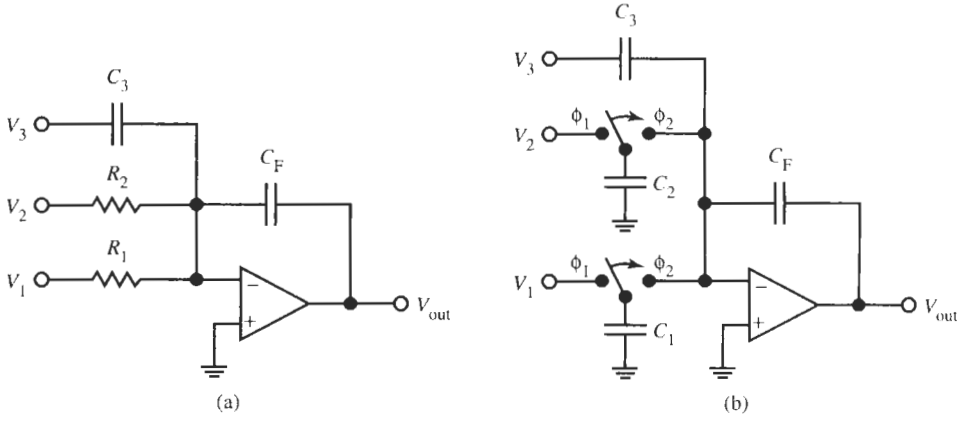

Figure 17.7 (a) An active RC integrating summer; (b) its SC equivalent.

$$V_{out} = -\frac{1}{j\omega C_F}(f_c C_1 V_1 + f_c C_2 V_2) - \frac{C_3}{C_F}V_3$$
$$= -\frac{f_c}{j\omega C_F}(C_1 V_1 + C_2 V_2) - \frac{C_3}{C_F}V_3 \qquad (17.6)$$

The one-to-one correspondence between the terms in Eqs. (17.5) and (17.6) for the two realizations is apparent. Extensions to additional capacitive or resistive inputs are obvious.

Just as in this example, we can design SC circuits from active *RC* prototypes by use of the simple analogy of Eq. (17.4). We can do this for relatively undemanding specifications, provided only that the condition in Eq. (17.2) is satisfied, that is, the clock frequency f_c must be "much larger" than the highest signal frequency f. In the following sections, we will introduce a number of SC building blocks and helpful procedures for the design of filters based on the simple switched-capacitor–resistor equivalent. This material will allow us to design simple SC filters by making use of the many active *RC* design techniques presented in this book. It will allow us to arrive at preliminary designs with circuit structures and component values without having to resort to more complicated mathematical treatment. But to be able to design high-performance precision circuits, we must understand the meaning of "much larger" in $f_c \gg 2\pi f$, and the resulting limitations and approximations. The difficulties arise because, although analog, the signals are not processed in a *continuous-time* fashion. Rather, they are *sampled* by the clocked switches at the frequency f_c, i.e., we are dealing with a *sampled-data system*. We shall investigate the fundamentals and some consequences of sampling and sampled-data operation in Section 17.5.

17.3 FIRST-ORDER BUILDING BLOCKS

A problem arises when implementing the simple switched capacitor in Fig. 17.4a. Integrated capacitors are typically constructed as two polysilicon electrodes separated by a thin oxide on the IC chip, so-called double-poly capacitors. This configuration rests on the thick oxide on top of the substrate. Figure 17.8 shows a sketch of the integrated capacitor C_R with metal connections and several parasitic capacitors. As we discussed in Chapter 16, the largest of these is the capacitor C_b between bottom plate and substrate (ac ground). C_b may be as large as 10 to 20% of the nominal capacitor C_R. The capacitor C_m from the top plate (various metal interconnections) to the substrate (1 to 2% of C_R) must be considered as well, in addition to parasitic capacitors C_{sw} arising from the switches. Thus, the capacitor can be represented by the small-signal model in Fig. 17.8b. Figure 17.9a illustrates how all these parasitics enter an SC integrator. Notice that all capacitors at the inverting input node of the opamp are connected to virtual ground; thus, they and also the bottom plate capacitor of C_R are always shorted. The bottom plate capacitor of C_F as well as C_{sw} at the left side of switch ϕ_1 are voltage driven and, therefore, have no effect. Thus, the relevant circuit is that of Fig. 17.9b, which shows that C_R is in parallel with an unknown and likely nonlinear parasitic capacitor C_p that may be as large as 0.2 pF and prevents us from achieving accurate designs with minimum-size capacitors. Since the realized SC resistor is now $1/[f_c(C_R + C_p)]$, the incorrect integrator time constant of this circuit is

$$\tau = \frac{C_F}{f_c(C_R + C_p)} = \frac{1}{f_c}\frac{C_F}{C_R}\frac{1}{1 + C_p/C_R} = \tau_0\frac{1}{1 + C_p/C_R}$$

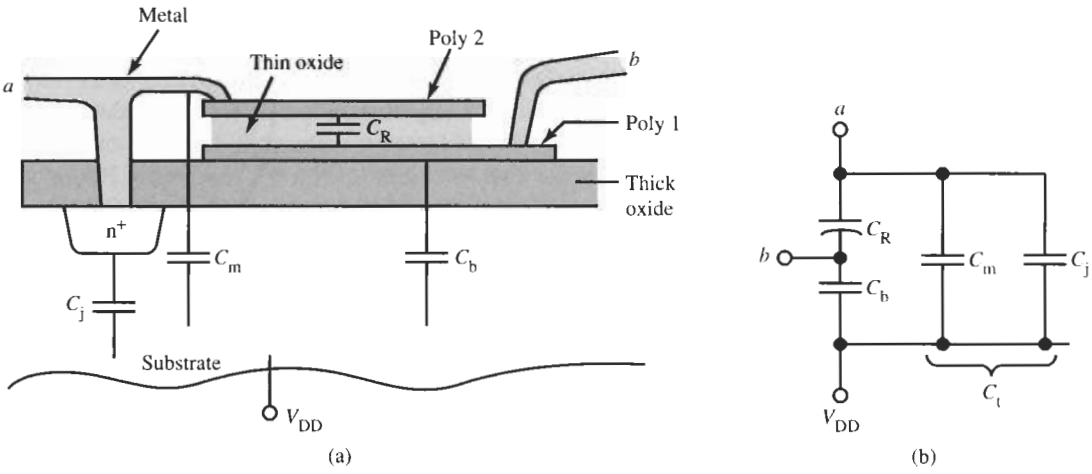

Figure 17.8 (a) Implementation of a double-poly integrated capacitor; (b) small-signal model.

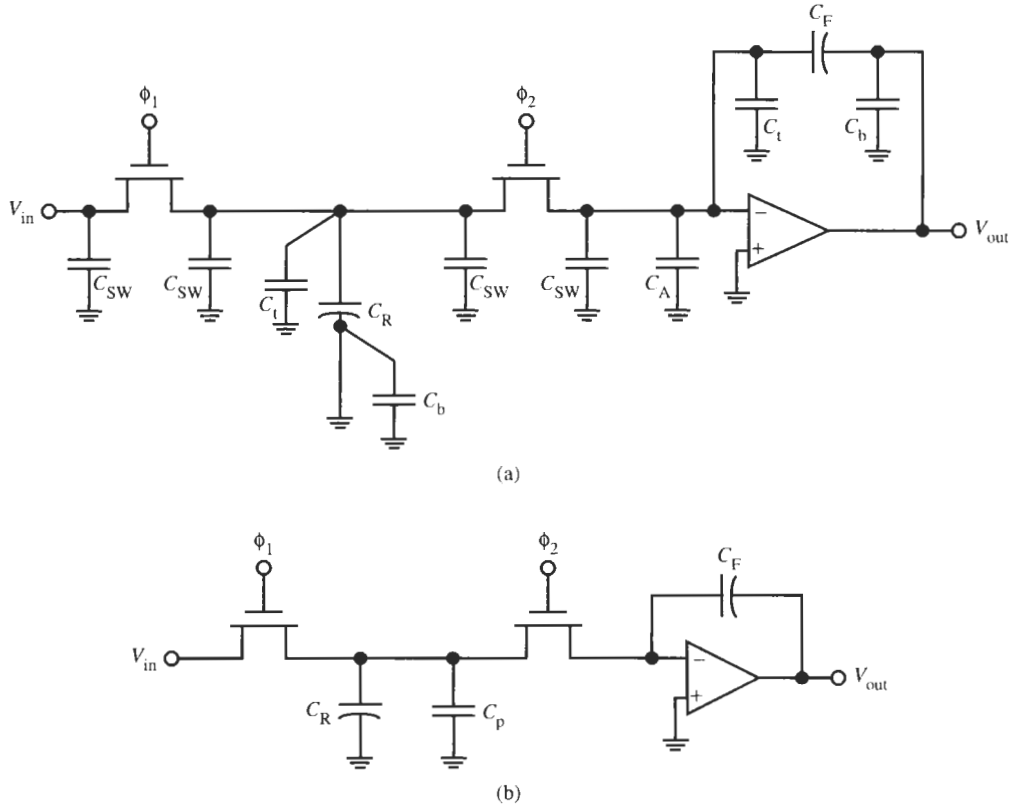

Figure 17.9 (a) SC integrator with all parasitic capacitors: C_{sw}, switch parasitics; C_t, C_b, top plate, bottom plate parasitic; C_A, opamp input parasitic; (b) SC integrator with operative parasitics.

For minimum-size capacitors, this error may be too large to accept.

Fortunately, circuit techniques were invented to eliminate the effects of any remaining parasitic capacitors. These so-called *parasitics-insensitive* circuits make use of a different switch configuration that prevents any charges on parasitic capacitors from contributing to the useful signal. Figure 17.10 shows the parasitics-insensitive SC resistors at the input of integrators. When the two switches in Fig. 17.10a are in Position 1 as shown ($\phi = \phi_1$ in the MOS version), the charge on C_R equals $\Delta Q = C_R(V_1 - 0)$ (remember that the opamp input is virtual ground). As the opamp input is an open circuit, the current to charge C_R has to flow to the right through C_F where it changes the charge on C_F by subtracting ΔQ from its charge $C_F V_{out}$. When the switches are in Position 2 ($\phi = \phi_2$), C_R discharges completely and C_F retains its charge until the next phase ϕ_1. Therefore, when the switching frequency is f_c, the average current $I = +f_c \Delta Q = +f_c C_R V_1$ flows to the right into C_F and the integrator is inverting as we expect from the active *RC* analog:

$$\frac{V_{out}}{V_1} = -\frac{f_c C_R}{j\omega C_F} \tag{17.7}$$

This is the result in Eq. (17.6) with $V_2 = V_3 = 0$. The MOS implementation of the inverting integrator is also shown in Fig. 17.10a along with the relevant parasitics $C_{p1} = C_{sw} + C_t$ and $C_{p2} = C_{sw} + C_b$, respectively. Note that although during phase ϕ_1 these two parasitic capacitors

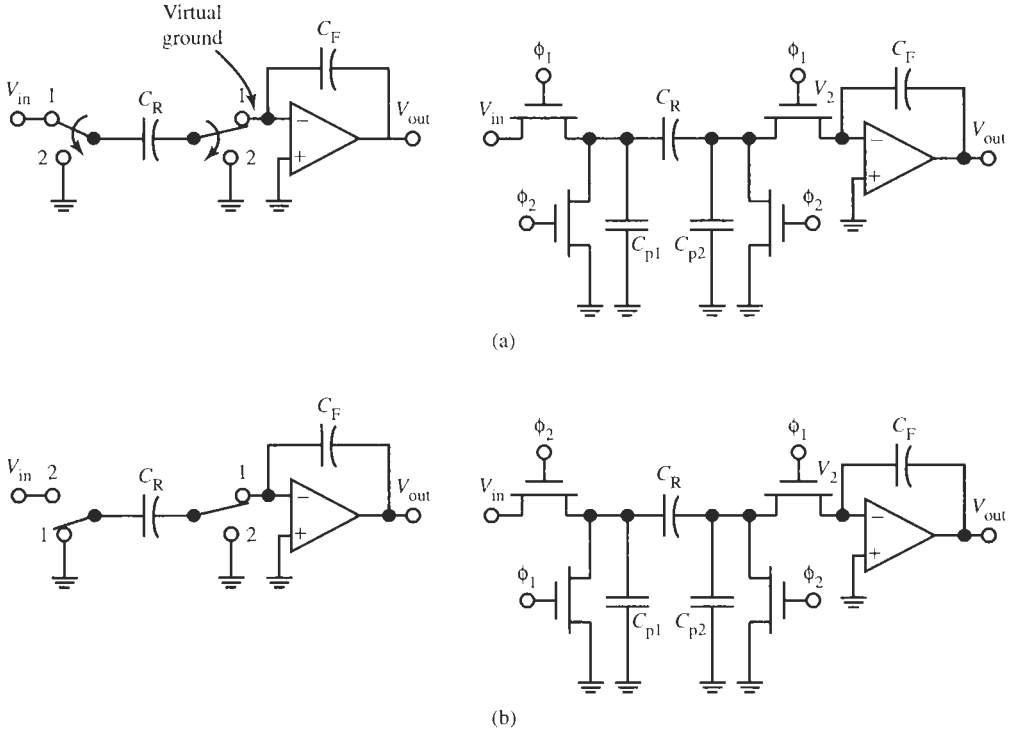

Figure 17.10 Parasitics-insensitive SC integrators: (a) inverting; (b) noninverting. The output voltage is sampled during phase ϕ_1.

are charged[2] to V_{in} and V_2, respectively, during phase ϕ_2 they both discharge harmlessly to ground without transferring any charges to node V_{in} or to C_F.

A small but very useful modification of this topology is shown in Fig. 17.10b. By having inverted the switch phases at the circuit input we observe that during phase ϕ_2 C_R is again charged with $Q_1 = C_R V_1$ but no current flows through C_F to change its charge. During ϕ_1 the capacitor C_R is connected with reversed polarity to the opamp input and has to discharge because it is now connected between ground and virtual ground. The *negative* discharging current $I = -f_c \Delta Q = -f_c C_R V_1$ flows into C_F, adding to its charge. It follows that by a simple change of switch phasing the integrator is now noninverting:

$$\frac{V_{out}}{V_1} = \frac{f_c C_R}{j\omega C_F} \tag{17.8}$$

The obtained effect is as if we had replaced the input resistor in the active *RC* integrator by a negative resistor. If we examine the operation of the switches in Fig. 17.10b carefully, it becomes clear that any charges imparted on the parasitic capacitors are again discharged harmlessly to ground. During ϕ_2, C_{p1} charges to $C_{p1} V_{in}$ and C_{p2} is shorted; during ϕ_1 the charge on C_{p1} is shorted to ground and C_{p2} stays discharged between ground and virtual ground. Because of the importance of eliminating parasitic effects from SC filter operation, in practice, all SC circuits are designed with parasitics-insensitive switch configurations.

EXAMPLE 17.1

Construct a first-order SC lowpass filter to process the difference of two voltages V_1 and V_2. V_1 is to be multiplied by a low-frequency gain of 2 dB and V_2 by 0 dB. The lowpass filter should have the cut-off frequency $f_0 = 3.6$ kHz. Assume that the clock frequency $f_c = 128$ kHz is large enough so that simple design based on active *RC* prototypes is adequate.

Solution

Because we can implement effective negative resistors in SC filters, we may start the design from the active *RC* prototype circuit in Fig. 17.11a. It is described by the equation

$$G_1 V_1 - G_2 V_2 + (sC_F + G_3) V_{out} = 0$$

or

$$V_{out} = -\frac{1}{sC_F + G_3} (G_1 V_1 - G_2 V_2) \tag{17.9}$$

R_3 is determined from the cut-off frequency f_0 as $R_3 = 1/(\omega_0 C_F)$; choosing $C_F = 2$ pF, we obtain

$$R_3 = 1/\left(2\pi \times 3600 \times 2 \times 10^{-12}\right)\ \Omega = 22.10\ \text{M}\Omega$$

[2] Of course $V_2 = 0$ because of the virtual ground node.

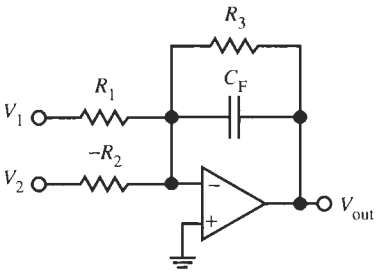

(a)

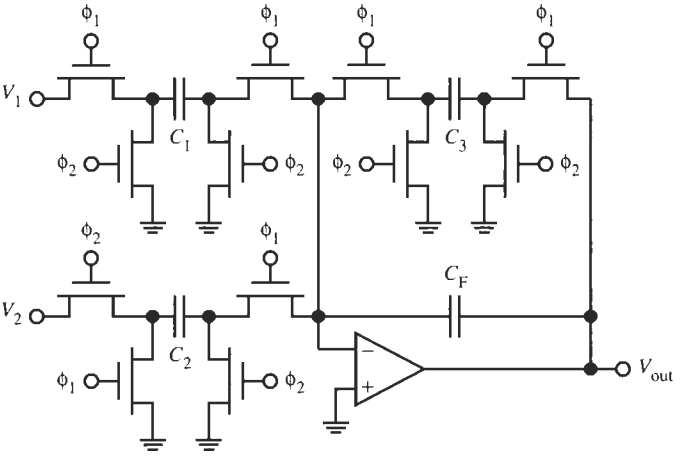

(b)

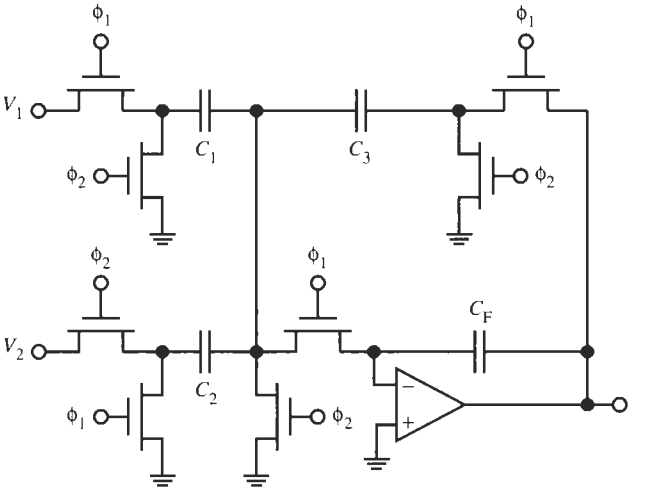

(c)

Figure 17.11 Circuits for Example 17.1: (a) active *RC* prototype; (b) SC lowpass filter; (c) the circuit of (b) after using switch sharing. The output voltage is sampled during phase ϕ_1.

The specified low-frequency gain constants of the filter for V_1 and V_2, respectively, are $R_3/R_1 = 1.259$ (2 dB) and $R_3/R_2 = 1$ (0 dB). The two resistors are, therefore, $R_1 = R_3/1.259 = 17.55\ \text{M}\Omega$ and $R_2 = R_3 = 22.19\ \text{M}\Omega$. The prescribed clock frequency is 128 kHz with switched capacitors of value $C_i = 1/(f_c R_i), i = 1, 2, 3$. The numbers are

$$C_1 = 0.445\ \text{pF}, \quad C_2 = C_3 = 0.354\ \text{pF}$$

We use parasitics-insensitive switch arrangements so parasitics are of no concern, even if the nominal capacitors are very small. Paying attention to phasing the switches appropriately for the "negative resistor," we obtain the final SC circuit in Fig. 17.11b.

If we examine the SC circuit in Fig. 17.11b carefully we notice that it contains redundant switches: during ϕ_1, the capacitors C_1, C_2, and C_3 are connected to the inverting opamp input terminal, and during ϕ_2 they are connected to ground. This means that the three pairs of switches to the right of C_1 and C_2 and to the left of C_3 perform the same function and can be shared by the three capacitors. The resulting simplified circuit is shown in Fig. 17.11c. It is an example of *switch sharing* that is employed in many practical situations to yield simpler circuitry.

We have now designed inverting and noninverting integrators and have seen how lossy integrators and integrators with differential inputs (Fig. 17.11) can be realized. A special case of the circuit in Fig. 17.11 is the bilinear filter in Fig. 17.12. The active *RC* prototype in Fig. 17.12a realizes

$$\frac{V_{\text{out}}}{V_1} = -\frac{sC_1 + G_2}{sC_F + G_3} \tag{17.10}$$

If we assume a sufficiently high clock frequency f_c, the approximate SC equivalent in Fig. 17.12b realizes

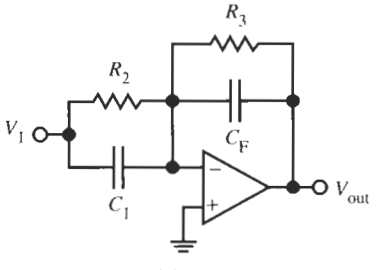

(a)

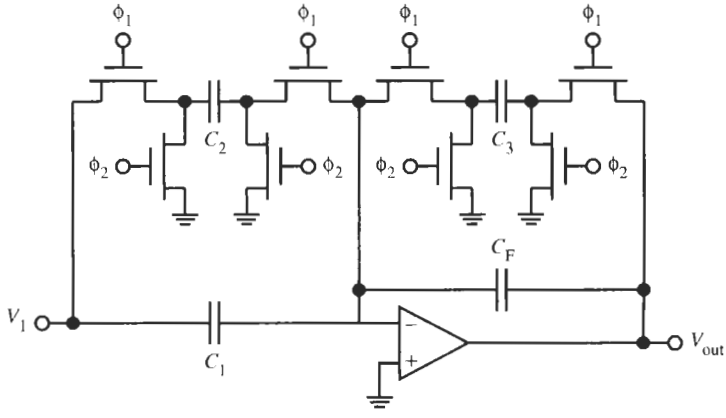

(b)

Figure 17.12 (a) A first-order active *RC* filter; (b) the SC equivalent of the circuit in (a) where switch sharing can, of course, be used; (c) changing the switch phasing results in a right half-plane zero. The output voltage is sampled during phase ϕ_1.

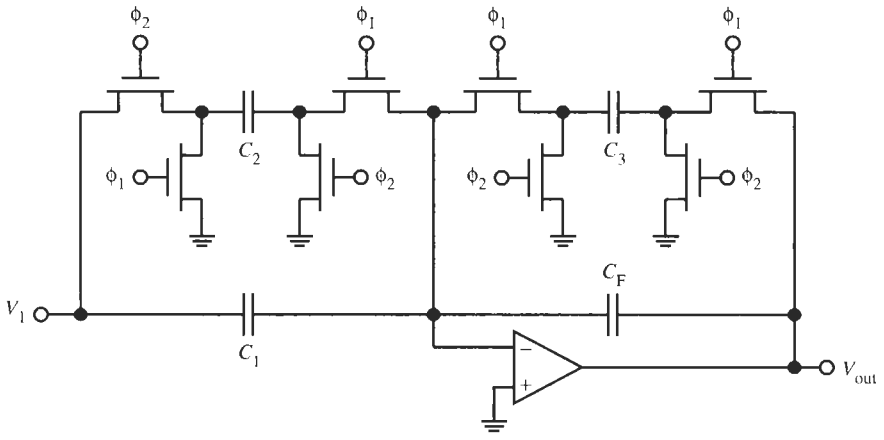

(c)

Figure 17.12 Continued

$$\frac{V_{out}}{V_1} = -\frac{sC_1 + f_c C_2}{sC_F + f_c C_3} \tag{17.11a}$$

If we change the switch phasing to the left of capacitor C_2 as is shown in Fig. 17.12c we obtain a minus sign in the numerator

$$\frac{V_{out}}{V_1} = -\frac{sC_1 - f_c C_2}{sC_F + f_c C_3} \tag{17.11b}$$

with a right half-plane zero and the possibility of realizing a first-order SC allpass circuit.

EXAMPLE 17.2

Design an SC filter to realize the transfer function

$$T(s) = \frac{(s + 100)(s + 400)}{(s + 200)^2}$$

It is a band-enhancement circuit that finds application in the gain equalization of transmission systems. The frequency is not normalized, i.e., the zeros are at 19.9 and 63.7 Hz, and the double pole is at 31.8 Hz. The Bode plot is shown in Fig. 17.13.

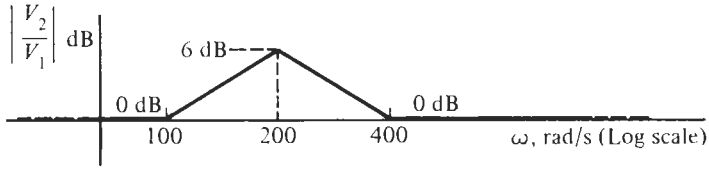

Figure 17.13 Bode plot of the gain equalizer of Example 17.2.

Solution

Since the frequencies of interest are very low, a direct translation of the active *RC* prototype can be used, allowing us to apply design techniques we studied earlier. We factor the transfer function into the product of two first-order terms,

$$T(s) = T_1 T_2 = \frac{s + 100}{s + 200}\frac{s + 400}{s + 200}$$

and use the circuit in Fig. 17.12a described by Eq. (17.11a). Let us use $C_1 = C_F = C = 10$ pF in both sections to give

$$R_{21} = \frac{1}{100C} = 10^9\ \Omega, \quad R_{22} = \frac{1}{400C} = 250\ \text{M}\Omega, \quad R_{31} = R_{32} = \frac{1}{200C} = 500\ \text{M}\Omega$$

Let us use $f_c = 10$ kHz to get the switched capacitors $C_i = 1/(f_c R_i)$:

$$C_{21} = \frac{1}{10{,}000R_{21}} = 0.1\ \text{pF}, C_{22} = \frac{1}{10{,}000R_{22}} = 0.4\ \text{pF}, C_{31} = C_{32} = \frac{1}{10{,}000R_{31}} = 0.2\ \text{pF}$$

The cascade circuit is shown in Fig. 17.14, both without and with switch sharing.

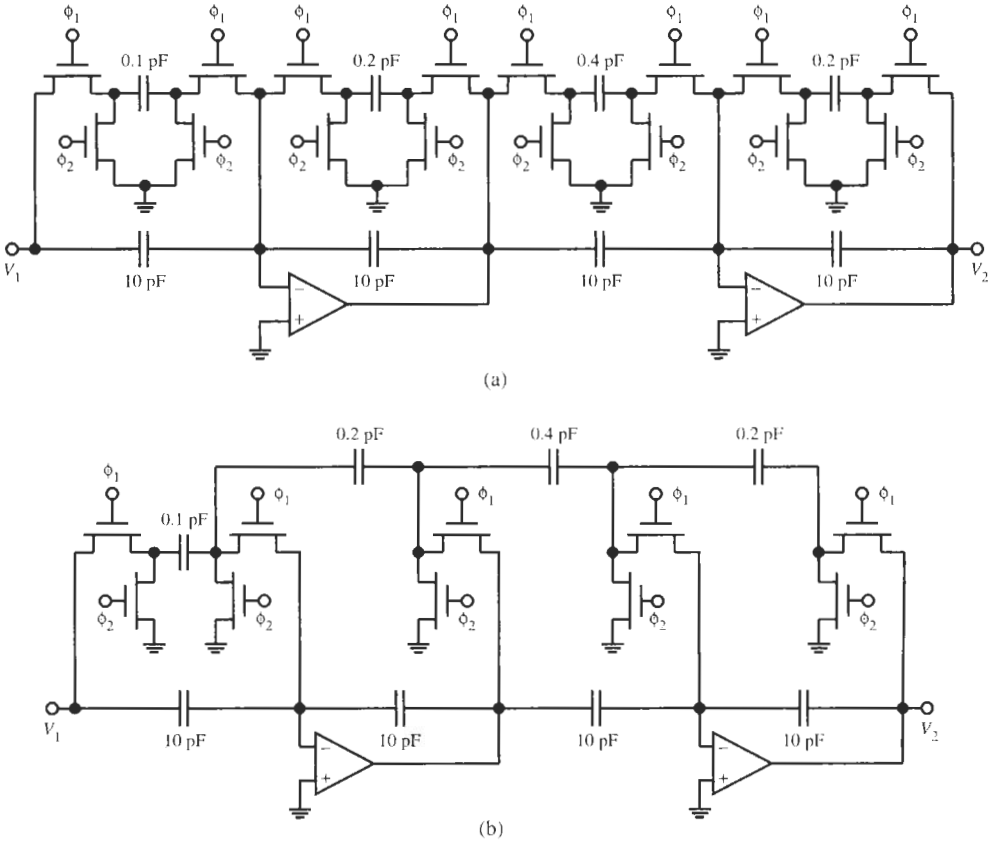

Figure 17.14 (a) The SC gain equalizer for Example 17.2; (b) the circuit with switch sharing.

The circuit in Fig 17.12b can also be used to build a circuit with frequency-independent gain. If we pick $C_1 = KC_F$ and $C_2 = KC_3$ in the transfer function in Eq. (17.11a) we obtain

$$\frac{V_2}{V_1} = -\frac{sKC_F + f_cKC_3}{sC_F + f_cC_3} = -K \tag{17.12}$$

Note that from this equation it appears that we could also delete the unswitched capacitors C_1 and C_F *or* the switched capacitors C_2 and C_3. This is not recommended because with C_F absent, the opamp would operate in open loop during phase ϕ_2 and with the switched capacitor C_3 absent, the opamp is in open loop at dc. In either case the opamp can possibly go into saturation so that the circuit will not function. A problem with the circuit is that the opamp's dc offset will be amplified by K as well. Modified gain circuits exist which avoid this problem (Gregorian, 1981; Matsumoto and Watanabe, 1987).

17.4 SECOND-ORDER SECTIONS

To realize second-order SC filters, it is intuitive and convenient to start again from a well-known good active *RC* filter and use the switched-capacitor–resistor equivalent to transform the circuit into the SC domain. This circuit is then usable if we remember the approximation made ($f_c \gg 2\pi f$) and that for precision design the sampled-data procedures to be discussed in Section 17.5 must be followed.

A suitable starting point is the Tow–Thomas biquad of Fig. 4.10. This is a circuit with an inverting and a noninverting integrator in a loop. The noninverting integrator was realized as a Miller integrator in cascade in an inverter. As we have seen in Figs. 17.10 and 17.11, in the present case the inverter is not needed because with SC techniques we can realize a noninverting integrator simply by phasing the switches appropriately and, in effect, implement negative resistors. Thus, we combine two of the integrators in Fig. 17.7, add loss and use negative resistors to make one integrator noninverting. To obtain a general transfer function with arbitrary transmission zeros, we also allow capacitors and positive and negative resistors as feed-in components into both opamps. Figure 17.15a shows the configuration. If we write node equations for the inverting input of the two opamps, we obtain under the assumption of ideal opamps, i.e., $V_{1-} = V_{2-} = 0$:

$$V_{in}(sC_4 + G_6 - G_7) + V_1sC_1 + V_2(sC_3 + G_8) = 0 \tag{17.13a}$$

$$V_{in}(sC_5 + G_{11} - G_{12}) - V_1G_9 + V_2(sC_2 + G_{10}) = 0 \tag{17.13b}$$

These two equations we can solve for V_1 and V_2; the result for V_2 is

$$\frac{V_2}{V_{in}} = -\frac{s^2C_1C_5 + s[C_1(G_{11} - G_{12}) + C_4G_9] + G_9(G_6 - G_7)}{s^2C_1C_2 + s(C_1G_{10} + C_3G_9) + G_8G_9} \tag{17.14}$$

At the output V_1 we also obtain a fully biquadratic transfer function but not substantially more flexibility. It is clear that this circuit can realize arbitrary transmission zeros because the numerator coefficients in Eq. (17.14) can be positive, negative, or zero. Every coefficient has an exclusive parameter to realize that coefficient without affecting the remaining ones. Replacing each resistor by its SC equivalent, $G_i = f_cC_i$, $i = 6, \ldots, 12$, results in the general switched-capacitor biquads in Fig. 17.15b and, after switch sharing, in Fig. 17.15c. Observe the

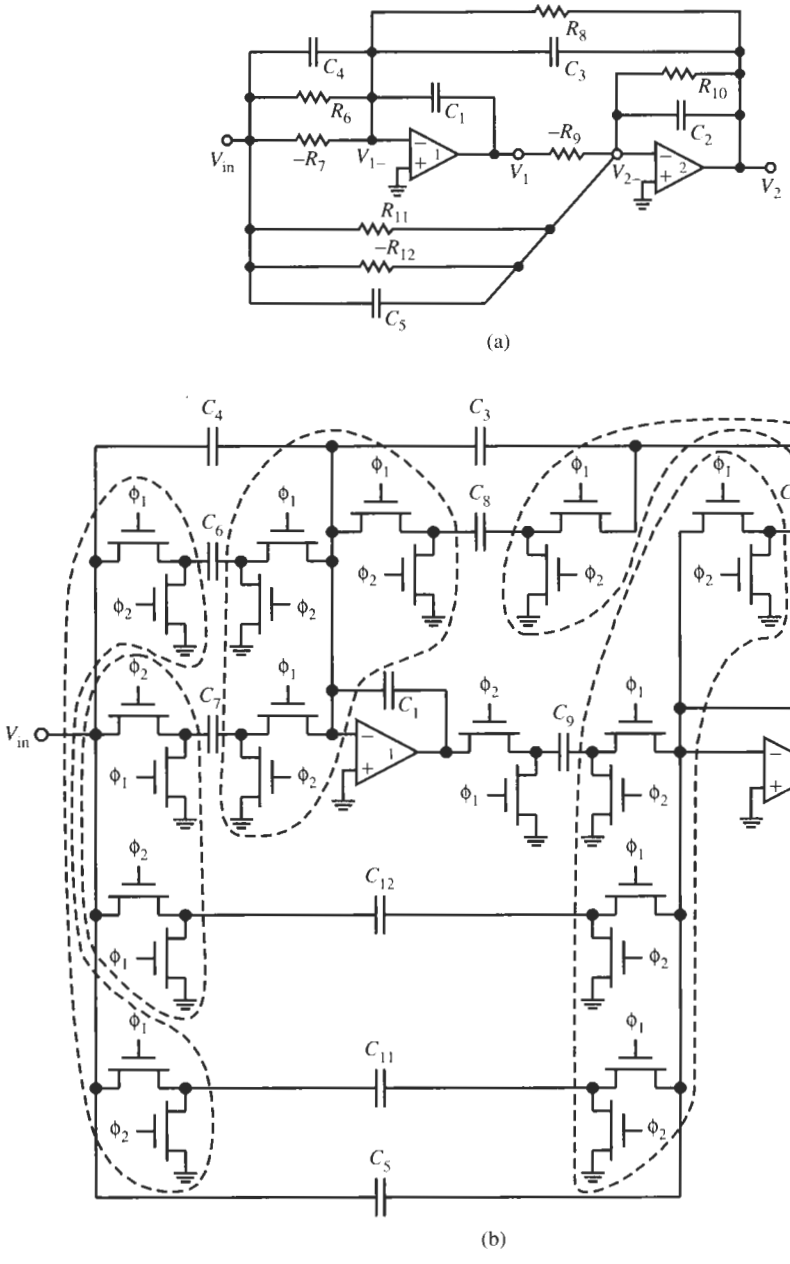

Figure 17.15 (a) General active *RC* biquad as a prototype for an SC biquad; (b) the SC version of the circuit in (a); the five sets of switches that can be shared are enclosed in dashed lines. (c) Simplified version of the circuit in (b) after using switch sharing. The output voltage is sampled during phase ϕ_1.

considerable reduction in the number of switches: from 28 in Fig. 17.15b to 12 in Fig. 17.15c. Switch sharing not only reduces the number of transistors, but, more importantly, it lessens the number of wires and simplifies significantly any routing problems on the chip. The approximate transfer function of the SC circuits is

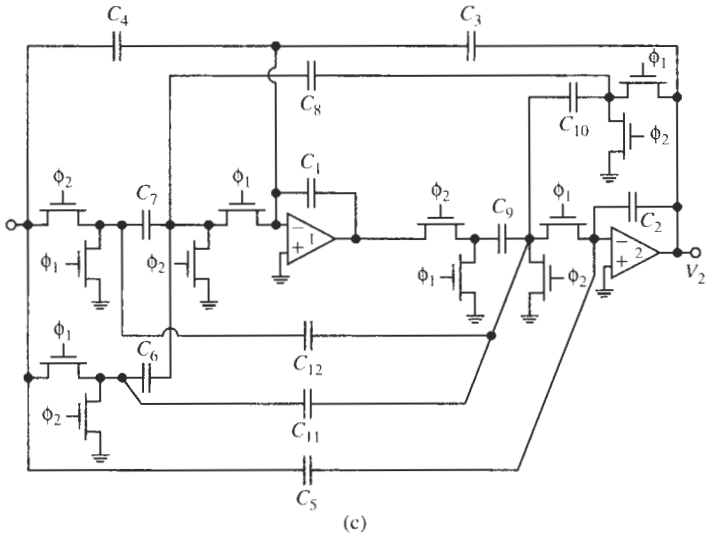

(c)

Figure 17.15 Continued

$$\frac{V_2}{V_{in}} = -\frac{s^2C_1C_5 + sf_c\left[C_1\left(C_{11} - C_{12}\right) + C_4C_9\right] + f_c^2C_9\left(C_6 - C_7\right)}{s^2C_1C_2 + sf_c\left(C_1C_{10} + C_3C_9\right) + f_c^2C_8C_9} \tag{17.15}$$

EXAMPLE 17.3

Realize a second-order SC lowpass filter with cut-off frequency $f_0 = 7.8$ kHz, quality factor $Q = 3.5$, and dc gain equal to 0 dB, noninverting. The clock frequency should be at least 20 times the signal frequency.

Solution

With the lowpass bandwidth equal to 7.8 kHz, assume the highest frequency of interest is 10 kHz so the clock frequency should be at least 200 kHz. Let us take $f_c = 200$ kHz. We use the transfer function of Eq. (17.15) and set $C_3 = C_4 = C_5 = C_6 = C_{11} = C_{12} = 0$. The result is

$$\frac{V_2}{V_{in}} = +\frac{f_c^2C_7C_9}{s^2C_1C_2 + sf_cC_1C_{10} + f_c^2C_8C_9} = \frac{f_c^2\dfrac{C_7C_9}{C_1C_2}}{s^2 + sf_c\dfrac{C_{10}}{C_2} + f_c^2\dfrac{C_8C_9}{C_1C_2}}$$

0-dB dc gain requires $C_7 = C_8$. Further we have

$$f_c\frac{C_{10}}{C_2} = \frac{\omega_0}{Q} \quad \text{and} \quad \omega_0^2 = f_c^2\frac{C_8C_9}{C_1C_2},$$

that is

$$Q = \frac{\omega_0}{f_c}\frac{C_2}{C_{10}} = \sqrt{\frac{C_2C_8C_9}{C_1}}\frac{1}{C_{10}} = 3.5 \quad \text{and} \quad f_c\sqrt{\frac{C_8C_9}{C_1C_2}} = 2\pi \times 7800\text{s}^{-1}$$

Let us select $C_1 = C_2$ and $C_8 = C_9$ to get

$$\frac{C_8}{C_1} = \frac{2\pi \times 7800\text{s}^{-1}}{f_c} = \frac{2\pi \times 7800}{200{,}000} = 0.245 \quad \text{and} \quad \frac{C_8}{C_{10}} = 3.5$$

We choose $C_1 = 5$ pF, $C_8 = 1.225$ pF, $C_{10} = 0.35$ pF to arrive at the final circuit in Fig. 17.16.

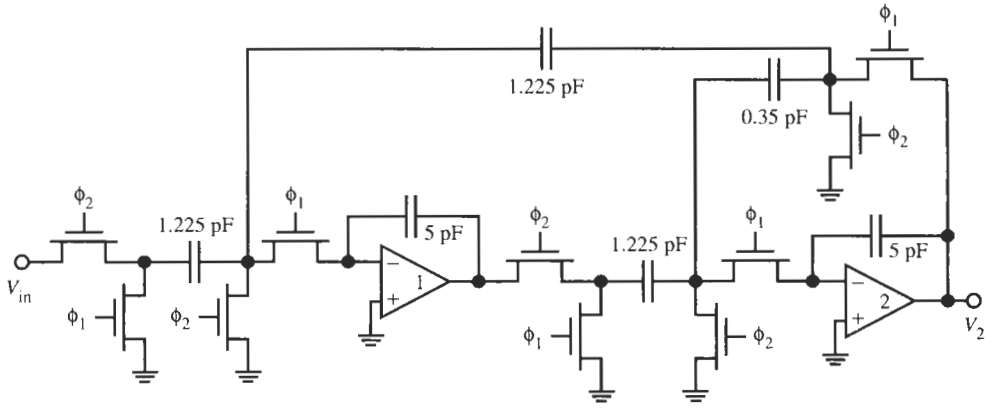

Figure 17.16 Switched-capacitor lowpass circuit for Example 17.3 with switch sharing. As always, the output voltage is sampled during phase ϕ_1.

Exactly as discussed in Section 5.3, the first- and second-order circuits we presented in this and the previous section can be connected in cascade to obtain higher order transfer functions.

We emphasized repeatedly that all circuits and transfer characteristics derived so far for the SC configurations are based on the assumption of Eq. (17.2), namely that the switching or clock frequency is much larger than the signal frequency, $f_c \gg 2\pi f$. Under this condition, the input branches of the SC integrators in Fig. 17.10 behave as positive or negative resistors, $R \approx \pm 1/(f_c C_R)$, and circuit operation is almost continuous. We used this approximation to permit us to derive SC circuits intuitively for undemanding applications from continuous-time active RC filters. However, as operating frequencies increase relative to the clock frequency, there are increasing deviations in the filters' characteristics from the specified performance. Thus, a more careful analysis is needed. In the next section we review the fundamental concepts of sampled-data operation, which will improve our understanding of switched-capacitor filters and let us assess the meaning of "f_c must be much larger than the signal frequency f." The material should be familiar to most students from elementary courses in system theory. A more thorough treatment is available in the literature (Oppenheim and Willsky, 1983).

17.5 SAMPLED-DATA OPERATION

For the following discussion refer to the two-phase clock waveforms in Fig. 17.3. Let us look at the operation of the inverting lossy integrator in Fig. 17.11b with $V_2 = 0$. The circuit is redrawn in Fig. 17.17a. For the two switch phases ϕ_1 and ϕ_2 the circuit looks like the configurations in Figs. 17.17b and 17.17c. It is perhaps easiest to obtain an exact analysis of the circuit by calculating the current $i(t)$ through the capacitor C_1 *during* ϕ_1 (Fig. 17.17b):

$$i(t) = C_1 \frac{dv_1(t)}{dt} = -(C_F + C_3) \frac{dv_{out}(t)}{dt} \tag{17.16}$$

To obtain an expression for the charges in the capacitors, we integrate this equation over time from the previous switch status $(n - 1/2)T$ during ϕ_2 until the present status nT in ϕ_1: We find

$$C_1 v_1(t)\Big|_{(n-1/2)T}^{nT} = -(C_F + C_3)\, v_{out}(t)\Big|_{(n-1/2)T}^{nT}$$

or

$$C_1 \{v_1(nT) - v_1[(n - 1/2)T]\} = -(C_F + C_3)\{v_{out}(nT) - v_{out}[(n - 1/2)T]\} \tag{17.17}$$

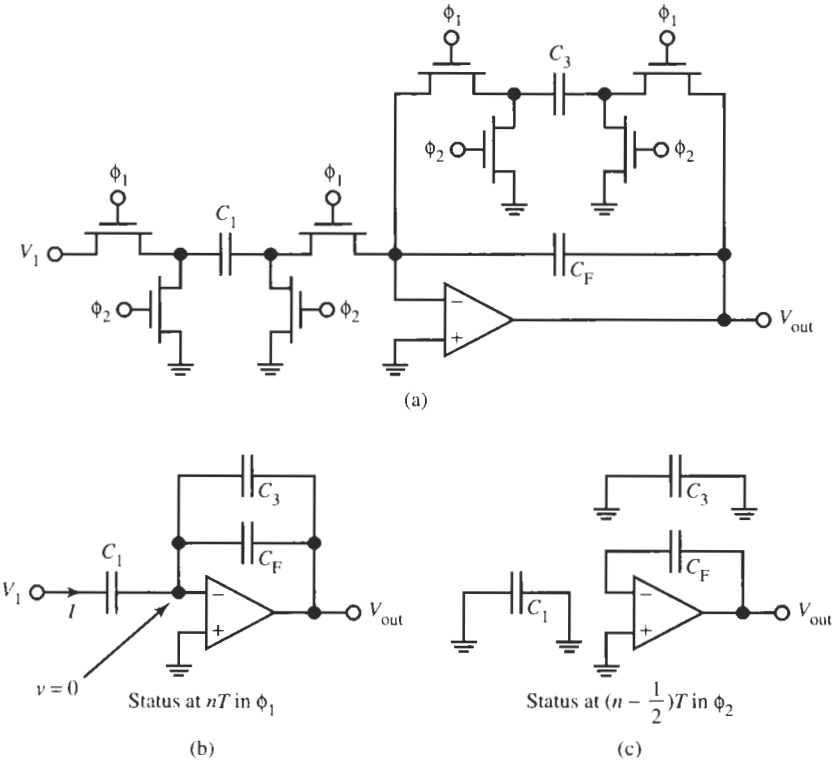

Figure 17.17 (a) The inverting lossy integrator; (b) and (c) configurations during the two switch phases.

The initial conditions at $t = (n - 1/2)T$ can be found from Fig. 17.17c: the capacitors C_1 and C_3 are discharged to ground, i.e., their charges are zero:

$$C_1 v_1[(n - 1/2)T] = 0 \quad \text{and} \quad C_3 v_{out}[(n - 1/2)T] = 0$$

Thus, we have from Eq. (17.17)

$$(C_F + C_3)\, v_{out}(nT) - C_F v_{out}[(n - 1/2)T] = -C_1 v_1(nT) \tag{17.18}$$

Further note that since the opamp was isolated since the time $(n - 1)T$, the voltage v_{out} maintained its value and $v_{out}[(n - 1/2)T] = v_{out}[(n - 1)T]$. Disconnecting C_3 does not change v_{out} because C_3 and C_F were in parallel. Thus, Eq. (17.18) can be rewritten as

$$C_F\{v_{out}(nT) - v_{out}[(n - 1)T]\} + C_3 v_{out}(nT) = -C_1 v_1(nT) \tag{17.19}$$

This is a *difference equation* for the relationship between the sample values of v_1 and v_2, rather than a differential equation that we would obtain for a continuous-time circuit.

In a similar fashion, we can analyze the noninverting lossy integrator of Fig. 17.11b, repeated in Fig. 17.18a, with $v_1 = 0$; it is shown for the two switch phases in Figs. 17.18b and c. Note that at time $t = (n - 1/2)T$, Fig. 17.18c, the charge $C_2 v_2[(n - 1/2)T]$ is established on

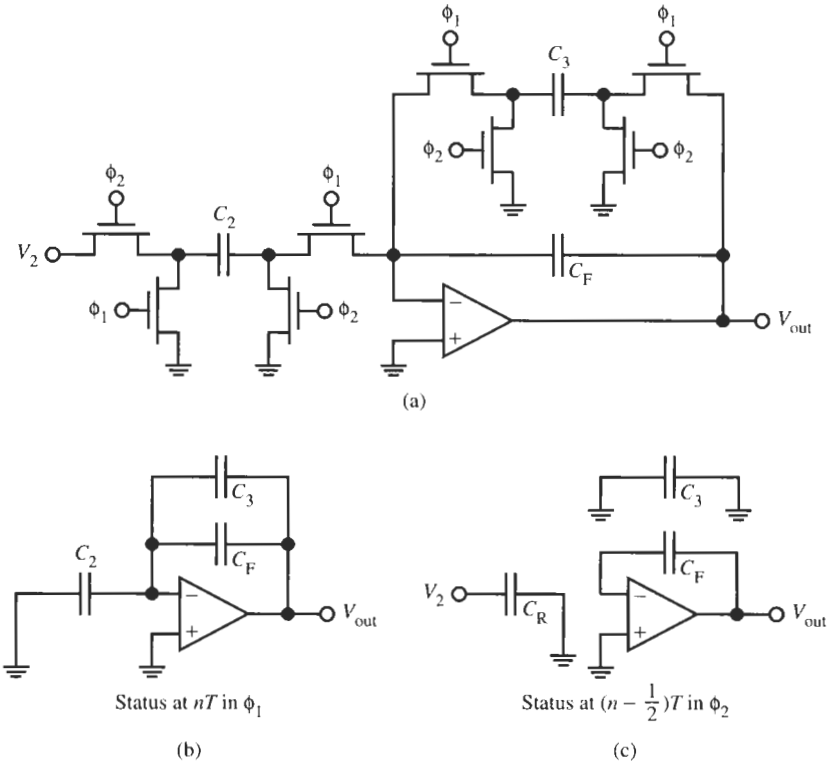

Figure 17.18 (a) The noninverting lossy integrator shown during the two switch phases: (b) ϕ_1 and (c) ϕ_2.

C_2 and $C_F v_{out}[(n-1/2)T]$ on C_F. Then, at time nT the polarity of the capacitor C_2 is inverted and C_2 and C_3 are added to the remaining circuitry, Fig. 17.18b. C_2 discharges because it is connected between ground and virtual ground, and adds its charge $-C_2 v_2[(n-1/2)T]$ to the charge on $(C_F + C_3)$. Thus, by charge conservation we obtain

$$(C_F + C_3)\, v_{out}(nT) = C_F v_{out}[(n-1/2)T] + C_2 v_2[(n-1/2)T]$$

Because we assumed that the switches flip instantaneously at the end (the falling edge, Fig. 17.3) of the ON periods, and no charges are transferred between time $(n-1)T$ and $(n-1/2)T$, we have $v_2[(n-1/2)T] = v_2[(n-1)T]$ and $v_{out}[(n-1/2)T] = v_{out}[(n-1)T]$. Consequently, the previous equation becomes

$$C_F\{v_{out}(nT) - v_{out}[(n-1)T]\} + C_3 v_{out}(nT) = C_2 v_2[(n-1)T] \tag{17.20}$$

We still simplify the two equations (17.19) and (17.20) by assuming a normalized time axis as in Fig. 17.3. This step corresponds to setting $T = 1$ and we obtain the difference equations

$$C_F\,[v_{out}(n) - v_{out}(n-1)] + C_3 v_{out}(n) = -C_1 v_1(n) \tag{17.21a}$$

for the inverting lossy integrator, and

$$C_F\,[v_{out}(n) - v_{out}(n-1)] + C_3 v_{out}(n) = C_2 v_2(n-1) \tag{17.21b}$$

for the noninverting lossy integrator.

Such difference equations in the sampled-data domain give us relationships between the sample values of v at the instants in time $t/T = n, n-1, n-2$, and so on. These difference equations are analogous to differential equations in the continuous-time domain; their solutions let us find the frequency response of the circuit. Without detailing rigorous mathematical conditions and proofs, let us use the Laplace transform and denote $\mathcal{L}\{v(t)\} = V(s)$ and recall that a function delayed by the time nT has the transform $\mathcal{L}\{v(t-nT)\} = V(s)e^{-snT}$. If we apply this formula to Eq. (17.21a), we obtain

$$C_F\left[V_{out}(n) - V_{out}(n)e^{-sT}\right] + C_3 V_{out}(n) = -C_1 V_1(n)$$

or

$$\frac{V_{out}(n)}{V_1(n)} = -\frac{C_1}{C_F\left(1 - e^{-sT}\right) + C_3} \tag{17.22a}$$

Similarly, we find from Eq. (17.21b),

$$C_F\left[V_{out}(n) - V_{out}(n)e^{-sT}\right] + C_3 V_{out}(n) = C_2 V_2(n)e^{-sT}$$

or

$$\frac{V_{out}(n)}{V_2(n)} = \frac{C_2 e^{-sT}}{C_F\left(1 - e^{-sT}\right) + C_3} \tag{17.22b}$$

It is interesting to evaluate the transfer functions of these two integrators on the $j\omega$-axis with our assumption that $f_c = 1/T \gg 2\pi f = \omega$, i.e., $\omega T \ll 1$, so that $e^{-j\omega T} \approx 1 - j\omega T$. For the inverting lossy integrator, Eq. (17.22a), we obtain

$$\frac{V_{out}}{V_1} = -\frac{C_1}{C_F\left(1 - e^{-j\omega T}\right) + C_3} \approx -\frac{C_1}{C_F(1 - 1 + j\omega T) + C_3}$$
$$= -\frac{C_1}{j\omega T C_F + C_3} = -\frac{f_c C_1}{j\omega C_F + f_c C_3}$$

Observe that this equation is equal to Eq. (17.9) with $V_2 = 0$, if we use the switched-capacitor–resistor equivalent $G_1 = f_c C_1$ and $G_3 = f_c C_3$. Similarly, we obtain for the noninverting lossy integrator, Eq. (17.22b),

$$\frac{V_{out}}{V_2} \approx \frac{C_2(1 - j\omega T)}{j\omega T C_F + C_3} \approx \frac{f_c C_2}{j\omega C_F + f_c C_3}$$

which we see is equal to Eq. (17.9) for $V_1 = 0$, $G_2 = f_c C_2$ and $G_3 = f_c C_3$. We observe, therefore, that as a first approximation we are justified in deriving an SC filter from a continuous-time active *RC* filter by simply substituting $G_i = f_c C_i$, provided that $f_c = 1/T \gg \omega$.

17.5.1 The z-Transform

It is customary to call

$$e^{sT} = z \tag{17.23}$$

Equation (17.23) defines the z-transform variable and one labels customarily $V(n) \Rightarrow V(z)$, where $V(z)$ is the (single-sided) z-transform of $V(n)$:

$$\mathcal{Z}\{v(n)\} = V(z) = \sum_{n=0}^{\infty} v(n)e^{-snT} = \sum_{n=0}^{\infty} v(n)z^{-n} \tag{17.24}$$

With this notation, in the z-domain the transfer function of the discrete-time inverting integrator, Eq. (17.22a), becomes

$$T_I(z) = \frac{V_{out}(z)}{V_1(z)} = -\frac{C_1}{C_F\left(1 - z^{-1}\right) + C_3} \tag{17.25a}$$

This equation provides the solution for the difference equation (17.21a). In the same manner, we find for the noninverting discrete-time integrator, Eq. (17.22b),

$$T_N(z) = \frac{V_{out}(z)}{V_2(z)} = \frac{C_2 z^{-1}}{C_F\left(1 - z^{-1}\right) + C_3} \tag{17.25b}$$

In a similar fashion, the general difference equation

$$a_0 y(n) + a_1 y(n-1) + \cdots + a_n y(0) = b_0 x(n) + b_1 x(n-1) + \cdots + b_n x(0)$$

which relates the samples of the output y to those of the input x has the z-transform solution

$$Y(z)\left(a_0 + a_1 z^{-1} + \cdots + a_n z^{-n}\right) = X(z)\left(b_0 + b_1 z^{-1} + \cdots + b_n z^{-n}\right)$$

or

$$T(z) = \frac{Y(z)}{X(z)} = \frac{b_0 + b_1 z^{-1} + \cdots + b_n z^{-n}}{a_0 + a_1 z^{-1} + \cdots + a_n z^{-n}} = \frac{b_0 z^n + b_1 z^{n-1} + \cdots + b_n}{a_0 z^n + a_1 z^{n-1} + \cdots + a_n} \tag{17.26}$$

$T(z)$ is the sampled-data transfer function in the z-domain.

Let us look again at the z-transform, $z = e^{sT}$ for $s = \sigma + j\omega$:

$$z = e^{(\sigma + j\omega)T} = e^{\sigma T} e^{j\omega T} = e^{\sigma T}(\cos\ \omega T + j\ \sin\ \omega T) \tag{17.27}$$

On the $j\omega$-axis, $\sigma = 0$, we recognize that $z^{-1} = e^{-j\omega T}$ is a pure delay of T seconds. Intuitively, this makes sense because the sample $y(n-1)$ in the sampled-data system is delayed from the sample $y(n)$ by exactly T seconds. Also, we note that on the $j\omega$-axis z has the magnitude $|z| = 1$. This means that a frequency on the $j\omega$-axis is transformed onto the unit circle in the complex z-plane. Any point in the left half s-plane, $\sigma < 0$, is transformed onto the interior of the unit circle:

$$|z| = e^{\sigma T} < 1 \quad \text{for} \quad \sigma < 0$$

Finally observe from Eq. (17.27) that z is a periodic function: the range $-\pi \leq \omega T \leq +\pi$ is transformed into one complete circumference of the unit circle. Extending ωT beyond $\pm\pi$ repeatedly covers the unit circle. These relationships are depicted in Fig. 17.19. The periodicity of the z-domain transfer function in $-\pi \leq \omega T \leq +\pi$ also means that only the (positive) frequency components in $\omega T = 2\pi f T \leq \pi$, that is,

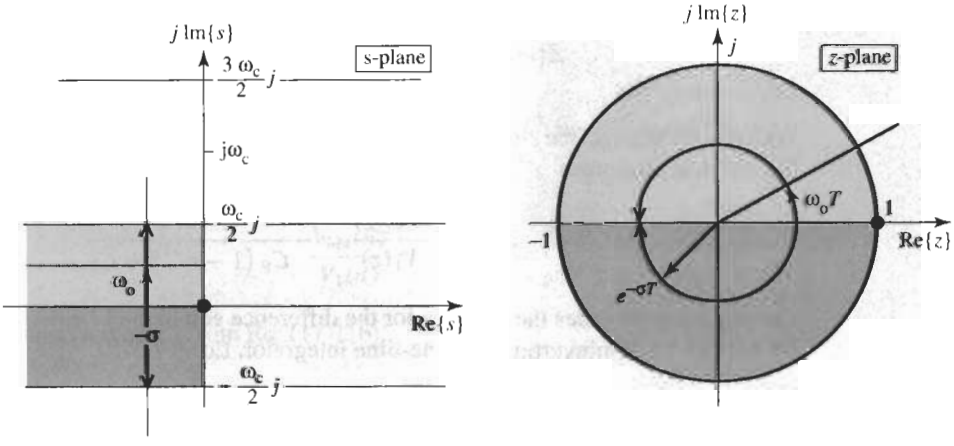

Figure 17.19 Transformation of the s plane onto the z plane by $z = e^{sT}$. Additional strips of width $j\omega_c$ in the s plane are transformed into the same unit circle as the strip in $-j\omega_c/2 \leq j\omega \leq +j\omega_c/2$, or as one says, "they are mapped onto separate sheets of the z-plane." The shaded areas in the s-plane are mapped into areas of the z-plane with the same shading. The lines at ω_0 and at $-\sigma$ are mapped into the corresponding lines indicated in the z-plane.

$$f \leq f_c/2 \tag{17.28}$$

have a unique representation in the z-domain. In words: the frequency f of a sampled signal must be at most equal to one-half the sampling or clock frequency f_c to be uniquely identifiable. We will reinforce this insight below when we look at the spectrum of a sampled signal.

For instance, to see clearly the periodicity of the response of an SC filter in the z-domain, let us express the response of the lossless integrator, Eq. (17.25a) with $C_3 = 0$, on the $j\omega$-axis. We obtain

$$\begin{aligned} T_{\text{I,lossless}}(z) = \frac{V_{\text{out}}}{V_1} &= -\frac{C_1}{C_F}\left.\frac{1}{1-z^{-1}}\right|_{z=e^{j\omega T}} \\ &= -\frac{C_1}{C_F}\left.\frac{z^{1/2}}{z^{1/2}-z^{-1/2}}\right|_{z=e^{j\omega T}} = -\frac{C_1}{C_F}\frac{1}{2j\,\sin\,\omega T/2}e^{+j\omega T/2} \end{aligned} \tag{17.29}$$

From this expression we observe also that the integrator is ideal only for $\omega T \ll 1$,

$$T_{\text{I,lossless}}\big|_{\omega T \ll 1} \approx -\frac{C_1}{C_F}\frac{1}{2j\omega T/2} = -\frac{f_c C_1}{j\omega C_F} \tag{17.30a}$$

as in Eq. (17.7). Apart from a delay $z^{-1/2} = e^{-j\omega T/2}$, the same results apply to the noninverting integrator, Eq. (17.25b),

$$T_{\text{N,lossless}}(z) = \frac{V_{\text{out}}(z)}{V_2(z)} = +\frac{C_2}{C_F}\left.\frac{z^{-1}}{1-z^{-1}}\right|_{z=e^{j\omega T}} = +\frac{C_2}{C_F}\frac{e^{-j\omega T}}{2j\,\sin\,\omega T/2}$$

and for $\omega T \ll 1$:

$$T_{\text{N,lossless}}\big|_{\omega T \ll 1} \approx +\frac{f_c C_2}{j\omega C_F} \tag{17.30b}$$

17.5.2 The Spectrum of a Sampled Signal

Sampling a signal $x(t)$ can be understood as representing $x(t)$ by its values at the instants nT at the falling edge of the clock waveform ϕ_1 in Fig. 17.3. Mathematically, we can perform this operation by multiplying $x(t)$ by a train of impulses, $s(t)$, as shown in Fig. 17.20. The sampled function $x_s(t)$ is then expressed as

$$x_s(t) = x(t)s(t) = x(t)\sum_{n=-\infty}^{+\infty}\delta(t-nT) = x(nT)\sum_{n=-\infty}^{+\infty}\delta(t-nT) \tag{17.31}$$

$\delta(t)$ is the *Dirac delta function,* which is zero everywhere except at $t = 0$ and has the *sifting* property, that is, it sifts that value out of the function $x(t)$ that is at the location of the impulse, $t = nT$. For this so-called impulse sampling $x_s(t)$ is, therefore, represented by a sequence of numbers, each delayed from the previous one by T seconds.

The filter operations we deal with in this book are concerned with shaping the spectrum of a signal. To find the spectrum of the sampled version, $x_s(t)$, of the continuous signal, $x(t)$,

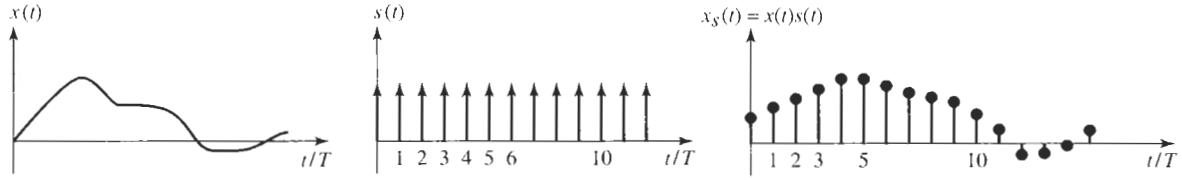

Figure 17.20 Sampling interpreted as a multiplication by a train of impulses.

we compute first the Fourier transform, $\mathcal{F}\{x\} = X(j\omega)$, of the periodic pulse train $s(t)$ in Eq. (17.31):

$$s(t) = \sum_{n=-\infty}^{+\infty} C_n e^{jn\omega_c t}$$

where the Fourier coefficients C_n can be shown to be equal to $1/T$. If we use this result in Eq. (17.31), we obtain

$$\mathcal{F}\{x_s(t)\} = X_s(j\omega) = \frac{1}{T} \sum_{n=-\infty}^{+\infty} \mathcal{F}\left\{x(t)e^{jn\omega_c t}\right\}$$

Using the time-delay property of the Fourier transform, this equation can be solved to yield

$$X_s(j\omega) = \frac{1}{T} \sum_{n=-\infty}^{+\infty} X[j(\omega - n\omega_c)] \tag{17.32}$$

Equation (17.32) is a very important result. It indicates that when a signal $x(t)$ has the spectrum $X(j\omega)$, the sampled signal $x_s(t)$ has the spectrum $X_s(j\omega)$, which consists of infinitely many copies of $X(j\omega)$, shifted on the frequency axis by integer multiples of the sampling (or clock) frequency ω_c. In addition, for the assumed impulse sampling all spectra are multiplied by the constant factor $1/T$. This is illustrated in Fig. 17.21. Figure 17.21a shows the spectrum $X(j\omega)$ of an assumed continuous-time band-limited signal $x(t)$ with bandwidth ω_B, or rather $\pm\omega_B$ because the magnitude is an even function. In Fig. 17.21b we have illustrated $X_s(j\omega)$ for the case when $\omega_B > \omega_c/2$ and we notice that the repeated spectra overlap. For example, components of $X[j(\omega - \omega_c)]$ appear in the base-band range $0 \leq \omega \leq \omega_B$; they are said to be *aliased* into the base band and cannot be separated in $X_s(j\omega)$ from those of $X(j\omega)$. In that case $X_s(j\omega)$ (solid line) in $|\omega| \leq \omega_B$ is different from the original $X(j\omega)$ in Fig. 17.21a. Similar statements can be made for the contributions to $X_s(j\omega)$ for larger values of n. Clearly, to avoid aliasing and to have the base-band spectrum $X(j\omega)$ appear uniquely in the sampled signal, we need to have $\omega_B \leq \omega_c/2$ or $f_B \leq f_c/2$. In that case $X(j\omega)$ can be extracted from $X_s(j\omega)$ by a lowpass filter, a so-called *reconstruction* or *smoothing filter*. Notice that the condition $f_B \leq f_c/2$ is the same result that we obtained in Eq. (17.28): all frequency components of the signal to be sampled must be less than one-half of the sampling frequency. Or expressed differently, the sampling frequency must be at least twice the highest frequency of the signal to be sampled:

$$f_c \geq 2f_B \tag{17.33}$$

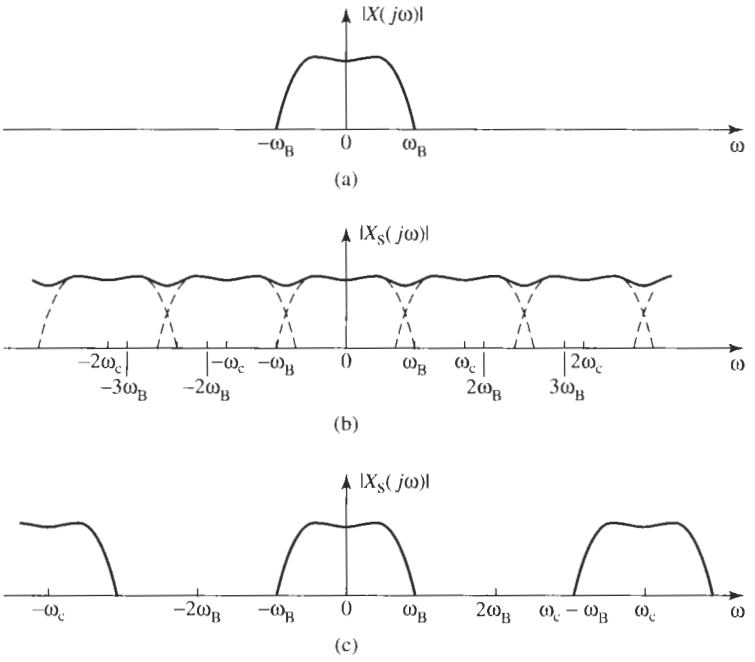

Figure 17.21 (a) Spectrum of the continuous-time signal with bandwidth f_B; (b) spectrum of the sampled signal for $f_B > f_c/2$, showing aliasing; (c) spectrum of the sampled signal for $f_B < f_c/2$ with no aliasing.

This statement, formalized in Eq. (17.33), is a way of expressing the important *sampling theorem* attributed to Claude Shannon (Oliver et al., 1948).

If a function $x(t)$ has a band-limited spectrum $X(j\omega)$ such that $X(j\omega) = 0$ for $|\omega| > \omega_B$, then $x(t)$ is uniquely described by its values at uniformly spaced time instants $T = 2\pi/\omega_c$ seconds apart, where $\omega_c \geq 2\omega_B$.

In the communications literature, the minimum sampling frequency $\omega_c = 2\omega_B$ is also called the *Nyquist* rate. The case satisfying this condition is depicted in Fig. 17.21c, which shows that the original spectrum of $x(t)$ is present with no overlap from an adjacent spectrum and can be recovered by a continuous-time lowpass filter.

Equation (17.33) together with Fig. 17.21 indicates the steps we have to take when processing a continuous-time signal in sampled-data format, such as in switched-capacitor filters:

1. The signal must be band limited, say $f \leq f_B$. If it is not naturally band limited, a continuous-time *antialiasing* lowpass filter with passband in $f \leq f_B$ must be used to eliminate any signal components in the frequency range $|f| > f_B$.
2. The sampling or clock frequency must be at least twice f_B, $f_c \geq 2f_B$.
3. The sampled-data signal is processed in the specified SC filter. The desired output signal of the SC filter is also band limited in $f \leq f_B$.

4. The baseband of the output signal is extracted by a continuous-time reconstruction lowpass filter that attenuates all frequencies in the multiple spectra for $n > 0$ sufficiently so that their contributions are negligible. The output signal of the system is then in the continuous-time domain.

The passband shape of antialiasing and reconstruction filters is shown in Fig. 17.22. Since the spectra for $n = 0$ and $n = 1$ will just touch for Nyquist-rate sampling, $f_c = 2f_B$, we are advised to choose f_c larger than $2f_B$, say $f_c > 8f_B$. Otherwise an expensive high-order "brick wall" lowpass filter would be needed to avoid aliasing. Clearly, the greater the separation between ω_B and ω_c, the wider the transition band (TB) can be between passband (PB) and stopband (SB) for the filters. We have seen in earlier chapters that widening the transition band results in lower order and, therefore, less expensive filter realizations.

Based on our foregoing discussion, we can now sketch a diagram of the signal path[3] in a sampled-data system (Fig. 17.23): Because real signals are generally not band-limited, a continuous-time antialiasing filter is required at the input in order to attenuate any unwanted high-frequency components beyond $f = f_B < f_c/2$. It is followed by the SC filter that samples the signal and performs the specified filtering operation to generate the output samples. If the output must also be in the continuous-time domain, a continuous-time reconstruction or smoothing filter eliminates or at least sufficiently attenuates the translated components of the output sampled-data spectrum. Of course, no antialiasing and smoothing filters are needed if the input signal is already sampled and the output does not have to be in continuous-time format.

17.5.3 The Frequency Response for a z-Domain Transfer Function

We have seen that the design of sampled-data circuits, or specifically of switched-capacitor filters, should be performed in the z-domain. In other words we need to work with z-domain transfer functions $T(z)$ as shown in Eq. (17.26). To ensure that the z-domain function is stable, its poles must lie inside the unit circle so that the response $Y(z)$ stays bounded. Because the left half-plane of the s-plane maps onto the interior of the unit circle in the z-plane and vice

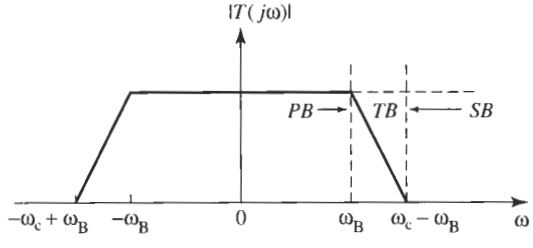

Figure 17.22 Transfer characteristic of antialiasing and reconstruction filters. The indicated transition bandwidth, $TB = (\omega_c - \omega_B) - \omega_B = \omega_c - 2\omega_B$, is the minimum necessary to avoid aliasing.

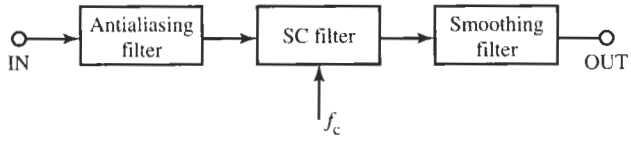

Figure 17.23 Block diagram of a sampled-data system including antialiasing and reconstruction lowpass filters.

[3] In practice a sample-and-hold (S/H) stage may precede the SC filter and an equalizer may follow the smoothing filter. For details, see, e.g., Johns and Martin (1998).

versa, we can be assured that stable s-domain transfer functions, $T(s)$, are converted into stable sampled-data transfer functions $T(z)$ by the s-to-z transformation. Before we develop the z-domain transfer functions for first- and second-order sections, let us consider how to obtain the frequency response of a filter characterized by the discrete-time transfer function $T(z)$, i.e., we need to determine gain $G(\omega)$

$$G(\omega) = 20 \log |T(z)|_{z=e^{j\omega T}} \tag{17.34}$$

and phase $\theta(\omega)$

$$\theta(\omega) = \tan^{-1} \left. \frac{\text{Im}\{T(z)\}}{\text{Re}\{T(z)\}} \right|_{z=e^{j\omega T}} \tag{17.35}$$

of $T(z)$. As we indicated in these equations this means, of course, that $T(z)$ must be evaluated along the unit circle in the z-plane. We encountered this method before in Eq. (17.29) where we found the frequency response for a lossless integrator.

As an example, let us evaluate these functions for the inverting and noninverting integrators in Eq. (17.25).

EXAMPLE 17.4

Evaluate the frequency-domain response of lossy z-domain integrators.

Solution

Starting from Eq. (17.25a), it is convenient to multiply the transfer function by $z^{1/2}$ in the numerator and denominator. The inverting lossy integrator function then becomes

$$T_I(z) = \frac{V_{out}(z)}{V_I(z)} = -\frac{C}{C_F\left(1 - z^{-1}\right) + C_3} = -\frac{Cz^{1/2}}{C_F\left(z^{1/2} - z^{-1/2}\right) + z^{1/2}C_3}$$

where we labeled the capacitor $C_1 = C$. We evaluate this expression on the unit circle:

$$T_I(z)|_{z=e^{j\omega T}} = -\frac{C}{2jC_F \sin\dfrac{\omega T}{2} + C_3\left(\cos\dfrac{\omega T}{2} + j \sin\dfrac{\omega T}{2}\right)} e^{j\omega T/2} \tag{17.36}$$

Next we collect real and imaginary parts in the denominator:

$$\begin{aligned} T_I(z)|_{z=e^{j\omega T}} &= -\frac{C}{j\,(2C_F + C_3) \sin\dfrac{\omega T}{2} + C_3 \cos\dfrac{\omega T}{2}} e^{j\omega T/2} \\ &= -\frac{C}{C_F} \frac{1}{j(2+c) \sin\dfrac{\omega T}{2} + c \cos\dfrac{\omega T}{2}} e^{j\omega T/2} \end{aligned} \tag{17.37a}$$

where we labeled the ratio C_3/C_F by c. Notice that the function has a frequency-dependent loss term $c \cos(\omega T/2)$. The gain becomes by Eq. (17.34)

$$G_{\mathrm{I}}(\omega) = 20 \log \frac{C}{C_{\mathrm{F}}} \frac{1}{\sqrt{4(1+c)\,\sin^2(\omega T/2) + c^2}} \tag{17.38a}$$

and the phase is

$$\theta_{\mathrm{I}}(\omega) = \pi - \tan^{-1} \frac{(2+c)\,\sin\dfrac{\omega T}{2}}{c\,\cos\dfrac{\omega T}{2}} + \frac{\omega T}{2} \tag{17.39a}$$

The term π in Eq. (17–39a) represents the minus sign in Eq. (17–37a).

We use a similar sequence of steps for the noninverting integrator in Eq. (17.25b); labeling now the capacitor $C_2 = C$, we obtain

$$\begin{aligned} T_{\mathrm{N}}(z)|_{z=e^{j\omega T}} &= \left.\frac{Cz^{-1/2}}{C_{\mathrm{F}}\left(z^{1/2} - z^{-1/2}\right) + C_3 z^{-1/2}}\right|_{z=e^{j\omega T}} \\ &= \frac{C}{j\,(2C_{\mathrm{F}} + C_3)\,\sin(\omega T/2) + C_3\,\cos(\omega T/2)} e^{-j\omega T/2} \end{aligned} \tag{17.37b}$$

Using again the notation $c = C_3/C_{\mathrm{F}}$, gain and phase are

$$G_{\mathrm{N}}(\omega) = 20 \log \frac{C}{C_{\mathrm{F}}} \frac{1}{\sqrt{4(1+c)\,\sin^2(\omega T/2) + c^2}} \tag{17.38b}$$

$$\theta_{\mathrm{N}}(\omega) = -\tan^{-1} \frac{(2+c)\,\sin\dfrac{\omega T}{2}}{c\,\cos\dfrac{\omega T}{2}} - \frac{\omega T}{2} \tag{17.39b}$$

Notice from Eqs. (17.38a, b) and (17.39a, b) that the two integrators have identical magnitudes. Disregarding the 180° phase shift because the first integrator is inverting, the phases differ by $\pm\omega T/2$: the inverting integrator has a *phase lead error* of $+\omega T/2$ and the noninverting integrator has a *phase lag error* of $-\omega T/2$. Drawing on our experience with two-integrator-loop filters, we recognize this as an advantage of sampled-data integrators because the errors just cancel when inverting and noninverting integrators are paired in biquads or in ladders.

To conclude the example, let us still consider the two lossless integrators with $C_3 = 0$. From Eq. (17.37),

$$T_{\mathrm{I,lossless}}(z) = -\frac{C}{C_{\mathrm{F}}} \frac{z^{1/2}}{z^{1/2} - z^{-1/2}} = -\frac{C}{C_{\mathrm{F}}} \frac{e^{j\omega T/2}}{2j\,\sin(\omega T/2)} \tag{17.40a}$$

$$T_{\mathrm{N,lossless}}(z) = \frac{C}{C_{\mathrm{F}}} \frac{z^{-1/2}}{z^{1/2} - z^{-1/2}} = \frac{C}{C_{\mathrm{F}}} \frac{e^{-j\omega T/2}}{2j\,\sin(\omega T/2)} \tag{17.40b}$$

or using Eqs. (17.38) and (17.39) directly, we obtain

$$G_{\mathrm{I,lossless}}(\omega) = G_{\mathrm{N,lossless}}(\omega) = 20 \log \frac{C}{C_{\mathrm{F}}} \left.\frac{1}{2\,\sin(\omega T/2)}\right|_{\frac{\omega T}{2} \ll 1} \approx 20 \log \frac{C}{C_{\mathrm{F}}} \frac{1}{\omega T} \tag{17.41}$$

$$\theta_{I,\text{lossless}}(\omega) = \pi - \frac{\pi}{2} + \frac{\omega T}{2}, \quad \theta_{N,\text{lossless}}(\omega) = -\frac{\pi}{2} - \frac{\omega T}{2} \tag{17.42}$$

We leave it to the student in the homework problems to sketch these frequency responses versus ω.

17.6 SWITCHED-CAPACITOR FIRST- AND SECOND-ORDER SECTIONS

Earlier we developed first- and second-order sections (Figs. 17.12 and 17.15), based on the intuitive approximate equivalence between a switched capacitor and a resistor: $G \approx f_c C$. To put these circuits on a sounder footing we need to determine the corresponding z-domain transfer functions. To this end we have to derive the difference equations for the various node voltages at the sampling instants, similar to our treatment in Eqs. (17.17) through (17.21). Clearly, this promises to be a laborious and quite tedious undertaking. In addition, keeping track of initial conditions and the charge transfers during various switch phases is prone to errors. It will be much simpler and methodical if we use the results available for the integrators and use superposition to develop an expression for the SC version of the three-input circuit in Fig. 17.7, letting one input be inverting. It is shown in Fig. 17.24. The circuit is linear in the z-domain and we can use superposition.

If $V_2 = V_3 = 0$ and V_1 is the input, we obtain simply

$$V_{\text{out}}(z) = -\frac{C_1}{C_F} V_1(z) \tag{17.43}$$

If V_2 is the input and $V_1 = V_3 = 0$, we have, from Eq. (17.40b),

$$V_{\text{out}}(z) = \frac{C_2}{C_F} \frac{z^{-1}}{1 - z^{-1}} V_2(z) \tag{17.44}$$

Finally, for $V_1 = V_2 = 0$ and the input at V_3, we use Eq. (17.40a) to get

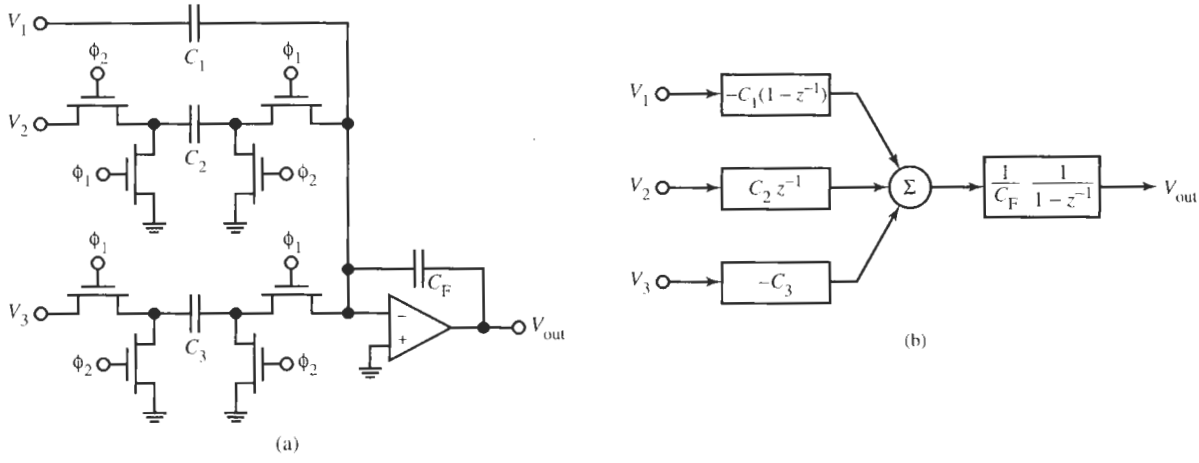

Figure 17.24 (a) A three-input SC integrator; (b) block diagram (or signal-flow graph) representation.

$$V_{out}(z) = -\frac{C_3}{C_F}\frac{1}{1-z^{-1}}V_3(z) \tag{17.45}$$

Adding these three results we have

$$V_{out}(z) = -\frac{C_1}{C_F}V_1(z) + \frac{C_2}{C_F}\frac{z^{-1}}{1-z^{-1}}V_2(z) - \frac{C_3}{C_F}\frac{1}{1-z^{-1}}V_3(z) \tag{17.46a}$$

which we can reformat as follows:

$$V_{out} = \frac{1}{C_F}\frac{1}{1-z^{-1}}\left\{\left[-C_1\left(1-z^{-1}\right)V_1\right] + C_2z^{-1}V_2 + (-C_3V_3)\right\} \tag{17.46b}$$

This equation is represented as a block diagram in Fig. 17.24b. If additional input branches of the same type are needed in a circuit, they can, of course, simply be added.

EXAMPLE 17.5

Use the signal-flow graph model in Fig. 17.24b to construct a noninverting lossy integrator.

Solution

To build a noninverting lossy integrator, we set $V_1 = 0$ and connect V_3 to the output, $V_3 = V_{out}$, as shown in Fig. 17.25a. From Eq. (17.46) we obtain

$$V_{out} = \frac{1}{C_F}\frac{1}{1-z^{-1}}\left[C_2z^{-1}V_2 + (-C_3V_{out})\right]$$

which is solved for the transfer function

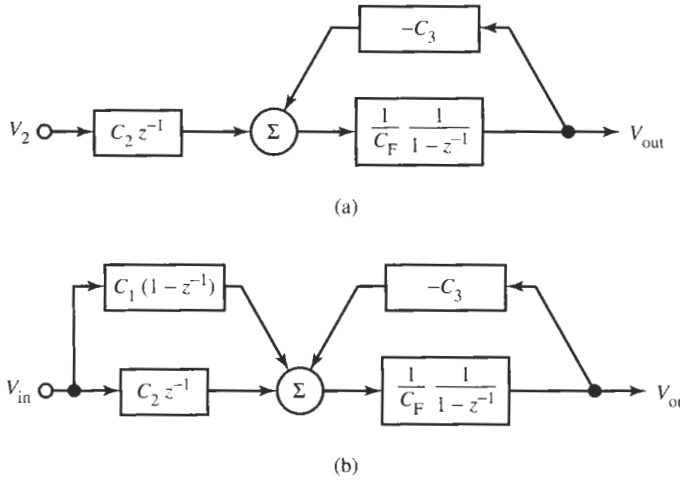

Figure 17.25 (a) A noninverting lossy integrator (the MOS circuit version is shown in Fig. 17.18a); (b) a bilinear circuit (Fig. 17.12c shows the MOS version).

$$\frac{V_{out}}{V_2} = \frac{C_2 z^{-1}}{C_F\left(1 - z^{-1}\right) + C_3}$$

This equation is, of course, the same as Eq. (17.25b).

17.6.1 Bilinear Sections

The technique demonstrated in Example 17.5 is used also to construct the bilinear circuit: in Fig. 17.24 we set $V_1 = V_2 = V_{in}$ and connect V_3 to V_{out}. The result is the block diagram in Fig. 17.25b, representing the circuit in Fig. 17.12c. We find from Eq. (17.46b)

$$V_{out} = \frac{1}{C_F}\frac{1}{1 - z^{-1}}\left\{\left[C_2 z^{-1} - C_1\left(1 - z^{-1}\right)\right]V_{in} + \left(-C_3 V_{out}\right)\right\}$$

or

$$\frac{V_{out}}{V_{in}} = -\frac{C_1\left(1 - z^{-1}\right) - C_2 z^{-1}}{C_F\left(1 - z^{-1}\right) + C_3} = -\frac{C_1 z - (C_1 + C_2)}{(C_F + C_3)\, z - C_F} \tag{17.47}$$

The right-hand side of Eq. (17.47) is often more convenient because filter specifications will be given as ratios of polynomials in z.

As expected, for $z = e^{j\omega T}$ and $\omega T \ll 1$, Eq. (17.47) is the same as Eq. (17.11b), which we found earlier by the approximate method from Fig. 17.12:

$$\frac{V_{out}}{V_{in}} = -\frac{C_1\left(1 - z^{-1}\right) - C_2 z^{-1}}{C_F\left(1 - z^{-1}\right) + C_3} \approx -\frac{C_1(1 - 1 + j\omega T) - C_2(1 - j\omega T)}{C_F(1 - 1 + j\omega T) + C_3} \approx -\frac{j\omega C_1 - f_c C_2}{j\omega C_F + f_c C_3}$$

Let us calculate the frequency response of the bilinear filter more carefully. As demonstrated in Example 17.4, we multiply the transfer function by $z^{1/2}$ in numerator and denominator to obtain

$$\begin{aligned}\frac{V_{out}}{V_{in}} &= -\frac{C_1\left(z^{1/2} - z^{-1/2}\right) - C_2 z^{-1/2}}{C_F\left(z^{1/2} - z^{-1/2}\right) + C_3 z^{1/2}} \\ &= -\frac{(2C_1 + C_2)\, j\, \sin(\omega T/2) - C_2\, \cos(\omega T/2)}{(2C_F - C_3)\, j\, \sin(\omega T/2) + C_3\, \cos(\omega T/2)}\end{aligned} \tag{17.48}$$

From this equation, gain and phase can be computed by using Eqs. (17.34) and (17.35). Let us emphasize again that the function is periodic. The frequency response is unique only in $\omega T/2 < \pi$ or $f < f_c$; for larger frequencies, the response repeats itself (see Fig. 17.21c).

Fully Differential Circuits

We discussed in the previous chapter the benefits of implementing analog integrated filters in fully differential form. These same advantages, such as better noise immunity and wider signal swing, are valid also here for switched-capacitor circuits. Consequently, SC circuits are normally built in differential form. The design procedures are very straightforward: we simply

have two parallel signal paths, one for positive voltages and one for the inverted (negative) ones. Figure 17.26a shows the differential configuration for the three-input integrator of Fig. 17.24a and Fig. 17.26b shows the corresponding block diagram. Analogous to Eq. (17.46), the circuit is described by

$$V_{\text{out}}^{+} - V_{\text{out}}^{-} = \frac{1}{C_F}\frac{1}{1-z^{-1}}\left\{\left[-C_1\left(1-z^{-1}\right)\left(V_1^{+}-V_1^{-}\right)\right] + \left[C_2 z^{-1}\left(V_2^{+}-V_2^{-}\right)\right] + \left[-C_3\left(V_3^{+}-V_3^{-}\right)\right]\right\} \tag{17.49}$$

The same equation is valid for the block diagram in Fig. 17.26b that can be used to develop higher order circuits.

A convenience afforded by the differential topology is that effectively negative components can be implemented by interchanging the (±) input connections. For instance, if we interchange the input connections of the branch $C_2 z^{-1}$ we have in effect realized a negative capacitor C_2. Thus, the first-order circuit in Fig. 17.27a, the differential version of Fig. 17.12c, realizes

$$V_{\text{out}}^{+} - V_{\text{out}}^{-} = \frac{1}{C_F}\frac{1}{1-z^{-1}}\left\{\left[-C_1\left(1-z^{-1}\right) - C_2 z^{-1}\right]\left(V_{\text{in}}^{+}-V_{\text{in}}^{-}\right) + \left[-C_3\left(V_{\text{out}}^{+}-V_{\text{out}}^{-}\right)\right]\right\}$$

or

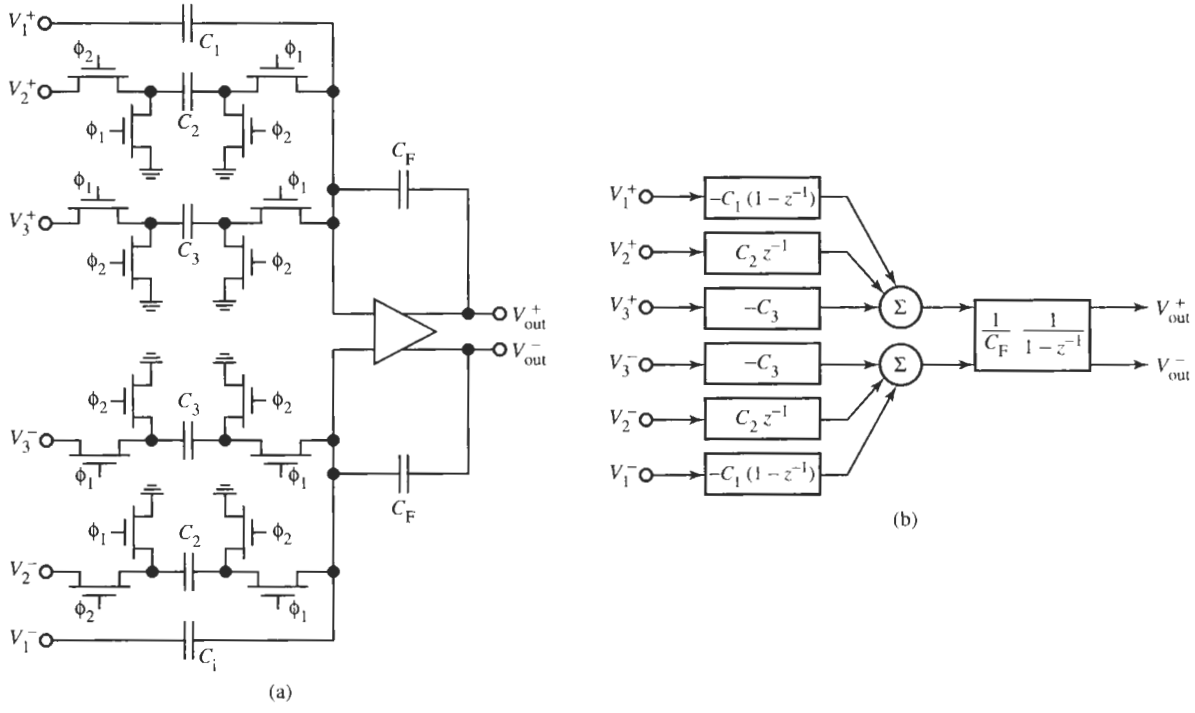

Figure 17.26 (a) Differential version of the three-input SC integrator; (b) block diagram (or signal-flow graph) representation.

$$\frac{V_{out}^{+}-V_{out}^{-}}{V_{in}^{+}-V_{in}^{-}}=-\frac{C_1\left(1-z^{-1}\right)+C_2z^{-1}}{C_F\left(1-z^{-1}\right)+C_3}=-\frac{C_1z-(C_1-C_2)}{(C_F+C_3)\,z-C_F} \tag{17.50}$$

In the circuit in Fig. 17.27b C_2 is replaced by $-C_2$ and it realizes

$$V_{out}^{+}-V_{out}^{-}=\frac{1}{C_F}\frac{1}{1-z^{-1}}\left\{\left[-C_1\left(1-z^{-1}\right)+C_2z^{-1}\right]\left(V_{in}^{+}-V_{in}^{-}\right)+\left[-C_3\left(V_{out}^{+}-V_{out}^{-}\right)\right]\right\}$$

or

$$\frac{V_{out}^{+}-V_{out}^{-}}{V_{in}^{+}-V_{in}^{-}}=-\frac{C_1\left(1-z^{-1}\right)-C_2z^{-1}}{C_F\left(1-z^{-1}\right)+C_3}=-\frac{C_1z-(C_1+C_2)}{(C_F+C_3)\,z-C_F} \tag{17.51}$$

Notice that the zero of Eq. (17.50), $z=(C_1-C_2)/C_1$, is in the range $|z|\le 1$; the zero of Eq. (17.51), $z=(C_1+C_2)/C_1$, on the other hand is in $|z|\ge 1$. Consequently, zeros anywhere on the real axis can be realized with the circuit of Fig. 17.27.

We will in the following assume that our circuits are realized in fully differential form, but we will draw only single-ended circuit diagrams because the topologies are more transparent and easier to understand. If negative components are needed we will assume they can be obtained from a differential version of the circuit.

17.6.2 Second-Order Sections

To determine the z-domain transfer function of the two-integrator-loop biquad in Fig. 17.15 we use the first-order circuit of Fig. 17.24b. We start by expanding Fig. 17.24b to obtain the necessary additional inputs. Let us use the same subscripts for the components as in Fig. 17.15 so that we can better compare the results obtained. Figure 17.28 shows the signal-flow diagrams of the two integrators. The first integrator in Fig. 17.28a is described by

$$\begin{aligned}V_1&=\frac{1}{C_1}\frac{1}{1-z^{-1}}\left\{C_7z^{-1}V_{in}+(-C_6V_{in})+\left[-C_4\left(1-z^{-1}\right)V_{in}\right]+(-C_8V_2)\right.\\&\quad\left.+\left[-C_3\left(1-z^{-1}\right)V_2\right]\right\}\\&=\frac{1}{C_1}\frac{1}{1-z^{-1}}\left\{\left[C_7z^{-1}-C_6-C_4\left(1-z^{-1}\right)\right]V_{in}-\left[C_8+C_3\left(1-z^{-1}\right)\right]V_2\right\}\end{aligned}$$

and for the second integrator, Fig. 17.28b, we find

$$\begin{aligned}V_2&=\frac{1}{C_2}\frac{1}{1-z^{-1}}\left\{C_9z^{-1}V_1+(-C_{10}V_2)+\left[-C_5\left(1-z^{-1}\right)V_{in}\right]+(-C_{11}V_{in})+C_{12}z^{-1}V_{in}\right\}\\&=\frac{1}{C_2}\frac{1}{1-z^{-1}}\left\{C_9z^{-1}V_1-C_{10}V_2-\left[C_5\left(1-z^{-1}\right)+C_{11}-C_{12}z^{-1}\right]V_{in}\right\}\end{aligned}$$

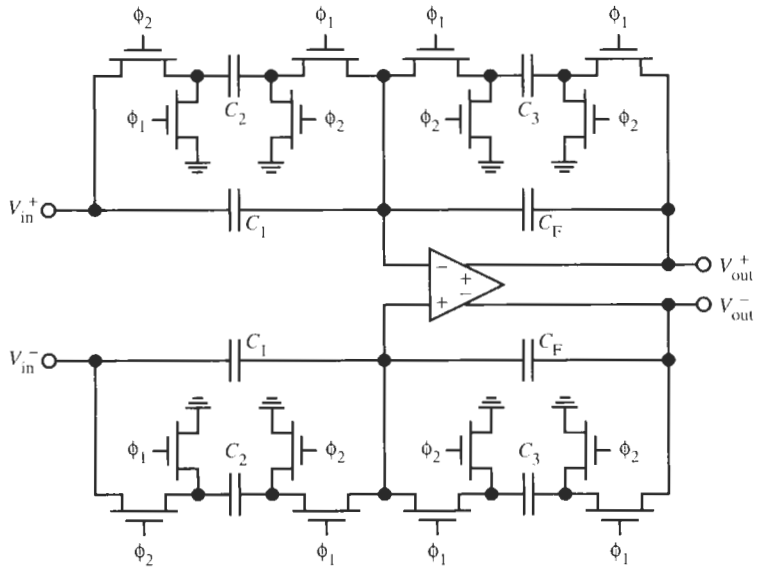

(a)

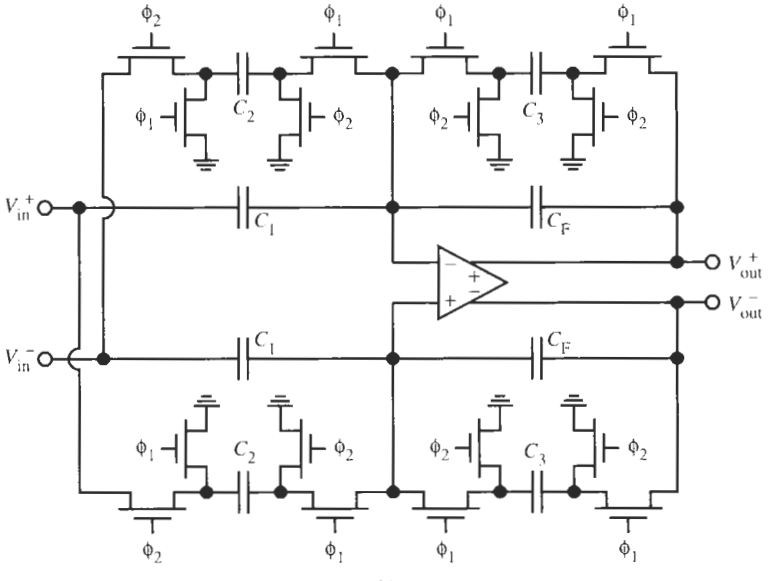

(b)

Figure 17.27 Two fully differential first-order circuits. (a) C_2 is positive [Eq. (17.50)]; (b) C_2 appears negative [Eq. (17.51)].

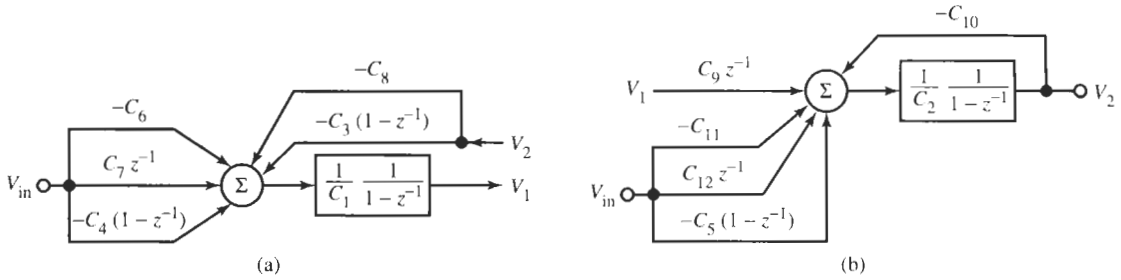

Figure 17.28 Signal-flow graphs of z-domain integrators for building a general sampled-data biquad: (a) the left integrator of Fig. 17.15b; (b) the right integrator of Fig. 17.15b.

To solve these two expressions for V_2, we substitute V_1 from the first into the second equation and obtain after some algebra:

$$\frac{V_2}{V_{in}} = -\frac{C_1C_5(1-z^{-1})^2 + [C_1(C_{11}-C_{12}z^{-1}) + C_4C_9z^{-1}](1-z^{-1}) + C_9z^{-1}(C_6-C_7z^{-1})}{C_1C_2(1-z^{-1})^2 + (C_1C_{10}+C_3C_9z^{-1})(1-z^{-1}) + C_8C_9z^{-1}} \tag{17.52a}$$

Again, if the frequency response is required, we use Eqs. (17.34) and (17.35). To check Eq. (17.52a) against our earlier work, derived for very fast sampling, we set the terms $z \approx 1$ and $1 - z^{-1} \approx j\omega T$ for $\omega T \ll 1$. This results in

$$\frac{V_2}{V_{in}} = -\frac{C_1C_5(j\omega T)^2 + [C_1(C_{11}-C_{12}) + C_4C_9]j\omega T + C_9(C_6-C_7)}{C_1C_2(j\omega T)^2 + (C_1C_{10}+C_3C_9)j\omega T + C_8C_9}$$

For $j\omega = s$, this equation is identical to Eq. (17.15) derived earlier for the circuit in Fig. 17.16 under the condition $\omega T \ll 1$.

When we wish to design a biquad from given specifications, the form of V_2/V_{in} in Eq. (17.52a) is not normally very useful. Because the prescribed transfer function will usually be given in the form of a ratio of polynomials in z, it will be preferable to collect the coefficients of z^2 and z in Eq. (17.52a) to obtain

$$\frac{V_2}{V_{in}} = -\frac{N(z)}{D(z)} \tag{17.52b}$$

$$= -\frac{z^2C_1(C_5+C_{11}) + z[C_9(C_4+C_6) - C_1(2C_5+C_{11}+C_{12})] + C_1(C_5+C_{12}) - C_9(C_7+C_4)}{z^2C_1(C_2+C_{10}) + z[C_9(C_3+C_8) - C_1(C_{10}+2C_2)] + (C_1C_2 - C_3C_9)}$$

From this form we recognize that there is a considerable redundancy in components. If we examine Eq. (17.52b) carefully, we notice that we may choose capacitors $C_4 = C_5 = 0$ and $C_1 = C_2 = C_9 = C$. Then Eq. (17.52) reduces to

$$\frac{V_2}{V_{in}} = -\frac{N(z)}{D(z)} = -\frac{(zC_{11}-C_{12})(z-1) + (C_6z - C_7)}{C(z-1)^2 + (C_{10}z + C_3)(z-1) + C_8z}$$

$$= -\frac{z^2C_{11} + z(C_6 - C_{11} - C_{12}) + (C_{12} - C_7)}{z^2(C+C_{10}) + z(C_3 + C_8 - C_{10} - 2C) + (C - C_3)} \tag{17.53}$$

Evidently this equation can realize arbitrary biquadratic z-domain functions. The corresponding SC circuit with switch sharing is shown in Fig. 17.29.

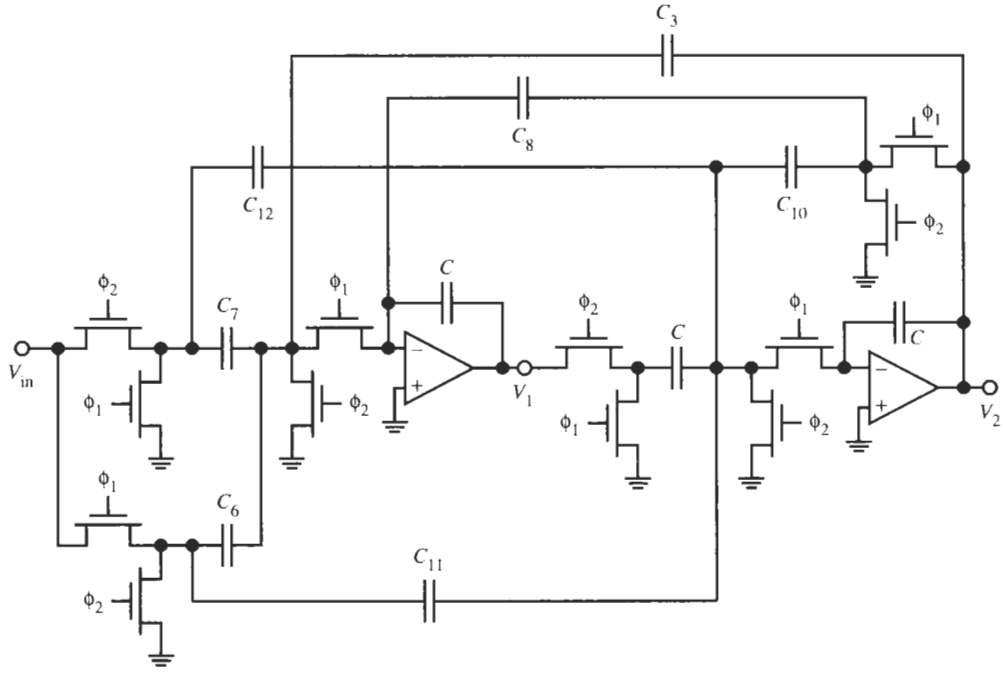

Figure 17.29 A special case of the biquad in Fig. 17.15c. The circuit realizes Eq. (17.53).

EXAMPLE 17.6

Realize a z-domain lowpass filter that has zeros z_1 and poles p_1 at

$$z_1 = e^{j1.24}, \quad p_1 = 0.8e^{j0.52}$$

the gain constant is $K = 0.185$. Sketch the magnitude response.

Solution

The z-domain transfer function is rational with real coefficients and hence has conjugate complex poles and zeros. Without concerning ourselves at this time with how such a function might arise, we note that it has two zeros on the unit circle and two poles inside the unit circle as is shown in Fig. 17.30. Thus we have

$$T(z) = K\frac{(z-z_1)(z-z_1^*)}{(z-p_1)(z-p_1^*)} = 0.185\frac{(z-e^{j1.24})(z-e^{-j1.24})}{(z-0.8e^{j0.52})(z-0.8e^{-j0.52})}$$

$$= 0.185\frac{z^2-(2\ \cos\ 1.24)z+1}{z^2-(1.6\ \cos\ 0.52)z+0.64} = 0.185\frac{z^2-0.6495z+1}{z^2-1.3890z+0.64}$$

$T(z)$ is to be matched with the biquad function of Eq. (17.53), which we reformat as follows to be able to compare coefficients:

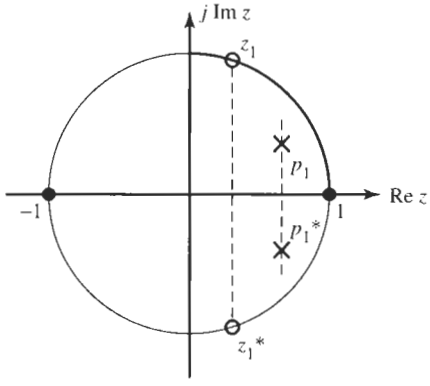

Figure 17.30 Pole-zero plot for Example 17.6.

$$\frac{V_2}{V_{in}} = \frac{C_{11}}{C + C_{10}} \frac{z^2 + z\left(\frac{C_6 - C_{11} - C_{12}}{C_{11}}\right) + \left(\frac{C_{12} - C_7}{C_{11}}\right)}{z^2 + z\left(\frac{C_3 + C_8 - C_{10} - 2C}{C + C_{10}}\right) + \left(\frac{C - C_3}{C + C_{10}}\right)}$$

The comparison gives the equations

$$\frac{C_{11}}{C + C_{10}} = 0.185, \quad \frac{C_6 - C_{11} - C_{12}}{C_{11}} = -0.6495, \quad \frac{C_{12} - C_7}{C_{11}} = 1,$$
$$\frac{C_3 + C_8 - C_{10} - 2C}{C + C_{10}} = -1.3890, \quad \frac{C - C_3}{C + C_{10}} = 0.64$$

or

$$C + C_{10} = 5.4054C_{11}, \quad C_6 - C_{12} = 0.3505C_{11}, \quad C_{12} - C_7 = C_{11},$$
$$C_3 + C_8 = 0.6110C - 0.3890C_{10}, \quad C_3 = 0.36C - 0.64C_{10}$$

These equations must be solved for the capacitor values; clearly the solution is not unique. Let us choose $C_3 = 0.2C$ and $C_7 = 0.1C$, then we find

$$C_6 = 0.4124C, \quad C_8 = 0.3138C, \quad C_{10} = 0.25C, \quad C_{11} = 0.2313C, \quad C_{12} = 0.3313C$$

Finally, we pick $C = 2$ pF to obtain the circuit using switch sharing in Fig. 17.29, with the elements $C = 2$ pF, $C_3 = 0.4$ pF, $C_6 = 0.82$ pF, $C_7 = 0.2$ pF, $C_8 = 0.63$ pF, $C_{10} = 0.50$ pF, $C_{11} = 0.46$ pF, and $C_{12} = 0.66$ pF.

To sketch the magnitude response we note that in the z-plane we need to move along the unit circle. Starting from $z = 1$, i.e., $\omega = 0$, we first pass the pole inside, but close to, the unit circle where can expect some peaking in the passband. Then we move across the zero on the unit circle where transmission is blocked, and on to the point $z = -1$. The process is exactly analogous to moving along the $j\omega$-axis in the continuous-time domain. The base band of the function is in $0 \leq \omega T \leq \omega_c T/2 = \pi$. We need to remember, of course, that the function is periodic. Thus, if we move on the unit circle from π to 2π the plot repeats, mirrored at the line π. Then, if we continue around the unit circle, multiple passbands and stopbands appear as is shown in Fig. 17.31.

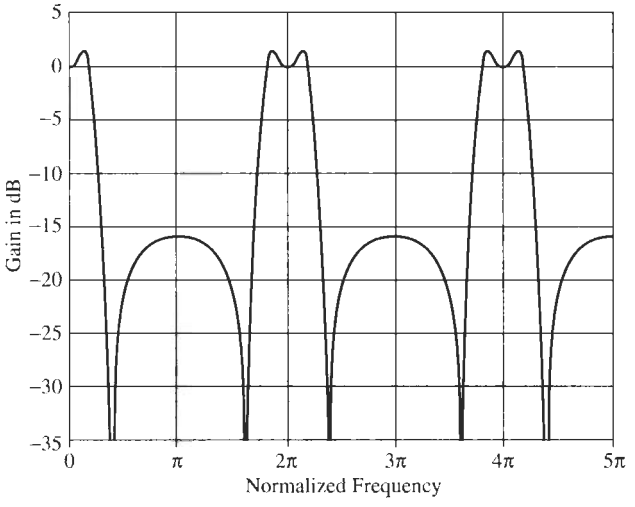

Figure 17.31 The magnitude response of the SC lowpass filter designed in Example 17.6. The passbands and stopbands are repeated as ω increases to the range $\omega T > \pi$.

An alternative way of simplifying the general SC biquad of Fig. 17.15, described by Eq. (17.52), is obtained by setting $C_7 = C_{10} = C_{11} = 0$ and, again, $C_1 = C_2 = C_9 = C$. The circuit is shown in Fig. 17.32; its transfer function is

$$\frac{V_2}{V_{\text{in}}} = -\frac{N(z)}{D(z)} = -\frac{z^2C_5 + z\,[(C_4 + C_6) - (2C_5 + C_{12})] + (C_5 + C_{12}) - C_4}{z^2C + z\,[(C_3 + C_8) - 2C] + (C - C_3)} \tag{17.54}$$

Observe that also this circuit can realize an arbitrary biquadratic function in the z-domain. Compared to the circuit in Fig. 17.29 it saves one capacitor.

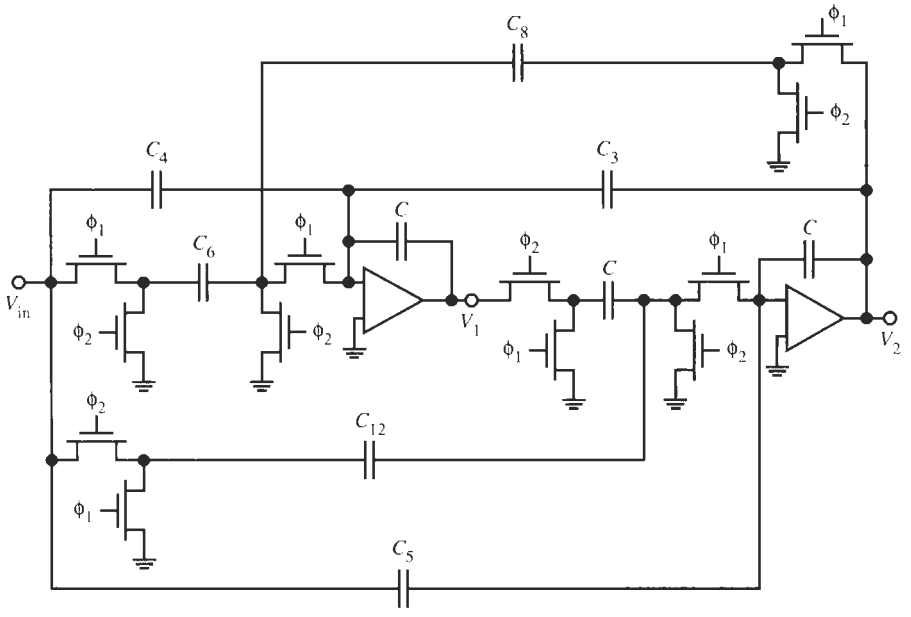

Figure 17.32 Switched-capacitor biquad realizing Eq. (17.54).

We have seen that the simple three-input z-domain integrator in Fig 17.24 together with its signal-flow graph and Eq. (17.46) can be used with ease to derive transfer functions of more complicated circuits as long as they are based on the interconnection of integrators. For example, we will find the method very useful for the design of simulated lossless ladders that are based on lossless and lossy integrators in the same way as in the continuous-time case.

In Example 17.6 we started from a given z-domain transfer function with prescribed poles and zeros without concerning ourselves with how this function would be derived from specified attenuation requirements. We shall introduce in the next section a frequency transformation that converts the regular continuous-time frequency s_{ct} into the frequency s that is valid in the sampled-data domain. We will then be able to transform well-known continuous-time filter specifications into the sampled-data domain where an SC filter can be designed. A complete example for a cascade design of an SC filter will illustrate the method.

17.7 THE BILINEAR TRANSFORMATION

The periodic nature of $T(z) = T(e^{j\omega T})$ will potentially give rise to problems and errors because in the continuous-time domain a transfer characteristic $T(j\omega)$ is prescribed along the *whole* frequency axis, $0 \leq \omega \leq \infty$, and not just in $0 \leq \omega \leq \omega_c/2$. To realize the desired attenuation characteristics with switched-capacitor circuits in the sampled-data domain, we need to find a frequency transformation that "compresses" the range $0 \leq \omega \leq \infty$ into $0 \leq \omega \leq \omega_c/2$. This transformation will also let us use the numerous results and tables, see chapters 6 to 8, that were developed for filter design in the continuous-time domain.

To be able to keep track of the different frequency variables, let us refer to the frequency that is valid in the sampled-data domain as ω or f and label the frequency for the continuous-time domain as ω_{ct} or f_{ct}. Then we need a function that can transform the frequency range $-\omega_c/2 \leq \omega \leq +\omega_c/2$ into the whole frequency axis $-\infty \leq \omega_{ct} \leq +\infty$; the function should also be periodic so that repeated bands of width ω_c are transformed into $-\infty \leq \omega_{ct} \leq \infty$ as well. A periodic transformation that maps an angle φ between $-\pi$ and π into the infinite interval $-\infty \leq \omega_{ct} \leq \infty$ is accomplished by the trigonometric function

$$\omega_{ct} = \frac{2}{T} \tan \frac{\varphi}{2} = \frac{2}{T} \tan \left(\frac{1}{2} \frac{2\pi f}{f_c} \right) = \frac{2}{T} \tan \frac{\omega T}{2} \tag{17.55}$$

as shown in Fig. 17.33. We defined the angle φ as $2\pi f/f_c$ so that $-\pi/2 \leq \varphi \leq +\pi/2$ when the frequency traverses the range $-f_c/2 \leq f \leq +f_c/2$. We have introduced the factor $2/T$, not only to make both sides of Eq. (17.55) frequencies with units of 1/time, but also to ensure that for very small ωT, that is, for *very fast sampling*, the two frequency axes ω and ω_{ct} coincide:

$$\omega_{ct} = \frac{2}{T} \tan \frac{\omega T}{2} \bigg|_{\omega T \ll 1} \approx \frac{T}{2} \frac{\omega T}{2} = \omega \tag{17.56}$$

This condition of very fast sampling was the basis of the approximate equivalence $G \approx f_c C$ on which we based our initial SC filter circuits. Equation (17.55) is *nonlinear* because the infinite frequency interval $-\infty \leq \omega_{ct} \leq \infty$ is compressed into the finite range $-\omega_c/2 \leq \omega \leq \omega_c/2$. We say that the axis is "*warped*."

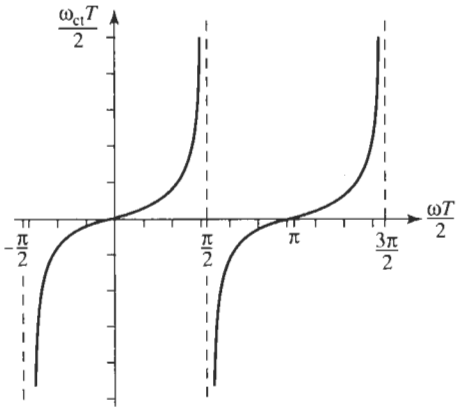

Figure 17.33 The nonlinear periodic transformation of Eq. (17.55) between ω_{ct} and ω.

We need now to make the connection between s_{ct} and z. We do this with Eq. (17.55) by using trigonometric identities, the relation between trigonometric and exponential functions, and Eq. (17.23):

$$\tan\frac{\omega T}{2} = \frac{\sin\dfrac{\omega T}{2}}{\cos\dfrac{\omega T}{2}} = \frac{\dfrac{1}{2j}\left(e^{j\omega T/2} - e^{-j\omega T/2}\right)}{\dfrac{1}{2}\left(e^{j\omega T/2} + e^{-j\omega T/2}\right)} = \frac{1}{j}\left.\frac{z^{1/2} - z^{-1/2}}{z^{1/2} + z^{-1/2}}\right|_{s=j\omega}$$

Therefore, from Eq. (17.55) we have

$$j\omega_{ct} = \frac{2}{T}\left.\frac{z^{1/2} - z^{-1/2}}{z^{1/2} + z^{-1/2}}\right|_{s=j\omega} \tag{17.57}$$

After so-called *analytic continuation* from the $j\omega_{ct}$-axis into the s_{ct}-plane and from the unit circle into the z-plane we find the desired *bilinear transformation*

$$s_{ct} = \frac{2}{T}\frac{z-1}{z+1} \quad \text{or} \quad z = \frac{1 + s_{ct}T/2}{1 - s_{ct}T/2} \tag{17.58}$$

The two expressions in Eq. (17.58) give the frequency transformations between the continuous-time domain, s_{ct}, and the sampled-data domain, z. Specifically, the physical frequencies are related by the nonlinear equations:

$$\frac{\omega_{ct}T}{2} = \tan\frac{\omega T}{2} \quad \text{and} \quad \frac{\omega T}{2} = \tan^{-1}\frac{\omega_{ct}T}{2} \tag{17.59}$$

Observe also from Eq. (17.58) that the bilinear transformation is a *rational* function. It follows that a rational continuous-time transfer function in s_{ct} will give a rational discrete-time transfer function in z of the same order. For instance, assume an analog approximation procedure resulted in the second-order transfer function in the s_{ct} domain

$$T(s_{ct}) = \frac{as_{ct}^2 + \tilde{b}s_{ct} + \tilde{c}}{s_{ct}^2 + \tilde{d}s_{ct} + \tilde{e}} \tag{17.60}$$

We can then multiply the numerator and denominator by $(T/2)^2$,

$$T(s_{ct}) = \frac{a(s_{ct}T/2)^2 + \tilde{b}T/2(s_{ct}T/2) + \tilde{c}(T/2)^2}{(s_{ct}T/2)^2 + \tilde{d}T/2(s_{ct}T/2) + \tilde{e}(T/2)^2} = \frac{a\lambda^2 + b\lambda + c}{\lambda^2 + d\lambda + e}$$

where we have labeled the normalized frequency parameter $s_{ct}T/2 = \lambda$, and where the definitions of the coefficients include the normalization factor $T/2$ as is clear from the equation. By Eq. (17.58) we see that $\lambda = (z-1)/(z+1)$ so that we obtain the second-order rational function in z:

$$\begin{aligned} T(z) = T(s_{ct})|_{s_{ct}=\frac{2}{T}\frac{z-1}{z+1}} &= \frac{a\left(\frac{z-1}{z+1}\right)^2 + b\left(\frac{z-1}{z+1}\right) + c}{\left(\frac{z-1}{z+1}\right)^2 + d\left(\frac{z-1}{z+1}\right) + e} \\ &= \frac{(a+b+c)z^2 + 2(c-a)z + (a-b+c)}{(1+d+e)z^2 + 2(e-1)z + e(1-d+e)} \end{aligned} \tag{17.61}$$

Comparing coefficients between Eq. (17.61) and Eqs. (17.53) or (17.54) then yields the capacitor values for the chosen SC biquad.

Further, we can show also that the *left* half s_{ct}-plane, $\sigma_{ct} < 0$, is mapped onto the *inside* of the unit circle, $|z| < 1$, in the z plane. From Eq. (17.58) we have

$$|z| = \left|\frac{1 + \sigma_{ct}T/2 + j\omega_{ct}T/2}{1 - \sigma_{ct}T/2 - j\omega_{ct}T/2}\right| = \sqrt{\frac{(1+\sigma_{ct}T/2)^2 + (\omega_{ct}T/2)^2}{(1-\sigma_{ct}T/2)^2 + (\omega_{ct}T/2)^2}} < 1 \quad \text{for} \quad \sigma_{ct} < 0$$

Thus, stable s_{ct}-plane poles are transformed into stable z-plane poles. The bilinear transformation is used to obtain the z-domain transfer function from a given s_{ct}-domain specification or transfer function: when $T(s_{ct})$ is given, we use Eq. (17.58) to obtain

$$T(z) = T(s_{ct})|_{s_{ct}=\frac{2}{T}\frac{z-1}{z+1}} \tag{17.62}$$

Note that $T(z)$ and $T(s_{ct})$ are *not* the same functions as we saw in Eqs. (17.60) and (17.61). The notation $T(\cdot)$ has been retained only for convenience of reference. When applying the bilinear transformation no attention needs to be paid to the attenuation specifications, such as passband ripple width, and the type of the transfer function (equiripple, maximally flat, etc.) because $s_{ct} = F(z)$ is a transformation of the independent variable. Recall from Chapter 9 that such a frequency transformation does not distort the ordinate, $T(\cdot)$, so that all attenuation specifications are maintained.

Most often it is convenient to handle the approximation problem on the continuous-time axis ω_{ct} where, as we have learned, passband and stopband corners or other frequencies critical to the filter operation are identified and used in the approximation procedure. However, since we are interested in building a switched-capacitor filter whose response is observed not on the ω_{ct}-axis but along the sampled-data axis ω, we need to make certain that the critical frequency points are correct when the ω_{ct}-axis is transformed, i.e., *warped*, into the ω-axis. This is accomplished by *prewarping* the ω_{ct}-axis by Eq. (17.59). The specified critical frequency points ω_k, say passband corners ω_p and stopband edges ω_s, that the SC filter must realize

correctly on the ω-axis are converted, that is prewarped, by Eq. (17.59) into the corresponding values $\omega_{ct,\,k}$, for example,

$$\omega_{ct,\,p} = \frac{2}{T}\tan\frac{\omega_p T}{2} \quad \text{and} \quad \omega_{ct,\,s} = \frac{2}{T}\tan\frac{\omega_s T}{2} \tag{17.63}$$

Note specifically that the frequency $\omega_c/2$, the end of the useful range in the periodic sampled-data domain, is transformed into ∞ on the continuous-time axis:

$$\omega_{ct} = \frac{2}{T}\tan\frac{(\omega_c/2)\,T}{2} = \frac{2}{T}\tan\frac{\pi f_c T}{2} = \frac{2}{T}\tan\frac{\pi}{2} = \infty$$

The approximation problem is now handled on the prewarped ω_{ct}-axis and the resulting transfer function $T(s_{ct})$ is converted by the bilinear transformation, Eq. (17.62), into the z-domain where the SC filter is implemented. Notice that applying the bilinear transformation then *warps* the *prewarped* ω_{ct}-axis so that in the SC filter we get precisely the desired critical frequencies; by Eq. (17.59) we have

$$\omega_k = \frac{2}{T}\tan^{-1}\frac{\omega_{ct,k}T}{2} = \frac{2}{T}\tan^{-1}\left(\tan\frac{\omega_k T}{2}\right) \to \omega_k$$

Figure 17.34 shows the corresponding behavior in the transformation of a third-order elliptic filter in the sampled-data domain.

We are now ready to apply the procedures we discussed, the bilinear transformation, warping, and prewarping, to the design of a switched-capacitor filter. We shall use a cascade design to illustrate that the methods presented in connection with active *RC* filters are valid here as well.

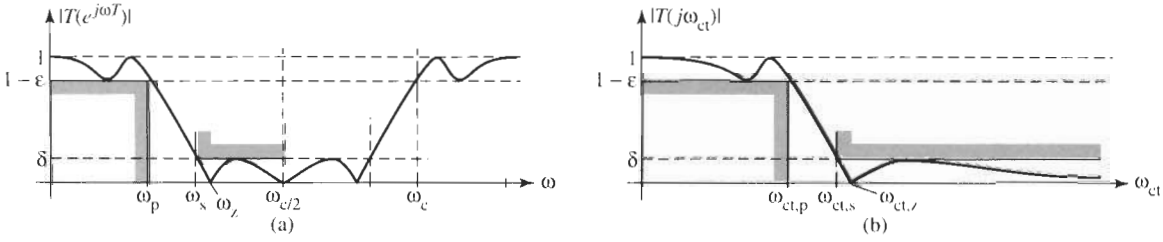

Figure 17.34 Filter specifications (a) in the sampled-data domain and (b) in the continuous-time domain obtained by prewarping.

17.8 DESIGN OF SWITCHED-CAPACITOR CASCADE FILTERS

For the design of a switched-capacitor filter we may start from a prescribed z-domain transfer characteristic and match it to the z-domain transfer function realized by a given SC filter topology. This coefficient matching technique is the customary procedure followed in s-domain active *RC* designs. It was the method used in Example 17.6 and it has also been adopted in much of the switched-capacitor literature. However, to facilitate the student's understanding of the derivations and design procedures, and to make the connection with the continuous-time procedures we studied in earlier chapters of this book, we shall in our discussion follow as

far as possible the analogous development for continuous-time filters. We pointed out in the beginning of this chapter that uncritical SC filters could be realized simply by replacing each resistor in an active *RC* realization by its SC equivalent, $G = f_c C$. However, as we have seen, these designs are based on the assumption of very fast sampling, $f_c \gg 2\pi f$, and are only approximate. Since exact methods are now available to us, let us present an example for such an approach. We shall design a cascade circuit and leave ladder simulations to the next section.

After prewarping the ω-axis into the ω_{ct}-axis by the transformation of Eq. (17.59), we complete the approximation procedure and then use Eq. (17.62) to give us the desired z-domain transfer function $T(z)$, which satisfies the prescribed behavior exactly. Analogous to the continuous-time domain, Eq. (1.12), the function $T(z)$ can be written in polynomial form or in factored form:

$$T(z) = \frac{V_{out}(z)}{V_{in}(z)} = \frac{\sum_{n=0}^{M} b_n z^n}{\sum_{n=1}^{N} a_n z^n + 1} = K \frac{\prod_{n=1}^{M} (z - z_n)}{\prod_{n=1}^{N} (z - p_n)} = K \frac{\prod_{n=1}^{M/2} \left(\beta_{2n} z^2 + \beta_{1n} z + \beta_{0n}\right)}{\prod_{n=1}^{N/2} \left(z^2 + \alpha_{1n} z + \alpha_{0n}\right)} \tag{17.64}$$

In Eq. (17.64) we assumed that M and N are even and we have combined the (usually) conjugate complex roots into second-order factors with real coefficients. The coefficient β_{2n} is either zero or one. Naturally, if M and/or N are odd, a first-order factor will appear in the numerator and/or denominator. There is no difference in principle from our familiar treatment of a continuous-time transfer function $T(s_{ct})$. The high-order function is factored into first-order

$$T_1(z) = \frac{b_1 z + b_0}{a_1 z + 1} \tag{17.65}$$

and second-order

$$T_2(z) = \frac{b_2 z^2 + b_1 z + b_0}{a_2 z^2 + a_1 z + 1} \tag{17.66}$$

factors in the z domain which are realized by a suitable SC module, such as the circuits in Fig. 17.12, 17.29, or 17.32.

EXAMPLE 17.7

We need to realize an SC lowpass filter with the specifications

passband attenuation: $\alpha_{max} \leq 0.9$ dB in $0 \leq f = f_p = 3.2$ kHz

stopband attenuation: $\alpha_{min} \geq 22$ dB in $4.3 \text{ kHz} = f_s \leq f \leq f_c/2$

The clock frequency is $f_c = 24$ kHz. Find and realize the z-domain transfer function.

Solution

Note that the switching frequency is fairly small here so that we cannot use a design based on the assumption of fast switching, $f_c \gg 2\pi f$. The first step in the solution is to find

the z-domain transfer function. To this end we prewarp the f-axis specifications to the f_{ct}-axis in the continuous-time domain by applying Eq. (17.59):

$$\omega_{ct,p} = \frac{2}{T}\tan\frac{\omega_p T}{2} = 2f_c\tan\left(\pi\frac{f_p}{f_c}\right) = 48{,}000\tan\left(\frac{3.2}{24}\pi\right) = 2\pi\cdot 3401.3\text{rad/s}$$

$$\omega_{ct,s} = \frac{2}{T}\tan\frac{\omega_s T}{2} = 2f_c\tan\left(\pi\frac{f_s}{f_c}\right) = 48{,}000\tan\left(\frac{4.3}{24}\pi\right) = 2\pi\cdot 4820.1\text{rad/s}$$

Thus, along the ω_{ct}-axis, the specifications are

passband attenuation: $\alpha_{max} \le 0.9$ dB in $0 \le f_{ct} \le f_{ct,p} = 3.401$ kHz

stopband attenuation: $\alpha_{min} \ge 22$ dB in $4.820\text{ kHz} = f_{ct,s} \le f_{ct} \le f_c/2$

Next we solve the approximation problem. Since no phase performance is specified, let us choose an elliptic (Cauer) approximation, Chapter 8, to keep the filter order as low as possible. With $f_{ct,s}/f_{ct,p} = 4.82/3.4 \approx 1.42$ and $\alpha_{max} \le 0.9$ dB we find from Table 8.4 the third-order Cauer function

$$T(\bar{s}_{ct}) = \frac{0.2745\left(\bar{s}_{ct}^2 + 2.41363\right)}{\left(\bar{s}_{ct} + 0.63584\right)\left(\bar{s}_{ct}^2 + 0.36139\bar{s}_{ct} + 1.04183\right)} \tag{17.67}$$

where $\bar{s}_{ct}$ is normalized with respect to the passband corner, $f_{ct,p}$. The transformation into the z-domain is obtained by Eq. (17.58):

$$\bar{s}_{ct} = \frac{s_{ct}}{\omega_{ct,p}} = \frac{1}{\omega_{ct,p}}\frac{2}{T}\frac{z-1}{z+1} = \frac{f_c}{\pi f_{ct,p}}\frac{z-1}{z+1} = 2.2460\frac{z-1}{z+1} \tag{17.68}$$

If we now substitute Eq. (17.68) into Eq. (17.67) we obtain the desired z-domain transfer function that has the prescribed behavior along the unit circle in the z-plane:

$$T(z) = \frac{0.2745\left[\left(2.246\dfrac{z-1}{z+1}\right)^2 + 2.41363\right]}{\left(2.246\dfrac{z-1}{z+1} + 0.63584\right)\left[\left(2.246\dfrac{z-1}{z+1}\right)^2 + 0.36139\times 2.246\dfrac{z-1}{z+1} + 1.04183\right]}$$

To be able to realize this function as a cascade of a first- and a second-order section we need to bring it into the form of a ratio of polynomials in factored form. Carrying out the necessary algebra, we obtain

$$T(z) = \frac{0.1029(z+1)\left(z^2 - 0.7055z + 1\right)}{(z - 0.5582)\left(z^2 - 1.1605z + 0.7647\right)} \tag{17.69}$$

Notice that $T(z)$ has a zero at $z = -1$, corresponding to $\omega_{ct} = \infty$, and a pair of complex zeros on the unit circle, $z_{2,3} = e^{\pm j\omega_{2,3}T} = e^{\pm j1.2103}$. In the sampled-data domain, these zeros are at

$$\omega_{2,3} = \pm\frac{1.2103}{T} = \pm 1.2103\cdot 24\text{krad/s} = \pm 2\pi\cdot 4.623\text{krad/s}$$

and in the continuous-time domain at

$$\omega_{ct} = \pm\frac{2}{T}\tan\frac{\omega T}{2} = 48{,}000\tan\left(\pi\frac{4623}{24{,}000}\right) = 33.203\text{krad/s} = \pm 2\pi \cdot 5.284\text{krad/s}$$

in agreement with Eq. (17.67): $\sqrt{2.41363} \times 3.401$ kHz $= 5.284$ kHz. A Bode plot of the base band, $\omega T < \pi$, is shown in Fig. 17.35. (Remember that the function is periodic as was illustrated in Fig. 17.31.)

In the next step of the design we realize the SC filter. We factor the transfer function of Eq. (17.69) into a product of a first- and a second-order section:

$$T(z) = T_1(z) \times T_2(z) = 0.221\frac{z+1}{z-0.5582} \times 0.466\frac{z^2 - 0.7055z + 1}{z^2 - 1.1605z + 0.7647} \tag{17.70}$$

The gain constant 0.1029 was factored into 0.221×0.466 so that each section has unity gain at $z = 1(\omega = 0)$.

The first-order block is realized by the circuit in Fig. 17.12b. Its transfer function is derived from Fig. 17.24 where the switch phases to the left of C_2 are interchanged ($C_2 z^{-1}$ is replaced by $-C_2$), and the connections $V_1 = V_2 = V_{in}$ and $V_3 = V_{out}$ are made. This process results in Eq. (17.47) with $C_2 z^{-1}$ replaced by $-C_2$:

$$T_1(z) = -\frac{C_1\left(1 - z^{-1}\right) + C_2}{C_F\left(1 - z^{-1}\right) + C_3} = -\frac{C_1 + C_2}{C_F + C_3}\frac{z - \dfrac{C_1}{C_1 + C_2}}{z - \dfrac{C_F}{C_F + C_3}} = 0.221\frac{z+1}{z - 0.5582}$$

Comparing coefficients we find that we must choose[4] $C_2 = -2C_1$ to obtain

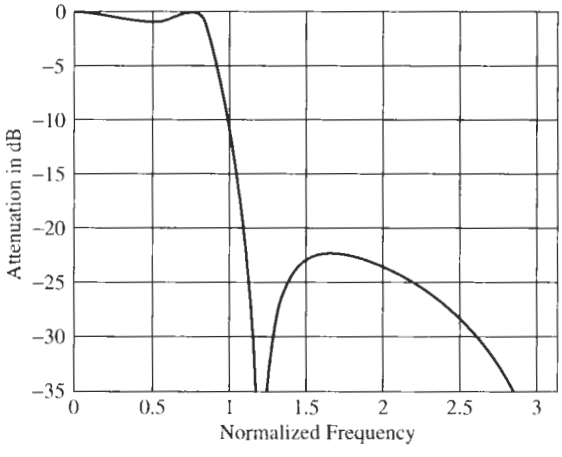

Figure 17.35 The base band ($0 \geq \omega T \geq \pi$) magnitude of the elliptic transfer function of Eq. (17.69).

[4]Recall our agreement that negative components are obtained from differential circuits, that is, in the present case the circuit with input connections as in Fig. 17.27b would be used so that C_2 is negative.

$$T_1(z) = \frac{C_1}{C_F + C_3} \frac{z+1}{z - \dfrac{C_F}{C_F + C_3}} = 0.221 \frac{z+1}{z - 0.5582}$$

which gives $C_1/C_F = 0.3959$, $C_3/C_F = 0.7915$. Let us choose $C_F = 2$ pF so that $C_1 = 0.792$ pF and $C_3 = 1.583$ pF.

Next we design the biquad. We choose the circuit in Fig. 17.29 and compare Eq. (17.53)[5] with $T_2(z)$ in Eq. (17.70). Disregarding the minus sign in Eq. (17.53), we obtain

$$T_2(z) = \frac{C_{11}}{C + C_{10}} \frac{z^2 + z\dfrac{C_6 - C_{11} - C_{12}}{C_{11}} + \dfrac{C_{12} - C_7}{C_{11}}}{z^2 + z\dfrac{C_3 + C_8 - C_{10} - 2C}{C + C_{10}} + \dfrac{C - C_3}{C + C_{10}}} = 0.466 \frac{z^2 - 0.7055z + 1}{z^2 - 1.1605z + 0.7647}$$

Comparing coefficients results in the equations

$$\frac{C_{11}}{C + C_{10}} = 0.466, \quad \frac{C_6 - C_{12}}{C_{11}} = 0.2945, \quad \frac{C_{12} - C_7}{C_{11}} = 1,$$
$$\frac{C_3 + C_8 + C_{10}}{C + C_{10}} = 0.8395, \quad \frac{C - C_3}{C + C_{10}} = 0.7647$$

From these equations we find

$$C + C_{10} = 2.1459C_{11}, \quad C_6 - C_{12} = 0.2945C_{11}, \quad C_{12} - C_7 = C_{11},$$
$$C_3 + C_8 = 0.8395C - 0.1605C_{10}, \quad C_3 = 0.2353C - 0.7647C_{10} \tag{17.71}$$

Although effectively negative capacitors may be implemented we will try to solve these equations such that all capacitors are positive. An examination of Eq. (17.71) reveals that we may choose two capacitors at our convenience because we have more unknown components than equations. Let us select $C_7 = 0$ and $C_{10} = 0.3077C$. Then we have

$$C_3 = 0, \quad C_6 = 0.7889C, \quad C_8 = 0.7901C, \quad C_{11} = C_{12} = 0.6094C$$

Finally we select $C = 2$ pF to arrive at the circuit in Fig. 17.36.

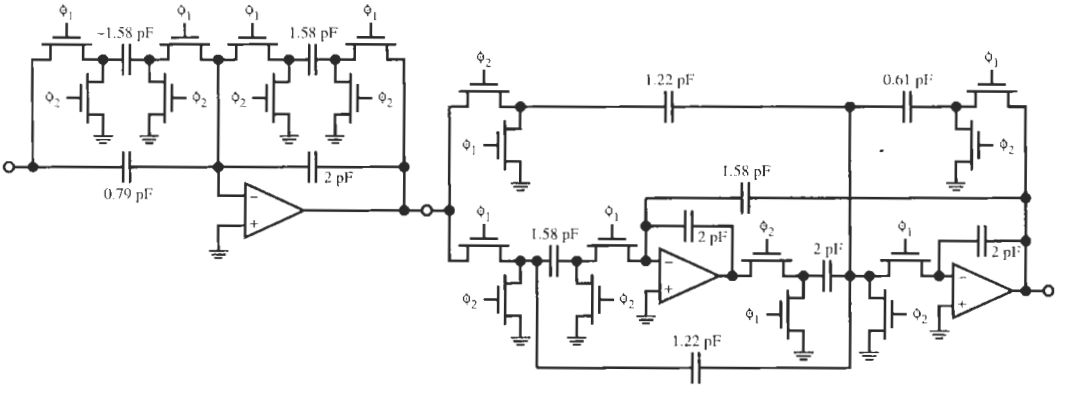

Figure 17.36 The third-order elliptic SC filter of Example 17.7.

[5]Equation (17.54) and the circuit in Fig. 17.32 could also be taken.

17.9 DESIGN OF SWITCHED-CAPACITOR LADDER FILTERS

We have pointed out a number of times in this book that *LC* ladders are the best possible filter realization for many applications because of their low passband sensitivities to component tolerances. Consequently, we hope to be able to develop switched-capacitor filters that simulate the performance of lossless ladders. From the study of SC design methods up to this point in our discussion, the student will correctly anticipate that an SC realization of *LC* ladder structures should indeed be possible: we only have to note that inverting and noninverting, lossy or lossless, summing SC integrators can be built (see Figs. 17.11 and 17.12) and that these are the only "components" necessary for obtaining a ladder via the signal-flow graph (SFG) method. The SFG method was discussed in Chapter 15 for continuous-time active *RC* designs. As it will be used for SC ladder implementations in an almost identical fashion in the following, the student may wish to review the relevant material at this time. As a matter of fact, *for very fast sampling* we could just take a continuous-time domain active *RC* design and replace the resistors R by their SC equivalent $1/(f_c C)$. But as we have learned, the sampled-data method of signal processing entails the periodic nature of the transfer characteristic, and unless $f_c \gg \omega_{ct}$, causes a number of errors that we need to address in precision designs.

As is normally the case in SC filter design, we start a ladder simulation from a transfer characteristic specified on the discrete-time frequency axis ω in $0 \leq \omega \leq \omega_c/2$. From the ω-axis, the specifications are transformed (prewarped) onto the continuous-time axis ω_{ct} by applying Eq. (17.59). The prewarping process was explained in Section 17.7 and in Example 17.7. Then, as was also explained in Example 17.7, we solve the approximation problem on the normalized $\bar{\omega}_{ct}$-axis and obtain a transfer function of the form

$$T(\bar{s}_{ct}) = \frac{b_m \bar{s}_{ct}^m + \cdots + b_1 \bar{s}_{ct} + b_0}{\bar{s}_{ct}^n + a_{n-1}\bar{s}_{ct}^{n-1} + a_{n-2}\bar{s}_{ct}^{n-2} + \cdots + a_1 \bar{s}_{ct} + a_0} \tag{17.72}$$

Note that $\bar{s}_{ct}$ is usually a frequency normalized to the passband corner. $T(\bar{s}_{ct})$ is then realized as an *LC* ladder by the methods discussed in Chapter 13 or a realization is found from tables, such as tables 13.1 or 13.2. The process yields the series branches $Y(\bar{s}_{ct})$ and the shunt branches $Z(\bar{s}_{ct})$ of the *LC* ladder as shown in Fig. 15.2. The equations describing the ladder are Eqs. (15.11) through (15.16). We chose a normalizing resistor R_p and now need to find a way to implement the transfer functions $t_Y(\bar{s}_{ct}) = R_p Y(\bar{s}_{ct})$ and $t_Z(\bar{s}_{ct}) = Z(\bar{s}_{ct})/R_p$. We recall that for simple all-pole lowpass ladders with series inductors and shunt capacitors, the functions t_Y and t_Z are integrators but that for general ladders more complicated structures are needed, such as the ones in Fig. 15.13. We now intend to perform switched-capacitor ladder design by following the active-*RC* signal-flow graph method in Chapter 15 exactly.

Since we are here interested in using switched-capacitor integrators in the sampled-data domain let us first make a few modifications to the transfer function of Eq. (17.72) so that we can identify the SC integrators in the z-domain. To this end we introduce three variables that prove useful in the development. The first of these we encountered earlier: after normalizing s_{ct} by $T/2$ we label the bilinear transformation as λ:

$$\lambda = \frac{s_{ct}T}{2} = \frac{z-1}{z+1} = \frac{z^{1/2} - z^{-1/2}}{z^{1/2} + z^{-1/2}} = \tanh \frac{sT}{2} \tag{17.73a}$$

We recognize the hyperbolic tangent by recalling that $z = e^{sT}$. Also we introduce the two variables

$$\gamma = \frac{1}{2}\left(z^{1/2} - z^{-1/2}\right) = \sinh\frac{sT}{2} \tag{17.73b}$$

$$\mu = \frac{1}{2}\left(z^{1/2} + z^{-1/2}\right) = \cosh\frac{sT}{2} \tag{17.73c}$$

and we note that

$$\lambda = \frac{\gamma}{\mu}, \quad \mu^2 - \gamma^2 = 1, \quad z^{1/2} = \mu + \gamma \tag{17.73d}$$

λ, γ, and μ are nothing but different nonlinearly transformed frequency variables.

EXAMPLE 17.8

Express the discrete-time inverting and noninverting lossy integrators in terms of the frequency variables λ, γ, and μ. The circuits are given in Figs. 17.17a and 17.18a and the z-domain equations are Eqs. (17.25a,b).

Solution

We find directly

$$T_I(z) = -\frac{C_1}{C_F\left(1 - z^{-1}\right) + C_3} = -\frac{C_1 z^{1/2}}{C_F\left(z^{1/2} - z^{-1/2}\right) + C_3 z^{1/2}}$$

$$= -\frac{C_1 z^{1/2}}{(2C_F + C_3)\gamma + C_3\mu} \tag{17.74a}$$

$$T_N(z) = \frac{C_2 z^{-1}}{C_F\left(1 - z^{-1}\right) + C_3} = \frac{C_2 z^{-1/2}}{C_F\left(z^{1/2} - z^{-1/2}\right) + C_3 z^{1/2}}$$

$$= \frac{C_2 z^{-1/2}}{(2C_F + C_3)\gamma + C_3\mu} \tag{17.74b}$$

Notice that we obtained integrators in the γ-domain with *frequency-dependent* loss $C_3\mu$. The integration capacitor C_F has *doubled* in value and the loss term C_3 affects the integration time constant. If $C_3 = 0$, the integrators in the γ-domain are ideal:

$$T_I(z) = -\frac{C_1}{2C_F\gamma} z^{1/2}, \quad T_N(z) = \frac{C_2}{2C_F\gamma} z^{-1/2} \tag{17.75}$$

As we observed earlier, the inverting and noninverting integrators, respectively, have a leading or lagging phase error $\pm\omega T/2$. This error will be of no concern to us in the design because for stability reasons we will always pair an inverting and a noninverting integrator in a loop, so that the net phase error is zero: $z^{1/2}z^{-1/2} = 1$.

EXAMPLE 17.9

Express the discrete-time three-input integrator of Fig. 17.24a in terms of the frequency variable γ and develop a small-signal model analogous to the one in Fig. 17.24b for the circuit. Use the result to develop (1) an inverting lossy two-input summing integrator and (2) a noninverting lossy two-input summing integrator.

Solution

We start by reformatting the z-domain equation (17.46a) that describes the integrator:

$$V_{out}(z) = -\frac{C_1}{C_F}V_1(z) + \frac{C_2}{C_F}\frac{z^{-1}}{1-z^{-1}}V_2(z) - \frac{C_3}{C_F}\frac{1}{1-z^{-1}}V_3(z)$$

and obtain

$$\begin{aligned} V_{out}(z) &= -\frac{C_1}{C_F}V_1(z) + \frac{C_2}{C_F}\frac{z^{-1/2}}{z^{1/2}-z^{-1/2}}V_2(z) - \frac{C_3}{C_F}\frac{z^{1/2}}{z^{1/2}-z^{-1/2}}V_3(z) \\ &= \frac{1}{C_F}\frac{1}{z^{1/2}-z^{-1/2}}\left[-C_1\left(z^{1/2}-z^{-1/2}\right)V_1(z) + C_2 z^{-1/2}V_2(z) - C_3 z^{1/2}V_3(z)\right] \end{aligned} \quad (17.76)$$

In this expression we identify the parameter γ from Eq. (17.73b) so that we can write

$$V_{out}(z) = \frac{1}{2C_F}\frac{1}{\gamma}\left[-2C_1\gamma V_1(z) + C_2 z^{-1/2}V_2(z) - C_3 z^{1/2}V_3(z)\right] \quad (17.77)$$

A model for Eq. (17.77) is shown in Fig. 17.37.

To create an inverting lossy summing integrator, we connect V_3 to the output. Then we remove the two inputs V_1 and V_2 and generate two new inputs V_{in1} and V_{in2} through capacitors C_{11} and C_{12}, respectively, of the type connected to V_3 in Fig. 17.37 (the switching configuration connected to V_3 in Fig. 17.24a). The result is

$$\begin{aligned} V_{out}(z) &= \frac{1}{2C_F\gamma + C_3 z^{1/2}}\left[-C_{11}z^{1/2}V_{in1}(z) - C_{12}z^{1/2}V_{in2}(z)\right] \\ &= -\frac{z^{1/2}}{(2C_F + C_3)\gamma + C_3\mu}\left[C_{11}V_{in1}(z) + C_{12}V_{in2}(z)\right] \end{aligned} \quad (17.78a)$$

Figure 17.38a shows the circuit. Observe that $z^{1/2}$ realizes a leading phase error in the integrator as we would expect from Eq. (17.74a). For the noninverting integrator we follow the same steps but create two inputs V_{in1} and V_{in2} through capacitors C_{21} and C_{22} of the type connected to V_2 in Fig. 17.37:

$$V_{out}(z) = \frac{z^{-1/2}}{(2C_F + C_3)\gamma + C_3\mu}\left[C_{21}V_{in1}(z) + C_{22}V_{in2}(z)\right] \quad (17.78b)$$

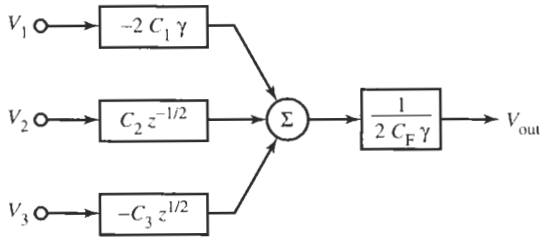

Figure 17.37 The γ-plane model for the three-input integrator of Fig. 17.24.

Here we have a lagging phase error as in Eq. (17.74b). Also observe that in both circuits the loss (C_3) affects the integration time constant and the loss term ($C_3\mu$) depends on frequency. The noninverting circuit is seen in Fig. 17. 38b.

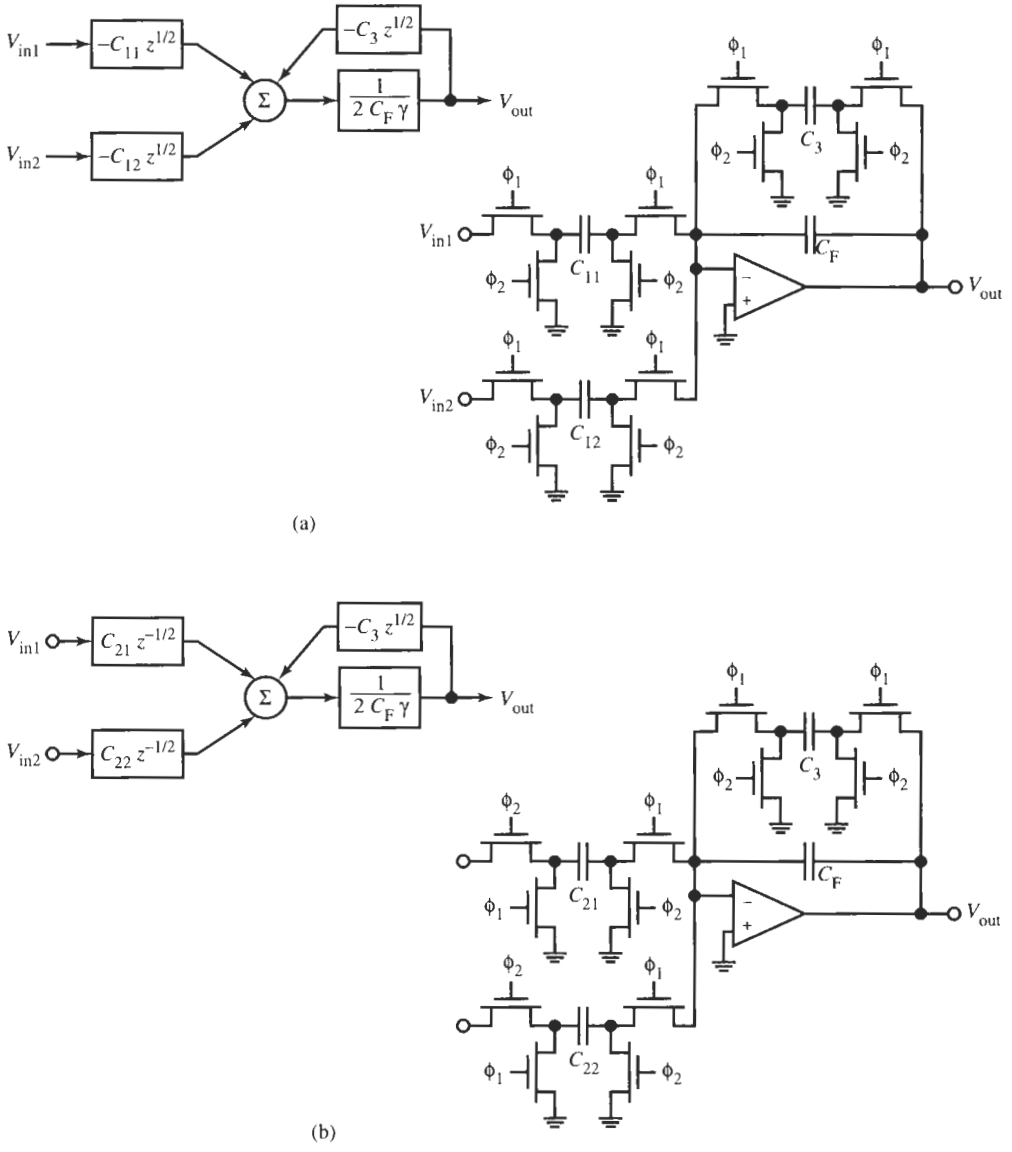

Figure 17.38 Two-input summing integrators: (a) inverting; (b) noninverting.

With our newly defined variables, the synthesis of the function $T(\bar{s}_{ct})$ of Eq. (17.72) now proceeds as follows. We assumed that $T(\bar{s}_{ct})$ was obtained from an approximation problem and $\bar{s}_{ct}$ will, therefore, be normalized, say, to the prewarped passband edge ω_0, $\bar{s}_{ct} = s_{ct}/\omega_0$. We will first denormalize the frequency $\bar{s}_{ct}$ by multiplying it by ω_0, $s_{ct} = \bar{s}_{ct}\omega_0$. Then we make a formal change of variables, replacing the denormalized frequency s_{ct} by $2\lambda/T$ per Eq. (17.73a):

$$s_{ct} = \bar{s}_{ct}\omega_0 = \frac{2}{T}\lambda \tag{17.79}$$

Although the bilinear transformation is hidden in λ, see Eq. (17.73a), for now we consider λ as just an abbreviation for $s_{ct}T/2$. Combining these steps means that we need to replace the normalized continuous-time frequency $\bar{s}_{ct}$ in Eq. (17.72) by

$$\bar{s}_{ct} = \frac{s_{ct}}{\omega_0} = \frac{2}{\omega_0 T}\lambda \tag{17.80}$$

We do this by multiplying the numerator and denominator of Eq. (17.72) by $[2/(\omega_0 T)]^n$. The result is

$$T(\lambda) = \frac{\left(\frac{\omega_0 T}{2}\right)^{n-m}\left[b_m\lambda^m + \cdots + \left(\frac{\omega_0 T}{2}\right)^{m-1} b_1\lambda + \left(\frac{\omega_0 T}{2}\right)^m b_0\right]}{\lambda^n + a_{n-1}\left(\frac{\omega_0 T}{2}\right)\lambda^{n-1} + a_{n-2}\left(\frac{\omega_0 T}{2}\right)^2\lambda^{n-2} + \cdots + a_1\left(\frac{\omega_0 T}{2}\right)^{n-1}\lambda + \left(\frac{\omega_0 T}{2}\right)^n a_0} \tag{17.81}$$

To simplify the equation, let us introduce the following notation for the coefficients:

$$K = \left(\frac{\omega_0 T}{2}\right)^{n-m}, \quad B_j = K\left(\frac{\omega_0 T}{2}\right)^{m-j} b_j, \quad \text{and} \quad A_{n-k} = a_{n-k}\left(\frac{\omega_0 T}{2}\right)^k \tag{17.82}$$

Then we have the transfer function

$$T(\lambda) = \frac{B_m\lambda^m + \cdots + B_1\lambda + B_0}{\lambda^n + A_{n-1}\lambda^{n-1} + A_{n-2}\lambda^{n-2} + \cdots + A_1\lambda + A_0} \tag{17.83}$$

in the continuous-time λ-plane. We wish to realize this function as a lossless ladder. Let us illustrate the steps taken with an example.

EXAMPLE 17.10

Design a lowpass filter with elliptic magnitude to satisfy the following:

passband attenuation: $\alpha_{max} \leq 0.5$ dB in $0 \leq f \leq f_p = 4.43$ kHz

stopband attenuation: $\alpha_{min} \geq 23$ dB in $f_s = 7.36$ kHz $\leq f \leq f_c/2$

dc gain: 0 dB

clock frequency: $f_c = 64$ kHz

Solution

We start by prewarping the frequency axis; with Eq. (17.59) we find

$$\omega_{ct,p} = \frac{2}{T}\tan\frac{\omega_p T}{2} = 128{,}000\tan\left(\pi\frac{4.43}{64}\right) = 2\pi \cdot 4501 \text{ rad/s}$$

$$\omega_{ct,s} = \frac{2}{T}\tan\frac{\omega_s T}{2} = 128{,}000\tan\left(\pi\frac{7.36}{64}\right) = 2\pi \cdot 7698 \text{ rad/s}$$

The transfer function for these requirements, $\alpha_{max} \leq 0.5$ dB in $f_{ct} \leq 4.501$ kHz and $\alpha_{min} \geq 23$ dB in $f_{ct} \geq 7.698$ kHz, can be found from a table:

$$T(\bar{s}_{ct}) = \frac{0.2816\left(\bar{s}_{ct}^2 + 3.2236\right)}{\left(\bar{s}_{ct} + 0.7732\right)\left(\bar{s}_{ct}^2 + 0.4916\bar{s}_{ct} + 1.1742\right)} \tag{17.84}$$

where $\bar{s}_{ct} = s_{ct}/\omega_{ct,p}$. This result corresponds to the general equation (17.72). We then need to replace $\bar{s}_{ct}$ by $[2/(\omega_0 T)]\lambda$ per Eq. (17.80). For this third-order function ($n = 3$) this means we multiply the numerator and denominator of Eq. (17.84) by

$$\left(\frac{\omega_0 T}{2}\right)^3 = \left(\pi\frac{f_{ct,p}}{f_c}\right)^3 = \left(\pi\frac{4.501}{64}\right)^3 = 0.22094^3 = 0.01079$$

as in Eq. (17.81). The result is

$$T(\lambda) = \frac{0.0622\left(\lambda^2 + 0.1626\right)}{\left(\lambda + 0.1708\right)\left(\lambda^2 + 0.1086\lambda + 0.0592\right)} \tag{17.85}$$

which corresponds to Eq. (17.83) and must be realized as a lossless ladder.

The transfer function $T(\lambda)$, Eq. (17.83), we obtained at this point satisfies the prescribed filter requirements along the λ-axis in $0 \leq \lambda \leq \infty$ *exactly*. These requirements are then transformed *exactly* onto the unit-circle in the z-plane by the bilinear transformation of Eq. (17.73a), i.e., by substituting

$$\lambda = \frac{z-1}{z+1}$$

Our task at this point is to realize the resulting z-domain transfer function as an SC ladder simulation. The problem is addressed most easily and intuitively by staying in the continuous-time λ-domain, i.e., by realizing $T(\lambda)$ instead of $T(z)$.[6] It should be clear to the student that it makes no difference to the realization procedure which label, s, s_{ct}, or λ, we attach to the independent variable. The process in the λ-plane is identical to the one in the s-plane; we simply change notation from s to λ.

We explained in Section 15.2 that in general the realization process leads to the typical ladder branches shown in Fig. 15.10 and further to the transmittances $t_Y(\lambda)$ for the series and $-t_Z(\lambda)$ for the shunt ladder arms; they were defined in Eqs. (15.40) and (15.41) in the s-plane and we repeat them for convenience here with suitable notation in the λ-plane:

[6] As was pointed out earlier, for ease of reference we labeled all transfer functions as $T(\cdot)$ regardless of their arguments. Actually, the frequency transformations result, of course, in different functions. $T(\lambda)$ and $T(z)$ have the same degree but different coefficients.

$$t_Y(\lambda) = \cfrac{1}{\lambda l_1 + \cfrac{1}{\lambda c_1} + \cfrac{1}{\lambda c_2 + \cfrac{1}{\lambda l_2}}} \tag{17.86}$$

$$-t_Z(\lambda) = -\cfrac{1}{g_1 + \lambda c_1 + \cfrac{1}{\lambda l_1} + \cfrac{1}{\lambda l_2 + \cfrac{1}{\lambda c_2}}} \tag{17.87}$$

The corresponding ladder branches are sketched in Fig. 17.39. Because we are dealing with lossless ladders we have no resistors in the series branches and we have elected to eliminate the loss term from the series branch t_Y. The only resistors are source and load resistors that we treat as shunt elements in the input and output admittance arms t_Z.

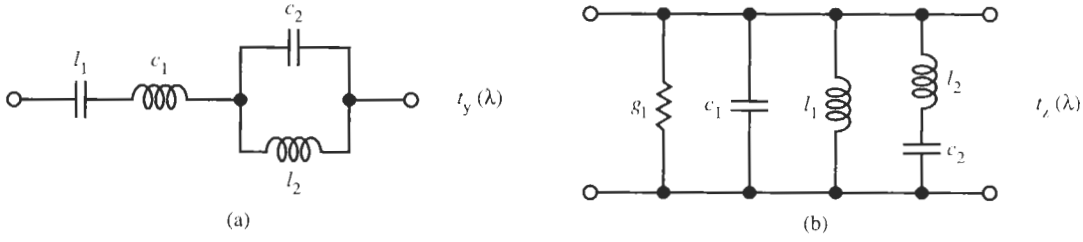

Figure 17.39 Series (a) and shunt (b) ladder arms in the λ-plane.

EXAMPLE 17.11

Realize the function of Eq. (17.85) as a lossless ladder in the λ-plane.

Solution

The ladder can be obtained by the method discussed in Chapter 13; Example 13.3 contains the detailed procedure. Figure 17.40 shows the circuit. For our example in Fig. 17.40 with $R_S = R_L = R$, $t_Y(\lambda)$ and $-t_Z(\lambda)$ for the three branches are

$$\begin{aligned}
\frac{V_1}{RI_0 - RI_2} &= \frac{Z_1}{R} = t_{Z1}(\lambda) = \frac{1}{1 + \lambda c_1} = \frac{1}{1 + 5.8535\lambda} \\
\frac{RI_2}{V_1 - V_3} &= Y_2 R = t_Y(\lambda) = \cfrac{1}{\cfrac{1}{c_2\lambda + \cfrac{1}{l_2\lambda}}} = \cfrac{1}{\cfrac{1}{1.6773\lambda + \cfrac{1}{3.7905\lambda}}} \\
\frac{V_3}{RI_2} &= \frac{Z_3}{R} = t_{Z3}(\lambda) = \frac{1}{1 + 5.8535\lambda}
\end{aligned} \tag{17.88}$$

Following the procedure in Chapter 15 for simulating ladders, we have normalized all parameters in the circuit by R so that currents become voltage signals, and have used lower-case symbols for the normalized elements.

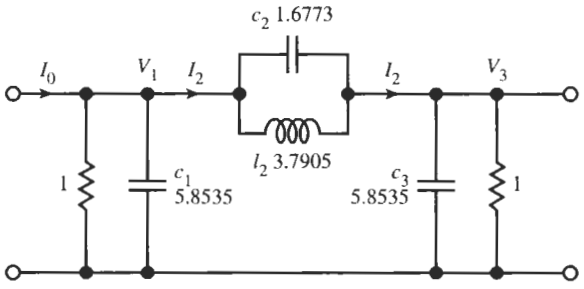

Figure 17.40 The third-order ladder for Example 17.11 in the λ-plane.

17.9.1 The γ-Plane Circuit

If we proceed with the signal-flow graph method of Section 15.2 to realize t_Y and t_Z using the circuits of Fig. 15.11, we need to build summing integrators *in the* λ*-plane*. However, the integrators available to us in Fig. 17.38 are *in the* γ*-plane* [see also Eqs. (17.74), (17.75), and (17.78)]. To be able to use these blocks, we need to modify (transform) t_Y and t_Z and make use of the identity $\lambda\mu = \gamma$ per Eq. (17.73d). The suggested transformation multiplies t_Y and divides t_Z by μ; in other words we scale the ladder impedances by the frequency parameter μ. We saw in Section 14.5 that such a scaling step does not change the transfer function. Performing the scaling by μ we obtain from Eqs. (17.86) and (17.87)

$$\mu t_Y(\lambda) = \cfrac{1}{\cfrac{\lambda}{\mu}l_1 + \cfrac{1}{\lambda\mu c_1} + \cfrac{1}{\lambda\mu c_2 + \cfrac{1}{\cfrac{\lambda}{\mu}l_2}}}$$

$$-\frac{1}{\mu}t_Z(\lambda) = -\cfrac{1}{\mu g_l + \lambda\mu c_1 + \cfrac{1}{\cfrac{\lambda}{\mu}l_1} + \cfrac{1}{\cfrac{\lambda}{\mu}l_2 + \cfrac{1}{\lambda\mu c_2}}}$$

If we make use next of Eq. (17.73d), $\mu^2 = 1 + \gamma^2$, then λ/μ becomes $\lambda/\mu = \lambda\mu/\mu^2 = \gamma/(1+\gamma^2)$ and both functions are expressed entirely in terms of γ. We obtain for the series branch:

$$\mu t_Y(\lambda) = t_Y(\gamma) = \cfrac{1}{\cfrac{\gamma}{1+\gamma^2}l_1 + \cfrac{1}{\gamma c_1} + \cfrac{1}{\gamma c_2 + \cfrac{1}{\cfrac{\gamma}{1+\gamma^2}l_2}}}$$

$$= \cfrac{1}{\cfrac{1}{1/(\gamma l_1) + \gamma/l_1} + \cfrac{1}{\gamma c_1} + \cfrac{1}{\gamma\,(c_2 + 1/l_2) + 1/(\gamma l_2)}} \tag{17.89a}$$

The realization of this series branch in the γ-plane is shown in Fig. 17.41a. An alternative way of writing t_Y is

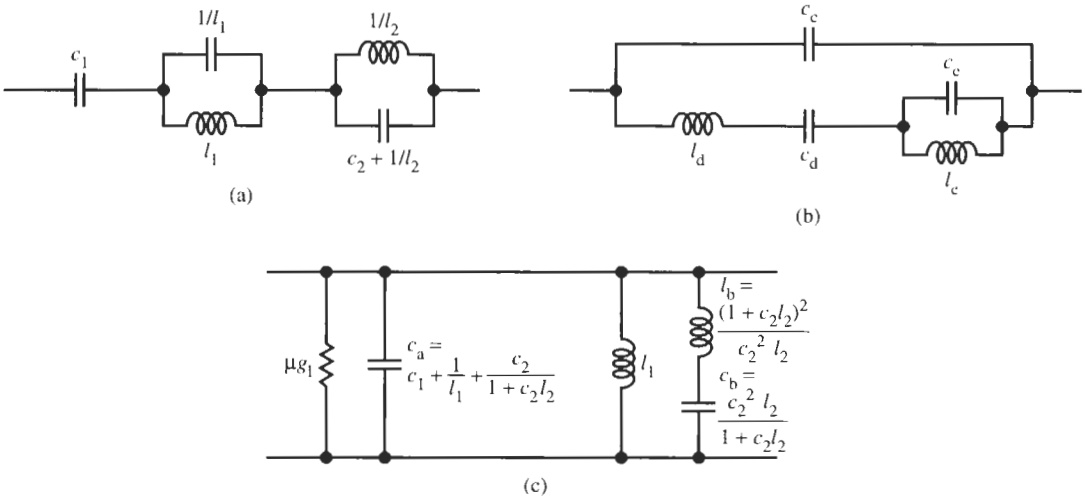

Figure 17.41 Realization of the lossless ladder arms in the γ-plane: (a) and (b): described by Eqs. (17.89a, b); (c) by Eq. (17.90).

$$t_Y(\gamma) = \frac{\gamma c_1 \left(1+\gamma^2\right)\left[\gamma^2 (l_2 c_2 + 1) + 1\right]}{\gamma^4 \left[(c_1 l_1 + 1)(l_2 c_2 + 1) + c_1 l_2\right] + \gamma^2 \left[c_1 (l_1 + l_2) + c_2 l_2 + 2\right] + 1}$$
$$= \gamma c_c + \cfrac{1}{\gamma l_d + \cfrac{1}{\gamma c_d + \cfrac{1}{\gamma c_e + \cfrac{1}{\gamma l_e}}}} \tag{17.89b}$$

which is realized by the circuit in Fig 17.41b.

For the shunt branch we find

$$-\frac{1}{\mu} t_Z(\lambda) = -t_Z(\gamma) = -\cfrac{1}{\mu g_1 + \gamma c_1 + \cfrac{1}{\cfrac{\gamma}{1+\gamma^2} l_1} + \cfrac{1}{\cfrac{\gamma}{1+\gamma^2} l_2 + \cfrac{1}{\gamma c_2}}}$$
$$= -\frac{1}{\mu g_1 + \gamma \left(c_1 + \dfrac{1}{l_1}\right) + \dfrac{1}{\gamma l_1} + \left(\dfrac{c_2}{c_2 l_2 + 1}\right) \dfrac{\gamma \left(1+\gamma^2\right)}{\gamma^2 + 1/(c_2 l_2 + 1)}}$$

The last term in the denominator of this equation can be brought into the form

$$\left(\frac{c_2}{c_2 l_2 + 1}\right) \frac{\gamma^3 + \gamma}{\gamma^2 + 1/(c_2 l_2 + 1)} = \frac{c_2}{c_2 l_2 + 1} \gamma + \cfrac{1}{\cfrac{(c_2 l_2 + 1)^2}{c_2^2 l_2} \gamma + \cfrac{1}{\cfrac{c_2^2 l_2}{c_2 l_2 + 1} \gamma}}$$
$$= \frac{c_2}{c_2 l_2 + 1} \gamma + \cfrac{1}{l_b \gamma + \cfrac{1}{c_b \gamma}}$$

so that

$$-t_Z(\gamma) = -\frac{1}{\mu g_1 + \gamma\left(c_1 + \dfrac{1}{l_1} + \dfrac{c_2}{c_2 l_2 + 1}\right) + \dfrac{1}{\gamma l_1} + \dfrac{1}{l_b\gamma + 1/(c_b\gamma)}}$$

$$= -\frac{1}{\mu g_1 + c_a\gamma + \dfrac{1}{\gamma l_1} + \dfrac{1}{l_b\gamma + 1/(c_b\gamma)}} \tag{17.90}$$

Figure 17.41c shows a realization of Eq. (17.90) in the γ-plane. Observe that the loss term in Eq. (17.90) is frequency dependent in exactly the way we need for realizing the function with our SC integrator circuits [see Eq. (17.78) and Fig. 17.38].

EXAMPLE 17.12

Transform the ladder branches of Example 17.11 into the γ-plane.

Solution

The functions are given in Eq. (17.88). Using the transformations in Eqs. (17.89b) and (17.90) we obtain

$$\frac{1}{\mu}t_{Z1}(\lambda) = t_{Z1}(\gamma) = \frac{1}{\mu + \lambda\mu c_1} = \frac{1}{\mu + \gamma c_1} = \frac{1}{\mu + 5.8535\gamma}$$

$$\frac{1}{\mu}t_{Z3}(\lambda) = t_{Z3}(\gamma) = t_{Z1}(\gamma) = \frac{1}{\mu + 5.8535\gamma} \tag{17.91a}$$

and

$$\mu t_Y(\lambda) = t_Y(\gamma) = \frac{1}{\dfrac{1}{\mu\lambda c_2 + \dfrac{\mu}{\lambda l_2}}} = \frac{1}{\dfrac{1}{\gamma c_2 + \dfrac{1+\gamma^2}{\gamma l_2}}}$$

$$= \frac{1}{\dfrac{1}{\gamma\left(c_2 + \dfrac{1}{l_2}\right) + \dfrac{1}{\gamma l_2}}} = \frac{1}{\dfrac{1}{1.9411\gamma + \dfrac{1}{3.7905\gamma}}} \tag{17.91b}$$

The realization of these functions in the γ-plane follows the methods discussed in Chapter 13; they are shown in Fig. 17.42.

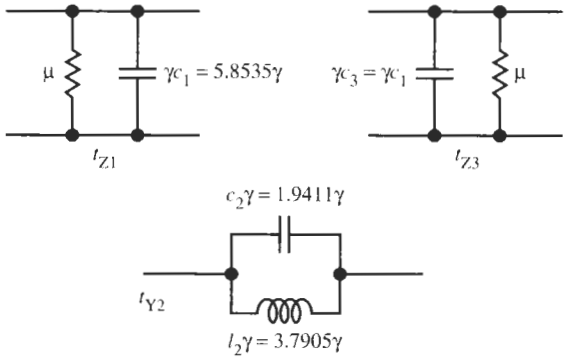

Figure 17.42 The realization of Eq. (17.91) in the γ-plane.

Let us summarize where we are in our SC ladder design process: We started from a specified filter requirement on the sampled-data frequency axis ω and prewarped the specifications into the continuous-time domain ω_{ct}. We then transformed $T(s_{ct})$ into $T(\lambda)$ with the implied bilinear transformation to get $T(z)$ in the z-domain. We proposed, however, to stay in the continuous-time λ-plane for the realization because it turns out to be more intuitive. Next we proceeded to realize the lossless ladder in the λ-plane using standard passive *LC* synthesis procedures or available tables. This gives us the series and shunt branches of the λ-plane ladder, which we can now translate into an active *RC* signal-flow graph implementation exactly as in Chapter 15, specifically Section 15.2. To avoid the complication of designing λ-plane integrators, we transformed the ladder arms into the γ-plane, where we can use the known integrators of Fig. 17.38, described by Eq. (17.78). We will now proceed to realize the γ-plane ladder, that is, we need to find implementations of the typical ladder branches of Fig. 17.41 that are described by Eqs. (17.89) and (17.90).

Referring to the discussion in Chapter 15, we must realize a typical ladder as depicted in Fig. 17.43a with the signal flow-graph in Fig. 17.43b. The signal-flow graph indicates that we must find circuits to implement the two operations

$$v_{out}(\gamma) = t_Y(\gamma)\,(v_{in1} + v_{in2}) \quad \text{and} \quad v_{out}(\gamma) = -t_Z(\gamma)\,(v_{in1} + v_{in2}) \tag{17.92}$$

and then interconnect the circuits as in Fig. 17.43b. Note the alternating signs in the flow graph in Fig. 17.43 so that each loop has negative loop gain and is stable. As in Chapter 15, we label by lower-case voltages the signals derived either from normalized currents or from voltages, depending on which node in the circuit the equation refers to. The series branches

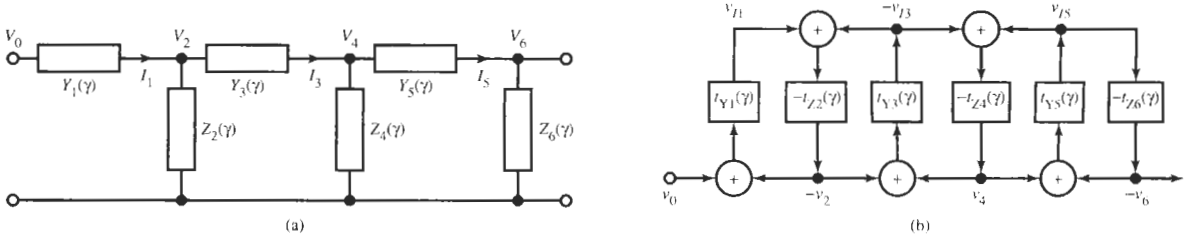

Figure 17.43 The ladder (a) and its signal-flow graph (b) in the γ plane.

t_Y are described by Eq. (17.89b) and the shunt arms t_Z by Eq. (17.90). Thus, for t_Y we must realize

$$v_{out}(\gamma) = t_Y\,(v_{in1} + v_{in2}) = \gamma c_c\,(v_{in1} + v_{in2}) + \frac{1}{\gamma l_d + \dfrac{1}{\gamma c_d} + \dfrac{1}{\gamma c_e + \dfrac{1}{\gamma l_e}}}\,(v_{in1} + v_{in2})$$

$$= v_{out1}(\gamma) + v_{out2}(\gamma) \tag{17.93}$$

A comment is appropriate at this point: Notice that in case the element c_c is present it can be connected directly as an unswitched capacitor between the node voltages v_{in1} and v_{in2}. Thus, for the series arm we can concentrate on realizing just the part $v_{out2}(\gamma)$:

$$v_{out2}(\gamma) = \frac{1}{\gamma l_d + \dfrac{1}{\gamma c_d} + \dfrac{1}{\gamma c_e + \dfrac{1}{\gamma l_e}}}\,(v_{in1} + v_{in2}) \tag{17.94}$$

Similarly, for the shunt arm t_Z, by Eq. (17.90) we must implement

$$v_{out}(\gamma) = t_Z(\gamma)\,(v_{in1} + v_{in2}) = -\frac{1}{\mu g_1 + c_a\gamma + \dfrac{1}{\gamma l_1} + \dfrac{1}{l_b\gamma + \dfrac{1}{c_b\gamma}}}\,(v_{in1} + v_{in2}) \tag{17.95}$$

Observe that apart from the sign inversion and the loss term in Eq. (17.95), Eqs. (17.94) and (17.95) are essentially the same functions. Both can be realized by expanding the SC circuits in Fig. 17.38.

We stated that we choose to realize the ladder branches in the continuous-time γ-plane. The general procedure follows Section 15.2 with the opamp circuit of Fig. 15.12. For the series arm in Eq. (17.94) specifically, we obtain the circuit in Fig. 17.44. We have drawn the circuit with inputs "at the bottom" and output "at the top" to conform to the direction of t_Y in Fig. 17.43. Notice that for the realization of noninverting integrators we used negative resistors because negative resistors can be obtained in SC circuits by appropriate switch phasing (see Fig. 17.10). In contrast to the continuous-time active *RC* circuits designed in Chapter 15, no second opamp is needed for noninverting integrators in the SC realization. The circuit is analyzed readily by writing Kirchhoff's current law at the inverting opamp input nodes. We find

$$\begin{aligned} -G_a v_{in1} - G_b v_{in2} + \gamma l_d v_{out} - G_c v_1 - G_e v_2 &= 0 \\ \gamma c_d v_1 + G_d v_{out} &= 0 \\ \gamma c_c v_2 + G_f v_{out} + G_h v_3 &= 0 \\ \gamma l_e v_3 - G_g v_2 &= 0 \end{aligned} \tag{17.96}$$

If we eliminate v_1, v_2, and v_3 from these equations we obtain

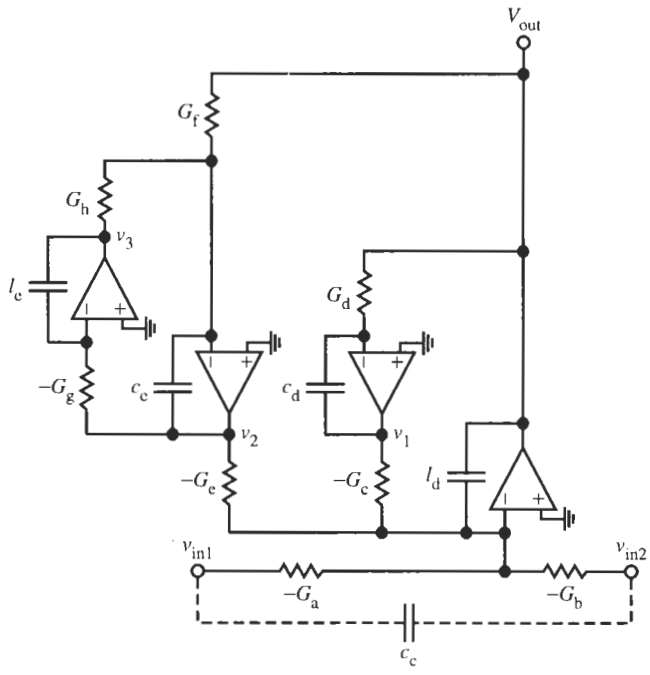

Figure 17.44 The series ladder arm, realizing t_Y in the continuous-time γ-plane. The dashed connection shows how to connect the capacitor c_c in case this term is present in Eq. (17.93).

$$v_{out} = \frac{1}{\gamma l_d + \dfrac{G_c G_d}{\gamma c_d} + \dfrac{G_e G_f}{\gamma c_e + \dfrac{G_g G_h}{\gamma l_e}}} (G_a v_{in1} + G_b v_{in2}) \tag{17.97}$$

In case the component c_c is present in Eq. (17.93), a capacitor c_c is connected between the two input nodes of the circuit in Fig. 17.44 as is shown in dashed form in the figure.

Next we address the realization of the shunt branches $-t_Z$ of Eq. (17.95). It is no different from the series branch t_Y with two exceptions: it has a loss term and it is inverting. The *RC* realization is shown in Fig. 17.45, pointing "downward" as does t_Z in Fig. 17.43. It is largely the same as Fig. 17.44 but there is a loss branch g_l in parallel with capacitor c_a and the input conductors are positive. The analysis of this circuit proceeds exactly as before. The circuit is described by the equations

$$\begin{aligned} G_a v_{in1} + G_b v_{in2} + \gamma(c_a + g_l) v_{out} + G_c v_1 + G_e v_2 &= 0 \\ \gamma l_1 v_1 - G_d v_{out} &= 0 \\ \gamma l_b v_2 - G_f v_{out} - G_h v_3 &= 0 \\ \gamma c_b v_3 + G_g v_2 &= 0 \end{aligned} \tag{17.98}$$

They can be solved for the output voltage of the shunt branch:

$$v_{out} = -t_Z (G_a v_{in1} + G_b v_{in2})$$

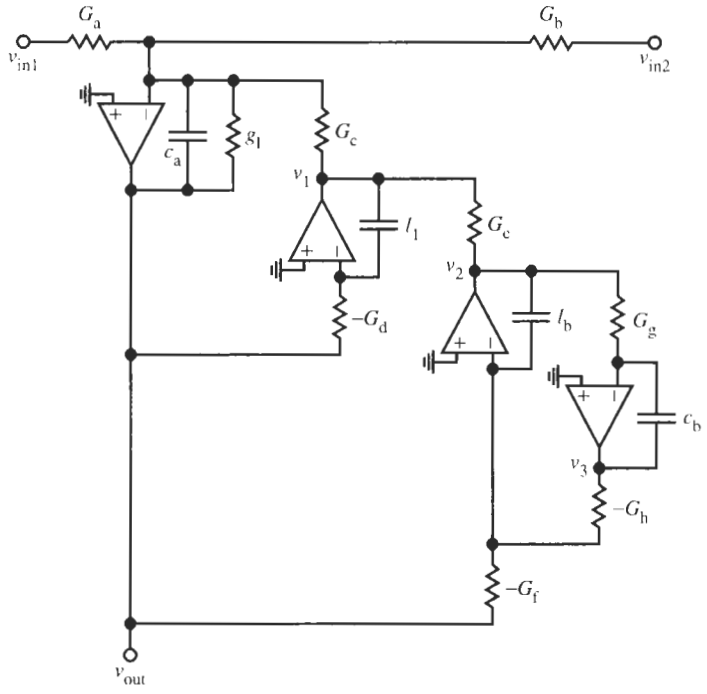

Figure 17.45 The shunt ladder arm realizing $-t_Z$ in the continuous-time γ-plane.

$$= -\frac{1}{(g_l + \gamma c_a) + \dfrac{G_c G_d}{\gamma l_1} + \dfrac{G_e G_f}{\gamma l_b + \dfrac{G_g G_h}{\gamma c_b}}} (G_a v_{in1} + G_b v_{in2}) \tag{17.99}$$

EXAMPLE 17.13

Implement the ladder branches of Example 17.12 as an active *RC* signal-flow graph realization in the γ-plane.

Solution

The γ-plane ladder branches were given in Eq. (17.91) and Fig. 17.42 and the complete *LC* circuit is shown in Fig. 17.46a. With $G_a = G_b = G$ we obtain from Eq. (17.97) for the series branch

$$t_{Y2}(\gamma) = \frac{1}{\dfrac{1}{1.9411\gamma + \dfrac{1}{3.7905\gamma}}} = \frac{G}{\dfrac{G_e G_f}{\gamma c_e + \dfrac{G_g G_h}{\gamma l_e}}}$$

In general, the different conductors in this equation can be used to scale component values or signal levels; here let us simply set $G_e = G_f = G_g = G_h = G$. Also we use the notation for this example, c_2 and l_2, and obtain

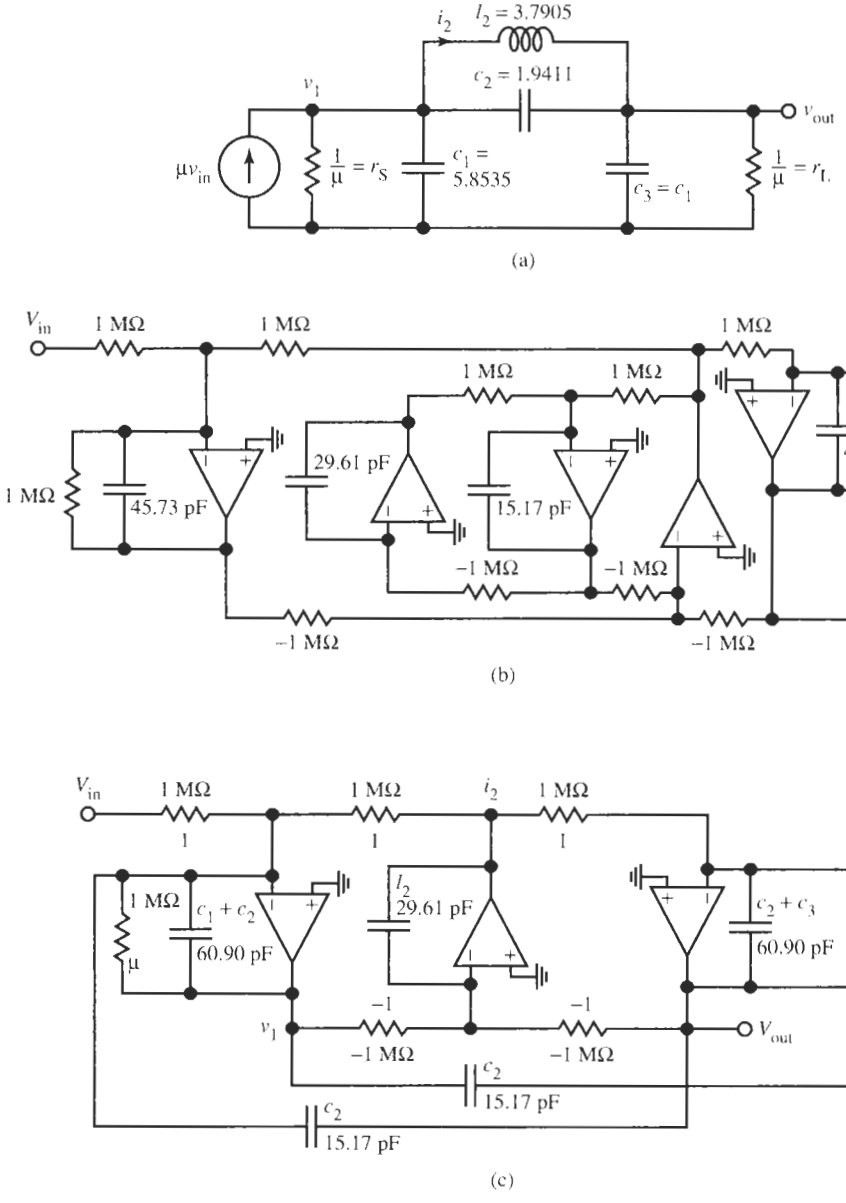

Figure 17.46 (a) The *LC* ladder of Example 17.12 in the γ-plane; (b) the signal-flow graph implementation; (c) a more economical realization saving two opamps.

$$t_{Y2}(\gamma) = \frac{1}{\dfrac{1}{1.9411\gamma + \dfrac{1}{3.7905\gamma}}} = \frac{1}{\dfrac{G}{\gamma c_2 + \dfrac{G^2}{\gamma l_2}}}$$

Thus we have $c_2/G = 1.9411$ and $l_2/G = 3.7905$.

Choosing again $G_a = G_b = G$, we obtain for the two shunt branches from Eq. (17.99)

$$t_{Z1} = t_{Z3} = \frac{1}{\mu + 5.8535\gamma} = \frac{G}{g_1 + \gamma c_1} = \frac{G}{g_1 + \gamma c_3}$$

which yields $g_1 = \mu G$ and $c_1 = c_3 = 5.8535G$. We need to pay no attention to the fact that g_1 is a function of frequency, $g_1 = \mu$G, because in the final realization in switched-capacitor form this frequency dependence is taken care of automatically [refer for example to Eq. (17.78)].

We still need to denormalize the component values. Since μ is dimensionless by Eq. (17.73c), we get back from the γ-plane via the λ-plane to the s_{ct}-plane by multiplying the normalized capacitors by $T/2$ [see Eq. (17.79)]. Let us choose $R = 1/G = 1$ MΩ; in Example 17.10 we were given $f_c = 1/T = 64$ kHz. With these numbers we find

$$C_1 = C_3 = 5.8535\frac{T}{2R} = 45.730 \text{ pF}$$

$$C_2 = 1.9411\frac{T}{2R} = 15.165 \text{ pF}, \quad C_{12} = 3.7905\frac{T}{2R} = 29.613 \text{ pF}$$

The circuit is shown in Fig. 17.46b. Notice that for the conventions and signs we adopted for the SFG configuration, the circuit configuration can be drawn with simple guidelines:

1. Draw the *current* signal[7] line on *top* and the *voltage* signal line on the *bottom* of the signal-flow graph diagram and position all opamps vertically. Then
2. All resistors above the opamps are positive.
3. All resistors below the opamps are negative.
4. Any resistor connected directly between current and voltage lines is positive.

In this realization we have used the generally valid method to obtain the SFG circuit. Often, a less expensive circuit can be achieved by taking advantage of the particular situation at hand. For instance, we may save two operational amplifiers and a few passive elements (and switches in the final SC realization) by carefully examining the structure of the passive *LC* prototype circuit and its equations. In our case we find from the circuit in Fig. 17.46a the equations

$$v_1\left[\mu + \gamma\,(c_1 + c_2)\right] - \gamma c_2 v_{out} = \mu v_{in} - i_2$$

or

$$v_1 = \frac{1}{\mu + \gamma\,(c_1 + c_2)}\,(\mu v_{in} - i_2 + \gamma c_2 v_{out}) \tag{17.100a}$$

and

[7]"Current signals" are those voltages that are derived from a current in the ladder.

$$i_2 = \frac{1}{\gamma l_2}(v_1 - v_{out}) \tag{17.100b}$$

$$v_{out} = \frac{1}{\mu + \gamma(c_2 + c_3)}(i_2 + \gamma c_2 v_1) \tag{17.100c}$$

Recall that all lower-case signals represent voltages. These equations are realized by the SFG circuit in Fig. 17.46c. The two terms, $\gamma c_2 v_{out}$, and $\gamma c_2 v_1$, are implemented by connecting the capacitor c_2 as indicated in the figure. Two opamps are saved for the price of an additional capacitor.

17.9.2 The z-Domain Circuit

From the expressions in Eqs. (17.97) and (17.99) we can derive the z-domain transfer functions most easily by replacing the positive and negative resistors and the opamp integrator blocks by their block diagram equivalents from Figs. 17.37 or 17.38. For a negative resistor (conductor) $-G_x$ we use the block $C_x z^{-1/2}$ and for a positive resistor G_y we substitute $-C_y z^{+1/2}$; the model for the opamp with an unswitched capacitor C in the feedback loop is a block $1/(2C\gamma)$. The resulting diagram is shown in Fig. 17.47, from which we can derive the following equations by inspection:

$$v_{out}(z) = \frac{1}{2C_A\gamma}\left[C_a z^{-1/2} v_{in1}(z) + C_b z^{-1/2} v_{in2}(z) + C_c z^{-1/2} v_1(z) + C_c z^{-1/2} v_2(z)\right]$$

$$v_1(z) = \frac{1}{2C_B\gamma}\left[-C_d z^{1/2} v_{out}(z)\right]$$

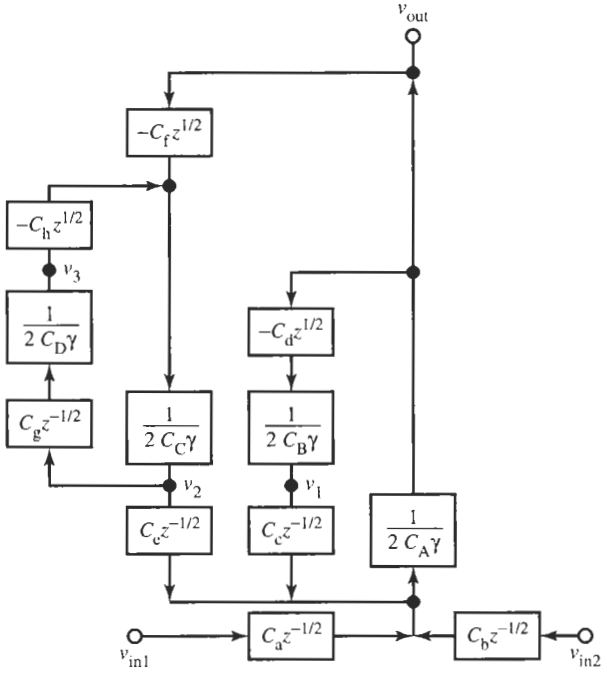

Figure 17.47 Block diagram model for the z-domain realization of the series ladder arm in Fig. 17.44.

$$v_2(z) = \frac{1}{2C_C\gamma}\left[-C_f z^{1/2} v_{out}(z) - C_h z^{1/2} v_3(z)\right]$$

$$v_3(z) = \frac{1}{2C_D\gamma}\left[C_g z^{-1/2} v_2(z)\right] \tag{17.101}$$

These equations are comparable to Eq. (17.96); they can be solved for the output voltage of the ladder's series branches,

$$v_{out}(z) = \frac{z^{-1/2}}{2C_A\gamma + \dfrac{C_c C_d}{2C_B\gamma} + \dfrac{C_c C_f}{2C_C\gamma + \dfrac{C_g C_h}{2C_D\gamma}}}\left[C_a v_{in1}(z) + C_b v_{in2}(z)\right] \tag{17.102}$$

It is worth pointing out that the leading or lagging phase terms $z^{\pm 1/2}$ in Eq. (17.101) cancel everywhere in the circuit because inverting and noninverting integrators are paired. The only remaining phase error is $z^{-1/2}$ for the whole noninverting branch.

As the final step in the realization of the series impedance branch we replace the model in Fig. 17.47 by the parasitics-insensitive switched-capacitor circuit in Fig. 17.48. Notice that Eq. (17.102) has a large number of capacitors in addition to the integrating capacitors C_A, C_B, C_C, and C_D. These component values for the SC series branch must be determined by comparing Eq. (17.102) with Eq. (17.94). The degrees of freedom can be used to equalize the signal levels in the SC circuit for designs with optimum dynamic range (Schaumann et al., 1990). Similar to Example 17.13, we shall not address this issue here but simply use the available freedom for obtaining convenient element values.

The modification of the circuit in Fig. 17.45 for the shunt branch is similarly easy: we replace the input blocks to account for the positive resistors and we add a positive resistor block $-C_1 z^{1/2}$ across $1/(2C_A\gamma)$ to account for the loss. The resulting model is given in Fig. 17.49. The analysis leads to a set of equations similar to Eq. (17.101); for example, the first of them is modified to read

$$v_{out}(z) = \frac{1}{2C_A\gamma}\left[-C_a z^{1/2} v_{in1}(z) - C_b z^{1/2} v_{in2}(z) - C_1 z^{1/2} v_{out}(z) - C_c z^{1/2} v_1(z) - C_e z^{1/2} v_2(z)\right]$$

which results in

$$v_{out}(z) = \frac{1}{(2C_A + C_1)\gamma + C_1\mu} \times \left[-C_a z^{1/2} v_{in1}(z) - C_b z^{1/2} v_{in2}(z) - C_c z^{1/2} v_1(z) - C_e z^{1/2} v_2(z)\right] \tag{17.103}$$

The structure of the denominator term is as expected for a lossy integrator [compare Eq. (17.78)]. If we solve Eq. (17.103) along with the remaining equations for the model in Fig. 17.49 to get the z-domain transfer function of the shunt branch, we obtain the result

$$v_{out}(z) = -\frac{z^{1/2}}{C_1\mu + (2C_A + C_1)\gamma + \dfrac{C_c C_d}{2C_B\gamma} + \dfrac{C_e C_f}{2C_C\gamma + \dfrac{C_g C_h}{2C_D\gamma}}} \times \left[C_a v_{in1}(z) + C_b v_{in2}(z)\right] \tag{17.104}$$

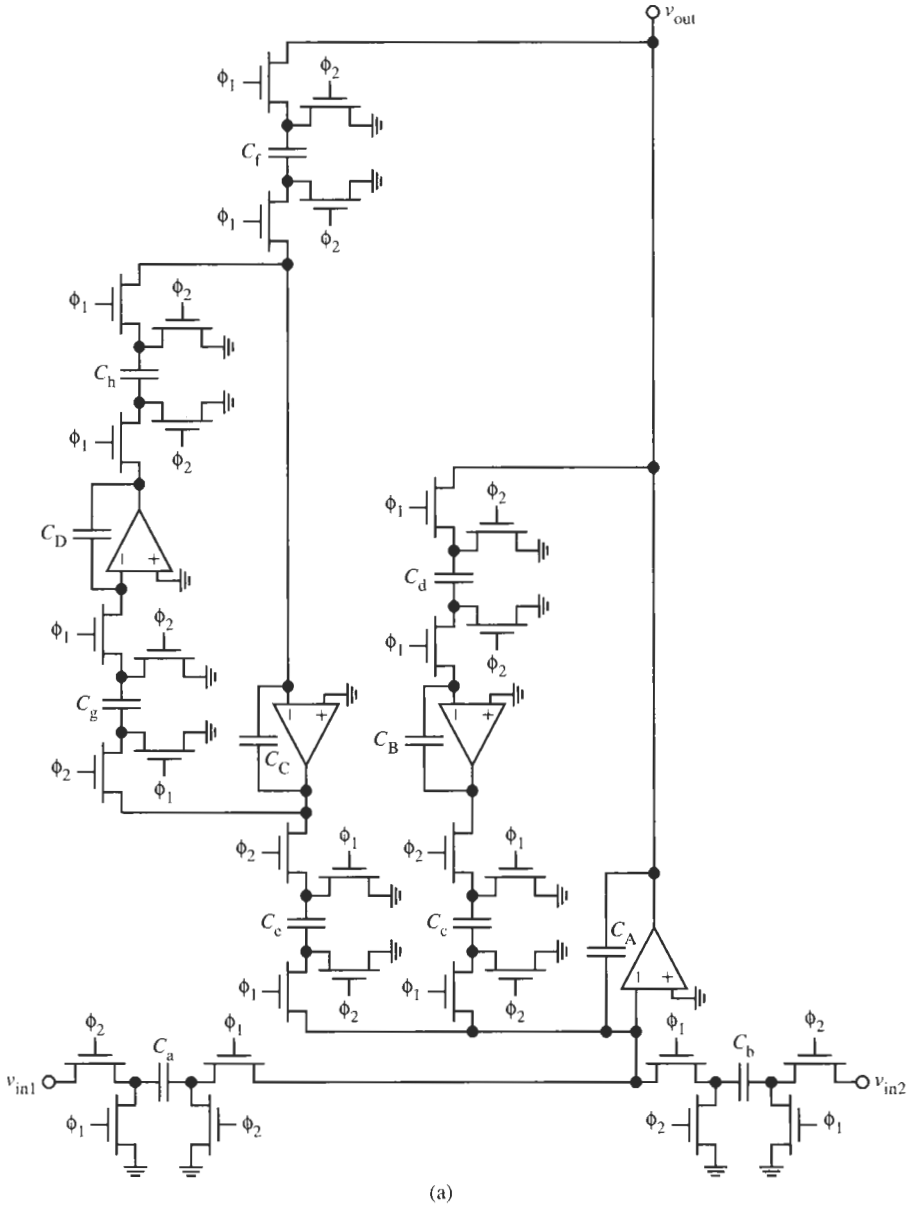

Figure 17.48 (a) The SC series ladder arm realizing t_Y; (b) the circuit with switch sharing.

This equation is compared to Eq. (17.95) to find the component values.

The SC circuit of the shunt branch is shown in Fig. 17.50. The leading and lagging phase terms $z^{\pm 1/2}$ cancel again everywhere in the circuit because inverting and noninverting integrators are paired. The only remaining phase error is $z^{+1/2}$ for the complete inverting branch. Thus, when t_Y and $-t_Z$ branches of Eqs. (17.102) and (17.104) are paired in loops in

Figure 17.48 Continued

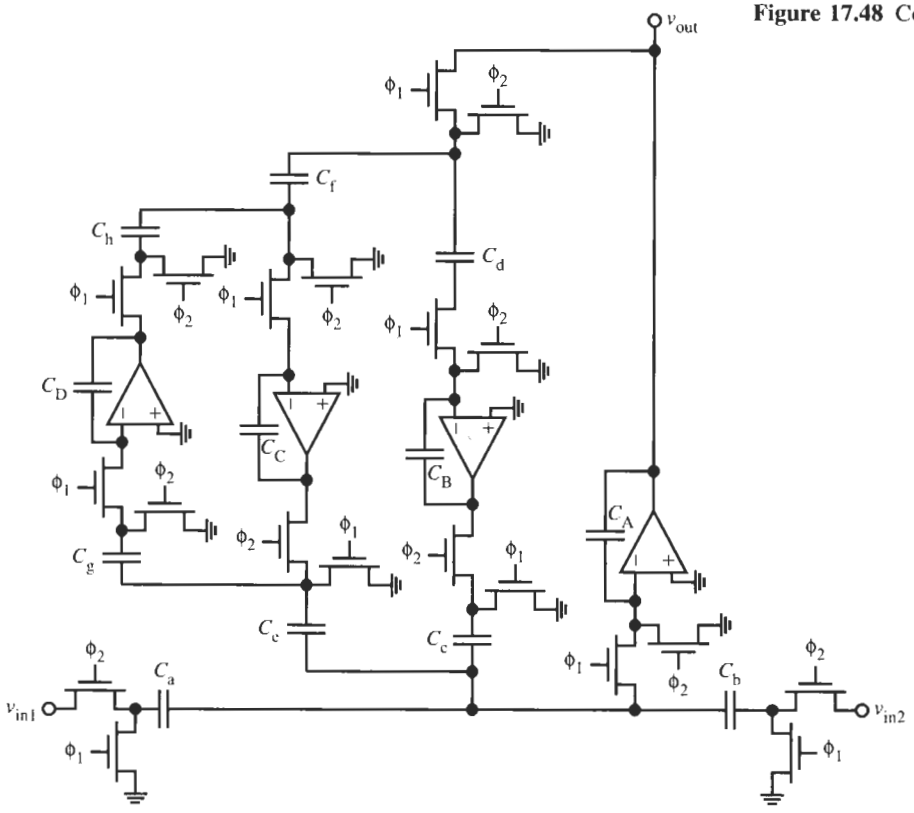

(b)

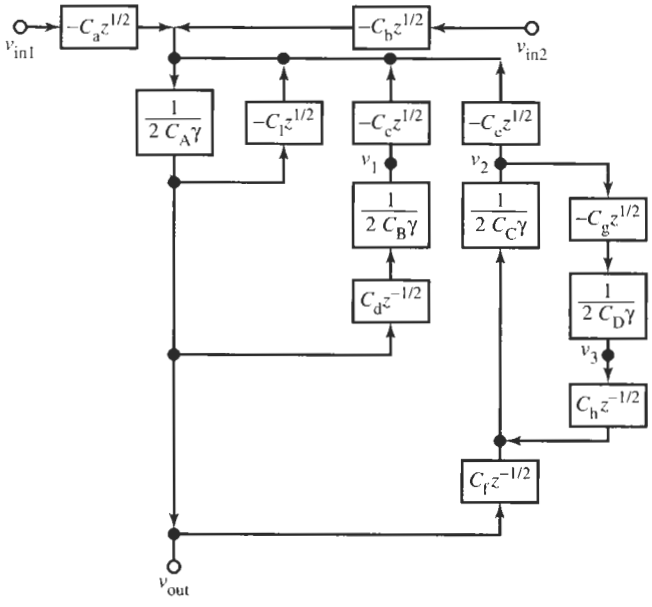

Figure 17.49 Block diagram model for the z-domain realization of the shunt ladder arm in Fig. 17.45.

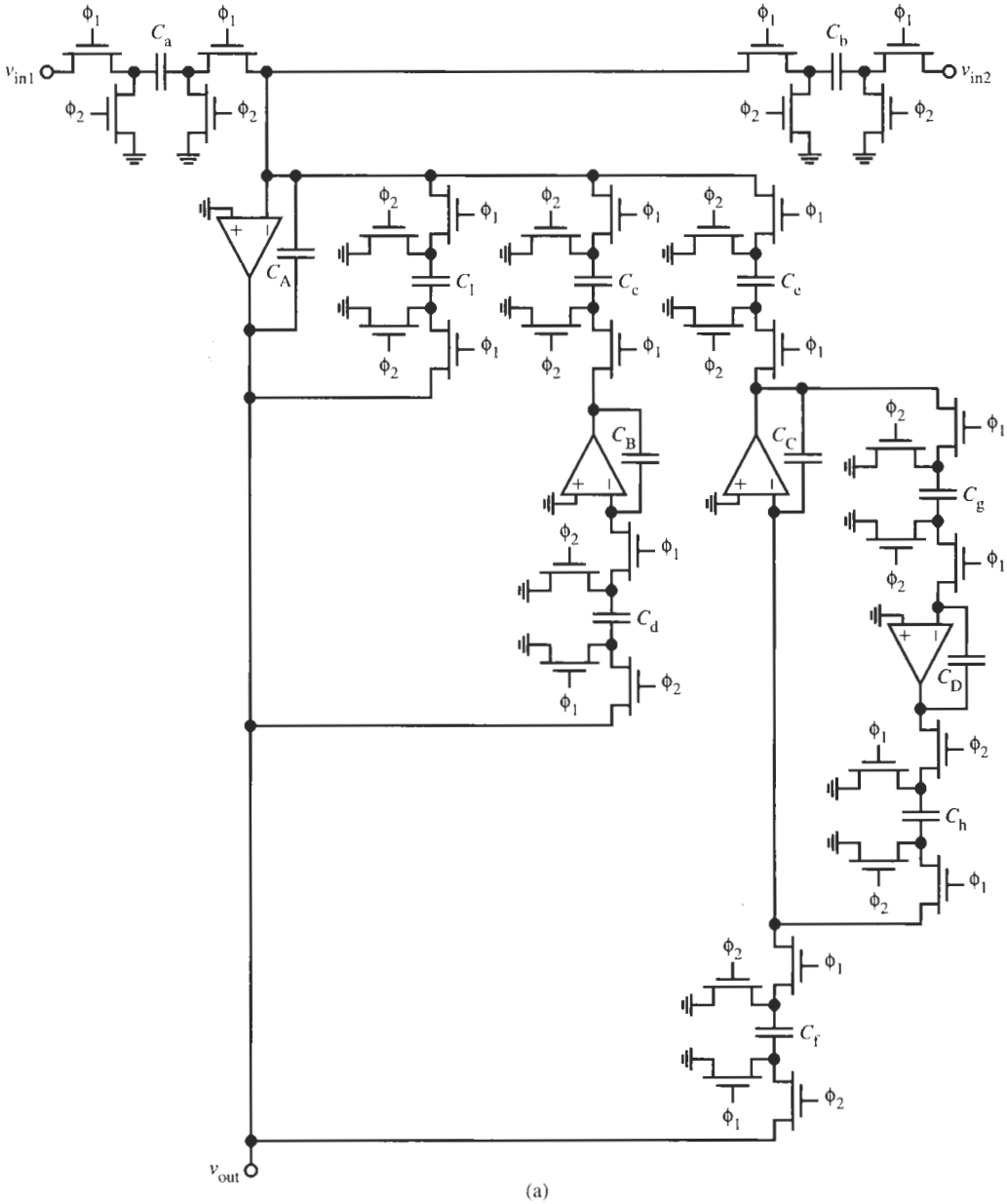

Figure 17.50 (a) The SC shunt ladder arm realizing t_Z; (b) the circuit with switch sharing.

the total signal-flow graph realization illustrated in Fig. 17.43, the phase errors in each loop cancel also in the total filter because $z^{+1/2}z^{-1/2} = 1$.

Before we demonstrate the conversion of our ladder into SC format on an example we need to attend to an additional problem that is caused by our choice of incorporating the source resistor r_{in} as a shunt element in the first shunt admittance. Recall that after scaling t_Z by μ,

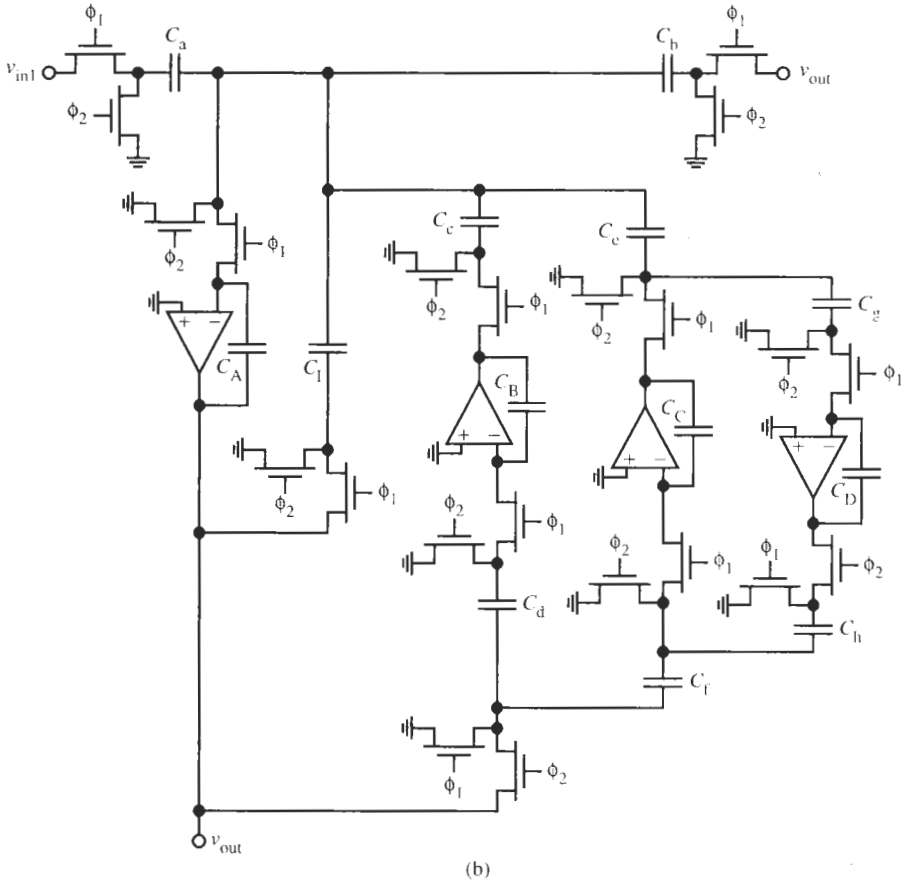

Figure 17.50 Continued

any loss term g_1 becomes μg_1 [see Eq. (17.90) and Fig. 17.41c]. The same happens to the normalized source resistor r_{in}: it is represented as r_{in}/μ. A consequence of this transformation from a voltage source to a current source and the frequency scaling by μ is that the source is also multiplied by μ (see also Fig. 17.46a). Figure 17.51 illustrates the transformation. Routine analysis shows that the circuit in the γ-plane is described by

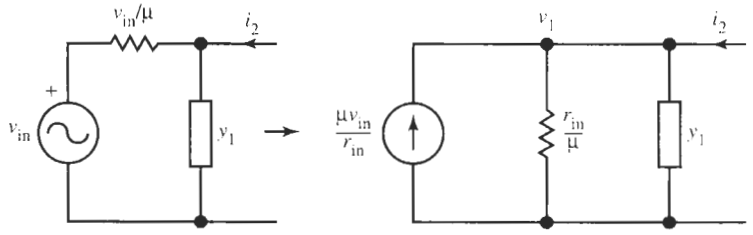

Figure 17.51 The result of scaling and source transformation at the ladder input.

$$v_1(\gamma) = \frac{g_{in}\mu v_{in}(\gamma) + i_2(\gamma)}{y_1(\gamma) + g_{in}\mu} \tag{17.105}$$

It is clear then that we cannot simply apply the input signal v_{in} to the transformed SC ladder, say, as v_{in1} in Fig. 17.49, because the frequency-dependent scale factor $\mu = \cosh(sT/2)$ will alter the transfer function. We need to find a method to generate μv_{in1} as input. A solution is obtained by adding to the block diagram in Fig. 17.49 an additional input that implements a negative resistor. The modified (partial) block diagram is shown in Fig. 17.52a; it is described by

$$\hat{v}_{out}(\gamma) = \frac{-C_{a1}z^{1/2}v_{in11}(\gamma) + C_{a2}z^{-1/2}v_{in12}(\gamma)}{(2C_A + C_1)\gamma + C_1\mu} \tag{17.106}$$

To attain the factor $\mu = (z^{1/2} + z^{-1/2})/2$, we now choose $v_{in11} = -v_{in12} = v_{in1}$, $C_{a1} = C_{a2} = C_a/2$ and make use of Eq. (17.73c). We obtain

$$\hat{v}_{out}(\gamma) = \frac{-C_a\frac{1}{2}\left(z^{1/2} + z^{-1/2}\right)v_{in1}(\gamma)}{(2C_A + C_1)\gamma + C_1\mu} = -\frac{-C_a\mu v_{in1}(\gamma)}{(2C_A + C_1)\gamma + C_1\mu} \tag{17.107}$$

Since the inverting branch $-t_Z(\gamma)$ will be paired in the ladder with a noninverting branch t_Y, it should have a leading phase error $z^{1/2}$ that will cancel the lagging phase error $z^{-1/2}$ of t_Y. To this end we rewrite Eq. (17.107) as

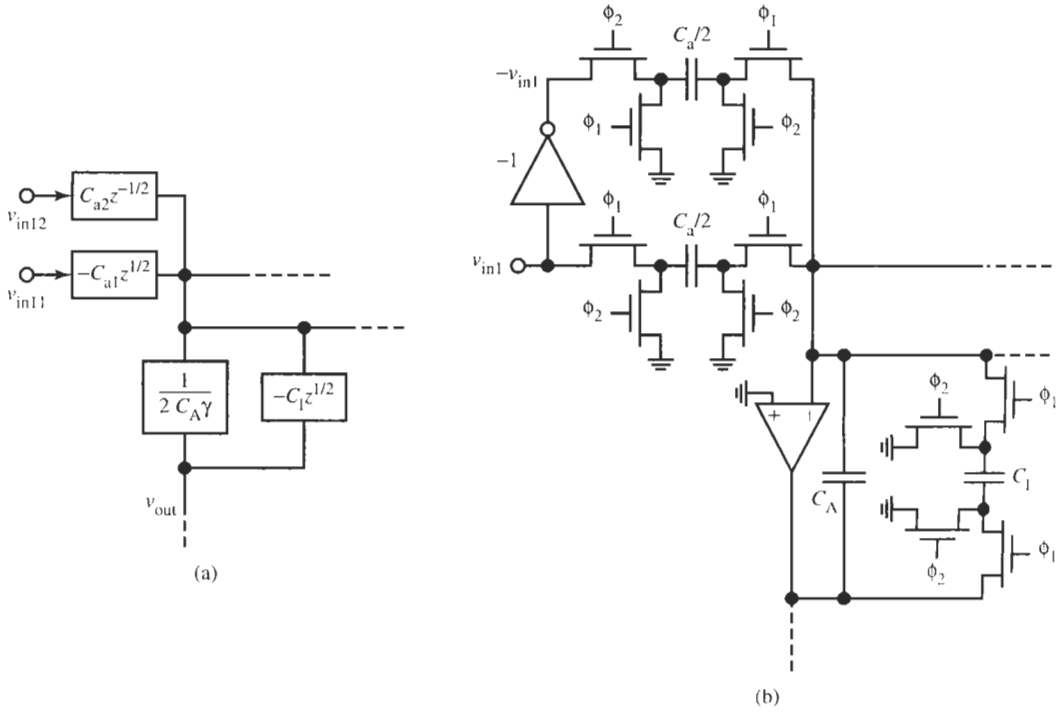

Figure 17.52 The input stage to implement scaling the input voltage by μ: (a) block diagram; (b) final circuit. Using switch sharing permits the six switches at the opamp input to be replaced by two.

$$\hat{v}_{out}(\gamma) = \frac{z^{1/2}}{(2C_A + C_1)\gamma + C_1\mu}\left[-C_{a1}\mu v_{in1}(\gamma)z^{-1/2}\right] \tag{17.108}$$

If we compare Eqs. (17.108) and (17.105), we notice that we have achieved the desired scaling of the input voltage by μ and all delay errors cancel in the ladder. The remaining uncompensated factor $z^{-1/2}$ of the input signal is an unimportant *constant* delay $T/2$ that propagates through to the filter output.

To realize the scaling by μ requires an inversion of the input signal, $v_{in12} = -v_{in11}$, as is illustrated in Fig. 17.52b. The inversion can be accomplished by a switched capacitor as is illustrated in Fig. 17.5. Alternatively, since SC circuits are normally realized in differential form, the inverted signal may simply be obtained from the inverted signal path as was done in Fig. 17.27.

EXAMPLE 17.14

Convert the continuous-time λ-domain circuit obtained in Example 17.13 into switched-capacitor form.

Solution

Let us use the simpler circuit in Fig. 17.46c. Compared to the implementation in Fig. 17.46b it costs one additional capacitor but saves two opamps and five SC resistors along with their associated switches when the resistors are realized in SC form. The corresponding block diagram is shown in Fig. 17.53. It can be used to obtain the z-domain transfer function of the circuit and for converting the γ-plane active RC circuit into switched-capacitor form. Figure 17.54 shows the resulting SC circuit.

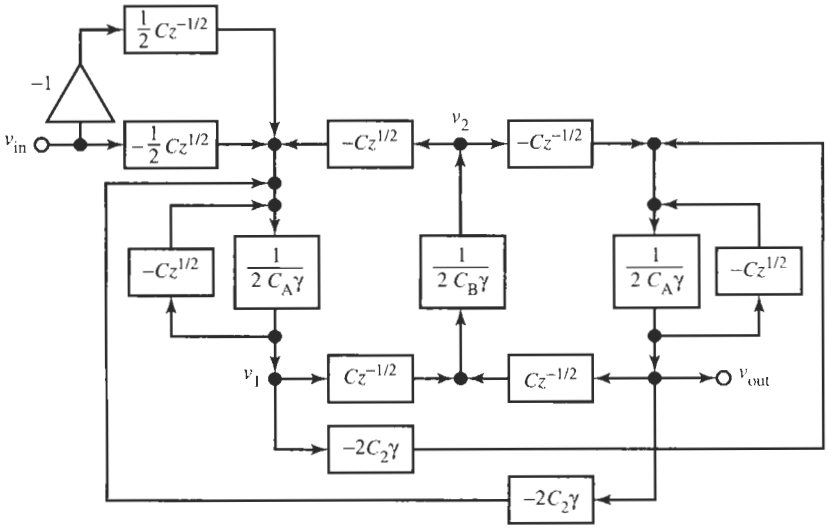

Figure 17.53 The block diagram to represent the circuit in Fig. 17.46c.

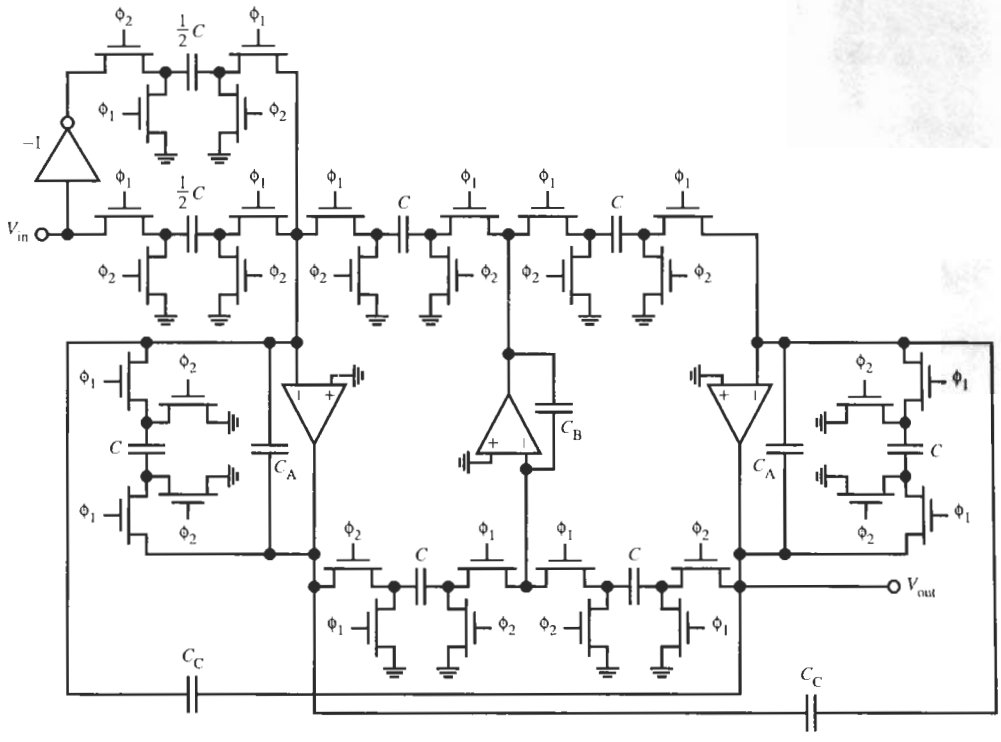

Figure 17.54 The switched-capacitor circuit for Example 17.14.

When we compare Eqs. (17.102) and (17.104) with the prescribed equations (17.100) to find the element values, we must observe two points:

- All *unswitched* capacitors are effectively doubled. It follows that the values in the continuous-time γ-plane circuit in Fig. 17.46c should be halved in the SC circuit.
- If an integrator is lossy, the value C_1 of the capacitor that represents the loss is added to the doubled integrating capacitor. This leads to the coefficient $(2C_A + C_1)$ in Eq. (17.104). In the SC realization, this effect must be corrected by subtracting the value C_1. For instance, a comparison of Eqs. (17.104) and (17.95), after denormalizing c_a, results in $2C_A + C_1 = c_a T/(2R)$, or $C_A = [c_a T/(2R) - C_1]/2$.

Thus, the components in Fig. 17.54 are obtained as follows.

The switched capacitors C that represent resistors R have the value $C = 1/(f_c R) = TG$. Because we chose for simplicity all resistors equal to 1 MΩ, we find with $f_c = 64$ kHz the capacitor values

$$C = \left(64{,}000 \cdot 10^6\right)^{-1} F = 15.625 \text{ pF}$$

Note that it does not matter whether R is positive or negative; the sign of R is taken care of by appropriate switch phasing. The two unswitched capacitors C_C in Fig. 17.54 are equal to $C_C = C_2/2 = 7.58$ pF. For the integrating capacitors C_A in blocks t_{Z1} and t_{Z3} we have

$$2C_A = 60.90 \text{ pF} - C = 45.275 \text{ pF}, \quad \text{that is,} \quad C_A = 22.64 \text{ pF}$$

Finally, we have $2C_B = 29.61$ pF, i.e., $C_B = 14.81$ pF. This completes the design; remember that the two capacitors in the input stage that implements μv_{in} have the value $C/2$. The student may still wish to redraw the circuit with switch sharing to demonstrate that a total of 12 switches can be saved.

Let us summarize the discussion of switched-capacitor ladder synthesis by providing a step-by-step design procedure:

STEP 1: Using Eq. (17.55), prewarp the filter specifications from the sampled-data frequency axis ω into the continuous-time axis ω_{ct}. Then use any convenient approximation routine to obtain $T(\bar{s}_{ct})$, where $\bar{s}_{ct}$ is a frequency parameter normalized by a frequency $\omega_0 = 2\pi f_0$. Typically f_0 is the corner of a lowpass prototype. Refer to the discussion in Chapters 6, 7, and 8. Transform $T(\bar{s}_{ct})$ into $T(\lambda)$ by Eq. (17.80), i.e., by setting $\bar{s}_{ct}(\omega_0 T/2) = \lambda$. The resulting transfer function is given in Eq. (17.83) [Eq. (17.85) in Example 17.10].

STEP 2: Realize $T(\lambda)$ as an LC-ladder in the continuous-time λ-domain with normalized admittances g_{in}, $1/(\lambda l)$, λc, and g_{out}. Perform impedance-level normalization by using any convenient resistor R. The equations for the resulting shunt and series ladder branches, t_Z and t_Y, respectively, are Eqs. (17.86) and (17.87), and the ladder arms are shown in Fig. 17.39 [Eq. (17.88) and Fig. 17.40 in Example 17.11].

STEP 3: Scale the impedance level by μ to obtain the admittances μg_{in}, $\mu/(\lambda l) = (1 + \gamma^2)/(\gamma l)$, γc, and μg_{out} in the γ-plane. Perform a source transformation, if necessary, to obtain g_{in} as a shunt element. This results in Eqs. (17.89) and (17.90) and the ladder arms in Fig. 17.41 [Eqs. (17.91) and Fig. 17.42 in Example 17.12].

STEP 4: Realize the γ-plane lossless ladder circuit as an active RC filter in the γ-plane, using the SFG technique of Section 15.2 in all its details, such as topology, component values, and scaling for element values. Figures 17.44 and 17.45 show the general ladder arms. Denormalize the elements by multiplying r_{in} and r_{out} by the chosen value R; denormalize the capacitors c as $C = c[T/(2R)]$. [Example 17.13 provides an illustration of the procedure.] An important difference in the present case from the active RC case is that we may use negative resistors because they are easy to implement in the final SC conversion. During this process, disregard the fact that the source and load resistors are frequency dependent, r_{in}/μ and r_{out}/μ, that is, assume $\mu = 1$. The terminations will become automatically correct in the final transformation to SC form.

STEP 5: Convert the active RC filter into a block diagram, using a $-Cz^{1/2}$ block for each positive conductor and $Cz^{-1/2}$ blocks for negative conductors. An opamp with an unswitched integrating capacitor C_X becomes a block $1/(2C_X\gamma)$. All unswitched capacitors, including the integrating capacitors, are effectively doubled. A capacitor C_l representing loss is effectively added to the doubled integrating capacitor. This process converts

- the circuit for a series branch in Fig. 17.44 described by Eq. (17.97) to the diagram in Fig. 17.47 described by Eq. (17.102), and
- the circuit for a shunt branch in Fig. 17.45 described by Eq. (17.99) to the diagram in Fig. 17.49 described by Eq. (17.104).

STEP 6: Convert the γ-plane active RC circuit into the SC domain as follows:

- Replace the positive and negative conductors G by properly phased switched capacitors of value TG; $f_c = 1/T$ is the clock frequency. (Converting the active RC branches of Figs. 17.44 and 17.45 first into the SC block diagrams of Fig. 17.47 and 17.49, respectively, may help in the conversion process.)

- To compensate for the effective doubling of all *unswitched* capacitors and for the effective addition of the damping capacitor to the integrating capacitor of a *lossy* integrator,
  - subtract the capacitor representing the loss from the integrating capacitor of a *lossy* integrator in the continuous-time γ domain and then
  - halve each *unswitched* capacitor.
- For the "SC resistors," use the strays-insensitive realizations of Fig. 17.10a or Fig. 17.10b, depending on whether inverting or noninverting integrators, respectively, are to be implemented.
- Realize the input signal branch as shown in Fig. 17.52b; remember to halve the nominal capacitor of the input branch.
- Choose a convenient resistor R for scaling the impedance level so that practical capacitor values are obtained.

REFERENCES

R. Gregorian, "High-Resolution Switched-Capacitor D/A Converter," *Microelectr. J.*, Vol. 12, No. 2, pp. 10–13, 1981.

D. A. Johns and K. Martin, *Analog Integrated Circuit Design*, Chapters 8 and 9. John Wiley, New York, 1998.

H. Matsumoto and K. Watanabe, "Spike-Free Switched-Capacitor Circuits," *Electr. Lett.*, Vol. 23, No. 8. pp. 428–429, 1987.

B. M. Oliver, J. R. Pierce, and C. E. Shannon, "The Philosophy of PCM," *Proc. IRE*, Vol. 36 (November 1948), pp. 1324–1331.

A. V. Oppenheim and A. S. Willsky, *Signals and Systems*. Prentice Hall, New York, 1983.

R. Schaumann, M. S. Ghausi, and K. R. Laker, *Design of Analog Filters: Passive, Active RC and Switched Capacitor*. Chapter 8. Prentice Hall, Englewood Cliffs, NJ, 1990.

PROBLEMS

17.1 A lowpass filter for an implantable device for medical applications has a bandwidth of 125 Hz. As the circuit is to be integrated, the largest capacitor that may be used is 15 pF. Approximately what are the resistor values needed to realize the required time constants in this low-frequency active *RC* filter? The filter is to be realized as a switched-capacitor circuit, clocked at 100 times the filter's bandwidth. What is the size of the switched capacitors C_R needed to implement the resistors?

17.2 To save switches and wiring on the integrated circuit, a designer attempts to implement a switched-capacitor integrator as in Fig. 17.9 with an SC resistor shown in Fig. 17.6a. The required values of C_F and C_R are $C_F = 2.5$ pF and $C_R = 0.3$ pF. The technology provides symmetrical switches with $C_{sw} \approx 0.01$ pF and top- and bottom-plate parasitic capacitors are $C_t \approx 0.04C$ and $C_b \approx 0.12C$, where C is the designed capacitor. Estimate the error in the integrator time constant that must be expected.

17.3 Design a switched-capacitor circuit to realize the three-phase output voltages of Example 3.8. Use $f_c = 12.5$ kHz for the switching frequency and $C_{max} = 25$ pF. At the low frequencies required in the problem, you may assume the opamps to be ideal. Also, since f_c is more than 200 times faster than the signal frequency, the simple switched-capacitor–resistor equivalent of Eq. (17.4) may be used. Of course, stray-insensitive switch configurations should always be employed.

17.4 Realize the function of Example 3.5 in switched-capacitor form. Use the circuit in Fig. 3.24 with stray-insensitive switch configurations so that minimum-sized capacitors can be used. Assume the opamp

bandwidth is large enough so that the opamp may be considered ideal. Pick a clock frequency at least 20 times the signal frequencies and use Eq. (17.4) for the resistor equivalent. Your final circuit should employ switch sharing.

17.5 Repeat Problem 17.4 for Example 3.11.

17.6 Repeat Problem 17.4 for Example 3.12.

17.7 Repeat Problem 17.4 for the circuit in Problem 3.23.

17.8 Design an SC filter to realize the requirements of Problem 3.43.

17.9 Starting from Eqs. (17.13a) and (17.13b), verify Eq. (17.14) and

(a) derive the transfer function V_1/V_{in},

(b) derive the SC version of V_1/V_{in} analogous to V_2/V_{in} in Eq. (17.15).

17.10 Design a second-order switched-capacitor filter based on the circuit in Fig. 17.15c, described by Eq. (17.14), to realize the following requirements. Choose $f_c = 256$ kHz for the clock frequency, large enough so that we may neglect that the filters work in sampled-data mode, as was done in Example 17.3 [the switched-capacitor–resistor equivalence of Eq. (17.4) can be used]. It is also specified that the largest capacitor must be less than 20 pF:

(a) lowpass with $f_0 = 600$ Hz, $Q = 0.707$, and dc gain of 0 dB

(b) lowpass with $f_0 = 3.4$ kHz, $Q = 1.3$, and dc gain of 0 dB

(c) lowpass with $f_0 = 12$ kHz, $Q = 0.707$, and dc gain of 3 dB

(d) bandpass with $f_0 = 3.4$ kHz, $Q = 4.5$, and midband gain of 10 dB

(e) bandpass with $f_0 = 120$ Hz, $Q = 16$, and midband gain of 6 dB

(f) highpass with $f_0 = 1.2$ kHz, $Q = \sqrt{2}$, and high-frequency band gain of 1 dB

(g) notch filter with $f_z = 2$ kHz, $Q = 5$, and low- and high-frequency band gain of 2 dB

(h) lowpass notch with $f_0 = 3.6$ kHz, $Q = \sqrt{2}$, $f_z = 8.7$ kHz, and dc gain of 0 dB

(i) allpass with $f_0 = 1.2$ kHz, $Q = 2$, and phase shift of $\phi = 125°$ at 9 kHz

17.11 Sketch the gain and phase responses, Eqs. (17.41) and (17.42), of the lossless inverting and noninverting integrators of Eqs. (17.40a) and (17.40b).

17.12 Use the SC biquad of Fig. 17.15c to design a filter with the specifications of Example 4.2. Use the simple SC–resistor of Eq. (17.4), i.e., assume the switched capacitor acts like a continuous-time resistor so that the circuit is described by Eq. (17.14). Let $f_c = 128$ kHz and $C_{max} = 20$ pF.

17.13 Use the SC biquad of Fig. 17.15c to design a filter with the specifications of Example 4.3. Assume the circuit is described by Eq. (17.14). Let $f_c = 12$ kHz and $C_{max} = 20$ pF.

17.14 Use the SC biquad of Fig. 17.15c to design a filter with the specifications of Example 4.4. Use the simple SC–resistor of Eq. (17.4) and assume that $f_c = 128$ kHz and $C_{max} = 20$ pF. (*Note*: f_c is very low relative to the signal frequency, so that the circuit, based on the switched capacitor acting like a continuous-time resistor, will likely not work satisfactorily; see also Problem 17.20.)

17.15 Use the SC biquad of Fig. 17.15c to design a filter with the specifications of Example 4.9. Assume the circuit is described by Eq. (17.14). Let $f_c = 256$ kHz and $C_{max} = 20$ pF.

17.16 Use the SC biquad of Fig. 17.15c to design a filter with the specifications of Example 5.2. Assume the circuit is described by Eq. (17.14). Let $f_c = 32$ kHz and $C_{max} = 20$ pF.

17.17 Use the SC biquad of Fig. 17.15c to design a filter with the specifications of Example 5.3. Assume the circuit is described by Eq. (17.14). Let $f_c = 32$ kHz and $C_{max} = 20$ pF.

17.18 Use the SC biquad of Fig. 17.15c to design a filter with the specifications of Example 5.5. Assume the circuit is described by Eq. (17.14). Let $f_c = 32$ kHz and $C_{max} = 20$ pF.

17.19 Repeat Problem 17.14 but now consider that the switching frequency of $f_c = 128$ kHz is not very low relative to the signal frequency of 38 kHz. Consequently, the approximate techniques of Sections 17.3 and 17.4 cannot be used with dependable results. Rather, proper sampled-data methods must be employed:

(a) Assume the specifications of Example 4.4 are in the sampled-data domain ω. Prewarp them into the continuous-time domain ω_{ct}.

(b) Find the continuous-time transfer function $T(s_{ct})$.

(c) Use the bilinear transformation to derive the transfer function $T(z)$ in the z-domain.

(d) The realization of the function derived in (c) is still based on the circuit in Fig. 17.15c, but now described more accurately in the z-domain by Eq. (17.52b). More particularly, use the circuit in Fig. 17.29, described by Eq. (17.53), to realize the transfer function derived in (c).

(e) Compare the two realizations in this problem and Problem 17.15. If you have access to a suitable software package, such as MATLAB®, prepare a plot of the two frequency responses.

17.20 Use the SC circuit of Fig. 17.29 to design a filter with the specification of Example 5.1. The specifications are understood to be in the sampled-data domain. Use $f_c = 512$ kHz and proper sampled-data techniques in your design.

17.21 Use the SC biquad of Fig. 17.29 to design a filter with the specifications of Example 5.11. Assume that $f_c = 64$ kHz, $C_{max} = 20$ pF, and use proper sampled-data techniques in your design.

17.22 Realize the transfer function of Eq. (5.83) of Example 5.16 as a cascade connection of three SC biquads as shown in the following:

(a) Figure 17.15c, described by Eq. (17.14), using approximate SC techniques. Use switch sharing.

(b) Figure 17.29, described by Eq. (17.53), using proper sampled-data techniques.

(c) Compare the two designs. If you have access to a suitable software package, such as MATLAB®, plot the two frequency responses.

17.23 Realize the specifications of Example 5.17 as a cascade connection of three SC sections. Select $f_c = 126$ kHz and use proper sampled-data techniques in your design. The final circuit should use switch sharing and no capacitor must be larger than 12 pF.

17.24 Realize the specifications of Example 6.2

(a) as a cascade connection of three SC sections,

(b) as a simulated SC ladder filter.

Use sampled-data design techniques, choose $f_c = 24$ kHz, and make certain that the component values are practical.

17.25 Design an SC circuit to realize the lowpass specifications of Example 6.3. Since the passband corner frequency is 18 kHz and $f_c = 64$ kHz is prescribed, proper sampled-data design techniques must be employed. To reduce the total capacitance as much as possible, choose $C_{min} = 0.4$ pF. Show the final design with switch sharing, based on

(a) a cascade connection of three SC sections,

(b) a simulated SC ladder filter.

17.26 Realize the specifications of Example 8.1

(a) as a cascade connection of three SC sections,

(b) as a simulated SC ladder filter.

Choose $f_c = 512$ kHz and make certain that the component values are practical. Show the final realizations with switch sharing.

17.27 Design an SC circuit to realize the delay specifications of Example 10.4. Use $f_c = 256$ kHz and $C_{max} = 25$ pF. Proper sampled-data design techniques should be employed.

17.28 Design a fifth-order Chebyshev lowpass filter with $\alpha_{max} = 0.1$ dB in $0 \leq f \leq 3.8$ kHz as a switched-capacitor ladder. The clock frequency is 64 kHz. The LC prototype can be obtained from Table 13.3. Show the circuit with switch sharing.

17.29 Realize the lowpass ladder of Examples 13.3 and 13.5 such that the lowpass bandwidth is $f_p = 21$ kHz. For the SC ladder implementation the clock frequency is $f_c = 128$ kHz. Realize the ladder following the discussion in Section 17.9.

17.30 Realize the LC circuit of Fig. 14.15a as an SC ladder. (Neglect the two 0.1-resistors.) Assume $f_c = 128$ kHz, use $C_{max} = 20$ pF, and show the final circuit implementation with switch sharing.

17.31 Realize an SC ladder filter to satisfy the specifications of Example 14.7. The LC circuit is shown in Fig. 14.22a. Assume $f_c = 128$ kHz, use $C_{max} = 20$ pF, and show the final circuit implementation with switch sharing.

17.32 Realize an SC ladder filter for the LC circuit of Problem 14.9. Assume $f_c = 64$ kHz, use $C_{max} = 20$ pF, and show the final circuit implementation with switch sharing.

17.33 Realize an SC ladder filter for the LC circuit of Problem 15.8. Assume $f_c = 128$ kHz, use $C_{max} = 20$ pF, and show the final circuit implementation with switch sharing.

17.34 Repeat Problem 17.33 for the circuit in Problem 15.19. Assume that $f_c = 512$ kHz.

INDEX

Written for advanced undergraduate and first-year graduate courses in analog filter design and signal processing, *Design of Analog Filters* integrates theory and practice to provide a modern and practical "how-to" approach to design. A complete revision of Mac Van Valkenburg's classic work, *Analog Filter Design* (1982), this text builds on the presentation and style of its predecessor, updating it to meet the needs of today's engineering students. Reflecting recent developments in the field and emphasizing intuitive understanding, it provides readers with an up-to-date introduction and design guidelines and also helps them to develop a "feel" for analog circuit behavior.

Design of Analog Filters moves beyond the simple treatment of active filters built with opamps to discuss the more recent design of filters based on transconductors. Topics covered include fundamental concepts; opamps; first- and second-order filters; second-order filters with arbitrary transmission zeros; filters with maximally flat magnitude, with equal-ripple (Chebyshev) magnitude, and with inverse Chebyshev and Cauer response functions; frequency transformation; cascade designs; delay filters and delay equalization; sensitivity; *LC* ladder filters; ladder simulations by element replacement and by operational simulation; transconductance-*C* filters; and switched-capacitor filters.

Features

- Includes a wealth of examples, all of which have been tested on simulators or in actual industrial use
- Employs MATLAB® to minimize algebraic and other computational needs
- Uses Electronics Workbench® to help students simulate actual experimental behavior
- Provides sample design tables and design and performance curves
- Avoids sophisticated mathematics wherever possible in favor of algebraic or intuitive derivations

About the Authors

Rolf Schaumann was Chairman of the Department of Electrical and Computer Engineering at Portland State University and is now Professor Emeritus. He is a coeditor of *Modern Active Filter Design* (1981) and coauthor, with M. S. Ghausi and K. R. Laker, of *Design of Analog Filters: Passive, Active RC, and Switched Capacitor* (1990). Professor Schaumann is a Fellow of the IEEE and a recipient of the IEEE Millennium Medal. He is the author of over 150 refereed technical articles and conference presentations and several book chapters in the area of analog filters and circuit design.

The late Mac E. Van Valkenburg was Distinguished Professor in the Department of Electrical Engineering at the University of Illinois and the author of *Analog Filter Design* (OUP, 1982), *Introduction to Modern Network Synthesis* (1960), *Network Analysis, 3/e* (1974), *Signals in Linear Circuits* (with Jose B. Cruz, 1974), and *Reference Data for Engineers, 8/e* (1996). Professor Van Valkenburg was the author of hundreds of technical articles and a beloved teacher.

Cover design: Eve Siegel

OXFORD
UNIVERSITY PRESS
www.oup.com

90000
9 780195 118773
ISBN 0-19-511877-4